



Mašinski fakultet
Podgorica

UNIVERSITY OF MONTENEGRO
Faculty of Mechanical Engineering

UNIVERSITY OF EAST SARAJEVO
Production and Management Faculty at Trebinje
Faculty of Mechanical Engineering



8th International Scientific Conference

Research and development of mechanical
elements and systems



PROCEEDINGS

**MACHINE ELEMENTS AND SYSTEMS IN ENERGY SECTOR
DEVELOPMENT OF POWER PRODUCTION SYSTEMS**

Trebinje, September 2017

Organised by:

Asocijacija za Dizajn, Elemente i Konstrukcije
Association for Design, Elements and Constructions
Association für Design, Elementen und Konstruktionen



Partner organisations:



IFTOMM
International Federation
for the Promotion of
Mechanism and Machine
Science



Trebinje
Municipality
in Bosnia and Herzegovina



Power Utility of
Republic of Srpska



Mine and Thermal power
plant Gacko



Hydroelectric Power Plant at
Trebišnjica

UNIVERSITY OF MONTENEGRO
Faculty of Mechanical Engineering

UNIVERSITY OF EAST SARAJEVO
Production and Management Faculty at Trebinje
Faculty of Mechanical Engineering

8th International Scientific Conference

Research and development of mechanical
elements and systems



PROCEEDINGS

MACHINE ELEMENTS AND SYSTEMS
IN ENERGY SECTOR
DEVELOPMENT OF POWER PRODUCTION SYSTEMS

Trebinje, September 2017

PROCEEDINGS OF THE 8th INTERNATIONAL SCIENTIFIC CONFERENCE
"Research and development of mechanical elements and systems"
IRMES 2017,
"Machine elements and systems in energy sector, Development of power production systems"
Trebinje 2017.

Editor:

Prof. dr – Ing. Radoslav Tomović,
University of Montenegro, Faculty of Mechanical Engineering

Publisher:

University of Montenegro, Faculty of Mechanical Engineering

For publisher:

Prof. dr Igor Vušanović, dean

Reviewers:

Prof. dr Radivoje Mitrović
Prof. dr Igor Vušanović
Prof. dr Dušan Jokanović
Prof. dr Ranko Antunović

Technical preparation and design:

Ing. Aleksandar Tomović, BsC
Ing. Vidosava Vilotijević, BsC
Aleksandra Tomović, architect

Printing:

MatPrint d.o.o. - Trebinje

Number of copies: 150

CIP - Каталогизација у публикацији
Национална библиотека Црне Горе, Цетиње

ISBN 978-9940-527-53-2
COBISS.CG-ID 33677328

ISBN 978-9940-527-53-2



All the publications in this Proceedings have the authorship, whereas the authors of the papers carry entire responsibility for originality and content.

8th INTERNATIONAL SCIENTIFIC CONFERENCE

”Research and development of mechanical elements and systems“

IRMES 2017

*“Machine elements and systems in energy sector
Development of power production systems”*

Trebinje, Republika Srpska, Bosnia and Herzegovina
September 7th - 9th, 2017

Organizer:

ADEKO

Association for Design, Elements and Construction

Faculty of Mechanical Engineering, University of Belgrade, Serbia
Faculty of Mechanical Engineering, University of Montenegro, Montenegro
Institute of Structural and Computational Mechanics, Berlin
Institute of Technology (TU Berlin), Germany
Faculty of Mechanical Engineering, University of Niš, Serbia
Faculty of Technical Sciences, University of Novi Sad, Serbia
Faculty of Engineering, University of Kragujevac, Serbia
Faculty of Mechanical and Civil Engineering in Kraljevo, University of Kragujevac, Serbia
School of Mechanical Engineering, Aristotle University of Thessaloniki, Greece
Faculty of Mechanical Engineering, Slovak University of Technology in Bratislava, Slovakia
Faculty of Engineering, University Politehnica Timisoara, Hunedoara, Romania
Faculty of Mechanical Engineering, University of Technology and Economics Budapest, Hungary
Faculty of Mechanical Engineering, University of Ljubljana, Slovenia
Faculty of Mechanical Engineering, Technical University of Sofia, Bulgaria
Faculty of Mechanical Engineering, University of East Sarajevo, RS, Bosnia and Herzegovina
Faculty of Mechanical Engineering, University of Banja Luka, RS, Bosnia and Herzegovina
Faculty of Mechanical Engineering, Ss. Cyril and Methodius University in Skopje, FYROM
Technical Faculty Bitola, University St. Kliment Ohridski in Bitola, FYROM
Faculty of Mechanical Engineering, University Džemal Bijedić of Mostar, Bosnia and Herzegovina
Faculty of Mechanical Engineering and Computing, University of Mostar, Bosnia and Herzegovina
"Logos Centar" College Mostar, Bosnia and Herzegovina
Production and Management Faculty at Trebinje, University of East Sarajevo, RS, Bosnia and Herzegovina

Host organizer:

FACULTY OF MECHANICAL ENGINEERING
UNIVERSITY OF MONTENEGRO

Co-organizer:

PRODUCTION AND MANAGEMENT FACULTY AT TREBINJE,
FACULTY OF MECHANICAL ENGINEERING
UNIVERSITY OF EAST SARAJEVO, RS, BOSNIA AND HERZEGOVINA

Supported by:

IFToMM
International Federation for the Promotion of Mechanism and Machine Science
TREBINJE
Municipality in Bosnia and Herzegovina

REVIEWERS

Prof.dr.-Ing., Milorad Burić, University of Montenegro, Montenegro
Prof.dr.-Ing., Milosav Ognjanović, University of Belgrade, Serbia
Prof.dr.-Ing., Lozica Ivanović, University of Kragujevac , Serbia
Prof.dr.-Ing., Radoslav Tomović, University of Montenegro, Montenegro
Prof.dr.-Ing., Biljana Marković, University of East Sarajevo, RS, Bosnia and Herzegovina
Prof.dr.-Ing., Blaža Stojanović, University of Kragujevac , Serbia
Prof.dr.-Ing., Ranko Antunović, University of East Sarajevo, RS, Bosnia and Herzegovina
Prof.dr.-Ing., Safet Isić, University Džemal Bijedić of Mostar, Bosnia and Herzegovina
Prof.dr.-Ing., Janko Jovanović, University of Montenegro, Montenegro
Prof.dr.-Ing., Marina Mijanović Markuš, University of Montenegro, Montenegro
Prof.dr.-Ing., Radoš Bulatović, University of Montenegro, Montenegro
Prof.dr.-Ing., Uroš Karadžić, University of Montenegro, Montenegro
Prof.dr.-Ing., Mirko Blagojević, University of Kragujevac , Serbia
Doc.dr.-Ing., Milan Banić, University of Niš, Serbia
Doc.dr.-Ing., Milan Rackov, University of Novi Sad, Serbia
Doc.dr.-Ing., Radoje Vujadinović, University of Montenegro, Montenegro
Doc.dr.-Ing., Obrad Spaić, University of East Sarajevo, RS, Bosnia and Herzegovina

International Scientific Committee

President:

Prof.dr.-Ing., Radivoje Mitrović, University of Belgrade, Serbia

Secretary:

Prof.dr.-Ing., Blaza Stojanovic, University of Kragujevac , Serbia

Members:

Prof. dr.-Ing. Marco Ceccarelli, IFToMM President, University of Cassino, Italy

Prof. dr.-Ing. Veniamin Goldfarb, Izhevsk State Technical University, Russia

Prof. dr.-Ing. Daizhong Su, Nottingham Trent University, United Kingdom

Prof. dr.-Ing. Dragan Marinković, Technische Universität Berlin, Germany

Prof. dr.-Ing. Manfred Zehn, Technische Universität Berlin, Germany

Prof. dr.-Ing. Dragan Đurđanović, University of Texas at Austin, USA

Prof. dr.-Ing. Vlado Lubarda, University of California, San Diego, USA

Prof. dr.-Ing. Miki Hondžo, University of Minnesota, USA

Prof. dr.-Ing. Victor E. Starzhinsky, National Academy of Sciences of Belarus, Belarus

Prof. dr.-Ing. Aleksandar Subić, Swinburne University of Technology, Melbourne, Australia

Prof. dr.-Ing. Pavan Kumar Kankar, Indian Institute of Information Technology, India

Prof. dr.-Ing. Prof. Ling Zhou, Hohai University, China

Prof. dr.-Ing. Miroslav Vereš, Slovak University of Technology in Bratislava, Slovakia

Prof. dr.-Ing. Mikael Möller, Lulea University of Technology, Sweden

Prof. dr.-Ing. Nikolai Balc, Technical University of Cluj-Napoca, Romania

Prof. dr.-Ing. Marian Borzan, Technical University of Cluj-Napoca, Romania

Prof. dr. Lucian Tudose, Technical University of Cluj-Napoca, Romania

Prof. dr.-Ing. Athanassios Mihailidis, Aristotle University of Thessaloniki, Greece

Prof. dr.-Ing. Vilmos Simon, Budapest University of Technology and Economics, Hungary

Prof. dr.-Ing. József Sárosi, University of Szeged, Hungary

Prof. dr.-Ing. Tamas Mankovits, University of Debrecen, Hungary

Prof. dr.-Ing. Ljubomir Dimitrov, Technical University of Sofia, Bulgaria

Prof. dr.-Ing. Jože Duhovnik, University of Ljubljana, Slovenia

Prof. dr.-Ing. Božidar Križan, University of Rijeka, Croatia

Prof. dr.-Ing. Vladeta Radović, University of Montenegro, Montenegro

Prof. dr.-Ing. Radoš Bulatović, University of Montenegro, Montenegro

Prof. dr.-Ing. Radoslav Tomović, University of Montenegro, Montenegro

Prof. dr.-Ing. Milorad Burić, University of Montenegro, Montenegro
Prof. dr.-Ing. Igor Vušanović, University of Montenegro, Montenegro
Prof. dr.-Ing. Bozidar Rosić, University of Belgrade, Serbia
Prof. dr.-Ing. Milosav Ognjanović, University of Belgrade, Serbia
Prof. dr.-Ing. Mileta Ristivojević, University of Belgrade, Serbia
Prof. dr.-Ing. Mirko Blagojević, University of Kragujevac. Serbia
Prof. dr.-Ing. Nenad Marjanović, University of Kragujevac. Serbia, Serbia
Prof. dr.-Ing. Dragan Milčić, University of Niš, Serbia
Prof. dr.-Ing. Dušan Stamenković, University of Niš, Serbia
Prof. dr.-Ing. Vojislav Miltenović, University of Niš, Serbia
Prof. dr.-Ing. Sinisa Kuzmanović, University of Novi Sad, Serbia
Prof.dr.-Ing., Biljana Markovic, University of East Sarajevo, RS, Bosnia and Herzegovina
Prof. dr.-Ing. Remzo Dedić, University of Mostar, Bosnia and Herzegovina

International Programme Committee

President:

Prof.dr.-Ing., Radoslav Tomović, University of Montenegro, Montenegro

Secretary:

Dipl.-Ing. Žarko Mišković, M.Sc., University of Belgrade, Serbia

Members:

Prof. dr.-Ing. Radivoje Mitrović, University of Belgrade, Serbia
Prof.dr.-Ing., Safet Isić, University Džemal Bijedić of Mostar, Bosnia and Herzegovina
Prof. dr.-Ing. Ljubomir Dimitrov, Technical University of Sofia, Bulgaria
Prof. dr.-Ing. Biljana Marković, University of East Sarajevo, RS, Bosnia and Herzegovina
Prof. dr.-Ing. Adisa Vučina, University of Mostar, Bosnia and Herzegovina
Prof. dr.-Ing. Uroš Karadžić, University of Montenegro, Montenegro
Prof. dr.-Ing. Janko Jovanović, University of Montenegro, Montenegro
Prof. dr.-Ing. Lozica Ivanović, University of Kragujevac. Serbia
Prof. dr.-Ing. Blaža Stojanović, University of Kragujevac. Serbia
Doc. dr.-Ing. Milan Tica, University of Banja Luka, RS, Bosnia and Herzegovina
Doc. dr.-Ing. Milan Banić, University of Niš, Serbia
Doc. dr.-Ing. Milan Rackov, University of Novi Sad, Serbia
Doc. dr.-Ing. Radoje Vujadinović, University of Montenegro, Montenegro

Organizing Committee

President:

Prof.dr.-Ing., Radoslav Tomović, University of Montenegro, Montenegro

Secretary:

Ing. Vidosava Vilotijević, University of Montenegro, Montenegro

Members:

Prof. dr.-Ing. Igor Vušanović, University of Montenegro, Montenegro

Prof.dr.-Ing., Ranko Antunović, University of East Sarajevo, RS, Bosnia and Herzegovina

Prof. dr. Dušan Jokanović, University of East Sarajevo, RS, Bosnia and Herzegovina

Prof. dr.-Ing. Janko Jovanović, University of Montenegro, Montenegro

Doc. dr.-Ing. Zoran Stamenić, University of Belgrade, Serbia

Doc. dr.-Ing. Aleksandar Košarac, University of East Sarajevo, RS, Bosnia and Herzegovina

Doc. dr. Blagoje Šupić, University of East Sarajevo, RS, Bosnia and Herzegovina

Doc. dr.-Ing. Budimirka Marinović, University of East Sarajevo, RS, Bosnia and Herzegovina

Mr.-Ing. Luka Petrović, Municipality of Trebinje, RS, Bosnia and Herzegovina

Dipl.-Ing. Gordan Mišeljić, Hydroelectric Power Plant at Trebišnjica, RS, Bosnia and Herzegovina

Dipl.-Ing. Ilija Tamindžija, Hydroelectric Power Plant at Trebišnjica, RS, Bosnia and Herzegovina

Mr.-Ing. Boro Vujučić, Mine and Thermal power plant Gacko, RS, Bosnia and Herzegovina

Ing. Marko Mumović, University of Montenegro, Montenegro

Ing. Aleksandar Tomović, University of Montenegro, Montenegro

Marko Radić, Tourist Organization Of Trebinje, RS, Bosnia and Herzegovina

General sponsors



***Power Utility of Republic of
Srpska - Trebnje***



***Mine and Thermal power plant
Gacko***



***Hydroelectric Power Plant at
Trebišnjica – Trebinje***

Sponsors



***BerDiz Consulting AB
Göteborg - Sverige***



ANDRITZ HYDRO GmbH



***EMG Engineering Tomović
Nevesinje***



***TRC pro - d.o.o
PETROVARADIN***



Dear Ladies and Gentlemen, participants and sympathizers of the IRMES 2017 Conference,

It is our pleasure to introduce you Proceedings of the 8th International Scientific Conference „Research and development of mechanical elements and systems“ – IRMES 2017, which is being organized in Trebinje in the period from 7th to 9th September, 2017.

IRMES is one of the most important and largest conferences in the area of mechanical engineering in South-Eastern Europe. The conference is organized under the auspices of the "Association for Design, Elements and Constructions" (ADEKO), which brings together 22 higher education and scientific institutions and a large number of researchers and engineers from Central and South-Eastern Europe.

We are proud to point out that this year's IRMES has been supported by the International federation for the Promotion of Mechanisms and Machine Science - IFToMM, one of the most important world associations of scientists and engineers. Entering for the second time in a row in the official calendar of IFToMM, the IRMES conference is slowly expanding its boundaries and becoming recognizable to the scientific community around the world. The evidence for this is that the conference papers were submitted by researchers which coming from 16 different countries, from 4 continents.

The honor to host the conference was awarded to the University of Montenegro (Faculty of Mechanical Engineering, Podgorica), and co-organizers are the University of East Sarajevo (Faculty of Production and Management in Trebinje and Faculty of Mechanical Engineering in East Sarajevo). The joint organization of this conference is just another step in a series of successful cooperation between this two Universities.

The topic of the conference is: MACHINE ELEMENTS AND SYSTEMS IN ENERGY SECTOR – DEVELOPMENT OF POWER PRODUCTION SYSTEMS.

The goal of the conference is:

- To connect the academic community, professors and researchers with engineers and businessmen, to share their experiences and establish new business relationships, in order to encourage better cooperation and industrial activity in the region.*
- To introduce new technologies, products and solutions with the aim of better utilization of available resources, increasing energy efficiency, reducing maintenance and production costs, extending working life and availability of energy facilities, and reducing the cost of electricity.*

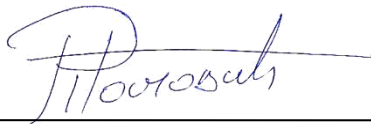
The papers presented in this Proceedings represent the source of the latest and most relevant information primarily in the areas of product development and machine design, construction calculations, power transfer and motion, 3D modeling and analysis by finite element method, rapid production prototyping, new production technologies and materials, maintenance, reparation and monitoring of mechanical elements and systems. A widely was accepted approach in which product development, new technology and innovation are the most important drivers of the development of the economy, ranging from small enterprises to the state level. Of particular importance are the papers dealing with sustainable development with an accent on increasing the efficiency of production, energy efficiency, exploitation of renewable energy sources and environmental protection.

By starting a discussion related to current issues in the field of energy, the conference organizer intends to contribute to overcoming the gap between science and practice through the exchange of new co-habits, forasmuch as the necessity for modern solutions developed in this field to be best applied in our economy, primarily in the real sector. Special attention is paid to the thematic areas within the framework of a round table (panel) in order to better understand and solve current problems.

The papers from the IRMES 2017 Conference are divided into seven different thematic areas: Mechanical systems and Elements, Power and motion transmission systems, New production technologies and materials, Hydro and Thermal power plants, Mechanical systems monitoring and maintenance, Sustainable development in the energy industry. A part in the conference took 225 authors from 16 countries, with a total of 88 papers, including 5 plenary lectures. All papers contained in the Proceedings have been reviewed and accepted for publication by the Program Committee. At the conference, the organization of one work meeting is planned, as well as several presentations from very recognized world companies.

On behalf of the organizer of the IRMES 2017 conference, I would like to thank all the authors, reviewers, members of the Scientific and Program Committee, institutions, sponsors and everyone who in any way contributed to the realization of the conference. Our greatest pleasure is if we have contributed to the expansion of the ADEKO mission at the local, regional and global level through the organization of the conference.

Podgorica, Belgrade, 25th August 2017.



Prof. Dr.-Ing. Radoslav Tomović

Faculty of Mechanical Engineering,
University of Montenegro
President of the IRMES 2017
the Programme and Organizing Committee



Prof. Dr.-Ing. Radivoje Mitrović

Faculty of Mechanical Engineering,
University of Belgrade
President of the IRMES 2017
the International Scientific Committee



International Federation for the Promotion of Mechanism and Machine Science

www.iftomm.net

PRESIDENT	Prof. Marco Ceccarelli, Department of Civil and Mechanical Engineering, University of Cassino and South Latium, Via G. Di Biasio 43, 03043 Cassino, Italy Tel: +39 0776-2993663, Fax: +39 0776-2993689, E-mail: ceccarelli@unicas.it
VICE-PRESIDENT- (acting)	Prof. Tian Huang, School of Mechanical Engineering, Tianjin University, Tianjin 300072, China Tel: +86 22 2740 5280, Fax: +86 22 2740 5280 Email: tianhuang@tju.edu.cn
SECRETARY-GENERAL	Prof. Teresa Zielinska, Warsaw University of Technology, Faculty of Power and Aeronautical Engineering, ITLiMS, ul. Nowowiejska 24, 00-665 Warsaw, Poland Tel: +48 234 7790, Fax: +48 234 7513, E-mail: teresaz@meil.pw.edu.pl
TREASURER	Prof. Juan Antonio Carretero, Department of Mechanical Engineering, University of New Brunswick, 15 Dineen Dr., Fredericton, NB, E3B 5A3, Canada Tel: +1 506 458-7454, Fax: +1 506 453-5025, E-mail: juan.carretero@unb.ca

Trebinje, Bosnia and Herzegovina 8th International Scientific Conference – Research and Development of Mechanical Elements and Systems, IRMES 2017 http://www.irmes2017.ac.me/organizacioni.php?jezik=en	Radoslav Tomovic radoslav@ac.me	September 7-9, 2017
--	---	---------------------

Dear Organizers and Participants of IFTToMM sponsored conference **IRMES 2017**

I am very sorry not be there with you as I originally planned with my participation to **IRMES 2017** event.

It is an honour for me, as IFTToMM President, to address these few words of welcome and wishes to the participants for a fruitful conference time during this conference **IRMES 2017**, the conference organized of the IFTToMM MO Serbia and Montenegro. Let's remind also the IFTToMM distinguished figure of Alexander Veg and pay tribute to his efforts and contribution to the IFTToMM mission!

This conference is an important conference forum for discussing specific topics of the IFTToMM activity, even with the aim to promote IFTToMM and MMS not only by involved MO and TC. The IFTToMM patronage of this conference event has a particular significance for the fact that this conference event has been organized successfully with the typical IFTToMM atmosphere in a regional area in order to provide suitable environment for enhancing and starting collaborations and disseminating last advances in MMS and in specific fields.

I congratulate the organizers and their teams for the very successful organization of this **IRMES 2017!**

IFTToMM is particularly careful to aspects both of scientific and social activity as intended to promote both MMS disciplines and IFTToMM Community. I am sure that all the participants will contribute successfully to the abovementioned goals by sharing studies and results with other colleagues not only from the IFTToMM Community. Therefore, I thank the participants and organizers for having supported the IFTToMM traditional high-quality standard for this conference with your active participation.

Another important event will be the 2019 IFTToMM World Congress that will be held in Krakow, Poland in June 2019 as 50th Jubilee IFTToMM anniversary where we hope to have a large participation of colleagues from all around the world, even from those countries that have not yet IFTToMM Member Organizations. There we could also have more advances on MMS and therefore this is to invite all you participants to join the IFTToMM World Congress 2019 too.

I wish you a wonderful time at this IFTToMM sponsored conference event, both from technical and social viewpoints

prof. Marco Ceccarelli
President of IFTToMM (2016-2019)

Cassino, 16 August 2017
www.iftomm.net

EXECUTIVE COUNCIL

Prof. M. Ceccarelli (President), prof. Y. Nakamura (Past-President), prof. Tian Huang, (Vice-President- acting), prof. T. Zielinska (Secretary General), prof. J.A. Carretero (Treasurer), prof. B. Corves, prof. C. I. Dede, prof. A. Ghosal, dr. J.P. Merlet, prof. F. Viadero.

CONTENTS:

LECTURES BY INVITATION

1. **INNOVATING MMS AND IFTOMM IN INNOVATION CHALLENGES**
Marco CECCARELLI 3
2. **MICRO SYSTEM TECHNOLOGY AND INDUSTRIAL APPLICATION - STATE OF THE ART AND CURRENT TRENDS**
Klaus - Peter KAEMPER 9

INTRODUCTORY LECTURES

3. **ROLE, IMPORTANCE AND MISSION OF ADEKO**
Vojislav MILTENović 13
4. **GEAR TRANSMISSION FAILURES AND FAILURE BASED DESIGN**
Milosav OGNJANOVIĆ, Nenad KOLAREVIĆ, Miloš STANKOVIĆ, Sanja VASIN 21
5. **THE INFLUENCE F THE DESIGN FLOW RATE ON THE ECONOMICAL AND ECOLOGICAL ASPECTS OF SHP - SMALL HYDROPOWER PLANTS**
Petar V. VUKOSLAVČEVIĆ 27

MECHANICAL SYSTEMS AND ELEMENTS

6. **ROOT CAUSE ANALYSIS OF MICRO CRACKS OF HYDROGEN REFORMER HG**
Samir DIZDAR, Radoslav TOMOVIĆ, Adisa VUČINA 37
7. **EXAMINATION OF ULTIMATE BENDING STRENGTH OF POWDER METALLUGRY GEARS**
Lubomir DIMITROV, Georgi DIMCHEV, Pancho TOMOV, Kiril NIKOLOV 43
8. **OPTIMAL PROFILES OF CYLINDRICAL ROLLERS OF ROLLING BEARINGS**
Lucian TUDOSE, Cristina TUDOSE, Constantin URSACHE 47
9. **COMPARABILITY OF EXERIMENTAL AND ANALYTICAL STUDY OFTHE EFFECT RADIAL LOAD AND ROTATION SPEED ON FRICTION COEFFICIENT OF RADIAL PLAIN BEARING UNDER LUBRICANT CONDITIONS USING RAIMONDI AND BOYD'S CHARTS**
Amir Al-SAMMARRAIE, Dragan MILČIĆ, Milan BANIĆ, Sulaiman AL-BASAQR, Sabah SALIH..... 53
10. **RELIABILITY OF NECESSARY PRESSURE FROM THE REQUIRED LIQUID QUANTITY FOR LUBRICATION OF ENGINE CYLINDER IN THE PERIOD OF ONE WORKING CYCLE FOR UNSTEADY FLUID FLOW**
Dečan IVANOVIĆ 59

11. THE COMPARE OF ANGLES OF REPOSE WITH DISCRETE ELEMENT METHOD AND MEASUREMENT	
Tibor POÓS, Dániel HORVÁTH, Kornél TAMÁSH	65
12. DETERMINATION OF WEAR IN CONTACT OF WHEEL-RAIL SET USING FEM	
Milan BANIĆ, Dušan STAMENKOVIĆ, Miloš MILOŠEVIĆ, Aleksandar MILTENOVIĆ	71
13. DETERMINING THE BOUNDARIES OF PREDICTION INTERVALS IN SERVICE NETWORKS USING SIMULATION	
Vladimir JERZ	75
14. VEHICLE DRIVING SAFETY AND RIDE COMFORT IMPROVEMENT WITH MAGNETORHEOLOGICAL SHOCK ABSORBERS	
Ján DANKO, Tomáš MILESICH, Jozef BUCHA	81
15. IMPACT OF THE SUSPENSION PARAMETERS ON THE VERTICAL DYNAMICS OF THE VW E-UP	
Jozef BUCHA, Ján DANKO, Tomáš MILESICH	85
16. THE NEW METHOD OF INCREASING THE AMOUNT OF RESIN IN THE WINDING OF MOTOR	
Bohumil KOTLARIK, Janka SULOVA, Zuzana FILOVÁ, Alena KOZAKOVA, Katarína KUBALOVÁ, Daša KRUPJEJOVÁ	91
17. STATICAL ANALYSIS OF MEASUREMENTS IN A VEHICLE BRAKE TESTER	
Radoš BULATOVIĆ, Janko JOVANOVIĆ, Radoslav TOMOVIĆ	97
18. INFLUENCE OF LEAKAGE CLEARANCE ON PRESSURE VARIATION IN GEROTOR PUMP CHAMBERS	
Lozica IVANOVIĆ, Andreja ILIĆ, Blaža STOJANOVIĆ, Jasna GLIŠOVIĆ, Miloš MATEJJIĆ	105
19. OPTIMAL SYNTHESIS OF THE ROBOT EYES DRIVE SYSTEM WITH 7 DOFs	
Marko PENČIĆ, Maja ČAVIĆ, Milan RACKOV	111
20. HUMAN ACTION RECOGNITION BY ROBOT VISION SYSTEM BASED ON KALMAN FILTER AND NEURAL NETWORK CLASSIFICATION	
Emina PETROVIĆ, Miloš SIMONOVIĆ, Ivan ĆIRIĆ, Vlastimir NIKOLIĆ	117
21. VIBRATION CHARACTERISTICS STUDY OF SELF-PROPELLED MACHINE FOR CORN SPRAYING AND DETASSELING	
Boris STOJIĆ	123
22. CAD/CAM INTEGRATION OF THE FORKED ROD DESIGN OF THE SERVICE ROBOT CONTROL MECHANISM	
Milan VUKČEVIĆ, Nikola ŠIBALIĆ, Marina MIJANOVIĆ, Darko SKUPNJAK	129
23. MODELLING AND CALCULATION OF A BELT CONVEYOR	
Nenad MILORADOVIĆ, Igor ANTIĆ, Rodoljub VUJANAC	135
24. DEVELOPMENT OF THE CONSTRUCTION FOR THE EXAMINATION OF ROLLING BEARINGS	
Radoslav TOMOVIĆ	141

25. PRODUCT DEVELOPMENT PROCESS REGARDING TO CUSTOMER EMOTIONAL	
Biljana MARKOVIĆ, Lozica IVANOVIĆ, Aleksija ĐURIĆ	149
26. A NEW MODIFICATION OF GENETIC ALGORITHM FOR SOLVING ENGINEERING OPTIMIZATION PROBLEMS	
Nenad MARJANOVIĆ, Nenad KOSTIĆ, Nenad PETROVIĆ, Mirko BLAGOJEVIĆ, Miloš MATEJIĆ.....	153
27. CONTEMPORARY DESIGN AND RECONSTRUCTIVE ENGINEERING BY FDM METHOD	
Saša RANĐELOVIĆ, Dejan MOVRIN, Mladimir MILUTINOVIĆ, Srđan MLADENOVIĆ, Vladislav BLAGOJEVIĆ	157
28. DETERMINATION OF MUSCLE TISSUE PROPERTIES FOR FEA APPLICATIONS	
Branislav DIMITRIJEVIĆ, Milan BANIĆ, Žarko MIŠKOVIĆ, Radivoje MITROVIĆ, Aleksandar MILTENOVIĆ, Miša TOMIĆ	161
29. ADJUSTED DESIGN OF A COMPUTER MOUSE WITH ERGONOMIC REQUIREMENTS	
Inga KREŠIĆ, Nebojša RAŠOVIĆ	165
30. EFFECTS OF OUTLET NOZZLE SLOPE ANGLE ON ACCURACY OF MACHINE PARTS' GEOMETRICAL CONTROL	
Dragiša SKOKO, Mileta RISTIVOJEVIĆ, Cvetko CRNOJEVIĆ	169
31. CONCEPT SOLUTION OF THE SAFETY SYSTEM FOR AVOIDING WRONG FUEL USING IN CARS AND PREVENTION OF DAMAGE	
Milan TICA, Milan RACKOV, Djordje MILTENOVIĆ, Aleksandar MILTENOVIĆ, Milan BANIĆ	175

POWER AND MOTION TRANSMISSION SYSTEMS

32. THE INFLUENCE OF HELIX ANGLE ON THE LOAD CAPACITY OF CYLINDRICAL GEAR TEETH FLANKS	
Mileta RISTIVOJEVIĆ, Bozidar ROSIĆ, Aleksandar DIMIĆ	183
33. INFLUENCE TEMPERATURE ON STIFFNESS MATRIX FOR PAIRED (DUPLEX) ANGULAR CONTACT BALL BEARINGS	
Aleksandar ŽIVKOVIĆ, Milan ZELJKOVIĆ, Slobodan TABAKOVIĆ	189
34. ON THE FRICTIONAL HEATING OF SPUR GEARS OPERATING UNDER LOW ROTATIONAL SPEEDS	
Janko JOVANOVIĆ, Radoš BULATOVIĆ	195
35. NEW METHODOLOGIES FOR GEAR DESIGN IN ENERGY EFFICIENT POWER TRANSMISSIONS	
Ivana ATANASOVSKA, Saravanan KARUPPANAN, Santosh PATIL	203
36. COMPARATIVE ANALYSIS OF VIBRO-IMPACT OSCILLATIONS OF SPUR GEAR PAIR FOR VARIATION OF GEARS TRANSMISSION RATIO	
Ivana ATANASOVSKA, Katica R. (STEVANOVIĆ) HEDRIH	209
37. OPTIMAL SELECTION OF A TWO-SPEED TWO-CARRIER PLANETARY TRAIN	
Jelena STEFANOVIĆ-MARINOVIĆ, Sanjin TROHA, Miloš MILOVANČEVIĆ	215

38. THE INFLUENCE OF LUBRICANT VISCOSITY ON THE EFFICIENCY OF WORM GEAR REDUCER	
Blaža STOJANOVIĆ, Saša RADOSAVLJEVIĆ, Sandra VELIČKOVIĆ, Slavica MILADINOVIĆ, Milan BUKVIĆ	219
39. ANALYSIS OF THE TEETH NUMBER INFLUENCE ON THE GEAR MODULE SIZE AND LOAD CARRYING CAPACITY OF GEAR PAIR OF UNIVERSAL HELICAL GEAR DRIVES	
Milan RACKOV, Mirko BLAGOJEVIĆ, Siniša KUZMANOVIĆ, Miloš MATEJIĆ, Ivan KNEŽEVIĆ, Maja ČAVIĆ, Marko PENČIĆ	225
40. IMPROVING THE PERFORMANCE OF BALL ROLLER BEARINGS USING NEW MATERIALS	
Vesna JELIĆ, Nataša SOLDAT, Zoran STAMENIĆ	231
NEW PRODUCTION TECHNOLOGIES AND MATERIALS	
41. DETERMINATION OF KINEMATIC STATE IN BULK METAL FORMING	
Mileta JANJIĆ, Milan VUKČEVIĆ	237
42. TOPOGRAPHY OF CHARACTERISTIC SURFACES OF MODEL HOB MILLING TOOLS FOR MACHINING OF GEAR SERRATION	
Ivan SOVILJ-NIKIĆ, Sandra SOVILJ-NIKIĆ, Bogdan SOVILJ, Vladimir BLANUŠA	241
43. IMPACT TOUGHNESS OF HIGH-STRENGTH LOW-ALLOY STEEL WELDED JOINTS	
Andreja ILIĆ, Lozica IVANOVIĆ, Blaža STOJANOVIĆ, Danica JOSIFOVIĆ, Eleonora DESNICA	247
44. FAILURE MODE AND STRENGTH ANALYSES OF RESISTANCE SPOT WELD JOINTS OF ALUMINIUM AND AUSTENITIC STAINLESS STEEL SHEET	
Aleksija ĐURIĆ, Biljana MARKOVIĆ	253
45. ADVANCED FW AND AFP/ATL TECHNOLOGIES FOR PRODUCTION OF COMPLEX PARTS OF COMPOSITE MATERIALS	
Svetlana RISTESKA, Blagoja SAMAKOSKI, Vladimir DUKOVSKI	259
46. APPLICATION OF TAGUCHI METHODS WITH OPTIMIZATION OF FIBRE ORIENTATION ANGLE OF LAMINATED AL/ARAMID/EPOXY COMPOSITE CARDAN SHAFT	
Jasmina BLAGOJEVIĆ, Zorica DJORDJEVIĆ, Sandra VELIČKOVIĆ	265
47. RAPID PROTOTYPING AND MANUFACTURING FOR MODEL OF HUMAN HEAD	
Saša ŽIVANOVIĆ	271
48. PREDICTION OF THE OPTIMAL MICRO HARDNESS AND CRYSTALLINE SIZE OF NANOSTRUCTURE VIA MACHINING AND NEURO-FUZZY TECHNIQUE	
Dalibor PETKOVIĆ, Miloš MILOVANČEVIĆ	277
49. PREDICTION OF THE OPTIMAL MICRO HARDNESS AND CRYSTALLINE SIZE OF NANOSTRUCTURE VIA MACHINING AND NEURO-FUZZY TECHNIQUE	
Miloš MILOVANČEVIĆ, Dalibor PETKOVIĆ	281

50. THE INFLUENCE OF THE INPUT PARAMETERS TO THE DIMENSIONAL ACCURACY OF THE 3D PRINTED PROTOTYPE	
Obrad SPAIĆ, Aleksandra KOPRIVICA, Mirjana JOKANOVIĆ, Srđan ĆURIĆ	285
51. CUTTING FORCES DURING ULTRASONIC ASSISTED TURNING OF HARD TO MACHINE MATERIAL SPM10	
Vladimir PUCOVSKI, Milenko SEKULIĆ, Marin GOSTIMIROVIĆ, Pavel KOVAČ, Borislav SAVKOVIĆ, Darko JOVANOVIĆ	291
52. THE USE OF MODERN INFORMATION TECHNOLOGIES IN THE EDUCATIONAL PROCESS OF GRAPHIC ENGINEERS AND DESIGNERS	
Gojko VLADIĆ, Dragoljub NOVAKOVIĆ, Nemanja KAŠIKOVIĆ, Neda MILIĆ, Sandra DEDIJER	297
53. LASERES WITH THE SOLID EASY AND THEIR APPLICATIONS FOR GRAVING ON TRANSPARENT MATERIALS	
Dragana ĐURAŠKOVIĆ, Mileta JANJIĆ	301

HYDRO AND THERMAL POWER PLANTS

54. DESIGN OF WATER HAMMER CONTROL STRATEGIES IN HYDRPOWER PLANTS	
Anton BERGANT, Jernej MAZIJ, Uroš KARADŽIĆ	309
55. THE NUMERICAL CALCULATION BIFURCATION A6 OF PIPELINE C3 AT HPP “PERUCICA”	
Milorad BURIĆ, Radoje VUJADINOVIĆ, Igor KRESOJEVIĆ, Slaviša ĐURIŠIĆ, Marko LUČIĆ	315
56. ANALYSIS OF ECONOMIC JUSTIFICATION OF CONSTRUCTING A SMALL HYDRO POWER PLANT	
Darko SKUPNJAK, Milan VUKČEVIĆ	321
57. APPLICATION OF PROMETHEE METHOD AS SUPORT IN THE PLANNING PROCESS OF SMALL HYDROPOWER PLANTS	
Branka GVOZDENAC UROŠEVIĆ, Budimirka MARINOVIĆ, Radislav BRĐANIN, Željko ĐURIĆ	325
58. DEVELOPMENT OF WORK PLATFORMS FOR MAINTENANCE OF PENSTOCK HPP PIROT	
Dragan MILČIĆ, Miodrag VELIMIROVIĆ, Miodrag MILČIĆ	329
59. NUMERICAL ANALYSES OF TRASH RACKS CHARACTERISTICS UNDER DIFFERENT EXPLOITATION CONDITIONS IN HYDROPOWER PLANTS	
Miloš KRUNIĆ, Ivan BOŽIĆ	333
60. ANALYSIS OF TRANSIENTS IN HYDROELECTRIC POWER PLANTS FOR SPECIFICIED OPERATIONAL REGIMES	
Jovan ILIĆ, Ivan BOŽIĆ	339
61. THE FIRST FLUE GAS DESULPHURIZATION PLANT FOR THE COAL-BURNING THERMAL POWER PLANTS IN SERBIA	
Miroslav CRNČEVIĆ, Dragan ŽIVIĆ, Aleksandar GLIŠIĆ, Perica KRSTIĆ	343

62. THERMODYNAMIC ANALYSIS OF SYSTEM OF LOW-PRESSURE HEATERS THERMO-ENERGY PLANT	
Ivana KECMAN, Mirko DOBRNJAC	349

MECHANICAL SYSTEMS MONITORING AND MAINTENANCE

63. DETERMINATION OF CRITICAL SIZE OF CORROSION PIT ON MECHANICAL ELEMENTS IN HYDRO POWER PLANTS	
Radivoje MITROVIĆ, Dejan MOMČILOVIĆ, Ivana ATANASOVSKA	355
64. METHODOLOGY FOR THE REPAIR OF DAMAGES THAT OCCURRED ON THE WELDED JOINTS AT THE BODY OF GUIDE VANE APPARATUS VANES OF THE VERTICAL KAPLAN TURBINE	
Miodrag ARSIĆ, Srđan BOŠNJAK, Mladen MLADENOVIĆ, Zoranka MALEŠEVIĆ, Zoran SAVIĆ	359
65. REPAIR WELDING OF GEAR SHAFTS OF SERVICE ROLLERS AT THE ŽELEZARA SMEDEREVO	
Drakče TANASKOVIĆ, Branislav ĐORĐEVIĆ, Uroš TATIĆ, Aleksandar SEDMAK, Mirjana OPAČIĆ	365
66. THE CASE OF UNSUCCESSFUL REPAIR WELDING OF A TREIBER ROLL	
Drakče TANASKOVIĆ, Branislav ĐORĐEVIĆ, Simon SEDMAK, Uroš TATIĆ, , Marko GAJIN	371
67. MAINTENANCE OF AXIAL BEARING OF KAPLAN TURBINE	
Safet ISIĆ, Mensud ĐIDELIJA	375
68. CHALLENGES OF ROLLING ELEMENT BEARINGS FAULT DETECTION BASED ON VIBRATION SIGNAL MEASUREMENT AND ANALYSIS	
Ninoslav ZUBER	379
69. SELECTION OF RELIABLE VBRODIAGNOSTIC MODEL ROTATION MACHINES	
Ranko ANTUNOVIĆ, Nikola VUČETIĆ	385
70. VIBRATION ANALYSIS AND REPAIR PROCESS FOR THE VENTILATION SYSTEM FOR SMOKE DRAIN IN THE THERMAL POWER PLANT	
Emir NEZIRIĆ, Safet ISIĆ, Edin DŽIHO	391

SUSTAINABLE DEVELOPMENT IN THE ENERGY INDUSTRY

71. CONTEMPORARY APPROACH TO AUXILIARY MECHANIZATION OPERATIONS AND MAINTENANCE AT AN OPEN-PIT COAL MINE	
Radivoje MITROVIĆ, Dragan JOVANOVIĆ, Gradimir IVANOVIĆ, Dragan STOŠIĆ, Snežana PANTELIC, Dragan STEVIĆ	399
72. FUEL MANAGEMENT AT AUXILIARY MECHANIZATION OF OPEN-PIT COAL MINE SUPPORTED BY MODERN ICT	
Dragan STOŠIĆ, Dragan STEVIĆ, Snežana PANTELIC, Nenad NIKOLIĆ, Rastko NEGOIČIĆ, Filip TODOROVIĆ	405

73. CONTRIBUTION OF THERMAL POWER PLANT TO THE IMMISION OF PM10 IN THE CENTER OF PLJEVLJA	
Vladan IVANOVIĆ, Esad TOMBAREVIĆ	411
74. APPLICATION OF NEW TECHNOLOGIES IN THE DEVELOPMENT AND INCREASE OF WIND POWER PLANT CAPACITY	
Isak KARABEGOVIĆ	417
75. APPLICATION OF RENEWABLE ENERGY SOURCES IN TERMS OF ECONOMIC, ENVIRONMENTAL AND SOCIAL SUSTAINABILITY	
Mirjana JOKANOVIĆ, Dušan GOLUBOVIĆ, Blagoje ŠUPIĆ, Aleksandra KOPRIVICA	423
76. RESEARCH OF DEVELOPMENT AND PRODUCTION EFFECTS MACHINERY AND ELECTRIC SYSTEM FOR HYDRO POWER PLANTS ON THE BASIS OF ITS TECHNOLOGIES	
Zdravko BIJELIĆ, Biljana MILANOVIĆ, Mijana JOVIŠIĆ, Bojan JELAČIĆ	429
77. HYDRAULIC ANALYSIS OF THE WATER SUPPLY SYSTEM IN TOWN NEVESINJE	
Stanka KULJIĆ, Uroš KARADŽIĆ	437
78. SIMPLIFIED EQUILIBRIUM MODEL FOR BIOMASS AND WASTE GASIFICATION	
Beno ARBITER, Filip KOKALJ, Aleksandar JOVOVIĆ, Niko SAMEC	443
79. ANALYSIS COMBUSTION LIGNITE OF GACKO IN THE STEAM BOILER P - 64	
Borivoje VUJIČIĆ, Ženja VUJOVIĆ	449

STUDENT SESSION

80. MINI HYDRO POWER PLANT BASED ON PELTON TURBINE	
Marko MUMOVIĆ, Aleksandar TOMOVIĆ, Vuk VUJOŠEVIĆ, Marko RAŠOVIĆ, Vasilije SAMARDŽIĆ, Nikola ĆIRKOVIĆ, Radoslav TOMOVIĆ	457
81. CONSTRUCTION OF PELTONS MINI HYDROPOWER PLANT - MF MOSTAR	
Kenan PELKO, Edmin HAKALOVIĆ, Arnel MAKSUMIĆ, Muhamed GOSTO, Jasmina ŠENDRO, Safet ISIĆ	459
82. ACHIEVING LOW COST, HIGH EFFICIENCY PELTON TURBINE	
Enis HABUL, Armin MUŠIĆ, Muhamed GRAČIĆ, Sven BOREC, Mirsad BERBEROVIĆ, Emir NEZIRIĆ	461
83. HYDROTURBINE MADE FROM RECYCLED SCRAP MATERIALS	
Ahmed TAJAR, Samir RUSTEMPAŠIĆ, Amir OMERAGIĆ, Sead IMAMOVIĆ, Alem KARAOSMANOVIĆ, Emir NEZIRIĆ	463
84. MINI HYDRO POWER PLANT	
Kenan STARČEVIĆ, Nihad BEŠIĆ, Izet AHMIČEVIĆ, Dragi TIRO	465
85. CNC PLOTTER	
Aleksandar TOMOVIĆ, Vasilije SAMARDŽIĆ, Marko RAŠOVIĆ, Marko MUMOVIĆ, Vuk VUJOŠEVIĆ, Zoran MIJANOVIĆ	467
86. DEVELOPMENT OF A THERMAL POWER PLANT TUBULAR BOILER CLEANING MACHINE	
Slavoljub MARKOVIĆ, Dino TIHIĆ, Srđan ĐERIĆ, Biljana MARKOVIĆ	469

87. MOBILE NXT ROBOT THAT IS MANAGED VIA A BLUETOOTH CONNECTION	
Aleksandar TOMOVIĆ, Marko MUMOVIĆ, Vasilije SAMARDŽIĆ, Vuk VUJOŠEVIĆ, Marko RAŠOVIĆ, Marina MIJANOVIĆ MARKUŠ	471
88. TRAINABLE ROBOTIC ARM	
Marko MUMOVIĆ, Vuk VUJOŠEVIĆ, Vasilije SAMARDŽIĆ, Aleksandar TOMOVIĆ, Marko RAŠOVIĆ, Zoran MIJANOVIĆ	473
89. TACHOMETER BASED ON A HALL EFFECT	
Vasilije SAMARDŽIĆ, Vuk VUJOŠEVIĆ, Marko RAŠOVIĆ, Aleksandar TOMOVIĆ, Marko MUMOVIĆ, Marina MIJANOVIĆ MARKUŠ	475
INDEX OF AUTHORS	479
PRESENTATIONS OF SPONSOR	483

LECTURES BY INVITATION

INNOVATING MMS AND IFTOMM IN INNOVATION CHALLENGES

Marco CECCARELLI

Abstract: *In this paper concepts and activities for innovation challenges are presented as function of a significant role of technical contents on MMS (Mechanism and Machine Science) and IFToMM community. Examples are discussed to show past and present challenges in the areas of mechanical systems, including concerns on real novelty of today solutions. Innovation of MMS is highlighted in terms of community of the IFToMM federation by indicating IFToMM activities as results and aims in knowledge transfer and worldwide coordination.*

Key words: *Mechanism and Machine Science, IFToMM, mechanical systems, Innovation*

1. INTRODUCTION

Everywhere is asked for innovation in technological developments.

But what does innovation mean? What is the role of MMS (Mechanism and Machine Science) in innovation challenges?

Innovation is a complex activity with multidisciplinary contents to improve technological developments with practical implementations for benefits both of their producers and users. In the last decades Science achievements have made possible new engineering developments (and vice versa!) in many fields with fast evolutions more than in the past. This has produced even competition in developing solutions and innovation has raised to be fundamental for further developments in products, manufacturing and communities (scientists, engineers, and entrepreneurs). Those aspects and trends are today discussed and solicited from many viewpoints of innovation multidisciplinary activity and sometimes some aspects are overestimated as due to specific experience and expertise of the actors of discussions. A rich literature is available even from each aspect of the innovation activity. References are not included in the paper since its general character and as based on personal experience of the author.

MMS achievements are developed in theoretical, numerical, and design works that once implemented in engineering practice or in science applications they contribute to innovation or even they are innovation themselves. In this paper, a short presentation is attempted to clarify innovation mainly as related to technical aspects that are linked to MMS and IFToMM.

2. INNOVATION MEANING

In general, innovation can be understood as a transfer of knowledge and its applications into market sales. *Fig 1a*) summarizes the concept of innovation as a multi-

disciplinary complex of activities and actors. Innovation is achieved not only with novel ideas but mainly when the knowledge transfer reaches successfully the real world with users' acceptance. This complex of activities includes a variety of skills and when just one is weak or fails, the whole transfer process will fail. Innovation can be started when a technical idea or solution has potential contents. Thus, initiators of innovation are designers or scientists with engineering skills, but in general the main exploiters are business experts or enterprise leaders, who produce the idea at proper levels of market valorisation and users' acceptance. But, not only new solutions make innovation, since very often is the exploitation plan that produces innovation, like for example when a product reaches the market sales with no other competitors. Therefore, the success of innovation requires a full understanding of what can be transferred with enterprise perspectives for market sales toward properly solicited / identified users. Summarizing: Science and Technology are the fundamentals, but Economics and Administration are the motors, and Education and Publicity are important tools of Innovation. University frames can be involved both in fundamentals and tools when referring to technical contents since Education and Formation are essential areas both for conceiving new ideas and preparing users to the acceptance of those new ideas.

Procedures for innovation are proposed from different perspectives but always requiring:

- Technical novelty
- Production feasibility
- Operation efficiency
- Market exploitation

Technical aspects are often emphasized as due to design creativity and ingenuity for which patent production is considered one of the main means both of innovation defence and dissemination.

Understanding innovation concepts both in frames and activity plans can be considered fundamental for challenging innovation with well aware goals.

3. INNOVATION IN MMS

All the above considerations for understanding innovation can be referred also to MMS when innovative ideas are related to machines and their operations, and users are identified not only in general users but even in stakeholders and technique developers of mechanical/mechatronic systems. Thus, the general concept of Fig. 1.a) can be reshaped as in Fig. 1.b) when it refers to the modern concept of service machines that are designed for helping or servicing human operators in work tasks or diary life.

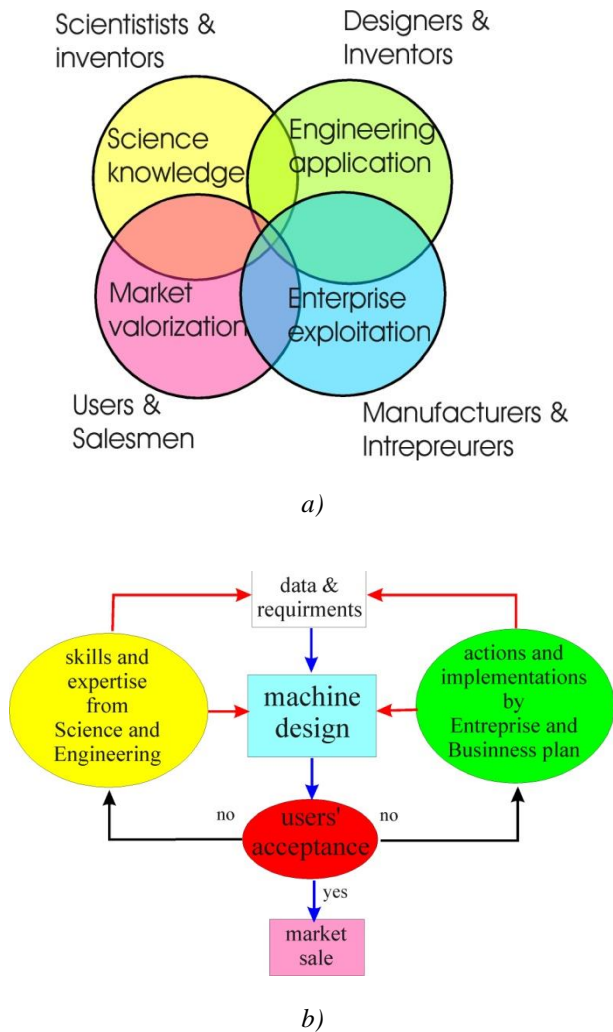


Fig. 1 Conceptual schemes for innovation challenges: a) a general meaning; b) in MMS areas.

In Fig. 1.b) the traditional engineering process is synthetically indicated in the central block of the diagram as the core of machine developments/designs. But the multidisciplinary aspects can be considered very influential in the design development of machines as coming from the two lateral blocks that summarize all those other aspects that are necessary to have a machine design and an innovation proposal with potential success results. The peculiarity of MMS areas can be summarized in the above-mentioned concept of service machines by which goals of MMS developments are finalized to improve and/or to solve new or evolved needs in users' activities both in diary life and technological labour.

4. EXAMPLES OF MMS INNOVATIVE SOLUTIONS

The following examples in Figs. 2 to 5 can clarify the above aspects of innovation meaning and challenges in MMS area with an illustrated approach. The innovation value of achievements and results in MMS is presented through few significant examples in order to stress the variety of innovation forms in MMS in terms of theory and practice of technological developments as well as in terms of knowledge acquisition and formation of next generations, involving IFToMM activities.

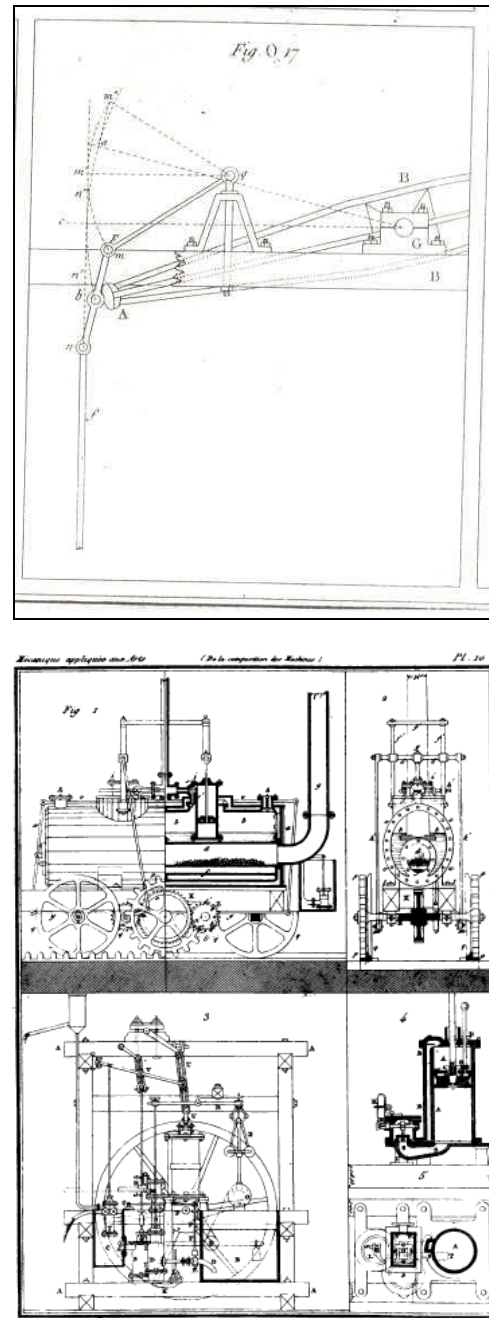


Fig. 2 Past innovation with Watt mechanism: a) early kinematic study of kinematic properties in the book by Lanz and Betancourt in 1808; b) applications for locomotives (top) and industrial plants (bottom) in the book on Composition of Machines by G.A. Borgnis in 1818.

Fig. 2 refers to the design of today very famous Watt mechanism that was used to increase the efficiency of steam motors thanks to the better accuracy in piston guidance. The success led to wide application of steam motors also in new machines for transportation and other industrial applications like the reported example in Fig. 2b). Technical novelty that is related to MMS of the time can be recognized in using coupler curve for motion guiding purposes. This is an emblematic example from the past in which knowledge, expertise, and ingenuity have produced innovation in machinery with strong impacts not only in technological developments but in social and economic evolutions.

While in the past technical contents were prominent in innovations with MMS values, today the commercial exploitation reduces the merit of technical valorisation.

Only partially this is limited with patent protections that help to give proper significance to MMS conceptions.

Fig. 3 refers to deployable mechanisms by showing the several solutions of the innovation success. The MMS theory of deployable mechanism is still a topic of intense research activity and new design solutions are continuously conceived with or without practical applications purposes, being an emblematic example of how much a technical achievement with theoretical MMS bases can be a complete innovation. The examples in Fig.3 refer to different fields of applications with specific innovation aspects. The very different fields of application can indicate how a mechanism design can contribute to innovation and technological achievements with different applications demonstrating the richness and indeed great potentiality of mechanisms.

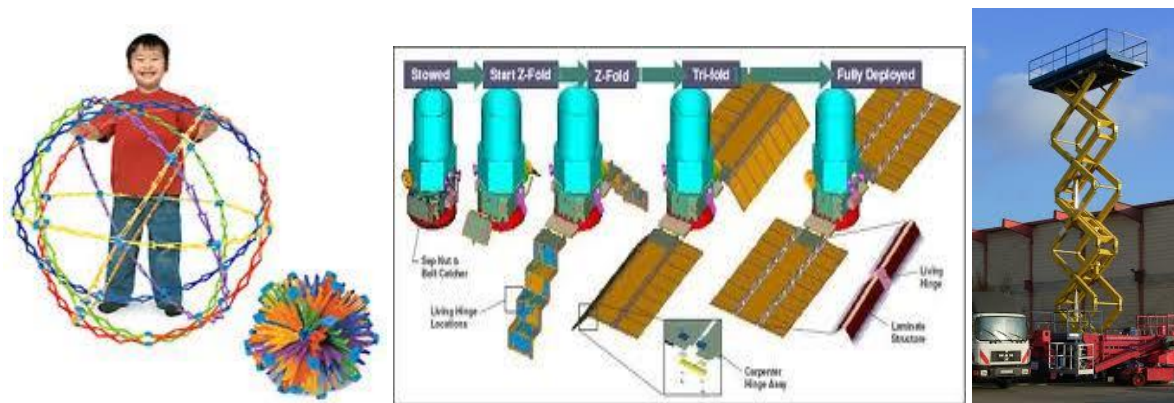


Fig.3 Deployable mechanisms in innovative applications: a) in toy design; b) for space antenna structures; c) in load lifters for civil engineering

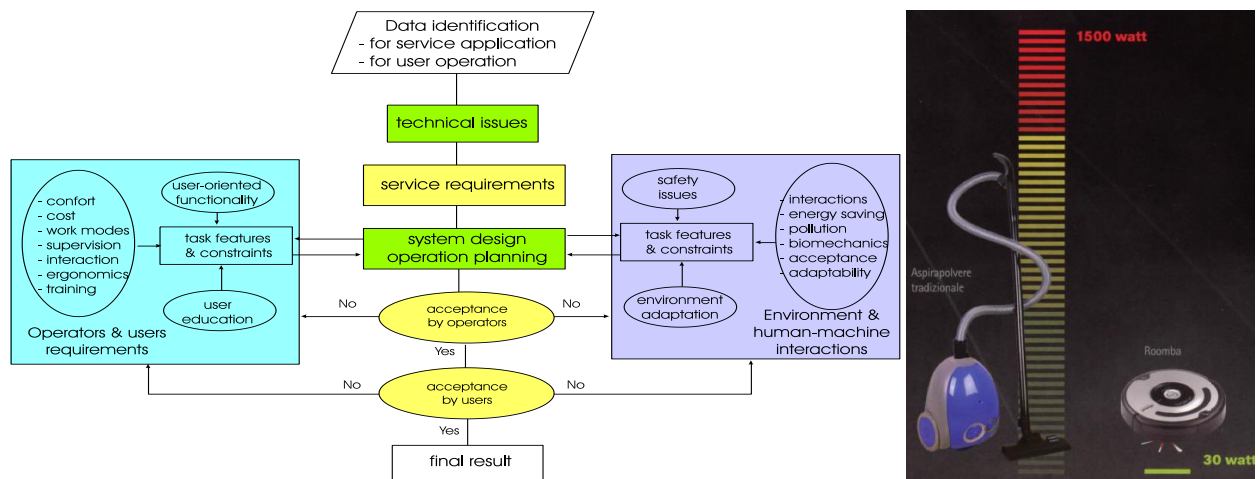


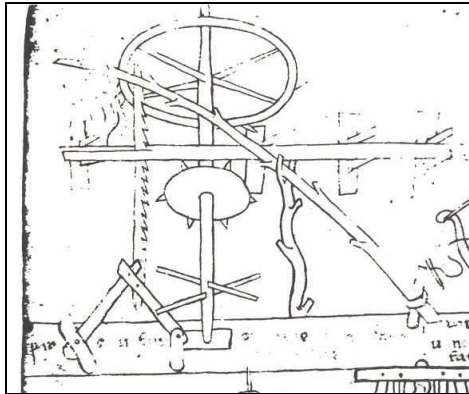
Fig.4 Innovation with service robots: a) a general scheme; b) Roomba market product.

In Fig.4 b) Roomba house cleaning robot is shown as an example of service robot. A general scheme for designing and operating service robots is reported in Fig.4 a) to show the complexity of the service robots which includes indeed aspects of the innovation products as a specific development of the service concept in Fig. 1 b). The current market Roomba robot is a mobile intelligent robot with a device for house

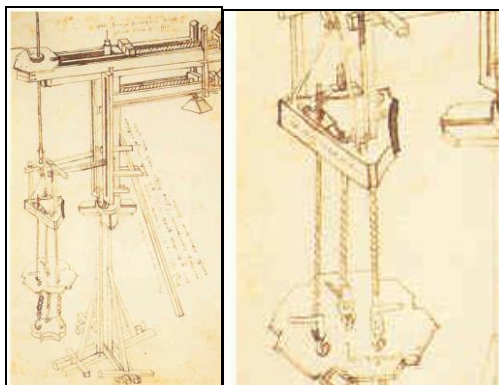
cleaning. Its design was started in 1990s' but only in the 2000s' it reached a large market success with millions of sales. Today versions are built also for other applications like garden grass cleaning and cutting. This is an example of how much users' education is influential in accepting innovation.

Fig.5 shows examples of past mechanism designs that were considered/recognized

innovation only much later. They concern with solutions with very modern concepts, like the coupler motion guidance in *Fig. 5 a)* and cable-based parallel architectures in *Fig. 5 b)*, that are today well understood and exploited in modern innovations. But the conceptual technical ideas were developed much before: this is the case for several modern inventions! And the past can be a source of inspiration!



a)



b)

Fig. 5 Examples of modern mechanism innovations in past designs: a) 2dof linkage with coupler guiding point by Villard de Honnecourt in 13th century; b) cable-base parallel manipulators by Filippo Brunelleschi (1377-1446)

5. IFTOMM ACTIVITIES FOR MMS INNOVATION

Significance of MMS innovation is produced and supported by related community and particularly significant is the role of IFToMM, even at the level of local frames.

The current structure of IFToMM is summarized in Fig. 6 in terms of the action of IFToMM bodies that are established in the IFToMM constitution for a worldwide flow of activities (www.iftomm.net). According to IFToMM mission as in the article 1 of the constitution, IFToMM activity is finalized to provide leadership for cooperation and development of modern results in

Mechanism and Machine Sciences by assisting and enhancing international collaboration.

The bodies of IFToMM can be described as:

- General Assembly: it is the supreme body of the Federation and determines its policy. It is composed of the Chief Delegates of IFToMM Organization Members (in 2017 they are 49 from countries of all the continents as national or territory associations) and members of the Executive Council with no vote rights.
- Executive Council: it manages the affairs of the Federation between the sessions of the General Assembly. It is elected every four years, meets annually, and is composed of the President, Vice-President, Secretary-General, Treasurer, Past President, and six ordinary members.
- 3 GACs (Committees of the General Assembly) that are appointed for the basic specific duty relating to GA in dealing with Constitution, EC Nominating procedure, Honours and Awards.
- 13 TCs (Technical Committees) are today active in the fields of Biomechanical Engineering, Computational Kinematics, Gearing and Transmissions, Linkages and Mechanical Controls, Micromachines, Multibody Dynamics, Reliability, Robotics and Mechatronics, Rotordynamics, Sustainable Energy Systems, Transportation Machinery, Tribology, and Vibrations. Additional TCs are under consideration for future activation in hot topics with an IFToMM significant community.
- The 4 PCs (Permanent Commissions) are on Communications, Publications and Archiving; Education; History of MMS; and Standardization of Terminology.

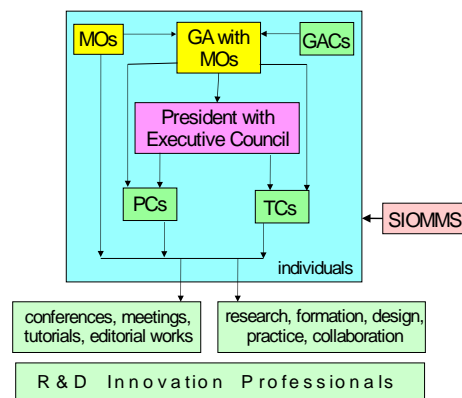


Fig. 6 IFToMM bodies and activities

Each PC and TC is composed of a Chairperson, appointed by the Executive Council, a Secretary and members, who are representatives of MOs and, once nominated by the Chairperson they are appointed by the Executive Council. A Chairperson shall not serve for more than two terms consecutively. The general goals for the work of the PCs and TCs are aimed at promoting their specific fields of interest by attracting researchers and practitioners, including young individuals, in order to:

- define new directions in research and development within their technical areas;
- establish contacts between researchers and engineers;

- initiate and develop bases and procedures for modern problems;
- promote the exchange of information;
- organize national and international symposia, conferences, summer schools, and meetings.

The mission of IFToMM is ‘to promote research, development, and education in the field of Machines and Mechanisms by using theoretical and experimental methods, along with their practical application’. This mission statement indicates the engineering aspects but also the practical scope of implementation of the activity of the community in technological developments for the benefit of the society with clear aims toward innovation.

Main activities can be summarized in, *Fig.6*:

- conference initiatives that are organized both for wide international participation and specific topic forums; conferences are held on local, national and international frames as organized by any body of IFToMM or by individuals, who are affiliated to IFToMM MOs under a given patronage of IFToMM; in general, each TC and PC has its own specific series of conference
- meetings of the IFToMM bodies for planning the activities and indicating new trends and initiatives; all TCs and PCs have an annual meeting and some other forums
- publications that include proceedings of IFToMM sponsored conferences, editorial works, and textbooks. A special Springer book series on MMS (available in the Springer website for book series at code 8779) has been started in 2011 for book projects on MMS topics as linked mainly from IFToMM community. Specific attention is devoted to journal paper publications that are organized mainly but not only within the 4 IFToMM affiliated Journals: Mechanism and Machine Theory, Open-access Mechanical Sciences, Chinese Journal of Mechanical Engineering, Advances in Vibration Engineering.
- knowledge transfer that is worked out through several actions including contacts and projects with professional and industrial frames, seminars, and tutorials.
- collaborations that are executed not only within the activities of PCs and TCs but also through actions for teaching, research and application among IFToMMists and institutions that are linked with IFToMM MOs; a special plan is established with SIOMMS (the student Olympiad in MMS) and Young Delegate Program to help young researchers in participating at IFToMM sponsored activities with specific grants from IFToMM budget.

Those activities are duties and benefits both for MOs and individuals, who are affiliated to IFToMM through a MO that is active in their territories.

A special attention is addressed to the IFToMM World Congress that is organized every 4 years. Last World Congress was held in 2015 in Taipei, China-Taipei and next World Congress will be held in 2019 in Cracow, Poland celebrating the 50th anniversary of IFToMM.

IFToMM activity has grown in many aspects, as for example concerning the number of Member Organizations (from the 13 founder organizations to the

current 49 organizations), the size and scale of conference events (with many other conferences, even on specific topics, at national and international levels, in addition to the MMS World Congress), and the number and focus of technical committees working on specific discipline areas of MMS. IFToMM was founded in 1969 and today a fourth generation of IFToMMists is active, who can be named as those persons working with international activity within the IFToMM community. Individuals have paid and still pay an important role on the activity and significance of IFToMM since the federation is made of people and its bodies are just an expression of the international aggregation of persons with commonly agreed rules for functioning and perspectives of activities. All the IFToMM activities are stimulated and directed to innovation in MMS technical fields with a clear impact also in other areas and ultimately in the society welfare evolutions. IFToMM itself can be considered an innovation result when it is recognized as a product of new attention to a community working for technological developments of MMS.

The IFToMM community evolved in character from that of a family of a few enthusiastic pioneers/visionaries and founders into a scientific worldwide community through the following generations:

- 1950s-1975 – First generation: founding fathers and their friend colleagues up to the 4th IFToMM World Congress in New Castle upon Tyne in 1975 with Prof. Leonard Maunder as Congress Chair.
- 1976-1995 – Second Generation: pupils and people, who were educated in TMM by founding fathers and their friend colleagues; up to the 9th World Congress in Milan in 1995 with Prof. Alberto Rovetta (Bianchi’s pupil) as Congress Chair.
- 1996-2011 – Third Generation: educated people with MMS activity in the frames of IFToMM and within IFToMM activity with 48 national organizations as IFToMM members, up to the 13th World Congress in 2011 in Guanajuato, Mexico with Prof. Carlos Lopez-Cajùn as Congress Chair.
- 2011 – Today – Fourth Generation: educated people working in frames that are linked to IFToMM and within IFToMM activity with 49 organizations as IFToMM members.

IFToMM officers (who are the Chairs of IFToMM Member Organizations, the Chairs of TCs and PCs, and the members of the Executive Council) have contributed and still contribute as leaders for the mission of IFToMM, which is stated in the first article of the Constitution as: ‘The mission of IFToMM is the promotion of Mechanism and Machine Science’.

6. EXAMPLES OF IFTO MM CONTRIBUTIONS TO MMS INNOVATION

IFToMM community works for innovation in MMS but through developments and applications of mechanical systems by means of an action of leadership and coordination of activities and trends in worldwide international frames.

Significant examples of contributions of IFToMM with innovation contents can be summarized both in

community aggregation and identification as well as in specific activities such as:

- TCs for new research subjects of large interest
- New forums and publication frames
- New demands for formation in research and profession

Innovation can be focused in new research subjects that in IFToMM can be motivation for establishing new TCs in order to focus and coordinate trends and developments. New subjects are arising that could permit/require the creation or enlargement of TCs with suitable groups of interested persons and institutions from Member Organizations. In addition, in each of the existing TCs, activities are continuously worked out to stimulate new trends and challenges together with the usual activities of meetings, conferences, and information flows.

Similarly, innovation in IFToMM is stimulated and also disseminated through publications in international frames that can be considered themselves innovation. Thus, IFToMM looks for more affiliated international journals with the aim to facilitate aggregation of publications of works from the IFToMM community as also the Springer book series does as focused on MMS.

Formation with advanced issues is of great interest since the early days of IFToMM. New results can be considered the planning of several specific tutorials, mainly as Summer schools by TCs and even a Student Olympiad that in 2018 has been planned in its fourth event.

Beside the above, innovation of MMS is obtained in IFToMM through specific results in new theories, designs, and applications that are achieved for new solutions.

7. CONCLUSION

Achievements and solutions in MMS as well as the corresponding IFToMM community can be considered important bases for innovation with technical contents and backgrounds, without which no innovation is possible in machine areas and even in more fields. But a full modern innovation exploitation up to users' satisfaction requires a community with more multi-disciplinary skills, even from Business and Administration areas and IFToMM community can work such an influential role in stimulating/guiding innovation activity since it was established with vision of international frames for collaboration purposes in the growth of MMS with impacts and application of technological developments for the benefits of the society.

REFERENCES

- [1] CECCARELLI M. (Ed.), *Role of MMS and IFToMM in Technology Development*, Book series on Machines and Machine Science, Vol.1, Springer, Dordrecht, 2011. ISBN 978-94-007-1299-7, DOI: <http://dx.doi.org/10.1007/978-94-007-1300-0>
- [2] BAUTISTA PAZ E., CECCARELLI M., ECHAVARRI OTERO J., MUNOZ SANZ, J.J., *A brief illustrated history of machines and mechanisms, Science and Engineering*, Book series on History of Machines and Machine Science, Vol.10, Springer, Dordrecht, 2010. DOI 10.1007/978-90-481-2512-8. ISBN: 978-90-481-2511-1
- [3] CECCARELLI M., *Problems and issues for service robots in new applications*, International Journal of Social Robotics: Volume 3, Issue 3 (2011), Page 299-312, DOI: 10.1007/s12369-011-0097-8.
- [4] CECCARELLI M., "*The Challenges for Machine and Mechanism Design at the Beginning of the Third Millennium as Viewed from the Past*", Proceedings of Brazilian Congress on Mechanical Engineering COBEM2001, Uberlandia, 2001, Invited Lectures, Vol.20, pp.132-151.
- [5] CECCARELLI M., *History and Challenges of Mechanism and Machine Science within IFToMM Community*, in: Towards Intelligent Engineering & Information Technology, Springer, Berlin, 2009, pp. 469-488.
- [6] CECCARELLI M., *Twenty-five year of activity in IFToMM*, journal Theory of Mechanism and Machine (<http://tmm.spbstu.ru>), St Petersburg State University, Vol.11. No.2, pp.3-14.
- [7] CECCARELLI M., *An Outline of History of Mechanism Design in servicing Science, In Physics, Astronomy and Engineering: critical problems in the History of Science and Society – Proc. of SISFA 2012*, The Scientia Socialis Press Siauliai, (Invited lecture) pp.1-10.
- [8] CECCARELLI M., A short account of History of IFToMM and its role in MMS, Mechanism and Machine Theory, Vol. 89, 2015, pp.75-91, 10.1016/j.mechmachtheory.2014.09.007
- [9] [M. CECCARELLI](#), *Figures and achievements in MMS as landmarks in history of MMS for inspiration of IFToMM activity*, [Mechanism and Machine Theory, Volume 105](#), 2016, Pages 529–539. [doi: 10.1016/j.mechmachtheory.2016.07.012](https://doi.org/10.1016/j.mechmachtheory.2016.07.012)

CORRESPONDANCE



Marco CECCARELLI, Prof. D.Sc. Eng.
University of Cassino and South Latium
Cassino, Italy
ceccarelli@unicas.it

ABOUT THE AUTHOR:

Marco Ceccarelli is Professor of Mechanics of Machinery and Director of LARM, the Laboratory of Robotics and Mechatronics at Cassino University <http://larmlaboratory.net>). He has been President of IFToMM, the International Federation for the Promotion of Machine and Mechanism Science for terms 2008-2011 and 2016-2019, and Secretary General in 2003-2007. He is editor of the Springer book series on MMS and History of MMS. His research interests cover aspects of Mechanics of Mechanisms and Robots, History of MMS, and Mechanism Design. He authored more than seven hundred papers, and he has authored 4 books and edited 20 books for proceedings and specific topic issues.

MICRO SYSTEM TECHNOLOGY AND INDUSTRIAL APPLICATION, STATE OF THE ART AND CURRENT TRENDS

Klaus Peter KÄMPER

CORRESPONDANCE



Klaus Peter KÄMPER, Prof. D.Sc. Eng.
University of Applied Sciences Aachen
Faculty of mechanical engineering and
mechatronics
Goethestr. 1
D 52064 Aachen, Germany
kaemper@fh-aachen.de

ABOUT THE AUTHOR:

Dr. Klaus-Peter Kämper is Professor at the Faculty of mechanical engineering and mechatronics at the University of Applied Sciences Aachen, Germany, (*FH Aachen - Fachhochschule Aachen*), working in the field of microsystem technology and MEMS, mechatronics, sensors and new actuators. He studied Physics at the University of Cologne, Germany and Oregon State University, Corvallis, USA. He received his Ph.D. in the field of surface and ultrathin film magnetism at RWTH Aachen, Germany (*RWTH Aachen - Rheinisch-Westfälische Technische Hochschule Aachen*). He continued to work in this field at University of California Irvine, USA before switching to microsystems technology and MEMS at IMM GmbH, Mainz, Germany (*Institute für Mikrotechnik Mainz GmbH*). In 1997 he joined FH Aachen, where he built up

and is responsible for the study programs in mechatronics. He authored more than 55 publications and supervised more than 145 Bachelor and Master thesis. He organized numerous national and international R&D projects in collaboration with industrial and academic partners. At the university, he served as dean of his faculty and as head of the academic senate of his university. He organized a number of international collaborations, including a double degree program in mechatronics with CIDESI, Mexico (*CIDESI - Centro de Ingeniería y Desarrollo Industrial = Center for Engineering and Industrial Development*) and a Tempus project on mechatronics education in the Western Balkan region (*Development of Regional Interdisciplinary Mechatronic Studies - DRIMS*).

INTRODUCTORY LECTURES



ROLE, IMPORTANCE AND MISSION OF ADEKO

Vojislav MILTENOVIĆ

Abstract: *A company success in modern conditions is possible to achieve by introducing innovative products and product processes. In conditions of fierce competition and saturated markets, companies that do not innovate are stagnating and disappear from the market. Innovation is therefore every intervention which can reduce production costs, enables optimum utilization of available human, energy and material resources, improve product quality, improve the placement, which leads to an increase in competitiveness. A prerequisite for fulfilment of the above-mentioned tasks is that the companies have engineers with the appropriate competencies. Likewise, the abovementioned essentially defines the goals of the ADEKO Association, and they are reflected in encouraging education which would enable engineers to create new, sophisticated and competitive products by means of creativity, innovation and fascinating technique. Moreover, it should encourage activities relating to the relevant and efficient application of research results to business entities.*

Key words: *ADEKO, product development, competence, education*

1. ESTABLISHMENT, ACTIVITIES AND WORK RESULTS

In modern conditions education is a key factor behind the development and competitiveness of the economy of every country, i.e. it plays an essential role in the socio-economic development of the economy and society. In that respect, the role of education provided by faculties of technology, i.e. the education of engineers is of utmost importance. This particular role of education was recognised in the Socialist Federal Republic of Yugoslavia in the previous century. After 1960 a series of faculties and higher education institutions have been established around the country which signified a sudden increase in the number of people with a university degree in a relatively short period of time. Being aware of the role and significance of education for the society, professors of several universities recognised the need for establishing a closer co-operation among educated people from universities and work fields, as well as the necessity of establishing connections with appropriate personnel abroad. Acting on the initiative of professor Zoran Savić from the Faculty of Mechanical Engineering in Belgrade, professor Eugen Oberšmit from the Faculty of Mechanical Engineering and Naval Architecture in Zagreb, professor Jože Hlebanja from the Faculty of Mechanical Engineering in Ljubljana and professor Dimitar Stamboliev from the Faculty of Mechanical Engineering in Skopje, on February 19th, 1973 the **Yugoslav Society for Machines and Elements (JuDEKO)** was founded at the Faculty of Mechanical Engineering in Belgrade. Professor Zoran Savić was elected President of the Society, professor Jože Hlebanja became the vice-president, while assistant professor

Milan Nedeljković was appointed secretary of the Society.

The goals of the JuDEKO Society defined by the Statute were as follows: encouraging the development of the science of machine elements and mechanical constructions, of theoretical and experimental research as well as of the application of new knowledge and research results to mechanical construction; establishing co-operation between experts and organisations in this field, both in the country and abroad; organising professional and scientific gatherings in this field; stimulating the exchange of scientific and professional information and publishing scientific papers; suggesting improvements in the process of teaching in the aforementioned fields at higher education institutions.

In the period between 1973 and 1990 the JuDEKO Society achieved significant results, not only in organising scientific conferences and improving the teaching process, but also in connecting professionals in this field, both in the country and abroad. Eight scientific gatherings and two international conferences have been organised (Table 1). One of the most significant gatherings was the **World Symposium on Gears and Gear Transmission** which was held from September 13th to September 16th in 1978, in the village of Kupari, Croatia.

Due to the outbreak of war on the territory of former Yugoslavia, the Society ceased with its activities in the period between 1991 and 1995. Acting on the initiative of professors from the universities in Belgrade, Novi Sad, Niš, Kragujevac and Podgorica, a scientific gathering named **Research and Development of Machine Elements and the IRMES-95 System** was held from April 19th to April 21st, 1995 comprising 250 participants and 137 papers from the country and abroad.

The new Founding Assembly of the JuDEKO Society was held on February 8th, 1997 on the Faculty of Mechanical Engineering in Belgrade. Professor Vojislav Miltenović was elected president, while professors Milosav Ognjanović and Radoš Bulatović were appointed vice-presidents.

Table 1. Overview of JuDEKO - conference 1973-1990

No	Conference title, location and time, organizer (con. type)
1.	Actual problems of gear manufacturing , Beograd 26. April 73, MF Beograd, (scient,-prof.)
2.	Symposium on gears and sliding bearings , Zagreb 22-24. Jan.74, JuDEKO-FSB Zagreb (scient,-prof.)
3.	General problems of machine design , Ljubljana 6-7 Sept.76, JuDEKO- FS Ljubljana (Workshop)
4.	World Symposium on Gears and Gear Transmissions , Kupari 13-16 Sept.78, JuDEKO-IFTToMM (World Symp.)
5.	Design Science and Computer Aided Design , Zagreb June 1981., JuDEKO-FSB Zagreb (scient,-prof.)
6.	Scientific-expert Symposium on Design , Zagreb June 1984., JuDEKO-FSB Zagreb, (scient,-prof.)
7.	Actual problems of machine elements and constructions , Ohrid 3-6-June 1985., JuDEKO-MF Skoplje, (sc.,-prof.)
8.	Science, Research and Development of Mechanical Systems and Elements , Beograd,14-16.May 87., JuDEKO-MF Beograd, (scient,-prof.)
9.	Symposium on Design “88, Zagreb 8-10-June 88., JuDEKO-FSB Zagreb, (scient,-prof.)
10.	International Conference on Engine-ering Design – ICED, Cavtat 28.-30. Aug.90.,JuDEKO-WDK CiriH, (Int.Con.)

The activities and results of the JuDEKO Society in the period between 1995 and 2005:

- there were 15 gatherings in total, comprising 5 IRMES scientific gatherings, 5 SEVER symposia, 3 KOD gatherings and 2 workshops (Table 2);
- since 1997, under the immediate auspices of the JuDEKO Society, a bilingual journal *Machine Construction* was being published in Serbian and English;
- the Balkan Association for Power Transmission (BAPT) has been established, whereby the JuDEKO Society was a member
- on several occasions, the syllabi in Machine Elements and the Basics of Construction had been reconsidered and conclusions were submitted to various departments of Mechanical Construction and faculties of Mechanical Engineering.

Table 2. Overview of JuDEKO - conference 1995-2005

No	Conference title, location and time, organizer (con. type)
1.	Research and Development of Mechanical Elements and Systems - IRMES'95 , Niš,19-21. April 1995. JuDEKO-MF Niš (1th-scient,-prof.)
2.	Symposium on electromechanical transmissions, SEVER-95 , Subotica, 12-13. Okt.1995. JuDEKO-Sever-Sub., (5th –Sym.)
3.	Application of CAD system in design , Niš,17-18. Okt. 1996, JuDEKO-MF Niš, (Workshop)
4.	Modern methods in teaching design , Beograd, 15.March 97., JuDEKO-Min. prosv., (Workshop)
5.	Symposium on electromechanical transmissions, SEVER-97 , Subotica, 15.Okt. 97. JuDEKO-Sever-Sub. (6th –Sym.)
6.	Research and Development of Mechanical Elements and Systems - IRMES'98 , Beograd, 10.-11. Sept. 1998., JuDEKO-MF Beograd, (2th-scient,-prof.)
7.	Symposium on electromechanical transmissions, SEVER-99 , Subotica, 13.Okt. 99., JuDEKO-Sever-Sub., (7th –Sym.)
8.	“Forming and Design in mechanical Engineering” - KOD-2000 , Novi Sad, May 2000., JuDEKO-FTN Novi Sad, (1th-scient.-prof.)
9.	Research and Development of Mechanical Elements and Systems - IRMES'2000 , Kotor, 13-15. Sept.2000, JuDEKO-MF Podgorica, (3th-scient,-prof.)
10.	Symposium on electromechanical transmissions. SEVER-01 , Subotica, Okt. 2001, JuDEKO-Sever-Sub., (8th –Sym.)
11.	“Forming and Design in mechanical Engineering” KOD-2002 , Novi Kneževac, May 2002., JuDEKO-FTN Novi Sad, (2th-scient.-prof.)
12.	Research and Development of Mechanical Elements and Systems -IRMES'2002 , Jahorina, 19.-20.Sept. 2002, JuDEKO-MF-S.Sarajevo, (4th-Scient.-proff. with intern. part.)
13.	Symposium on electromechanical transmissions – SEVER-03 , Subotica, 10.Okt.2003., JuDEKO-Sever-Sub., (9th –Sym.)
14.	“Forming and Design in mechanical Engineering”- KOD-2004 , Novi Sad, May 2004. JuDEKO-FTN Novi Sad, (3th-scient.-prof.)
15.	Research and Development of Mechanical Elements and Systems - IRMES'2004 , Kragujevac, 16.-17. Sept.2004., JuDEKO-MF Kragujevac, (5th-Scient.-proff. with intern. part.)

At the meeting of the Executive Board of the Society held on September 29th, 2005 in Banja Luka a decision has been made to transform the JuDEKO Society into ADEKO – the Association for Design, Elements and Construction (Association für Design, Elementen und Konstruktionen), as well as to transform the Executive Board of the JuDEKO Society into the Co-ordination Board of the ADEKO Association.

Table 3. Overview of ADEKO - conference 2006-2016

No	Conference title, location and time, organizer (con. type)
1.	International Conference POWER TRANSMISSIONS'06 BAPT , Novi Sad, 25.-26. April.2006, ADEKO-FTN Novi Sad, (4th Intern. Con.)
2.	Research and Development of Mechanical Elements and Systems - IRMES-2006 , Banja Luka, 28.-29. Sept.2006, ADEKO-MF Banja Luka, (6th-Scient.-proff. with intern. part.)
3.	Design in mechanical Engineering – KOD 2008 , Novi Sad, 15.-16. April.2008, ADEKO-FTN Novi Sad, (5th Intern. Con.)
4.	Forming and Design in mechanical Engineering – KOD 2010 , Novi Sad, 29.-30. Sept.2010, ADEKO-FTN Novi Sad, (6th Intern. Con.)
5.	Research and Development of Mechanical Elements and Systems - IRMES 2011 , Zlatibor, 27-28. April 2011. ADEKO-MF Niš, (6th-Int. Scientific Con.)
6.	“Conference on Mechanical Engineering Technologies and Applications” COMET-a , 28-30. Nov. 2012., Jahorina, BiH, ADEKO-MF I.Sarajevo, (1th Intern. Con.)
7.	KOD 2012 “Machine and Industrial Design in Mechanical Engineering” , 24 - 26 May 2012, Balaton, Hungary, ADEKO-FTN Novi Sad – MF Bratislava, (7th Int. Sym.)
8.	Modern Approach to Product Development and Business Improvement , 16 - 19 May 2013, Balaton, Hungary. ADEKO-FTN Novi Sad – MF Bratislava, (Workshop)
9.	KOD 2014 “Machine and Industrial Design in Mechanical Engineering” , 12 - 15 June 2014, Balaton Hungary, ADEKO-FTN Novi Sad – MF Bratislava, (8th Int. Sym.)
10.	“Conference on Mechanical Engineering Technologies and Applications” COMET-a , 2-5. Decem. 2014., Jahorina, BiH, ADEKO-MF I.Sarajevo, (2th Intern. Con.)
11.	Where does the mechanical engineering go? , 11 - 14 June 2015, Balaton, Hungary, ADEKO-FTN Novi Sad – MF Bratislava, (Workshop)
12.	KOD 2016 “Constuction Machine and Industrial Design in Mechanical Engineering” , 9 - 12 June 2016, Balaton, Hungary, ADEKO-FTN Novi Sad – MF Brat-, (9th Int. Sym.)
13.	“Conference on Mechanical Engineering Technologies and Applications” COMET-a , 7-9. Decem. 2016., Jahorina, BiH, ADEKO-MF I.Sarajevo, (3th Intern. Con.)
14.	Mechanical Engineering Today , 22 - 25 June 2017, Balaton Hungary, ADEKO-FTN Novi Sad – MF Bratislava, (Workshop)

On the basis of written recommendations from universities/faculties, at the meeting held on September

29th, 2006 in the town of Palić, the Co-ordination Board of the ADEKO Association was founded and it included the following Board members: professor Milosav Ognjanović (Faculty of Mechanical Engineering in Belgrade), professor Siniša Kuzmanović (Faculty of Technical Sciences in Novi Sad), professor Vojislav Miltenović (Faculty of Mechanical Engineering in Niš), professor Vera Nikolić (Faculty of Mechanical Engineering in Kragujevac), professor Radoš Bulatović (Faculty of Mechanical Engineering in Podgorica), professor Milosav Đurđević (Faculty of Mechanical Engineering in Banja Luka), professor Momir Šarenac (Faculty of Mechanical Engineering in Eastern Sarajevo), professor Kosta Krsmanović (University of Arts in Belgrade), an engineer Vladeta Kostić (Zastava Automobile Company). The co-ordination of the Board, as well as the task of writing the ADEKO Declaration was placed in charge of professor Vojislav Miltenović.

Table 4. Membre od ADEKO

No	Name of institution
1.	Karlsruher Institut für Technologie (KIT)- IPEK – Institut für Produktentwicklung, Deutschland,
2.	Faculty of Technical Sciences, University of Novi Sad, Serbia
3.	Mechanical Engineering Faculty, University of Belgrade, Serbia
4.	Faculty of Engineering, University of Kragujevac, Serbia
5.	Mechanical Engineering Faculty, University of Nis, Serbia
6.	School of Mechanical Engineering, Aristotle University of Thessaloniki, Greece
7.	Faculty of Mechanical Engineering, Slovak University of Technology in Bratislava, Slovak Republic
8.	Faculty of Mechanical Engineering, University of Maribor, Slovenia
9.	Faculty of Mechanical Engineering, Technical University of Sofia, Bulgaria
10.	Mechanical Engineering Faculty, University of Banja Luka, Bosnia and Herzegovina
11.	Mechanical Engineering Faculty, University of Oest Sarajevo, Bosnia and Herzegovina
12.	Mechanical Engineering Faculty, University of Montenegro, Montenegro
13.	Faculty of Mechanical Engineering, Ss. Cyril and Methodius University in Skopje, FYROM
14.	Technical Faculty Bitola, University St. Kliment Ohridski in Bitola, FYROM

The goals of the Association defined by the ADEKO Declaration:

- To stir up development of science about machine elements, construction and product development.
- To stir up theoretical and experimental research in this area.

- Restoration and expanding of contacts, visits and cooperation of expert and organisations from this region.
- To stir up mobility, education and science and expert informations.
- Organization of scientific and expert's gatherings – congresses, symposiums, seminars and other expert meetings in this field.

Activities and results of the ADEKO Association in the period between 2005 and 2017 <http://adeko.omk.in.rs/>:

- there were 14 gatherings in total, comprising 2 IRMES conferences, 6 KOD conferences, 3 COMET-a conferences and 3 wrokshops: (Table 3);
- since 2007, as a result of co-operation between the ADEKO Association and the Faculty of Mechanical Engineering in Novi Sad, the journal *Machine Design* has been published in English, and since 2016 this journal has been categorised as one of the leading domestic scientific journals (M51): <http://www.mdesign.ftn.uns.ac.rs/>;
- co-operation and assistance regarding international projects such as CEEPUS, TEMPUS, etc.;
- activities regarding innovations in the teaching process in the field of product development;
- the number of members has been increased to 14 (Table 4).

At the meeting of the Co-ordination Board of the ADEKO Association, held on December 2nd, 2014 on the mountain of Jahorina, the unanimously elected president was dr Radivoje Mitrović, a tenured professor of the Faculty of Mechanical Engineering in Belgrade.

2. ROLE, IMPORTANCE AND MISSION

A company success in modern conditions is possible to achieve by introducing innovative products and product processes. It is necessary to consider market needs, customer wishes, concurrence etc. Innovative products in mechanical engineering are different from other products, in one hand it is assembly of mechanical, electronic and informatics components and on the other mechanical product development must consider all product life cycle phases. Under the conditions of industry 4., the structure of the product is drastically changed, primarily from the aspect of perpetrators of basic and partial functions (Fig.1). Application of micro mechanical, microelectronic and micro optical components in combination with software components, manufacturing and assembly process are completely automated. Innovative products are characterized by strong logistic backup related to product exploitation maintenance and recycling.

Therefore application of innovative products and product processes is very complex and demands new work approach, which is primarily related to resource optimization, precision defining of competence and cooperative work approach. In comparison to convectional primarily functional oriented approach, cooperative work process is based on interdisciplinary project teams, methodical work approach is connected to specific parallel process structure (simulate engineering) with use of modern information technologies. This approach has influence on shortening time period for

creating and lunching new product (time to market), reduction of prices (design to cost) and to insure quality (best quality).

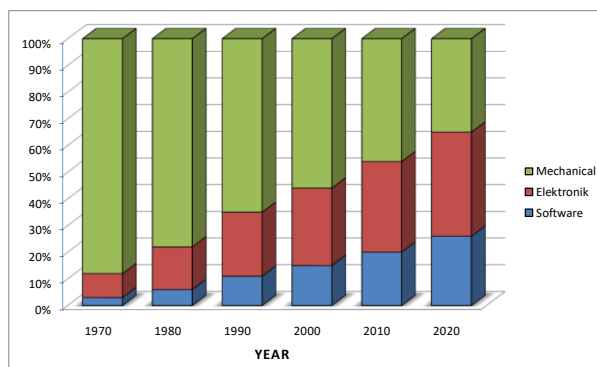


Fig.1: Perpetrators of functions by modern products

Modern companies must have access to comprehensively educated engineers so that they can solve complex problems.

The development engineer tasks in the field of product development are varied. They deal with the entire life cycle of a product, from a product idea to its concretization through manufacturing, distribution and recycling. The development is about developing new products or improving existing products and to fulfil market needs through creativity, innovation and technology. For realization of this tasks of develop engineers has to possess knowledge of which technologies for successful creation of products and production are available and to take in account available material and energetic resources as well as environmental protection.

The issue of educating development engineers, as well as activities regarding the development of new products are directly related to the goals of the ADEKO Association. On the basis of the aforementioned, one can discern the role and significance of the mission of the ADEKO Association in modern times. Hence, the unequivocal tasks of ADEKO are related to encouraging activities in the field of development, i.e. making new products in the regional business entities, defining goals for the purposes of improving the teaching process at universities, as well as clearly defining the relevant competences of development engineers. In further text the authors shall present straightforward facts and guidelines in these fields.

3. PRODUCT CREATION, PRODUCT DEVELOPMENT, CONSTRUCTION

Development of successful product represents important factor for value of today's companies. The product creation is the part of the product life cycle (Fig. 2). It starts by determining needs, developing ideas for products and finishes with production.

Under the product development involves the interdisciplinary process in the company. This process is based on product planning, begins by defining the product profile, within this process continuously running further development, and ends with the product that is feasible for production and it can properly work. Therefore, the

iterative procedures of the analysis and synthesis are performed, which are represented on Figure 3 through 7 activities. This process should aim at close cooperation between the various departments and divisions.

The development process is carried out in the core of the organizational unit "product development", but also in various other departments such as design, testing, analysis, prototyping and with support of Department for Standardization and Patent Department.

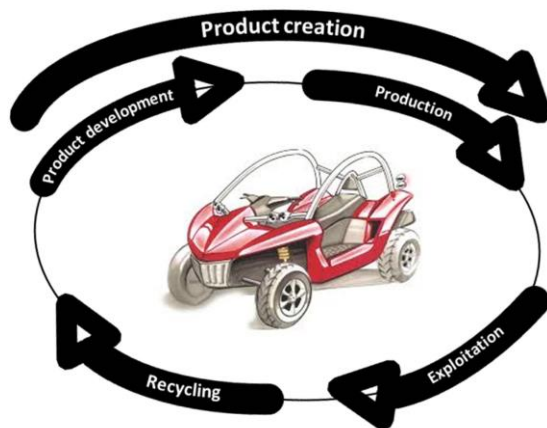


Fig.2: Product life cycle

So, organizational unit Design should be considered as part of product development. It is located next to other organizational units, such as Testing. On the other hand, the expression Design in the company includes the process. This iterative process begins by clarifying the task and ends with the production documentation.

In product development there are different professions such as, for example, designers, CAD engineers, test engineers, standardization and patent engineers. Various activities oriented towards synthesis or analyses are performed depending on the profession.

University -educated engineers in the field of Product Development does not have to be specialists in all the seven fields of activity (Fig. 3), but they need to be able to take into account all of the above.

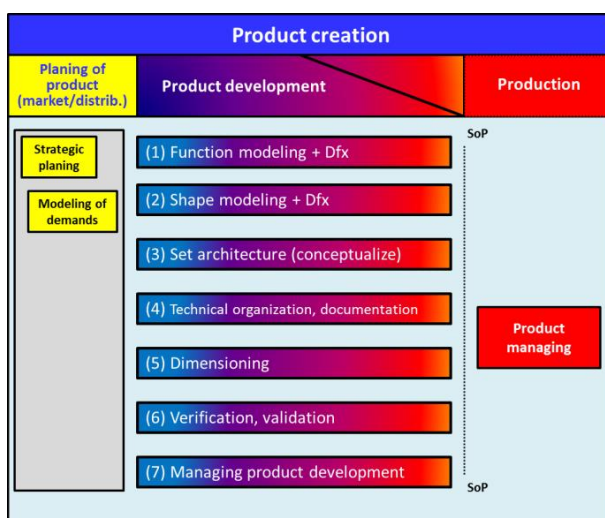


Fig.3: Position of Product Development in process of Product Creation

Product Development engineers, whose main task is in modeling of functions, to determine the form, choose the material, dimensioned product and its components and preparation of production documentation, referred to as designers. Designer therefore mainly takes steps of synthesis, with a focus on budgets and testing. Designers are therefore in the process of formation of new mechanical and mechatronic products involved in the development, management and embodiment design.

4. TASKS AND GOALS OF UNIVERSITY TEACHING IN PRODUCT DEVELOPMENT

One of the key areas related directly to product development are machine elements. Lectures of machine elements have to provide an overview of machine elements, to describe the main stresses, to give knowledge of methods of dimensioning and design and to deepen their knowledge in selected examples.

Priority in education of product development engineers makes the teaching of machine elements and design methods. In the basic (bachelor) studies in education is used a structured methodological approach. This includes the methodological development of products at a basic level, a systematic approach for designing and shaping including CAD as well as arrangement of elements and transfers to other machine elements. Scientific specialization methodological approach in solving structural problems and switching of used methods as the focus of teaching methodological product development in subsequent semesters.

Basic knowledge of production with the corresponding parameters of the production process, shaping and material processing is a prerequisite for understanding the machine elements as well as production-oriented and cost effective design. Students must at an early stage identify and detect opportunities and constraints of modern production processes. Industrial practice has the same importance for learning the theoretical basis from the beginning of the actual education of machine elements.

Content of teaching in the field of machine elements must constantly be updated and aligned with trends in industrial practice. In addition to conventional mechanical machine elements should be taken into account and a number of pneumatic, electric, electromagnetic, electronic, optical, biological, and other elements.

The study of mechanical machine elements such as, for example, joints, springs, bearings, guides and gears are a central part of the class of Machine elements. The goal of learning machine elements is that in variable terms of the spectrum of application of machine elements (many classic elements become obsolete) tends to their correct application in industrial practice.

Teaching in machine elements should be organized as a separate structure - a combination of lectures with intensive exercises in groups - with appropriate forms of training such as team work, project work and tests.

Design of technical systems in terms of price (Design to Cost) is a priority in the product development process. Design to cost as the basis for a successful construction must be methodically examined. It is important from the very beginning to future mechanical engineers to

demonstrate the importance of product prices, they have to adopt as a significant factor in his work. Exclusive transfer ideal technical solution does not correspond to the professional reality. Discussion of possible alternative solutions in terms of costs, having in mind the possible disadvantages and risks must be constantly present in practical training.

Special significance for the individual activities of design and interdisciplinary communication between engineers and others involved in the process of industrial product development and production is the ability to sketch. 2D and 3D drawings can be quickly in any situation to convey important information. Despite the implementation of CAD, the practice of sketching layouts, sections and spatial representation is very important. Drawings are an important element of communication to discuss alternative solutions to the team and the starting point for further CAD modeling.

CAD technology is now further advanced and offers powerful features to create 2D drawings and 3D models for products. Thus it provides information about the product that are essential in the chain of product development process (eg. \Leftrightarrow FEM CAD, CAD \Leftrightarrow simulation, CAD \Leftrightarrow Rapid- Prototyping, CAD \Leftrightarrow PPS, CAD \Leftrightarrow CAM). CAD technology applied today as a standard tool in product development. Therefore, CAD technologies have to be involved in the teaching of Product Development. It must also be taken into account through the use of new technology of virtual product development which leads to changes in procedures regarding the product development process. For mastering the field of CAD technology must be provided additional teaching in education in the field of product development. The scope and content, and applied systems must be coordinated with the capacity and capabilities of a

particular university.

5. AUTHORITATIVE COMPETENCES OF DEVELOPMENT ENGINEERS

Task of teams in Product Development is to achieve multiple compliance, exchange of information to debate, dispute resolution and formal decision. It is important to establish the personal competencies, which are very important for the successful operation of the team. It is also important real competence, which team members have in relation to the upcoming task, only to be successfully solved. After extensive research in this direction, clearly defined following relevant competencies: professional competence, methodological competence, social competence, creative potential and ability elaboration. Furthermore will be defined the above mentioned competences.

Under **social competences** are following parameters or social behavior and personal characteristics:

- Endurance
- Motivational parameters (initiatives, work motivation)
- Work styles (analytical way of thinking and working, orientation towards target)
- Penetrability (the possibility of implementation)
- Problem solving (organizational skills)
- Determination (determination of behaviour)
- Creativity
- Team behaviour (cooperation, coordination, willingness to discuss, competence for discussion)
- The behaviour in social situations

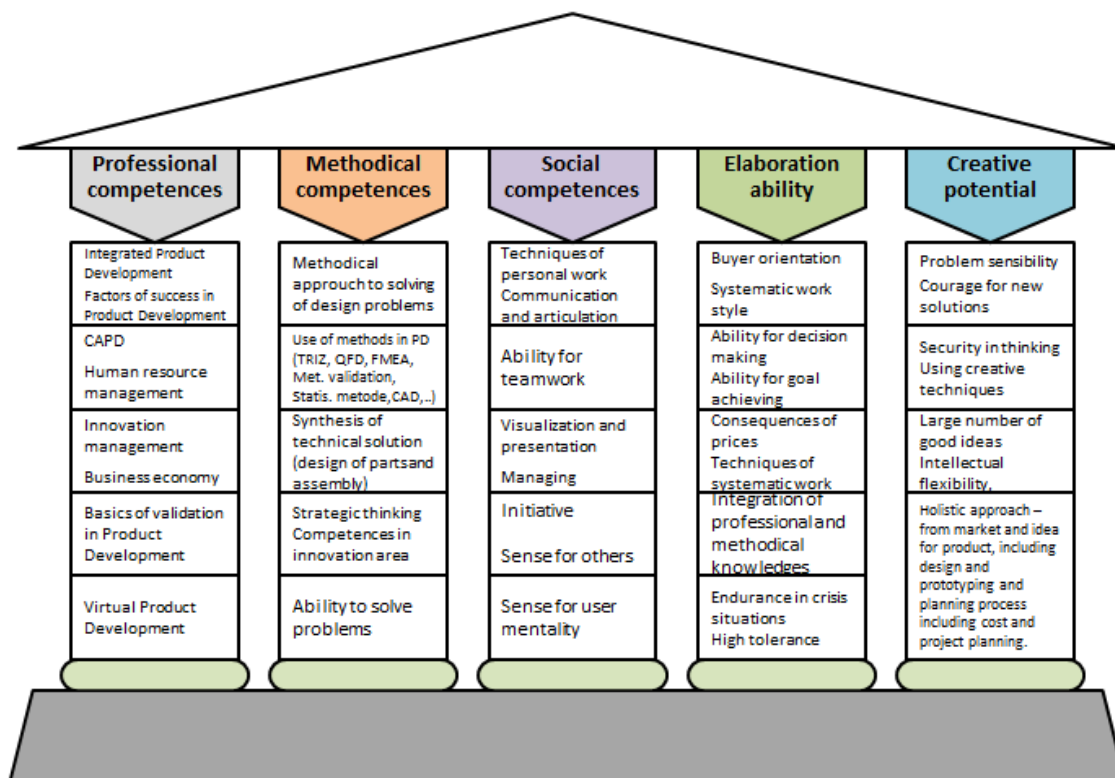


Fig.4. Authoritative competences in field Product Development on master studies

The term **professional competencies** include the practical knowledge and professional experience, as well as theoretical knowledge that an engineer in his own work uses. It can be defined as "the willingness and ability to take on the basis of professional knowledge and skills of tasks and problems oriented towards a goal, if done correctly, methodically and independently solved and the results obtained adequate evaluation."

Methodical competence includes methods and proper procedures used by experienced specialists in resolving known and partially unknown problems.

Social competence is more or less subjective but it is a very important factor, so it can not be easily determined. It can be determined through answers to indirect questions. There is a difference between direct and indirect questions. In direct questions it is possible to estimate its own performance and skills of the tested person. In indirect questions, tested persons are required to on the question choose between several possible answers. The rating is then performed through a personality test based on the long experience of psychologists. The team members are different personality types according to their personal and social characteristics.

Creative potential includes the following abilities:

- Sensitivity to problems,
- The appropriate use of creative techniques
- Availability of a large number of good ideas,
- Intellectual flexibility,
- Ability to abstract thinking.

Elaboration ability includes:

- Ability to achieve goals
- Orientation towards the customer,
- Keep in mind the requirements of the user,
- Knowledge of the consequences of costs and prices,
- Knowledge of the techniques of systematic work,
- Durability in crisis situations,
- Enthusiasm in decision-making,
- A high level of tolerance.

Based on the above given, in Figures 4 are presented the authoritative competencies that need to be gained as master's studies.

At the basic studies, priority is acquisition of technical and methodological competencies, which are the basis for further upgrading and acquiring other competences at master studies. At this stage of education are acquired a certain extent and social competence primarily through teamwork in the exercise, through the organization of workshops and learning active work.

The main part of the education of product development engineers and acquiring the necessary competencies are achieved during the master studies. Competencies listed in Figure 5 are possible to obtain on the two-year master studies. Professional competence leaning on the knowledge acquired at the bachelor level are primarily oriented to obtain knowledge and skills in the areas of product development and the processes which are carried out at the same time. To acquire methodological competencies presented is the practical application of a

number of methods to solve problems in Product Development, the ability to synthesize technical solutions, as well as the successful implementation of innovations. Social competences are focused on communication and articulation skills, teamwork and leadership as well as the ability to solve problems through their own initiatives. Very important are the competences related to the ability of elaboration. These competencies are expressed through the skills of systematic work style, integration of technical and methodological knowledge and managing in crisis situations. Competencies related to the creative potential include acquiring skills for applying creative techniques, safety at work and the implementation of new solutions as well as a holistic approach to product development.

6. CONCLUSION

Through its activities in the period between 1973 and 2016 the JuDEKO Society and its successor, the ADEKO Association, achieved significant results which are reflected in the following:

- encouraging experimental and theoretical research, as well as developing the science of machine elements, mechanical construction and product development;
- establishing co-operation between professionals and organisations in this field, both in the country and abroad, by means of exchanging scientific information, publishing scientific papers and journals, as well as by working on joint projects;
- improving the teaching process in these fields in higher education institutions;
- organising over forty scientific meetings – conventions, conferences, symposia, seminars and other professional gatherings in this field.

In the light of the current conditions of globalisation and the Industrie 4., the mission of the ADEKO Association becomes even more important and it is reflected in the following:

- intensifying activities of professionals in science and work fields with respect to developing, i.e. making new products in regional business entities;
- defining goals for improving the teaching practice at the universities, as well as providing a precise definition of relevant competences of development engineers according to the requirements of the economy
- co-ordinating activities in the field of excellence, relevance and efficient application of research results at faculties and research organisations for the purposes of developing regional economies
- establishing and expanding contacts and co-operation between professionals and organisations in the region with the EU countries by means of organising professional gatherings and conferences in this field.

REFERENCES

- [1]. SAVIĆ, Z.: (2000) *Jugoslovensko društvo za mašinske elemente i konstrukcije - JuDEKO od 1973. do 2000. Godine*. Naučno-stručni skup "Istraživanje i razvoj mašinskih elemenata i sistema"-IRMES'2000, Zbornik radova: pp.8-14. Kotor.
- [2]. MILTENOVIĆ, V., IANICI, S., BANIC, M., MILTENOVIĆ, A.: (2014) *University Teaching and Authoritative Competences of Product Development Engineers*. Proc. of 8th International Symposium KOD 2014 - Machine and Industrial Design in Mechanical Engineering, Balatonfüred, Hungary.
- [3]. MILTENOVIĆ, V., VEREŠ, M., BANIC, M.: (2012) *Concept of virtual Product Development*. Proceedings of 6th Int.Sym. about Forming and Design in mechanical Engineering – KOD 2010. (ISBN 978-86-7892-278-7) Novi ad, Serbia, pp.7-12.
- [4]. MILTENOVIĆ, V., MITROVIĆ, R.: (2011) *Ingenieurausbildung im Gebiet Produktentwicklung*. Proceedings of the 7th International Scientific "Conference Research and Development of Mechanical Elements and Systems", Zlatibor, Serbia. Plenary Session S. I-VI.
- [5]. MILTENOVIC, V., MARKOVIC, B., BANIC, M., MILTENOVIC, A., (2012) *Future Technology and Education of Engineers*. Proc of 1st Int.Con. COMETA 2012, East Sarajevo – Jahorina, Bosnia and Herzegovina.
- [6]. MILTENOVIĆ, V., IANICI, S., BANIĆ, M., MILTENOVIĆ, A, (2014) *University Teaching and Authoritative Competences of Product Development Engineers*, 8th KOD 2014, Balatonfüered, Hungary, pp. 1-8.
- [7]. BINZ, H., ALBERS, A., (2013). *Universitäre Lehre in der Produktentwicklung. Leitfaden der Wissenschaftlichen Gesellschaft für Produktentwicklung (WiGeP)*. Stuttgart, Germany.

CORRESPONDANCE



Vojislav MILTENOVIĆ, Prof. D.Sc. Eng.
University of Niš
Inovation Center of the University in Nis
Univerzitetski Trg 2
18000 Niš, Serbia
vojamiltenovic@yahoo.com

GEAR TRANSMISSION FAILURES AND FAILURE BASED DESIGN

Milosav OGNJANOVIĆ
Nenad KOLAREVIĆ
Miloš STANKOVIĆ
Sanja VASIN

Property based design - PBD approach provides improvement of various properties and characteristics. In the area of transmission units', by applying PBD, significantly are increased service life and reliability, including vibration and noise reduction. Together with these improvements, operating conditions of gear unit components got significantly worst and possible failure relations are changed and needs the new approaches in analysis in comparison to the traditional one.

This article has intention to create relation between possible failures of gearbox components, according to mentioned trends. The main trend is significant reduction of dimensions which is in strong contradiction with gear lubrication and cooling. Together with increase of rotation speed, these contradictory effects transforms pitting as the dominant gear failure into the scoring of the teeth contact surfaces. This and similar failure transitions are presented. In order to prevent it, specific cooling and lubrication systems have to be developed. This is the reason that design structure of gear transmission units getting more and more complex.

*From presented point of view, failures of gear transmission components interaction is important design constraint and it justifies the introduction of the term **Failure based Design - FBD** of gear transmission units. Presented cases study of transmission units for various applications, contains mentioned analysis and FBD application.*

Key words: Gear transmission units, Engineering design, Failures of gear units components

1. INTRODUCTION

Nowadays is actual approach to increase the quality of action and behaviour of TS with existing principle of action. This Effect-based design approach is oriented to expand the domain of TS functions– F , domain of structures– S and domain of behaviour– B , using integration of mechanical structure with electronic, software and mental action [1]. In Fig.1 is presented FBS model [1] with activities in all of them in the area of gear transmission units design. Also this figure shows that transformation of function– F into structure– S is Function-based Design which performs according to linear design model. Relation between structure– S and behaviour– B is Property-based design approach with the aim to improve behaviour of existing TS, according to V-design model. In order to increase the level of TS, the area of function– F spreads out with electronic, software and mental action. Relation between function area– F and behaviour area– B is the approach Behaviour-based Design.

Perfection of TS implies the new secondary functions, the new structure and increase of TS behavior. It can be achieved by application of hybrid structure which except of mechanical, contains electronic, software and similar components, in a word by development of intelligent TS.

This kind of reverse engineering with the objective to increase existing TS behavior, performs with the pressure (force) to increase certain indicator of behavior such as efficiency, convenient control, comfort etc. The limitations which define design parameters, got *design constraints*. These are forced directions and objectives which have to be fulfilled in order to increase the level of TS. The design limitations are the passive limits which have to be satisfied, but design constraints are active and forced directions of design action and for activities which lead to objectives which are not precisely defined in advance, uncertain and will be fulfilled in the measure which allow level of knowledge, available technology and market conditions.

The basic design model established by J. Gero [1] is FBS-model (Fig.1) which shows that in design process it is necessary to bring in close relation function F , behaviour B and structure S . From generation to generation of power transmission units, by presented design constraints action, the level of design quality is increased, especially in the area of design behaviour in exploitation. Majority of constraints are in the strong contradictions, especially structural and behaviour constraints. The typical example is contradiction between lightweight design i.e. mass reduction and reliability and durability increase and vibration and noise reduction.

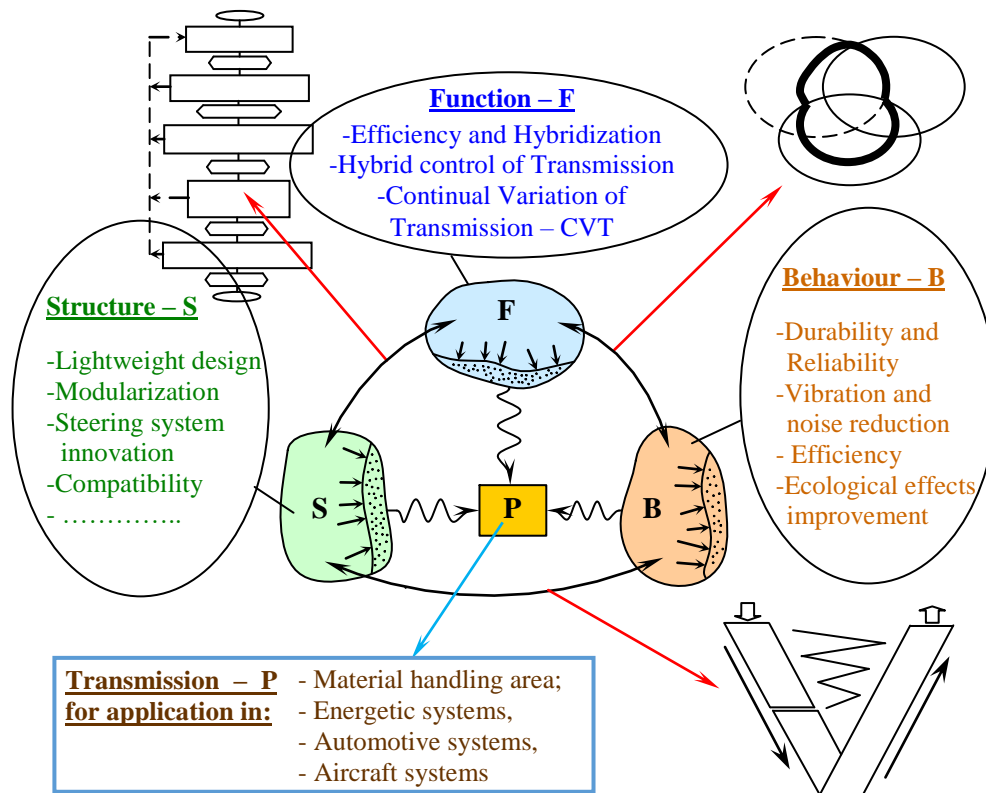


Fig. 1: Design aspects of gear transmission units, constraints and approaches

Functional design constraints in the case of vehicle gearboxes arise in order to increase vehicle efficiency by reduction of mechanical power dissipation and to transform surplus of this power in electricity and use it when it is necessary. It was beginning of hybridization but it continued for various necessity by adding of electronic and software control.

Structural design constraints such as lightweight design and high level of compatibility, modularization, etc. got very important. These constraints are in strong contradiction between each other and with behavioural constraints. In *Lightweight design* the weight reduction is the complex activity which involves all phases of design process, starting from conceptual design, material selection, dimensions and shape selection, application of various technological methods such as thermal and plastic treatment etc. Application of these approaches can significantly reduce the mass but also can significantly increase product cost. This contradiction is very often a limit for mass reduction. *Modularization* is structural design constraint directed to the cost reduction. Modularization contains transformation of complex technical system into the set of modular components which can be installed in various design structures. Solving of this contradictions produces various specific design solutions and innovations.

Behavioural design constraints are oriented to increase quality of action, market quality, environmental and ecological quality etc. Behaviour of the system is result of developed structure and required field of functions. In reverse direction, desired behaviour imposed necessary functions, design parameters and structure, interrelations

inside the system, etc. *Durability and reliability* are the main indicators for market competition. Furthermore increase of durability and reliability are in strong contradiction with other constraints such as cost reduction, lightweight design, compatibility, etc. *Vibration and noise* level reduction is also the design constraint which provides increase of TS quality and better position in the market competition. This action constrains development of technical solution which satisfies legal limitations and also in reverse, provides effect at the legal limitations to be stronger in the future.

Satisfaction of design constraints cause change of operating conditions of gear unit components. Speed of rotation, loads and stresses significantly increases. The space for components installation and surface for heat reflection, decreases. These are conditions for gear teeth failure transition from pitting to scoring. Lubrication of gears and bearings together with cooling needs specific approaches which can significantly increase design complexity and cost. This is the trend in all areas of gear transmission units' application: material handling, energy production, automotive and aircrafts. The intensity of contradictory interaction are not the same and effects are the different and design solutions are also different.

Failure-based Design-FBD is result of worsened conditions and endeavour to avoid any kind of failures. This means if these contradictions cause the new kinds of failure, to find some kind of design approach and solution which can prevent expected and possible failure. This is the set of design activities which provide reliable and steady operation of gear transmission unit.

2. TRANSITION OF GEAR UNITS FAILURES

By application of design constraints presented in Fig.1, operating conditions of gear units components getting worse and worse. Reduction of dimensions significantly increase the loads and stresses. Together with very high speed of rotation and reduced volume, heating inside of gear unit, makes extreme difficult *operating conditions*. This transition of operating conditions causes transitions of component failures.

Gear failures, very known, tested and recognized in standards for gear design, transit from the state which provides usual gear unit behavior (vibration, reliability, etc.) to the state of progressive damage and reduction of service life. Its' need additional design improvement with the aim to prevent effects such this one. In Fig.2 is presented possible trends in gear teeth failures in relation to load limits according to various failures. It is known that involute teeth fracture limit is higher in relation to teeth flank failures. Teeth pitting load limit is common for gear design. For this purpose it is necessary to provide lubrication with permanent and stabile oil film in teeth contacts and corresponding pressure and stress distribution (Fig.2). Missing of oil film transit teeth flank failures from pitting or micro-pitting to spalling (in the range of small speeds) or to scoring in the range of high circular speeds. Losing of oil film in conditions of high

speed and high load produce local welding and particles and pitting roughness's produces very intensive scoring process, overheating and reduction of service life. In order to avoid losing of oil film it is necessary to apply corresponding lubrication system. Gear sinking in oil (Fig.3a) can provides oil film for relative small speed and stabile gear unit position, not in vehicles and aircrafts. Centrifugal effects produces oil dispersion and it is not possible to create oil film when the speed is high. Spraying by oil under the pressure provides possibility for stabile oil film and for teeth cooling (Fig.3b). When peripheral speed is very high such us 80m/s and more, centrifugal effects can prevent possibility of oil film creation. For these conditions oil film can be survived by bilateral spraying of gear connection area (Fig.3c).

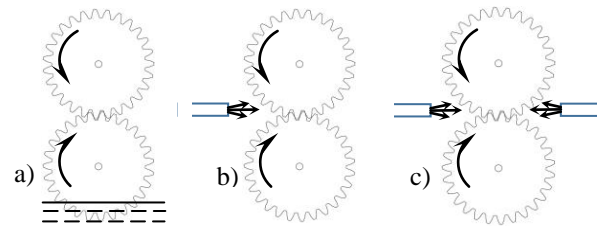


Fig. 3: Principles of lubrication and cooling

Lubrication by spraying (Fig.3b and c) provides possibility to avoid scoring failure but makes design structure much more complex and expensive.

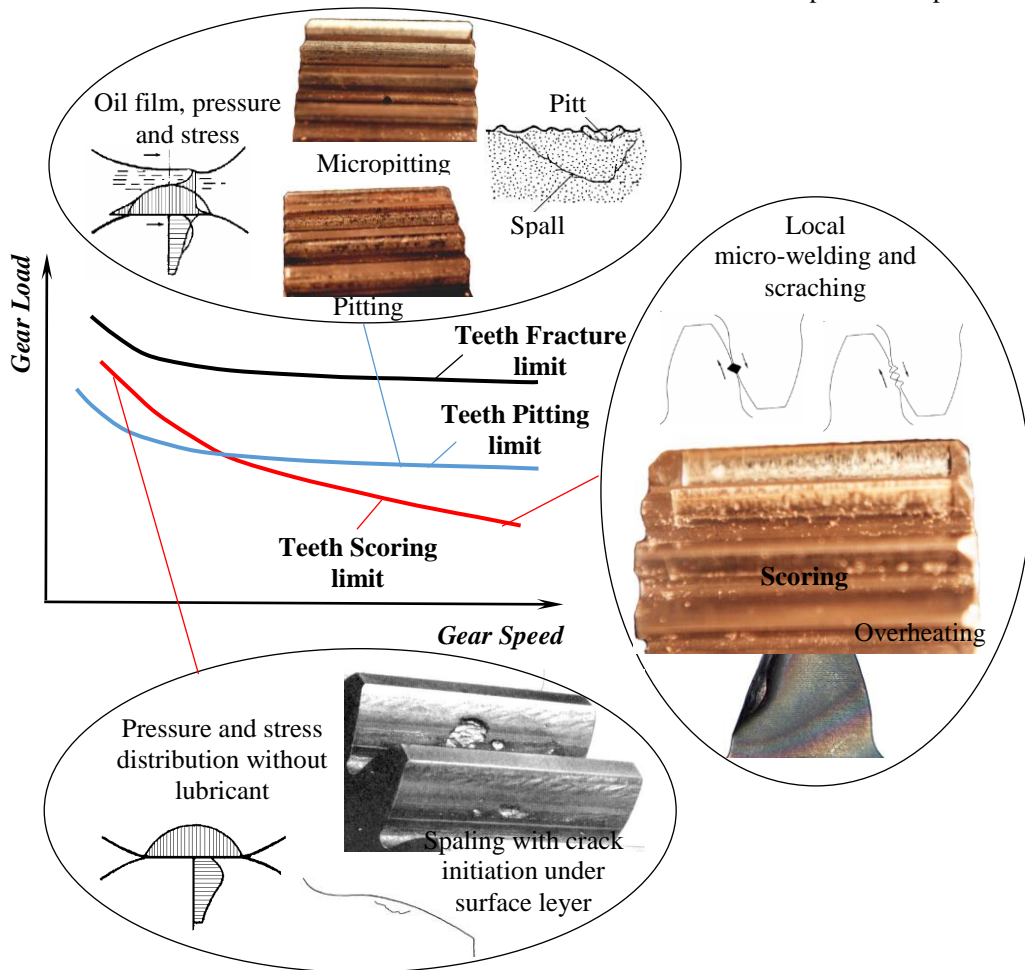


Fig.2: Relation between types of failure, gear speed and gear load limit

Bearing failures do not significantly transits in those extreme operating conditions but the service life has reduces. Reduction of gear dimensions increase bearing loads and necessary bearing dimensions. The main contradiction in lightweight design that reduction of gear dimensions is limited by the necessary space for bearings. Approach in design to solving of this problem is specific. For this purpose various kinds of bearing designs of small volume and high speed is developed. Additional problem is that this solutions needs specific way of lubrication and cooling. Furthermore, rolling bearings for extreme operating conditions replace hydrostatic, aerodynamic or aerostatic plane bearings.

Caring structure failures in the new designs are important for analysis. Lightweight design together with design volume reduction impose the need for design of complex shape and light caring structure of gear units. Inside structure of gear unit getting complex and compact. It is not easy to make difference between the shafts and gears (see Fig.5-7). Also housings are made from lightweight alloys, have small wall thicknesses with a lot of ribs. The ribs have to increase housing strength and stiffness. Reduction of gear dimensions has effect to increase gear forces and bearing and housing loads. In contradiction to reduce housing mass arises possibility of the **crack initiation in the housing walls**. Together with residual stresses as a casting result, the crack initiation in the housing walls getting very probable.

Reduction of dimensions reduces housing outside surface for heat radiation. The ribs provides relative small improvement but very often it is not enough. Really high quantity of heat relished inside of gear unit has to be taken out using additional design solutions.

Gear resonances in the case of high speed of rotation are also probable. Gear rotating masses connected with gear teeth in mesh stiffness presents harmonic oscillator. When teeth mesh frequency comes close to natural frequency of harmonic oscillator, arises gear in mesh resonance. This resonance produces significantly increase of dynamic loads of complete structure and level of vibrations. Gear transmission units consists of a few gear pairs in mesh and everyone has teeth mesh resonance. Additionally gear unit structure has modal shapes of natural vibrations. Teeth mesh frequencies of gears have to be different in relation to natural frequencies. From this point of view, dynamic analysis of gear unit with high speed of rotation is really complex for analysis.

3. FAILURE-BASED DESIGN

Property-based design is general approach in engineering design oriented to improve certain property of developed or existing technical system. The set of technical system properties identify behaviour-B of the system (Fig.1). In order to increase the level of TS behaviour, relation between structure-S and behaviour-B is the task of Property-based design which is carry out according to V-model presented in Fig.1. Since the possible failures belongs to the group of design properties or indicators of design properties, Failure-based design corresponds to this design approach.

Property-based design with the task to increase TS reliability, to increase aesthetic level, to reduce vibrations and noise, etc., presents the set of minor or large design activities which lead to the aim. Failure-based design also contains the set of design activities which correspond to technical system type and to failure or cause of failure. In Fig. 4 is presented this procedure which consists of a few groups of activities. The first group includes analysis of operating conditions, causes of failures and failure processes. Systematic search for details of causes is the base of search for the solution which can prevent certain failure. The next group of activities is search for these design or other solutions by application of innovative technics such as TRIZ or WOIS. Since the failures are results of no harmonized contradictions in technical systems, the TRIZ technique leads to contradiction harmonisation and WOIS leads to solution without compromise. Both imply perforation of thinking barrier and search for the new innovative solution. This means spreadsheet area of function-F, structure-S and behaviour-B. The thread group of activities is development of the new design structure with improved mechanical structure, electronic structure and software. This is enhanced existing TS or the new one and present higher level of TS perfection. The fourth group of activities, according to Fig. 4, contains systematic conditions analysis and testing in relation to expected influences. For this purpose the process needs various models and experimental installation for simulation of conditions in service life. Very often results of these analysis are not satisfactory. In the meantime information and knowledge level got higher and the next iteration of failure-based design procedure can be successful. This means that procedure is iterative and every iteration leads to higher level of TS perfection.

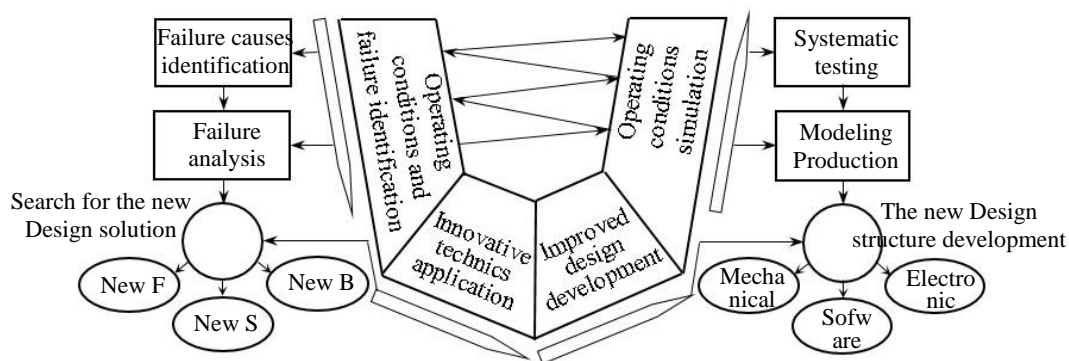


Fig. 4: Failure-based Design procedure

4. CASES STUDY

The set of innovative gear units are developed according to presented methodology. Principles of development are the same but depending of operating conditions and design constraints, the results are with design specificity.

4.1. Area of energetic systems

Production of electricity from alternative resources makes wider the area of gear units' application. Various functions have to be carried out by gear units. In Fig. 5a is presented gear unit applied at wind turbine. In combination with electronic system and motor-generator, gear transmission variates transmission ratio according to wind speed in order to provides permanent speed of electricity generator and 50Hz current, ready for synchronization at public electric net. Mechanical part of this hybrid system consists of the two planetary stages. Outside gear ring at the second stage is not fixed. By motor-generator this ring rotates with the speed which corresponds to necessary transmission ratio in dependence of wind speed. Motor-generator tracking or braking gear ring, spend or produces electricity using additional batteries.

Mechanical structure is developed according to lightweight design principles. Materials, dimensions, shape, volume and other features are selected to provide minimal mass and volume of complete structure. That is the reason for possibility of mechanical failures especially at gears and bearings. Sinking of gears in oil provides lubrication of this relative slow gears. Cooling of this compact gearbox is solved by specific solution using heat superconductors in the form of sheets which covers gear unit and outside turbine box. This solutions provides possibility to avoid gear failure in the form of scoring and put back to the pitting (Fig.2). In Fig. 5c is presented testing installation with power circulation and load, speed and transmission ratio variation for testing to the failure arises, by operating conditions variation according to service conditions.

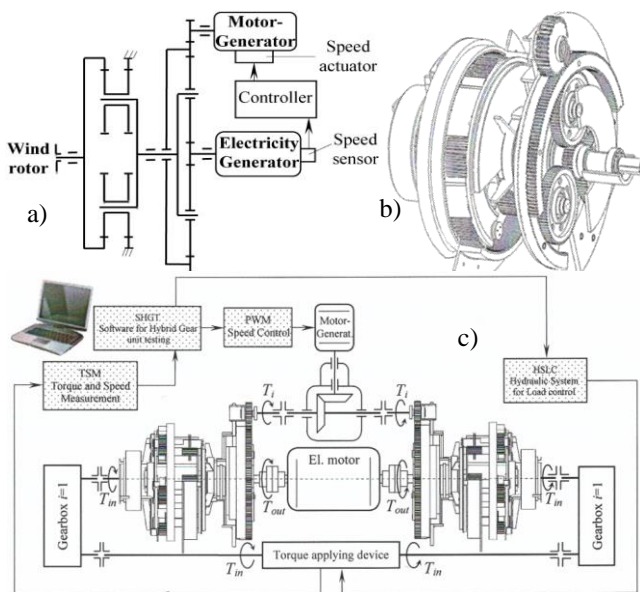


Fig. 5: Wind turbine gearbox with continual variation of transmission ratio: a) turbine concept, b) gearbox design, c) test installation with power circulation

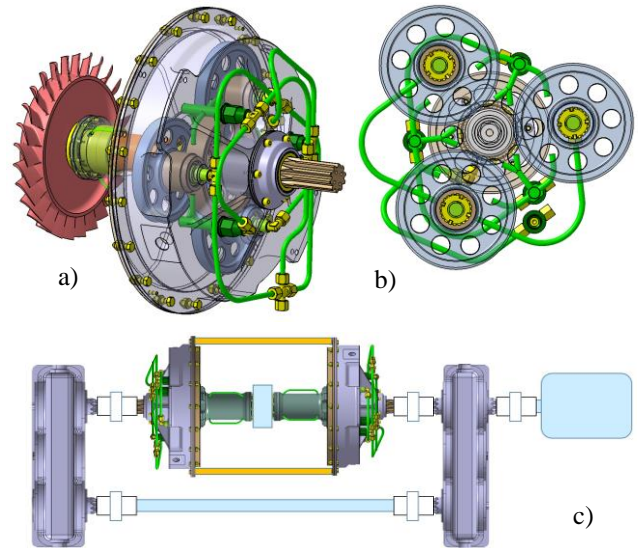


Fig. 6: Reducer of turbo-shaft motor: a) reducer design, b) bilateral lubrication of gears, c) test stand with power circulation

Electricity production from biomass fuel can be carried out by gas-generator and turbo-shaft motor. Very high speed of rotation, 40.000-65.000 rpm have to be reduced to the level of 6000 rpm suitable for electric generator operation. Design solution of reducer for this purpose is presented in Fig.6a. Peripheral gear speed of input gear is higher than 100 m/s. In order to maintain the oil film between gear flanks is applied bilateral oil injection in gear meshes (Fig.6b). Besides of oil film provision, the oil has the task to take out significant quantity of heat produced in the teeth contacts. For carrying out these functions reducer has to be equipped with hydraulic oil system and with cooling system. The question is the optimal balance between reducer volumes, speed and load capacity in relation to additional complex equipment which it is necessary to apply in order to avoid gear scoring and provide conditions for pitting failure (Fig.2). In Fig. 6c is presented the test stand for reducer testing until to failure according to principle of Failure-based design presented in Fig.4. The stand consists of the two opposite connected reducers with input shafts. Output shafts are connected to the gearboxes which provide power circulation, speed of output shafts of 6000 rpm and corresponding load. Test stand is equipped by system for lubrication and cooling and by system for operation conditions monitoring. Testing prolongs until to the gears failure with testing time not less than expected reducer service life.

4.2. Area of automotive application

Innovative design of automotive hybrid gearbox with continual variation of transmission ratio 1...10 is presented in Fig.7. This is the two stage planetary transmission connected by motor generator which consumes and produces electricity in the course of transmission ratio variation. Gearbox is extreme compact with outside diameter about 300 mm, transmission power 315 kW and input speed 6000 rpm. Gears operates with very high speed and are in very high risk of scoring failure. It is necessary to find out solution for lubrication and cooling in order to avoid scoring failure.

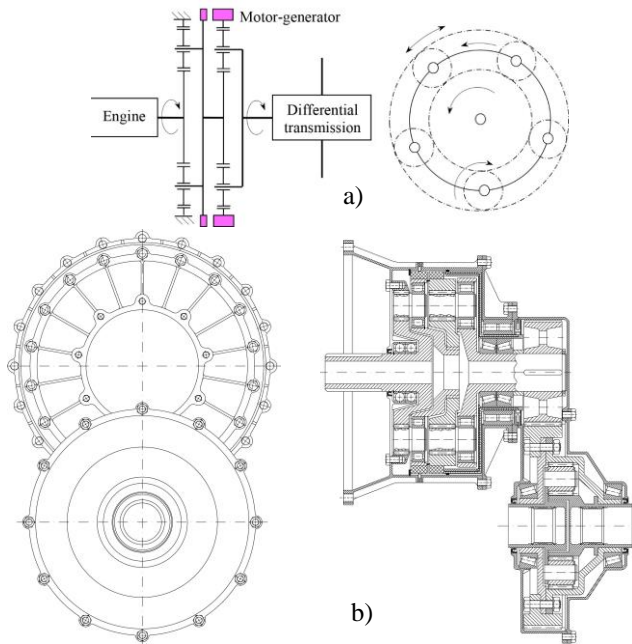


Fig.7: Hybrid design of automotive gearbox with continual variation of transmission ratio

4.3. Area of aircrafts

Design constraints presented in Fig.1 in the area of aircrafts are of significant importance especially lightweight, reliability, vibration etc. Power sources are of extreme high speed and specific loads of transmission unit parts are also high. Turboshaft engines provides high level of power with extreme high speed of rotation and have relatively small mass. Helicopters or propeller airplanes needs 20...100 times less speed of propeller rotation. Very light and reliable gear units have to provide corresponding speeds. In Fig. 6 and 8 are presented gear units for this purpose. In Fig. 6 is presented gearbox for turboshaft engine which can be used for propeller aircrafts propulsion or for ground energetic application. In Fig. 8 is presented design for additional speed reduction for helicopter propulsion. Both of them need application of Failure-based Design approach (Fig.4) in order to find corresponding design solution which will provides gear pitting failure instead of scoring failure. Lateral or bilateral forced lubrication (Fig.3) and conduction of teeth local heat is the main target of design. Delivery and return of oil together with the cleaning and cooling is the task of complex oil system with the pumps, oil tank, filters, valves etc. (Fig.8). The main topic in design and testing of this gearboxes is transferred from the gears and bearings to lubrication and cooling system, very important for reliable operation.

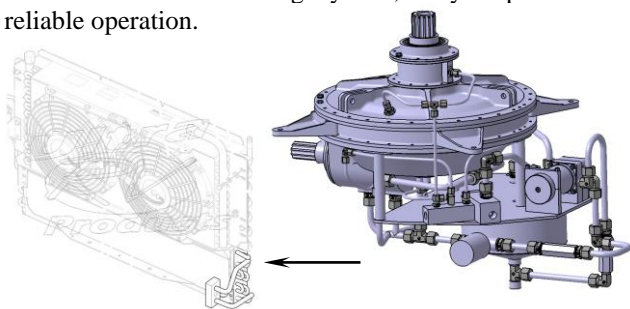


Fig. 8: Additional design structure applied for lubrication and cooling which provides gear unit operation in aircraft field

5. CONCLUSION

Actual design constraints in the area of gear transmission units such as continual variation of transmission ratio, lightweight, reliability, vibration, etc., cause transition of failure processes and also present the top topic of gear units design. The article offer the next contributions.

- 1) Transition of gear teeth failure process caused by application of actual design constraints.
- 2) Failure-based design of gear units in order to prevent failure transition from gear pitting to gear scoring.
- 3) For energetic application, in the area of alternative sources of electricity (wind energy and biomass), the two innovative gearboxes are presented and discussed.
- 4) For automotive and aircraft areas are also presented innovative designs of gear boxes together with discussion according to presented methodology of Failure-based design.

REFERENCES

- [1] VREMAS, P.E., DORST, K. (2007) *On the conceptual framework of John Gero's FBS-model and the prescriptive aims of design methodology*, Design Studies, vol. 28, 133-157.
- [2] ASLANTAS, K., TASGETIREN. S (2004) *Tasgetiren S.: A study of spur gear pitting formation and life prediction*. Wear 257, 1167-1175
- [3] FISCHER, R. BESTE, F. (2014) *AVL Future Hybrid Transmission – the holistic approach for hybrid drivetrains - The new AVL 7-Mode transmission - E-Proceedings of the 14th International VDI Congress*.

CORRESPONDANCE



Milosav OGNJANOVIĆ, Prof. D.Sc. Eng. **Professor emeritus**, University of Beograd Faculty of Mechanical Engineering Full member of **Academy of engineering sciences of Serbia** - AINS milosav.ognjanovic@gmail.com



Nenad KOLAREVIĆ, Ass. M.Sc. Eng. University of Belgrade Faculty of Mechanical Engineering Kraljice Marije 16. 11120 Beograd, Serbia nkolarevic@mas.bg.ac.rs



Miloš STANKOVIĆ, Eng. PhD-student University of Belgrade Faculty of Mechanical Engineering Kraljice Marije 16. 11120 Beograd, Serbia mstankovic@mas.bg.ac.rs



Sanja VASIN, M.Sc. Eng., Ph.D Student University of Beograd Faculty of Mechanical Engineering Kraljice Marije 16 11200 Beograd, Serbia vasinsanja@gmail.com

THE INFLUENCE OF THE DESIGN FLOW RATE ON THE ECONOMICAL AND ECOLOGICAL ASPECTS OF SHP - SMALL HYDROPOWER PLANTS

Petar V. VUKOSLAVČEVIĆ

***Abstract:** The negative impacts of the design flow rate, as one of the most significant design parameters of SHP, are analyzed. It is shown that the negative influence of this parameter on the local as well as on state level is mainly underestimated and not presented transparently. It is clear from the given examples that this influence strongly depends on the national strategies in the SHP developments. It is also shown that the design flow rate can have as strong environmental impacts as the reserved flow rate. The real impact on the final consumer prices of electrical energy of the design flow rate is also analyzed and some recommendations how to reduce the negative influence presented.*

***Key words:** small HPP, design flow rate, installation ratio, environmental impacts, grid connection, FIT*

1. INTRODUCTION

The document "Blue Age for a Green Europe", completed in 2002, represents a foundation of a strategy for the development of Small Hydropower Plants (SHP) in the European Union. The target set by this document was an increase in power of 1111 MW by upgrading existing SHP and an increase of 4828 MW by building new units, what will result in a production of 24153 GWh of electrical energy. This was a realistic target, because a real technical potential offered almost a double capacity of upgrading existing and building new SHP. As a result a reduction of CO₂ emission of about 20 million tones could be achieved (based on a prudential value of gas fired plants, 0.43 kg_{CO2} /kWh). It must be emphasized that two world conferences on environment protections and climate change: Rio Conference on Environment and Development in June 1992 [1] and Kyoto Conference on Climate Change in December 1997 [2], as well as Directive/77/EC of the European Parliament, of 27 September 2001 [3], have preceded this document. EU 20-20-20 strategy set in 2007 and enacted in legislation in 2009, also contributed to the strategy of the SHP's development.

Although SHP's do not produce carbon dioxide or any significant water pollutants, they can have strong environmental impacts on local level. As stated by ESHA [4], "The significant global advantages of small hydropower must not prevent the identification of burdens and impacts at local level and the taking of necessary mitigation actions". Identification of the environmental impacts usually does not make a problem, but to meet the agreements on the mitigation measures can create serious difficulties not only due to the objective, but also due to subjective arguments.

Implementation of the mitigation measure in order to reduce the environmental impact and meet the demands in ecological terms, have serious cost implications reducing the viability of SHP. Besides the environmental impact on local level, depending on the national strategies of the SHP developments, a strong economic impact on the state level can be also present. The economic impacts are usually in the shadow of the environmental one.

2. THE ENVIRONMENTAL AND OTHER NEGATIVE IMPACTS OF SHP

A nice survey of environmental impact is given in a guideline of ESHA (European Small Hydropower Association) [4]. The most significant one, depending on the designed flow rate or installation ratio (ratio of the designed and mean flowrate) and reserved or ecological flow rate, will be addressed here.

2.1. Influence on the streambed

The most of the SHP are of the diversion type, especially in the Western Balkan region. A great amount of water is diverted from the stream in penstocks what results in the reduction of flow in the streambed between the position of intake and powerhouse, affecting incubation, rearing, and the passage of fish and other living spaces in streambed. A conflict between the potential investors and local community is unavoidable. In order to increase the electricity production and profit, the investors tend to take as much water from the streambed as possible from technical point of view, while the local community tends to preserve the flora and fauna of streambed and its surroundings as well as to have enough water for irrigation and other purposes.

It is very important to emphasize that the high flow rates in raining seasons are as important as the minimum flow

rates in dry seasons for the wildlife of the streambed. While a wide range of guidelines, methodologies and formulas exist for determination of minimal flow rate, there are hardly any guidelines for the minimal amount of the high flow rates in raining seasons. Both of these flow rates will be analyzed in separate chapters of this presentation.

2.2. Influence on the energy cost

Purchase prices of electrical energy from renewable energy source are based on generation cost. As a result, the prices for different technologies and for projects of varying sizes are different. This is known as a feed-in tariff, FIT, or advanced renewable tariff [5] or renewable energy payment [6]. FIT is a policy mechanism designed to motivate the investment in renewable energy source technologies. Tariffs are formed in different way in negotiation between energy producers and suppliers with strong influence of national policies. They vary from one to the other country and frequently change over time. For a given time period the prices are subsidized to a great extent comparing to the market prices and afterward they are subject to the market only. The difference between market and renewable energy subsidized price is also known as green certificate. The green certificate can be up to three times of the market prices. Besides the subsidies in energy prices, the renewable energy producers has guaranteed greed access. This means that in some situations the prices from renewable energy source can be over five times of market energy prices. Such rather high price difference is finally paid by energy consumers. The final consumers energy prices will depend not only on the subsidies for green energy but also on the participation of the green energy to the overall energy productions. The subsidized prices of electrical energy from SHP in Montenegro depends on the SHP's power at the connection point to the greed system. They are arranged in five groups, Table.1. [7].

Table 1: The subsidies energy prices of the electrical energy from SHP's in Montenegro

Power P_{SHP} [MW]	Group	Subsidized prices [c€/kWh]
< 1 MW	1	10,44
$1 \leq P_{SHP} < 3$ MW	2	$10.44 - 0.7 * P_{SHP}$
$3 \leq P_{SHP} < 5$ MW	3	$8.87 - 0.24 * P_{SHP}$
$5 \leq P_{SHP} < 8$ MW	4	$8.35 - 0.18 * P_{SHP}$
$8 \leq P_{SHP} \leq 10$ MW	5	6,8

The prices are guaranteed for a period of 12 years. The FIT is not the only cause that will increase the bills of final consumers. They are many others, depending on design parameters, that are almost never presented transparently. The most important one are construction and maintaining of the grid as well as the grid balancing.

3. BASIC PARAMETERS OF A STREAM FLOW CHARACTERISTICS

A program of flow rate measurements, at a particular site over a period of at least one year, should provide a table of flow rates which has to be organized into a usable

forms as hydrographs and various versions of flow duration curves (FDC).

3.1. Hydrograph

Hydrographs show discharge Q [m^3/s] as a function of time in chronological order at a given sight of streambed. The input data are the discharge values, usually mean day values, over a year. Several hydrographs, typical for Western Balkan's countries are presented in following figures [8].

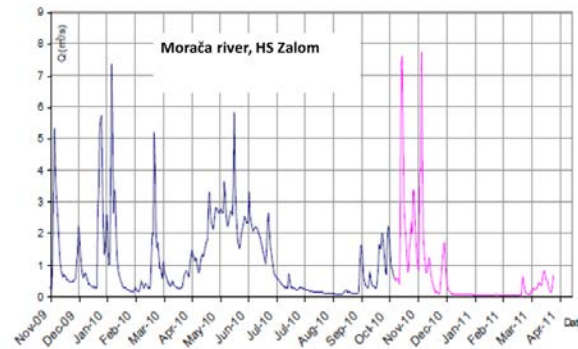


Fig.1: Hydrograph of river Morača, HS Zalom

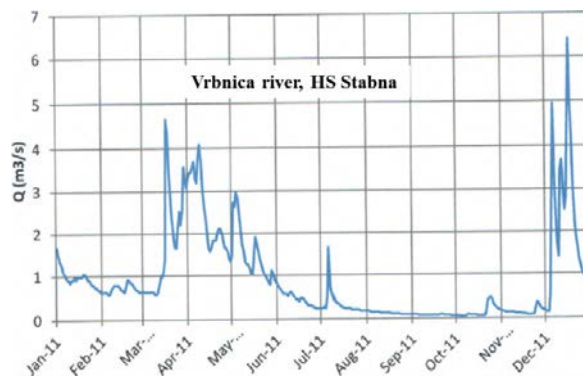


Fig.2: Hydrograph of river Vrbnica, HS Stabna

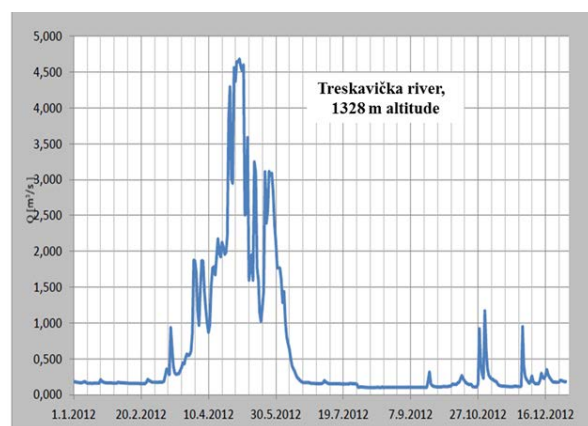


Fig.3: Hydrograph of river Treskavička at 1328 altitude

The main characteristics of these hydrographs are strong discharge variation, with high picks in raining seasons and almost dry stream bed in summer time. It is typical even for rivers of moderate mean discharge, like Morača, and much more exaggerated for streams with low mean

flow rates. It also depends on the regions; seaside, inland or high mountains range. The high flow picks can appear one, Fig.3, or several times over a year (Fig.1 and Fig.2). The high flow rates don't have to appear always in the same time each year, as it can be seen in a case of Morača, Fig.2. In January 2010 the flow rate was well above an average, while in January 2011 the river bed was almost dry. Having that in mind, it is clear that, in order to have reliable information, it is necessary to take the data over several years period and then use the mean value of the flow obtained by averaging the measured data of each year at the same date. The other way is to correct one year data by the proportion of the mean participation rate over several years period for a given region. A difference up to 20% can appear in the Western Balkan region.

3.2. Flow duration curves - FDC

FDC is a useful way of organizing the discharge data given in hydrographs. For a particular section of streambed, FDC shows the time period or the time proportion in a year, during which the discharge equals or exceeds certain values. It can be obtained from the hydrograph by ordering the daily mean flows by its magnitude. It can be also estimated at given sight using the measurement data from other sights. Various approaches of estimation procedures can be found in [16]. Plant energy output as well as the percentage of time that a power output can be generated, can be obtained from FDC. If it is necessary to know when it happens, the hydrograph has to be used.

The FDC of the hydrographs shown in Fig.1, Fig.2 and Fig.3 are presented in Fig.4, Fig.5 and Fig.6.

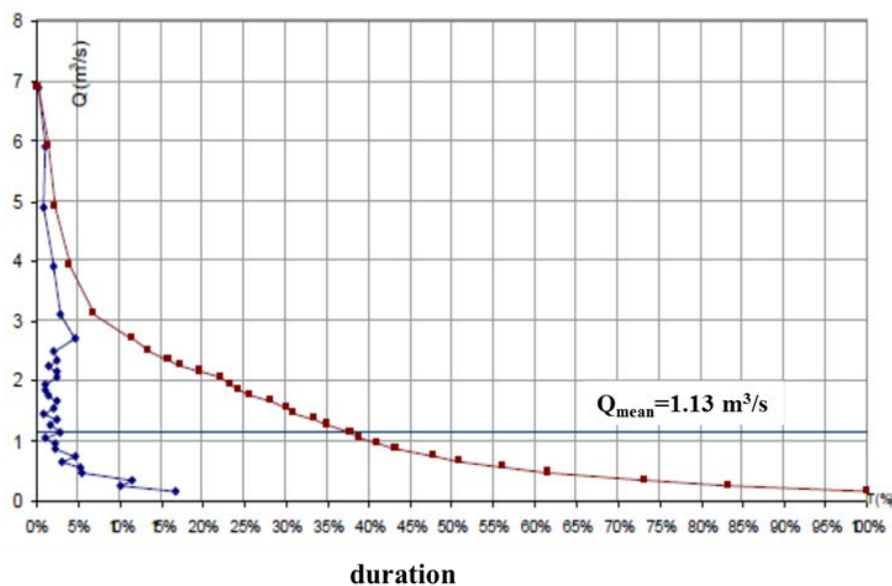


Fig.4: FDC of river Morača at HS Zalom

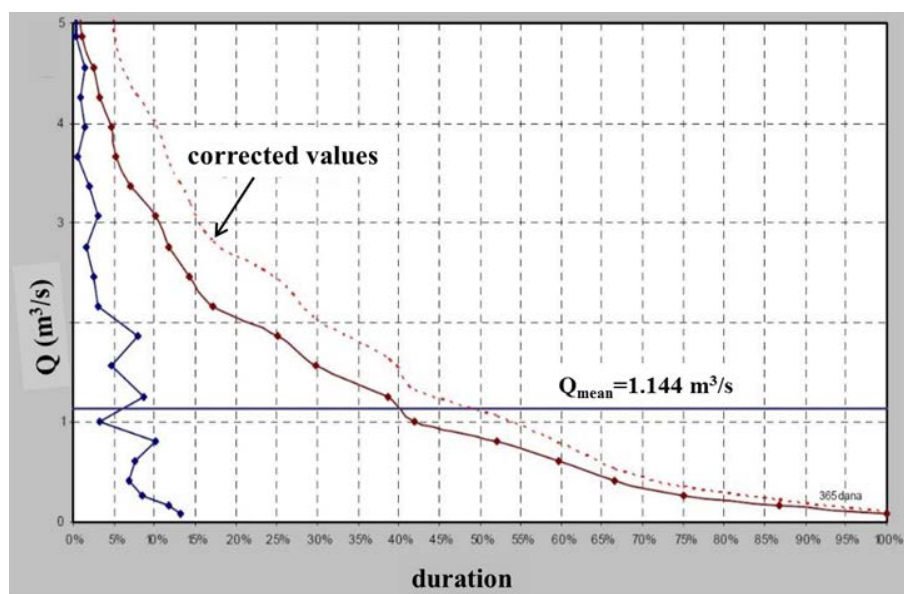


Fig.5: FDC of river Vrbnica at HS Stabna

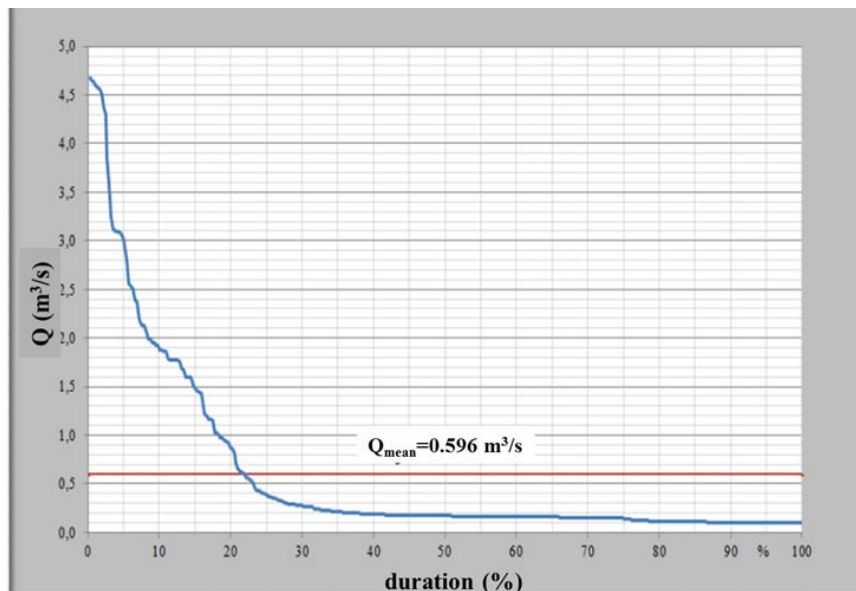


Fig.6: FDC of river Treskavička at 1328 mnm

A correction due to the variation of the participation over a 10 year time period is shown in Fig.5.

One of the main characteristics of FDC curves is their slope. The higher the slope is the smaller is the time with flow rate equal or higher than the mean flow rate. In a case of Vrbnica river, Fig.5, the flow rate is equal or higher than mean one 40% of the time, while in a case of Treskavička it is only 22%. As it will be shown in the following paragraphs, all negative impacts of SHP are going up with increase of the slope of FDC.

4. BASIC DESIGN PARAMETERS THAT INFLUENCE NEGATIVE IMPACTS OF SHP

The design and reserved flow rates are the designed parameters that strongly affect not only the final price of electrical energy but also the flora and fauna in and around the river bed.

4.1. Design flow rate – installation ratio

The designed flow rate represents the ratio of design and mean flow rate or discharge. It should be define through an optimization process which can results in a flow rate much larger than a mean one. Various optimization parameters can be used like: specific investment cost per installed power, EU/kW, specific investment cost per annual production, EU/MWh, net present value – NPV or revenue reduced for investment, operational and maintain costs over the SHP lifetime, NPV over a subsidized price time period, simple payback period - SPP or the time period when NPV reach zero, internal interest rate – IRR and others, [4], [9]. It is interesting that depending on the priorities given to SHP investors (regarding to the greed connection, level and period of subsidized prices) and optimization parameters the designed flow rate can strongly vary in comparison to the mean flow rate giving different values of installation ratios. The choice of investors is also different, depending on their financial capabilities, bank interested rates, possibility of investing

money in other projects and so on. They are almost never guided by negative impacts of SHP's, if they do not have to do that.

There are hardly any reliable information about the range of installation factor in the Western Balkan countries. A systematic analysis of available data has not been done so far except for Montenegro. Even these data are not publicly available. From various, mainly private sources, unofficial recommendations of the recognized investors and states institutions for Western Balkan and Austria, it looks that the installation factor is in the range of $i = 1,1 - 1,6$, for high or moderate head, which prevails in these regions. The recommendation from a study made by HMZ of Motenegro and UNDP [10], for the Montenegrin SHP, is close to that range; $i = 1,2 - 1,6$. The operational time with designed flow rate (or full capacity), for a given FDC, depends on instalation factor. A recommended value, given in [11] is 35% yearly or $Q_i = Q_{35\%}$. A minimum value of 33% yearly is recommended by [12]. A recommendation in the range of 25-45% is given in [13].

Based on this data, a conclusion can be drawn that the instalation factor should not go over 1.6 or that the full capacity operational time should be over 25% yearly. The priorities of privity investors are, unfortunately, very often out of that range, going to the side that increase the negativ impact of SHP.

A few typical investor proposals from Montenegro are given below. They are assigned with corresponding numbers because of the possibility that some of the data might be confidential. The optimization is based on three parameters: simple payback period, specific investment cost per annual production and NPV or net profit over 12 years' time period. The results for SHP2 are shown in Fig.8 and Fig.9.

It can be seen from these figures that the optimal design flow rate based on Simple pay back and specific investment is practically the same, $Q_i = 0.8 \text{ m}^3/\text{s}$, giving an installation ratio of $i = 1.48$, inside the recommended range. The optimal design flow rate based on net profit over 12 years subsidized price period is $Q_i = 1.1 \text{ m}^3/\text{s}$, giving

an installation ratio of $i=1.84$, above the recommended range. It is clear that the investor choice is based on net profit. The operational time with designated flow rate for

the examples given in Fig.7 varies from 9% yearly for SHP3 to 18% for SHP1.

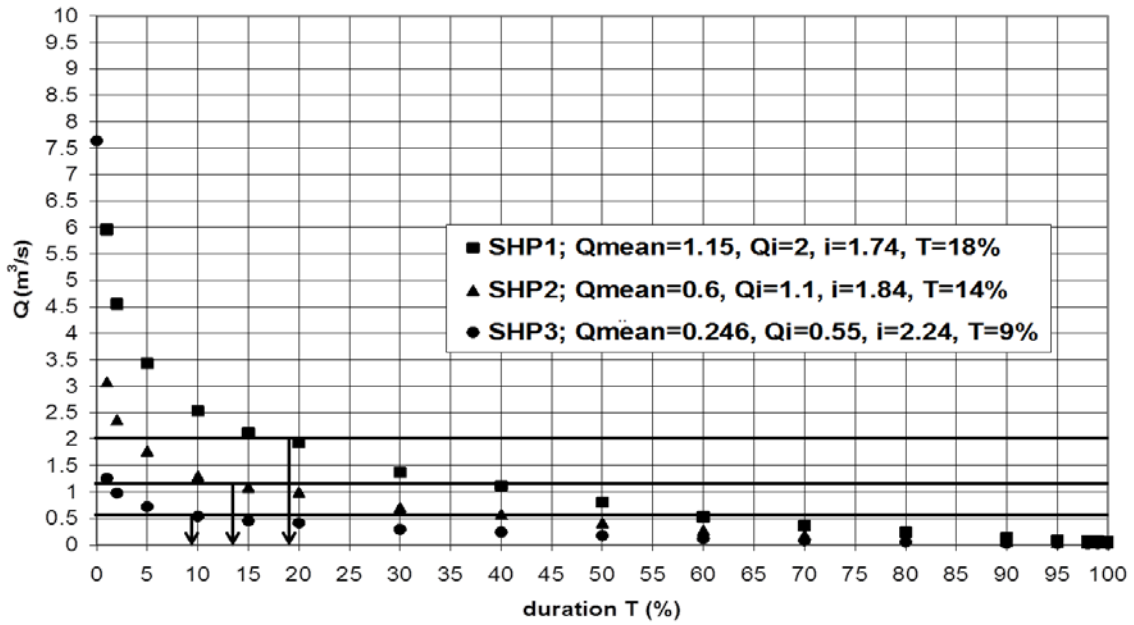


Fig.7: FDC with proposed installation factor for SHP1, SHP2 and SHP

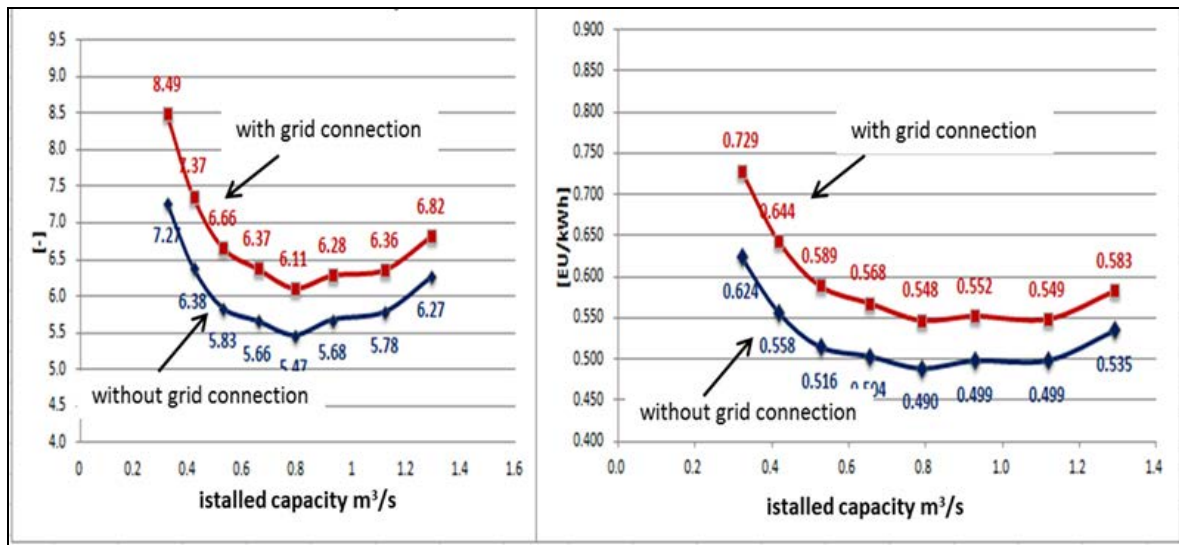


Fig.8: Simple pay back and specific investment as a function of designed flow rate for SHP2

Another example is given in Fig.10. The recommended installation ratio was 1.6, giving a period of 25% yearly operation with full capacity of $P=2.75$ MW. The proposed value of installation ratio is 2.6 what increases the installed power to $P=6.5$ MW, but reduces the operational time with full capacity to only 11% yearly.

It is clear that the proposed installation factors are above the recommended values for SHP, going in the range characteristics for impoundment (with accumulations) HPP, $i=1.6-3.8$ [14].

An economic analysis of SHP5 for 12 years subsidized prices period time, given in Table 2, clearly shows the legal investors motivation to increase the installation factor and reduce the full capacity operational time below an acceptable level.

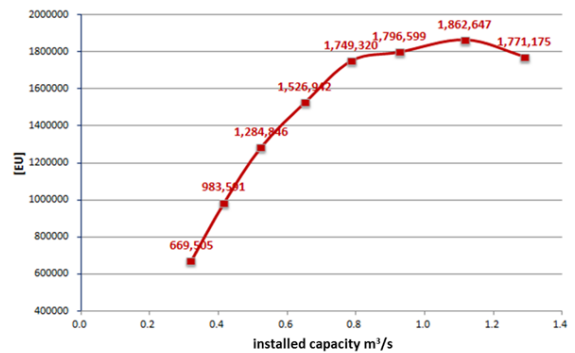


Fig.9: Net profit over 12 years subsidized prices time period for SHP2

Table 1: Economical analysis of SHP5

Q_i (m ³ /s)	i (-)	Full capacity operational time (%)	Investment (mil EU)	Production (GWh/year)	Revenue (EU/year)	Net income (EU/Year)
0.334	1.36	28	1.154	1.879	176000	145000
0.56	2.27	10	1.31	2.166	213000	178000
			17%	20.6%	21%	22.7%

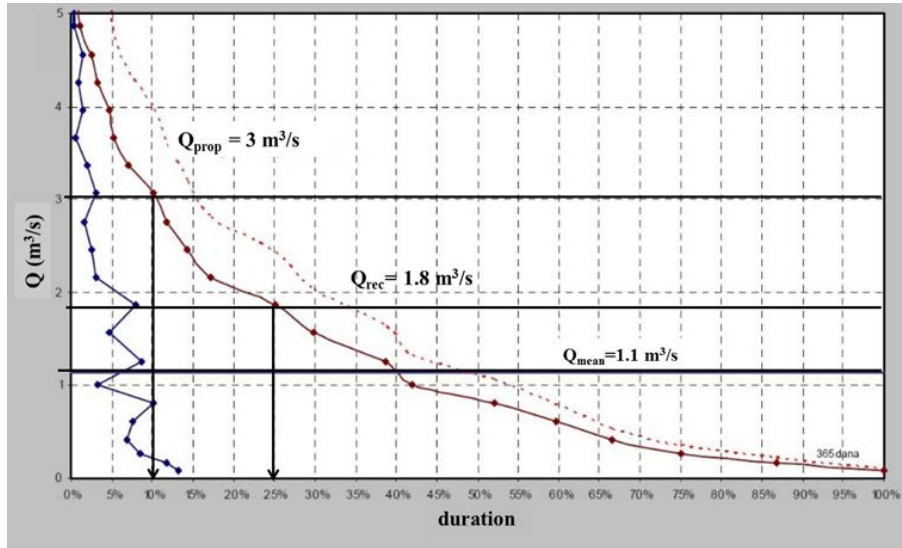


Fig.10: FDC with recommended and proposed installation factor for SHP4

To better understanding of these results it is necessary to analyze the cost of each segment of a SHP. A nice analysis of these partial costs is given in [15].

Presented results strongly depend on the benefits and priorities given by state national politics in the field of SHP development. A frequent appearance of strong deviation from the recommended values is a good indication that such a policy has to be revised.

4.2. Reserved flow rate and minimum of high flow rates

Diversion of water from the watercourse can make a strong impact on the living organism of flora and fauna in and around the stream bed even if it is not left completely dry. To avoid this, a certain amount of water should remain in streambed. This amount of water is named different way depending on the country like: reserved flow, prescribed flow, compensation flow, ecological minimum and minimum flow. The term reserved flow will be used in subsequent text. Not only that this reserved flow is important from ecological point of view, but also a minimum of high flow rates during the raining season are of great importance. While various recommendations related to the reserved flow can be found in literature, there are hardly any information about the minimum level and duration period of high flow rates that have to be preserved. It is clear that both of these flow rates have serious cost implication and that they can strongly reduce the viability of SHP.

Various formulas defining the reserved flow can be found in literature and websites like [4], [16]. Their number is going up almost every year showing that a reliable methodology has not be found yet and that the ecological

demands are increasing every year. A brief review of the best known formulas based on various stream parameters will be present here.

Average flow rate Q_{mean} . Reserved flow is in a wide range of Q_{mean} , going from 2.5% in France to 60% in Montana (USA). A typical value of $10\%Q_{mean}$ is mostly used. This value is also adopted in the most of the Western Balkan countries.

Minimum flow rate Q_{min} . Reserved flow rate varies in the range from 20% to 100% of river Q_{min} . Such a method should never be applied in a case when the riverbed can get dry or the water goes underground during dry season.

Prescribed flow rate. This method is based on prefixed values on the FDC. For example Q_{300} refers to the values of 300 days on the FDC. The number of days varies from one to the other country; 300 in Switzerland, 347 in Germany and so on.

In addition to the presented one there are methods that prescribed the minimum of velocity and depth of water. It usually goes from 0.3 to 2.5 m/s and from 10 to 24 cm. An optimization method taking in consideration of both, economic and ecological parameters can be also used. Some methods prescribed various reserved flow rates at various sections of the same riverbed.

One of the rare methods that prescribed both, the reserved and minimum of high flow rates is proposed by Green home NGO from Montenegro [17]. Although the presented idea deserve attention, it turns out that in some cases obtained results are worse from the ecological point of view than the $10\%Q_{mean}$ for reserved flow and a minimum of high flow rate determined by recommended values of installation ratio.

5. NEGATIVE IMPACTS OF HIGH INSTALLATION FACTOR AND UNDEFINED MINIMUM OF HIGH FLOW RATES

Negative impacts of SHP are presented in almost each book related to the SHPs like [18], [4], [19] and others and an enormous number of articles and websites. They can be divided in two groups; the one that appear during the construction of SHP and the one present during its operation. The most of the negative impacts that characterized the operation time of SHP depends mainly on the installation ratio. The minimum of high flow rates and its impacts on living organism is also strongly correlated to the level of installation ratio.

High installation ratio will strongly affect:

- greed connection,
- greed balancing,
- quality of the electrical energy,
- river bed morphology and deposits,
- the real price difference in raining season
- final price of electrical energy.

Power line from SHP to the nearest transformer station as well as transformer capacity has to be designed according to the designed power. In a case of high installed ratio, see Fig.10 for example, it is clear that full capacity of these facilities will be used about 10% of the year only. Investors will take this problem in consideration if they have to pay for the connection construction and maintenance expenses. Otherwise, if the greed operator guaranties free connection, as it is the case in some countries, the investor are not limited in increasing of the installation ratio from this point of view.

SHP has the priority in delivering the produced energy to the greed. Having in mind uncertainty of the energy production from SHP, greed operator has to have a reserved energy source to balance the grid. This is the most expensive energy that enters the greed. The higher installation ratio, the smaller is the period of the known energy production rate and higher the need for energy balance.

It is well known that SHP can affect the quality of electrical energy having in mind its influence on frequency and reactive power. The higher is the frequency of variation of energy production rate the most serious are this problem. This variation will obviously increase by increasing the installation ratio.

The river morphology as well as structure and level of various deposits, crucial for the life of many organisms and species strongly depend on high flow rates. During the high flow rate periods, various organisms (plants for example) that decays in the water will be washed away, preventing the river bet to become a dead swamp and new deposit will create necessary condition for developing new life in the river bed.

Having in mind the priority of the SHPs related to the grid connection, it can happen that they deliver energy with subsidized prices while the energy prices from the other sources are well below the average one or almost free. This makes the differences of green energy and market

prices much higher than the average one. The higher is the installation ratio, the higher could be this difference. If the investors are not limited by regulations they will hardly consider any of the presented problems. Having in mind the priorities given to the investors in SHP, the cost of the most of cited problems is paid by final consumers. Unfortunately, the most of them are not presented transparently. For the difference from the FIT, that is transparent, the consumers are not very often aware of the expenses of the greed construction and maintenance, losses in the greed, the expense of grid balancing and real price difference in the raining seasons.

6. CONCLUSION

1. The installation ratio is the most important design parameter that strongly affects the economic and ecological aspects of SHP.
2. The upper limit of installation ratio has to be strongly bounded, otherwise it can create enormous negative impacts on the living organisms in and around river bed and on final price of electrical energy.
3. The most of the consequences on the energy price created by high level of installation ratio are not presented transparently.
4. Besides the reserved flow rate in dry season, a minimum in high flow rate in raining season has to be defined to. The best way to define this flow rate is by limiting the installation ratio.
5. All priorities given to the investors in SHP, has to be revised each years. Besides the FIT, that has been slowly decreased each year, the participation of the investors in the expenses of greed construction, maintenance and balancing should be revised to.
6. In order to reach the national goals in green energy production, the priority of the energy sources that should be subsidized, should be reconsider every year.
7. The Western Balkan countries should take in consideration the possibility some of the SHP could become the monuments of a wrong policy in the field of green energy production, after the subsidized prices period expiries

REFERENCES

- [1] *The United Nation Conference on Environmental and development*, Rio de Janeiro, 1992.
- [2] *Kyoto Climate Change Conference*, Kyoto, 1997.
- [3] *Directive 2001/77/EC of Renewable electricity*, European Parliament and Council, 2001.
- [4] *Guide on How to Develop a Small Hydropower Plant*, ESHA, 2004.
- [5] GIPE P. (2006) *Renewable Energy Policy Mechanisms*, www.wind-works.org
- [6] MENDONÇA, M., JACOBS, D., SOVACOO, B. (2009) *The Feed-in Tariff Handbook--a Review*, ISBN 9781844078585, Earthscan, London.

- [7] *Uredba o tarifnom sistemu za utvrđivanje podsticajne cijene električne energije iz obnovljivih izvora energije i visokoefikasne kogeneracije*, Službeni list CG“, br. 28/10, 6/13 i 10/15, 2015.
- [8] *Preliminarna obrada hidropotencijala na pritokama glavnih vodotoka Pive i Lima u Crnoj Gori*, Hidrometeorološki zavod Crne Gore, 2008.
- [9] INVERSION, A. *Micro-hydropower source book*, NRECA international foundation, Washington, 1990.
- [10] *Hidrološka obrada za profile malih hidroelektrana na pritokama glavnih vodotokova u Crnoj Gori*, Hidrometeorološki zavod Crne Gore, 2012.
- [11] Guidelines for layout for SHP, AHEC/MNRE/SHP standards/civil work, 2008.
- [12] *Zgradimo majhno hidroelektrarno*, Zveza organizacija tehnično kulturo, Ljubljana 1986.
- [13] WARNICK C.C., *Hydropower engineering*, Prentice-Hall Inc., NJ 07632.
- [14] ĐORĐEVIĆ B., *Hydroenergetsko korišćenje voda*, Građevinski fakultet Univerziteta u Beogradu, Beograd, 2001.
- [15] *Cost base for small-scale hydropower plants*, Norwegian Water Resources and Energy, Directorate, 2012.
- [16] www.esha.be
- [17] *Pravilnik o načinu određivanja ekološki prihvatljivog protoka površinskih voda*, Službeni list CG, br.023/16 od 05.04.2016.
- [18] SHAPES M., et al. (2010) Work package 2: SHP Research and Development activities within the EU and associated states, Small Hydro Action for the Promotion of Efficient Solution.
- [19] RAMOS H., et all. (1999) Guideline for Design of Small Hydropower Plants, WREAN and DED, Belfast.

CORRESPONDANCE



Petar V. VUKOSLAVČEVIĆ,
 Prof. D.Sc. Eng., Academician
 Montenegrin Academy of Sciences
 and Arts
 81000 Podgorica, Montenegro
petarvuk@ac.me

**MECHANICAL SYSTEMS
AND ELEMENTS**

ROOT CAUSE ANALYSIS OF MICRO CRACKS OF HYDROGEN REFORMER HG

Samir DIZDAR
Radoslav TOMOVIĆ
Adisa VUČINA

Abstract: Micro cracks have been found near some of the welds on the Hydrogen Reformer HG unit at Refinery AB. This paper investigates the root cause of this damage and suggests improvements to prevent such damage from occurring.

The investigation includes several simulations using Pipestress and Ansys Mechanical, a welding and materials investigation, and a more theoretical creep investigation using the Larson-Miller parameter. A sensitivity study of the outlet pigtail installation and support configuration is performed as well as a cyclic plastic analysis. A complementary analysis of the catalyst tubes, inlet and outlet system shows that the only areas where the stress and strain indicate an elevated risk of damage are the areas around the ends of the outlet pigtails.

Suggested improvements include reconfiguration and load reduction of constant hanger supports, improving welding procedures in order to lower residual stresses and undertake more material and on site investigations to verify causes of failure

Key words: cracks, creep, fatigue, plastic analysis.

1. Introduction

Micro cracks have been found on several of the pipes in the HF system unit [1]. To continue to operate, the root cause need to be determined and potential actions need to be taken.

1.1. Purpose

The purpose of this paper is to analyze the micro cracks in the outlet system and try to establish a root cause for this damage, as well as suggesting how to avoid further damage or prevent such damage in future installations. In addition, a complimentary evaluation, presented in Section 3.

1.2. Scope

The scope of this paper contains an investigation into different damage mechanisms such as creep, fatigue and welding procedure to find a root cause for the micro cracks. An investigation into the previously made calculations is made to establish whether this damage could have been predicted. Using the results of the different analyses, suggestions on improvements are made.

This paper treats the most highly stressed areas and where the damages have been observed. Hence, not all parts of the system are evaluated in detail. The focus lies on the parts containing the welds where micro crack damages have been found, in particular three locations where the most severe damages are observed. Following the notation of [1], these three welds are called S3, S4 and S7. Their locations are shown in Fig.1.

Several different methods are used to try to determine the cause of the observed damages. The system is investigated with numerical finite element (FE) analyses as well as with analytical and theoretical methods. Welding and inspection books are studied to analyze the choice of materials and welding procedure. The different methods are meant to provide a substantial width in the investigation and hopefully increase the understanding and to prevent damages like these from occurring in the future.

The system is evaluated according to the ASME B31.3 standards [2]. API papers are also considered. ASME B31.3 is used for process piping and will be used to evaluate stresses in the system for design purposes. A Swedish code BSV97 [3] is used for calculation of wind and snow loads on different structures.

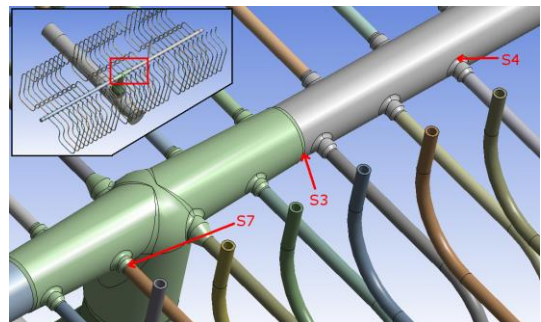


Fig.1: The location of the three most severe damages. The damages at S3, S4 and S7 are all located on the southern side of the mid-section of the manifold

1.3. Pipestress Analysis

The software Pipestress [4] is used to make a model of the piping system and to obtain loads and movements at different points throughout the system.

Pipestress is a one dimensional software that is used to model large piping systems including supports of different kinds. The software is very efficient at calculating the response of the system to different loads and thereby identifying weak points in its design. It is also very useful when wanting to investigate different design solutions.

1.4. ANSYS FE-analysis

The software ANSYS Mechanical [5] is used as a verification of the Pipestress results as well as to provide detailed results regarding stress concentrations and stress directions at points of interest. Furthermore, thermal transients and effects due to creep properties of the material are investigated using ANSYS.

1.5. Loads

The system is evaluated for sustained loads and thermal range loads. The sustained loads considered are internal pressure and dead weight. The loads are evaluated in accordance with reference [2]. No wind loads have been applied in the calculation, but recorded data suggest that the contribution is small. The temperatures (T) and

pressure for the different parts of the system, according to specifications, are presented in Table 1.

The load combinations are presented in Table 2. Thermal range is the load resulting from Thermal Expansion (TE). Thermal Range is defined as the difference between the cold and hot states of the system. In these cases, Dead Weight (DW) is included with together with TE.

Table 2: Load Cases

Load case	Loads	Allowed stress
Sustained Loads	DW+DP	S_A (from table)
Thermal Range	TE (+DW)	$S_A=1.25 S_c+0.25 S_h$
Sustained Loads	DW+OP	S_A (from table)
Thermal Range	TE (+DW)	$S_A=1.25 S_c+0.25 S_h$
Combined (Creep)	DW+OP+TE	-

1.6. Welding and Materials Investigation

An investigation into what impact welding procedure and material quality may have had on the occurrence of damages is made using installation and inspection books together with comparisons with literature.

The materials used for the different parts are shown in Table 3.

Table 1: Temperature and Pressure conditions according to specifications

Part	Design		Operation	
	Temperature [°C]	Pressure [MPa]	Temperature [°C]	Pressure [MPa]
Transfer Line	300	2.8	250	2.48
Manifold (Sub Header)	890	2.8	860	2.48
Pig Tails	890	2.8	860	2.48

Table 3: Parts and Materials

Part	Material	Temperature [°C]	Allowable Stress [MPa]	Young's Modulus [GPa]	Thermal Expansion Coefficient [mm/m]
Transfer Line	A 387 GR. 11 CL. 2	20	172	204	0
		250	130	190	2.6
		300	125	186	3.8
Manifold (Sub Header)	PARALLOY CR32W	20	116.7	196	0
		860	15.18	143	15.54
		890	12.64	141	16.1
Pig Tails	ASTM B 407 N08811	20	115	196	0
		860	9	143	15.35
		890	6.9	141	15.59

2. RESULTS

Many of the results are presented with the term utilization. The utilization U for a component is the fraction between the actual and allowed stress,

$$U = S_{\text{actual}}/S_{\text{allowed}} \quad (1)$$

A utilization below 1 ($U < 1$) means the component is qualified, a utilization above 1 ($U > 1$) means that a more

detailed analysis needs to be performed or requires a change in design.

2.1. Pipestress Results

Results are presented for Sustained Loads and Thermal Range Loads with utilization in accordance with ASME B31.3 302.3.5 (c) and (d) [2]. The load cases considered are the conditions for design and operation. Temperature and pressure conditions according to specifications are given in Table 1 and utilizations for the different load cases for the different models are given in Table 4. The

model of the current state of the system is also run with the sliding boundary condition at the top of the Pig Tails. Table 5 shows the stresses at the welds S4, S7 described in the Inspecta report, reference [1], as well as the stress at the node with highest utilization in the model. The pressure causes a stress of 1.68 MPa in design and 1.48

MPa during operation conditions. Adding the moment stress gives the total sustained stress presented in the table.

Note that the node SS02 is in the Manifold (Sub Header) and therefore uses a different material with higher allowable stress.

Table 4: Utilization

Part	Design		Operation	
	Sustained	Thermal Range	Sustained	Thermal Range
Current State	1.36	0.90	1.02	0.83
C.S. Sliding		0.82		0.77
Improved State	0.84	0.90	0.63	0.83

Table 5: Stresses at S4, S7 and the highest utilization stress MPa. The node number where the stress occurs in Pipestress is presented in parenthesis

		Design stress [MPa]		Operation stress [MPa]	
		Sustained	Thermal Range	Sustained	Thermal Range
Current State	Maximum	9.36 (PO3L)	130.4 (PJ27)	9.16 (PO3L)	120.4 (PJ27)
	S4 (S518-PD10)	7.45	110.2	7.25	104.4
	S7 (S004-PE30)	7.39	117.1	7.19	110.7
Current State (Sliding)	Maximum	11.64 (PM1L)	119.1 (S002)	11.45 (PM1L)	112.5 (S002)
	S4 (S518-PD10)	7.46	108.3	7.26	102.5
	S7 (S004-PE30)	7.4	118.7	7.2	112.1
Improved State	Maximum	5.76 (PQ82)	130.4 (PJ27)	9.49 (SS02)	120.4 (PJ27)
	S4 (S518-PD10)	4.17	110.2	3.97	104.4
	S7 (S004-PE30)	3.88	117.1	3.68	110.7

2.2. ANSYS Results

Overall, the ANSYS results are in good agreement with the Pipestress results. However, more details are modeled in ANSYS, which results in stress concentrations and higher peak stresses. Another fundamental difference from the Pipestress results is that circumferential stresses due to inner pressure is included in the ANSYS results. The absence of these stresses in Pipestress is a result of Pipestress only being concerned with evaluating longitudinal stresses.

Three different types of analyses are performed with ANSYS:

1. Static structural analyses of the sustained (pressure + dead weight) loads and the thermal expansion load (including dead weight)
2. Creep analyses, to study the creep strain over time at different temperatures.
3. Thermal transient analyses, to study the temperature and local thermal stress distributions at start-ups, shut-downs and trips.

The maximum stresses observed in the considered system parts for the static structural and thermal transient analyses are summarized in Table 6 for the respective load cases. The stresses on the inside and outside of the pipes are presented separately. The internal pressure has little effect on the outside but may cause high stresses on the inside while the dead weight typically affects the outside most. The von Mises stress on the inside and outside surface of a section of the manifold is plotted in Figure 2. One may note in Table 6 and Figure 2 that the stress under sustained loads is significant on the inside.

This occurs on the inside of the manifold at the pig tail connection.

Table 6: Load Cases

		Maximum stress [MPa]	
		Inside	Outside
Design	Sustained (PD+DW)	36	13
	Thermal expansion (TE _{890 °C} +DW)	75	150
Operation	Sustained (PO+DW)	32	12
	Thermal expansion (TE _{820 °C} +DW)	70	137
Thermal Transient	Increasing (860 – 20)°C/4h	40	25
	Decreasing (20 – 860)°C/4h	130	60

One may also in Table 6 note the large stress due to thermal expansion. This stress arises at the end of the pig tails by the manifold and is considered in detail in the context of the observed damage at the S7 weld.

The main results concern the observed damages at S3, S4 and S7. An overview of the maximum principal stresses at these points for different load cases is presented in Table 7, where also the maximum utilization among the points is given for each load case.

The non-linear behavior of creep makes the results from the creep analyses very sensitive to the particular values used for the temperature and material properties. Thus, the creep results are here chosen to be summarized with a plot rather than a table. In this way, one may judge the

behavior of the creep in the model. One of the locations found to be quite sensitive to creep is the upper part of the weld between manifold and pig tail weldolets, e.g. where the damage at S4 where found. The strain at such a point is plotted against time for various temperatures in Figure 3. The strong temperature dependence is evident from the plot where it can be seen that changing the temperature from 820 °C to 860 °C reduces the time to reach a particular strain almost by a factor of 10.

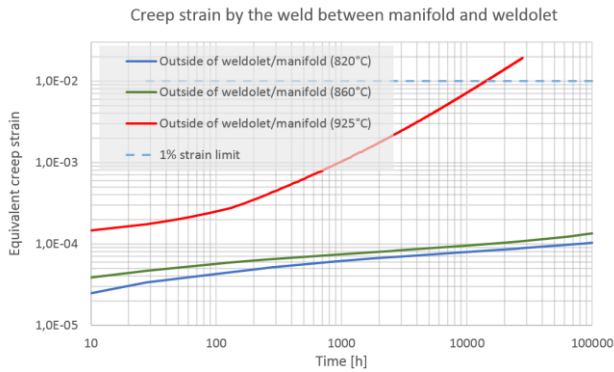


Fig.3: The strain over time at the weld between manifold and weldolet, e.g. S4's location. The 1% strain limit at which creep damages might emerge is plotted as a dashed line

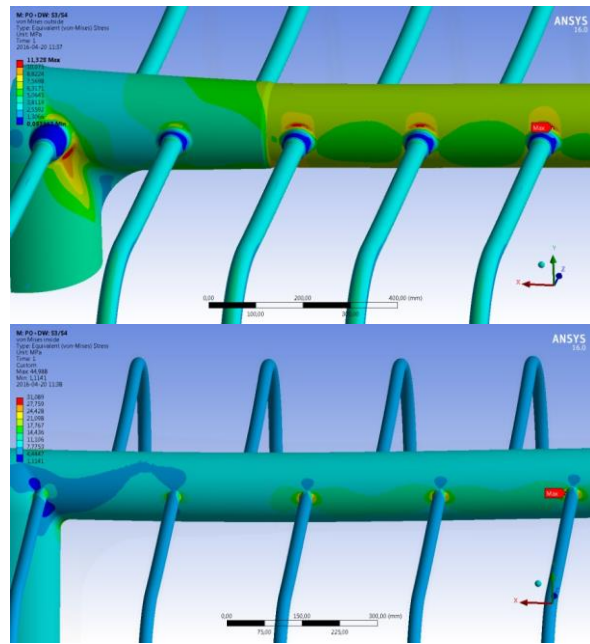


Fig.2: The von Mises stress on a section of the manifold's outer surface (top) and its inner surface (bottom) under PO+DW loads. The central southern pig tail group is on the bottom of the plots and thus S4 is where the maximum is labelled.

Table 7: Overview of the maximum principal stress, which roughly coincides with the longitudinal direction, at the areas around the observed damages.

		Maximum Principal stress (Longitudinal) [MPa]			Utilization	
		S3	S4	S7	Overall	Stress limit [MPa]
Design	Sustained (PD+DW)	7.5*	14.7	7	1.16	12.64
	Thermal expansion (TE _{890 °C} +DW)	20	63	175	-	-
	Thermal range (890-20 °C)	14	50	168	1.15	145.5
Operation	Sustained (PO+DW)	8.5*	13.3	7	0.88	15.18**
	Thermal expansion (TE _{820 °C} +DW)	19	54	158	-	-
	Thermal Range (820-20 °C)	13	41	151	0.98	154

*The maximum principal stress is not longitudinal here. The longitudinal (middle) principal stress is 6.5 MPa for both design and operation.

**Allowed stress at 860 °C

The outside of weldolet/manifold was one of the most highly stressed points under sustained loads, which is why it is susceptible to creep. The point on the inside, mentioned earlier, where the maximum stress occurs during sustained loads, is located on the inside of the manifold by the pig tail connection. Due to its higher stress, this point is even more susceptible to creep. Therefore, creep damages might be worse on the inside and it is not unlikely that micro cracks also could be found on the inside of the manifold.

The following list summarizes the conclusions which can be drawn from the ANSYS results regarding the damages at S3, S4 and S7.

S3: The evaluated stresses around S3 for the different load cases do not on their own suggest that there would be any damages there at this time nor in the near future. Perhaps together with the residual stresses, discussed in the next section, they could contribute to damages.

S4: The stresses due to sustained loads around S4 exceed the allowed limit in the design case and are highly

utilized in the operational case. However, the region is shown to be sensitive to creep strain but with current data it is difficult to make accurate predictions regarding its life time. Furthermore, the thermal stress range is moderate and fatigue will thus give negligible contributions.

S7: The thermal stress range at this weld is large but lie 2% below the allowed limit in the operational case. However, this limit is rather conservative, in particular in this case where the actual number of cycles is so small. Furthermore, a comparison of the strain range with the low-cycle fatigue data of the similar INCOLOY 800H alloy [6] shows that the evaluated strain is roughly 50 times smaller than that which would cause failure.

Even though the magnitude of the evaluated stresses at the damaged regions do not provide striking, conclusive evidence of the cause of micro cracks, their directions correspond well with the orientation of the cracks. The number of tests and observed cracks do not provide a

good statistical basis but there seems to be a correlation between the directions of stresses and cracks. This may suggest that the stress have had an impact on the crack formation, perhaps in combination with factors not accounted for here, e.g. residual stresses in the welds.

2.3. Creep Analysis Results

The evaluated utilization at the current time with regard to expected lifetime varies by use of data from references[2], [6] and [7]. The results for the two stresses 10 MPa and 14.7 MPa at different operational temperatures are presented in Table 8 for the different references. The corresponding expected lifetime for these temperatures at the stress of 14.7 MPa is presented in Table 9.

From the results, it is clear that the materials differ in rupture life, with the ASME material being considerably weaker. The ASME material has a safety factor applied to it to get the allowable stress given in the code [2]. This explains most of the difference but since the determining material value is unknown a compensation for the safety factors cannot be made. Furthermore, the ASME material is specified for the weldolets, to which two of the critical welds are connected.

The contribution from fatigue is very low. Considering that the utilization from fatigue is combined with the utilization from creep as a sum of squares, when the creep-fatigue utilization is evaluated, the contribution from fatigue becomes completely dismissible.

Table 8: Utilization at present time of operation for different operational temperatures

Operational Temperature	PARALLOY, reference [8]		INCOLOY, reference [5]		ASME B31.3, reference [2]	
	10 MPa	14.7 MPa	10 MPa	10 MPa	14.7 MPa	10 MPa
820 °C	0.002	0.005	0.002	0.01	0.16	0.43
840 °C	0.006	0.01	0.006	0.03	0.38	0.99
860 °C	0.02	0.04	0.02	0.11	0.86	2.20
880 °C	0.05	0.1	0.07	0.35	1.89	4.75

Table 9: Expected life (rupture life) [h] at constant stress 14.7 MPa

Operational Temperature	PARALLOY, reference [8]	INCOLOY, reference [5]	ASME B31.3, reference [2]
	14.7 MPa h	14.7 MPa	14.7 MPa
820 °C	9610000 h	4320000 h	100000 h
840 °C	3250000 h	1270000 h	43700 h
860 °C	1140000 h	391000 h	19700 h
880 °C	417000 h	125000 h	9100 h

3. COMPLEMENTARY ANALYSIS OF THE INLET SYSTEM AND CATALYST TUBES

The additional analysis presented in this section serves as a current status check and verification of the inlet system and catalyst tubes of HG. To take into account interactions between the different system parts, the outlet parts are considered in this analysis as well.

The Pipestress software is used to determine the stress levels in the inlet system. Furthermore, Pipestress provides displacement results, which are used as input in the more detailed Ansys analysis of the Pig Tails and Catalyst Tubes, which also models the development of creep strains in the materials.

The loads considered are the same as for the previous analyses, Dead Weight (DW), Thermal Expansion (TE) and Operational Pressure (OP). The Pipestress analysis evaluates both the Design case as well as the operational conditions while Ansys only considers the operational case. A summary of the temperatures and pressures in the system is presented in Table 10.

Table 10: Temperature and Pressure conditions

Part	Design		Operation	
	Temp. [°C]	Press. [MPa]	Temp. [°C]	Press. [MPa]
Inlet	540	3.15	450	2.8
Catalyst	922	2.8	880	2.48
Outlet	890	2.8	860	2.48

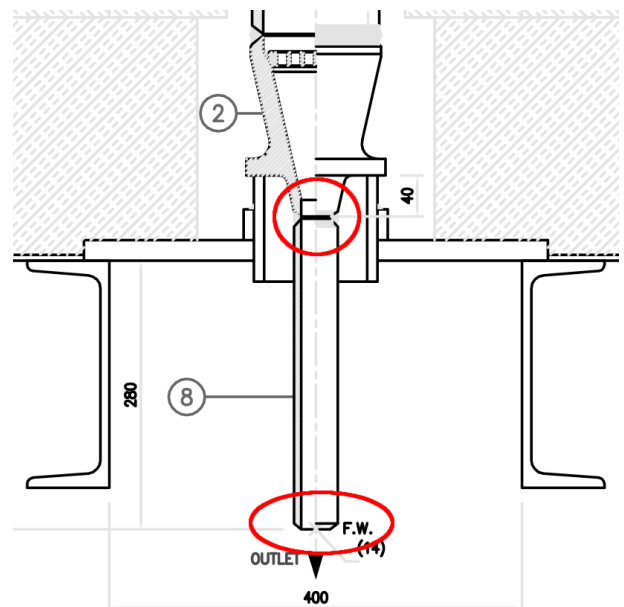


Fig.4: Regions at the upper end of outlet pigtails considered to have an elevated risk of damage

The results of the Ansys analysis, show that no severe stresses or strains are found in the catalyst tubes or the inlet pigtails. The maximum creep strain in the inlet system is 0.07 % and is not in the vicinity of any weld which might affect crack formation and is thus not considered a risk area. The only significant strain in connection to the catalyst tubes is at the bottom of the

reducer to the outlet pigtail where comparatively large stresses and creep strains occur. It is at the upper end of the outlet pigtail where the maximum creep strains occur. These are approximately 0.2 % after 100 000 h, and are at the same levels as at lower end of the pigtail towards the manifold, where cracks have been observed. These creep strain levels are not on their own worrying, but taking into account the fact that cracks have been observed at locations showing the same levels of stress and strain in combination with close proximity welds, these are considered risk areas. The areas with elevated risk for damage are encircled in Figure 4.

4. CONCLUSION

The HG unit seems to have been manufactured and evaluated in accordance with applicable standards and codes, save the questionable existence of an applied wind load, which would not influence the result significantly.

Moving the constant hanger supports according to the improved Pipestress model would greatly reduce the creep driving forces, e.g. sustained loads. The analyses over all shows that the system is very sensitive to the loads from the constant hangers. The movements of the pipes from sustained loads are very small; this indicates that the system is very sensitive to small changes during installation, e.g. mounting of insulation and cladding as well as the relative position on the pipes in relation to the constant hanger support.

The Ansys analysis indicates that creep could be the root cause of the damage at the S4 weld. However, the point most sensitive to creep in the model lies on the inside of the manifold, which suggests that creep damages could be worse there. In general, the observed crack orientations are consistent with the direction of the principal stresses. However, the magnitude of the principal stresses are typically not large enough to, by themselves, be the cause of the observed damages, indicating the presence of unknown stresses, for example residual stresses.

The complementary analysis of the inlet system and catalyst tubes show that there are no regions of significant stress or creep strain in these parts. The analysis shows that the ends of the outlet pigtails (and adjacent reducer and manifold respectively) acquire the largest creep strains. Because of their similarity (in terms of creep strain, material and close proximity to welds) to the locations where cracks are observed these locations are considered as areas with risk for damage.

REFERENCES

- [1] INSPECTA TEKNISK RAPPORT, *Replikprovning HG*, 2015,
- [2] ASME B31.3, 2012
- [3] Boverket, *Boverkets handbok om snö och vindlast*, 1997, 2nd edition.
- [4] DST Computer Services S.A., PIPESTRESS, version 5.0
- [5] ANSYS® Mechanical™, Release 16.0, ANSYS, Inc.
- [6] INCOLOY® alloy 800T & 800HT®, *Special Metals Corporation*, 2004
- [7] DONCASTER PARALLOY, Heat resistant alloy technology centrifuged tubes and statically cast fittings, fabricated coils, catalyst tubes and manifolds

CORRESPONDANCE



Samir DIZDAR, M.Sc. Eng.
BerDiz Consulting AB
Ranängsgatan 8-10
416 64 Göteborg
Sverige
samir.dizdar@berdiz.se



Radoslav TOMOVIĆ, Prof. D.Sc. Eng.
University of Montenegro
Mechanical Engineering Faculty
Bul. Džordža Vašingtona bb
81000 Podgorica, Montenegro
radoslav@ac.me



Adisa VUČINA, Prof. D.Sc. Eng.
University of Mostar
Faculty of Mechanical Engineering and Computing
Matice hrvatske bb
88000 Mostar, B&H
adisa@sve-mo.ba

EXAMINATION OF ULTIMATE BENDING STRENGTH OF POWDER METALLURGY GEARS

Lubomir DIMITROV
Georgi DIMCHEV
Pancho TOMOV
Kiril NIKOLOV

Abstract: Nonmetallic gears are widely used in modern industry. Metal-ceramic gears (MCG) particularly, successfully replace metal gears because of their relatively good mechanical properties and relatively low cost. This paper concentrates on experimental examination of bending stress of maximum loaded metal-ceramic gears. The experimental settings and stress calculations are based on the international standard ISO 6336, which takes into consideration the specifics of MCG. and the results of the conducted experiments.

Key words: gears, metal-ceramic gears, ultimate bending strength

1. INTRODUCTION

One of widely used method for production of metal-ceramic gears is powder metallurgy method [1,2]. The peculiarities of this technology for producing metal-ceramic gears (MCG) – different grain size, mixture composition, inhomogeneity, porosity, deviations of the technological process (environment and sintering temperature, additional heat treatment, wear of the matrix) lead to significant scattering of the geometrical and strength parameters of the MCG. This leads to the requirement that their strength properties be tested experimentally for each batch.

This article presents the results of the experimental determination of the static bending strength of manufactured small module involute MCG and describes the methodology and the test rig for this study. The authors suggest accomplishing the stress and strength calculations based on the available Bulgarian standard BDS 17108-89 [3] as well as the international standard ISO 6336 [8] and to reckon the specifics of MCG (accuracy, pinhole porosity, composition and differences in homogeneity of powders, heat treatment, etc.). MCG strength data in sources [4,5,7,9] is insufficient and refer only to fixed mixture-composition and technology of production which is usually the manufacturer's "know how". This fact imposes to make experiments for each producer and for each group of gears.

2. DESCRIPTION OF THE TEST RIG AND THE EXPERIMENTAL METHODOLOGY

The static teeth bending strength of MCG is determined on a test rig that consists of a device, a dynamometer and a hydraulic press. The body of the device shown in Fig.1

is a U-shaped profile, in the short sides of which two coaxial holes are drilled. In the upper opening, the sleeve 2 is press fitted, which acts as a guide for the piston 3 and in the lower part is the bracket 6, which is press fitted as well. The piston has a cylindrical shape, the lower part of which is square and the upper part is also square. The working faces of the piston and the bracket are hardened (heat treated). In the piston body, there is a groove in which the screw 7 is inserted, thus the piston cannot rotate freely during operation.

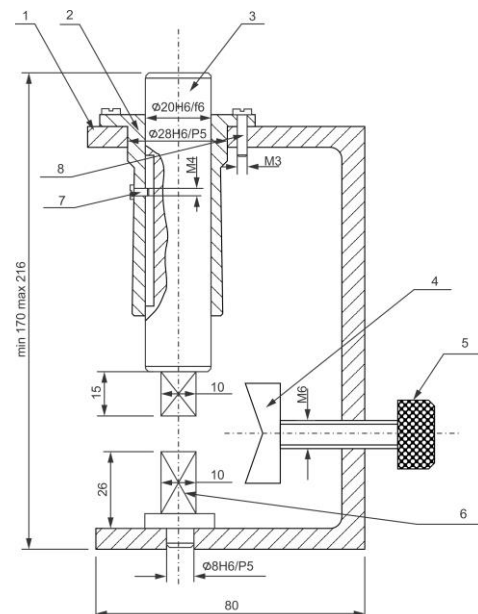


Fig.1 Scheme of the test rig

The tested gear is fixed by interchangeable prisms 4 and is tightened with the screw 5 so that there is a certain

number of teeth between the working surfaces of the piston and the bracket. In this way, it is ensured that the direction of the teeth load is at their common normal. A dynamometer is attached to the device. The gradual loading of the tested tooth is achieved by increasing the pressure in the hydraulic cylinder of the press. The maximum load is measured by the dynamometer at the moment of the teeth breakage. In this case, there is a breakage of the upper tooth (which rests on the piston) or the lower tooth (which rests on the bracket). There is no regularity in this, which shows that the force acts on the common normal. In all cases, the tooth breaks at its base. In the test of a single tooth, the neighboring of which is already broken, it is found that this does not affect the strength of the tooth tested and the results being within the overall scattering, i.e. the strength does not change significantly.

Three groups of MCG having different chemical compositions were subjected to an experimental study of static bending strength (Table 1). The porosity of the samples in all groups is no more than 20% and their metallographic study shows a uniform pore distribution of 250-300 μm . In each group, experiments were performed with 10 gears, with 10 broken teeth from gears with 20 teeth and 20 broken teeth from gears with 35 teeth.

Table 1. Description of investigated gear groups

Group №	Mark of mixtures	Composition of mixtures	Geometrical Parameters			Technological Parameters	
			m [mm]	z [-]	b [mm]	p [MPa]	t [°C]
1.	ИКМ-I-21	Steel, C 0,4%, Cu 5%	0,8	45	4 + 0,15	3,55	1150
2.	ИКМ-I-21	Steel, C 0,4%, Cu 0,8%, Ni 1,0%	0,8	52	4 + 0,15	3,55	1170
3.	ИКМ-I-21	Steel, C 0,4%, Cu 0,8%, Ni 1,0%	0,8	45	4 + 0,15	3,55	1170
4.	ИКМ-I-21	Steel, C 0,4%, Cu 0,8%, Ni 1,0%	0,8	52	4 + 0,15	5,70	1170
5.	ИКМ-I-21	Steel, C 0,4%, Cu 0,8%, Ni 1,0%	0,8	52	4 + 0,15	5,70	1150
6.	ПРЖ 2 Russian	Alloy steel, C 0,4%	1,0	35	8 + 0,18	4,50	1200
7.	ПРЖ 2 Russian	Alloy steel, C 0,4%	1,0	20	8 + 0,18	4,50	1200
8.	Distalloy Swedish	Alloy steel, Mo, Cu, Ni	1,0	20	8 + 0,18	4,50	1200

In the experiment, the force needed to break a tooth is measured and the value of the tooth bending limit at maximum load σ_{Fs} is determined, which is calculated using the formula:

$$\sigma_{Fs} = Y_{Fs} \cdot Y_{\varepsilon} \cdot \frac{F_t}{m_n \cdot b_w} \cdot k_F \quad (1)$$

where:

Y_{Fs} - factor taking into account the shape of the tooth and the stress concentration at its base;

Y_{ε} - coefficient taking into account the overlap of the teeth;

F_t - tangential force acting on the tooth;

b_w - working width of the gear wreath;

m_n - normal module;

k_F - coefficient taking into account the additional bending stress.

Since the load is carried out in static mode, it is assumed that $Y_{\varepsilon} = 1$ and $k_F = 1$.

The coefficient Y_{Fs} is determined by the dependence:

$$Y_{Fs} = 7,32 \cdot \frac{h_{Fa} \cdot \cos \alpha_{Fan}}{m_n} \cdot \sqrt[3]{\frac{S_{Fn}}{2 \cdot \rho_{Fn}}} \cdot \left(\frac{S_{Fn}}{m_n}\right)^2 \cdot \cos \alpha_n$$

where (Fig.2):

h_{Fa} - cantilevered shoulder of the force that

loads the teeth in bending and is applied to its tip;

S_{Fn} - thickness of the tooth at its base;

ρ_{Fn} - radius of curvature of the transverse curve

(for the studied MCG this transition curve is an arc of a circle);

α_{Fan} - angle of action of the force at the tip of the tooth of the equivalent gear.

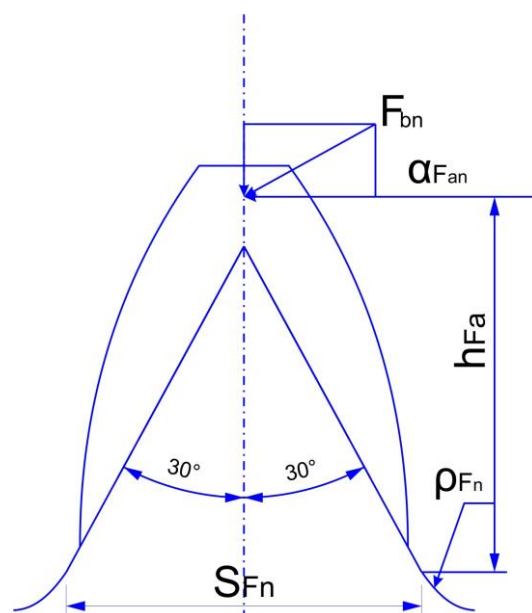


Fig.2 Forces in the tooth

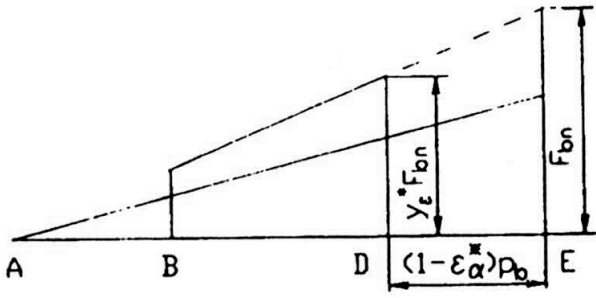


Fig.3 Distribution of the force F_{bn} in points A, B, D and E

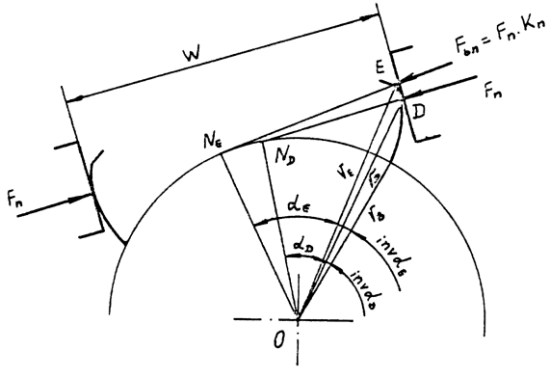


Fig.4 Loading of the teeth

These parameters were measured using an instrument microscope manufactured by Zeiss, Germany. The coefficient Y_{Fs} calculated in this way and the theoretical coefficient reported by the graphs in [1] differs within +15%, which is explained by errors in the measurements. The bending stress is determined by the dependence (1) provided that the force F_{bn} acts on the tooth tip as shown in Fig.3. In the experimental setting, the force acts on the common normal - at point D in Fig.4. This requires the load reported by experimental research to be brought down to a computing one, i.e. when the force F_{bn} acts at point E. To measure the difference in bending moments from the force applied at point D and at point E, a conditional coefficient Y_{ϵ}^* is introduced. By analogy with the adopted methodology, this coefficient it is determined by:

$$Y_{\epsilon}^* = \frac{1}{\epsilon_{\alpha}^*}$$

where ϵ_{α}^* is a conditional coefficient of overlap, which corresponds to a particular arc of the main pitch. This factor is determined by the scheme shown in Fig.5, where the following abbreviations are used:

- r_b - radius of the base circle;
- α_E, α_D - profile angles of the respective points;
- Q_E, Q_D - polar angles of the involute at the respective points;
- α - profile angle of the basic rack tooth profile.

$$N_E N_D = \frac{(\alpha_E + Q_E) - (\alpha_D + Q_D)}{r_b} = \frac{\epsilon_{\alpha} - 1}{P_b}$$

$$P_b = \pi \cdot m \cdot \cos \alpha = 2\pi \cdot \frac{r_b}{Z}$$

$$\epsilon_{\alpha}^* = \frac{2\pi \cdot [(\alpha_E + Q_E) - (\alpha_D + Q_D)]}{Z} + 1$$

If we add Y_{ϵ}^* to formula (1), the final formula for calculating the static bending strength of the teeth of the gears is:

$$\sigma_{Fs} = Y_{Fs} \cdot Y_{\epsilon}^* \cdot \left(\frac{F_{bn} \cdot \cos \alpha}{m_n \cdot b_w} \right) = K \cdot F_{bn}$$

where:

K - constant determined for each group of tested gears;

F_{bn} - measured force by the dynamometer.

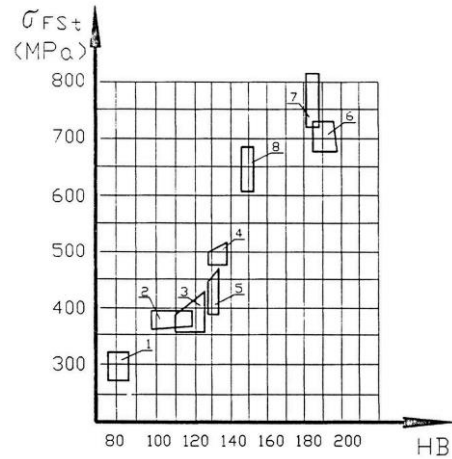


Fig.5 Influence of the hardness of MCG to their strength (The number of the groups are according to Table 1)

3. EXPERIMENT RESULTS AND DISCUSSION

The experiment results are given in Fig.2. Looking at the figure the following conclusions can be made:

- a) Gear-tooth-bending ultimate strength σ_{Fs} is a function of the hardness of the tooth surface and it increases with hardness.
- b) Alterations in technological processes make essential changes in gear-tooth-bending ultimate strength. For instance:
 - if the technological pressure for mixture ИКМ-I-40 increases with 60%, σ_{Fs} increases with approximately 18% (groups 3 and 4 in Fig.2);
 - if the sintering temperature for the same mixture is reduced to 20%, σ_{Fs} reduces with 10% (groups 4 and 5 in Fig.2);
- c) Gear-tooth-bending ultimate strength significantly changes in function of the size of the gears in the same module and the same technological parameters (groups 2-3 and 6-7 in Fig.2);
- d) Considerable dispersion in σ_{Fs} can be observed not only in the gear groups but also in the gears and gear teeth in each group.

The methodologies of BDS 17108-89 [3] and ISO 6336 [8] can be used for permissible bending stress calculations. In comparison with metal gears, the only difference is in determination of the tip factor Y_{Fs} . The author's research shows that formulae and graphics for given in [7,8] are appropriate for calculating stresses of MCG. However, the real value of bending stress can be obtained if the minimum safety factor σ_{Fstmin} is increased.

As a result of these experiments and according to the international standards we suggest calculating the permissible bending stress PM-Gear-Tooth using the following formula from [8]:

$$\sigma_{FPmax} = \frac{\sigma_{FSt}}{S_{FStmin}}$$

Because of the big dispersion of accuracy and strength of MCG (Fig.2) the authors suggest the minimum safety factor to be bigger than 2,2 ($S_{FStmin} > 2,2$). For MCG produced from those mixtures related to ones examined (see Table 1), gear-tooth-bending ultimate strength can be obtained from Fig.2.

4. CONCLUSION

The results of the experimental studies have shown that the static teeth bending strength of the above-mentioned MCG is between 1,5 and 2 times less than that of gears made from gray iron and about 3-5 times lower than that of steel gears. This makes it imperative to recommend that the use of such MCG to be utilized in lighter loaded gears.

The significant scattering of the strength of the gears requires experimentally testing of each group of MCG made from a given material and specific technology used. The results obtained can be used in the development of a methodology for improving the load capacity of MCG based on the standards BDS 17108-89 [3] and ISO 6336 [8].

The credibility of the results of these experiments allows them to be used for composite gears (POM, PA6, UHMWPE, CNTs).

REFERENCES

- [1] DATTA, B. (2014) *Powder Metallurgy. An Advanced Technique of Processing Engineering Materials*. 2ed, PHI Learning.
- [2] WHITE D. (2002) State of the North American Powder Metallurgy Industry. *Advances in Powder Metallurgy and Particulate Materials*, part 8, Princeton, pp. 1-12.

- [3] BDS 17108-89. Predavki zybni tzilindrichni evolventi s vynshno zatzeptyvane. Jakostno izchislyavane na zybite. (in Bulgarian)
- [4] DIMCHEV, G. (1990): „*Ekspiermentalno izsledvane na tovaronosimostta na metalokeramichni zybni kolela*“, in Proceedings of "Novi materiyali i tehnologii v prahovata metalurgiya". Sofia, 13-15 X 1990. p.51. (in Bulgarian)
- [5] KUZMIN I., RAZJIKOV S. (1987): „*Melkomodulnii tzilindricheskie zybchati peredachi*“, Mashinostroene, Moscow. (in Russian)
- [6] BS 436. Part 3: 1986. Method of calculation < contact and root bending stress limitation for metallic, involute gears; British Standards Institution. London. 1987.
- [7] Design of parallel axis straight spur and helical non-metallic gears – choice of material and load capacity. Engineering Sciences Data Unit. Item 68001. September 1997
- [8] ISO 6336. Calculation of load capacity of spur and helical gears.
- [9] WALSON D., SHI Y. (1989): “*A comparison of ratings for plastic gears*”, Proc. Int. Mech. Eng. C. 203, N 1. 31-38.

CORRESPONDANCE



Lubomir DIMITROV, Prof., PhD, Department of Machine Elements and Non-metal Constructions; Faculty of Mechanical Engineering, Technical University of Sofia, Bulgaria, E-mail address: lubomir_dimitrov@tu-sofia.bg



Georgi DIMCHEV, Prof., PhD, Department of Machine Elements and Non-metal Constructions; Faculty of Mechanical Engineering, Technical University of Sofia, Bulgaria, E-mail address: gnd@tu-sofia.bg



Pancho TOMOV, assist. Prof., PhD, Department of Automation of Discrete Manufacturing; Faculty of Mechanical Engineering, Technical University of Sofia, Bulgaria, E-mail address pkt@tu-sofia.bg

Kiril NIKOLOV, MEng, PhD student, Department of Machine Elements and Non-metal Constructions; Faculty of Mechanical Engineering, Technical University of Sofia, Bulgaria, E-mail address: knikolov90@tu-sofia.bg

OPTIMAL PROFILES OF CYLINDRICAL ROLLERS OF ROLLING BEARINGS

Lucian TUDOSE
 Cristina TUDOSE
 Constantin URSACHE

Abstract: Obtaining an optimal profile for rollers is of paramount importance in rolling bearing design. Such a profile, under most conditions of loading, should yield lower stresses and provide longer bearing life. But, unfortunately, it is impossible to find a universal optimal profile for a certain cylindrical roller whatever is the actual radial force that loads the roller. In this paper a complex procedure to find the optimal profiles of the cylindrical rollers of a rolling bearing (appropriate to specific loading ranges) is presented. The purpose is defined as an approximative-optimization problem and solved by means of a evolutionary algorithm which manipulates the objective function by means of the Kriging regression method.

Key words: Cylindrical roller bearings, Roller optimal profile, Evolutionary Algorithms

1. INTRODUCTION

The life of any rolling bearing is strongly related to the stress state developed at the contact surface between the rollers and raceways, as well as within the material of mating parts. Unfortunately, an analytical relationship between the geometry of the mating surfaces and the contact pressure exists only for a limited number of ideal shapes (Hertz's theory). For other shapes of the contact surfaces, a lot of efforts were done to achieve an appropriate algorithm to obtain the pressure distribution along the contact area. In this paper, for this purpose, the conjugate gradient method (CGM) coupled with discrete convolution fast Fourier transform (DC-FFT) it was used [4], [7], [9].

Regarding the roller bearings, when a roller of finite length is pressed against a certain ring raceway (wider than the roller length) the constant pressure distribution along the roller is altered, and the end pressure tends to be significantly higher than that in the center of contact (Fig.1). This phenomenon of stress concentration is referred to as "edge loading" or "edge effect". This undesired condition is further aggravated if the rollers are misaligned for any reason: bearing mounting errors, thermal distortion of a bearing housing, elastic bending of the shaft under external loads, etc.

To counteract this condition, cylindrical rollers (and/or the raceways) should be axially "profiled", to thereby make the stress distribution as uniform as possible, without edge peaks. It was Lundberg [6] who suggested for the first time such kind of profile. He found, that a profile expressed with a mathematically logarithmic curve may form, between two aligned cylinders in contact:

- an axially uniform and
- elliptical transversely stress distribution, and
- a rectangular contact area.

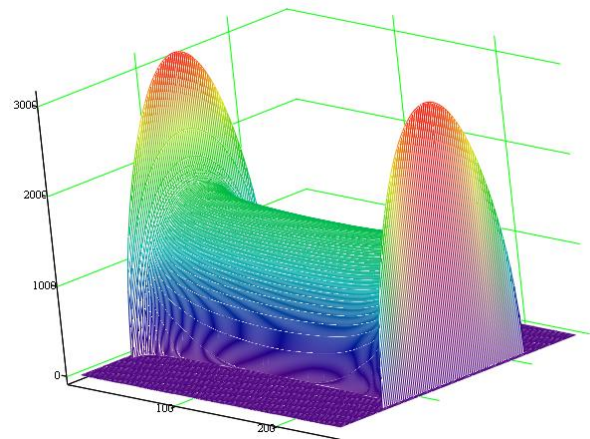


Fig.1: Pressure distribution along a roller without profile

Note that ISO/TS 16281: 2008(E) standard [11] provides an equation of the logarithmic profile for cylindrical rollers which is essentially identical to the one proposed by Lundberg:

$$f_L(y) = -0.00035D_{we} \ln \left[1 - \left(\frac{2y}{L_w} \right)^2 \right] \quad (1)$$

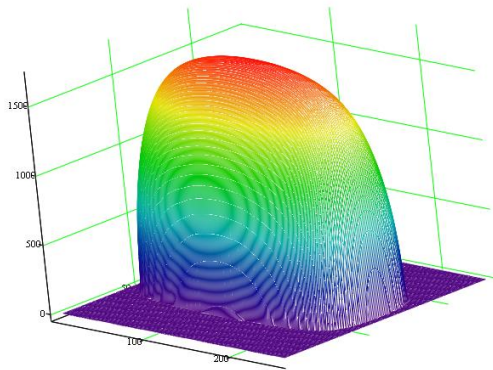
where:

- $f_L(y)$ – drop (mm) of the profile at the abscissa y (mm);
- D_{we} – roller diameter (mm);
- L_w – roller length (mm).

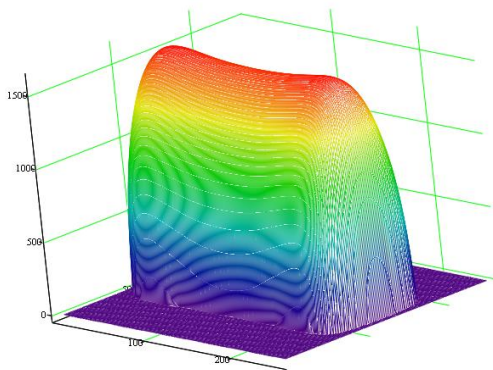
However, Lundberg's logarithmic profile has a major drawback: the roller radius reduction (crown drop) is theoretically infinite at the roller ends. Lundberg himself proposed an approximation to avoid this issue, but the fact that a roller has chamfers at the ends seems to solve the

problem. In fact, the point where the roller profile meets the chamfer profile is a “sharp point” and, even if the resulting curve is continuous in this point, this is an important stress concentration point.

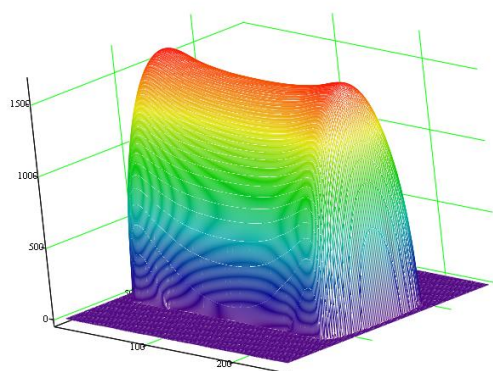
During the time, many researchers modified the Lundberg’s profile to satisfy different requirements. Johns and Gohar [3] revised the basic logarithmic function presented by Lundberg, but the crowning profile based on their equation inevitably yields edge loading when the rollers are tilted. Later, Lösche [5] brought important improvements, but his work was mostly dedicated to taper roller logarithmic profiles and it was mentioned here only for historical reasons.



a) $e = 2$



b) $e = 7$



c) $e = 12$

Fig.2: Pressure distribution along log-profiled rollers

Fujiwara et al. [2] provided a logarithmic crowning equation by introducing three design parameters into Johns and Gohar’s formula to improve the flexibility of the profile design. That was convenient for engineering applications and offered a new design approach that prevents edge loading due to misalignment. As the authors claimed these three parameters could be optimized by applying a mathematical technique according to the operating conditions of the bearing.

On the other hand, the manufacturing of a logarithmic profile requests an expensive technology and for this reason simplified profiles were introduced. Today, there are plenty of crowning cross-section profiles including: linear profile with one crowning radius, circular crowning with large radius, ZB type roller with linear profile and two crowning radii at the end, B-TAN (3 crowning radii) and CIR (2 crowning radii), and so on. The author of this paper proposed also a simplified profile, called 2ZB [8].

Coming back to the known logarithmic profiles it must be noticed that there are several attempts to improve the carrying capacity of the contact, mainly by:

- minimization of the maximum of the contact pressure;
- maximization of rigid body displacement;
- maximization of torque or contact resultant force between the bodies;
- minimization of frictional power loss.

In this context, this research intends to draw attention to another aspect. The way in which the basic curve was obtained suggests clearly that a “logarithm” function must be involved. However, there were used a lot of simplifications and approximations, and eliminating them, probably, an analytical general equation cannot be developed. In Fig. 2 the same cylindrical roller, pressed against the same inner raceway, with the same radial load is presented. The difference consists in the axial profile: in Fig. 2 a) the profile is given by eq. (1), and in Fig. 2 b) and 2 c) the exponent of the term $(2y/L_w)$ was turned to 7 and 12, respectively (instead of 2). It is very clear that the real 3D distribution of the pressure along the contact area between the roller and raceway changes significantly, and eq. (1) does not seem to be the best solution. Values of the exponent higher than 2 could provide a better (constant) distribution of the pressure. Obviously, natural questions arise: what about the constant in front of the logarithm? Can it modify significantly the pressure distribution? And finally: which is the best combination? The aim of this paper is to answer to these questions.

In what follows, let any roller crowning profile be called “log-profile” if it is expressed logarithmically.

2. ROLLER OPTIMAL PROFILES

It was mentioned from the beginning the fact that it is impossible to find a universal optimal profile for a certain cylindrical roller since this optimum is close connected to the level of the radial force that loads the roller. The levels of the considered loads were determined according to some imposed values of the Hertzian pressure (when the so called “edge effect” does not appear).

2.1. Equation of roller optimal profile

In our approach, we considered the optimal profile of a cylindrical roller (Fig. 3) having the following form:

$$f(y) = K \ln \left[1 - \left(\frac{2y}{L_w} \right)^e \right] \quad (2)$$

where:

K – constant;

e – exponent lying in the range 2 ... 12.

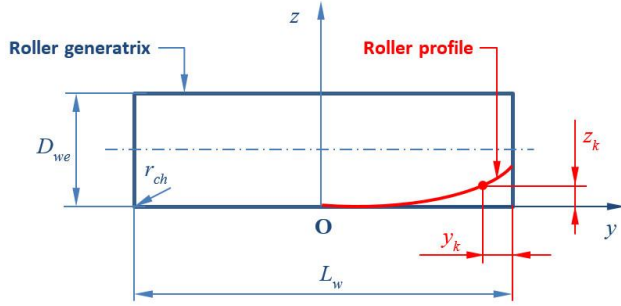


Fig.3: Parameters of the optimal profile

From technological point of view, it is better to connect the constant K to a certain point (y_k, z_k) belonging to the roller profile. This specific point further will be used in the control of the machined profile. Therefore, the constant K becomes:

$$K = \frac{z_k \cdot 10^{-3}}{\ln \left[1 - \left(\frac{L_w - 2y_k}{L_w} \right)^e \right]} \quad (3)$$

where:

y_k – distance from the lateral side of the roller where the profile drop will be measured (mm);

z_k – value of the profile drop at the measuring distance y_k (μm).

In this way, for an accepted value of y_k , the equation of the profile is governed by only two parameters: the exponent e and the drop z_k , that must be set so that a certain purpose is achieved.

Note that, according to ISO 16281: 2008(E), the logarithmic profile equation has $e = 2$ and the drop can be calculated as:

$$z_{k_L} = -0.35 D_{we} \ln \left[1 - \left(\frac{L_w - 2y_k}{L_w} \right)^2 \right] \quad (4)$$

2.2. Procedure for obtaining optimal profile

The considered procedure used in finding the parameters of the optimal profile equation of the cylindrical roller is the following:

1. Consider a certain value of the maximum Hertzian pressure, σ_H .
2. Calculate, using Eq. (5), the normal force necessary to load the roller in order to obtain, from the classical

Hertz's theory, the same value of the maximum contact pressure.

$$Q = (L_w - 2r_{ch}) \cdot \frac{\pi^2 \sigma_H^2}{E_{red} \cdot \Sigma \rho} \quad (5)$$

where:

Q – normal force necessary that load the roller (N);

E_{red} – reduced modulus of elasticity (MPa):

$$E_{red} = \frac{\pi}{\frac{1 - \nu_r^2}{E_r} + \frac{1 - \nu_{rw}^2}{E_{rw}}} \quad (6)$$

E_r – Young's modulus of elasticity of the roller material (MPa);

ν_r – Poisson's ratio of the roller material;

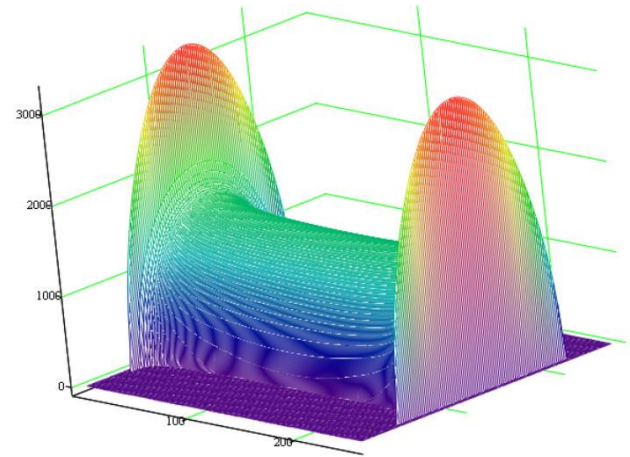
E_{rw} – Young's modulus of elasticity of the inner ring material (MPa);

ν_{rw} – Poisson's ratio of the inner ring material;

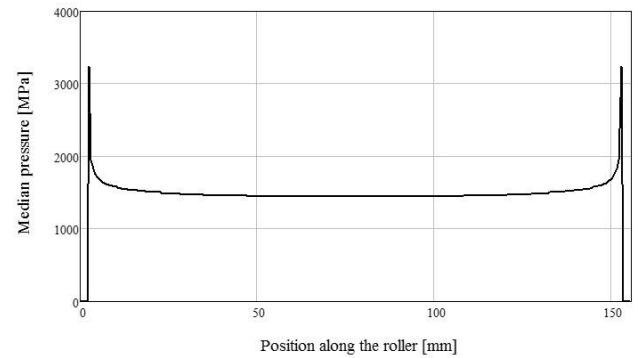
$\Sigma \rho$ – curvature sum (1/mm):

$$\Sigma \rho = \frac{2}{D_{we}} + \frac{2}{F_w} \quad (7)$$

F_w – inner ring raceway diameter (mm).



a) 3D pressure distribution



b) Maximum pressure in axial section

Fig.4: Grid cell real pressure distribution in the axial section of the real 3D pressure distribution (example)

3. For this value of the load find e and z_k so that the value of the standard deviation (SD) of the grid cell pressures values (in the axial section of the real 3D pressure distribution), is minimum. To accomplish this objective, the following sequences should be performed:
 - 3.1. Consider several values for the exponent e and the drop z_k ;
 - 3.2. For every combination $e \times z_k$ consider the roller manufactured with the resulting profile and find the real distribution of the contact pressure between this roller and inner ring raceway using a grid (for the contact area) as large as possible;
 - 3.3. Calculate the standard deviation of the values of pressures of the cells along the axial section through the roller (see, for example, Fig.4, where the roller without profile was loaded with a normal force that create a maximum theoretical pressure of 1500 MPa);
 - 3.4. Construct the “map” of coordinates $e \times z_k$ having as values the obtained standard deviations;
 - 3.5. Using Kriging regression method [1] and an optimization software based on Evolutionary Algorithms (in fact we used a relatively new cuckoo search optimization algorithm [11]) find the values of the drop z_k and exponent e for which the standard deviation reaches its minimum.

In the following sub-section the above procedure is exemplified on a specific bearing case.

3. CASE STUDY

For this study, the four-row cylindrical roller bearing 4CRB 334633 F2CIIHB4ZBA (Fig. 5), produced by RKB Group (Switzerland), was chosen. The choice is interesting because the bearing has long rollers, difficult to be optimized (from the profile point of view). The main dimensions of the cylindrical rollers and of the linear raceway of the inner ring are given in Table 1. The roller (index r) and inner ring (index rw) material properties are given in Table 2.

Table 1: Roller and inner ring raceway main dimensions

Dimension	Symbol	Value	UM
Length	L_w	156	mm
Diameter	D_{we}	80	mm
Chamfer radius	r_{ch}	2.5	mm
Distance from the side of the roller to the section where the profile is measured	y_k	4.6	mm
Inner ring raceway diameter	F_w	940	mm

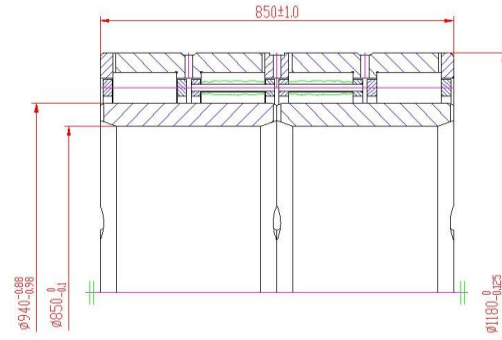


Fig.5: Assembly drawing of the four-row cylindrical roller bearing 4CRB 334633 F2CIIHB4ZBA

For the construction of the $e \times z_k \times SD$ maps, 25 values of the Hertzian pressure (in the range 1000 ... 3000 MPa), 11 values for the exponent e (in the range 2 ... 12), and 20 values of the drop z_k (in the range 5 ... 100 μm , with a step of 5 μm) were used. For each map using Kriging interpolation to estimate the value of SD in any point and running an Evolutionary Algorithm software the optimal values for $e \times z_k$ were found. The results are given in Table 2 and Fig. 6. Note that for this roller the ISO logarithmic profile must have a drop of about 61 μm at 4.6 mm from the side end of the roller (eq. (4) was used).

Table 2: Roller main dimensions

Parameter	Symbol	Value	UM
Young's modulus of elasticity	E_r, E_{rw}	208000	MPa
Poisson's ratio	ν_r, ν_{rw}	0.3	-

First observation that can be made is that only for very high contact pressures the value of the exponent is 2 (as ISO recommends). Contrary, for the most contact pressure values of the optimal points the exponent is 7. The shape of two optimal profiles, called here Profile A (optimized for an estimated Hertzian pressure of about 2500 MPa) and Profile B (optimized for an estimated Hertzian pressure of about 1500 MPa), respectively, found during the optimization are presented in Fig. 7.

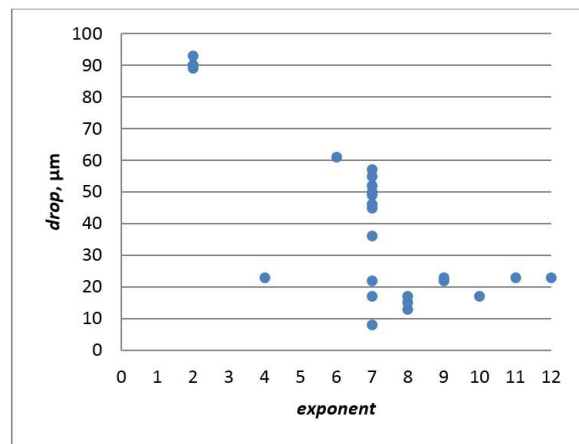


Fig.6: Scatter of $e \times z_k$ optimal points

Table 3: Parameters of the optimal profile (for different values of the considered maximum Hertzian pressure),

Estimated Hertzian pressure σ_H [MPa]	Exponent e	Drop z_k [μm]
1000	7	8
1250	8	13
1300	8	15
1350	7	17
1400	8	17
1450	10	17
1500	7	22
1550	9	22
1600	4	23
1650	9	23
1700	11	23
1750	12	23
2000	7	36
2250	7	45
2300	7	46
2350	7	49
2400	7	50
2450	7	52
2500	7	55
2550	7	57
2600	6	61
2650	2	93
2700	2	89
2750	2	90
3000	2	90

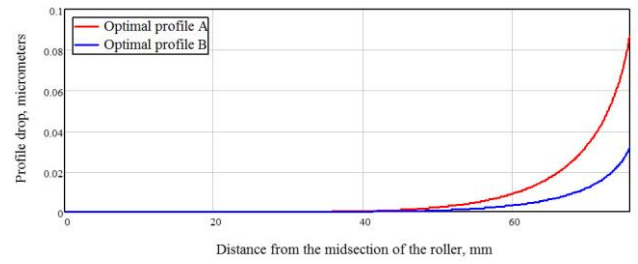
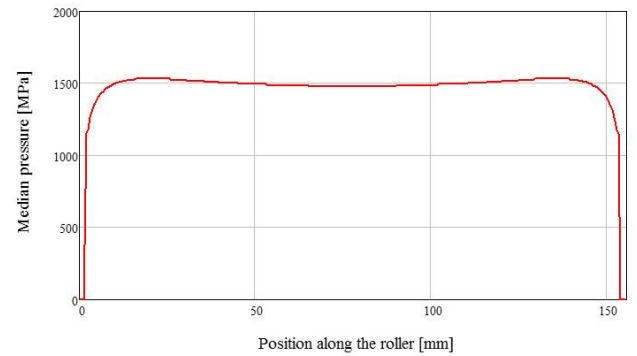
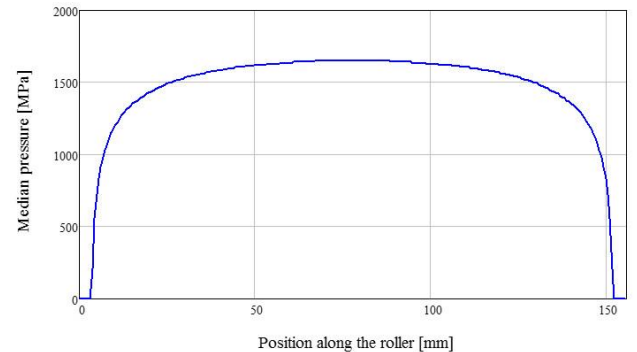


Fig.7: Optimal profiles A (optimized for about 2500 MPa) and B (optimized for about 1500 MPa)

It is now clear that for reasons of simplification of roller manufacturing it is a good idea to adopt the value $e = 7$ as standard and through optimization (much simpler now) to find the optimal drop.



a) Optimized profile (profile B)

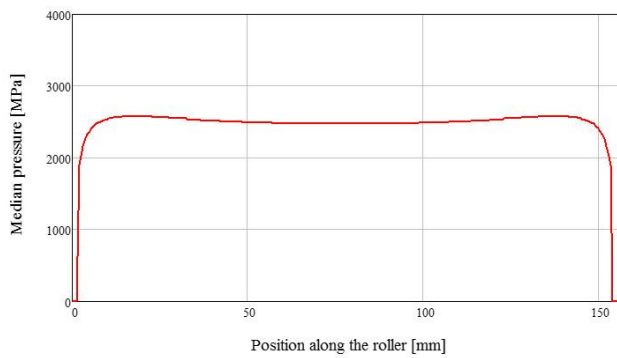


b) ISO profile

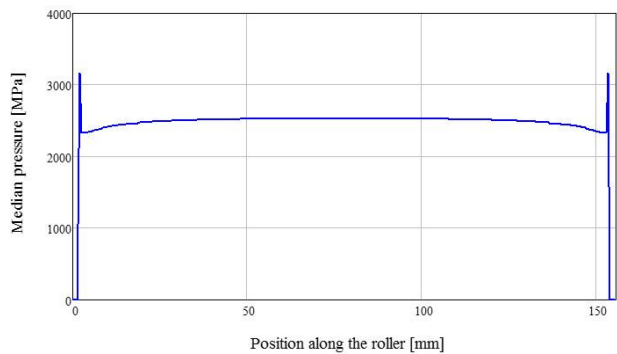
Fig.8: Comparison between the maximum pressure distribution (expected Hertzian pressure of 1500 MPa)

In Fig. 8 and Fig. 9 comparisons between the optimal profiles obtained through the depicted procedure and the Lundberg's (ISO) profile, for expected Hertzian pressure of 1500 MPa and 2500 MPa, respectively, are presented. The advantages of the optimal profiles A and B, respectively, are more than evident.

Profiles A and B, respectively, presented above, were selected by purpose, because within the RKB Group a decision was made. For general purposes the optimal profiles will be established according to two expected pressures: 1500 MPa and 2500 MPa, respectively. For special cases the optimal profile will be obtained considering the actual level of bearing loading.



a) Optimized profile (profile A)



b) ISO profile

Fig.9: Comparison between the maximum pressure distribution (expected Hertzian pressure of 2500 MPa)

4. CONCLUSIONS

Lundberg's (or ISO) logarithmic curve is not always the best profile for cylindrical rollers. Better solutions of log-profiles can be obtained through the approximative-optimization procedure described above. In addition, almost always is possible to group the obtained optimal solutions in two categories of profiles, fact that will ease significantly the bearing manufacturing.

5. ACKNOWLEDGMENTS

The authors would like to thank the RKB Group, the Swiss bearing manufacturer, for the permission to publish these results and the RKB staff for their great interest and support during the development of this project.

REFERENCES

[1] van BEERS, W. C. M., and KLRIJNEN, J. P. C. (2004) *Kriging interpolation in simulation: A survey*, Proceedings of the 36th Conference on Winter Simulation WSC '04, Washington, DC, USA, pp. 113–121

[2] FUJIWARA, H., KOBAYASHI, T., KAWASE, and T., YAMAUCHI K. (2010) *Optimized Logarithmic Roller Crowning Design of Cylindrical Roller Bearings and Its Experimental Demonstration*, Tribology Transactions, Vol. 53, No 6, pp. 909-916

[3] JOHNS, P. M., and GOHAR, R. (1981) *Roller bearings under radial and eccentric loads*, Tribology International, Vol. 14, pp. 131-136

[4] LIU, S., WANG, Q., and LIU, G. (2000) *A Versatile Method of Discrete Convolution and FFT (DC-FFT) for Contact Analyses*, Wear, Vol. 243, pp. 101-111

[5] LOSCHE, T. (1987), *Capacity increase due to modified line contact in cylindrical and tapered roller bearing*, Ball and Roller Bearings Engineering, Vol. 1, pp. 4-9

[6] LUNDBERG, G. (1961) *Elastic contact between two semi-infinite bodies*, Fur Schung auf dem Gebieto des Engenienswesens, Vol. 10, No 5, pp 165–174

[7] POLONSKY, I., and KEER, L.M. (1999) *A Numerical Method for Solving Rough Contact Problems Based on the Multi-Level Multi-Summation and Conjugate Gradient Techniques*, Wear, Vol. 231, pp. 206-219

[8] TUDOSE, L., URSACHE, C., TUDOSE, C., and RUSU, F. (2016) *Optimal 2ZB approximation of Optimal Profile of Rolling Bearings Cylindrical Rollers*, Proceedings of the 5th International Conference "Power Transmissions" BAPT2016, Ohrid, Macedonia, pp. 99-113

[9] WANG, Q. J., and CHUNG Y.-W. (Eds.) (2013) *Encyclopedia of Tribology*, Springer.

[10] ZHENG, H., and ZHOU, Y. (2012) *A novel cuckoo search optimization algorithm based on Gauss distribution*, Journal of Computer Information Systems, Vol. 8, No 10, pp. 4193-4200

[11] *** ISO/TS 16281: 2008(E) *Rolling bearings — Methods for calculating the modified reference rating life for universally loaded bearings*

CORRESPONDANCE



Lucian TUDOSE, Prof. D.Sc. Eng.
 Technical University of Cluj-Napoca
 Machine Building Faculty
 St. Memorandumului Nr. 28
 400114 Cluj-Napoca, Romania
Lucian.Tudose@omt.utcluj.ro



Cristina TUDOSE, D.Sc. Eng.
 RKB Group
 Technical Team Unit
 Via Primo Agosto 1
 6828 Balerna, Switzerland
Cristina.Tudose@rkbeurope.com



Constantin URSACHE, D.Sc. Eng.
 Technical University of Cluj-Napoca
 Machine Building Faculty
 St. Memorandumului Nr. 28
 400114 Cluj-Napoca, Romania
Constantin.Ursache@omt.utcluj.ro

COMPARABILITY OF EXPERIMENTAL AND ANALYTICAL STUDY OF THE EFFECT OF RADIAL LOAD AND ROTATION SPEED ON FRICTION COEFFICIENT OF RADIAL PLAIN BEARING UNDER LUBRICANT CONDITIONS USING RAIMONDI AND BOYD'S CHARTS

Amir ALSAMMARRAIE

Dragan MILČIĆ

Milan BANIĆ

Sulaiman E. AL-BASAQR

Sabah M. SALIH

Abstract: *The present paper investigates experimentally the effect of rotation speed of shaft and normal load on coefficient of friction of bearing inner surface made of tin-based alloys, sliding was carried out against stainless steel shaft, to do that, a test rig apparatus was designed and fabricated. Experiments were performed under lubricant condition, normal load 1000-4000 N and speed 1000-3000 rpm. Results show that friction coefficient increases with the increase of sliding speed and decreases with increase normal load for tin-based white material. The experimental results of friction coefficient were compared with the Raimondi and Boyd's charts, there is a difference in the value of the friction coefficient obtained analytically (using Raimondi and Boyd's charts) and experimentally, the error rate was up to 6-13 %.*

Key words: *coefficient of friction; rotation speed; radial load; viscosity; Raimondi and Boyd's charts*

1. INTRODUCTION

Under conditions of full-film lubrication, the thickness of the lubricant film is supposed to be large enough to separate the roughness peaks on the surfaces of journal and bushing completely. The coefficient of friction and wear rate of the bearing material is an important quality criterion that should be taken into account by designers and users.

The process of friction as the most common physical phenomenon causes a lot of negative effects in production systems and constructor attempts to reduce them to a minimum. One of the basic parameters which characterize the process of friction shaft and sliding sleeve is friction. The measurement of this ratio can be realized by using experimental methods. R. Đuriš [1] and Labašová [2] the experimental tests came up to the value of the coefficient of friction of the sliding pair of aluminum – Steel. The value of the coefficient of friction is sharply reduced from 0.8 to 0.1. Tests were conducted on Tribotestor M '89. Adjusted the input parameters: sliding speed and load.

So, Nada Bojić, Dragan Milčić [3], they carried out modification of journal bearing test rig under self-lubricant condition to conduct identification of the coefficient of friction and temperature as well as their correlations. The experimental research showed that the increase of the percentage of graphite coverage reduces friction. Tested bearings contain lead, tin, aluminum and copper. These elements are coated to steel foundation due

to their superior antifriction properties. These alloys are produced by casting and spray deposition method.

Many experiments under different static loads by using the purpose-built journal bearing test rig were performed. Hakan Adatepe, Aydın Bıyıklıoğlu [4], conducted a study on Performances of plain and micro-grooved engine journal bearings, they modified laboratory journal bearings test rig to use in determining frictional properties of the bearings, the results showed that the highest value of coefficient of friction as well as the frictional torque was obtained on the transversal micro-grooved journal bearings.

Application of the above method E. Labašová [5] and [6] in his two papers examined the coefficient of friction for the bronze (CuZn25Al6) with inserted graphite blades. The results showed that the friction coefficient decreases with increasing normal load. Some research coefficient of sliding friction in the joint were performed on the sleeve of brass, aluminum and polyamide for the chosen load. Eva Labašová E., R. Đuriš [7] noted that the greatest drop in the size of the coefficient of friction observed in isolators of aluminum. Reducing the friction coefficient is recorded about 82% of isolator made of brass and about 72% for the insulator made of polyamide. Production and overhaul of the drive bay and their assembly and disassembly is often cheaper than repair and assembling shafts. In such cases, bearings must have good technological properties of the bearing parts obtained by casting, low melting temperature, high accuracy, low shrinkage, high purity surface of the casting. Mičić [8] performed a comparison of individual elements important

for bearings that import from the influence of two different technologies making bearings - pouring, surfacing and soft sliding layers based on high strength (steel).

The purpose of this study is to investigate the coefficient of friction of tin-based bearing alloy used particularly in heavy industrial service conditions by Manufactures and develop a testing device, and Comparison of experimental results of friction coefficient with Raimondi and Boyd's charts which obtained numerically.

2. THEORETICAL FOUNDATION OF THE FRICTIONAL HYDRODYNAMICALLY

2.1. Reynolds equation

Journal bearings are termed full bearings when the bearing surface completely surrounds the journal. The mathematical theory of hydrodynamic lubrication is based upon Reynolds work [11]. Therefore, the differential equation governing the pressure in the lubricating film is called the Reynolds equation. The Reynolds equation for most machine design applications for a steadily running bearing is given by Eq. 1.

$$\frac{d}{dx} \left(\frac{h^3}{\mu} \cdot \frac{dp}{dx} \right) + \frac{d}{dz} \left(\frac{h^3}{\mu} \cdot \frac{dp}{dz} \right) = 6 \cdot U \cdot \frac{dh}{dx} \quad (1)$$

As a role, three form of circumferential boundary conditions are utilized in solving the Reynolds equation Raimondi A. A., Boyd J., A. [9]. In case of long bearings, here $B/D > 2$, the pressure does not change in the axial direction (z -axis), i.e. there is no side leakage. Therefore, neglecting the axial pressure flow term, Equation 1 reduces to Kalani A. et al [10]:

$$\frac{d}{dz} \left(\frac{h^3}{\mu} \cdot \frac{dp}{dz} \right) = 6 \cdot U \cdot \frac{dh}{dx} \quad (2)$$

which is the classical Reynolds equation for one-dimensional flow. This equation has been solved by Sommerfield and Gumbel.

In case of short bearings ($B/D < 1/4$), all of the entering lubricant is diverted to side leakage. Under this condition the axial pressure flow in the z -direction will dominate over the circumferential flow in the x - direction. Also 'h' is usually not a function of z (only a function of x). Therefore, the Reynolds equation may be written:

$$\frac{d}{dz} \left(\frac{dp}{dz} \right) = 6 \cdot U \cdot \frac{dh}{dx} \cdot \frac{\mu}{h^3} \quad (3)$$

This is known as Ocvirk equation. If the boundary conditions are taken as.

- at $z = 0$, $dp/dz=0$ (symmetry about $z = 0$),
- at $z = \pm B/2$, $p = 0$, then Equation 1 may be:

$$p = 3 \cdot U \cdot \frac{\mu}{h^3} \cdot \left(z^2 - \frac{U^2}{4} \right) \quad (4)$$

where are, p is film pressure[MPa], U is surface speed of the shaft[m/s], h is variable film thickness [m], x is coordinate in the direction of motion, z is coordinate in the axial direction, μ is absolute viscosity of the lubricant [Pa·s], B is axial bearing length [m]. For finite-length of bearings $B/D=1$ has been solved by this paper

2.2. 2.2 Petroff's equation for bearing friction

Regarding Fig.1, an expression for viscous friction drag torque is derived by considering the entire cylindrical oil film as the "liquid block" acted upon by force F .

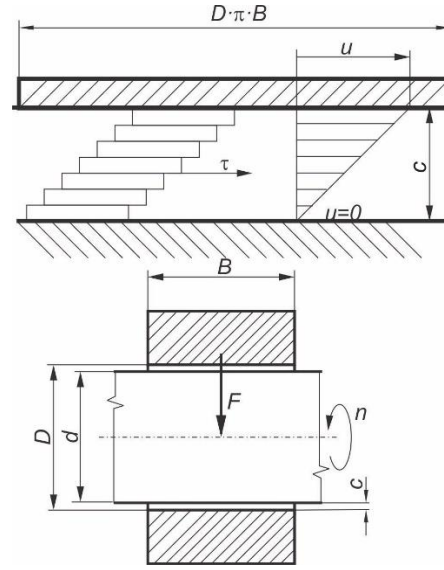


Fig. 1: Laminar flow of fluid in clearance space

From Newton's law of viscosity:

$$\tau = \eta \cdot \frac{du}{dy} \quad (5)$$

If the supposition is made that the rate of change of velocity or the rate of shear stress is a constant, then $du/dy = u/c$ and Eq. (5) becomes:

$$\tau = \eta \cdot \frac{u}{c}, \quad (6)$$

$$u = \omega \cdot r \quad (7)$$

As well:

$$\tau = \frac{F_t}{A} \quad (8)$$

From Eqs. (6), (7) and (8) the frictional force can be derived as:

$$\begin{aligned} F_t &= \tau \cdot A = \frac{\eta \cdot u}{c} \cdot 2 \cdot \pi \cdot r \cdot B \\ &= \frac{\eta \cdot \omega \cdot r}{c} \cdot 2 \cdot \pi \cdot r \cdot B \end{aligned} \quad (9)$$

The frictional torque is then:

$$M = F_t \cdot r = 2 \cdot \pi \cdot \frac{r^2 \cdot B}{c} \cdot \eta \cdot \omega \quad (10)$$

And bearing load (normal force) can be expressed in another way:

$$M = \mu \cdot F \cdot r \quad (11)$$

Then Eqs. (10) and (11) give the coefficient of friction and the bearing pressure, respectively, as:

$$\mu = 2 \cdot \pi \cdot \frac{r^2 \cdot B}{c} \cdot \frac{\eta \cdot \omega}{F} \quad (12)$$

$$p = \frac{F}{2 \cdot r \cdot B} \quad (13)$$

The coefficient of friction can also be presented as the Petroff's law:

$$\mu = 2 \cdot \pi \cdot \frac{r^2 \cdot B}{c} \cdot \frac{\eta \cdot \omega}{2 \cdot p \cdot r \cdot B} = \pi \cdot \frac{r}{c} \cdot \frac{\eta \cdot \omega}{p} \quad (14)$$

The first quantity in the bracket stands for bearing modulus and the second one stands for clearance ratio. Both are dimensionless parameters of the bearing.

3. EXPERIMENTAL STUDIES

3.1. Preparation of experimental materials and conditions

In this study, tin-based white metal bearing specimens were used as journal bearing and AISI 440C stainless steel was used as shaft. The chemical compositions of the journal and bearing materials used in the experiments were given in Table 1. Dimensions of bearing specimens were as follows: inner diameter is $40^{+0.05}$ mm, width is 40 mm, and outer diameter is 60mm. The bearing was drilled with hole (dimension $r = 1.5$ mm) in radial direction to ease lubrication oil flow into the contact zone. Circumferential

groove was also made onto the outer surface of bush (width 2 mm, depth 0.5 mm) to include that lubrication oil arrives into the radial hole. as well, the spiral groove is made onto inner surface of sample (width 2 mm, average depth of 30 μ m) to improve the lubrication process between the shaft and the bush as shown in Fig. 2. The specimens were tested by radial journal bearing test rig under lubricated condition.

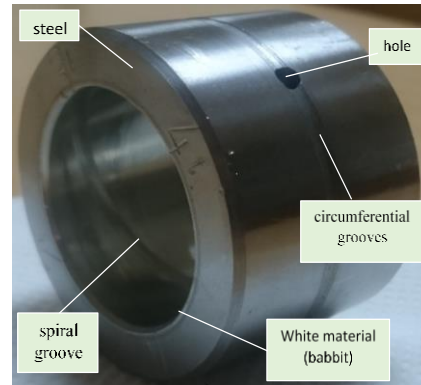


Fig.2: Tested plain journal bearing

Table 1: Chemical composition of AISI440C wt-(%), and bearings materials wt- (%)

TEGOTENAX (V480) (big sticks), in TKL NOVA TVORNICA KLIZNIH LEZAJEVA (SLIDING BEARING MANUFACTURING), CROATIA											
WM	Sn	Sb	Cu	As	Bi	Ni	Pb	Cd	Fe	Al	Zn
Actual Value %	88.7	7.6	3.7	0.009	0.002	0.003	0.008	0.010	0.009	0.000	0.002
The alloy is free of lead and free of cadmium in compliance with RoHS Regulation (EU-Directive 2002/95/EC)											
AISI 440C	C	Si	Mn	Ni	Cr	Mo	P	S			
	1.2	1	1	1	18	0.75	0.04	0.03			
Mechanical Property Requirements For Material in the Annealed Condition to 1) AS2837 - 1986 440C and 2) ASTM A276-98b 440C											

The tribological parameter were measured under lubricated conditions of (1000, 2000, 3000, 4000) N loads, (1000, 2000, 3000) rpm equals to (2.09, 4.2, 3.6) m/s and every 5 h for change coefficient friction, the lubrication was achieved by using ISO VG32 oil.

3.2. Radial journal bearing test rig

Bearings materials in journal bearings are generally selected from materials, which have lower wear strength than the shaft material, that way dropping the wearing of the shaft safely. Therefore, journal bearing wear test apparatus are designed to examine the wearing of bearing materials. In Fig. 3. Shows the test rig which was modified specifically for this research to use in determining tribological properties of the bearings [3]. Therefore, it is possible to investigate different bearing and shaft materials and the effects of heat treatments on these materials. This test rig is divided into three main systems: Hydraulic Loading System, Rotation System, Lubrication system of the bush as shown in Fig. 3.

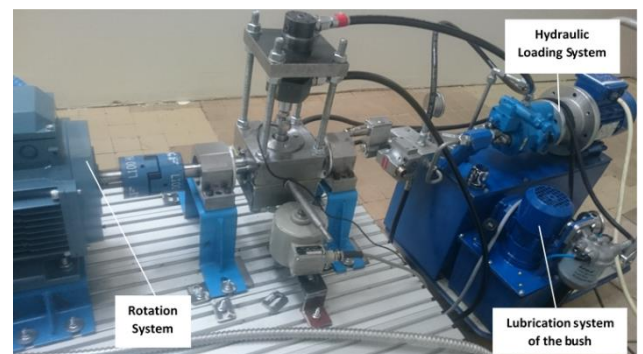


Fig.3: View of hydrodynamic journal bearing test rig

Hydraulic Loading System includes rotating electrical machines (REM) type CEM, IEC (0.75KW, 380V, 1420-1745 rpm, 50Hz), which is mounted on the hydraulic tank 20l and connected into high-pressure hydraulic flexible tubes which feed hydraulic into the hydraulic cylinder. The hydraulic cylinder is in contact with radial force sensor (U9c/10kN) which is located below it. The testing was done with the oil type ISO VG32. The Rotation System is consists of an asynchronous induction motor (AIM) (ABB, 400V, 3Ph, 50Hz, 3KW, 2860 rpm), which is attached by a flexible coupling to a shaft. The

shaft is supported by two roller bearings and the test bearing is mounted between these two bearings as shown as Fig. 3. Lubrication system of the bush contains electric lubrication pump (ELP) AMGP-03C, 05C Series (1450rpm, 500W, 220V, 50Hz) which was mounted on the hydraulic tank (10l). The lubricant is supplied by the ELP to the housing bearing through two flexible tubes which are threaded up the housing through an assembly steel tube. E540 - Wireless / Point laser was used for shaft alignment. The same type of oil, ISO VG32, was used in the testing.

3.3. Test Specimen and Procedure

load and friction coefficient as a function of time in the touch of two real bodies is associated by Coulomb equations:

$$F_f(t) = \mu(t) \cdot F_N(t) \quad (15)$$

As a function of time the moment of friction was calculated as the result of the normal force of the sleeve (using reaction force transducer) and the distance on lever between the center of the bush and contact point of the force transducer.

$$M_f(t) = F_s(t) \cdot l_{ac} = F_f(t) \cdot r, \quad (16)$$

as shown in Fig. 4. From Eqs.15 and 16

$$\mu(t) = \frac{M_f(t)}{r \cdot F_N(t)} = \frac{F_s(t) \cdot l_{ac}}{r \cdot F_N(t)}, \quad (17)$$

where M_f is Frictional moment [Nm], F_s is Reactional force sensor [N], l_{ab} leg distance of lever [m]. The temperature change and the values of the radial force on the bush were calculated by LabVIEW program which is installed into the computer. The data was transmitted to the recorder and this enabled monitoring and recording of the signals. The data about coefficient friction, radial load and sensor force were applied for 1/20 s, temperature of lubricating oil and load for 5 s. The most common solution is to begging operate the bearing with no apparent pressure at the test rig's maximum speed as in [10]. This pattern of operation causes the shaft to converge as near to zero eccentricity as possible and ideally provides a measurement of the location at which the shaft and the bearing centers identify. Tests were performed for 5 hours' duration regarding coefficient of friction test.

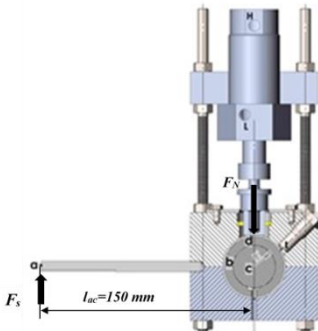


Fig.4.: Scheme of the frictional force measurement system for journal bearing determine the coefficient of friction

4. RESULTS AND DISCUSSION

4.1. Change coefficient of friction with radial load obtained experimentally

Typical curves of variations in friction coefficient with test duration (5 hour) for different average normal loads 1000, 2000, 3000 and 4000 N and different sliding speeds 1000, 2000 and 3000 rpm are shown in Fig. 5.

Friction coefficient was specific as a function of radial and friction force as in Eq. 14. It has been observed that the coefficient of friction decreases extremely when increasing the radial load of journal bearing for all average impact radial load and each sliding speed, the highest friction coefficients 0.083 occurred in average radial load 1000 N and 3000 rpm sliding speed, whereas the lowest friction coefficients 0.021 occurred in highest average radial load i.e. 4000N and rotate shaft speed 1000 rpm. Change coefficient of friction values take the form of converging curve toward increasing the radial load at increasing rotate shaft speeds 1000, 2000 and 3000 rpm as shown in Fig. 5.

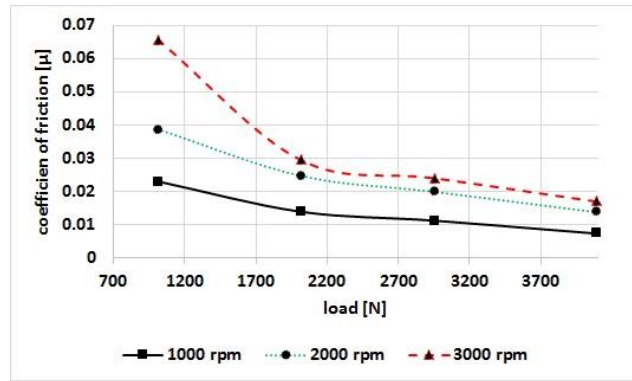


Fig.5: Change coefficient of friction with radial load experimentally

Fig. 6 illustrates the relationship between friction coefficient and rotation speeds of shaft, friction coefficient increases slightly with the increase of rotating shaft speed for same average radial load. The friction between rotate shaft, bush and lubricant causes temperature growth of lubricant which results decrease in the shear stress of lubricant that lead to lowering viscosity of lubricant thus decrease coefficient of friction as shown in Eq. 14.

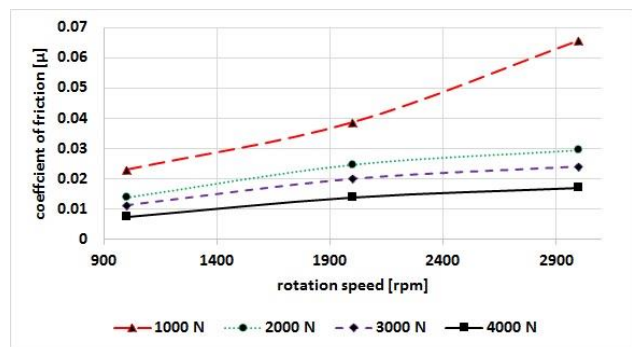


Fig.6: Change coefficient of friction with sliding speed experimentally

Therefore, the coefficient of friction at highest load and lowest rotation speed of shaft have been lowest values, Vice versa as regards lowest radial load and highest sliding speed coefficient of friction have highest values. In Fig. 6, it was noted increases slightly coefficient of friction with increasing sliding speed of shaft which may be attributable to larger shear layers lubricant thus increases friction drag i.e. coefficient of friction.

4.2. Change coefficient of friction with radial load obtained analytically using Raimondi and Boyd's charts

Raimondi and Boyd have obtained computerized solutions for Reynolds Eq. 1 and reduced them to chart form which provide accurate solutions for bearings of all proportions. All these charts are plots of non-dimensional bearing parameters as functions of the bearing characteristic number, or the Sommerfield variable S which itself is a dimensionless parameter. A comparison of experimental and analytical results can be made by investing Raimondi and Boyd's charts. In the following example, a typical solution is to find the analytical values of the coefficient of friction using Raimondi and Boyd's charts.

Example:

- Oil used has dynamic viscosity $\eta=28.37$ mPas at 40°C ,
- radial load $F_N=1000$ N.
- apparent pressure $(p = F_N / B \cdot d) = 0.625$ MPa,
- $n=1000$ rpm $= 1000/60 = 16.7$ rps
- radius shaft $(r = d/2) = 20$ mm,
- clearance $(c = (D-d)/2) = 0.0125$ mm,

$$S = \left(\frac{r}{c}\right)^2 \cdot \left(\frac{\eta \cdot n}{p}\right) = \left(\frac{20}{0.0125}\right)^2 \cdot \left(\frac{28.37 \cdot 10^{-3} \cdot 16.7}{0.625 \cdot 10^6}\right) = 1.97, \quad (16)$$

Use Chart for coefficient of friction variable as shown in Fig. 7 to determined coefficient of friction.

$(r/c) \cdot f = 35$, from chat

$$\mu_{an} = f = 35 \cdot (0.0125/20) = 0.021875$$

Examples of solutions to other cases have been included in the Appendix. Table 3 has included experimental and analytical results for comparative purposes.

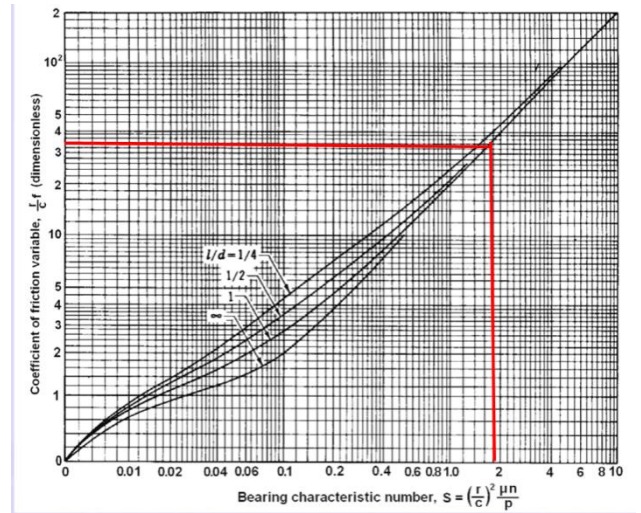


Fig.7: Chart for coefficient of friction variable

4.3. Comparison of experimental and analytical (Raimondi and Boyd's charts) results of friction coefficient values

Table 2 shows that there is a difference in the value of the friction coefficient obtained analytically and experimentally, this is something expected and the reasons can be identified, including the following:

- a) The inaccuracy of Raimondi and Boyds' charts available.
- b) Raimondi and Boyds' charts do not take into account changes in the coefficient of friction in the unsteady state.
- c) The values of the coefficient of friction obtained from the practical experiments, which are included in the table 3, are in fact the values of the average coefficient of friction for a large amount of data, obtained for five hours.
- d) The force sensors used in the experiments have specific accuracy associated with their technical specifications. This also affects the accuracy of experimental results data.

Nevertheless, the data compared to the experimental results with analytical results were acceptable, error did not exceed the 13% in cases fare worse.

Table 2: Experimental and analytical results of friction coefficient values

Rotation speed [rpm]	Rotation speed [rps]	Load [N]	Apparent pressure [MPa]	Sommerfield variable S	μ_{ex}	μ_{an}	$E_r = (\mu_{an} - \mu_{ex}) / (\mu_{an} \cdot 100)$ [%]
1000	16.7	1000	0.625	1.97	0.0259	0.023875	8.4816754
		2000	1.25	0.96	0.0168	0.01525	10.1639344
		3000	1.875	0.64	0.0118	0.0103125	14.4242424
		4000	2.5	0.485	0.0048	0.00562	14.5907473
2000	33.3	1000	0.625	3.8	0.0459	0.047	2.3404255
		2000	1.25	1.92	0.0278	0.024	15.8333333
		3000	1.875	1.3	0.0178	0.017	4.7058824
		4000	2.5	0.93	0.0148	0.01325	11.6981132
3000	50	1000	0.625	4.7	0.0713	0.063	13.1746032
		2000	1.25	2.9	0.0307	0.03475	11.6546763
		3000	1.875	1.8	0.0217	0.02	8.5
		4000	2.5	1.3	0.0192	0.018	6.6666667

5. CONCLUSION

Tribological properties in lubrication conditions of radial load and sliding speed change can vary over many orders of magnitude. In this study, comparability of experimental and analytical study of the effect normal load and sliding speed on friction coefficient of Radial Plain Bearing under lubricant conditions using Raimondi and Boyd's charts were carried out, the following conclusions can be drawn:

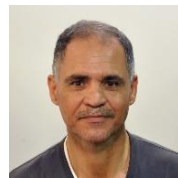
1. Friction coefficient with respect to radial load is lowest in highest radial load for each shaft rotational speed, it decreases extremely when increasing the radial load of journal bearing.
2. Change coefficient of friction values take the form of converging curve toward increasing the radial load at increasing rotate shaft speeds.
3. Coefficient of friction increases slightly with an increase of shaft rotational speed for same average radial load.
4. The coefficient of friction at highest load and lowest rotation speed of shaft have been lowest values, Vice versa as regards lowest radial load and highest sliding speed coefficient of friction have highest values.
5. The equivalent values of the friction coefficient were calculated using Raimondi and Boyd's charts, according to the certain radial load and rotation speed used into experimental test.
6. A comparison of the experimental and analytical results has shown an error of 2-13% for all cases, due to experimental conditions and Raimondi and Boyd's charts.

REFERENCES

- [1] Labašová E., Ďuriš R. (2014) *Measurement of Tribological Parameters*, Advanced Materials Research, Volumes 875 - 877, pp 496-499.
- [2] Labašová E. (2014) *The Dependence of the Friction Coefficient on the Size and Course of Sliding Speed*, Applied Mechanics and Materials, (Volume 693), pp 305-310.
- [3] Bojić, N. Milčić, D., Banić, M., Milčić, M. (2015) *Effect of coverage of graphite on self-lubricating plain bearings*, 14th International Conference on Tribology SERBIATRIB '15, p. 309-313.
- [4] Adatepe, H., Bıyıklıoğlu, A., Sofuoğlu, H. (2011) *An experimental investigation on frictional behavior of statically loaded micro-grooved journal bearing*, Elsevier Tribology International Volume 44, Issue 12, pp. 1942-1948.
- [5] Labašová E. (2014) *The Dependence of the Friction Coefficient on the Size and Course of Sliding Speed*, Applied Mechanics and Materials, Volume 693, pp 305-310.
- [6] Labašová E. (2014) *The Size of the Friction Coefficient Depending on the Size and Course of Normal Load*, Applied Mechanics and Materials, Vol 474, pp.303-308.

- [7] Labašová E., Ďuriš R. (2014) *Measurement of Tribological Parameters*, Advanced Materials Research, Vols. 875 - 877, pp 496-499.
- [8] Mičić, M., Đorđević, M., Đajić, G. (2002) *Svojstva ležaja proizvedenih nalivanjem i navarivanjem kliznog sloja belog metala*, MJoM METALURGIJA - JOURNAL OF METALLURGY, pp 225-236.
- [9] Raimondi A.A., Boyd J., A. (1958) *Solution for the Finite Journal Bearing and its Application to analysis and Design: I'*, ASLE Transactions, 1(1), V.1958, pp 175 – 193.
- [10] Kalani A., Soni S., Jani R. (2015) *Expert knowledge-base system for Computer Aided Design of Full Hydrodynamic Journal Bearing*", IJMET, Volume 6, Issue 8, pp. 46-58.
- [11] Harnoy, A. (2003) *Bearing Design in Machinery: Engineering Tribology and Lubrication*, Marcel Dekker, Inc. New York.

CORRESPONDANCE



Amir Al-SAMMARRAIE, lucture sc Eng.
University of Tiktít, Mechanical
Engineering Faculty, Department of
Mechanics,
Bagdad, IRAQ,
amircraft2014@gmail.com.



Dragan MILČIĆ, Prof. D.Sc. Eng.
University of Niš
Faculty of Mechanical Engineering
Aleksandra Medvedeva 14
18000 Niš, Serbia
dragan.milcic@masfak.ni.ac.rs



Milan BANIĆ, Prof. D.Sc. Eng.
University of Niš
Faculty of Mechanical Engineering
Aleksandra Medvedeva 14
18000 Niš, Serbia
banicmilan@hotmail.com



Sulaiman E. AL-BASAQR, lucture sc
Eng.
University of Tiktít, Mechanical
Engineering Faculty, Department of
Mechanics,
Tikrit, IRAQ,
sulimaninad@gmail.com



Sabah M. SALIH, lucture sc Eng.
University of Tiktít, Mechanical
Engineering Faculty, Department of
Mechanics,
Tikrit, IRAQ,
sabahmehdi_69@yahoo.com.

RELIABILITY OF NECESSARY PRESSURE FROM THE REQUIRED LIQUID QUANTITY FOR LUBRICATION OF ENGINE CYLINDER IN THE PERIOD OF ONE WORKING CYCLE FOR UNSTEADY FLUID FLOW

Dečan IVANOVIĆ

Abstract: The paper presents the nonstationary flow of oil for lubrication between the piston and the cylinder tube wall, through a pipe of known length and a known diameter. For a known amount of lubricating oil and for the known duration of the working and return stroke of the piston in the cylinder, the pressure is determined above the oil level in the oil trap, which allows such a flow. A mathematical model for the problem described is set. For known cylinder design values, if a known amount of oil for lubrication and pressure above the oil level in the oil trap, through the embodied integral the best length of the pipe from the oil trap to the cylinder can be found, or its most optimal diameter.

Key words: Nonstationary flow of oil for lubrication, piston movement in the cylinder, oil pressure, energy losses

1. INTRODUCTION

In designing internal combustion engines, it is very important to accurately determine the required amount of lubricating oil, i.e. its volume $V_{ulja} (m^3)$, which is fed through a thin tube of length $l(m)$ and diameter $d(m)$ into the cylinder, to create a thin layer of lubricating oil between the piston and the cylinder wall itself, all in a cycle that lasts $t_0(s)$, where $t_0/2(s)$ is the lifetime of the piston stroke from the upper to the lower dead point, as well as the duration of the return of the piston from the bottom to the upper dead point. For known constructional values such as cylinder and piston diameter $D(m)$, the piston stroke speed in a cylinder $v_k(m/s)$, the duration of one cycle $t_0(s)$, it is necessary to determine the pressure $p^*(Pa)$ that must be above the level of the lubricating oil placed in the oil trap, from which the oil will flow unsteady through the tube of length $l(m)$ and diameter $d(m)$, to the cylinder, providing the required amount of oil $V_{ulja} (m^3)$, therefore it is necessary to find a functional dependence between p^* and V_{ulja} in the presence of a number of constructive quantities, i.e. $p^* = p^*(V_{ulja}.const.)$

2. MATHEMATICAL MODEL OF A MISCELLANEOUS PROBLEM

In the upper dead center of the piston, the gas pressure is p_1 , and the gas is located in the volume $V_1 = \frac{D^2 \pi}{4} l_1$,

Fig. 1, where l_1 is the piston distance from the cylinder head. When designing the engine, for the upper dead point of the piston, the pressure p_1 and volume V_1 are of a known sizes. The opening hole on the cylinder through the lubricating oil enters in the cylinder is removed from the front of the cylinder for l_3 . At the moment when the piston is in section 3, and that is the moment when the piston releases the hole on the cylinder of the d diameter, the gas pressure is p_3 and the gas is in volume

$V_3 = \frac{D^2 \pi}{4} l_3$. During the working walk, the piston goes

further, from section 3 to the intersection 2, i.e. to their lower dead spot. When the piston comes into section 2, the gas pressure is p_2 , and it occupies the volume

$V_2 = \frac{D^2 \pi}{4} l_2$. During the working stroke, the piston

crosses the path from section 1 and over crosses section 3 to the section 2, and this takes time $\frac{t_0}{2}$, while in the

return stroke that also takes place $\frac{t_0}{2}$, the piston moves from the cross section 2 and over cross section 3 to the cross section 1, which means that the total cycle time is lasting t_0 . For example, when the engine rotates at 3000 rpm, which means 50 rps, it follows that the total cycle (working and return stroke in the cylinder) lasts 0.02 seconds in duration.

It is clear, then, that for such a very short time, and during the working stroke of the piston, $\frac{t_0}{2} = 0,01\text{sec}$, the change in the gas temperature is almost negligible, so it can be stated that $T_1 = T_2 = T_3$, where $T_1(K)$ is the gas temperature in volume V_1 , $T_2(K)$ is gas temperature in volume V_2 and $T_3(K)$ is gas temperature in volume V_3 . It states that $T_1 = T_2 = T_3$, during the working stroke, the piston gas propagation process from volume V_1 over volume V_3 to the volume V_2 , is typically isothermal, and isothermal is also the compression of the gas for return of the piston from volume V_2 , over volume V_3 up to volume V_1 . The equation of gas in volume V_1 is $\frac{p_1}{\rho_1} = RT_1$, where the gas constant is $R(m^2s^{-2}K^{-1} = J/kgK)$ and $\rho_1(kg/m^3)$ is density of the gas in that volume that amounts $\rho_1 = \frac{m}{V_1}$, whereby the mass of that gas $m(kg)$ is located in that volume V_1 so that it can be placed $\frac{p_1V_1}{m} = RT_1$ either $p_1V_1 = mRT_1$. The gas equation of the state in volume V_2 is $\frac{p_2}{\rho_2} = RT_2$, where the gas density $\rho_2(kg/m^3)$ is in that volume which is the amount $\rho_2 = \frac{m}{V_2}$, whereby the $m(kg)$ is mass of that gas which fills the volume V_2 , and is the same as the mass that filled the volume V_1 , so that it can be placed $\frac{p_2V_2}{m} = RT_2$, either $p_2V_2 = mRT_2$. Similarly, for the equation of the gas state in volume V_3 , it can be stated that $\frac{p_3}{\rho_3} = RT_3$ where $\rho_3(kg/m^3)$ is gas density in that volume which is the amount of $\rho_3 = \frac{m}{V_3}$, whereby the mass of that gas $m(kg)$ fills volume V_3 which is the same as the mass

that is filled the volume V_1 as well as the volume V_3 , so it can be put that is $\frac{p_3V_3}{m} = RT_3$, or $p_3V_3 = mRT_3$.

How are all three temperatures the same, $T_1 = T_2 = T_3$, i.e. these three terms have the same right sides, so it can be stated that:

$$p_1V_1 = p_2V_2 = p_3V_3, \quad (1)$$

respectively:

$$p_2 = p_1 \frac{V_1}{V_2}; \quad p_3 = p_1 \frac{V_1}{V_3}. \quad (2)$$

The pressure of gas p_1 , as well as the volumes V_1 , V_2 and V_3 , is known as constructive quantities, and, from expression (2), one can see that pressures ratio is $p_1 > p_3 > p_2$.

At the moment when the piston arrives in section 3, the small hole on the cylinder is opening, which surface $\frac{d^2\pi}{4}$ becomes free, and through the hole the quantity of oil for lubrication is entered through the tube of length l and diameter d , where $v(m/s)$ is the fluid flow velocity which is the same, on the basis of the equation of continuity, along the entire tube. When the piston moves its operating stroke from section 3 to cross section 2 and in the return stroke from section 2 to cross section 3, the oil continuously expands from the pipe to the cylinder, with the oil pressure p_3 at the end of the pipe when the piston is in cross-section 1, and p_2 when piston is in the lower dead point or section 2. For a very short interval when the piston moves from section 1 to cross section 3 in its operating stroke, and from section 3 to section 1 in reverse, the opening hole $\frac{d^2\pi}{4}$ at the end of the pipe is closed and there is no fluid flow through the tube of length l and diameter d . Therefore, during the duration of the working and return stroke of the piston which is t_0 , the gas pressure in an arbitrary volume V of the cylinder, amounts p , and at the same time it is the pressure of the oil at the end of the pipe, i.e. at the entrance to the cylinder. When the piston is in section 3, this pressure is $p = p_3$, and when is in section 2 it is pressure $p = p_2$. At some point in time t , and it is in an interval $0 < t < t_0$, i.e. when a piston is found at an arbitrary cross-section, and let's say it is a cross-section t because it corresponds to that moment, the arbitrary volume of the cylinder V , in which the gas is located with pressure p , is: $V = V_3 + \frac{d^2\pi}{4}s_k$, where $s_k = v_k t$ is the length of the piston has exceeded with velocity v_k for arbitrary time interval t . The gas temperature in that volume V is T ,

and since the whole process of propagation and compression of gas in the cylinder is isothermal, it is possible to put on the basis of relation (1) and (2):

$$p(t) = p_1 \frac{V_1}{V} = p_1 \frac{V_1}{V_3 + \frac{D^2 \pi}{4} v_k t}. \quad (3)$$

It is obvious that the flow of oil for lubrication in the pipe length l and diameter d , Fig. 1, is non-stationary, because for the entire operating cycle that takes place t_0 , the oil pressure p at the exit from the

pipe surface $\frac{d^2 \pi}{4}$ is the function from the time t shown

by the relation (3). Therefore, if Bernoulli's equation from the Fluid Mechanics [1,2,3,4,5,6] is set for nonstationary fluid flow, for the level of oil in the oil trap located at a vertical distance H_0 from the axis of the cylinder above which pressure is p^* , and for the outlet of the pipe which surface is $\frac{d^2 \pi}{4}$, it receives:

$$\frac{p^*}{\rho g} + H_0 = \frac{p}{\rho g} + (1 + \xi + \xi_t) \frac{v^2}{2g} + \frac{1}{g} \int_0^l \frac{\partial v}{\partial t} dl, \quad (4)$$

where the coefficient of local energy loss ξ at the input in

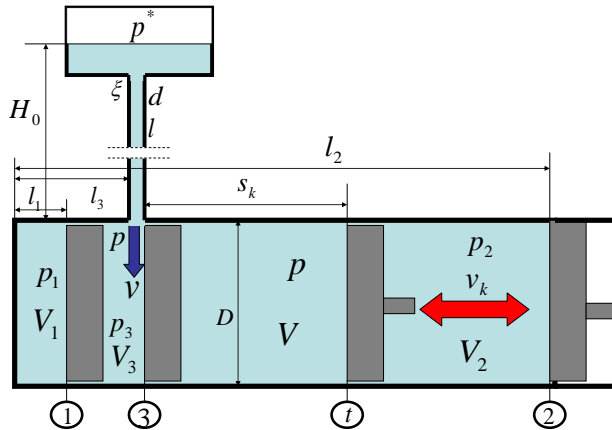


Fig. 1: Piston movement in the cylinder

pipe, and ξ_t the friction coefficient which, bearing in mind that the flow of oil in the pipe is laminar, is $\xi_t = \frac{64}{R_e}$. For this pipe R_e is Reynolds number and he is

$R_e = \frac{vd}{\nu}$. Here is ρ (kg/m^3) the density of the oil,

and ν (m^2/s) the coefficient of the kinematic viscosity of the oil. The partial derivative $\frac{\partial v}{\partial t}$ goes into the $\frac{dv}{dt}$

derivation, because in this case the flow velocity v , which is in principle a function of the longitudinal coordinate x ($0 < x < l$) and time t , is a function only from time t , since the entire length of the pipe in each cross-section

is the same. Similarly, this derivative $\frac{dv}{dt}$ is the same on

each elementary length dl of the pipe, and it goes in front of the integral in (4).

Having this in mind, the integral $\int_0^l \frac{\partial v}{\partial t} dl$ now reads

$$\int_0^l \frac{\partial v}{\partial t} dl = \int_0^l dl = l \frac{dv}{dt},$$

so that the equation (4) gets its appearance:

$$\frac{p^*}{\rho g} + H_0 = \frac{p}{\rho g} + (1 + \xi) \frac{v^2}{2g} + \xi_t \frac{l}{d} \frac{v^2}{2g} + \frac{l}{g} \frac{dv}{dt}. \quad (5)$$

When for ξ_t puts $\xi_t = \frac{64}{R_e} = \frac{64\nu}{vd}$, then a member

$$\xi_t \frac{l}{d} \frac{v^2}{2g}$$

in equation (5) goes to $\xi_t \frac{l}{d} \frac{v^2}{2g} = \frac{64\nu}{vd} \frac{l}{d} \frac{v^2}{2g}$

$\frac{v^2}{2g} = \frac{32\nu l}{gd^2} v = kv$, where is $k = \frac{32\nu l}{gd^2}$. By placing this

expression for $\xi_t \frac{l}{d} \frac{v^2}{2g} = kv$ and expression (3) for the

pressure p at the pipe outlet, in equation (5), we obtain:

$$\frac{dv}{dt} = \frac{p^*}{\rho l} + \frac{H_0 g}{l} - \frac{p_1}{\rho l} \frac{V_1}{V_3 + \frac{D^2 \pi}{4} v_k t} - (1 + \xi) \frac{v^2}{2l} - \frac{g}{l} kv, \quad (6)$$

which after the introduction:

$$a = -\frac{(1 + \xi)}{2l}; \quad b = -\frac{32\nu}{d^2}; \quad c = \frac{p^*}{\rho l} + \frac{H_0 g}{l};$$

$$e = -\frac{p_1 V_1}{\rho l}; \quad f = V_3;$$

$$h = \frac{D^2 \pi}{4} v_k; \quad j = c + \frac{e}{f + ht}, \quad (7)$$

reads:

$$\frac{dv}{dt} = av^2 + bv + j. \quad (8)$$

After the separation of the variable differential equation

(8), it follows: $dt = \frac{dv}{av^2 + bv + j}$ and after integration:

$$\int_0^t dt = \int_0^v \frac{dv}{av^2 + bv + j}. \quad (9)$$

The boundaries for the integral in the equation (9) are based on the fact that at the moment $t = 0$, the flow through the pipe has not yet begun, so the oil velocity is $v = 0$, because the small opening hole on the cylinder of

the surface $\frac{d^2\pi}{4}$ is closed and the piston is in section 3,

at some arbitrary time t within the limits $0 < t < \frac{t_0}{2}$,

the oil speed through the tube is v . The integral on the left side of the equation (9) is t , while the integral on the right-hand side is from the integral table, which reads:

$$\frac{1}{\sqrt{-\Delta}} \ln \left[\frac{2av+b-\sqrt{-\Delta}}{2av+b+\sqrt{-\Delta}} \right], \text{ so that the equation (9)}$$

now looks:

$$t = \frac{1}{\sqrt{-\Delta}} \ln \left[\frac{2av+b-\sqrt{-\Delta}}{2av+b+\sqrt{-\Delta}} \right], \quad (10)$$

where is:

$$\Delta = 4aj - b^2. \quad (11)$$

In order to exist the expression (10), it needs $-\Delta$ to be greater than zero, i.e. $-\Delta > 0$, which means $\Delta < 0$, so the expression (11) is:

$$\Delta = 4aj - b^2 < 0. \quad (12)$$

By placing the marks (7) in (12) we obtain:

$$\Delta = 4 \left[-\frac{(1+\xi)}{2l} \right] \left[\left(\frac{p^*}{\rho l} + \frac{H_0 g}{l} \right) + \frac{-\frac{p_1 V_1}{\rho l}}{V_3 + \frac{D^2 \pi}{4} v_k t} \right]$$

$$- \left(-\frac{32v}{d^2} \right)^2 < 0,$$

or inequality:

$$4 \left[\frac{(1+\xi)}{2l} \right] \left[\left(\frac{p^*}{\rho l} + \frac{H_0 g}{l} \right) + \frac{-\frac{p_1 V_1}{\rho l}}{V_3 + \frac{D^2 \pi}{4} v_k t} \right]$$

$$+ \left(-\frac{32v}{d^2} \right)^2 > 0,$$

which, after the introduction of tags:

$$a^* = \frac{2(1+\xi)p^*}{\rho l^2} + \frac{2(1+\xi)H_0}{l^2} + \left(\frac{32v}{d^2} \right)^2;$$

$$b^* = -4(1+\xi)p_1 V_1;$$

$$c^* = 2\rho l^2 V_3;$$

$$d^* = 2\rho l^2 \frac{D^2 \pi}{4} v_k, \quad (13)$$

reads:

$$a^* + \frac{b^*}{c^* + d^* t} > 0. \quad (14)$$

In the labels (13), it is seen that b^* , c^* and d^* are the constants for the adopted cylinder and the pipe, while the a^* is function of pressure p^* , i.e. $a^* = a^*(p^*)$, so for any found p^* , which will be determined in a further

proceeding, and for any arbitrary time t within the boundaries $0 < t < \frac{t_0}{2}$, the inequality (14) must be

satisfied. If betting (14) for $-\Delta$, it gives.

$$-\Delta = a^* + \frac{b^*}{c^* + d^* t}, \quad (15)$$

and after placing (15) in (10), the decision reads as follows:

$$t = \frac{1}{\sqrt{a^* + \frac{b^*}{c^* + d^* t}}} \ln \left[\frac{2av+b-\sqrt{a^* + \frac{b^*}{c^* + d^* t}}}{2av+b+\sqrt{a^* + \frac{b^*}{c^* + d^* t}}} \right], \quad (16)$$

from where it is obtained:

$$\ln \left[\frac{2av+b-\sqrt{a^* + \frac{b^*}{c^* + d^* t}}}{2av+b+\sqrt{a^* + \frac{b^*}{c^* + d^* t}}} \right] = \left(\sqrt{a^* + \frac{b^*}{c^* + d^* t}} t \right),$$

respectively:

$$\left[\frac{2av+b-\sqrt{a^* + \frac{b^*}{c^* + d^* t}}}{2av+b+\sqrt{a^* + \frac{b^*}{c^* + d^* t}}} \right] = \exp$$

$$\left[\left(\sqrt{a^* + \frac{b^*}{c^* + d^* t}} t \right) \right], \text{ which further provides:}$$

$$2av+b - \sqrt{a^* + \frac{b^*}{c^* + d^* t}} =$$

$$2av \cdot \exp \left[\left(\sqrt{a^* + \frac{b^*}{c^* + d^* t}} t \right) \right] +$$

$$+ b \cdot \exp \left[\left(\sqrt{a^* + \frac{b^*}{c^* + d^* t}} t \right) \right] + \left(\sqrt{a^* + \frac{b^*}{c^* + d^* t}} t \right)$$

$$\cdot \exp \left[\left(\sqrt{a^* + \frac{b^*}{c^* + d^* t}} t \right) \right],$$

so that the speed v , which is a function of time t ,

where is $0 < t < \frac{t_0}{2}$, i.e. $v = v(t)$, which will be

marked for the working cycle as $v_1 = v_1(t)$, is:

$$v_1(t) = \frac{\left(b + \sqrt{a^* + \frac{b^*}{c^* + d^* t}} \right) \exp \left(t \sqrt{a^* + \frac{b^*}{c^* + d^* t}} \right) + \sqrt{a^* + \frac{b^*}{c^* + d^* t}} - b}{2a \left[1 - \exp \left(t \sqrt{a^* + \frac{b^*}{c^* + d^* t}} \right) \right]}$$

. (17)

And for the return of the piston, from position 2 to position 3, the speed will be $v_2 = v_2(t)$ valid for the time interval t ($\frac{t_0}{2} < t < t_0$), and it is the same as $v_1 = v_1(t)$ shown with (17).

If for elemental time dt , through the outlet of the pipe, where cross surface is $\frac{d^2\pi}{4}$, with velocity $v_1(t)$, flow out elementary oil volume $dV_{ulja1} = v_1(t) \frac{d^2\pi}{4} dt$, then the volume of the oil entering the cylinder during the working stroke of the piston from position 3 to position 2, therefore for the time interval $0 < t < \frac{t_0}{2}$, will be:

$$V_{ulja1} = \int_0^{\frac{t_0}{2}} v_1(t) \frac{d^2\pi}{4} dt,$$

which, after putting expression (17), gives:

$$V_{ulja1} = \frac{d^2\pi}{4} \int_0^{\frac{t_0}{2}} \frac{\left(b + \sqrt{a^* + \frac{b^*}{c^* + d^*t}} \right) \exp\left(t \sqrt{a^* + \frac{b^*}{c^* + d^*t}} \right) + \sqrt{a^* + \frac{b^*}{c^* + d^*t}} - b}{2a \left[1 - \exp\left(t \sqrt{a^* + \frac{b^*}{c^* + d^*t}} \right) \right]} dt.$$

Also, for elemental time dt through the outlet of the pipe, where cross surface is $\frac{d^2\pi}{4}$, with velocity $v_2(t)$ flow out elementary oil volume $dV_{ulja2} = v_2(t) \frac{d^2\pi}{4} dt$, then the volume of the oil entering the cylinder during the return of the piston from position 2 to the position 3, therefore for the time interval $\frac{t_0}{2} < t < t_0$, is: $V_{ulja2} = \int_{\frac{t_0}{2}}^{t_0} v_2(t) \frac{d^2\pi}{4} dt$

which, after putting expression (17), gives:

$$V_{ulja2} = \frac{d^2\pi}{4} \int_{\frac{t_0}{2}}^{t_0} \frac{\left(b + \sqrt{a^* + \frac{b^*}{c^* + d^*t}} \right) \exp\left(t \sqrt{a^* + \frac{b^*}{c^* + d^*t}} \right) + \sqrt{a^* + \frac{b^*}{c^* + d^*t}} - b}{2a \left[1 - \exp\left(t \sqrt{a^* + \frac{b^*}{c^* + d^*t}} \right) \right]} dt.$$

It is clear that the total volume V_{ulja} of oil entering the cylinder during the working and return stroke of the piston, for the time interval $0 < t < t_0$, is:

is:

$$V_{ulja} = V_{ulja1} + V_{ulja2} = \frac{d^2\pi}{4} \int_0^{\frac{t_0}{2}} v_1(t) dt + \frac{d^2\pi}{4} \int_{\frac{t_0}{2}}^{t_0} v_2(t) dt$$

so after putting the expressions (18) and (19) into (20) we obtain:

$$V_{ulja} = \frac{d^2\pi}{2} \int_0^{\frac{t_0}{2}} \frac{\left(b + \sqrt{a^* + \frac{b^*}{c^* + d^*t}} \right) \exp\left(t \sqrt{a^* + \frac{b^*}{c^* + d^*t}} \right) + \sqrt{a^* + \frac{b^*}{c^* + d^*t}} - b}{2a \left[1 - \exp\left(t \sqrt{a^* + \frac{b^*}{c^* + d^*t}} \right) \right]} dt.$$

3. CONCLUSION

This integral (21) can only be numerically solved, and it can be seen that the amount of lubricating oil V_{ulja} (m^3) between the piston and the cylinder walls depends on the pressure p^* (Pa) that prevails above the level of the oil placed in the oil trap, i.e. $V_{ulja} = V_{ulja}(p^*)$. In the subintegral function $F = F(const_1; p^*)$ of integral (21), a some value of p^* is entered, so it is calculated for a time interval t_0 , and if it differs from the known value, V_{ulja} , same numerically procedure is repeated, it is understood under different values for pressure p^* until the left and right sides are not equal. If it is also known V_{ulja} and p^* , then over the integral (21) must be find the optimal length of the pipe $l(m)$ from the oil trap to the

cylinder, or its most optimal diameter $d(m)$. In this case, subintegral function of integral (21) is $F = F(const_2; l)$ if the optimal length of the pipe $l(m)$ is required, or $F = F(const_3; d)$ if its most optimal diameter $d(m)$ is required.

These three constants $const_1$, $const_2$ and $const_3$, are functions of known sizes, i.e.

$$const_1 = const_1(l, d, v_k, D, l_1, l_2, l_3, H_0, \nu, \rho);$$

$$const_2 = const_2(p^*, d, v_k, D, l_1, l_2, l_3, H_0, \nu, \rho);$$

$$const_3 = const_3(p^*, l, v_k, D, l_1, l_2, l_3, H_0, \nu, \rho).$$

REFERENCES

- [1] WHITE, F, (2008) *Fluid mechanics*, McGraw-Hill, 6th Ed., New York.
- [2] BATCHELOR, G, (2002) *An introduction to fluid Dynamics*, Cambridge University Press, 20th Ed., New York.
- [3] FOX, R, McDonald, A, (1978) *Introduction to Fluid Mechanics*, John Wiley and sons, New York
- [4] FOX, R, McDonald, A, (1978) *Introduction to Fluid Mechanics*, John Wiley and sons, New York
- [5] VUKOSLAVČEVIĆ, P, KARADŽIĆ, U, (2010) *Introduction to Fluid Mechanics*, Faculty of Mechanical Engineering, University of Montenegro, Podgorica.
- [6] IVANOVIĆ, D, (2012) *Applied Fluid Mechanics*, Faculty of Mechanical Engineering, University of Montenegro, Podgorica

CORRESPONDANCE



Dečan IVANOVIĆ, Prof. D.Sc. Eng.
University of Montenegro
Mechanical Engineering Faculty
Bul. Džordža Vašingtona bb
81000 Podgorica, Montenegro
decan@ac.me

THE COMPARE OF ANGLES OF REPOSE WITH DISCRETE ELEMENT METHOD AND MEASUREMENT

Tibor POÓS
Dániel HORVÁTH
Kornél TAMÁS

Abstract: In this study the angle of repose of hulled millet with different moisture content was investigated with measurement and discrete element method. The result of the simulation and measurement were compared. The aim of this study to define the unknown micromechanical parameter set of the discrete element model. In further studies the calibrated parameter set of the modelling of equipment could be used for the chosen granular material.

Key words: angle of repose, discrete element method, cohesion, moisture, hulled millet

1. INTRODUCTION

There are several technologies in the food and pharmaceutical industry which include mixing, drying and the transportation of granular materials.

The aim of this study is to compare angle of repose measurements on granular material processing equipment with simulations using the discrete element method. The angle of repose has a role in the design and maintenance of agricultural machines. These include equipment and vessels used in sowing, harvest, the transportation of material, drying and rationing. By determining the angle of repose we can describe the internal friction inside granular material. This is the preferred method to provide fast, cost-efficient approximation of the kinetic and thermodynamic processes in granular materials with sufficient accuracy. The material properties of the test material (hulled millet) and some simulation parameters were unknown, e.g. the cohesion forces and dimensionless numbers referring to the moisture value of the material. Hulled millet was chosen as a granular material for the purpose of this study because of being nearly homogeneous in the scale of the study and the fact that the geometry of the granules can be approximated by spheres made it a good choice as test material.

2. THE DISCRETE ELEMENT METHOD

Currently there are a number of discrete element method software available for research, e.g. EDEM [1], SAMADII [2], Yade [3], PFC3D [4].

2.1. The DEM simulation software

In this study, the Yade [5] open source discrete element method software was used, in which the simulation model was built in Python.

Several models are available to describe the rheological processes between granules in the program (e.g. friction, cohesive, capillary). During the simulation the software uses an explicit integral system with respect to time, which iterates between the movement and the force-displacement law, the cycle can be seen in Fig. 1.

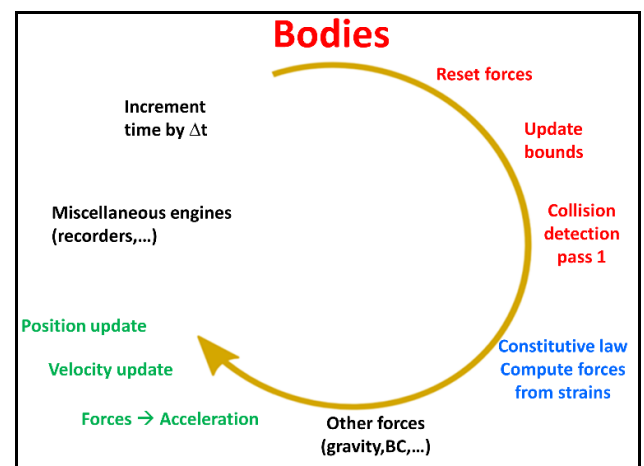


Fig.1: Calculation cycle in Yade discrete element software [5]

The first step in explicit time integral is to set the value of forces to default, then refresh the bonds. Afterwards the collisions are detected. The software then calculates the forces from displacements based on the engine settings. From these forces the acceleration is calculated, the velocity is refreshed, then these data (forces, displacements) are recorded. Finally, the time step is increased by Δt_i and the bodies on the program display are refreshed, then the cycle starts again. To provide the stability of the integral, an upper limit for Δt_i is calculated [6]:

$$\Delta t_{cr}^{(p)} = R_i \cdot \sqrt{\frac{\rho_i}{E_i}} \quad (1)$$

where:

$\Delta t_{cr}^{(p)}$ – critical time step (PWaveTimeStep) [s]

R_i – radius of particles [m]

ρ_i – particle density [kg/m³]

E_i – micromechanical Young modulus of particles [Pa]

The time step which was calculated is only an estimation, so it has to be validated.

2.2. The setup of the DEM simulation

The granular material used in this study was hulled millet, that can be seen in Fig.2., with a characteristic diameter of $d_p=1.7$ mm

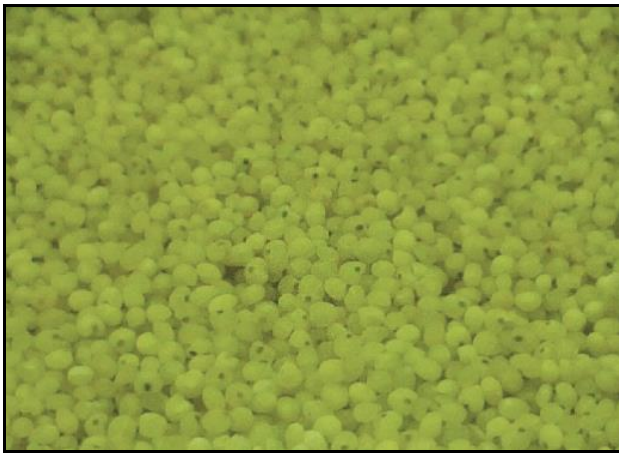


Fig.2: Hulled millet

The aim of the study is to determine the effect of moisture on the mechanical properties of the material. The shape of granules was approximated using spheres. Because the moisture content varied during the study, a cohesion engine was used in simulations, which takes adhesion into account, as this cohesion contact model can show the effect of different moisture contents. For cohesion contact models in DEM, the forces are calculated for each degree of freedom using stiffness coefficients [7]. The normal force can be described by the following equation:

$$F_n = k_n \cdot u_n \quad (2)$$

where:

F_n – normal force [N]

k_n – normal elastic stiffness [Pa]

u_n – normal displacement [m].

While macroscale stiffness is not related to the granule size, the normal stiffness is a function of the granule size:

$$k_n = 2E_c \cdot \frac{R_1 R_2}{R_1 + R_2}, \quad (3)$$

where:

E_c – macroscale stiffness [Pa]

R_1 – radius of an interacting particle [m]

R_2 – radius of the other interacting particle [m].

Shear and normal elastic stiffness can be scaled [7] using the following equation:

$$k_s = \alpha \cdot k_n \quad (4)$$

where:

k_s – shear elastic strength [Pa]

α – non-dimensional factor [1]

The DEM also calculates the maximal forces (5)-(6) and torques (7)-(8) in comparison with the normal and shear strengths [7]. If the tension exceeds the maximum strength during the simulation, the bond breaks, the connection ceases to exist. On certain settings a new a connection automatically forms on next contact. The maximal normal force is calculated as following in DEM model:

$$F_n \leq \sigma_n^l \cdot A \quad (5)$$

The maximal shear force:

$$\|F_s\| \leq F_n \cdot \tan \varphi_c + \sigma_s^l \cdot A \quad (6)$$

The bending moment:

$$M_b \leq \frac{\sigma_n^l \cdot I_b}{R_c} \quad (7)$$

A twisting moment:

$$M_t \leq \frac{\sigma_s^l \cdot I_t}{R_c} \quad (8)$$

where:

A – the reference surface area [m²]

F_s – shear force [N]

σ_n^l – tensile strength [Pa]

σ_s^l – shear strength [Pa]

φ_c – friction angle [°]

I_b – the reference bending moment of inertia [m⁴]

I_t – the reference polar moment of inertia [m⁴]

R_c – the reference radius of the contact [m]

In Table 1. the computer specifications used in the study and the maximal time requirements for simulations are shown.

Table 1. Computer specifications and time requirements of simulations

No	Processor Number	Processor base frequency	Memory	Max time
		[GHz]	[Gbyte]	[min]
1.	Intel® Core™ i7-4710HQ	2.5	8	52
2.	Intel® Core™ i5-6500	3.2	16	40

In Fig 3. the model of the measuring equipment built in Yade can be seen.

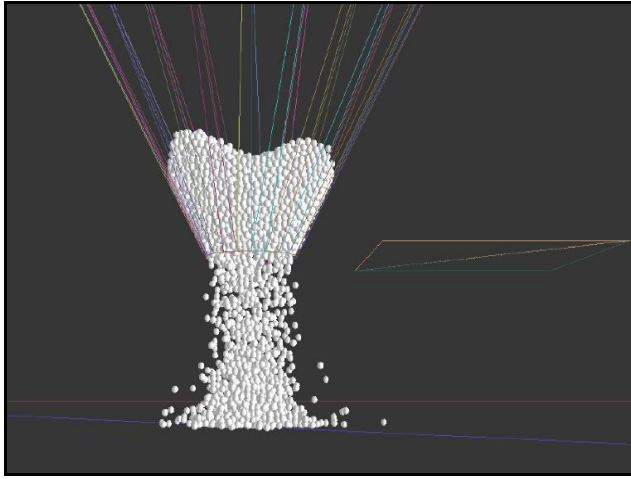


Fig. 3. The measuring equipment in Yade software

The model consists of a cylinder and two sides of a box in the z direction, which make up the upper and the lower surfaces. The first step in the simulation is the sedimentation of particles in the cylinder. When the unbalanced forced decreased to a sufficient value, cohesion was turned on with the setCohesionNow command. Then the outlet opened and the millet started flowing, while a harmonic engine was resonating the cylinder. After a number of iterations, the outlet closed because of the particles stuck on the surface of the cylinder, this way the simulation time decreased and the poured granule pile stabilized quicker. When the particles reached a sufficiently low velocity, the simulation stopped and the screen display was saved.

To further lower the simulation time requirement, the height of the cone outlet was decreased to 0.4 m, as in a 1:1 scale the simulation would have taken days with the specifications listed in Table 1.

2.3. The parameter sets of the simulation

Some of the unknown parameters have been previously determined by measurements. Friction angles have been determined for different moisture contents using direct shear box test [2]. Sieve analysis was used to determine the granule sizes and distribution, and granule density was calculated from porosity. The micromechanical Young modulus used in the DEM, and the shear and tensile strengths from the shear box test was based on previous simulation experience and literature [9-11]. According to previous shear box measurements [8], the increase in moisture content resulted in the decrease of cohesion forces and the friction angle. The parameters which have to be calculated are the dimensionless bending (etaRoll) and twisting (etaTwist) strengths, which were made equal and changed together during the simulation. [4]. These are marked as eta in the following pages. These settings can be seen in Table 2.

Table 2. Settings for the DEM system

No	x	d _p	ρ _p	Φ _p	E _p	ν _p	τ _{shear}	σ _{normal}
	$\frac{\text{kg H}_2\text{O} \cdot 100\%}{\text{kg wet product}}$	[mm]	$\frac{\text{kg}}{\text{m}^3}$	[°]	[MPa]	[1]	[kPa]	[kPa]
1.	12.5	1.7±0.1	1381	42.2	20	0.2	6.1	6
2.	14.5	1.7±0.1	1385	42.2	20	0.2	5.2	5
3.	19.4	1.7±0.1	1394	41.5	20	0.2	4.2	4
4.	21.9	1.7±0.1	1399	40.5	20	0.2	3.4	3
5.	24.7	1.7±0.1	1404	39.3	20	0.2	1.7	1.5
6.	29.8	1.7±0.1	1413	36.1	20	0.2	2.2	2

where:

x – moisture content based on the wet material $\frac{\text{kg H}_2\text{O} \cdot 100\%}{\text{kg wet product}}$

d_p – particle diameter [mm]

ρ_p – particle density $\frac{\text{kg}}{\text{m}^3}$

E_p – micromechanical Young modulus [MPa]

ν_p – particle Poisson's ratio [1]

Φ_p – particle friction angle [°]

τ_{shear} – the shear strength of the cohesion [kPa]

σ_{normal} – the tensile strength of the cohesion [kPa]

There are two ways in the software to simulate cohesion forces. The first, which is used in this study is to make cohesion connections once in a moment in time between the currently particles in contact (setCohesionNow). This way, no new connections are formed after a time step. The other way is the continuous making of cohesion connections with every new contact (setCohesionOnNewContacts). The global damping which was used to decrease particle acceleration was set to 0.4 for each run. The time step value was $1.42 \cdot 10^{-5}$ s, which is the double of the value from the PWaveTimeStep (1) equation. These parameter sets provided numerically stable particles.

The cylinder and surfaces used in the DEM model are based on the properties of steel, which can be seen in Table 3. Between the wall and the particles the Mohr-Coulomb plasticity [6] was used instead of the cohesion model. In this case, only the equation (2)-(4) shown in section 2.2 were used by the DEM software.

Table 3. Material properties of the measuring equipments in the DEM software

No	ρ _E	E _E	ν _E	Φ _E
	$\frac{\text{kg}}{\text{m}^3}$	[GPa]	[1]	[°]
1.	7750	200	0.3	40.1

where:

ρ_E – equipment density $\frac{\text{kg}}{\text{m}^3}$

E_E – equipment Young modulus [GPa]

ν_E – equipment Poisson's ratio [1]

Φ_E – equipment friction angle [°]

3. MEASUREMENT AND METHOD

The calculation of angle of repose is regulated by a standard. Different measuring equipment are recommended for

different granule sizes. The equipment for 1.7 mm hulled millet is described below.

3.1. Measurement equipment

The measurement equipment was built according to MSZ EN standard [12] both the sematic and real device can be seen in Fig. 4.

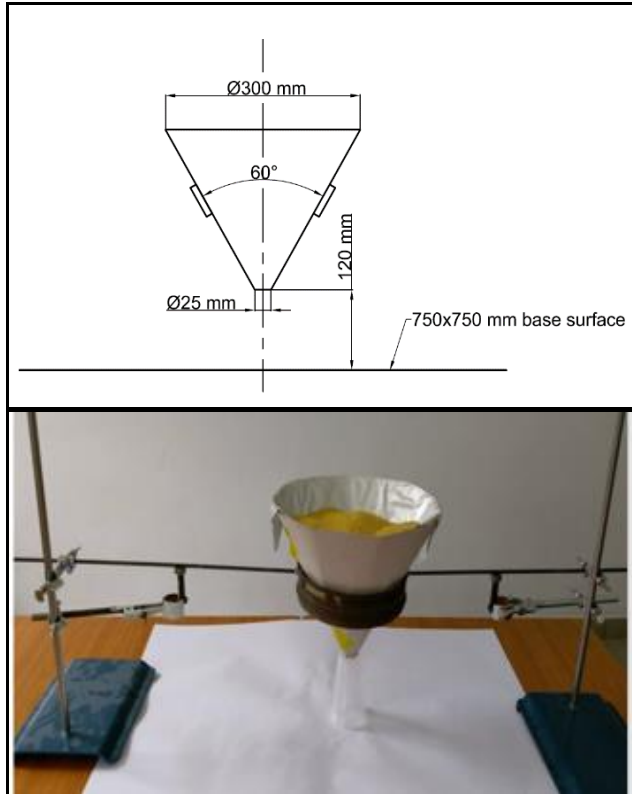


Fig. 4. In the upper part the size according to standard is shown, the real device is seen at the bottom

The cone is made of 1.5 mm thick cardboard, the inside is covered with aluminum foil, because of the moisture content of the material. It was fixed to the post using a retaining ring.

3.2. Measurements

First the hulled millet was put in a wind sorter to provide nearly constant granule size. Then water is added and the mixture is stirred every hour for 24 hours before measuring (the moisture content were 12,5%, 14,5%, 19,4%, 21,9%, 24,7%, 29,8%). The measurement was done according to the standard [12]. The millet had to be poured out of the cone until the pile of millet reached the outlet.

3.3. Method

There are two ways to evaluate the collected data. One is shown in Fig 5. where the tangent line is drawn on the pile of granules, and the angle of repose can be determined from the enclosed angle between the tangent and a horizontal line. This was used in the simulation evaluation because the calculating capacity only allowed the use of less granules, and the height of the outlet was lowered.

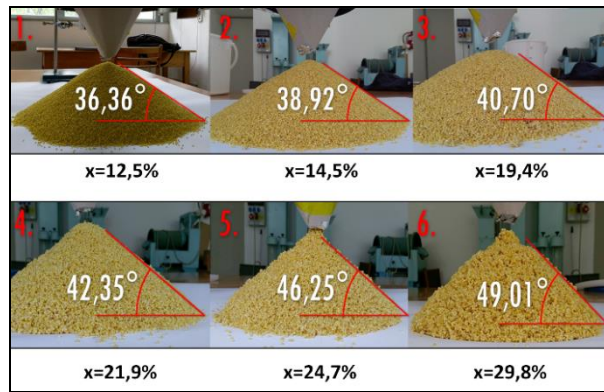


Fig. 5: The drawing of tangents for different moisture values

The other way to evaluate is stated in the standard [12], this was used for the data of a laboratory measurements. A circle is drawn on the paper under the cone, and a series of 45° lines are drawn in the circle, then the diameters of the pile are measured along the lines and the average value was taken. Then Eq. 2 was taken from the standard to calculate the angle of repose:

$$\alpha = \tan^{-1} \left(\frac{240}{\bar{d} - 25} \right) \quad (2)$$

where:

α – the calculated angle of repose [°]

\bar{d} – the average diameter [mm].

4. RESULTS

Using result from a measurement regulated by standard, the dimensionless bending and twisting strengths were calculated which are used in the discrete element method.

4.1. Results of the simulation and measurement

First sensitivity tests were simulated with the smallest and largest moisture values based on Table 2., changing eta values on a logarithmical scale, the effect of this can be seen on Fig. 6. The reason of these tests was to lower the time of the simulations. From this we can approximate the range of eta values worth using for simulation, as they are between the minimum ($x=12.5\%$) and maximum ($x=29.8\%$) moisture values.

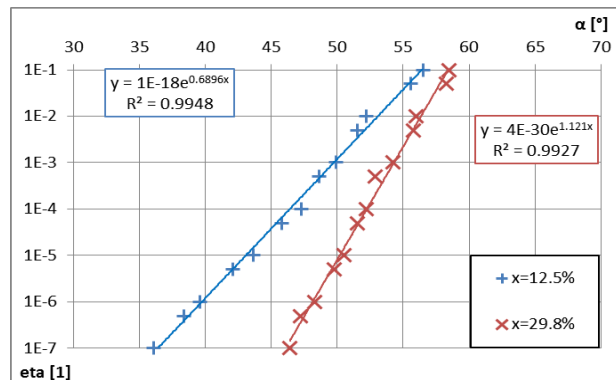


Fig 6: Eta values on a logarithmic scale as a function of angles of repose, for moisture values of $x=12,5\%$ and $x=29,8\%$

For both moisture values $R^2 > 0.99$, which means the trendlines fit the values well. Statistical analysis [13]-[14] was conducted on the data seen in Table 6. During the Abbe-test for 95%, 99%, and 99.9% the null-hypothesis was false, the measured data are not constant, so there is a tendency between them. During regression testing the error of sum squares (SSE) was 2.6 and 1.4 for moisture contents of 12.5% and 29.8% respectively. As both values are larger than 1, the results are sufficient. A confidence interval was determined for the data, which is shown in Fig. 7 for two moisture values.

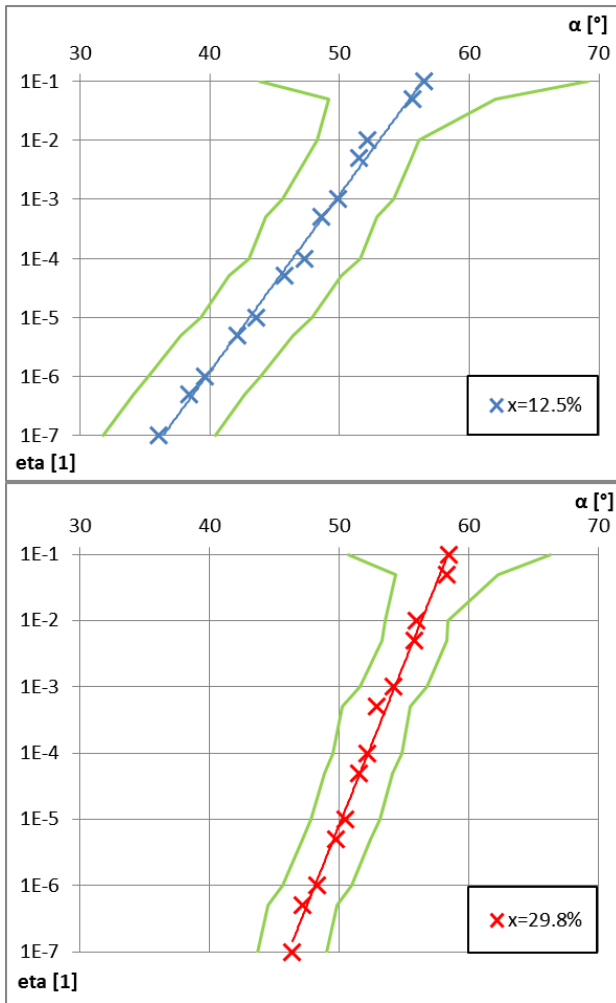


Fig 7. Eta parameter as a function of the angle of repose with confidence intervals (green), for moisture values of 12.5% (upper) and 29.8%(lower)

The simulation results are inside the confidence intervals with a 95% probability. The measured and simulated angles of repose are shown in Table 4., where the modeled values were given in intervals due to uncertainties in evaluation and reading.

Table 4. Results of measurement and simulation

No	1.	2.	3.	4.	5.	6.
x [%]	12.5	14.5	19.4	21.9	24.7	29.8

Measurement	α_m [°]	36.4	38.9	40.7	42.4	46.3	49
Simulation	α_{sz} [°]	36.1-38.4	37.6-39.4	39.8-41.9	41-43.3	45.4-47.3	48.3-49.8
	eta [10 ⁻⁶]	1-5	0.1-0.5	0.1-0.5	0.5-1	0.5-1	0.1-0.5

where:

α_m – angle of repose by measurement [°]

α_{sz} – angle of repose by DEM simulation [°]

eta – dimensionless bending and twisting strengths [10⁻⁶]

The measured angles of repose can be seen in Fig. 8., these where also analyzed using statistic methods. [12-13].

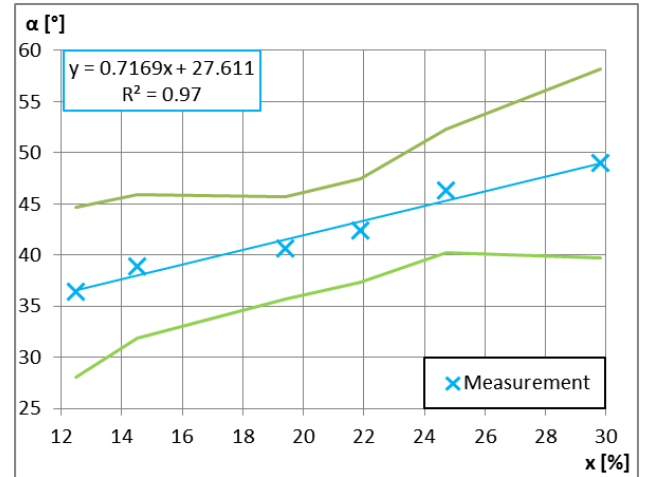


Fig 8. Angles of repose by measurement with confidence interval (green), in case of 95% probability

During the Abbe-test the null hypothesis was false for 95%, 99%, 99.9% cases, so the data series show a tendency. The error of sum squares (SSE) is 3.3, which is sufficient because it is larger than 1. Confidence intervals for 95% probability are shown in Fig. 8.

4.2. Comparison of angles of repose by measurement and simulation

The angles of repose by measurement and simulation are approved by using statistical methods in Chapter 4.1. The results of the angles of repose can be seen in Fig. 9., where blue and red marking the measured and simulated data respectively.

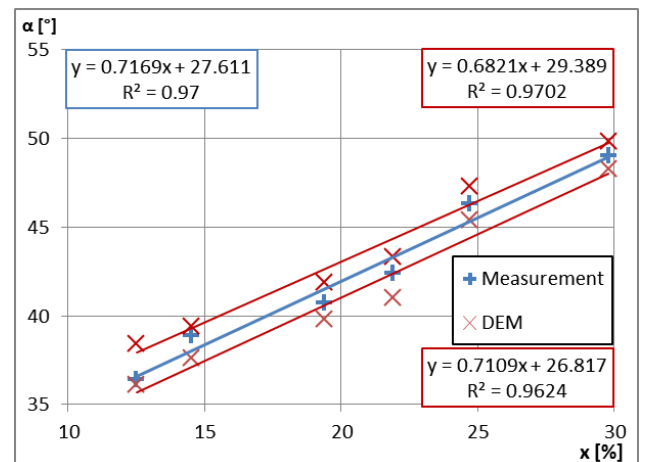


Fig 9: Angles of repose by measurement and simulation in the function of moisture content based on wet material

The results show that with the increase in moisture content the angle of repose increased, and this can also be seen in the simulated results as expected. While the granules stuck together more when increasing the shear and tensile strengths using sphere shaped granules, the increase in moisture content resulted in decreasing strengths. We can clearly state that the eta parameters are the main factors influencing angles of repose.

5. CONCLUSION

During this study the angles of repose were given for hulled millet using standard-regulated measurements and discrete element modeling (DEM) for different moisture contents. The geometry of the granules was approximated by a sphere for the purpose of this study. Increasing the moisture content resulted to an increase in the angle of repose, which was modeled with good accuracy on computer using the correct simulation parameters. Using the data from measurements, the dimensionless bending and twisting strengths were given (eta) for different moisture contents. The results of the sensitivity tests can be used in future studies. The study also showed that increasing the micromechanical stiffness in the simulation resulted the increase in the angles of repose. During the DEM simulations the cohesion between granules provided by shear and normal stiffness did not influence the results considerably, while changing the eta parameter had a larger effect on the results. Finally, statistical methods were used to analyze the measured angles of repose and the results of the sensitivity tests, and both proved to be satisfactory.

ACKNOWLEDGEMENTS

We would like to express our thanks to László Iván and Tamás Kovács for their assistance in creating this publication. We also greatly appreciate the financial funding provided Richter Gedeon Talentum Alapítvány, Richter Gedeon Nyrt. Centenárium Alapítvány (1103 Budapest, Gyömrői út 19-21.) and Nemzeti Kutatási, Fejlesztési és Innovációs Hivatal (NKFIH/PD-116326).

REFERENCES

- [1] Edem software, <https://www.edemsimulation.com>
- [2] Samadii™/DEM software, <http://www.metariver.kr>
Yade DEM software, <https://yade-dem.org>
- [3] PFC3D software, www.itascacg.com
- [4] ŠMILAUER, V., et al. (2015) *Reference manual. In Yade Documentation 2nd ed The Yade Project*, DOI 10.5281/zenodo.34073, <http://yade-dem.org/doc/>
- [5] ŠMILAUER, V., et al. (2015), *DEM formulation. In Yade Documentation 2nd ed The Yade Project*, DOI 10.5281/zenodo.34044, <http://yade-dem.org/doc/>
- [6] BOURRIER, F., KNEIB, F., CHAREYRE, B., FOURCAUD, T. (2013) *Discrete modeling of granular soils reinforcement by plant roots*, Ecological Engineering, pp 646– 657.
- [7] HORVÁTH, D., HEGEDŰS, K., VARJU, E. (2016) *Keverős dobszárító keverési teljesítmény szükségletének meghatározása, (Determination of*

Power Requirement of Mixing Drum Dryer), Scientific Students' Associations, Budapest University of Technology and Economics

- [8] HORABIK, J., MOLENDÁ, M. (2016) *Parameters and contact models for DEM simulations of agricultural granular materials: A review*, Biosystems Engineering 147, pp 206-225
- [9] TAMÁS, K., FÖLDESI, B., RÁDICS, J. P., JÓRI, J. I., FENYVESI, L. (2015) *A Simulation Model for Determining the Mechanical Properties of Rapeseed using the Discrete Element Method*, Periodica Polytechnica Civil Engineering, pp 575-582, DOI: 10.3311/PPci.8173
- [10] CUNDALL, P. A., STRACK, O. D. L. (1979) *A discrete numerical model for granular assemblies*, Geotechnique 29, pp 47-65
- [11] MSZ EN 12047:1998 standard: *Solid fertilizers - Measurement of static angle of repose (ISO 8398:1989 modified)*, 1998.
- [12] HALÁSZ, G., VARGA, R., TILL, S. (2016) *Műszaki és gazdasági adatok elemzése, (Analysis of Technical and Economic Data)*, http://www.hds.bme.hu/letoltesek/targyak/BMEGEV_GAG14/mugaz_ea_jegyzet_jav.pdf
- [13] LUKÁCS, O. (1987) *Matematikai statisztika, (Mathematical Statistics)*, Műszaki könyvkiadó, ETO: 519.22, ISBN:963 10 6848 X

CORRESPONDANCE



Tibor POÓS, PhD Eng.
Budapest University of Technology and Economics
Faculty of Mechanical Engineering
Department of Building Services Process Engineering
H-1111 Budapest, Hungary
Bertalan Lajos u. 4-6. D. ép. 110.
poos@mail.bme.hu



Dániel HORVÁTH, M.Sc. Eng. Student
Budapest University of Technology and Economics
Department of Building Services and Process Engineering
H-1111 Budapest, Hungary
Bertalan Lajos u. 4-6. D. ép. 110.
daniel.horvath.nk@gmail.com



Kornél TAMÁS, PhD Eng.
Budapest University of Technology and Economics
Faculty of Mechanical Engineering
Department of Machine- and Product Design
H-1111 Budapest, Hungary
Bertalan Lajos u. 4-6. MG. ép. 300.
tamas.kornel@gt3.bme.hu

DETERMINATION OF WEAR IN CONTACT OF WHEEL-RAIL SET USING FEM

Milan BANIĆ
Dušan STAMENKOVIĆ
Miloš MILOŠEVIĆ
Aleksandar MILTENOVIĆ

Abstract: The modelling of the wear has become increasingly important in product design process including areas such as automotive, aerospace, railway (e.g. wheel and rail rolling contact, braking systems, etc.). Determination of wear volume in the contact of wheel and rail is important for understanding the damage mechanisms on this two bodies. This paper presents a procedure to determine the wear in contact of wheel and rail during normal operation using transient structural analysis in ANSYS WORKBENCH software.

Key words: wheel-rail contact, wear, FEM

1. INTRODUCTION

Today, computer simulation has allowed engineers and researchers to optimize product design process efficiency and explore new designs, while at the same time reduce costly experimental trials. Wear volume in contact of rail and wheel is important factor for determination of life span of wheel and rail. An accurate wear prediction can have both economic and safety implications [1].

The railway wheel wear is usually predicted by using Archard's equation [1, 2], or by using the energy dissipation effect [3]. Archard's equation is more commonly used in railway industry as determined by Cremona [1], which proposed a novel wear prediction methodology that accounts for dependence of wear coefficient K on contact pressure and sliding speed. Xia [4] proposed a rail wear prediction model using Archard's model in the procedure includes a coupled dynamics model of freight vehicle and track, Non-Hertzian contact model, and a material wear model.

Archard's equation is now incorporated into commercial FEA software like ANSYS, which enables quick and relatively easy prediction of wear for mechanical systems. This paper presents a procedure for assessment of wear volume in contact of railway wheel and rail by using the Archard wear model in ANSYS WORKBENCH software.

2. WEAR MODELLING

Wear is erosion or sideways displacement of material from its "derivative" and original position on a solid surface performed by the action of another surface. Material erosion/removal is limited to the small volume in the contact zone. In that way comes to gradual reduction of dimensions and changing shape on one or both

elements of friction pair in normal direction on the friction surface.

There are different few mechanism theories how wear process occur but there are always three characteristic phases that are shown on Fig. 1.

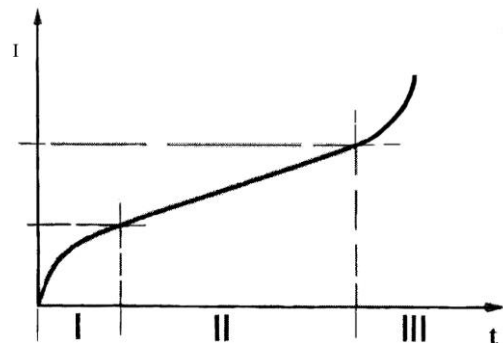


Fig. 1: Three characteristic phases of wear process

This law of wear process that is used for all tribomechanical systems is given by V.F. Lorenz in 1934. First phase is the period of adaptation of friction elements. After this phase, the wear intensity is decreasing and process is stabilized which is characteristic of second phase. This is exploitation period of tribomechanical system. Third phase is characterized with increased wear intensity similar to first phase but process strive to catastrophic wear and total destruction of the system.

2.1. Archard wear equation

First equation for calculation of wear material volume is given in 1953, based on the adhesion theory of friction. This was made by J.F. Archard who started from the assumption that the contact of two bodies is discreet and that real contact surfaces are circular and that diameter is $2r$. He also had assumption that all wear particles occur

on the sliding path that is equal to $2r$ and that they always have the shape of half sphere with volume [5]:

$$\Delta V_i = \frac{2}{3} \pi r^3 \quad (1)$$

Total wear volume for the unit of path length is:

$$\Delta V = \frac{\pi r^2 n}{3} \quad (2)$$

where n – number of contacts (number of friction connections) on sliding path under condition that outside load is equally arranged on all contact elements and it is:

$$N = \sigma_T \pi r^2 n \quad (3)$$

where σ_T – yield strength of material with lower hardness. From previous Eq-s can be concluded that the wear volume is:

$$\Delta V = \frac{N}{3\sigma_T} \quad (4)$$

However, since wear is not going to occur in all the contacts, Archard introduced constant K that take into account possibility of destruction of adhesion connections. The Eq. for total wear volume that appear on the path L is:

$$V = K \frac{N}{3\sigma_T} L \quad (5)$$

Constant K is coefficient of adhesion wear. Like friction coefficient it is dimensionless and it can be determined experimentally.

Archard's equation is not universal and it can be used approximately for the second phase of wear in the case when wear intensity is relatively low. Regardless, this equation has advantages like that it is simple and it gives possibility to calculate the wear volume without expensive experiments.

3. WHEEL-RAIL GEOMETRY

3.1. Rail profile

Standard EN 13674-1:2011 specified 23 rail profiles. This European Standard specifies Vignole railway rails of 46 kg/m and greater linear mass, for conventional and high speed railway track usage.

Two classes of rail straightness are specified, differing in requirements for straightness, surface flatness and crown profile. Two classes of profile tolerances are specified. Figure 2. shows the rail profile 50E2 which is used in further analysis.

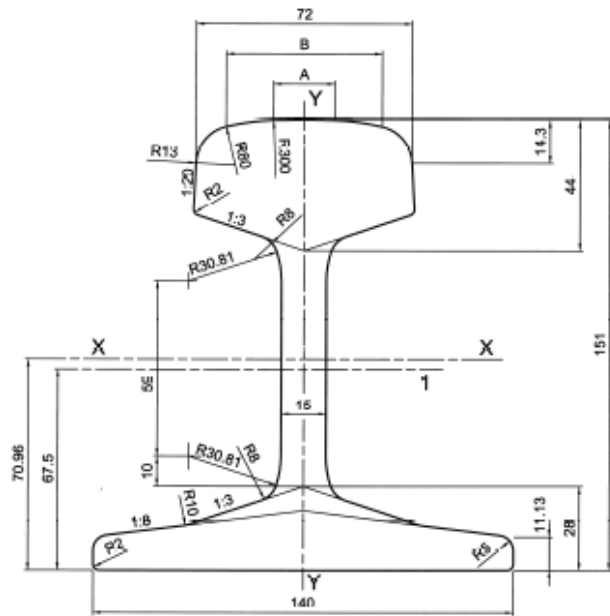


Fig. 2: Rail profile 50E2 [4]

3.2. Wheel profile

UIC CODE 510-2 [7] contains the conditions relating to the design and maintenance of wheels and wheelsets for coaches and wagons used on international services. It covers wheel diameters from 330 to 1000 mm, and indicates the permissible axle loads from the standpoint of stresses of the metal used for the wheel and the rail.

UIC CODE 510-2 contains detail coordinates of wheel rim line. It is valid for a nominal track gauge of 1435 mm and cannot be readily transposed to apply to other track gauges. Figure 3. shows the wheel profile which is used in further analysis.

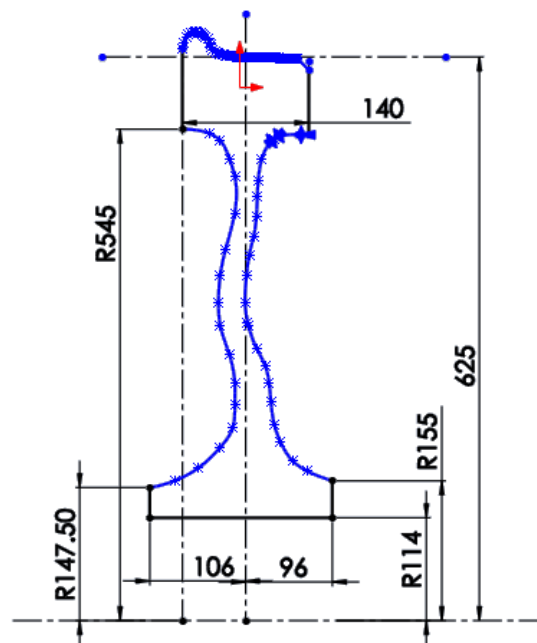


Fig. 3: Wheel profile

4. ANALISYS SETUP

Basic model of wheel-rail set was defined in SOLIDWORKS and then exported in ANSYS WORKBENCH software. To speed up the analysis time only a fraction of wheel model (outer rim) was considered in analysis. Due to same reasons only upper part of the rail was used in analysis. Such simplifications does not influence contact pressure and sliding speed so they don't influence the accuracy of wear prediction. The FEA mesh (Figure 4) was defined with 211506 nodes which form 134678 elements. All mesh quality parameters were in allowable boundaries.

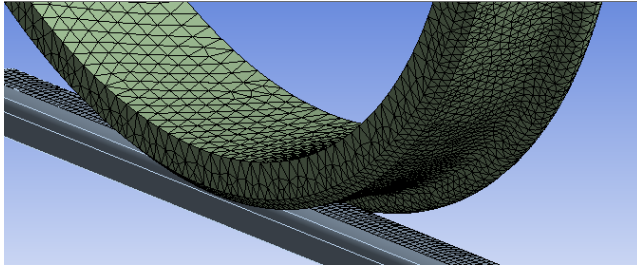


Fig. 4. Mesh of wheel and rail

The properties of the wheel material used in the analysis are listed in Table 1.

Table 1. The mechanical properties of material used in this study

Density, kg/m ³	7850
Young's modulus, Pa	$2 \cdot 10^{11}$
Poisson's Ratio	0.3
Hardness, Pa	2549820000
Wear coefficient [8]	$3.56 \cdot 10^{-4}$

Analysis was defined as transient structural analysis. The loads and boundary conditions were defined via joints as shown in Figure 5.

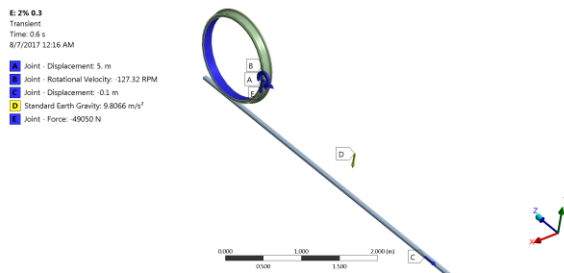


Fig. 5. Load and boundary conditions

The parameters of the Archard model were defined via the ANSYS command interface for the contact setup. The analysis was performed for a friction coefficient value of $\mu = 0.3$ and 2% slip between the wheel and the rail. Furthermore, the analysis was performed for a locomotive speed of 30 km/h. Due to slip between the wheel and the rail, the wheel speed was recalculated as 29.4 km/h for 2% sliding. The wheel circumferential speed defines the

length of simulation as the analysis is performed for one revolution of the wheel, as well as the RPM of the wheel. The normal load was 49050 N which corresponds to distribution of locomotive weight on one wheel.

5. RESULTS

Figure 6. shows contact pressure on wheel surface for a simulation setup described in the previous chapter. The contact pressure values and the shape of the contact surface are in line with expected and with results obtained by other authors.

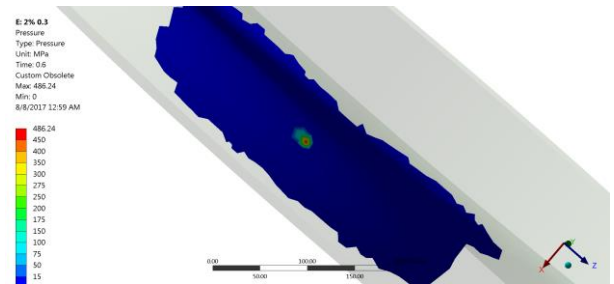


Fig. 6: Contact pressure on wheel surface

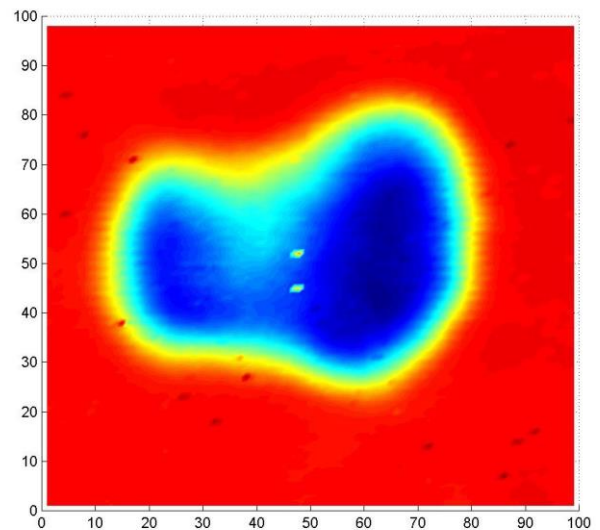


Fig. 7: An example of real contact surface obtained by ultrasonic measurement [9]

Figure 7 shows the real contact surface obtained by ultrasonic measurement. In theory the contact surface should have an elliptic shape but due to wear, slip and geometrical irregularities it has a shape of “multi-point contact” [10]. The software accounts for wear of the surface also, so the contact surface shape obtained by simulation is similar to contact surface shape obtained by ultrasonic measurements. With prolonged wear in simulation (more than one revolution) the shape of the contact surface from simulation would further approach the contact shape obtained by ultrasonic measurements. The software calculates the remaining wheel volume so the wear volume for one revolution can be obtained by subtracting the remaining wheel volume from the wheel volume at the start of the simulation. From the obtained data, it can be calculated that the wear volume per one

revolution is 0.02 mm^3 . It must be emphasised that such results are obtained for specific conditions locomotive speed 30 km/h, slip ratio 2% and friction coefficient of $\mu = 0.3$. Based on obtained data for one revolution the wear volume can be easily calculated for any running distance. For instance, for 50000 km the wear volume would be 202839 mm^3 .

Further research should be directed to estimate wear for different tribological conditions and for change of wear coefficient with contact pressure and sliding speed.

6. CONCLUSION

The paper present approach to determine the wear volume in wheel rail contact by using of FEM. It was found that for locomotive speed of 30 km/h, slip ratio 2% and friction coefficient of $\mu = 0.3$ the wear volume for one wheel revolution is 0.02 mm^3 . The presented research is a first step in a broader research focused to wear estimation at different vehicles speeds, as well as for different tribological conditions.

REFERENCES

- [1] CREMONA, M.A., BINBIN, L., YUNG. H., BRUNIB, S., LEWIS, R. (2016) *Predicting railway wheel wear under uncertainty of wear coefficient, using universal kriging*, Reliability Engineering & System Safety, Vol. 154, pp. 49-59.
- [2] JENDEL T. (2002) *Prediction of wheel profile wear - comparisons with field measurements*, Wear, Vol. 253 (1-2), pp. 89-99.
- [3] ELKINS J., EICKHOFF B. (1982) *Prediction of wheel profile wear – comparisons with field measurements*, Journal of Dynamic Systems, Measurement and Control, Vol. 104 (2), pp. 133-142.
- [4] XIA L., TAO Y., JUAN Z., YABO C., ZEFENG W., XUESONG, J. (2016) *Rail wear on the curve of a heavy haul line - Numerical simulations and comparison with field measurements*, Wear, Vol. 366–367 (15), pp. 131-138.
- [5] ARCHARD J.F. (1953) *Contact and rubbing of flat surfaces*, J. Appl. Phys., Vol. 24(8), pp. 981–988.
- [6] EN 13674-1:2011: Railway applications - Track - Rail - Part 1: Vignole railway rails 46 kg/m and above, 2010.
- [7] UIC CODE 510-2: Trailing stock: wheels and wheelsets. Conditions concerning the use of wheels

of various diameters, 2004

- [8] ASADI A., BROWN M. (2008) *Rail vehicle wheel wear prediction: a comparison between analytical and experimental approaches*, Vehicle System Dynamics Vol. 46 (6), pp. 541–549.
- [9] PAU M., AYMERICH F., GINESU F., ISHIDA M., CHEN H. (2001) *Evaluation of the Influence of Surface Conditions on Wheel-Rail Contact Performances*, WCRR 2001, Cologne
- [10] ĐURĐANOVIĆ M., STAMENKOVIĆ D. (2007) *Static friction – a movement prerequisite*, 10th International Conference on Tribology – SERBIATRIB 2007, Kragujevac, pp. 215-218.

CORRESPONDANCE



Milan BANIĆ, Ass. Prof.
University of Niš
Faculty of Mechanical Engineering
A.Medvedeva 14
18000 Niš, Serbia
milan.banic@masfak.ni.ac.rs



Dušan STAMENKOVIĆ, Full Prof.
University of Niš
Faculty of Mechanical Engineering
A.Medvedeva 14
18000 Niš, Serbia
dusan.stamenkovic@masfak.ni.ac.rs



Miloš MILOŠEVIĆ, Asoc. Prof.
University of Niš
Faculty of Mechanical Engineering
A.Medvedeva 14
18000 Niš, Serbia
milos.milosevic@masfak.ni.ac.rs



Aleksandar MILTENOVIĆ, Ass. Prof.
University of Niš
Faculty of Mechanical Engineering
A.Medvedeva 14
18000 Niš, Serbia
aleksnadar.miltenovici@masfak.ni.ac.rs

DETERMINING THE BOUNDARIES OF PREDICTION INTERVALS IN SERVICE NETWORKS USING SIMULATION

Vladimir JERZ

Abstract: The paper describes the purpose of using prediction intervals when interpreting the results of simulation experiments as well as differences resulting from using confidence intervals. A method for obtaining data for prediction interval determination is provided when experimenting with the simulation model. Attention is paid to particular factors which may affect the veracity of the results. A special simulation model of the queuing systems network was created for the purpose of experimentation and presentation of the proposal.

Key words: queuing systems network, prediction interval, simulation, Witness

1. INTRODUCTION

The frequent drawback of using simulation to predict the behavior of the queuing systems network is the misrepresentation of outcomes in simulation experiments and the inappropriate form of presented results. The output of the simulation experiment is usually the value of observed output variable or values of more output variables $y_1, y_2, \dots, y_b, \dots, y_n$. It is fairly well known that when random variables are present in the model, which is quite common in the case of a queuing systems network, sequences of simulation experiments of the same model tend to be performed. However, these sequences are made with different streams of random numbers to generate values of random variables. This method allows us to gain statistical sets of output variable values, which illustrates the variation due to the presence of random variables in the model. The results of experimentation can then be presented, for example, in the form of spot characteristics (mean, standard deviation, median, etc.). The mean value provides intelligible information, but says nothing about the variations caused by the presence of random variables. The standard deviation provides some information about the degree of stochasticity, but for the average user it is quite incomprehensible. It is therefore preferable to take advantage of interval estimates. The width of interval estimation also serves as a measurement of errors and of the inaccuracy of the point estimate [4, 6].

2. INTERVAL ESTIMATES

The most important result in the statistical evaluation of the simulation experiment results are average values. When evaluating the sequence k of discrete values, these are calculated using the relation

$$\mu_i = \frac{1}{k} \sum_{j=1}^k y_{ij} \quad (1)$$

in case of evaluation of continuous values in the interval $(0, T)$, calculation is made using the following equation

$$\mu_i = \frac{1}{T} \int_0^T y_i(t) dt \quad (2)$$

Additional information is the standard deviation or sampling variance of values of this parameter, or median (50% quantile), or quantiles that specify limits for different probability types [7].

The purpose of the simulation is to estimate which value certain parameter will obtain in real conditions, e.g. how many products are produced in one day. If it is a random variable, this number can fluctuate around a certain value. If we merely want to know how many products will be produced over a longer period of time, provision of information such as average (mean) value and confidence interval within which this value is specified will be sufficient, along with the given probability. But if it is important how many products will be produced in a particular day, this characteristic will not be sufficient. The number of products determined by simulation per day will be $(y_{i1}, y_{i2}, \dots, y_{ik})$. Let's assume that these values are characterized by the normal distribution. Sampling variance can be calculated according to the equation

$$S_i^2 = \frac{1}{k-1} \sum_{j=1}^k (y_{ij} - \mu_i)^2 \quad (3)$$

The boundaries of the confidence interval for that parameter can be calculated by the equation

$$\mu_i \pm u \left(1 - \frac{\alpha}{2} \right) \cdot \frac{S_i}{\sqrt{k}} \quad (4)$$

where $u\left(1-\frac{\alpha}{2}\right)$ is $\left(1-\frac{\alpha}{2}\right)\%$ quantile of considered probability distribution (in case of Student distribution with $k-1$ degrees of freedom). The preselected number α is called the significance level. In practice, this number is most often adjusted to values of 0.01 or 0.05, which corresponds to 99 or 95% probability that the calculated random variable would be from the found interval. It should be noted that this calculated confidence interval indicates the range in which the actual mean value of observed variable occurs with given probability. From this relationship it is clear that along with increasing the value k , the confidence interval is narrowing, which means that the accuracy of the mean value estimation is proportional to the range of the evaluated set of values. Due to practical needs, it is sometimes important to use the interval, in which the actual observed value of the variable (not its mean) would occur with a certain probability - prediction interval. In the example above, it is the information that says how many products will be produced with a given probability in a particular day. **The prediction interval can be regarded as a measure of risk, while the confidence interval is a measure of error.** Boundaries of prediction interval can be calculated by the equation

$$\mu_i \pm u\left(1-\frac{\alpha}{2}\right) \cdot S_i \cdot \sqrt{1+\frac{1}{k}} \quad (5)$$

It is clear that unlike the confidence interval, its width does not converge to zero [2].

3. PROPOSAL FOR A DATA GATHERING METHOD

The standard way to obtain a statistical set of values of observed output variable is a procedure that involves the performance of the sequence l experiments (simulation runs) with different streams of random numbers used in the model. These streams are used to generate the values of the input parameters of the model within the rules inside the model. Obtained values l of output variables can be statistically processed. According to the nature of the monitored output variables, the individual values of this sequence are obtained by means of status and statistical functions applied at the end of each simulation run.

The need for large-scale statistical data sets raises the need to generate a sequence of simulation runs automatically. In the case of the Witness simulation system it is possible, for example, to use the Scenario Manager module, but there are other ways, such as the use of an optimization Optimizer module in a non-standard way. A useful tool of Witness is the ability to record the values of observed output variable in the appropriate simulation periods of time into a file, which can then be statistically processed using other software.

This paper will present a detailed analysis of a method, which would allow us to get all the values of observed output variable, i.e. complete statistical set, from one simulation run. The simulation run with a duration length T of unit simulation time will be divided into more sub-interval lengths T/k of the same length. From each sub-

interval one value of the observed output variable will be obtained, which will be written to the file. Then the file will be statistically processed using the appropriate software (e.g. Excel). However, it is also possible to process and subsequently present results of the assessment directly via simulation software at the end of a simulation run.

The methods for obtaining the values of the monitored output variable from sub-intervals depend on the nature of these variables.

Some values are given in units of "number per time" For instance, the number of manufactured products for a period of time at a steady state of service operation, the number of objects which passed through a certain point in a given time interval, the number of operations performed on a given machine, the number of defect products (which does not always result from the input percentage specified on the simulation experiment, but may be due to temporal relationships in the model, e.g. inappropriate or unacceptably long delays of produced parts in a certain point of the model, or a late method of equipment failure detection on the assembly line during the inspection of products after a certain time interval), the number of operator interventions caused by different situations in the model, and so on. This number is most commonly related to the entire sub-interval with the length T/k . To record this number it is appropriate to use a global variable, which is set to zero at the beginning of the sub-interval and at the end of this interval its value is saved to a file.

This group may also include variables that indicate the "maximum value" or "minimum value", which the given variable achieved during the period of time under consideration, for example the maximum number of parts in a certain queue, minimum stock of semi-products, the maximum waiting time for repairing a breakdown, etc. In that case, the variable at the beginning of the sub-interval is also set to zero and if the value of the observed variable is higher than the latest recorded one (or lower, in case of searching for the minimum value), it is constantly updated during the simulation within the given sub-interval. At the end of the sub-interval it is written (added) into the file.

If the value of observed output variable is obtained as the value of the statistical function that is non-decreasing over the entire simulation run (e.g., "the number of products which have left the model"), it is appropriate to use an approach where the value of the observed output variable is transcribed into the variable designated for this purpose at the beginning of the sub-interval. At the end of the interval the difference between the current value of the monitored output variable and the value included in the variable designated for this purpose is recorded into the file.

The second group includes variables that are mostly expressed as average values, for example, the average utilization of the machine or of the worker, the average throughput time of parts, etc. This is a variable whose values are normally provided at the output of the simulation experiment, but which would be tedious to count when using the procedure described, since the data for statistical analysis are derived from a single simulation run of the length T , divided into k intervals. In this case, it is possible to express the average value of the i^{th} observed output variable in j^{th} interval by the equation:

$$y_{ij} = \frac{1}{T} \int_{\frac{(j-1)T}{k}}^{\frac{jT}{k}} y_i(t) dt, \quad (6)$$

The obtained values may be statistically processed. In certain cases these values, cannot be considered statistically independent of each other (e.g. the average queue length in the $(j+1)^{\text{th}}$ interval depends on the average queue length in the j^{th} interval). This fact, however, usually does not affect the accuracy of the experiment results.

Obviously, the method of obtaining the average values of the observed variables depends on whether the value of the observed variable in the sub-interval changes in a discrete or a continuous way. Even in the case of discrete changes which occur at any (continuously increasing time), the average value cannot be obtained by a conventional procedure for obtaining the average value, because the observed output variable achieves different values in various time intervals (sub-intervals of a given interval). Only when value changes of the observed output variables occur in a finite number of discrete time points which divide the sub-interval into n equal length sub-intervals, can the average value be obtained as follows:

$$y_{ij} = \frac{1}{n} \sum_{m=1}^n y_{ijm}, \quad (7)$$

where y_{ijm} is an amount that the observed output variable achieves within the m^{th} sub-interval of j^{th} partial interval [3].

4. FORMATION OF THE MODEL AND DESIGN OF THE SIMULATION EXPERIMENT

For the purpose of experimentation and design verification, a simple model of the service network was created in the Witness system. It is, however, characterized by a strong influence of fluctuations in the values of random variables on the values of the observed output variable. This variable is represented by the number of processed requests (processed items) for a certain period, which in practical application equals, for example, the number of products produced in the manufacturing system per day. As mentioned above, a statistical set of output variable values - the number of processed requests, processed products for a certain time interval, is obtained from one simulation run of length T , divided into k equal intervals of length T/k .

The simulation run will start with an empty model. Since the aim is to monitor the behavior of the system in a steady state, it would be appropriate to determine and set the appropriate length of onset time, in which the observed data will not be collected. In this case we can simply exclude the output from the first interval of the statistical set. At the beginning of other intervals some parts can wait for operation in queues and service channels can be filled by processed products. For more complex and larger models several values can thus be

neglected. The number of intervals that were not considered can be estimated intuitively or we can apply other popular procedures which track when queue length becomes stable. In the case of longer throughput times of products, the queues to reach the end of the process must become stable.

When experimenting with the simulation model, it is generally assumed that during the simulation run all kinds of events should occur at least 10 times. In the proposed procedure this would mean that the length of each interval should be at least long enough so that this condition can be met at each interval. However, this holds in the case, when the data are used in the calculation of boundaries of confidence intervals. As prediction intervals have different meanings, it is more appropriate to violate this rule in this case, which leads us to use prediction intervals that take into consideration the impact of occasional occurrence of such events, hence using a larger (wider) interval. An experiment which illustrates and tests our proposed approach was performed in both situations, without the occurrence of such events, and consequently with the occurrence of failure, which happens on average only in every fourth interval.

The following experiments were designed to determine:

1. how the boundaries of both confidence and of prediction intervals are changed depending on significant changes in the range of the statistical data set,
2. how the boundaries of both confidence and of prediction intervals are changed depending on significant changes in the length of each sub interval,
3. how the boundaries of both confidence and of prediction intervals are changed if certain events do not occur even once at a certain interval.

In all cases, the results will be compared with the results of the initial variant. In all three figures, the 99% and 95% confidence intervals (CI) and the prediction intervals (PI) are graphed for the experiments with the initial model and corresponding intervals below them, obtained from the experiments after modifications.

5. DOING EXPERIMENTS WITH THE MODEL AND CALCULATING THE BOUNDARIES OF CONFIDENCE INTERVALS AND PREDICTION INTERVALS

The length of the simulation experiment with the initial model was set to 48,480 units of simulation time and this run was divided into 101 intervals with equal length. This confirmed the rule that each type of event occurs in each sub-interval at least 10 times. The values of the observed output variable obtained within particular intervals, with the exception of the first value, were entered into the file (via File element), then transferred into an Excel chart, and were evaluated there.

Subsequently, the model was modified so that the length of the simulation experiment was increased to 4,800,480 units of simulation time (approximately a hundredfold increase), while the length of the sub-intervals wasn't changed. This led to a hundredfold increase in their number and the extent of statistical data set too. The impact of this change to the mean values and the

boundaries of confidence and prediction intervals is evident in Table 1.

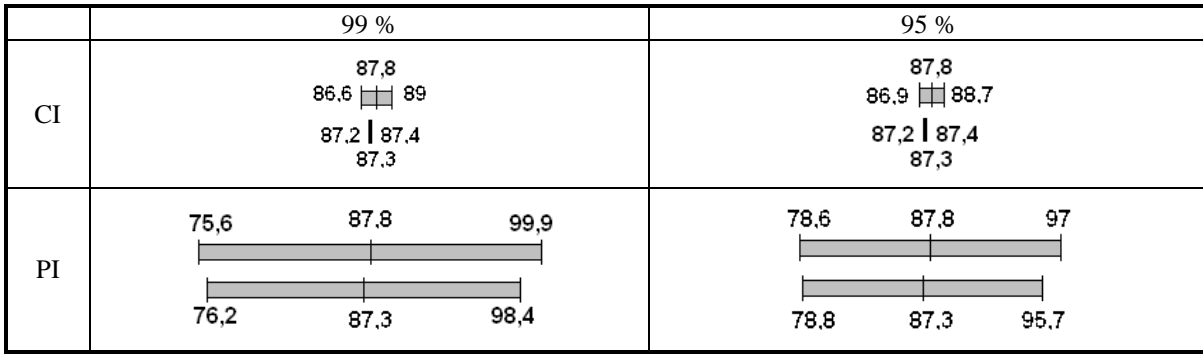


Fig.1: Boundaries of intervals after changing the extent of the statistical set

Conclusion of the 1st experiment

A significant increase in the extent of the statistical set led to a significant reduction of the confidence interval. This confirmed the fact that the width of the confidence interval is a measurement of the error. The boundaries of the prediction interval, that express 5%, respectively 1% chance that the observed output variable will not occur within the stated interval, have changed only slightly – due to more precise values achieved by greater extent of the statistical set.

During further experimentation, the length of the simulation experiment, in comparison to the initial model, was increased to 4,848,000 units of simulation time (approximately one hundred times), while the number of sub-intervals did not change, thereby the length of each sub-interval was increased a hundredfold. A subsequent comparison with the initial model will be clearer, if the confidence and prediction intervals are shown in the scale of 100:1, in comparison to the results of the initial variant. The impact of this change on the mean values and the boundaries of confidence and prediction intervals is apparent from Fig.2.

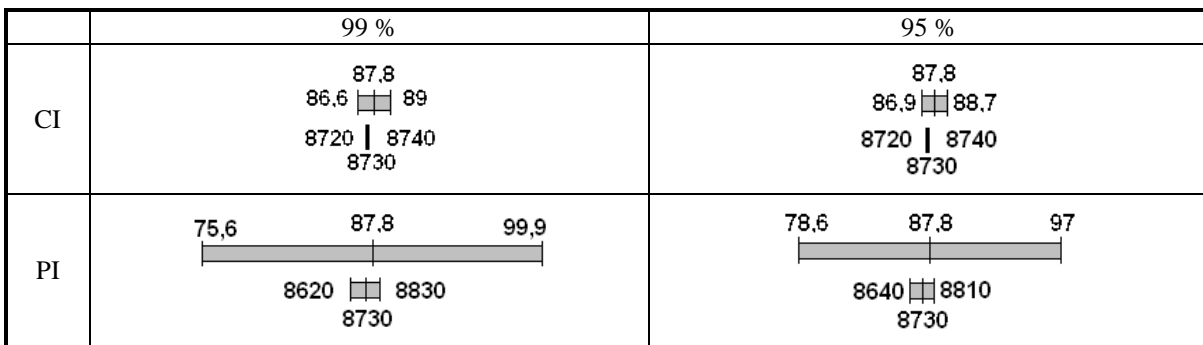


Fig.2: Boundaries of intervals after changing the length of sub-intervals

Conclusion of the 2nd experiment

Similarly to the previous experiment, the width of the confidence intervals was significantly reduced. Thus, it is clear that the estimation error of the mean value of the observed output variable can be minimized by multiple repetition of the simulation run, or by its significant lengthening. Unlike the previous experiment, the results should show that the width of the prediction interval was significantly reduced. This is obvious when looking at the Figure-2, as well as when comparing it in the percentage (in the first case, the width of the prediction interval is approximately 20% of the mean value of the observed variable, in the second case 2%). In fact, the value of the observed variable (i.e. the number of processed requests) refers to a one hundred times longer period. Thus, in absolute terms, the width of the prediction interval is 18.4 in the first case, and 170 in the second case.

Finally, the initial model was modified in such a way that the events that didn't occur within each interval were added into the model (in real conditions, represented for example by breakdowns in the production system, which occur rarely, but when they occur, they may significantly affect the behavior of the system). In addition, this model was investigated in two variants – in the first case, the events occurred regularly in every fourth interval, in the second case, they occurred in an equal frequency, but irregularly. The first case has to provide an answer, which is not affected by an accidental nature of this phenomenon. The impact of this change on the mean values and boundaries of confidence and prediction intervals is shown in Fig.3. (the intervals are listed below each other in the order: a starting model - a regular occurrence of rare events - irregular occurrence of rare events).

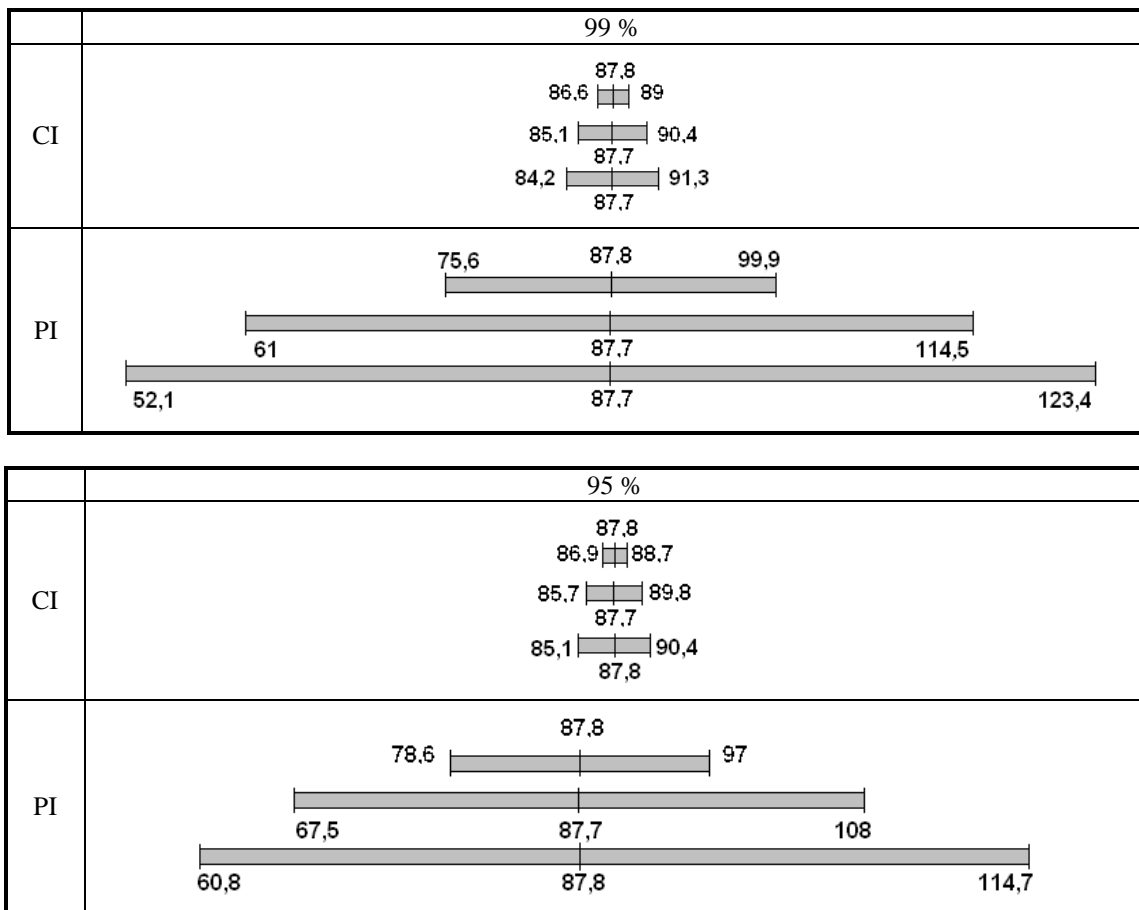


Fig.3: Boundaries of intervals with occasional occurrence of rare events

Conclusion of the 3rd experiment

The change in the model increases the uncertainty and thus the estimation error of the mean value of the observed output variable and also the width of the confidence interval. This is caused by the fact that the observed output variable is significantly different in approximately every fourth sub-interval. It is clear that if the observed variable was investigated separately in the intervals when a rare event occurred and when it did not occur, we would obtain two significantly narrower confidence intervals with different mean values. In the second variant, the error is slightly increased by random nature of implemented changes. Unlike previous experiments, this change increases dramatically the width of the prediction interval, too. As in case of the confidence intervals, it would also be possible here to consider separately the sub-intervals in which a rare event occurred and did not occur and to present two different prediction intervals. The first would correspond to the results of the experiment with the original model and the second would have a similar width, but a displaced mean value (as in the case of the confidence intervals). The result of experimentation could be presented as "dependent on the occurrence of the rare events." Thus, the importance of prediction intervals would be denied in cases when the occurrence of rare events is very irregular and unpredictable.

6. CONCLUSION, RECOMMENDATIONS AND FURTHER OBJECTIVES

Performing these experiments has resulted in recommendations primarily for solving practical tasks within the simulation studies. Using the proposed approach raises the question of the optimal determination of the number and the length of sub-intervals. It would be useful to find out how to determine these experimentation parameters for certain types of practical tasks and to prepare a spreadsheet editor application for calculating the boundaries of intervals with the interactive selection of relevant quantiles. When determining confidence intervals the experiments showed that under given circumstances, such a significant extension of the length of the simulation run, or of the length of sub-intervals is unnecessary. However, it can be assumed that with more complex models, including the models used for commercial purposes, certain extension of time simulation is useful. Nonetheless, it is important to analyze the occurrence of rare events – their frequency and regularity, as these can significantly affect the veracity of the results of experimentation.

This study was supported by the Cultural and Educational Agency of the Ministry of Education of the Slovak Republic under the contract KEGA 035STU-4/2017 The introduction of progressive educational methods for manufacturing systems to car production.

REFERENCES

- [1] JAŠUREK, J., KRÁLIK, M. (2010) *Simulation of production systems in virtual reality of programme Witness*, Mechanical Engineering 2010: 13th international conference on the occasion of the 70th anniversary of the beginning of education of mechanical engineering students at the Slovak University of Technology in Bratislava. Bratislava, 21.10. 2010. Proceedings of the papers. - Bratislava: Slovak University of Technology in Bratislava, 2010. - ISBN 978-80-227-3304-5. pp S3-103 - S3-108.
- [2] JERZ, V. (2009) *Intervaly spoľahlivosti a predikčné intervaly pri experimentovaní v systéme Witness*, Zborník z 12. ročníka medzinárodnej konferencie Witness 2009. Brno: Humusoft & VUT Brno 2009, pp 45-50, ISBN 978-80-214-3900-9
- [3] JERZ, V. (2012) *Niektoré možnosti interpretácie výsledkov simulácie v systéme Witness*, WITNESS 2012. Diskrétní simulace. 15. ročník mezinárodní konference. Sborník příspěvků. 7.- 8.6.2012, hotel Akademie, Hlubočky u Olomouce. Brno: Vysoké učení technické v Brně, 2012. ISBN 978-80-214-4538-3
- [4] JERZ, V. (2009) *Simulácia a optimalizácia v procese prijímania rozhodnutí*, Habilitation thesis. Bratislava: Sjf STU, 2009.
- [5] JERZ, V. (2008) *Simulácia a optimalizácia výrobných systémov*, Bratislava: FX s.r.o. 2008, 128 p., ISBN 978-80-89313-16-7
- [6] JERZ, V., KRÁLIK, M. (2014) *The use of meta models to interpret the results of simulation studies*, International Journal of Mechanical Engineering and Computer Applications. ISSN 2320-6349 (E), Vol. 2, Iss. 6 (2014), pp 177-181.
- [7] POTOCKÝ, R., KALAS, J., KOMORNÍK, J., LAMOŠ, F. (1986) *Zbierka úloh z pravdepodobnosti a matematickej štatistiky*, Bratislava: Alfa/SNTL 1986
- [8] VAŽAN, P., TANUŠKA, P. (2012) *A short Reflection on the Strengths and Weaknesses of Simulation Optimization*, World Academy of Science, Engineering and Technology 65/2012, eISSN 2010-3778, pp 892-896, www.waset.org/proceedings.php

CORRESPONDANCE



Vladimír JERZ, Assoc.Prof. Ph.D.
Slovak University of Technology
in Bratislava
Faculty of Mechanical Engineering
Namestie slobody 17
81231 Bratislava, Slovakia
vladimir.jerz@stuba.sk

VEHICLE DRIVING SAFETY AND RIDE COMFORT IMPROVEMENT WITH MAGNETORHEOLOGICAL SHOCK ABSORBERS

Ján DANKO
 Tomáš MILESICH
 Jozef BUCHA

Abstract: Paper deals with modelling of vehicle suspension system with magnetorheological damper. The driving safety and ride comfort can be improved by using of magnetorheological dampers to vehicle suspension system. Parametric mathematical model of magnetorheological damper is described. Experimental measurements of magnetorheological damper are realized. Cosimulation of virtual vehicle suspension system with magnetorheological system is made in MSC.ADAMS/Car and MATLAB/Simulink. Final part includes evaluation of simulation results of vehicle passive suspension system with vehicle semi-active suspension system.

Key words: magnetorheological damper, cosimulation, comfort and safety.

1. INTRODUCTION

Modern vehicles have to satisfy high driving safety and comfort requirements. It could be problem to satisfy these contradictory requirements with standard passive vehicle suspension. Therefore it is better to use adjustable suspension elements such variable dampers.

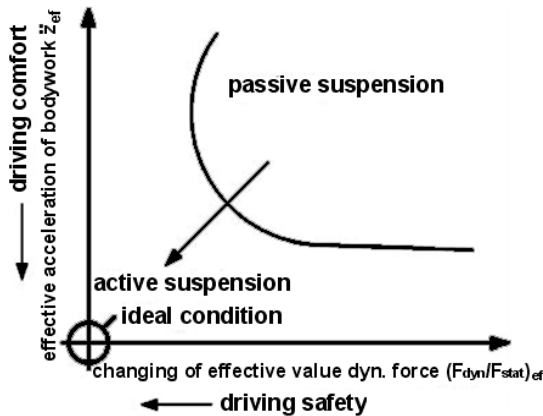


Fig. 1: The curve of conflict between comfort and safety

Using controllable suspension systems it is possible to achieve various characteristics and get under the limiting curve which is in the Fig. 1. Controllable suspension systems are adaptive, semi-active and active. Adaptive system is additive to passive suspension which has predefined step change damping characteristics. Semi-active system is suspension with variable changing of damper characteristics. Active system uses actuators to eliminate relative displacement between axes and bodywork and needs energy to run [1].

2. MATHEMATICAL MODEL OF VEHICLE SEMI-ACTIVE SUSPENSION WITH MAGNETORHEOLOGICAL DAMPER

A 3D mathematical model of a vehicle is described such as five mass system. The model presents the vehicle with the four wheels and the suspension units which are linked by the dynamics. The interaction is caused by the center of gravity, moments of inertia in longitudinal and transverse directions. The model includes real behavior of the vehicle such as rolling, acceleration and effect of braking. In the Fig. 2 is 3D model of a vehicle.

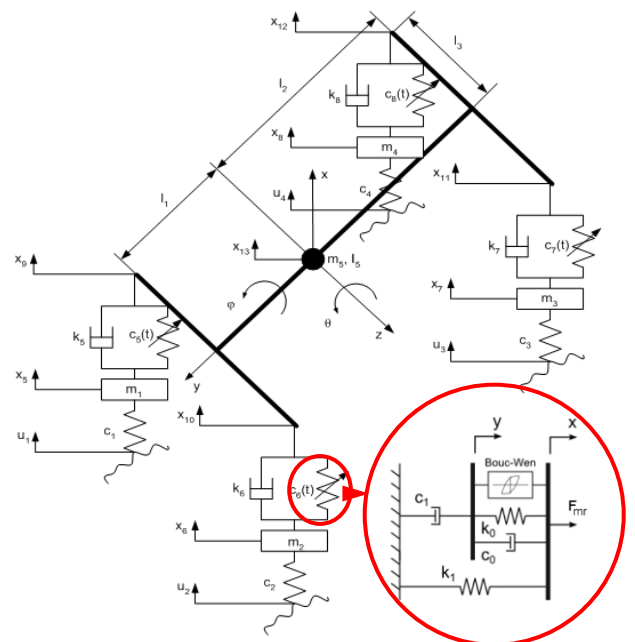


Fig. 2: 3D mathematical model of the vehicle with Spencer model of magnetorheological damper

The semi-active suspension system uses magnetorheological damper, but it is not possible to supply energy to the system and achieve the required minimum tilting [1]. Magnetorheological damper is described by Spencer mathematical model equations (1,2,3) [4], which are implemented to the MATLAB/Simulink.

$$F_{MR} = c_1 \dot{y} + k_1(x - x_0) \quad (1)$$

$$\dot{y} = \frac{1}{(c_0 + c_1)} [\alpha z + c_0 \dot{x} + k_0(x - y)] \quad (2)$$

$$\dot{z} = -\gamma |\dot{x} - \dot{y}| |z|^{n-1} - \beta (\dot{x} - \dot{y}) |z|^n + A(\dot{x} - \dot{y}) \quad (3)$$

Parameters c_0 and c_1 are coefficients of viscous dampers. Parameters k_1 and k_2 are spring rates. Parameters x' and y' are velocities on damper. Parameter x represents the deflection of the spring and x_0 initial compression of the spring. Parameter z is variable of hysteresis and it is affected by parameters $\alpha, \beta, \gamma, n, A$. Parameters α, β, γ affect linearity during stretching and smoothing the transition from compressed to expanded state. Parameter α represents the stiffness of damping force and is related to variable z . Parameter n depends on the damping force and velocity [1,4].

3. EXPERIMENTAL MEASURING OF MAGNETORHEOLOGICAL DAMPER

Experimental measurement was performed on our measurement test rig. On test bed EDYZ 4 was kinematically excited MR damper, displacement was measure with potentiometer sensor of displacement and force was measured using strain gauges.

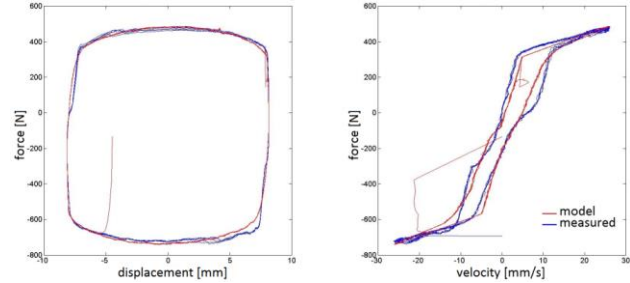


Fig.3: Schematic diagram of measurement and excitation system

The measurements are carried out according to the scheme in Fig. 3, which schematically shown the involvement of measuring input cards and output PCI card. Output PCI card generates a signal and sends it to the servovalve. Force response is measured by strain gauges, Fig. 4. The signals from the potentiometer and strain gauges are recorded through the input card in PC2, which is processed by the LabVIEW Signal Express [6].

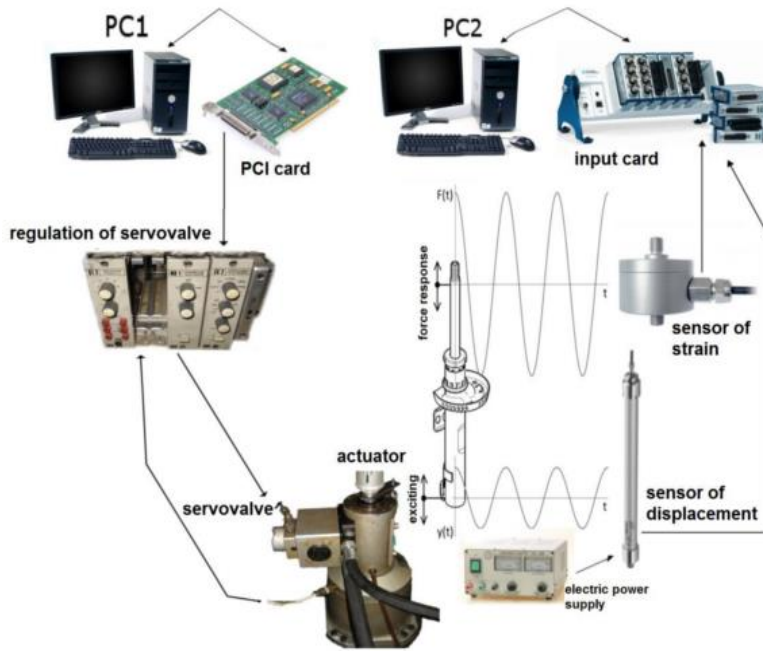


Fig.4: MR damper characteristics of modelled and measured data

4. COSIMULATION OF MSC.ADAMS AND MATLAB/SIMULINK

4.1. Modeling of magnetorheological damper in MATLAB/Simulink

The main goal in creating the model of MR damper in MATLAB/Simulink, Fig. 5, is to get closer to the real

values of damper behavior. Creating a more accurate model of the damper helps facilitate development and can be reliably operated in the management of semi-active dampers.

Parameters of the model are searched by Control and Estimation Tools Manager in Matlab/Simulink [5]. It is possible to estimate the parameters of models which describe the characteristics of the damper, Fig. 4.

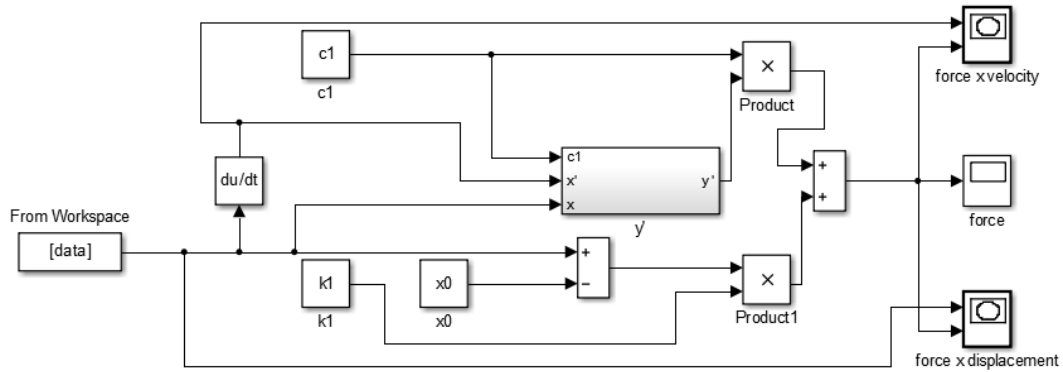


Fig.5: Spencer model in MATLAB/Simulink

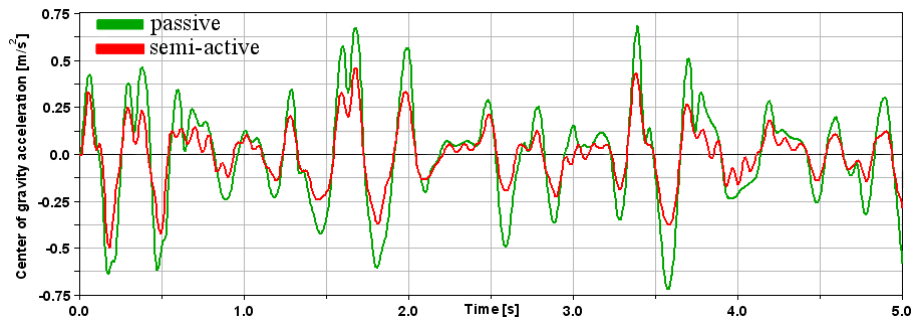


Fig.7: Comparison of body center of gravity acceleration with passive and semi-active suspension

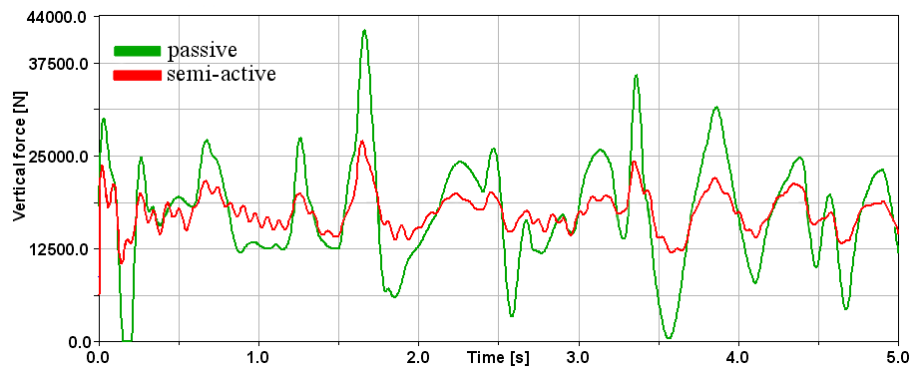


Fig.8: Comparison of wheel force with passive and semi-active suspension

4.2. Modeling of vehicle in MSC.ADAMS/Car

The model of a virtual vehicle is made in the MSC.ADAMS/Car, by using the Ride environment, Fig.6. The virtual vehicle is tested by a four-post test rig, which is a virtual simulator of the road. The control system and the model of magnetorheological damper were executed by MATLAB/Simulink [1,7].

For magnetorheological damper is necessary to use an optimal dynamic range. The optimal dynamic range is managed by the system which generates a control signal to the demands of the suspension system of the vehicle. In this case is used Skyhook control system which is most widely used control system in vehicles [2].

4.3. Results of cosimulations

Virtual vehicle goes through the terrain with random excitation and the velocity is 50 km/h. Fig. 7 and Fig. 8 show the results of cosimulations of virtual vehicle with passive and semi-active suspension.

Semi-active suspension has beneficial effects on vertical vehicle dynamics, Fig. 9. Suspension improves ride comfort, increase contact among road and wheel, which increases driving safety [1].

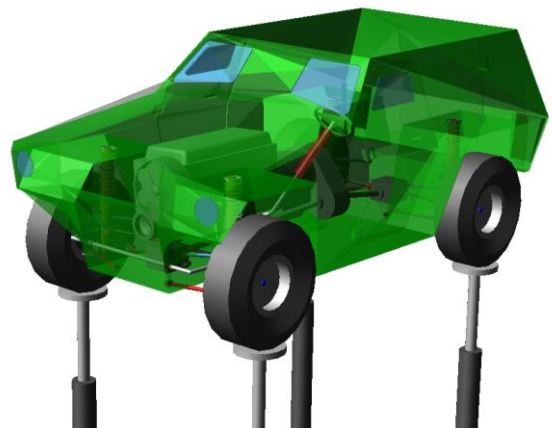


Fig.6: The virtual vehicle four-post test rig in MSC.ADAMS/Car with magnetorheological dampers

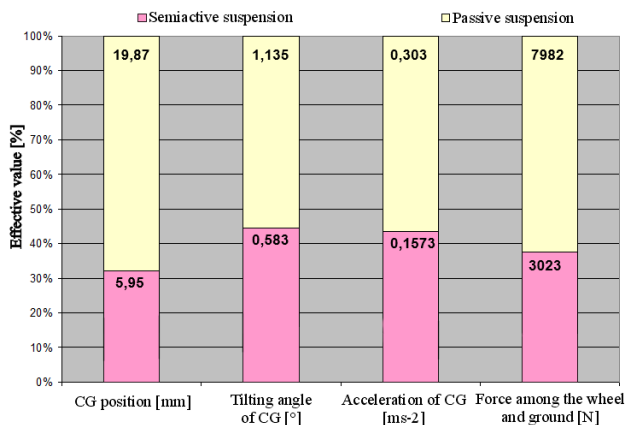


Fig.9: Effective value of selected parameters

5. CONCLUSION

Designing the ideal vehicle suspension system is a difficult task for automotive engineers. This is the reason why semi-active dampers are used. For reliable management of their behavior it is necessary to use a suitable mathematical description. Simulation results are important for automotive engineers. Simulation is the cheapest way how to improve the driving safety and vehicle comfort without the expensive real measurements. With cooperation mathematical model of MATLAB/Simulink and using environment MSC.ADAMS/Car for simulation engineers could design the ideal suspension system for designing vehicle. Nowadays the semi-active dampers like magnetorheological are the best way to increase vehicle safety and comfort without using actuators such as in the active suspension.

This work was supported by the R&D Agency: APVV-15-0524

REFERENCES

- [1] WANG D. H., LIAO W. H.. Magnetorheological fluid dampers a review of parametric. -Hong Kong : CUHK, 2011, 35 p.
- [2] ERSOY M., HEISSING B.. Chassis Handbook: Fundamentals, Driving Dynamics, Components, Mechatronics, Perspectives. -Berlin : MercedesDruck, 2011. 616 p. ISBN 978-3-8348-0994-0
- [3] FERENCY V., MADARÁS J., BUGÁR M.. Modelling of Energy and Powertrain System of the

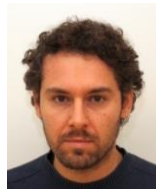
Electric Vehicle. In: Transport Means 2012 : 16th International Conference. Kaunas, Lithuania, October 25-26, 2012. - Kaunas : University of Technology, 2012. - p. 73-76. - ISBN 1822-296X.

- [4] SPENCER JR. B. F., DYKE S. J., SAIN M. K., CARLSON J. D.. Phenomenological Model of a Magnetorheological Damper. Journal of Engineering Mechanics. 1997. p. 230-238. ISSN 0733-9399.
- [5] BIGOŠ P., PUŠKÁR M., KOPAS M.. Design of Mechatronic System Specified for Feedback Required in Development of Combustion Engines. Procedia Engineering. Volume 48, 2012, p. 30-34. ISSN 1877-7058.
- [6] MLYNÁR P., MASARYK M.. Air-conditioning of battery powered electromobiles - a serious engineering challenge. In Heat engines and environmental protection : Proceedings of the 11th international conference. Balatonfüred, Hungary, June 3-5, 2013. Budapest : Budapest University of Technology and Economics, 2013, p.25-29. ISBN 978-963-313-091-9.
- [7] GUGLIELMINO E., SIRETEANU T., STAMMERS CH. W., GHITA G., GIUCLEA M. Semi-active Suspension Control, Springer-Verlag London Limited 2008. p 302. ISBN 978-1-84800-230-2.

CORRESPONDANCE



Ján DANKO, Ing., PhD.
Slovak University of Technology
Faculty of Mechanical Engineering
Námestie Slobody 18
812 31 Bratislava, Slovakia
jan.danko@stuba.sk



Tomáš MILESICH, Ing., PhD.
Slovak University of Technology
Faculty of Mechanical Engineering
Námestie Slobody 18
812 31 Bratislava, Slovakia
tomas.milesich@stuba.sk



Jozef BUCHA, Ing., PhD.
Slovak University of Technology
Faculty of Mechanical Engineering
Námestie Slobody 18
812 31 Bratislava, Slovakia
jozef.bucha@stuba.sk

Impact of the suspension parameters on the vertical dynamics of the VW E-UP

Jozef BUCHA
 Ján DANKO
 Tomáš MILESICH

Abstract: The paper deals with effect of suspension parameters on vertical dynamics of the VW E-UP vehicle. To examine vehicle dynamics, a virtual vehicle model was developed in the MSC ADAMS/ Car environment. The vehicle's virtual model was based on the VW E-UP CAD model, from which the suspension and body parts were used. To enhance the accuracy of the model, the rear axle twist beam was designed as a flexible body. The virtual vehicle model was set up according the actual parameters of the springs, dampers, tire stiffness and silent blocks from VW E-UP. Subsequently, the model was tuned up according the results from real measurements of the vertical dynamics of VW E-UP. Frequency analysis was performed to evaluate the effect of modifying vehicle parameters on vertical vehicle dynamics

Key words: Virtual vehicle, MSC ADAMS/CAR, Vertical dynamics, Frequency analysis

1. INTRODUCTION

At present time, vehicle producers are forced to bring new vehicle models to market as quickly as possible and at the lowest cost. Companies, if they want to succeed in competitive struggle, put pressure on designers. One of the tools used in CAE in car development is the use of MBD (i.e. Adams / Car program by MSC Software) simulations at all stages of vehicle development.

Vertical dynamics of the vehicle is influenced by number of parameters, where is need to know their effect on the whole assembly and on the individual subassemblies of the vehicle. Through variation of these parameters, it is possible to tune the model for its higher efficiency.

2. SIMULATION VEHICLE MODEL

The MBD simulation software ADAMS/CAR was used to create a virtual MBD vehicle model. Fig. 1 shows the modeling process in ADAMS/CAR [1].

The basic building block of the model is the so-called template. Based on the templates, the vehicle subsystems are then defined. The group of subsystems group is then assembled together with the appropriate stand into the vehicle assembly. Fig. 2 shows the used templates and subsystems in virtual vehicle VW E-UP [2].

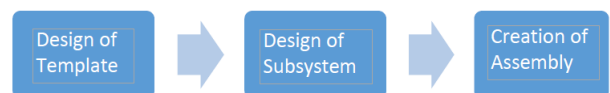


Fig.1: Philosophy of vehicle modelling in ADAMS/CAR

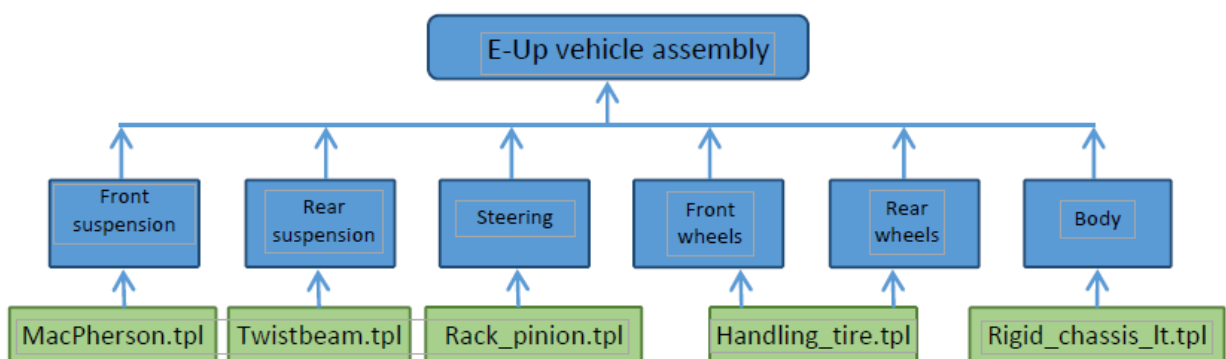


Fig.2: Used templates and subsystems in virtual vehicle

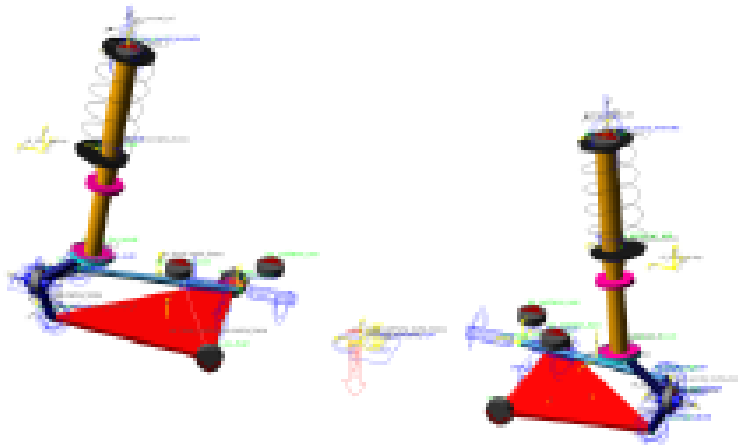


Fig.3: MacPherson template



Fig.4: MacPherson template with imported parts

The front suspension subsystem is based on the MacPherson.tpl template (Fig. 3). In the template, the coordinates of hardpoints point according to the cad model of the vehicle (Fig. 3) and then the cad parts of the individual suspension components where imported (Fig. 4).

The rear suspension subsystem is based on the Twistbeam.tpl template. The main part of suspension was modelled as flexible part. For the steering subsystem, the Rack_pinion.tpl template is used. Both the front and rear wheels are using the same template Handling_tire.tpl template. The body subsystem is based on the Rigid_chassis.tpl template.

The body of vehicle was imported as surfaces into the template. The position of the center of gravity was set by static simulation to match the values obtained by measuring the weight of actual vehicle.

The properties of a flexible body in an external FEM program are described in a Modal neutral file (*.mnf) that contains all the important data of inertia and flexible properties of the flexible body, as well as the information needed to integrate the flexible body into the ADAMS program. To determine the minimum number of mode shapes, a modified Craig-Bampton method (CMS) is used. This method reduces the size of the FEM model. It allows the selection of a subset of those degrees of freedom that are not subject to modal superposition - boundary degrees of freedom. The advantage of the modal superposition is that the modal flexible body, even after the modal reduction of the number of its mode

shapes, replaces the deformation of the elastic body, which has many nodal degrees of freedom with a much smaller number of modal degrees of freedom [1] [2]. The torsion part of the axle bridge Fig. 5, its FEM representation is shown in Fig. 6. As a pre and post processor, Patran was used, as solver Nastran was used.

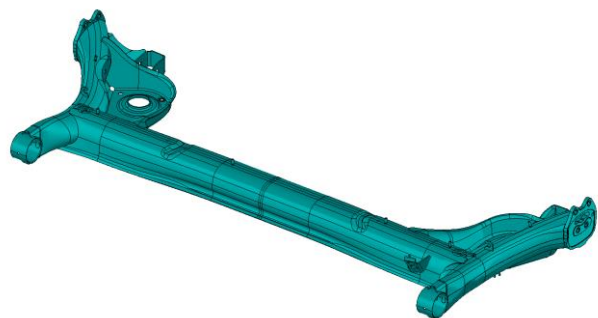


Fig.5: CAD model of twisted beam

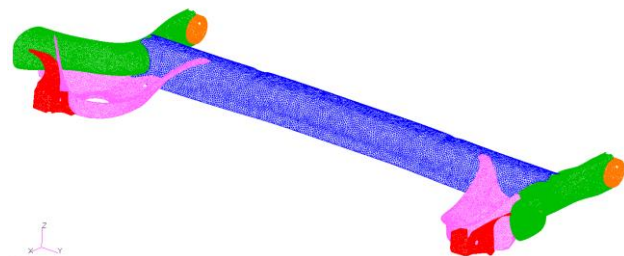


Fig.6: FEM model of twisted beam

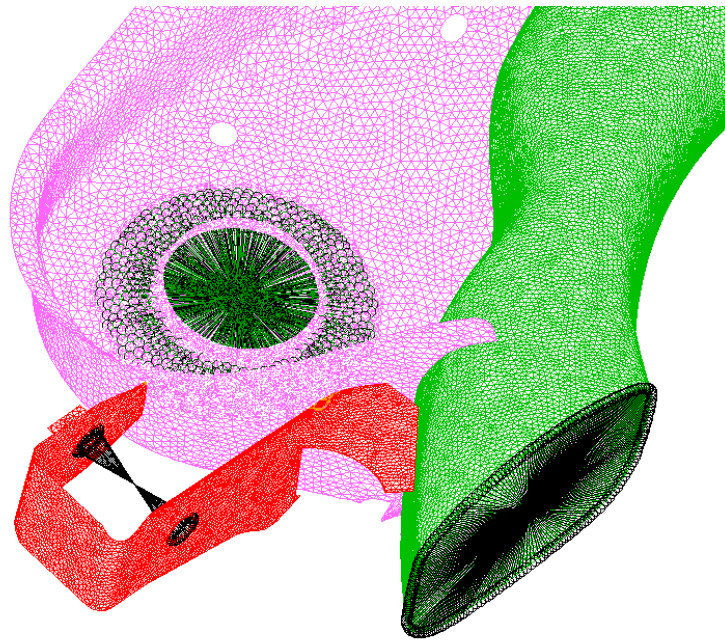


Fig.7: Connections of boundary node with internal node

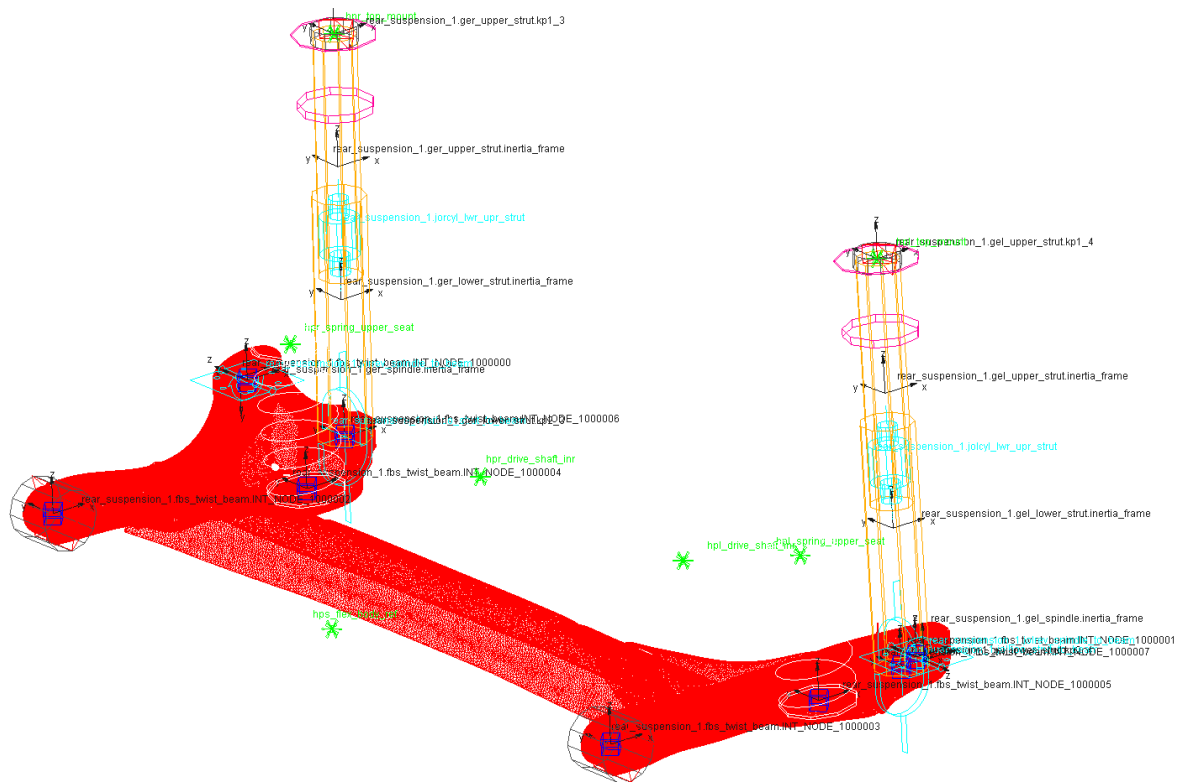


Fig.8: Template of rear suspension

In FEM model a shell element type was used. The model contains also 8 boundary nodes. For connection of the inner nodes, with boundary nodes the element RBE2 was used. The degree of freedom of border nodes were removed using the DOF List. Fig. 7 shows detail of the resulting boundary node connections with internal nodes. Fig. 8 shows template with flexible component. Fig 9 shows finished virtual vehicle VW E-UP.

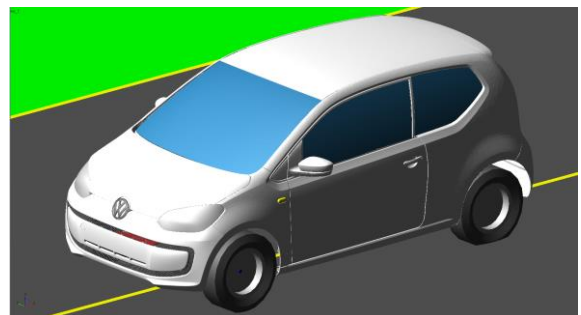


Fig.9: Virtual VW E-UP vehicle

3. SETTING UP THE VEHICLE MODEL

The virtual VW e-UP model has to be tuned up to describe its properties as precisely as possible. This tuned virtual model can then be used in simulations with acceptable accuracy of results.

The individual parameters (springs characteristics, dampers characteristics, bushing properties, wheel properties) were defined in the virtual model based on the real parameters of the VW E-UP vehicle, according manufacturers data.

Verification of the accuracy of the virtual vehicle model was carried out based on the results of the VW e-UP experimental measurements. Vehicle passes over speed bump, where acceleration was recorded on the front (Fig. 10) and rear suspensions, several points of the chassis and the driver's seat. For the analysis of the measurements, a camera record with the 240 pictures per second was recorded [6]



Fig.10: Comparison of simulation and camera record

The accuracy of the virtual vehicle model with the results of real vehicle measurements was performed by comparing the acceleration of the vehicle chassis obtained from the simulation and the experimental measurements (Fig. 11).

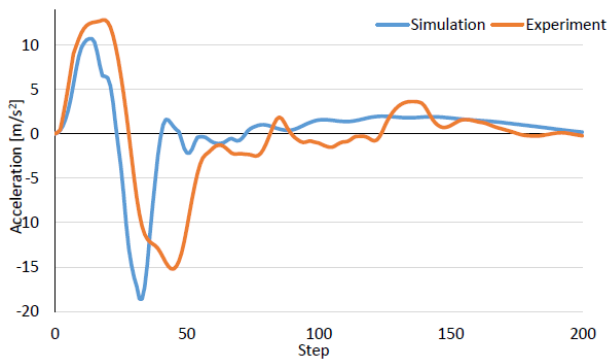


Fig.11: Acceleration of vehicle chassis

The accuracy of the virtual model was determined by the smallest squares method from the acceleration times obtained from the simulation and from the experimental measurement. The difference between simulated and measured data is 21.6%, which can be considered as sufficient accuracy [6].

4. IMPACT OF THE SUSPENSION PARAMETERS ON THE VERTICAL DYNAMIC

The vehicle's virtual model was used to analyze the impact of the suspension parameters on the vertical dynamics of the vehicle. The impact of the suspension

parameters was evaluated by frequency-amplitude response of vehicle chassis acceleration. The frequency-amplitude response of the acceleration of the vehicle chassis was realized by changing the selected vehicle suspension parameters, namely the stiffness of the springs, the characteristics of the dampers and the radial stiffness of the tires.

The virtual vehicle model was excited with a swept signal with a frequency range of 0 to 20 Hz and a constant amplitude. Subsequently, the time domain data was transformed by the FFT method into a frequency domain in which the effect of the change of the suspension parameters on the vehicle frequency of the sprung and unsprung mass can be assessed, as well as the acceleration amplitude of the vehicle chassis. The result is a course that has two distinct maxima, first defining the natural frequency of the suspended mass - the chassis of the vehicle, and the second maximum defining the natural frequency of the unsprung mass - the suspension, the brakes and the wheels [6].

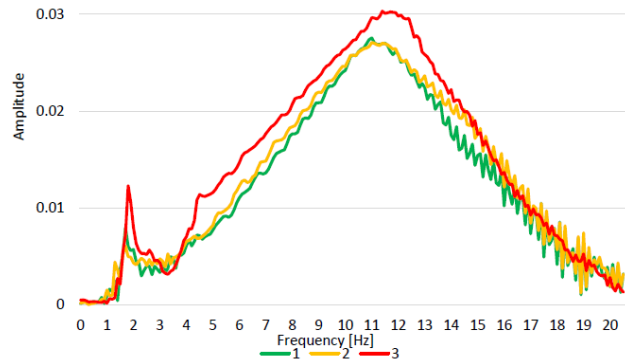


Fig.12: Amplitude-frequency response of chassis CG acceleration – impact of spring stiffness

Fig. 12 shows a graph of the frequency analysis when the stiffness of springs is changed. The original spring stiffness value is 1 (green color), decreased spring stiffness 2 (orange) and increased spring stiffness 3 (red), Tab. 1.

Table 1: Spring stiffness values and eigenfrequencies

1		2		3	
Stiffness 28 N/mm		Stiffness 25 N/mm		Stiffness 56 N/mm	
Chassis	Suspension	Chassis	Suspension	Chassis	Suspension
1,660 Hz	10,742 Hz	1,660 Hz	10,742 Hz	1,758 Hz	11,133 Hz

The greatest differences in the change in stiffness of the springs arise in the area of the natural frequency of chassis. The acceleration of the chassis in the area of the first resonant peak decreases when the stiffness of the

springs decreases. This will increase the driving comfort and also the safety of driving in the area of low excitation frequencies, but this is limited by vehicle design constraints. In the area of the second resonant peak, the change in stiffness of the springs is not as significant as in the previous region [5].

Fig. 13 shows a graph of the frequency analysis when the characteristic of dampers is changed Tab. 2.

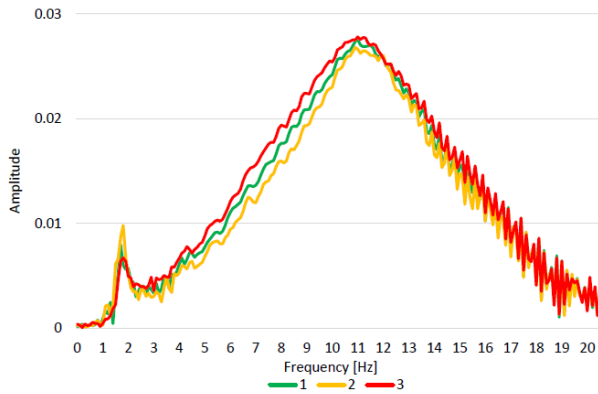


Fig.13: Amplitude-frequency response of chassis CG acceleration – impact of damper characteristic

The original characteristics of the damper 1 (green color), reduced characteristic 2 (orange) and increased characteristic 3 (red); is shown in Fig.14.

Near the first resonant tip, increased damping reduces the amplitude of chassis acceleration. In the region of the second resonant tip, increased damping slightly increases the acceleration of the chassis, tab. 2, Fig. 13.

Fig. 14 shows the amplitude frequency response of the chassis acceleration of the vehicle, which describe the change in radial stiffness of the tire. The original tire's radial stiffness value is 1 (green), decreased tire stiffness 2 (orange) and increased tire stiffness 3 (red).

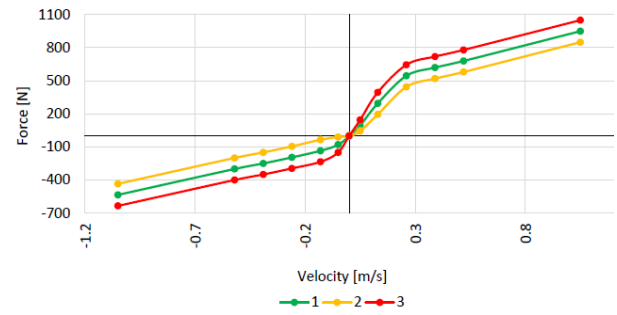


Fig.14: Damper characteristics

The higher radial stiffness of the tire increases eigenvalue of suspension. The acceleration amplitudes of the chassis are rising and shifting to higher exciting frequencies. The soft tire can therefore substantially reduce the amplitudes in the area of the second resonant tip as the soft springs of the spring unit reduce the amplitudes in the area of the first resonant tip [3], [4], [5].

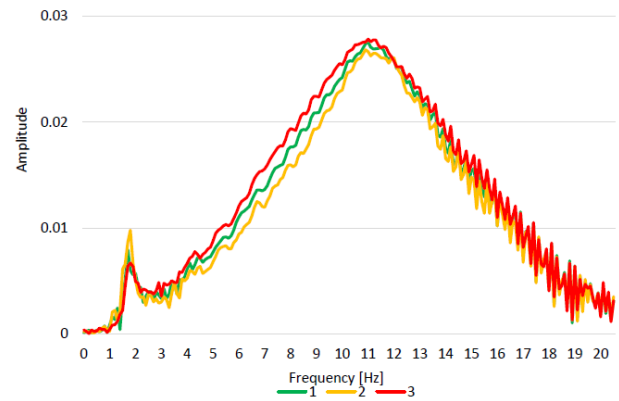


Fig.14: Amplitude-frequency response of chassis CG acceleration – impact of damper characteristic

Table 2: Eigenfrequencies

1		2		3	
Chassis	Suspension	Chassis	Suspension	Chassis	Suspension
1,660 Hz	10,742 Hz	1,758 Hz	10,645 Hz	1,758 Hz	10,742 Hz

Table 3: Values of radial tire stiffness and eigenfrequencies

1		2		3	
Stiffness 150 N/mm		Stiffness 100 N/mm		Stiffness 200 N/mm	
Chassis	Suspension	Chassis	Suspension	Chassis	Suspension
1,660 Hz	10,742 Hz	1,563 Hz	10,254 Hz	1,660 Hz	11,426 Hz

5. CONCLUSION

The VW E-Up Virtual Vehicle was built in the ADAMS/CAR environment based on the CAD model of the vehicle. In the CAD models, the coordinates of the points of interest (hardpoints), the mass and the moments of inertia of the individual components of the subsystems

were measured. The characteristics of the force elements (springs, dampers, silent blocks, tires) were defined according to the manufacturer's data. The model was tuned to the results of experimental measurement, which provided sufficient accuracy for the virtual model. The precision of the model could be further increased by using a more accurate chassis model (flexible chassis),

use front antiroll bar, using a more accurate tire model (ftire) [3] [5].

The virtual model of vehicle will also be used to simulate and compare with experimental measurements of other riding maneuvers. The flexible rear suspension beam will also be verified by tensometric measurement.

The results of the effect of the spring parameters on the vertical dynamics of the vehicle can be summarized as follows:

- The stiffness of the springs should be small in terms of driving comfort and driving safety. However, the small stiffness of the spring increases its deflection, which is limited by the design conditions.
- The damping coefficient of the dampers should be relatively larger so that the relative attenuation is in the range of 0.2 to 0.3.
- The weight of the unsprung mass does not affect the comfort of the ride but should be small in terms of driving safety.
- radial stiffness of the tire should be in terms of comfort and driving safety as small as possible, but this in turn worsens the transverse stability.

This work was supported by the R&D Agency: APVV-15-0524

REFERENCES

- [1] BUCHA, J. (2009) Modelovanie prognózovania zostatkovej životnosti vybraných súčastok špeciálnej techniky, Alexander Dubcek University of Trencin, Faculty of Special Technology, Dissertation thesis, Trencin
- [2] BUCHA, J., GAVAČOVÁ, J., MILESICH, T. (2015) Application of Skeleton Method in Interconnection of Cae Programs Used in Vehicle Design, Scientific Proceedings Faculty of Mechanical Engineering. Volume 22, Issue 1, ISSN 1338-5011
- [3] BLUNDELL, M., HARTY, D. (2004) The multibody system approach to vehicle dynamics, Elsevier Butterworth-Heinemann, ISBN 0-7506-5112-1
- [4] Vlk, F. (2006) Podvozky motorových vozidel : Pneumatiky a kola, Zavěšení kol, nápravy, Odpružení, Řídicí ústrojí, Brzdové systémy. 3. Vyd. Brno: nakladatelství a vydavatelství VLK ISBN 80-239-6464-X
- [5] Vlk, F. (2003) Dynamika motorových vozidel. Brno: nakladatelství a vydavatelství VLK, 3. ISBN 80-239-0024-2
- [6] FRANKO, V. (2017) Vplyv parametrov pruženia na zvislú dynamiku vozidla, Diploma thesis, Faculty of Mechanical Engineering, STU in Bratislava

CORRESPONDANCE



Jozef BUCHA, Ing., PhD.
Slovak University of Technology
Faculty of Mechanical Engineering
Námestie Slobody 18
812 31 Bratislava, Slovakia
jozef.bucha@stuba.sk



Ján DANKO, Ing., PhD.
Slovak University of Technology
Faculty of Mechanical Engineering
Námestie Slobody 18
812 31 Bratislava, Slovakia
jan.danko@stuba.sk



Tomáš MILESICH, Ing., PhD.
Slovak University of Technology
Faculty of Mechanical Engineering
Námestie Slobody 18
812 31 Bratislava, Slovakia
tomas.milesich@stuba.sk

THE NEW METHOD OF INCREASING THE AMOUNT OF RESIN IN THE WINDING OF MOTOR

Bohumil KOTLÁRIK
Janka SULOVIÁ
Zuzana FILOVIÁ
Alena KOZÁKOVÁ
Katarína KUBALOVÁ
Daša KRUPEJOVIÁ

Abstract: *Dynamic progress is supposed to drive all areas of industry inexorably forward, especially referring to the electrical industry and modernization and expansion of production of electrical rotating machines and transformers in particular.*

In terms of operational life of each electrical appliance, the most important component is its insulation system. Primary and secondary insulation forms the basic insulation of electrical system. Secondary insulation, known as secondary impregnation process is considered to define the process of wire insulation, usually followed by primary insulation. This is a chemical process by application of which impregnating resins increases mechanical stability of windings and protect insulated windings against mechanical damage, moisture and other environmental influences. The role of impregnating resins in windings is mostly strengthening of windings and heat transfer. The operational life of insulation system however is significantly dependent on its influence on electrical insulating properties (varnish compatibility, compatibility with other materials of insulation system based on construction) and an exact type of motor or transformer. Last but not the least, is inertness against metal components of engine, transformer tin sheets or resistance to oil, or freon's when using electrical rotating machines and transformers are required in specifically defined environment conditions: oil standards at transformers, CFCs in engines operating in an environment of refrigerants Research to further modify the impregnating resin to increase the life of electrical rotating and non-rotating machines (increasing content of resin in the motor windings) for better heat dissipation, improving the hydrophobicity of the impregnating resin and the better protection of metal transformers from corrosion caused by moisture and other conditions are caused by the legislation. In order to reduce energy consumption and thus CO₂ emissions produced by the European Union relevant legislation. Energy use and efficiency of induction motors deals EuP (Energy using Product) - Part 11 respectively of Directive EU2009 / 125 / EC. These guidelines have been incorporated into the legislation of all European Union countries. To provide more resin in motor winding, we tested a number of ways, but only one met the stringent criteria: In an existing technology, by dipping after one impregnation at least 20% increase of the resin's content in the winding. The purity of the stator core has to be good in order to avoid the need of cleaning the core.

Key words: *Impregnating resin, viscosity behavior, stators frame size to 160 mm*

1. INTRODUCTION

The requirement for an increase of cured resin in the winding by 20 % was motivating for us. For these reason, several possibilities were tested, excluding the increase of the resin in the winding we also observed the increase of the capacity measured [1] between the winding and the ground before impregnation and after impregnation. This methodology is used to control the quality of impregnation of winding. It allows relatively easy to check the quality of impregnation (amount of resin in the winding and its degree of curing). The requirement to

increase the resin content in the winding is related to the requirement for better resistance of the engine surges when speed-controlled frequency converter is used, to improve the heat transfer from the winding and to require of a slower increase temperature in the winding after the rotor stops, thermal protection to be able to respond to this situation with disconnection from the electrical supply and thereby prevent an engine breakdown. To control the increase of the resin content in the winding, stators with shaft height 132 mm were used. As the reference standard, a commonly used resin with the styrene monomer was used and to increase the resin content in the winding by increasing the viscosity,

respectively, by increasing of the flow time was tested. At the same time, it was tried to impregnate stators with other types of resins (epoxy and acrylic resins). Subsequently, to increase the resin content in the winding by increasing the degree of condensation of the basic esterimid base resin was tried. [2] Even if these measurements have not led to the desired results, the flow properties of the resin were modified. Its thixotropic properties were improved and so the desired result was achieved.

2. BACKGROUND

For impregnation of stators, dipping technology was used. The temperature of the resin and the stator depending on the viscosity of the resin used were adjusted. With styrene types non-heated stators were dipped in resin with ambient temperature and with other resins with higher viscosity preheated stators were impregnated at a temperature of 30 – 60 °C in resin with a temperature 32 – 35 °C. The temperature was chosen according to the viscosity of the resin to achieve good wetting of the stator windings for the required time of impregnation. Table 1 shows the types of resins used for impregnation with their basic processing properties.

Table 1: Used resins and their processing properties

Type of resin	Viscosity at 25 °C [mPa·s]	Gelling time at 120 °C [min/s]	Gelling time at 130 °C [min/s]	Gelling time at 150 °C [min/s]
Styrene no. 1	87s *	4/45	3	1/45
Styrene no. 2	34s*	4/30	3	1/45
Epoxy no. 3	576		25/15	10/45
Acrylate no. 4	1403,5	17	6	2/15
Acrylate no. 5	866,7	15	5/45	2
Acrylate no. 6	1403,5	17	6	2/15
Acrylate no. 7	866,7	15	5/45	2
Acrylate no. 8	1403,5	17	6	2/15
Acrylate no. 9	559		6	
Acrylate no. 10	673	13/45	5/45	2/30
Acrylate no. 11	955,5		5	

* Flow time according to DIN 53211 through 4 mm nozzle at temperature 23°C.

The stators of shaft height of 132 mm were impregnated. Table 2 contains material balance of impregnation.

Table 2: Material balance of impregnation

St. no.	Resin	Mass of stator before impreg. [kg]	Mass of stator after impreg. [kg]	Mass of stator after curing [kg]	Mass of resin in stator [g]
4	St. no.1	18,043	18,371	18,192	149
5	St. no. 1	18,040	18,363	18,189	149
6	St. no. 2	18,050	18,312	18,165	115
7	Epox. no. 3	18,053	18,355	18,162	109
8	Ac. no. 4	18,007	18,416	18,147	140
9	Ac. no. 5	18,043	18,415	18,180	137
10	Ac. no. 6	18,059	18,470	18,177	118
11	Ac. no. 7	18,055	18,414	18,175	120
12	Ac. no. 8	18,044	18,433	18,166	122
13	Ac. no. 9	18,044	18,355	18,169	125
14	Ac. no. 10	18,046	18,370	18,163	117
15	Ac. no. 11	18,040	18,404	18,182	143

With styrene resin with flow time of 87 s the desired increase of resin in the winding, but cleanliness of core was not good. Resin with flow time of 87 s forms a thicker layer on the skeleton. Due to the requirement to increase the growth of capacity between the wires connected to the node and ground, capacity was measured before impregnation and after curing resin in the winding. The results are shown in Table 3.

Table 3: Increase of capacity between the phases and ground

Stator no.	Resin	Increase of capacity [%]
4	Styrene no. 1	10,54
5	Styrene no. 1	11,14
6	Styrene no. 2	8,58
7	Epoxy no. 3	21,08
8	Acrylate no. 4	22,02
9	Acrylate no. 5	15
10	Acrylate no. 6	18,17
11	Acrylate no. 7	16,92
12	Acrylate no. 8	18,21
13	Acrylate no. 9	16,33
14	Acrylate no. 10	15,02
15	Acrylate no. 11	16,02

Table 2 and 3 shows that the increase of capacity after impregnation does not always coincide with the material balance. This fact can be explained so that part of resin may remain on the skeleton, so it does not fill the air space between the winding and the ground as much as the other resin with a higher capacity increase, but the most significant effect on the increase of capacity after impregnation has the relative permittivity of cured resin. The higher is the relative resin permittivity, the higher is the increase in capacity after impregnation at the same content of the resin in the winding. The relative permittivity of resin also depends on the degree of cure. This fact was confirmed on the stator no. 7, where the capacity increase was measured after the basic curing for 3 hours at 160 °C and followed by 15 hours curing at 160 °C.

Table 4: Effect of post curing on capacity increase after impregnation

Stator no.	Resin	Increase of capacity [%]
7	Epoxy no. 3	21,08
7	Epoxy no. 3 post cured	14,46

Despite the same amount of resin in the winding after post curing, the measured capacity increase dropped from 21,08 % to 14,46% which is a decrease of approximately 31,5%. Based on these measurements, we have come to a finding that a method of measuring the increase of capacity is suitable for the quality control of impregnation for the used type of resin. However, it is not possible to evaluate the amount of different resins in the winding by this method since even at higher resin contents in the winding, the capacity increase may be less after impregnation. The increase of capacity is not affected only by the amount of resin in the winding, but also its relative permittivity. It depends on the type of resin and on the degree of its cure. Whereas the best increase in the amount of resin in the winding has been achieved with the styrene resin of higher viscosity, it has been attempted to

increase the content of the resin in the winding by increasing the condensation degree of basic polyesterimide resin dissolved in styrene while maintaining the flow time of resin suitable for dipping technology. Four types of resins were prepared, one with a basic degree of condensation and three with an increase of 55 %, 100 % and 148 %. Resins had the same flow time and the same gelling time. However the increase in the amount of resins was, only between 1,2 to 3 %. After this finding, it has been decided to increase the amount of resin in the winding by changing its flow properties.

3. ADJUSTMENT OF FLOW PROPERTIES

In the impregnation process, it is important that the resin quickly penetrated into the winding, that is, it has the lowest viscosity when entering the winding, but it has the highest viscosity to drop as much as possible from the winding. This property is called thixotropy. Four types of thixotropic agents in various amounts were tested and these resin increment was compared after impregnation twisted coils prepared according to IEC 61037 Met. A. While the growth of untreated cured resin in the winding twisted coil was 61,73 % wet resin, at the modified resin with thixotropic agent, it was up 72,08 %. Some types have been discarded because of worsening stability of the resin, by some there have been a problem with their incorporation in to the system. Finally, the problem of sedimentation of thixotropic agent had to be solved. Three types of anti-sedimentation additives in various amounts have been tested. Some have influenced the stability of the resin and shortened the time of gelling. In Table 6 there is compared the stability of the thixotropic resin and the original resin at 40 °C.

Table 5: Stability of resins

Resin	NK 50/1K		NK 50/1KTxn	
	Gelling time at 100 °C [min/s]	Viscosity at 23 °C [mPa.s]	Gelling time at 100 °C [min/s]	Viscosity at 23 °C [mPa.s]
Start	25 – 25/30	155,9	27/45 – 28/45	144,1
1 week	20/15 – 21	187,3	22/30 – 23/30	170,4
2 week	14/15 – 14/30	192,8	14/15 – 14/30	190,1
3 week	10/15 – 10/30	203	13/30 – 14	220,1
4 week	gelled	gelled	gelled	gelled

As shown in Table 5 the stability of both resins was practically the same. In monitoring the stability of both resins there was for six months no changing of the behaviour occurred due to the thixotropic adjustment. Table 6 compares the dependence of viscosity classical NK 50/1K and thixotropic NK 50/1KTxn on speed gradient. Table 6 shows that at low speed gradient thixotropic treatment achieves a higher viscosity than the original resin and at higher gradient it achieves a lower viscosity than the original resin. The dependence is also identified in Figure 1.

Table 6: Comparison of viscosity versus the speed gradient for NK 50/1K and NK 50/1K Txn

Speed gradient [s ⁻¹]	NK 50/1K Txn Viscosity at 25 °C [mPa.s]	NK 50/1K Viscosity at 25 °C [mPa.s]
11,7	220	165
19,5	181	181
32,5	158	158
54,3	154	160
90,6	145	156
152,1	137	156
251,6	135	158
421,2	131	159
702	128	158
1170	126	157

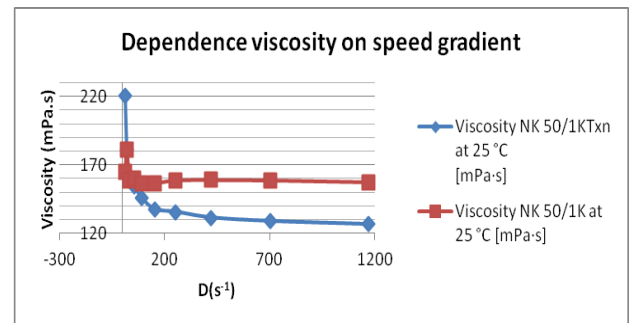


Fig. 1: Dependence of viscosity on speed gradient

Thixotropic properties were measured according to STN 67 3020 at 25 °C. From the measurements, viscosity for brushing, the viscosity at the beginning of leveling and the end of levelling and also thixotropic and relative thixotropic increase in viscosity were calculated according to the above standard. The data are presented in Table 7.

Table 7: Comparison of thixotropic properties of NK 50/1K Txn and NK 50/1K

Sample	η_b [mPa.s]	η_l [mPa.s]	η_s [mPa.s]	$\Delta\eta$ [mPa.s]	T
NK 50/1K	146,6	1252,5	1739,9	487,4	38,9
NK 50/1K Txn	130,9	1252,5	2549,4	1297	104,0

Viscosity η_b – with brush is viscosity of the resin when it start flow into the winding, η_l – viscosity at the start of leveling and η_s – viscosity on the end of levelling is viscosity of the resin on the end of dropping from winding, $\Delta\eta$ – thixotropic viscosity increase, T – relative thixotropic increase. It can be seen that on the start of impregnation of winding is viscosity of the thixotropic resin lower, so it flows into winding more quickly, but on the end of dropping its viscosity rises and it flows from winding more slowly.

3.1 Thin layer curing

NK 50/1K and NK 50/1K Txn resins were cured on Al plate for 2 hours at 140 °C. Layer thickness was measured. The results are shown in Table 8.

Table 8 Comparison of the coating thicknesses of NK 50/1K and NK 50/1K Txn

Resin	Thickness of layer up [mm]	Thickness of layer middle [mm]	Thickness of layer down [mm]
NK 50/1K	15,9	23,3	26,6
NK 50/1K Txn	26,2	40,0	43,6

From the Table 8 it can be seen, that on Al plate the thixotropic resin forms thicker film.

Strength of reinforcement the twisted and helical coil by impregnation

The most important role of the resin is reinforcement of the winding. In Table 9 are shown the values of bonding strength on the helical and twisted coils. It is measured according to EN 61033 – article 2.1 Method A and 2.2 Method B. The coils were cured for 2 hours at 140 °C.

Table 9 Bonding strength on twisted and helical coil

Resin	Temperature [°C]	Twisted coil Met. A	Helical coil Met. B
		Bonding strength [N]	Bonding strength [N]
NK 50/1K	23	167	118
	155	28	16
	180	28	14
NK 50/1K Txn	23	165	111
	155	24	17
	180	27	17

Table 9 shows that the bonding strength is comparable for NK 50/1K and NK 50/1K Txn and is very good for styrene resin.

Dielectric strength of the coating film

Dielectric strength of the coating film is measured according to EN 60243-1 (curing for 2 hours at 140 °C). For NK 50/1K, this property is defined in the technical specifications listed in Table 10. The measured values for the thixotropic version comply with the intervals as required for classic NK 50/1K. Thixotropic treatment does not affect this property.

Table 10 Electrical strength of the coating film NK 50/1K and NK 50/1K Txn

Sample	Conditions	Dielectric strength [kV/mm]
NK 50/1K property defined in the technical specifications	23 °C	>70
	155 °C	> 60
	after 24 h. in water	> 35
NK 50/1K Txn	23 °C	112
	180 °C	88
	after 24 h. in water	61

Breakdown voltage and insulation resistance of the twisted pairs

The values of breakdown voltage and insulation resistance of the twisted pairs prepared according to the EN 60317-13 Gr. 2 Ø 0,85 mm impregnated in the resins NK 50/1K and NK 50/1K Txn are summarized in Table 11 and 12.

Table 11 Comparison of breakdown voltage NK 50/1K and NK 50/1K Txn

Resin	Breakdown voltage [V]
NK 50/1K	12 234
NK 50/1K Txn	12 352

Table 12 Comparison of the insulation resistance NK 50/1K and NK 50/1K Txn

Resin	Insulation resistance [Ω]
NK 50/1K	$3,8 \times 10^{11}$
NK 50/1K Txn	$3,2 \times 10^{11}$

From these measurements it can be seen that the thixotropic treatment NK 50/1K Txn does not deteriorate the value of breakdown voltage and insulation resistance compared to NK 50/1K.

Volume resistance

Volume resistance was measured according to STN 34 6460. The results are shown in Table 13.

Table 13 Volume resistance

Sample	Thickness [mm]	Volume resistivity [Ω·m]	Volume resistivity [Ω·m]	Temp. [°C]
NK50/1K	2,40	$6,1 \cdot 10^{14}$	$5,7 \cdot 10^{14}$	23
NK50/1K	2,66	$5,2 \cdot 10^{14}$		23
NK50/1K after 168 h in water	2,44	$6,3 \cdot 10^{13}$	$6,1 \cdot 10^{13}$	23
NK50/1K after 168 h in water	2,66	$5,9 \cdot 10^{13}$		23
NK50/1K at 180 °C	2,40	$8,2 \cdot 10^9$	$7,3 \cdot 10^9$	180
NK50/1K at 180 °C	2,66	$6,4 \cdot 10^9$		180
NK50/1K Txn	2,71	$6,2 \cdot 10^{14}$	$5,9 \cdot 10^{14}$	23
NK50/1K Txn	2,63	$5,5 \cdot 10^{14}$		23
NK50/1K Txn after 168 h in water	2,32	$3,6 \cdot 10^{13}$	$4,3 \cdot 10^{13}$	23
NK50/1K Txn after 168 h in water	2,41	$4,9 \cdot 10^{13}$		23
NK50/1K Txn at 180 °C	2,71	$6,0 \cdot 10^9$	$6,1 \cdot 10^9$	180
NK50/1K Txn at 180 °C	2,63	$6,2 \cdot 10^9$		180

The Table 13 shows that the thixotropic adjustment after a prescribed curing does not affect the volume resistance. Samples NK 50/1K Txn prepared from a sample NK 50/1K reach after prescribed curing the same values as impregnating NK 50/1K.

Comparison of the properties by DSC and TGA

Differential scanning calorimeter DSC-7 Perkin-Elmer was used for the DSC measurements. TGA measurements

were performed on a Seiko Extar termoanalyser simultaneous TG/DTA 6300 [3]. Uncured NK 50/1K and NK 50/1K Txn samples and the samples cured for 2 hours at 140 °C were analysed. In Table 14 there are the basic parameters for the curing of the both samples. The curing of thixotropic resin begins almost at the same temperature as the original resin and curing takes place at a temperature of about 2 °C higher.

Samples NK 50/1K Txn prepared from a sample NK 50/1K reach a prescribed curing the same values as impregnating NK 50/1K.

On the DSC measurements of the cured NK 50/1K and NK 50/1KTxn samples a complete cure of both resins after prescribed curing can be seen because they both have not expressed an exothermic peak, which was apparent in the uncured samples.

DTA/TGA measurements showed that the NK 50/1K have the same weight loss at lower temperatures than the NK 50/1K Txn. Table 15 and the Figure 2 show the dependence of the temperature at which both of the resins achieve the same material losses.

Table 14: Uncured samples NK 50/1K and NK 50/1K Txn

Sample	Curing temperature [°C]	Onset temperature [°C]
NK 50/1K	123 – 173	126,8
NK 50/1K Txn	125 – 178	126,5

Table 15: Cured samples NK 50/1K and NK 50/1K Txn

Losses of resin [%]	Temperature [°C]	
	NK 50/1K	NK 50/1K Txn
1	143	162
2	174	216
5	247	304

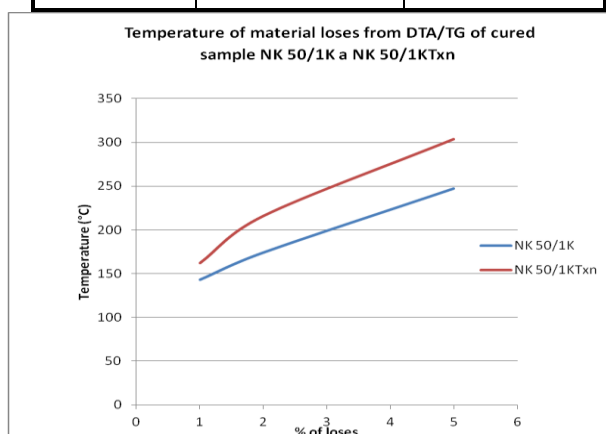


Fig.2 Temperature of material losses

DTA/TGA measurements of cured samples were used to determine at 1 %, 2 % and 5 % weight losses. From the measured results shown in Table 15 and Figure 2 the thixotropic treatment improves the thermos-oxidation stability of the cured resin.

Technological tests

Material balance of resin on the stator and increasing of capacity

After completing of all measurements that proved that thixotropic treatment of NK 50/1K resin in all aspects meets the qualities that good resin must have. The technological tests on stator have been performed. Stators of frame size 132 mm were used. Flow time of both resins at 23 °C was measured on DIN cup 4 = 40s, the gelling time at 100 °C of NK 50/1K was 24 minutes and NK 50/1K Txn was 30 minutes. The process of impregnation was: 5 minutes dipping into resin, stator was dipped in resin 10 minutes, 5 minutes emergence, dropping 20 minutes, 2 hours curing at 140 °C. After impregnation of stators and curing, increase of the cured resin in winding, capacity (measured before impregnation and after curing, in the Table 16 is mentioned only increase) and the purity of stator core (important in practice, minimizing cleaning during assembly) was evaluated. The results of these tests are summarized in Table 16.

Table 16: Increase of cured the resin NK 50/1K and NK 50/1K Txn in the stator frame sizes 132 mm and capacity increase after impregnation

Sample	Increase after curing [g]	Capacity increase [%]
NK 50/1K	128	9,45
	127	8,84
	127	10,75
NK 50/1K Txn	240	21,25
	246	23,02
	251	20,19

On stator frame size, the effect of thixotropy was even more pronounced than in laboratory tests It's probably because of the conductors of the test samples have a diameter of 0,315 mm and a stator winding wire have a diameter of 0,85 mm. Increase the amount of resin NK 50/1K Txn in the winding is significant compared to NK 50/1K. Also stator capacity at NK 50/1K Txn increased by about 11 % compared to NK 50/1K.

Cleanliness of stators

The purity of stators impregnated with NK 50/1K Txn (DIN 4/23 = 40 s, TS₁₀₀ = 30 min) is shown in the Figures 3 and 4. The purity itself stator, winding pre-impregnated faces, cut tipping winding and winding the stator grooves were checked.



Fig.3: Stator frame sizes 132 mm

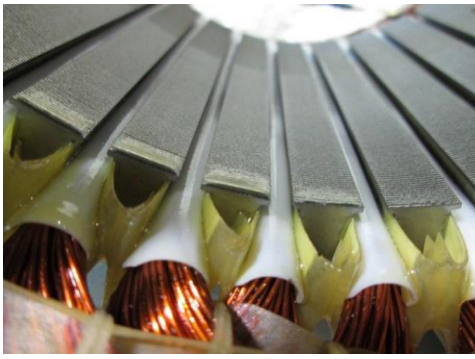


Fig. 4: Bottom inside part of the frame



Fig.5: Cut from upper side of winding



Fig.6: Segment of winding from slot

Compactness of winding on upper part of stator and of winding in slot with resin NK 50/1K Txn was very good. Stator pollution was minimal.

4. CONCLUSION

Increase the amount of resin in the winding while maintaining the purity of the core, has been managed by changing of flow properties of resin. Increase the amount of resin was checked on the stator of shaft height 80 mm, 132 mm and 160 mm. After impregnation with the resin with flow time of 43 s at 23 °C, the increase of the amount of the resin in the winding relative to the original was the following.

Table 17 Increase of resin and capacity

Frame size [mm]	Original content of resin [g]	Content of resin with thixotropic adjustment [g]	Increase of resin in winding [%]
80	54	71	32
132	130	240	85
160	240	400	66

Cleanliness of stator cores of all frame sizes impregnated with thixotropic treatment was better than with the original resin.

ACKNOWLEDGEMENT

This contribution was supported by APVV under contract no. APVV-14-0125 and APVV-15-0108

REFERENCES

- [1] KOTLÁRIK, B., VAŇKOVÁ, R., FILOVÁ, Z., *A new ERM winding impregnation quality assessment method* Diagnostika '11, Kašperské hory, 6-8 sept.2011 s 167-172
- [2] FILOVA, Z., KOZÁKOVÁ, A., KUBALOVÁ, K BOČKAJ, J UJHELYIOVÁ, A: *THIXOTROPIC ADJUSTMENT OF IMPREGNANTS WITH NANOADDITIVES AND its EFFECT TO PROCESSING AND FUNCTIONAL PROPERTIES*, IX. Slovensko - Česká konferencia POLYMÉRY, Stará Lesná, SR
- [3] ŠIMON,P.,DUBAJ,T.,: *DSC,DTA and TG measurements of samples NK 50/1K and NK 50/1KTxn*, STU FCHPT Bratislava May 2015

CORRESPONDANCE



Bohumil Kotlárík, p.ch., CSc.
VUKI a.s.
Rybničná 38
831 07 Bratislava
Slovakia
kotlarik@vuki.sk



Janka Sulová, Ing..
VUKI a.s.
Rybničná 38
831 07 Bratislava
Slovakia
sulova@vuki.sk

STATICAL ANALYSIS OF MEASUREMENTS IN A VEHICLE BRAKE TESTER

Radoš Bulatović
Janko Jovanović
Radoslav Tomović

Abstract: : This paper introduce a methodology of statical analysis of a measurements in a vehicle brake tester. On the base of 15 repeatedly conducted measurements, which is considered to be a large sample, it was shown that results of mesuremets are in accordance with the Gaussian distribution. Parameters of Gaussian distribution are determined by means of probability paper and the least square method that are used to calculate parameters of optimal approximating straigth line. Finally, a comparison of the results of conducted measuremets and the calculated values is performed.

Key words: mjerenje, greške mjerenja, normalna raspodjela, statistički test

OBRADA REZULTATA MJERENJA KOD UREĐAJA ZA PROVJERU SILE KOČENJA KOD MOTORNH VOZILA

Abstract: : U radu je data metodologija obrade rezultata mjerenja sile kod uređaja za provjeru sile kočenja kod motornih vozila. Na osnovu 15 puta ponovljenih mjerenja za jednu tačku, što je u ovom radu tretirano kao veliki uzorak, pokazano je da se mjerni rezultati pokoravaju normalnom zakonu raspodjele. Izvršeno je određivanje parametara normalne raspodjele pomoću vjerovatnosnog papira normalne raspodjele i na osnovu metode najmanjih kvadrata, određivanjem parametara optimalne prave. Na kraju je izvršeno upoređivanje rezultata sprovedenih mjerenja sa tačnim vrijednostima koji su dobijeni proračunom.

Ključne riječi: mjerenje, greške mjerenja, normalna raspodjela, statistički test

1. UVOD

Mjerenje neke veličine je samo prvi korak u saznanju i identifikaciji mjernog objekta. Sledeći, vrlo važan korak je matematička obrada dobijenih rezultata mjerenja. Kod samog mjerenja, bez obzira koliko je upotrijebljena opreme savršena i odgovarajuća, rezultati mjerenja u sebi sadrže, u manjoj ili većoj mjeri, greške mjerenja. Dakle, na osnovu neobrađenih rezultata mjerenja, ne može se pouzdano zaključiti o objektu mjerenja. Takođe, netačni i grubi rezultati mjerenja mogu iskriviti saznanje i isključiti mogućnost saznanja o objektima mjerenja odnosno ciljevima samog ispitivanja. Znači, samo dovoljno tačne rezultate mjerenja ima smisla matematički obrađivati, analizirati i na kraju ocjenjivati.

2. GREŠKA MJERENJA

Apsolutna greška mjerenja G_a je razlika između rezultata mjerenja i prave vrijednosti mjerene veličine:

$$G_a = x - x_0 \quad (1)$$

gde su:

- x izmjerena vrijednost;
- x_0 prava vrijednost mjerene veličine.

Apsolutna greška je algebarska vrijednost koja ima istu dimenziju kao i mjerene veličina.

Relativna greška mjerenja G_r je jednaka odnosu apsolutne greške mjerenja G_a i prave vrijednosti mjerene veličine x_0 :

$$G_r = \frac{x - x_0}{x_0} \quad (2)$$

Obadviije prethodne definicije ne pomažu dovoljno, jer se zapravo ne zna prava vrijednost mjerene veličine. S obzirom na to mora da se procijeni vrijednost mjerene veličine, koristeći rezultate mjerenja. Procijenjena vrijednost mjerene veličine naziva se **usvojena (dogovorena) vrijednost** mjerene veličine. Najčešće za dogovorenu vrijednost uzima aritmetička sredina rezultata mjerenja \bar{x} . Koristeći dogovorenu vrijednost umjesto tačne vrijednosti dobija se da su apsolutna i relativna greška mjerenja:

$$G_a = x - \bar{x}; G_r = \frac{x - \bar{x}}{\bar{x}} \quad (3)$$

Jasno je, da ako se želi da se procijeni vrijednost kao i greška pri mjerenjima, mora da se uradi niz mjerenja pod istim ili vrlo sličnim uslovima.

Pri mjerenjima, treba da se razlikuju:

1) **Grube greške mjerenja** koje nastaju nepažnjom ili nepravilnim rukovanjem instrumentom, i one se neće razmatrati.

2) **Sistematske greške mjerenja** nastaju zbog nesavršenosti metoda mjerenja i mjernih sredstava i mjera, nesavršenosti mjernog objekta, i predvidivih uticaja sredine i uticaja lica koje mjeri. Većina sistematskih grešaka ima stalnu vrijednost, pa se mogu eliminisati već definisanim korigovanjem rezultata. Cilj mjerenja je da se minimiziraju sistematske greške, ili da se usavrši postupak obrade rezultata na takav način da se automatski eliminiše sistematska greška mjerenja.

3) **Slučajne greške mjerenja** nastaju pri mjerenju pod istim uslovima, pravilno rukujući instrumentacijom i posledica su stohastičkog ponašanja u mjernom sistemu. Slučajna greška se mijenja i nije predvidljiva u toku mjerenja. Slučajne greške mjerenja čine rezultat nepouzdanim i nesigurnim, i njihov uticaj se ne može potpuno eliminisati, već samo značajno smanjiti.

Primenjujući statističke metode analize može se korigovati rezultat mjerenja i minimizirati uticaj slučajnih grešaka ako je obavljen dovoljno veliki broj mjerenja.

3. STATISTIČKA OBRADA REZULTATA REZULTATA MJERENJA

Zadatak statističke obrade rezultata je procjena prave vrijednosti mjerene veličine i procjena mjerne nesigurnosti korigovanog rezultata mjerenja.

Procjena prave vrijednosti mjerene veličine uključuje:

- 1) Određivanje najvjerovatnije vrijednosti mjerene veličine, za koju se pokazuje da je jednaka aritmetičkoj sredini rezultata mjerenja;
- 2) Korigovanje ove vrijednosti za poznate sistematske greške mjerenja.

Procjena mjerne nesigurnosti uključuje određivanje njene slučajne komponente na osnovu ponovljenih mjerenja, i sistematske komponente kao posledice nepoznatih (neisključenih) sistematskih grešaka.

Ponavljajući mjerenja jedne iste veličine pod istim uslovima, koristeći pri tome isto mjereno sredstvo sa dovoljno velikom rezolucijom, dobijaju se razne vrijednosti rezultata. Ako se poče od pretpostavke da su sve sistematske greške eliminisane, u tom slučaju aritmetička sredina rezultata mjerenja se može smatrati pravom vrijednošću.

Srednja vrijednost mjerne veličine ili aritmetička sredina je:

$$\bar{x} = \frac{x_1 + x_2 + \dots + x_n}{n} = \frac{1}{n} \cdot \sum_{i=1}^n x_i \quad (4)$$

gdje su x_i rezultati mjerenja, a n broj mjerenja.

Stvarne greške pojedinačnih mjerenja ili apsolutne greške su:

$$\Delta x_i = x_i - x_0 \quad (5)$$

gde je x_0 nepoznata prava vrijednost.

Ako se saberu sve apsolutne greške, dobija se:

$$\sum_{i=1}^n \Delta x_i = \sum_{i=1}^n x_i - \sum_{i=1}^n x_0 = \sum_{i=1}^n x_i - n \cdot x_0 \quad (6)$$

Prava vrijednost mjerene veličine je prema tome:

$$x_0 = \frac{1}{n} \cdot \sum_{i=1}^n x_i - \frac{1}{n} \cdot \sum_{i=1}^n \Delta x_i \quad (7)$$

Prvi član sa desne strane jednačine je srednja vrijednost \bar{x} , a drugi član se može obilježiti sa ε i on je:

$$\varepsilon = \frac{1}{n} \cdot \sum_{i=1}^n \Delta x_i \quad (8)$$

aritmetička sredina stvarnih apsolutnih grešaka pojedinačnih mjerenja.

S obzirom da je podjednaka vjerovatnoća pojavljivanja pozitivnih i negativnih apsolutnih grešaka (ako su sistematske greške eliminisane), može se napisati:

$$x_0 = \bar{x} - \frac{1}{n} \cdot \sum_{i=1}^n \Delta x_i = \bar{x} \pm |\varepsilon| \quad (9)$$

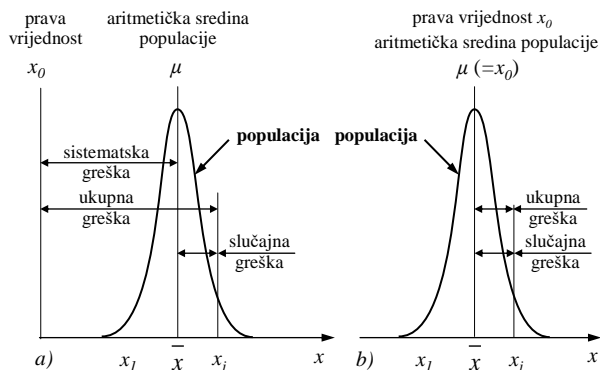
Prema Gausovoj teoriji slučajnih grešaka, pri proučavanju slučajnih grešaka na rezultate mjerenja, treba početi od dvije pretpostavke:

1. Pri velikom broju ponovljenih mjerenja jednako vjerovatno nastaju slučajne greške jednakih vrijednosti, ali suprotnog znaka;
2. Vjerovatnoća pojavljivanja malih grešaka veća je od vjerovatnoće pojavljivanja velikih grešaka.

Na osnovu prve pretpostavke može se zaključiti da je $\lim_{n \rightarrow \infty} \varepsilon = 0$, što znači da je pri velikom broju ponovljenih

mjerenja aritmetička sredina rezultata mjerenja jednaka pravoj vrijednosti mjerene veličine.

Pretpostavljajući da je raspodjela grešaka slučajna može se sa grafikom jasno uočiti mjerenje u kome je prisutna sistematska greška (lijevo), u odnosu na mjerenje u kome su eliminisane sistematske greške (desno). U slučaju mjerenja u kome postoje sistematske greške, aritmetička sredina populacije nije jednaka pravoj vrijednosti mjerene veličine i odstupanje je jednako sistematskoj greški, a greške mjerenja su jednake zbiru slučajne i sistematske greške.



Sl.1: Rezultat mjerenja

Aritmetička sredina populacije i mjerenja se uvijek razlikuju, jer je broj uzoraka u populaciji mnogo veći u odnosu na uzorak, pa greške pri mjerenju uzorka zapravo ne ispunjavaju ranije navedene osobine slučajne veličine.

Bliskost srednjih vrijednosti populacije i uzorka se kvantitativno određuje koristeći standardnu devijaciju.

4. GRAFIČKO PREDSTAVLJANJE RASPODJELE REZULTATA MJERENJA

Pri ponavljanju mjerenja iste veličine pri istim uslovima, s obzirom da se koristi mjerni instrument određene tačnosti, izmjeriće se ista vrijednost više puta, što znači da će se ista greška mjerenja ponavljati.

4.1. Gustina raspodjele vjerovatnoće mjerenja

Najjednostavnija mogućnost za grafičko predstavljanje mjerenja služi histogram učestalosti pojave rezultata mjerenja (sl.2). Mjerenjem se registruju rezultati mjerenja (sl.2a). Grupisanjem ovih rezultata mjerenja dobija se prikaz dat na sl.2b. Da bi se dobila grafička predstava o učestalosti pojave rezultata mjerenja crta se histogram. Apscisa se dijeli na intervale, koji se označavaju kao klase. Rezultati mjerenja se sređuju po klasama. Rezultati mjerenja u različitim klasama predstavljaju se preko različitih visina stubića.

Za vrijednost na ordinati histograma može se uzeti apsolutna učestalost:

$$f_{abs} = N(\Delta x) \quad (10)$$

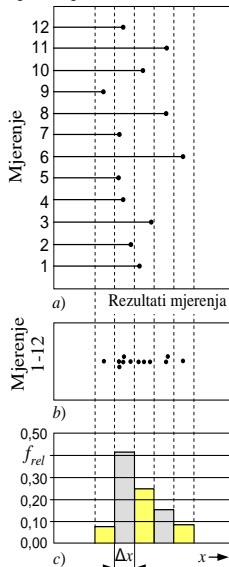
Uobičajeno se koristi relativna učestalost:

$$f_{rel} = \frac{N(\Delta x)}{n} \quad (11)$$

Ovdje su:

- $N(\Delta x)$ - broj rezultata mjerenja u klasi odnosno u intervalu Δx ,
- n - ukupan broj izvršenih mjerenja.

Na sl.2c prikazan je histogram učestalosti pojave rezultata mjerenja.



Podjela apcise na klase i uređenje rezultata mjerenja u pojedine klase označava se kao klasiranje. Pitanje broja klasa je važno pitanje. Broj klasa se ne može uvijek jednostavno ustanoviti. Broj klasa se bira tako da se ne izgubi suviše mnogo informacija.

Kao grubo približenje, odnosno prva procijenjena vrijednost za broj klasa z mogu da posluže sledeći izrazi:

$$\begin{aligned} z &\approx \sqrt{n} ; \\ z &\approx \sqrt{n} + 1 \\ z &\approx 1 + 3,3 \cdot \log n \\ z &\approx 5 \cdot \log n \end{aligned} \quad (12)$$

Sl.2 Histogram učestalosti pojave rezultata mjerenja

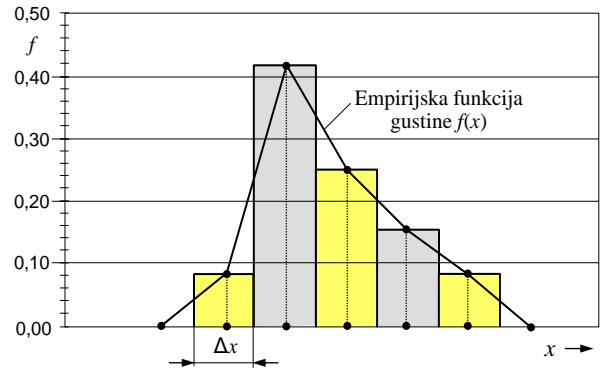
Širina intervala Δx određuje se izrazom:

$$\Delta x = \frac{x_{max} - x_{min}}{z} \quad \text{ili} \quad \Delta x = \frac{x_{max}}{z} \quad (13)$$

Ovdje su:

- x_{min} - najmanja izmjerena veličina;
- x_{max} - najveća izmjerena veličina.

Umjesto sa histogramom, pojava rezultata mjerenja se može opisati empirijskom funkcijom gustine raspodjele vjerovatnoće mjerenja $f(x)$ (sl.3). Empirijska funkcija gustine $f(x)$ se dobija tako što se sredine stubića u histogramu povezuju pravim linijama. Empirijski dodatak kod funkcije gustine znači da je funkcija gustine nacrtana na osnovu podataka registrovanih rezultata mjerenja.

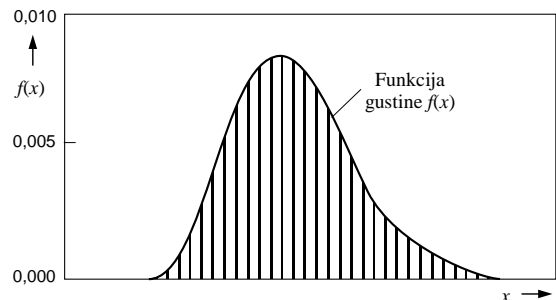


Sl.3 Histogram učestalosti rezultata mjerenja i empirijska funkcija gustine

Empirijska funkcija gustine može se odrediti izrazom:

$$f(x) = \frac{N(\Delta x)}{n \cdot \Delta x} \quad (14)$$

Kako se eksperiment vrši na malom uzorku, to je empirijska funkcija gustine raspodjele vjerovatnoće mjerenja dobijena na osnovu relativno malog broja podataka registrovanih rezultata mjerenja. Idealna funkcija gustine raspodjele vjerovatnoće mjerenja se dobija, kada se broj n mjerenja dodatno poveća. Povećavanjem broja mjerenja i broj klasa se takođe na osnovu izraza (12) povećava. Za slučaj $n \rightarrow \infty$ kontura histograma se približava glatkoj, kontinuiranoj krivoj (sl.4). Ova kriva predstavlja stvarnu krivu funkcije gustine raspodjele vjerovatnoće mjerenja $f(x)$.



Sl.4 Funkcija gustine raspodjele vjerovatnoće mjerenja

Na osnovu realnih mjerenja mogu se uvijek odrediti samo empirijske funkcije gustine raspodjele vjerovatnoće mjerenja $f(x)$. Posebno u slučaju malog uzorka, empirijska funkcija gustine raspodjele vjerovatnoće mjerenja može značajno da odstupa od idealne funkcije gustine.

Cilj teorije statistike i vjerovatnoće je, između ostalog, da se provjeri mogućnost interpretacije empirijske funkcije gustine, teorijskom funkcijom gustine raspodjele vjerovatnoće mjerenja.

5. KONTROLA TAČNOSTI MJERENJA UREĐAJA ZA PROVJERU SILE KOČENJA KOD MOTORNH VOZILA

Sa stanovišta sigurnosti sistem za kočenje je sigurno jedan od najvažnijih i najodgovornijih sistema na motornom vozilu. Njegova ispravnost i efikasnost su ključni elementi za sigurno zaustavljanje vozila u svim uslovima eksploatacije. Stoga se provjeri ispravnosti i efikasnosti sistema za kočenje vozila poklanja velika pažnja, što je između ostalog regulisano i zakonskom regulativom.

Uobičajeno se efikasnost sistema za kočenje provjerava ispitivanjem vozila u statičkim uslovima, na valjcima za ispitivanje sile kočenja, pri čemu sistem mora da zadovolji zakonom propisane norme.

Valjci za provjeru sile kočenja su najvažniji dijelovi opreme u stanicama za tehnički pregled vozila i njihovoj ispravnosti se posvećuje posebna pažnja. Zakonom su pripisani zahtjevi u pogledu tačnosti ovih uređaja i stanice tehničkog pregleda imaju obavezu da rade periodičnu kontrolu svojih uređaja od strane ovlaštene laboratorije na nivou države. U Crnoj Gori periodična provjera ispravnosti uređaja na liniji tehničkog pregleda vozila se obavlja dva puta godišnje.

5.1. Postupak kontrole

Postupak kontrole uređaja za provjeru sile kočenja zasniva se na poređenju vrijednosti koje pokazuje mjerni instrument sa referentnim vrijednostima dobijenim proračunom.

Na Sl.5 je prikazana mjerna oprema za kontrolu uređaja za provjeru sile kočenja kod motornih vozila. Zahvaljujući svojoj konstrukciji kao i dodatnom priboru za montažu, oprema je pogodna za provjeru većine postojećih uređaja.

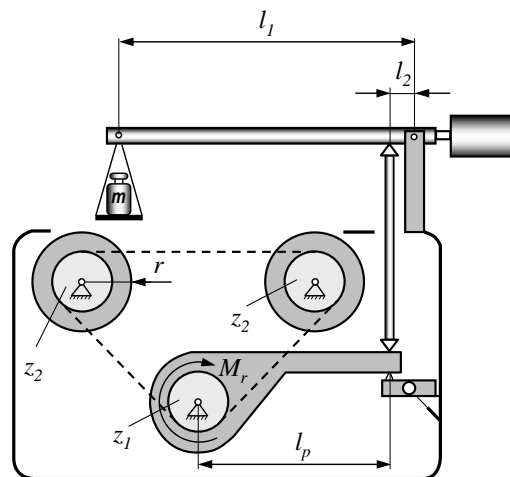
Smisao je u nanošenju tačno definisanog opterećenja na mehanički dio sistema za mjerenje sile kočenja, a zatim poređenje pokazivanja dobijenog na mjernom uređaju, sa vrijednostima dobijenim na osnovu proračuna.

Opterećenje se zadaje pomoću tegova različitih težina. Obično se koriste težine od 1, 2, 3, 5, 10, 15, 20, 25 i 30 kilograma.

Koristeći zakon poluge, sila koju daje opterećenje od težine se višestruko pojačava i preko trna se prenosi na mjerni dio uređaja za kontrolu sile kočenja. Na osnovu poznatih geometrijskih odnosa i poznavanjem brojeva zubaca z_1 i z_2 na lančanicima koji služe za prenos snage od motora do valjaka, moguće je izračunati računске vrijednosti mjerene veličine.



Sl.5. Mjerna oprema za kontrolu uređajaza provjeru sile kočenja kod motornih vozila



Sl.6. Šematski prikaz postavljenje aparature prilikom kontrole uređaja za mjerenje sile kočenja kod motornih vozila

Računski dobijene vrijednosti predstavljaju očekivane vrijednosti pokazivanja uređaja, odnosno predstavljaju tačnu vrijednost (x_0) mjerene veličine. Dobijaju se na osnovu geometrijskih veličina uređaja za mjerenje sile kočenja, geometrijskih odnosa kontrolnog uređaja i nanesenog opterećenja (Sl.6.), prema jednačini:

$$x_0 = m \cdot g \cdot \frac{l_1 \cdot l_p \cdot z_2}{l_2 \cdot r \cdot z_1} \quad (15)$$

U daljoj analizi će biti obrađeni rezultati za opterećenje na kontrolnom uređaju od 2 kg. Na sličan način, u cilju dobijana relevantnih zaključaka o tačnosti mjernog uređaja, je potrebno obraditi rezultate za sve mjerne etalone, odnosno za sva nanesena opterećenja.

5.2. Ocjena rezultata mjerenja za etalon od 2 kg

Ponavljanjem mjerenja etalomom od 2 kg dobijeni su rezultati poređani u rastućem nizu i prikazani u Tabeli 1.:

Tabela 1: Rezultati mjerenja

Broj mjer.	Sila daN	Broj mjer.	Sila daN	Broj mjer.	Sila daN
1	36,78	6	37,04	11	37,14
2	36,81	7	37,06	12	37,17
3	36,90	8	37,08	13	37,18
4	36,92	9	37,09	14	37,27
5	36,95	10	37,10	15	37,33

Na osnovu izraza (12), za uzorak $n=15$, usvaja se broj klasa $z=5$.

Širina intervala shodno izrazu (13) je:

$$\Delta x = \frac{x_{max} - x_{min}}{z} = \frac{37,33 - 36,78}{5} = 0,11 \quad (16)$$

Rezultati mjerenja intervalno su sređeni i prikazani u Tabeli 2.

Tabela 2: Podaci o rezultatima mjerenja dati tabelarno

i	Δx (daN)	$N(\Delta x)$
1	36,78÷36,89	2
2	36,89÷37,00	3
3	37,00÷37,11	5
4	37,11÷37,22	3
5	37,22÷37,33	2

Kako su podaci o rezultatima mjerenja tabelarno sređeni u 5 intervala, neophodno je tabelu sa podacima dopuniti podacima o broju mjerenja koji odgovaraju krajevima intervala $N_i(x)$ i vrijednostima kumulativne učestalosti $F(x_i)$ koje su date u Tabeli 3., gdje je ukupan broj mjerenja $n=15$.

Proračunom vjerovatnoće pojave rezultata mjerenja $F(x_i)$, unošenjem tačaka $[x_i, F(x_i)]$ u vjerovatnosni papir normalne raspodjele i konstatuje se mogućnost povlačenja prave linije između ovih tačaka (Sl.7.). Donosi se zaključak o prihvatanju hipoteze o normalnom zakonu raspodjele.

Očitane vrijednosti parametara raspodjele sa vjerovatnosnog papira su:

– Srednja vrijednost $x_{50\%} = \mu = 37,074 \text{ daN}$;

Standardna devijacija σ se sračunava kao:

$$\sigma = x_{84,13\%} - x_{50\%} = 37,237 - 37,074 = 0,163 \text{ daN} \quad (17)$$

Tabela 3: Vrijednosti za određivanje parametara normalne raspodjele

i	Δx daN	x daN	$N_i(\Delta x)$	$N_i(x)$	$F(x_i) = \frac{N_i(x)}{n+1}$
1	36,78÷36,89	36,89	2	2	0,12500
2	36,89÷37,00	37,00	3	5	0,31250
3	37,00÷37,11	37,11	5	10	0,62500
4	37,11÷37,22	37,22	3	13	0,81250
5	37,22÷37,33	37,33	2	15	0,93750

Skup statističkih metoda koje utvrđuju oblik i smjer povezanosti dvije veličine, kao i njenu jačinu, naziva se teorija korelacije, a jedan od osnovnih pokazatelja je jednačina optimalne prave. Optimalna prava $y=a \cdot x+b$ je jednačina koja se praktično određuje koristeći metodu najmanjih kvadrata. Koristeći podatke iz Tabele 3, mogu se sračunati veličine a i b :

$$a = \frac{n \cdot \sum_{i=1}^{n=15} (x_i \cdot y_i) - \sum_{i=1}^{n=15} x_i \cdot \sum_{i=1}^{n=15} y_i}{n \cdot \sum_{i=1}^{n=15} x_i^2 - \left(\sum_{i=1}^{n=15} x_i \right)^2} \quad (18)$$

$$a = \frac{15 \cdot 41,59 - 185,55 \cdot 1,1}{15 \cdot 6885,882 - (185,55)^2} \approx 6,132 \quad (19)$$

$$b = \frac{\sum_{i=1}^{n=15} x_i^2 \cdot \sum_{i=1}^{n=15} y_i - \sum_{i=1}^{n=15} x_i \cdot \sum_{i=1}^{n=15} (x_i \cdot y_i)}{n \cdot \sum_{i=1}^{n=15} x_i^2 - \left(\sum_{i=1}^{n=15} x_i \right)^2} \quad (20)$$

$$b = \frac{6885,882 \cdot 1,1 - 185,55 \cdot 41,59}{15 \cdot 6885,882 - (185,55)^2} = -227,327 \quad (21)$$

Jednačina prave je:

$$y = a \cdot x + b = 6,132 \cdot x - 227,327 \quad (22)$$

Srednja vrijednost se određuje za:

$$F(x) = 0,5 \rightarrow y = 0 \quad (23)$$

Iz jednačine prave $y = a \cdot x + b$ se dobija srednja vrijednost:

$$\mu = x = \frac{y - b}{a} = \frac{0 - (-227,327)}{6,132} = 37,074 \text{ daN} \quad (24)$$

Standardna devijacija se određuje, ako se stavi da je:

$$F(x) = 0,8413 \rightarrow y = \text{NORMSINV}[F(x)]$$

$$y = \text{NORMSINV}[0,8413] = 0,999815 \text{ (EXELL);}$$

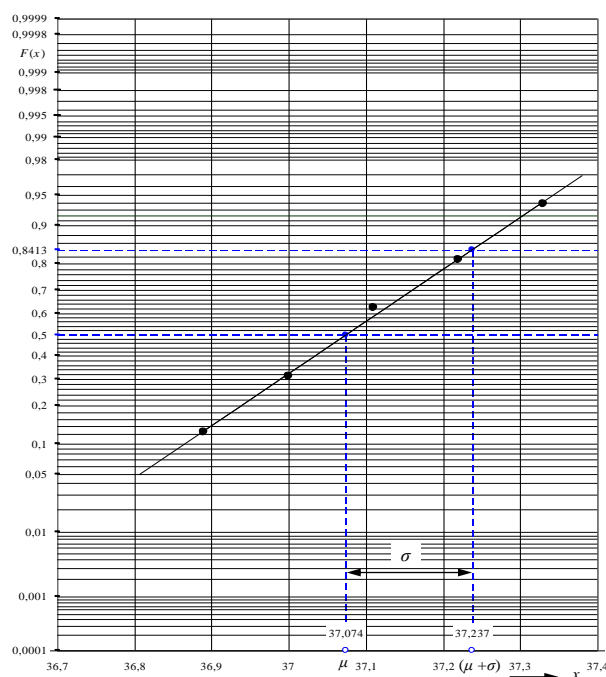
Iz jednačine prave $y = a \cdot x + b$ dobija se vrijednost $(\mu + \sigma)$:

$$\mu + \sigma = x = \frac{y - b}{a} \quad (25)$$

$$\mu + \sigma = \frac{0,999815 - (-227,327)}{6,132} = 37,237 \text{ daN}$$

Sada se može odrediti standardna devijacija:

$$\sigma = (\mu + \sigma) - \mu = 37,237 - 37,074 = 0,163 \text{ daN} \quad (26)$$



Sl.7: Vjerovatnosni papir normalne raspodjele

Tabela 4: Podaci za određivanje apsolutne vrijednosti razlike $[F_e(x) - F_i(x)]$

i	x_i daN	$F_e(x) = \frac{N(x)}{n+1}$	$f_e(x) = \frac{N_i(\Delta x)}{n \cdot \Delta x}$	$z_i = \frac{x_i - \mu}{\sigma}$	$F_i(z) = \frac{1}{\sqrt{2\pi}} \cdot \int_{-\infty}^z e^{-\frac{1}{2}z^2} dz$ $F_i(z) = \text{NORMSDIST}(z)$	$f_i(x) = \frac{1}{\sigma \cdot \sqrt{2 \cdot \pi}} \cdot e^{-\frac{1}{2} \left(\frac{x - \mu}{\sigma} \right)^2}$	$ F_e(x) - F_i(x) $
1	36,89	0,1250	1,2121	-1,1290	0,1294	1,2935	0,0044
2	37,00	0,3125	1,8182	-0,4544	0,3248	2,2066	0,0123
3	37,11	0,6250	3,0303	0,2202	0,5871	2,3880	0,0379
4	37,22	0,8125	1,8182	0,8948	0,8146	1,6395	0,0021
5	37,33	0,9375	1,2121	1,5694	0,9417	0,7140	0,0042

6. STATISTIČKI TESTOVI

Ocjena polazne hipoteze o važnosti određenog zakona raspodjele vrši se na vjerovatnosnom papiru procjenjivanjem da li sve unijete tačke odgovaraju pravoj liniji. Pri tom mogu da se tolerišu određena odstupanja, bez obzira iz kojih izvora potiču. Ovo se posebno odnosi na tačke koje odgovaraju najmanjim relativnim učestanostima.

Da bi se u ocjeni ovih odstupanja dobila potrebna sigurnost mogu da se koriste tzv. statistički testovi. Ovakvih testova ima više, a najviše se koriste test Kolmogorov – Smirnov ili d_α – test, Pirsonov χ^2 – test i Studentov t – test.

6.1. Test Kolmogorov-Smirnov (d_α -test)

Test Kolmogorov-Smirnov se zasniva na pretpostavci da dobijena raspodjela zaista odgovara teorijskoj, i to za cijelu populaciju. Stepem saglasnosti se ocjenjuje na bazi odstupanja pojedinih tačaka od pretpostavljene raspodjele, upoređujući ova odstupanja sa dozvoljenim koeficijentom povjerenja d_α koji je dat tablično, za veličinu uzorka n i nivo značajnosti α :

$$D_{max} = \max |F_e(x) - F_t(x)| \leq d_\alpha \quad (27)$$

gdje su $F_e(x)$ i $F_t(x)$ - empirijska i teorijska funkcija raspodjele vjerovatnoće rezultata mjerenja.

Ukoliko je $D_{max} > d_\alpha$, hipoteza o pretpostavljenoj raspodjeli se odbacuje. Test Kolmogorov-Smirnov može da se primijeni na sve raspodjele koje se definišu u vidu kontinualnog zakona, kao i za relativno male uzorke, odnosno mali broj podataka.

Prilikom primjene ove metode treba poštovati:

- Poredati podatke u rastućem nizu;
- Utvrđiti ukupan broj podataka mjerenja n ;
- Izračunati vrijednosti empirijske funkcije raspodjele vjerovatnoće rezultata mjerenja $F_e(x)$;
- Izračunati odgovarajuće vrijednosti teorijske funkcije raspodjele vjerovatnoće rezultata mjerenja $F_t(x)$;
- Odrediti apsolutnu vrijednost razlike $[F_e(x) - F_t(x)]$;
- Odrediti maksimalnu apsolutnu vrijednost razlike D_{max} ;
- Uporediti D_{max} sa tabličnom vrijednošću d_α . Ako je $D_{max} < d_\alpha$ prihvata se hipoteza o datoj raspodjeli na datom nivou značajnosti α .

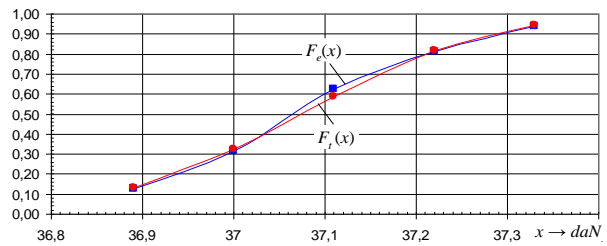
U predhodnom mjerenju sile 2 kg, poslije $n=15$ ponovljenih mjerenja je izvršeno određivanje vjerovatnoće pojave rezultata mjerenja $F(x_i)$, za veličinu ranga $n=15$.

Na osnovu podataka za x_i i $F(x_i)$, sračunate su vrijednosti pomoću kojih su određeni parametri Normalne raspodjele:

- $\mu = 37,074 \text{ daN}$ – srednja vrijednost i
- $\sigma = 0,163 \text{ daN}$ – standardna devijacija

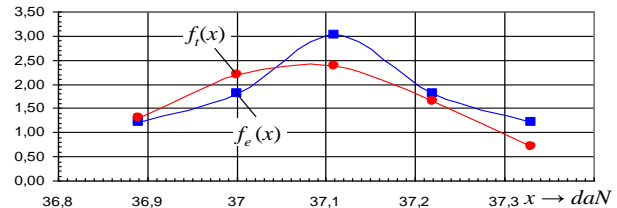
Rezultati su prikazani u Tabeli 4.

Maksimalna apsolutna vrijednost razlike prema tabeli iznosi $D_{max} = 0,0379$. Za faktor značajnosti $\alpha = 0,05$ i uzorak $n = 15$, koeficijent povjerenja $d_\alpha = 0,338$ iz odgovarajuće tablice. Kako je $D_{max} = 0,0379 < d_\alpha = 0,338$, prihvata se Normalna raspodjela sa parametrima $\mu = 37,074 \text{ daN}$ i $\sigma = 0,163 \text{ daN}$. Na Sl.8., na osnovu podataka iz Tabele 4, su date funkcije empirijske i teorijske vjerovatnoće pojave rezultata mjerenja.



Sl.8: Funkcije empirijske i teorijske vjerovatnoće pojave rezultata mjerenja

Na sl.9, na osnovu rezultata iz Tabele 4, prikazana je teorijska $f_t(x)$ i eksperimentalna $f_e(x)$ funkcija gustine raspodjele vjerovatnoće rezultata mjerenja.



Sl.9 Teorijska i eksperimentalna funkcija gustine raspodjele vjerovatnoće rezultata mjerenja

6.2. Pirsonov χ^2 (HI kvadrat) test

Pirsonov χ^2 (HI kvadrat) test je najstarija i najčešće korišćena metoda za procjenjivanje valjanosti, pretpostavljene raspodjele za date podatke. Glavna prednost χ^2 metode je njena fleksibilnost. Može se primijeniti za ispitivanje bilo koje pretpostavljene raspodjele, kako diskretne, tako kontinualne.

Tabela 5: Podaci za određivanje statistiku χ^2

i	1	2	3	4	5
ΔN_{ei}	2	3	5	3	2
x_d u daN	36,78	36,89	37	37,11	37,22
$z_d = \frac{x_d - \mu}{\sigma}$	-1,80	-1,12	-0,45	0,22	0,89
$F_{xi}(x_d) = \text{NORMDIST}(z_d)$	0,035	0,129	0,324	0,587	0,814
x_g u daN	36,89	37	37,11	37,22	37,33
$z_g = \frac{x_g - \mu}{\sigma}$	-1,12	-0,45	0,220	0,894	1,569
$F_{xi}(x_g) = \text{NORMDIST}(z_g)$	0,12	0,32	0,587	0,81	0,941
$\Delta F_{xi} = F_{xi}(x_d) - F_{xi}(x_g) $	0,094	0,195	0,262	0,227	0,127
$\Delta N_{xi} = n \cdot \Delta F_{xi}$	1,407	2,930	3,936	3,411	1,908
$(\Delta N_{ei} - \Delta N_{xi})$	0,593	0,070	1,064	-0,411	0,092
$(\Delta N_{ei} - \Delta N_{xi})^2$	0,352	0,005	1,133	0,169	0,009
$\frac{(\Delta N_{ei} - \Delta N_{xi})^2}{\Delta N_{xi}}$	0,250	0,002	0,288	0,050	0,004
$\chi^2 = \sum_{i=1}^k \frac{(\Delta N_{ei} - \Delta N_{xi})^2}{\Delta N_{xi}} = 0,250 + 0,002 + 0,288 + 0,050 + 0,004 = 0,594$					

Za mjeru odstupanja između empirijske i teorijske funkcije raspodjele uvodi se veličina χ^2 :

$$\chi^2 = \sum_{i=1}^k \frac{(\Delta N_{ei} - \Delta N_{xi})^2}{\Delta N_{xi}} = \sum_{i=1}^k \frac{(\Delta N_{ei} - \Delta N_{xi})^2}{n \cdot \Delta F_{xi}} \leq \chi_{\alpha; v}^2 = \chi_{\alpha; k-1}^2 \quad (28)$$

Ovdje je:

- ☞ ΔN_{ei} - empirijski broj rezultata mjerenja u i -tom intervalu;
- ☞ ΔN_{xi} - očekivani teorijski broj broj rezultata mjerenja u i -tom intervalu;
- ☞ $n=15$ - broj mjerenja;
- ☞ $\Delta F_{xi}=F_{xg}-F_{xd}$ - vjerovatnoća pojave rezultata mjerenja u granicama i -tog intervala;
- ☞ $\chi_{\alpha, v}^2 = \text{CHINV}(\alpha; v) = \text{CHINV}(0,05; 2) = 5,991$ - kritična vrijednost statistike, komandom u **EXCELL**-u, za dato mjerenje, za dati nivo značajnosti $\alpha=0,05$ i poznati broj stepeni slobode $v=2$;
- ☞ $v=k-l-1=5-2-1=2$ - broj stepeni slobode;
- ☞ $k=5$ - broj intervala;
- ☞ $l=2$ - broj nepoznatih parametara pretpostavljene raspodjele (μ i σ);
- ☞ $P=0,95$ - vjerovatnoća realizacije;
- ☞ $\alpha=1-P=1-0,95=0,05$ - faktor značajnosti (kritički koeficijent hipoteze o slaganju empirijske i teorijske raspodjele, odnosno rizik prihvatanja hipoteze).

Za slučaj $\chi^2 \leq \chi_{\alpha}^2$ prihvata se hipoteza o teorijskom zakonu raspodjele, u suprotnom se odbacuje. Pošto je:

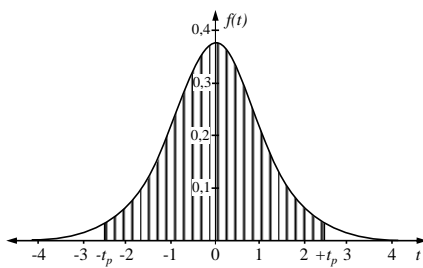
$$\chi^2 = 0,594 < \chi_{0,05; 2}^2 = 5,991 \quad (29)$$

to znači da se prihvata hipoteza o normalnom zakonu raspodjele rezultata mjerenja.

Rezultati za statistiku χ^2 su dati u Tabeli 5.

6.3. Studentov t -test

Ako je broj mjerenja mali ($n < 30$), da bi se ocijenilo da li je pretpostavljena normalna raspodjela valjana, primjenjuje se Studentov t -test, koji se zasniva na Studentovoj raspodjeli. Do ovoga testa je došao 1908. godine William Sealy Gosset u radu kojega je objavio pod pseudonimom Student. Po tome je i test dobio naziv Studentov test. Kao što je χ^2 test baziran na gama raspodjeli, tako je i t -test baziran na t -raspodjeli.



Sl.10 Funkcija gustine Studentove raspodjele

Na sl. 10 je prikazana Studentova raspodjela vjerovatnoće rezultata mjerenja za broj stepeni slobode $v=5$.

Ako se poče od izraza za normalnu raspodjelu:

$$f(z) = \frac{1}{\sqrt{2 \cdot \pi}} \cdot e^{-\frac{z^2}{2}} \quad (30)$$

kao i izraza za χ^2 raspodjelu:

$$f(\chi_v^2) = \frac{1}{2^{\frac{v}{2}} \cdot \Gamma\left(\frac{v}{2}\right)} \cdot (\chi_v^2)^{\frac{v-2}{2}} \cdot e^{-\frac{\chi_v^2}{2}} \quad (31)$$

dobija se nova raspodjela $f(z, \chi_v^2) = f(z) \cdot f(\chi_v^2)$:

$$f(z, \chi_v^2) = \frac{1}{\sqrt{2 \cdot \pi} \cdot 2^{\frac{v}{2}} \cdot \Gamma\left(\frac{v}{2}\right)} \cdot (\chi_v^2)^{\frac{v-2}{2}} \cdot e^{-\frac{1}{2}(\chi_v^2 + z^2)} \quad (32)$$

Ako se uvede promjenljiva t :

$$t = \frac{z}{\sqrt{\frac{\chi_d^2}{v}}} \quad (33)$$

dobija se t -gustina raspodjele vjerovatnoće $f(t)$:

$$f(t) = \frac{1}{\sqrt{v \cdot \pi}} \cdot \frac{\Gamma\left(\frac{v+1}{2}\right)}{\Gamma\left(\frac{v}{2}\right)} \cdot \left(1 + \frac{t^2}{v}\right)^{-\frac{v+1}{2}} \quad (34)$$

gdje su:

- ☞ $\Gamma(v)$ - gama funkcija;
- ☞ $v=n-1$ - broj stepeni slobode.

Za poznate vrijednosti \bar{x} - srednje vrijednosti i σ - standardne devijacije, može se prema Studentovom kriterijumu procijeniti prava vrijednost mjerene veličine:

$$x_0 = \bar{x} \pm t_{v,p} \cdot \frac{\sigma}{\sqrt{n}} \quad (35)$$

gdje su:

- ♦ \bar{x} - srednja vrijednost mjerene veličine;
- ♦ σ - standardna devijacija mjerene veličine;
- ♦ $t_{\alpha, v}$ - vrijednost t - raspodjele koja se vadi iz odgovarajuće tablice za:
 - ☞ $v=n-1$ - broj stepeni slobode;
 - ☞ $P=95\%$ - vjerovatnoća realizacije (ili $\alpha=0,05$ - faktor značajnosti).

U predhodnom mjerenju sile 2 kg, poslije $n=15$ ponovljenih mjerenja, srednja vrijednost mjerene veličine je:

$$\bar{x} = \frac{1}{n} \cdot \sum_{i=1}^n x_i = \frac{1}{15} \cdot \sum_{i=1}^{15} x_i \quad (36)$$

Poslije zamjene izmjenjenih veličina prema Tabeli 1, dobija se:

$$\bar{x} = \frac{x_1 + \dots + x_{15}}{15} = \frac{36,78 + \dots + 37,33}{15} = 37,055 \text{ daN} \quad (37)$$

Standardna devijacija mjerene veličine (sila) je:

$$\sigma = \sqrt{\frac{1}{n-1} \cdot \sum_{i=1}^n (x_i - \bar{x})^2} = \sqrt{\frac{1}{15-1} \cdot \sum_{i=1}^{15} (x_i - \bar{x})^2} \quad (38)$$

Poslije zamjene izmjenjenih veličina prema Tabeli 1, dobija se:

$$\sigma = \sqrt{\frac{1}{14} \cdot [(36,78 - 37,055)^2 + \dots]} = 0,158 \text{ daN} \quad (39)$$

- ♦ $t_{\alpha, v} = t_{0,05,14} = 2,145$ - vrijednost t - raspodjele koja se dobija komandom u EXCELL-u;
- ♦ $t_{\alpha, v} = \text{TINV}(\alpha; v) = \text{TINV}(0,05; 14) = 2,145$ za:
 - ☞ $v=15-1=14$ - broj stepeni slobode;
 - ☞ $\alpha=0,05$ - faktor značajnosti.

Dakle, sila se procjenjuje kao:

$$x = \bar{x} \pm t_{v,p} \cdot \frac{\sigma}{\sqrt{n}} = 37,055 \pm 2,145 \cdot \frac{0,158}{\sqrt{15}} \quad (40)$$

$$x = 37,055 \pm 0,0877$$

Znači, sledeće mjerenje sile se procjenjuje, sa 95% vjerovatnoće, da će da bude u granicama:

$$\begin{aligned} x_{\min} &= 37,055 - 0,0877 = 36,967 \text{ daN} \\ x_{\max} &= 37,055 + 0,0877 = 37,142 \text{ daN} \end{aligned} \quad (41)$$

6.4. Standardna devijacija aritmetičke sredine

Aritmetička sredina mjerenja $\bar{x} (\mu)$ nije jednaka pravoj vrijednosti mjerene veličine x_0 . Odstupanje aritmetičke sredine u odnosu na pravu vrijednost je ε .

Prava vrijednost mjerene veličine je:

$$x_0 = \bar{x} - \frac{1}{n} \cdot \sigma \cdot \sqrt{n} = \bar{x} - \frac{\sigma}{\sqrt{n}} \quad (42)$$

Drugi član sa desne strane jednačine se naziva standardna devijacija aritmetičke sredine, i on opada sa recipročnom vrijednošću korijena iz broja mjerenja.

Standardna devijacija aritmetičke sredine je:

$$\sigma_{\bar{x}} = \frac{\sigma}{\sqrt{n}} = \frac{0,163}{\sqrt{15}} = 0,0421 \quad (43)$$

U jednačini su:

– σ – standardna devijacija i n – broj mjerenja.

Iz naprijed navedenog slijedi da se prava vrijednost mjerene veličine nalazi u granicama:

$$\begin{aligned} \bar{x} - |\sigma_{\bar{x}}| &\leq x_0 \leq \bar{x} + |\sigma_{\bar{x}}| \\ 37,074 - |0,0421| &\leq x_0 \leq 37,074 + |0,0421| \\ 37,0319 &\leq x_0 \leq 37,1161 \end{aligned} \quad (44)$$

Definisani interval se često naziva interval povjerenja. Ako greške ispunjavaju navedene Gausove uslove (slučajni proces), vjerovatnoća da se mjereni rezultat nađe u intervalu poverenja je 68,3% ($\mu \pm \sigma$), odnosno $\sigma = 34,15\%$.

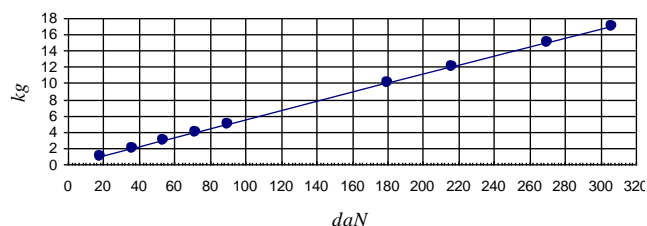
Standardna devijacija aritmetičke sredine je manja od standardne devijacije pojedinog mjerenja. U praksi, nema smisla povećavati broj mjerenja preko $n=10$.

7. TAČNE VRIJEDNOSTI SILE

Na osnovu proračuna, dobijeni su rezultati koji su prikazani u Tabeli 6.

Tabela 6: Rezultati proračuna

Teg kg	Sila daN	Teg kg	Sila daN	Teg kg	Sila daN
1	18,01	4	72,06	12	216,18
2	36,03	5	90,07	15	270,22
3	54,04	10	180,15	15	306,25



Sl.11: Baždarna karakteristika uređaja

Na osnovu podataka iz Tabele 4 je nacrtana baždarna karakteristika koja je prikazana na sl.11. Kao što se iz Tabele 4 vidi, tačna vrijednost za opterećenje etalonom od 2 kg je sila od 36,03 daN.

8. ZAKLJUČAK

Na osnovu sprovedenog kontrolnog mjerenja sa etalonom od 2 kg, ponavljajući mjerenje 15 puta ($n=15$), dobijena je zavisnost koja se pokorava normalnom zakonu raspodjele, što je potvrđeno testom Kolmogorov-Smirnov (d_α -test), χ^2 (HI kvadrat) testom kao i Studentovim t -testom.

Dakle, određena je je srednja vrijednost $\mu=x=37,074 \text{ daN}$ i standardna devijacija $\sigma=0,163 \text{ daN}$.

Proračunom je za etalon od 2 kg je dobijena tačna vrijednost $x_0=36,03 \text{ daN}$. Na osnovu izraza (2), može se odrediti relativna greška mjerenja:

$$G_r = \frac{x - x_0}{x_0} = \frac{37,074 - 36,03}{36,03} = 0,0297 = 2,897 \%$$

Dakle, može se zaključiti da se tačna vrijednost nalazi u dozvoljenim granicama.

LITERATURA

- [1] DUNN, P. (2005) *Measurement and Data Analysis for Engineering and Science*, McGraw – Hill, New York.
- [2] ZAIMOVIĆ-UZUNOVIĆ N. (2006) *Mjerna tehnika*, Zenica, Univerzitet u Zenici.
- [3] BENEDICT, R. (1984) *Fundamentals of temperature, pressure, and flow measurements*, A Wpley-Interscience Publication, JOHN WILEY & SONS, New York – Chichester – Brisbane – Toronto – Singapore, pp 172-196.
- [4] SIMONOVIĆ, V. (1991) *Uvod u teoriju verovatnoće i matematičku statistiku*, Gradjevinska knjiga, Beograd.

KORESPONDENCIJA



Radoš BULATOVIĆ, Prof. Dr. Eng.
University of Montenegro
Mechanical Engineering Faculty
Bul. Džordža Vašingtona bb
81000 Podgorica, Montenegro
rados@ac.me



Janko JOVANOVIĆ, Prof. Dr. Eng.
University of Montenegro
Mechanical Engineering Faculty
Bul. Džordža Vašingtona bb
81000 Podgorica, Montenegro
janko@ac.me



Radoslav TOMOVIĆ, Prof. Dr. Eng.
University of Montenegro
Mechanical Engineering Faculty
Bul. Džordža Vašingtona bb
81000 Podgorica, Montenegro
radoslav@ac.me

INFLUENCE OF LEAKAGE CLEARANCE ON PRESSURE VARIATION IN GEROTOR PUMP CHAMBERS

Lozica IVANOVIĆ
Andreja ILIĆ
Blaža STOJANOVIĆ
Jasna GLIŠOVIĆ
Miloš MATEJIĆ

Abstract: Gerotors are used as pumps, motors, compressors, etc. and used in a wide range of industrial areas. Gerotors are, as pumps suitable for automotive industry as elements of lubricating systems, steering mechanisms and engines. The main component of gerotor pumps is a pair of toothed rotors. Usually, the outer rotor has a circular profile, while inner one has related coupled trochoid profile. In case of the theoretical ideal profile, contacts are simultaneous at all teeth. However, for a real profile, technological clearance and gaps are unavoidable. The existence of these gaps and clearances causes volumetric losses and consequently, variation of pressure in gerotor pump chambers. For the full understanding of real processes of fluid flow in gerotor pumps, the analytical model of fluid leaking through clearance between the profiles of teeth is presented in this paper. Due to the complexity of the fluid flow process, only volumetric losses caused by gaps between profiles of teeth and losses caused by an act of viscosity forces along the gap are analyzed. The effects of variation of geometrical parameters of profiles on the value of volumetric losses and variation of pressure in chambers of gerotor pumps are analyzed in this paper. Besides, the mutual comparison of pressure variation due to current flow obtained analytically in the pump with a theoretical ideal profile of teeth and with a real profile with gaps and clearances is done. Results and conclusions presented in this paper by highlighting real processes during exploitation bring very important perspectives for gerotor pump design that provides an effective constructional solution.

Keywords: gerotor pump, trochoid, leakage clearance, pressure variation

1. INTRODUCTION

The object of research presented in this paper is the gerotor pump used for the lubrication of the internal combustion motor. The basic components of gerotor pump are two toothed rotors, one outer usually with a circular profile and one inner with the corresponding coupled trochoid profile. In case of trochoid gear pairs with theoretical (ideal) profiles, the simultaneous contact of all teeth is achieved. In real constructions, simultaneous meshing of all the teeth at all times is not possible for the following reasons: real profiles are produced with technological tolerances, there are production and assembly errors, and due to the wear of profiles, there is a gap between the profiles. Despite the inevitable existence of gaps between the teeth, they can lead to fluid loss, reduce stability and increase noise and vibrations, especially at high speeds. Due to the presented reasons, the modeling of the meshing of the real profiles will be considered in this paper. In addition, it is assumed that all deviations from the theoretical measures

are reflected in the equidistant modification of inner gear's trochoid profile.

In accordance with the subject and goals of this paper, the influence of the geometrical and kinematical parameters of mated gear profiles on the volumetric losses and the pressure variation in the pump chambers will be done primarily.

Basic research in the area of trochoid profiles was performed by *Ansdal* [1]. On these bases, modern research related to the gerotor pump is based. *Manco* et al. [2-4] investigated the implementation of gerotor pumps in internal combustion engines as an element of its lubrication system. The same group of authors also worked on improving the profiles of gerotor pump teeth as well as on the automatic generation of the gear profile. *Maiti* and *Sinha* [5] analyzed the kinematic of modified epitrochoid profiles. *Shung* and *Pennock* [6] are evaluated in detail and extended this research to more contact aspects than only kinematics. *Raush* et al. [7] experimentally tested of damages and failures of gerotor pumps during exploitation. *Buono* [8] et al. performed a simulation of cavitation phenomena during exploitation of gerotors. *Ivanović* with a group of authors [9-12]

investigate processes that occur on the gerotor teeth due to pressure during its exploitation. The same group of authors worked on the gerotor pumps models with technological gaps as well as with theoretical determination of pump flow.

In this paper, the model of the kinematic pair with fixed axis of gear shafts is considered. The input drive shaft is connected to the inner gear. For determination of current surface of the cross-section of the pump chamber, the method presented in reference [9] is used, while the minimal dimension of the gap is determined by the method presented in reference [11]. The determination of pressure variation in pump chambers is done by the method presented in reference [10] with certain modifications. The scientific significance of this paper is reflected in the setup and testing of the mathematical model of pressure variation in pump chambers under conditions very similar to the real ones. This precise simulation of exploitative conditions was done by introducing a technological gap into the mathematical model.

2. FLOW LOSSES AND PRESSURE VARIATION IN GEROTOR PUMP CHAMBERS WITH CLEARANCE

In the case of the considered gear pair of the trochoid pump, the theoretical profile of inner gear is in the form of an equidistant peritrochoid, while the outer gear is in form of a circular arc with radius, r_c . The profile of inner gear, which represents a realistic profile, will be generated in the form of an equidistant of the basis trochoid with an radius of equidistant, which is in relation to the theoretical one for assumed value of technological gap, ε . Due to the specific geometry of gear profiles and the exceptional complexity of the gerotor pump operational process, in this paper, only losses due to the gap between gear profiles and losses due to the viscosity of working fluid (as a consequence of adhesion forces, fluid particles are paste to the side of gear tooth) are considered [2]. The volume loss analysis will be carried out for the pump model shown in Fig. 1. With the pump shown, both outer and inner gears rotate around their axis in the same direction, counterclockwise. When considering the pressure variation in pump chamber K_i , it is assumed that the flow $Q_{(in)i}$ that comes from the adjacent chamber is positive (inflows into the chamber K_i), while the flow $Q_{(out)i}$ is negative, since it is pushed from the chamber K_i to the adjacent chamber.

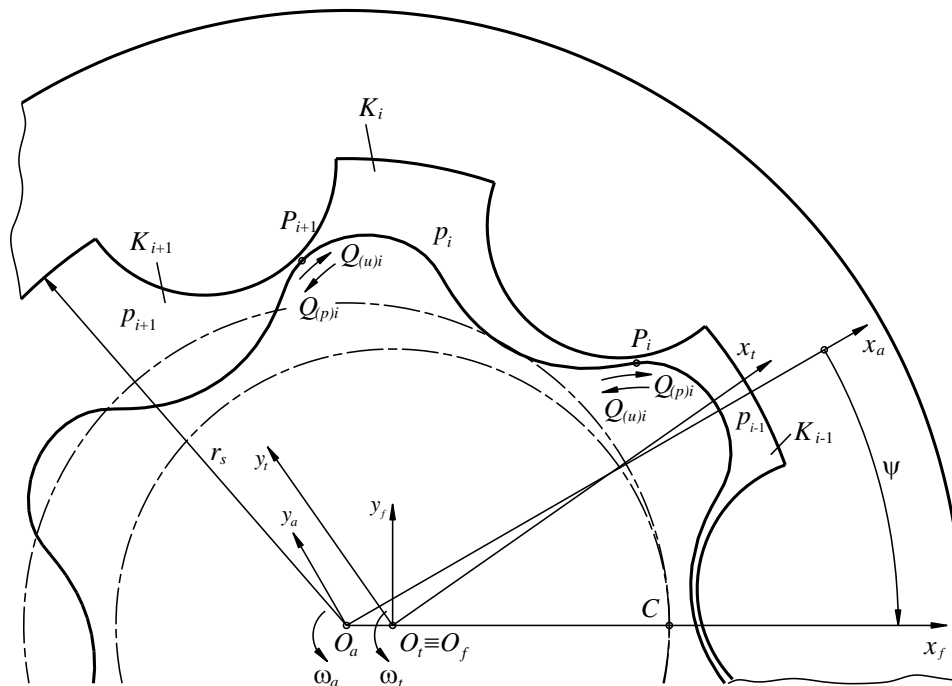


Fig.1: Model of pump with technological gap

The flowing of the fluid through the gap between the profiles of the teeth is caused by the difference of pressures between the two adjacent pump chambers. To calculate these losses, a hydraulic fluid flow model through rectangular notch with variable dimensions is adopted. Basic geometrical relations for determining the height of the gap between gear profiles are presented in Fig. 2.

Coordinate system Oxy is introduced, whose coordinate start point O is set at the point P_{ai} , the axis x has the direction of tangent, the axis y is has the direction of common normal of the profile, and are oriented as shown in Fig. 2. For calculating the height of the gap, the profile of inner gear is approximated by a circular arc of the radius ρ_{ci} which is equal to the radius of curvature of the trochoid profile at the point P_{ii} . On the basis of this, an

equation can be written for calculating the height of the gap depending on the x coordinate in following form [2]:

$$h_i(x) = (h_{\min})_i + r_c + \rho_{ci} - \sqrt{r_c^2 - x^2} \mp \sqrt{\rho_{ci}^2 - x^2}, \quad (1)$$

Where the radius of curvature ρ_{ci} of equidistant trochoid profile is defined by the following equation

$$\rho_{ci} = \frac{ez[1 + \lambda^2 - 2\lambda \cos(\tau_i - \psi_i)]}{z + \lambda^2 - \lambda(z+1)\cos(\tau_i - \psi_i)}^{\frac{3}{2}} - r_c^*, \quad (2)$$

Where ψ_i is the angle which defines the current position of the point P_{ii} [11]. In equation (1) the sign "-" refers to the convex, and the sign "+" is refers to the concave zone of the profile. All other parameters that are used in this equation are described in detail in reference [9, 11].

The basic relation for calculation of volume losses is principal equation for hydrodynamic lubrication, which can be derivate from the basic principles of fluid mechanic, or from Navier-Stocks equations [13]. The following assumptions have been made:

- the pressure is constant at the cross-section,
- the curvature of the surfaces are large in relation to the thickness of the lubrication layer,
- the lubricant is the Newtonian fluid,
- the fluid flow is laminar,
- the viscosity of the fluid is constant.

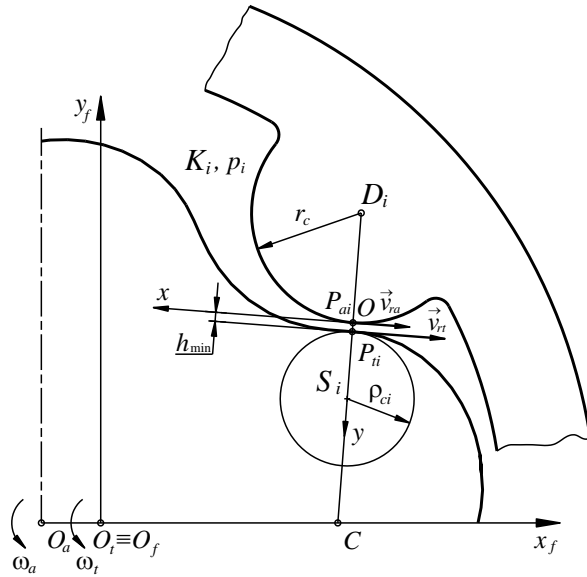


Fig.2: Basic geometrical relations for determining the height of the gap

Starting from the presented assumptions for calculation of total fluid flow through the gap with height $h(x)$, the following equation can be used [13]:

$$Q = \frac{v_r b h}{2} - \frac{b h^3}{12\eta} \frac{dp}{dx}, \quad (3)$$

where

- η - Coefficient of fluid dynamic viscosity,
- v_r - Speed intensity of the relative movement of inner gear profile relative to the outer gear [14].

The first member of the right side of expression (3) reflects the effect of viscous forces on the flow, while the second member indicates the effect of the pressure force. Starting from the fact that flow has a constant value along the gap, equation for calculation of the flow can be written for the minimal cross-section of the gap with height h_{\min} . Accordingly, a variation of the flow in the pump chamber due to the action of the viscous forces along the gap can be determined by following relation:

$$Q_{i(v)} = \frac{(v_r)_i b (h_{\min})_i}{2}. \quad (4)$$

The fluid flow through the gap due to the action of the pressure forces is determined by the following expression:

$$Q_{i(\Delta p)} = \frac{b(h_{\min})_i^3}{12\eta} \frac{dp}{dx}. \quad (5)$$

To calculate the variation in the pressure of the fluid during its flow through the gap in direction of x axis, the following assumption is made: in a limited segment defined by $[-a, a]$ around h_{\min} , the cross-section of the gap between profiles of gears through which fluid flow can be modeled with rectangles of constant dimensions. For the limit value of a , the value of coordinate x are used for which related gap height according to equation (1), which is not much larger than h_{\min} , means $x = a \rightarrow h \approx h_{\min}$. In order to make a deviation from the accurate calculation of cross-section surface negligible, limits of the relative error are set in advance, in particular:

$$\frac{P_r - P_a}{P_a} 100 \leq 2\%, \quad (6)$$

where P_r is the value of the real surface of the cross-section of the gap and P_a is the approximate value of surface obtained by approximating the geometrical form of the gap. Starting from the assumption made, the equation (5) can be written as follows:

$$Q_{i(\Delta p)} = \frac{b(h_{\min})_i^3}{24\eta} \frac{\Delta p}{a_i}, \quad (7)$$

where Δp is the difference in the pressure between the two adjacent chambers of the pump [15].

Upon the presented analysis, the final form of equation for the calculation of flow rate through the gaps between related profiles of gears for the considered active chamber K_i can be formed as follow:

$$Q_{i\Sigma} = \text{sign}(\psi) \left[\frac{(v_r)_{i+1} b (h_{\min})_{i+1}}{2} - \frac{(v_r)_i b (h_{\min})_i}{2} \right] - \frac{b(h_{\min})_i^3 [p_i - p_{i-1}]}{24\eta a_i} - \frac{b(h_{\min})_{i+1}^3 [p_i - p_{i+1}]}{24\eta a_{i+1}}. \quad (8)$$

Volumetric losses affect the pressure variation in pump working chambers. In a pump with fixed shaft axes, the fluid distribution is done through the holes with variable fluid flow area. In such constructions, we assume that fluid flow area is equal to instantaneous chamber area. This assumption leads to expression for calculation of the

pressure variation during the fluid flow in the chamber K_i in the following form,

$$\Delta p_i = \frac{\rho_f b^2}{A_i^2} \left[\frac{dA_i}{dt} \right]^2. \quad (9)$$

In expression (9), ρ_f is the fluid density and dA_i/dt is the gradient of the instantaneous area A_i of the chamber K_i [5, 9]. Now, the equation for calculation of pressure in the intake chamber can be done as:

$$p_i = p_{in} - \Delta p_i, \quad (10)$$

While in the output chamber is

$$p_i = p_{out} + \Delta p_i. \quad (11)$$

The current theoretical flow in the chamber K_i represents the variation in the volume at the working chamber in the time and is calculated using the following general form [6]:

$$Q_i = \frac{dV_i}{dt} = C_p A_0 \left[\frac{2\Delta p_i}{\rho_f} \right]^{\frac{1}{2}}, \quad (12)$$

where

Δp_i - Pressure drop due to the fluid flow,

A_0 - cross-section surface of the distribution valve opening,

ρ_f - fluid density.

During the intake phase, the volume of the chamber increases and the current theoretical flow is positive. Accordingly, the following expression for determining the theoretical flow for the chamber K_i during intake phase:

$$Q_i = C_p A_0 \left[\frac{2(p_{in} - p_i)}{\rho_f} \right]^{\frac{1}{2}}, \quad (13)$$

During the thrust phase, the volume of the chamber decreases and the current theoretical flow is negative. Therefore, the following expression for determining the theoretical flow for the chamber K_i during thrust phase:

$$Q_i = -C_p A_0 \left[\frac{2(p_i - p_{out})}{\rho_f} \right]^{\frac{1}{2}}. \quad (14)$$

On the basis of equation (13) the expression for determining the pressure in the chamber K_i during intake phase can be done as follows:

$$p_i = p_{in} - \frac{\rho_f [dV/dt]^2}{2C_p^2 A_0^2} \quad (15)$$

Respectively, according to the equation (14), during thrust phase:

$$p_i = p_{out} + \frac{\rho_f [dV/dt]^2}{2C_p^2 A_0^2}. \quad (16)$$

Starting from the equation (9) and taking into account the flow losses defined by the expression (8), the following equation for the calculation of the pressure

variation in the chamber is obtained, depending on the height of the gap between gears profiles, can be done as follows:

$$\Delta p_{i\Sigma} = \frac{\rho_f}{A_i^2} \left[\frac{dV_i}{dt} + Q_{i\Sigma} \right]^2 \text{ or } \Delta p_{i\Sigma} = \frac{\rho_f}{A_i^2} [Q_i + Q_{i\Sigma}]^2. \quad (17)$$

For considered model of the pump, the following equation for calculation of current flow can be used in the following form:

$$Q_i = -2\pi n_i e^2 z b \left\{ 2\lambda \sin \frac{\pi}{z} \sin \left(\frac{2\pi i}{z} - \psi \right) - \frac{c}{z} \left[1 + \lambda^2 - 2\lambda \cos(\tau - \psi) \right]^{\frac{1}{2}} \right\}_{\tau_i}^{\tau_{i+1}}. \quad (18)$$

Based on the established relations between the geometric parameters and the functional characteristics of the gerotor pump, a computer program composed of several specific modules has been developed. The values of pressure variation in the pump chambers are calculated and graphic interpretation of the obtained results are done using the appropriate software package AutoLISP and Mathematica. The results are presented in next section of this paper.

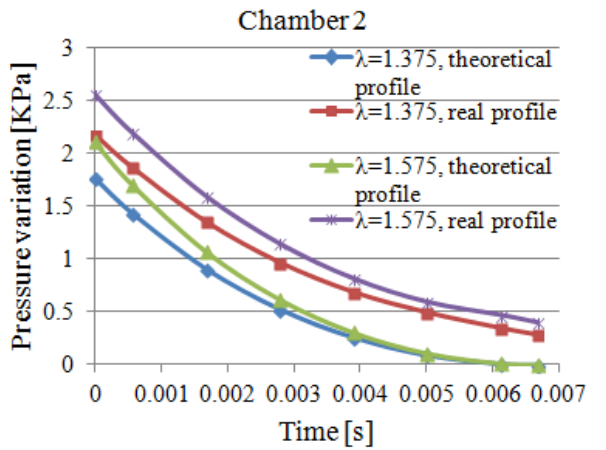
3. TESTING OF MATHEMATICAL MODEL OF PRESSURE VARIATION IN PUMP CHAMBERS

The previously presented mathematical model was tested on two concrete examples of the gear pairs of the considered pump model, one is existing commercial, and the second gear pair with a profile obtained on the basis of the calculated results in order to improve existing design of the gerotor pump used as part of a system for lubrication of internal combustion engine [11]. The geometric parameters of the gear pairs are as follows: $z = 6$, $e = 3.56$ mm, $b = 16.46$ mm, $c = 2.75$, $r_s = 26.94$ mm. For a newly generated gear pair, parameters are as follow: $\lambda = 1.375$, $c = 2.75$ while for current commercial one parameters are as follow: $\lambda = 1.575$, $c = 3.95$. Other pump parameters are: $\Delta p = 0.6$ MPa, $\rho_f = 900$ kg/m³, $n_i = 1500$ rpm, $\omega_i = 2\pi n_i = 50\pi$ s⁻¹.

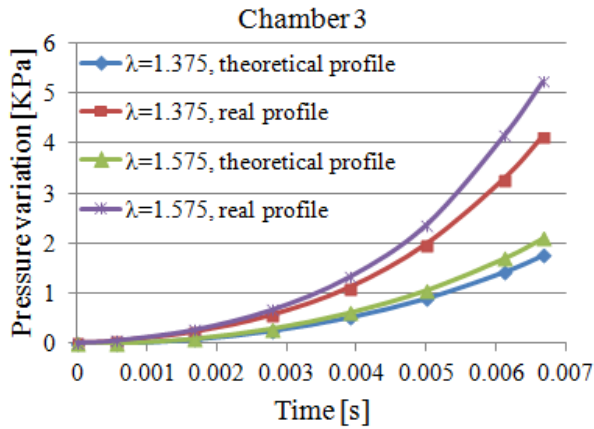
In order to better understand the influence of trochoidal coefficient λ and the height of the gap on the pressure variation in the pump chambers, comparative diagrams are presented in Fig. 3. The analysis was performed for theoretically ideal profile and for a profile with tolerances, over a period of time corresponding to one phase of the working cycle of the gerotor pump. the graphic interpretation of pressure variation in pump chambers as a function of time is presented only for a transition zone between intake and thrust phase due to significant differences in pressures.

In the diagram shown, the symmetry of the pressure variation distribution, in the case of an ideal profile, is observed for chambers that are symmetrically arranged in relation to the transition of the intake and thrust phase. With the increase of the coefficient λ , the value of these variations increases. In the case of real profile meshing,

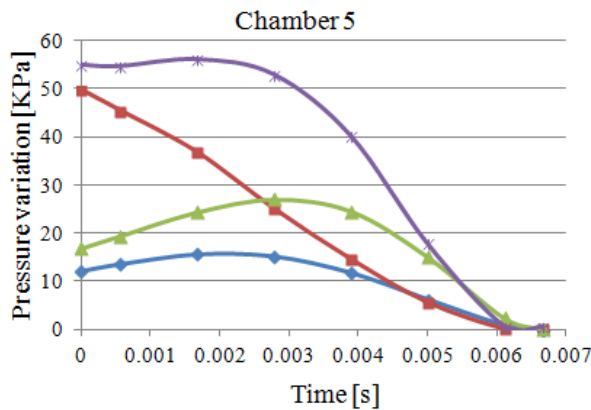
the value of these variation increases, but the trend of increase of those variations with an increase of coefficient λ remains.



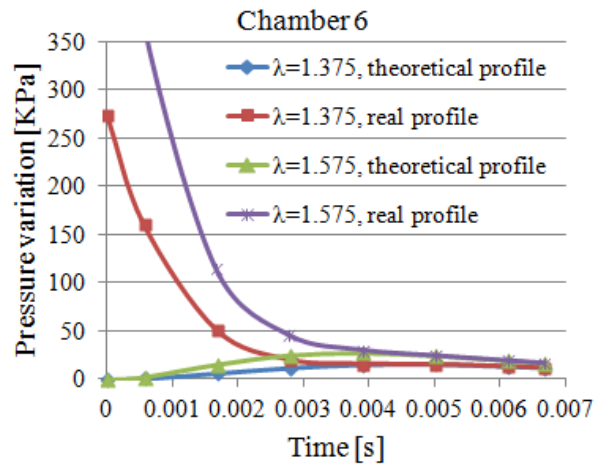
a)



b)



c)



d)

Fig.3: Comparative diagrams of pressure variation in pump chambers between intake and output zone

Based on the presented graphical interpretation, it can be concluded that the influence of the gap height on the pressure variation is greatest at the end of thrust (intake) zone and at entering the intake (thrust) phase. This can be explained by the greatest difference in the pressure between adjacent pump chambers. Highest values of pressure variations occur at the beginning of the considered phase period, in the chamber 6, in the commercial model. Based on the presented results the conclusion was made that more beneficial indicators are derived from the model ($\lambda = 1.375$) proposed as a solution with improved characteristics compared to the existing commercial ones ($\lambda = 1.575$).

After carrying out the theoretical analysis of the gerotor pump gear pair, it is necessary to verify and evaluate the formed models through the production of concrete gear pairs and the performance of the laboratory testing with the simulation of the working conditions of the pump.

4. CONCLUSION

Comparative analysis of pressure variation in pump chambers with different trochoidal coefficient λ is presented in this paper. The analysis was performed both for theoretical and realistic profiles. It has been presented that in the case of gerotor pumps with the same number of chambers z and same longitudinal base radius r_s , by selecting smaller value of trochoidal coefficient λ , smaller variation of pressure in pump chambers are obtained. The same conclusions are done on results obtained by analysis of ideal theoretical profile and in the real profiles with technological gaps and tolerances.

The scientific results of this paper establish new valuable guidelines and perspectives for constructors to creating more efficient construction solutions of the gerotor pumps. By implementing the results presented in this paper, it is possible to achieve more smoothly operation of gerotor. The main guideline for future research on this topic will be focused on experimental testing of presented models and their comparative analysis with theoretical models.

ACKNOWLEDGMENT

This paper is a result of the research activities conducted under the projects "Sustainable development of technology and equipment for motor vehicles recycling" TR 35033 and "The research of vehicle safety as part of a cybernetic system: Driver-Vehicle-Environment" TR 35041, which are financed by the Ministry of Education, Science and Technological Development of Republic of Serbia.

REFERENCES

- [1] ANSDALE, R. F., LOCKLEY, D. J. (1970) *The Wankel RC Engine*, Iliffe Books Ltd., London
- [2] MANCO, S., NERVEGNA, N., RUNDO, M., ARMENIO, G., PACHETTI, C., TRICHILO, R. (1998) *Gerotor Lubricating Oil Pump for IC Engines*, SAE Paper 982689, International Fall Fuels & Lubricants Meeting and Exposition, October 19-22, San Francisco, USA and SAE Transactions
- [3] MANCO, G., MANCO, S., RUNDO, M., NERVEGNA, N. (2001) *Computerized generation of novel gearings for internal combustion engines lubricating pumps*, The International Journal of Fluid Power, Vol. 1 – No 1 - ISBN 1493-9776, pp 49-58
- [4] MANCÒ, S., NERVEGNA, N., RUNDO, M. (2001) *Critical issues on performance of lubricating gerotor pumps at high rotational speed*, Proceedings, The 7th Scandinavian International Conference on Fluid Power, SICFP, Linköping, Sweden, Vol. 2, pp 23-38.
- [5] MAITI, R. AND SINHA, G. L. (1998) *Kinematics of active contact in modified epitrochoid generated rotary piston machines*, Mechanism and Machine Theory, Vol. 23 No 1, pp 39-45.
- [6] SHUNG J. B., PENNOCK G. R. (1994) *The direct contact problem in a Trochoid-Type Machines*, Mechanism and Machine Theory, Vol. 29, No 5, pp. 673-689.
- [7] RAUSH, G., GAMEZ-MONTERO, P. J., CASTILLA, R., CODINA, E. (2017) *Experimental study on the impulsion port of a trochoid wheeled pump*, Flow Measurement and Instrumentation, Vol. 55, pp 13-22.
- [8] BUONO, D., SCHIANO DI COLA, D., SENATORE, A., FROSINA, E., BUCCILLI G., HARRISON, J. (2016) *Modelling approach on a Gerotor pump working in cavitation conditions*, Energy Procedia, Vol. 101, pp 701-709.
- [9] IVANOVIĆ, L., DEVEDŽIĆ, G., MIRIĆ, N., ČUKOVIC, S. (2010) *Analysis of forces and moments in the gerotor pumps*, Proc. Instn Mech. Engrs, Part C: J. Mechanical Engineering Science, Vol. 224, No 10, pp 2257-2269 DOI: 10.1243/09544062JMES2041, ISSN 0954-4062.
- [10] IVANOVIĆ, L., JOSIFOVIĆ, D., ILIĆ, A., STOJANOVIĆ, B. (2013) *Analytical model of the pressure variation in the gerotor pump chambers*, Technics Technologies Education Management / TTEM, Vol.8, No1, pp 323-331, ISSN 1840-1503.
- [11] IVANOVIĆ, L., DEVEDŽIĆ, G., ČUKOVIC, S., MIRIĆ, N. (2012) *Modeling of the Meshing of Trochoid Profiles With Clearances*, Journal of Mechanical Design, Vol.134, No 4, pp 041003-1 / 041003-9, ISSN 1050-0472, Doi 10.1115/1.4005621
- [12] IVANOVIĆ, L., JOSIFOVIĆ, D., BLAGOJEVIĆ, M., STOJANOVIĆ, B., ILIĆ, A. (2012) *Determination of gerotor pump theoretical flow*, Proceedings, COMETA 2012 1st international scientific conference, Jahorina, B&H Republic of Srpska, 28th-30th November, pp. 243-250.
- [13] TIPEI, N. (1962) *Theory of lubrication*, Stanford university press, Stanford, California
- [14] IVANOVIĆ, L., JOSIFOVIĆ, D., ILIĆ, A., STOJANOVIĆ, B. (2011) *Tribological aspect of the kinematical analysis at trochoid gearing in contact*, Journal of the Balkan Tribological Association (JBTA), Vol. 17, No 1, pp. 37-47, ISSN 1310-4772.
- [15] BAŠTA, T. M. (1990) *Engineering hydraulic*, Faculty of mechanical engineering, Belgrade, Serbia

CORRESPONDANCE



Lozica IVANOVIĆ, Full Prof PhD,
University of Kragujevac,
Faculty of Engineering,
Sestre Janjić 6,
34000 Kragujevac, Serbia,
E-mail: lozica@kg.ac.rs



Andreja ILIĆ, PhD,
University of Kragujevac,
Faculty of Engineering,
Sestre Janjić 6,
34000 Kragujevac, Serbia,
E-mail: andreja.coka@gmail.com



Blaža STOJANOVIĆ, Assist. Prof PhD,
University of Kragujevac,
Faculty of Engineering,
Sestre Janjić 6,
34000 Kragujevac, Serbia,
E-mail: blaza@kg.ac.rs



Jasna GLIŠOVIĆ, Assist. Prof PhD,
University of Kragujevac,
Faculty of Engineering,
Sestre Janjić 6,
34000 Kragujevac, Serbia,
E-mail: jaca@kg.ac.rs



Miloš MATEJIĆ, Teaching Assistant
University of Kragujevac
Faculty of Engineering
Sestre Janjić 6
34000 Kragujevac, Serbia
E-mail: mmatejic@kg.ac.rs

OPTIMAL SYNTHESIS OF THE ROBOT EYES DRIVE SYSTEM WITH 7 DOFs

Marko PENČIĆ
Maja ČAVIĆ
Milan RACKOV

Abstract: This paper presents the optimal synthesis of the eyelids/eyeballs drive system with 7 DOFs for humanoid robots. Eyeballs drive system has 3 DOFs and consists of two identical and interconnected spatial mechanisms which enable motion of the both eyeballs around the pitch axis – elevation/depression movements and out of two identical planar mechanisms which enable independent motion of the eyeballs around the yaw axis – abduction/adduction movements. Eyelids drive system has 4 DOFs and consists of four spatial mechanisms which enable independent motion of each eyelid. Based on the set requirements, an optimization problem has been formed and optimal synthesis was performed. Using optimized parameters of the lower/upper eyelid and eyeball drive systems, kinematic model of the mechanisms has been formed and motion simulation was performed. Obtained angular velocities of the eyelids/eyeball are within the parameters of the human eye. Influence of the pressure angle on the dynamic efficiency of the eyelids/eyeball mechanisms was investigated. All mechanisms have high efficiency because the values of the pressure angle during the entire movement are less than the prescribed maximum. Proposed solution enables the installation of a camera in the eyeball, enabling the artificial vision function of the robot.

Key words: optimal synthesis, robot eyes drive system, planar linkage mechanism, spatial linkage mechanism

1. INTRODUCTION

The eyes are the most expressive part of the face and represent an important functionality aspect of socially interactive robots. If a robot were to look at the face of the person in front of it, an impression of attention and focus would be given. Blinking gives the impression of naturalness. In addition, the intensity of openness and the eyelids position enable expressing various emotions such as surprise, happiness, tiredness, sadness etc. All of this gains importance if the rest of the robot face is rigid and immovable, as is the case with most robots. Therefore, special attention should be given to the design and realization of the eyes.

This paper presents the optimal synthesis of the eyelids/eyeballs drive system for humanoid robots. The paper is structured as follows – the first section shows the research motivation and anatomy of the human eye; the second section represents the analysis of realized solutions of the robotic eyes and their actuation; the third section shows robot eyes drive system; the fourth section presents optimal synthesis of the eyeballs/eyelids drive systems – based on the set requirements, objective function was formed, constraints were prescribed and optimal synthesis is performed; fifth section summarizes the paper contribution and outlooks future work.

1.1. Human eye

The eye is a pair organ that consists of the eyeball, optic nerve and supporting structures – Fig. 1. The eyeball is approximately spherical and is, for the most part,

surrounded with the fat tissue. Due to the transparent structure of its media, the diopter system and the presence of neuroepithelial elements in the retina, the eyeball enables the reception of visual impressions. Visual paths connect the eyeball respectively the nerve membrane – retina, with the visual centers in the brain, and thus the visual stimulus created on the retina is transmitted in the corresponding centers of the brain cortex, where they are interpreted. Additional structures of the eye are eyelids, tear apparatus, muscles, eye socket etc. Their function is to protect the eyeball and to enable complex functioning of the eye. Eyelids are formed of skin, muscles and connective tissue. They protect eyeball and enable the tear flow. Upper eyelid is twice as wide as the lower one [1, 2].

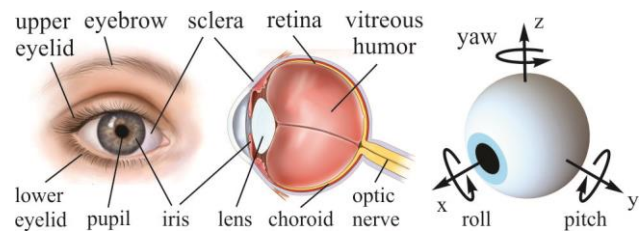


Fig. 1: Human eye anatomy and eyeball movements

The eyeball has 3 DOFs and enables the abduction/adduction movements – rotation around the yaw axis, elevation/depression movements – rotation around the pitch axis and excyclotorsion/incyclotorsion movements – rotation around the roll axis. Mobility is the largest around the yaw axis – approximately 100°, then around the pitch axis – approximately 75°, and at least around the roll axis –

approximately 10° [3]. Maximal velocity of the eyeball occurs during saccadic movements – simultaneous movement of both eyes between two or more phases of fixation in the same direction. This movement lasts 0.2 s, and velocity interval is from 400 to 800°/s [4]. The average duration for a single blink of eye is 0.1 to 0.4 s [5].

2. STATE OF THE ART

There are two basic groups of robots that are able to move eyeballs and/or eyelids independently from the face. The first group of the robots has eyeballs with 3 DOFs which enable movements of both eyeballs around the pitch axis and independent motion of the eyeballs around the yaw axis – Flobi [6], iCat [7], iCub [8], Kismet [9], Melvin [10], Infanoid [11], Muecas [12], Fritz [13], Domo [14], Probo [15], Twente Humanoid Head [16], EDDIE [17], CB² [18], MERTZ [19], WE-4RII [20], KOBIAN [21], BARTHOC [22] etc. The second group of the robots has eyeballs with 4 DOFs which enable independent motion of eyeball around the pitch and yaw axes – James [23], Romeo [24], Robotinho [25], EveR-1 [26], EveR-2 [27], ARMAR-4 [28], ROMAN [29], KIBO [30], HUBO [31] etc. Upper eyelids can be actuated together with the eyeballs or separately from them – it is possible to move both eyelids together or individually, while the lower eyelids are usually immovable. Power transmission and motion from actuators to the output members of the eyes drive system – eyeballs and eyelids, is most frequently done with belt mechanisms, lever mechanisms and low backlash gear mechanisms which secure high positioning accuracy and repeatability of movements, which is essential for motion control. Beside this, there are robot eyes realizations based on the biological principles using pneumatic artificial muscles – PAMs [32].

3. ROBOT EYES DRIVE SYSTEM

Fig. 2 shows a kinematic scheme of the eyeballs drive system which has 3 DOFs and enables the rotation of both eyeballs around the pitch axis – angles θ_L and θ_R , and independent motion of the eyeballs around the yaw axis – angles ϕ_L and ϕ_R . Eyeball 1 and 2 are spheres of radius r with center in the point O_L and O_R , respectively. Movements of the eyeballs around the pitch axis are generated by two identical spatial mechanisms 3 and 4 which are interconnected with the planar mechanism 7. Actuation is performed by the motor 10 – joint D_{OR} . Movements of the eyeballs around the yaw axis are generated by two identical planar mechanisms 5 and 6 which are actuated by motors 8 and 9 – joints A_{OL} and A_{OR} . Given that the mechanisms 3 and 4, respectively 5 and 6, are identical, only one eyeball is further considered, so the indices L – left and R – right, can be neglected.

Fig. 3 shows the kinematic scheme of the eyelids drive system which has 4 DOFs and enables independent motion of the each eyelid around the pitch axis – angles ψ_{UL} , ψ_{UR} , ψ_{LL} and ψ_{LR} . It consists of four spatial mechanisms 5, 6, 7 and 8, which are actuated by motors 9, 10, 11 and 12 – joints M_{OL} , P_{OL} , M_{OR} and P_{OR} . Given that the mechanisms 5 and 7, respectively 6 and 8, are identical, only one eyelid is further considered, so the indices L – left and R – right, can be neglected.

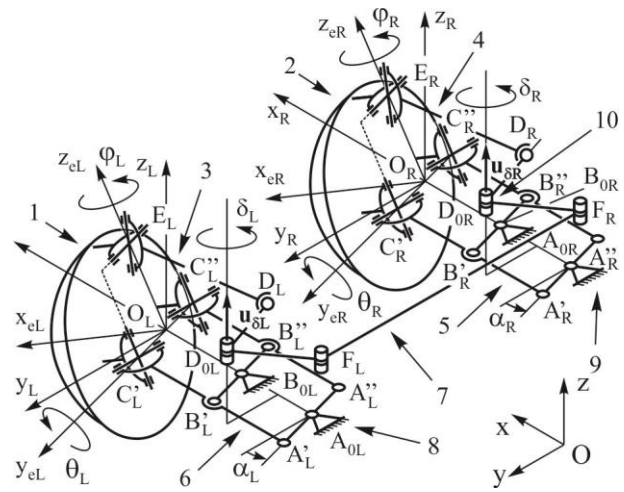


Fig. 2: Kinematic scheme of the eyeballs drive system: 1 and 2 – left and right eyeball, 3 and 4 – spatial mechanisms, 5, 6 and 7 – planar mechanisms, 8 and 9 – motors for abduction/adduction movements and 10 – motor for elevation/depression movements

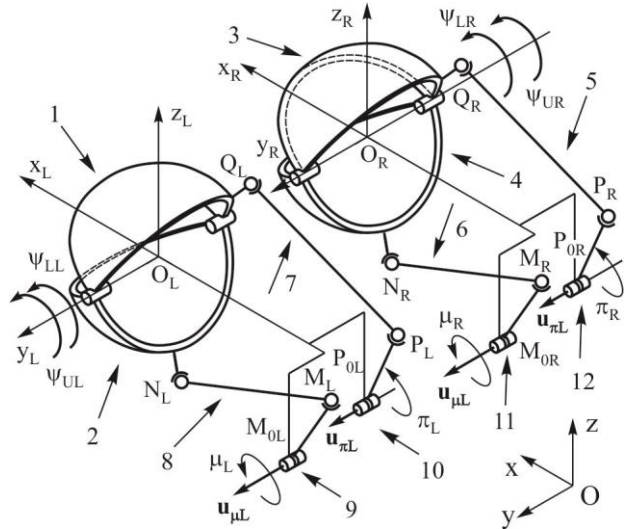


Fig. 3: Kinematic scheme of the eyelids drive system: 1 and 3 – upper left and right eyelid, 2 and 4 – lower left and right eyelid, 5, 6, 7 and 8 – spatial mechanisms, 9 and 11 – motors for driving lower eyelids, and 10 and 12 – motors for driving upper eyelids

3.1. Eyeball drive system

Fig. 4 is shows the kinematic scheme of the eyeball drive system consisting of a planar and spatial mechanism. Due to the structure of the links, the mechanisms can function independently. Local coordinate system with the center in point O and axes x_e, y_e, z_e is fixed to the eyeball and in the initial position coincides with the axis of main – immovable coordinate system Oxyz.

Planar mechanism consists of two four-bar linkages $A_0A'B'B_0$ and $A_0A''B''B_0$. Points A', A_0 and A'' as well as points B', B_0 and B'' are located on the same lever. Angle α is an input parameter and represents the rotation of lever $A'A''$ around the point A_0 . Four-bar linkages are of the parallelogram configurations, so $A_0A'=B'B_0$ and $A_0A''=B''B_0$. In addition, $A_0A'=A_0A''$, $B'B_0=B''B_0$, $A'B'=A''B''$ and $C'B'=C''B''$. Connections between the

eyeballs and the mechanisms – points C' and C'', are of the second order and enable two rotations whereby the axes of rotation are mutually perpendicular. One axis is parallel to the y axis and the other with the z_e axis. Centers of links – points C' and C'' are on y_e axis. Spatial mechanism represents a four-bar linkage of RSCR configuration. The input link is a lever D₀D which is by a cylindrical joint connected to an immovable link in the point D₀. Lever D₀D performs a rotation by angle δ around an axis whose unit vector is **u**_δ. Lever D₀D is connected by spherical joint to the floating link DE in the point D. Link DE is connected to the output link – eyeball at point E with a second order connection, which is on the z_e axis. Rotation axes are mutually perpendicular – one axis is parallel to the y_e axis, and the other is, at the initial position, parallel to z axis.

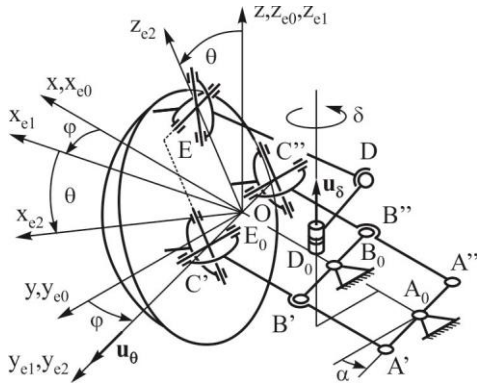


Fig. 4: Kinematic scheme of the eyeball drive system

3.2. Eyelid mechanism

Fig. 4 shows the kinematic scheme of eyelid mechanism – spatial four-bar mechanism. Movable links are input link M₀M, floating link MN and output link – lower eyelid. In order to simplify, a lever N₀N is considered as the output link. Mechanism is RSSR type. The connection between the immovable link and the input link M₀M is a cylindrical joint in point M₀ enabling the rotation of one link relative to another around an axis whose unit vector is **u**_μ. The connection between the input link M₀M and the floating link MN is a spherical joint in the point M. The connection between the floating link MN and the output link N₀N is the spherical joint in the point N. The connection

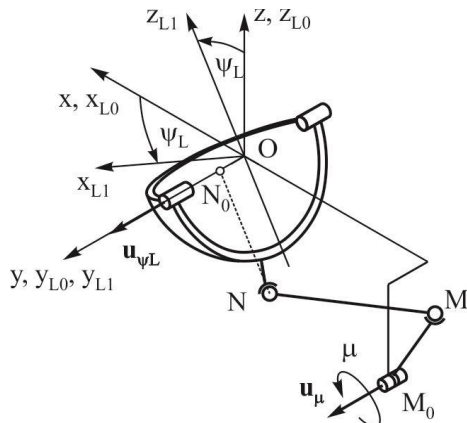


Fig. 5: Kinematic scheme of the eyelid mechanism

between the output and immovable link is a cylindrical joint in the point N₀ with the axis of rotation which is defined by unit vector **u**_{ψL}.

4. OPTIMAL SYNTHESIS

Optimization goal is to maximize angular velocity of the eyelids/eyeball so that they can perform movements similar to those of the human eyelids/eyeball. Angular velocity of the eyeball around the yaw axis is equal to the angular velocity of the motors 8 and 9 – joints A_{0L} and A_{0R}, due to the planar mechanism of parallelogram configuration – see Fig. 2, so it will not be considered in optimization process.

Optimization problem presents minimization of the objective function for the set constraints:

$$\text{MIN } f(x), x \in D \quad (1)$$

where:

$x = (x_1, x_2, \dots, x_m)$ - vector variables,

$D = \{x \in R^n \mid g(x) \leq 0 \wedge h(x) = 0\}$ - a set of solutions that fulfills the defined constraints,

$g(x) \leq 0$ and $h(x) = 0$ - constraint vectors.

Objective function is formed as:

$$f(x) = \frac{1}{|\dot{\theta}|_{\max}} + \frac{1}{|\dot{\psi}_U|_{\max}} + \frac{1}{|\dot{\psi}_L|_{\max}} \quad (2)$$

where:

$|\dot{\theta}|_{\max}, |\dot{\psi}_U|_{\max}, |\dot{\psi}_L|_{\max}$ - maximum absolute values of the corresponding angular velocities during analyzed movement – see Fig. 6. Eyelids perform a blink moving from $\psi_{U\text{ OPEN}}, \psi_{L\text{ OPEN}}$ to $\psi_{U\text{ CLOSED}}, \psi_{L\text{ CLOSED}}$ and then back to $\psi_{U\text{ OPEN}}, \psi_{L\text{ OPEN}}$, respectively. Eyeball moves from θ_{START} to θ_{END} .

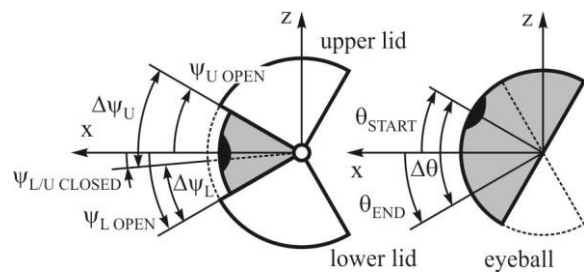


Fig. 6: Lower/upper eyelid and eyeball – change of position

As for constraints, desired intervals of motion for eyelids/eyeball are defined first:

$$h_1 = \Delta\psi_U - 35^\circ = 0 \quad (3)$$

$$h_2 = \Delta\psi_L - 25^\circ = 0 \quad (4)$$

$$h_3 = \Delta\theta - 60^\circ = 0 \quad (5)$$

Eyelids must not overlap, so:

$$h_4 = \psi_{U\text{ CLOSED}} - 5^\circ = 0 \quad (6)$$

$$h_5 = \psi_{L\text{ CLOSED}} - 5^\circ = 0 \quad (7)$$

Eyeball movement is symmetric with respect to the pitch axis:

$$h_6 = |\theta_{START}| - |\theta_{END}| = 0 \quad (8)$$

By decreasing pressure angle most of the power is used for overcoming workload, and lesser for internal loads, so the mechanism is more efficient. As high values of pressure angle can lead to the jamming of the mechanism, following constraints are defined – maximum pressure angles must not exceed 45° :

$$g_1(x) = \alpha_{UPPLIDMAX} - 45^\circ \leq 0 \quad (9)$$

$$g_2(x) = \alpha_{LOWLIDMAX} - 45^\circ \leq 0 \quad (10)$$

$$g_3(x) = \alpha_{EYEBALLMAX} - 45^\circ \leq 0 \quad (11)$$

Kinematic analysis of the eyeballs/eyelids drive systems and determination of all kinematic parameters are presented in [33]. Head of the robot has to accommodate the robot eyes drive system, so constraints concerning the dimensions of the mechanism in form of equalities and inequalities are set – Tables 1, 2 and 3.

Table 1. Lower eyelid parameters – lower/upper bounds

	$\overline{M_0M}$ [mm]	\overline{MN} [mm]	$\overline{N_0N}$ [mm]	x_{M0} [mm]	y_{M0} [mm]	z_{M0} [mm]	μ_{START} [°]	$\Delta\mu$ [°]
Lower	15	80	32	-80	27.5	-37.5	20	25
Upper	25	110	38	-120	27.5	-37.5	40	45

Table 2. Upper eyelid parameters – lower/upper bounds

	$\overline{P_0P}$ [mm]	\overline{PQ} [mm]	$\overline{Q_0Q}$ [mm]	x_{P0} [mm]	y_{P0} [mm]	z_{P0} [mm]	π_{START} [°]	$\Delta\pi$ [°]
Lower	15	80	32	-80	29	-17.5	40	45
Upper	25	110	38	-120	29	-17.5	60	65

Table 3. Eyeball parameters – lower/upper bounds

	$\overline{D_0D}$ [mm]	\overline{DE} [mm]	$\overline{E_0E}$ [mm]	x_{D0} [mm]	y_{D0} [mm]	z_{D0} [mm]	δ_{START} [°]	$\Delta\delta$ [°]
Lower	15	80	15	-60	10	7.5	50	50
Upper	25	110	25	-100	10	7.5	70	70

With defined objective function and constraints, optimal synthesis of the eyeballs/eyelids drive systems was performed in MATLAB and optimized design and kinematic parameters were obtained – Tables 4, 5 and 6.

Table 4. Lower eyelid parameters after optimization

$\overline{M_0M}$ [mm]	\overline{MN} [mm]	$\overline{N_0N}$ [mm]	x_{M0} [mm]	y_{M0} [mm]	z_{M0} [mm]	μ_{START} [°]	$\Delta\mu$ [°]
17.71	104.03	37.10	-119.06	27.5	-37.5	38.43	44.40

Table 5. Upper eyelid parameters after optimization

$\overline{P_0P}$ [mm]	\overline{PQ} [mm]	$\overline{Q_0Q}$ [mm]	x_{P0} [mm]	y_{P0} [mm]	z_{P0} [mm]	π_{START} [°]	$\Delta\pi$ [°]
20.10	94.54	33.88	-99.80	29	-17.5	49.65	56.16

Table 6. Eyeball parameters after optimization

$\overline{D_0D}$ [mm]	\overline{DE} [mm]	$\overline{E_0E}$ [mm]	x_{D0} [mm]	y_{D0} [mm]	z_{D0} [mm]	δ_{START} [°]	$\Delta\delta$ [°]
20.04	80.61	20.40	-80.01	10	7.5	60.70	61.09

Using optimized parameters of the lower/upper eyelid and eyeball drive systems, kinematic model has been formed and motion simulation was conducted – Figs. 7 and 8. Duration of all movements is adopted to be 0.3 s.

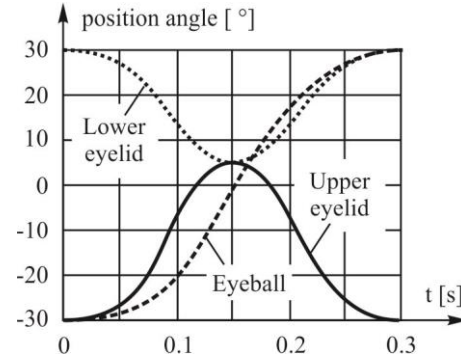


Fig. 7: Time histories of the position angles

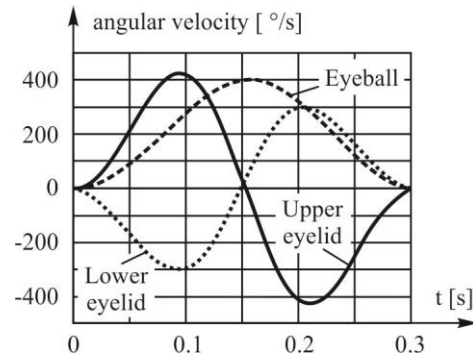


Fig. 8: Time histories of the angular velocities

The lower eyelid performs a movement from 30° to 5° – closing the eyelid and from 5° to 30° – opening the eyelid. In the initial position, the lower eyelid is opened and is rotated by 30° around the y axis, i.e. the eyelid is in the lower end position. The maximum value of angular velocity is $298.14^\circ/s$.

The upper eyelid performs a movement from -30° to 5° – closing the eyelid and from 5° to -30° – opening the eyelid. In the initial position, the upper eyelid is opened and is rotated by -30° around the y axis, i.e. the eyelid is in the upper end position. The maximum value of angular velocity is $425.46^\circ/s$.

Eyeball movement in the direction of elevation/depression is 60° . In the initial position, the eyeball is rotated by -30° around the y axis. The maximum value of angular velocity is $401.4^\circ/s$.

Robot eyes drive system must be movable and efficient in all positions during the motion. Therefore, the influence of the pressure angle on the dynamic efficiency during the entire movement of the eyelids/eyeball mechanisms was investigated. Pressure angle for all mechanisms are less than the prescribed maximum which is 45° . Pressure angles time histories are shown in Fig. 9.

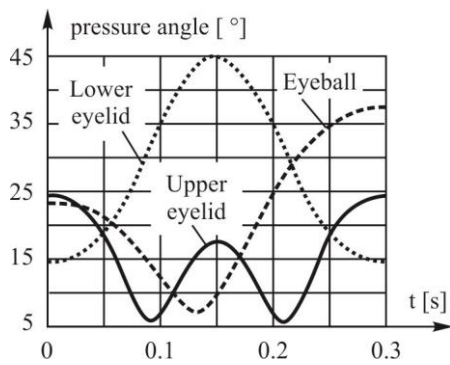


Fig. 9: Time histories of the pressure angles

5. CONCLUSION

This paper presents the optimal synthesis of the eyelids/eyeballs drive system with 7 DOFs for humanoid robots. Eyeballs drive system has 3 DOFs and consists of two identical and interconnected spatial mechanisms which enable motion of the both eyeballs around the pitch axis – elevation/depression movements and out of two identical planar mechanisms which enable independent motion of the eyeballs around the yaw axis – abduction/adduction movements. Eyelids drive system has 4 DOFs and consists of four spatial mechanisms which enable independent motion of each eyelid. Based on the set requirements, an optimization problem has been formed and objective function was defined – angular velocity of the eyelids/eyeball has to be as large as possible. Constraints in form of equalities and inequalities were prescribed and optimal synthesis of the robot eyes drive system was performed. Using optimized parameters of the lower/upper eyelid and eyeball drive systems, kinematic model of the mechanisms has been formed and motion simulation was conducted. Duration of all movements is adopted to be equal and has value of 0.3 s. Movements which were observed are closing and opening of the eye. For lower eyelid and interval of motion $\pm 25^\circ$, maximal angular velocity is $298.14^\circ/\text{s}$, while for upper eyelid and interval of motion $\pm 35^\circ$, maximal angular velocity is $425.46^\circ/\text{s}$. For eyeball movement around pitch axis and interval of motion $\pm 30^\circ$, maximal angular velocity is $401.4^\circ/\text{s}$. Angular velocities of the eyelids/eyeball are within the parameters of the human eye. Robot eyes drive system must be movable and efficient in all positions during movement, so influence of the pressure angle on the dynamic efficiency of the eyelids/eyeball mechanisms was investigated. All mechanisms have high efficiency because the values of the pressure angle during the entire movement are less than the prescribed maximum. In addition, the proposed solution enables the installation of a camera in the eyeball, enabling the artificial vision function of the robot. In the further work, possibility to reduce additionally the dimensions, the pressure angles as well as the time duration of the movements, will be investigated.

REFERENCES

[1] Cvetković, D., Golubović, S., Hentova-Senčanić, P., Ignjačev, M., Jovanović, M., Kontić, Đ., Latković, Z., Milenković, S., Misita, V., Risović, D.,

Stanojević-Paović A. (2010) *Ophthalmology for Medical Students*, Faculty of Medicine, Belgrade

[2] Litričin, O., Blagojević, M., Cvetković, D. (2004) *Ophthalmology*, Elit Medica, Belgrade

[3] Shin, Y., Lim, H.W., Kang, M.H., Seong, M., Cho, H., Kim, J.H. (2013) *Normal range of eye movement and its relationship to age*, Acta Ophthalmologica, Vol. 94, Suppl. 256, pp. n/a–n/a

[4] Schiffman, H.R. (2001) *Sensation and Perception: An Integrated Approach*, John Wiley & Sons, New York, NY, USA

[5] Sparks, D.L. (2002) *The Brainstem Control of Saccadic Eye Movements*, Nature Reviews Neuroscience, Vol. 3, pp. 952–964

[6] Hegel, F., Eyssel, F., Wrede, B. (2010) *The Social Robot 'Flobi': Key Concepts of Industrial Design*, Proceedings of the 19th International Symposium in Robot and Human Interactive Communication (RO-MAN 2010), Viareggio, Italy, pp. 107–112

[7] van Breemen, A.J.N. (2004) *Animation Engine for Believable Interactive User-Interface Robots*, Proceedings of the IEEE/RSJ International Conference on Intelligent Robots and Systems (IROS 2004), Sandai, Japan, Vol. 3, pp. 2873–2878

[8] Parmiggiani, A., Maggiali, M., Natale, L., Nori, F., Schmitz, A., Tsagarakis, N., Santos-Victor, J., Becchi, F., Sandini, G., Metta, G. (2011) *The Design of the iCub Humanoid Robot*, International Journal of Humanoid Robotics, Vol. 9, No. 4, pp. 1–24

[9] Breazeal, C. (2003) *Emotion and Sociable Humanoid Robots*, International Journal of Human-Computer Studies, Vol. 59, No. 1-2, pp. 119–155

[10] Shayganfar, M., Rich, C., Sidner, C.L. (2012) *A Design Methodology for Expressing Emotion on Robot Faces*, Proceedings of the IEEE/RSJ International Conference on Intelligent Robots and Systems (IROS 2012), Vilamoura, Portugal, pp. 4577–4583

[11] Kozima, H. (2002) *Infanoid: A Babybot that Explores the Social Environment*, In book: Dautenhahn, K., Bond, A., Cañamero, L., Edmonds B. (Eds.) *Socially Intelligent Agents: Creating Relationships with Computers and Robots*. MSASSO, Vol. 3, pp. 157–164, Springer

[12] Cid, F., Moreno, J., Bustos, P., Núñez, P. (2014) *Muecas: A Multi-Sensor Robotic Head for Affective Human Robot Interaction and Imitation*, Sensors, Vol. 14, No. 5, pp. 7711–7737

[13] Bennewitz, M., Faber, F., Joho, D., Behnke, S. (2007) *Fritz – A Humanoid Communication Robot*, Proceedings of the 16th IEEE International Conference on Robot and Human Interactive Communication (RO-MAN 2007), Jeju, Korea, pp. 1072–1077

[14] Edsinger-Gonzales, A., Weber, J. (2004) *Domo: A Force Sensing Humanoid Robot for Manipulation Research*, Proceedings of the 4th IEEE-RAS International Conference on Humanoid Robots (Humanoids 2004), Santa Monica, pp. 273–291

[15] Goris, K., Saldien, J., Vanderborght, B., Lefeber, D. (2011) *Mechanical Design of the huggable Robot Probo*, International Journal of Humanoid Robotics, Vol. 8, No. 3, pp. 481–511

- [16] Reilink, R., Visser, L.C., Brouwer, D.M., Carloni, R., Stramigioli, S. (2011) *Mechatronic Design of the Twente Humanoid Head*, Intelligent Service Robotics, Vol. 4, No. 2, pp. 107–118
- [17] Sosnowski, S., Bittermann, A., Kuhnlenz, K., Buss, M. (2006) *Design and Evaluation of Emotion-Display EDDIE*, Proceedings of the IEEE/RSJ International Conference on Intelligent Robots and Systems (IROS 2006), Beijing, pp. 3113–3118
- [18] Minato, T., Yoshikawa, Y., Noda, T., Ikemoto, S., Ishiguro, H., Asada M. (2007) *CB²: A Child Robot with Biomimetic Body for Cognitive Developmental Robotics*, Proceedings of the 7th IEEE-RAS International Conference on Humanoid Robots (Humanoids 2007), Pittsburgh, PA, USA, pp. 557–562
- [19] Aryananda, L., Weber, J. (2004) *MERTZ: A Quest for a Robust and Scalable Active Vision Humanoid Head Robot*, Proceedings of the 4th IEEE-RAS International Conference on Humanoid Robots (Humanoids 2004), Santa Monica, CA, USA, pp. 513–532
- [20] Itoh, K., Miwa, H., Zecca, M., Takanobu, H., Roccella, S., Carrozza, M.C., Dario, P., Takanishi, A. (2006) *Mechanical Design of Emotion Expression Humanoid Robot WE-4RII*, In book: Zielinska, T., Zielinski, C. (Eds.) ROMANSY 16: Robot Design, Dynamics and Control. CISM, Vol. 487, pp. 255–262, Springer
- [21] Zecca, M., Endo, N., Momoki, S., Itoh, K., Takanishi, A. (2008) *Design of the Humanoid Robot KOBIAN – Preliminary Analysis of Facial and Whole Body Emotion Expression Capabilities*, Proceedings of the 8th IEEE-RAS International Conference on Humanoid Robots (Humanoids 2008), Daejeon, Korea, pp. 487–492
- [22] Spexard, T.P., Hanheide, M., Sagerer G. (2007) *Human-Oriented Interaction with an Anthropomorphic Robot*, IEEE Transactions on Robotics, Vol. 23, No. 5, pp. 852–862
- [23] Jamone, L., Metta, G., Nori, F., Sandini, G. (2006) *James: A Humanoid Robot Acting over an Unstructured World*, Proceedings of the 6th IEEE-RAS International Conference on Humanoid Robots (Humanoids 2006), Genova, Italy, pp. 143–150
- [24] Pateromichelakis, N., Mazel, A., Hache, M.A., Koumpogiannis, T., Gelin, R., Maisonnier, B., Berthoz, A. (2014) *Head-Eyes System and Gaze Analysis of the Humanoid Robot Romeo*, Proceedings of the IEEE/RSJ International Conference on Intelligent Robots and Systems (IROS 2014), Chicago, IL, USA, pp. 1374–1379
- [25] Faber, F., Bennewitz, M., Eppner, C., Gorog, A., Gonsior, C., Joho, D., Schreiber, M., Behnke, S. (2009) *The Humanoid Museum Tour Guide Robotinho*, Proceedings of the IEEE International Symposium on Robot and Human Interactive Communication (RO-MAN 2009), Toyama, Japan, pp. 891–896
- [26] Hirth, J., Schmitz, N., Berns, K. (2007) *Emotional Architecture for the Humanoid Robot Head ROMAN*, Proceedings of the IEEE International Conference on Robotics and Automation (ICRA 2007), Roma, Italy, pp. 2150–2155
- [27] Ahn, H.S., Lee, D.-W., Choi, D., Lee, D.Y., Hur, M.H., Lee, H., Shon, W.H. (2011) *Development of an Android for Singing with Facial Expression*, Proceedings of the 37th Annual Conference of the IEEE Industrial Electronics Society (IECON 2011), Melbourne, Australia, pp. 104–109
- [28] Asfour, T., Schill, J., Peters, H., Klas, C., Bucker, J., Sander, C., Schulz, S., Kargov, A., Werner, T., Bartenbach, V. (2013) *ARMAR-4: A 63 DOF Torque Controlled Humanoid Robot*, Proceedings of the 13th IEEE-RAS International Conference on Humanoid Robots (Humanoids 2013), Atlanta, GA, USA, pp. 390–396
- [29] Hirth, J., Schmitz, N., Berns, K. (2007) *Emotional Architecture for the Humanoid Robot Head ROMAN*, Proceedings of the IEEE International Conference on Robotics and Automation (ICRA 2007), Roma, Italy, pp. 2150–2155
- [30] Lee, S., Kim, J.-Y., Kim, M. (2013) *Development and Walking Control of Emotional Humanoid Robot*, KIBO, International Journal of Humanoid Robotics, Vol. 10, No. 4, pp. 1–35
- [31] Park, I.-W., Kim, J.-Y., Lee, J., Oh, J.-H. (2007) *Mechanical Design of the Humanoid Robot Platform, HUBO*, Advanced Robotics, Vol. 21, No. 11, pp. 1305–1322
- [32] Wang, X.-Y., Zhang, Y., Fu, X.-J., Xiang, G.-S. (2008) *Design and Kinematic Analysis of a Novel Humanoid Robot Eye using Pneumatic Artificial Muscles*, Journal of Bionic Engineering, Vol. 5, No. 3, pp. 264–270
- [33] Penčić, M., Čavić, M., Rackov, M., Borovac, B., Knežević, I., Zlokolica, M. (2017) *Kinematic Analysis of the Robot Eyes Drive System with 7 DOFs*, Proceedings of the 8th PSU-UNS International Conference on Engineering and Technology (ICET 2017), Novi Sad, Serbia, pp. PS-1.14-1– PS-1.14-5

CORRESPONDANCE



Marko PENČIĆ, Res. Assoc. M.Sc.
University of Novi Sad
Faculty of Technical Sciences
Trg Dositeja Obradovica 6
21000 Novi Sad, Serbia
mpencic@uns.ac.rs



Maja ČAVIĆ, Assoc. Prof. Ph.D.
University of Novi Sad
Faculty of Technical Sciences
Trg Dositeja Obradovica 6
21000 Novi Sad, Serbia
scomaja@uns.ac.rs



Milan RACKOV, Assis. Prof. Ph.D.
University of Novi Sad
Faculty of Technical Sciences
Trg Dositeja Obradovica 6
21000 Novi Sad, Serbia
racmil@uns.ac.rs

HUMAN ACTION RECOGNITION BY ROBOT VISION SYSTEM BASED ON KALMAN FILTER AND NEURAL NETWORK CLASSIFICATION

Emina PETROVIĆ
Miloš SIMONOVIĆ
Ivan ĆIRIĆ
Vlastimir NIKOLIĆ

Abstract: *There is growing interest in the research of human action recognition in human-robot interactive applications. A lot of attention is devoted to a human action recognition based on the trajectory of human tracking where it is necessary to transform quantitative data of the human movements into qualitative data. In the other words, the numerical characteristics such as speed, direction, etc., of the observed person can be presented as "moving towards something" or "moving away from something" or "standing relative to something". In this paper, the problem of identifying human action based on information received from robust vision system, in order to carry out tasks when a robot behaves as a human's assistant, helping the human co-worker with transportation of different objects is presented. A 3D Asus Xtion Pro Live camera was used as a robotic vision sensor in the laboratory experimental scenario. Since one of the key requirements in the field of service robotics is a robotic vision system, which provides reliable outputs in order to control the mobile human-collaboration robot, the robust vision system for human tracking based on Kalman filter was developed.*

Key words: *neural network, human action recognition, robust robotic vision, Kalman filter*

1. INTRODUCTION

In the future years, it is expected that service robots will become a part of human's everyday life, and will play an important role as human's appliances, servants and assistants [1].

In human-robot interactive applications it is expected from robots to be able to track human motion to avoid colliding with them, to acquire a sufficient understanding of the environment, to detect and track people with minimum instruction and with high precision and also to be able to make decisions based on their recognition of human action in order to become functional collaborators in different situations. [2,3,4]. For example, a mobile robot which works in a team helping the human co-worker in investigation of contaminated / hazardous environments carrying containers with collected samples from the environment.

In the literature, there are many number classification methods for human action recognition such as vector machines (SVM) [5], decision trees classifiers [6], k-nearest neighbour (kNN) classifier [7], hidden Markov models [8], neural networks [9], as well as data mining algorithms such as Naïve Bayes classifier [10] and Bayesian Network Classifiers [11].

Human action recognition based on trajectory of human motion also attracted a lot of attention.

In the other words, quantitative data of the human movements such as speed, direction, etc., of the observed person, is necessary to transform into qualitative numerical characteristics to represent an action [12].

The research presented in this paper, refers to the problem of human action recognition based on the information received from the robust robotic vision system that uses a 3D Asus Xtion Pro Live camera [13] as the sensor of robotic vision, in order to perform tasks in which a robot behaves as a human assistant.

In order to build a system of robotic vision that is robust in relation to various external influences such as change of lighting, changing the angle of recording and the presence of many different objects on the scene, it is necessary to perform the prediction of the position of the human who is tracked by a mobile robot. For that purpose the robust vision system for human tracking based on Kalman filter that provides reliable outputs, even in cases when the vision does not provide data due to various disturbances in the system, was developed.

The robotic system presented in this paper should be able to detect and follow a single person in the working scenario, maintaining a constant distance from the human, based on the information obtained by a robotic vision. In addition, the robot should be able to "predict" the intendancy of a human to come closer to the robot and in this case, it should stop and let the human to put something on the mobile robotic platform.

In order for robot to understand the human actions and to behave in accordance with them, it is necessary to semantically translate the information provided by a sensor robot vision. In other words, information about the position of human have to be translated into human

action. Human actions are identified as a "moving away from the robot", "stands in relation to the robot" and "moving towards the robot". The classification of the human action recognition is performed by using the neural network-based classifier.

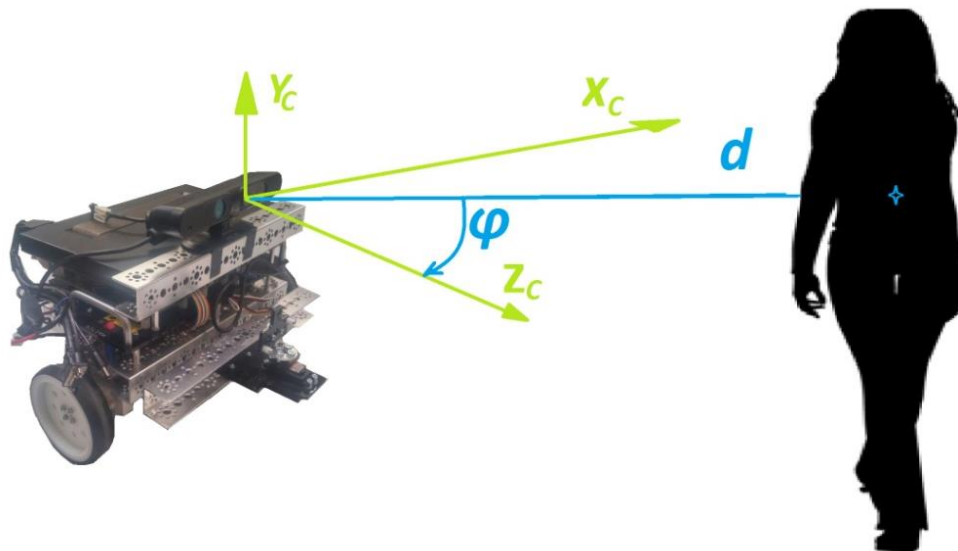
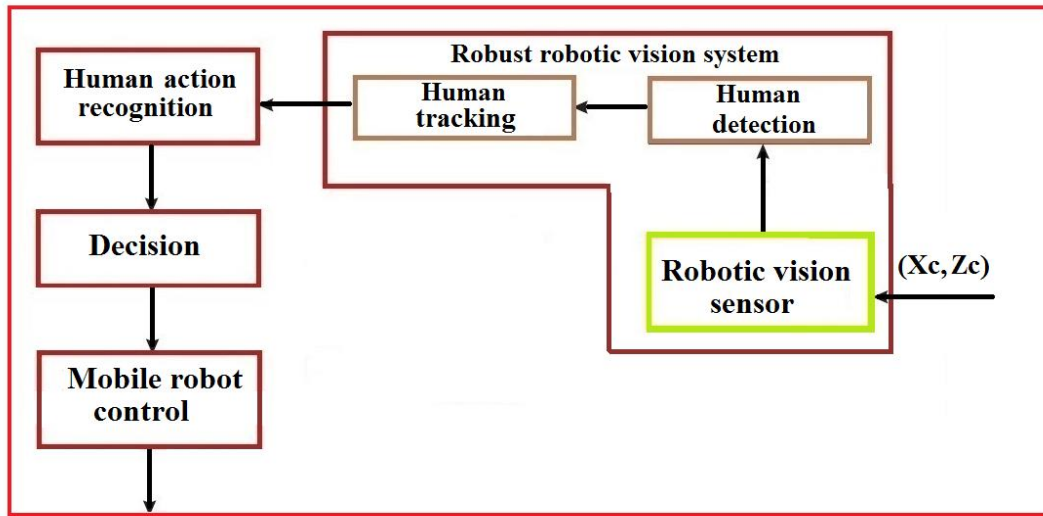


Fig.1: Principal layout of the robotic system for following the human co-worker

2. EXPERIMENTAL SETUP

The mobile robot platform NI Robotics Starter Kit 2.0, known as DaNI robot developed by National Instruments [14] is used as the platform for robotic system. The robot has sensors, motors and NI Single-Board RIO-9632 control panel with the processor for work in real time. The mobile robot we used has two wheels driven by two motors and one auxiliary wheel without the drive. As a robot vision sensor, Asus Xtion PRO LIVE 3D camera was used, which is connected to the embedded PC (Intel Core i7 3517UE 1.7GHz, 16GB RAM) [15] placed on a mobile robotic platform, which communicates over the LAN cable to the robot (Fig.1).

In order to obtain valid data for further processing and finally to control the mobile robotic platform, it was

necessary to develop a model for data acquisition and human detection from images obtained by a robotic vision sensor.

In Figure 3 it is shown the model for data acquisition by ASUS Xtion PRO LIVE camera. Obtained data is used for human detection as well as for calculation of the 2D coordinates of human's center of mass in camera coordinate system (X_{HC}, Z_{HC}).

Determining of 2D position of the walking person in front of the robot was done with respect to the horizontal plane coordinate system with the center placed on the camera mounted on the robotic platform.

The frame rate of the used camera is 30 frames per second (fps).

One example of original, depth image, and image with detected human obtained by ASUS Xtion PRO LIVE 3D camera is shown in figure 4.

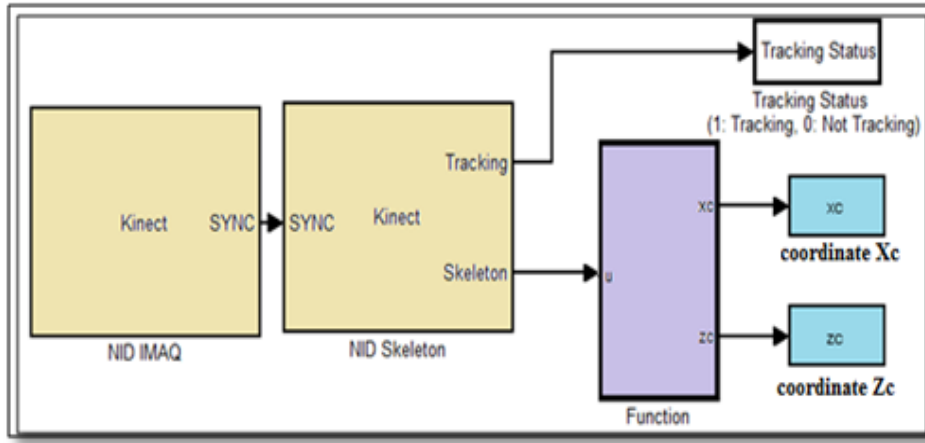


Fig. 3: Model for acquisition data of 2D human position by ASUS Xtion PRO LIVE camera

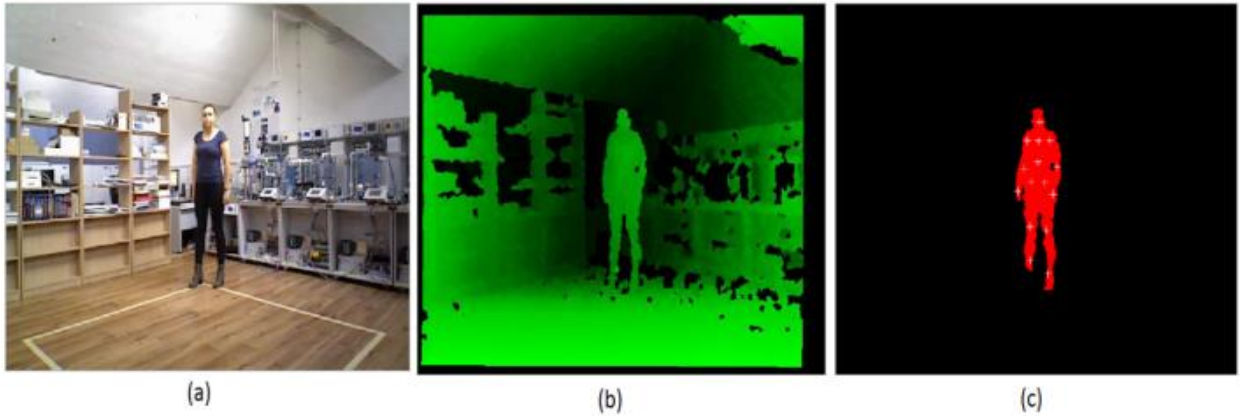


Fig. 4: Data recording for neural network training: a) Original image, b) Depth image, c) Detected human

The presented robotic system should be able to detect and follow a single person in the working scenario, maintaining a constant distance of 1.5 m from the human and be oriented so that the human is always in front of the camera and aligned with the Z_C axis.

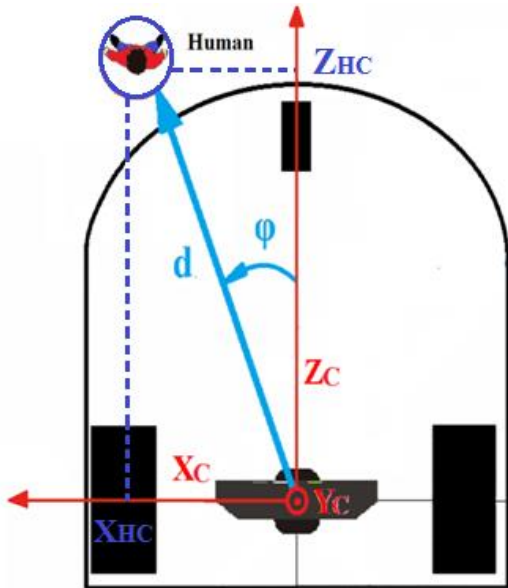


Fig.5: Distance d and the alignment angle φ with respect to the horizontal plane coordinate system with the center placed on the camera mounted on the robotic platform

Based on 2D position of the human (Fig.5), the distance d and the alignment angle φ are calculated according to:

$$d = \sqrt{X_{HC}^2 + Z_{HC}^2} \quad (1)$$

$$\varphi = \arctg \frac{X_{HC}}{Z_{HC}} \quad (2)$$

3. ROBUST ROBOTIC VISION SYSTEM BASED ON KALMAN FILTER

A robotic vision system that provides reliable inputs to the control module of the mobile robot due to various disturbances in the system, is one of the key requirements in robot-human applications.

For that purpose in this paper, the robust vision system for human tracking based on Kalman filter was developed. In the Kalman Filter approach [16], it is presumed that the behavior of a moving object could be characterized by the following predefined motion and measurement models:

$$\mathbf{x}_k = \mathbf{F}\mathbf{x}_{k-1} + \mathbf{w}_k \quad (3)$$

$$\mathbf{y}_k = \mathbf{H}\mathbf{x}_k + \mathbf{v}_k \quad (4)$$

The models can be represented in terms of a state vector \mathbf{x}_k that corresponds to image frame k . In (3) \mathbf{F} represents

the state transition matrix which determines the relationship between the present state \mathbf{x}_k and the previous one \mathbf{x}_{k-1} and the matrix \mathbf{H} describes the relationship between the measurement vector \mathbf{y}_k and the state vector \mathbf{x}_k . The vectors \mathbf{w}_k and \mathbf{v}_k are noise terms which are assumed to be independent of each other, Gaussians with zero mean and covariance matrices $\mathbf{Q} = E[\mathbf{w}_k \mathbf{w}_k^T]$ and $\mathbf{R} = E[\mathbf{v}_k \mathbf{v}_k^T]$.

We assume that the velocity of the tracked human is constant between the subsequent video frames, so the state vector is simplified and does not include the acceleration term. By considering a constant velocity, the state transition matrix \mathbf{F} can be determined from the basic kinematic equations as follows:

$$\mathbf{S}_k = \mathbf{S}_{k-1} + \mathbf{V}_{k-1} \cdot \Delta t \quad (5)$$

$$\mathbf{V}_k = \mathbf{V}_{k-1} \quad (6)$$

where the vector \mathbf{S}_k represents the position (X_{HC}, Z_{HC}) of a human in frame k , in relation to the coordinate system of camera, the vector \mathbf{V}_k represents the velocities in the X_c and Z_c direction and the Δt represents the sampling interval.

In the presented system, we want to predict and estimate the state of vector \mathbf{x}_k , defined as:

$$\mathbf{x}_k = [\mathbf{S}_k \quad \mathbf{V}_k]^T = [X_{HC} \quad Z_{HC} \quad \dot{X}_{HC} \quad \dot{Z}_{HC}]^T \quad (7)$$

$$\mathbf{y}_k = [\mathbf{S}_k]^T = [X_{HC} \quad Z_{HC}]^T \quad (8)$$

$$e_d = 1,5 - d \quad (9)$$

$$e_\varphi = 0 - \varphi \quad (10)$$

The measurement vector \mathbf{y}_k in frame k is defined as:

The performance of the presented robotic vision system with Kalman filter based tracker was tested within the working scenario where a mobile robot intended to follow human co-worker in indoor applications.

Experiments were conducted where a human walking in front of the mobile robot was imaged by a ASUS Xtion PRO LIVE camera mounted on the robot.

Figure 6 shows the result of the experiment where the reference path in form of a square of 2x2 m is represented by the red line, while the output of the proposed robotic

vision based human detection without and with tracking filter (Kalman estimation and prediction) is represented by blue and green line respectively.

In the Figure 6, it can be seen that there is a region in the reconstructed path that is marked by a purple ellipse where human detection does not give results. As evident Kalman filter estimates and predicts the position of the human in these frames, so that at any moment the proposed tracker outputs valid data.

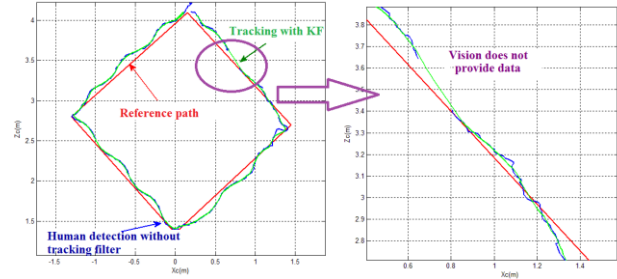


Fig.6: Comparison of the reference human's path and the human's paths reconstructed with the proposed robotic vision based tracker with and without tracking filter

Based on experimental result, it can be concluded that the proposed robotic vision system is robust and provides reliable outputs in order to control the mobile robot. Valid output data of the proposed robust vision system can be now used for development of human action classifier in order for robot to understand the human actions and to behave in accordance with them.

4. NEURAL NETWORK-BASED CLASIFFIAER

In order to classify human actions, a classifier based on neural network pattern recognition with 10 neurons in the hidden layer was proposed, and its architecture is shown in Figure 7. A feed forward neural network with one hidden layer with sigmoid activation function is used.

The distance error e_d and the alignment angle error e_φ was used as input into the classifier and they are calculated as: The output from the classifier is a probability that the human action belongs to one of the three classes that are presented as "moving away from the robot", "stands in relation to the robot" and "moving toward the robot".

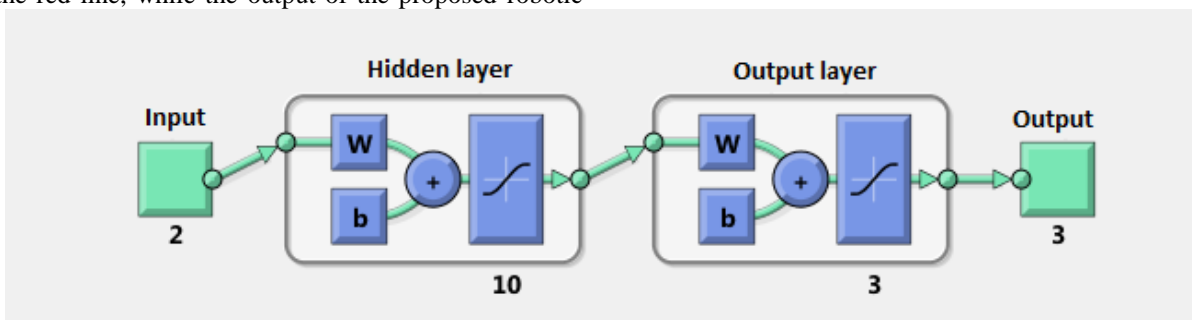


Fig. 7: Architecture of the NN classifier for human action recognition

For the training, a validation and testing of the neural network, 1730 samples with hand-specific labels was used. 70% of data sets for training were arbitrarily chosen, and 15% of randomly selected sets were used for validation and testing. For the training is used scaled conjugate gradient with back propagation error which updates the weights and belonging status to the Levenberg-Marquardt optimization, while the mean square error MSE is used as a measure of performance during the training of the network. The purpose of training network is to forecast the human action in real time.



Fig. 8: Confusion matrix classifier

Training of the proposed classifier was performed through 47 iterations, and the results of the classification are satisfying. The results of the training, validation and testing of the network can be seen on confusion matrix shown in Figure 8.

The accuracy of the trained classifier is over 99%, thus it can be concluded that the proposed classifier based on neural network gives good results, and implementation of this classifier can do human action recognition and accordingly to that, adequately control the movement of a mobile robot.

The results of the experiment where a human approached the robot are displayed. Experiments were done in a working scenario where a robot tracks the human who moved along the square path, which is drawn on the floor, and it is divided at the distance of 0.5 m, in order to facilitate visual monitoring of the distance between the robots and the human. Stationary camera recorded the movement of robots and the human.

In Figure 10 it can be seen that the robot "permitted" human to approach it. Only when the human walked away from the robot, with more than 1.5 m, the robot started tracking the human. The images are taken in the form of a series of images at every 30th frame from a video recorded by the stationary camera



Fig. 10: The results of the experiment where the human approached to the robot

5. CONCLUSION

Based on experimental results, it can be concluded that the proposed robotic vision system is robust and provides reliable outputs in order to control the mobile robot.

The presented robotic system is able to detect and follow a single person in the working scenario, maintaining a constant distance from the human based on information obtained by robotic vision, which use ASUS Xtion PRO LIVE camera as sensor of robotic vision.

The developed neural network based classifier is able to recognize human's actions in order to carry out tasks where the robot behaves like a human's collaborator.

The robot is able to "predict" the intendancy of a human to come closer to the robot and in this case, to stop and let the human to put something on the mobile robotic platform, in order to perform tasks when a robot behaves as a human's assistant, helping the human co-worker with transportation of different objects as containers with collected samples from the contaminated / hazardous environment.

REFERENCES

- [1] Ćirić I., Ćojbašić Ž., Nikolić V., Ćirić M., Tomić M., Petrović E., Simonović M., Neural network prediction of preson position for human following mobile robot platform, DEMI 2015, ISBN 978-99938-39-53-8, pp.577-582.
- [2] Alvarez-Santos, V., Pardo, X.M., Iglesias, R., Canedo-Rodriguez, A., Regueiro, C.V., Feature analysis for human recognition and discrimination: Application to a person-following behaviour in a mobile robot, Robotics and Autonomous Systems, 60 (2012), 8, pp. 1021-1036
- [3] Böhme, H.-J., Wilhelm, T., Key, J., Schauer, C., Schröter, C., Groß, H.-M., Hempel, T., An approach to multi-modal human-machine interaction for intelligent service robots, Robotics and Autonomous Systems, 44 (2003), 1, pp. 83-96
- [4] Ćirić, I., Ćojbašić, Ž., Nikolić, V., Antić, D., Computationally Intelligent System for Thermal Vision People Detection and Tracking in Robotic Applications, Proceedings, 11th International Conference on Telecommunications in Modern Satellite, Cable and Broadcasting Services - TELSIS 2013, Niš, Serbia, 2013, pp 587-590.
- [5] Anguita, D., Ghio, A., Oneto, L., Parra, X., & Reyes-Ortiz, J. L. (2012, December). Human activity recognition on smartphones using a multiclass hardware-friendly support vector machine. In International Workshop on Ambient Assisted Living (pp. 216-223). Springer Berlin Heidelberg.
- [6] Simon, C., Meessen, J., & De Vleeschouwer, C. (2010). Visual event recognition using decision trees. Multimedia Tools and Applications, 50(1), 95-121.
- [7] Preece, S.J., Goulermas, J.Y., Kenney, L.P., Howard, D. (2009). A comparison of feature extraction methods for the classification of dynamic activities from accelerometer data. IEEE Transactions on Biomedical Engineering, 56 (3), 871-879.
- [8] Oniga, S., & József, S. (2015). Optimal Recognition Method of Human Activities Using Artificial Neural Networks. Measurement Science Review, 15(6), 323-327.
- [9] Benyacoub, B., ElBernoussi, S., Zoglat, A., & Ismail, E. M. (2014). Classification with Hidden Markov Model. Applied Mathematical Sciences, 8(50), 2483-2496.

- [10] Gao, L., Bourke, A.K., Nelson, J. (2011). A system for activity recognition using multisensor fusion. In Annual International Conference of the IEEE - Engineering in Medicine and Biology Society (EMBC 2011), Boston, MA. IEEE, 7869-7872.
- [11] Magnanimo, V., Saveriano, M., Rossi, S., & Lee, D. (2014, August). A Bayesian approach for task recognition and future human activity prediction. In The 23rd IEEE International Symposium on Robot and Human Interactive Communication (pp. 726-731). IEEE.
- [12] Bellotto, N. (2012). Robot control based on qualitative representation of human trajectories.
- [13] Asus Xtion PRO LIVE product description [online] Available at: <http://www.asus.com/Multimedia/Xtion_PRO_LIVE/> [Accessed May 2013]
- [14] <http://www.ni.com/datasheet/pdf/en/ds-217>
- [15] <http://www.acrosser.com/Products/Embedded-Computer/Fanless-Embedded-Systems/AES-HM76Z1FL/Intel-Core-i3/i7-AES-HM76Z1FL.html>
- [16] Petrović E., (2017), Development of hierarchical control structure of a mobile robot for human tracking based on robust robotic stereo vision, *PhD thesis*.

CORRESPONDANCE



Emina PETROVIĆ, D.Sc. Eng.
University of Niš
Mechanical Engineering Faculty
Aleksandra Medvedeva 14
18000 Niš, Serbia
emina.petrovic@masfak.ni.ac.rs



Miloš SIMONOVIĆ, D.Sc. Eng.
University of Niš
Mechanical Engineering Faculty
Aleksandra Medvedeva 14
18000 Niš, Serbia
milos.simonovic@masfak.ni.ac.rs



Ivan ĆIRIĆ, D.Sc. Eng.
University of Niš
Mechanical Engineering Faculty
Aleksandra Medvedeva 14
18000 Niš, Serbia
ivan.ciric@masfak.ni.ac.rs



Vlastimir NIKOLIĆ, Prof. D.Sc. Eng.
University of Niš
Mechanical Engineering Faculty
Aleksandra Medvedeva 14
18000 Niš, Serbia
vlastimir.nikolic@masfak.ni.ac.rs

VIBRATION CHARACTERISTICS STUDY OF SELF-PROPELLED MACHINE FOR CORN SPRAYING AND DETASSELING

Boris STOJIC

Abstract: *This paper deals with preliminary assessment of whole-body vibration properties of specialized agricultural self-propelled machine used for corn spraying and detasseling. Due to highly specific tasks of the machine and low-volume, on-demand production, vibration properties were not taken into consideration within the machine design process. With the aim to define recommendations for future design enhancement, especially in view of human operator exposure to vibrations, parameters of vehicle ride model for machine vibration response were assessed and RMS values of acceleration at the seat calculated for in-field operation and country lane driving. It was concluded that, in order to carry out thorough analysis of vibration impact on operator and define directions for design improvement, it will be necessary to carry out experimental investigations, which will be used for model validation*

Key words: *Self-propelled machine, whole-body vibration, vehicle dynamic response*

1. INTRODUCTION

Absence of elastic wheel suspension is common characteristic of agricultural tractors and self-propelled agricultural machines. Thereby these vehicles by their nature use mainly off-road terrain or local roads of low quality. For this reason, human operator is exposed to significant level of vibrations arising from terrain irregularities. Despite intensive technological development of those vehicle categories in past decades that led to series of highly sophisticated solutions, vibration impact mitigation is still one of the most challenging engineering tasks in this field [7].

In this paper vibration behaviour of specialized agricultural self-propelled machine used for corn spraying and detasseling is analyzed in view of whole-body vibration response. Due to highly specific tasks of the machine and low-volume, on-demand production, vibration properties were not taken into consideration within the machine design process. Aim of this paper is to carry out preliminary numerical assessment of vibration behaviour of the machine, especially in view of human operator exposure to vibrations. Conclusions based of this preliminary assessment should be used to define further directions of research, with further goal of defining recommendations for future design enhancements. Calculations carried out subsequently are based on presumptions of certain operating conditions and known design parameters. Values that are not known are assessed on the basis of available data for similar machines and/or their components.

2. MACHINE DESCRIPTION

Machine description is given based on previously published paper [6]. Self-propelled agricultural machine with high clearance Hidromatiks S-PST has been developed for the implementation of agro-technical measures in crop production. It is primarily specialized in the production of corn seeds. Primary tasks of the machine are pesticide spraying and some specialized mechanical operations carried out in the scope of corn and seed production. The machine and its main components are shown in Figures 1 and 2.

At the front end of the machine there are mechanical tools for appropriate agrotechnical operations. The pesticide treatment is carried out by using the sprayer mounted on the rear of the machine, and the tank is placed in the middle of the vehicle. The powertrain consists of diesel engine and hydrostatic transmission enabling maximum speed of up to 25 km/h. Main braking is realized on the basis of differential pressure in the hydrostatic installation of the powertrain. The parking brake is made by mechanical locking mechanism. The steering system consists of orbitrol steering unit and two-way hydraulic cylinder that imparts steering angle to the road wheels. Machine has no elastic wheel suspension i.e. the wheels are connected rigidly to the chassis. Front wheels can move vertically in opposite directions to one another to accommodate for the side slope of the terrain. This solution is realized by using interconnected hydraulic cylinders mounted vertically. This system itself introduces no significant elastic properties and therefore can be considered to exert no influence on main vibration properties of the machine.



Fig. 1: Self-propelled agricultural machine with high clearance Hidromatiks S-PST

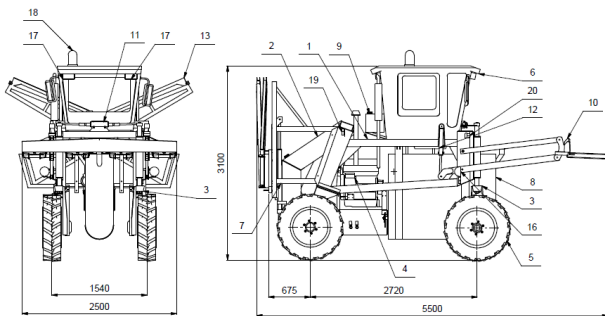


Fig. 2: Basic components and dimensions of the machine Hidromatiks S-PST. 1 - main frame box, also used as hydraulic oil tank (2), 3 - wheel holder, 4 - drive unit, 5 - steering assembly, 6 - cabin, 9 - fuel tank, 11 - steering mechanism, 10 and 12 - working device for cutting operations, 8 - tank for pesticides, 13 - sprayer, 16, 17, 18, 19, 20 - light-signalling equipment

3. VEHICLE MODEL AND ASSUMPTIONS

In order to carry out thorough analysis of vibration properties of regarded agricultural machine, an in-plane 3-DOF model shown in Figure 3 can be regarded as adequate basis at the initial stage of the study.

Since the self-propelled machine is not equipped with elastic suspension of the wheels, the only elasticity between the vehicle body and the ground is represented by front and rear tires, which are modelled as linear Voigt-Kelvin model characterized by stiffness and damping coefficients for front and rear tire, $c_{F/R}$ and $k_{F/R}$ respectively.

Furthermore, operator's seat is elastically suspended at location S_0 , which is also modelled by linear Voigt-Kelvin element having stiffness and damping coefficients c_S and k_S respectively.

Model degrees of freedom are defined through vertical displacement of front (z_F) and rear (z_R) axle, as well as that of the seat (z_S). Model further takes into account vehicle mass and inertial properties through three lumped masses, located at each axle (front and rear - m_F and m_R) and at vehicle's true centre of mass (m_C - coupling mass). These masses can be calculated from the conditions of identical total vehicle mass, centre of mass location and appropriate moment of inertia about lateral axis that passes centre of mass. Vibration excitation is introduced at the front and rear tire contact patch by the ground irregularities, as the vehicle passes ground at some velocity. Road profile is defined as function of longitudinal displacement x by its ordinate $q(x)$. Taking vehicle speed into account, road irregularities are transferred from spatial to time domain, i.e. from $q(x)$ to $q(t)$. A condition is present that value of $q(t)$ at rear axle - $q_R(t)$ - is identical to that at the front axle - $q_F(t)$, shifted in time domain by the value τ that depends on vehicle speed and wheel base ($q_R(t) = q_F(t - \tau)$). Furthermore, tire enveloping properties have to be taken into account due to short wavelength of road irregularities that are low-pass filtered by the action of tire geometry and elasticity. Allowing for different filtering properties at front and rear tire, effective excitations $q_{Fef}(t)$ i.e. $q_{Ref}(t)$ are introduced to the point-contact tire models at front and rear axle respectively. Appropriate tire enveloping model is required in order to switch from $q_{F/R}$ to $q_{Fef/Ref}$.

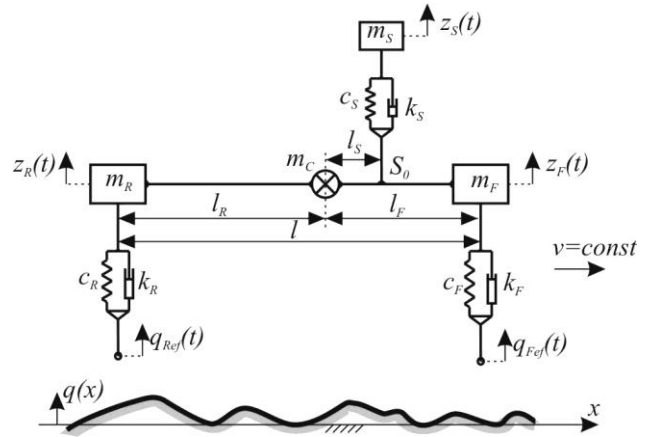


Fig. 3: vehicle ride model

Since the purpose of this paper is not to concentrate on exact and detailed prediction of vehicle vibration response, but to make its preliminary assessment in order to draw conclusions for further investigation directions, some assumptions and significant reduction of model complexity will be adopted subsequently, that enable significant simplifications of further analysis. Firstly, relying on publications about agricultural tractors dynamic behaviour (e.g. [2]), and taking into account similarity of self-propelled machine treated in this work with this kind of vehicles, it can be regarded allowed to adopt that coupling mass can be neglected:

$$\triangleright m_C \approx 0$$

This means that, neglecting impact of operator's suspended mass being much lower than the vehicle mass, masses at front and rear axle m_F and m_R vibrate independently of each other, i.e. in such case z_F and z_R will be mutually independent.

Since by the present vehicle concept operator's seat is located near the front axle, second simplification will be made by adopting that the system behaves as if front axle and the seat were located at the same longitudinal position, meaning that the point S_0 can be considered to be located approximately above the front axle (which further means $l_S \approx l_F$, Figure 3).

Under these assumptions, rear axle displacement z_R can be left out of the consideration and model reduces to ordinary "quarter-vehicle" model without wheel suspension. On the basis of adopted simplifications it will be assumed that for drawing basic conclusions in the scope of this paper, this reduced model can be used as well. Quarter-vehicle model for the given system is governed by the following system of equations:

$$\begin{aligned} m_S \ddot{z}_S + k_S (\dot{z}_S - \dot{z}_F) + c_S (z_S - z_F) &= 0 \\ m_F \ddot{z}_F + k_S (\dot{z}_F - \dot{z}_S) + c_S (z_F - z_S) + k_F \dot{z}_F + \\ + c_F z_F &= k_F \dot{q}_{Fef} + c_F q_{Fef} \end{aligned} \quad (1)$$

Carrying out Laplace transform and solving for appropriate relations yields transfer function between effective excitation and seat displacement H_{qzs} :

$$\begin{aligned} H_{qzs}(s) &= \frac{Z_S(s)}{Q_{Fef}(s)} = \\ &= \frac{N_2 \cdot s^2 + N_1 \cdot s + N_0}{D_4 \cdot s^4 + D_3 \cdot s^3 + D_2 \cdot s^2 + D_1 \cdot s + D_0} \end{aligned} \quad (2)$$

Where:

$$\begin{aligned} N_2 &= k_F \cdot k_S \\ N_1 &= c_S \cdot k_F + c_F \cdot k_S \\ N_0 &= c_F \cdot c_S \\ D_4 &= m_S \cdot m_F \\ D_3 &= m_S \cdot (k_S + k_F) + k_S \cdot m_F \\ D_2 &= m_S \cdot (c_S + c_F) + k_S \cdot k_F + c_S \cdot m_F \\ D_1 &= k_S \cdot c_F + c_S \cdot k_F \\ D_0 &= c_S \cdot c_F \end{aligned}$$

This enables subsequent analysis in frequency domain, which can be considered appropriate technique due to stochastic nature of road irregularities from which the vibration excitation is exerted to the vehicle. Later can hence be best described in term of their spectral content. Numerous investigations have revealed that PSD function of most ground profiles, prepared or unprepared for vehicle motion, can be modelled by the decay of profile height power density $S_q(\Omega)$ with increase spatial frequency Ω [3]. One of the most frequently used relationships (e.g. [3, 5, 10 etc.]) that will be used herein is:

$$S_q(\Omega) = S_q(\Omega_0) \cdot \left(\frac{\Omega}{\Omega_0} \right)^{-w} \quad (3)$$

Where:

$S_q(\Omega_0)$ - profile roughness coefficient
 Ω - spatial frequency of road irregularities
 Ω_0 - reference spatial frequency
 w - frequency index

When vehicle is moving in longitudinal direction at constant velocity v , spectral content of ground irregularities in temporal frequency domain in term of PSD function $S_q(\omega)$ is obtained through relationship:

$$S_q(\omega) = \frac{1}{v} \cdot S_q(\Omega) \quad (4)$$

Applying index "F" for the front axle, notation:

$$S_{qF}(\omega)$$

will be used subsequently for road irregularities PSD.

Thereby spatial frequency Ω switches to temporal frequency ω by using relation:

$$\omega = v \cdot \Omega \quad (5)$$

Where:

ω, Ω - temporal and spatial frequencies respectively
 v - motion velocity

For tire enveloping properties, empirical model in frequency domain given in [2] will be used that is given by modulus of appropriate frequency response function, comprising impact of vehicle velocity v and tire contact patch length $2a_0$:

$$|H_{env}(j\omega)|^2 = \frac{(1, l \cdot v)^2}{(1, l \cdot v)^2 + (a_0 \cdot \omega)^2} \quad (6)$$

Such function structure assumes constant length of tire contact patch. However in reality this is not the case, due to continuous dynamic wheel load fluctuations. This represents another modelling simplification in this analysis.

Shape of the function of $|H_{env}(j\omega)|^2$ with a_0 as parameter is displayed in Figure 4.

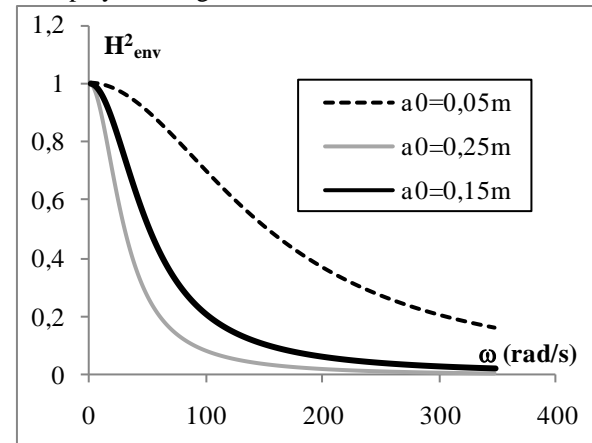


Fig. 4: Quadratic modulus of frequency response function for tyre enveloping model

By using function $|H_{env}(j\omega)|$, PSD of effective excitation at the front axle q_{Fef} is obtained from the relation:

$$S_{qFef} = |H_{env}(j\omega)|^2 \cdot S_{qF}(\omega) \quad (7)$$

Finally, seat displacement PSD is obtained by applying:

$$S_{zS} = |H_{qzs}(j\omega)|^2 \cdot S_{qFef}(\omega) \quad (8)$$

Thereby transfer function $H_{qzs}(j\omega)$ is obtained by substituting s with $j\omega$ in transfer function (2). This will have shape:

$$H_{qzs}(j\omega) = A(\omega) + jB(\omega) \quad (9)$$

Where:

$$A(\omega) = \frac{A_N \cdot A_D + B_N \cdot B_D}{A_D^2 + B_D^2}, \quad B(\omega) = \frac{B_N \cdot A_D - A_N \cdot B_D}{A_D^2 + B_D^2}$$

$$A_N = N_0 - N_2 \cdot \omega^2; \quad B_N = N_1 \cdot \omega; \quad A_D = D_0 - D_2 \cdot \omega^2 + D_4 \cdot \omega^4; \quad B_D = D_1 \cdot \omega - D_3 \cdot \omega^3$$

Thereby, quadratic modulus of $H_{qzs}(j\omega)$ is:

$$|H_{qzs}(j\omega)|^2 = A^2(\omega) + B^2(\omega) \quad (10)$$

Shape of the function of $|H_{qzs}(j\omega)|^2$ is displayed in Figure 5.

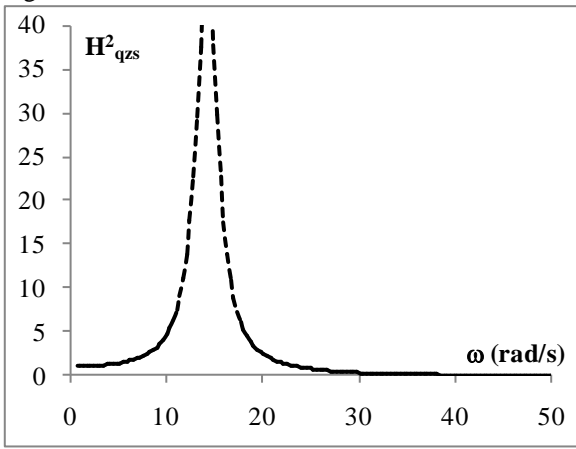


Fig. 5: Quadratic modulus of frequency response function between displacement at the front axle as input and displacement at the seat as output

Introducing expression (7) into (8) yields direct relation between input PSD S_{qF} and output PSD S_{zS} :

$$S_{zS} = |H_{qzs}(j\omega)|^2 \cdot |H_{env}(j\omega)|^2 \cdot S_{qF}(\omega) \quad (11)$$

Finally, mean square value of vertical acceleration at the operator seat that is used to evaluate operator's exposure to vibrations is obtained from:

$$\bar{z}_S^2 = \int_0^{\infty} \omega^4 \cdot S_{zS}(\omega) d\omega \quad (12)$$

Term $\omega^4 \cdot S_{zS}(\omega)$ represents seat acceleration PSD function.

4. MACHINE DESIGN AND OPERATING PARAMETERS

In order to accomplish this study, i.e. to obtain assessment of vertical acceleration at the operator seat i.e. its impact on the operator, numerical values of model parameters named in previous chapter are required in order to carry out necessary calculations.

Front axle weight, i.e. proportion of the vehicle mass carried by the front axle was determined by measurement:

- $m_{Fmin} = 1580$ kg - front axle load for unladen vehicle

- $m_{Fmax} = 2050$ kg - front axle load for fully laden vehicle
- $m_F = 1800$ kg - front axle load assumed for further calculations

For the mass of the seat including the driver, 120 kg is assumed as reasonable typical value:

- $m_s = 120$ kg

Stiffness of the front tyre c_F will be substantially influenced by tyre pressure, but for the given pressure it will also depend on tyre dimensions and design parameters. Thereby it is also significantly affected by excitation amplitude, frequency and rolling velocity. Determination of these unknown relationships lays far out of the scope of this paper. Therefore assumption will be made based on available data. Previous studies (e.g. [4, 8, 10]) revealed that for nominal tyre load and pressure the stiffness coefficient will lay roughly somewhere between 300 and 500 kN/m, so the value of 400 kN/m will be assumed for further calculations:

- $c_F = 400$ kN/m

As there is no elastic suspension system, tyre damping has to be taken into account and is therefore included in the vehicle model. Investigation of tractor tyre behaviour [8] shown that damping ratio D of agricultural vehicles "suspended" only on their tyres can be expected to be approximately around 0.1, so that from this data tyre damping coefficient k_F is calculated:

- $k_F = 2 \cdot D \cdot \sqrt{c_F \cdot m_F} \approx 5$ kNs/m

Assessed value is similar to available published data (e.g. [10]).

Unknown parameters of the seat suspension will be assessed from typical values of seat damping ratio D_S and natural frequency f_{S0} , which according to [5] are in the order of 0.35 i.e. 4.5Hz respectively. Therefore it applies:

- $c_S = 4 \cdot \pi^2 \cdot f_{S0}^2 \cdot m_S \approx 100$ kN/m
- $k_S = 2 \cdot D_S \cdot \sqrt{c_S \cdot m_S} \approx 2.5$ kNs/m

In order to evaluate tyre enveloping model $|H_{env}(j\omega)|^2$, it is also required to know half contact length of the tyre a_0 as well. As in this case there is also lack of information, arbitrary assumption of some reasonable value is made base on experience and taking into account data obtained from the study carried out previously [8]:

- $a_0 \sim 150$ mm

Having determined or assessed all numerical parameters of the model, it is possible to carry out necessary calculations.

Parameters of road unevenness in spatial frequency domain and velocity value, necessary for shifting between temporal and frequency domain, will be adopted subsequently for two different operating regimes:

- a) in-field agrotechnical operations
- b) road driving

5. METHOD OF NUMERICAL CALCULATIONS

In order to carry out numerical evaluation of definite integral (12), upper limit have to be replaced with finite

value. For lower limit also some positive (i.e. non-zero) value has to be assumed, because the value of the road irregularities PSD, S_{z_s} , according to theoretical model given by equation (3) would approach infinity for vanishing frequency. Here, arbitrary choice was made for spatial frequency limits as:

- $\Omega_{min} = 0.1 \text{ m}^{-1}$ - lower integration limit
- $\Omega_{max} = 50 \text{ m}^{-1}$ - upper integration limit

Chosen interval of spatial frequency values corresponds to interval of road undulations wavelengths between 0.12 and 62.8 m.

Further, definite integral (12) has to be replaced by finite sum, whereby $d\omega$ i.e. $d\Omega$ switches to finite $\Delta\Omega$. For N points used for numerical evaluation it applies:

$$\Delta\Omega = \frac{\Omega_{max} - \Omega_{min}}{N - 1} \quad (13)$$

Replacing definite integral (12) by sum of finite values yields:

$$\begin{aligned} \overline{z_s}^2 &\approx \sum \frac{1}{2} [S_{z_s}(\omega_i) + S_{z_s}(\omega_{i-1})] \cdot (\omega_i - \omega_{i-1}) \cdot \omega_i^4 \\ \omega_i &= \omega_{min} + i \cdot \Delta\omega, i = 0 \div N \end{aligned} \quad (14)$$

Thereby relation (5) can be applied:

$$\begin{aligned} (\omega_i - \omega_{i-1}) &= \Delta\omega = v \cdot \Delta\Omega \\ \omega_{min/max} &= v \cdot \Omega_{min/max} \\ \omega_i &= v \cdot \Omega_i \end{aligned} \quad (15)$$

6. NUMERICAL ASSESMENT OF OPERATOR'S EXPOSURE TO VIBRATIONS

6.1. In-field agrotechnical operations

Series of published data for PSD function of rough terrain unevenness was summarized in [8] so assumed typical values for the ploughed field will be taken herein:

- $S_q(\Omega_0) = 650 \text{ cm}^3$
- $\Omega_0 = 1 \text{ m}^{-1}$
- $w = 1.7$

For plant cultivation carried out by the machine, velocity value is assumed according to [1]:

- $v = 5 \text{ km/h}$

Root mean square value of the vertical acceleration at the operator's seat obtained for in-field conditions is:

$$\sqrt{\overline{z_s}^2} = 4.9 \text{ m/s}^2$$

6.2. Road driving

In order to bring the machine from and to the agricultural field, public or internal road network has to be used. For this assessment it is assumed that machine drives at maximum velocity:

- $v = 25 \text{ km/h}$

Choice of the road terrain parameters was again made based on [8], assuming that it uses country lane of low quality:

- $S_q(\Omega_0) = 145 \text{ cm}^3$
- $\Omega_0 = 1 \text{ m}^{-1}$

- $w = 1.5$

Root mean square value of the vertical acceleration at the operator's seat obtained for low-quality road condition is:

$$\sqrt{\overline{z_s}^2} = 7.8 \text{ m/s}^2$$

7. DISCUSSION AND CONCLUSIONS

Ride properties of self-propelled agricultural machine were analyzed by using quarter-vehicle ride model for the vehicle without elastic suspension and with elastically suspended operator's seat included. This model describes system behaviour by using product of two transfer functions, connecting road profile geometry shifted to time domain as input with displacement at the operator's seat as output. Thereby the spatial frequency of road irregularities is shifted to temporal excitation frequency based on vehicle velocity.

First transfer function (given by its FRF quadratic modulus (6)) represents tyre enveloping model, which accounts for low-pass filtering of short-wavelength road irregularities due to geometric and elastic properties of the tyre. This function actually takes real road geometry as input and returns filtered i.e. effective road profile as output, which is further used as vibration excitation for elastically suspended masses. Figure 4 indicates that there is significant reduction of high-frequency content of real road profile due to named properties of tyre, whereby value of the tyre contact length itself seems to exert moderate impact.

Second transfer function (2) i.e. appropriate FRF (10) represents the gain of seat displacement due to effective excitation imparted to the front axle. This FRF shows significant dynamic gain approximately between 20 and 30 Hz, caused by natural frequency of the front axle being approximately 15 Hz, and almost complete vibration isolation for excitation frequencies from above 30 Hz.

By using this reduced vehicle ride model, vertical acceleration RMS values at the operator's seat are calculated for both in-field use and country lane driving. Results are 4.9 m/s^2 for the first case i.e. 7.8 m/s^2 for the later. These numbers by themselves are though not sufficient to give final conclusions about vehicle vibration behaviour with regard to operator's exposure. This would require some appropriate approach for analysis that takes into account characteristics of the human body by using standard tolerance curves. This further includes determination of vibration frequency content and application of techniques such as filtering, frequency weighting, calculation of acceleration RMS around series of central frequencies etc.

However, in order to obtain practically usable results from such analysis, used ride model has to be validated at first. In this paper theoretical background was developed, but almost all model parameters have been not known and could only be roughly assessed. It is, further, still under the question if adopted level of model simplification can lead to valid predictions of system behaviour with respect to the topic regarded. These considerations give clear directions of further work: further experimental investigations are required that will either enable validation of reduced model used herein (together with

determination of real parameters' values) or reveal the need for more sophisticated approach in order to draw valid conclusions, and to overcome possible shortcomings of the approach used. Such further work would then represent appropriate basis for thorough analysis of machine vibration response and determining directions for design improvements.

8. ACKNOWLEDGEMENTS

This paper was done as a part of the researches on the project TR35041 – "Investigation of the safety of the vehicle as part of cybernetic system: Driver-Vehicle-Environment" and the project TR31046 "Improvement of the quality of tractors and mobile systems with the aim of increasing competitiveness and preserving soil and environment", supported by Serbian Ministry of Education, Science and Technological Development.

REFERENCES

- [1] BÖTTINGER S., *Ackerschlepper - Vorlesung*, Institut für Agrartechnik Hohenheim, <https://www.uni-hohenheim.de/LT/Vorlesung/Vorlesung.html>, accessed 2.10.2010
- [2] ČASNJI F. (1984). *Ogibljeno traktorsko sedište sa inercijalnim prigušivačem oscilacija (Suspended tractor seat with inertial vibration damper)*, Doctoral thesis, FTN Novi Sad
- [3] HORST, B.: (1969). *Untersuchungen von Fahrbahnunebenheiten und Anwendungen der Ergebnisse*, Doctoral thesis, Braunschweig, T. U., F. f. Maschinenbau u. Elektrotechnik
- [4] KISSING A., GÖHLICH H. (1988). *Ackerschlepper-Reifendynamik, Teil 1: Fahrbahn- und Prüfstandsergebnisse*, Grundlagen Landtechnik 38 (1988) 3, 78-87, ISSN 0017-4920
- [5] MITSCHKE M., WALLENTOWITZ H.: *Dynamik der Kraftfahrzeuge*, Springer-Verlag Berlin Heidelberg New York, ISBN 978-3540420118
- [6] RUŽIĆ D., STOJIC B., MILISAVIĆ P. (2016) *Design features of farm self-propelled working machine relevant for working and traffic safety*, Proceedings of the National conference with international participation "UNAPREĐENJE SISTEMA ZAŠTITE NA RADU (Improvement of the occupational safety system)", Tara, Serbia, pp 166-175, ISBN 978-86-919221-1-5
- [7] SCARLETT, A.J. et al (2005). *Whole-body vibration on agricultural vehicles*, Research report, Silsoe Research Institute and RMS Vibration Test Laboratory for the Health and Safety Executive, HSE Books, ISBN 0 7176 2970 8, Silsoe
- [8] STOJIC B. (2014). *Modeliranje oscilatornog ponašanja traktorskih pneumatika veštačkim neuronskim mrežama (Tractor tire vibration behaviour modelling by using artificial neural networks)*, Doctoral thesis, FTN Novi Sad
- [9] STOJIC B., POZNANOVIĆ N., POZNIĆ A. (2015). *Research and Modeling of the Tractor Tire Enveloping Behavior*, Journal of Vibration and Control, DOI: 10.1177/1077546315576302, ISSN: 1741-2986
- [10] WONG J. Y. (2001). *Theory of Ground Vehicles*, John Wiley & Sons Inc., New York Toronto 2001., ISBN 0-471-35461-9

CORRESPONDANCE



Dr Boris STOJIC, Assistant professor
University of Novi sad
Faculty of Technical Sciences
Trg Dositeja Obradovica 6
21000 Novi Sad, Serbia
bstojic@uns.ac.rs

CAD/CAM INTEGRATION OF THE FORKED ROD DESIGN OF THE SERVICE ROBOT CONTROL MECHANISM

Milan VUKCEVIC
Nikola SIBALIC
Marina MIJANOVIC
Darko SKUPNJAK

Abstract: The paper presents a design of the forked rod being an integral element of the control mechanism of the service robot, using CAD/CAM program application. For the mobile service platform which leans on 4 wheels, a unique mechanism for turning control has been designed. A design of the mechanism itself has been made in CAD technology. Technology of manufacturing relies on the existing machining park. The processing systems have been integrated, of one CNC milling machine (three axes) and two conventional machines (tool shop milling machine and machine for round grinding). For CNC milling machine technology was prepared by using software with CAM module and G-code was generated. Considering that the forked rod geometry is complex, an additional jig was designed for the second clamping on CNC machine and it was used on the tool shop milling machine for making a keyway in hub of the forked rod.

Key words: CAD/CAM, Product designing, Processing system, Processing systems integration

1. INTRODUCTION

The most common techniques of the project designing are: robust designing, modular designing, computer designing, computer production of technology of virtual reality and the value analysis.

In order to have this robot realized (MNE ROBECO) one of several product designing techniques, known as computer designing CAD (*Computer Aided Design*). CAD is application of computers in designing and preparation of technical documentation.

For making certain elements of complex assemblies of the mobile platform, a technique of computer production CAM (*Computer Aided Manufacturing*) will be applied. By connecting CAD and CAM, CAD/CAM technology has been got. Advantages of CAD/CAM technology are: quality of the product, less time for designing, reduction of production expenses, availability of data base and the new scope of capability [1, 2].

CAD/CAM is a requirement of the modern market. Modern development of the product and the process is an essential pre-request for the success and survival on the market [1, 2].

Strategy of development is of internal character and it is development of the completely new product.

For the robot, it is necessary to design a mobile platform where a manipulator will be possible to install. The robot is intended to move on open space, not only along the flat road, but over uneven terrain and to perform certain assignments. The robot might be requested to take the samples (water, gas, earth) from contaminated zone,

recording dangerous terrain, finding and marking mine-explosive devices, etc.

Service mobile platform MNE ROBECO is a complex product and it consists of three basic complex assemblies (systems), such as: system for turning control, the mobile platform leaning system and the system for the drive control (motors).

One of basic parts of designed control system is a forked rod of the control mechanism for turning the mobile platform, which has been made by using modern CAD/CAM integration.

2. DESCRIPTION OF THE CAD SYSTEM

Development of the product using CAD/CAM/CAPP/CAE system speeds up development, analysis, redesigning of the model and making of decision on proper solutions as optimal or original ones that meet requirements, with minimum price and maximum quality. Product designing is a key activity of the manufacturing process, because its part is estimated to cover 70-80% of the development and the production price. CAD is a program which uses computer graphics for development, analyses and changes during procedure of the product designing.

According to definition of CAD applications (tool), any application which contains computer graphics and application adjusted to engineering functions in designing process is classified as CAD application. This actually means that CAD applications may be versatile, varying from geometric tools for shape manipulation to the tool for visualization of the results we are analyzing.

Service robot consists of a mobile platform and a manipulator. The mobile platform will be a special

vehicle with four wheels drive, while direction will be controlled by turning all four wheels. Also, a construction of the mobile platform will be solved by providing a high clearance (distance from the base), independent hanging of each wheel and turning a wheel for $\pm 45^\circ$, thus enabling good performances for turning outside the roads (off-

road). It is important to point out that the forked rod of the mechanism for controlling mobile platform turning, will be designed and its construction optimized in order to transmit the forces that appear when turning to the levers of the mechanism. Figure 1 shows a mobile CAD service platform.

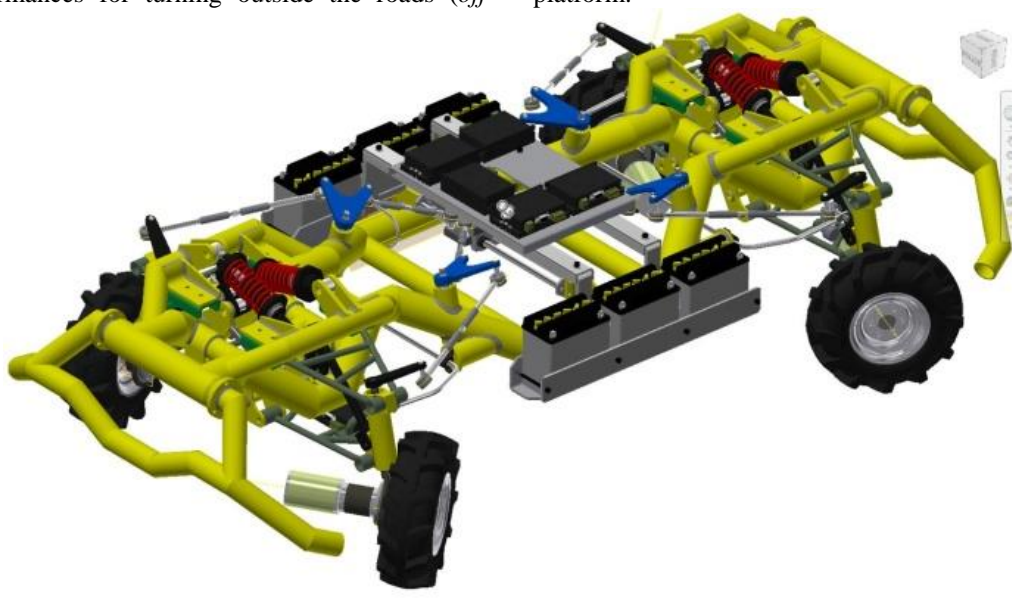


Fig.1: Mobile CAD platform of the service robot

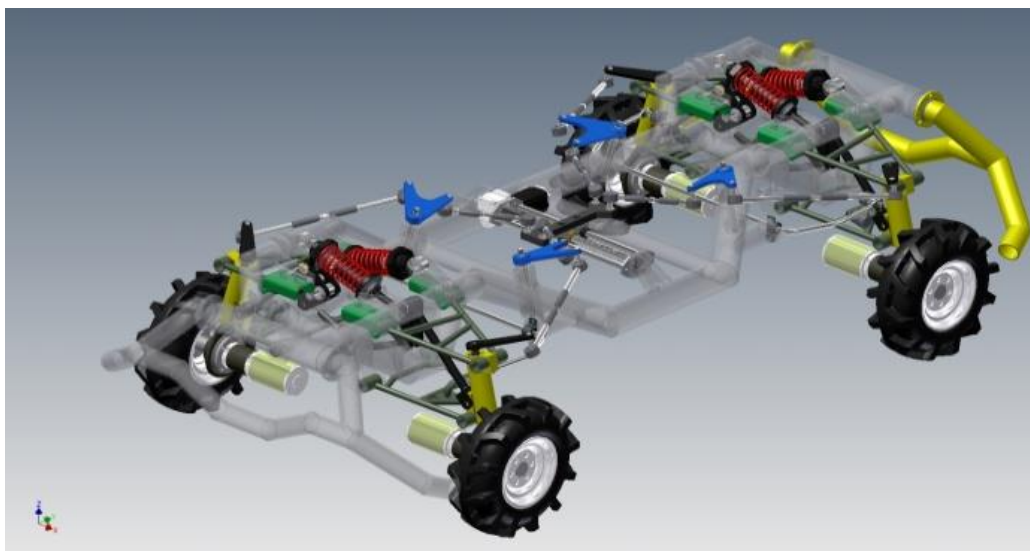


Fig.2: System for control of turning of the mobile platform “MNE ROBECO”

2.1. CAD design of the control mechanism

Designing, i.e. CAD design of the mechanism for controlling mobile platform turning has been done by using software package Autodesk Inventor Professional 2016.

Figure 2 presents a scheme of designed control mechanism. This refers to symmetric mechanism against to two normal planes. Figure 3 presents a view on the mechanism for control of the mobile platform turning in XOY plane.

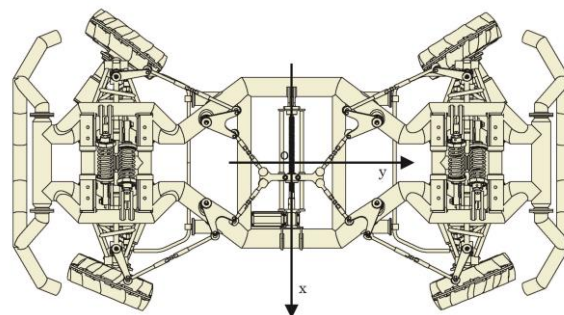


Fig.3: The mechanism in XOY plane

2.2. CAD design of the control mechanism forked rod

The forked rod is also designed by using software package of Autodesk Inventor Professional. It is possible to create elements (Part), assemblies (Assembly), drawings (Drawings) and presentations [4, 5, 8]. Figure 4 presents a drawing of a forked rod in the sketch level.

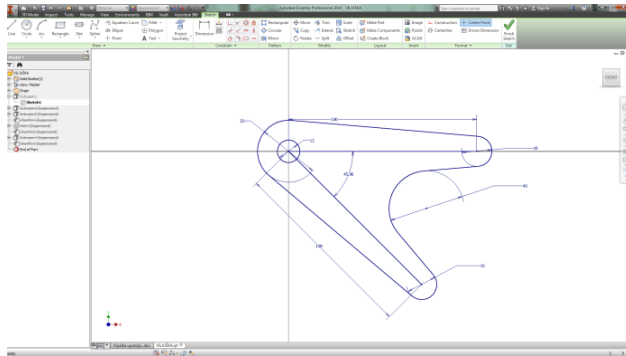


Fig.4: Creating a forked rod draft

A base is drawn using a range of tools placed over the working space and it is similar to the ones with other software packages (Catia, Solid Works, Esprit, CREO...). 3D model of the forked rod is shown in Figure 5.

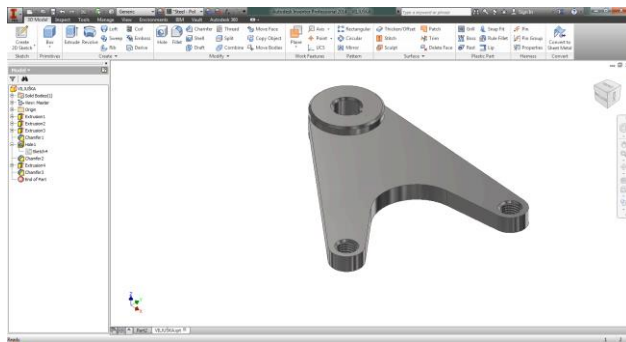


Fig.5: 3D Model of the forked rod

Creation of the drawing is done in Inventor Professional. Figure 6 shows a drawing of the forked rod of the control mechanism.

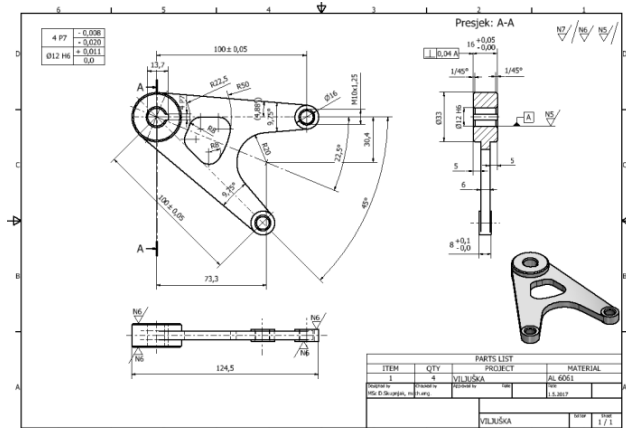


Fig.6: Detail drawing of the forked rod

3. CONNECTION BETWEEN CAD/CAM SYSTEMS

There are a lot of connections between CAD and CAM systems. CAD system provides information on the product and the construction, which is an input for CAM system. Connection between CAD and CAM systems can be realized in several ways. The first method is to realize connection between CAD and CAM systems using documentation, the next method is connecting CAD and CAM systems by constant link through proper interfaces, and the third method is integration of CAD/CAM systems through a data base. Connection between CAD/CAM systems is shown in Figure 7.

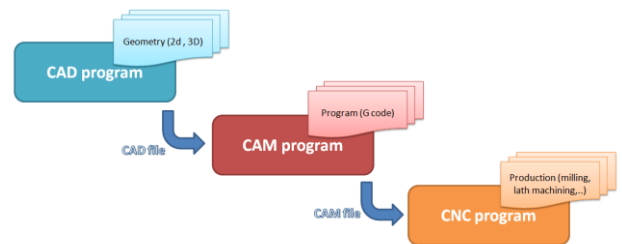


Fig. 7: Connection between CAD and CAM systems

CAM systems present program tools which support intensive use of computers for planning and projecting the production and technology processes and operations and controlling production, i.e. the production process.

CAM systems in automatization of designing and manufacturing make an important factor, as they establish a connection of CAD model and machines numerically controlled.

Basic functions of CAM systems are related to production-technological processes.

These are as follows:

- Generate a preparation part
- Generate and optimize a tool path
- Create and use of data base and catalogue of regime and the tools,
- Calculation of the production time,
- Generating NC program,
- Simulation and visualization of the production process
- Generating production documentation
- Managing production processes.

4. INTEGRATED SYSTEMS OF MACHING

Systems of machining by cutting or otherwise called a system of machining consists of: means of work and machining processes, with characteristic inputs and outputs, as shown in Figure 8. Supportive processes do not directly affect the condition of the processed part (positioning and clamping of the processed part, laying down the processed part, putting it into function and stopping the machine), while the machining processes present direct transformation of the preparation part to the processed part (change of geometry, physical and chemical features, measures, quality of surface) [1, 3, 6].

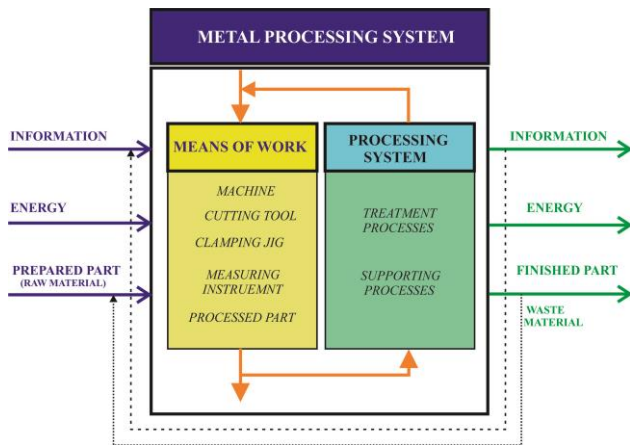


Fig. 8: Structure of the machining system

4.1. Example of making a forked rod of the control mechanism

For the forked rod of the control mechanism for turning the mobile platform "MNE ROBECO", it is necessary to

design technology of production based on a defined detail drawing.

For designing technology, it is necessary to:

1. Complete an analysis of geometry of shape - Forked rod,
2. Define a basic material,
3. Define machining operations,
4. Select a tooling machine, integrate machining systems
5. Define tools, auxiliary tool and clamping plan,
6. Design technology in a software package Autodesk Inventor Professional 2016,
7. For used CAM technology, generate G code

For production [7] of the forked rod of the control mechanism, three machining systems will be integrated (Figure 9):

1. CNC Milling machine
2. Universal tool milling machine
3. Milling machine for round milling (hole)

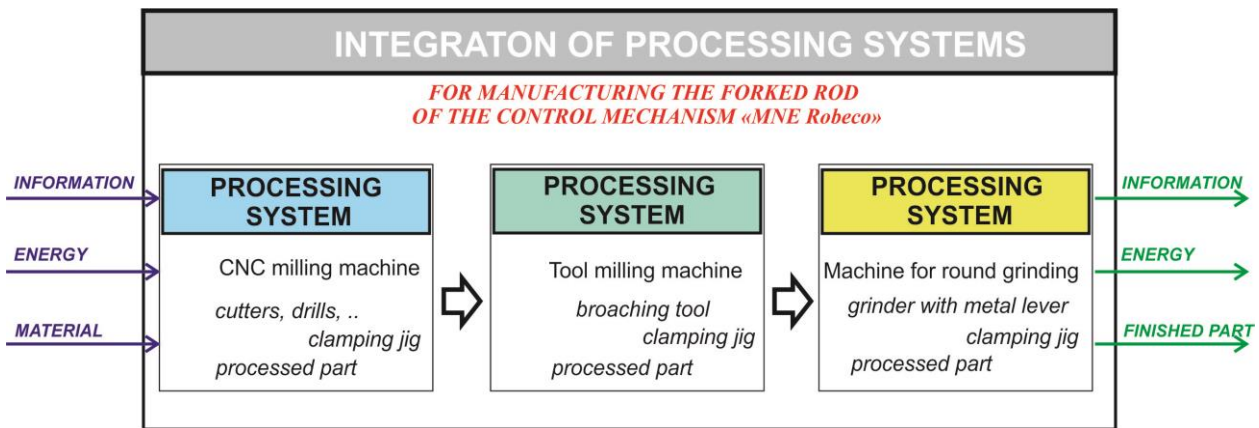


Fig. 9: Integration of the machining systems for producing a forked rod

Machining on CNC milling machine

For milling of the forked rod of the control mechanism, succession of operations and actions is as follows:

First clamping

Preparatory operations:

1. Prepare CNC machine,
2. Install and set all tools,
3. Clamp the prepared part and set it,
4. Set a zero point of the treated part,

Machining operations:

5. Front operation,
6. Hole boring (without rough drilling),
7. Contour machining,
8. Corner chamfering (outside),
9. Inner corner chamfering (hole thread),
10. Tapping (M10x1.25),

Final operations:

11. To release a treated part,
12. To clean a treated part,
13. Check achieved dimensions and quality of surface.

Second clamping

Preparatory operations:

1. Prepare CNC machine (clean),

2. Clamp the prepared part in the auxiliary jig and adjust it,
3. Set the zero point of the treated part,

Machining operations:

4. Front machining,
5. Contour machining,
6. Corner chamfering (outer),
7. Inner corner chamfering,

Final operations:

8. Release the treated part,
9. Remove a treated part from the auxiliary tool,
10. Clean a treated part,
11. Check achieved dimensions or quality of surface.

Operation sheet is a basic document of technological preparation. Every individual part is made for every individual part of the product. There is a defined technological process in it. The most common contents of the operation sheet are: operation, capture, machine, tooling – regimes of operation, i.e. cutting speed, feeding speed, cutting depth, number of passes, technological and backing time, etc. Figure 10 shows an example of operation sheet, milling a contour, the second clamping.

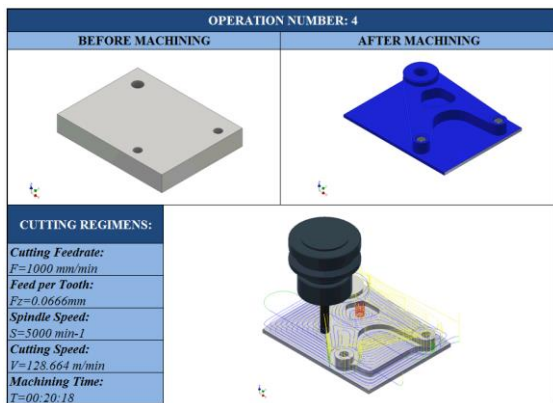


Fig. 10: Operation sheet of the contour milling

Table 1 shows a survey of generated G-code for the first and the second clamping [4, 5].

Table1. Generated G-code

I CLAMPING	II CLAMPING
O0001	O0002
(Milling I)	(Milling II)
G98 G18	G98 G18
G21	G21
M31	M31
G53 G0 U0.	G53 G0 U0.
G53 W0.	G53 W0.
(Face2)	(Face2)
T101	T101
S955 M3	S955 M3
G54	G54
M8	M8
M154	M154
G98	G98
(Milling from Z+ G17)	(Milling from Z+ G17)
G0 X195. Y-41.092 Z15.	G0 X195. Y-41.092
Z5.	Z15.
G1 Z4. F460.	Z5.
G18 G3 X185. Z-1. R5.	G1 Z2. F460.
G1 X130.	G18 G3 X185. Z-3. R5.
X-130.	G1 X130.
.	X-130.
.	.
.	.
X131.591 Y27.686	.
X131.589 Y23.789	.
Y14.534	.
	M155
	G53 W0.
	G53 U0.
	M9
	M1

Machining on the tool milling machine ALG 200B with head for grooving

For grooving a cleat, of the control mechanism forked, sequence of operations and captures is as follows:

The first clamping

Preparatory operations:

1. Prepare the machine,
2. Set the tool,
3. Clamp the prepared part in the auxiliary jig and clamp

- the auxiliary jig in the press,
 4. Adjust a tool axis to the opening axis,
- Machining operations:
5. Grooving,
- Final operations:
6. Release the auxiliary jig,
 7. Release a treated part from the auxiliary jig,
 8. Clean a treated part,
 9. Check achieved dimensions and quality of surfaces.

Figure 11 shows operation sheets for contour milling in the second clamping.



Fig. 11: Operation sheet grooving

Grinding operation on the machine for inside and outside round grinding

When grinding a tolerated hole $\varnothing 12$ H6, on the forked rod of the control mechanism, a sequence of operations and captures is the following:

The first clamping

Preparatory operations:

1. Prepare the machine,
 2. Install and adjust the tool,
 3. Clamp a prepared part in the chuck and enter a treated part,
 4. Set delimiters for moving of the grinder desk,
- Machining operations:
5. Hole grinding (control measures using a gauge block),
- Final operations:
6. Release a treated part,
 7. Clean a treated part,
 9. Control of the achieved dimensions and quality surfaces.

Figure 12 shows an example of the operation sheet, grinding the hole to tolerated measure.

OPERATION NUMBER: 1	
BEFORE MACHINING	AFTER MACHINING
	
CUTTING REGIMENS: Speed of Auxiliary Motion: $F_2=130 \text{ min}^{-2}$ Feed per Pace: $F_2=0.01 \text{ mm/pace}$ Spindle Speed: $S=10,000 \text{ min}^{-2}$ Cutting Speed: $V=50 \text{ m/min}$ Machining Time: $T=00:20:00$	

Fig. 12: Operation sheet Opening grinding

5. CONCLUSION

Designing a control mechanism of the service mobile platform required necessary knowledge from different technical disciplines in order to realize set goals.

Due to complexity of producing a forked rod of the control mechanism, the systems of processing have been integrated. The processing system consists of: CNC Milling machine (with three axes), universal tool milling machine ALG 200B and a grinder for round inside and outside grinding.

Using software Inventor Professional 2016 in module CAM, technology has been designed of making a forked rod of the mechanism on CNC milling machine for which a G-code for two clamping actions has been post-processed. Considering that geometry of the forked rod is complex, it has been required to design an auxiliary jig for the second clamping. The same auxiliary jig was used for clamping and positioning of the forked rod on Universal tool milling machine (machining system) where the head for boring the hub had been installed. Final operation, grinding of the hole has been done on the machine for round inside grinding being the third machining system in an integrated order. This example shows that modern CNC machine can be integrated with conventional existing capacities with technology of manufacturing carefully selected.

Of course, for serial and mass production, machining park would be additionally equipped with CNC, CAM, CAPP technologies.

REFERENCES

- [1] MCMAHON, C., BROWNE, J. (1998) CAD/CAM principles, practice and manufacturing management, Addison-Wesley, Harlow
- [2] LINGAIAH, K. (1994) Machine design data handbook, McGraw-Hill, USA
- [3] VUKČEVIĆ, M., ŠIBALIĆ, N. (2017) Tehnologija mašinske obrade, Univerzitet Crne Gore, Mašinski fakultet Podgorica
- [4] ĆIRKOVIĆ, R. (2015) Programiranje CNC mašina, Mikro knjiga, Beograd
- [5] OGRIZOVIĆ, M. (2012) Programiranje CNC mašina, Kompjuter biblioteka, Čačak
- [6] STANKOVIĆ, P. (1970) Mašine i alatke - konceptijske i eksploatacione analize mašina za obradu rezanjem, Građanska knjiga, Beograd
- [7] BOROJEVIĆ, Lj., ZELJKOVIĆ, M. (2008) Glavne karakteristike i struktura obradnih sistema, Fakultet tehničkih nauka, Novi Sad
- [8] TOOGOOD, R. (2006) Pro Engineer wildfire 3.0, Kompjuter biblioteka, Čačak.

CORRESPONDENCE

Milan VUKČEVIĆ, Prof. D.Sc. Eng.
 University of Montenegro
 Faculty of Mechanical Engineering
 Bul. Džordža Vašingtona bb
 81000 Podgorica, Montenegro
 milanvu@ac.me

Nikola ŠIBALIĆ, Prof. D.Sc. Eng.
 University of Montenegro
 Faculty of Mechanical Engineering
 Bul. Džordža Vašingtona bb
 81000 Podgorica, Montenegro
 nikola@ac.me

Marina MIJANOVIĆ, Prof. D.Sc. Eng.
 University of Montenegro
 Faculty of Mechanical Engineering
 Bul. Džordža Vašingtona bb
 81000 Podgorica, Montenegro
 marina@ac.me

Darko SKUPNJAK, M.Sc. Mech. Eng.
 Daido Metal Kotor AD
 85330 Kotor, Montenegro
 skupnjak@daidokotor.com

MODELLING AND CALCULATION OF A BELT CONVEYOR

Nenad MILORADOVIĆ

Igor ANTIĆ

Rodoljub VUJANAC

Abstract: Belt conveyors have important position in continuous transport of bulk materials due to their advantages such as economy and safety of operation, reliability and broad range of capacities. A 3D model of a belt conveyor construction was developed in this paper using Autodesk Inventor software package. Detailed calculations and selection of conveyors main elements were performed according to given demands and required capacity of transport. Dimensions and parameters of the most important elements of the design (belt width, types of belt conveyor idlers, belt conveyor drive equipment and other elements necessary for handling bulk materials) were determined based on previous calculations. Modelling of the complete belt conveyor was carried out according to the dimensions obtained by calculation. Finally, manufacture of the belt conveyor's elements based on the results of calculations and modelling as well as the complete assembly of the conveyor on the separation of gravel and sand were performed and presented in the paper.

Key words: belt conveyor, 3D model, bulk materials

1. INTRODUCTION

Belt conveyors are the most common material handling conveyors in use today. In this paper, a belt conveyor used for handling bulk materials is considered.

Bulk materials are powdery, granular or lumpy in nature and are stored in heaps. Examples of bulk materials are: minerals (ores, coals, etc.), earthly materials (gravel, sand, clay, etc.) processed materials (cement, salt, chemicals, etc.), agricultural products (grain, sugar, flour, etc.) and similar other materials.

Major characteristics of bulk materials in view of their handling are: lump-size, bulk weight, specific weight, moisture content, mobility of its particles, angles of repose, abrasiveness, temperature, proneness to explosion, stickiness, corrosivity, hygroscopic properties, etc [1].

2. CALCULATION

The design of a belt conveyor begins with an estimate of the characteristics of the material to be transported. The belt conveyor shown in Fig. 1 is used for transportation of separated gravel with 16-32.5 mm particle size.

Considering that characteristics of material considerably influence the material handling, corresponding belt conveyor travel paths, loading and discharging arrangements and overall conveyor configuration were adopted. Discharge over end pulley was applied.

All influencing factors were considered to arrive to the optimal solution, which would provide efficient and safe movement of materials in accordance with initial technical demands.

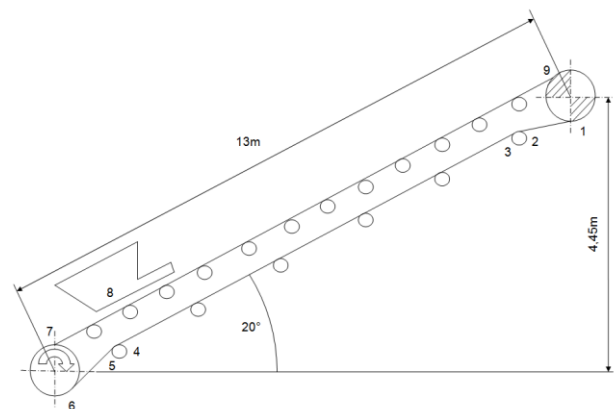


Fig.1: Belt conveyor travel path

The nominal cross section of the material on the inclined conveyor belt was considered in a vertical plane in order to maintain the total width of the material load on the belt and to maintain unchanged surcharge angles. When applying inclines and declines, it is important not to make the angle steeper than the product can safely navigate. The angle of inclination at which a belt conveyor conveys a bulk material depends upon the material particle size, shape of lumps, moisture content, angle of repose and flowability.

Design factors will affect the behaviour of materials on an inclined belt, including belt speed, whether material is ascending or descending, how fully the belt is loaded and how it is loaded. When the incline is too steep, some part of the material may slide, flow, or roll back, resulting in spillage.

Belt conveyor speed was selected in accordance with the characteristics of the material to be conveyed and desired capacity.

Based on the required technical and exploitation parameters of the conveyor, calculation of drive and resistive forces was conducted using the contour method [2]. By this method, numbering of the characteristic points of the conveyor's closed contour in direction of the drive element's movement was conducted starting from the point with minimal belt tension, Fig. 1.

All belt tension forces were calculated as they occur along the conveyor. Thus, the location of maximum belt tension force may be determined. The power required to drive or restrain the conveyor is derived from the tension, which represents the amount of pull at the drive pulley necessary to propel or retard the loaded belt. The components of belt tension were summarized to determine the effective tension required at the driving pulley.

The concept of calculations is based on DIN 22101 and FEM 2.124 standards [3-4].

The major steps in belt conveyor calculation were:

- definition of capacity of a conveyor,
- calculation of maximum belt tension required to convey the load,
- selection of belt,
- selection of drive pulley,
- determination of motor power,
- selection of idlers and their spacing.

The main technical parameters of the belt conveyor are: capacity of transport, $Q=90$ t/h, belt width, $B=400$ mm, belt velocity, $v=1.5$ m/s.

3. 3D MODEL FORMING

Calculations of the belt conveyor provided all data and dimensions of the belt conveyor elements. After that, modelling of elements and final assembly of the belt conveyor were conducted [5]. Designed 3D model of the belt conveyor was created using „Autodesk Inventor“ software [6]. The model was created having in mind the order of the assembling of the elements into the final device. Most of the adopted elements (conveyor rollers, drive and tensioning devices, bearings) are mounted on the carrying structure of the belt conveyor.

The adopted carrying structure of the belt conveyor is presented in Fig. 2. This construction was made of circular tubes, which create two frames connected with the smaller tube ribs.

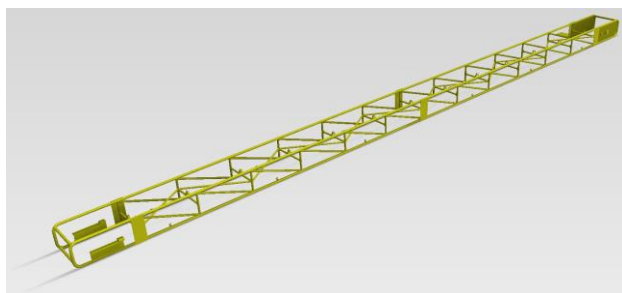


Fig.2: Basic carrying structure of the belt conveyor

At both ends of the construction, appropriate bearing profiles are designed for the installation of the elements of the drive and tension pulley. Each of these parts is easily and quickly mounted on the adjacent part, using steel plates and screw connections.

The tension pulley is located at the end of the belt conveyor. Because the endless conveyor belt needs to be tightened so that sufficient frictional force is developed between the drive pulley and the belt, to make the belt move, a belt tensioning device was built on the tension drum, Fig. 3. The belt conveyor has a screw-type (mechanical) belt tensioning device. The bearing blocks for the tail end pulley are located in guide ways, so that these may be moved by rotating two screws as and when belt tension needs to be increased.

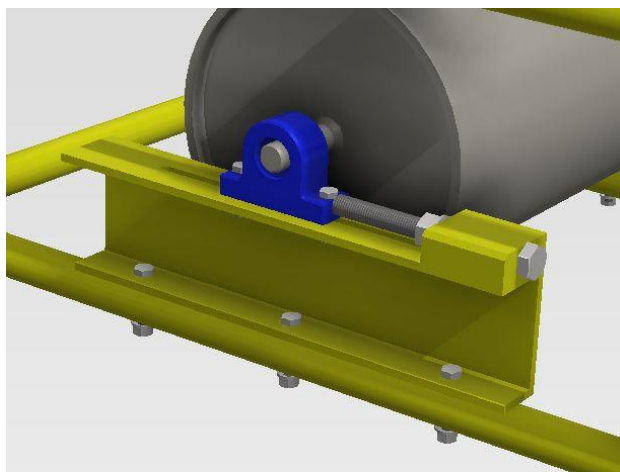


Fig.3: Belt tensioning device

The belt conveyor is supported by troughed carrying idlers so that the two edges of the active side of the belt are elevated from the middle part to form a trough. This provides a greater carrying capacity than a flat belt of equal width for conveying bulk materials or those materials which would slide off flat belts. The return side of the belt is kept flat supported on cylindrical rollers.

The carrying part of the conveyor belt is supported by twelve sets of two carrying rollers, while the return part of the belt is supported by six return rollers, Fig. 4. The return rollers with fixed shafts are horizontal, positioned between brackets which are attached to the support structure.

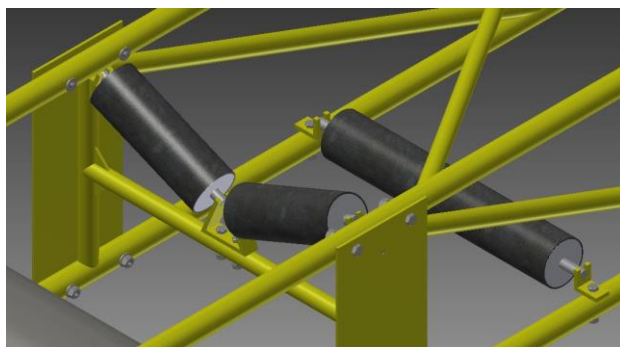


Fig.4: Belt conveyor rollers

The dimensions of the straight or troughed roller set are based on the selected width of belt and recommended edge clearance between belt and roller edges. Spacing of rollers in the loaded run is a function of bulk weight of materials and width of belt. These rollers are made of seamless tubes, side covers and bearing housings, which allow their movement.

A shaft with a profiled end portion secured at the edges of the basic structure of the belt conveyor passes through the roller. The two roller's set is positioned by one eyelid at both sides, as well as by the inner eyelid that are attached to the basic structure of the conveyor, Fig. 4. The return roller placed at the return run of the conveyor belt relies on the two eyelets through which the axle is mounted, thus allowing the movement of the rollers.

The conveyor belt drive device is an electric motor adopted from the standard catalogues of the electric motors. Power from the drive motor is transferred to the drive shaft via the coupling and the belt drive, Fig. 5.

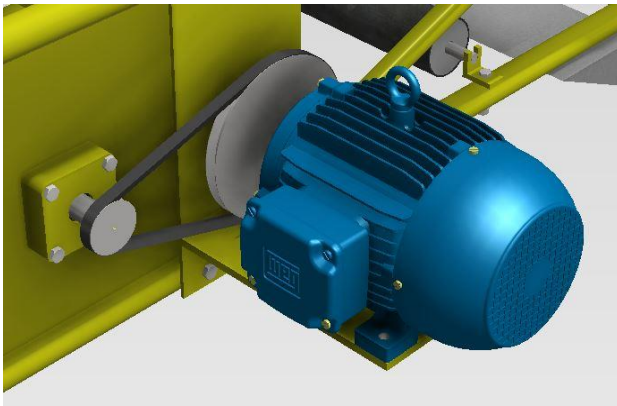


Fig.5: Electric motor and belt drive

The electrical equipment must be capable not only of propelling the fully loaded conveyor at its designed speed, but also of controlling starting acceleration within design limits to prevent excessive tension in the belt.

The power required for the belt conveyor drive is derived from the effective tension force required at the pulley to propel or restrain the loaded conveyor at the designed velocity of the belt.

To determine the effective tension force it is necessary to calculate each of the individual forces acting on the conveyor belt at the characteristic points and contributing to the tension required to drive the belt at the driving pulley. The effective tension force is the final sum of the belt tensions produced by forces such as:

- the gravitational load to lift the material being transported,
- the frictional resistance of the conveyor components, drive and all accessories while operating at design capacity,
- the frictional resistance of the material being conveyed and
- the force required to accelerate the material continuously as it is fed onto the conveyor by a feeder.

While a belt conveyor system is composed of many important parts, none is more economically important

than the conveyor belt itself, which, in most cases, will represent a substantial part of the initial cost. Therefore, the selection of the conveyor belt must be made with great care. Fig. 6 illustrates the selected conveyor belt design.

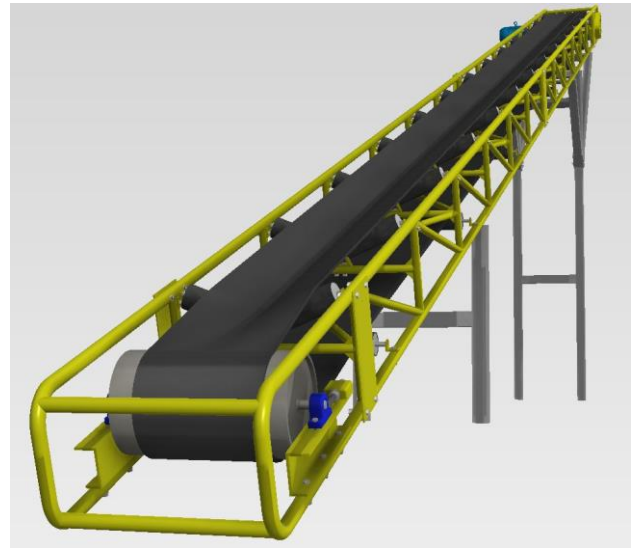


Fig.6: Conveyor belt design

The conveyor belt consists of three elements: top cover, carcass and bottom cover. The primary purpose of the covers is to protect the belt carcass against damage and any special damaging factors that may be present in the working environment. The belt carcass carries the tension forces necessary in starting and moving the loaded belt, absorbs the impact energy of material loading, and provides the necessary stability for proper alignment and load support over rollers under all conditions of loading.

An extremely important point in belt conveyor design is the proper loading of the conveyor belt. Improper loading may result in accelerated belt wear, spillage, and/or reduced capacity.

After all elements were assembled, an overall model of the belt conveyor for continuous transport of bulk materials was obtained, Fig. 7.



Fig.7: Overall model of the belt conveyor

Standard elements (screws, nuts, washers, bearing, seals, etc.) were used during assembly of belt conveyor. All of them play an important role in achieving belt conveyor functionality and protection against dirt particles.

4. MANUFACTURE

The manufacture phase followed after the calculation, modeling and making corresponding technical documentation.

The rollers, Fig. 8, were manufactured, greased and mounted on the belt conveyor carrying structure using eyelids.



Fig.8: Manufactured rollers

The rollers are fitted with antifriction bearings and seals, and are mounted on shafts.

Fig. 9 shows the carrying idler mounted on the belt conveyor carrying structure. Important requirements for idlers are proper support and protection for the belt and proper support for the load being conveyed.



Fig.9: Belt conveyor carrying idler

The next step was the mounting of the welded steel drum pulley with grooved lagging, Fig. 10. The pulley is mounted on heavy duty antifriction bearings in suitable bearing housings.

Belt conveyors are driven by the friction of the belt wrapped around the drive pulley. The drive pulley is typically rubber lagged to provide the traction needed to pull the belt. The rubber covers are made to resist abrasion and cutting. More wrap and greater contact area provide better performance.

The drive pulley is connected to the drive motor through suitable transmission elements. All the components that make up the pulley and shaft assembly must be integrated to provide a fully capable power transmission system.



Fig.10: The drive pulley mounted on the belt conveyor carrying structure

The tension pulley is mounted at the discharge end of the conveyor.

Assembly of chain transmission is presented in Fig. 11. The chain transmission has the role to reduce the speed of the drive device (electric motor) and to transfer the power to the driven device (drive pulley). It is enclosed in metal protection grid due to safety reasons.



Fig.11: Chain transmission

After all carrying idlers were mounted, the whole belt conveyor construction was moved to the working site, Fig. 12.

A welded steel frame design of belt conveyor structure was adopted, based on formed model.

The conveyor structure supporting the pulleys and idlers consists of suitable sized channel stringers, with supporting legs to the main structure or floor.

Fig. 13 shows a final appearance of the belt conveyor carrying structure with a mechanism having possibility of changing the height of the conveyor legs.



Fig.12: Carrying structure of the belt conveyor at the working site



Fig.13: The conveyor legs

Final look of the belt conveyor after assembly of all elements is presented in Fig. 14.

The belt conveyor is designed, constructed, and must be maintained so that the belt consistently runs centrally on its mechanical system of idlers and pulleys.



Fig.14: Belt conveyor after assembly

The belt conveyor with the loading device and complete crushing mill unit are shown in Fig. 15.



Fig.15: Complete transport line

Material can simply be discharged over the head end of the conveyor or anywhere along its length by means of plows or travelling trippers.

5. CONCLUSION

Belt conveyors are environmentally more acceptable than other means of transporting bulk materials. The belt conveyor labour hours and operating cost per ton are usually the fewest of any method of transporting bulk materials. Maintenance costs for belt conveyors are also extremely low compared with the other means of transporting bulk materials. Usually, they need only scheduled inspection and lubrication. Component parts are small and accessible so replacements can be made on the site quickly and with minimal service equipment.

Detailed calculation of the belt conveyor according to the set requirements in terms of size and the required transport capacity was conducted. According to the dimensions obtained by calculation, modeling of the complete belt conveyor was carried out and technical documentation showing the complete model was generated. The calculation and selection of main elements of the belt conveyor were also presented.

In the final stage, manufacturing of the belt conveyor's elements in the workshop was shown, as well as the complete assembly of the conveyor on the separation of gravel and sand site.

The presented model has universal validity and after minimal modifications it can be used for analysis of different constructions of belt conveyors. Thanks to the adopted construction, it is possible to increase or decrease the number of carrying rollers per unit length in a quick and easy manner and to modify the model in accordance with the new user requirements.

With the use of special modules within the framework of the software program, it is possible to perform a detailed analysis in terms of deformation and stress of carrying structure of the belt conveyor.

Depending on the new requirements and working conditions, the model can be adjusted and the solutions of conveyor drive units defined.

Considering the manner of loading and discharging materials from the conveyor, it is possible to include other devices and means of continuous transport and, in that way, further improve the system model.

REFERENCES

- [1] CEMA. (2007) *Belt Conveyors for Bulk Materials* 6th Ed., Conveyor Equipment Manufacturers Association, USA
- [2] Гашић, М. (1997) *Transport devices – continuous transport*, (in Serbian), Faculty of Mechanical Engineering, Kraljevo
- [3] DIN 22101 *Continuous conveyors - Belt conveyors for loose bulk materials - Basic for calculation and dimensioning*
- [4] FEM 2.124 *Influence of the characteristics of bulk material on the design of troughed belt conveyors*, The European Federation of Materials Handling “FEM”
- [5] Antić, I. (2014) *The calculation of the belt conveyor for transport of bulk materials* (in Serbian), M. Sc. thesis, Faculty of engineering of the University of Kragujevac

- [6] Waguespack, C. (2014) *Mastering Autodesk Inventor 2015 and Autodesk Inventor LT 2015*, John Wiley & Sons, Inc. Indianapolis, Indiana

CORRESPONDANCE



Nenad MILORADOVIĆ, Assist. Prof. Ph. D.
University of Kragujevac
Faculty of Engineering
6, Sestre Janjic Str.
34000 Kragujevac, Serbia
mnenad@kg.ac.rs



Igor ANTIĆ, M.Sc.
University of Kragujevac
Faculty of Engineering
6, Sestre Janjic Str.
34000 Kragujevac, Serbia
igor.antic@yahoo.com



Rodoljub VUJANAC, Assist. Prof. Ph. D.
University of Kragujevac
Faculty of Engineering
6, Sestre Janjic Str.
34000 Kragujevac, Serbia
vujanac@kg.ac.rs

DEVELOPMENT OF THE CONSTRUCTION FOR THE EXAMINATION OF ROLLING BEARINGS

Radoslav TOMOVIĆ

Abstract: *Rolling bearings are one of the most important sources of noise and vibration in mechanical structures. Therefore, it is of particular importance to know the causes of the formation and noise and vibration intensities generated by the bearings. The noise and vibration test for rolling bearings is carried out during laboratory testing, during production, for the purpose of assessing the quality of the finished bearings, but also in exploitation for the purpose of assessing the condition of the built-in bearings in constructions, as well as for diagnostic purposes. In this paper the construction of a working table for vibration testing for roller bearings is presented. It is pointed to the advantages of the developed construction in relation to the solutions developed so far. The shown construction can be used for laboratory purposes, but it can also be a good basis for the development of the equipment for quality testing rolling bearings after production.*

Key words: *rolling element bearing, rotor vibrations, ball passage frequency, examination*

RAZVOJ KONSTRUKCIJE ZA ISPITIVANJE KOTRLJAJNIH LEŽAJEVA

Abstract: *Kotrljajni ležajevi su jedni od najvažnijih izvora buke i vibracija kod mašinskih konstrukcija. Zbog toga je od posebnog značaja poznavanje uzroka nastajanja i inteziteta buke i vibracija koju generišu ležajevi. Ispitivanje buke i vibracija kod kotrljajnih ležajeva vrši se tokom istraživanja u laboratorijama, u toku proizvodnje radi ocjene kvaliteta izrađenih ležajeva, ali i u eksploataciji radi procjene stanja ugrađenih ležajeva u konstrukcijama, kao i u dijagnostičke svrhe. U ovome radu je predstavljena konstrukcija radnog stola za ispitivanje vibracija kod kotrljajnih ležajeva. Ukazano je na prednosti razvijene konstrukcije u odnosu na do sada razvijena rješenja. Prikazana konstrukcija se može koristiti u laboratorijske svrhe, ali može predstavljati i dobru osnovu za razvoj uređaja za ispitivanje kvaliteta kotrljajnih ležajeva nakon proizvodnje.*

Key words: *kotrljajni ležaj, vibracije rotora, frekvencija prolaska kuglice, ispitivanje*

1. UVOD

Sve oštriji zahtjevi u pogledu kvaliteta kotrljajnih ležajeva, kao i složenost fizičkih i hemijskih procesa koji se dešavaju u njihovoj unutrašnjosti, a koje nije moguće razjasniti samo na osnovu poznatih teorijskih saznanja, usloveli su intenzivan razvoj eksperimentalnih metoda i uređaja za ispitivanje i dijagnozu stanja kotrljajnih ležajeva, kako u laboratorijskim tako i u radnim uslovima. Putem ovih metoda istražuju se uticaji pojedinih parametara na radnu sposobnost kotrljajnih ležajeva i definišu pokazatelji njihovog tehno-ekonomskog kvaliteta.

Obimna saznanja do kojih se dolazi primjenom ovih ispitivanja imaju veliki značaj za rješavanje tehničkih problema, razvoj novih i poboljšanje postojećih konstrukcija i tehnologija u oblasti proizvodnje, eksploatacije i održavanja kotrljajnih ležajeva. Do

saznanja se dolazi periodičnim ili permanentnim praćenjem stanja ležajeva u laboratorijskim uslovima, ali i u samoj eksploataciji.

Pojava savremenih dijagnostičkih instrumenata i softverskih paketa za analizu stanja ležajeva omogućila je da se na licu mjesta "on site", za vrijeme rada ležaja u realnim uslovima eksploatacije "on line", ispituju i donose relevantni zaključci o radnoj sposobnosti i stanju ležajeva.

Najadekvatnija primjena metoda za ispitivanje i dijagnozu kotrljajnih ležajeva vezana je za poslove nadzora stanja, koji se zasnivaju na periodičnom ili kontinualnom praćenju stanja (monitoringu) tehničkih sistema i njihovih dijelova i registrovanju problema koji dovode do otkaza. Ležajevi su karakteristični mašinski elementi i po tome, što je praćenjem njihovog stanja moguće dati ocjenu o stanju cjelokupne mašine u koju je ležaj ugrađen. Gotovo svi otkazi i nepravilnosti u radu mašina se odslikavaju upravo na ponašanju ležajeva.

Pravilna dijagnoza stanja u prvom redu zavisi od pravilnog izbora dijagnostičkih tehnika i parametara relevantnih za stanje ležaja, pravilnog izbora mjernih mjesta na objektu, nivoa pouzdanosti mjerne opreme, kao i kvaliteta primijenjenog softvera za akviziciju i analizu podataka i stručnosti lica koje obavlja dijagnozu.

Najpotpuniju i najdetaljniju dijagnostiku stanja kotrljajnog ležaja sa identifikacijom uzroka toga stanja, moguće je dobiti na osnovu analize dinamičkog ponašanja kotrljajnog ležaja. Analizom dinamičkog ponašanja ležaja moguće je veoma pouzdano i vrlo rano predvidjeti najveći broj kvarova koji su vezani za kotrljajne ležajeve, te iste na vrijeme otkloniti. Obzirom da su kotrljajni ležajevi jedni od najzastupljenijih mašinskih elemenata i da otkaz ležaja najčešće proizvodi veoma skupe i neplanirane zastoja cijelog mašinskog sistema, koji redovno višestruko prevazilaze cijenu samih ležajeva, ovoj problematici se danas pridaje poseban značaj. Ovo i zbog toga što se analizom dinamičkog ponašanja ležajeva mogu dati ocjene i o stanju cjelokupne mašine u koju je ležaj ugrađen.

Pristup istraživanju dinamičkog ponašanja ležajeva u suštini se odvija u dva pravca. Prvi se zasniva na kombinaciji matematičkog modeliranja i kompjuterskih simulacija, a drugi na kombinaciji eksperimentalnih metoda i inženjerskog iskustva. Na osnovu teorijskih analiza, kompjuterskih simulacija i eksperimentalnih ispitivanja određuju se sopstvene frekvencije elemenata sistema, analiziraju mehanizmi generisanja vibracija i određuju parametri za njihovu identifikaciju, analiziraju

aspekti prigušenja, izrađuju dinamički modeli kompletnog uležištenja, samog ležaja i njegovih komponenti i sl.

Eksperimentalna istraživanja se izvode i u laboratorijskim uslovima i u uslovima eksploatacije. Laboratorijska ispitivanja se obično obavljaju na specijalnim, za tu svrhu namijenjenim probnim stolovima, na kojima se simuliraju različiti radni režimi rada ležajeva. Ova ispitivanja se vrše u cilju smanjenja troškova i skraćivanja vremena ispitivanja, posebno u početnoj fazi istraživanja i osvajanja novih proizvoda i tehnologija izrade ležajeva.

U ovome radu je prikazan sasvim novi pristup u eksperimentalnom ispitivanju dinamičkog ponašanja kotrljajnih ležajeva, primjenom bezkontaktnih senzora, za mjerenje reletivnog vibracijskog pomjeranja između spoljašnjeg prstena ležaja i rotora. Primjena uređaja je pokazala veliku pogodnost ovakvog pristupa kod analize vibracija kod ležajeva, jer se dobija bolji uvid u dinamičko ponašanje i način generisanja poremećajnih sila kod ležajeva.

Uređaj omogućava zadavanje i mjerenje spoljašnjeg radijalnog opterećenja i praćenje promjene relativnih vibracija između spoljašnjeg i unutrašnjeg prstena ležaja i apsolutnih vibracija spoljašnjeg prstena ležaja.

Razvijeno rješenje ima niz prednosti u odnosu na do sada poznata i primjenjivana rješenja. Da bi se to pokazalo u narednom poglavlju će biti opisane karakteristika uređaja za ispitivanje kotrljajnih ležajeva koji je razvio SKF i koji se masovno koristi za ispitivanje vibracija tek proizvedenih ležajeva, nakon montaže na proizvodnim trakama.

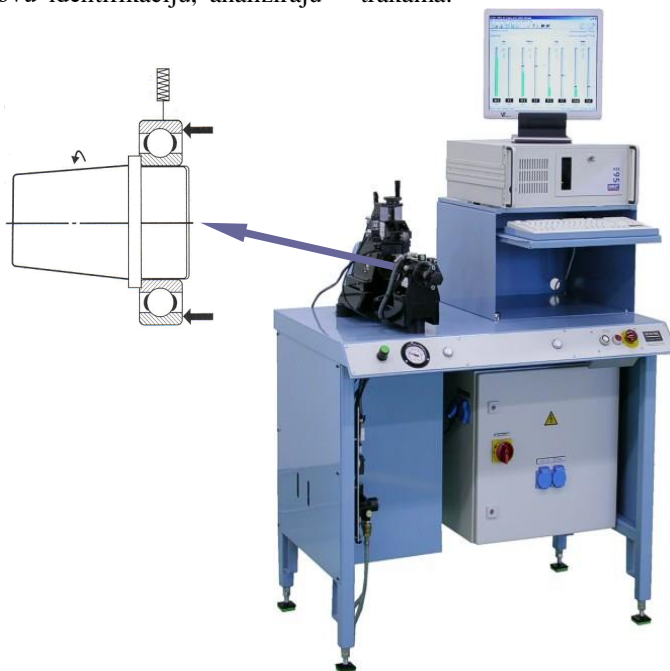


Fig.1. Uređaj za ispitivanje vibracija kod ležajeva
a) Probni sto, b) šema opterećenja i davač na spoljnjem obimu ležaja

2. SKF PROBNI STO ZA ISPITIVANJE KOTRLJAJNIH LEŽAJEVA

Na slici Fig.1. prikazan je probni sto za ispitivanje vibracija koji je razvio SKF. Haris je u referenci [1] dao opis ovoga uređaja. Analiza vibracija i ocjena stanja ležaja pomoću ovoga uređaja je napravljena u odnosu na

smjernice koje propisuje ISO 15242-1-2004(E) standard [2].

Probni sto na slici Fig.1. služi prvenstveno za testiranje vibracija relativno malih ležajeva, npr. do veličine 100 mm za spoljni prečnik. Slična oprema se koristi za testiranje ležajeva većih prečnika i primjenjuju se automatizovane verzije ovog uređaja na proizvodnim trakama. Glavni djelovi sistema su testna stanica i

instrument za analizu signala vibracija. Testna stanica se sastoji od hidrodinamičkog vratila, vazdušnog klipa koji služi za primjenjivanje opterećenja na testirani ležaj i podešavajućeg klizača za pozicioniranje pretvarača brzine. Osovina se preko kaiša pogoni motorom koji je monitoran ispod stola za testiranje. Šematski prikaz sistema je dat na slici *Fig.1.* lijevo. Unutrašnji prsten se postavlja na preciznu osovinu koja je pričvršćena za glavnu osovinu koja se rotira sa 1800 obr/min. Spoljašnji prsten, koji se ne rotira, opterećuje se određenom bočnom silom, kako je to prikazano na šemi. Vrh davača vibracijske brzine, koji je lagano opterećen sa oprugom se stavlja na spoljni obim spoljašnjeg prstena ležaja. Alat za za zadavanje opterećenja ima oblik tankozidnog čeličnog prstena koji dodiruje bočnu stranu spoljašnjeg prstena ležaja. Alat i kombinacija opterećenja su dovoljno prilagodljivi da dozvole radijalno kretanje spoljnog prstena dok se kuglice kotrljaju preko talasavih površina ili defekata u stazama. Naponski signal iz pretvarača je ulazni podatak za pojačalo, koji se posle pretvara u digitalni signal za unos u računar, koji filtrira signal kroz propusnik opsega i prikazuje RMS vrijednost brzine vibracija u svakom opsegu. Nivo vibracija se analizira u tri frekventna opsega: 50–300, 300–1800 i 1800–10.000 Hz. Veći ležajevi se testiraju na manjim brzinama rotiranja (700 obr/min) sa odgovarajućim manjim opsegom filtriranja: 20–120, 120–700 i 700–4000 Hz.

Uređaj na slici *Fig.1.* je veoma pogodan za dijagnozu grešaka mikro i makrogeometrije radnih površina ležaja, kao i za detekciju oštećenja elemenata ležaja nastalih prilikom proizvodnje ili sklapanja ležaja. Nedostatak uređaja je što se radijalni ležajevi ispituju pod dejstvom aksijalnog opterećenja. Pored toga, usled aksijalnog pomjeranja spoljašnjeg prstena ležaja pomjera se i linija dodira između kotrljajnih staza i kotrljajnih tijela ležaja, pa registrovane vibracije tehnološkog porijekla ne odgovaraju dodirnim površinama koje bi se javile kada bi

ležaj bio opterećen radijalnim opterećenjem. Dakle, ne odgovaraju dodirnim površinama koje bi se javile tokom eksploatacije ležaja.

3. NOVA KONSTRUKCIJA ISPITNOG STOLA

Na slici *Fig.2.* prikazan je raspored osnovnih elemenata koji sačinjavaju konstrukciju novog Uređaja za dinamičko ispitivanje kotrljajnih ležajeva [3]. Brojčanim oznakama su obilježeni pojedini dijelovi uređaja i to:

1. Elektromotor, snage 1,5 kW i broja obrtaja $n=2780 \text{ min}^{-1}$, proizvođača Pedrollo-Italija
2. Vratilo sa remenicom
3. Ležajne jedinice za oslanjanje vratila (FAG P56210)
4. Ležaj za ispitivanje
5. Poklopac ležaja za ispitivanje
6. Zavrtnji sa navrtkama za pričvršćivanje poklopca
7. Davač vibracijskog ubrzanja
8. Sklop mjernog pribora za mjerenje relativnih vibracija
9. Sklop za zadavanje opterećenja sa mjernim priborom
10. Stroboskop za mjerenje broja obrtaja
11. Uređaj za prikazivanje rezultata mjerenja broja obrtaja
12. Noseća konstrukcija
13. Uređaj za akviziciju i obradu rezultata ispitivanja
14. Monitor za prikazivanje rezultata ispitivanja
15. Pribor za montiranje i demontiranje ležajeva.

Elektromotor (1) preko remenog prenosa pogoni vratilo (2) na kome se postavljaju ležajevi za ispitivanje (4). Remeni prenosnik vrši redukciju broja obrtaja, tako da je broj obrtaja vratila $n=1476 \text{ min}^{-1}$, odnosno njegova kružna frekvencija je $\omega=154,5 \text{ s}^{-1}$. Broj obrtaja se mjeri pomoću stroboskopske lampe (10), a rezultati se prikazuju na posebnoj mjernom uređaju (11).

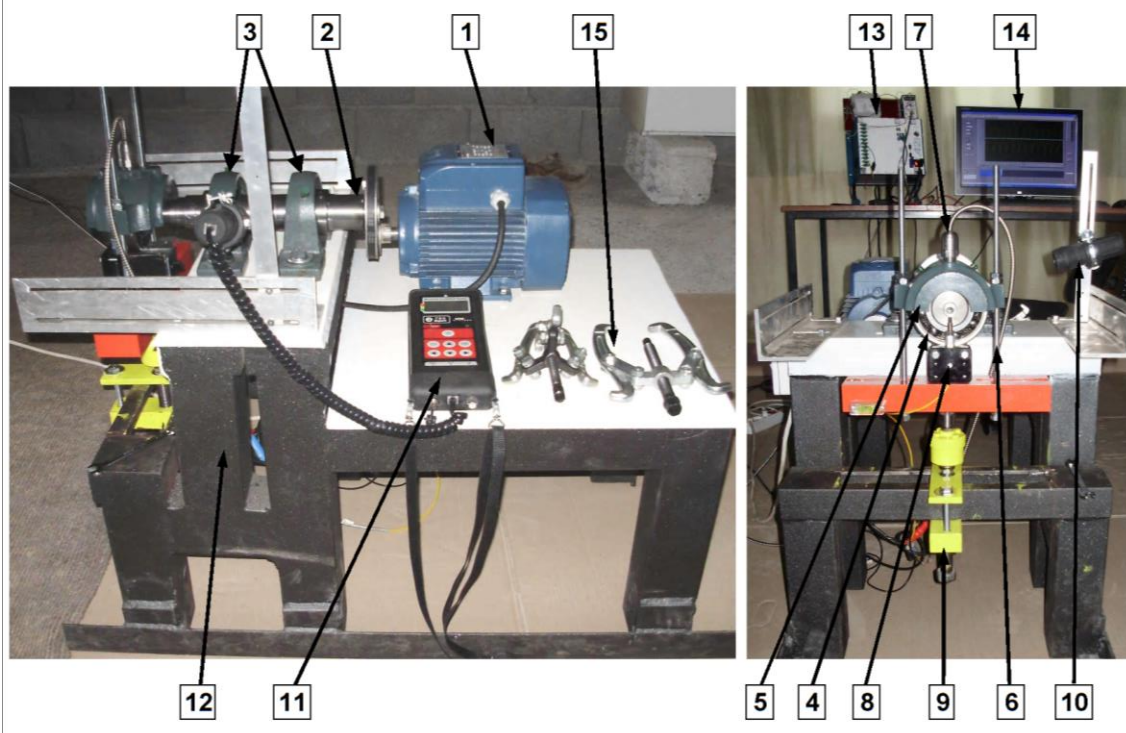


Fig.2. Sastavni elementi uređaja za dinamičko ispitivanje kotrljajnih ležajeva [3]

Sa druge strane vratila postavljaju se ležajevi na kojima se vrši ispitivanje (4). Ležajevi se montiraju na vratilo sa laganim preklomom. Prečnik vratila na mjestu montiranja ležaja koji se ispituje je $d=20$ mm. Za ležajeve većih prečnika, prethodno se na mjesto za montiranje postave čaure za namještanje. Čaure za namještanje služe za premošćavanje razlike između prečnika vratila i nazivnog prečnika ležaja. Spoljašnji prečnik čaura za namještanje odgovara nazivnom prečniku ležaja koji se ispituje. Čaure se na noseće vratilo montiraju sa manjim preklomom. Na čelu vratila je urezan navoj, koji uz primjenu odgovarajućih čaura za postavljanje, služi za montiranje ležajeva i čaura za namještanje. Skidanje ležajeva i čaura za namještanje se vrši pomoću odgovarajućih izvlačača (15).

Ispitivanje ležajeva je moguće obavljati pri čisto radijalnom opterećenju konstantnog pravca i intenziteta. Za zadavanje spoljašnjeg opterećenja služi sklop sa navojnim vretenom (9). Nivo spoljašnjeg opterećenja se mjeri pomoću davača za mjerenje aksijalne sile. Spoljašnje opterećenje se na ležaj prenosi preko poklopca ležaja (5). Unutrašnji prečnik poklopca mora odgovarati spoljašnjem prečniku ležaja. Na taj način se ostvaruje ravnomjerniji prenos opterećenja na spoljašnji prsten ležaja. Kao poklopac ležaja koriste se poklopci odgovarajućih FAG-SNV kućišta. Spoljašnje opterećenje se od sklopa za zadavanje spoljašnjeg opterećenja (9) do poklopca ležaja prenosi preko zavrtnjeva za pričvršćivanje (6). Zavrtnji za pričvršćivanje (6) ujedno služe i za fiksiranje poklopca na ležaju i osiguranje od aksijalnog pomjeranja ispitivanog ležaja, poklopca i mjernog pribora.

Dinamičko ponašanje ležaja se prati pomoću davača vibracijskog ubrzanja (7) i davača za mjerenje vibracijskog pomjeranja (8). Rezultati mjerenja se pomoću odgovarajućih kablova prenose do uređaja za akviziciju (13), gdje se vrši obrada, memorisanje i prikazivanje rezultata ispitivanja na monitoru (14).

U daljim izlaganjima će zbog svog značaja biti detaljnije opisani postupci za mjerenje vibracija, mjerenje broja obrtaja i zadavanje spoljašnjeg opterećenja, kao i sistem za prikupljanje, memorisanje, obradu i prikazivanje rezultata ispitivanja.

3.1. Sistem za akviziciju, obradu i prikazivanje rezultata mjerenja

Za prikupljanje, obradu i prikazivanje rezultata kod Uređaja za dinamičko ispitivanje kotrljajnih ležajeva služi sistem za akviziciju **A2 logger**, proizvođača Electronic Desing iz Beograda (Fig. 3.). A2 Logger je specijalno modeliran prenosni računar, sa plag-in sistemom za akviziciju podataka, monitoring, mjerenje, snimanje i prikazivanje rezultata ispitivanja.

Sistem za akviziciju A2 Logger se sastoji od četiri, osnovne komponente:

1. Aluminijske kutije sa pasivnim bekpanelom sa 8 ISA slotova i sistemom za električno napajanje. U krajnji desni slot je instaliran plag-in PC modul sa procesorom Pentium III od 1.3 GHz sa 256 MB memorije. Hard disk je 2,5 inča, 80 GB i on je otporniji na vibracije i udare od standardnih 3,5 inčnih diskova.
2. A/D modula A2-28-MS, za akviziciju podataka. Modul ima 12 analognih ulaznih kanala. Analogno/digitalni

konvertor ima šesnaestobitnu rezoluciju sa brzinom uzorkovanja od 200 kHz. Modul podržava rad u DMA modu.

3. Monitor za prikazivanje rezultata mjerenja.
4. Na kućište logera je još instalirano i 24-voltno napajanje (4) i transponder za pojačanje signala od vibracijskog pomjeranja (5).

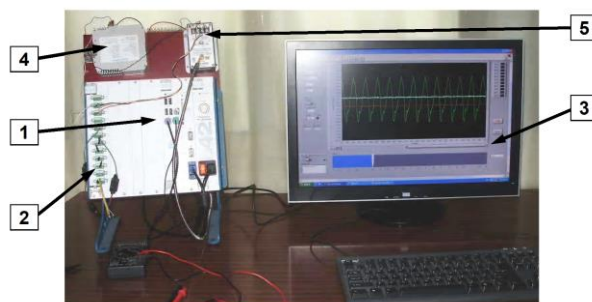


Fig.3. Sistem za akviziciju podataka [3]

Upravljanje akvizicijom podataka kod A2 Loggera je ostvareno pomoću softverskog paketa LabVIEW. LabVIEW je revolucionarno grafičko programsko razvojno okruženje, bazirano na programskom jeziku G, namijenjeno za upravljanje instrumentacionim sistemima i za akviziciju podataka, kao i za analizu i prezentaciju rezultata mjerenja. Akviziciju podataka je moguće obavljati na svih 12 kanala istovremeno, potom je podatke moguće kontinualno snimati na disk i grafički prikazivati na monitoru. Na monitoru se mogu prikazivati jedan ili više kanala istovremeno (Fig. 4). Kontrolu i upravljanje procesom moguće je pratiti pomoću korisničkog interfejsa, koji se vrlo lako može kreirati pomoću funkcija LabVIEW-a.

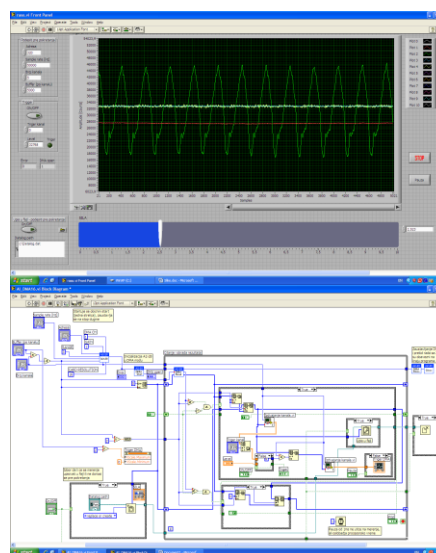


Fig.4. Front panel i blok dijagram uređaja za akviziciju podataka [3]

3.2. Postupak mjerenja vibracija

U odnosu na referentnu tačku Uređaj za dinamičko ispitivanje kotrljajnih ležajeva omogućuje primjenu dva pristupa za mjerenje i analizu vibracija i to:

- Mjerenje relativnih vibracija (pomjeranja) između spoljašnjeg prstena ležaja i rotora.

– Mjerenje apsolutnih vibracija spoljašnjeg prstena ležaja.

Za mjerenje apsolutnih vibracija spoljašnjeg prstena ležaja moguće je koristiti mjerenje vibracijske brzine ili vibracijskog ubrzanja. Za istraživanja u ovome radu su korištena mjerenja vibracijskog ubrzanja.

Na slici (Fig.5) je prikazana šema ova dva pristupa mjerenja vibracija, kao i položaj i izgled davača koji su korišteni u toku ovoga istraživanja.

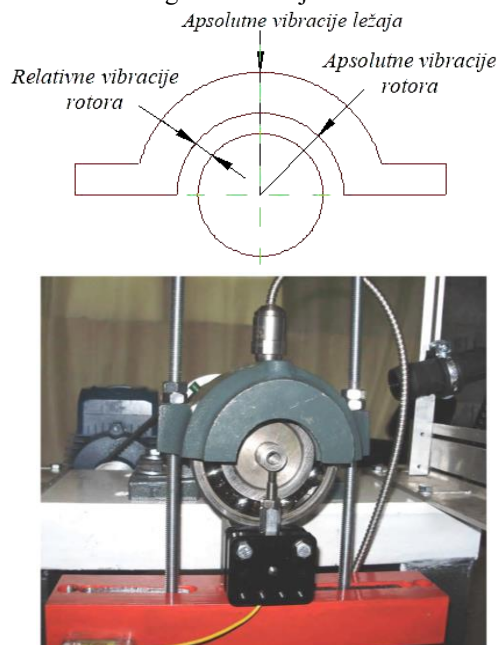


Fig.5. Šema mjerenja i položaj davača [3]

Uopšteno, mehaničke vibracije je najbolje mjeriti što bliže mjestu generisanja poremećajnih sila. Dakle, u ovome slučaju bi to bilo na samom ležaju. Međutim, zbog velike tvrdoće materijala spoljašnjeg prstena ležaja, kao i zbog opasnosti da ne dođe do oštećenja radnih površina kotrljajnih staza ležaja, navoj za fiksiranje davača vibracijskog ubrzanja je urezan u poklopac ležaja, a nosač davača za mjerenje relativnog pomjeranja rotora je pomoću magneta spojen sa spoljašnjim prstenom ležaja, kao što to pokazuje Fig.6.

3.3.1. Mjerenje relativnih vibracija (pomjeranja) između spoljašnjeg prstena ležaja i rotora

Za mjerenje relativnog vibracijskog pomjeranja između spoljašnjeg prstena ležaja i rotora, korišten je bezkontaktni davač serije 10000, proizvođača Metrix-SAD. Davač radi na principu vrtložnih struja. Za mjerenje vibracija, osa davača se postavlja radijalno u odnosu na rukavac, sa udaljenošću vrha sonde od površine rukavca za oko 1.25 mm (Fig.6).

Na slici Fig.7. prikazana je šema mjernog lanca za mjerenje relativnih vibracija rotora. U zavisnosti od rastojanja između vrha sonde i površine rukavca rotora, u sondi se indukuje električni napon. Indukovani napon je proporcionalan rastojanju između vrha sonde i površine rotora. Dobijeni signal se nakon toga pomoću transmitera ispravlja i pojačava. Transmitter šalje signal dalje u sistem za akviziciju podataka, gdje se vrši njegova konverzija u digitalni oblik, zatim njegova obrada, arhiviranje i prezentacija. Za ispravljanje i pojačanje signala korišćen

je Metrix-ov transmitter 5465E. Ovaj transmitter omogućuje praćenje vibracijskog signala čije je frekventni opseg od 5-3000 Hz. Transmitter sistem za akviziciju šalje dva oblika mjernog signala. Prvi je naponski signal, opsega ± 1 V, što odgovara mjernom opsegu vibracijskog pomjeranja od ± 125 μm . Ovaj signal opisuje relativno pomjeranje rotora u odnosu na spoljašnji prsten ležaja. Drugi signal je strujni, opsega od 4-20 mA. Ovaj signal opisuje promjenu pp-amplitude oscilovanja rotora u dijapazonu od 0-250 μm .

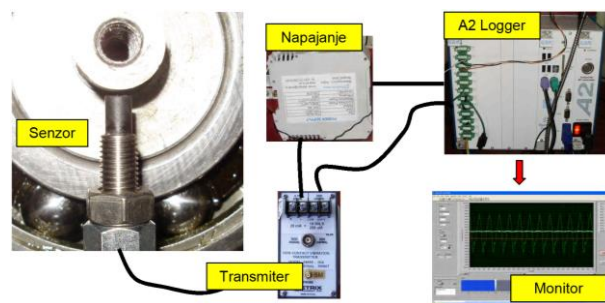


Fig 6. Mjerni lanac za mjerenje relativnih vibracija rotora [3]

3.3.2. Mjerenje apsolutnih vibracija spoljašnjeg prstena ležaja

Za mjerenje apsolutnih vibracija spoljašnjeg prstena ležaja korišten je seizmički senzor, Metrix SA6200B. Senzor registruje vibracije u opsegu frekvencija od 0,5-10000 Hz. Osjetljivost senzora je 100 mV/g, što odgovara 10.2 mV/m/s². Davač sistem za akviziciju šalje signal opsega ± 5 V, što odgovara punoj skali vibracijskog ubrzanja od $\pm 490,5$ m/s². Na slici Fig.7. prikazana je šema mjernog lanca za mjerenje apsolutnih vibracija spoljašnjeg prstena ležaja.

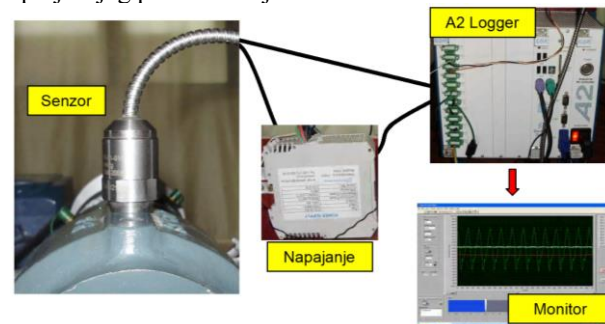


Fig 7. Mjerni lanac za mjerenje apsolutnih vibracija spoljašnjeg prstena ležaja

3.3. Mjerenje broja obrtaja

Na Uređaju za dinamičko ispitivanje kotrljajnih ležajeva moguće je kontinualno pratiti broj obrtaja vratila. Poznavanje broja obrtaja vratila je potrebno za frekventnu analizu spektra vibracija. Broj obrtaja se mjeri pomoću stroboskopske lampe model TAD 18, proizvođača SPM-Švedska. Rezultati mjerenja se zapisuju pomoću uređaja za ispitivanje mašina T30, istog proizvođača. Na slici Fig 8. prikazan je izgled uređaja T30 povezanog sa lampom. Mjerni opseg uređaja je 10-19999 $^{\circ}/\text{min}$, sa rezolucijom od 1 $^{\circ}/\text{min}$ i tačnošću od 1%.

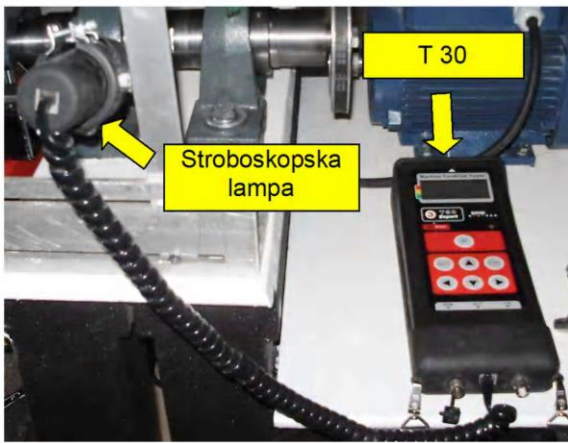


Fig 8. Mjerni lanac za mjerenje broja obrtaja vratila [3]

3.4. Postupak zadavanja opterećenja

Na slici Fig.9. prikazan je sklop za zadavanje spoljašnjeg opterećenja. Pored slike dat je šematski prikaz načina zadavanja spoljašnjeg opterećenja koje se predaje ispitivanom ležaju.

Potrebno radijalno opterećenje zadaje se pomoću navojnog vretena (1) i ploče (2), koja u sredini ima rupu sa urezanim navojem. Aksijalna sila se dalje preko sklopa (4) i davača (5) prenosi na kruti nosač (6). Sa nosača se dalje pomoću dva zavrtnja sa navrtkama (7), prenosi na poklopac ležaja (8), gdje se raspoređuje na spoljašnji prsten ležaja. Ploča (2) zajedno sa pločom (3) i pripadajućim zavrtnjevima služi i za horizontalno podešavanje položaja sklopa za zadavanje spoljašnjeg opterećenja. Sklop (4) obezbeđuje da se na davač (5) prenosi samo aksijalno pomjeranje navojnog vretena, a ne i njegovo obrtanje.

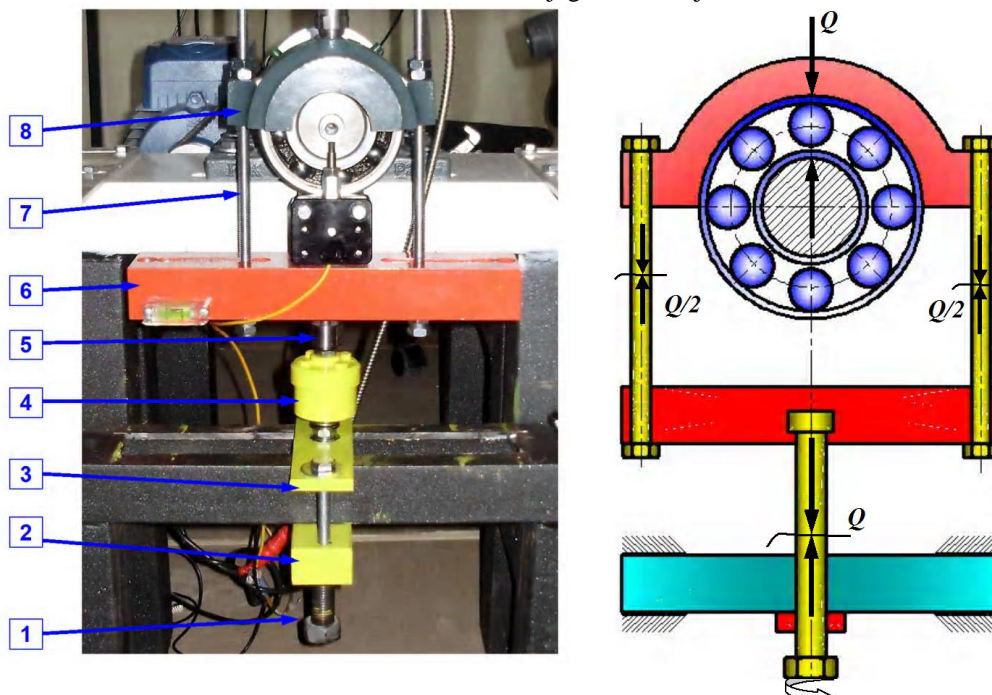


Fig 9. Sklop za zadavanje spoljašnjeg radijalnog opterećenja [3]

Šema opterećenja prikazana na slici Fig.9. pokazuje da su navojno vreteno (1) i zavrtnjevi (7) opterećeni aksijalnom silom na zatezanje. Veličina ove sile se mjeri pomoću HBM-ovog davača aksijalne sile (5), tipa U9B, mjernog opsega od ± 10 kN. Prema šemi prikazanoj na slici Fig.10.. aksijalna sila u navojnom vretenu je jednaka spoljašnjoj radijalnoj sili koja opterećuje ležaj.

Na Fig.10. prikazana je šema mjernog lanca za mjerenje spoljašnjeg radijalnog opterećenja ležaja.

Maksimalno opterećenje ležaja računa se u odnosu na nominalni radni vijek izražen u brojevima obrtaja prema jednačini [4]:

$$N = N_c \cdot \left(\frac{C}{F} \right)^\alpha \quad (1)$$

Ovdje su: N – radni vijek ležaja izražen u min-1, $N_c=10^6$ – nominalni broj obrtaja, C – dinamička nosivost ispitivanog ležaja, F – ekvivalentno dinamičko opterećenje, α – eksponent koji zavisi od tipa ležaja ($\alpha=3$

za kuglične i $\alpha=10/3$ za ležajeve sa valjcima). Međutim, prilikom ispitivanja opterećenja ne smije preći statičku nosivost ležaja (C_0), koja je uvijek manja od dinamičke, odnosno ne smije preći maksimalnu nosivost davača od 10 kN.

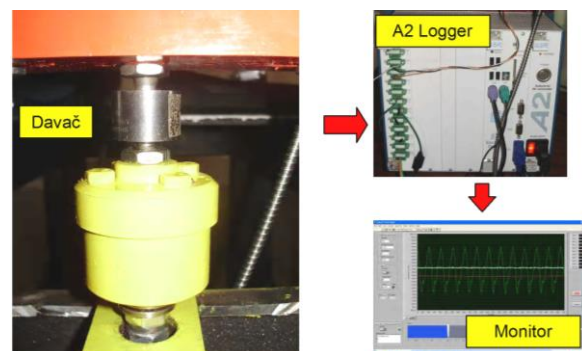


Fig 10. Mjerni lanac za mjerenje nivoa spoljašnjeg radijalnog opterećenja [3]

Kod ispitivanja ležajeva bez spoljašnjeg radijalnog opterećenja, za ostvarivanje neprestanog kontakta prstenova ležaja i kotrljajnih tijela potrebna radijalna sila se dobija pomoću opruga (Fig.11.). Pritezanjem navrtki (1), sabijaju se opruge (2) i na taj način se zadaje potrebna radijalna sila na poklopac ležaja (5). Zadana sila se do poklopca ležaja prenosi pomoću dva zavrtnja (4). Vrijednost zadate radijalne sile i ovdje je moguće pratiti pomoću davača (3). Za ovaj slučaj ispitivanja, da bi radne površine ležaja bile stalno u kontaktu, dovoljna je radijalna sila koja se kreće u dijapazonu od 1-2 N.

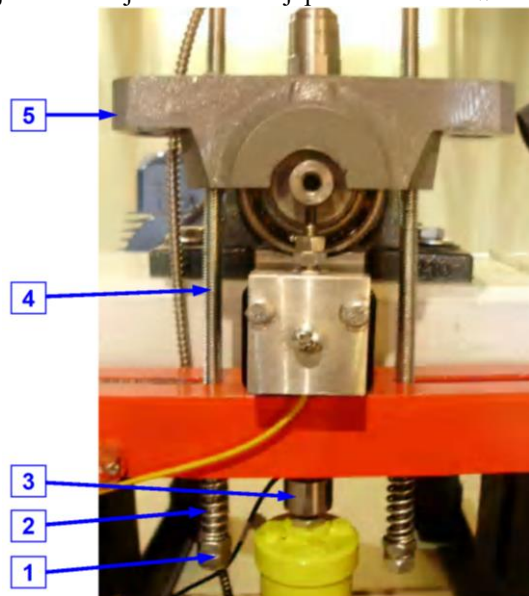


Fig 11. Ispitivanje ležaja u neopterećenom stanju [3]

4. OPIS POSTUPKA ISPITIVANJA

4.1. Priprema ležajeva za ispitivanje

Postupak eksperimentalnih ispitivanja ležajeva često predstavlja veoma kompleksan problem, koji zahtijeva ispitivanje različitih grupa ležajeva, koji se često u okviru jedne grupe moraju razlikovati kako po tipu, tako i po osnovnim parametrima konstrukcije ležaja. Zbog toga je prije početka ispitivanja potrebno izvršiti određenu pripremu uzoraka ležajeva za ispitivanje, koja se sastoji iz:

- Analize traženog cilja pojedinačnih eksperimenata,
- Izboru tipa ležaja s obzirom na traženi cilj,
- Izboru potrebne veličine unutrašnjeg radijalnog zazora s obzirom na postavljeni cilj eksperimenta,
- Obilježavanja ležajeva s obzirom na pripadajuću grupu u odnosu na postavljeni cilj eksperimenta,
- Mjerenja i zapisivanja veličine radijalnog zazora u protokol za svaki ispitivani ležaj,
- Zapisivanje u protokol ostalih karakterističnih parametara ležaja s obzirom na cilj eksperimenta.

Sve ležajeve je prije ugradnje potrebno napuniti određenom količinom masti za podmazivanje.

4.2. Procedura ispitivanja

Postupak ispitivanja svakog od ležajeva sastoji se iz sledećih radnih koraka:

1. Postavljanja čaure za namještanje,

2. Montaže kotrljajnog ležaja za ispitivanje,
3. Postavljanja odgovarajućeg poklopca ležaja i zavrtnjeva za prčvršćivanje,
4. Zadavanja željenog nivoa spoljašnjeg radijalnog opterećenja,
5. Dobijanja vremenskog zapisa vibracija sa ispitivanog ležaja,
6. FFT-analize vibracionog odziva ispitivanog ležaja.

Sva mjerenja su obavljena pri konstantnoj učestalosti obrtanja vratila koja iznosi $n=1476 \text{ min}^{-1}$, odnosno $\omega=154,5 \text{ s}^{-1}$. Pri tome se mijenjala samo veličina spoljašnjeg radijalnog opterećenja. Početna mjerenja se obavljaju na neopterećenom ležaju. Nakon toga u zavisnosti od tipa ležaja i postavljenog cilja postepeno se povećavao nivo opterećenja, sve do statičke nosivosti ležaja odnosno maksimalnog dozvoljenog opterećenja konstrukcije koje iznosi 10 kN.

Kao rezultat svakog mjerenja na ispitivanim ležajevima dobija se vremenski zapis relativnih vibracija između rotora i spoljašnjeg prstena ležaja i apsolutnih vibracija spoljašnjeg prstena ležaja. Prikaz tih zapisa je prikazan na slici Fig.12. Prilikom uzorkovanja treba voditi računa da budu zadovoljene preporuke da frekvencija uzorkovanja bude deset puta veća od maksimalne frekvencije od interesa, kako bi se izbjegao aliasing. Kako se maksimalna računaska vrijednost BPF ispitivanih ležajeva kretala u granicama do 800 Hz, usvojena vrijednost frekvencije uzorkovanja od 20 kHz je višestruko ispunjavala ovaj zahtjev. Sa svakog od ispitivanih ležajeva sniman je nivo relativnih vibracija u trajanju od 15 sekundi. Tako su dobijeni vibracioni zapisi od 300000 podataka za svako ponovljeno ispitivanje.

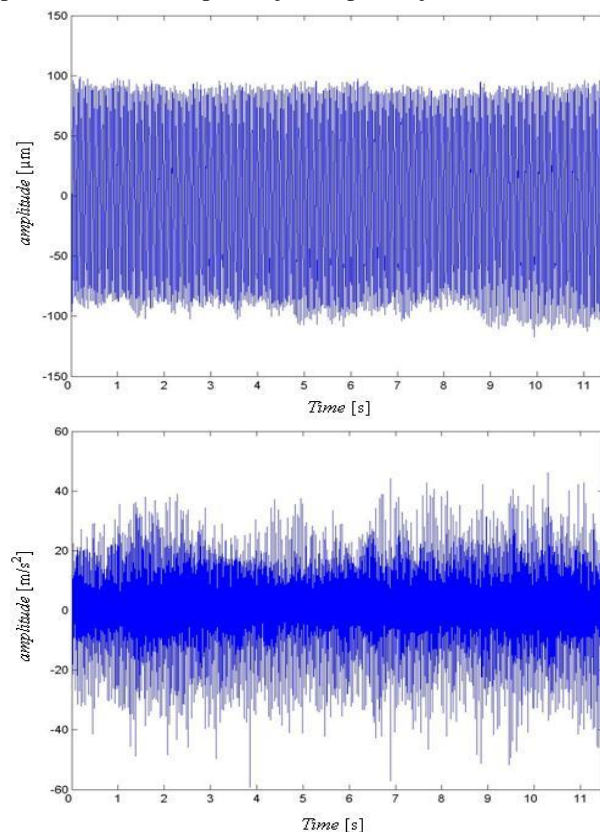


Fig 12. Ispitivanje ležaja u neopterećenom stanju [3]

Rezultati mjerenja dalje su obrađivani FFT-tehnikom pomoću MATLAB-ove biblioteke funkcija za digitalnu obradu signala Signal Processing Toolbox. Frekventni spektar relativnih je prikazan na slici Fig.13. Na ovim dijagramima su sa f_{bp} naznačeni prvi harmonici prolazne učestalosti kuglice i sa $1x\omega$ kružne frekvencije vratila. U spektru vibracija se javljaju pikovi i na višim harmonicima BPF. Međutim, za analizu u razmatranje se najčešće uzimaju samo amplitude vibracija na primarnim frekvencijama, koje su u najvećem broju slučajeva i navažniji za ocjenu vibracionog ponašanja mašinskih konstrukcija.

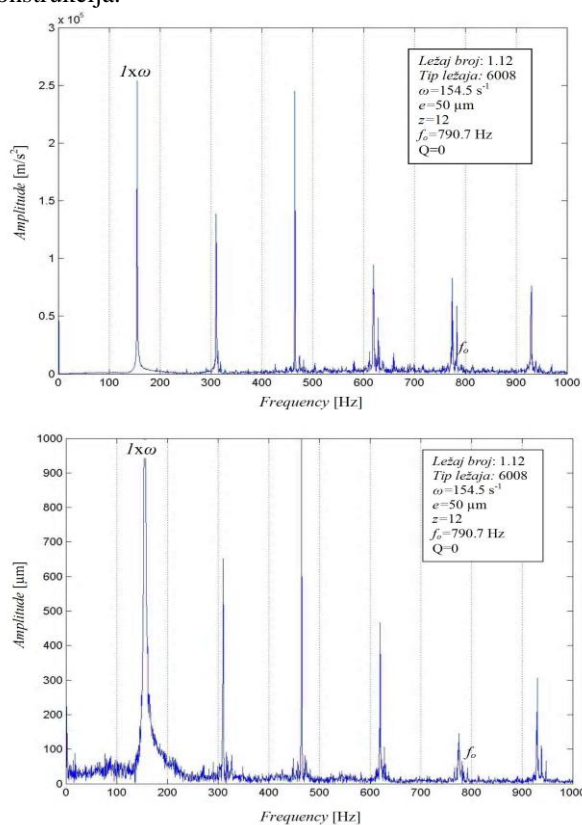


Fig 13. Spektralni zapis vibracija ležaja a)relativne, b)apsolutne [3]

Na frekventnim dijagramima uočavaju se visoke vrijednosti amplitude vibracija na frekvenciji obrtanja rotora i njenim harmonicima, kao i na BPF. Visok nivo vibracija na frekvenciji obrtanja rotora je posledica

zaostalog debalansa u sistemu, dok su vibracije na BPF posledica specifične konstrukcije i načina rada kotrljajnog ležaja. Ove vibracije se nazivaju strukturnim i ne mogu se izbjeći i javljaju kod svih kotrljajnih ležajeva, čak i onih idealne konstrukcije. Strukturne vibracije se mogu jedino značajnije smanjiti, smanjenjem radijalnog zazora ili odgovarajućom kombinacijom spoljašnjeg radijalnog opterećenja i radijalnog zazora u ležaju.

5. ZAKLJUČAK

Konstrukcija probnog stola koja je razvijena u okviru ovoga istraživanja prikazanog omogućuje sveobuhvatno istraživanje dinamičkog ponašanja kotrljajnih ležajeva, različitih dimenzija i različitih tipova, uz efikasno zadavanje i mjerenje spoljašnjeg radijalnog opterećenja i praćenje promjene relativnih vibracija između spoljašnjeg i unutrašnjeg prstena ležaja i apsolutnih vibracija spoljašnjeg prstena ležaja. Uz dodavanje sklopa za varijaciju broja obrtaja rotora, razvijena konstrukcija daje dobru podlogu za dalja eksperimentalna istraživanja u ovoj oblasti.

REFERENCES

- [1] HARRIS T.A., KOTZALAS M.N., (2007), *Rolling Bearing Analysis*, Taylor & Francis Group, USA,
- [2] ISO 15242-1:2004(E), *Rolling bearings-Measuring methods for vibration*, ISO, 2004
- [3] TOMOVIĆ R., (2010), *Istraživanje uticaja konstrukcionih parametara kotrljajnih ležaja na stanje njihove radne ispravnosti*, Doktorska disertacija, Mašinski fakultet Niš

CORRESPONDANCE



Radoslav TOMOVIĆ, Prof. D.Sc. Eng.
University of Montenegro
Mechanical Engineering Faculty
Bul. Džordža Vašingtona bb
81000 Podgorica, Montenegro
radoslav@ac.me

PRODUCT DEVELOPMENT PROCESS REGARDING TO CUSTOMER EMOTIONAL NEEDS

Biljana MARKOVIĆ
Lozica IVANOVIĆ
Aleksija ĐURIĆ

Abstract: A successful development of a new product implies satisfaction of customer's requirements to the level of their individual wishes which include emotions as well. A new or innovative product should be designed to support customer needs, including the customer's persona which can be done by including feelings or emotions into interaction with the product. Customers tend to make a decision about a product based on their perception, values and reflections, so designers and manufacturers should consider making emotional design a bottom line in a product development. Therefore, the aim of this paper is to describe evaluation of customer needs regarding to product development process.

Key words: product development, emotional design, customer needs, evaluation

1. INTRODUCTION

Design, as a term that has been used for many years in the field of mechanical engineering, has had various interpretations and translations over the years. The understanding of the notion was usually based on the aesthetic experience of the object (product), and its interpretation was largely related to art, architecture, fashion, etc.

Incorporating the technical persons in the story of the design, the term is brought into the field of the design process, even projecting, as a wider term. Design is understood as a process that involves visual identification, but also any other design of constructions, including different aspects of observation and study, by authors, constructors. Today, in the literature, various definitions can be found, i.e. interpretations of the concept of design in mechanical engineering, which include the various fields of research and learning, such as: industrial design, product aesthetics, development of machine elements and systems (including development methods), ergonomic design, decision making methods and problem solving, bionics in design, specific development methods, axiomatic methods, etc. The ultimate goal of an optimal, or adequate design, lies in satisfying the requirements of customers, i.e. users, to the level of their individual wishes.

In the spirit of such interpretation, during previous last years the term of emotional design appears, as the means of expression users needs, from the standpoint of satisfying their emotional needs. This means that the designers, the constructors, are tasked to understand the needs of customers, including the emotional aspect, which is not easy to interpret and understand.

When speaking about emotional design, from the standpoint of the development of new products, then it is interesting to look at the approach of Arron Walter's theory, the author of the book "Designing for emotion", Fig.1.

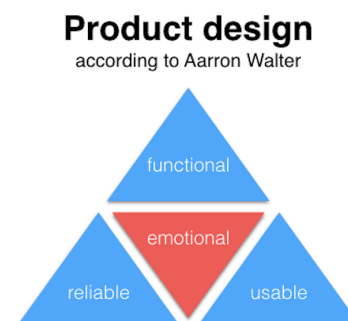


Fig.1: Product design, [1]

According to Aarron Walters theory, a product should be functional, reliable and usable, in that order. Emotional design is another level that adds an to a product when mere functionality is secured. Emotional design should evoke a positive reaction in their users and should make the experience of using a product pleasant and memorable. Great design can evoke positive emotions, these could be: curiosity, gratitude, surprise, originality, success, satisfaction.

1.1. Engineer and emotions

Emotions, during the design process, if judged on the basis of years of experience in dealing with students or mechanical engineers, are not logical for engineers. They are expected to be immune to external influences or to

something that can make them happy or sad during the realization of the disadvantages. Why? Emotions are for the weak. Engineers work in a defined, strict and analytical way, while emotions are for everyday problems that "ordinary" people have.

However, it seems that things turn around a little. Recent studies suggest that the success of designing new products largely depends on the emotional perception of product users.

Naturally, based on this future engineers, they must seek techniques for integrating emotional perception into their product, and educators have to find a way to present to students the importance of this aspect and techniques for integrating emotional perception into product development methods. Reading these lines many young students or future engineers can wonder if they are, in fact, such non-emotional robots?

Design according to emotions requires the analysis of potential emotional reactions which can cause their product, therefore, to do something that they probably have never done before. The design of today's product must be more human, human oriented, and it arises by assimilating conceptual emotions into design principles. Designing products that are psychologically "satisfying" and attractive in terms of the emotional perspective of the users, they are guaranteed to become more attractive than the competition. So, how does a tangible product have a positive, immaterial, emotional effect on users? Easy. An attractive product designed to be aesthetically appealing to human emotions establishes a strong competitive advantage as users will be very satisfied [1].

Studying Wolters' approach, it can be concluded that he believes that the product can be personalized, which makes them much more human, related to people and their emotions. Considering that emotional design is essentially a detailed, complex process, it is important to integrate various aspects of human thinking into the very appearance, which is obvious in some engineering results of the process of developing a new product, such as interface, graphic design, customer service, development strategies, etc.

The most important thing, in fact, is to have a full understanding of the expectations, motivations and intentions of the target market. These are the data that lead engineers in achieving a comprehensive understanding of user needs, and engineers can then design a suitable brand interface to meet these requirements.

The ability of a person to rationalize easily exceeds the power of emotions, and this is precisely what emotional design intends to do, to cause an emotional response in communication with the user, in order to establish a sense of attachment. The emotional design, the segment of the humanistic design, is based on the fact that the products increase their usefulness with aesthetic customer satisfaction, which is used as a tactic that makes users more tolerant towards minor difficulties. The issue of emotion and aesthetics: attractive things work better because emotional design is equal to the identity of satisfying all the user's senses.

According to the original model of the hierarchy of needs, presented as a pyramid, people need health and safety for their existence, than love and self-esteem, before starting

to think about higher - level needs, such as self-actualization, i.e., the need for reaching one owns potentials (Fig.2 a).

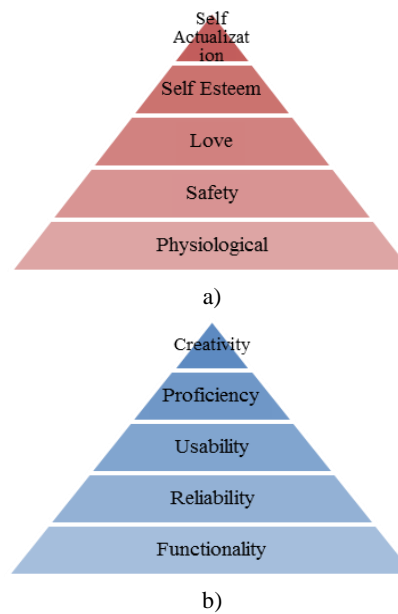


Fig.2: a) Maslow's hierarchy of needs b) Design hierarchy of needs

In design hierarchy of needs, for a customer to be satisfied, a product has to be functional at first place, reliable and simple for usage (Fig.2b). Level of satisfaction which can be reached at the level higher than the mentioned levels is expressed through emotional design. Thus, at the top of the design pyramid are proficiency (professionalism) and creativity which are necessary to generate innovative solutions [5].

Maslow's hierarchy of needs, join with shortcomings, is a framework of thinking reflection, in order to add new value to the product.

2. EDUCATION OF DEVELOPMENT ENGINEERS

In the contemporary era of technical and technological, socio-economic and cultural development of society, the role and importance of theoretical and methodological training of students in the field of product development is increasing. The mission of education of mechanical engineers today is much wider, as well as the challenges they face during professional activities. In this context, both the industry and the academic community have a need for the latest knowledge, techniques and methods in the field of product development. In the past years, the concept of education based on innovative competences has been developed with the aim of developing students' creativity and shaping their thinking in the context of customizing the shape of products to needs and the wishes of the users.

A design engineer or "the one who is developing the project", a central designer and the one who is capable of designing product. Requirements of such position are high engineering understanding, as well as high competencies with respect to the process understanding. Designers must mutually differ by methodological knowledge paired with

social competencies and potential in order to realize ideas. Industry is in search for engineers who are able to continually overcome problematic situations that occur during development of a new product, besides their good established basic training for acquiring methodic skills and ability to abstract and design models. What is important is understanding of competences of control of complicated challenges referring to product development. These competences comprise fundamental knowledge of field of general development of a neutral product and appropriate skills, in respective specific technical fields of product development.

It is evident that great deficit in general engineering education [9] is existent, which is reflected in engineers' inability to transfer their theoretical knowledge to practice. In order to use potential capacities of engineers' personality capacities, as team members, in the best possible manner, it is necessary to use existent, or develop new or different evaluation methods, and/or evaluation of key personality characteristics of every engineer, all according to environment. Also, it is very important to affect the system of thinking, according to which it is crucial for an engineer to possess only professional, technical skills, not to have necessary knowledge of all segments included in product production, as well as innovative management or emotional design influences.

The aim of university education of mechanical engineers is implementation of complex knowledge necessary for efficient development of a product in industrial environment, and students to learn which are the key skills required in their professional work.

If results of study, which has been conducted by VDI, regarding to reasons why engineers did not adapt during probation period, are taken into consideration, it is logical conclusion that the basic goal and request of education of engineers should be improvement of key personal competences.

Engineers have to be „team players“, they should be trained in technical, „now-how“ and business management, making and implementing decisions.

A creative engineer is a visualiser, a diligent worker and a constructive nonconformist with knowledge in his field and the ability to analyze things in his head.

It is important to emphasize that a problem of need for „closing space“ between engineer education and practice requests is not just evident in immediate surrounding (former Yugoslavian republics), but solution of this problem represents challenge to most of big developed countries and their mechanical engineers education system. The basic reason why this space appeared is lack of „rational“ and „detailed“. That is why modern approach to education of mechanical engineers has to assure capabilities: **Conceive, design, implement and operate.**

2.1. Design as socio-cultural way of thinking

Over the last 15 years, changes in world trends have contributed to changes in the sphere of design and reflected that professional capabilities are at a critical stage today more than before.

This was prompted by rapid changes in technologies, especially information, external sources, globalization of the market, which has made a great impact on

professional skills.

The next four major trends have a crucial impact on technical practice and knowledge acquisition in skills that are much more than technical:

- Changing the relationship of forces (leading forces) in a world-sensitive (fragile) economy;
- Mobility of professors and students;
- Using communication and teaching technologies,
- Strengthening the impact of the social imperative.

The previously mentioned "soft" skills, which are much more than the ability of public expression, managerial skills, teamwork skills, are the needs of understanding how the growth of social consequences worldwide is an imperative for mechanical engineers, which helps them to understand the implications of their work.

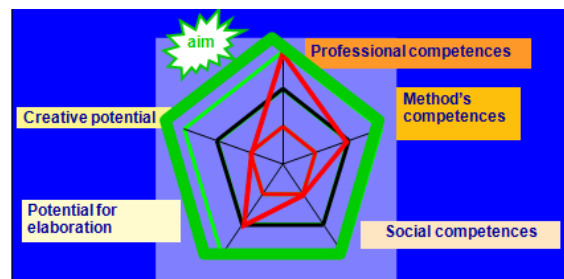


Fig.3: Competences evaluation of engineer's profile [10]

Figure 3. shows one of the methods used in engineering practice to evaluate the overall performance of engineers, taking into account both "hard" and "soft" skills.

Globalization also implies the globalization of the profession of engineers, it is to consider the future role of machine engineers and education must meet this role. Today, it is clear, however, that many US companies are looking for talented engineers anywhere around the world, where possible. Quality in design, low cost of engineering services and production capabilities determine the place where such personnel can be located and sought.

In order to consider "soft" skills, it is possible to divide them into two groups:

- Process skills: ability to communicate, teamwork, the ability to recognize and solve ethical dilemmas,
- Conscious Skills: understanding the impact of global and social factors, knowledge from modern sources, lifelong learning, including adapting to changing trends, tracking contemporary demands from screening users, which also means the skills to comprehend and use the postulate of emotional design.

Teams of people are designing new products today. Reciprocity between transfers of new knowledge on individual level is cognitive distributing process.

This is so-called "socio-cultural" cognitive phenomena, which is a base for management of individuals, i.e. human resource management, in process of product development, in phase of design, and in the rest phases.

In the first place, it is necessary to understand three levels of thinking process. First level is in connection with cognitive behavior of individuals, designers. The second level is the level when the group of people are going to meet design conditions. The «hard» skills of every person

are becoming visible in that level. The third level is level where subject of analyzing is process of individual thinking, in the context of group design.

Generally, a relation between these levels of thinking is a link between technical design tools and mental processes, because designers can reach their ideas only by usage of technical design tools and equipment. Generally, a conclusion is – technical tools and methods are in the strong and intensive link with a social context (depends on boundary conditions of social context itself).

Accordingly, entering a new value into the product, through the design process, not only involves consideration of the emotions of potential users of the new product, but also of the social context in which the process occurs.

3. CONCLUSION

Facing the difference between scientific and practical engineering demands and needs, it is necessary to accept the challenge of reforming engineering education, especially in the field of construction, beyond design. This implies a reversible process, where the starting point for reforming engineering education of design engineers is to consider the demands of users (customers), including their emotions.

Every successful product is the result of the research in the process of product development which requires a special methodological approach. A modern approach to product design which is quality life improvement oriented, is emotional design. Such approach identifies and analyzes emotional responses of customers in order to create an innovative product and solve the problem of the effective usage of the product. In such way, emotional design can be helpful to many companies in implementation of creative strategies and integration of concepts directed to emotions and satisfaction of customers [5].

Therefore, the imperative of each company is to conquer the modern market, by placing an innovative product before the competition, which will in every sense, and even emotionally, satisfy the needs of the users. For this reason, the concept of developing an innovative product, from idea to realization, with the support of all purposeful methods of development and teamwork, must also include consideration of the emotional demands of users. Students and young engineers must be familiar with these needs before engaging in practical work.

Therefore, the goal of engineering education today is far more than transferring knowledge in the conditions of classical university practice, it is a challenge that is being set up every day by professors who prepare young engineers for a modern knowledge market and the acquisition of new products.

REFERENCES

- [1] WALTER, A. Designing for Emotion, <http://www.abookapart.com/products/designing-for-emotion>
- [2] NORMAN, D. (1990) *The design of everyday things*, Doubleday Business

- [3] IVANOVIC, L., KUZMANOVIC, S., VERES, M., RACKOV, M., & MARKOVIC, B. (2015) *Industrial Design*, Faculty of Engineering, University of Kragujevac, Kragujevac, ISBN 978-86-6335-017-5.
- [4] NORMAN, D. A. (2004) *Emotional Design: Why We Love (or Hate) Everyday Things*. New York: Basic Books.
- [5] IVANOVIC, L., MARKOVIC, B., ARSOVSKI, S., RACKOV, M., KUZMANOVIC, S., (2017) *Emotional design and quality of life*, Proceedings of the International conference „2nd Interational conference on Quality of life“, Kragujevac, Serbia.
- [6] CHAKRBARTI, A., ASHISH GUPTA, A. (2007) *Design for emotions*, “International conference on engineering design, ICED’07”, 28 - 31 august 2007, Cite des sciences et de l'industrie, Paris, France.
- [7] DESMET, P. M. A., PORCELIJN, R. & DIJK, M. B. (2007) *Emotional Design*; Application of a Research-Based Design Approach Know Techn Pol 20:141–155, DOI 10.1007/s12130-007-9018-4
- [8] SHARMA, V., PRAKASH, N. R., KALRA, P. (2016) *User Sensory Oriented Product Form Design Using KANSEI Engineering and Its Methodology for Laptop Design*, “International Journal of Scientific Research in Science, Engineering and Technology”, Vol.2, No.1, pp 161-164
- [9] MARKOVIĆ. B. *Doktorski rad - Metodološki pristup upravljanju ljudskim resursima u procesu razvoja proizvoda*, juli 2008., Mašinski fakultet, Univerzitet u Nišu, Niš, Serbia.
- [10] MARKOVIC, B., (2008), *Konstruisanje kroz interoragnizacine projekte putem virtualnih timova*, Proceedings of the International conference KOD 2008, FTN Novi Sad , Serbia.

CORRESPONDANCE



Biljana MARKOVIĆ, Prof. D.Sc. Eng.
University of East Sarajevo
Mechanical Engineering Faculty
Vuka Karadžića 30,
71000 East Sarajevo, B&H
E-mail: biljana46m@gmail.com



Lozica IVANOVIĆ, Full Prof PhD,
University of Kragujevac,
Faculty of Engineering,
Sestre Janjić 6,
34000 Kragujevac, Serbia,
E-mail: lozica@kg.ac.rs



Aleksija ĐURIC, M.Sc. ass
University of East Sarajevo
Mechanical Engineering Faculty
Vuka Karadžića 30,
71000 East Sarajevo, B&H
E-mail: aleksijadjuric@gmail.com

A NEW MODIFICATION OF GENETIC ALGORITHM FOR SOLVING ENGINEERING OPTIMIZATION PROBLEMS

Nenad MARJANOVIĆ
Nenad KOSTIĆ
Nenad PETROVIĆ
Mirko BLAGOJEVIĆ
Miloš MATEJIĆ

***Abstract:** Today, for solving complex engineering problems it is necessary to use optimization methods. Popular methods for finding optimal characteristics are heuristic methods, and the most predominant in use is the genetic algorithm. This paper presents a new modification of the genetic algorithm (iGA) and its testing on complex engineering problems. Results are compared to relevant results from literature for genetic algorithm and other modern optimization methods. The developed modification represents a contribution for practical optimization of engineering problems.*

***Key words:** genetic algorithm, iGA, optimization, engineering problems, heuristic*

1. INTRODUCTION

Engineering problems are clearly defined and must comply with certain constraints. For their adequate operation, adapted for real world application, the need for implementing optimization which grows with the increase of the problems complexity arises. Optimization is used with a clearly defined objective function, optimization variables, existing constraints, feasible solutions and optimization method. Heuristic methods are preferred when it comes to engineering problems due to their favorable characteristics, such as their capability to operate with a large number of variables, overcoming local extremes, speed and efficiency of work, field of use, low threshold of needed facts about the problem in order to find a solution, etc. Optimization is finding solutions from a group of alternative possible solutions. These solutions entail better characteristics of the construction, while at the same time decreasing invested work and expended costs.

There is a large number of heuristic methods such as the Genetic Algorithm (GA) [1], Particle Swarm Optimization (PSO) [2], Artificial Bee Colony (ABC) [3, 4], Ant Colony Optimization (ACO) [5], Teaching-Learning-Based Optimization (TLBO) [6], etc. What is common for these methods is that they work on the principle of mimicking natural occurrences and processes. The most commonly used method is GA, and it is used for solving complex problems with a large number of variables and constrains. The use of this method implies adequate control of algorithm parameters, such as population size, number of generations, selection, crossbreeding and mutation with referencing. Changing parameters of optimization in any method changes the

efficiency of the methods operation for solving optimization problems.

The motivation behind this research is the development of a new modification of the genetic algorithm method, in order to achieve better performances for solving complex engineering problems. This approach improves the optimization process and removes shortcomings which the genetic algorithm has.

2. PROPOSED MODIFICATION OF GA

The principle of operation of the genetic algorithm is based on the mechanism of genetics and natural selection. The algorithm has three phases in its structure: selection, crossbreeding, and mutation. The current versions of GA are based on operation with real numbers (RCGA – real coded genetic algorithm), simulating genetic structure in the evolutionary process. This method was developed for a long time and has a large number of modifications and versions. For the purposes of this research the basic goal is to decrease the number of influencing algorithm parameters. Control of a large number of parameters presents a serious task for adequate use of this method, which limits use.

The development of a modification implies the change of structure and operation of some algorithm, which would achieve better optimization characteristics. This procedure is very complex and requires absolute knowledge of the algorithm in question, its advantages, shortcomings, only after which the new version can be created to improve processes by which the algorithm can be improved. This process requires a large number of tests, checks, attempts and settings, in order to achieve the desired effect. Aside from that, regardless of invested efforts there is no full guarantee that the algorithms convergence will be as the development intended. The modification developed based

on classic GA is based only on managing the population size and number of generations, which widens practical application possibilities of this method. The problem of managing the algorithm and the influence of the user on the results is decreased. The structure of the suggested iGA is presented in fig.1.

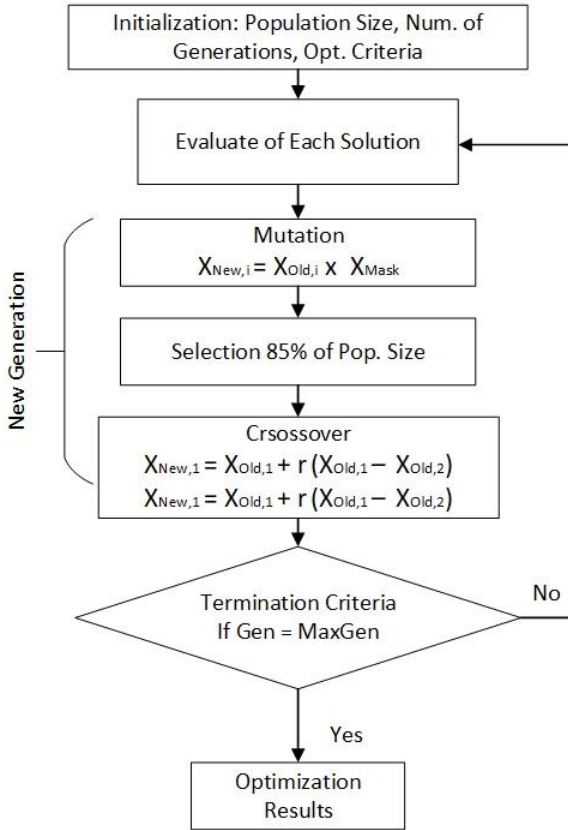


Fig.1: GA structure

This modification can perform like modern heuristic methods, and its operation is simplified for use with practical problems. This modification is efficient, easy for software implementation and most importantly useful for practical application in solving complex engineering problems.

3. EXPERIMENTAL SIMULATION

Every new method, modified method, or hybrid, must be tested on a group of test problems from literature and be compared to results achieved to date. An original software written in C++ for testing this method was developed. Testing was done according to suggestions from literature, with 25 consecutive repetitions of the experiment and for standard engineering problems for testing [7]. Testing was done for problems weld beam, tension compression spring, and gear train. These problems classify algorithms, dependent on whether they are adequate for solving practical engineering problems or not.

3.1. Welded beam

The welded beam problem is a standard test example for engineering optimization. A schematic view of this problem is shown in fig.2.

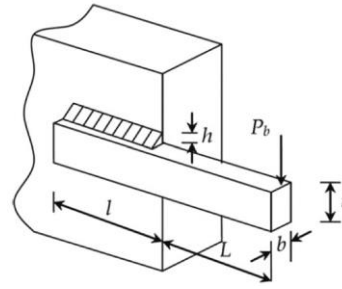


Fig.2: Schematic view of the welded beam problem

This problem is very complex and contains for variables and seven complex constraints. The goal is to minimize costs using the following objective function:

$$f(x) = 1.10471x_1^2x_2 + 0.04811x_3x_4(14 + x_2) \quad (1)$$

The following constraints must be met:

$$\begin{aligned} g_1(x) &= \tau(x) - \tau_{\max} \leq 0, & g_2(x) &= \sigma(x) - \sigma_{\max} \leq 0, \\ g_3(x) &= x_1 - x_4 \leq 0, \\ g_4(x) &= 0.10471x_1^2 + 0.04811x_3x_4(14 + x_2) - 5 \leq 0, \\ g_5(x) &= 0.125 - x_1 \leq 0, & g_6(x) &= \delta(x) - \delta_{\max} \leq 0, \\ g_7(x) &= P - P_c(x) \leq 0 \end{aligned} \quad (2)$$

Where:

$$\begin{aligned} \tau(x) &= \sqrt{(\tau')^2 + 2\tau't''\frac{x_2}{2R} + (t'')^2}, & \tau' &= \frac{P}{\sqrt{2}x_1x_2}, \\ \tau'' &= \frac{MR}{J}, & \sigma(x) &= \frac{6PL}{x_4x_3^2}, & \delta(x) &= \frac{4PL^3}{Ex_3^3x_4}, \\ P_c(x) &= \frac{4.013E\sqrt{\frac{x_3^2x_4^6}{36}}}{L^2} \left(1 - \frac{x_3}{2L}\sqrt{\frac{E}{4G}}\right) \end{aligned}$$

$$\begin{aligned} x_1 &= h, & x_2 &= l, & x_3 &= t, & x_4 &= b, \\ P &= 6000lb, & L &= 14in, & E &= 30 \times 10^6 \text{ psi}, \\ G &= 12 \times 10^6 \text{ psi}, & \tau_{\max} &= 13600 \text{ psi}, \\ \sigma_{\max} &= 30000 \text{ psi}, & E &= 30 \times 10^6 \text{ psi}, & \delta_{\max} &= 0.25in \\ 0.1 &\leq x_1 \leq 2, & 0.1 &\leq x_2 \leq 10, & 0.1 &\leq x_3 \leq 10, & 0.1 &\leq x_4 \leq 2 \end{aligned} \quad (3)$$

The best known value of this problem is $f(X) = 1.724852$.

3.2. Tension / compression spring

On fig.3 the tension/compression spring problem is shown schematically. This problem falls in the group of standard engineering problems for testing optimization methods. The expected optimal value (best known) is $f(X) = 0.012665$.



Fig.3: Schematic view of tension/compression spring problem

The problem is to optimize the objective function:

$$f(x) = (x_3 + 2)x_2x_1^2 \quad (4)$$

The following constraints must be met:

$$\begin{aligned}
g_1(x) &= 1 - \frac{x_2^3 x_3}{71785 x_1^4} \leq 0, \\
g_2(x) &= \frac{4x_2^2 - x_1 x_2}{12566(x_2 x_1^3 - x_1^4)} + \frac{1}{5108 x_1^2} - 1 \leq 0, \\
g_3(x) &= 1 - \frac{140.45 x_1}{x_2^2 x_3} \leq 0, \quad g_4(x) = \frac{x_1 + x_2}{1.5} \leq 0, \\
x_1 &= d, \quad x_2 = D, \quad x_3 = P, \\
0.05 &\leq x_1 \leq 2, \quad 0.25 \leq x_2 \leq 1.3, \quad 2 \leq x_3 \leq 15, \\
x_1 &= d, \quad x_2 = D, \quad x_3 = \text{spring length},
\end{aligned} \tag{5}$$

3.3. Gear train

This problem is formulated to contain one discrete, and six continual variables. The best known solution for this problem is $f(X) = 2996.348465$. The problem also contains 4 linear and 7 non linear constraints in forms of inequality.

The goal function for this problem is:

$$\begin{aligned}
f(x) &= 0.7854 x_1 x_2^2 (3.3333 x_3^2 + 14.9334 x_3 - 43.0934) \\
&\quad - 1.508 x_1 (x_6^2 + x_7^2) + 7.4777 (x_6^3 + x_7^3) + 0.7854 (x_4 x_6^2 + x_5 x_7^2)
\end{aligned} \tag{6}$$

Following the constraints given as:

$$\begin{aligned}
g_1(x) &= \frac{27}{x_1 x_2^2 x_3} - 1 \leq 0, \quad g_2(x) = \frac{397.5}{x_1 x_2^2 x_3^2} - 1 \leq 0, \\
g_3(x) &= \frac{1.93 x_3^3}{x_2 x_3 x_6^4} - 1 \leq 0, \quad g_4(x) = \frac{1.93 x_5^3}{x_2 x_3 x_7^4} - 1 \leq 0, \\
g_5(x) &= \frac{\sqrt{\left(\frac{745 x_4}{x_2 x_3}\right)^2 + 16.9e6}}{110 x_6^3} - 1 \leq 0, \\
g_6(x) &= \frac{\sqrt{\left(\frac{745 x_5}{x_2 x_3}\right)^2 + 157.5e6}}{85 x_7^3} - 1 \leq 0, \\
g_7(x) &= \frac{x_2 x_3}{40} - 1 \leq 0, \quad g_8(x) = \frac{5 x_2}{x_1} - 1 \leq 0, \\
g_9(x) &= \frac{x_1}{12 x_2} - 1 \leq 0, \quad g_{10}(x) = \frac{1.5 x_2 + 1.9}{x_4} - 1 \leq 0, \\
g_{11}(x) &= \frac{1.1 x_7 + 1.9}{x_5} - 1 \leq 0, \\
2.6 &\leq x_1 \leq 3.6, \quad 0.7 \leq x_2 \leq 0.8, \quad 17 \leq x_3 \leq 28, \quad 7.3 \leq x_4 \leq 8.3, \\
7.8 &\leq x_5 \leq 8.3, \quad 2.9 \leq x_6 \leq 3.9, \quad 5 \leq x_7 \leq 5.5.
\end{aligned} \tag{7}$$

4. RESULTS

By comparing the developed modification its efficiency can be noted. For all 25 repeated simulations the best value, worst value, mean value and number of calculations is given for the goal function (FEs) in the optimization process. These values are considered as an evaluation of the method with standard algorithm testing. In table 1 the results of the analyzed methods of optimization of the welded beam are given. The methods analyzed are: GA (Matlab GA-toolbox), PSO-DE, TLBO, ABC, WCA and the developed modification iGA. The FEs value is different for each method. It is obvious that

the iGA is a contender to modern heuristic methods of optimization and that it gives much better results compared to traditional GA. The used values for FEs is 20000, as iGA achieves optimum at that value, and the increase of this value leads the mean value closer to the optimum.

Table 1: Results of analyzed methods for the welded beam problem

Method	Best	Worst	Mean	FEs
GA[8]	2,026769	3,162137	2,760333	25000
PSO-DE [9]	1,724852	1,724852	1,72485	66600
TLBO [6]	1,724852	N/A	1,72844	20000
ABC [10]	1,724852	N/A	1,74191	30000
WCA 1 [7]	1,724856	1,744697	1,72642	46450
WCA 2 [7]	1,724857	1,801127	1,73594	30000
iGA	1,724852	2,134913	1,75364	20000

For the problem of tension/compression spring, the analyzed methods are GA (Matlab GA-toolbox), PSO, PSO-DE, TLBO, ABC, WCA, and the developed iGA (table 2). The used values for FEs is 20000 for this problem as well. Results for this value converge to optimal, and the increase of this value may lead to increased precision.

Table 2: Results of analyzed methods for the tension / compression spring problem

Method	Best	Worst	Mean	FEs
GA [8]	0,012671	0,012693	0,012683	25000
PSO [9]	0,012857	0,071802	0,019555	2000
PSO-DE [9]	0,012665	0,012665	0,012665	42100
TLBO [6]	0,012665	N/A	0,012666	20000
ABC [10]	0,012665	N/A	0,012709	30000
WCA 1 [7]	0,012665	0,012952	0,012746	11750
WCA 2 [7]	0,012665	0,015021	0,013013	2000
iGA	0,012784	0,016049	0,014155	20000

Table 3 gives the results of optimization for the geared speed reducer problem for different optimization methods. Used methods are GA (Matlab GA-toolbox), PSO-DE, ABC, TLBO, and the developed iGA. The method performs perfectly with this problem, which is confirmed by achieving the optimal value in every repetition with only 6500 FEs.

Table 3: Results of analyzed methods for the geared speed reducer problem

Method	Best	Worst	Mean	FEs
GA [8]	2996,41544	2997,57529	2996,627632	25000
PSO-DE [9]	2996,34817	2996,348174	2996,348174	54350
ABC [10]	2997,058	N/A	2997,058	30000
TLBO [6]	2996,34817	N/A	3996,34817	20000
iGA	2996,348165	2996,348165	2996,348165	6500

The developed modification of the genetic algorithm has potential for use with practical engineering optimization problems. The method is available for implementation and is easy to use. It operates rapidly and efficiently, and achieves the optimum in a finite number of iterations, which are the basic requirements for practical application of a method.

5. CONCLUSION

This research is oriented on the development of a new modification of the genetic algorithm called iGA. This problem is very complex. The basic goal is to decrease the influence of parameters, changes in structure and method of using the algorithm. The algorithm is developed for use on engineering problems with constraints, and its testing is done on this group of problems. Tests show that the developed modification works significantly better than certain traditional methods, and that it can answer to application needs with the same quality as current heuristic methods. Testing was conducted on three engineering examples. These examples present standard test examples, which are in literature used to verify the operation of optimization methods. Changes made to the algorithm structure, decrease parameters, and its ease of use have proven to be better compared to the initial algorithm, which verifies the modification as successful. The perspective for use of this modification in engineering practice is creating constructions of optimal characteristics, which will be the subject of future research.

REFERENCES

- [1] HOLLAND, J. (1975) *Adaptation in Natural and Artificial Systems*, University of Michigan Press, Ann Arbor
- [2] KENNEDY, J., EBERHART, R. (1995) *Particle swarm optimization*, Proceedings of IEEE International Conference on Neural Networks, vol.1944, pp 1942-1948
- [3] KARABOGA, D. (2005) *An Idea Based on Honey Bee Swarm for Numerical Optimization*, Erciyes University, Engineering Faculty Computer Engineering Department Kayseri, Türkiye
- [4] KARABOGA, D., BASTURK, B., (2008) *On the performance of artificial bee colony (ABC) algorithm*, Applied Soft Computing, Vol. 8, pp 687-697
- [5] DORIGO, M. (1992) *Optimization, Learning and Natural Algorithms*, Polit.di Milano.
- [6] RAO, R.V., SAVSANI, V.J., VAKHARIA, D.P. (2011) *Teaching-learning-based optimization: A novel method for constrained mechanical design optimization problems*, Computer-Aided Design, Vol. 43, pp 303-315
- [7] ESKANDAR, H., SADOLLAH, A., BAHREININEJAD, A., HAMDY, M. (2012) *Water cycle algorithm – A novel metaheuristic optimization method for solving constrained engineering optimization problems*, Computers & Structures, Vol. 110-111, pp 151-166
- [8] SAVSANI, P., SAVSANI, V. (2016) *Passing vehicle search (PVS): A novel metaheuristic algorithm*, Applied Mathematical Modelling, Vol. 40, pp 3951-3978
- [9] LIU, H., CAI, Z., WANG, Y. (2010) *Hybridizing particle swarm optimization with differential evolution for constrained numerical and engineering optimization*, Applied Soft Computing, Vol. 10, pp 629-640
- [10] AKAY, B., KARABOGA, D. (2010) *Artificial bee colony algorithm for large-scale problems and engineering design optimization*, Journal of Intelligent Manufacturing, Vol. 23, pp 1001-1014

CORRESPONDANCE



Nenad MARJANOVIĆ, Prof. D.Sc. Eng.
University of Kragujevac
Faculty of Engineering
Sestre Janjić 6.
34000 Kragujevac, Serbia
nesam@kg.ac.rs



Nenad KOSTIĆ, MSc. Eng.
University of Kragujevac
Faculty of Engineering
Sestre Janjić 6.
34000 Kragujevac, Serbia
nkostic@kg.ac.rs



Nenad PETROVIĆ, Ass. MSc. Eng.
University of Kragujevac
Faculty of Engineering
Sestre Janjić 6.
34000 Kragujevac, Serbia
npetrovic@kg.ac.rs



Mirko BLAGOJEVIĆ, Prof. D.Sc. Eng.
University of Kragujevac
Faculty of Engineering
Sestre Janjić 6.
34000 Kragujevac, Serbia
mirkob@kg.ac.rs



Miloš MATEJIĆ, Ass. MSc. Eng.
University of Kragujevac
Faculty of Engineering
Sestre Janjić 6.
34000 Kragujevac, Serbia
mmatejic@kg.ac.rs

CONTEMPORARY DESIGN AND RECONSTRUCTIVE ENGINEERING BY FDM METHOD

Saša RANĐELOVIĆ
Dejan MOVRIN
Mladomir MILUTINOVIĆ
Srđan MLADENOVIĆ
Vladislav BLAGOJEVIĆ

Abstract: *Modern reconstructive engineering methods are becoming more and more important in the production of elements of complex spatial surfaces. Using the FDM (Fused Deposition Modeling) procedure, it is possible to make a more or less successful copy of a complex spatial 3D geometry very quickly, which largely meets the set criteria. The whole process consists in identifying spatial surfaces and shapes that must be recognized from an existing model in order to obtain an initial CAD model. After that, with more or less corrections to the 3D model obtained, the existing structural requirements necessary for further assembly and the function itself can be fully met.*

Key words: *Reverse engineering, FDM, quality,*

1. INTRODUCTION

Modern business conditions impose and demand in every sense new approaches that largely change existing constructive rules but also a way of thinking. Namely, we live in a time when new products are quickly released to the market with a predetermined goal that, in the conditions of the environment, must be more or less fulfilled. Defined conditions at the very start determine the entire process of development and production that is decisive for the next stages of the product life cycle. When it comes to reconstructive engineering, the situation is exactly the same only that all this needs to be repeated, but most often with much smaller deadlines and in an environment with imposed restrictions [1].

Reverse engineering is the opposite of forward engineering. It takes an existing product, and creates a CAD model, for modification or reproduction to the design aspect of the product. It can also be defined as the process or duplicating an existing component by capturing the components physical dimensions. Reverse engineering is usually undertaken in order to redesign the system for better maintainability or to produce a copy of a system without access to the design from which it was originally produced [2].

Some of following are reasons for reverse engineering a part or product. First of all the original manufacturer of a product no longer produces a product or there is inadequate documentation of the original design. Third the original manufacturer no longer exists, but a customer needs the product or the original design documentation has been lost or never existed. Some bad features of a product need to be designed out, for example, excessive wear or deformations might indicate where a product should be improved. To strengthen the good features of a

product based on long-term usage of the product. In order to analyze the good and bad features of competitor's products. To explore new avenues to improve product performance and features and to gain competitive benchmarking methods to understand competitor's products and develop better products. The original CAD model is not sufficient to support modifications or current manufacturing methods and the original supplier is unable or unwilling to provide additional parts. The original equipment manufacturers are either unwilling or unable to supply replacement parts, or demand inflated costs for sole-source parts. To update obsolete materials or antiquated manufacturing processes with more current, less-expensive technologies.

Today's production is characterized by remarkable product customization and product quality adjustment for the selected customer. Less or more all product range in one brand offer is similar and for the same purpose. But when a bit deeper analysis is made, there are essential differences that precisely define a particular product for a particular customer. Thus we arrive at the real market situation that certain products are made for a particular customer, that is, certain quality is for a particular customer.

2. CONSTRUCTIVE SOLUTIONS FOR THE TOP CARVING SKI

Modern constructive solutions for new products are often found in a very complex geometric form. Manufacturers intend to protect themselves and accelerate the process of manufacturing and assembly of complex products, combining different functions and purposes of certain elements into more complex and complex products. So we get very complex geometric forms (Fig.1) that now combine different functions and purposes of individual

parts. Combined complex part, complex geometry and production technology is a challenge in every sense.



Fig.1: Top skis with metal and plastic protection

For example, a very simple and simple part is used for its basic function, but also for an effective advertising message. Namely, the top of the skis always represented the most sensitive part that is exposed to frequent hits and damages. Thus, manufacturers in almost all brands decided that there is a need for physical protection and security at the very top of the ski. As the most desirable solution, metal protection solutions appear very quickly (Fig.1), which can fully fulfill this function due to small, very frequent impacts, i.e. strikes on less unpredictable obstacles in the snow race itself. The process of shaping this metal part can be different, but with certain limitations and set conditions very quickly comes to the technology of molding the sheet or the bending process, possibly deep drawing. As the most commonly today is a very complex spatial contour, which suffers permanent damage and damage, it is subject to constructive changes and new requirements to be met. Today, there are completely new solutions that largely change the overall problem-solving approach and production technology that is necessary [3]. The plastic top offers much less protection for the top of the ski, which is the primary goal of the core idea. An eventual impact with a coated metal tip is much safer and the damage is very small. Plastic in these extreme conditions is certainly not able to meet such a requirement. But the question arises, how many such cases actually have and when will that metal summit fulfill such a purpose? Such an analysis comes to a

solution with a plastic tip (ABS - Acrylonitrile Butadene Styrene) that only fits this to a certain extent.

What's more, the metal top of the ski offers almost no chance of advertising the brand itself, that is, it leaves no space for the message in such an attractive and visible place. This is very important for the user, but it is even more important for the future user and potential customer. When things are considered creator of a new product, they will just use this part to mark their brand. This may be a problem with a metal product, but the injection molding techniques of plastics represent a technologically very easy to apply solution. In order to further customization products, we come to the most demanding customer, who may be looking for the initials of his skiing idol (Bode Miller, Hermann Maier, Lindsey Von) at the same place, or full personalization of the product with his own initials and messages (Fig.2).

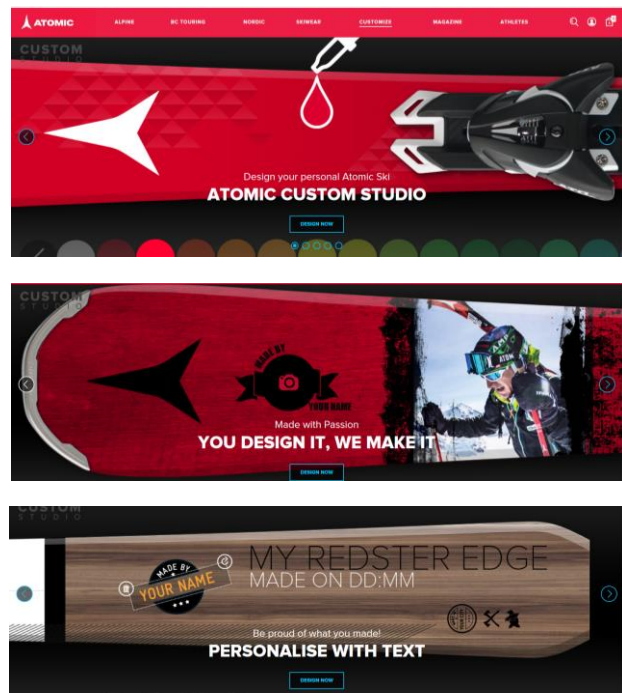


Fig.2: Product customization and personification of users

It is precisely this requirements that demands a completely new approach and production process that will be completely customized with a response to each market demand. Additive technologies, or in this case FDM methods, this requirement can largely fulfill.

3. CHARACTERISTIC OF THE FDM METHOD

The FDM starts with an STL or IGS file from a CAD software like all other additive manufacturing technologies. Fused Deposition Modeling is an additive manufacturing technique commonly used in the rapid prototyping industry. It has a variety of applications but is most often used for modeling, prototyping and production applications. Fused deposition modeling is an additive process that layers the material to produce the finished prototype [4]. A plastic or metal coil is unwound through a heated nozzle, melting the material in the desired shape (Fig.3). One material is for support, while the other is for

the 3D model itself. A 3D CAD file defines a calculated path for melted thermoplastics (print material) to travel and the model is built up, layer-by-layer, which is eventually cooled into a solid. Although different materials cannot be combined in this form of rapid prototyping, different materials can be used to create custom finishes, effects, product specifications and appearance.

Horizontal build layers can be built in three options ranging from 0.2 mm to 3.0 mm. The minimum wall thickness must exceed 0.5mm. Models made from ABS material maintain tolerances of ± 0.13 mm for the first 20 mm, and ± 0.05 mm for each additional 20 mm. In the z axis (vertical), there are standard tolerances of ± 0.25 mm for the first 20 mm, ± 0.05 mm on every 20 mm thereafter. The build size for a single piece is 285 mm \times 155 mm \times 155 mm. This does not restrain you, however, because models that are larger than the build enclosure can be divided, printed as separate pieces and assembled after completion [5].

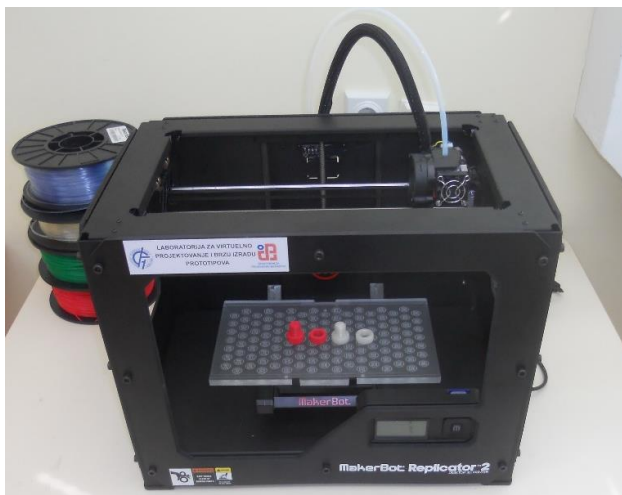


Fig.3: FDM 3D printer

The ability to get every 3D shape and detail in a certain random space (a bounding box) provides great opportunities and fulfill every requirement of the customer when it comes to individual products with short deadlines.

Different requirements and very fast production in small quantities are the main advantage of such processes. Today, this is very simple and close to every user who can very easily take on the role of designers and creators of shapes, but also their own symbol and symbol. That is precisely the goal of such technologies that now offer the possibility of the most diverse solutions that are being created and produced in many places because preconditions of a technical nature have been created.

4. GENERATION OF 3D MODELS AND FDM PRODUCTION

To create a 3D geometric model, SOLID WORKS was used in which a geometric model was created based on the existing geometry at the level based on which the spatial model was obtained (Fig.4). The external

dimensions fully correspond to the existing model, primarily due to the same shape and design. The internal dimensions are very important in functional terms, which provide easy assembly and fixing for the existing profile surface of the top of the ski itself. It's mostly about the Features obtained by the Boss extrude function (Fig.4) based on drawing in the plane.

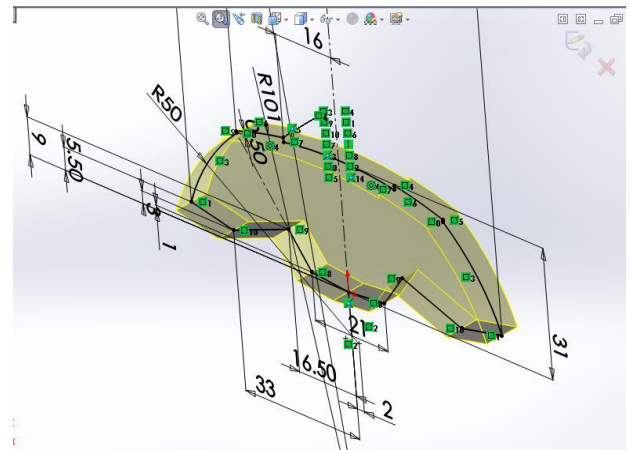


Fig.4: The 3D model of top skis generation

All outer edges and passes are rounded by the fillet function in order to get as close as possible and identical to the original. For the purpose of the same product, which will completely replace the part of the missing part, a sign of the brand is created (Fig.5), which is fully integrated with both the front and the back as per the original.

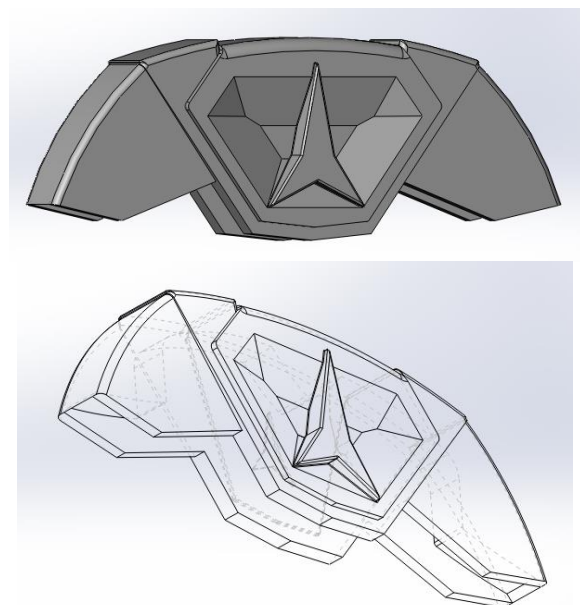


Fig.5: Front and back surface with sign of brand

One of the most popular 3D printers in this class is the Makerbot Replicator 2, which is based on FDM technology and can work with 0.1, 0.2 and 0.3 layers, allowing user to vary a broad range of production parameters (Fig.6). In this 3D printing, Makerbot Replicator 2 was used to produce space specimens with characteristic outside and inside geometry (Fig.6).

The FDM method described gave a satisfactory level of quality in every respect. The demand for the accuracy of the geometry and the quality of the outer surfaces has been met. In these technologies, a lot of attention is paid to surface quality and depth of roughness that directly depend on the temperature and speed of extrusion. A number of papers deal with these problems, where their interaction is explained to detail [6].

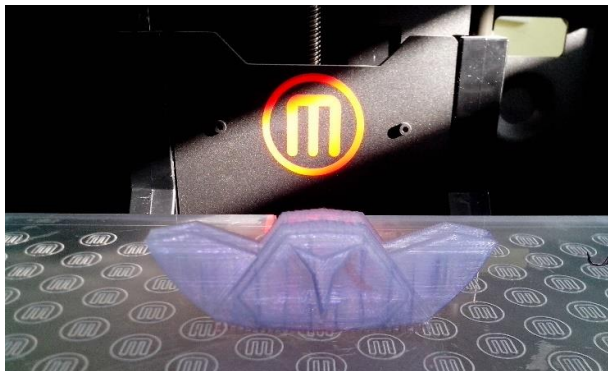


Fig.6: Appearance of the finished work obtained by the FDM method

5. CONCLUSION

The FDM method of production and production provides great opportunities and the freedom to create different spatial surfaces. The model can have very complex surfaces that can be obtained for the first time or reproduced in order to obtain a copy of the existing model. Limitations in terms of curvature, transient radius and surface quality should be respected so that the final shape would have the desired geometry and strength of the boundary surfaces the object of which is to achieve the layering process in several successive passages.

REFERENCES

- [1] PEREZ, C. L. (2002) *Analysis of the surface roughness and dimensional accuracy capability of fused deposition modelling processes*, International Journal of Production Research, Vol. 40, No 12, pp 2865-2881
- [2] GALANTUCCI, L. M., LAVECCHIA, F., PERCOCO, G. (2009) *Experimental study aiming to enhance the surface finish of fused deposition modeled parts*, CIRP Annals - Manufacturing Technology, 49 (2), pp 189-192
- [3] ULBRICH, B., et al. (2012) *Comparison of five rapid prototype techniques (SLS/FDM/DLP/3DP/Polyjet)*, Innovative Development of Virtual and Physical Prototyping - Bartolo et al. (Eds.), Taylor & Francis Group, London, ISBN 978-0-415-68418-7, pp 573-580

- [4] MAHESH, M., et al. (2004) *Benchmarking for comparative evaluation of RP systems and Processes*, Rapid Prototyping Journal, 30(2), pp 123-135
- [5] UPCRAFT, S., FLETCHER, R. (2003) *The rapid prototyping technologies*, Rapid Prototyping Journal, 23(4), pp 318-330
- [6] LUŽANIN, O., MOVRIN, D., PLANČAK, M. (2013) *Experimental investigation of extrusion speed and temperature effects on arithmetic mean surface roughness in FDM built specimens*, Journal for Technology Plasticity, Vol.38, No 2, pp 179-190, Novi Sad, Srbija

CORRESPONDANCE



Saša RANĐELOVIĆ, Prof. D.Sc. Eng.
University of Niš
Faculty of Mechanical Engineering
Aleksandra Medvedeva 14
18000 Niš, Serbia
sassa@masfak.ni.ac.rs



Dejan MOVRIN, M.Sc.
University of Novi Sad
Faculty of Technical Sciencel Engineering
Trg Dositeja Obradovića 6
21000 Novi Sad, Serbia
dmovrin@uns.ac.rs



Mladimir MILUTINOVIĆ, Prof. D.Sc. Eng.
University of Novi Sad
Faculty of Technical Sciencel Engineering
Trg Dositeja Obradovića 6
21000 Novi Sad, Serbia
mladomil@uns.ac.rs



Srđan MLADENOVIĆ, PhD
University of Niš
Faculty of Mechanical Engineering
Aleksandra Medvedeva 14
18000 Niš, Serbia
maki@masfak.ni.ac.rs



Vladislav BLAGOJEVIĆ, Prof. D.Sc. Eng.
University of Niš
Faculty of Mechanical Engineering
Aleksandra Medvedeva 14
18000 Niš, Serbia
sassa@masfak.ni.ac.rs

DETERMINATION OF MUSCLE TISSUE PROPERTIES FOR FEA APPLICATIONS

Branislav DIMITRIJEVIĆ
Milan BANIĆ
Žarko MIŠKOVIĆ
Radivoje MITROVIĆ
Aleksandar MILTENOVIC
Miša TOMIĆ

Abstract: *The paper presents an experimental procedure for compression testing and determination of viscoelastic characteristic of porcine muscle tissue. Uniaxial compression tests were performed on fresh porcine muscle samples at various fibre orientations to determine muscle viscoelastic behaviour. The experimental test were performed with a goal to obtain parameters of Bergström–Boyce constitutive model, which will be used in future research of vibration influence on human musculature and vibration suppression of hand held machinery.*

Key words: *muscle tissue, uniaxial compression, Bergström–Boyce material model, HAVS*

1. INTRODUCTION

Vibration white finger (VWF), also known as hand-arm vibration syndrome (HAVS) or dead finger, is a secondary form of Raynaud's syndrome, an industrial injury triggered by continuous use of vibrating hand-held machinery. HAVS is a widespread recognized industrial disease affecting tens of thousands of workers. It is a disorder that affects the blood vessels, nerves, muscles, and joints, of the hand, wrist, and arm. The hand-arm vibration syndrome causes changes in sensory perception which can lead to permanent numbness of fingers, muscle weakness and, in some cases, bouts of white finger. The mechanisms of how vibration causes the condition is not clear yet. It is believed that slight but repeated injury to the small nerves and blood vessels in the fingers cause the HAVS. Because of this problems, it is necessary to develop a machines/devices which are going to be used to protect people from vibration influence of hand tools.

Virtual product development (VPR) and simulations can be used to evaluate vibration influence on people and to develop new vibration suppression devices. In order to simulate influence of hand tools to human hand-arm system it is necessary to determine mechanical properties of muscle tissue. Numerous authors worked on determination of properties of musculature. Researchers usually tested the porcine muscle tissue because it is most similar to human muscle tissue. Most of the authors used hyperelastic models to describe the mechanical behaviour of muscular tissue [1, 2]. Bol [3] tested porcine skeletal muscle until 112 hours post mortem using a semi-confined compression device that included fascicles to enter one of the states of compression, tension or constant length. The anisotropic mechanical behaviour of the tissue was analysed with a special focus on the testing time post

mortem. Moerman [4] tested the tension-compression asymmetry properties of Ogden hyperelastic formulation. Although it is well established that biological tissues exhibit viscoelastic/viscoplastic behaviour [5, 6, 7], only few researchers used viscoelastic models recently to model the constitutive behaviour of tissues [8, 9, 10].

Usually two different approaches are adopted to obtain viscoelastic parameters of biological tissues - creep/stress relaxation (quasi-static/low-rate) and dynamic tests. The results from quasi-static tension/compression tests are most often correlated by Prony series, although other fitting techniques have been used (transfer function in Laplace space, splines) [11]. As for dynamic tests, the system is subjected to a predefined displacement function over a range of frequencies and temperatures. The amplitude of the force response and phase lag between the displacement and force signals can then be measured [11]. In quasi-static/low-rate tests the authors are calibrating the constitutive model parameters based on uniaxial, biaxial, tensile plane stretching and tension relaxation testing which is very complicated to perform and requires specialised testing equipment.

One of basic ideas in this research was to replace complicated standard tests procedures (uniaxial, biaxial, plane stretching tensile and tension relaxation testing), which are usually conducted in specialized laboratories, with simple uniaxial compression on universal testing machine. This paper gives an procedure for testing tissue to determine parameters Bergstrom-Boyce material model.

2. BERGSTRÖM-BOYCE MATERIAL MODEL

The Bergström-Boyce material model is a phenomenological based, highly nonlinear model used to

model behaviour of viscoelastic/viscoplastic materials [14]. The model allows for a nonlinear stress-strain relationship, strain rate dependence and can capture the hysteresis effect of tissue. The time dependent behaviour of tissue can be mechanically described by decoupling it into two parts: an equilibrium response and time depended deviation from the equilibrium response. Tissue can then be modelled as two parallel polymer networks (Figure 1).

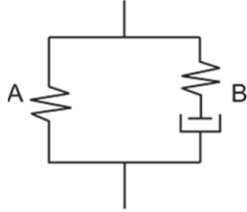


Fig 1: Representation of Bergstrom-Boyce model

The first network (A) captures the equilibrium response and can be modeled by using any of the known hyperelastic material models. The second network (B) represents a perfect network in series with a time dependent element which acts to relieve the strain in the network over time. The deformation gradient F acts on both networks, so it can be represented as [15]:

$$F = F_A = F_B = \nabla_x x \quad (1)$$

The deformation gradient of the time dependent network (B) F_B can be further decomposed to elastic F_{Be} and inelastic F_{Bi} parts:

$$F = F_{Be} \cdot F_{Bi} \quad (2)$$

The stress in network A (T_A) can be obtained from the 8-chain network model given by Arruda [14]:

$$T_A = \frac{\mu_A^0}{J_A \lambda_A^*} \frac{\mathbf{L}^{-1} \left(\frac{\lambda_A^*}{\lambda_A^{lock}} \right)}{\mathbf{L}^{-1} \left(\frac{1}{\lambda_A^{lock}} \right)} dev[B_A^*] + K[J_A - 1]I \quad (3)$$

The initial shear modulus of the equilibrium network μ_A^0 and limiting stretch of the equilibrium network λ_A^{lock} are the material constants, which are determined experimentally.

The stress in the elastic part of network B can be obtained similarly as stress in network A, by the 8-chain network model [14]:

$$T_B = \frac{s\mu_B^0}{J_{Be} \lambda_{Be}^*} \frac{\mathbf{L}^{-1} \left(\frac{\lambda_{Be}^*}{\lambda_{Be}^{lock}} \right)}{\mathbf{L}^{-1} \left(\frac{1}{\lambda_{Be}^{lock}} \right)} dev[B_{Be}^*] + K[J_{Be} - 1]I \quad (4)$$

The components of eq. (4) are analogous to components of eq. (3) and they are computed in the same way as for eq. (3). The initial shear modulus of the time depended network μ_B^0 and limiting stretch of the time depended network λ_{Be}^{lock} are the material constants, which are determined experimentally.

Currently the Bergström-Boyce model is only nonlinear viscoelastic model of elastomers which is implemented in commercial software packages for analysis using the

finite element method. Precision of forecasting mechanical behaviour by Bergström-Boyce model was proved by many authors [14].

3. EXPERIMENTAL PROCEDURE

Mechanical behaviour of muscle tissue was experimentally tested on a porcine meat sample, as it well established that porcine muscle tissue is the most similar to human muscle tissue of a finger.

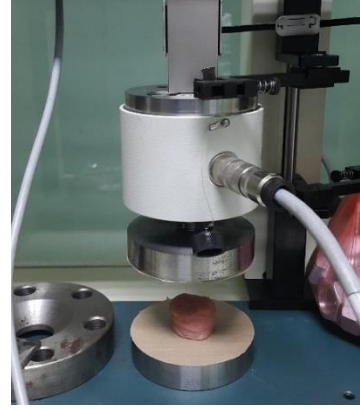


Fig 2: Experimental setting on universal testing machine

Compression testing is easier to perform compared to standard tests and can be done in any laboratory which has a universal testing machine. Uniaxial compression is alternative method for two-axial stretching, because it doesn't require special tools for sample testing. During compression testing, it's not necessary to use extension meter to determine sample deformation. Test program definition is based on general recommendations for compression testing is given in the reference [16]. It was decided that tests will be performed with value of the maximum relative deformation (ϵ) equal to 0.5. All experimental testing is conducted on universal testing machine (Figure 2) between plates made of hardened steel. A special tool was created for cutting the sample from the porcine gluteus.

Table 1. Sample dimensions for experimental uniaxial compression testing of the muscle tissue

Sample dimensions	Ø35.7 ± 0.5 x 17.8 ± 0.5 mm
Test temperature	23 ± 2 °C
Maximum compression force	300 N (depends on the sample)
Maximum deformation	9 mm
Number of samples	6 (3 per fibre direction)
Testing machine control method	Manual deformation control

The samples were cutted in two directions – normal to the direction of the fibres of the musculature and along the direction of the fibres.

Test specification is defined as shown in Table 1. Before the tests, samples were conditioned on a room temperature (test temperature) for at least 24 hours. Before testing process was started, dimensions of all samples were checked (Table 1). Samples are set between hardened plates which are coated with Teflon. Mild liquid

soap solution is applied to both sample and plates. Usage of Teflon wraps and lubrication of both plate and sample, reduces friction influence on the process as the barrelling of the sample is avoided. Thus, influence of friction on the resulting force and change of sample's shape is reduced by achieving above mentioned tribological conditions. Noted conditions allow minimal slide resistance of sample's base when sample is pressed between steel plates.

During the test, the acquisition of data on the value of force and deflection is carried out to obtain a mechanical characteristics of the sample.

Table 2. Procedure for muscle tissue testing

Test N°	Procedure
1	From starting position, load is applied with a deformation speed of 10 mm/min until maximum deformation (9 mm) is achieved. Same speed is applied during sample unloading.
2	From starting position, load is applied with a deformation speed of 100 mm/min, until maximum deformation (9 mm) is achieved. Same speed is applied during sample unloading.
3	From starting position, load is applied with a deformation rate of 10 mm/min until one third of maximum deformation (3 mm) is achieved, and at that point, is retained for 30 seconds. After 30 s pass, load is reapplied with same deformation rate until two thirds of maximum deformation (6 mm) are achieved. When required deformation is achieved, load is retained for 30 more seconds; after that period is over, load is reapplied until maximum deformation (9 mm) is achieved. Without changing of the speed, perform the relief in the reverse order.

All samples were tested according to the procedure described in table 2. The tests were performed for two strain speeds which defer for a factor of 10. Noted test have a function to capture strain rate dependence of the mechanical response. The third test has a function to capture relaxation parameters.

4. RESULTS

The results of experimental testing of porcine meat sample are shown on Figures 3 to 5.

It can be observed from the obtained results that the specimens exhibit significant hysteresis value. Due to high internal friction of the tissue the absorbed energy is than very high. Thus hysteresis dampening of vibrations of the skeletal muscle tissue is very high. Furthermore, the specimens exhibit viscoplastic behaviour as the resisting force quickly drops zero during the unloading phase. The specimens do not return to original dimensions before the tests even after the prolonged time.

The viscoplastic behaviour of the tested specimens is a consequence of the large deformation as there is evidently some damage to muscular protein chains.

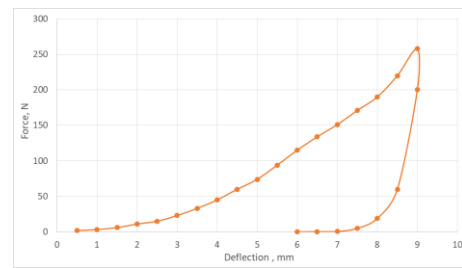


Fig 3: Compression of sample at deformation speed of 10 mm/min

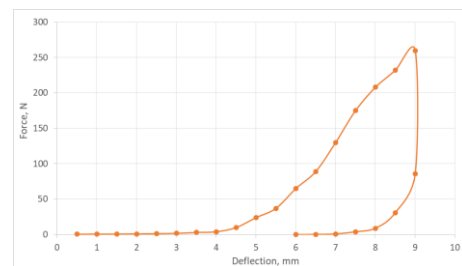


Fig 4: Compression of sample at deformation speed of 100 mm/min

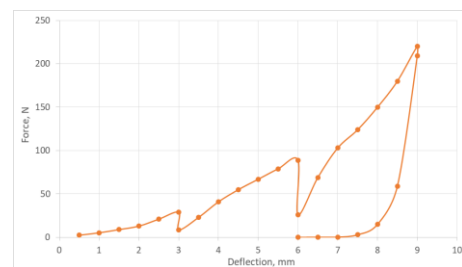


Fig 5: Compression with relaxation at deformation speed of 10 mm/min

The obtained resisting force is increasing with the increase of the deformation speed. The load and unload curves are also more steep for a larger deformation speed. From the obtained results it was also observed that fibres orientation doesn't have a significant influence on the mechanical response of the porcine gluteus musculature. The reasons for behaviour this should be further investigated as gluteus belongs to a group of skeletal muscles which are "striated" in that they contain sarcomeres that are packed into highly regular arrangements of bundles.

The relaxation test (Figure 5) shows that there is a pronounced specimen relaxation at larger deformations. Due to viscoplasticity of the behaviour the relaxation cannot be observed during the relaxation phase.

5. CONCLUSION

The paper presents the procedure for testing of skeletal musculature tissue in order to obtain parameters of the advanced viscoelastic/viscoplastic Bergström-Boyce constitutive. The testing was performed on a porcine gluteus muscle as it is most similar to the musculature of the human hand. The specimens exhibited the viscoplastic behaviour during the testing due to large deformation which led to damage of the musculature molecular chains. It is further observed that the absorbed energy is very

high, which suggests that there is a significant damping of vibrations due to internal friction of the muscle protein chains.

The described procedure will be used in future research of vibration influence on human musculature and vibration suppression of hand held machinery to obtain parameters of Bergström–Boyce constitutive model at different strain levels and FEA simulations in noted research.

REFERENCES

- [1] ALI A., HOSSEINI M., SHARA B.B. (2010) *A review of constitutive models for rubber-like materials*, Am. J. Eng. Appl. Sci., Vol. 3, pp. 232-239
- [2] BEDA T. (2007) *Modeling hyperelastic behavior of rubber: a novel invariant-based and a review of constitutive models*, J. Polym. Sci., Part B: Polym. Phys., Vol. 45, pp. 1713-1732
- [3] BOL M., LEICHSENRING K., ERNST M., EHRET A. (2016) *Long-term mechanical behaviour of skeletal muscle tissue in semi-confined compression experiments*, Journal of the mechanical behavior of biomedical materials, Vol 63, pp 115-124.
- [4] MOERMAN M., CIARIAN S., NAGEL T. (2016) *Control of tension-compression asymmetry in Ogden hiperelasticity with application to soft tissue modelling*, Journal of the mechanical behavior of biomedical materials, Vol 56, pp 218-228
- [5] BAYLISS L.E., ROBERTSON G.W. (1939) *The visco-elastic properties of the lungs*, Q. J. Exp. Physiol., Vol 29, pp. 27-47.
- [6] HUANG C.Y., MOW V.C., ATESHIAN G.A. (2001) *The role of flow-independent viscoelasticity in the biphasic tensile and compressive responses of articular cartilage* J. Biomech. Eng., Vol 123, p. 410
- [7] HOLZAPFEL G.A. (2000) *Biomechanics of soft tissue* LEMAITRE J. (Ed.), *Handbook of Material Behavior, Nonlinear Models and Properties*, LMT-Cachan, France
- [8] BERGSTRÖM J.S., BOYCE M.C. (2001), *Constitutive modeling of the time-dependent and cyclic loading of elastomers and application to soft biological tissues*, Mech. Mater., Vol. 33, pp. 523-530
- [9] PARK S.W., SCHAPRZ R.A. (1999) *Methods of interconversion between linear viscoelastic material functions. Part I—A numerical method based on Prony series* Int. J. Solids Struct., Vol. 36, pp. 1653-1675
- [10] ANSSARI-BENAM A., BADER D.L., SCREEN H.R. (2011) *A combined experimental and modelling approach to aortic valve viscoelasticity in tensile deformation*, J. Mater. Sci.—Mater. Med., Vol. 22, pp. 253-262
- [11] PALCIO-TORRALBA J., HAMMER S., GOOD W.D., McNEILL S.A., STEWART D.G., REUBEN L.R., CHEN Y., (2015) *Quantitative diagnostics of soft tissue through viscoelastic characterization using time-based instrumented palpation*, Journal of the Mechanical Behavior of Biomedical Materials, Vol. 41, pp. 149-160.
- [12] COONEY M.G., MOERMAN M.K., TAKAZA M., WINTER C.D., SIMMS K.C. (2015) *Uniaxial and biaxial mechanical properties of porcine linea alba,*

Journal of the Mechanical Behavior of Biomedical Materials, Vol. 41, pp. 68-82

- [13] KAHLON A., HURTIG M.B., GORDON K.D. (2015) *Regional and depth variability of porcine meniscal mechanical properties through biaxial testing*, Journal of the Mechanical Behavior of Biomedical Materials, Vol. 41, pp. 108-114
- [14] BANIC M., STAMENKOVIC D., MILTENOVIC V., MILOSEVIC M., MILTENOVIC A., DJEKIC P., RACKOV M. (2012) *et al.: Prediction of Heat Generation in Rubber or Rubber-Metal Springs*, Thermal science, Vol. 16, Suppl. 2, pp. S527-S539
- [15] BERGSTROM JS. (1999) *Large strain time-dependent behavior of elastomeric materials* [Ph.D.]. Massachusetts, USA: Massachusetts Institute of Technology
- [16] BANIĆ M. (2015) *A methological approach to development of rubber-metal springs* [Ph.D.]. Niš, Serbia: University of Niš

CORRESPONDANCE



Branislav DIMITRIJEVIĆ, PhD student
University of Nis
Faculty of Mechanical Engineering
Aleksandra Medvedeva 14
18000 Nis, Republic of Serbia
b.dimitrijevicvr@gmail.com



Milan BANIĆ, Assis. Prof. Ph.D.
University of Niš
Faculty of Mechanical Engineering
Aleksandra Medvedeva 14
18000 Niš, Republic of Serbia
milanbanic@hottmail.com.rs



Žarko MIŠKOVIĆ, Ass. M.Sc. Eng.
University of Belgrade
Faculty of Mechanical Engineering
Kraljice Marije 16.
11120 Beograd, Serbia
zmiskovic@mas.bg.ac.rs



Radivoje MITROVIĆ, Prof. Ph.D.
University of Belgrade
Faculty of Mechanical Engineering
Kraljice Marije 16.
11120 Beograd, Serbia
rmitrovic@mas.bg.ac.rs



Aleksandar MILTENOVIC, Assis. Prof. Ph.D.
University of Niš
Faculty of Mechanical Engineering
Aleksandra Medvedeva 14
18000 Niš, Republic of Serbia
amiltenovic@yahoo.com



Miša TOMIĆ, PhD student
University of Niš
Faculty of Mechanical Engineering
Aleksandra Medvedeva 14
18000 Niš, Republic of Serbia
mishatomic@gmail.com

ADJUSTED DESIGN OF A COMPUTER MOUSE WITH ERGONOMIC REQUIREMENTS

Inga KREŠIĆ
Nebojša RAŠOVIĆ

Abstract: This paper presents the adjusted design of a computer mouse. Experimental measurements are performed by ZEBRIS measuring plate in order to obtain anthropometric sizes. These values have been used to get optimal information for creating appropriate mouse design. Prototype model has done in the software package SolidWorks. Finally, the case study has been conducted and the benefits of this research are presented.

Key words: surface modelling, CAD model of mouse, ergonomics features of mouse

1. INTRODUCTION

The main idea of this paper came from the results of the European Agency for Safety & Health at Work (EU-OSHA) [1]. 62% of injuries are caused by constant and recurring movements, of which 7,5% including typing and moving of a computer mouse. Using a computer mouse, 33% of people feel pain in the wrist. Also, 7% of people have problems with elbows [1]. It's the right, dominant arm. Some papers are based on experimental data of fatigue of using mouse and in-depth analysis was conducted on the bone and meridian of the arm using traditional mouse as well as the wrist force [2]. Some analyses show effects of forearm and palm supports on the upper extremity during PC mouse use [3]. This paper shows optimal hand position in order to get usable shape in the mouse design process. Experimental measurements have been conducted in order to get starting parameters in this analyse of a computer mouse design.

2. CARPAL TUNNEL SYNDROME

The consequence of recurring movements is Repetitive Strain Injury (RSI). It is also known as cumulative trauma disorders. The most common example of RSI is Carpal Tunnel Syndrome which has shown in Figure 1.

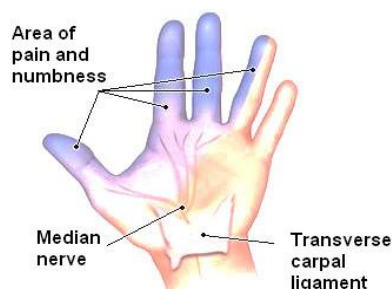


Fig.1: Carpal Tunnel Syndrome [4]

Carpal Tunnel Syndrome is a condition in which the median nerve is squeezed where it passes through the wrist. This often happens because the tendons in the wrist have become swollen and they press on the nerve. The median nerve controls some of the muscles that move the thumb and it carries information back to the brain about sensations in your thumb and fingers.

When the nerve is squeezed it can cause pain, tingling and numbness in the affected hand [5]. The primary task is to devise an ergonomically designed computer mouse for the general population.

3. EXPERIMENTAL MEASUREMENTS

At the Faculty of Mechanical Engineering and Computing, University of Mostar, in Biomechanical Testing Laboratory, there are equipment for measuring anthropometric sizes.

Two goals are defined:

1. To measure the force of the arm pressure on the main fit surface of mouse,
2. To get the optimum position of the hand at work.

The measuring equipment were a ZEBRIS measuring plate, a video camera Panasonic and a computer with a peripheral part (Figure 2).



Fig.2: Experimental measuring equipment

ZEBRIS Software was used on a computer. A Dynamic Test and FDM + Video configuration were selected for experimental measurement. The stress scale was adapted to the weight of the computer mouse (cca 5 N/m²). The user interface is divided into three parts. On the left side is a measuring plate. The move of the computer mouse will be displayed. On the right side is image that the camera shoots and the force diagram (Figure 3).

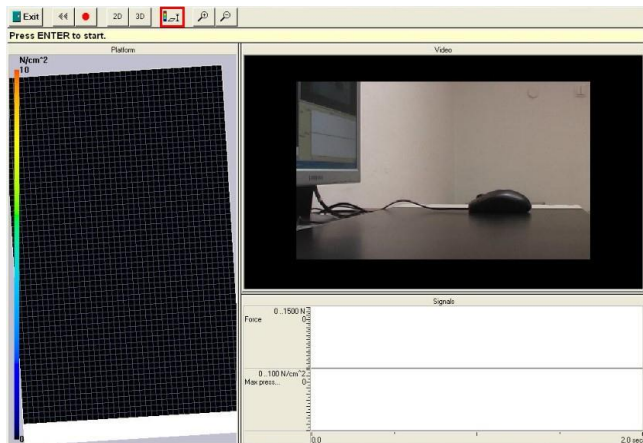


Fig.3: The user interface

3.1. Analysis of a standard computer mouse

Logitech RX 250 is taken for example of a standard computer mouse (Figure 4).



Fig.4: Logitech RX 250

The hand is placed on the computer mouse so that it touches the working surface. The parabola is given to describe the shape of the hand (Figure 5).

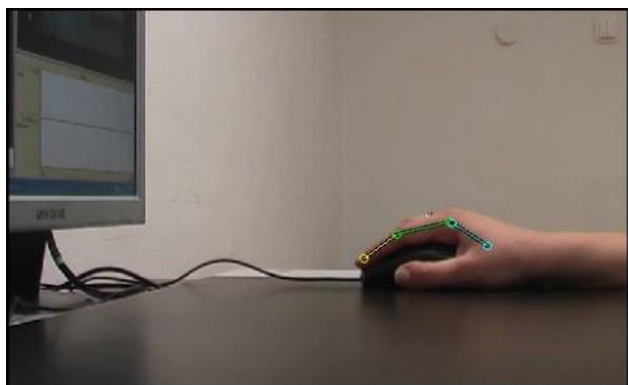


Fig.5: Parabola is obtained by experimental measurement

The goal of the diagram was to show the force of index finger press on the left key of the computer mouse. The force constant in the range from 1N to 5N is measured. The maximum value of the force is 6N (Figure 6).

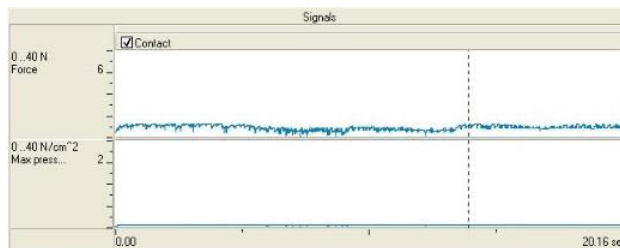


Fig.6: The layout of diagram is obtained by experimental measurement

3.2. Analysis of a standard computer mouse with an ergonomic wrist support

A wrist support helps keep the wrists in the proper positions during typing and can be used to support the wrists during intermittent rests. Keeping the wrists at the proper height is important since it keeps the wrists in a neutral position. Users can rest their wrists on the gel height instead of the hard work desk (Figure 7).



Fig.7: Ergonomic wrist support for a computer mouse

The user doesn't feel the load because everything is transmitted to a gel height. The parabola is sketched by placing a hand on a mouse with an ergonomic support (Figure 8).

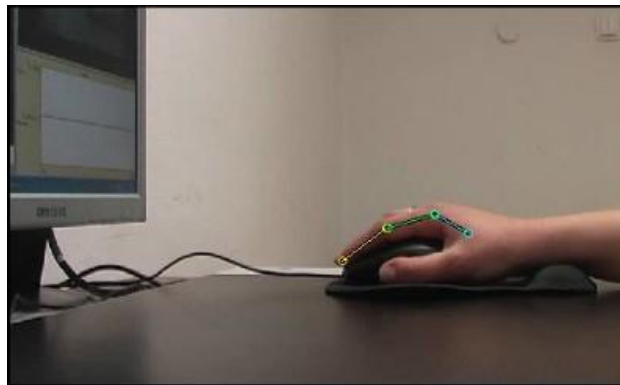


Fig.8: Parabola is obtained by experimental measurement with an ergonomic support

Using a computer mouse, the force constant in the range from 6N to 10N is measured. The maximum value of force is 11N (Figure 9).

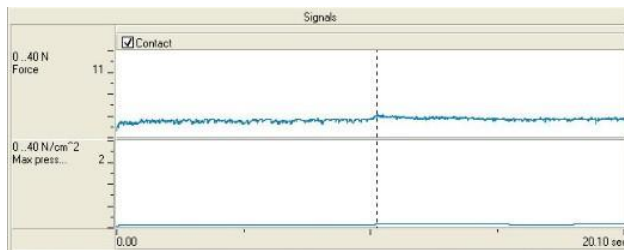


Fig.9: The layout of diagram is obtained by experimental measurement with an ergonomic support

3.3. Ergonomic analysis of a computer mouse

Ergonomic requirements in the workplace promote worker productivity, safety and health. Some of them are described in the following list [6-7]:

1. The work desk must be stable and the devices are at your fingertips. The minimum distance of the mouse from the edge of the table must be 150 mm.
2. On the same work desk there are a computer mouse and a keyboard. In front of the user is the keyboard and mouse is up to it.
3. The shape of a computer mouse must be adapted to the shape of a user's hand.
4. The squeeze of the mouse must be relaxed.
5. Arm and forearm should be parallel to the work desk. Hand wrists should be kept flat so that forearms, wrists and fingers create a straight line.
6. Keys must be adopted with user's fingers. The thumb must control the work of a computer mouse.

4. MODELING A COMPUTER MOUSE INCLUDING EXPERIMENTAL MEASUREMENTS AND ERGONOMIC ANALYSIS

The prototype model was made in the program of SolidWorks. In this chapter, it was used surface modelling techniques to create a model of a computer mouse.

Surface modelling is the part of advanced technology in program of SolidWorks. Using surfaces is a way to describe more complex part shapes. It is still widely used in CAD/CAM systems [8-10].

The basic difference in SolidWorks between solids and surfaces is that surfaces don't have volume. The surface model produces surfaces only with "zero" thickness.

Ergonomically designed computer mouse has shown in Figure 10. Some key stages in the modelling process of this part are given in the following list:

- Extruded Surfaces (to use a base curve or surface to make an open or closed shape),
- Boundary Surfaces (to create surfaces that can be tangent or curvature continuous in both directions),
- Knit Surfaces (to combine two or more faces and surfaces into one),

- Filled Surfaces (to use this feature to construct a surface to fill a gap in a model),
- Trim Surfaces (to use a surface, plane or sketch as a trim tool to trim intersecting surfaces).

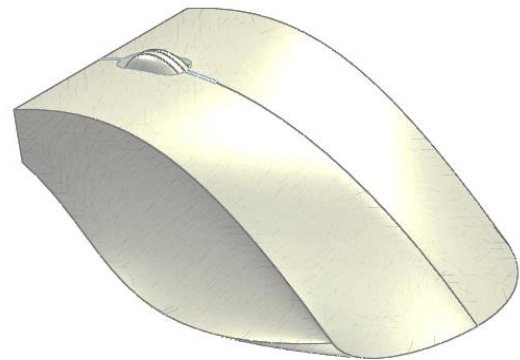


Fig.10: Ergonomically designed computer mouse

5. CASE STUDY

Case study has conducted to combine theory, experimental measurements and ergonomic analysis into modelling procedures of a computer mouse. In this chapter, surfaces of interest have been described.

There is a gap between the hand and the computer mouse that was made by an irregular design of a computer mouse. The starting point for modelling a new variant is a parabola. It is obtained by experimental measurement, which has shown in Figure 5.

Ergonomic request 5 is difficult to implement in practise. When the arm and forearm are parallel to the work desk, it looks like that the arm hangs in the air. The quick tiredness of the hand and the first pains are appeared. In Figure 8. the surface allows to lean the hands on the work desk. The pains will reduce and the hand will be in the correct position (Figure 11).

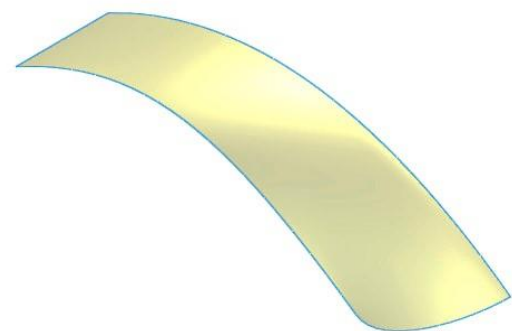


Fig.11: Surface for index finger position

Using a standard computer mouse, the index finger is fully loaded. The surface for the position of the thumb is created because it is stronger than the index finger.

Ergonomic request 6 is realized. User's thumb will move the cursor on the screen. Also, there will be a labelling button. It will be possible to move the mouse on the left or right side (Figure 12).

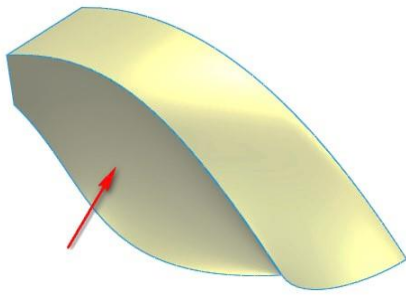


Fig.12: Surface for thumb position

Figure 13 shows the surface for the position of the small finger. Ergonomic request 3 is reason why all fingers must have own their positions. The texture of surface is important. The mouse shouldn't fall out of the user's hand.

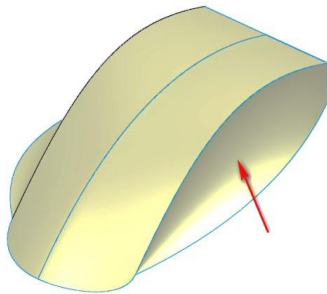


Fig.13: Surface for little finger position

The squeeze depends on design of computer mouse (ergonomic request 4). By combing ways, curved lines, position for palms, the pains are reduced. The lines are marked in Figure 14.

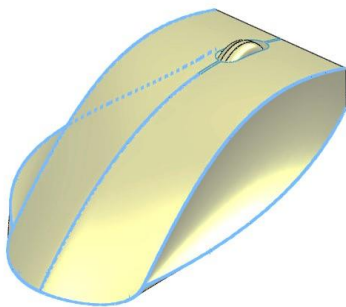


Fig.14: Curved lines have been used in a mouse modeling

There are also tips for use a computer mouse. Take a short but frequent breaks. If the arm is in the same position for too long or repeats the same movements, there will be fatigue and injury.

6. CONCLUSION

Making a variant solution of a computer mouse is a complex and demanding job. The product can't be realized all the requirements, wishes and regulations. In this paper, the computer mouse is created. It isn't the best, but the optimal variant solution. Analyses can be used for

a new variant of ergonomically designed computer mouse. They can help to make a computer mouse for people with protected hand. Then, it follows the production phase. The 3D printing process has been planned in the further research.

REFERENCES

- [1] BOGADI ŠARE, A., *Health Aspects of Working by a Computer*, Available from: <http://hzzsr.hr>
- [2] Sun H. (2016) *Research on Mouse Design Based on Ergonomics*. In: Long S., Dhillon B. (eds) *Man-Machine-Environment System Engineering. Lecture Notes in Electrical Engineering*, vol 406. Springer, Singapore
- [3] Onyebek, L.C., Young, J.G., Trudeau, M.B. & Dennerlein, J.T. (2014) *Effects of forearm and palm supports on the upper extremity during computer mouse use*. *Applied Ergonomics*. 45(3): p. 564-570.
- [4] *Healthcare media publishing company*, Available from: <http://www.medicinenet.com>
- [5] *The Chartered Society of Physiotherapy*, Available from: <http://www.csp.org.uk>
- [6] *Safety and Health Protection in Working by Computer*, Available from: <http://iusinfo.hr>
- [7] *Department of Applied Mathematics*, Available from: <http://web.zpr.fer.hr>
- [8] RAŠOVIĆ, N. & OBAD, M. (2013) *Layered Manufacturing Process Supported By Expert System*. *Machine Design*. 5(2): p. 93-98
- [9] CEKIC, A., RASOVIC N., OBAD M., KALJUN J., DOLSAK, B. & BEGIC-HAJDAREVIC, D. (2015) *Production of optimized layered products using intelligent support*. *Proceedings of the 26th International DAAAM Symposium*, 271-279. DOI: 10.2507/26th.daaam.proceedings.037
- [10] RAŠOVIĆ N. & OBAD, M. (2012) *Adaptive slicing in 3D printing process*. *Proceedings of The 7th International Symposium on Machine And Industrial Design in Mechanical Engineering KOD 2012*, Faculty of Technical Sciences, Novi Sad, p. 243-246

CORRESPONDANCE



Inga KREŠIĆ, M.Sc. Eng.
University of Mostar
Faculty of Mechanical Engineering and Computing
Matice hrvatske bb
88000 Mostar, BiH
inga.kresic@student.fsr.ba



Nebojša RAŠOVIĆ, Assistant Professor
University of Mostar
Faculty of Mechanical Engineering and Computing
Matice hrvatske bb
88000 Mostar, BiH
nebojsa.rasovic@sve-mo.ba

EFFECTS OF OUTLET NOZZLE SLOPE ANGLE ON ACCURACY OF MACHINE PARTS' GEOMETRICAL CONTROL

Dragiša SKOKO
Mileta RISTIVOJEVIĆ
Cvetko CRNOJEVIĆ

Abstract: All to date studies of pneumatic metrology have been carried out under so-called normal operating conditions when there is no inclination of outlet nozzle, i.e. when the outlet nozzle axis of symmetry is normal to the measuring part flat face. Under normal conditions, compressible fluid flow in a jet impinging on a baffle is symmetric, whereas in the case of leaned jet the flow is asymmetric and considerably more complex. Studies of effects of outlet nozzle inclination, i.e. oblique jet shock, relative to a measuring part represent a new effect in studying pneumatic comparators' operation, having only research significance for the time being. In this paper, the effects of outlet nozzle slope angle and supply pressure on the radial pressure field on the measuring part flat face were experimentally analyzed for measuring branch nozzle and outlet nozzle specified diameters. Based on results obtained, it has been shown that with the increase of outlet nozzle slope angle the intensity of radial pressure on a measuring part decreases, while radial pressure field becomes less symmetric. Also, it has been shown that the subpressure value and zone on the measuring part flat face depend on the size of the outlet nozzle slope angle.

Key words: pneumatic metrology, outlet nozzle, slope angle, radial pressure field

1. INTRODUCTION

In the era of increasing automation and robotization of production processes, control of geometrical accuracy of machine parts, subassemblies and assemblies by applying pneumatic metrology gains in prominence in mechanical engineering, ref. [1]. There are growing requirements for safe and reliable operation of contemporary constructions. Accordingly, the requirements for geometrical accuracy control of constructions' components are becoming stricter. To increase the accuracy and reliability level of pneumatic metrology in control of machine parts, it is necessary to gain as detailed insight as possible into the effects, geometrical and flow, on pneumatic control accuracy, ref. [2], [3] and [4]. To this end, the paper considered the effects of outlet nozzle inclination on the accuracy degree of pneumatic control of machine parts' geometrical parameters, ref. [5]. In [5] a key dependence $\rho(\delta)$ is also given for different supply pressures, used as a basis for definition of pneumatic sensitivity. Under real conditions of control, the outlet nozzle inclination may occur due to a likely error in the measuring head assembly, its wear due to long-term use, or great deviations of surface controlled for flatness. Under normal conditions of control, when there is no outlet nozzle inclination, compressible fluid jet impingement on a machine part flat face is symmetric. In outlet nozzle inclination, air flow becomes asymmetric and considerably more complex.

All to date studies of compressible flow jet impinging on an inclined solid face have not been for pneumatic metrology needs but for other applications, as reported in ref. [6]: multi-stage rocket separation, deep-space docking, jet-engine exhaust impingement, gas-turbine blade failure, terrestrial rocket launch, etc. Studying the effects of the outlet nozzle inclination, i.e. the oblique jet shock, relative to a measuring part represents a new effect in studying the pneumatic comparator operation. Apart from research significance, the oblique outlet jet may be used for creating new geometric shapes of measuring outlet head. In this paper, the effect of outlet nozzle slope angle and supply pressure on the radial pressure field, i.e. position and size of the vortex zone was experimentally studied for measuring branch nozzle and outlet nozzle specified diameters, ref. [3]. Fluid pressure measurements were performed when outlet nozzle deviates from normal position by: 1° consecutively to 7° , for supply pressure values $p_0 = 2, 3$ and 4 bar and throttling nozzle diameter $D = 1.0$ mm.

2. EXPERIMENTAL SETUP

Determination of $p(r, \alpha)$ and $p(\delta, \alpha)$ pressure fields on the measuring part flat face in the radial and axial direction is performed using the installation shown in Fig. 1. It consists of a pneumatic comparator PC that contains a measuring branch BM and reference branch BR, pressure air source AL and the system for fine horizontal (DH) and vertical (DV) displacement of a flat measuring

machine part. In the measuring branch there is a nozzle M1 of diameter D in the throat of which a critical flow at a Mach number $M=1$ is realized. In this paper, nozzle M1 diameter is $D=1\text{mm}$, outlet nozzle M2 inner diameter $D=2\text{mm}$ and outer diameter is 4mm , supply pressure $p_0=2, 3$ and 4 bar. All pressure measurements were done using manometers with accuracy of 0.001bar . The nozzle

M2 slope angle was varied in the range of $\alpha=0\div 7^\circ$, pitch 1° . By inclining the outlet nozzle M2, relative to the vertical axis, by angle α , the region of the flow between the nozzle and the measuring part is divided into convergent part – side A ($r < 0 \mu\text{m}$) and divergent part – side B ($r \geq 0 \mu\text{m}$).

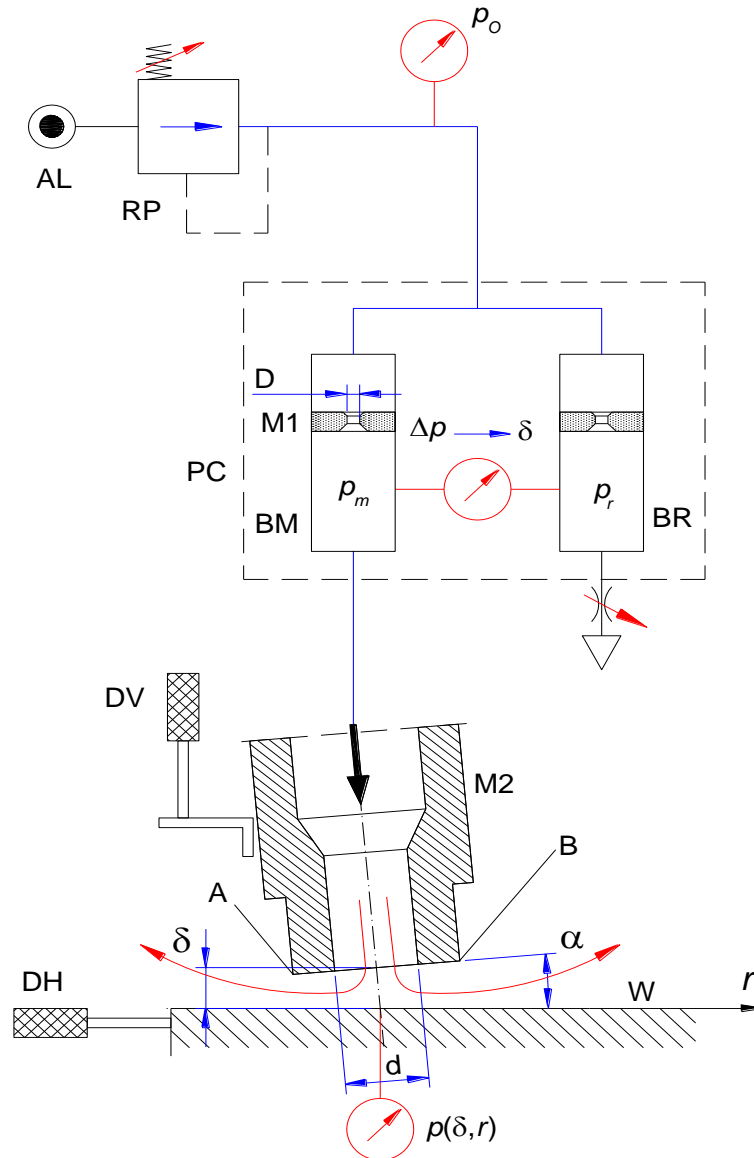


Fig.1: Experimental setup

3. EFFECT OF OUTLET NOZZLE INCLINATION ON RADIAL PRESSURE FIELD

Effect of outlet nozzle inclination on radial pressure field was analyzed for different values of supply pressure p_0 and slope angles $\alpha=0\div 7^\circ$. First, considerations included radial pressure field $p(r, \alpha)$ at compressed air supply pressure $p_0=2\text{bar}$ and axial distance of the outlet nozzle tip from the measuring part face $\delta=250\mu\text{m}$ at different nozzle slope angles α . The region of nozzle radial

displacement is $-3000 \leq r \leq 3000\mu\text{m}$. This measuring region is chosen so that it involves the expected effects. Effect of nozzle slope angle and displacement in radial direction towards the radial pressure field $p(r, \alpha)$ is shown in diagrams in Fig. 2. Radial pressure referenced curve $p(r, 0^\circ)$ is symmetric relative to the nozzle axis and it represents radial pressure referenced field $p(r, \alpha)=p(r, 0^\circ)$, a benchmark for the analysis of obtained diagrams. It has been shown by the curves in Fig. 2 that compared to referenced pressure field the radial pressure significantly changes with nozzle slope angle α increment in such way that the pressure drops in the environment of the air jet

axis with the nozzle slope angle increment. Simultaneously, as the nozzle slope angle α increases the curve becomes more asymmetric in distant zone parts of sides A and B. On the nozzle M2 side B, the subpressure zone is retained at all slope angles, Fig. 2, which may cause potential deposition of dirt during the geometrical accuracy control of machine parts. On the nozzle M2 side A, curve asymmetricity increases with respect to

referenced curve, while subpressure zone decreases, and at a certain nozzle inclination subpressure is converted into superpressure, Fig. 2.

The basic parameters of radial pressure field, pressure limit values – maximum and minimum, and radial direction distances characteristic of pressure change, are shown in Fig. 3. All parameters for side A of diagrams in Figs 2 and 4 are designated as (·) prim.

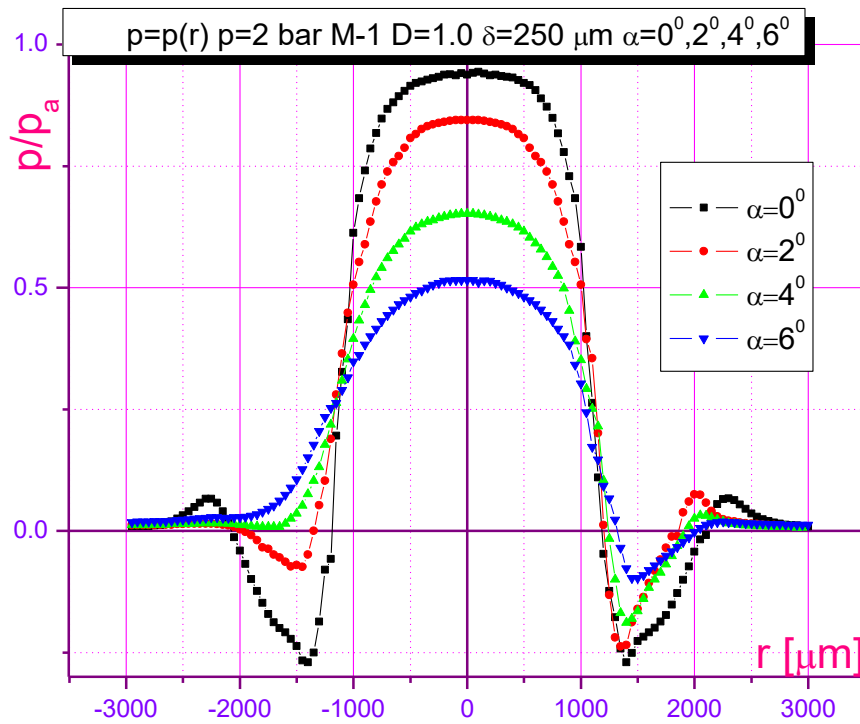


Fig.2: Radial pressure field $p(r, \alpha)$ at supply pressure $p_0=2\text{bar}$ and for angles $\alpha=0^\circ, 2^\circ, 4^\circ$ and 6°

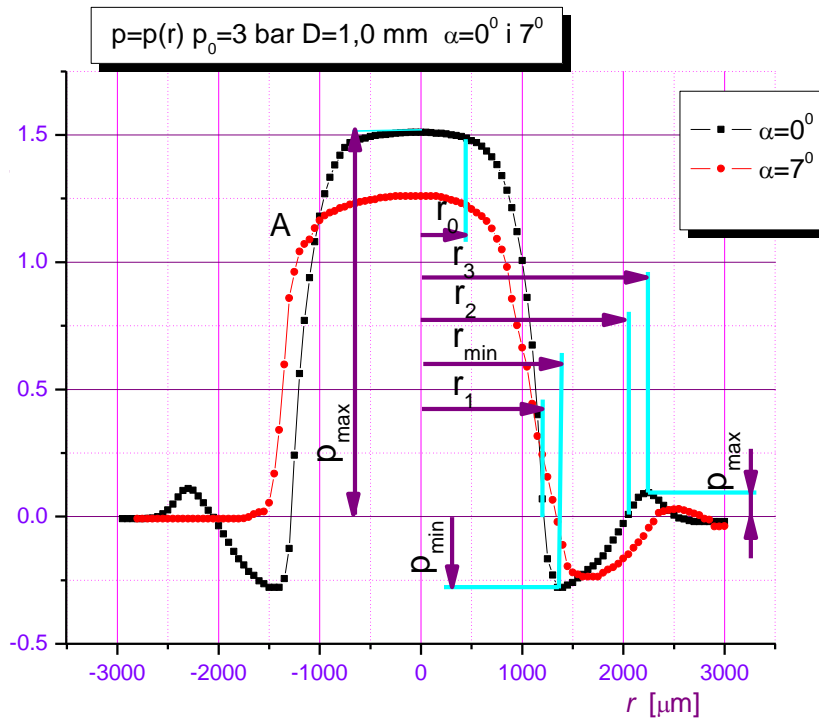


Fig.3: Basic parameters of radial pressure field

3.1 Analysis of radial pressure field on the outlet nozzle side A

Experimental values of basic parameters of the radial pressure field, on side A of the outlet nozzle, are given in Tab. 1. Referenced radial pressure field $p(r, \alpha) = p(0, 0)$ has max value $p_{\max} = 0.944 \text{ bar}$, and as the nozzle slope angle α increases the pressure drops to the value of $p = 0.483 \text{ bar}$ for $\alpha = 7^\circ$. With respect to the referenced curve $\alpha = 0^\circ$, max relative pressure decreased by 95%, while min, i.e. subpressure, by 3.5 times.

On the nozzle side A the pressure has constant max value with the increase of outlet nozzle tip radial distance to the value of r'_0 . This distance of the diagram straight-line segment decreases as the outlet nozzle slope angle increases, Fig. 2 and Tab. 1. Max pressure values are identical on both diagram sides, i.e. $p'_0 = p_0$. Also, the curve for $\alpha = 0^\circ$ is completely symmetric relative to the referenced axis, Tab.1. As radial distance further increases, relative pressure on the measuring part flat face abruptly decreases, reaching negative values in one segment. Radial distance from the axis of nozzle referenced position, when relative pressure becomes negative, is denoted with r'_1 , i.e. with the point on curve $p(r', 0)$. This distance is the lowest for $\alpha = 0^\circ$ and amounts to $r'_1 = -1189 \mu\text{m}$, i.e. for the nozzle referenced position. As the nozzle slope angle increases the distance $r'_1(\alpha)$ increases too as follows: for slopes $r'_1(1^\circ) = 1234 \mu\text{m}$, $r'_1(2^\circ) = 1349 \mu\text{m}$ and $r'_1(3^\circ) = 1496 \mu\text{m}$. For outlet nozzle slope angles $\alpha = 4^\circ$, $\alpha = 5^\circ$, $\alpha = 6^\circ$ and $\alpha = 7^\circ$ the pressure in radial direction, on the measuring part face, is positive.

Table 1: Parameters of radial pressure field for $p = 2 \text{ bar}$ side A

α°	μm					bar	
	r'_0	r'_1	r'_2	r'_{\min}	Δr	$p(0,0)$	p_{\min}
0	288	-1189	-2078	-1400	889	0.944	-0.269
1	255	-1234	-1978	-1456	744	0.898	-0.265
2	239	-1349	-2005	-1504	656	0.841	-0.076
3	223	-1496	-1854	-1651	358	0.748	-0.001
4	206					0.652	
5	190					0.583	
6	174					0.518	
7	156					0.483	

The referenced curve has the highest subpressure or min absolute pressure r'_{\min} . For $\alpha = 0^\circ$ $p_{\min} = -0,269$ at $r_{\min} = -1400 \mu\text{m}$. The value of subpressure drops with the outlet nozzle slope angle increment, Tab. 1. For supply pressure $p_0 = 2 \text{ bar}$ the values of subpressure $\alpha = 0^\circ, 1^\circ, 2^\circ$ are relatively high. In the regions of high subpressure values on the nozzle wall above a flat wall, the vortex zones may be formed, undesirable in pneumatic metrology, because they reduce accuracy and reliability level of geometrical quantities' control in machine parts. As the outlet nozzle slope angle increases $\alpha > 3^\circ$ subpressure disappears. Subpressure on the measuring part face decreases with increase of radial distance and at some distance r'_2 it equals zero, i.e. $p = 0 \text{ bar}$, Fig.3. From the diagram in Fig.

2 it is evident that radial distance r'_2 is the longest for the nozzle referenced position $r'_1(0^\circ) = -2078 \mu\text{m}$. The outlet nozzle slope angle increment causes changes in distance values r'_2 , Tab. 1.

Apart from subpressure intensity, pneumatic control accuracy and reliability is also affected by the subpressure zone size, i.e. length of distance $\Delta r = r_2 - r_1$, Tab. 1. As the outlet nozzle slope angle increased, the subpressure zone decreased, and for slope angles $\alpha = 4^\circ, 5^\circ, 6^\circ$ and 7° it is $\Delta r = 0$, the subpressure zone disappears. This measurement result is in complete agreement with well-known conclusion from gas dynamics that pressure drops at subsonic compressible gas flow due to acceleration of a flow (side A in Figs 1 and 2). Obtained results lead to the conclusion that in pneumatic control of machine parts under conditions of increased dirt concentration, nozzle optimum slope angle should be defined, in accordance with supply pressure that would not generate subpressure and vortex zones on the measuring part face

As radial distance increases the pressure increases, and at radial distance r'_3 it reaches the highest local value. Further increase of radial distance $r \geq -2500 \mu\text{m}$ approximates asymptotically the pressure curve to the line $p = 0 \text{ bar}$. In the radial distance region $-2500 \leq r \leq -1500 \mu\text{m}$ the highest pressure is for the nozzle referenced position, however with the nozzle slope angle increase its value is increased. The outlet nozzle tip radial distance position in the region $-1500 \leq r < -2500 \mu\text{m}$ is denoted with r'_3 , when local pressure is the highest.

Based on obtained experimental results it can be concluded that on the outlet nozzle side A subpressure is generated at small outlet nozzle slope angles $\alpha = 0^\circ, 1^\circ, 2^\circ$ and 3° and that at larger slope angles it disappears and is converted into superpressure. This means that at higher values of outlet nozzle slope angle potential deposition of dirt at the nozzle tip is prevented, which results in increased geometrical control accuracy of machine parts by pneumatic procedure.

3.2 Analysis of radial pressure field on the outlet nozzle side B

On side B of inclined nozzle, in the diagram segment $p(r_0, p_0)$, with increase of radial distance to the value of r_0 , i.e. on the measuring part in the environment of the jet air axis, the pressure has constant value, Fig. 3. This distance of the diagram straight-line segment is decreased with increase of the nozzle slope angle. The largest distance is for the curve referenced position $r_0 = 288 \mu\text{m}$. As the nozzle slope angle increases the straight-line segment zone is decreased Fig. 3 and Tab. 2.

With increase of radial distance, relative pressure on the measuring part face declines rapidly, and in one segment it becomes negative, Fig. 3. The distance from the nozzle referenced position axis to the radial distance, when the pressure becomes negative $p(r_1, p)$, is denoted with r_1 . For the nozzle referenced position $\alpha = 0^\circ$ the distance is $r_1 = 1188 \mu\text{m}$. The distance r_1 increases with the nozzle slope angle increase, Fig. 3, Tab.2. The highest subpressure or min pressure $p(r_{\min}, p_{\min})$ is in referenced curve. As the nozzle slope angle increases min pressure decreases, Fig. 3, Tab.2. For supply pressure $p_0 = 2 \text{ bar}$, these values of subpressure are relatively high,

undesirable in pneumatic metrology, due to the occurrence of vortex zones.

As radial distance increases, subpressure decreases and in some segment of the curve $p(r_2,0)$, at distance r_2 , it is $p=0$ bar. From the diagram in Fig. 3 it is noticeable that distance r_2 is the longest for the nozzle referenced position. Distance r_2 increases with increase of the nozzle slope angle.

Table 2: Parameters of radial pressure field for $p = 2$ bar side B

α^0	μm					bar	
	r_0	r_1	r_2	r_{min}	Δr	ρ	ρ_{min}
0	288	1188	2112	1403	924	0.944	-0.269
1	255	1193	1864	1347	671	0.898	-0.256
2	239	1208	1869	1355	661	0.841	-0.239
3	223	1236	1936	1403	700	0.748	-0.221
4	206	1239	1932	1399	693	0.652	-0.188
5	190	1263	1981	1419	718	0.583	-0.133
6	174	1315	2024	1482	709	0.518	-0.099
7	156	1343	1989	1495	646	0.483	-0.075

The subpressure region on a measuring part is defined by distance $\Delta r=r_2-r_1$. From the aspect of pneumatic metrology this region is undesirable and should have as low value as possible. In the referenced curve this region is the largest and with increase of the outlet nozzle slope angle the size of the subpressure-region is decreased, Fig.3, Tab.2.

Further increase of radial distance causes pressure rise and it reaches the highest local value at distance r_3 . In radial distances $r \geq 2500 \mu\text{m}$ the relative pressure curve

decreases and approximates asymptotically the line $p=0$ bar. In the radial distance segment $1500 \leq r \leq 2500 \mu\text{m}$ the pressure is the highest for the nozzle referenced position, while with nozzle slope angle increment it declines.

Obtained results lead to the conclusion that on the nozzle side B subpressure is generated at all values of the nozzle slope angle on the measuring part face. Furthermore, the subpressure value is smaller than subpressure that corresponds to the nozzle referenced position. Also, it can be stated that as the nozzle slope angle increases the value of subpressure decreases.

4. EFFECT OF SUPPLY PRESSURE ON RADIAL PRESSURE FIELD

In order to provide better understanding of supply pressure effect on radial pressure field on a measuring part face, experimental studies were carried out at supply pressure of $p_0=2, 3$ and 4 bar. Results are presented by diagrams in Figs 2, 3 and 4.

Obtained results lead to the conclusion that with pressure supply increase p_0 the intensity of max pressure is increased on the measuring part face and simultaneously the zone of its action is reduced. Also, on the nozzle side A subpressure disappears only at the nozzle slope of 6° . On the nozzle side B with supply pressure increase the value of subpressure is significantly increased. In general, it can be concluded that with increase of supply pressure p_0 , the conditions of machine parts' geometrical control deteriorate due to dirt deposition on the outlet nozzle tip. This negative effect can be alleviated by more frequent cleaning of the nozzle tip.

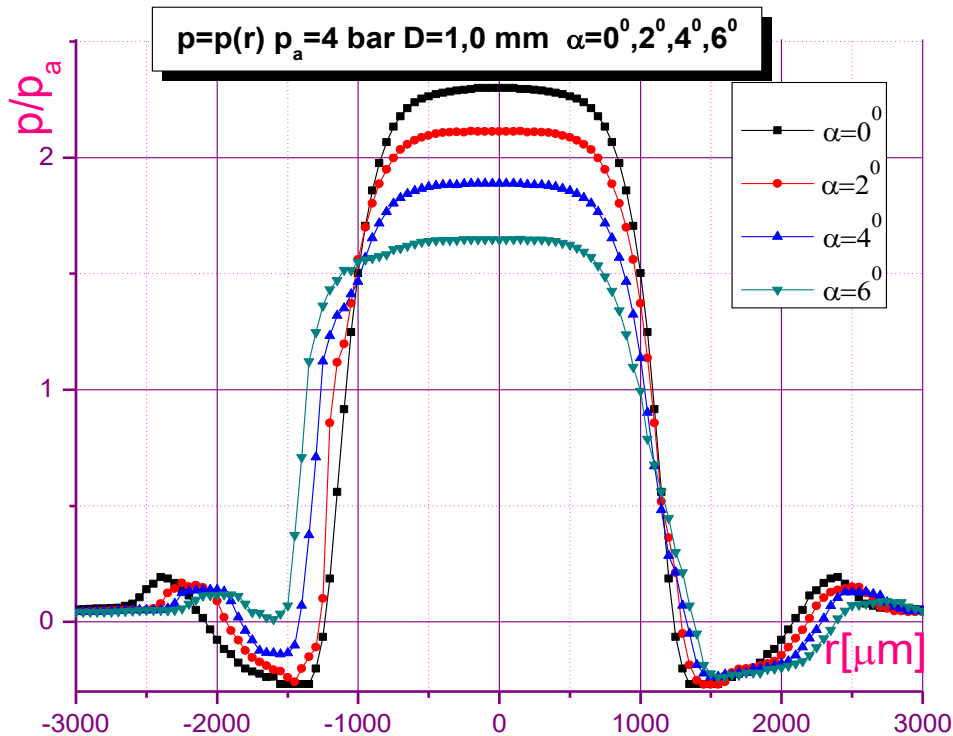


Fig.4: Radial pressure field $p(r, \alpha)$ at supply pressure $p_0=4\text{bar}$ and for angles $\alpha=0^\circ, 2^\circ, 4^\circ$ and 6°

5. CONCLUSION

Based on carried out experimental studies, it has been shown that the choice of outlet nozzle slope angle and supply pressure can significantly affect pneumatic control accuracy and reliability of machine parts' geometrical quantities, primarily by using the outlet nozzle side A. On the nozzle side A, at supply pressure of 2 bar, with increase of the outlet nozzle slope angle the intensity of subpressure is decreased, while at the slope angle greater than 3° subpressure is converted into superpressure. Subpressure disappearance eliminates conditions for dirt deposition on the outlet nozzle tip, resulting in the increase of accuracy and reliability of machine parts' geometrical control. Compared to side A, on side B subpressure and vortex zone are generated on the measuring part face. Furthermore, both subpressure and vortex zone are smaller relative to the referenced curve. The intensity of subpressure increases on both side A and side B with the increase of supply pressure. Due to this fact, the accuracy of machine parts' geometrical control is reduced. More frequent accuracy control of differential pneumatic comparator and more frequent cleaning of the outlet nozzle tip may significantly affect the level of geometrical control accuracy and reliability by applying pneumatic metrology. Apart from research significance, the oblique outlet jet can be also used for manufacturing new geometrical shapes of the measuring head outlet nozzle

6. REFERENCES

- [1] <http://www.etamic.com>.
- [2] CRNOJEVIC C., ROY G., BETTAHAR A. AND FLORENT P.: Influence of regulator diameter and injection nozzle geometry on flow structure in pneumatic dimensional control systems. Transactions of ASME, Journal of Fluids Engineering, Vol. 119. (1997), pp. 609-615
- [3] ROY G., CRNOJEVIC C., BETTAHAR A., FLORENT. P. AND VO-NGOC D.: "Influence of nozzle geometry in pneumatic metrology applications." International Conference on Fluid and Thermal Energy Conversion, Proc. Vol. 1, pp.363-368, Bali, Indonesia, (1994)
- [4] SKOKO D., (2007), Investigation of the effects of flow fluid to control the accuracy of machine parts. Master thesis, Faculty of Mechanical Engineering, University of Belgrade.
- [5] SKOKO D., CRNOJEVIĆ C., RISTIVOJEVIĆ M., Inclination effects of outlet nozzle on sensitivitz of pneumatic comparator. 29th Int. Conference DANUBIA-ADRIA, BELGRADE 2012, Serbia, , Proceedings pp. 222 – 225, Septembar 26 – 29. 2012
- [6] LAMONT P., HUNT B.: The impingement of underexpanded, axisymmetric jets on perpendicular and inclined flat plates. J. Fluid Mech. (1980), vol. 100, part 3, pp.471-511
- [7] SKOKO D., CRNOJEVIĆ C., RISTIVOJEVIĆ M., Influence of supply pressure and geometry of meassurin branch's nozzle on the work of differential pneumatic controller. 4th Int. Conference on Manufacturing Eng., October 2011, Thessaloniki, Greece, Proceedings pp. 423-430

CORRESPONDANCE



Dragiša SKOKO, . M.Sc. Eng.
University of Belgrade
Mechanical Engineering Faculty
Kraljice Marije 16.
11120 Beograd, Serbia
dskoko@mas.bg.ac.rs



Mileta RISTIVOJEVIĆ, Prof. D.Sc. Eng.
University of Belgrade
Mechanical Engineering Faculty
Kraljice Marije 16.
11120 Beograd, Serbia
mristivojevic@mas.bg.ac.rs



Cvetko CRNOJEVIĆ, Prof. D.Sc. Eng.
University of Belgrade
Mechanical Engineering Faculty
Kraljice Marije 16.
11120 Beograd, Serbia
ccrnojevic@mas.bg.ac.rs

CONCEPT SOLUTION OF THE SAFETY SYSTEM FOR AVOIDING WRONG FUEL USING IN CARS AND PREVENTION OF DAMAGE

Milan TICA
Milan RACKOV
Djordje MILTENOVIC
Aleksandar MILTENOVIC
Milan BANIC

Abstract: *The occurrence of wrong refuelling in cars is very common. Car manufacturers offer a very large number of technological innovations in cars, but they still have not dealt enough with this case sufficiently. Manufacturers have still not found an adequate solution to prevent misfuelling, nor have they found a solution to prevent damage. The paper presents the analysis of the frequency of occurrence of incorrect refuelling and risk of ignition of the vehicle. We analyzed the specific case and given some of the conceptual solutions.*

Key words: *safety, car, conceptual solutions*

1. INTRODUCTION

Every fifth Englishman at least once poured the wrong fuel in his car. There are about two hundred thousand cases of pouring the wrong fuel per year in England and Germany. The pouring of wrong fuel occurs even though the cap of the reservoir is in most cars written with warning of the type of used fuel (Figure 1).

Pouring the gasoline (petrol) into the tank of diesel vehicles is more often. Pipe diameter of machines for pouring gasoline is smaller than the pipe diameter of machines for pouring diesel fuel, and the hole diameter of the gasoline tank is usually smaller than the pipe diameter of machines for pouring diesel. This prevented the putting pipes of machines for pouring diesel fuel into the opening of the gasoline tank.

Vehicle manufacturers pay great attention and develop a variety of sophisticated car models with many different functions. Great attention is paid to the safety of passengers in the car. Different security systems are developed which should prevent driver error occurring, as well as systems which should prevent harmful event if this driver error occurs. Therefore, there are numerous safety systems in the vehicle, starting from the simplest until the intelligent safety system. For example, the system Attention assist can recognize and warn the driver about tiredness and force him to rest. Then, cruise control with the function of maintaining a space. There is a warning system about the vehicles in the blind spot of mirrors and warning of sudden lane change that will alert the driver with the subtle, but perceptible vibration of the steering wheel. For even better security, there is an additional safety element, which in the case that car assesses the accident is unavoidable, it takes over the control of braking, seat belts are automatically tightened and puts the seats in the proper position during emergency braking. Developing these systems, designers of some vehicle manufacturers have neglected the development of systems to prevent incorrect refueling, as well as systems



Fig.1: Display of inscription on the cap of the fuel tank

that prevent damaging consequences if to the wrong refueling occurs.

This paper presents several concept solutions for a system that will prevent wrong refuelling, as well as a system that will prevent harmful consequences if the wrong fuelling still occurs.

2. POSSIBLE CONSEQUENCES

The reverse is possible, so setting the pipe of machines for pouring petrol into the opening of diesel vehicles tank can occur. If incorrect pouring of gasoline into diesel vehicle is happened, damage of the assemblies' parts for injecting and operating assemblies of engine can occur (eg . filters, injectors, etc ...). This is so-called "driving damage". Beside to the material damage, in a very small number of cases this can lead to ignition of the vehicle. In this paper a real case of ignition of the vehicle is analyzed.

The principle of operation of diesel engines is shown in Figure 2. Each movement of the piston in the cylinder from one end point to another is called a stroke. In four-stroke diesel engine piston moves down in the cylinder in the first stroke, and fresh air enters through the open suction valve. In the second stroke the suction valve closes, the piston moves up and compresses the air above it, so the temperature of air is increased. At the end of the second stroke fuel is injected through the holes on top of the cylinder. Since the air is hot due to compression, fuel explodes and pushes the piston down. It is the third stroke and is called working stroke. In the fourth stroke the piston again moves upwards and forces the gases out through the exhaust valve at the top of the cylinder. The exhaust valve closes when the piston reaches the top of the cylinder and the first stroke starts again. The revolution speed of the engine is regulated by the fuel volume injected into the air in the cylinder.

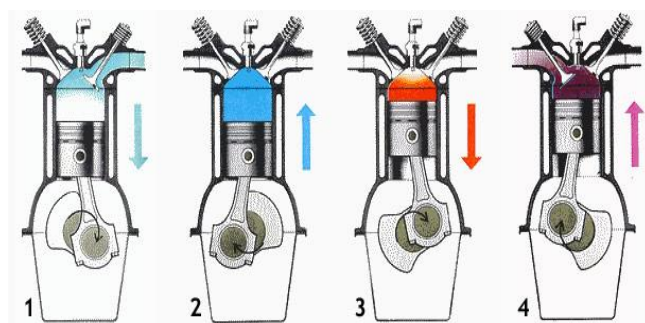


Fig.2: Schematic view of diesel engine strokes

The main difference between diesel and gasoline engines is in the way of ignition of fuel and air (Table 1, Table 2). In a gasoline engine spark that occurs at the spark plug burns the mixture, while in diesel engine air in the cylinder is heated to a temperature higher than 500°C due to compression. When the fuel is injected into the air, it is selfignited due to a high temperature with no spark. Diesel engines can have built heaters that help fuel is injected when the engine is started cold.

If it is considered only theoretically, it is impossible that vehicle ignition occurs due to pouring the wrong fuel.

The following case shows that it happened, and therefore it is possible. In this case, beside a damage caused to the vehicle, the safety of passengers was directly threatened.

Table 1. Four-stroke petrol engines:

Stroke	Piston moving	Petrol engine
1. suction	downward	Suction valve is opened, the mixture of air and fuel enters the cylinder
2. compression	upward	Both valves are closed, the piston forces and compresses the mixture
3. stroke	downward	Both valves are closed, a spark plug ignites compressed mixture, the pressure and temperature are increased, the piston is pushed down
4. stroke	upward	The exhaust valve is opened, burned mixture comes out of the cylinder

Table 2. Four-stroke diesel engines:

Stroke	Piston moving	Diesel engine
1. suction	downward	Suction valve is opened, only air enters the cylinder
2. compression	upward	Both valves are closed, the air is compressed to a very high pressure, the air temperature is increased, the fuel is injected
3. stroke	downward	Both valves are closed, it comes to selfignition, the pressure and temperature are increased, the piston is pushed down
4. stroke	upward	The exhaust valve is opened, burned mixture comes out of the cylinder

3. CASE STUDY OF VEHICLE INFLAMMATION DUE TO POURING OF WRONG FUEL

Damaging accident

Damaging accident happened when EUROSUPER was poured in a car reservoir instead EURODIESEL. After 7 km of driving the inflammation of the vehicle was happened. The police statement from the point of accident claims the center of the fire front was located in right part of the underside of the car, where the particles catcher ("particle filter") is located. The fire had already caught outside of the car reservoir and only thanking to the quick intervention and timely fire extinguishing, the worst was avoided. The vehicle was from a high-class and from a well-known automobile manufacturer, age less than one year. Damaging accident happened within the warranty period.

Price of a new vehicle was approximately 65,000.00 EUR. Photos of vehicle parts are shown in Figures 3, 4 and 5.

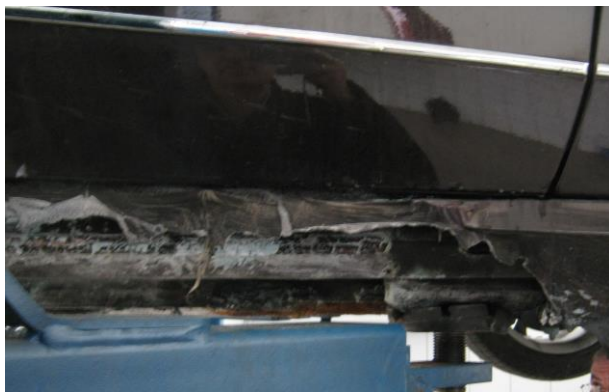
After disassembling the parts around the place where the fire occurred, it has been found that all sensors are burnt. Figure 5 shows dismantled exhaust manifold with individual parts that are burnt.



Fig.3: Showing the inside of the vehicle affected by fire



a) rear lower part of the vehicle



b) vehicle threshold



c) front lower part of the vehicle - a place where fire occurred, "fire center"

Fig.4: Photos of underside of the car with the marked fire center



a) exhaust manifold



b) catalytic converter



c) exhaust pipe



d) particles catcher („dieselpartikelfilter“)

Fig.5: Photos of exhaust manifold with particular details

During the vehicle inspection it was found out the engine is a V-engine with "common rail" supply system (Figure 6). Characteristic of this system is much higher supply pressure than previously used systems (for example: the system pump-injector). Supply pressure in these systems is up to 1850 bar. Complete process control of engine operation is performed by central processing unit (CPU) and electric control unit (ECU). These units perform complete control and management of the working process starting from the supply of engine until the control exhaust system. Large number of sensors and encoders send the basic information about the process parameters on the basis of which ECU is managed. During the inspection of the exhaust system it was found out that the exhaust system was with catalytic converter and particles catcher ("Dieselpartikelfilter") and also with temperature sensors of exhaust gases and lambda probe. In every moment those sensors send data to ECU about measured values.

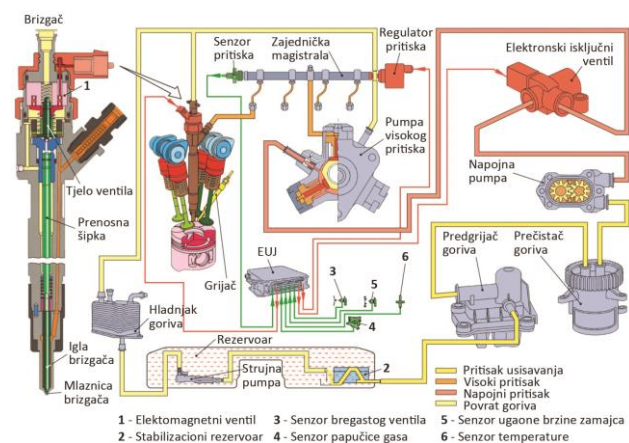


Figure 6. Common rail system of supplying diesel engine by fuel

The scenario of the process from the moment of pouring the wrong fuel to the fire occurring in vehicle

Based on the analysis of the sample extracted from the fuel reservoir, it can be concluded that after pouring petrol into the reservoir of diesel vehicle, the formed mixture was with a majority part of petrol. In that moment a clean diesel was in the piping and wiring between the tank and the engine. When starting the engine, it was normally started since in the fuel pipeline there was a clean diesel. In the case that petrol was in the fuel system, the engine could not get start. While driving and during engine operation, the mixture from reservoir with the prevailing petrol came in the power system. It is known that gasoline has more explosive power than diesel but it needed a spark to ignite the mixture as described above. Theoretically after finishing the fourth stroke (when exhaust is completed and there is no combustion), when the petrol enters in the cylinder, the engine should be shut down because there is no spark to ignite in third stroke. Thus, in the case of pouring gasoline instead of diesel, theoretically in most cases, the engine should be stopped with a small chance that fire occurs. In this case, it may cause damage to the engine parts.

Since it is evident that the engine is not shut down in this case, it is possible that the combustion of the mixture gave a completely different image of the process parameters, in particular pressure and temperature, and it is possible that ECU failed to respond adequately and disrupted the process control and the whole engine process, so some valves and some of the injectors could remain open at the end of the fourth stroke, and combustion continued with uninterrupted supply of fuel. It is also possible that the mixture contained so many diesels that it had made the selfignition, or that some of the exhaust valve stuck and made it possible combustion transferring from the cylinder to exhaust manifold. According to the color of exhaust pipe, and that catalytic converter and temperature sensor are burned, it is evident that the process of combustion passed from the cylinder into the exhaust system (exhaust manifold). In that case, all the sensors measured the values that were beyond the allowed limits. Electric control unit (ECU-processor) was not programmed to stop the engine power supply and turn off the engine, or to do anything to prevent the continuation of this process. After long term operation of engines and burning the mixture in the exhaust system, exhaust system heated up and the fire was transferred from the particles catcher to the surrounding flammable parts, where it was spreaded to the upper and rear parts of the vehicle under the influence of air flow. Based on the examination of the place of fire origin, it was not found that exhaust system was broken and the flames burnt the surrounding parts, but that thermal insulation around the exhaust system was not sufficient to prevent the transfer of fire from glowing particles catcher.

Given description presents a potential and the most likely scenario of the process occurring. In order to describe the process with greater precision and certainty, some clarification was required from the manufacturer through a representative in B&H. The answers from the main representative of the manufacturer's vehicles are not obtained. It was particularly important to clarify the behavior of the central control unit in the case when sensors located on the exhaust manifold obtain it with information about the extreme deviations of the measured values. Since the information about the programmed behavior of ECU and whole systems with information from sensors about the parameters above permitted limits was not received from main representative, it is impossible to determine whether the cause of the fire was failure of a sensor or some of the functions of the central control unit. It can be noticed that inflammation of the vehicle due to incorrect refuelling could prevented by various measures.

4. CONCEPT SOLUTION OF THE SAFETY SYSTEM FOR AVOIDING WRONG REFUELLING IN CARS AND PREVENTION OF DAMAGE

As it is seen from the previous paragraphs, the display of inscription on the cap of the fuel tank is not sufficient to prevent the pouring of the wrong fuel. In the previous paragraph, the frequency of wrong refuelling and the harmful consequences are shown.

Consequences can be different, from the damage of driving engine to the fire and total damage. In the event of fire, the health and life of passengers in the vehicle can come in danger. This problem is not adequately solved even by the leading car manufacturers. Based on all of the above, it is clear that there is a need to analyze possible solutions of this problem.

The searching of concept solutions can be made in two directions (Fig.7). The first direction of searching a solution refers to prevent the wrong refuelling. The second direction would include searching for concept solution that would prevent the damage.

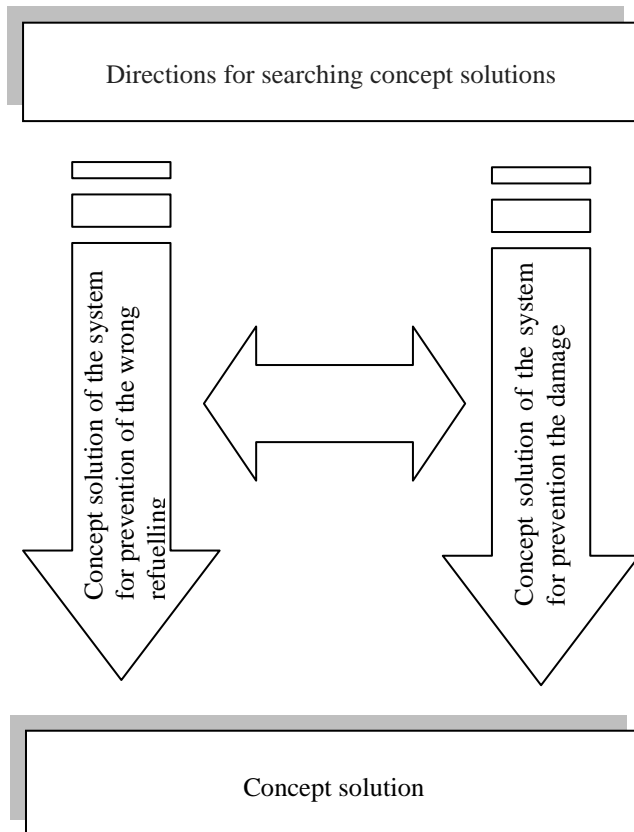


Fig.7: The directions of searching concept solution

There are also solutions that include both aspects; prevention of wrong refuelling, but also prevention of the occurrence of damage due to a fire resulting from another cause. From the analysis shown in the previous paragraphs, it is obvious that car manufacturers did not pay enough attention to prevent the fire in the vehicle. For the most car producers, except the fire extinguisher intended for fire extinguishing in car, there is no any autonomous system to prevent the occurrence and extinguish the fire occurred in the car.

Concept solutions for preventing the wrong refuelling can be very simple (Fig.8.). The simplest solution would be that the profile of the pipes of the diesel fuel dispensers is different from the profile of the pipes of the petrol dispensers. The profiles of the openings of the diesel and petrol fuel tanks would correspond to the pipe diameter profiles.

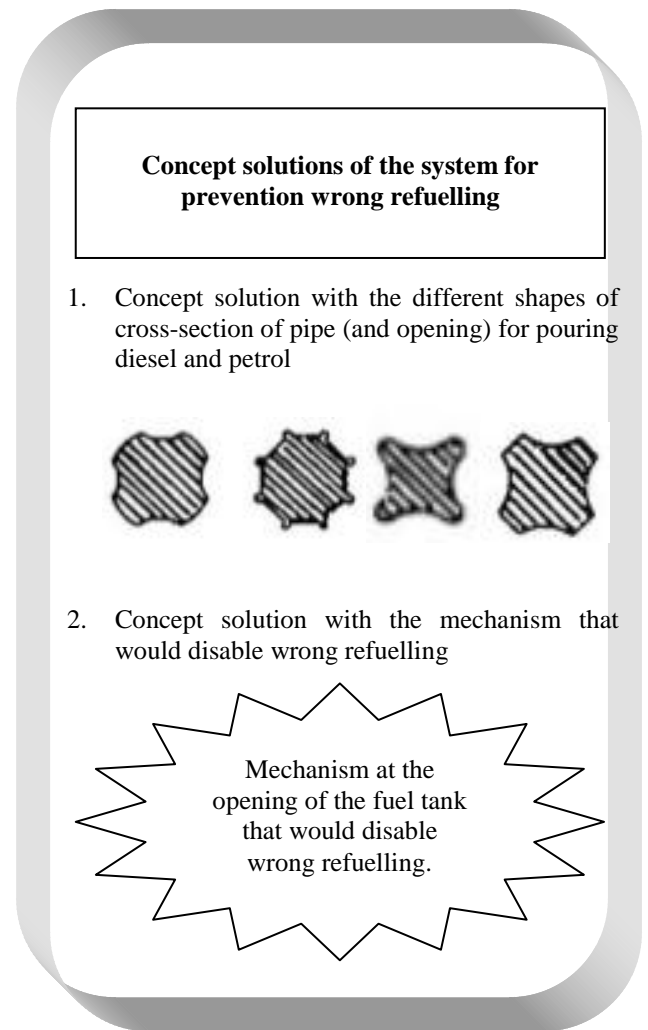


Fig.8: Concept solutions of the system for prevention wrong refuelling

It is simpler to solve the problem by preventing the wrong refuelling; but if this already happens, there should be a system that would identify the wrong refuelling and prevent the damage. Concept solutions of the system for preventing damage due to incorrect refuelling are shown in Fig.9. The concept solution of the system for pouring the fuel should include a system of fuel identification, a warning system and an active system for preventing damage.

Beside the inscription on the cap (cover) of reservoir, wrong refueling can be prevented through appropriate construction solution of opening and cap of reservoir. Pouring the wrong fuel could be prevented using the reservoir opening structurally designed in such a way that it cannot accept the tube device for pouring gasoline, but only tube device for pouring diesel. Pipes of mentioned devices have different diameters and it is possible to perform this system. If it still happens the wrong fuel is poured, as soon as possible it is required to notice this and prevent the engine starting. This is possible by setting the identification sensor and measuring features of poured fuel.

Concept solution of the system for identification wrong fuel and prevention the damage

Identification of pouring wrong fuel:

- Sound and visual signaling to the driver that the wrong fuel has been poured.

Prevention the damage:

- Stopping the fuel supply to the engine;
- Automatic engine shutdown;
- Starting the safety fire alarm system.

Fig.9: Concept solution of the system for identification wrong fuel and prevention the damage

However, if it comes to the starting of engine, damage can be reduced and especially fire can be avoided in the way that the central processing unit stops fueling and turns off the engine at the moment when it receives information from sensors and transmitters from the exhaust manifold. It is essential that the central processing unit sends signal to the driver to stop the vehicle and shut off the engine. Particular attention should be given to thermal insulation of the engine components and exhaust system in which the high temperature may occur.

5. CONCLUSION

The occurrence of wrong refuelling spills in cars is very common. Car manufacturers offer a very large number of technological innovations in cars, but they still have not dealt enough with this case sufficiently. Manufacturers have still not found an adequate solution to prevent misfuelling, nor have they found a solution to prevent damage. The paper presents the analysis of the frequency of occurrence of incorrect refueling and risk of ignition of the vehicle. We analyzed the specific case and given some of the conceptual solutions.

This paper presents several concept solutions for a system that will prevent wrong refuelling, as well as a system that will prevent harmful consequences if the wrong fuelling still occurs. Based on the given analysis, it is evident that

it is possible to introduce a lot of simple solutions that would be universal and quickly applicable. Some of these solutions have already been elaborated and the concept is presented in this paper. Further research should be directed to concrete development of several variants of the system for prevention of wrong refuelling in cars and systems for preventing damaging consequences.

REFERENCES

- [1] Tica, M., (2010.) , Vještačenje zapaljenja putničkog motornog vozila, Banja Luka,
- [2] Tica, M., Rackov, M., Miltenović A., Banić, M., Mišković Ž. (2015.), *Safety car - ignition risk due to misuse of fuel scattering, XL naučno stručni skup ODRŽAVANJE MAŠINA I OPREME, Budva*
- [3] Milašinović, A., Knežević, D., (2010.) , Tehnologija tehničkog pregleda vozila, Doboju, Saobraćajni fakultet u Doboju
- [4] Tica, M., (2014.) , Sigurnosna tehnika-skripta, Banja Luka, Mašinski Fakultet Banja Luka

CORRESPONDANCE



Milan TICA, PhD
University of Banja Luka
Mechanical Engineering Faculty
S. Stepanovića 71,
78000Banja Luka
milan.tica@mf.unibl.org



Milan RACKOV, PhD
University of Novi Sad
Faculty of Technical Sciences
Trg Dositeja Obradovića 6,
21101 Novi Sad
racmil@uns.ac.rs



Djordje MILTENOVIĆ, PhD
High Technologic and Artistic School in Leskovac
Vilema Pušmena 17,
16000 Leskovac
milten2004@yahoo.com



Aleksandar MILTENOVIĆ, PhD
University of Niš
Mechanical Engineering Faculty
A. Medvedeva 14,
18000 Niš
amiltenovic@yahoo.com



Milan BANIĆ, PhD
University of Niš
Mechanical Engineering Faculty
A. Medvedeva 14,
18000 Niš
milan.banic@outlook.com

**POWER AND MOTION
TRANSMISSION SYSTEMS**

THE INFLUENCE OF HELIX ANGLE ON THE LOAD CAPACITY OF CYLINDRICAL GEAR TEETH FLANKS

Mileta RISTIVOJEVIĆ
 Bozidar ROSIĆ
 Aleksandar DIMIĆ

Abstract: Load capacity of gear pairs is primarily limited by tooth root strength and surface durability of the flanks of gear teeth. It is well known that, considering volume strength and surface durability of cylindrical gears, load capacity of helical gears is greater than the one of spur gears. For the manufacturing of these gears the same manufacturing tool can be used – basic tooth rack. Thereby, these two types of cylindrical gears have same teeth profiles, from the aspect of shape and dimensions in normal plane, i.e. plane which is perpendicular to a helix of gear tooth. The difference between two profiles occurs in transverse plane, i.e. plane which is perpendicular to a rotational axis of gear, and it is a consequence of tilt of manufacturing tool – basic tooth rack, for the value of helix angle. For the load capacity analysis the surface contact stress of gear teeth flanks is more valid. According to that fact, this paper analyses the influence of helix angle on the load capacity of cylindrical gear teeth flanks.

Key words: Helical gears, spur gears, load capacity, helix angle

1. INTRODUCTION

The most commonly used profile for power transmission gear teeth is involute profile. The most important characteristic of involute profile is the fact that the straight edge part of manufacturing tool – basic tooth rack is used when generating of involute profile occur. Gears that were manufactured by the tool in the form of basic tooth rack can be meshed correctly regardless of the number of the teeth [1]. Thus, a single tool may be used for the generation of a family of gears. Because of that, a basic tooth profile is accepted as the basis for a gear standard, defined for a gear with an infinite diameter – a basic tooth rack. The parameters of the basic tooth rack are standardized according to [2], and theoretical form and dimensions of the involute tooth and gear are determined by that standard [3]. The method of generating the gear teeth with the tool in the form of a basic tooth rack allows the manufacture of spur and helical cylindrical gears. Such division was made according to the position of the helix of the tooth and straight line element of reference cylinder, which is parallel with gear axis of rotation (Fig.1). This means that a spur gear can be thought of a special case of a helical gear [4]. This position is determined by helix angle β . For cylindrical spur gears tooth helix is parallel to the axis of rotation of the gear, thus $\beta = 0^\circ$. Tooth helix of the helical gear, relative to the one of the spur gear, is “tilted” for the value of the helix angle ($0 < \beta < 45^\circ$). As a result, the geometrical characteristics of the tooth profile in the normal and transverse plane do not match [1]. This paper analyses the influence of the helix angle to the amount of

contact stress at the teeth flanks, for the contact of the meshed teeth profiles at the pitch point. Conducted analysis of contact stress ratio of the flanks of spur and helical gears makes it possible to quantify the influence of the helix angle on the load capacity of cylindrical gear flanks.

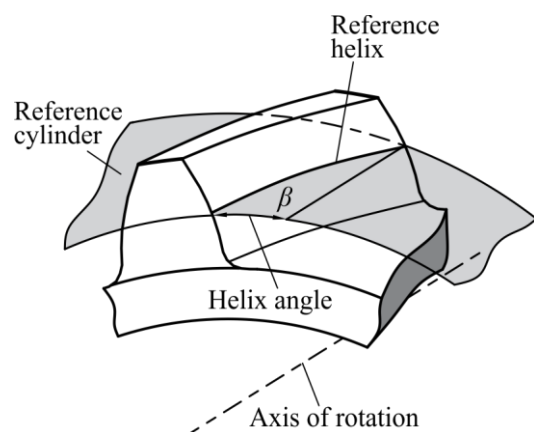


Fig.1: Tooth helix and helix angle

2. CONTACT STRESS ON THE CYLINDRICAL GEAR TEETH FLANKS

In this paper the contact stress on the teeth flanks is considered, when the contacting of the meshed teeth profiles occurs in pitch point. The ratio of nominal contact stresses at the pitch point for the spur and helical gears is observed. According to that, for the purposes of this

analysis, only the influence of geometrical and kinematic dimensions, which are dependent on the helix angle are considered. The expression for calculating nominal contact stress at the pitch point of cylindrical gears, expressed as a function of center distance has the following shape:

$$\sigma_{H0} = Z_H Z_E Z_\varepsilon Z_\beta \sqrt{\frac{F_t (u+1)^2 \cos \alpha}{b \cdot a \cdot 2u \cos \alpha_w}}, \quad (1)$$

where:

- Z_H is the zone factor,
- Z_E is the elasticity factor,
- Z_ε is the contact ratio factor,
- Z_β is the helix angle factor,
- F_t is the nominal tangential load,
- a is the center distance,
- b is the face width,
- u is the gear ratio,
- α_n is the normal pressure angle,
- α_w is pressure angle at the pitch cylinder,

according to [5]. The ratio of the nominal working contact stresses at the pitch point for the spur and helical gears, for the same nominal load in the form of a torque T , is:

$$\frac{\sigma_{H0}}{\sigma_{H0,\beta}} = \frac{Z_H}{Z_{H,\beta}} \cdot \frac{Z_\varepsilon}{Z_{\varepsilon,\beta}} \cdot \frac{1}{Z_{\beta,\beta}} \cdot \frac{1}{\cos \beta} = \xi_H \cdot \xi_\varepsilon \cdot \xi_\beta \cdot \xi_a \quad (2)$$

Dimensions related to helical gears ($\beta > 0^\circ$) appear with the attached symbol β in the subscript. The ratio of nominal contact stresses at the pitch point for the spur and helical gears comes down to ratios of two analytically obtained factors: ratio of the zone factors ξ_H , and ratio of the contact ratio factors ξ_ε , which can be concluded by looking at equation (2). Member ξ_a in equation (2) is the result of the difference in the center distance of spur and helical gear pairs. According to [6] the influence of gradual meshing entrance of the helical gear teeth in reference to spur gear teeth is taken into account with the use of special factor Z_β . Accordingly, in expression (2), this influence is taken into account with the introduction of factor ξ_β . The following analysis was carried out over the cylindrical gear pair with geometric and kinematic dimensions which are given in table 1.

Table 1: Characteristics of the considered gear pair

Dimension	Symbol	Value
Normal module	m_n	5 mm
Normal pressure angle	α_n	20°
Number of teeth	z_1	25
	z_2	25
Gear ratio	u	1
Helix angle	β	$0 \dots 45^\circ$
Center distance	a	125 ... 176,78 mm

3. ANALYSIS OF INFLUENCE FACTORS ON THE NOMINAL CONTACT STRESS OF THE CYLINDRICAL GEAR TEETH FLANKS

3.1. Analysis of the influence of factor ξ_a

Due to the variation of the helix angle β , the value of the center distance of the helical gear pair is changed in relation to center distance of the spur gear pair. Accordingly, the value of factor ξ_a also changes. Graphical representation of the dependence of the factor ξ_a from the helix angle is given in Fig.2, for the values of axle angle in the range of $0^\circ - 45^\circ$.

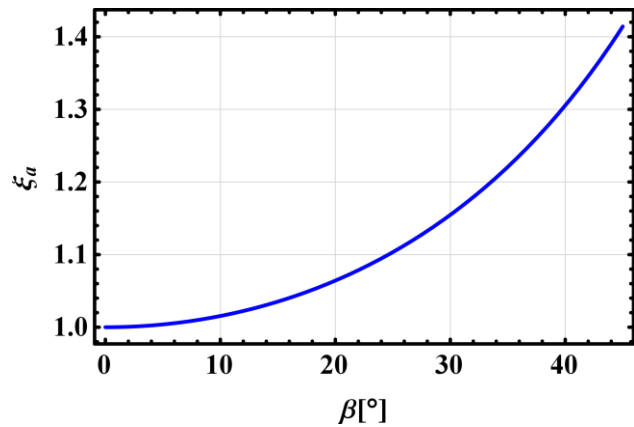


Fig.2: The influence of helix angle on the ξ_a factor

The influence of the helix angle on the change of center distance of the helical gear pair is significantly present for the values of helix angle above 20° (Fig.2.). For the mostly used values of helix angle, i.e. $\beta = 10^\circ - 20^\circ$, changes in center distance, and therefore factor ξ_a are about 5%. This means that with increase of helix angle, difference in load capacity of helical and spur gear pair is increased.

3.2. Analysis of the influence of factor ξ_H

This factor accounts for the influence of tooth flank curvature on contact stress [5]. The general form for the determination of this factor has the following appearance:

$$Z_H = \frac{1}{\cos \alpha} \sqrt{\frac{2 \cos \beta_b}{\tan \alpha_w}} \quad (3)$$

Analyzing the term given by the equation (3) it can be concluded that the ratio of the zone factors of the spur and helical gears, beside parameters given in Table 1, is a function of three variables dimensions:

$$\xi_H = \frac{Z_H}{Z_{H,\beta}} = f(x_1, x_2, \beta) \quad (4)$$

Graphical representation of the dependence of the factor ξ_H in relation to the helix angle is given on Fig.3, for different cases of the shift profile coefficient sums for gear 1 and gear 2. Based on the diagram shown in Fig.4 it can be noticed that for different helix angle values ratio of zone factors can vary up, in extreme cases, up to 55%, for certain cases of the shift profile coefficient sums. It also

can be noticed, that for values of helix angle up to 10° , the zone factors ratio is negligible. In the domain of the most common engineering practice ($\beta = 10^\circ - 20^\circ$), difference in load capacity ranges between 2 – 10%, wherein the influence of the helix angle is more pronounced for the gear pairs which are made with larger negative shift coefficients.

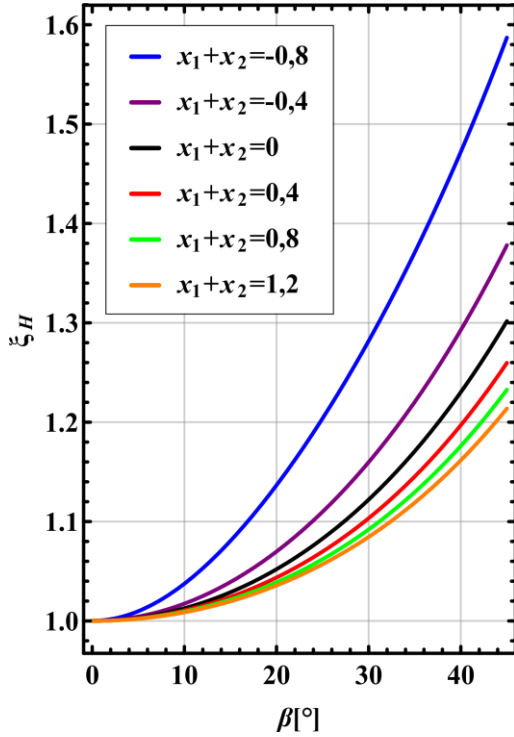


Fig.3: The influence of helix angle on the ζ_H factor

The individual influence of profile shift coefficients, for fixed value of helix angle $\beta = 20^\circ$, on the ratio of zone factors for spur and helical gears is given graphically in Fig.4.

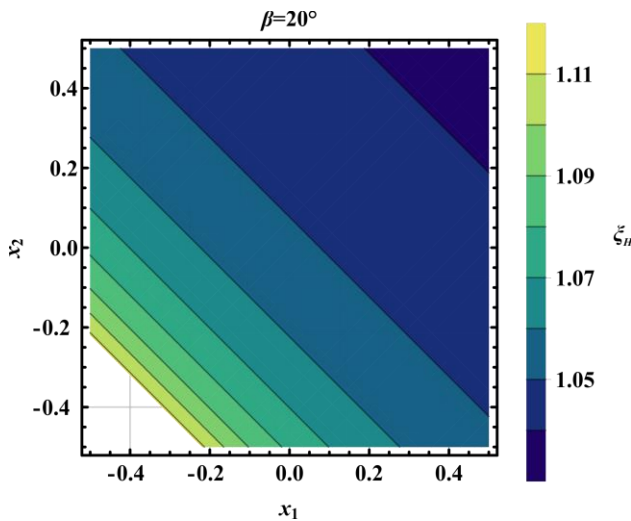


Fig.4: The individual influence of profile shift coefficients on the ζ_H factor

For cylindrical helical gear pair with the helix angle $\beta = 20^\circ$, it can be noticed based on the graphics on the Fig. 4., that load capacity of helical gear pair in reference to spur gear pair can vary up to 11%, for certain values of profile shift coefficients. However, it must be borne in mind that the profile shift coefficients must be carefully selected because their influence on the appearance of surface damage on the flanks of the teeth of cylindrical gears is very pronounced [7].

3.3. Analysis of the influence of factor ζ_ε

The contact ratio factor, Z_ε , accounts for the influence of the transverse contact and overlap ratios on the surface load capacity of cylindrical gears [5]. The general form for the determination of this factor has the following appearance:

$$Z_\varepsilon = \sqrt{\frac{4 - \varepsilon_\alpha (1 - \varepsilon_\beta) + \frac{\varepsilon_\alpha}{\varepsilon_\beta}}{3}} \quad (5)$$

The ratio of contact ratio factors ζ_ε , depends on the overlap ratio ε_β and ,after arranging equation (5), can take the following values:

$$\zeta_\varepsilon = \frac{Z_\varepsilon}{Z_{\varepsilon,\beta}} = \begin{cases} 1, & \text{for } \varepsilon_\beta = 0 \\ \frac{1}{\sqrt{\frac{(1 - \varepsilon_\beta) + \frac{3\varepsilon_\beta}{\varepsilon_\alpha(4 - \varepsilon_\alpha)}}{3}}}, & \text{for } \varepsilon_\beta < 1, \\ \frac{1}{\sqrt{\frac{3}{\varepsilon_\alpha(4 - \varepsilon_\alpha)}}}, & \text{for } \varepsilon_\beta > 1 \end{cases} \quad (6)$$

i.e. the ratio of contact ratio factors between spur and helical gears is dimension that is functionally dependent on four variable dimensions:

$$\zeta_\varepsilon = \frac{Z_\varepsilon}{Z_{\varepsilon,\beta}} = f(x_1, x_2, \beta, b). \quad (7)$$

For the cylindrical gear pairs for which the condition $x_1 + x_2 = 0$ applies, the ratio of contact ratio factors can be graphically displayed as a function of gear face width b and helix angle β (Fig.5).

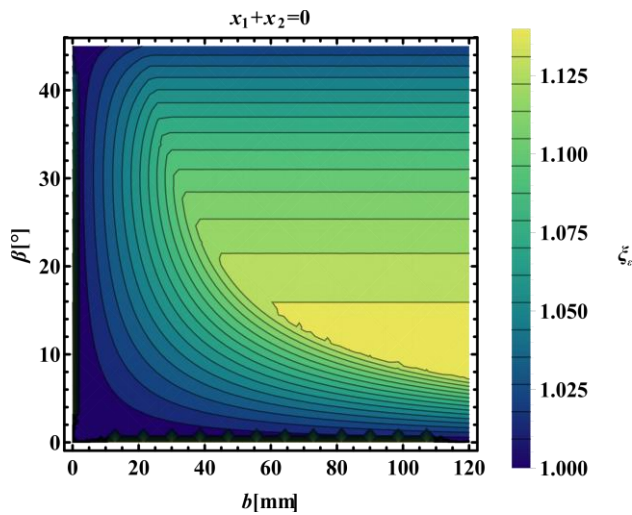


Fig.5: The influence of helix angle and the gear face width on the ξ_ϵ factor

Infection points which can be noticed in the diagram shown in Fig.5 occur when a condition $\epsilon_a = \epsilon_\beta$ is met. In this case maximal length of the line of contact B , which depends on gear face width, transverse contact ratio, overlap ratio and helix angle, appears at the matting flanks of the gear teeth only once during meshing (Fig.6b.). In case when condition $\epsilon_a > \epsilon_\beta$ is met, maximal length of the line of contact B begins at tooth profile of front gear surface, and ends up at the tooth profile of back gear surface (Fig.6a.). In case when condition $\epsilon_a < \epsilon_\beta$ is met maximal length of the line of contact B extends from top land of tooth to the line near bottom end which is limited by its active part (Fig.6c.) [8].

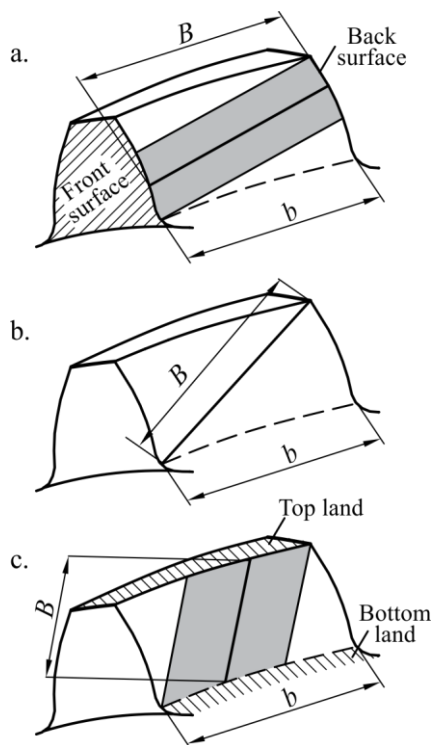


Fig.6: The influence of transverse contact ratio and overlap ratio on the maximal length of the line of contact

The graphic shown in the Fig.5. indicates that, for certain values of gear face width b and helix angle β , difference in load capacity between spur and helical gears can arise up to 12,5%. For helical gear pair with the helix angle $\beta = 20^\circ$, and gear face width $b = 40\text{mm}$, the influence of profile shift coefficients on the factor ξ_ϵ is shown in Fig. 7 i.e., in this case the load capacity also varies in the interval 0 – 12,5%.

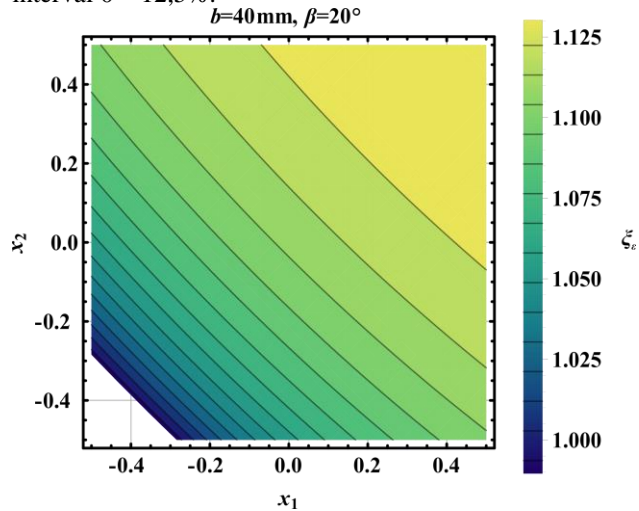


Fig.7: The influence of profile shift coefficients on the factor ξ_ϵ

Bearing in mind that factors ξ_H , ξ_ϵ and ξ_a from equation (2) are obtained by analytical method as opposed to factor ξ_β , and since the factor $Z_{\beta,\beta}$ is a subject of recent debate [9], it is desirable to define the auxiliary dimension k :

$$k = \frac{Z_H}{Z_{H,\beta}} \cdot \frac{Z_\epsilon}{Z_{\epsilon,\beta}} \cdot \frac{1}{\cos \beta} = \xi_H \cdot \xi_\epsilon \cdot \xi_a, \quad (8)$$

thus, it can be said that the ratio of the nominal working contact stresses at the pitch point for the spur and helical gears is reduced to the following term

$$\frac{\sigma_{H0}}{\sigma_{H0,\beta}} = k \cdot \frac{1}{Z_{\beta,\beta}} = k \cdot \xi_\beta. \quad (9)$$

An auxiliary dimension k is functionally dependent on four variable dimensions:

$$k = f(x_1, x_2, \beta, b). \quad (10)$$

An auxiliary dimension k represents the difference in contact stresses on teeth flanks which is a consequence of analytically derived zone and contact ratio factors of the spur and helical gear, as well as kinematic difference between observed gear pairs. The way in which the auxiliary size k changes with respect to helix angle β and gear face width b , in case when $x_1+x_2=0$, can be seen in the Fig.8. For helical gear pair with the helix angle $\beta = 20^\circ$ and gear face width $b = 40\text{mm}$, the influence of profile shift coefficients on the auxiliary dimension k is shown in Fig.9.

When taking into account all influential dimensions, apart from the ratio of factor $Z_{\beta,\beta}$, it can be noticed that the difference in the load capacity of teeth flanks between spur and helical cylindrical gears can vary

up to 80%, analyzing the graphic from the Fig.8. This means that this kind of analysis can be exploited for the optimisation of parameters x_1 , x_2 , β and b in order to achieve greater load capacity and efficiency of cylindrical gear pairs, in the way it is shown in [10,11]. For the observed helical gear pair when $\beta = 20^\circ$ and $b = 40\text{mm}$, this difference can vary from 20% to 28%, which depends on the values of profile shift coefficients x_1 and x_2 .

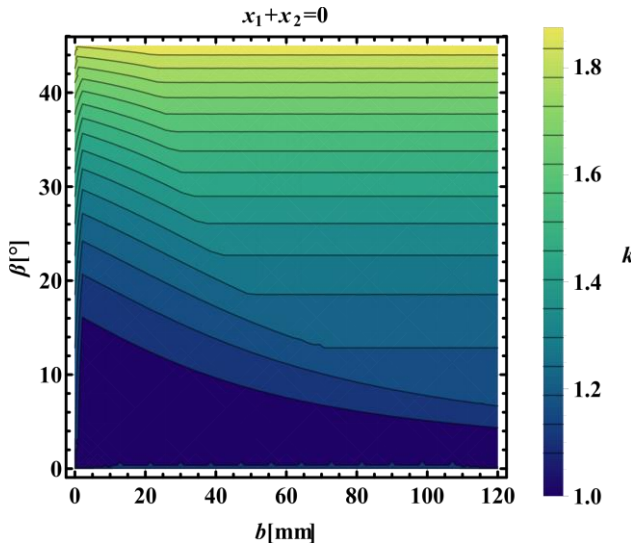


Fig.8: The influence of helix angle and the gear face width on the auxiliary dimension k

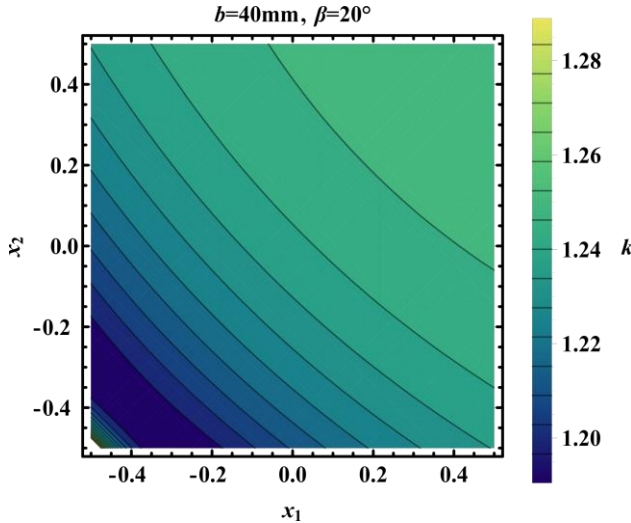


Fig.9: The influence of profile shift coefficients on the auxiliary size k

3.4. Analysis of the influence of factor ξ_β

In the previous analysis, the helix angle β was also figurative in the factors ξ_H , ξ_c and ξ_a to a certain extent, however its influence is also included in the factor ξ_β . The helix angle factor Z_β has empirical nature, and according to the recommendations of [5] it can be calculated using expression:

$$Z_{\beta,\beta} = \sqrt{\cos \beta}. \quad (11)$$

Since its origin is unknown, it is desirable to carry out load capacity analysis of the spur and helical gears considering the impact of this factor. Diagram of the contact stresses ratio change, depending on helix angle β and the gear face width b , in the case when $x_1+x_2=0$, is shown on Fig.10 for the cases when the factor Z_β is taken into account (blue surface on Fig.10) and when it is excluded from consideration (orange surface on Fig.10).

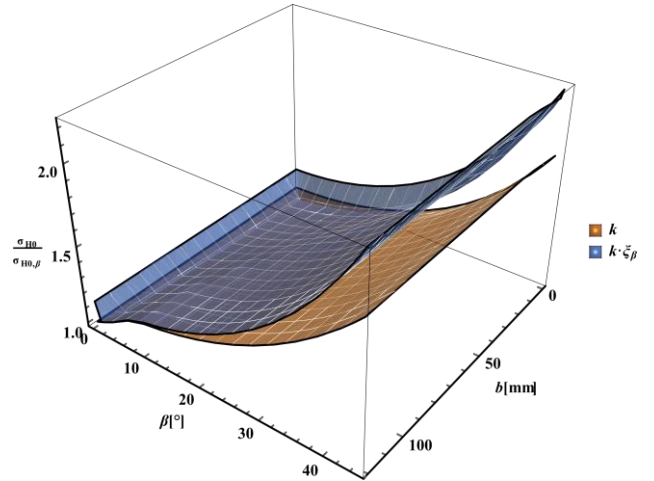


Fig.10: The influence of helix angle, the gear face width and helix angle factor on the contact stresses ratio of spur and helical gears

For the observed helical gear pair when $\beta = 20^\circ$ and $b = 40\text{mm}$, and $x_1+x_2 \neq 0$, contact stresses ratio change depends of the values of the profile shift coefficients, and it is shown in Fig.11 for the cases when the factor Z_β is taken into account (blue surface on Fig.11) and when it is excluded from consideration (orange surface on Fig.11).

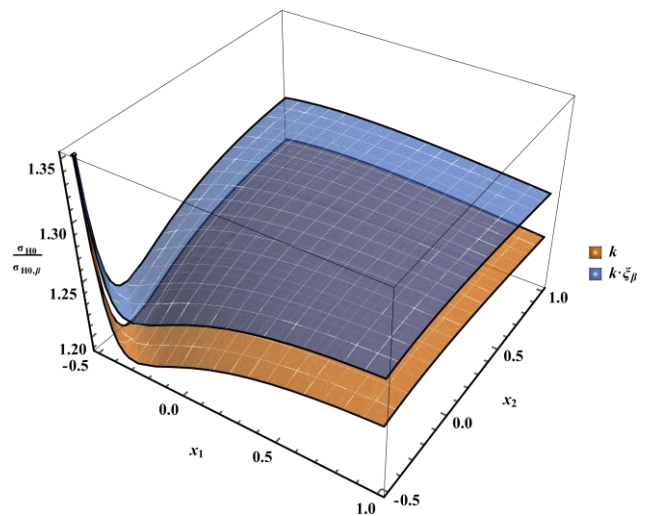


Fig.11: The influence of profile shift coefficients and helix angle factor on the contact stresses ratio of spur and helical gears

Analyzing Fig.10 and Fig.11 it can be concluded that the influence of the helix angle factor leads to an additional load capacity increase, when used in the form suggested in [5], however, it should be kept in mind that such a form is the topic of discussion [9].

4. CONCLUSION

The nominal values of the contact stresses on the gear teeth flanks of the cylindrical gears are multiply dependent on the helix angle. As the helix angle increases, the central distance of the gear pair also increases. As a result, the dimensions of the gear pair increase in the radial direction, but at the same time the load capacity of the tooth flanks of the helical gear pair is increased in relation to the spur gear pair, the diagram in Fig. 2. The helix angle also affects the shape of the teeth profile. In the area of small angles (up to 10°), its influence on the load capacity of the teeth flanks is small, below 5%. The maximum increase of 30% is at a maximum helix angle of 45° , however, in this case, high-intensity axial forces are generated. In addition to the partial impact of the helix angle on the load capacity of the teeth flanks, its influence may be more or less expressed in combination with certain values of the profile shift coefficients, the diagram in Figure 4. The helix angle also influences the contact stresses of gear teeth flanks through transverse contact ratio and overlap ratio. In the area of small gear face widths, the influence of the helix angle on the load capacity of the gear teeth flanks is also small. With the increase in the gear face width, this effect also increases, but with a small gradient. The helix angle also influences the load capacity of the gear teeth flanks through length of the line of contact. All of the above-mentioned impacts of the helix angle on the load capacity of gear teeth flanks were given in analytical form. The influence of the phenomena of gradual entry into the meshing of the helical gear teeth on the load capacity of the teeth flanks, according to the ISO standard is quantified by a special factor Z_β .

REFERENCES

- [1] RISTIVOJEVIC, M. (2006) *Zupcanici 1 – Kinematika i kontrola*, Zavod za udzbenike i nastavna sredstva.
- [2] ISO 53 (1998) – Cylindrical gears for general and heavy engineering – standard basic rack tooth.
- [3] JELASKA, D. (2012) *Gears and gear drives*, John Wiley & Sons Ltd.
- [4] RADZEVICH, S.P. (2012) *Dudley's handbook of practical gear design and manufacture*, Taylor & Francis Group.

- [5] ISO 6336-2 (2006) – *Calculation of load capacity of spur and helical gears – Part 2. Calculation of surface durability*.
- [6] ISO 6336-1 (2006) – *Calculation of load capacity of spur and helical gears – Part 1. Basic principles, introduction and general influence factors*.
- [7] RISTIVOJEVIC M., LAZOVIC, T., VENCL, A. (2013) *Studying the load carrying capacity of spur gear tooth flanks*, Mechanism and Machine Theory, Vol. 59, pp 125-137.
- [8] RISTIVOJEVIC, M., MITROVIC, R. (2002) *Raspodela opterecenja – Zupcasti parovi i kotrljajni lezaji*, Masinski fakultet.
- [9] HOHN, B.R., OSTER, P., STEINBERGER, G. (2007) *Influences of load distribution and tooth flank modifications as considered in a new DIN/ISO compatible calculation method*, Proceedings of IDETC/CIE 2007, Las Vegas, Nevada.
- [10] ROSIC, B., RISTIVOJEVIC, M., RADOVIC, D., MARKOVIC, D., VASIC, Z. (2012) *Analysis and multiobjective design optimization of planetary gear train*, TECHNICS TECHNOLOGIES EDUCATION MANAGEMENT-TTEM, (2012), vol. 7 pp. 975-984.
- [11] DOBRATIC, P., RISTIVOJEVIC, M., ROSIC, B. (2014) *An analysis of the efficiency of utilization of involute cylindrical gear pairs*, 6th International Scientific Conference on Defensive Technologies, Belgrade, Serbia.

CORRESPONDANCE



Mileta RISTIVOJEVIĆ, Prof. D.Sc. Eng.
University of Belgrade
Mechanical Engineering Faculty
Kraljice Marije 16.
11120 Belgrade, Serbia
mrstivojevic@mas.bg.ac.rs



Bozidar ROSIĆ, Prof. D.Sc. Eng.
University of Belgrade
Mechanical Engineering Faculty
Kraljice Marije 16.
11120 Belgrade, Serbia
brosic@mas.bg.ac.rs



Aleksandar DIMIĆ, Ass. M.Sc. Eng.
University of Belgrade
Mechanical Engineering Faculty
Kraljice Marije 16.
11120 Beograd, Serbia
adimic@mas.bg.ac.rs

INFLUENCE TEMPERATURE ON STIFFNESS MATRIX FOR PAIRED (DUPLEX) ANGULAR CONTACT BALL BEARINGS

Aleksandar ŽIVKOVIĆ
 Milan ZELJKOVIĆ
 Slobodan TABAKOVIĆ

Abstract: Although angular contact ball bearings are widely used for the support of high speed machine tools spindles, the scientific literature on paired ball bearings is scarce. To overcome the deficiency in the literature, an comprehensive, analytical approach based on the Hertzian theory and John-Harris's quasi-static equilibrium equations for back-to-back, face-to-face, and tandem arrangements is proposed. The elements of the five-dimensional stiffness matrix for angular contact ball bearings are computed, under influence of temperature. The diagonal elements of the proposed stiffness matrix are verified with a data of commercial ball bearing for all arrangements. For angular contact ball bearings mounting in paired, the angular stiffness and cross-coupling stiffness are significant, and the contact angle changes under external inertial and thermal loads. The proposed model is also valid for double row ball bearings.

Key words: Ball bearing, Bearing stiffness, Spindle unit, Machine tool

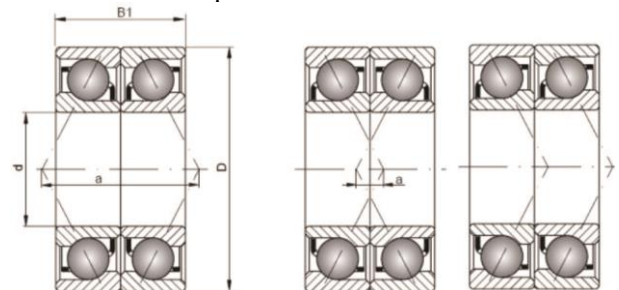
1. INTRODUCTION

Ball bearings with angular contact are the most commonly used type of bearing for high-speed spindle support, due to the small friction coefficient and the economical maintenance. The contact forces within the bearing consist of four interconnected components: initial axial preload, thermal preload, external load and the inertial force (e.g. centrifugal force). Permissible spindle speed, reliability and performance are usually limited by the bearing characteristics. As such, bearing support modeling is crucial for predicting thermo-mechanical behavior of the spindle.

In the early '60s Jones [5] presented the model of the bearing, while taking into account the effect of high-speed on the ball due to the inertial force. Houpert [4] determined the forces and moments on ball bearings based on relative ring displacements. In this model, the influence of inertial forces and the contact angle change have been neglected. Harris *et al.* [3] developed the quasi-static model of high speed bearings. Cao [1] showed the matrix formulation of Harris's model. Comprehensive analytical bearing model for determining the stiffness matrix for different bearing arrangements based on Hertz's contact theory and Jones-Harris [3] quasi-static equilibrium equation, without considering the effect of inertial forces, was shown by Gunduz. [2]. Besides the influence of preload and load, in high speed bearings, inertial forces significantly affect bearing stiffness due to change in contact load and contact angle with outer and inner raceway.

This paper focuses on duplex angular contact ball bearings which can be categorized into three arrangements as shown in Fig. 1: "O" arrangement, in

which the load lines meet outside of the bearing; "X" arrangement, where the load lines converge toward the bore of the bearing; "TANDEM" arrangement, in which the load lines act in parallel.



"O" arrangm. "X" arrangm. "Tandem" arrangm.

Fig. 1 Arrangements of duplex angular contact ball bearings

The angular stiffness terms of angular contact ball bearings mounting in pair are significant and highly dependent on the configuration of the ball bearings.

2. MATHEMATICAL MODEL OF THE BEARING

The mechanical and thermal processes in the bearing are connected. As the speed of bearing rotation increases, so does the heat generated on the contact surfaces of the bearing. Likewise external load, preload, lubricant characteristics, bearing arrangement and the surrounding area affect the increase in temperature. On the other hand, variable heat sources and sinks cause complex thermal expansion, which creates additional thermal load. Thermal load changes the contact pressure in the bearing, thus it affects heat development, thermal contact

conductivity, dynamic stiffness, and damping in the bearing.

2.1. Internal loading of the bearing

The bearing can be illustrated in a simple manner, as shown in Figure 2. The bearing's ability to transfer load largely depends on its inner geometry. Also, Figure 2(a) shows that the initial contact angle can be defined by the line which goes through the contact points of the ball and the raceway, with the plane orthogonal to the bearing rotation axis. When there is no load the raceway curvature centers (C_0) i (C_i) are located at the distance $A=Bd_b=(f_i+f_0-1)d_b$ as can be seen in Fig. 2 (b).

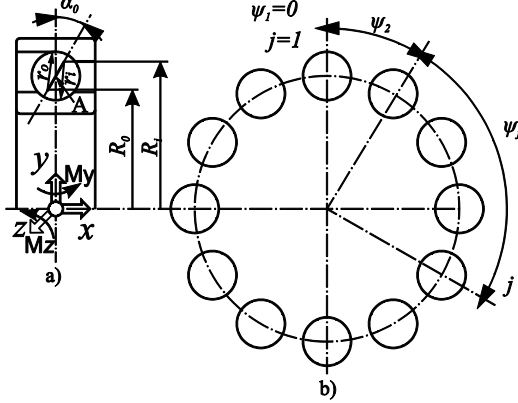


Fig. 2 Schematic of ball bearing. (a) Parameters of a ball bearing. (b) Angular position of the ball

After the bearings are mounted, due to applied initial preload there is axial displacement of inner raceway groove curvature center from C_i to $C_{i(1)}$. Following this, the nominal angle of contact increases from α_0 to α_p (the contact angle after preload) as shown in Fig. 3.

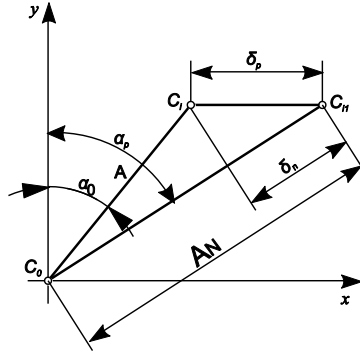


Fig. 3 The ball bearing under applied initial preload

Likewise, the distance between raceway curvature centers (A) increases and new distance A_N can be defined as:

$$A_N = A \left(\cos(\alpha_p - \alpha_0) + \left(\frac{\cos \alpha_0}{\cos \alpha_p} - 1 \right) \right) \quad (1)$$

The contact angle after preload α_p is defined via $\cos \alpha_p$ [9]:

$$\cos \alpha_p = \cos \alpha_0 \left[1 + \left(\frac{F_p}{ZK_n A^{3/2} \sqrt{1 - \cos^2 \alpha_p}} \right)^{2/3} \right]^{-1} \quad (2)$$

In high speed bearings the inertial forces cause the change in contact angle with the raceways, due to the line of action between the raceway groove curvature centers will not be collinear with the distance between centers A_N as depicted in Fig. 4 (a). The inner raceway groove curvature

center (C_{i1}) moves relatively compared to the center (C_o) which is fixed.

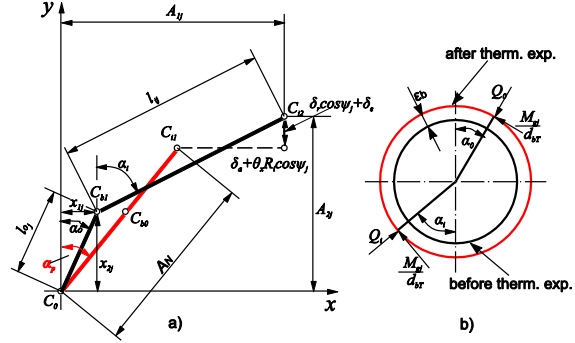


Fig. 4. (a) Position of raceway curvature centers, (b) Ball loading at angular position ψ_j

Due to the effect of external load, inertial load and taking into account the thermal expansion of the balls as a result of temperature increase, the distance between inner raceway groove curvature center (C_{i2}) and the new position of the center of the ball (C_{b1}) and the distance between the fixed center of outer raceway groove curvature (C_0) and the new position of the ball center (C_{b1}) is:

$$l_{m,j} = (f_{m,T} - 0.5) d_{bT} + \delta_{m,j}; m = i, o; j = 1, 2, \dots, Z \quad (3)$$

where $f_{m,T}$ in the function of thermal expansion of bearing elements $f_{m,T} = r_m/d_{bT}$, and d_{bT} is diameter of the balls after thermal expansion $d_{bT} = d_b(1/2\alpha_b\Delta T + 1)$.

Radial and axial distance between the position of curvature centers, when applying preload and thermal expansion effect, according to Fig. 4 (b) is:

$$A_{1j} = A_N \sin \alpha_p + \delta_a + \delta_{ea} + \theta_y R_i \cos(\psi_j) - \theta_z R_i \cos(\psi_j) \quad (4)$$

$$A_{2j} = A_N \cos \alpha_p + \delta_r \cos(\psi_j) + \delta_z \sin(\psi_j) + \delta_{er}$$

The increase of temperatures of the outer ring/the housing/distance ring, inner ring/spindle shaft, and balls due to heat generated in the bearings, causes the expansion of distance rings, balls and spindle shaft in axial and radial direction, resulting in thermal preload. The relative displacement between the inner and outer rings of each bearing originates from the distribution of axial thermal displacement of spindle and housing. In Fig. 5 the thermal expansion of spindle elements for lock-ring preload can be seen.

Based on Fig. 5 the thermal displacement in axial (δ_{ea}) and radial direction (δ_{er}), depending on the bearing arrangement [7] and can be represented as [8]:

$$\delta_{ea} = \alpha_s \left(x_b \pm \frac{1}{2} d_{bT} \sin \alpha_p \right) \cdot (\Delta T_s) - \alpha_h \left(x_b \mp \frac{1}{2} d_{bT} \sin \alpha_p \right) \cdot (\Delta T_h) \quad (5)$$

$$\delta_{er} = \frac{1}{2} \alpha_r [D_{io}(\Delta T_r) - D_{oi}(\Delta T_{or})]$$

For "Tandem" arrangement the thermal displacement in axial (δ_{ea}) is:

$$\delta_{ea} = \alpha_s(x_s) \cdot (\Delta T_s) - \alpha_h(x_h) \cdot (\Delta T_h) \quad (6)$$

where α_s, α_h are the linear expansion coefficient of the shaft and housing; $\Delta T_s, \Delta T_h$, are the increases in temperature of the spindle shaft and housing respectively; α_r is the linear expansion coefficient of the rings; D_{io} and D_{oi} are the inner diameter of the outer ring and outer diameter of inner ring, respectively.

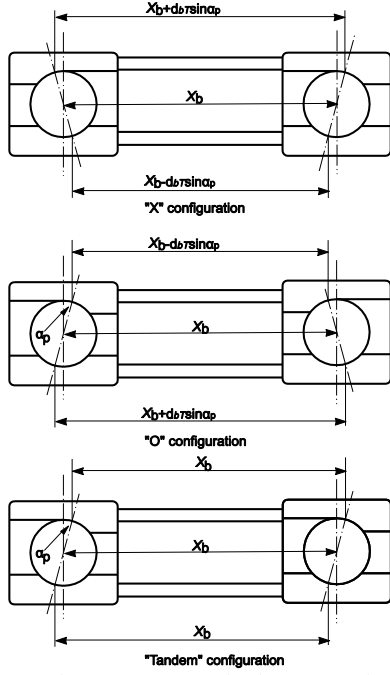


Fig. 5 Thermal expansion for lock-ring preload bearing configuration

According to Pythagoras's theory the equation of kinematic constraints between balls and raceways in Fig. 4 (a) is:

$$\begin{aligned} [A_{1j} - X_{1j}]^2 + [A_{2j} - X_{2j}]^2 + l_{ij}^2 &= 0 \\ X_{1j}^2 + X_{2j}^2 + l_{oj}^2 &= 0 \end{aligned} \quad (7)$$

Based on Fig. 3 (d), in accordance with Newton's 2nd law, for every ball the equation of forces in horizontal and vertical direction is defined as:

$$\begin{aligned} Q_{oj} \cos \alpha_{oj} - Q_{ij} \cos \alpha_{ij} - \frac{M_{gj}}{d_{br}} (\sin \alpha_o - \sin \alpha_i) - F_{cj} &= 0 \\ Q_{oj} \sin \alpha_{oj} - Q_{ij} \sin \alpha_{ij} + \frac{M_{gj}}{d_{br}} (\sin \alpha_o - \sin \alpha_i) &= 0 \end{aligned} \quad (8)$$

The method of determining gyroscopic moment and centrifugal force of a ball is shown in [3] in greater detail. The relation between local Hertz's contact forces $Q_{(j)}$ and deflection $\delta_{(j)}$ between ball and inner/outer raceway is defined as:

$$Q_{m,j} = K_m \delta_{m,j}^{3/2}; m = i, o; j = 1, 2, \dots, Z \quad (9)$$

In order to find the value of δ_a , δ_r i θ_y the conditions of equilibrium applied to the entire bearing must be set. Considering the combination of uniform preload action and the external load of the bearing, the equations of equilibrium for the inner ring are:

$$\begin{aligned} F_x - \sum_{i=1}^N \sum_{j=1}^Z \left(Q_{i(j)} \sin \alpha_{i(j)} + \frac{M_{gj}}{d_k} \cos \alpha_{i(j)} \right) + F_p &= 0 \\ F_y - \sum_{i=1}^N \sum_{j=1}^Z \left(Q_{i(j)} \cos \alpha_{i(j)} - \frac{M_{gj}}{d_{br}} \sin \alpha_{i(j)} \right) \cos \psi_j &= 0 \\ F_z - \sum_{i=1}^N \sum_{j=1}^Z \left(Q_{i(j)} \sin \alpha_{i(j)} - \frac{M_{gj}}{d_{br}} \cos \alpha_{i(j)} \right) \sin \psi_j &= 0 \\ M_y - \sum_{i=1}^N \sum_{j=1}^Z \left\{ r_i \left(Q_{i(j)} \sin \alpha_{i(j)} + \frac{M_{gj}}{d_{br}} \cos \alpha_{i(j)} \right) - f_i M_{gj} \right\} \sin \psi_j &= 0 \\ M_z - \sum_{i=1}^N \sum_{j=1}^Z \left\{ -r_i \left(Q_{i(j)} \sin \alpha_{i(j)} + \frac{M_{gj}}{d_{br}} \cos \alpha_{i(j)} \right) + f_i M_{gj} \right\} \cos \psi_j &= 0 \end{aligned} \quad (10)$$

After obtaining the primary variables δ_a , δ_r , δ_z and θ_y , θ_z , a new set of values X_{1j} , X_{2j} , $\delta_{i(j)}$, $\delta_{o(j)}$, must be determined in

order to be compatible with the primary values. After all the values X_{1j} , X_{2j} , $\delta_{i(j)}$, $\delta_{o(j)}$, are determined, contact parameters such as contact forces, contact angle contact deformations and the contact areas for each position of the ball are calculated. Following that, the angle of contact with the outer and inner raceway in Fig. 4 (a) is:

$$\begin{aligned} \tan \alpha_{oj} &= X_{1j} / X_{2j} \\ \tan \alpha_{ij} &= (A_{1j} - X_{1j}) / (A_{2j} - X_{2j}) \end{aligned} \quad (11)$$

2.2. Stiffness matrix

This paper presents the stiffness coefficients for every ball as the combination of the effects of kinematic, elastic and thermal properties on the bearing. The bearing stiffness consists of an array of combined stiffness of the ball/inner raceway and ball/outer raceway. If the relative displacement of the bearing is denoted by δ_k^m where is $k=x, y, z, \theta_y, \theta_z$ i $m = i, o$, then the stiffness of the bearing can be expressed by:

$$K_{i,k}^L = \frac{\partial F_k^i}{\partial \delta_k^i} = \left(- \sum_{j=1}^Z [T]_j^T \frac{\partial Q_j}{\partial u_j} [T]_j \right)_i, \text{ or,} \quad (12)$$

$$K_{o,k}^L = \frac{\partial F_k^o}{\partial \delta_k^o} = \left(- \sum_{j=1}^Z [T]_j^T \frac{\partial Q_j}{\partial u_j} [T]_j \right)_o$$

$$[K]^L = \begin{bmatrix} k_{xx} & k_{xy} & k_{xz} & k_{x\theta_y} & k_{x\theta_z} \\ & k_{yy} & k_{yz} & k_{y\theta_y} & k_{y\theta_z} \\ s & & k_{zz} & k_{z\theta_y} & k_{z\theta_z} \\ & i & & k_{\theta_y\theta_y} & k_{\theta_y\theta_z} \\ & & m. & & k_{\theta_z\theta_z} \end{bmatrix}_{5 \times 5} \quad (13)$$

where is $[T]_j$ - matrix transformation in the form:

$$[T]_j = \begin{bmatrix} \cos \psi_j & \sin \psi_j & 0 & -\sin \psi_j & \cos \psi_j \\ 0 & 0 & 1 & r_{i,o} \cos \psi_j & -r_{i,o} \sin \psi_j \\ 0 & 0 & 0 & -\sin \psi_j & \cos \psi_j \end{bmatrix} \quad (14)$$

3. RESULTS AND DISCUSSION

Analysis of stiffness was carried out on the hybrid bearing SKF 7011 CDGA/HC P4. The analysis covered changes in stiffness for the axial preload and radial loads $F_p = 100 - 1000$ [N], $F_r = 1000 - 4000$ [N] in the steady state and for speeds $n = 0$ to 11200 [rpm]. Radial load is determined on the basis of the maximum torque that can be transferred with ISO tapered inner surface of the main spindle, which is supported with mentioned bearing in front support. Bearing speed is defined based on the recommendation from the bearing manufacturers. The analysis was carried out in the example of the main spindle (Fig. 6). In order to test the bearing itself, it is assumed that the spindle is absolutely rigid, in which case the loads acting at the spindle nose are directly transferred to bearings, on the basis of which: $F_p = F_x$, $F_r = F_y$. The temperatures required in the equation (5) and (6) were used from the paper [8].

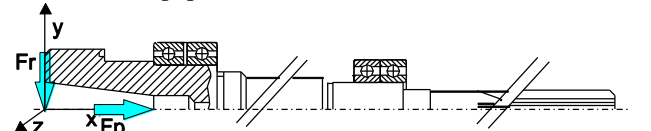


Fig. 6. Rigid spindle subjected to radial and axial load at spindle nose

3.1. Effect of preload and temperature on the stiffness

In order to verify the proposed model, first, axial and radial stiffness k_{xx} , k_{yy} are compared with a data of commercial ball bearing for “O” arrangements. Secondary the effect of pure preload and temperature is analyzed for all arrangements. Table 1 and Table 2 shows the comparison of the axial and radial stiffness determined by propose model with the catalog bearing values of the series 7011 CDGA/HC P4 for “O” arrangement.

Table 1. Comparison of axial stiffness with catalog values

	SKF	SNFA	FAG	Propose model
Preload	Axial stiffness k_{xx} N/ μ m			
small	71	56	61.9	67.4
middle	110	82	107.2	109.8
high	155	102	155.6	154.6

Table 2. Comparison of radial stiff. with catalog values

	SKF	SNFA	FAG	Propose model
Preload	Axial stiffness k_{xx} N/ μ m			
small	426	336	371.4	393.4
middle	660	492	643.2	550.2
high	930	612	933.6	676.4

Zeljko came to similar data [6] on the basis of the data from the bearing manufacturer's catalog. On the other hand, according to Zverev [10], certain stiffness values can vary from 10 to 15% depending on the bearing manufacturer.

In the absence of radial or moment load, the radial stiffness (k_{yy} and k_{zz}) as well as the angular stiffness ($k_{\theta_y\theta_y}$ and $k_{\theta_z\theta_z}$) are equal, yielding independent diagonal stiffness coefficient k_{xx} , k_{yy} and $k_{\theta_z\theta_z}$, for all consider arrangement are shows in Fig. 7 to Fig. 9. As seen from the Fig 7 and Fig. 8, the axial and radial stiffness for the “O” and “X” arrangement is the same, while the stiffness for the “TANDEM” arrangement is greater by about 10 to 30%. Angular stiffness $k_{\theta_z\theta_z}$ of the “O” and “TANDEM” arrangement is approximately the same, while the “X” arrangement is significantly lower. In all considered of the bearing arrangements, the temperature significantly influences of the increase in stiffness in all direction.

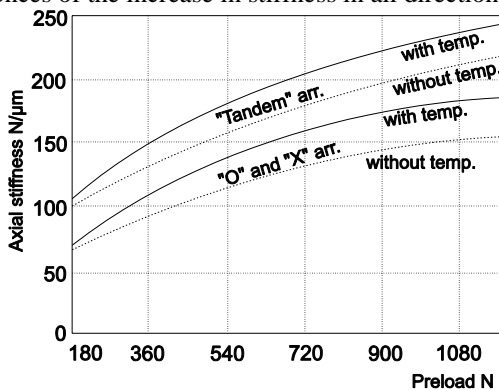


Fig.7. Axial stiffness with respect preload for consider the bearing arrangement

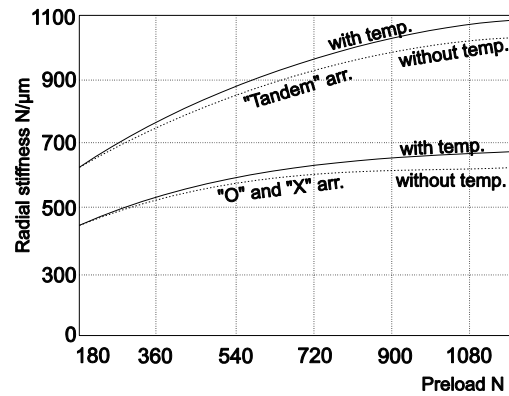


Fig.8. Radial stiffness with respect preload for consider the bearing arrangement

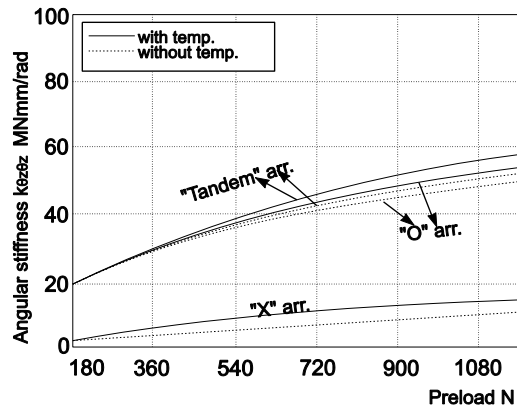


Fig.9. Angular stiffness with respect preload for consider the bearing arrangement

Other hand, rise in the temperature of spindle units produces thermal expansion of bearing elements, which causes preload increase, which is often called thermal preload. The temperatures of the balls are larger than the temperatures of the raceways.

As time passes, the larger amount of generated heat goes through the housing and the spindle, and the temperature between the balls and the raceways decreases. All of this causes larger or smaller changes of the bearing elements. Thus, thermal expansion in the housing is greater than that in the shaft leading to a negative thermal expansion δ_{ea} between the shaft and housing. This is the reason why both the axial displacement d_a in Eq. (5) and the preload F_p in Eq. (10) are increased. In time the spindle shaft's temperature gradient approaches the temperature gradient of the housing. This causes the reduction of negative value δ_{ea} , which leads to the decrease of bearing preload during time. By taking the maximal increase in preload from Figure 10, the change in radial bearing stiffness has been determined for different rotation speeds. From Figure 11, it can be seen that the initial preload of the bearing is 194 N when the spindle does not rotate with the corresponding stiffness of 392 N/ μ m. Preload then increases to 274 N, as shown in Figure 14, for 6000 rpm with the stiffness of 435.6 N/ μ m. As the result of increase in maximal thermal preload by 41.23 % for 6000 rpm, the bearing stiffness increases by 11 %. Finally, after reaching the stationary thermal state, the bearing elements' expansion is nearly constant, therefore it can be said that the change in preload for stationary thermal state is negligibly small.

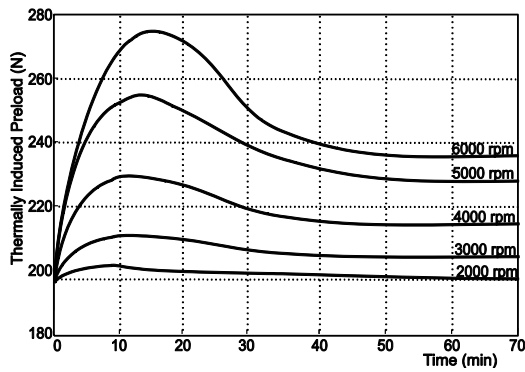


Fig. 10 Prediction of thermally induced preload of the bearing

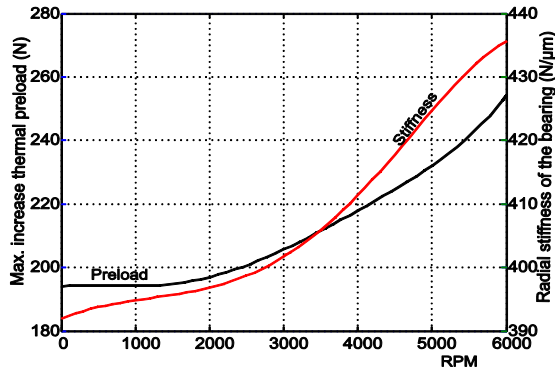


Fig. 11 Maximum thermal induced preload and radial stiffness of the bearing

3.2. Effect of inertial load and temperature on the stiffness

Centrifugal force decreases bearing stiffness for two reasons. Firstly, due to the influence of centrifugal force on the balls, the contact force between balls and outer raceways decreases. Hence, Hertz's contact stiffness will be proportional to contact force. Secondly, because of centrifugal forces, the contact angle between balls and outer or inner raceway changes. The contact angle with the inner raceway increases, while the one with the outer raceway decreases. The influence of inertia force increases significantly on higher speeds, as seen from the Figure 12 and Figure 13. On the other hand, the increase of the speed increases the temperature on the bearings, which leads to an increase in stiffness.

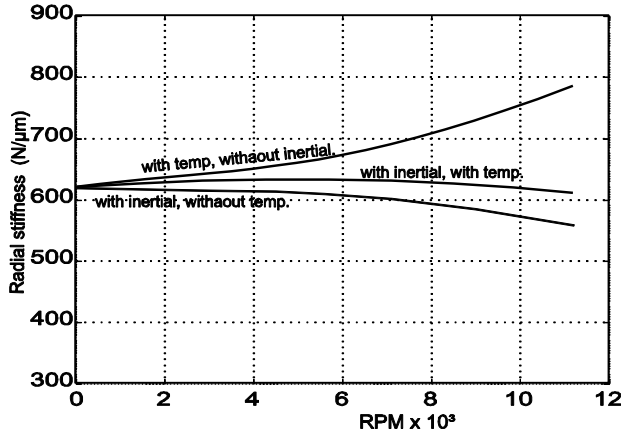


Fig. 12 Radial stiffness depending on the inertial force and temperature

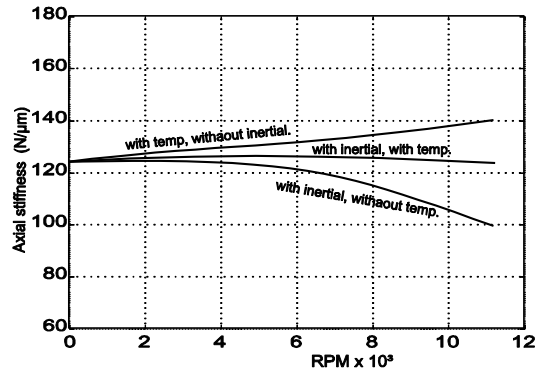


Fig. 13 Axial stiffness depending on the inertial force and temperature

3.3. Effect of contact angle on the stiffness coefficient

A radial force of $F_r = 3000$ N applied to the bearing, and the effect of contact angle (α) on the stiffness coefficients are investigated and shown in the Figures 14, 15 and 16 for diagonal and off-diagonal elements of matrix, respectively. The stiffness coefficients k_{xx} , k_{yy} and k_{zz} of all three arrangements are identical under a pure radial load (Fig. 14). Radial stiffness k_{yy} and k_{zz} have a similar trend, as they have a maximum value for $\alpha = 0^\circ$ (deep groove ball bearing). On the other hand, axial stiffness k_{xx} has minimum when $\alpha = 0^\circ$, reaches its maximum about $\alpha = 60^\circ$ to 65° , and then decreases for higher α values. The bearings with $\alpha \geq 45^\circ$ are often called “thrust bearings”, and thus, an increase in k_{xx} for higher α is an expected result. On Figure 15 and 16 are shown angular stiffness $k_{\theta_y\theta_y}$ and $k_{\theta_z\theta_z}$, which depend on the bearing configuration. $k_{\theta_y\theta_y}$ and $k_{\theta_z\theta_z}$ of the “O” arrangement are higher than the other consider arrangements on all α values. As well $k_{\theta_z\theta_z}$ is greater than $k_{\theta_y\theta_y}$ for all consider bearing arrangements.

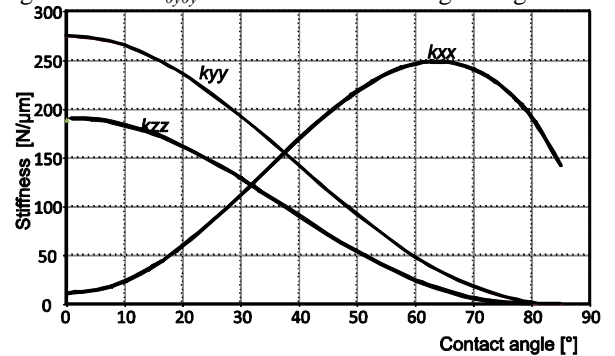


Fig. 14. Variations in the diagonal stiffness elements for all arrangement

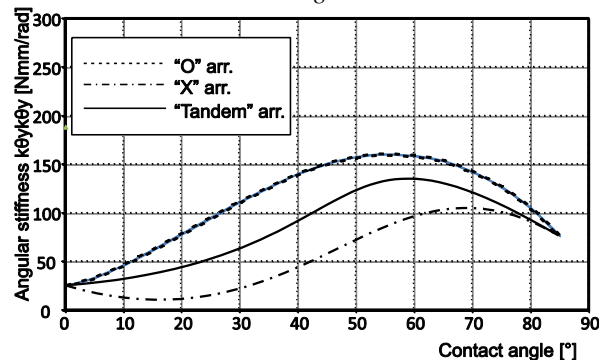


Fig. 15. Variations in the angular stiffness $k_{\theta_y\theta_y}$

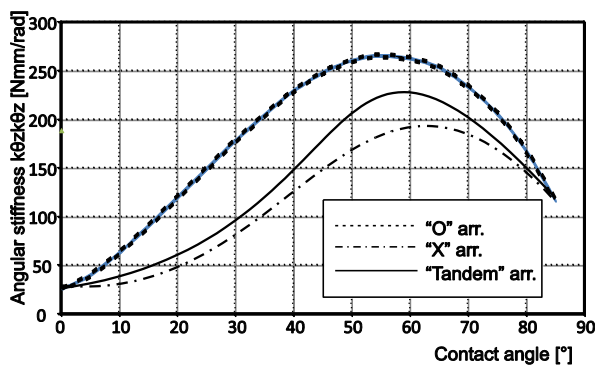


Fig. 16. Variations in the angular stiffness $k_{\theta z}$

4. CONCLUSION

The main goal contribution of this paper is the development of the five dimensional stiffness matrix for duplex angular contact ball bearings of “O”, “X”, and “TANDEM” arrangements. Proposed model of the bearing provides a useful tool in the static and dynamic analyses of angular contact ball bearings, such as the vibration analysis of machine tool spindle (shaft-bearing systems). The diagonal elements of the stiffness matrix k_{xx} and k_{yy} are verified with the catalog's stiffness of the most important bearing manufacturers. Excellent agreement between the proposed model and the catalog values has been obtained. Some changes in matrix elements are further investigated with the proposed model by varying bearing loads and preload, and contact angle, of the bearing to provide some insight.

This mathematical model is also valid for double row angular contact ball bearings or HUB unit bearings (integrate unit) when the surrounding structural elements (shaft, housing and bearing rings) are sufficiently rigid.

ACKNOWLEDGMENTS

In this paper, some results of the project *Contemporary approaches to the development of special solutions related to bearing supports in mechanical engineering and medical prosthetics*–TR 35025, carried out by the Faculty of Technical Sciences, University of Novi Sad, Serbia, are presented. The project is supported by the Ministry of Science and Technological Development of the Republic of Serbia.

REFERENCES

- [1] CAO, Y. (2006) *Modeling of high-speed machine tools spindle system*, Doctoral Dissertation, The University of British Columbia
- [2] GUNDUZ, A. (2012) *Multi-dimensional stiffness characteristics of double row angular contact ball bearings and their role in influencing vibration modes*, Doctoral Dissertation, The Ohio State University
- [3] HARRIS, T., A., MICHAEL, N. K. (2007) *Rolling bearing analysis: Advanced Concepts of Bearing Technology*, Taylor & Francis Group

- [4] HOUPERT, L. (1997) *A Uniform Analytical Approach for Ball and Roller Bearings Calculations*, Journal of Tribology, Vol. 119, No. 4, pp. 851-858
- [5] JONES, A., B. (1960) *A general theory for elastically constrained ball and roller bearings under arbitrary load and speed conditions*, Journal of Basic Engineering Transactions of the ASME, Vol., No. 82, pp. 309-320
- [6] ZELJKOVIC, M. (1996) *System for Automated Design and Behavior Identification of Machine Tool Spindle Assembly*, Doctoral Dissertation, University of Novi Sad, Faculty of Technical Sciences, Novi Sad, , 1996
- [7] ZELJKOVIC, M., ZIVKOVIC, A., BOROJEV, L. (2005) *Influence of the bearing configuration on the high-speed main spindle behavior*, Machine Engineering Vol. 3, No. 1-2, pp. 165-176.
- [8] ŽIVKOVIĆ, A. (2013): *Computer and experimental analysis of behavior ball bearings for special applications*, Doctoral Dissertation, Faculty of technical science, University of Novi Sad, Serbia.
- [9] ZIVKOVIC, A., ZELJKOVIC, M. TABAKOVIC, S., MILOJEVIC, Z. (2015): *Mathematical modeling and experimental testing of high-speed spindle behavior*, Int J Adv Manuf Technol, Vol. 77, pp. 1071-1086
- [10] ZVERV, I., PYOUN, Y.S., LEE, B. K., KIM, J. D., JO, I., COMBS, A. (2005) *An elastic deformation model of high speed spindles built into ball bearings*, Journal of Materials Processing Technology, Vol. 170, pp. 570-578

CORRESPONDANCE



Aleksandar ŽIVKOVIĆ, Ass. Prof.
University of Novi Sad
Faculty of technical science
Trg Dositeja Obradovića 6
21000 Novi Sad, Serbia
acoz@uns.ac.rs



Milan ZELJKOVIC, Prof.
University of Novi Sad
Faculty of technical science
Trg Dositeja Obradovića 6
21000 Novi Sad, Serbia
milanz@uns.ac.rs



Slobodan TABAKOVIC, Ass. Prof.
University of Novi Sad
Faculty of technical science
Trg Dositeja Obradovića 6
21000 Novi Sad, Serbia
tabak@uns.ac.rs

ON THE FRICTIONAL HEATING OF SPUR GEARS OPERATING UNDER LOW ROTATIONAL SPEEDS

Janko D. JOVANOVIĆ
Radoš B. BULATOVIĆ

Abstract: *The most significant problem encountered while running a gear under continuous operation is the thermal effects on the surface failure, such as hot scoring, wear, surface pitting, micropitting and thermal cracking. Continuous operation of gear transmissions running under low rotational speeds, causing mixed lubrication, generates a high temperature rise within tooth contacts and heats up the gear surface, which can cause thermal shock on the tooth surface as well as lubrication breakdown. For these reasons the surface temperature holds the critical information about the condition of a gear. This paper deals with numerical simulation of spur gear frictional heating based on control volume finite element method in order to establish a valid numerical model for investigation of temperature distribution in spur gear operating under mixed lubrication conditions.*

Key words: *spur gear, mixed lubrication, frictional heat, control volume finite element method*

1. INTRODUCTION

Mechanical power transmission by multiplying the angular speed under a constant transmission ratio represents the function of a large group of products known as speed multipliers. Most wind turbines, Fig.1, and hydro systems drive trains include a gearbox to increase the speed of the turbine shaft to the generator.



Fig.1: Wind turbine

An increase in speed is needed because the turbine shaft turns at low rotational speed much lower than is required by most electrical generators. Typical wind turbine input shaft rotational speed for a 2 MW machine is between 14 and 20 rpm with output shaft rotational speed up to 1800 rpm [1]. Larger hydroelectric turbines rotate at 35-75 rpm, and smaller ones as fast as 150 rpm [2].

One stage planetary and two-stage parallel shaft wind turbine gearbox, consisted of spur and helical gears, is shown in Fig.2 [3].

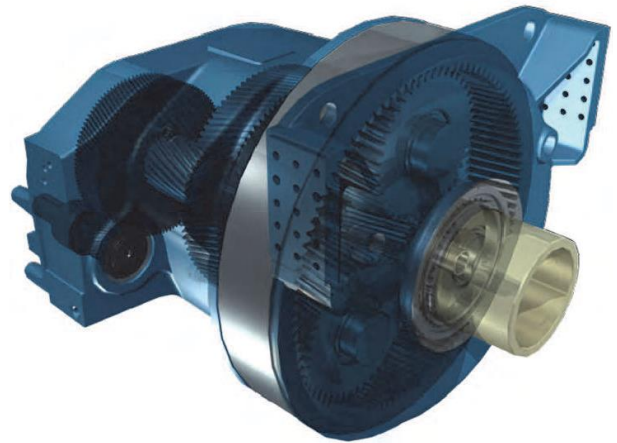


Fig.2: Wind turbine gearbox

The increasing development of tribological studies has improved our knowledge of the mechanisms of lubrication that take place in low rotational speed or/and highly loaded contacts such as those that occur in gears and rolling bearings of wind and hydroelectric turbine gearboxes. These contacts operate in elastohydrodynamic lubrication when there is a complete separation of surfaces, resulting in fluid film lubrication. However, demanding working conditions often cause a loss in continuity of the lubrication film and the existence of direct contacts between surface asperities. Mixed lubrication takes place in these conditions and the interactions between the surfaces lead to an increase in the friction coefficient and the working temperature. Tooth surface temperature has a significant effects on gear performance and failure. Tooth temperature and

thermal behaviour of gears are affected by gear geometry, rotational speed, applied loads, lubrication and operational conditions. Gear parameters and tooth profile have direct influences on load sharing and pressure distribution, and tooth sliding along the contact path of the meshing teeth. Relative sliding of the meshing teeth under mixed lubrication results in significant frictional heat generation, which is determined by the load sustained, rotational speed and coefficient of friction. Heat generated is conducted into the gear teeth and is also taken away by the cooling lubricant applied on the gear wheel and tooth flank. The frictional heat flux generated on the tooth flank and heat transfer on the gear surface and tooth flanks have a significant influence on the temperature variation and distributions. Consequently they affect the surface failure, such as hot scoring, wear, surface pitting, micropitting and thermal cracking. Experimental techniques, theoretical approaches and numerical modeling methods have been used to investigate interactions in relation to heat generation, heat transfer and lubrication effects under combined conditions of rotational speed and load.

Townsend et al. [4] have conducted tooth temperature analysis of spur gear using the finite element method as well as experimental measurements using infrared radiometric microscope. The effects of oil pressure on the jet cooling, oil inlet temperature and oil jet impingement depth with consideration of load applied and operating speed on average and surface temperatures have been investigated in their research. Wang et al. [5] have developed numerical and analytical approach to determine spur gear dynamic load, lubricant film thickness, bulk equilibrium and tooth flash temperatures in gear contacts. Wang et al. [6] have derived the distribution of bulk equilibrium temperature and flash temperature along the contact path for pinion and gear teeth. Koshigoe et al. [7] developed computer program for the computation of running gear temperature using Green's functions to predict the gear surface temperature. Long et al. [8] have conducted tooth temperature analysis of spur gear using the finite element method as well as experimental measurements using infrared camera and thermocouples. The effects of gear parameters, such as tooth width, tooth module with consideration of load applied and operating speed on average and surface temperatures have been investigated in their research. Yi et al. [9] have conducted spur gear surface temperature monitoring by using miniature thermocouples. They have investigated various effects of load, rotational speed, and meshing point on surface temperature. However, a general approach to temperature analysis for engineering applications and an investigation of the impact of operational conditions on surface temperature are currently limited.

The development of numerical modeling procedure to evaluate thermal behaviour and tooth temperature under mixed lubrication is described in this paper. Frictional heat generation at the meshing teeth along contact path is estimated and analysed. Two-dimensional control volume finite element model of the gear tooth is established to investigate temperature distributions and variations along contact path over a range of applied loads and operating speeds with consideration of lubrication conditions.

2. METHODS

2.1. Heat equations and boundary conditions

As a result of the frictional heat between the teeth engaged in a pair of gears, the temperature of the tooth surface changes during the meshing process. However, the bulk temperatures of gears can achieve a thermal equilibrium after many cycles at a fixed load. After reaching an equilibrium state, the temperature changes in the gear tooth body during one revolution are very small. This is because most of the heat generated on the surface is taken away by the cooling lubricant and the time is very limited for heat conduction from surface into body under high-speed operations. By assuming every single tooth of the gear follows the same cycle, i.e. heating, then convective cooling and conduction, the heat balance of the gear can be analysed by establishing a single-tooth model (Fig.3).

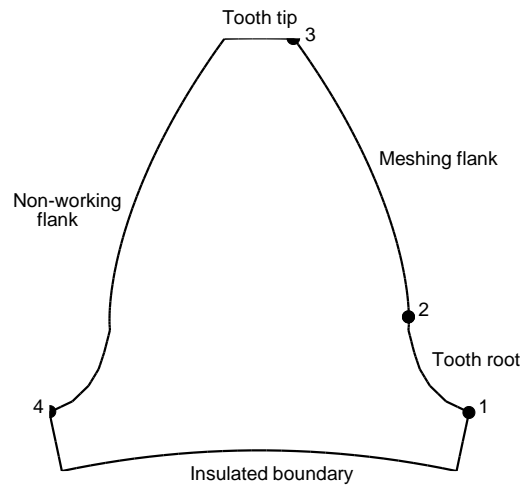


Fig.3: Simulated gear tooth geometry and all boundaries with different conditions

The transient heating of the gear tooth is described by [7,8]:

$$\frac{\partial T}{\partial t} = \alpha_{TD} \cdot \nabla^2 T \quad (1)$$

where $\nabla^2 = \partial^2/\partial x^2 + \partial^2/\partial y^2$, α_{TD} is thermal diffusivity and $T=T(x,y)$ is temperature changing with time t and position x,y . Convective boundary conditions for different boundaries are specified as follows [8]:

$$-\left. \frac{\partial T}{\partial n} \right|_{1-2} = -\left. \frac{\partial T}{\partial n} \right|_{3-4} = h_{TC} \cdot (T - T_b)$$

$$-\left. \frac{\partial T}{\partial n} \right|_{2-3} = h_{TC} \cdot (T - T_b) + q_F \quad (2)$$

$$\left. \frac{\partial T}{\partial n} \right|_{4-1} = 0$$

where h_{TC} is heat transfer coefficient, T_b is bath temperature of cooling lubricant and q_F is frictional heat flux.

2.2. Frictional heat

Frictional heat generation during gear meshing is determined by applied load, rotational speed and lubrication on the tooth flank. The frictional heat flux varies over the tooth flank due to changes of sliding velocity, normal load and coefficient of friction along the contact path.

The differences in rotational speed and sizes of the pinion and gear result in unequal velocities of the pinion and gear in the direction of motion. Therefore, absolute velocities of the meshing teeth on the pinion and gear in the direction of contact tangents are different and consequently relative sliding between the tooth flanks of the pinion and gear occurs and causes frictional heat generation. The absolute velocities of the meshing point on the pinion and gear in the direction of contact tangents, u_1 and u_2 , and the sliding velocity of the meshing points Δu can be expressed as [8]:

$$\begin{aligned} u_1 &= 2 \cdot \pi \cdot n_1 \cdot \left(\frac{1}{2} \cdot d_1 \cdot \sin \alpha_p \pm g \right) \\ u_2 &= 2 \cdot \pi \cdot n_2 \cdot \left(\frac{1}{2} \cdot d_2 \cdot \sin \alpha_p \mp g \right) \end{aligned} \quad (3)$$

$$\Delta u = u_1 - u_2$$

where n_1 and n_2 are the rotational speed of pinion and gear, d_1 and d_2 the pitch diameter of pinion and gear, α_p the pressure angle and g the distance of meshing point from pitch point, that could be expressed as [8]:

$$g = \mp \frac{1}{2} \cdot d_1 \cdot \sin \alpha_p \pm \sqrt{\left(\frac{1}{2} \cdot d_1 \cdot \sin \alpha_p \right)^2 - \left(\frac{1}{2} \cdot d_1 \right)^2} + r \quad (4)$$

where r is the radius of meshing point on the pinion. The upper signs in equations (3) and (4) are for a contact point on the addendum flank of the pinion or the dedendum flank of the gear. The lower signs are for a contact point on the dedendum flank of the pinion or the addendum flank of the gear.

The contact pressure on the tooth flank could be determined by normal load applied on the tooth, gear material properties and the tooth profile. Based on Hertzian contact theory, the average compressive pressure for an arbitrary meshing pair of teeth p_N can be expressed as [8]:

$$p_N = \frac{\pi}{4} \cdot \sqrt{\frac{F_N \cdot E}{2 \cdot \pi \cdot R \cdot b \cdot (1 - \nu^2)}} \quad (5)$$

where F_N is the normal load at meshing point, E the reduced modulus of elasticity, ν the Poisson's ratio and R the equivalent curvature radius of meshing point.

It is very common for machine elements such as gears to operate in elastohydrodynamic (EHD), mixed or even boundary film lubrication. These regimes of lubrication correspond to different ranges of specific film thickness Λ [10]:

$$\Lambda = \frac{h_0}{\sqrt{\sigma_1^2 + \sigma_2^2}} \quad (6)$$

where σ_1 and σ_2 are the root mean square roughness parameter of pinion and gear and h_0 the minimum lubricant film thickness. The EHD lubrication corresponds to Λ values greater than 2, for lower values, the contact operates under mixed lubrication $0.5 < \Lambda < 2$, or under boundary lubrication $\Lambda < 0.5$ [11]. Depending on the specific film thickness a load share function for spur gear line contact f_Λ can be established for the normal load supported by the lubricant film F_L and supported by the roughness asperities in boundary lubrication F_B [12]:

$$f_\Lambda = 0.84 \cdot \Lambda^{0.23} \quad (7)$$

$$F_L = f_\Lambda \cdot F_N \quad , \quad F_B = (1 - f_\Lambda) \cdot F_N$$

Friction force F_T and coefficient of friction μ under mixed lubrication is given by equation [13,14]:

$$\begin{aligned} F_T &= \mu_E \cdot f_\Lambda^{1.2} \cdot F_N + \mu_B \cdot (1 - f_\Lambda) \cdot F_N \\ \mu &= \frac{F_T}{F_N} = \mu_E \cdot f_\Lambda^{1.2} + \mu_B \cdot (1 - f_\Lambda) \end{aligned} \quad (8)$$

where μ_E and μ_B are the coefficients of friction in full film lubrication and boundary lubrication.

Regarding the coefficient of friction, various results have been published for boundary lubrication, in the case of steel-steel contacts, values have been determined around $\mu_B = (0.07 \div 0.15)$ which depend on the type and amplitude of roughness [15].

In elastohydrodynamic lubrication regime, the viscous properties of the lubricant play a fundamental role on friction. The Carreau model is one of the most used to determine generalised viscosity η_G for shear-thinning lubricants under severe working conditions typical of elastohydrodynamic lubrication [16]:

$$\eta_G = \eta \cdot \left[1 + \left(\frac{\eta \cdot \dot{\gamma}}{G} \right)^2 \right]^{\frac{n-1}{2}} \quad \text{with } \eta = \eta_o \cdot e^{\alpha \cdot p} \quad (9)$$

$$\alpha = \left[\int_0^\infty \frac{\eta_o}{\eta(p)} dp \right]^{-1} \quad \text{and } \dot{\gamma} = \frac{\Delta u}{h}$$

where η_o is the viscosity at ambient pressure ($p=0.1$ MPa), p the elastohydrodynamic pressure, G the shear modulus, n the power-law exponent, Δu the sliding velocity, h the film thickness and α is reciprocal asymptotic isoviscous pressure coefficient, which is determined within the pressure range bounded not by the infinity but by the maximum Hertzian pressure. The integral in equation (8) is evaluated, piecewise, by assuming that the response for pressure greater than p_N follows the exponential rule with coefficient α_N . The formula for α is then [17]:

$$\alpha \approx \left[\frac{\eta_o}{\alpha_N \cdot \eta_N} + \sum_{i=1}^N \frac{\eta_o}{\alpha_i} \cdot \frac{\eta_i - \eta_{i-1}}{\eta_i \cdot \eta_{i-1}} \right] \quad (10)$$

Afterwards shear stress distribution τ_E can be determined by the following equation:

$$\tau_E = \eta_G \cdot \dot{\gamma} \quad (11)$$

Taking into account two simplifying hypotheses that have been proven to be reasonable in elastohydrodynamic lubrication [18]: a pressure based on Hertzian distribution and a constant film thickness, the coefficient of friction in full film lubrication can be determined by integrating shear stress distribution in the contact area which gives the force of friction and dividing it by normal load supported by the lubricant film [13,14]:

$$\mu_E = \frac{A}{F_L} \cdot \left(\frac{\eta_o \cdot \Delta u}{h} \right)^n \cdot G^{1-n} \cdot e^{n \cdot \alpha \cdot p_{ef}} \quad (12)$$

where p_{ef} is the effective pressure [19]:

$$p_{ef} = \frac{1}{n \cdot \alpha} \cdot \ln \left[\begin{array}{l} 1 + \frac{\pi \cdot n \cdot \alpha \cdot p_o}{12} \cdot \left(\frac{2 + \sqrt{3}}{2} \cdot e^{n \cdot \alpha \cdot p_o \cdot \sqrt{\frac{1+\sqrt{3}}{2}}} + \frac{2 - \sqrt{3}}{2} \cdot e^{n \cdot \alpha \cdot p_o \cdot \sqrt{\frac{1-\sqrt{3}}{2}}} \right) \end{array} \right] \quad (13)$$

where p_o it the maximum Hertzian pressure and A is contact area of line contact:

$$p_o = \frac{2 \cdot \left(\frac{F_L}{L} \right)}{\pi \cdot a}, \quad A = 2 \cdot a \cdot L$$

$$a = \sqrt{\frac{8 \cdot \left(\frac{F_L}{L} \right) \cdot R}{\pi \cdot E}}$$

where a is the halfwidth of Hertzian contact zone, L the length of line contact.

The film thickness depends primarily on the inlet conditions in the contact and can be approximated as the central value h_c [13,14]:

$$h_c = h_{Nct} \cdot \left[\left(1 + 0.79 \cdot \left(\left(1 + \frac{SRR}{100} \right) \cdot \frac{u_m \cdot \eta_o}{h_{Nct} \cdot G} \right)^{\frac{1}{1+0.002 \cdot SRR}} \right)^{-3.6(1-n)^{1.7}} \right] \quad (15)$$

$$h_{Nct} = \varphi_i \cdot h_{Ncb} \quad \text{and} \quad SRR = \frac{\Delta u}{u_m} \cdot 100$$

where SRR is the slide to roll ratio, u_m the average velocity and h_{Nct} the Newtonian central film thickness at inlet temperature. Unlike bath temperature, inlet temperature is initially unknown and the use of a thermal

factor φ_i is therefore needed to consider the shear heating effects in the inlet zone:

$$\varphi_i = \frac{1 - 13.2 \cdot \left(\frac{p_o}{E} \right) \cdot L_t^{0.42}}{1 + 0.213 \cdot \left[1 + 2.23 \cdot \left(\frac{\Delta u}{u_m} \right)^{0.83} \right] \cdot L_t^{0.64}} \quad (16)$$

$$L_t = \frac{\beta \cdot \eta_o \cdot u_m^2}{K_l}$$

where β is the temperature-viscosity coefficient, K_l the lubricant thermal conductivity. The Newtonian central film thickness at bath temperature h_{Ncb} can be determined by the well known Hamrock equation for line contact:

$$h_{Nc} = 2.154 \cdot \alpha^{0.47} \cdot (\eta_o \cdot u_m)^{0.692} \cdot E^{0.110} \cdot R^{0.308} \cdot p_o^{-0.332} \quad (17)$$

$$h_{Ncb} = h_{Nc}(T_b)$$

The properties of the lubricant are assessed at contact temperature T , that is, the average temperature of the lubricant within the high pressure contact zone. This temperature is calculated using the classic flash theory for dry contact [20] generalised for lubricated contact [21] which for low film thickness, typical for mixed lubrication, can be expressed in the following way:

$$T = T_{in} + T_f \quad (18)$$

where T_{in} is the inlet temperature of lubricant which may be calculated using the following equation:

$$\left[\alpha(T_{in}) \right]^{0.47} \cdot \left[\eta_o(T_{in}) \right]^{0.692} = \varphi_i(T_b) \cdot \left[\alpha(T_b) \right]^{0.47} \cdot \left[\eta_o(T_b) \right]^{0.692} \quad (19)$$

The flash temperature rise T_f can be estimated as the average flash temperature for each contact surface T_{fi} ($i=1,2$) which are separately calculated as if all the heat generated was conducted to both surfaces:

$$\frac{1}{T_f} = \frac{1}{T_{f1}} + \frac{1}{T_{f2}} \quad (20)$$

The average flash temperature depend on the Peclet number P_{ei} ($i=1,2$) which is related to heat transferred into the bulk of each contacting body [22]:

$$P_{ei} = \frac{u_i \cdot a}{2 \cdot \chi_i} \quad (21)$$

$$\chi_i = \frac{K_i}{\rho_i \cdot c_i}$$

where χ_i is the thermal diffusivity, K_i the thermal conductivity, ρ_i the density, c_i the specific heat and u_i the velocity of the surface. The average flash temperature for line contacts is calculated in the following way [22]:

$$T_{fi} = 0.318 \cdot \frac{\mu \cdot \left(\frac{F_N}{L}\right) \cdot \Delta u}{K_i \cdot P_{ei}} \quad \text{if } P_{ei} < 0.1$$

$$\left(\frac{-2.303 \cdot P_{ei} \cdot \log_{10}(2 \cdot P_{ei}) + 1.616 \cdot P_{ei}}{1.616 \cdot P_{ei}} \right)$$

$$T_{fi} = 0.159 \cdot \frac{\mu \cdot \left(\frac{F_N}{L}\right) \cdot \Delta u}{K_i \cdot P_{ei}} \quad \text{if } 0.1 < P_{ei} < 5$$

$$\left(\frac{0.423 + 2.663 \cdot P_{ei} - 0.649 \cdot P_{ei}^2 + 0.062 \cdot P_{ei}^3}{0.649 \cdot P_{ei}^2 + 0.062 \cdot P_{ei}^3} \right)$$

$$T_{fi} = 0.376 \cdot \frac{\mu \cdot \left(\frac{F_N}{L}\right) \cdot \Delta u}{K_i \cdot P_{ei}^{0.5}} \quad \text{if } P_{ei} > 5$$

Lubricant density at atmospheric pressure and different temperatures ρ_l can be determined by the following empirical relationship:

$$\rho_l = \rho_{l,o} \cdot [1 - \beta \cdot (T - T_o)] \quad (23)$$

where $T_o = 20^\circ\text{C}$ is the room temperature and ρ_o the density at the room temperature.

The heat flux on the contact area of the pinion and gear, q_1 and q_2 , generated by frictional sliding of the meshing teeth could be expressed as [8]:

$$q_1 = \gamma \cdot \mu \cdot p_N \cdot \Delta u \quad (24)$$

$$q_2 = (1 - \gamma) \cdot \mu \cdot p_N \cdot \Delta u$$

where γ is the partition constant of the heat flux between the contact areas of two engaged teeth. During rotation every tooth of the pinion or gear receives the heat input once over each revolution. Thus averaged frictional heat flux for the meshing areas on the pinion and gear teeth over one revolution can be expressed as [8]:

$$q_{F1} = \frac{2 \cdot a \cdot n_1}{u_1} \cdot q_1 \quad (25)$$

$$q_{F2} = \frac{2 \cdot a \cdot n_2}{u_2} \cdot q_2$$

Heat transfer coefficient

The method of cooling for the gear transmission is bath cooling, by which the oil is supplied to each tooth flank once per revolution. This process is characterized as intermittent fling-off cooling with a sequence of transient and forced heat convection as described by DeWinter and Blok [23]. An approach for estimating the heat transfer coefficient on the tooth flank is developed based on a model where the frictional heat is withdrawn from the tooth flank by centrifugal fling-off process. The heat transfer coefficient h_{TC} then can be expressed as [8,23]:

$$h_{TC} = \frac{\sqrt{\omega}}{2 \cdot \pi} \cdot \sqrt{K_l \cdot \rho_l \cdot c_l} \cdot \left(\frac{v_o \cdot H}{\alpha_p \cdot r} \right)^{1/4} \cdot q_n \quad (26)$$

where ω is the angular speed, K_l the lubricant conductivity, c_l the lubricant specific heat, v_o the lubricant kinematic viscosity, ρ_l the lubricant density, H is height of contact point on the tooth and q_n is normalized cooling capacity.

2.3. Control volume finite element method

Control volume methods are viewed as bridging between finite difference and finite element methods, with ability to adopt and adapt the advantage of these methods while neglecting the drawbacks. The control volume method that seems to obtain the maximum advantage of this hybrid view of point are those based on finite element method, referred to as control volume finite element method. A notable feature of this method is the relative ease by which it can be applied to both solids and fluids problems.

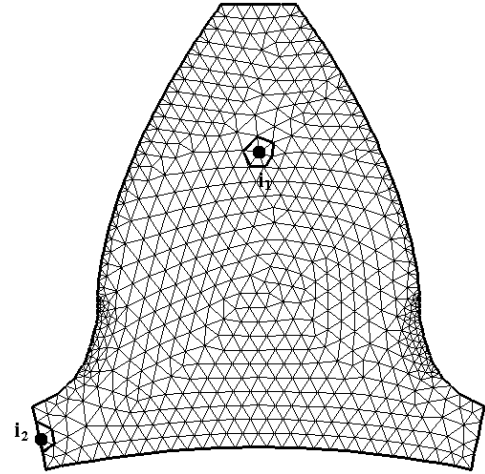


Fig.4: Gear tooth geometry with mesh of triangular elements

The key feature of this method is that control volumes can be constructed around the node points on an unstructured finite element mesh that conforms to an arbitrarily shaped domain. With this construction, the fluxes across control volume faces can be approximated by using finite element interpolation. Balancing these fluxes, leads to a physically based representation of the governing equation as a discrete set of equations in terms of mesh nodal values. Equation (1) could be alternatively expressed in the integral form [24]:

$$\frac{d}{dt} \int_{\Omega} T \cdot dA = \oint_S \alpha \cdot \nabla T \cdot n \cdot dS, \quad x \in \Omega \quad (27)$$

where Ω is arbitrary two dimensional domain. In this paper this domain is gear tooth geometry shown in Fig.3. The integral form of conservation equation (12) is most suitable for developing numerical solution based on control volume finite element method (CVFEM) [24]. The key objective of CVFEM is to reduce the integral form of governing field equation (12) to set of discrete algebraic equations in the unknown nodal values of T .

First step of this procedure is meshing two dimensional domain into mesh of linear triangular elements, Fig.4.

The continuous unknown field of temperature over triangular elements, can be expressed as the linear combination of the temperature values at nodes placed at the vertices of triangular elements [24]:

$$T(x, y) = \sum_{j=1}^3 N_j(x, y) \cdot T_j \quad (28)$$

where $N_j(x, y)$ are shape functions and T_j are nodal temperature values.

Then, the regions of support and control volumes attached to each node i are identified. The domains of the integral in (26) are associated with the regions of support. Regions of support for internal node 1 and boundary node 2 are shown in Fig.4. For each node i in the mesh the region of support is identified by counting and listing all the neighboring nodes k that share a common element side with node i . Using numerical integration and shape function approximations (27) of T in each element of i^{th} support, equation (26) is expanded in terms of nodal values of T in the support. On gathering terms, the resulting equation for node i can be written in the general discrete form [24]:

$$a_i \cdot T_i = \sum_{nb} a_{nb} \cdot T_{nb} + b_i \quad (29)$$

where a_i is coefficient associated with the unknown nodal values of T_i and a_{nb} are coefficients associated with the unknown nodal values of T_{nb} at neighboring nodes in the i^{th} support, and the additional coefficient b_i accounts for the contribution from sources, transients and boundaries. Equation (28) provides an algebraic relationship between the value of T at node i and the neighboring nodes nb in its support. More details on determination of coefficients a_i , a_{nb} and b_i could be found in [24]. The final step is to solve equation (28) and to determine the nodal field values T_i . Gauss-Seidel iterative solver is used to find solution with specified tolerance.

2.4. Meshing gear tooth geometry

A special programme is developed in Visual Lisp to generate gear tooth geometry in AutoCAD (AutoDesk, San Rafael, California, USA) environment. Generated tooth profile is then exported in the ACIS format file.

Output AutoCAD file, in ACIS format, is then imported in Ansys (Ansys, Canonsburg, Pennsylvania, USA) and gear tooth profile is meshed with finite element mesh of linear triangular elements. Meshed model of gear tooth profile is consisted of 1584 finite elements with 838 nodes, Fig.4. Data on mesh nodes and elements are then exported in the ASCII format files.

Finally, a special programme is developed in Matlab (MathWorks, Natick, Massachusetts, USA) to process output Ansys files, in ASCII format, and to prepare adequate data structure on mesh nodes and elements for the CVFEM modeling.

3. RESULTS AND DISCUSSION

Analysis of frictional heating of spur gear under low rotational speed is conducted for gears of intermediate stage of wind turbine gearbox shown in Fig.2. Basic

running conditions of gearbox for the calculations: power $P=2$ MW, input torque $T_{input}=1273$ kNm, input speed $n_{input}=15$ rpm, total gear ratio $i_E \approx 108$, planetary stage ratio $i_{PS}=5.67$, intermediate stage ratio $i_{IS}=4.25$, high stage ratio $i_{HS}=4.48$ [3]. Basic dimensions and running conditions of intermediate stage spur gears for the calculations: $z_1=85$, $z_2=20$, module $m=12$ mm, face width $b=400$ mm, pressure angle $\alpha_p=26^\circ$, $T_f \approx 225$ kNm, $n_f \approx 85$ rpm [3], corresponding distributions of normal load and sliding velocity along the line of action – LoA is shown in the following figures.

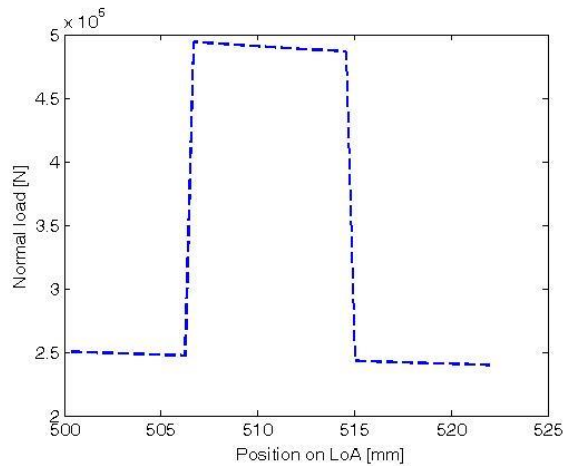


Fig.5: Distribution of normal load along LoA

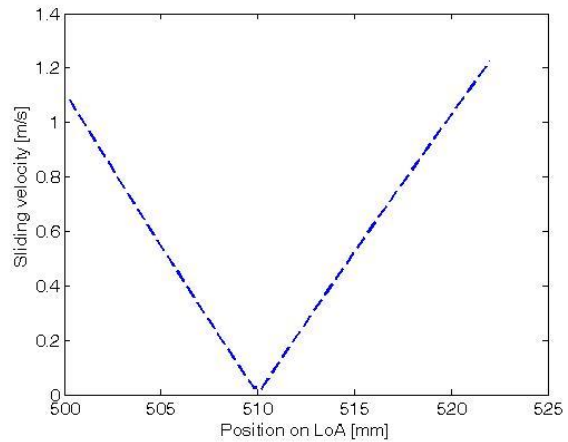


Fig.6: Sliding velocity along LoA

Both gears are made of 665M17 (EN-34) steel with the following basic mechanical and thermal properties: modulus of elasticity $E=185.42$ GPa, Poisson's ratio $\nu=0.3$, thermal conductivity $K=41.8$ W/m·K, thermal diffusivity $\chi=1.077 \cdot 10^{-5}$ m²/s, specific heat $c=493$ J/kg·K [8]. This gear set is case-hardened and ground to a surface finish of $\sigma_1=\sigma_2=0.6$ μ m.

Synthetic oil poly-alfa-olefine PAO-6, with following properties at bath temperature $T_b=80^\circ$ C, is used as lubricant in gearbox: $\rho_l=0.83$ kg/dm³ temperature-viscosity coefficient $\beta=0.033$ K⁻¹, $n=0.81$, shear modulus $G=0.1$ MPa, thermal conductivity $K_f=0.15$ W/m·K, specific heat $c_f=2200$ J/kg·K [14]. Lubricant viscosity at ambient pressure and piezoviscous coefficient: $\eta_o=25$

m·Pa·s and $\alpha=11.5 \text{ GPa}^{-1}$ at $T=40^\circ\text{C}$, $\eta_o=12.57 \text{ m·Pa·s}$ and $\alpha=10.1 \text{ GPa}^{-1}$ at $T=60^\circ\text{C}$, $\eta_o=7.36 \text{ m·Pa·s}$ and $\alpha=9.0 \text{ GPa}^{-1}$ at $T=80^\circ\text{C}$, $\eta_o=4.78 \text{ m·Pa·s}$ and $\alpha=8.2 \text{ GPa}^{-1}$ at $T=100^\circ\text{C}$ [14].

The partition constant of the heat flux between the contact areas of two engaged teeth γ is 0.5 [8]. Boundary friction coefficient value is $\mu_B=0.13$ [14].

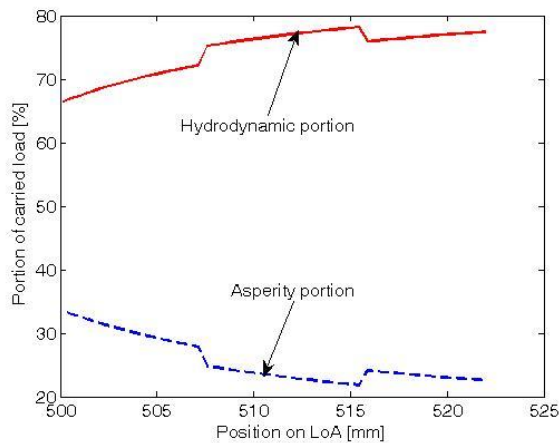


Fig.7: Portion of load taken by lubricant film and by asperities along LoA

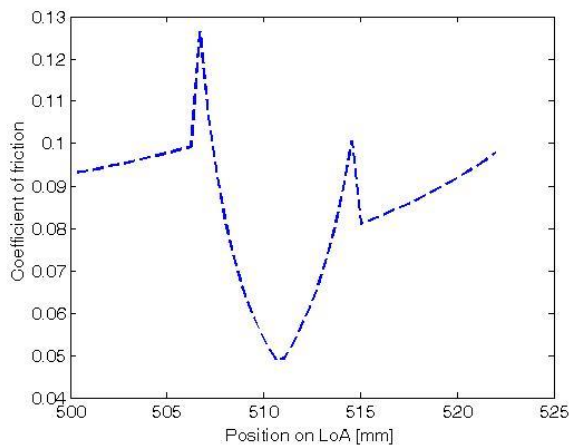


Fig.8: Distribution of coefficient of friction along LoA

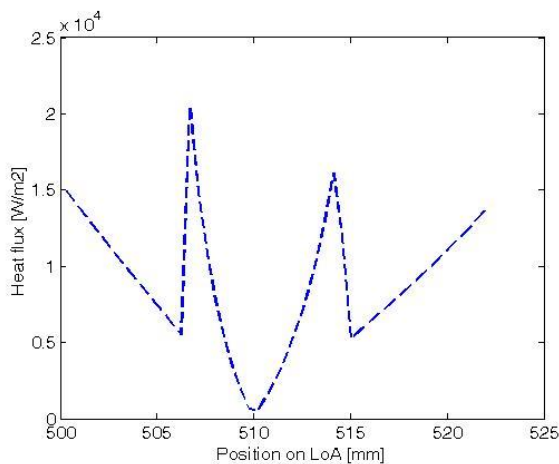


Fig.9: Distribution of heat flux along LoA

The variation of portion of carried load by lubricant film and by asperities along LoA is shown in Fig.7. The variation of coefficient of friction and corresponding heat flux under mixed lubrication are shown in Fig.8 and Fig.9. Determined CVFEM temperature distribution over the pinion tooth is illustrated in Fig.10.

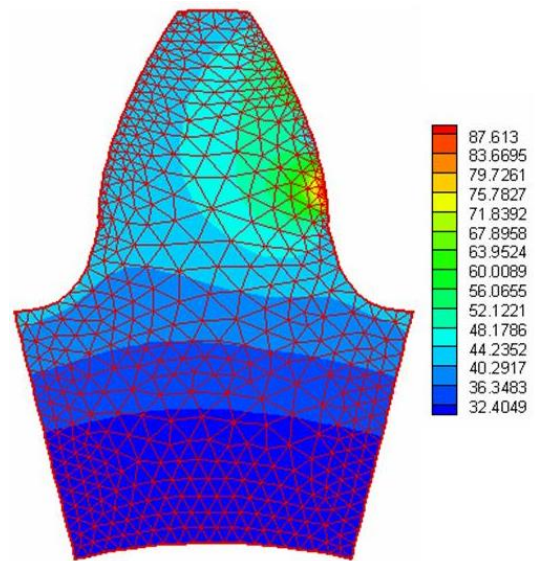


Fig.10: Distribution of pinion temperature

The temperature distribution matches the frictional heat flux distribution which results in the maximum temperature occurring at the dedendum close to the pitch line. The surface temperature on the tooth flank is substantially higher than the internal tooth temperature. Due to the non-uniform distribution of frictional heat flux (Fig.9), two peak values of surface temperature take place on the tooth flank.

4. CONCLUSION

A mixed lubrication model of spur gear has been presented for low rotational speeds, based on a simplified analytical procedure that considers the thermal effects in the contact and the rheology of the lubricant. The procedure described has shown its capacity to estimate the friction coefficient in a simple way. Simultaneously, it allows predicting temperature distribution over spur gear tooth, which improves the analysis of the quantitative influence of the physical phenomena involved and contributes to a better understanding of the results.

REFERENCES

- [1] UKONSAARI, J., BENNSTEDT, N. (2016) Wind turbine gearboxes: Maintenance effect on present and future gearboxes for wind turbines, Energiforsk, Sweden.
- [2] (2006) Power generation: Maximizing hydroelectric turbine performance and reliability, Pall Corporation, New York, USA.
- [3] CARRIVEAU, R. (2011) *Fundamentals and advanced topics in wind power*, InTech.

- [4] TOWNSEND, D.P., AKIN, L.S. (1981) *Analytical and experimental spur gear tooth temperature as affected by operating variables*, Journal of Mechanical Design, Vol.103, No.1, pp.219-226.
- [5] WANG, K.L., CHENG, H.S. (1981) *A numerical solution to the dynamic load, film thickness and surface temperatures in spur gears, Part I: analysis*, Journal of Mechanical Design, Vol.103, No.1, pp.177-187.
- [6] WANG, K.L., CHENG, H.S. (1981) *A numerical solution to the dynamic load, film thickness and surface temperatures in spur gears, Part I: results*, Journal of Mechanical Design, Vol.103, No.1, pp.188-194.
- [7] KOSHIGOE, S., MURDOCK, J.W., AKIN, L.S., TOWNSEND, D.P. (1996) *A computer program for the computation of running gear temperatures using Green's function*, 7th International Power Transmission and Gearing Conference, San Diego, California, USA, pp.1-8.
- [8] LONG, H., LORD, A.A., GETHLIN, D.T., ROYLANCE, B.J. (2003) *Operating temperatures of oil-lubricated medium-speed gears: numerical models and experimental results*, Proceedings of the Institution of Mechanical Engineers, Part G: Journal of Aerospace Engineering, Vol.217, pp.87-106.
- [9] YI, J., QUINONEZ, P.D. (2005) *Gear surface temperature monitoring*, Proceedings of the Institution of Mechanical Engineers, Part J: Journal of Engineering Tribology, Vol.219, pp.99-105.
- [10] TALLIAN, T.E. (1967) *On competing failure modes in rolling contact*, ASLE Transactions, 10(4):418-439.
- [11] BRANDAO, J.A. (2007) *Gear micropitting prediction using the Dang Van high-cycle fatigue criterion*, PhD Thesis, Porto.
- [12] CASTRO, J., SEABRA, J. (2007) *Coefficient of friction in mixed film lubrication: gears versus twin-discs*, Proc. IMechE, Part J: Journal of Engineering Tribology, 221:399-41
- [13] ECHAVARRI, J.O., GUERRA, E.O., CHACON, E.T., LANTADA, A.D., MUNOZ GUIJOSA, J.M. (2016) *Analytical model for predicting friction in line contact*, Lubrication Science, 28:189-205.
- [14] ECHAVARRI, J.O., GUERRA, E.O., CHACON, E.T., RIO LOPEZ, B. (2017) *Friction coefficient in mixed lubrication: A simplified analytical approach for highly loaded non-conformal contacts*, Advances in Mechanical Engineering, 7(7):1-11.
- [15] ZHU, D., HU, Y.A. (2001) *A computer program package for the prediction of EHL and mixed lubrication characteristics, friction, subsurface stresses and flash temperatures based on measured 3D surface roughness*, Tribology Transactions, 44:383-390.
- [16] CARREAU, P.J. (1972) *Rheological equations from molecular network theories*, Journal of Rheology, 16:99-27.
- [17] BAIR, S., LIU, Y., WANG, Q.J. (2006) *The pressure-viscosity coefficient for Newtonian EHL film thickness with general piezoviscous response*, Journal of Tribology, 128:624-631.
- [18] BAIR, S. (2007) *High pressure rheology for quantitative elastohydrodynamics*, Vol.54, Burlington, MA, Elsevier.
- [19] MURAKI, M., DONG, D. (1999) *Derivation of basic rheological parameters from experimental elastohydrodynamic lubrication traction curves of low-viscosity lubricants*, Proc IMechE, Part J: Journal of Engineering Tribology, 213:53-61.
- [20] ARCHARD, J.F. (1958) *The temperature of rubbing surfaces*, Wear, 2:438-455
- [21] OLIVER, A.V., SPIKES, H.A. (1998) *Prediction of traction in elastohydrodynamic lubrication*, Proc IMechE, Part J: Journal of Engineering Tribology, 212:321-332.
- [22] STACHOWIAK, G.W., BATCHELOR, A.W. (2005) *Engineering tribology*, Burlington, MA, Elsevier.
- [23] DEWINTER, A., BLOK, H. (1974) *Fling-off cooling of gear teeth*, Journal of Engineering for Industry, Vol.96, No.1, pp.60-70.
- [24] VOLLER, V.R. (2009) *Basic control volume finite element methods in fluids and solids*, World Scientific Publishing.

CORRESPONDANCE



Janko JOVANOVIĆ, Prof. D.Sc. Eng.
University of Montenegro
Faculty of Mechanical Engineering
Džordža Vašingtona bb
81000 Podgorica, Montenegro
janko@ac.me



Radoš BULATOVIĆ, Prof. D.Sc. Eng.
University of Montenegro
Faculty of Mechanical Engineering
Džordža Vašingtona bb
81000 Podgorica, Montenegro
rados@ac.me

NEW METHODOLOGIES FOR GEAR DESIGN IN ENERGY EFFICIENT POWER TRANSMISSIONS

Ivana D. ATANASOVSKA
Saravanan KARUPPANAN
Santosh PATIL

Abstract: *The optimal gear design with different requirements is imperative in the last few decades. In that sense, one of the main optimization requirements is energy efficiency. In the contemporary machine design procedures, the energy efficiency achieves potential savings of any form of natural resources. In this paper, a new algorithm for increasing the energy efficiency of power transmission systems and their main elements was developed and presented as an attempt to find a unique procedure for this purposes. Based on the detailed analysis of all major influential factors, it is clear that the increase of energy efficiency can be achieved by simultaneous application of new methodologies in all phases i.e. from design to the exploitation of gears and other machine elements and power transmission systems. In this paper a special attention was paid to the application of newly developed methods and development of new methodologies for gear design optimization. One of the highlights of this paper is the suggestion for improvement of the standard calculating procedures for gear pairs.*

Key words: *power transmissions, gears, energy efficiency, FEA*

1. INTRODUCTION

Energy efficiency is an important requirement in the last two decades in a variety of human activities from everyday life to general mechanical production. Everyday utilization of natural energy resources has decreased the availability of these resources. The use of natural resources for two centuries without control has imposed a modern industry's requirement i.e. decrease the consumption of natural resources and increase the energy efficiency of objects and machines in all areas of work and life. The development of equipment for the exploitation of sustainable energy resources is one of the main global tasks for the industries in all progressive countries. Working capacity, reliability and economy of the main elements in this equipment are the basic parameters to be considered by the present engineers. The mechanical, electrical and software engineers have to coordinate the work and effort in developing the machines, structures and factories of the future.

The standard machine elements and assemblies, such as beams, joints, springs, gears, bearings, shafts, etc. form the building blocks of all machines, equipment, structures, and electronic devices. Therefore, increases in efficiency of these main machine elements have a direct impact on the machine system's efficiency, productivity and reliability. Similarly, the energy efficiency of power transmission systems is improved by the optimization of the characteristics of standard machine elements and assemblies, on the basis of new methods.

In the last two decades, many authors have realized the importance of machine elements, assemblies and complex plants research with regards to their energy efficiency. Many projects have been dedicated to the improvements in production and maintenance of the machine's system and its subsystems in order to decrease the consumption of energy and other natural resources.

Ferrero [1] presented a procedure for increasing the energy efficiency of roller bearings. This was achieved by investigating the influences of lubricants, material and sealing on the service life of ball bearings, and mechanical systems related to the ball bearings. A similar approach was used by Kenneth [2], who displayed the advantages of helical gears over spur gears, viz. increased load capacity, reduced wear and low-cost maintenance. Atanasovska and Vuksic [3] developed a new procedure to compare spur and helical gears with regards to stability. Marques *et al.* [4] were taking into account elastic and frictional effects and developed gear load sharing models, which could be used for more precise estimations of gear friction losses and gear efficiency. Some authors have focused their research on investigating machines systems in order to increase the energy efficiency of the aforesaid systems. Mateos-Espejela *et al.* [5] focused their research on the procedures for mill energy efficiency improvement. Mitrovic *et al.* [6] developed new experimental setups to find innovative methods to reduce the maintenance costs for conveyer systems that are utilized in opencast mining. Zivkovic determined the energy loss sources in the case of planetary gear set [7].

2. DEFINITION OF THE ENERGY EFFICIENT POWER TRANSMISSION SYSTEM

Energy efficiency can be defined as “*saving of any kind of natural resources: energy, natural made materials, manpower and time*”. In terms of power transmission systems, energy efficiency means the reduction in consumption of natural resources, and product price; while simultaneously increasing life cycle period, reliability, applicability and decreasing the maintenance costs. Therefore, the lucid definition of energy efficiency within the context of power transmission systems and other similar machine equipment is “*Energy efficient power transmission system is one that causes the least possible environmental changes and has the best operating performances*”. Thus, it can be stated that energy efficiency goes hand in hand with environmental protection.

3. ALGORITHM FOR INCREASING THE ENERGY EFFICIENCY OF POWER TRANSMISSION SYSTEMS

Individual research and studies couldn't make a significant step forward; hence designers/manufactures were forced to accept the basic principles/postulates in developing energy efficient power transmission systems. Hence, an algorithm for designers/manufacturers to follow through the processes of development, design, manufacturing and maintenance of energy efficient machine parts and systems is necessary. Some authors have already discussed about how important is the methods and principles used during the design and development of mechanical systems, and tried to inform the mechanical engineers population with the present problem. In this regards, works published by Chandler and Petterson [8], Landry [9], and Worrell and Price [10] are excellent groundwork for future improvements regarding the development of unique procedures for increasing the energy efficiency of machine parts and systems.

Development and improvement of machine elements and systems always begin with conceptual designs which are carried out by mechanical engineers. The requirements for the increase in energy efficiency, reliability of machine parts and design that has low maintenance are the most common requirements defined by the manufacturers and users in the last few years. In order to meet the ever changing market requirements and address the issue of depleting natural resources, a new engineering profession known as “green technology engineer” was created. These engineers are designing the equipment using the ecological materials which have an effect to the reducing of environmental pollution and energy consumption, and in same time reduced or eliminated prescribed maintenance during the projected operation life. New technologies enable precise analyses of mechanical systems which in turn assist in achieving the aforementioned objectives. CAD (computer aided design) and computerized programs for numerical calculations of strains and stresses – FEA (Finite Element Analysis) are some of the new methods used for the selection of optimal

characteristics of machine parts and systems. Green technology engineers are involved in optimal material selection, and thus having an important role in design of energy efficient machine parts and systems. Furthermore, their research constitutes finding new materials which possess improved and advanced properties, as well as finding suitable applications for well-known materials.

New advancements in the area of CAD/CAM (computer aided design/computer aided manufacture) have solved numerous problems related to the application of new materials in machine elements manufacturing, and has also enabled high level dimension accuracies. Hence, these systems enable economical production of large series of energy efficient machine parts and systems. In that way the progress achieved in the last few decades in the procedures and methods for manufacturing tools production had a high impact on the quality of manufacturing processes and price.

The main problem based on the all above discussed requirements is in different directions in machine parts dimensioning. It is quite common that the use of low quality materials lead to an increase in the dimensions, which is opposite to the requirements. On the other hand, production of energy efficient parts using new materials can raise production costs. These basic aspects indicate that the design of energy efficient mechanical elements and systems is a task for a team of experts. The design defined on above mentioned premises also includes a very complex optimization task.

The only possible way to increase energy efficiency of mechanical system is through a holistic approach due to a large number of influential factors. The key influential factors can be organized in the following groups:

- Optimal design of mechanical elements
- Optimal dimensioning of mechanical system
- Decrease of loses (due to increased reliability and decreased overhaul periods)
- Decrease of heat losses
- Possibility of good installation and others

The basic responsibility for proper operation of energy efficient machine elements and systems is on the engineers, as any imperfection in mounting and maintenance can decrease efficiency, or lead to failure with huge loss. Furthermore, professional and educated staff is vital for efficient use of mechanical systems within design limits.

Further analysis of present situation shows a very important link between software and mechatronic engineers, as they are responsible for applying the new technological devices and software for monitoring the operating conditions of the mechanical systems. The coordination amongst the software and the mechatronic engineers is important for fast identification of any shift in the regular operating conditions in order to respond efficiently against system failure. Lastly, an increased energy efficient system can be achieved by qualified and motivated management with full understanding of all aspects of mechanical systems. This approach enables the utilization of embedded knowledge of all experts involved in design, production, mounting and maintenance of mechanical systems.

The development of a universal algorithm which considered all the influential factors is important for energy efficient power transmission. The basic guidelines of the developed and presented algorithm in this paper are: distinct, comprehensive and visually representable. For solving such a complex task, a certain level of simplification is required; however this is done without compromising the final aim – to increase energy efficiency. Figure 1 shows the algorithm in which all key influential factors are in context.

4. THE NEW METHODOLOGIES IN THE DESIGN OF GEARS FOR POWER TRANSMISSION SYSTEMS

From a power transmission perspective, one factor with a great potential to reduce energy usage and to boost sustainability is the gear design. Selection of low cost gearing material causes intensive wear, dissipates energy and causes premature failures.

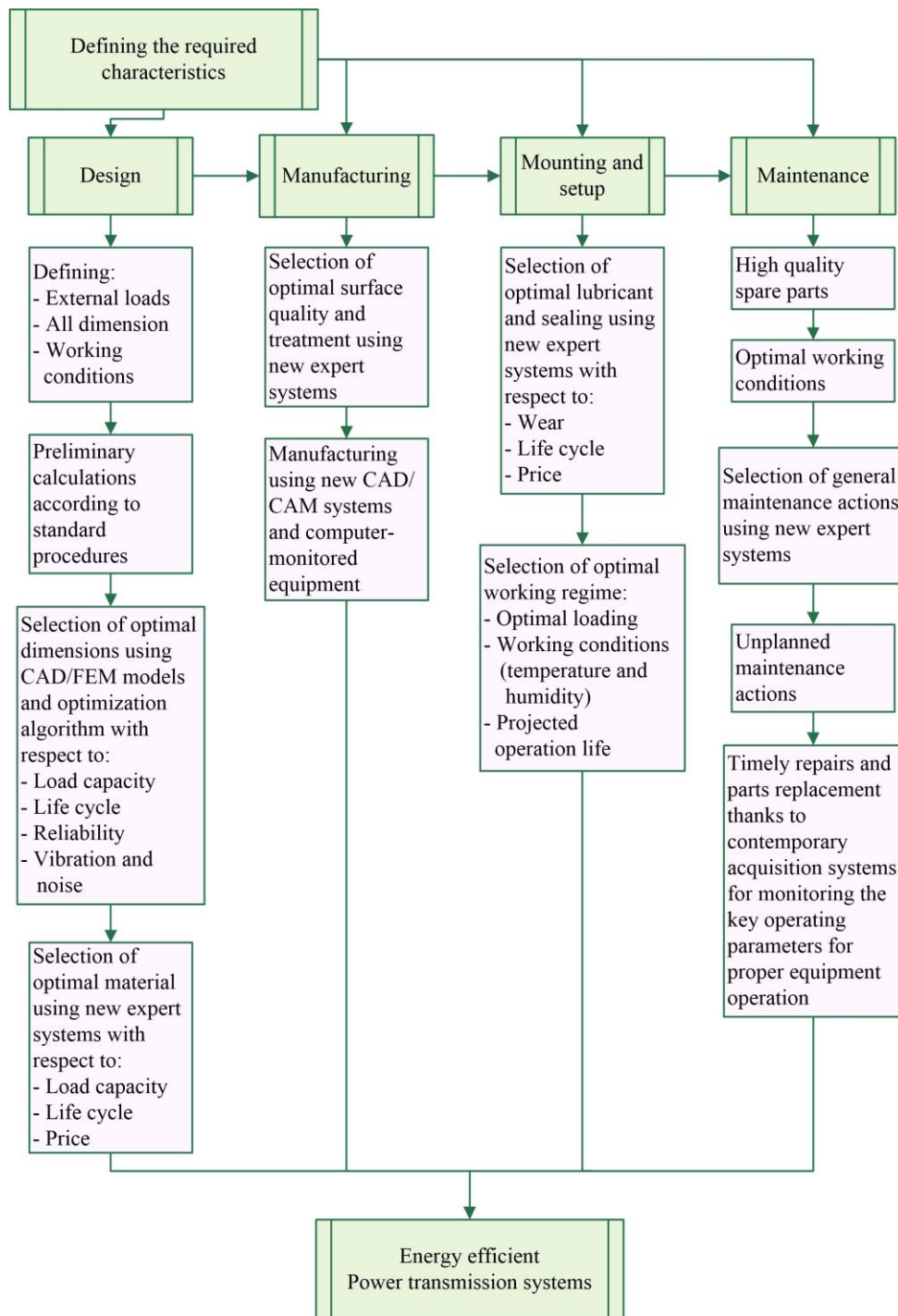


Fig.1: Algorithm for increasing the energy efficiency of power transmission systems

The result is machines which require extensively maintenance. To assist manufacturers, green technology

engineers produce equipment using materials efficiently and effectively. The latter is related to lower the operating

energy costs and the former is related to minimizing scrap. They are also developing highly efficient maintenance free components, and eliminating parts wherever possible. Energy usage is a key factor that affects power transmission system's sustainability. Sustainability is the effective management of resources with minimal waste, while also addressing issues such as workplace safety, product integrity, and reduction of

waste products. In this matter, it is very important to select optimal combination of gear pair characteristics. In the recent decades, new computer technologies and capabilities enable rapid development of new methods in gear calculations and data analysis. Figure 2 shows a few innovative methodologies developed for the selection of optimal gears design.

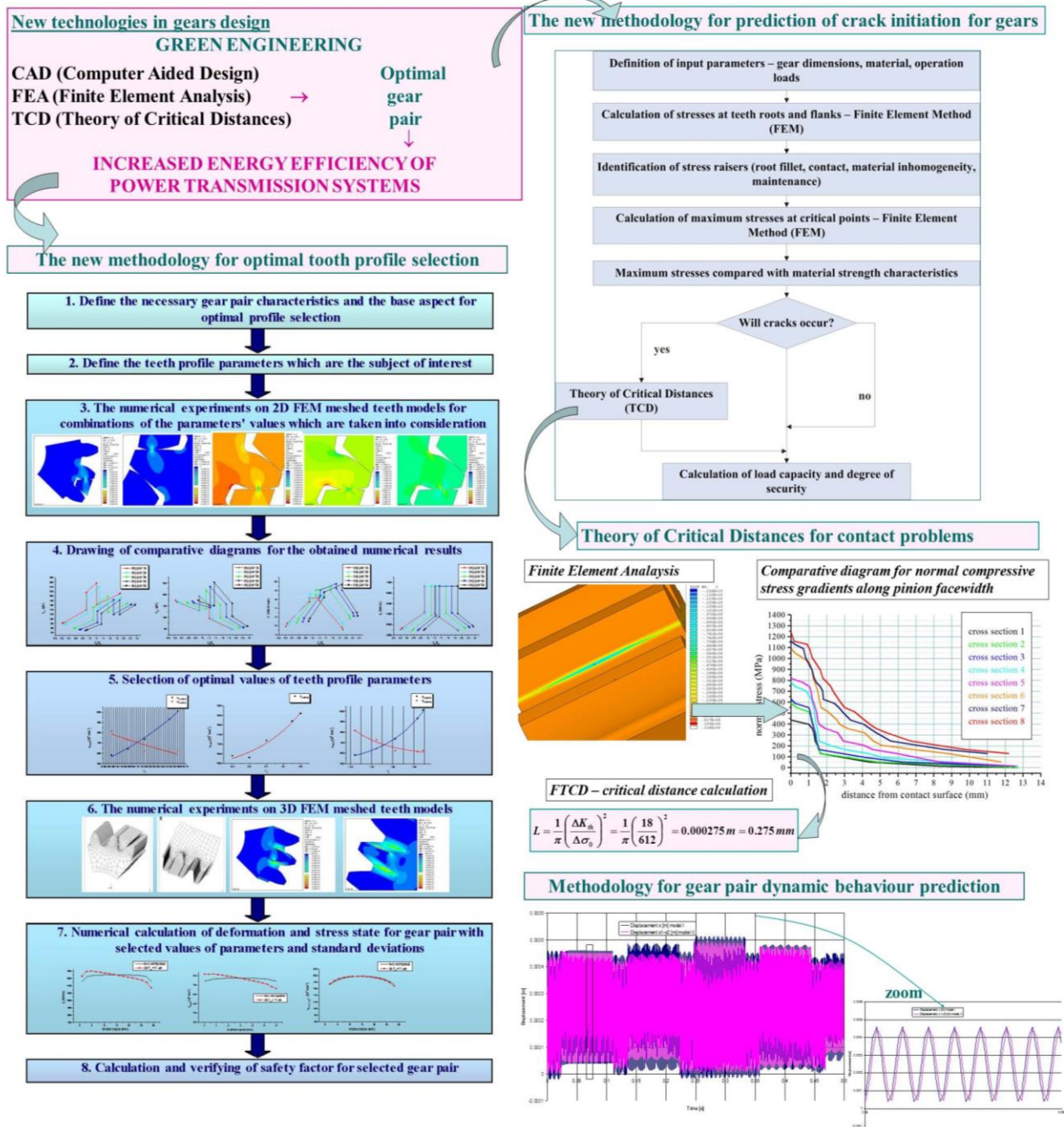


Fig.2: New methodologies for optimal gear designs using new methods

The methodologies are as follows:

- The new methodology for optimal tooth profile selection was developed by using CAD/FEA methods and a new graphically interactive method was generated – Explicit Parametric Method [11];
- The new methodology for prediction of crack initiation in gears [12] has been introduced, which uses the novel

theory of critical distances in order to design gear pairs with minimized possibilities for fatigue failures within the designed life.

- The new methodology for gear pair dynamic behaviour prediction technique [3, 13] has been developed, which uses numerical methods and developed computer

software for determining the dynamic responses of The combination of these methodologies gives the possibility of designing energy efficient gear pair for efficient power transmission, whilst adhering to the various requirements.

New methods for calculation of the strains and stresses also give the possibilities for correction in the standard

gears with various combination of main characteristics. calculation procedures, which are widely used by designers/engineers. A methodology that has been used for developing the new correction factor – friction factor in standard gears calculations is shown in Figure 3 and is explained in detail in previous authors' papers [14, 15].

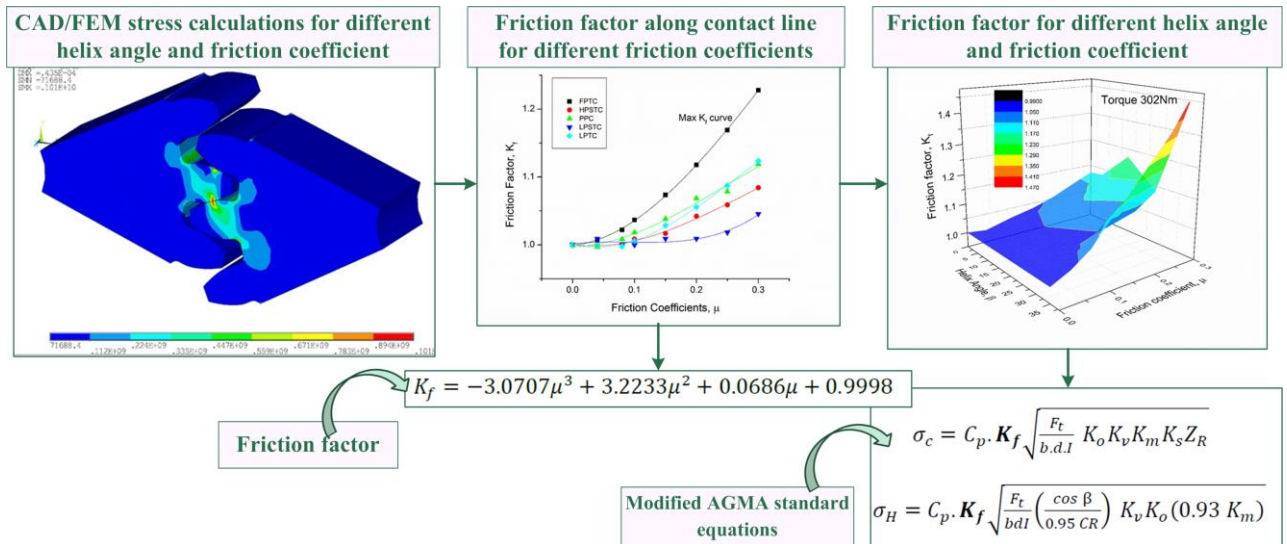


Fig.3: New methodology for modification of standard calculation

5. CONCLUSIONS

Energy efficiency is much more than protecting the environment. Saving energy requires cutting relative unit costs in all fields of everyday life and general mechanical production. The savings produced from designing energy efficient power transmission systems can be highly significant. Therefore, the development of basic principles and the algorithm for increasing the energy efficiency of power transmission systems is extremely important. The utilization of new technologies, methods and procedures allows for more accurate calculations of the elements of the system in question; this in turn leads to designs with higher efficiency. This is in accordance with one of the twelve principles of green engineering as a foundation for sustainability, which are presented by Anastas and Zimmerman [16]. One of the most crucial factors in the advancement of green engineering is the development of a new generation of future engineers with multidisciplinary knowledge, which includes the areas of mechanical, materials, electrical and software engineering [17]. However, the question that should be addressed with regards to energy efficiency should not be restricted to the utilization of new methods, but rather how best to exploit novel technologies, such as: CAD/FEA analysis, expert systems, new materials production, and new acquisition systems to achieve the aforementioned objectives.

ACKNOWLEDGEMENT

Parts of this research were supported by the Ministry of Sciences and Technology of Republic of Serbia through

Mathematical Institute of SASA, Belgrade, Grant ON174001 and Grant TR35029.

REFERENCES

- [1] FERRERO R. (2001) *Keeping it green*, Machine Design. 13. pp. 56-63
- [2] KENNETH J. K. (2011) *Helical gears help manufacturers go green*, Machine Design. May 5. pp. 58-59
- [3] ATANASOVSKA I., VUKSIC-POPOVIC M. (2013) *Dynamics of gear-pair systems with periodic varying mesh stiffness – spur gears vs helical gears*, Series: Scientific Review, Scientific and Engineering, Special Issue - Nonlinear Dynamics. Dedicated to Milutin Milanković (1879-1958). pp. 373-388
- [4] MARQUES P. M. T., MARTINS R. C., Seabra J. H. O. (2016) *Power loss and load distribution models including frictional effects for spur and helical gears*, Mechanism and Machine Theory. Vol.96. pp.1–25
- [5] MATEOS-ESPEJELA E., SAVULESCUB L., PARISA J. (2011) *Base case process development for energy efficiency improvement, application to a Kraft pulping mill. Part I: Definition and characterization*, Chemical Engineering Research and Design. Vol. 89. pp. 742–752
- [6] MITROVIC R. et al. (2011) *Instalation for carrier roller idlers of belt conveyors testing on the open pit mining*, Conference IRMES 2011., pp. 383-388
- [7] ZIVKOVIC P. (2009) *Analysis and calculation of energy losses in planetary gear set components*, Machine Design, University of Novi Sad, May 2009, pp. 249-254

- [8] CHANDLER P., PETERSON D. (2001) *Counting the losses in very high efficiency machine design*, Renewable Energy, No. 22, pp. 143-150
- [9] LANDRY J. (2011) *A Mechanical Engineer's Perspective on Energy Efficiency*, The Rockwell automation Journal, February 2011, pp. 40-42
- [10] WORRELL E., PRICE L. (2001) *Policy scenarios for energy efficiency improvement in industry*, Energy Policy, No.29, pp.1223-1241
- [11] ATANASOVSKA I., MITROVIC R., MOMCILOVIC D., 2013, *Explicit Parametric Method for Optimal Spur Gear Tooth Profile Definition*, Advanced Materials Research, Vol. 633, Trans Tech Publications, Switzerland, pp. 87-102
- [12] ATANASOVSKA I., MOMCILOVIC D. (2016) *Spur gear model for prediction of fatigue damage initiation in contact zone*, International Journal of Powertrains – „Special Issue on Technologies and Models for High Power Density Geared Powertrains“, Guest Editor: Prof. Dr. Christos Spitas, Delft University of Technology, Netherlands, ISSN online:1742-4275, ISSN print:1742-4267, doi: [10.1504/IJPT.2016.079073](https://doi.org/10.1504/IJPT.2016.079073), Publisher: Inderscience Publishers, Switzerland, Vol.5, No.3, pp.213-229
- [13] ATANASOVSKA I. (2016) *Influence of addendum modification on spur gears stability*, International Journal of Powertrains – „Special Issue on Technologies and Models for High Power Density Geared Powertrains“, Guest Editor: Prof. Dr. Christos Spitas, Delft University of Technology, Netherlands, ISSN online:1742-4275, ISSN print:1742-4267, doi: [10.1504/IJPT.2016.079074](https://doi.org/10.1504/IJPT.2016.079074), Publisher: Inderscience Publishers, Switzerland, Vol.5, No.3, pp.230-245
- [14] PATIL S., KARUPPANAN S., ATANASOVSKA I., WAHAB A. (2014) *Contact Stress Analysis of Helical Gear Pairs, Including Frictional Coefficients*, International Journal of Mechanical Sciences, Elsevier, Vol. 85, pp. 205-211
- [15] PATIL S., ATANASOVSKA I., KARUPPANAN S. (2015) *Contact stress evaluation of involute gear pairs, including the effects of friction*

and helix angle, Journal of Tribology, Transactions of the ASME, Vol. 137 (4), pp. 044501(1-5)

- [16] ANASTAS P. T., ZIMMERMAN J. B. (2006) *The Twelve Principles of Green Engineering as a Foundation for Sustainability*, Sustainability Science and Engineering, Defining principles, M.A. Abraham (Ed.). Elsevier. Amsterdam, 2006. pp.11-32
- [17] Reference Architecture Model Industrie 4.0 (RAMI 4.0). Status Report, July 2015. https://www.vdi.de/fileadmin/vdi_de/redakteur/dateien/gma_dateien/5305_Publikation_GMA_Status_Report_ZVEI_Reference_Architecture_Model.pdf

CORRESPONDANCE



Ivana ATANASOVSKA, Dr.Sc. Eng.
Mathematical Institute of the Serbian
Academy of Sciences and Arts
Kneza Mihaila 36
11000 Belgrade, Serbia
iviatanasov@yahoo.com
iatanasovska@mi.sanu.ac.rs



Saravanan KARUPPANAN, Prof. Dr.Sc.
Universiti Teknologi PETRONAS
Department of Mechanical Engineering
Perak Darul Ridzuan
32610 Seri Iskandar, Malaysia
saravanan_karuppanan@petronas.com.my



Santosh PATIL, Dr.Sc. Eng.
Manipal University Jaipur
Department of Mechanical Engineering
School of Automobile, Mechanical &
Mechatronics Engineering
Dehmi Kalan, Off Jaipur-Ajmer
Expressway, Jaipur, (Raj.), Rajasthan
303007, India
santosh045@gmail.com

COMPARATIVE ANALYSIS OF VIBRO-IMPACT OSCILLATIONS OF SPUR GEAR PAIR FOR VARIATION OF GEARS TRANSMISSION RATIO

Ivana D. ATANASOVSKA
Katica R. (STEVANOVIĆ) HEDRIH

Abstract: *The operation of spur gears with involute profile is characterized with total deformations variation particularly because of variable number of teeth pairs in contact. These variations and a tooth profile pitch deviations lead to the backlash, appearance of internal dynamic forces and impacts. Vibro-impact dynamics of spur gear pair caused by successive collisions of series of teeth pairs in forward-backward collision contacts are source of vibro-impact vibrations and noise in the spur gear pair system. A model of the central centric collision of two fictive rolling disks with radii equal to the radii of pitch diameters of pinion and wheel, and with instantaneous rolling axes in collision in the rotation axis of pinion and wheel, are used to describe the vibro-impact dynamics of gears.*

The angular velocities of the pinion and the wheel before and after each of successive collisions, and before and after every successive impact are calculated in accordance with the postulates of the extension of the classical theory of impact with theory of kinematics and dynamics of the collision of two rolling axially symmetric rigid bodies. The set of equations for calculation of the pinion disturbance angular velocity, called transmission error, are developed. This angular velocity has a role of an excitation in vibro-impact vibrations of gears.

A particular involute spur gear pair with such a geometry which could lead to vibro-impact and with different values of transmission ratio is used for the gears vibro-impact analysis. The main characteristic variables of vibro-impact oscillations are calculated for the pinion and the wheel. The comparative diagrams for monitoring of these variables are created and the appropriate conclusions are derived and discussed.

Key words: *Vibro-impact oscillations, successive collisions, spur gear pair, outgoing post-collision angular velocities*

1. INTRODUCTION

The extensive research of the gears vibrations is in the focus in last few decades. There are a lot of published models and procedures which attempted to explain some or all of the aspects in gears dynamics. Almost all of analysis research used the equation of motion to explain the gear pair as multi- DOF (degrees of freedom) dynamic system, [1]. However, a significant number of authors have verified the reduction on the system with two [2] or one degree of freedom [3 - 7]. A vibration of spur gear pair was simulated with two disks coupled by nonlinear mesh stiffness\mesh damping and excitation due to gear errors, [2 - 4, and 6 - 10]. Authors within their gear dynamics models use the Finite Element Method (FEM) for the calculations of a meshed gear teeth deformations and stiffness function, [5 - 7, 11 - 13].

The analysis of the present models for gear dynamics simulation, leads to the conclusion that there are still the room for improvements. However, it is more important to emphasize that there is an obviously requirements for developing new models for coupled phenomenon simulations.

In this paper, for investigation of a new model of vibro-impact dynamics of spur gear pair, a completely new and original application of the extension of classical theory of impact with theory of kinematics and dynamics of collision of two rolling axial-symmetric bodies was used, [14 - 18]. In this paper a new model of vibro-impact dynamic of spur gears is described in detail in accordance with the main postulates of a model of the central centric collision of two fictive rolling disks with radii equal to the radii of kinematic diameters of pinion and wheel, and with current rolling axes in collision coincide with the rotation axis of pinion and wheel [14-18].

2. A MODEL FOR VIBRO-IMPACT DYNAMICS OF SPUR GEARS

2.1. Collision and vibro-impact phenomena in gear teeth contact

The conditions for vibro-impact vibrations regime of spur gears operation exists only in the special cases of involute cylindrical gears, and is characterized with a vibro-impact behavior of pinion gear. The involute cylindrical gears are widely used primarily thanks to the approximately constant transmission ratio. Vibro-impact dynamics

occurs when a disturbance of angular velocities ration appears. The disturbance angular velocity of pinion can be defined as:

$$\Delta\omega_1 = \omega_1 - i\omega_2 > 0 \quad (1)$$

and considered as an excitation of vibro-impact vibrations when this phenomenon can appears. Whether the vibro-impact dynamics will occur in the coupling of gear pair depends primarily on the gear geometry, i.e. of teeth profile parameters and transmission ratio. These variables could have in some cases the values which lead to the arc distance between the pinion tooth and next wheel tooth with the very small dimensions. As a result, in the momentum of changes of number of teeth pairs in contact, the collision of pinion tooth and wheel tooth causes the backwards rejection of pinion tooth and its collision with next wheel tooth. A certain number of successive forward-backward collisions-impacts arise during very short time period and lead to the decreasing of the disturbance of the post-collision outgoing and next pre-collision arrival angular velocity. After few successive forward-backward collisions-impacts the regular operation regime returns and gears rotate without vibro-impact vibrations and followed noise. In the ideal stationary kinetic states, this phenomenon is repeating into infinity, and all of described operation disturbances have only the character of vibro-impact vibrations, but not of permanent disorders of angular velocities. However, the certain amounts of energy have to be loosed in these cases.

The calculation of the disturbance pinion angular velocity is of main character in developing of the model of vibro-impact oscillations of spur gears. We could start from the definition of tooth profile pitch deviation as a result of deformations and manufacturing deviations, as:

$$b = K_b m_n, [\text{mm}] \quad (2)$$

where: m_n - is a standard normal tooth profile module, while K_b -could be defined as error coefficient and has a value in the range (0.01-0.1), [2]. The time which is required by a pinion tooth to pass this deviation can be express as:

$$T(b) = \frac{K_b m_n}{r_1 \omega_1}, [\text{s}] \quad (3)$$

The pinion disturbance angular velocity can be calculated in accordance with the postulate that the rotation time of pinion gear will be the same in the cases with and without deviation b :

$$\frac{2\pi}{\omega_1} = \frac{2\pi + \frac{K_b m_n}{r_1}}{\omega_1 + \Delta\omega_1}, \text{ie } \Delta\omega_1 = \frac{K_b m_n}{2\pi r_1} \omega_1, [\text{rad/s}] \quad (4)$$

Coefficient K_b in general depends on variation of total deformation of meshed teeth pairs and base profile pitch deviation. Variation of total deformation u_s during contact period of a single teeth pair are very small and could be calculated as a sum of: deformation of pinion tooth u_1 , deformation of wheel tooth u_2 and contact deformation u_H . The point of force action moves from tooth root to tooth addendum at pinion gear tooth, therefore the moment arm relative to the root increases and consequently deflection increases. This leads to the

increasing of the deformation of pinion tooth u_1 . Contrary, the point of force action moves from tooth tip to tooth dedendum at wheel gear tooth, therefore the moment arm relative to the root decreases and consequently deflection decreases. This leads to the decreasing of the deformation of wheel tooth u_2 . The contact local deformation of meshed teeth flanks u_H is almost constant during the teeth pair contact period. Therefore, if the normal force acting at teeth flanks is constant during gears operating, i.e. if the single teeth pair contact exists during transmission, total deformation will be approximately unchanged.

However, the number of teeth pairs in contact is changing during the gear operation. In such the conditions the deformations of pinion tooth and wheel tooth, as well as the total deformation of teeth pair in contact, vary. Figure 1 shows the variation of deformations' variables during single contact period in the case without profile pitch deviations. The variations of the normal contact force intensity and deformations when base pitch deviation exists are given in [19].

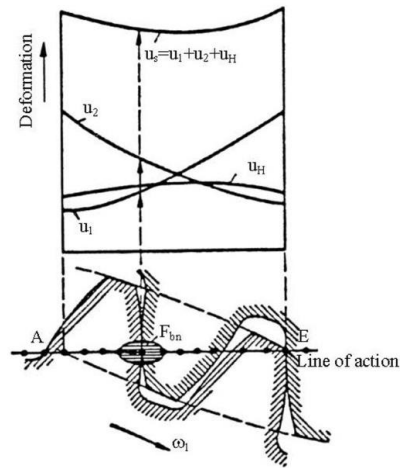


Fig.1: Variation of a single teeth pair deformations along the Line of action

If the start point of analysis is the beginning of the gear pair operation when the wheel (driven gear) is stationary, then the total deformation of starting meshing teeth pair causes backward moving of the pinion (drive gear). This movement would lead to a pinion profile pitch reduction and a wheel profile pitch increasing. In theoretically (geometric) point of view, the overlap of profile lines of next teeth pair that should come in contact would be appears. In real condition this leads to the collision of pinion tooth dedendum with a tip of next teeth pair's wheel tooth. In this way the wheel accelerates and its delay relative to pinion decreases. This corresponds to the momentum when the single teeth pair period pass to the double teeth pair period. If the contact is ideally elastic, after second - backward collision-impact, the outgoing angular velocities of pinion and wheel would be back to the values in the start point of analysis. The same phenomenon occurs when base pitch manufacturing deviation is less than 0. Similar analysis could be performed for the moment when the double teeth pair period pass to the single teeth pair period and single meshed teeth pair receives the full external load. This leads to new collision and wheel again delays relative to

the pinion as a result. The same phenomenon occurs when base pitch manufacturing deviation is greater than 0. Vibro-impact vibrations of gear pair would be generated due to these occurrences.

In following consideration the approximation of gear pair with two fictive rolling disks with radii equal to the radii of pitch diameters of pinion and wheel is used. The influence of gear masses is taking into account by axial mass moments of inertia for the current gear axis of rotation. The angular velocities of the pinion and the wheel before and after every collision, and before and after every successive collision-impact are calculated in accordance with the postulates of the extension of the classical theory of impact and collision of two rolling axially symmetric rigid bodies, [14-18]. These velocities depend of teeth profile pitch deviations as well as from the total deformations of teeth pair. The values of pinion tooth deformation, wheel tooth deformation and total teeth pair deformation should be precise calculated, therefore the Finite Element Analysis under the especially developed models are performed in presented research, [20 - 22].

2.2. Central centric collision of two rolling disks

In any point P with character of vibro-impact vibration behavior, the fictive rolling disks, which are used to simulate the teeth pair contact, represent a system with the rotation defined by the axial mass inertia moments \mathbf{J}_{p1} and \mathbf{J}_{p2} for corresponding instantaneous axis of fictive rolling-rotation. These disks have in the point P the arrival (before-impact) angular velocities: $\vec{\omega}_{p1,impact} = \vec{\omega}_{p1}(t_0)$ and $\vec{\omega}_{p2,impact} = \vec{\omega}_{p2}(t_0)$, and corresponding outgoing (after-impact) angular velocities: $\vec{\omega}_{p1,outgoing} = \vec{\omega}_{p1}(t_0 + \tau)$ and $\vec{\omega}_{p2,outgoing} = \vec{\omega}_{p2}(t_0 + \tau)$, [14 - 18].

A qualitative and mathematical analogy between the relations correspond to the system of translational dynamics and central collision (impact) dynamics of two bodies in translation, and to the system of rolling dynamics of two disks and central collision (impact) dynamics of two rolling disks in rolling motion could be indicated.

On the basis of mentioned qualitative and mathematical analogies, analogous kinetic parameters of these systems could be defined:

- The axial mass inertia moments \mathbf{J}_{p1} and \mathbf{J}_{p2} for corresponding instantaneous axis of rolling-rotation of two bodies in collision during rolling motion are analogous to the bodies' masses m_1 and m_2 of two bodies in collision during translation, [14 - 18].

- Before-impact (arrival) angular velocities at moment defined with t_0 ($\vec{\omega}_{p1,impact} = \vec{\omega}_{p1}(t_0)$ and $\vec{\omega}_{p2,impact} = \vec{\omega}_{p2}(t_0)$) of the rolling disks around corresponding instantaneously axis are analogous to corresponding before-impact velocities ($\vec{v}_1(t_0)$ and $\vec{v}_2(t_0)$) of two bodies in translation at the moment before collision.

- After-impact (outgoing) angular velocities at moment ($t_0 + \tau$) ($\vec{\omega}_{p1,outgoing} = \vec{\omega}_{p1}(t_0 + \tau)$ and

$\vec{\omega}_{p2,outgoing} = \vec{\omega}_{p2}(t_0 + \tau)$) of the rolling disks are analogous to corresponding after-impact (outgoing) velocities ($\vec{v}_1(t_0 + \tau)$ and $\vec{v}_2(t_0 + \tau)$) of two bodies in translation at the moment after collision.

The analogous *hypothesis* of conservation of sum of angular momentum (moment of impulse) before and after collision for impact dynamics of two disks in rolling motion is formulated by K. Hedrih [14 - 18] and is given with following relation:

$$\mathbf{J}_{p1}\vec{\omega}_{p1}(t_0) + \mathbf{J}_{p2}\vec{\omega}_{p2}(t_0) = \mathbf{J}_{p1}\vec{\omega}_{p1}(t_0 + \tau) + \mathbf{J}_{p2}\vec{\omega}_{p2}(t_0 + \tau) \quad (5)$$

Consequently, a new definition of coefficient of the restitution of collision of two rolling disks could be expressed as ratio between differences of angular velocities of rolling disks before collision and after collision in following form [14 - 18]:

$$k = \frac{\omega_r(t_0 + \tau)}{\omega_r(t_0)} = \frac{\omega_{p2}(t_0 + \tau) - \omega_{p1}(t_0 + \tau)}{\omega_{p1}(t_0) - \omega_{p2}(t_0)} \quad (6)$$

The coefficient of restitution of collision of two rolling bodies is real, dimensionless number which depends of bodies materials, with value between zero and one (0-1), and can be determined experimentally. In accordance with relations (7) and (8) the expressions of after-collision outgoing angular velocities of rolling disks or balls could be expressed with the following forms [14 - 18]:

$$\omega_{p1}(t_0 + \tau) = \omega_{p1}(t_0) - \frac{1+k}{1 + \frac{\mathbf{J}_{p1}}{\mathbf{J}_{p2}}} (\omega_{p1}(t_0) - \omega_{p2}(t_0)) \quad (7)$$

$$\omega_{p2}(t_0 + \tau) = \omega_{p2}(t_0) + \frac{1+k}{1 + \frac{\mathbf{J}_{p2}}{\mathbf{J}_{p1}}} (\omega_{p1}(t_0) - \omega_{p2}(t_0)) \quad (8)$$

3. VIBRO-IMPACT VIBRATIONS FOR A PARTICULAR GEAR PAIR WITH VARIABLE TRANSMISSION RATIO

The procedure for analysis a vibro-impact vibrations of spur gears described above is demonstrated on the particular series of spur gear pairs with main characteristics and dimensions given in Table 1, [21].

In order to calculate the coefficient K_b , the total deformation variation along the Line of action is calculated by Finite Element Analysis (FEA) developed for the particular spur gear pair [21]. The case without pitch deviations of meshed teeth pairs and base profile pitch deviation is assumed. In accordance with above explain theoretical model of vibro-impact vibrations of spur gears, the disturbance angular velocity defined with relation (4) has been calculated. Expressions (7) and (8) have been used for calculation of the angular velocities of the pinion and the wheel before and after every collision, and before and after every successive collision-impact. The algorithm for calculations of all main characteristic variables of vibro-impact oscillations of spur gear pair (each outgoing and next arrival angular velocities in successive forward-backlash collisions, angular momentum, kinetic energy, transmission ratio) is programmed in MathCAD software. For the spur gear

with characteristics given in Table 1, the obtained results for the variations of pinion angular velocity, pinion

angular momentum and kinetic energy of pinion during two contact periods are given in Figures 2-4.

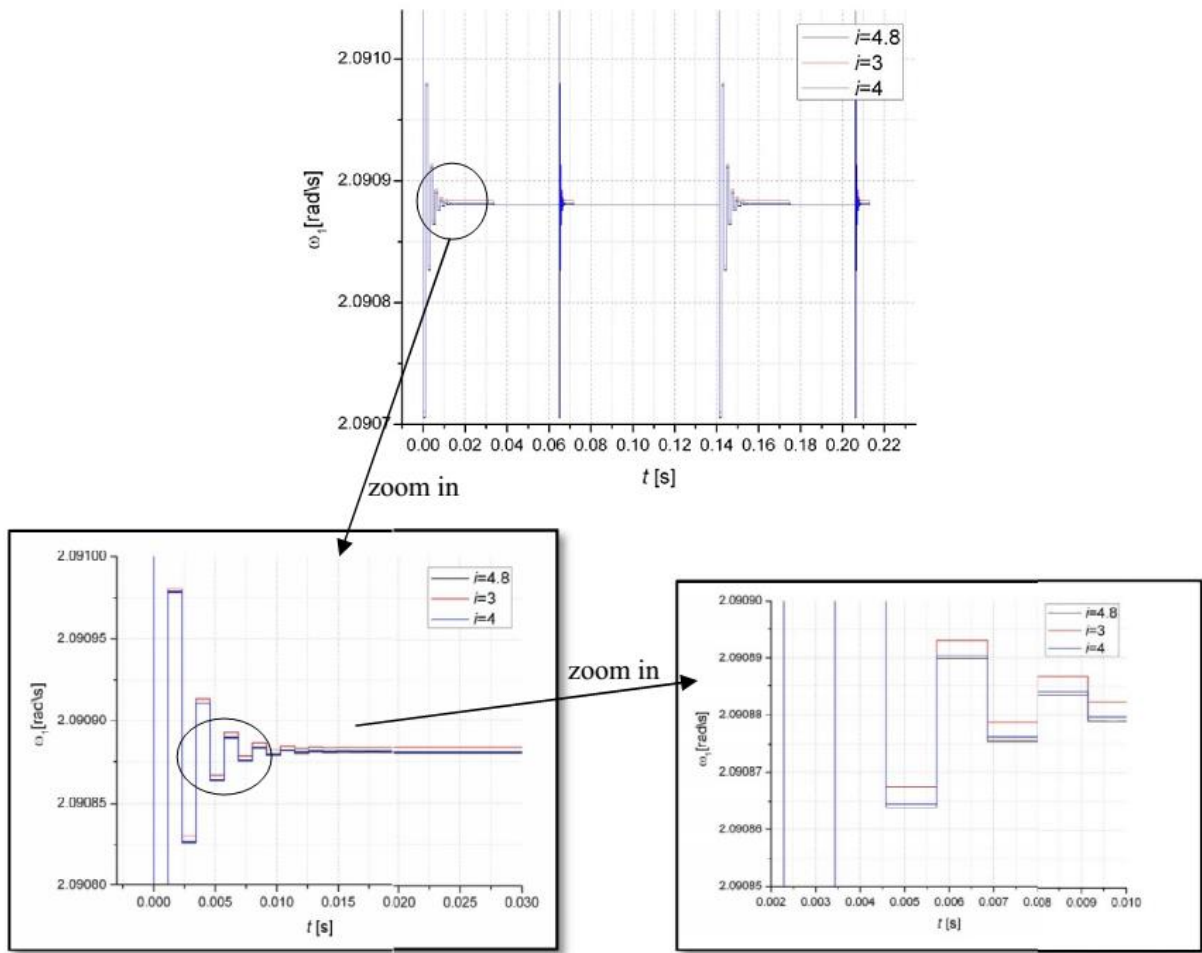


Fig.2: The variations of pinion angular velocity ω_1 during two contact periods for different transmission ratio (with zoom in details): ___ $i=4.8$; ___ $i=4$; ___ $i=3$

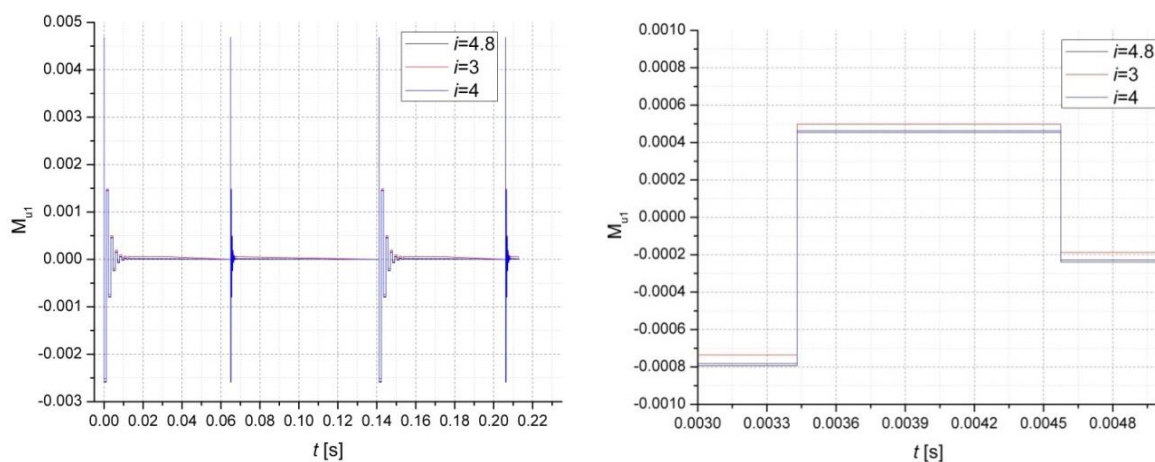


Fig.3: The variations of pinion angular momentum M_{u1} during two contact periods for different transmission ratio (with zoom in detail): ___ $i=4.8$; ___ $i=4$; ___ $i=3$

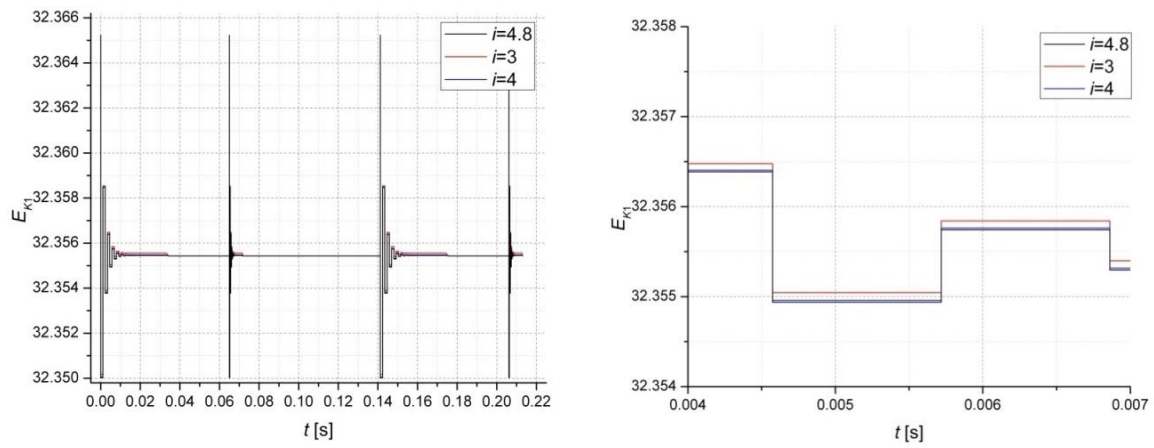


Fig.4: The variations of kinetic energy of pinion E_{kl} during two contact periods for different transmission ratio (with zoom in detail): ___ $i=4.8$; ___ $i=4$; ___ $i=3$

Table 1: Characteristics of analyzed spur gear pairs

Variable	Symbol and value		
Number of teeth	$z_1=20$; $z_2=96$	$z_1=20$; $z_2=80$	$z_1=20$; $z_2=60$
Transmission ratio	$i = z_2/z_1$ $=4.8$	$i = z_2/z_1$ $=4$	$i = z_2/z_1$ $=3$
The coefficients of profile modification	$x_1=0.7$; $x_2=-0.2$		
Gears facewidth	$b=350$ mm		
Profile module	$m=m_n=24$		
Rpm for wheel	$n_2=4.1596$ min ⁻¹		
Wheel torque	$T_2=2526.8$ KN·m		
Material characteristics	$E = 206\ 000$ N/mm ² ; $\nu = 0,3$		

4. DISCUSSIONS AND CONCLUSIONS

A new model for investigation of vibro-impact dynamics of gears is developed on the basis of approximation with two fictive rolling disks in successive centric central collisions and presents abstraction of real system under corresponding assumptions. Within this model the extension of the classical theory of impact by developed theory of kinematics and dynamics of collision of two rolling axially symmetric rigid bodies is used for determine the outgoing angular velocities of the pinion and the wheel before and after every collision from series of successive collisions, and before and after every successive forward-backward collision-impact between gears teeth. The explained theoretical model of vibro-impact phenomenon for spur gears, as an approximate abstraction of real vibro-impact system dynamics, has proved to be very suitable for the analyses of dynamics of the spur gears with profile parameters and deviations which lead to the backlash, appearance of internal dynamic forces and impacts or damages during operation. The obtained numerical results for a particular gear pair with variable transmission ratio are presented with comparative diagrams and lead to the conclusion that

variation of transmission ratio, when the contact ratio stays constant, doesn't provoke the variation in the amplitude of vibro-impact vibrations. The variation of transmission ratio leads only to the occurrence of shifts of the analyzed variables for small values. These shifts are not linear proportional with the transmission ratio variation. Decreasing of the transmission ratio leads to the very small incremental increasing of the pinion angular velocity of about 0.0005% and of the kinetic energy of pinion of about 0.0003%, but in the same time leads to the significant increasing of the pinion angular momentum of about 10%.

ACKNOWLEDGEMENT

Parts of this research were supported by the Ministry of Sciences and Technology of Republic of Serbia through Mathematical Institute of SASA, Belgrade, Grant OI174001 and Grant TR35029.

REFERENCES

- [1] SPITAS C., SPITAS V. (2016) *Coupled multi-DOF dynamic contact analysis model for the simulation of intermittent gear tooth contacts, impacts and rattling considering backlash and variable torque*, Journal of Mechanical Engineering Science, Vol. 230, No.7-8, pp.1022-1047.
- [2] ANDERSSON A., VEDMAR L. (2003) *A dynamic model to determine vibrations in involute helical gears*, Journal of Sound and Vibration, Elsevier, Vol. 260, pp. 195–212.
- [3] MORADI H., SALARIEH H. (2012) *Analysis of nonlinear oscillations in spur gear pairs with approximated modelling of backlash nonlinearity*, Mechanism and Machine Theory, Vol. 51, Elsevier, pp. 14–31.
- [4] AMABILI M, RIVOLA A. (1997) *Dynamic analysis of spur gear pairs: steady-state response and stability of the sDOF model with time-varying meshing damping*, Mechanical Systems and Signal Processing, Vol.11, No.3, Academic Press Limited, pp. 375-390.
- [5] PARKER R. G., VIJAYAKAR S. M. and IMAJO T. (2000) *Non-linear dynamic response of a spur gear pair modelling and experimental comparisons*, Journal

- of Sound and Vibration (2000), Vol. 237, No. 3, Accademic press, pp. 435-455.
- [6] ATANASOVSKA I., VUKŠIĆ POPOVIĆ M. (2013) *Dynamics of gear pair systems with periodic varying mesh stiffness - spur gears vs helical gears*, Series: Scientific Review, Scientific and Engineering - Special Issue - Nonlinear Dynamics S2 (2013) Dedicated to Milutin Milanković (1879-1958), Guest Editors: Katica R. (Stevanović) Hedrih and Željko Mijajlović, pp. 373-388.
- [7] ATANASOVSKA I. (2015) *The Mathematical Phenomenological Mapping in Nonlinear Dynamics of Spur Gear Pair and Radial Ball Bearing due to the Variable Stiffness*, International Journal of Non-linear Mechanics, Elements of mathematical phenomenology and phenomenological mapping in non-linear dynamics, Edited by Katica R. (Stevanovic) Hedrih, Ivan Kosenko, Pavel Krasilnikov and Pol D. Spanos, Vol. 73, pp. 114-120.
- [8] JELIĆ M., ATANASOVSKA I. (2012) *The New Approach for Calculation of Total Mesh Stiffness and Nonlinear Load Distribution for Helical Gears*, Mechanisms and Machine Science (Book Series), Power Transmissions (Proceedings of The 4th International Conference on Power Transmissions - PT 12, Sinaia, Romania), pp. 645-654.
- [9] ZHANG D., WANG S. (2014) *Parametric vibration of split gears induced by time-varying mesh stiffness*, Proc IMechE Part C: J Mechanical Engineering Science, doi:10.1177/0954406214531748.
- [10] THEODOSSIADES S. and NATSIAVAS S. (2000) *Non-linear dynamics of gear-pair systems with periodic stiffness and backlash*, Journal of Sound and Vibration, Vol. 229, No.2, pp. 287-310.
- [11] LIN T., OU H., LI R. (2007) *A finite element method for 3D static and dynamic contact/impact analysis of gear drives*, Computer Methods in Applied Mechanics and Engineering, Vol. 196, pp. 1716-1728.
- [12] SONG X., IAN H. (2016) *Dynamic modelling of flexibly supported gears using iterative convergence of tooth mesh stiffness*, Mechanical Systems and Signal Processing, Vol. 80, pp. 460-481.
- [13] LIU X., YANG Y., ZHANG J. (2016) *Investigation on coupling effects between surface wear and dynamics in a spur gear system*, Tribology International, Vol. 101, pp. 383-394.
- [14] HEDRIH (STEVANOVIĆ) K. R. (2015) *Elements of mathematical phenomenology: I. Mathematical and qualitative analogies*, Труды МАИ Выпуск №84, pp. 42 (1-42); II. Phenomenological approximate mappings, №84, pp. 29 (1- 29).
- [15] HEDRIH (STEVANOVIĆ) R. K. (2016) *Dynamics of Impacts and Collisions of the Rolling Balls*, Dynamical Systems: Theoretical and Experimental Analysis, Springer Proceedings in Mathematics & Statistics, Volume Number: 182, Chapter 13, pp. 157-168.
- [16] HEDRIH (STEVANOVIĆ) R. K. (2016) *Vibroimpact dynamics in systems with trigger of coupled three singular points: Collision of two rolling bodies*, Book of Papers, International Congress of Theoretical and Applied Mechanics (ICTAM 2016), Montreal, Canada, 21-26 August.
- [17] HEDRIH (STEVANOVIĆ) R. K. (2015) *Vibro-impact dynamics of the rolling disks along rotate circle in vertical plane*, Dynamical Systems, Control and Stability, Thematical Proceedings Editors: Jan Awewjcewicz, Marek Kazmierczak, Jerzy Mrozowski, Pawel Olejnik, 2015, Vol. 13/3, pp. 251-262.
- [18] HEDRIH (STEVANOVIĆ) R. K. (2016) *From geometry, kinematics and dynamics of billiards to the extended theory of skew collision between two rolling bodies and methodology of vibro-impact dynamics (Review paper)*, Plenary Lecture, The 5-th international conference on "Nonlinear Dynamics" in Kharkov, September 27-30, 2016, Dedicated to the 90th Anniversary of Academician V.L. Rvachov, National Technical University "Kharkov Polytechnic" et al., N49-Proceedings 538p, pp. 108-116.
- [19] OGNJANOVIĆ M. (1984) *Vibracije, šum i odstupanja mera zupčastih parova – istraživanje uzajamnih zavisnosti (Vibrations, noise and dimension deviations of gear pairs - research of dependences)*, PhD thesis, Faculty of Mechanical Engineering, Belgrade (in Serbian).
- [20] ATANASOVSKA I. et al. (2007) *Developing of gear FEM model for nonlinear contact analysis*, Proceedings of 1. International Congress of Serbian Society of Mechanics, Kopaonik, 10-13.04.2007., pp. 695-703.
- [21] ATANASOVSKA I. et al. (2013) *Explicit Parametric Method for Optimal Spur Gear Tooth Profile Definition*, Advanced Materials Research, Vol. 633: Advances in Engineering Materials, Product and Systems Design (Special topic volume with invited peer reviewed papers only), Editor: Aleksandar Subić, pp. 87-102.
- [22] PATIL S. S., KARUPPANAN S., ATANASOVSKA I., WAHAB A. A. (2014) *Contact Stress Analysis of Helical Gear Pairs, Including Frictional Coefficients*, International Journal of Mechanical Sciences, Vol. 85, pp. 205-211.

CORRESPONDANCE



Ivana ATANASOVSKA, Dr.Sc. Eng.
Mathematical Institute of the Serbian
Academy of Sciences and Arts
Kneza Mihaila 36
11000 Belgrade, Serbia
iviatanasov@yahoo.com
iatanasovska@mi.sanu.ac.rs



Katica R. (STEVANOVIĆ) HEDRIH, Prof.
Dr.Sc.
Mathematical Institute of the Serbian
Academy of Sciences and Arts
Kneza Mihaila 36
11000 Belgrade, Serbia
and
Faculty of Mechanical Engineering,
University of Niš, Serbia
khedrih@sbb.rs

OPTIMAL SELECTION OF A TWO-SPEED TWO-CARRIER PLANETARY TRAIN

Jelena STEFANOVIĆ-MARINOVIĆ

Sanjin TROHA

Miloš MILOVANČEVIĆ

Abstract: This paper considers two-speed planetary gear trains with four external shafts, composed of two simple planetary gear trains. A method of optimal selection of a two-speed two-carrier planetary train according to several criteria is presented. The shown methodology enable quick determining of structure and base parameters of two-speed PGT which can satisfy transmission requirements.

These transmissions have significant application in systems which require speed change under load.

The example of selection of optimal two-speed PGT is given and its structural and kinematic scheme is formed.

The shown methodology enable next step in PGT optimization: application of multicriteria optimization to the chosen PGT in order to define design parameters.

Key words: two-speed planetary gear trains, transmission ratio, ideal torque ratio

1. INTRODUCTION

Planetary gear trains (PGT) are a type of gear trains with many advantages. Since that their application is increasing in mechanical engineering and conveyor systems as single-stage and multi-stage. Multi-stage planetary gear trains are obtained from single stage gear trains by linking one or two planetary units shafts. A special type of multi-stage PGTs is two-speed two-carrier planetary gear trains which consist of two coupled and four external shafts and have brakes on single shafts. This type of compound gear trains has many advantages, first of all possibility of speed change under load. Speed change under load is request of mechanical system in some occasions (e.g. machine tools, cranes etc.).

The number and actuality of published studies indicate the importance and contemporaneity of these transmissions. Two-carrier transmissions with four external shafts used as two-speed transmissions are presented in the [1]. The review of possible schemes can be seen in [2, 3], but their convertible characteristics are barely investigated. Also, there are relatively small number of kinematic schemes which are practice realized. That is why establishing a quality method for selection optimal scheme and parameters of two-speed two-carrier planetary gear trains can be useful for both theoretical research and practice tasks.

This paper deals with these compound gear trains. The importance of mathematical optimization procedure and mathematical optimization methods to these transmissions is pointed in the paper. The first step is the optimal kinematic scheme choice. In the next step, the optimal solution determinant by design parameters can be obtained.

Since optimization procedures in the both steps required multi-criteria optimization, the weighted coefficient method is suitable for application.

2. STRUCTURES OF COMPOUND TWO-CARRIER PGT

The most often used single-carrier planetary gear train is basic type of PGT, Fig. 1. This type of a PGT is a design which has a central sun gear (external gearing - 1), central ring gear (internal gearing - 3), planets (satellites - 2) and carrier (h). Planets are in simultaneous contact with the sun gear and the ring gear.

It is appropriate to use the Wolf-Arnaudov's symbol for simple planetary gear train review [3].

By using this symbol the PGTs are shown with a circle and different width lines. Sun gear shaft 1 is shown by a thin line, ring gear shaft 3 by a thick line and the carrier shaft h by two parallel lines since the carrier shaft is summary element regarding by carrier stopping negative transmission ratio is obtained [1,3].

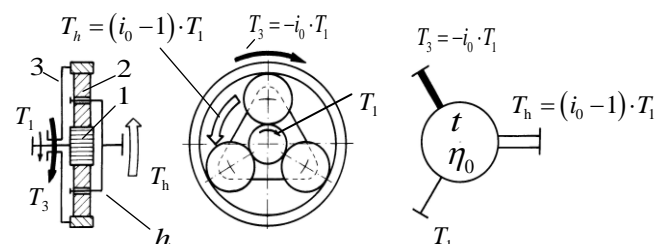


Fig.1: Wolf-Arnaudov's symbol and torque ratios of the basic type of PGT

The main force and kinematic characteristic of the simple planetary gear is the torque ratio t .
Ideal torque ratio is:

$$t = \frac{T_3}{T_1} = \frac{z_3}{z_1} = -i_0 > +1 \quad (1)$$

Torques on the ring gear shaft T_3 and on the carrier shaft T_h are given as a function of the ideal torque ratio t and the torque on the sun gear shaft T_1 .

Torques are in the relation:

$$T_1 : T_3 : T_h = +1 : (-i_0) : (i_0 - 1) \quad (2)$$

The relation between torques is:

$$T_1 \equiv T_{\min} < T_3 \equiv T_{\max} < |T_h| \equiv |T_{\Sigma}| \quad (3)$$

where:

$T_1 \equiv T_{\min}$ is the torque on the sun-gear (the lowest torque);

$T_3 \equiv T_{\max}$ is the torque on the ring-gear (the higher differential torque)

It is assumed:

$$\eta_0 = \eta_{13(h)} = \eta_{31(h)} = 1 \quad (4)$$

Its advantage over other PGT types lies, first of all, in its efficiency. The efficiency value varies negligibly in the whole range of the internal gear ratio, i.e. ideal torque ratio, $t = |z_3/z_1|$. Also, this type has small overall dimensions and mass, and its production costs are relatively low because of the relatively simplified production [6,7].

This type of a PGT is often used as single stage transmission, as a building block for higher compound planetary gear trains.

A special group of compound planetary gear trains is PGTs obtained by linking two shafts of one component planetary gear train with two shafts of the other component planetary gear train. In that way a mechanism with four external shafts is obtained (Fig. 2). Two external shafts are coupled external shafts and two are single external shafts.

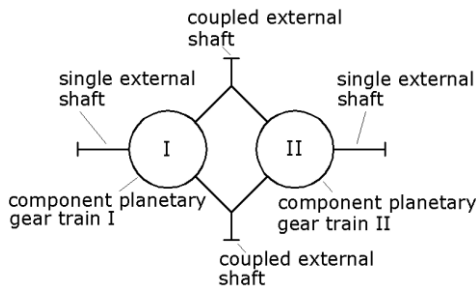


Fig.2: Planetary gear train with four external shafts (compound train)

There are many different ways of connecting the component planetary gear trains. Since that, there is isomorphism, there are only 12 different structural schemes for review. To each of 12 structural schemes an

alphanumerical label (S11...S56) is attached, which indicates the ways of connecting the shafts of the main elements of both component trains (Fig. 3)

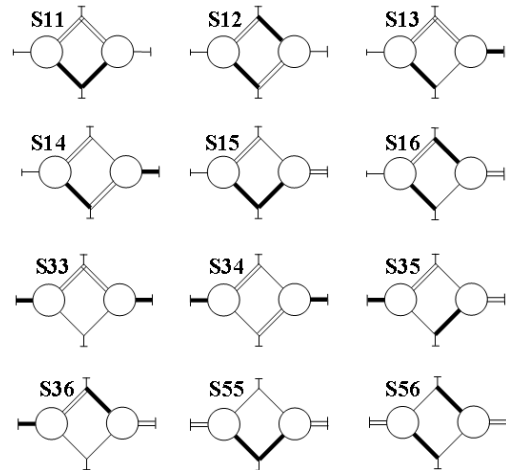
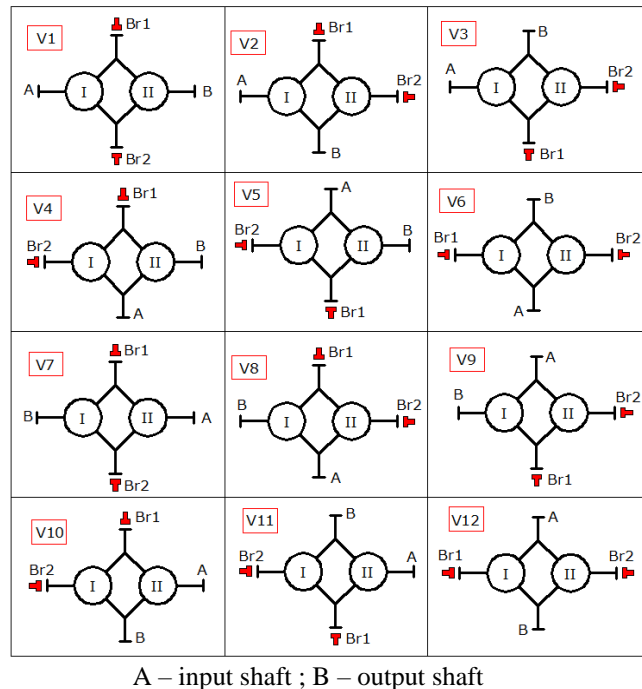


Fig.3: Systematization of all schemes of two-carrier planetary gear train with four external shafts

By placing the brakes on two shafts, a braking system is obtained in which the alternating activation of the brakes shifts the power flow through the planetary gear train, which causes a change in the transmission ratio.

In every presented scheme it is possible to put brakes (Br1 and Br2) as well as the driving and the operating machine on external shafts in 12 different ways (V1...V12) - layout variants (Fig. 4).



A – input shaft ; B – output shaft

Fig.4: Systematization of all layout variants of two-carrier planetary gear train with four external shafts

The application of these transmissions is important in mechanical systems which need speed change under load, like machine tools, cranes etc. Two-speed two-carrier planetary gears which consist of two coupled and four

external shafts and have brakes on single shafts could be used in the transport and stationary machines without limitation in power and velocity, for example in the vital parts of the helicopter, caterpillar, mining, agricultural and other machines and so on. Since that, the knowledge of methodology of synthesis of these transmissions is important.

3. THE METHODOLOGY OF SYNTHESIS OF TWO-SPEED PGT

By analyzing possibilities of two-speed two-carrier transmissions can be concluded that two speed driving systems defined by two transmission ratios can be reached by many different variants. Each of these variants has its own parameters which make possible kinematic requirements.

For the “best” solution choosing is necessary to define procedure and a computer program according the procedure [4].

The optimization process begins with generating all solutions for the assigned input data. Then, choosing optimal solution according objective functions. In this model, the following characteristics are chosen for objective functions [4]:

- minimal pitch diameter of greater ring gear
- minimal mass of all gears in the train
- maximal efficiency
- minimal relative number of revolution of the fastest satellite
- minimal satellite bearings dynamic load.

It is possible to choose one or more criteria (max 3). If user wants to select more than one criteria it is appropriate to applicate the weighted coefficient method.

In this method the following scalarized problem is constructed:

$$\max f^M(x) = w_1 \cdot f_1^0(x) + \dots + w_m \cdot f_m^0(x) \quad (5)$$

s.t. $x \in S$

Here, the weighted coefficients (or weights) w_i are positive real numbers and $f_i^0(x) = (f_i^0)^{-1} \cdot f_i(x)$ are normalized objective functions where f_i^0 are normalizing coefficients.

The input data is:

- the number of desired speed (“1” is the mark for one speed and “2” for two-speed)
- the tolerances of desired transmission ratios of each speeds ($i_{k1\min} \div i_{k1\max}, i_{k2\min} \div i_{k2\max}$)
- possibility of changing of driving shaft revolution direction
- desired satellite bearings service life
- the type of satellite bearings
- torque on input shaft
- number of revolution of input shaft
- limited intervals of the torque ratios of the two coupling gears t_1 and t_2 ($t_{1\min} \div t_{1\max}, t_{2\min} \div t_{2\max}$)
- number of teeth of sun gears of the first and second planetary gear sets (z_{11}, z_{112})

The developed computer program DVOBRZ determines values of transmission ratio functions in the frame of each

two-speed PGT for each possible combination of ideal torque ratios and checks if these values are found in the required intervals I_1 and I_2 . The intervals I_1 and I_2 are the intervals for the required transmission ratios, for which $i_{k1} \in I_1$ and $i_{k2} \in I_2$.

For the purpose of showing the computer program operation, the procedure of getting the solutions of two-speed PGT is shown. Some of the input data are:

- transmission ratio intervals $9.8 \leq i_{k1} \leq 10$;
 $3.9 \leq i_{k2} \leq 4$
- number of teeth of sun gears of the first and second planetary gear sets $z_{1I} = z_{1II} = 18$
- torque on input shaft of PGT $T_A = 50 \text{ Nm}$.
- torque ratio intervals $2 \leq t_1 \leq 12, 2 \leq t_2 \leq 12$
- the frequency of working with mentioned transmission ratios: 70% i 30%

The task is to find optimal solution according to only one criterion: minimal radial dimensions of planetary gear train. After entering input data and starting the program system DVOBRZ, 6 concepts of PGT are obtained (Tab. 1).

With the acquired data of the ideal torques ratio t_I and t_{II} , transmission ratios i_{k1} and i_{k2} , the teeth number of gears z_{3I} and z_{3II} as well as pitch diameter of the ring gears d_{3I} and d_{3II} , the computer program system determines the variant and breaks with which each transmission ratio is achieved. The PGT S16V3 ($t_1 = 3$ and $t_2 = 2$) is the optimal solution according to the criteria of minimal radial dimensions of planetary gear sets.

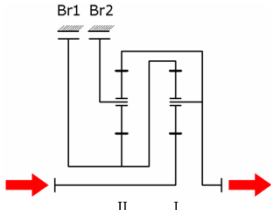
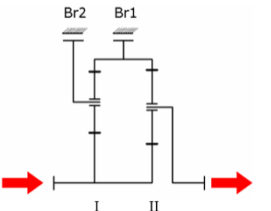
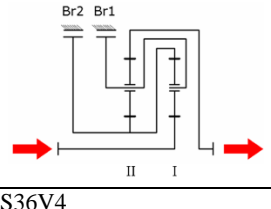
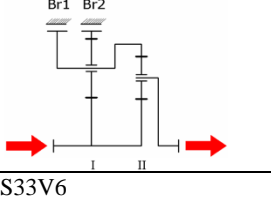
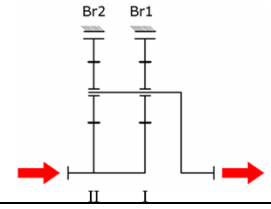
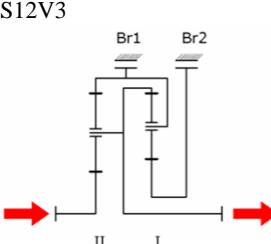
For the established solution, it is possible in the next step to define planetary gear train units by design parameters, as it implemented in [5] according the procedure described in [6,7].

The optimization process begins with generating all solutions for the assigned input data. For the given input data (transmission ratio, input number of revolution, input torque, service life in hours, application factor, accuracy grade (Q-DIN3961)), all 6-tuples of design parameters ($z_1, z_2, z_3, n_w, m_n, b$) satisfying the functional constraints are generated and the values of the objective functions for every 6-tuple are computed.

These 6-tuples form a set of feasible solutions. Based on the established objective functions and constraints, an optimal solution is selected, determined by variables. In this model the following characteristics are chosen for objective functions of a planetary gear train: volume, mass, efficiency and production cost of gear pairs [6,7], so we consider techno-economical optimization.

In this optimization application the weighted coefficient method is considered, too. The weighted coefficients method has very clear physical meaning and experience in application on technical systems optimization. This model is suitable in the case of priority functions existence, also in the case of equal priority functions.

Table 1: Solutions which conform to the given requirements

Labels and kinematic schemes	t_1, t_2	i_{k1}, i_{k2}	d / mm
S16V3 	3,2	10,4	117
S55V5 	5,3	10,4	157.5
S13V1 	5,2	10,4	157.5
S36V4 	4.8333, 8.8333	9.8333, 3.91098	238.5
S33V6 	3, 8.8333	9.8333, 4	238.5
S12V3 	8.8333, 2	9.8333, 3.94444	238.5

4. CONCLUSION

A method of optimal selection of a two-speed two-carrier planetary train according to several criteria is presented. By using program DVOBRZ, which was developed according presented procedure, we will receive the optimal two-carrier two-speed variant and its basic parameters easily.

The example of selection of optimal two-speed PGT by the computer program DVOBRZ is given. The shown methodology and the computer program enable quick

determining of structure and base parameters of two-speed PGT which can satisfy transmission requirements.

Also it is indicated the next step in the complete optimal solution definition: multi-criteria application for planetary gear units determination. In the both optimization application, the weighted coefficient method is implemented.

REFERENCES

- [1] KARAIVANOV, D., TROHA, S. (2006) Examining the possibilities for using coupled two-carrier planetary gears in two-speed mechanical transmissions, *Machinebuilding and electrical engineering*, Nr. 5 – 6, pp. 124 – 127.
- [2] KUDRJAVTSEV, V. N., KIRDYIASHEV, I. N. (1977) *Planetary gears*, Handbook, Mashinostroenie, Leningrad
- [3] ARNAUDOW, K., KARAIVANOV, D. (2005) Systematik, Eigenschaften und Möglichkeiten von zusammengesetzten Mehrsteg-Planetengeräten, *Antriebstechnik*, 5, pp. 58-65.
- [4] TROHA, S. (2011) *Analysis of a planetary change gear train's variants*, PhD Thesis, University of Rijeka, Engineering Faculty, Rijeka, Croatia.
- [5] STEFANOVIĆ-MARINOVIĆ, J., TROHA, S., MILOVANČEVIĆ, M. (2017) An Application of Multicriteria Optimization to The two-Carrier Two-Speed Planetary Gear Trains, *FACTA UNIVERSITATIS Series: Mechanical Engineering*, vol. 15, no. 1, p. 85-95.
- [6] STEFANOVIĆ-MARINOVIĆ, J. (2008), *Multicriterion optimization of planetary power transmission gear pairs*, PhD Thesis, University of Niš, Faculty of Mechanical Engineering, Niš, Serbia
- [7] STEFANOVIĆ-MARINOVIĆ, J., PETKOVIĆ, M., STANIMIROVIĆ I., MILOVANČEVIĆ, M. (2011), *A model of planetary gear multicriteria optimization*, *Transactions of FAMENA*, 35(4), pp. 21-34

CORRESPONDANCE



Jelena STEFANOVIĆ-MARINOVIĆ,
Assoc. prof. Ph.D.
University of Niš
Faculty of Mechanical Engineering
Aleksandra Medvedeva 14,
18000 Niš, Serbia
jelenas@masfak.ni.ac.rs



Sanjin TROHA, Assist. prof. Ph.D.
University of Rijeka
Faculty of Engineering
Vukovarska 58,
51000 Rijeka, Croatia,
sanjin.troha@riteh.hr



Miloš MILOVANČEVIĆ,
Assoc. prof. Ph.D.
University of Niš
Faculty of Mechanical Engineering
Aleksandra Medvedeva 14,
18000 Niš, Serbia
milovancevic@masfak.ni.ac.rs

THE INFLUENCE OF LUBRICANT VISCOSITY ON THE EFFICIENCY OF WORM GEAR REDUCER

Blaža STOJANOVIĆ
Saša RADOSAVLJEVIĆ
Sandra VELIČKOVIĆ
Slavica MILADINOVIĆ
Milan BUKVIĆ

Abstract: *The results of testing the influence of lubricant viscosity on the efficiency of the worm gear reducer are presented in this paper. The results are performed on the specialized testing device AT200 at the Center for testing power transmission at the Faculty of Engineering in Kragujevac, Serbia. The efficiency of worm gear reducer is determined for different values of input number of revolution, output torque and by variation of two types of oil. The lubricant of viscosity of 220 mm²/s and 680 mm²/s are used in the tests. The tests are performed according to the pre-defined experiment plan. The analysis of the results shows that the efficiency of the worm gear reducer increases with the increase of the number of revolutions of the input shaft, braking torque (current intensity of the brake), and the viscosity of the oil.*

Key words: *efficiency, worm gear, power.*

1. INTRODUCTION

Worm gears are widely used in technical systems both due to the possibility of achieving high speed ratios and due to the low cost of production. These gears generally have small dimensions, and they can also work as a reducer and as a multiplier. [1]

One of the main characteristics of the gear is the degree of efficiency. Despite the very low value of the degree of efficiency, the worm gears are widely applied. Numerous factors influence the degree of efficiency of worm gears, such as: the materials from which they are made, the viscosity and type of lubricants, the speed ratio, the gear type (reducer or multiplier), axial distance, operating conditions, temperatures, etc [2].

M.Turci et al. [1] were determining the degree of efficiency of worm gear reducer of the mutual distance of 50 mm, of the speed ratio of 49 and for the different types of lubricants they obtained the values of the degree of efficiency of $0.572 < \eta < 0.64$. Đ. Miltenović et al. [3] tested of the strength losses of the worm gear, in which there was a synthetic oil GH6-1500, at the value of the input number of revolutions of 5000 min^{-1} and different values of the output torque, and they obtained the value of degree of efficiency $0.52 < \eta < 0.71$. B.Magyar and B.Sauer [4] tested the values of the degree of efficiency at the lubricant temperature of 60°C and output torque of $T_2 = 430 \text{ Nm}$ by which they obtained the degree of efficiency of $0.65 < \eta < 0.74$ for different values of input number of revolutions. H.Siebert [5] determined different

types of lubricants on the degree of efficiency of the worm gear reducer, at the speed ratio of 39, the input number of revolutions of 350 min^{-1} , and the output torque of $T_2 = 200 \text{ Nm}$, and therefore he obtained the results of the degree of efficiency of $0.62 < \eta < 0.80$. According to the catalogue of the NORD Company [6], the value of the degree of efficiency of the worm gear reducers is within the range of $0.4 < \eta < 0.9$.

The influence of lubricant viscosity on the degree of efficiency of the worm gear reducer was analysed in this paper. Two types of lubricants were used in the testing, and the tests were performed for different types of values of input number of revolutions and output torque. The results show that the degree of efficiency of the worm gear reducer increases with the increase of the lubricant viscosity, input number of revolutions and output torque.

2. WORM GEARS

The worm gear pair or the worm gear is a type of gear whose axes pass by each other, mostly at the angle of 90°C . The worm gear consists of worm wheel and worm shown in the Figure 1. The angle at which the axes pass by each other can be greater and less than 90°C . If the driving part of the gear is a worm, than the reduction of the number of revolutions is done, and if the worm wheel is a driving part, than the multiplication of the number of revolutions is done. Since the values of the degree of efficiency are less than 0.5, the worm gear pair is rarely used as a multiplier [7].

It can be said that the worm gear pair is a sliding joint. One of the parts in the joint is made of a softer material

(worm wheel), and the other part of the material of the greater hardness (worm), in order to achieve the function according to the principle of intensive sliding. So therefore, the worm gear is made of bronze, aluminum alloys, zinc alloys, pearlite grey and nodular cast, brass, and the worm is made of cemented steel with a hardness of up to 62 HRC as well as of induction and flame hardened steel which are used for high loads [7,8].

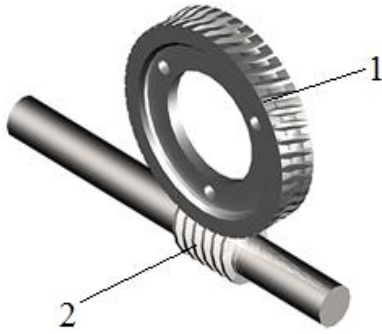


Figure 1. Worm wheel and worm

The basic characteristics and advantages of worm gears are:

- Very high speed ratio; In the case of reduction, the values of the speed ratio are $5 < i < 70$, and in the case of multiplication, they are $5 < i < 15$.
- Quieter operation and considerably lower dynamic shocks and vibrations that allow tooth on a tooth sliding.
- Long lifetime if the accuracy of the manufacture, assembly rules, good selection of materials and lubrication are respected.
- In comparison to other gears, they are usually smaller and cheaper.
- They could be a self-braking gears.
- The possibility of changing the direction of rotation of the worm wheel without structural changes so that the worm can be made with the right and left thread.
- It is possible to perform input and output power on the worm, as well as on the worm wheel from the both sides, which allows them to branch or distribute the energy by connecting a large number of worm gears [7,8,9].

The disadvantages of the worm gear are:

- Large amount of heat and energy loss due to high slide resistance.
- Relatively low degree of efficiency.

3. DEGREE OF EFFICIENCY OF WORM GEAR REDUCER

The ratio of invested and useful strength represents the degree of efficiency. In comparison to other types of gear reducers, the worm gear reducer has a lower value of the degree of efficiency. The reason for the deviation of the invested and useful strength are the strength losses occurring in the gear reducer.

If the strength on the worm is marked with P_1 , and the strength on the worm gear is marked with P_2 , in the case

where the worm is a drive element, the efficiency can be expressed as [7,8]:

$$\eta = \frac{P_2}{P_1} = \frac{T_2 \omega_2}{T_1 \omega_1} = \frac{\omega_2 F_{t2} \cdot d_2 / 2}{\omega_1 F_{t1} \cdot d_1 / 2} = \frac{F_{t2} \operatorname{tg} \gamma_m}{F_{t1} \operatorname{tg}(\gamma_m + \rho)} \quad (1)$$

The equalities were taken into account, when expressing the equation:

$$i = \frac{d_2}{(d_1 \operatorname{tg} \gamma_m)} \text{ and } F_{t2} = F_{a1} = \frac{F_{t1}}{\operatorname{tg}(\gamma_m + \rho)} \quad (2)$$

The equivalent angle of friction and the lead angle on the middle cylinder of the worm follow from the equation:

$$\operatorname{tg} \gamma_m = \frac{z_1}{q}; \quad \rho = \operatorname{arctg} \mu_z \quad (3)$$

where z_1 is a number of thread of the worm, q is a worm number and ρ is an equivalent angle of friction.

If assumed that $\rho \approx \gamma_m$, then the degree of efficiency can be expressed as following:

$$\eta = \frac{\operatorname{tg} \gamma_m}{\operatorname{tg}(\gamma_m + \rho)} = \frac{\operatorname{tg} \rho}{\operatorname{tg} 2\rho} = \frac{1 - \operatorname{tg}^2 \rho}{2} \quad (4)$$

$$\eta = \frac{\operatorname{tg} \gamma_m}{\operatorname{tg}(\gamma_m + \rho)} = \frac{\operatorname{tg} \gamma_m}{\operatorname{tg} 2\gamma_m} = \frac{1 - \operatorname{tg}^2 \gamma_m}{2}$$

The degree of efficiency increases with the increase of the lead angle to a certain maximum, and then it decreases. When the lead angle is $\gamma_m = 45^\circ$, the maximum value of the degree of efficiency of worm gear reducer is obtained. For the values of the lead angle $\gamma_m < 45^\circ$, the value of the degree of efficiency rapidly decreases, so it is recommended to use the higher angle values of the thread of the worm or to use the multi-start worms, but in doing so, the lower speed ratios are obtained [7,8].

A large number of parameters influence the degree of efficiency, among which there is one of the main types of materials, from which the worm and worm wheel are made. The extensive velocity is also an important factor that influences the degree of efficiency, because at higher extensive velocity, it is easier to create an oil film between the meshed flanks, which increases the degree of efficiency itself, as well as the worm type [8].

The total losses of energy or power occurring in the worm gear reducer consist of power losses due to the slide resistance of the worm gear pair during the movement P_{Gz} , the power loss occurring in the bearings P_{GL} and the power loss at idle motion P_{G0} . So that total power losses can be determined as following [7,8]:

$$P_G = P_{Gz} + P_{GL} + P_{G0} \quad (5)$$

If the power of the worm is marked as P_1 and the power on the worm wheel is marked with P_2 , then the degree of efficiency of the worm gear, in case when the worm is drive element, can be expressed as following [7,8]:

$$\eta = \frac{P_1 - P_G}{P_1} = \frac{P_2}{P_2 + P_G} \quad (6)$$

The power lost in overcoming the slide resistance at mashing the worm gear pair, can be determined as following [7,8]:

$$P_{Gz} = F_N \cdot \mu_z \cdot v_k \quad (7)$$

where F_N - is a normal force on the tooth flanks, μ_z - a coefficient of friction of worm gear pair, v_k - sliding velocity which can determined by following equation:

$$v_k = \frac{\pi \cdot d_{m1} \cdot n_1}{60 \cdot \cos \gamma_m} \quad (8)$$

If the diameter of the middle cylinder is in meters and the number of revolutions of the worm is expressed in minutes.

The power loss of the worm gear reducer at idle motion can be determined as [7,8]:

$$P_{G0} = 10^{-7} \cdot a \cdot \left(\frac{n_1}{60}\right)^{4/3} \cdot \left(\frac{v_{40}}{1.83} + 90\right) \quad (9)$$

where a [mm] – is a wheelbase, n_1 [min^{-1}] – number of revolutions of the worm, v_{40} [mm^2/s] - kinematic viscosity of oil on 40° C.

The following ratios are used for power loss in bearings depending on the bearing type used in the worm gear reducer [7,8]:

- $P_{GL} = P_1 \cdot (0.005 \dots 0.01)$ - if the roller bearings are built on the shaft of the worm and worm wheel.
- $P_{GL} = P_1 \cdot (0.02 \dots 0.03)$ - if the sliding bearing are built on the shaft of the worm and worm wheel.

4. DEVICE FOR TESTING THE DEGREE OF EFFICIENCY

The testing of the degree of efficiency was performed in the Center for testing power transmission at the Faculty of Engineering in Kragujevac, Serbia. Figure 2 shows the device AT200 on which the degree of efficiency was determined.

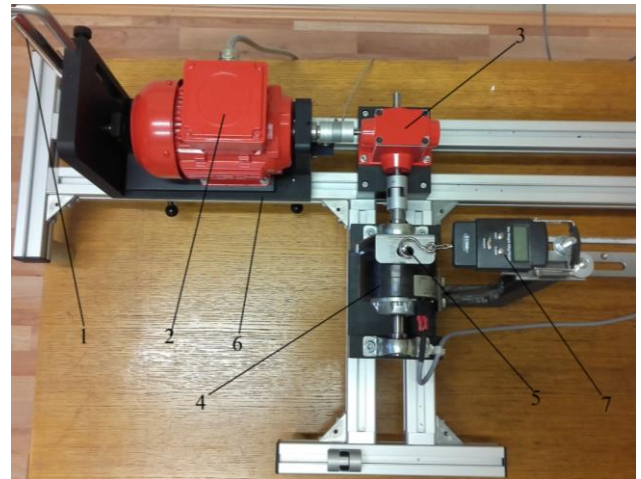


Fig.2: Device for testing the degree of efficiency - AT200

The device is used to determine the degree of efficiency of different gear transmissions and it contains the following parts (Figure 2):

- 1 - dynamometer at the input,
- 2 - motor,
- 3 - worm gear reducer,
- 4 - brake,
- 5 – brake lever,
- 6 - housing,
- 7 - dynamometer at the output.

The input torque of an electric motor is determined by using a 50 mm lever and a dynamometer. When the lever is placed in the horizontal position, and the force value on the dynamometer is read, with the help of the screw, the dynamometer remains locked at the given value. The electric motor is supported by two bearings. The tested worm gear reducer is connected to the electric motor via a claw coupling. The braking torque is calculated as the product of braking force and distance from the center of the brake to the place where the dynamometer is placed, and the length of this shaft is 100 mm. The brake consists of: the body of the brake and the shaft on which the brake is located. The brake is located on a multi-part stand, in order to allow the brakes to be connected to a different gear reducers. The entire device is placed on the frame.

The control unit (Figure 3) serves to adjust the input number of revolutions or the number of revolutions of the engine shaft as well as the braking force. The electric motor is powered from the control unit and the number of revolutions is adjusted by using a potentiometer. There is a sensor on the output shaft of the electric motor whose reading values are displayed on the control unit. The brake is also connected to the control unit and the braking force is regulated by the change of the current intensity.



Fig.3: Control unit

The degree of efficiency is calculated according to the following mathematical model [11]:

The input power is calculated according to:

$$P_1 = M_1 \cdot \omega_1$$

where:

$$M_1 = F_1 \cdot l_1$$

M_1 - is input torque EM [Nmm]; F_1 - balancing force [N]; l_1 - lever arm [mm];

ω_1 angular velocity [s^{-1}]:

$$\omega_1 = 2 \cdot \pi \cdot f_1$$

where:

$$f_1 = \frac{n}{60} \text{ - is frequency.}$$

Output power is calculated as:

$$P_2 = M_2 \cdot \omega_2$$

where:

$$M_2 = F_2 \cdot l_2$$

M_2 - output torque [Nmm] ; F_2 - balancing force [N];

l_2 - lever arm [mm]

ω_2 - angular velocity [s^{-1}]:

$$\omega_2 = 2 \cdot \pi \cdot f_2, \text{ where}$$

$$f_2 = \frac{n}{60} \text{ - is frequency.}$$

The degree of efficiency is determined as the ratio between the output and the input power:

$$\eta = \frac{P_2}{P_1} \cdot 100, \%$$

5. TEST RESULTS

The degree of efficiency was determined on the previously described device for different values of the input number of revolutions and the output torque regulated by the current intensity on the control unit.

Table 1 and Table 2 show the values of the degree of efficiency of the worm gear reducer, for the viscosity of the lubricant $220 \text{ mm}^2/\text{s}$ and $680 \text{ mm}^2/\text{s}$ for the values of the input number of revolutions of 1500, 1750 and 2000, all with different values of output torque regulated by the current intensity on the control unit.

Table 1: Degree of efficiency of worm gear reducer for viscosity of lubricant $v=220 \text{ mm}^2/\text{s}$

current intensity [A]	input number of revolutions [min^{-1}]		
	1500	1750	2000
0.1	0.568	0.581	0.592
0.125	0.603	0.616	0.623
0.15	0.62	0.636	0.643
0.175	0.636	0.655	0.662
0.2	0.647	0.663	0.669

Table 2: Degree of efficiency of worm gear reducer for viscosity of lubricant $v=680 \text{ mm}^2/\text{s}$

current intensity [A]	input number of revolutions [min^{-1}]		
	1500	1750	2000
0.1	0.582	0.599	0.61
0.125	0.623	0.636	0.644
0.15	0.65	0.665	0.671
0.175	0.674	0.686	0.692
0.2	0.684	0.695	0.701

Figure 4 shows the values of the degree of efficiency of the worm gear reducer for the viscosity of the lubricant of $220 \text{ mm}^2/\text{s}$ and the difference that occurs when changing the output torque, regulated by the current intensity, on the control unit, can be easily noticed.

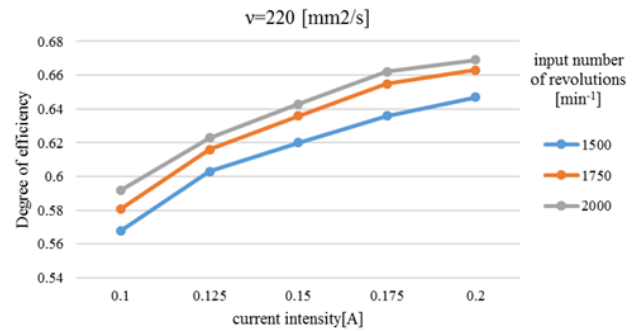


Fig.4: The value of degree of efficiency of worm gear reducer for viscosity of lubricants $v=220 \text{ mm}^2/\text{s}$

The values of the degree of efficiency of the worm gear reducer for the viscosity of the lubricant $680 \text{ mm}^2/\text{s}$ are shown in Figure 5. It is also noticed that the difference occurs when changing the output torque, regulated by the current intensity, on the control unit.

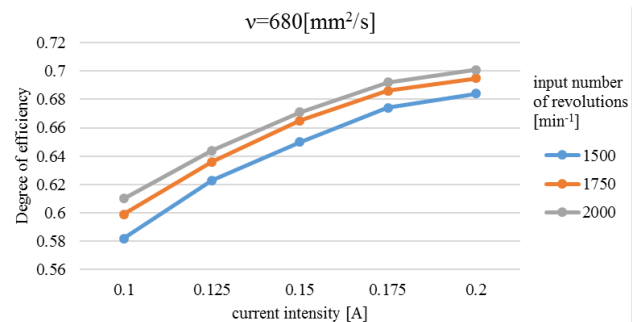


Fig.5: The value of degree of efficiency of worm gear reducer for viscosity of lubricants $v=680 \text{ mm}^2/\text{s}$

Figure 6 shows a comparative view of the values of the degree of efficiency for different viscosities depending on the input number of revolutions and current intensity, on the control unit.

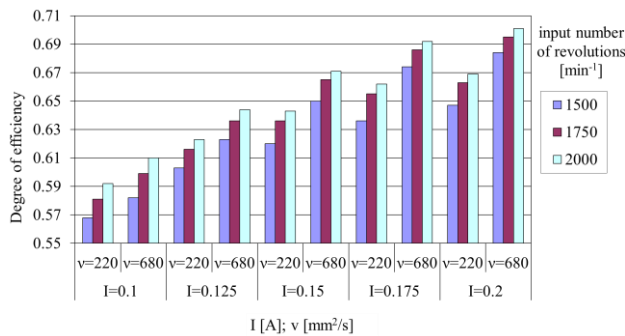


Fig.6: Comparative view of the values of degree of efficiency for different viscosities of lubricants

6. RESULT ANALYSIS

Table 1 and Figure 4 clearly show the proportional dependence of the value of the degree of efficiency from the output torque, regulated by the current intensity, on the control unit for the viscosity of the lubricant of 220mm²/s. The value of the degree of efficiency increases with the increase of the value of current intensity or output torque. Table 2 and Figure 5 show that the degree of efficiency increases by using the lubricants of higher viscosity (680 mm²/s) with the increase of the value of current intensity.

Likewise, it can be noticed that there is a difference in values of the degree of efficiency for a different values of the input number of revolutions. Figure 4 and Figure 5 clearly show that the degree of efficiency increases for the same current intensity, or the output torque, with the increase of value of the input number of revolutions, for the tested worm gear reducer. The highest values of the degree of efficiency of the worm gear reducer are obtained for the value of the input number of revolutions of 2000 min⁻¹, because the losses in the worm gear reducer decreases with the increase of number of revolutions.

The comparative view of the degree of efficiency for both types of lubricants is shown in the Figure 6 and it can be noticed that the degree of efficiency is always higher with the lubricants of higher viscosity than the one with lubricants of lower viscosity. The increase of the degree of efficiency for the both types of lubricants is noticed with the increase of the current intensity, and the highest degree of efficiency is obtained for the current intensity of 0.2 A, at the number of revolutions of 2000 min⁻¹, and for the lubricant viscosity of 680 mm²/s.

Also, the difference is clearly noticed in the trend of change of the degree of efficiency in relation to the current intensity for the lubricant viscosity of 220 mm²/s, in relation to lubricant viscosity of 680 mm²/s, because the lubricant viscosity of 220 mm²/s is a mineral oil, while the lubricant viscosity of 680 mm²/s is a synthetic grease.

The values of the degree of efficiency determined by the device AT200 are, for the most part, within the limits stated in the introduction of this paper. Somewhat higher values of the degree of efficiency occur due to the fact that the worm gear reducer is used for the purpose of testing, whose worm contains two threads. As shown in Figure 5, after the adjustment period, and if the worm contains two threads, the degree of efficiency is about 0.7, which are the values obtained by the experiment. Also, it is important to note that the slightly higher degree of efficiency is the consequence of the use of high viscosity lubricants.

7. CONCLUSION

Even though the worm gear reducers have the lower degree of efficiency than other reducers with the same speed ratio and sizes, they are still very interesting because they are simple and cheap.

The improvement of their degree of efficiency is done in pace with the continuous development of standard. If there is a tendency not to change the geometry of the worm gear reducer, the increase of the degree of efficiency can be made by the influence on the composition of the lubricant additive.

The tests have shown that the increase of the lubricants viscosity influence the increase of the degree of efficiency of the worm gear reducer. Also, the degree of efficiency increases with the increase of the number of revolutions of the input shaft and torque of the reducer output shaft. Make sure that the number of revolutions of the input shaft does not exceed 3000 min⁻¹, because then, the degree of efficiency decreases due to the inability to form the lubricant layer

ACKNOWLEDGEMENT

This paper presents the results obtained during research within the framework of the project TR 35021, supported by the Ministry of Education, Science and Technological Development of the Republic of Serbia.

REFERENCES

- [1] TURCI, M., FERRAMOLA, E., BISANTI, F., GIACOMOZZI, G. (2016) *Worm Gear Efficiency Estimation and Optimization*, Gear Technology, Vol. 33, No. 4, pp. 46-53.
- [2] SKULIĆ, A., KRSMANOVIĆ, D., RADOSAVLJEVIĆ, S., IVANOVIĆ, L., STOJANOVIĆ B. (2017) Power Losses of Worm Gear Pairs, ACTA TECHNICA CORVINIENSIS - Bulletin of Engineering, Vol.10, No. 3, pp. 39-45.
- [3] MILTENOVIC, Đ., BANIĆ, M., MILTENOVIC, A., TICA, M. (2016) *Power losses and efficiency of worm gears in extreme operating conditions*, Proceedings of the International conference „COMETA 2016”, pp. 169-176.
- [4] MAGYAR, B., SAUER, B. (2015) *Calculation of the Efficiency of Worm Gear Drives*, Power Transmission Engineering, Vol 9, No 4, pp. 52-56.

- [5] SIEBERT, H. (2011) Worm Gears-Higher Energy Efficiency and Less Strain on Resources, Gear Technology, pp. 26-30.
- [6] NORD Drivesystems; internet adres: <https://www.nord.com/content/worm-gear-efficiency>, accessed: 28.3.2017.
- [7] NIKOLIĆ, V.,: *Mašinski elementi*, Mašinski fakultet u Kragujevcu, 2004.
- [8] MILTENOVIĆ, V., OGNJANOVIĆ, M. (1995) *Mašinski elementi 2-elementi za prenos snage*, Mašinski fakultet Niš.
- [9] MILTENOVIĆ, Đ., TICA, M., MILTENOVIĆ, A., BANIC, M. (2016) *Load Capacity of Worm Gears with Compact Design*, International Journal of Engineering, pp. 25-30.
- [10] BOSTON GEAR, <http://www.bostongear.com/>, accessed: 25.3.2017.
- [11] GUNT (2011) Experiment Instructions, AT200 Apparatus for Determination of Gear Efficiency.

CORRESPONDANCE



Blaža STOJANOVIĆ, Assist. Prof PhD,
University of Kragujevac,
Faculty of Engineering,
Sestre Janjić 6,
34000 Kragujevac, Serbia,
E-mail: blaza@kg.ac.rs



Saša RADOSAVLJEVIĆ, Master Eng.
University of Kragujevac
Mechanical Engineering Faculty
Sestre Janjić 6.
34000 Kragujevac, Serbia
rsasa742@gmail.com



Sandra VELIČKOVIĆ, PhD student
University of Kragujevac
Faculty of Engineering
Sestre Janjić br. 6
34000 Kragujevac, Serbia
sandrav@kg.ac.rs



Slavica MILADINOVIĆ, PhD student
University of Kragujevac
Faculty of Engineering
Sestre Janjić br. 6
34000 Kragujevac, Serbia
slavicam@kg.ac.rs

Milan BUKVIĆ, PhD student
University of Kragujevac
Faculty of Engineering
Sestre Janjić br. 6
34000 Kragujevac, Serbia
milanbukvic76@gmail.com

ANALYSIS OF THE TEETH NUMBER INFLUENCE ON THE GEAR MODULE SIZE AND LOAD CARRYING CAPACITY OF GEAR PAIR OF UNIVERSAL HELICAL GEAR DRIVES

Milan RACKOV
Mirko BLAGOJEVIĆ
Siniša KUZMANOVIĆ
Miloš MATEJIĆ
Ivan KNEŽEVIĆ
Maja ČAVIĆ
Marko PENČIĆ

Abstract: *The basic parameters of the universal gear drives, except the axis height, are not defined by the standard, so the manufacturers of universal gear reducers can define them in their way. Most of the manufacturers followed the parameter values of universal gear reducers of leading world producers in order to ensure their interchangeability and the better positioning of their gear units at the market. This paper deals with the analysis of the influence of the gear pair teeth number on the size of the module, as well as on the load carrying capacity of single-stage universal gear units. For defined gear ratio values, different combinations of teeth number of pinion and driven gear were selected. Further, it was made calculation of the basic geometric dimensions of the gear pair, as well as the load capacity.*

Key words: *gear ratio, module, gear pair, load carrying capacity.*

1. INTRODUCTION

Axis heights of universal gear reducers are defined according to the standard row R20 (1; 1,12; 1,25; 1,4; 1,6; 1,8; 2; 2,24; 2,5; 2,8; 3,15; 3,55; 4; 4,5; 5; 5,6; 6,3; 7,1; 8; 9; 10). Since this row is very dense, for a while manufacturers of universal gear reducer produced reducers with axis height from a standard row R10 (1; 1,25; 1,6; 2; 2,5; 3,15; 4; 5; 6,3; 8; 10). But soon they increased axis heights in order to have larger dimensions to increase gear ratio, and now reducers are produced with axis height in a standard row R20/2 [1, 2]. However, in the area of the most used gearbox sizes, some manufacturers produce gear units with the axis heights in a row R20. Thus, today combined row is practically used. Defining the row R20/2, which means growth factor of height is $q_1 = 1.25$, it follows that growth factor of torque is $q_T = (q_1)^3 = 2$. This practically defines the row of output torques (R20/3 or R40/6), which is followed by almost all manufacturers of gear drives. On the basis of the axis height and the output torque, particular gear ratio values of the universal gear reducer are also defined [3, 4, 5, 6, 7]. However, for each value of gear ratio manufacturers specially define the load capacity, in order to use the gear unit in the most rational way (it is important to adopt as higher output torque as possible for each gear ratio) [1, 2, 3]. Of course, it should take into account the strength of all components, shafts, bearings, keys.

2. PROBLEM DESCRIPTION

The gear ratio of the gearbox depends on the adopted concept of the gear reducer family. Therefore, gear reducers can be manufactured in separate housing only for single-stage, two-stage, three-stage and four-stage gear unit. Such an approach is extremely expensive and nobody uses it. Generally, single-stage gear units are produced in a separate housing. However, due to lower demand for these reducers, there are manufacturers which do not produce single-stage gearbox at all, since they consider that single-stage gear units are not cost-effective. There are manufacturers who produce two-stage gearboxes in a special housing for two-stage gear units and three-stage gearboxes produce by adding one-stage gear unit to this special two-stage unit [4, 5, 6]. Most of manufacturers produce universal housing for two- and three-stage reducers, but this kind of two-stage gear unit is more expensive. Therefore, in this way, two- and three-stage gearboxes are produced in the same housing, with the same output gear pair and the same output shaft and bearings. According to this, it follows that the output nominal torque of two- and three-stage gearbox is the same. Since the output gear pair is much more expensive than the input (first) or the second gear pair, the number of different output gear pairs is reduced to a minimum (one or two gear pairs) and that the number of input gear pairs is increased in order to achieve different values of gear ratio within the first gear pair. These same first gear

pairs are also used within single-stage gear units. If it should provide the gear ratio values within the standard row R20 for a single-stage gear drive, it should have a lot of first gear pairs, and especially a lot of pinions (with different hole diameters in order to fit different sizes of electric motors). This production is more expensive, so some manufacturers offer gear ratio values of single-stage gearboxes within standard row R10. With two output gear pairs they provide gear ratio values of two- and three-stage gearbox within the standard row R20 (Fig.1).

Nevertheless, there are manufacturers which offer gear ratio within the row R20 for single-stage gear units. Today, the second approach is considered to be more justified, since it is possible to provide all gear ratio values with a small number of expensive gears. Also, it is possible to mount different requirements of the gear ratio and thus provide their faster delivery. It is considered today that it is necessary to deliver a gear reducer to the customer as soon as possible, usually within 72 hours.

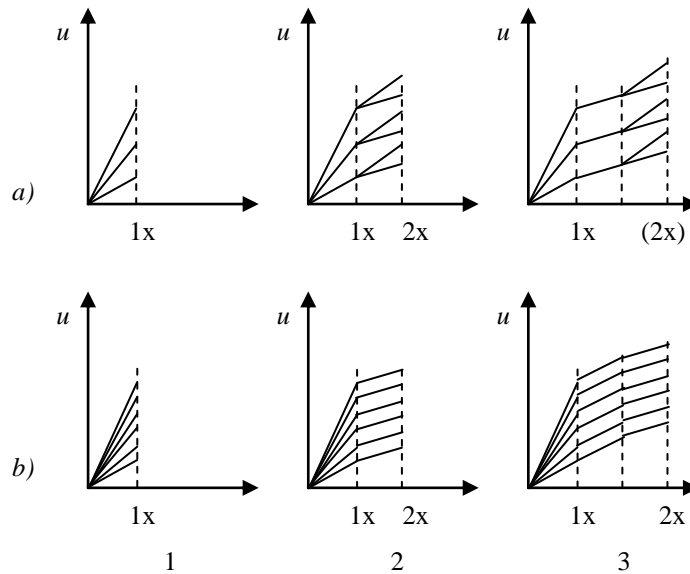


Fig.1: Performing of gear ratio for single-stage (1), two-stage (2) and three-stage (3) universal gear units; (a) first gear pair is performed with gear ratio in standard row R10 and (b) first gear pair is performed with gear ratio in standard row R20

Of course, the goal is to achieve as high as possible gear ratio within each number of gear stages. Therefore, most manufacturers of gear reducers use special reducer motor which has shaft with smaller diameter than standard IEC electric motor. This allows the installation of smaller

gears. Also, special reducer motor can have a hole in the free end of the shaft where small pinions are pressed, so gear ratio can have high values (Fig.2-1). Although, there are manufacturers which use standard IEC electric motor, but also achieve relatively high gear ratio (Fig.2-2).

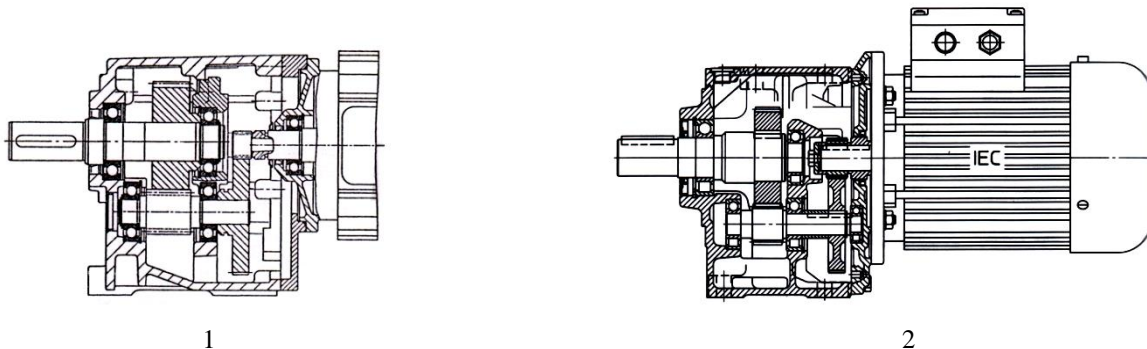


Fig.2: Gearmotor with special reducer motor Lenze (1) and gearmotor with standard electric motor ROSSI(2)[7, 8]

The great advantage of special reducer motors is that they have stronger bearings, which allow supporting of large radial and axial forces occurring on the pinion. Sealing problem is better and seriously solved for special motors, so there is no possibility of leaking oil from the gearbox into the electric motor housing. Additionally, these special electric motors are made with smaller flanges, making the gearmotor much more compact. Adopted concept of the housing with the common output gear pair for two- and three-stage solution allows the use

of first gear pair with smaller loadability in a three-stage variant to rationally utilize the first pair (Fig.3). This first pair is from the first smaller size of a two-stage gearbox. Otherwise, the first pair would be oversized in the three-stage variant. The load carrying capacity of the first gear pair is determined on the basis of the nominal output torque and the lowest gear ratio of the second pair, in the case of two-stage gearbox; and respectively, on the basis of the nominal output torque and the lowest gear ratio of the second and third pair of three-stage gearbox [1, 3].

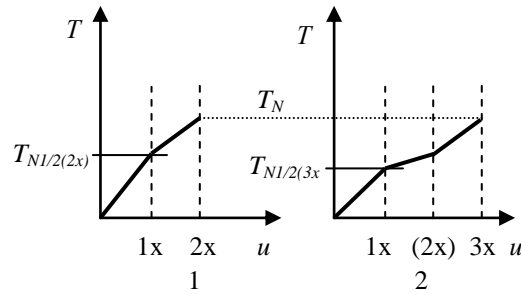


Fig.3: The way of performing output torque for two-stage (1) and three-stage (2) gear reducer

This paper defines the highest value of the gear ratio depending on the available space and it makes the variation of the modules for adopted helical angle in order to adopt the most favorable gear reducer solution.

3. EXAMPLE

For example, if single-stage gear reducer is considered for the axis height of 100 mm, it can be concluded that many

manufacturers (Table 1, 2 and 3) adopt a calculation output torque value of approx. 400 Nm. However, there are manufacturers who adopt higher values of nominal torque, but they have lower gear ratios, and vice versa.

It is evident that within the available space inside the housing, i.e. for the adopted central distance and the overall dimensions, manufacturers succeed to obtain relatively high gear ratio and large load carrying capacities.

Table 1: Nominal output torque values of single-stage gear units of manufacturer SEW for particular values of the gear ratio for different axis heights and central distances [4]

SEW, RX87, $h = 100$ mm, $a = 93,5$ mm																
u	8.65	7.63	7.20	6.45	5.56	5.07	4.50	3.78	3.48	3.09	2.76	2.48	2.15	1.93	1.60	1.39
T_{N2}	139	149	140	192	225	250	290	305	405	405	405	405	385	355	315	290

Table 2: Nominal output torque values of single-stage gear units of manufacturer NORD for particular values of the gear ratio for different axis heights and central distances [5]

NORD, SK51E, $h = 112$ mm, $a = 106$ mm														
u	13.27	9.09	6.82	5.50	4.04	3.31	2.86	2.5	2.06	1.82	1.64	1.52	1.44	1.24
T_{N2}	290	320	400	220	410	492	456	426	382	341	325	310	305	275

Table 3: Nominal output torque values of single-stage gear units of manufacturer SIEMENS for particular values of the gear ratio for different axis heights and central distances [6]

SIEMENS, E88, $h = 100$ mm, $a = 99$ mm																	
u	10.33	9.46	8.42	7.69	7.07	6.53	6.06	5.65	5.11	4.70	4.23	3.90	3.30	2.88	2.45	2.09	1.71
T_{N2}	230	210	245	245	290	300	280	320	370	385	400	385	450	435	420	420	365

Especially, it should be noted that today the values of gear ratio of single-stage gear units are adopted from the standard row R20. In the case of integer number, the teeth number of gear wheel is usually reduced by one to prevent the constant contact of the same teeth. Nowadays, eight teeth is usually adopted as the smallest number of teeth of pinion, since now the most of manufacturers of gear reducers have the technology for producing such kind of gears. Also, the distance between the outside diameter of the driven gear and the gear unit housing is reduced to approx. 2-3 mm. Also, for this axial height of 100 mm, the thickness of the wall housing between the driven gear and the floor is reduced from 6 mm to only 3-4 mm, in order to allow the installation of larger driven gears.

In this case, only the first gear pair, used for single-, two-, three- and multi-stages gearbox, will be analyzed. The diameter of the pinion is defined by preliminary calculation according to the equation defined by the standard [9]:

$$d_1 = 850 \sqrt[3]{\frac{T_1 K_A S_{H\min}^2 u + 1}{\psi_{b/d} \sigma_{H\lim}^2 u}} \quad (1)$$

where:

T_1 – torque on the pinion calculated according $T_1 = T_{N2} / u_{1/2}$. In this analyze, it is calculated as

$$T_1 = \frac{T_{N2}}{u_{1/2}} = \frac{200}{10} = 20 \text{ Nm} \quad (2)$$

Output nominal torque for universal gear units is defined by corresponding sizes of single-stage gear units. In this case, torque $T_{N2} = 200$ Nm will be adopted for this gear ratio, similar as the most other gear units manufacturers (Tables 1, 2 and 3). Standard value $u_{1/2} = 10$ is adopted as the value of the gear ratio, in this case.

K_A – impact factor; it is adopted that $K_A = 1.0$ for universal gear units, but all operation unbalances are taken into account when selecting the size of the gear unit through the service factor (f_B) [9].

$S_{H\min}$ – minimal value of safety factor. It is supposed by standard that its value is $S_{H\min} = 1.2$, although it is usually enough to have a value of 1 or something above it for universal gear units [9].

u – gear ratio for calculated gear pair; $u_{1/2} = 10$ is adopted as the value of the gear ratio.

$\psi_{b/d}$ – the ratio of the width and pinion diameter; it is adopted that $\psi_{b/d} = 1$.

σ_{Hlim} – permitted dynamic contact stress; for carburizing steel 16MnCr5 it is $\sigma_{Hlim} = 1470 \text{ N/mm}^2$.

Calculated value of pitched diameter is $d_1 = 18.43 \text{ mm}$. Different modules and different load carrying capacities of the gear pair are obtained for different pinion teeth numbers for its constant diameter and constant helical angle (Table 4) [9, 10, 11].

If the helical angle is 30° and pinion teeth number is 8, it follows that the value of module can be calculated as [9, 10]:

$$m_{n1/2} = \frac{d_1 \cos \beta_{1/2}}{z_1} = \frac{18.43 \cdot \cos 30^\circ}{8} = 2.05 \text{ mm} \quad (3)$$

On the basis of this, it is adopted the standard value of module $m_{n1/2} = 2 \text{ mm}$. For teeth numbers of other gear pairs, the values are given in Table 4.

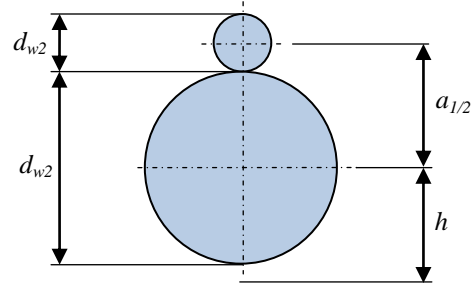


Fig.4: Characteristic dimensions of gears and gearbox housing

Table 4: Load carrying capacity of gear pairs for different teeth number and module of pinion, but for the same pinion diameter

u	z_1	z_2	u_r	$\beta_{1/2}$ [°]	$m_{n1/2 \text{ calc}}$ [mm]	$m_{n1/2 \text{ stan}}$ [mm]	b_2 [mm]	$a_{1/2}$ [mm]	T_{N2} [Nm]
10	7	69	9.86	30	2.28	2.25	19	100	259.66
10	8	79	9.88	30	2.00	2	19	100	260.14
10	9	89	9.89	30	1.77	1.75	19	99	260.5
10	10	99	9.90	30	1.60	1.5	19	95	234.71
10	11	109	9.91	30	1.45	1.5	19	104	306.72
10	12	119	9.92	30	1.33	1.25	19	95	228.58
10	13	129	9.92	30	1.23	1.25	19	103	300.61
10	14	139	9.93	30	1.14	1	19	90	202.7
10	15	149	9.93	30	1.06	1	19	95	228.96
10	16	159	9.94	30	1.00	1	19	101	274.87
10	17	169	9.94	30	0.94	0.9	19	97	242.24
10	18	179	9.94	30	0.89	0.9	19	103	301.26
10	19	189	9.95	30	0.84	0.8	19	97	235.84
10	20	199	9.95	30	0.80	0.8	19	101	255.56
10	21	209	9.95	30	0.76	0.8	19	105	301.5
10	22	219	9.95	30	0.73	0.7	19	97	203.23
10	23	229	9.96	30	0.69	0.7	19	101	236.06

Table 5: Load carrying capacity and dimensions of gear pairs for particular values of gear ratio and adopted central distance, for the same module value

u_{R20}	z_1	z_2	u_r	$\beta_{1/2}$ [°]	$m_{n1/2 \text{ stan}}$ [mm]	d_{w1} [mm]	d_{w2} [mm]	b_2 [mm]	$a_{1/2}$ [mm]	T_{N2} [Nm]
10	8	79	9.88	30	2	18.3908	181.609	19	100	253.63
9	9	80	8.89	30	2	20.2247	179.775	19	100	275.13
8	10	79	7.90	30	2	22.4719	177.528	19	100	322.57
7.1	11	78	7.09	30	2	24.7191	175.281	19	100	373.59
6.3	12	76	6.33	30	2	27.2727	172.727	19	100	458.8
5.6	13	73	5.62	30	2	30.2326	169.767	19	100	554.72
5	15	74	4.93	30	2	33.7079	166.292	19	100	536.08
4.5	16	72	4.50	30	2	36.3636	163.636	19	100	622.351
4	18	71	3.94	30	2	40.4494	159.551	19	100	623.45
3.55	20	70	3.50	30	2	44.4444	155.556	19	100	599.3
3.15	21	66	3.14	30	2	48.2759	151.724	19	100	703.73
2.8	23	64	2.78	30	2	52.8736	147.126	19	100	696.36
2.5	25	63	2.52	30	2	56.8182	143.182	19	100	697.03
2.24	27	61	2.26	30	2	61.3636	138.636	19	100	681.45
2	29	59	2.03	30	2	65.9091	134.091	19	100	656.52
1.8	31	56	1.81	30	2	71.2644	128.736	19	100	618.63
1.6	34	54	1.59	30	2	77.2727	122.727	19	100	585.74
1.4	36	51	1.42	30	2	82.7586	117.241	19	100	569.11
1.25	39	49	1.26	30	2	88.6364	111.364	19	100	521.28
1.12	41	46	1.12	30	2	94.2529	105.747	19	100	502.44

Notification: The calculation has a certain dissipation of the torque value because of the application of different profile shift coefficients, and this dissipation is neglected in this case.

If the pinion diameter and the gear ratio are defined, the diameter of the driven gear and the central distance are defined (Fig. 4 and Table 4) [9, 11]:

$$d_2 = u_{1/2} d_1 \quad (4a)$$

$$a_{1/2} = \frac{m_{n1/2}}{\cos \beta_{1/2}} \cdot \frac{z_1 + z_2}{2} \cdot \frac{\cos \alpha_t}{\cos \alpha_{wt}} \quad (4b)$$

where:

α_t – transverse pressure angle.

α_{wt} – transverse working pressure angle.

Based on the previous calculation (Table 4), it is evident that with the reduction of the module value, for the same central distance, the teeth number of gear increases, while the value of load capacity remains almost the same. In this case, the module can be reduced from 2 mm to 0.7 mm or less (Fig.5). Of course, there is no justification for the application of small modules, since the teeth are smaller then and thus their load capacity (Fig.6).

If it is adopted standard module value of 2 mm for gear pair with gear ratio according standard row R20 (Table 5), it can be concluded that the load capacity of the gear pairs with smaller gear ratio increases, which is logical since the pinion diameter has larger dimension (Fig.7).

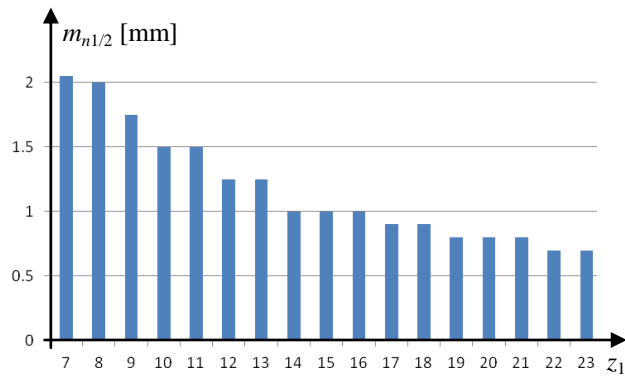


Fig.5: The values of required modules for the particular teeth number of pinion for approximately the same central distance $a \approx 100$ mm and the gear ratio $u \approx 10$

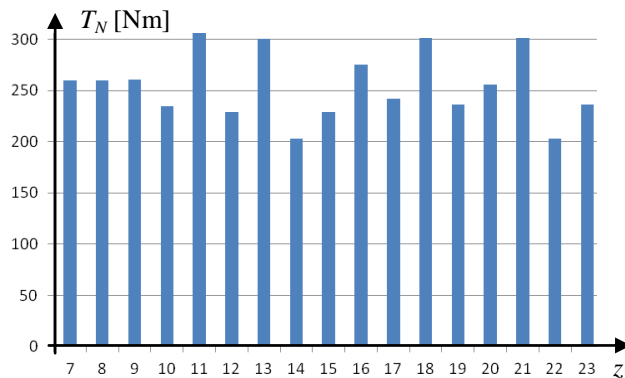


Fig.6: Load carrying capacities obtained for different teeth number of pinion for approximately the same central distance $a \approx 100$ mm and the minimum required module value

If the values of modules for gear pairs with lower gear ratio would be increased, it would significantly increase its load capacity (Fig.7). However, it is not necessary, since it would require more tools during production, and

also this increased load capacity could not be used, because with a large number of gear ratios this capacity is smaller and it is no reasonable to install other stronger components (shafts, bearings, keys, etc.) because they could not be used rationally. For very low gear ratios, the load capacity of gear pairs is not decreased, while the output torque of the gearbox is decreased due to reduced load capacity of the bearings at high speeds.

If this analysis of load carrying capacities is carried out for all gear ratio, it can be seen that with the change of the module there is a significant change in the load capacity of the gear pairs (Fig.8 and 9). The great difference in load capacity is not justified in this case, because stronger bearings, shafts, keys and other components should be installed, but they could not be used in all gear ratios.

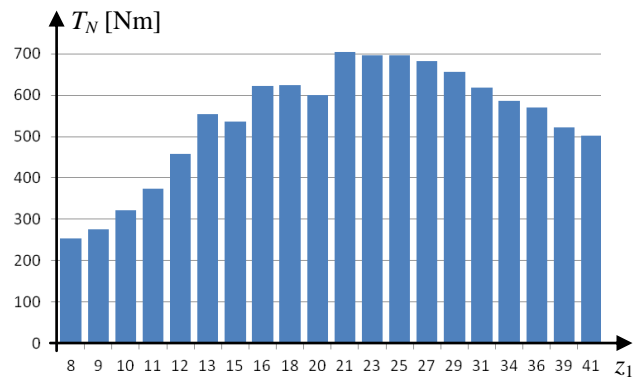


Fig.7: Load carrying capacities obtained for different teeth number of pinion for the same central distance $a = 100$ mm and adopted module $m_n = 2$ mm

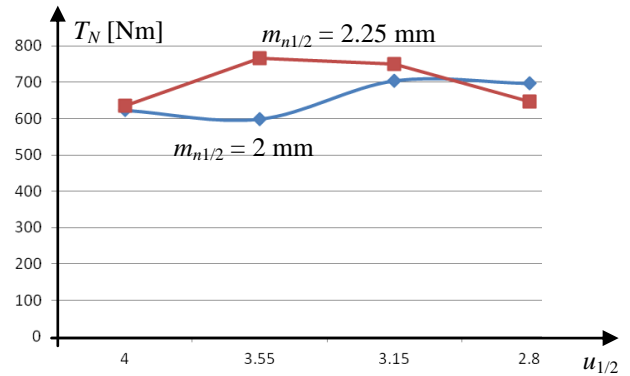


Fig.8: Comparison of load capacities obtained for different gear ratio for the same central distance $a = 100$ mm and two module values

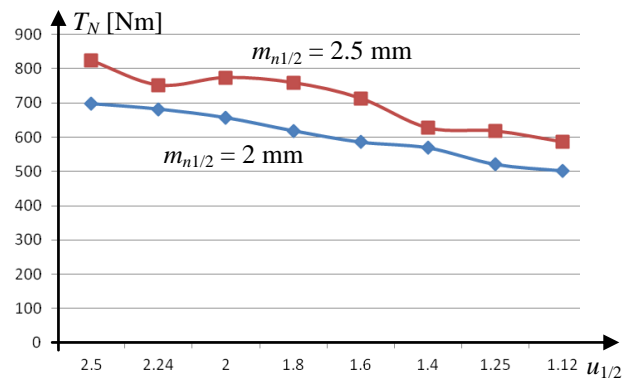


Fig.9: Comparison of load capacities obtained for different gear ratio for the same central distance $a = 100$ mm and two module values

4. CONCLUSION

This paper defines the way of preliminary calculation of gear pair inside the single-stage gearbox. Also, it defines a way for determination of gear ratio, teeth number and module values. On the basis of the carried out preliminary calculation of a gear pair in single-stage gear reducer with axial height of 100 mm, maximal nominal torque 200 Nm and the highest gear ratio 10, the minimal pinion diameter is 18.43 mm for the helical angle of 30° and different pinion teeth numbers (7, 8, 9, 10, 11, 12, 13, 14, 15, 16, 17, 18, 19, 20, 21, 22, 23). The actual value of the torque at the output is 200-300 Nm which indicates that the teeth number and the module has no major impact on the load carrying capacity of the gearbox. However, if the gear ratio values and module values are varied, it can be concluded that the change of load capacity is significant. Nevertheless, using the large module values is often not justified, since it provides great load capacity for small gear ratio. But the problem is that other gearbox components should carry this large load capacity which requires stronger and more expensive gearbox components.

In the final selection of the module value, it must be have in mind that larger modules provide greater load capacity, but also increase the production costs of the gearbox. Since the final load carrying capacity of the gearbox is also limited by the capacity of the other components within the gearbox, it can be concluded it is not justifiable to apply very large and different values of modules. In that case production of gearbox requires more different tools, more tools installation and set up, more complex control, etc. The aim of this paper is to point out the justification of a simple approach to the selection of the basic gears parameters and the benefits that are achieved.

REFERENCES

- [1] Kuzmanović, S. (2009) *Universal Gear Reducers with Cylindrical Gears* (in Serbian), University of Novi Sad, Faculty of Technical Sciences, Novi Sad.
- [2] Marjanovic, N., Isailovic, B., Marjanovic, V., Milojevic, Z., Blagojevic, M., Bojic, M. (2012) *A Practical Approach to the Optimization of Gear Trains With Spur Gears*, Mechanism and Machine Theory, Vol.53, No.July 2012, pp. 01-16, ISSN 0094-114.
- [3] Rackov, M. (2013) *Conceptions of Development of Universal Gear Reducers* (Ph.D. thesis in Serbian), University of Novi Sad, Faculty of Technical Sciences.
- [4] SEW EURODRIVE CATALOG DRN. Gearmotors (IE3) Edition 11/2015, 2133189/EN.
- [5] Catalog NORD DRIVERSYSTEMS G1000, constant speeds, www.nord.com.
- [6] SIEMENS, motox, GEARED MOTORS, Catalog D87.1.2007.
- [7] Lenze, L-force, Getriebemotoren, de 02/2016.
- [8] Rossi, E04 – *Coaxial Gear Reducers and Gearmotors*, Edition December 2015, 4002BRO.ECO-en 1210 HQM.
- [9] Kuzmanović, S. (2016) *Machine Elements* (in Serbian), University of Novi Sad, Faculty of Technical Sciences, Novi Sad.

- [10] Marjanovic, N., Ivkovic, B., Blagojevic, M., Stojanovic, B. (2010) *Experimental Determination of Friction Coefficient at Gear Drives*, Journal of the Balkan Tribological Association, Vol.16, No.4, pp. 517-526, ISSN 1310-4772.
- [11] Marjanovic, N., Kostic, N., Blagojevic, M., Marjanovic, V., Isailovic, B. (2013) *Automated Gear Train Modeling in CAD Environment*, Proceedings of the International conference "DEMI 2013", Banja Luka, 30.05.-01.06.2013, pp. 107-110, ISBN 978-99938-39-46-0.

CORRESPONDANCE



Milan RACKOV, Assist. Prof., Ph.D. Eng.
University of Novi Sad
Faculty of Technical Sciences
Trg Dositeja Obradovića 6
21000 Novi Sad, Serbia
racmil@uns.ac.rs



Mirko BLAGOJEVIĆ, Assoc. Prof. Ph.D.
University of Kragujevac
Faculty of Engineering
Sestre Janjic 6
34000 Kragujevac, Serbia
mirkob@kg.ac.rs



Siniša KUZMANOVIĆ, Prof. D.Sc. Eng
University of Novi Sad
Faculty of Technical Sciences
Trg Dositeja Obradovića 6
21000 Novi Sad, Serbia
kuzman@uns.ac.rs



Miloš MATEJIĆ, Teach. Ass., MSc. Eng.
University of Kragujevac
Faculty of Engineering
Sestre Janjic 6
34000 Kragujevac, Serbia
mmatejic@kg.ac.rs



Ivan KNEŽEVIĆ, Teach. Ass., MSc. Eng.
University of Novi sad
Faculty of Technical Sciences
Trg Dositeja Obradovica 6
21000 Novi Sad, Serbia
ivanknezevic@uns.ac.rs



Maja ČAVIĆ, Assoc. Prof. Ph.D.
University of Novi sad
Faculty of Technical Sciences
Trg Dositeja Obradovica 6
21000 Novi Sad, Serbia
scomaja@uns.ac.rs



Marko PENČIĆ, Res. Assoc., M.Sc. Eng.
University of Novi sad
Faculty of Technical Sciences
Trg Dositeja Obradovica 6
21000 Novi Sad, Serbia
mpencic@uns.ac.rs

IMPROVING THE PERFORMANCE OF BALL ROLLER BEARINGS USING NEW MATERIALS

Vesna JELIĆ
Nataša SOLDAT
Zoran STAMENIĆ

Abstract: *Rolling bearings, as integral parts of all machines, their operating characteristics directly affect on their operational ability. For this reason, it is imperative to improve the performance of these important machine elements and increase their service life. Manufacturers pay great attention to the improvement of existing and development of new, improved design and new bearing production technologies. From bearing is required dependable service, often at high rotation frequency, low vibration and increased wear resistance. In order to improve performance and increase efficiency, special attention is paid to the application of new materials for the production of ball roller bearings. Studies have shown that a combination of different types of materials can significantly increase their service life, reduce noise and vibration during exploitation, allowing their use in high-frequency rotation conditions.*

Hybrid bearings combine the rings made of steel with rolling bodies made of ceramics, which is characterized by high strength and resistance to wear. Such bearings can operate with higher angular speeds, better working conditions in poor lubrication, resistant on the adverse effects of contaminants and achieve a longer service life of bearings made entirely of steel. The aim of this paper is to highlight the performance improvement of ball roller bearings using new materials.

Key words: *Low-friction ball bearings, new materials, hybrid bearings, performance of steel and hybrid bearings*

1. INTRODUCTION

The first knowledge of bearings dates back to ancient Egypt until the oldest discovered bearings. Development bearings are chronologically built upon Aristotle's theory of rolling resistance, *Gaius Plinius* (Rome 23-79 a.c.) list of lubricants, Daidesus mechanism of rolling bearing to the first thrust bearing. Later, during the Renaissance, Leonardo da Vinci (16th century) designed the bearing, which was used until the late 19th century until the first modern design and construction of the first self-alignment bearing.

The specific use of bearing flourishes just after the industrial revolution. At the beginning, constructors were opted for plain bearings. As a technology of their making rapidly advances, during the sixties of 19th century, began the expansion of the use of roller bearings.

A great demand for ball bearings demanded better bearings. Introducing special steel in ball bearing production, as well as development of more precise machine tools, influenced on the bearing elements geometry accuracy, which considerably extended the life of the bearings, allowing the new industrial machinery to operate efficiently.

Rolling bearings are the most widely used machine elements. Almost no machinery, appliances or devices, which in its structure do not contain a certain number of rolling bearings. In most cases, there are considered as a critical element of assembly and of its operational abilities in many ways depends the functionality, reliability and properties of the entire assembly in which it is fitted. But the quality of the bearing itself is not sufficient to achieve all the demands that are placed before it. Just under ideal conditions roller bearings can achieve all of its design characteristics.

Because of the simplicity of construction, acceptable capacity, reliable operation at high rotation frequency, low vibration and wear resistance, there are a vast number of researches whose imperative was to improve ball bearings performance by using new materials. By combining the various types of materials it is possible to decrease the noise level, and make influence to the greater load capacity of mechanical and other structures. They are particularly characterized by resistance to wear and deformation at high temperatures and low density compared to steel. Those are hybrid bearings or ceramic ball bearings, which have different attributes and properties depending on their application.

2. ROLLING BEARINGS

Rolling bearings are standardized mechanical elements whose task is to allow relative movement of rotating parts and to transfer loads between them and to provide the accuracy of their positioning. They are consisting of rings or discs, which are attached to stationary or moving parts of the machine, and between them, are rolling elements.

Application of rolling bearings is much larger compared to plain bearings. This is primarily due to a high degree of standardization and mass production in factories. In the modern mechanical engineering, it is in use a few dozen types of rolling bearings, with over one million modifications.

According to the form of the rolling bodies, they are divided on:

- Ball;
- Cylindrical roller;
- Needles;
- Tapered roller;
- Barrel.[1]

2.1. Ball roller bearings

According to the form of the rolling bodies a bearings are named, as well as rolling ball bearings. They application are in mobile connection, as for example in the shaft and axle supports [1]. Mobility of ball bearings is based on the rolling principle of rolling bodies (balls), with two pint contact with the rings [6].

Advantages of rolling ball bearings reflected as follows:

- Simple imbedding design;
- Satisfy load capacity on lower and middle rotation speed;
- Easy lubrication and maintenance;
- They have accurate leading;
- Low cost of production.

Disadvantages of the application of steel rolling ball bearings compared to upgraded design are:

- The large mass;
- Unreliable operation in hevly exploitation conditions;
- Do not stand high rotation speed;
- Operating at intense vibration;
- Smaller lifetime.

3. IMPROVING THE PERFORMANCES OF BALL ROLLING BEARINGS

In late 1960, a number of researches led to the conclusion that the application of new materials can improve the performance of the bearing. Imperative was to meet the stringent requirements of development in aircraft industry, missile systems, the new design of turbine power plant and other mechanical systems.

Ceramic materials are hard and resistant to wear. In addition, ceramic is electrical insulator and chemically inert even in the harshest conditions (acid and various

chemical compounds). Defined as inorganic, nonmetallic materials, ceramic materials are fabricated by the sintering process, where the reinforced ceramic is compressed into a final shape during the thermal process.

The most frequently used ceramic materials for the ball bearings are a silicon nitride (Si_3N_4). This material has excellent properties, thanks to the covalent bonds within the atomic structure. There are particularly characterized by high strength, resistance to wear, has a resistance to wear at high temperatures and a lower density compared to steel [1].

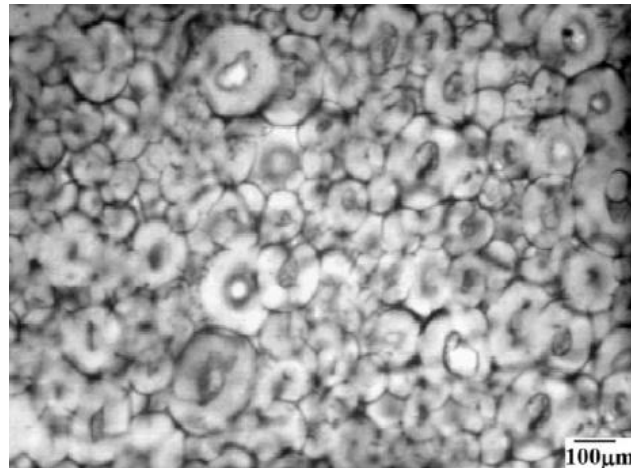


Fig.1: Microstructure of silicon nitride

3.1. Hybrid ball bearings

Hybrid ceramic ball bearings offer great promise in space applications but have not been rapidly adopted by industry perhaps partly due to the relatively low amount of published data on specific in-vacuum performance [1].

Combine the rings made of steel with rolling bodies made of ceramic (silicon nitride, Si_3N_4), and is also called a ceramic ball bearing, Fig. 2.



Fig.2: Hybrid ball bearing.

The advantages of hybrid bearings over a steel ball bearings are:

- *Low surface adhesive wear*
The lower affinity to steel reduces the adhesive wear, which is caused by the „cold welding effect” on irregularities in the raceway and ball surface.
- *Low abrasive wear out*
With steel balls, contaminants and particles from the process of running in are embedded into the surface. With every revolution of the ball, these foreign particles damage the raceway. These particles make little impact on the extremely hard ceramic ball.
- *Insensitivity to poor lubrication*
Low adhesion and friction allow the hybrid bearing to perform well even under poor lubrication.
- *Longer grease service life*
Lower operating temperature and favourable tribologic features, extend the service life of the grease
- *Higher rigidity*
The radial rigidity of hybrid bearings is approximately 15% higher at low speeds because of the higher Young's modulus.
With higher speeds, the centrifugal force affects the internal load distribution and the dynamic rigidity is reduced.
A high rigidity improves the accuracy and shifts the critical fundamental frequency of the bearing arrangement.
- *Improved machining accuracy*
The following factors lead to an improvement of the surface quality and accuracy of machined parts:
Higher rigidity of bearing arrangement.
Small thermal expansion.
Low vibration impulse by ceramic balls.

4. SCIENTIFIC BACKGROUND OF HYBRID BEARINGS

In the bearings design process is very important to systematically predict the interrelated effects of static, dynamic and thermal characteristics for different operating conditions.

A hybrid bearing is a complex system for modeling, with a large number of input and output parameters, complex physical and chemical processes that occur during their exploitation. From these reasons, it has been virtually impossible to form a comprehensive mathematical model. Therefore, in practical application, by setting the mathematical model, more attention is paid to parameters, which influence on the behavior of bearings in exploitation.

The most important parameters which determine the behavior of the bearing are as follows:

- Rolling bodies load distribution;
- Values of contact stresses and deformations;
- Changes of the contact angle;
- Temperature;
- Geometric imperfections of rolling surface [2].

Analyses of these parameters requires a dividing of comprehensive static – dynamic – thermal mathematical model on the sub-models, depending on the behavior that need to be investigated. In relation to bearings which are made of steel in various papers is shown, that the above parameters are different for hybrid bearings. Only a phenomenon of load distribution on bearing rolling bodies is the same.

4.1.1 Load distribution on rolling bodies of Hybrid bearings

The load distribution of hybrid bearing analysis is particularly investigated phenomenon. Department of General Machine Design, Faculty of Mechanical Engineering - University of Belgrade, for many years deal with this phenomenon. A significant contribution is presented through the master's theses, doctoral dissertations and scientific papers [4, 5, and 7].

A wide theoretical overview of the problem of roller bearings is provided by Harris [8], which is a foundation for most researchers for analysis of load distribution. The parallel analysis has performed, of the load distribution of the radially loaded rolling bodies of 6310 bearings made from steel and ceramics. Based on the already existing results [6] and published papers, the same principle is applied on load distribution of hybrid bearings.

Due to mathematical models of steel ball bearing and hybrid bearing exposed under external radial load, the analysis was performed. The two boundary conditions were considered: an ideal equal and extremely unequal load distribution.

Analysis of the existing results was obtained that the hybrid ball bearing load distribution match with the load distribution of the ball bearing made of steel. Only difference is in the exploitation life of steel rolling bearing and the hybrid ball bearing because the rolling bodies of a hybrid bearing on distribution lines suffer higher loads, Fig. 3.

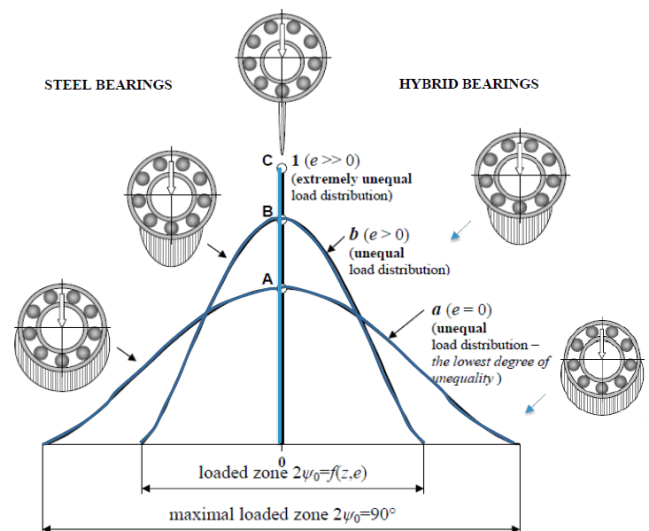


Fig.3: The load distribution of steel and hybrid ball bearings [4]

5. CONCLUSION

Evolution of bearing led to improved efficiency in all branches of technology, thus achieving satisfactory load capacity, a major shift in the development of bicycles, cars etc. and reduces energy losses.

The paper shows that the bearing is an irreplaceable part of mechanical systems. The performance improving the of ball rolling bearings with apply of new materials, for many scientists and large number of authors were the inspiration of researches which are still carried out. By combining the various types of materials it is possible to decrease the level of noise, provides reliable operation at high speed rotation and increase wear resistance. All of this enables a hybrid bearings, whose appearance, contribute that the machine systems operating under more extreme conditions. Thanks to its performance, many scientists call it "zero maintaining bearing".

It does not matter whether is bearing made of steel or other materials, today we can not imagine the world without this "small" machine element. As Mark Twain said, "Little things change the world".

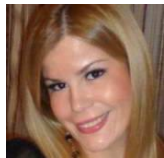
REFERENCES

- [1] MARKOVIC, N. (2015) *Istrazivanje kuglicnih lezjeva i njihovo unapredjenje*, 6.
- [2] ZIVKOVICI, A., ZELJKOVIC, M., TABAKOVIC, S. (2013) *Programsko resenje za analizu ponasanja kuglicnih lezaja, tehnicko crtanje*, Novi Sad
- [3] NATHAN KATZ, R.(1985) *Ceramics for High Performance Rolling Element Bearing: A Review and Assessment*, The Journal of Faculty of Tehnical Sciences, Vol.1, No 1, pp 69 - 79
- [4] LAZOVIC, T., RISTIVOJEVIC, M., MITROVIC, R., (2008) *Mathematical Model of Load Distribution in Rolling Bearing*, FME Transactions, Vol.36, No 4, pp 189-196
- [5] RISTIVOJEVIC, M., MITROVIC, R.,. (2002) *Monografija, Raspodela opterecenja (zupcasti parovi i kotrljajni lezaji)*, Masinski fakultet – Univerzitet u Beogradu.
- [6] KRSMANOVIC, V., MITROVIC, R.,(2015) *Klizni i kotrljajni lezaji*, Masinski fakultet – Univerzitet u Beogradu.
- [7] MITROVIC, R. *Istrazivanja uticaja konstruktivnih i triboloških parametara kugličnog kotrljajnog ležaja na radnu sposobnost pri velikim učestanostima obrtanja* Doktorska disertacija, Masinski fakultet – Univerzitet u Beogradu, 1992.
- [8] HARRIS, T.A., (1984) *Rolling Bearing Analysis*, John Wiely and Sons, New York.
- [9] http://www.vizijadanas.com/kuglicni_lezajevi.html, posećeno 20.06.2017.
- [10] <http://www.radijal.com/zanimljivo.htm>, posećeno 24.07.2017.

CORRESPONDANCE



Vesna JELIĆ, M.Sc. Eng.
University of Belgrade
Faculty of Mechanical Engineering
Kraljice Marije 16.
11120 Beograd, Serbia
vjelic@mas.bg.ac.rs



Nataša SOLDAT, M.Sc. Eng.
University of Belgrade
Faculty of Mechanical Engineering
Kraljice Marije 16.
11120 Beograd, Serbia
nsoldat@mas.bg.ac.rs



Zoran STAMENIĆ, Prof. dr Sci. Eng.
University of Belgrade
Faculty of Mechanical Engineering
Kraljice Marije 16.
11120 Beograd, Serbia
zstamenic@mas.bg.ac.rs

**NEW PRODUCTION
TECHNOLOGIES AND
MATERIALS**

DETERMINATION OF KINEMATIC STATE IN BULK METAL FORMING

Mileta JANJIĆ
 Milan VUKČEVIĆ

Abstract: Kinematic state of a working-piece at bulk metal forming of axial-symmetrical pieces has been determined in this paper. Strain rate tensor components are determined by the known theory, as partial strain rate component derivations. Displacement rate points of meridial section are basic for kinematic state determination. As non-stationary deformation process is concerned, it is necessary to determine initial and final points displacements when a relatively short observed interval is constant. Point displacements are determined by known geometry of groove-like plates before deformation and measured coordinate points out of digitalized picture of meridial section after deformation. Measurements are done by setting the lines with sufficient number of points. At the end, a graphic interpretation of the obtained results is given, their analysis and conclusions are made.

Key words: Bulk Metal Forming, Open Die, Finite Element Method (FEM), Strain Rate, Displacement Rate

1. INTRODUCTION

The importance of knowing the kinematic state of a working-piece in deformation process is pointed out by a hypothesis on similarity and coaxiality of deviators of stress tensor and strain rate tensor growth, being the base of Levy-Mises's theory of plastic yield [1].

Determining kinematic state is a quantitative determination of kinematic parameters in the form of components of strain rate tensor in all the points of the piece section. To reach the research goal, appropriate pieces were developed. After several trials, more or less successful ones, there resulted the idea of making pieces in segments of groove-plate forms. Plate grooves practically represent finite elements physical discretized, and this method is called Physical Discretization Method (PDM).

By a suitable mechanical and chemical forming after deformation, it is possible to get a deformed image of meridial section. First, a part of the piece till its symmetry axis, i.e. meridial section is removed by cutting. Then the surface is finely polished and chemically immersed into NaOH solution, after which deformed contours of groove plates become visible by a naked eye. The section is scanned and its digital version is obtained, being suitable for further computerization.

2. STRAIN RATES

To define strain rate displacement velocity is defined first as an expression of time displacement. Strain rate, in its general sense, represents the expression of time forming, or the ratio of strain rate of two points displacement to the distance of this points, when the distance tends to be zero.

For axis-symmetrical stress state of strain rate tensor components in cylindrical coordinate system are [2]:

$$\left. \begin{aligned} \dot{\epsilon}_r &= \frac{\partial v_r}{\partial r} & \dot{\gamma}_{r\theta} &= 0 \\ \dot{\epsilon}_\theta &= \frac{v_r}{r} & \dot{\gamma}_{\theta z} &= 0 \\ \dot{\epsilon}_z &= \frac{\partial v_z}{\partial z} & \dot{\gamma}_{rz} &= \frac{\partial v_r}{\partial z} + \frac{\partial v_z}{\partial r} \end{aligned} \right\} \quad (1)$$

Effective strain rate or intensity strain rate is a quantitative velocity change measure, expressed by [6]:

$$\dot{\epsilon}_e = \frac{2}{\sqrt{3}} \sqrt{I_2(\dot{T}_\epsilon)} = \frac{\sqrt{2}}{3} \sqrt{(\dot{\epsilon}_r - \dot{\epsilon}_\theta)^2 + (\dot{\epsilon}_\theta - \dot{\epsilon}_z)^2 + (\dot{\epsilon}_r - \dot{\epsilon}_z)^2 + \frac{3}{2} \dot{\gamma}_{rz}^2} \quad (2)$$

With unsteady processes such as bulk forming at open dies, kinematics and stress fields in an immovable space point where the forming originates are changed in the course of time. In such processes, an analysis of a forming growth can not illustrate kinematics and stress fields during the whole process, only the observed growth can be clear. Thus, it is necessary to determine an interval (step), at the end of which the stress state in the working piece volume could be determined.

Kinematics field is found by virtue of the known parameters of meridial cross-section point displacement and interval duration. Displacement velocity components are expressed by:

$$\left. \begin{aligned} v_r &= \frac{r_0 - r}{\Delta t} = \frac{\Delta r}{\Delta t} \\ v_z &= \frac{z_0 - z}{\Delta t} = \frac{\Delta z}{\Delta t} \end{aligned} \right\} \quad (3)$$

The hypothesis for such a velocity determination is the constant forming velocity.

If you know the kinematics field, i.e. displacement velocity arrangement, it is possible to determine forming

velocities to the cross-section meridial points (1), where partial derivates are determined for sufficiently small values of Δr , Δz and Δt , using these expressions [3]:

$$\left. \begin{aligned} \frac{\partial v_r}{\partial r} &= \frac{\Delta v_r}{\Delta r} \\ \frac{\partial v_z}{\partial z} &= \frac{\Delta v_z}{\Delta z} \\ \frac{\partial v_r}{\partial z} + \frac{\partial v_z}{\partial r} &= \frac{\Delta v_r}{\Delta z} + \frac{\Delta v_z}{\Delta r} \end{aligned} \right\} \quad (4)$$

3. EXPERIMENTAL RESEARCHES

There have been adopted two levels of height from the upper side and one level of height from the low side of the die plane [4,5,6].

Research works are carried out on a real material in laboratory conditions and are adjusted in the way to be as much similar to real (production) conditions being present in direct industrial environment. As the investigated material there has been used an aluminum alloy AlMgSi0,5, which is very often used in processes of bulk metal forming, above all in extrusion processes and bulk metal forming in open dies. Experiment is carried out at temperatures of hot forming of the mentioned alloy, namely at $t=440$ [°C]. Deformation is realized by constant deformation velocity: $v=2$ [mm/s]. Process is carried out by graphite grease lubrication, being applied in production conditions.

To determine kinematics state, compression of two working-pieces of $h_{va}=3$ [mm] wreath height and final $h_{vb}=h_v=1$ *mm* is done. An optimal forming interval at the end of forming process for tool stroke growth $\Delta z=2$ [mm] is chosen. These values are ensured by non-deformable steel rings. Otherwise, it is necessary for this interval to be little enough to maintain a real state of displacement velocities, but not too much little as to avoid the influence of anisotropy forming. The parameters at the end of the interval observed are marked with index b, whereas initial one is marked with a.

The process of preparing cross-section working-piece surface, and the image digitalization of deformed mesh in the meridial cross-section are described in the introductory part and papers [4,5]. The treated surface of the meridial cross-section with initial and final radial and axial lines are given in Fig.1.-Fig.4.

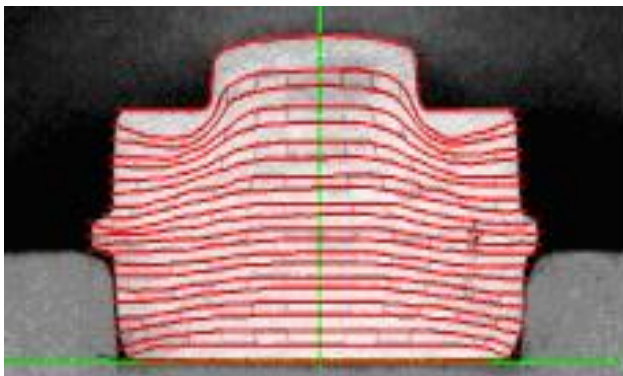


Fig.1: Initial interval radial lines

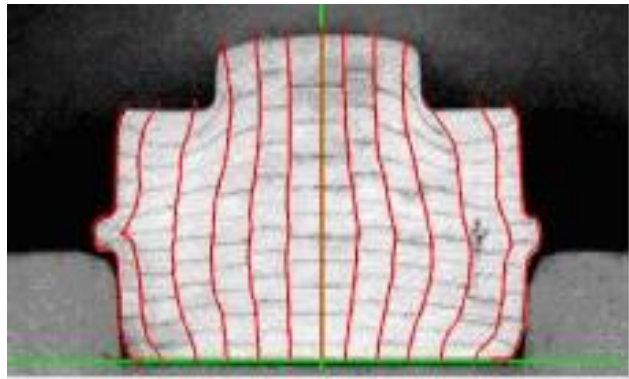


Fig.2: Initial interval axial lines

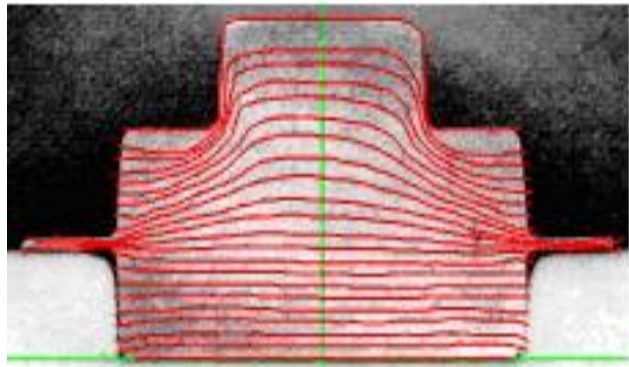


Fig.3: Final interval radial lines

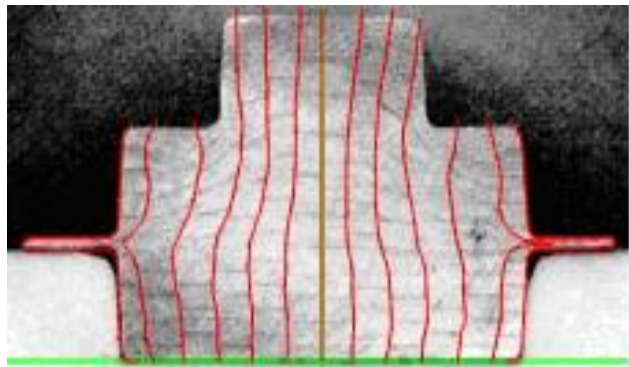


Fig.4: Final interval axial lines

4. RESULT PROCESSING

A program for complete kinematics analysis is made in MATLAB, input data are the values of coordinate points of deformed both radial and axial mesh. This program automatically determines node points of the deformed mesh, namely cross-section points of the deformed radial and axial lines, i.e. points whose displacement is determined.

The displacement growth in the node points of deformed mesh is determined as a displacement difference at the beginning and end of the observed interval:

$$\left. \begin{aligned} \Delta u_r &= u_{rb} - u_{ra} = r_{pb} - r_{pa} = \Delta r \\ \Delta u_z &= u_{zb} - u_{za} = z_{pb} - z_{pa} = \Delta z \end{aligned} \right\} \quad (5)$$

By expression (3) it is possible to determine displacement velocities in the node points of the deformed mesh. Displacement velocity values in other points are

approximated by the cube interpolation, thus a continual displacement velocity function in the meridial plane of the working-piece in function of radius and height coordinates are practically are obtained.

For the known displacement velocities of cross-section points, it is possible to determine partial expressions of velocity displacements per radius and height (4), to obtain forming velocities (1). The tangential strain rate component is not determined by partial derivate of displacement, the division result of radial displacement velocity and radius (1). Effective strain rate is obtained by expression (2).

Using cube interpolation radial, axial, tangential and shear components of strain rates and effective strain rate whose change in the meridial cross-section of the working-piece are given in the for of 3D diagrams in the function of radius and height of the working-piece in Fig.5.-Fig.9

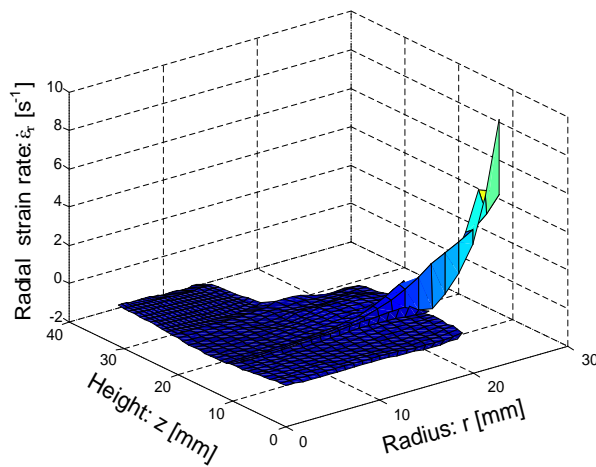


Fig.5: Radial strain rate

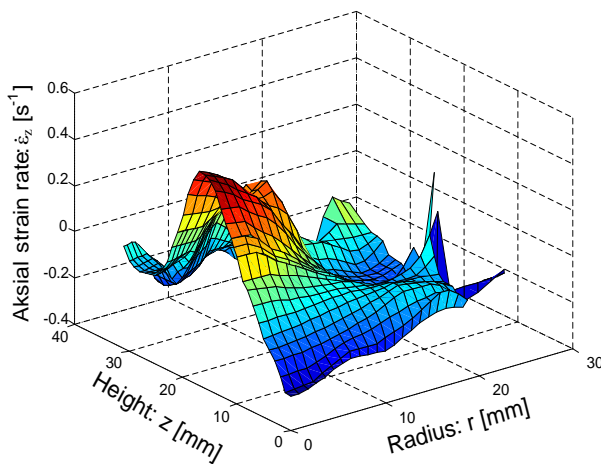


Fig.6: Aksial strain rate

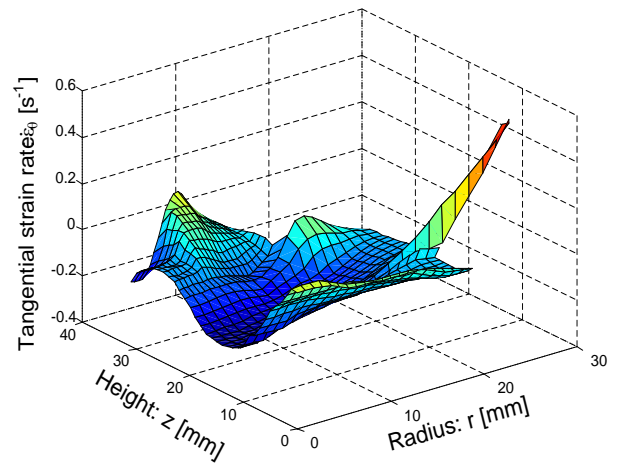


Fig.7: Tangential strain rate

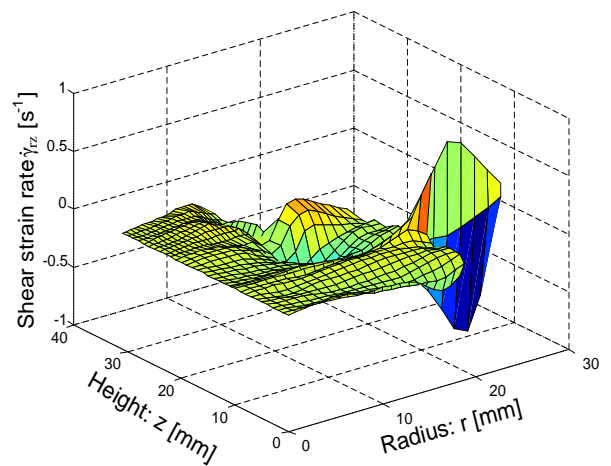


Fig.8: Shear strain rate

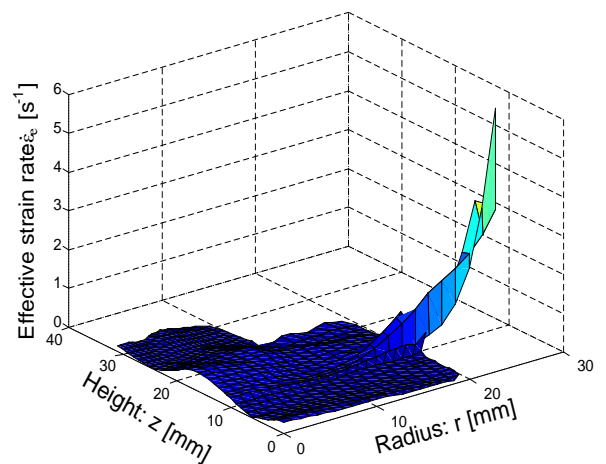


Fig.9: Effective strain rate

5. CONCLUSION

Using the Physical Discretization Method, it is possible to successfully obtain all the components of strain rates tensor and effective determination of meridial cross-section of axis-symmetrical working-piece formed in open dies.

With all components of strain rates, a zone is discretized clearly and it corresponds to the inner part of the die and wreath zone.

Radial and effective strain rates have an equal, very low absolute value in die zone whereas their extreme value is of the same size order and is in the end of the wreath. Tangential and axial strain rates have a less extreme value of the given components and are at the end of the wreath.

With shear strain rate extreme values are obtained for the middle wreath zone.

An expressive difference in the values of strain rates components in the die and wreath zones is due to the observing of final forming process when the material has filled a complete die engraving, which is not deformed any longer, if not distinguished in the wreath.

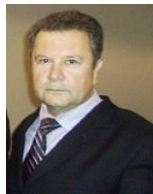
REFERENCES

- [1] КОЛМОГОРОВ В. Л. (1986) *Механика обработки металлов давлением*, "Металлургия", Москва
- [2] MUSAFIJA B. (1973) *Primijenjena teorija plastičnosti*, Univerzitet u Sarajevu, Sarajevo
- [3] PLANČAK M. (1984) *Naponsko-deformaciono stanje u procesima hladnog istiskivanja čelika*, Univerzitet u Novom Sadu, Fakultet Tehničkih Nauka, Novi Sad, 1984.
- [4] JANJIĆ M. (2005) *Stress Deformation Parameter Investigation in the Processes of the Bulk Metal Forming*, PhD Thesis, University of Montenegro, Faculty of Mechanical Engineering, Podgorica
- [5] JANJIC M., DOMAZETOVIC V., VUKCEVIC M., SAVICEVIC S. (2005) *Strain Determination by the Method of Physical Discretization*, Journal for Technology of Plasticity, Vol. 30, No 1-2, pp 83-93
- [6] JANJIĆ M., DOMAZETOVIĆ V., VUKČEVIĆ M., SAVIĆEVIĆ S. (2006) *The Regression Analysis of Deforming State by Physical Discretization Method of Bulk Forming in Open Die*, 10th International Research/Expert Conference TMT 2006, Barcelona, Spain, pp 1319-1322

CORRESPONDANCE



Mileta JANJIĆ, Prof. D.Sc. Eng.
University of Montenegro
Mechanical Engineering Faculty
Bul. Džordža Vašingtona bb
81000 Podgorica, Montenegro
mileta@ac.me



Milan VUKČEVIĆ, Prof. D.Sc. Eng.
University of Montenegro
Mechanical Engineering Faculty
Bul. Džordža Vašingtona bb
81000 Podgorica, Montenegro
milanvu@ac.me

TOPOGRAPHY OF CHARACTERISTIC SURFACES OF MODEL HOB MILLING TOOLS FOR MACHINING OF GEAR SERRATION

Ivan SOVILJ-NIKIĆ
Sandra SOVILJ-NIKIĆ
Bogdan SOVILJ
Vladimir BLANUŠA

Abstract: The problem of generating is analyzed in science and practice in various ways by identifying it once as an element of the machine, and the second time as a part of production, that is, a final product. The nature of the materials of the machine elements, the loads in the contact zone, the relative velocities, the topography of the contact surfaces, and the temperature in the contact zone influence on the tribological characteristics of the elements, and hence on the characteristics of the tribomechanical systems. There is a significant number of tribomechanical systems in the energy sector. Serration of gear machining is the most important operation in the production of gears. The gear is an element of a large number of tribomechanical systems.

In this paper, the topography of the characteristic surfaces of the model hob milling tools is analyzed before and after machining of serration of the gears.

Key words: tribomechanical systems, tribological characteristics, topography, roughness, model hob milling tools

1. INTRODUCTION

The contemporary characteristics of the society and the desire for continuous improvement of the quality of life require continuous improvement of the quality of production. The product is the most characteristic parameter of the technical development of a country. Analyzing the century-long coupling and mutual relations between man and the industrial product, at each stage of their life cycle, it can be concluded that the industrial product is material creation which is consciously developed and realized in industrial conditions of production. By directing the process of development of production to the development of various systems, it is especially important to find ways to improve the quality of products.

In tribological processes, the very small mass of the tool material and the large mass of the material of the work-piece are involved in the machining of serration of the gear. The consequences of the development of tribological processes in the zones of contact are the friction and wear of the cutting elements of hob milling tools. In the Figure 1 [1] examples of tribomechanical systems are given, and with the number one the critical element of each tribomechanical system is marked, that is, the element which is worn at the most in the process of achieving contact. The contact surface of the tribo elements after final machining is never absolutely smooth. Numerous unevennesses resulting from previous and final operations can have different geometric parameters and cause greater or minor irregularities in triboelements.

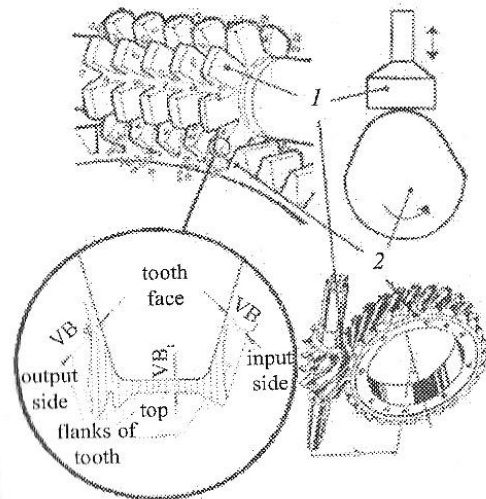


Fig.1: Example of tribomechanical systems with basic elements 1 and 2 and details with wear parameters of hob milling tool

It is indisputable that the change in system structure, energy losses and material losses are very complex processes and depend on a large number of factors. Numerous studies have shown that the quality of the contact surface significantly affects the wear resistance. Reducing the roughness increases the wear resistance. In this paper a part of the results of the research of tribological processes in the machining of serration of gears with uncoated and coated model hob milling tools is presented.

2. MACHINING OF GEAR SERRATION AND THE TOPOGRAPHY OF THE SURFACE

The occurrence of the power transmitter and movement dates back to ancient times. In China, Mesopotamia and Egypt, parts and assemblies of irrigation devices with toothed portable elements have been found, which according to the kinematic principle are still used today. In addition to agriculture, such devices have been developed for war and civil engineering purposes (Fig 2.) [2].

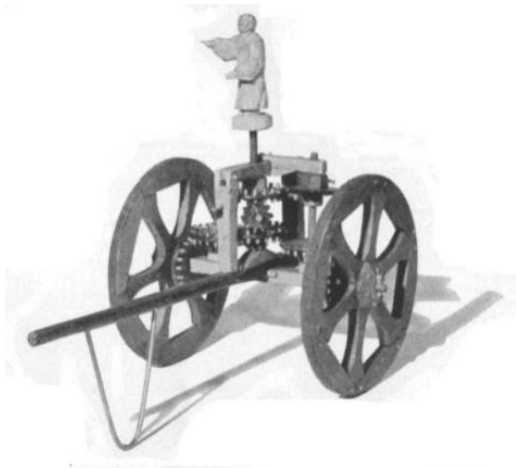


Fig.2: South pointing chariot

Machining of gear serration can be done by various methods and procedures. Thanks to the high productivity of the process, the hob milling has the widest application in the machining of serration of spur wheels. Integral hob milling tools are tools used in machining of gear serration by means of relative rolling method (Fig.3).

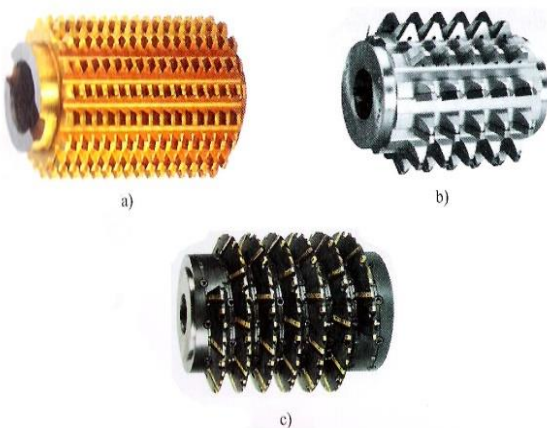


Fig.3: Hob milling tools (a. Integral, b. assembly, c. montage)

In defining the tool life of hob milling tool, it is necessary to perform long-term experimental tests which require considerable resources and efforts, and it is difficult to implement them in the real production process. In order to simplify this experimental research, there is a need for quick and cheaper testing procedures that will provide reliable information on the examined machining process. For the process of hob milling of gear serration, there is a possibility that instead of the integral hob milling tool,

model single-tooth hob milling tool can be used in research (Figure 4 [3]).

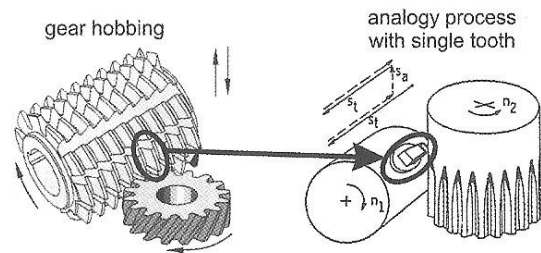


Fig.4: Gear hobbing represented by a single tooth fly-cutting analogous process

For the process of machining of gear serration, a method has been developed, device for accepting a cutting element (teeth) for model testing in laboratory conditions instead of an integral hob milling tool has been designed and manufactured (Figure 5 [1]).



Fig.5: Integral and model tools

Significantly the largest percentage of all breakdowns and slowdown in production is initiated through the surface of the elements of the tribomechanical system through mechanisms such as fatigue fracture, fracture due to stress corrosion, contact wear due to friction, erosion, etc. It is clear that it is important to know the properties of surfaces and zones near the surface of the elements. The answer to these problems can be given by tribology.

The interdisciplinary character of tribology and a wide array of possible aspects of the study have conditioned that in the process of tribologically correct design and construction, it has to be equipped with a large number of precisely defined tribological information. Due to the complexity of the tribological processes and the large number of influencing factors, it is necessary to possess information from various disciplines of this broad scientific field. In that sense, the development of triboinformatics encourages as the necessity of systematizing an increasing number of tribological information and the need for a more efficient exchange between scientific institutions and other potential users of tribological knowledge [4].

Technologists study technical drawings and they try to produce elements by defined dimensions within the limits of tolerance. Characteristic parameters formed during the technological process define macrogeometry and microgeometry of contact surfaces. For the correct analysis of tribological processes, but also tribologically correct construction, the roughness of the contact surfaces is especially significant. Macrogeometry can be repaired during the technological process itself by working properly on the system; machine-fittings-tool-work-piece. Roughness has a stochastic element and it is a consequence of random processes, it cannot be avoided,

but it can be managed to a large extent in the technological process of machining [5].

For analysis of the roughness of the machined surface of the elements, there are more than 30 parameters that are less and those that are more represented. The basic parameters of roughness are defined according to national and international standards. The first three parameters R_a , R_{max} and R_z represent a small group of the three most common parameters, while R_t , R_q and R_p are the parameters that are also used, but considerably less than the three previously mentioned roughness parameters.

Roughness significantly affects the actual surface of the contact, that is, the surface on which the contact of the micronuclei that forms the topography is realized. The actual surface of the contact depends on the micro and macro geometric characteristics of the surfaces in contact, from the corrugation, form errors, physical mechanical properties of the surface layer, from the load, etc. With the load parameter, the actual surface of the contact increases, and the growth is conditioned by the emergence of new contact points.

3. EXPERIMENTAL RESEARCH

According to research plan in the project entitled by Modeling and optimization of hob milling the analysis of the topography of tools for machining of serration and machined teeth of spur wheels was planned. Within this paper, only parts of the results related to the topography for machining of serration are given. Based on the experiment plan, the research was carried out on uncoated and coated model hob milling tools with modules $m = 3$ and $m = 5$.

At the beginning of experimental topography research 392 model hob milling tools were identified based on certain characteristics. The roughness parameters were first measured on unworn tools, and then on the same tools after reaching the wear criterion. Roughness parameters are measured on model tools, which were already worn before this research. From the group of 392 tools 104 model hob milling tools have been allocated with module $m = 3$ (Table 1) and $m = 5$ (Table 2). In each subtype, there are 13 model hob milling tools, and in Figure 6 a subtype of uncoated worn-out model hob milling tools with the module $m = 5$ is given.

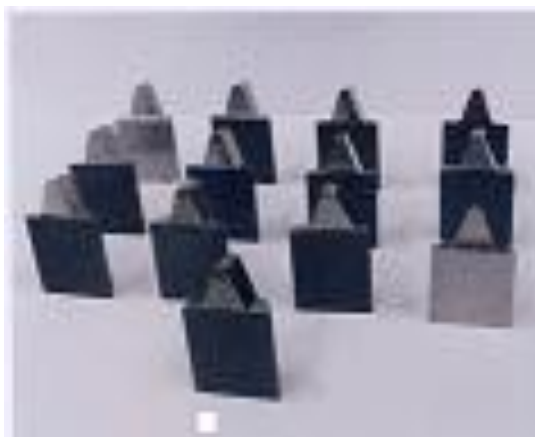


Fig. 6: Uncoated worn-out model hob milling tools with the module $m = 5$

Table 1: Subtypes of model hob milling tools $m=3$

MODUL $m=3$	1	2	3	4
UNCOATED	*	*		
COATED			*	*
UNWORN	*		*	
WORN-OUT		*		*

Table 2: Subtypes of model hob milling tools $m=5$

MODUL $m=5$	1	2	3	4
UNCOATED	*	*		
COATED			*	*
UNWORN	*		*	
WORN-OUT		*		*

In these experiments, a model hob milling tools made of HS 6-5-25 was used and a number of tools were coated with TiN. To measure roughness parameters, a MahrSurf PS1 device was connected to a computer, so the measurement results were obtained in electronic form (Figure 7).

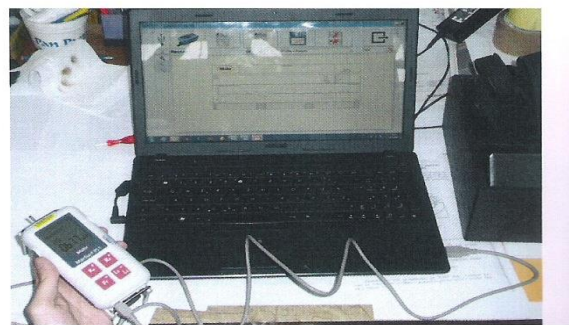


Fig. 7: Fig.:MahrSurf device connected to computer

Surfaces of model hob milling tools and measuring directions are shown in Figure 8.

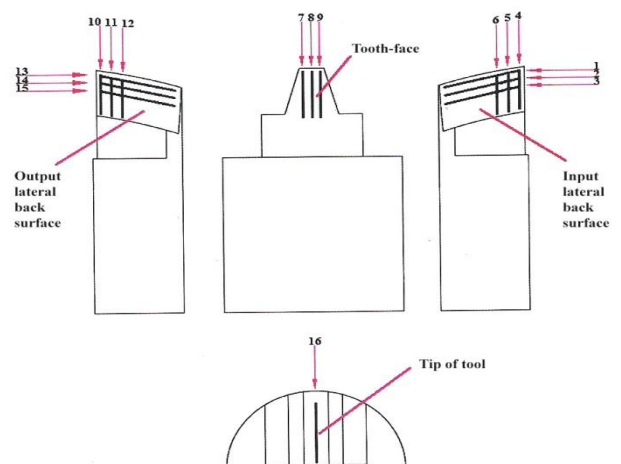


Fig. 8: Tool surfaces and directions of measuring

In this paper the roughness parameters for two characteristic surfaces: the input lateral back surface and the outlet lateral back surface were analyzed.

The results of the research are shown in diagrams and a part of the results is given in this paper in next figure.

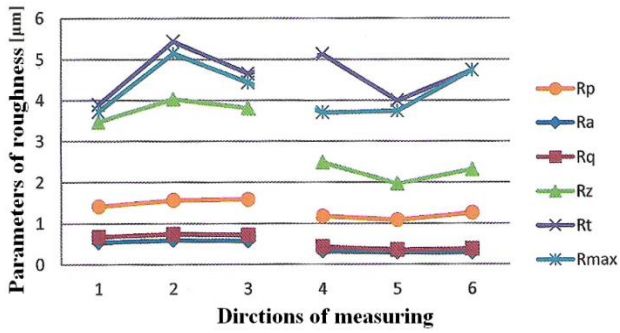


Fig.9: Diagram of roughness parameters the input lateral back surface of uncoated tool 7 unworn module $m=3$

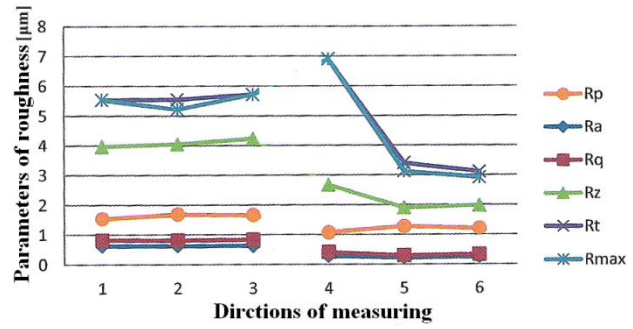


Fig.13: Diagram of roughness parameters the input lateral back surface of coated tool 13 unworn module $m=3$

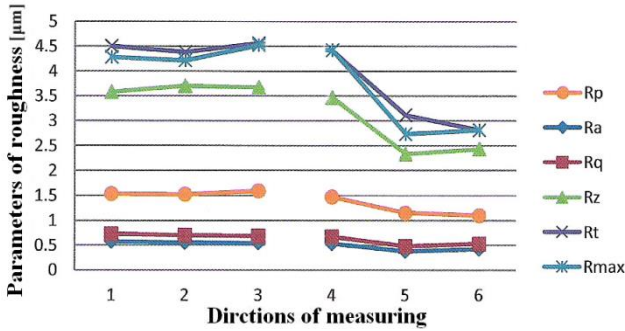


Fig.10: Diagram of roughness parameters the input lateral back surface of uncoated tool 7 worn-out module $m=3$

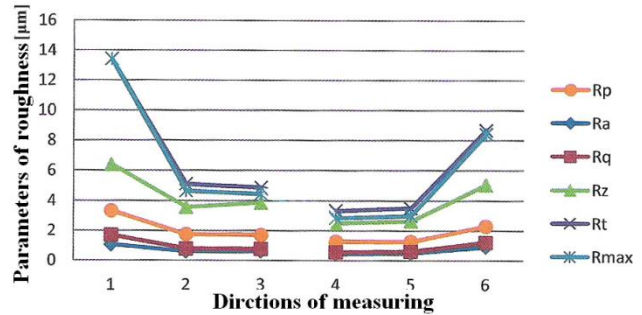


Fig.14: Diagram of roughness parameters the input lateral back surface of coated tool 13 worn-out module $m=3$

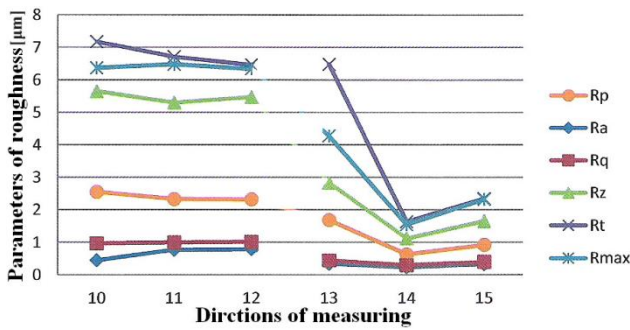


Fig.11: Diagram of roughness parameters the outlet lateral back surface of uncoated tool 7 unworn module $m=3$

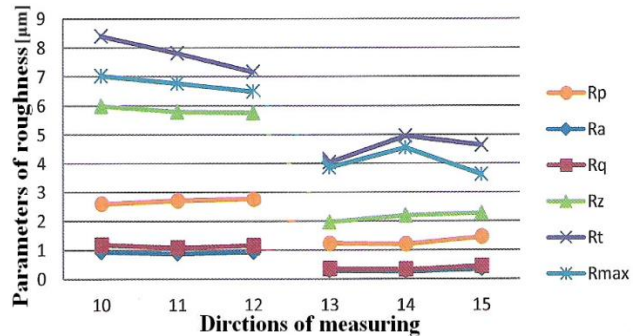


Fig.15: Diagram of roughness parameters the outlet lateral back surface of coated tool 13 unworn module $m=3$

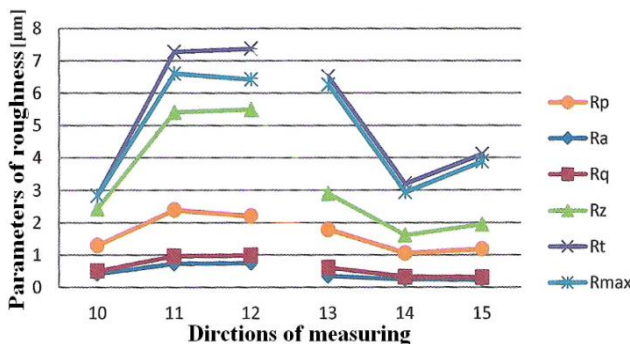


Fig.12: Diagram of roughness parameters the outlet lateral back surface of uncoated tool 7 worn-out module $m=3$

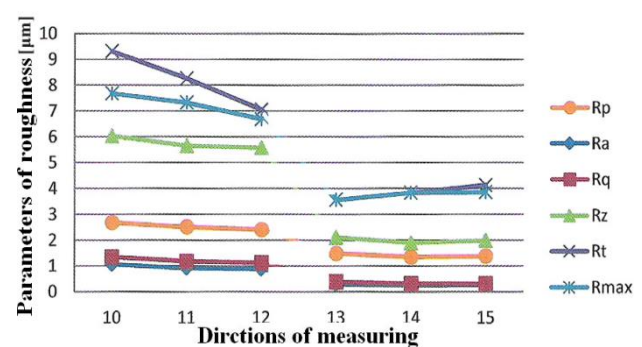


Fig.16: Diagram of roughness parameters the outlet lateral back surface of coated tool 13 worn-out module $m=3$

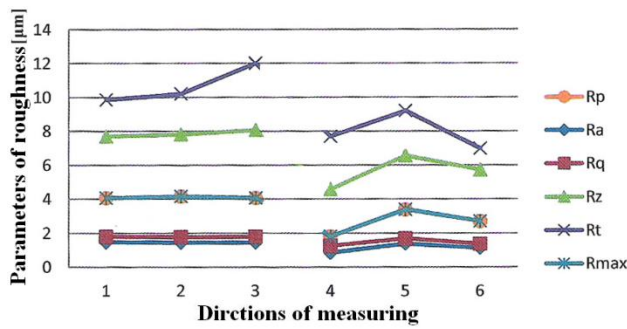


Fig.17: Diagram of roughness parameters the input lateral back surface of uncoated tool 22 worn-out module $m=3$

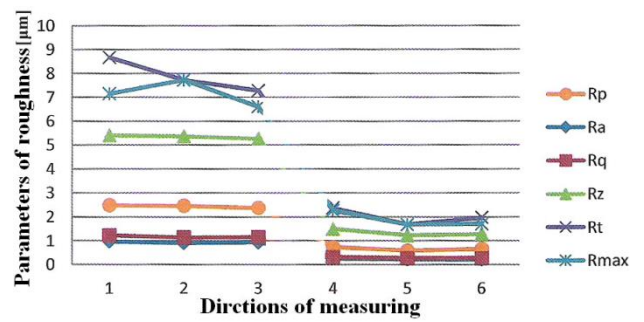


Fig.21: Diagram of roughness parameters the input lateral back surface of coated tool 73 worn-out module $m=5$

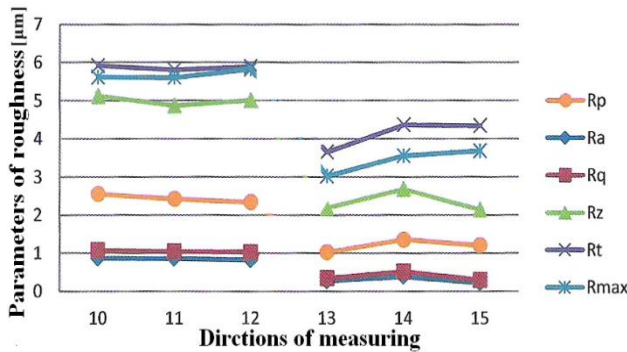


Fig.18: Diagram of roughness parameters the outlet lateral back surface of uncoated tool 22 worn-out module $m=3$

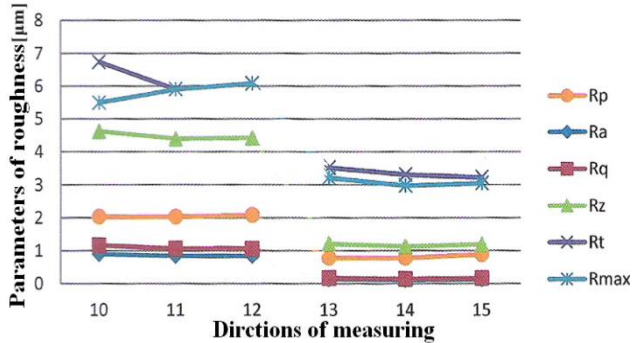


Fig.22: Diagram of roughness parameters the outlet lateral back surface of coated tool 73 worn-out module $m=5$

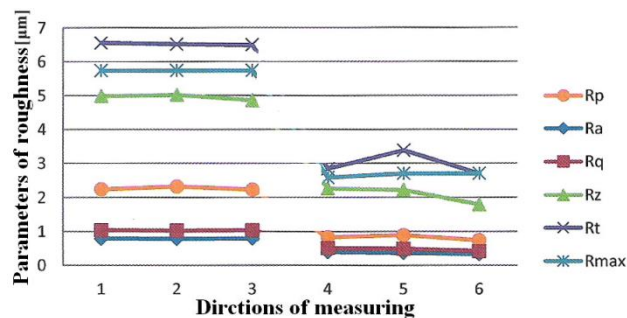


Fig.19: Diagram of roughness parameters the input lateral back surface of uncoated tool 55 worn-out module $m=5$

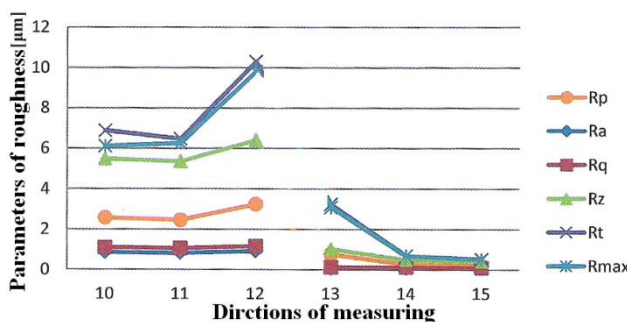


Fig.20: Diagram of roughness parameters the outlet lateral back surface of uncoated tool 55 worn-out module $m=5$

On the basis of the first and the second part of the experimental research it can be concluded that all the maximum values of roughness parameters at characteristic surfaces of the model hob milling tools are represented in longitudinal direction of measurement, while all minimum value of roughness parameters are represented in the cross-direction of measurement. Explanation arises from the fact that the measuring needle for measurements in the directions of 1, 2 and 3, respectively and 10, 11 and 12 was moving in the direction of the normal to the grooves resulting from the final machining of the characteristic surface of model hob milling tools. The movement of the measuring needle was parallel with the aforementioned grooves for the directions 4, 5 and 6, respectively and 13, 14 and 15.

4. CONCLUSION

Today, great efforts are being made to penetrate into the essence of the nature of the contact surface, and this is facilitated by new technologies and devices. The consequences of tribological processes are the changes that occur on the surface layer.

Research of the topography of the characteristic surfaces of the model hob milling tools have been performed on one of the most modern devices MahrSurf PS1 for testing the roughness parameters.

Based on the results of measuring the six most commonly used roughness parameters (R_a , R_q , R_z , R_p , R_{max} , R_p) or the entire experimental research in this paper it can be concluded that the topography of unworn coated model hob milling tools is better than the topography of worn coated model hob milling tools noting that the results of each of the parameters vary differently.

To complete the picture of the topography of the contact surfaces of the model hob milling tools, it is necessary in future investigations a precise definition of surface roughness through defining the distribution of the ordinates and the tops, the distribution of the inclination, the radius of the tops and recess of unevenness, carrying capacity curves of profile and others.

A two-dimensional analysis can often be used as a process monitoring that is limited in scope, but provides a simple indication, regardless of whether the topography changes. For a more complete understanding, a three-dimensional analysis of the topography of the characteristic surfaces of the model hob milling tools is necessary.

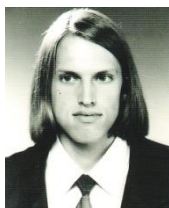
REFERENCES

- [1] SOVILJ-NIKIĆ, I., SOVILJ, B., KANDEVA, M., GAJIC, V., SOVILJ-NIKIĆ, S., LEGUTKO, S., KOVAC, P. (2012) *Tribological characteristics of hob milling tools from economic aspect*, Journal of the Balkan Tribological Association, Vol. 18, No 4, pp 577-585
- [2] OPALIC, M. (1998) *Prijenosnici snage i gibanja*, Sveučilište u Zagrebu, FSB, Zagreb
- [3] KARPUSCHEWSKI B., PIEPER, H.J. (2012) Innovations in tool development and manufacturing, Proceedings of 13th International Conference on Tools, Miskolc, Hungary, pp 21-26
- [4] TANASIJEVIC, S. (2004) *Tribološki ispravno konstruisanje*, Mašinski fakultet, Kragujevac
- [5] BLUNT, L., JIANG, X (2001) *Roughness, Waviness and Primary Profile, Geometrical Product Specification*, Warsaw University of Technology Printing House, Warsaw

ACKNOWLEDGEMENT

The research was funded by the Ministry of Education, Science and Technological Development of the Republic of Serbia, within the projects TR 35015 and III 43008, and it is also the result of the cooperation within CEEPUS project CIII- RO-0058-07-1415 supported by Secretary of Science and Technological Development of the Autonomous Province of Vojvodina.

CORRESPONDANCE



Ivan SOVILJ-NIKIĆ, PhD student
University of Novi Sad
Faculty of Technical Science
Trg Dositeja Obradovića 6
21000 Novi Sad, Srbija
diomed17@gmail.com



Sandra SOVILJ-NIKIĆ, D.Sc. Eng.
Iritel a.d. Beograd
Batajnički put 23
11080 Beograd, Serbia
sandrasn@eunet.rs



Bogdan SOVILJ, Prof. D.Sc.Eng.
University of Novi Sad
Faculty of Technical Science
Trg Dositeja Obradovića 6
21000 Novi Sad, Srbija
bsovilj@uns.ns.ac.yu



Vladimir BLANUŠA, PhD student
University of Novi Sad
Faculty of Technical Science
Trg Dositeja Obradovića 6
21000 Novi Sad, Srbija
blanusa@vtsns.edu.rs

IMPACT TOUGHNESS OF HIGH-STRENGTH LOW-ALLOY STEEL WELDED JOINTS

Andreja ILIĆ
Lozica IVANOVIĆ
Blaža STOJANOVIĆ
Danica JOSIFOVIĆ
Eleonora DESNICA

Abstract: Impact toughness of samples with three different relative positions of V-notch and multipass V-butt welded joint at high-strength low-alloy steel S690 are considered in this paper. The aim of this paper is to analyze the influence of material degradation due to welding to impact toughness of samples made of considered steel. Impact toughness was analyzed by experimental approach objected to including as many influential factors as it is possible. The main objective of impact toughness testing is to evaluate the influence of welding to overall load capacity and stability of welded mechanical construction made of high-strength low-alloy steels. Fully understanding of transformation processes provoked by welding of high-strength low-alloy steels and impact toughness testing as resulting property of those processes are crucial to perform integrity, safety and reliability analysis. This paper pointed out the necessity of analyzing the welded constructions on different dimension levels. Further investigations in this area have to be a continued through more quantitative analysis of welded joints which will, established precise analytical model of zones of welded joints, and furthermore, in involvement with adequate software, a complete evaluation of the experimentally obtained results. As the chemical composition and microstructural state of high-strength low-alloy steel originate from special production process their nature must be fully understood during selection and definition of welding even during the design process of mechanical construction. As experimentally obtained results of impact toughness that correlate to microstructure and microhardness distribution implicated that development of those steels must be followed with improving weld processes and development, adjusting and modification of the design.

Keywords: impact toughness, high-strength, low-alloy steel, welded joint

1. INTRODUCTION

Welding procedures are continually developing due to the intensive applications of the obtained results in fundamental and applied scientific disciplines to meet present demands in mechanical constructions. An ordinary welding process in present industry is based on localized heating and cooling, which creates inhomogeneous temperature fields at zones of welded joints. The consequences of applied welding technology processes are numerous and heterogeneous by its nature, such as material inhomogeneity, alteration of its chemical compositions, different microstructural transformations, etc.

On the other side, welded constructions are complex systems of heterogeneous elements with mechanical properties that are highly dependent on its welded joints. The present demands that are put on welded constructions caused significant increases in applications of high-strength low-alloy steels. Applications of those steels instead of conventional, general purpose structural steels provide many advantages. But, high-strength low-alloy steels due to specific chemical composition and

microstructure are highly sensitive to influences of welding. High-strength low-alloy steels, so as considered S690QL have beneficial mechanical properties, but full benefit of applications of those steels can be obtained only by its adequate welding. Optimal welding technology is the main condition for preserving characteristics and microstructural state of material after welding, which are the basis of beneficial mechanical properties, and condition of joining.

High-strength low-alloy steels due to conditional weldability often require additional procedures to obtain an intended characteristic of welded joints. The processes of material degradation due to welding at those steels can be related to increasing of hardness, a decrease of toughness, an increase of transition temperature, the presence of different material discontinuities and so on. Initialization of cracks and formation of brittle structures due to welding are related to the high cooling speed of weld metal and its surrounding zone in diapason of temperature in which austenite is highly unstable. Considerations of mechanical properties of high-strength low-alloy steels must be based on its specific characteristics, as limited plasticity reserve due to high strength of steels, possible formation of local zones with

lower plasticity in relation to rest of the construction and possibility of material discontinuities and initialization of cracks (primarily, hydrogen) during welding at weld metal and heat affected zone.

As material discontinuities (inclusions, defects, cracks, sharp cuts, etc.) and imperfections are usually present at zones of welded joints, those zones are most dangerous from the aspect of loss of structural integrity. From the aspect of structural integrity, safety and reliability analysis, the measure the amount of energy required to cause fracture is crucial. The welded construction ability to absorb energy without compromising of integrity comes in focus of many different types of research.

Pamnani with associates in ref. [1] evaluate the mechanical properties across the SMAW, SAW, FCAW and A-GTAW weld joints of micro-alloyed HSLA steel. The correlation between microstructure, microhardness and tensile properties obtained using automated ball indent has been undertaken.

Multi-pass submerged arc welding at high-strength low-alloy steels using multi micro-alloy electrodes with three different heat input processes was analyzed by Lan and associates in ref. [2] to investigate the microstructure evolution and corresponding mechanical properties of weldments. The emphasis was placed on studying the influence of microstructure aspects on impact toughness of weld metal and heat affected zone (HAZ) with different heat inputs to reveal fracture micro-mechanism and to optimize the welding system.

In ref. [3] Costa et al. present a study of the thermal behavior and its effect on phase transformations in the HAZ, depending on cooling rates to obtain continuous cooling transformation (CCT) curves for an high-strength low-alloy steel. The results presented in ref. [3] showed that, with the used cooling conditions, the steel did not provide formation of brittle structures.

The results of research presented in ref. [4] by Sadeghian et al. implicate that the results of impact tests revealed that the specimen with low heat input exhibited brittle fracture and that with high heat input had a higher strength than the base metals.

The presented results of researches in literature overview point out those properties of welded joints are a key element of structural integrity of the welded constructions. Welded structure is a complex system that can be considered from many aspects. Safety and reliability requirements for welded construction point out that welded joint zones have to be considered adequately.

The essence of determining impact toughness so as a type of fracture in zones of welded joints is the qualitative analysis of structural integrity due to the integrity of its welded joints. Capacity calculations analyze and prove mechanical resistance and stability of welded structures for the expected loads and exploitative conditions. The multiple stress concentrations at zones of welded joint and mechanical properties of welded joints are a major dominant factor to the precision of analytical models used for calculations. Data obtained from exploitation of welded constructions showed that mechanical properties of welded joints due to are nature were not adequately take in consideration in present analytical models and capacity calculations. Only results obtained by

experimental testing can be taken as relevant to a high degree.

2. EXPERIMENTAL TESTING

The testing was done on models made of high-strength low-alloy steel S690QL, as the parent metal, commercially nominated as Weldom 700. The used steel is produced by SSAB Oxelösund AB, 613 80 Oxelösund, Sweden and fulfills requirement classified for EN 10025-6:2004 [5]. The chemical composition of Weldom 700 steel, according to the producer is presented in Table 1.

Table 1. Chemical composition of Weldom 700 steel

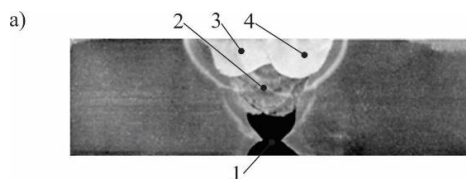
Chemical element	Content, %	Chemical element	Content, %
C	max 0,20	V	Max 0,09
Si	max 0,60	Cu	Max 0,30
Mn	max 1,6	Ti	Max 0,04
P	max 0,020	Al	Total max 0,015
S	max 0,010	Mo	Max 0,70
B	max 0,0005	Ni	max 2,0
Nb	max 0,04	N	max 0,010
Cr	max 0,07		

Mechanical properties of considered high-strength low-alloy steel S690QL related to specific plate thickness according to producer data are min. yield strength - $R_{p0,2} = 700$ MPa; tensile strength - $R_m = 780 - 930$ MPa; elongation - $A = 14\%$. The used steel is produced in two grades, nominated with suffix E and F in relation to impact toughness. Values of impact energy for Weldom 700 steel determined at V-notch Charpy specimens (EN ISO 148-1:2010 and EN 10045-1:1990) are presented at Tab. 2 [6 and 7].

Table 2. Impact energy of Weldom 700 steel

	Weldom 700E at -40°C	Weldom 700F at -60°C
Min. impact energy	69 J	27 J
Nom. according to EN 10025-6:2004	S690QL	S690QL1

Butt V-joint is done by welding at plates with a thickness of 15 mm. Microphotography of cross sections of considered welding joints after metallographic preparation and chemical etching by 4% nitric acid in alcohol is presented in Fig. 1.



1- root pass MMA, welding consumable INOX 18/8/6
2, 3, 4, 2', 3', 4' - other passes MAG, welding consumables MIG 75

Fig. 1. Microphotography of cross-sections of considered welded joint

The root pass is done by MMA welding process and welding consumables with a lower strength (pass - 1), while other passes are done by MAG welding process and welding consumables with higher strength (passes - 2, 3 and 4). Welding parameters for each pass and mechanical characteristics of related welding consumables are presented in Table 3.

Table 3. Welding parameters and mechanical characteristics of related welding consumables

Parameter	Root pass MMA	Root pass MIG
Current, I_z	$\approx 120 A$	$\approx 110 A$
Voltage, U	$\approx 24 V$	$\approx 24 V$
Welding speed, v_z	$\approx 0.2 cm/s$	$\approx 0.35 cm/s$
Heat input, q_l	$\approx 12 kJ/cm$	$\approx 13 kJ/cm$
Penetration, δ	$\approx 1.8 mm$	$\approx 1.8 mm$
Protective atmosphere	-	100% Ar (M11)
Welding consumables	INOX B 18/8/6; $\varnothing 3.25 mm$	MIG 18/8/6 Si; $\varnothing 1.2 mm$
Mechanical properties	R_m, MPa	590-690
	$R_{p0.2}, MPa$	> 350
	$A_5, \%$	> 40
	KV, J	> 80 (+ 20°C)
		560 - 660
		> 380
		> 35
		> 40 (+ 20°C)

Charpy V-notched samples are prepared according to related standards and norms. The preparation of samples is done with minimal additional heat input. The Charpy method of impact toughness test is a standardized high strain-rate test for determination of the energy absorbed by a sample to fracture. The standard dimensions of the sample for Charpy impact toughness test are presented in Fig. 2.

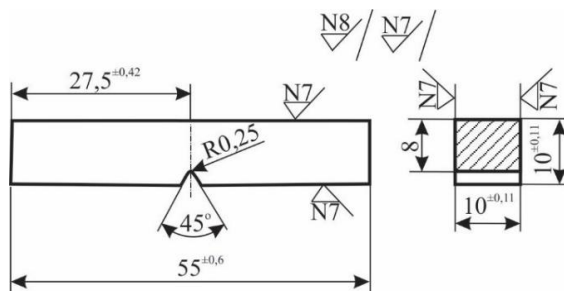


Fig. 2. Standard sample for Charpy impact testing

As the zone of welded joint is indicated as critical from the aspect of material degradation V-notch is done at its specific zones; weld metal, fusion zone, and heat affected zone. The method of the preparation of samples from the aspect of the relative positioning of V-notch and welded joint is presented in Fig. 3. Preparing of samples is done with special care in order to avoid additional heat input, corrosion and other types of material degradation. Visualization of welded joints is done by metallurgical preparation in order to obtain specific relative position between welded joint and V-notch. Testing procedure was design and done in order to obtained relevant tasting data related to current industrial practice and usual exploitative

conditions. Impact toughness is a very important mechanical characteristic of the material that can be defined as a measure of the energy need to be absorbed to cause fracture of the sample or the compromise the integrity of the structure of materials. When this energy is less material having a higher brittleness, and when this energy is greater material having a higher toughness.

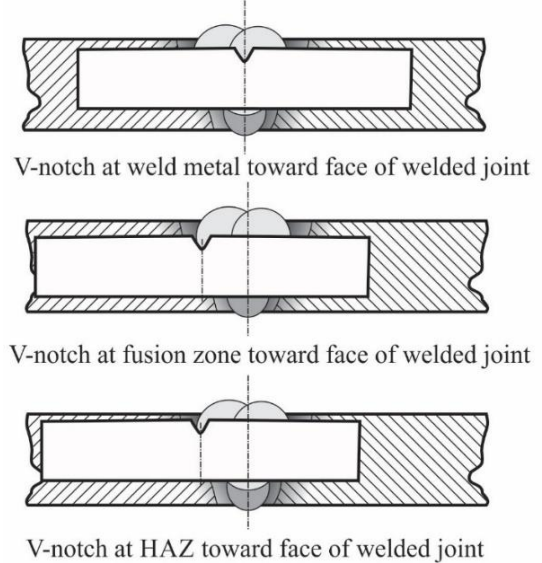


Fig. 3. Positions of V-notch for preparation of samples for impact toughness testing

The appearance of prepared samples after preparation for metallurgical preparation and chemical etching by 4% nitric acid in alcohol before testing are presented in Fig. 4. The metallurgical preparation and chemical etching were done in order to visualize specific zones of welded joint.

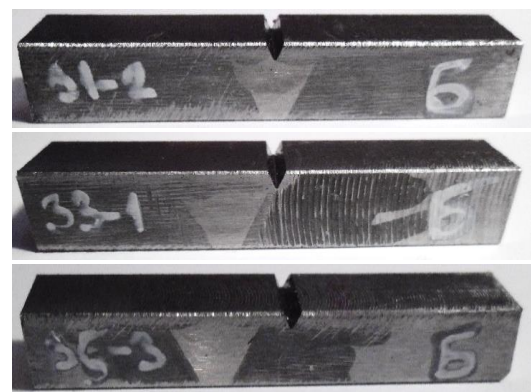


Fig.4. Charpy V-notched samples

Testing was done using a pre-defined standardized procedure on a series of samples for each position of V-notch at a temperature of 20°C. Testing machine is based on the computerized Charpy pendulum, presented at Fig. 5.

The used computerized Charpy pendulum is a device for measuring the energy absorbed by the samples to a fracture, which is a measure of toughness. The test procedure, the shape, and dimensions of the samples are defined by the standard EN ISO 148-1: 2010 and EN 10045-1: 1990 - Metallic materials - Test impact strength Charpy impact, i.e. SRPS EN ISO 148-1: 2012. Speed pendulum during impact strength test is from 5 to 5.5 m/s, while the energy losses are less than 1%.



Fig. 5. Computerized Charpy pendulum used for testing

The force and energy during testing of impact toughness were registered. The obtained results show very small relative exceptions and can be taken as relevant for further analysis.

3. TESTING RESULTS

The experimentally obtained values of fracture energy and force - time depending during the fracture of the tested samples show very small mutual deviations and consistent behavior so the results can be taken as relevant for further consideration. Experimental results indicate a mixed character of fracture of the tested samples. Force-time dependence to fracture during impact toughness testing of samples with V-notch at weld metal from the face of welded joint is presented in Fig. 6.

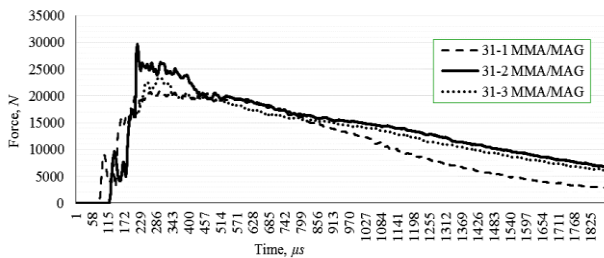


Fig. 6. Force-time dependence to fracture during impact toughness testing

The changing of the absorbed energy to fracture for the sample with V-notch at weld metal from the face of welded joint at testing temperature is shown diagrammatically in Fig. 7.

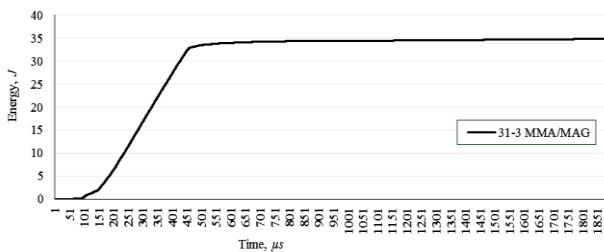


Fig. 7. Changing of energy to fracture during testing for samples with V-notch at weld metal

The appearance of sample with V-notch in welded joint after testing is presented in Fig. 8. The appearance of the surface created by fracture indicates its mixed character means both brittle and ductile fracture. The appearance of the fracture surfaces is in accordance with certain mechanical characteristics during testing impact toughness and character of force-time and energy-time relations. The test procedure is then done at specimens notched in the fusion zone, as at the test samples with the notch in the heat affected zone towards face of the welded joint.



Fig. 8. Sample with V-notch at welded joint after testing of impact toughness

Force-time dependence to fracture during impact toughness testing of samples with V-notch at fusion zone from the face of welded joint is presented in Fig. 9.

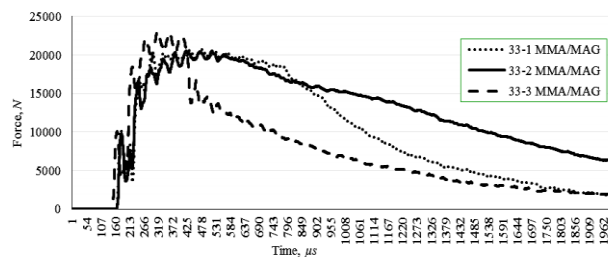


Fig. 9. Force-time dependence to fracture during impact toughness testing

The changing of the absorbed energy to fracture for the sample with V-notch at fusion zone from the face of welded joint at testing temperature is shown diagrammatically in Fig. 10.

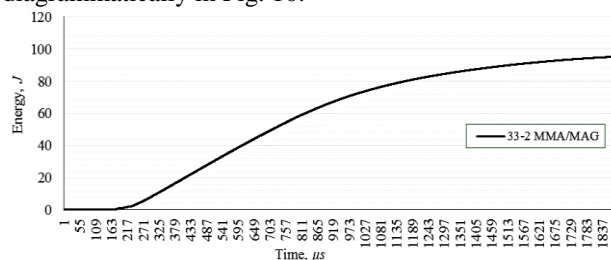


Fig. 10. Changing of energy to fracture during testing for samples with V-notch at fusion zone

Force-time dependence to fracture during impact toughness testing of samples with V-notch at HAZ from the face of welded joint is presented in Fig. 11.

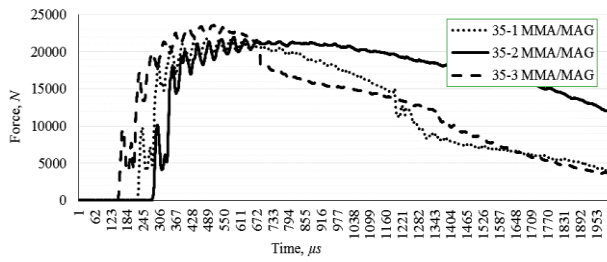


Fig. 11. Force-time dependence to fracture during impact toughness testing

The changing of the absorbed energy to fracture for the sample with V-notch at HAZ from the face of welded joint at testing temperature is shown diagrammatically in Fig. 12.

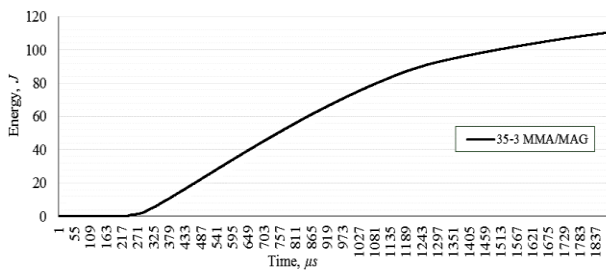


Fig. 12. Changing of energy to fracture during testing for samples with V-notch at HAZ

Experimentally determined values of fracture energy have small mutual deviation, the relations force - time show the same character, so testing results can be taken as relevant for further analysis. The histogram presented in Fig. 13 show experimentally obtained fracture energy for samples with different positions of V-notch towards to weld face.

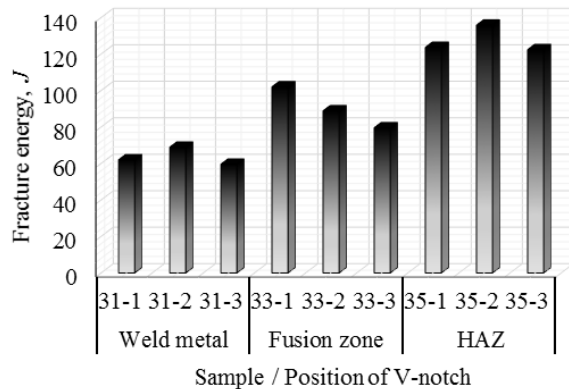


Fig. 13. Fracture energy of tested samples

4. EVALUATION OF THE OBTAINED RESULTS

Experimentally obtained the value of energy that is absorbed to fracture for different positions of V-notch toward to the face of welded joint it can be concluded that the maximal energy is obtained for samples with the V-notch in the heat affected zone, while slightly less for

samples with the V-notch at fusion zone. The lowest values of absorbed energy were obtained for samples with a notch at the axis of weld metal. The experimentally obtained values of energy are lower than at control samples made of parent material without welded joint. The appearance of the fracture surface for samples notched in the fusion zone toward the face of the welded joints after impact toughness testing at room temperature is presented in Fig. 14.



Fig. 14. Appearance of fracture surface after testing of samples notched at fusion zone

The appearance of the fracture surface shows a mixed character of fracture with distinct zones of brittle and ductile fracture. The appearance of the fracture surface for samples notched at the heat affected zone toward the face of the welded joints after impact toughness testing at room temperature is shown in Fig. 15.



Fig. 15. Appearance of fracture surface after testing of samples notched in HAZ

On fracture surface differ brittle and ductile fracture zone, indicating a mixed fracture character of tested sample, which is in agreement with the experimental values of impact strength and theoretical considerations related to this area.

5. CONCLUSION

Due to welding microstructural state at heat affected zone will be transformed in relation to the chemical composition of parent and filler metal, thermal cycles due to welding etc. High heat input affected the growth of metal grain that means degradation of strength and toughness, while low heat input during welding caused low penetration of fusion zone. As chemical compositions and microstructural state are complex altogether with high sensitivity to heat input, producers of those steels provide recommendations for filler metal and preheating temperatures, limitations for heat input and interpass temperatures [8, 9, 10].

Present norms, standards, and recommendations for the design of welding joints at high-strength low-alloy steels are based on heterogeneous backgrounds. Also, limitations are established for different reasons in order to

provide welded joint with adequate mechanical properties. On the other side, methods for improving the impact toughness and load capacity of welded joints to forming of defect and inclusions are based, primarily, on relaxing residual stress state, reducing hydrogen content and obtaining preferred thermal cycles during welding and cooling. Due to the complexity of factors and their interactions, present standards and recommendations are still not fully developed and precise, especially related to effects of specific welding parameters to chemical compositions and microstructural state at specific zones of welding joints and by that to impact toughness as complex general characteristic caused by a large number of factors. From the practical aspect and obtaining relevant data for design optimization, mechanical characteristics, and properties, stability and integrity analyses of welded joints at this steel grade is crucial. Due to complex nature of welded joints, only experimental testing can provide relevant data and information about the mechanical behavior of welded joints at high strength low alloyed steels during exploitation.

ACKNOWLEDGMENT

This paper is a result of the research activities conducted under the project "Sustainable development of technology and equipment for motor vehicles recycling" TR 35033, which is financed by the Ministry of Education, Science and Technological Development of Republic of Serbia.

REFERENCES

- [1] PAMNANI, R., KARTHIK, V., JAYAKUMAR, T., VASUDEVAN, M., & SAKTHIVEL, T. (2016). Evaluation of mechanical properties across micro alloyed HSLA steel weld joints using Automated Ball Indentation. *Materials Science and Engineering: A*, 651, 214-223.
- [2] LAN, L., KONG, X., QIU, C., & ZHAO, D. (2016). Influence of microstructural aspects on impact toughness of multi-pass submerged arc welded HSLA steel joints. *Materials & Design*, 90, 488-498.
- [3] COSTA, P. S., REYES-VALDÉS, F. A., SALDAÑA-GARCÉS, R., DELGADO, E. R., & SALINAS-RODRÍGUEZ, A. (2017). Thermal Behavior of an HSLA Steel and the Impact in Phase Transformation: Submerged Arc Welding (SAW) Process Approach to Pipelines. In *Characterization of Metals and Alloys* (pp. 85-98). Springer International Publishing.
- [4] SADEGHIAN, M., SHAMANIAN, M., & SHAFYEI, A. (2014). Effect of heat input on microstructure and mechanical properties of dissimilar joints between super duplex stainless steel and high strength low alloy steel. *Materials & Design*, 60, 678-684.
- [5] EN 10025-6:2004 - Technical delivery conditions for flat products of high yield strength structural steels in the quenched and tempered condition

- [6] ISO 148-1:2009 - Metallic materials - Charpy pendulum impact test - Part 1: Test method
- [7] EN 10045-1:1990 - Metallic materials - Charpy impact test - Part 1: Test method
- [8] ILIĆ, A. (2015) Influence of shape complexity, material, stress concentration and temperature to design of welded constructions, PhD thesis, Faculty of Engineering, Kragujevac (in Serbian)
- [9] ILIĆ, A. , IVANOVIĆ, L., RAKIĆ, B., JOSIFOVIĆ, D., LAZIĆ, V. (2014) Influence of welding technology to mechanical properties of welding joints at high strength low alloy steels, The 8th International Symposium KOD 2014, Machine and Industrial Design in Mechanical Engineering, Balatonfüred, Hungary,
- [10] LAZIĆ, V., ALEKSANDROVIĆ, S., ARSIĆ, D., SEDMAK, A., ILIĆ, A., IVANOVIĆ, A., ĐORĐEVIĆ, M. (2016) The influence of temperature on mechanical properties of the base material and welded joint made of steel S690QL, *Metalurgija*, Vol.55, No.2, pp. 213-216, ISSN 0543-5846

CORRESPONDANCE



Andreja ILIĆ, PhD,
University of Kragujevac,
Faculty of Engineering,
Sestre Janjić 6,
34000 Kragujevac, Serbia,
E-mail: andreja.coka@gmail.com



Lozica IVANOVIĆ, Full Prof PhD,
University of Kragujevac,
Faculty of Engineering,
Sestre Janjić 6,
34000 Kragujevac, Serbia,
E-mail: lozica@kg.ac.rs



Blaža STOJANOVIĆ, Assist. Prof PhD,
University of Kragujevac,
Faculty of Engineering,
Sestre Janjić 6,
34000 Kragujevac, Serbia,
E-mail: blaza@kg.ac.rs



Danica JOSIFOVIĆ, Full Prof PhD,
University of Kragujevac,
Faculty of Engineering,
Sestre Janjić 6,
34000 Kragujevac, Serbia,
E-mail: danaj@kg.ac.rs



Eleonora DESNICA, Assoc. Prof. Ph.D.
Department of Mechanical Engineering
University of Novi Sad
Technical faculty "Mihajlo Pupin"
Đure Đakovića bb
23000 Zrenjanin, Serbia
E-mail: desnica@tfzr.uns.ac.rs

FAILURE MODE AND STRENGTH ANALYSES OF RESISTANCE SPOT WELD JOINTS OF ALUMINIUM AND AUSTENITIC STAINLESS STEEL SHEET

Aleskija ĐURIĆ
 Biljana MARKOVIĆ

Abstract: Resistance spot welding (RSW) is considered as the dominant process for joining similar and dissimilar sheet metals in automotive industry. In this paper will be present the strength analyze of spot weld joint and analyze the transition between interfacial and pull-out failure modes for resistance spot weld joints of aluminium and austenitic stainless steel sheet, during the tensile–shear test, by usage analytical and experimental approach. For experimental testing, the specimen of 1 mm and 2 mm thickness were used, welded with different welding parameters.

Key words: resistance spot welding, failure mode, tensile-shear test

1. INTRODUCTION

Lightweight design (LW) is resulting from the need for sustainable design and product development [1]. Material, design and manufacturing technologies remain key technologies in vehicle development [2] and also in other products development. The essence of success at global world market is integration, so the multi-material design has been developed as a modern concept of LW design, aimed at integrating different types of materials into one structure. For example, vehicle body weight can be reduced by the use of multiple materials without cost increase [2]. Various lightweight automotive bodies have been developed using high strength steels, aluminium alloys, and composite materials. One prerequisite for multi-material structures for car bodies is the availability of material-capable and cost-efficient joining technologies [4].

Aluminium, aluminium alloys, and steel are often used in multi-material structures, so there are various studies [4,5] that analyze how these materials are bonded. Very often in these studies can be saw the resistance spot welding (RSW) [6-8] as one solution. Despite the emergence of new technologies, RSW is still a dominant process for joining similar and dissimilar sheet metals in automotive industry.

Joint failure, e.g. resistance spot weld (RSW) joint failure, was identified as one of the key failure types when a vehicle crash occurs [9]. Failure mode of resistance spot welds is indicator of weld quality. Two major types of spot weld failure are pull-out and interfacial fracture [9,10]. The aim of this paper is strength analyze of spot weld joint and analyze the transition between interfacial and pull-out failure modes for resistance spot weld joints of aluminium 99,5 (1050A) and austenitic stainless steel X2CrNi18-9 sheet during the tensile–shear test, by the use of analytical and experimental approach.

Austenitic stainless steels, and therefore the steel X2CrNi18-9 is often used as construction material in the chemical- and food-processing industry [11] and also, this steel is applied in the automotive industry [12]. In order to develop lightweight structures, stainless steel is tended to replace, primarily because of their weight. However, steel structures can not be completely replaced, it is possible to replace parts of constructions with lightweight materials, such as aluminium. In this case, it is necessary to join stainless steels and aluminium [13]. The chemical composition and basic mechanical properties of steel X2CrNi18-9 and aluminium 99.5 (1050A), that were used for research present in this paper, are given in Table 1.

Table 1: Chemical composition and basic mechanical properties of steel X2CrNi18-9 and aluminum 99.5 (1050A)

Material	Steel X2CrNi18-9		Al99,5	
Chemical composition [%]	C	0,03	Al	99,5
	Si	0,75	Si	0,25
	Mn	2,0	Fe	0,4
	Ni	8,0	Cu	0,05
	Cr	17,5	Mn	0,05
	N	0,1	Mg	0,05
	S	0,015	Zn	0,07
	P	0,045	Ti	0,05
Mech. properties	R _m [N/mm ²]	540	R _m [N/mm ²]	230
	R _{p0,2} [N/mm ²]	100-135	R _{p0,2} [N/mm ²]	75
	HB	92	HB	35

2. THEORETICAL STRESS ANALYSES AND FAILURE MODE TRANSITION

Basically, spot welds can fail in three distinct different modes, shown on figure 1, described as follows [9]:

- Interfacial failure (IF) in which, fracture propagates through the fusion zone (FZ)
- Pull-out failure (PF) in which, failure occurs via the withdrawal of weld nugget from one sheet. In this mode, fracture may initiate in base metal (BM), heat affected zone (HAZ) or HAZ/FZ depending on the base metal and the loading condition.
- Partial interfacial mode (PIF) in which, fracture first propagates in fusion zone (FZ) and then is redirected through thickness.

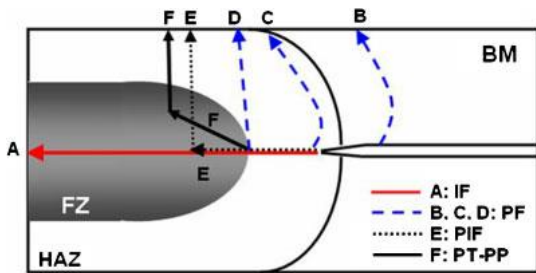


Fig.1: Schematic of various failure modes during mechanical testing [14]

The failure of resistance spot welds during the tensile-shear test can be described as a competition between the shear plastic deformation of the fusion zone (i.e. IF mode) and the necking in the base metal (i. e. PF mode) [9]. At the nugget circumference, shown on figure 2, stresses are shear tensile at position A and shear compression at position B [10].

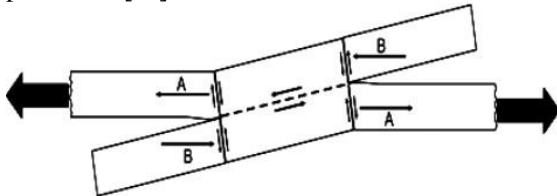


Fig.2: Distribution at nugget centerline and circumference during shear tensile test [16]

According to [9] the failure load at the interfacial failure mode (IF mode) can be expressed using Eq. 1:

$$F_{IF} = \frac{\pi}{4} \cdot d^2 \cdot \tau_{FZ} \quad (1)$$

where d is the diameter of the weld nugget and the τ_{FZ} is shear strength of the fusion zone.

For PM mode, failure is initiated when the maximum experienced radial tensile stress at nugget circumference reaches the ultimate tensile strength of the failure location. Therefore, failure load in the PF mode can be expressed using Eq. 2 [9]:

$$F_{PF} = \pi \cdot t \cdot d \cdot \sigma_{PFL} \quad (2)$$

where t is the thickness of the base metal sheet and σ_{PFL} is the ultimate tensile strength of the PF location.

For Sawhill and Baker, equation 2 can be written as Eq. 3 [10]:

$$F_{PF} = c \cdot t \cdot d \cdot \sigma_{BM} \quad (3)$$

Where σ_{BM} is the ultimate tensile strength of base material and c is a constant between 2,5 and 3,1.

According to previous equations, the comparative stress of spot weld joint can be calculated using Eq. 4:

$$\sigma_s = \max \left\langle \frac{4F}{i \cdot \pi \cdot d^2} \cdot \frac{1}{\alpha_1}, \frac{F}{i \cdot \pi \cdot t \cdot d} \cdot \frac{1}{\alpha_2} \right\rangle \quad (4)$$

where F is applied load, i number of welds and α coefficient of weld joint. Coefficient α_1 is 0,65 and α_2 is 0,5 [15].

Comparative stress is approach to calculate stresses in spot weld joint. Generally, the stress in welds has normal and tangential components. The method of comparative stresses is based on the fact that the shear strength of weld metal is lower than the tensile strength [15].

3. EXPERIMENTAL PROCEDURE

Specimens for this study are prepared in accordance with EN ISO 14273: 2001, the dimensions of specimens are shown on Figure 3.

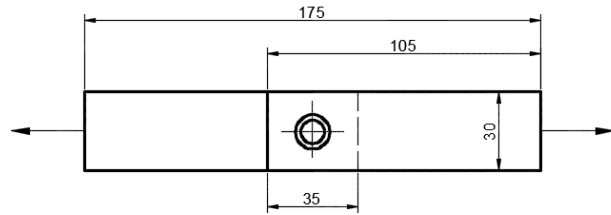


Fig. 3: Dimensions of specimen

The process of spot welding was done on the machine shown in Figure 4, manufactured by DALEX WERK, located in the TMD dommers factory in Gradačac, BiH. Welding parameters for all specimens are given in Table 2. For the welding of all specimen, class 2 electrodes (Cu + Zr + Cr) were used. The head of the upper electrode is 5 mm and the lower electrode type is beck-up. Also, the electrode force for all specimens was 2 kN.



Fig. 4: Spot weld machine and specimen after spot welding

Table 2: Welding parameters for all specimens

Marks	Mat. 1	Mat. 2	Thic. 1 t [mm]	Thic. 2 t [mm]	Weld current [kA]	Weld time [1/100 sec]	Number and position of weld
E24	Al 99,5	X2CrNi18-9	1	1	6	32	*
E26			1	1	6	32	*
E27			1	1	6	32	*
E28**			1	1	6	32	* *
E29**			1	1	6	32	* *
E30			1	1	6	32	* *
E40			1	1	6	32	* *
E32*			2	1	7	32	*
E33*			2	1	7	32	*
E34			2	1	7	32	*
E35			2	1	7	32	*
E49			2	1	7	72	* *
E50			2	1	7	72	* *
E51			2	1	7	72	* *

* The steel was in direct contact with the upper electrode
 ** For one spot steel was in contact with the upper electrode and for other one spot aluminum was in contact with the upper electrode

For further analysis, it is very important to know which material is in contact with the upper electrode. Steel and aluminum are not the same conductors of electricity, so different parameters are required in welding if the same quality of welding is desired. It is visually possible to perceive the difference in the appearance of the weld, depending on that which material is in a contact with the upper electrode, as shown in Figure 5.

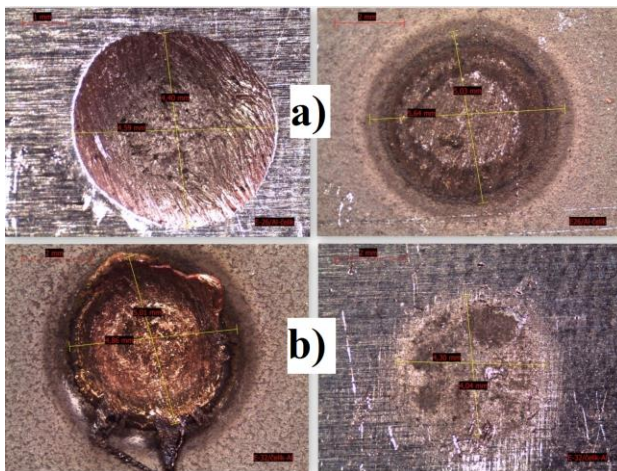


Fig. 4: a) Spot weld when aluminum is in a contact with upper electrode; b) Spot weld when steel is in a contact with upper electrode

The tensile -shear test of all specimens welded by RSW with welding parameters shown in Table 2., was carried out according to the recommendations of the aforementioned standard EN ISO 14273: 2001, on the test machine AGS-X 20 kN, manufactured by SCHIMDZU (Figure 5).

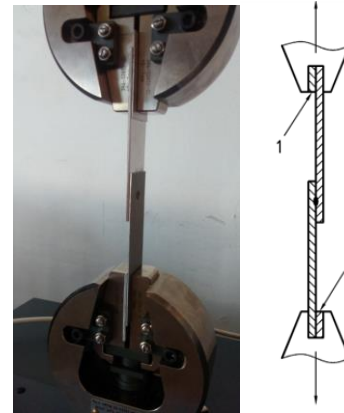


Fig. 5: Specimen prepared for testing set in jaws of test machine (1- shim plates)

4. RESULTS AND DISCUSSION

In this section it will be shown illustration of two major types of spot weld failure: pull-out (PF) and interfacial fracture (IF) and tensile-shear strength for previously shown specimens.

Pull-out failure (PF) is illustrated in Figure 6a for all three specimens marked as E24, E26 and E27. These are specimens with one spot and sheet thickness of both materials (aluminum and steel) of 1 mm. In standard EN ISO 14273:2001 pull-out failure shown on Figure 6a is called spot weld with partial pull-out failure.

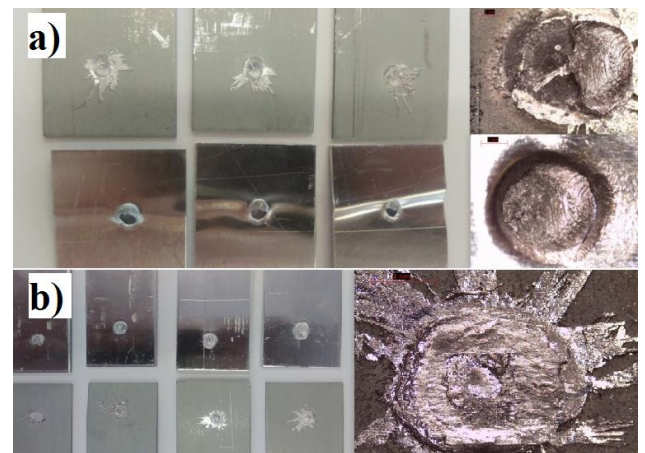


Fig. 6: Illustration of failures: a) pull-out failure (PF); b) interfacial failure (IF)

A specimen with one spot with aluminum thickness of 2 mm, and steel 1 mm marked E32-E35 after the testing are shown on Figure 6b, where interfacial failure (IF) can be seen. The force/displacement diagram for the E24 specimen for static tensile-shear test is shown in Figure 7.



Fig. 7: Force/displacement diagram for the E24 specimen

Specimens marked with E32 and E33 were welded so that the steel was in contact with the upper electrode, and the specimens E34 and E35 were welded so that the aluminum was in contact with the upper electrode. In terms of failure mode, this is not important. Figure 8a shows the force/displacement diagram for E32 specimen (steel in contact with the upper electrode) and Figure 8b shows same diagram for E35 specimen (aluminum in contact with the upper electrode).

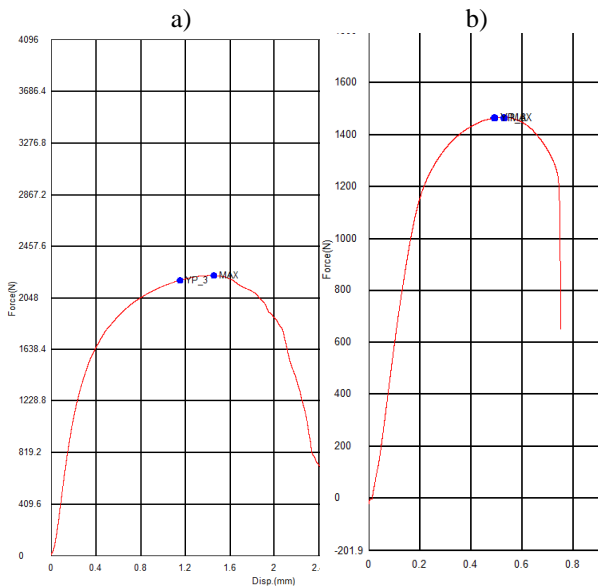


Fig. 8: Force/displacement diagram for the a) E32 specimen; b) E35 specimen

The fact that the specimens E32 and E33 were welded so that steel is in contact with the upper electrode was shown as a favorable case in terms of a tensile shear strength, what can be concluded when comparing Figures 8a and 8b.

One of very important parameter for spot weld obtained from force/displacement curves is energy absorption [16, 17]. The amount of energy absorption can be digitally calculated by measuring the area under the force/displacement curve up to failure using the Eq. 5 [16]:

$$Q = \sum_{n=1}^N F(n) \cdot [x(n) - x(n-1)] \quad (5)$$

where F is force, x the displacement, n the sampled data and N the peak failure load.

Load carrying capacity and energy absorption capability for those welds fail under interfacial mode, are much less than those which fail under pull-out mode. To ensure reliability of spot welds during vehicle lifetime, process parameters should be adjusted so that pull-out failure mode is guaranteed [10].

When the spot weld joint is with two spot, for the same specimen thickness, the fail is dominant in the PF mode, regardless of whether the spots are arranged vertically or horizontally (Figure 9a). For the same spot weld joint, but with different thickness of aluminum (2 mm) and steel (1 mm), the fail is dominant in the IF mode (Figure 9b).

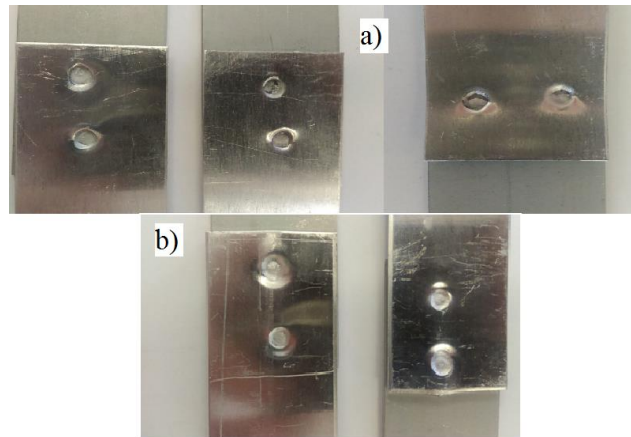


Fig. 9: Illustration of a) pull-out failure (PF); b) interfacial failure (IF) for spot weld with two spots

The tensile-shear strength of the specimens with the vertical spots marked E28 and E29 is somewhat higher than the specimens with horizontal spots E30 and E40, although the same welding parameters. One of the reasons is the fact that for a vertical weld joint one spot is welded when aluminum being in contact with the upper electrode and other one when steel being in contact with the upper electrode, differing from the horizontal layout, where both spots are welded when aluminum being in contact with the upper electrode.

The values of tensile-shear strength and comparative stress for all specimens are shown in Table 3.

Tensile-shear strength of specimen marked E49 i E50 is higher than tensile-shear strength of E28 i E29 specimens, especially because of different thickness, weld current and weld time. This four specimens have same layout of spots. The force/displacement diagram for the E29 specimen is shown in Figure 10a and for the E50 specimen is shown in Figure 10b.

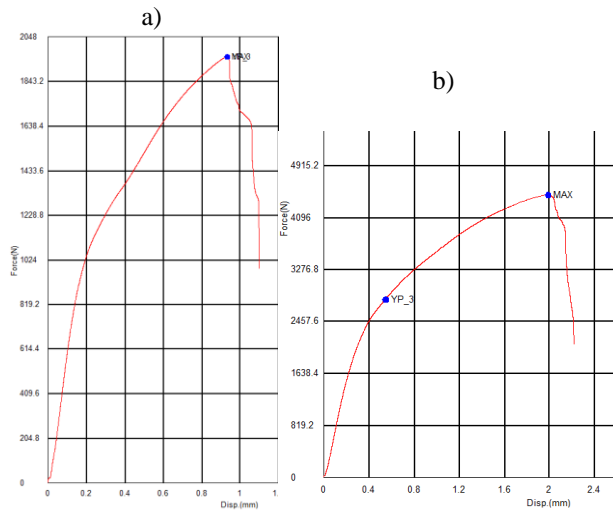


Fig. 8: Force/displacement diagram for the a) E29 specimen; b) E50 specimen

The influence of the weld time on the tensile-shear strength was shown in [18] and the analysis in [19] shows the percentage contribution of individual parameters on the weld strength. The percentage contribution of the welding current is 49.81%, the thickness of 37.94% and the cycle time of 2.61%.

Table 3: The values of tensile-shear strength and comparative stress

Mar.	F_{\max} [N]	i	$\frac{4F}{i \cdot \pi \cdot d^2} \cdot \frac{1}{\alpha_1}$ [N/mm ²]	$\frac{F}{i \cdot \pi \cdot t \cdot d} \cdot \frac{1}{\alpha_2}$ [N/mm ²]	σ_s [N/mm ²]
E24	797,494	1	62,52	101,59	101,59
E26	771,043	1	60,44	98,22	98,22
E27	811,536	1	63,62	103,38	103,38
E28	2203,63	2	86,37	140,36	140,36
E29	1996,20	2	78,24	127,15	127,15
E30	1347,91	2	52,83	85,85	85,85
E40	1665,5	2	65,28	106,08	106,08
E32	2224,33	1	174,37	141,68	174,37
E33	2073,79	1	162,57	132,09	162,57
E34	1645,35	1	128,98	104,80	128,98
E35	1472	1	115,39	93,76	115,38
E49	4380,55	2	171,70	139,51	171,70
E50	4453,22	2	174,55	141,82	174,55
E51	2810,55	2	110,16	89,51	110,16

The analytically obtained stress values based on equation 4 shown in Table 3 confirm the previous experimental test, in terms of failure mode. For example, specimens E24 to E30 and E40 have higher stress analytically obtained for PF mode, than stress analytically obtained for IF mode. Also, previous Figures (Fig. 6a and Fig 9a) confirm that these specimens fail in PF mode in experimentally test.

5. CONCLUSION

In this paper was analyzed the tensile-shear strength and failure mode of the spot weld joint of X2CrNi18-9 steel and aluminum 99.5. The theoretical analysis was showed,

that spot welds for tensile-shear load general can fail in two distinct different modes: IF (Interfacing) in which, fracture propagates through the fusion zone (FZ) and pull-out failure (PF). The analytical comparative stress of the spot weld joint is determined by selecting the maximal value between the stresses received by the IF and the PF mode.

The experimental testing of the spot weld joint of the aforementioned two materials for different welding parameters and the thickness of the material was done, as a confirmation of the theoretical analysis. After the experiment, it is easy to recognize which mode belongs to the fail of the specimen and it was found that comparative stress is analytical obtained from the same failure mode. The thickness of the material is one of the parameters that largely indicate in which failure mode will fail spot weld joint.

Many previous studies, referenced here, together with this one shown that, in terms of the tensile-shear, the strength material thickness and the welding current are very important. Also, the tensile-shear strength depends on which material is in contact with upper electrode, when dissimilar material welding, which has been shown here.

REFERENCES

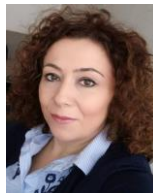
- [1] ĐURIĆ, A., MARKOVIĆ, B., VUČETIĆ, N., PELKIĆ, S. (2016) *Calculation of factors LBKz and its significance for the development of lightweight construction*, Proceedings of the International conference "Mechanical Engineering in XXI century", Niš, Serbia.
- [2] GOEDE, M., STEHLIN, M., RAFFLENBEUL, L., KOPP, G., BEEH, E. (2008) *Super Light Car—lightweight construction thanks to a multi-material design and function integration*, European Conference of Transport Research Institutes (ECTRI), pp 5-10
- [3] CUI, X., ZHANG, H., WANGB, S., ZHANG, L., KO, J. (2011) *Design of lightweight multi-material automotive bodies using new material performance indices of thin-walled beams for the material selection with crashworthiness consideration*, Journal of Materials and Design, Vol. 32, pp 815-821
- [4] MESCHUT, G., JANZEN, V., OLDFERMANN, T. (2013) *Innovative and Highly Productive Joining Technologies for Multi-Material Lightweight Car Body Structures*, Journal of Materials Engineering and Performance, Vol.23, No 5, pp 1515-1523
- [5] SAKIYAMA, T., NAITO, Y., MIYAZAKI, Y., NOSE, T., MURAYAMA, G., SAITA, K., OIKAWA, H., (2013) *Dissimilar Metal Joining Technologies for Steel Sheet and Aluminum Alloy Sheet in Auto Body*, Nippon steel technical report, No. 103, pp 91-98
- [6] SUN, X., STEPHENS, E. V., KHALEEL, M. A., SHAO, H., KIMCH, M. (2004) *Resistance Spot Welding of Aluminum Alloy to Steel with Transition Material - From Process to Performance - Part I: Experimental Study*, Welding journal, pp 188-195
- [7] QIU, R., IWAMOTO, C., SATONAKA, S. (2009) *Interfacial microstructure and strength of steel/aluminum alloy joints welded by resistance spot*

- welding with cover plate, Journal of Materials Processing Technology, Vpl. 209, pp 4186–4193
- [8] ZHANG, W. H., QIU, X. M., SUN, D. Q., HAN, L. J. (2011) *Effects of resistance spot welding parameters on microstructures and mechanical properties of dissimilar material joints of galvanised high strength steel and aluminium alloy*, Science and Technology of Welding and Joining, Vol.16, No 4, pp 153-161
- [9] POURANVARIA, M., MARASHIB, S.P.H. (2011) *Failure mode transition in AHSS resistance spot welds. Part I. Controlling factors*, Journal of Materials Science and Engineering A, Vol.528, pp 8337– 8343
- [10] POURANVARI, M., ASGARI, H. R., MOSAVIZADCH, S. M., MARASHI, P. H., GOODARZI, M. (2007) *Effect of weld nugget size on overload failure mode of resistance spot welds*, Science and Technology of Welding and Joining, Vol.12, No 3, pp 217-225
- [11] MULLER, D., WOLF, G.K., STAHL, B., AMARAL, L., BEHAR, M., CUNHAC, J.B.M. (2002) *Phase transformation and corrosion behavior of stainless steel bombarded by pulsed energetic ion beams*, Journal of Surface and Coatings Technology, Vol.158 –159, No 2, pp 604–608
- [12] CUNAT, P., (2002) *Stainless Steel In Structural Automotive Applications*, SAE Technical Paper 2002-01-2067
- [13] FUKUMOTO, S., TSUBAKINO, H., OKITA, K., ARITOSHI, M., TOMITA, T. (1999) *Friction welding process of 5052 aluminium alloy to 304 stainless steel*, Journal of Materials Science and Technology, Vol.15, pp 1080-1086
- [14] POURANVARI, M., MARASHI, S. P. H., MOUSAVIZADEH, S. M. (2010) *Failure mode transition and mechanical properties of similar and dissimilar resistance spot welds of DP600 and low carbon steels*, Science and Technology of Welding and Joining, Vol.15, No 7, pp 625-631
- [15] https://www.engineersedge.com/weld/spot_weld_joint_single_shear.htm , 26.07.2017.
- [16] KHAN, M. I., KUNTZ, M. L., ZHOU, Y. (2008) *Effects of weld microstructure on static and impact performance of resistance spot welded joints in advanced high strength steels*, Science and Technology of Welding and Joining, Vol.13, No 3, pp 294-304
- [17] HAN, L., THORNTON, M., SHERGOLD, M. (2010) *A comparison of the mechanical behaviour of self-piercing riveted and resistance spot welded aluminium sheets for the automotive industry*, Journal of Materials and Design, Vol.31, pp 1457–1467
- [18] ASLANLAR, S., OGUR, A., OZSARAC, U., ILHAN, E. (2008) *Welding time effect on mechanical properties of automotive sheets in electrical resistance spot welding*, Journal of Materials and Design, Vol.29, pp 1427–1431
- [19] Shah, D., Patel, P. D. (2013) *Prediction of Weld Strength of Resistance Spot Welding Using Artificial Neural Network*, Journal of Engineering Research and Applications, Vol. 3, No 5, pp1486-1491

CORRESPONDANCE



Aleksija ĐURIĆ, Ass. M.Sc. Eng.
University of East Sarajevo
Faculty of Mechanical Engineering
Vuka Karadzica 30,
71123 East Sarajevo, B&H
aleksijadjuric@gmail.com



Biljana MARKOVIĆ, Prof. D.Sc. Eng.
University of East Sarajevo
Faculty of Mechanical Engineering
Vuka Karadžića 30,
71000 East Sarajevo, B&H
biljana46m@gmail.com

ADVANCED FW AND AFP/ATL TECHNOLOGIES FOR PRODUCTION OF COMPLEX PARTS OF COMPOSITE MATERIALS

Svetlana RISTESKA
Blagoja SAMAKOSKI
Vladimir DUKOVSKI

Abstract: Composites have emerged in recent years as a valuable class of engineering materials. They offer many attributes not attainable with other materials – they are lightweight, yet offer stiffness – and as a result can be found in a range of tech application with advanced technologies.

One from advanced technology for manufacture a composite is FW. This process is primarily used for hollow, generally circular or oval sectioned components, such as pipes and tanks. Filament winding technology are use and in wind energy. A coupling and a torque shaft are normally part of a classic drive train configuration in wind power generators. Both parts are critical from a cost/performance and maintenance point of view. Steel as well as composite materials are involved in shaft designs. Flexible torque shaft from composite was developed for turbine to eliminate the need for a coupling for steel shaft. The new composite shaft combines the key features of a drive shaft with a coupling – in a single, integrated component provide maximum torque strength for high torque transmission, while offering low bending stiffness. The main advantage of composites is that they have a high strength and high stiffness to weight ratio. They are also corrosion resistant, are electrical insulators, and lend themselves to a variety of fabrication methods.

Second advanced technology is ATL machine, who is the capability for fast automated laying of tape. As the application of lasers in tape placement is relatively new, and laser heating has some distinct differences from other forms of heating such as hot gas or infrared heating, it is important to understand how the LAMP process influences the morphology development. Mikrosam enables high quality of the automated fiber/tape placement manufacturing process via its own tools: MikroPlace - an intelligent machine-independent software for off-line programming, design, simulation and analysis.

Key words: composite, shaft, machine, robot, laser,

1. INTRODUCTION

1.1. FW technology

Filament winding is a process for fabricating composite materials in which continuous fibers, either previously impregnated with a matrix material or impregnated during winding, are wound onto a rotating mandrel in a precise, predetermined pattern.

With help of design of experiment (DOE) can be investigated the complex interaction between filament winding manufacturing and design variables, which affect tensile strength and composite quality of specimens [1-4]. Tension control is important factor for better winding patterns, which is the main reason for composite high strength. Therefore, tension control system was designed and manufactured to understand the effect of it parameters on the end product. There are a number of parameters that affect the breaking of fiber during it transport in FW process, which influence the composites mechanical properties [5-10].

If a composite materials tower in wind energy industries is used instead of the existing steel tower, the production cost can be reduced by using of low cost composite materials, simple manufacturing process, easy transportation and easy assembly [11-14].

In this study will present and discuss some process variables parameters in final properties of composite specimens, manufactured with conventional filament winding equipment.

1.2. AFP/ATL (LAMP) machine for thermoplastics

Automated fiber placement and tape laying (AFP/ATL) are the technologies that for more than two decades have revolutionized the production of composite structures for the aviation and space industry, and nowadays are entering into new industries such as wind energy. While AFP places multiple individual tows, ATL lays unidirectional tapes or strips of fabric. Both processes apply thermoset, thermoplastic resin-impregnated or dry continuous fibers.

The laser-assisted tape placement (LATP) process is a promising manufacturing technology for thermoplastic composites [14-17], combining high productivity with the ability to manufacture complex geometries. The process comprises the automated lay-up and (in the ideal case) consolidation of pre-impregnated fiber reinforced thermoplastic tapes to incrementally shape a composite structure.

The present work aims to determine some parameters for to optimize the LATP process. Advanced parts can now be produced, whether flat or highly contoured, with automated computer controlled placement of the UD carbon thermoplastic prepreg tape. The temperature control of the thermoplastic material is controlled via a compaction surface laser (heating temperature up to 500°C) integrated to the ATL head. MikroPlace - an intelligent machine-independent software for off-line programming, design, simulation and analysis; and Mikro Automate - a software for online process control and data acquisition system tailored to the specific need of ATL production.

2. EKSPERIMENTAL PART

2.1. Example 1

Filament Winding machines nowadays are widely used in the production of high efficiency carbon fiber parts for the winding energy industry. This series of Filament Winding machines are specially designed to meet specific requirements and in the process of production of carbon fiber shaft. This composite shaft is ideal for the specific load requirements of a drive shaft in continuous operation between the ship's engine and the propellers. It's outstanding damping performance ensures propulsion at low-noise and low-vibration levels. Handling and transportation are much easier thanks to the much lighter construction compared to drive shafts made of steel.

The influence of parameters in the FW process, speed of winding, angles, and transport of fiber in the rollers are key parameters for determining high strength and high stiffness of composite shafts. Variable parameters who are using in this tests are show in Table 1.

Table 1: Composite shaft instructions

No	shaft prototype	
1.	Material	CFRP (carbon epoxy)
2.	Tension of fiber	20, 50N
3.	Winding speed	5, 21 m/min
4.	Angles	45/78/90 degrees

The aim of this study is to investigate the mechanical properties of continuous fiber reinforced composite tubes, produced by filament winding technique. For this purpose, the full factorial experimental design was implemented. When designing the filament winding composites, three major factors are the most important: fiber orientation, fiber tension and velocity of the filament winding. The ultimate target is to achieve the composite pipes with good characteristics as material for construction with the lowest possible weight. The filament winding composite pipes were made of carbon fiber and epoxy resin.

This study used highest strength, standard modulus single carbon fiber Torayca T700S 24K from Toray. Carbon fiber was impregnated into commercially available epoxy resin system with anhydride hardener and amine accelerator for filament winding processing from Huntsman, Araldite® LY 1135-1 / Aradur® 917 / Accelerator 960-1. Wet winding process was carried out on Filament winding machine with roller type resin bath and electrical creel manufactured from Mikrosam A.D (fig.1 and fig. 2).

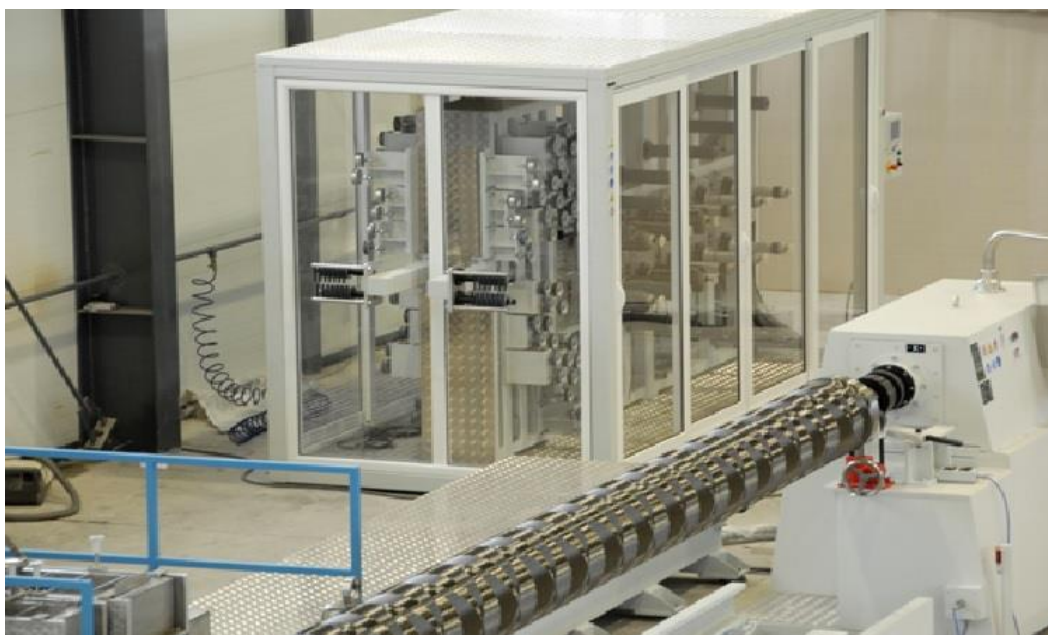


Fig.1: FW machine for composite shaft



Fig.2: manufacture of composite shaft with FW machine

The preparation of the composites was done by applying the 2^3 full factorial experimental design. For the purposes of these investigations, eight test specimen configurations are made and on the basis that test results should provide material properties useful in the design stage. The velocity of the filament winding was taken to be the first factor, the second – fiber tension and the third – winding angle. The effect of a filament-winding processing variables on longitudinal and hoop tensile and bending properties of the prepared composites will be investigated according to American Society for Testing and Materials (ASTM) standards ASTM D 2290 and D 790.

Different values of the process parameters have been considered by means of design of experiment (D.O.E) technique used for Carbon fiber/ epoxy with FW, as shown in Table 1.

Table 1: Carbon /epoxy with FW DOE 2^3

No. of samples	Tension of fiber (N)	Winding speed (V m/min)	Angle (α)
1.	50	21	90°
2.	20	21	90°
3.	50	5	90°
4.	20	5	90°
5.	50	21	45°
6.	20	21	45°
7.	50	5	45°
8.	20	5	45°

2.2. Example 2

The part of experimental research will be realized at AD Mikrosam from Prilep on their equipment for

manufacturing composite materials - LAMP machine (fig.3).

As the laser is mounted at a fixed point on the tape placement heat, the laser angle governs the distribution of the power between the tape and the laminate. The effect of the laser angle influence the mechanical properties of laminates. At lower angles the majority of energy is supplied to the tape, while at higher angles more energy is supplied to the laminate. In these experiments the laser angle is a constant $22, 5^0$. The LAMP equipment allowed the variation of some process parameters. Experimental studies were performed with changing parameters – temperature, pressure of contacted roller and placement velocity. A set of experimental tests have been carried out by a ATL machine.

Different values of the process parameters have been considered by means of design of experiment (D.O.E) technique for PEEK/Carbon and PPS/Carbon tape 25mm width, as shown in Table 2 and 3.

Table 2: PEEK/Carbon UD Prepreg DOE 2^3

No. of samples	Temperature (T °C)	Placement velocity (V m/min)	Pressure of contacted roller (P bar)	Angle
1.	420	9	3.8	0°
2.	360	9	3.8	0°
3.	420	3	3.8	0°
4.	360	3	3.8	0°
5.	420	9	2.8	0°
6.	360	9	2.8	0°
7.	420	3	2.8	0°
8.	360	3	2.8	0°

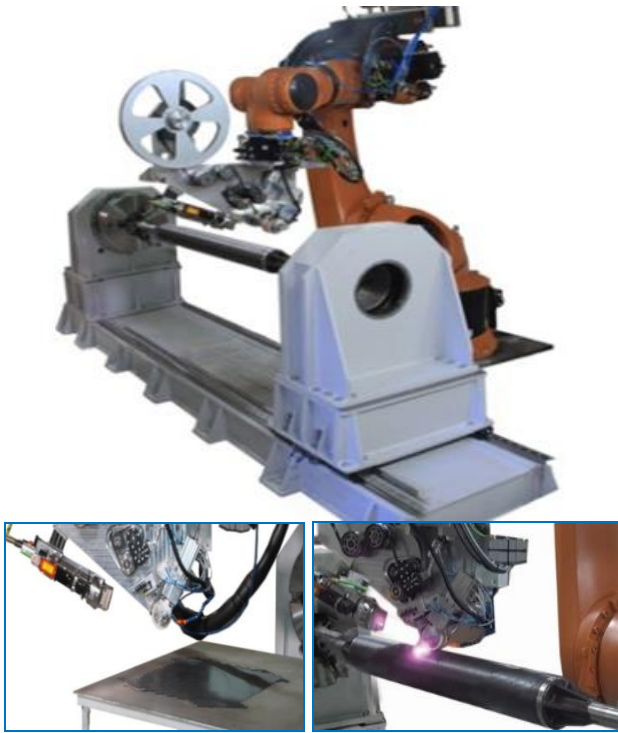


Fig.3: LAMP machine for thermoplastic UD prepreg

Table 3: PPS/Carbon UD Prepreg DOE 2³

No. of samples	Temperature (°C)	velocity (m/min)	Pressure (bar)	Angle
1.	350	9	3.8	0°
2.	280	9	3.8	0°
3.	350	3	3.8	0°
4.	280	3	3.8	0°
5.	350	9	2.8	0°
6.	280	9	2.8	0°
7.	350	3	2.8	0°
8.	280	3	2.8	0°

3. RESULTS AND DISCUSSION

3.1. FW technology

Tests describes optimal processing conditions that maximize the mechanical properties of the composites with different process parameters in FW technology. Higher speed, higher tension of fiber without carbon fiber breakage in transport in fiber creel and the use of angles of 40 to 80, give the best results at composite shafts. Larger tensions and angles decrease pores up to 1-2% in this technology, and increase mechanical properties to 20%.

With using composite shafts are reduces the weight of the shafts. The transmission energy is reduced by reducing the weight of the shaft. Replacement of transmission shafts of steel with carbon (positive experiences and benefits) Are examples where this is produced.

Composite shaft (tube) with FW technology with better process parameter can be used in shafts for wind power and other industry.

Some of the benefits are:

- ❑ Best results in mechanical properties obtained from winding speed V2, tension of fiber N2 and angle α_2
- ❑ Change of tension and angles increase mechanical properties to 20% in final mechanical results
- ❑ **Low upfront investment** (due to reduced design complexities and simplified layouts)
- ❑ **Significantly reduced weight** (for faster, simplified handling)
- ❑ **Outstanding damping** (for low noise and low vibration operation)
- ❑ **High operational reliability** (on account of a fully integrated in situ manufacturing process and significantly improved fatigue strength)

The process parameters of this technology are a key choice in the design of new advance materials for the replacement of conventional materials.

3.2. LAMP technology

Tests describes the investigation of the optimal processing conditions that maximize the mechanical properties of the composites. However, uncertainties exist on the mechanical performance of the final product which are associated with the process induced defects. Tests have revealed the minimal defects (void) and good interfacial properties in laminate.

From the present numerical and experimental studies, the following conclusions are made

- Obtained function from the factorial design concludes that researched parameters and the interaction between them has to be taken into account in LAMP process.

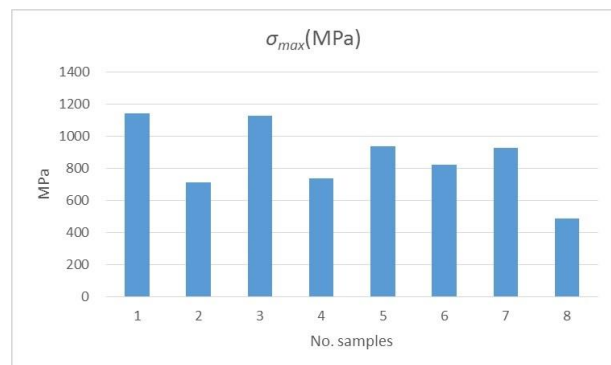


Fig.4: Flexural strength with no. of samples PEEK/Carbon UD Prepreg table 1

The experimental procedure described in the present work is suitable to study the consolidation behavior of thermoplastic matrix composite. The results shown, that good interaction between the layers is strongly dependent on the temperature of the laser, which should ideally be greater than the thermoplastic melt temperature. Rising of the temperature from 280oC to 350oC for PPS matrix and

from 360oC to 420oC for PEEK matrix is followed by sharp fall of voids percent due to the good melting of the PPS and PEEK. Also, higher pressure of the consolidation roller will decrease the percent of voids in the final composite, along with 9 m/min speed of the LATP machine.

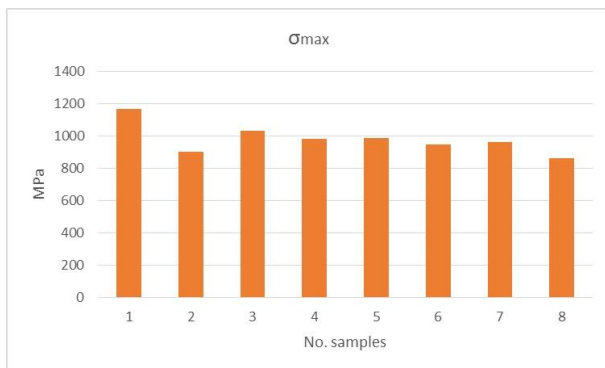


Fig.5: Flexural strength with no. of samples PPS/Carbon UD Prepreg table 2

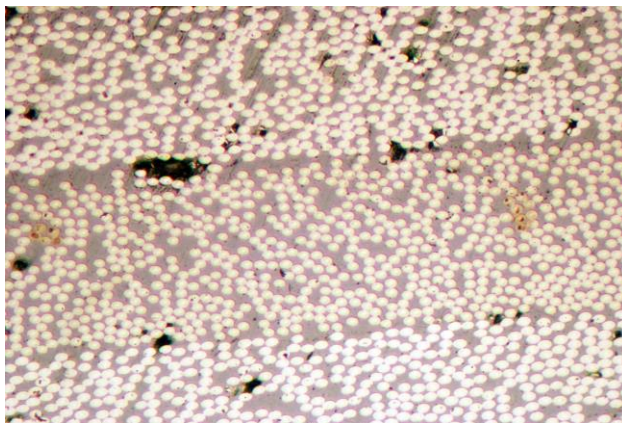


Fig. 6 1-3% void No.1 sample PPS/CF

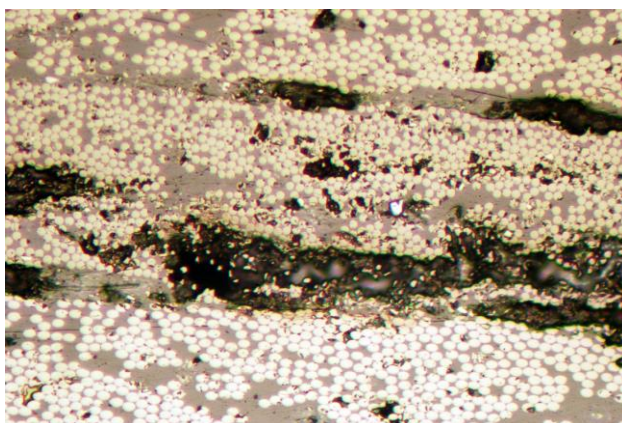


Fig. 7 void 14-30% No. 8 sample PEEK/CF

The large velocity allows different degree of crystallization in semi crystalline thermoplastics such as PPS and PEEK. From the selected parameters, the best results are shown with the number 1 for PPS and PEEK (see Figures 4 and 5).

These examples also have smaller falls compared with Example 8 for PEEK, where the sample has larger voids on the screens between the layers (Figures 6 and 7 for comparison).

High number of voids in the material causes a problem on the forces that influence the final product. Therefore, this study focused on these three parameters, and was done in two steps. Firstly, a two-factor central composite design of experiments was used to define the combination of processing parameters. The flexural strength was calculated according to ASTM D 790 standard (Fig 4 and Fig 5) and second the void content was calculated (Fig 6 and fig 7).

Some of the benefits are:

- ❑ Best results in flexural strength obtained from velocity V2, temperature T2 and P2
- ❑ Change of temperature causes variation from 1.9-9% to 60% in final mechanical results
- ❑ Pressure of the contact roller shows an influence in final mechanical results
- ❑ Researched parameters and interactions between them has to be taken into account in LATP process

4. CONCLUSION

From experimental work conducted in this research following conclusions can be made:

1. Larger tensions and angles decrease pores up to 1-2% in FW technology for thermosetting matrix, and increase mechanical properties to 20%.
2. Larger temperature, speed and pressure of contacted roller decrease pores up to 1-3% in LATP technology for thermoplastic matrix, and increase mechanical properties to 60%.

It is assumed that, lower mechanical properties of specimens by FW and LATL are caused from fiber breach or void content in the final composite, which were analyzed in this research. Statistical analysis of the data showed some very significant results, which should be very helpful in improving the composite parts.

Validity of this study lies in the expected results from the use of the different parameters in these technologies. Corresponding research made at this study, are in order to acquire full advantage of the quality of the composite products to avoid troubles when they are transformed into the final products from different parameters in these technologies. Mechanical, Aeronautical and Biomedical Engineering Department, University of Limerick, Limerick, Ireland

REFERENCES

- [1] POLINI,W and SORRENTINO,L. (2005) Influence of winding speed and winding trajectory on tension in robotized filament winding of full section parts. *Composites Science and Technology*, pp 1574-1581. DOI:10.1016, 2005.
- [2] MORGAN,P.H.(1969) Tensile and cyclic fatigue properties of graphite filament wound pressure vessels at ambient and cryogenic temperatures. NASA TN D-5354, 1969.
- [3] PLOCKI, M. HORN, S. and SAUZE, M. G., SCHARRINGHAUSEN, J. (2012) Failure Analysis of

- NOL-Ring Specimens by Acoustic Emission. *30th European Conference on Acoustic Emission Testing & 7th International Conference on Acoustic Emission University of Granada*, 2012.
- [4] AKKUS,N. GENÇ,G and GIRGIN,C. (2008) Control of the presentation in Filament winding process. *Acta mechanica et automatica*, vol.2 (3), 2008.
- [5] HARRY,N.E. (2012) *Clean Filament Winding-process optimization*. Doctor dissertation School of Metallurgy and Materials Sensors and Composites Group The University of Birmingham, 2012.
- [6] ERDILLER,M.S.(2004) Experimental investigation for mechanical properties of Filament Wound composite tubes. Master of science, 2004.
- [7] KOUSSIOS, S. (2004) *Filament Winding: a Unified Approach*. DUP Science is an imprint of Delft University Press, 2004.
- [8] SOBRINHOA,L.L. CALADOB,V.M and BASTIAN, F.L. (2011) Development and Characterization of Composite Materials for Production of Composite Risers by Filament Winding. *Materials Research*, 14(3): pp. 287-298, 2011.
- [9] DAVIJANI, A.A.B (2012) Experiments and prediction of the spreading behavior of fibrous tow by means of Discrete Element Method, Master Thesis, 2012.
- [10] GHIORSE, S.R.(1991) *A comparison of void measurement methods for carbon/epoxy composites*. U.S. Army materials Tehnology Laboratory Watertown, 1991.
- [11] SUNGJIN,L., CHANGDUK,K., HUYNBUM, P. (2013), A Study on Optimal Design of Filament Winding Composite Tower for 2 MW Class Horizontal Axis Wind Turbine Systems, *International Journal of Composite Materials* 2013, Vol 3, pp15-23
- [12] DANIL, P. (2010), Optimization of wind blade design including its energetic characteristics, master's thesis, Lappeenranta University of Technology Faculty of Technology, Degree Programme in Bioenergy, 2010 pp 82.
- [13] FRANCISCO J. B. (2006), Production of Large Wind Turbines in Latin America for Local Conditions, Eindhoven University of Technology, Faculty of Mechanical Engineering , 2006, pp.150.
- [14] WOUTER GROUVE. (2012), Weld strength of laser-assisted tape-placed thermoplastic composites, PhD Thesis, University of Twente, Enschede, the Netherlands, August 2012.
- [15] DENNIS MAURER and PETER MITSCHANG, Laser-powered tape placement process – simulation and optimization, (2016), *Advanced Manufacturing: Polymer & Composites Science*, 1:3, 129-137 pp.
- [16] ANTHONY COMER*, PETER HAMMOND, DIPA RAY, JOHN LYONS, WINIFRED OBANDE, DAVID JONES, RONAN O' HIGGINS, MICHAEL MCCARTHY, (2014), Wedge peel interlaminar toughness of carbon- fibre/peek thermoplastic laminates manufactured by laser-assisted automated-tape-placement (latp)
- [17] ANAHI PEREIRA DA COST, EDSON COCCHIERI BOTELHO, MICHELLE LEALI COSTA, NILSON EIJI NARITA, JOSÉ RICARDO TARPANI, (2012), A Review of Welding Technologies for Thermoplastic Composites in Aerospace Applications, *J. Aerosp. Technol. Manag.*, São José dos Campos, Vol.4, No 3, pp. 255-265, Jul.-Sep., 2012

CORRESPONDANCE

Svetlana Risteska, Prof. D.Sc. Eng.
IACR
Krusevski pat bb
7500 Prilep, Macedonia
svetlanar@iacr.edu.mk

Blagoja Samakoski, Prof. D.Sc. Eng.
IACR
Krusevski pat bb
7500 Prilep, Macedonia
blagojas@iacr.edu.mk

Vladimir Dukovski.Prof. D.Sc. Eng.
Faculty of Mechanical Engineering
1000 Skopje, Macedonia
vladimir.dukovski@mf.edu.mk

APPLICATION OF TAGUCHI METHODS WITH OPTIMIZATION OF FIBRE ORIENTATION ANGLE OF LAMINATED AL/ARAMID/EPOXY COMPOSITE CARDAN SHAFT

Jasmina BLAGOJEVIĆ
Zorica ĐORĐEVIĆ
Sandra VELIČKOVIĆ

Abstract: Optimization of fibre orientation angle of the laminated Al /aramid /epoxy composite cardan shaft using Taguchi methods was carried out in this paper. The aim of the study is to obtain values of fibre orientation angle at which the lowest value of angle of twist of shaft is obtained. The analysis of the fibre orientation angle of the laminated composite shaft has been carried out using ANOVA analysis. The laminated composite shaft consists of a layer of aluminum and eight layers of aramid /epoxy composite whose fibre orientation angle taken into consideration is -45° , 0° , 45° and 90° . To model the cardan shaft, programmes like FEMAP and NeNASTRAN were used, and they helped obtain angles of twist of Al /aramid /epoxy composite cardan shaft at appropriate factor levels. Predicted value of the angle of twist deviated from the experimental one by 1.805%, whereas the value obtained by confirmation test deviated by 1.491% from the experimental value of the angle of twist.

Key words: Al /aramid /epoxy composite, cardan shaft, Taguchi method, fibre orientation angle, angle of twist.

1. INTRODUCTION

The basis of the study of this paper is to determine the fibre orientation angle of the laminated Al /aramid /epoxy composite cardan shaft, more precisely, to find the optimal variation of the angles of the layers where the lowest value of the angle of twist of the shaft is obtained.

A review of the literature has shown that the two-piece steel cardan shafts are replaced by one-piece composite shafts due to the reduction of weight. A very large number of papers are referring to determining the fibre orientation angle of composite cardan shaft.

Rangaswamy and Vijayarangan performed the optimization of drive cardan shafts in the paper [1]. They used composite materials: E-glass/epoxy and HM carbon/epoxy. The weight savings for the composite E-glass/epoxy drive shaft is 48.36% compared to the steel shaft, while the weight savings of HM carbon/epoxy composites are 86.90% of the steel shaft.

In this paper [2], Dinesh and Anand Raju replaced the conventional two-piece steel drive shaft with one-piece E-glass/epoxy, HS carbon/epoxy and HM carbon/epoxy composite drive shafts. The shafts are subjected to restrictions, such as transmission torque, torsional buckling capacity and natural bending frequency. The weight savings of E-glass/epoxy, HS carbon/epoxy and HM carbon/epoxy composites are 48.36%, 86.90% and 86.90% of the weight of the steel shaft respectively.

Manjunath and Rangaswamy [3] performed the optimization of the layer stacking sequence of the composite multi-layers drive shaft by using PSO (*particle swarm optimization*) algorithm. They proposed the optimization process for the design of a multilayer single-piece drive composite shaft for a given torque, velocity and length in order to achieve minimum weight. The materials used for the one-piece drive shaft are: E-glass/epoxy, NM carbon/epoxy and boron/epoxy composites. They developed the PSO program in MATLAB V 7 to optimize the layer stacking sequence.

Srinivasa Moorthy *et al.* [4] designed and analysed carbon/epoxy and kevlar/epoxy composite shafts under conditions of torsional strength, natural bending frequency and torsional buckling, and they compared them with a conventional steel drive shaft under the same conditions. The emphasis was on aspects such as weight saving, number of layers and distribution of the layers. There is a reduction of weight in both types of composites compared to high-quality steel SM45C, but the carbon / epoxy for manufacturing an automotive drive shaft has multiple advantages. Its work is based exclusively on the analytical calculation. This approach focuses on the distribution of layers with standard orientations of 0° , 90° , $45^\circ +$ and -45° for the considered composites.

Kumar Rompicharla and Rambabu used kevlar / epoxy composite material of the cardan shaft [5]. They tried to determine the deflection, voltages, and natural bending frequency by using the Finite Element Methods (FEM). They concluded that the kevlar/epoxy composite had

good properties and that it could be used as a replacement for steel.

In this paper, Taguchi methods were used to determine the optimal variant of the factors. The fiber orientation angles of the layers of laminar composite shaft are factors, and the angle of twist of shaft is a response. The laminar composite shaft consists of a layer of aluminum and eight layers of aramid / epoxy composites. The shaft model and the values of angle of twist for the combined factor levels were obtained in the *FEMAP* and *NeNASTRAN* programs. The *Minitab 16* program was used for statistical processing of the results, and the confirmation of the experiment for determining the interval of the angle of twist of the composite shaft was used for the obtained optimal variant.

2. COMPOSITE CARDAN SHAFTS

The basic role of the cardan gears is transmission of the torque between shafts which are spatially at constantly variable angle, allowing their relative motion [6].

In modern aircrafts, airplanes, cars and boats, primarily in order to save the fuel and increase starting, intensive work is done to reduce the weight of the vehicle, by using aluminum or plastic materials in the construction of vehicles and engines or by using other lightweight materials of increased strength (light alloys, composite materials, etc.) [7, 8, 9]. The laminar composites have advantages due to their high specific stiffness. The composite drive shafts have a longer lifespan of the drive mechanism with a higher critical velocity [5, 10]. The fiber orientation angle in the laminar composite is shown in Figure 1 [1].

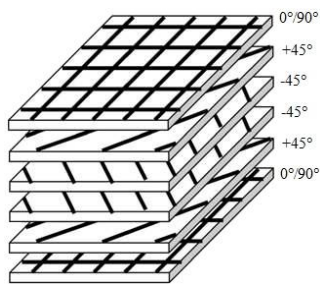


Fig.1: Fiber orientation angles

A laminar Al/aramid/epoxy composite shaft was used for testing in this paper. The basic characteristics of the aramid/epoxy composites are shown in Table 1, while the basic characteristics of the aluminum tubes are shown in Table 2 [11].

Table 1: Basic characteristics of aramid/epoxy composites

Longitudinal modulus	E_1	81.8 GPa
Transverse modulus	E_2	5.10 GPa
Shear modulus	G_{23}	1.82 GPa
Shear modulus	G_{12}	1.51 GPa
Poisson's ratio	ν	0.31
Density	ρ	1380 kg/m ³
Composite layer thickness	t_{sl}	0.12 mm

Table 2: Basic characteristics of aluminum tube

Tensile modulus	E	72000 MPa
Shear modulus	G	27000 MPa
Density	ρ	2659 kg/m ³
Tensile strength	R_m	350 MPa
Yielding strength	R_e	325 MPa
Shear strength		210MPa
Thickness of the aluminium tube		2.5 mm

3. TAGUCHI METHODS

Taguchi developed a method for designing experiments to examine how different parameters affect the mean value and variation of process performance characteristics that determine how well the process works. The experimental design that he proposed involves the use of orthogonal arrays for organization of parameters that affect the process and levels which are to be changed [12].

According to Taguchi, the selection of parameters is accomplished by methods of experiment planning, whereby Taguchi proposes using, along with ordinary indicators, a new quality indicator, the so-called signal/noise ratio (S/N).

The Taguchi method uses the loss function to calculate the deviation between the experimental value and the desired values. This loss function is converted into a S/N ratio. There are three types of S/N ratio: smaller the better, larger the better, and nominal the best, which serve to measure quality characteristics [13, 14, 15]. The S/N ratio the smaller the better was used in this paper:

$$S/N = -10 \log \left(\frac{1}{n} \sum_i^n y_i^2 \right), \quad (1)$$

where n is the repetition number of each trial and y_i is the result of the i-th experiment for each trial.

4. EXPERIMENTAL PART

The influence of the fibre orientation angle of aramid / epoxy composites on the angle of twist of the laminar combined Al/aramid/epoxy composite cardan shaft was tested in this paper. The aim of the paper is to obtain the values of the fibre orientation angle with the least torsion of the shaft.

The basic dimensions of the one-piece cardan shaft are: length of the shaft - 1.35 m, the mean radius of the shaft - 0.041 m, the thickness of the wall of the annular cross-section shaft - 0.003 m [11].

252 quadrangular finite elements of the shells were used for modelling the shaft. The maximum value of the maximum torque, at which the cardan shaft was tested, was 5000 Nm.

Table 3 shows the factors and levels of factors that are analysed. In this case, the factors are the fibre orientation angles of the composite laminar shaft. The first layer of the shaft is made of aluminum and the other layers are made of aramid/epoxy composites and the slopes of their fibres are on four levels (-45°, 0°, 45° and 90°).

Table 3: Factors and their levels

Factors (The fibre orientation angle)	Unit	Level			
		I	II	III	IV
(A) Layer 1	°	0	0	0	0
(B) Layer 2	°	-45	0	45	90
(C) Layer 3	°	-45	0	45	90
(D) Layer 4	°	-45	0	45	90
(E) Layer 5	°	-45	0	45	90
(F) Layer 6	°	-45	0	45	90
(G) Layer 7	°	-45	0	45	90
(H) Layer 8	°	-45	0	45	90
(J) Layer 9	°	-45	0	45	90

The first step in the application of Taguchi methods is to select the appropriate orthogonal array. Since a number of factors and levels are known, the appropriate orthogonal

Table 4: Orthogonal array L32 with experimental values of angle of twist and S/N values for Al/aramid/epoxy composite shaft

	A	B	C	D	E	F	G	H	J	Angle of twist [rad]	S/N ratio [dB]
1	0	-45	-45	-45	-45	-45	-45	-45	-45	0.187	14.5632
2	0	-45	0	0	0	0	0	0	0	0.219	13.1911
3	0	-45	45	45	45	45	45	45	45	0.185	14.6566
4	0	-45	90	90	90	90	90	90	90	0.219	13.1911
5	0	0	-45	-45	0	0	45	45	90	0.201	13.9361
6	0	0	0	0	-45	-45	90	90	45	0.207	13.6806
7	0	0	45	45	90	90	-45	-45	0	0.202	13.8930
8	0	0	90	90	45	45	0	0	-45	0.207	13.6806
9	0	45	-45	0	45	90	-45	0	45	0.197	14.1107
10	0	45	0	-45	90	45	0	-45	90	0.202	13.8930
11	0	45	45	90	-45	0	45	90	-45	0.197	14.1107
12	0	45	90	45	0	-45	90	45	0	0.202	13.8930
13	0	90	-45	0	90	45	45	90	0	0.207	13.6806
14	0	90	0	-45	45	90	90	45	-45	0.201	13.9361
15	0	90	45	90	0	-45	-45	0	90	0.207	13.6806
16	0	90	90	45	-45	0	0	-45	45	0.201	13.9361
17	0	-45	-45	90	-45	90	0	45	0	0.202	13.8930
18	0	-45	0	45	0	45	-45	90	-45	0.196	14.1549
19	0	-45	45	0	45	0	90	-45	90	0.202	13.8930
20	0	-45	90	-45	90	-45	45	0	45	0.197	14.1107
21	0	0	-45	90	0	45	90	-45	45	0.201	13.9361
22	0	0	0	45	-45	90	45	0	90	0.207	13.6806
23	0	0	45	0	90	-45	0	45	-45	0.201	13.9361
24	0	0	90	-45	45	0	-45	90	0	0.207	13.6806
25	0	45	-45	45	45	-45	0	90	90	0.197	14.1107
26	0	45	0	90	90	0	-45	45	45	0.202	13.8930
27	0	45	45	-45	-45	45	90	0	0	0.197	14.1107
28	0	45	90	0	0	90	45	-45	-45	0.201	13.9361
29	0	90	-45	45	90	0	90	0	-45	0.207	13.6806
30	0	90	0	90	45	-45	45	-45	0	0.201	13.9361
31	0	90	45	-45	0	90	0	90	45	0.207	13.6806
32	0	90	90	0	-45	45	-45	45	90	0.201	13.9361

Based on the results of the S/N ratio, it can be determined which of the control factors has the greatest influence on the angle of twist of the one-piece composite shaft (Table

array L32 has been selected for determining the optimal values of the fiber orientation angles of the layers of composite cardan shaft [16]. Since the factor A has only one level, it can be ignored in further analysis. The model of cardan shaft was made in the FEMAP and NeNASTRAN programs and the angles of twist of the Al/aramid/epoxy composite shaft are obtained by using those programs at the corresponding factor levels and they are shown in Table 4.

4.1. Statistical processing of the results

Table 4 shows the obtained S/N ratio values. S/N ratios were obtained by the use of Minitab 16 using the equation (1). This equation is used when it tends to the minimum target value, and in this case it is the angle of twist of the laminar composite shaft.

5). The optimal parameters of the angle of twist of these controlled factors can be determined based on the S/N ratios shown in Table 5 and Figure 2.

Parameter optimization of the angle of twist within the given factors and levels, considering the criterion “the smaller the better”, gives the combination of control factors: *A1, B3, C3, D3, E3, F3, G3, H3* and *J3*. In other

words, the combination of angles of aramid fiber slope is obtained in all layers of 45 ° for the lowest value of the angle of twist of Al/aramid/epoxy composite shaft.

Table 5: Response table for S/N ratio (for “the smaller the better” case)

Level	B	C	D	E	F	G	H	J
1	13.96	13.99	13.99	13.99	13.99	13.99	14.00	14.00
2	13.80	13.80	13.80	13.80	13.79	13.79	13.78	13.78
3	14.01	14.00	14.00	14.00	14.01	14.01	14.01	14.00
4	13.81	13.80	13.79	13.78	13.79	13.79	13.79	13.79
Delta	0.20	0.20	0.21	0.22	0.22	0.22	0.23	0.22
Rank	7	8	6	4	2	4	1	4

Experimental results are processed by applying the analysis of variance (ANOVA), which is used to identify the significance of the factors affecting the fibre orientation angles of the layers of composite shaft [17, 18]. The results of the ANOVA analysis are shown in Table 6.

Based on the ANOVA analysis of the S/N ratio, it can be concluded that all factors almost equally influence the angle of twist of the composite cardan shaft. Factor *H* has the greatest influence (14.46%), and factor *B* has the smallest influence (9.60%), while the influence of the error is almost negligible, amounting to 1.27%.

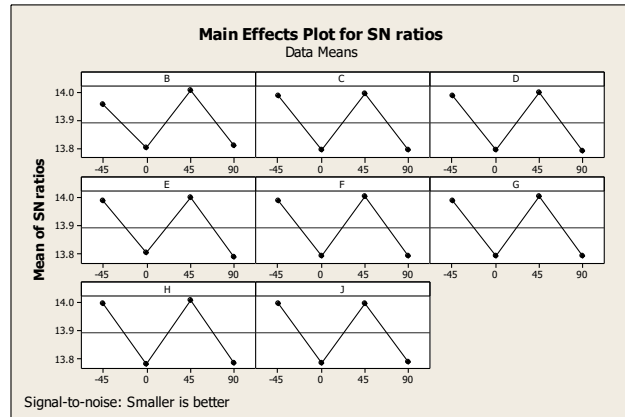


Fig.2: Diagram of the main effects of S/N ratio for angles of twist

Table 6: Results of ANOVA analysis of the S/N ratio

Source	DF	Seq SS	Adj SS	Adj MS	F	P	Pr
B	3	0.25900	0.25900	0.086333	17.63	0.001	9.60
C	3	0.30876	0.30876	0.102920	21.01	0.001	11.44
D	3	0.32688	0.32688	0.108961	22.25	0.001	12.11
E	3	0.32737	0.32737	0.109125	22.28	0.001	12.13
F	3	0.34503	0.34503	0.115011	23.48	0.000	12.79
G	3	0.34500	0.34500	0.114999	23.48	0.000	12.78
H	3	0.39028	0.39028	0.130094	26.56	0.000	14.46
J	3	0.36207	0.36207	0.120691	24.64	0.000	13.42
Residual Error	7	0.03429	0.03429	0.004898			1.27
Total	31	2.69869					100

4.2. Confirmation of the experiment

Besides Taguchi optimization technique, the experiment confirmation is used to confirm the statistically obtained optimal factor variant. The predicted optimal value of the angle of twist is obtained by considering the individual effects of the factors and their levels (*A1, B3, C3, D3, E3, F3, G3, H3* and *J3*). Estimated optimal value of the angle of twist may be obtained from the equation [17, 19]:

$$\varphi_p = T_\varphi + (A1 - T_\varphi) + (B3 - T_\varphi) + (C3 - T_\varphi) + (D3 - T_\varphi) + (E3 - T_\varphi) + (F3 - T_\varphi) + (G3 - T_\varphi) + (H3 - T_\varphi) + (J3 - T_\varphi) \quad (2)$$

where T_φ is the mean value of the angle of twist, and *A1, B3, C3, D3, E3, F3, G3, H3* and *J3* are the S/N responses

of the main factors at certain levels. The calculated optimal value of the angle of twist is 14.78333 dB. The confidence interval for the predicted optimal value is calculated by using the terms:

$$CI = \sqrt{F_{\alpha;1,V_2} \cdot V_e \cdot \left(\frac{1}{n_{eff}} + \frac{1}{r} \right)}, \quad (3)$$

where $F_{\alpha;1,V_2}$ is the table value F за ниво пове for confidence level α , V_2 is degree of freedom of pooled error, V_e is pooled error variance, r is the number of repetitions, and n_{eff} is the number of effective measured results defined as:

$$n_{eff} = \frac{\text{total experimental trials}}{1 + (\text{total degree of freedom of factors for prediction})}. \quad (4)$$

One confirmation experiment was performed for the evaluation of the performances of experimental tests for the angle of twist under optimal conditions, and because of that $r=1$. For the level of reliability 95%, $\alpha=0.05$ and $V_2=7$, value of $F_{\alpha,1,V_2}=5.59$. A confidence interval (± 0.221) was calculated based on the equations (3) and (4).

The experiment for the levels of factors $A1, B3, C3, D3, E3, F3, G3, H3$ and $J3$ was performed and the result is compared with the values obtained by the previous

equations and with the predicted values obtained in *Minitab 16* (Table 7).

The predicted value of the angle of twist of the shaft deviates from the experimental one by 1.805 %, while the value obtained by the confirmation of the experiment deviates by 1.491 % from the experimental value of the angle of twist.

Table 7: Results of the angle of twist and S/N ratio

	Predicted value	Experiment confirmation value	Experimental value
The angle of twist of the Al/aramid/epoxy composite cardan shaft [rad]	0.181719	0.1823	0.18506
S/N ratio [dB]	14.7695	14.78333	14.65347

The optimal values of the fibre orientation angles are also obtained in the *FEMAP* and *NeNASTRAN* programs. The fibre orientation angle of the aramid / epoxy composite is $Al/[\pm 454]$. For these optimal fibre orientation angles, the value of the angle of twist of the Al/aramid/epoxy composite cardan shaft is 0.182 rad [12].

The deviation of the optimum value of the angle of twist of the composite shaft obtained by Taguchi method is 1,685 % of the optimal value obtained in the *FEMAP* and *NeNASTRAN* programs. The fibre orientation of the aramid / epoxy composite is $Al/[\pm 454]$.

5. CONCLUSION

Based on the research in this paper, it can be concluded:

- ANOVA analysis of the S/N ratio shows that all factors have almost the same impact on the torsion of shaft and the error is 1.27 %.
- The lowest value of the angle of twist of the Al/aramid/epoxy composite cardan shaft by using the Taguchi method is obtained when the fibre orientation angles of aramid are in all layers of the aramide/epoxy composite + 45°.
- For optimal values of the fibre orientation in the *FEMAP* and *NeNASTRAN* programs, the obtained angle of twist of the shaft is 0.18506 rad (experimental value), and the obtained angle of twist in the *Minitab 16* program is 0.181719 rad (predicted value), while the angle of twist is obtained by confirming the experiment by 0.1823 rad.
- The predicted value of the experimental one deviates by 1.805 %, and the value of the angle of twist obtained by the experiment confirmation deviates by 1.491 % from the experimental one.
- The angle of twist obtained for the optimal variation of the fibre orientation angles in *FEMAP* and *NeNASTRAN* programs deviates from the angle of twist obtained by using the Taguchi method (experimental value) by 1.685 %.

- Taguchi methods can be used to analyse and optimize the fibre orientation angle of the laminar composite shaft layers that affect the angle of twist of the shaft.

REFERENCES

- [1] Rangaswamy, T., Vijayarangan, S. (2005) *Optimal Sizing and Stacking Sequence of Composite Drive Shafts*, MATERIALS SCIENCE, Vol.11, No 2, pp. 133-139
- [2] DINESH, D., RAJU, F. A. (2012) *Optimum Design And Analysis Of A Composite Drive Shaft For An Automobile By Using Genetic Algorithm And Ansys*, International Journal Of Engineering Research And Applications, Vol.2, Issue 4, pp.1874-1880
- [3] Manjunath, K., Rangaswamy, T. (2014) *Ply stacking sequence optimization of composite driveshaft using particle swarm optimization algorithm*, Published by EDP Sciences, DOI: 10.1051/smdo/2013001, pp. 1-6
- [4] Moorthy, R. S., Mitiku, Y., Sridhar, K. (2013) *Design of Automobile Driveshaft using Carbon/Epoxy and Kevlar/Epoxy Composites*, American Journal of Engineering Research (AJER), Vol.2, Issue 10, pp. 173-179
- [5] Rompicharla1, R. P. K., Rambabu, Dr. K. (2012) *Design and Optimization of Drive Shaft with Composite Materials*, International Journal of Modern Engineering Research, Vol.2, Issue 5, pp. 3422-3428
- [6] Nikolić, V. (2004) *Machine elements*, University of Kragujevac, Faculty of Engineering Kragujevac.
- [7] Mahajan, G. V., Aher, V. S. (2012) *Composite Material: A Review over Current Development and Automotive Application*, International Journal of Scientific and Research Publications, Vol.2, Issue 11, pp. 1-5
- [8] Satheesh Kumar Reddya, P., Nagarajub, Ch. (2017) *Weight optimization and Finite Element Analysis of Composite automotive drive shaft for Maximum Stiffness*, Materials Today: Proceedings, Vol.4, No 2, pp. 2390–2396

- [9] Djordjević, Z., Blagojević, M., Marjanović, V., Jovanovic, S. (2014) *The influence of material types on twist angles and torsion stability of a composite shaft*, Tech Gazette, Vol.21, No 5, pp. 917-923
- [10] Hargude, N.V., Ghatage k.D. (2012) *AN OVERVIEW OF GENETIC ALGORITHM BASED OPTIMUM DESIGN OF AN AUTOMOTIVE COMPOSITE (E-glass / epoxy and HM-carbon / epoxy) DRIVE SHAFT*, International Journal of Mechanical Engineering and Technology, Vol.3, Issue 1, pp. 110-119
- [11] Djordjević, Z. (2008) *Dynamic conduct composite shafts*, PhD Thesis, University of Kragujevac, Faculty of Engineering, Kragujevac.
- [12] Miković J., (2013) *Testing of mechanical properties of plastic mass using the Taguchi method*, Master's thesis, University of Kragujevac, Faculty of Engineering, Kragujevac.
- [13] Stojanović, B., Babić, M., Veličković, S., Blagojević, J. (2016) *Tribological behavior of aluminum hybrid composites studied by application of factorial techniques*, Tribology Transactions, Vol.59, No 3, pp. 522-529, Doi 10.1080/10402004.2015.1091535.
- [14] Kivak, T. (2014) *Optimization of surface roughness and flank wear using the Taguchi method in milling of Hadfield steel with PVD and CVD coated inserts*, Measurement, Vol.50, pp. 19-28
- [15] Dharmalingam, S., Subramanian, R., Somasundara Vinoth, K., Anandavel, B. (2011) *Optimization of tribological properties in aluminum hybrid metal matrix composites using Gray-Taguchi method*, Journal of Materials Engineering and Performance, Vol.20, No 8, pp. 1457-1466
- [16] Çiçek, A., Kivak, T., Samtaş, G. (2012) *Application of Taguchi method for surface roughness and roundness error in drilling of AISI 316 stainless steel*, Strojniški vestnik -Journal of Mechanical Engineering, Vol.58, No 3, pp. 165-174
- [17] Marwaha, R., Dev Gupta, R., Jain ,V., Kant Sharma, K. (2013) *Experimental investigation & analysis of wear parameters on Al/SiC/Gr - metal matrix hybrid composite by Taguchi method*, Global Journal of Researches in Engineering, Vol.13, No 9, pp. 15-22
- [18] Miladinović, S., Veličković S., Novaković, M. (2016) *APPLICATION OF TAGUCHI METHOD FOR THE SELECTION OF OPTIMAL PARAMETERS OF PLANETARY DRIVING GEAR*, Applied Engineering Letters, Vol.1, No 4, pp. 98-104
- [19] Soy, U., Ficici, F., Demir, A. (2011) *Evaluation of the Taguchi method for wear behavior of Al/SiC/B4C composites*, Journal of Composite Materials, Vol.46, No 7, pp. 851-859

CORRESPONDANCE



Jasmina BLAGOJEVIĆ, PhD student
University of Kragujevac
Faculty of Engineering
Sestre Janjić br. 6
34000 Kragujevac, Serbia
jacab@kg.ac.rs



Zorica DJORDJEVIĆ, Ph.D. Assoc. Prof.
University of Kragujevac
Faculty of Engineering
Sestre Janjić br. 6
34000 Kragujevac, Serbia
zoricadj@kg.ac.rs



Sandra VELIČKOVIĆ, PhD student
University of Kragujevac
Faculty of Engineering
Sestre Janjić br. 6
34000 Kragujevac, Serbia
sandrav@kg.ac.rs

RAPID PROTOTYPING AND MANUFACTURING FOR MODEL OF HUMAN HEAD

Saša ŽIVANOVIĆ

Abstract: Modeling of the human body has advanced in recent years with the rapid development of computer technology and the needs of the real digital and physical models. This paper describes an example of a rapid development of a model of a human head, on the basis of STL-format, which includes a digital information chain CAD / CAM / CNC, to a level which allows the successful realization of the physical models using new technology, by adding and subtracting material. In this paper is presented a photogrammetric method of obtaining STL model, where new technologies are applied for rapid prototyping. For several examples of 3D printing are shown and software for verification of programs and simulation of 3D printing.

Key words: rapid prototyping and manufacturing, STL, human head, 3D printing, verification, simulation

1. INTRODUCTION

Rapid prototyping has emerged as a key enabling technology, with its ability to shorten product design and development time. Rapid prototyping is a technology for quickly fabricating physical models, functional prototypes and small series of parts directly from CAD models. This technology has also been referred to as layer manufacturing, solid free-form fabrication, material addition manufacturing and 3D printing [1,2].

Rapid prototyping – an enabling technology for time compression engineering. If different design and manufacturing activities are carried out concurrently it is possible to compress the overall product development time, which will be shorter than in the serial activities, Fig.1. This can also allow engineers to be creative by providing more time for design, based on the time savings.

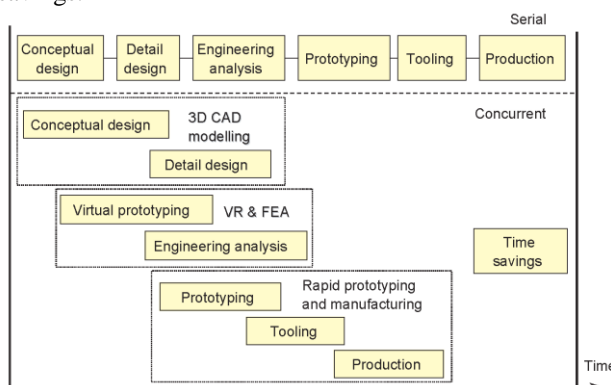


Fig.1: Time compression engineering [1,2]

With the development of computers and software for the CAD product design and 3D modeling of the human body is rapidly progressed, including technology to produce realistic models adequate for the needs of simulations and animations, or physical models.

3D models of the human head can be obtained in several ways: (i) using specialized software for modeling; (ii) obtaining a 3D scanning point cloud data for the model, using the reverse engineering method for getting a CAD model; (iii) using photogrammetric method, which is based on 2D images on the basis of which the obtained 3D CAD model.

Application of new technologies rapid prototyping based on models in STL format. In the first case this may be the additive technology that is using adding material in the layers. Another approach involves rapid prototyping technology based on subtraction of materials layer by layer, that is also based on a model in STL format.

2. RAPID PROTOTYPING AND MANUFACTURING

Rapid prototyping of different products, which includes machine parts is no longer a novelty, but is a real resource that provides processes and tools for rapid prototyping by adding and/or subtracting material. Rapid Prototyping in the present time is related to the beginnings of 3D Systems Company from the United States [3].

One of the definitions of rapid prototyping says that is the method of making 3D parts of a given shape using their models, usually made in CAD system environment, using a fast, repeatable and flexible processing operations [4]. Rapid prototyping is a process of joining materials to make physical objects from 3D CAD model, usually layer upon layer, as opposed to subtractive manufacturing or molding/casting technologies [5].

Although for rapid prototyping usually associated adding materials technologies, this can include the subtracting materials technologies, and the combination of adding and subtracting materials. One possible classification of these technologies is shown in Fig.2.

Now there are already many manufacturers of equipment for rapid prototyping, so there is a lot of different

technologies. Classification of RP technologies can be made upon different criteria. The most frequently applied is classification based on model material. Using this criteria all RP methods can be divided into three groups: 0D, 1D and 2D (Fig.2). These dimensions of material are: 0D for liquid/gas, 1D for powder form, and 2D for sheet form. More detailed information on every specific RP method can be found in the references [1], [2], [6].

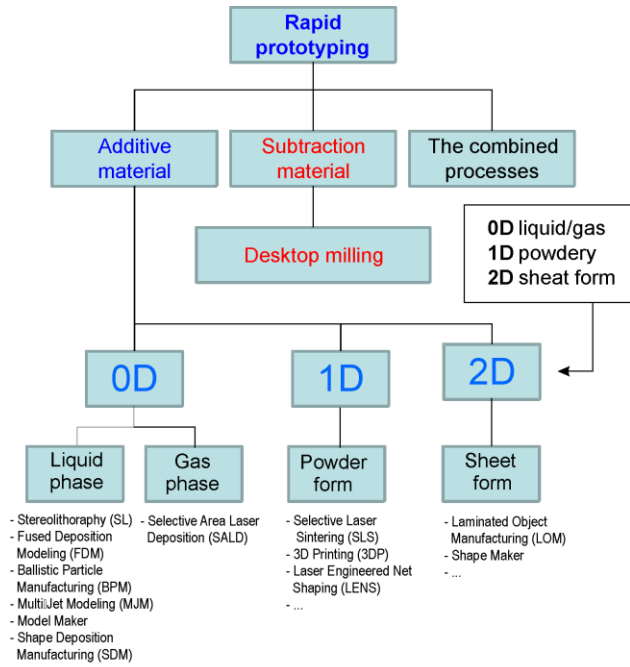


Fig.2: Basic classification of rapid prototyping

Methods of cutting, also one of the frequent method of rapid prototyping or rapid manufacturing. Some equipment manufacturers offer also systems for programming milling machines used for the first verification of the project mechanical parts for which there is already a model in STL format.

These milling machines, also known as a desktop milling machine, are usually cheaper than other machines for rapid prototyping so their low price is recommended as an alternative [4].

There is a third possibility, which is combining the technology of adding and subtracting material. In this case, additive technology preparing layers of the preform, and after that followed technology of cutting using finishing milling.

Prototypes in general can be divided into three main groups: (i) Form, (ii) Fit and (iii) Function, Fig.3. The phrase Form-Fit-Function, also referred to as 3F, is used in rapid prototyping to describe the identifying characteristics of a prototypes.

Group Form, are mainly reliefs. This group of prototypes serves to reach a conclusion on the usability and/or benefits in the form of prototype. This group is characterized: design verification, marketing and communication tool, high dimensional accuracy is not required, non-technical people see how product looks and feels.

Group Form, are mainly geometry of prototype. This group of prototypes used for various checks conclusion, however in this case, dimensional accuracy of this prototype is important in order after checking was

possible to continue further development. This group is characterized: fit verification of ability of a part to physically interface with, connect to, or become an integral part of another part, verification of manufacturability and assembly, required shape along with good dimensional tolerances, material choice is not important.

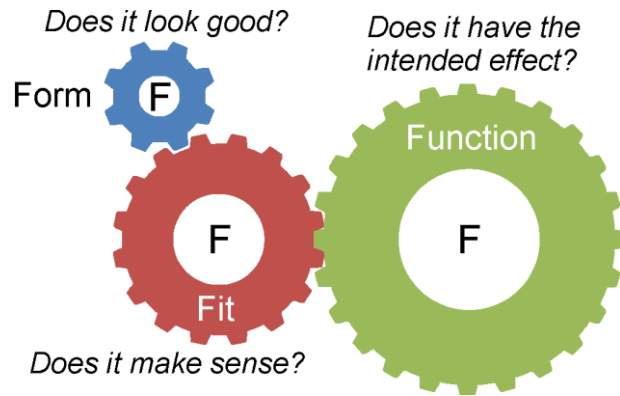


Fig.3: Prototype classifications (3F=FFF)

Group Function, are a prototypes that can be both relief and geometry. This group of prototypes used to test functionality of real part. Material should be similar to actual part. Function prototype should have same failure modes and levels as actual part. That is, should have similar characteristics to the real part.

Rapid prototyping is a typical additive technology, where models are formed layer by layer. Typical process stages for additive manufacturing is shown in Fig. 4 and includes the following stages: (i) CAD modeling of part, (ii) STL file is exported from CAD model and STL file is checked for defects, (iii) STL files are used as an input to slicing software, (iv) Machine setup, (v) simulation of 3D printing, (vi) building prototype, (vii) additional interventions on prototype (3D printed model) such as curing, surface polishing, finishing, etc.

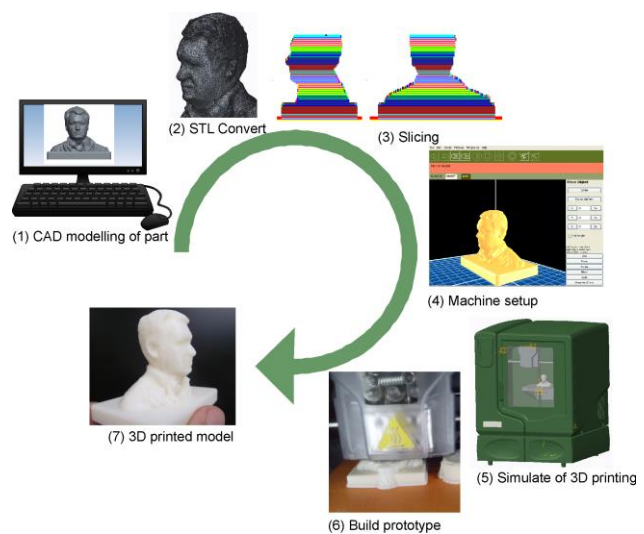


Fig.4: Stages for additive manufacturing process from CAD model to 3D part

In the next section, this procedure is applied in the case of the realization of a human head physical model.

3. RAPID PROTOTYPING AND MANUFACTURING PHYSICAL MODELS OF HUMAN HEAD

This section presents examples of rapid prototyping of several models of the human head. The first example is the realization of a model of human head on the basis of the finished CAD model. Based on this model prepared STL file using export option of CAD system. For this example are applied both technologies by adding and subtracting material.

For example, realization of model of human head with additive technology has been used the software Autodesk 123D Make [7]. This software is licensed as Freeware for Windows operating system without restrictions. Software allows creation of low-tech LOM (Laminated Object Manufacturing) -style solid models. Autodesk 123D Make loaded STL model based on which work slicing and preparation of layers for additive construction. The software can be prepared by different layouts for the construction of the physical model based on STL file. As the output of layout layers are available in formats *.DXF, *.EPS and *.PDF. There is also the possibility of simulation the adding layer by layer. The illustration of this kind of additive manufacturing was shown in one example of making of the head model from cardboard of a layer thickness of 2 mm, Fig. 5a.

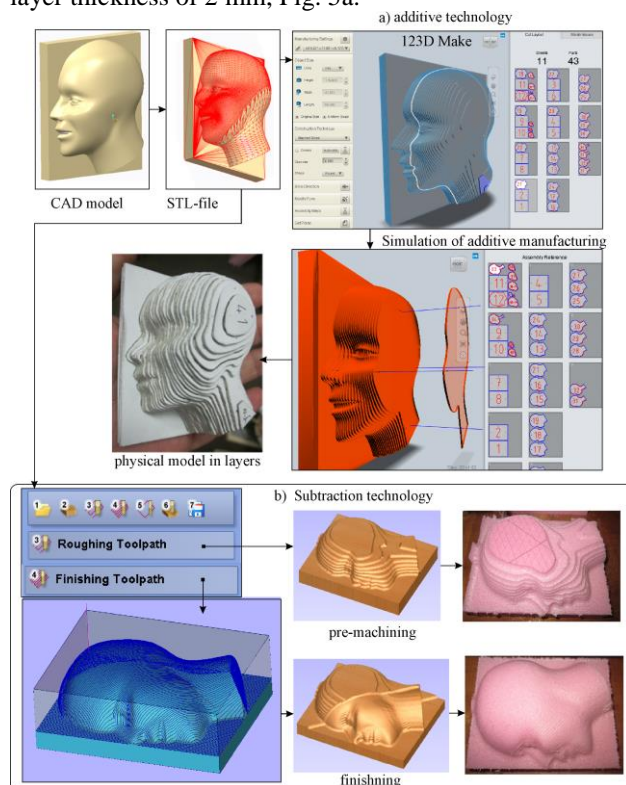


Fig.5: An example of building model of a human head using additive and subtraction technologies

For the same model were applied technology for rapid manufacturing with subtracting material. For this purpose is used specialized software for the rapid manufacturing based on STL file, which allows pre-machining layer by layer and finally finishing. Such similar specialized softwares for machining based on STL file has many and some of them are CUT3D, DeskPROTO, MeshCAM, etc. Usually this kind of softwares are presented as CNC

Software for Non-Machinists and working with them is very intuitive. These softwares enables the loading of the model in the STL format, orientate model for machining, tool selection, choosing machining strategies for roughing and finishing, simulation of material removal for machining cases from different materials, and finally postprocessing the tool path into G code. A sample of machining for the selected head model is shown in Fig. 5b. Machining is carried out on 3-axis vertical Parallel Kinematic Milling Machine LOLA pn101_4 V2, that is installed at the Faculty of Mechanical Engineering in Belgrade.

3.1. Autodesk 123D Catch and 123D Make

For the second example, is characteristic way of preparing model in STL format. In this case, the STL model obtained by the photogrammetric method based on 2D images using the software Autodesk 123D Catch [8] Fig.6.

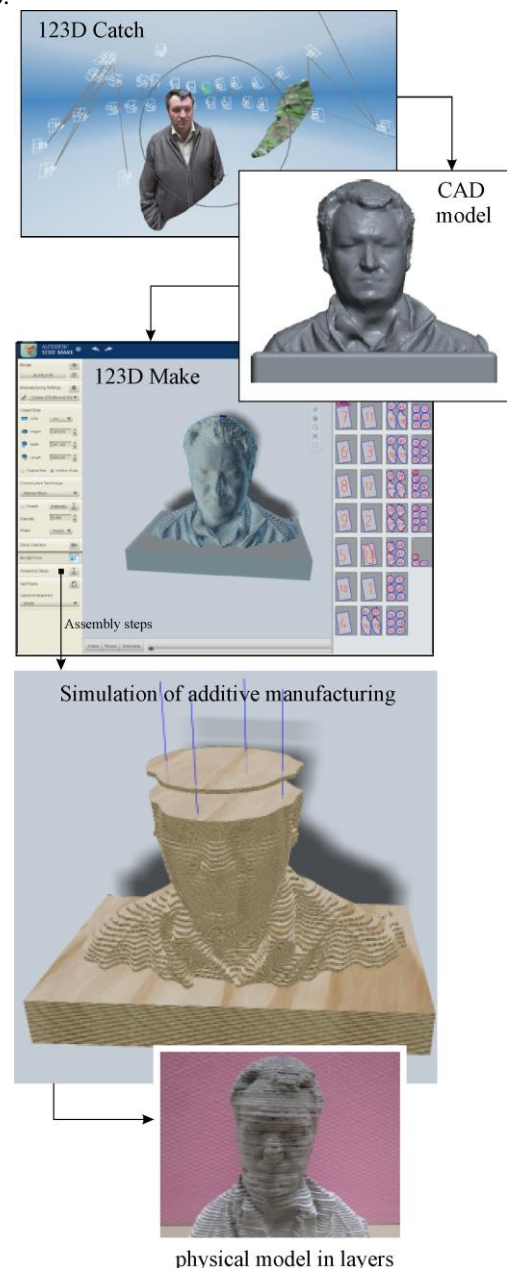


Fig.6: Building of the model of human head using 123D Catch and 123D Make

Autodesk 123D Catch is a handy, free Windows program, belonging to the category Design & photography software with subcategory 3D Design and has been published by Autodesk [8]. This software allows creating 3D models from series of photographs taken at various angles using photogrammetry method. After we get initial STL model, follow its completion in the CAD system and preparing corrected STL format for next step. This step is load STL file into the software Autodesk 123D Make [7] that makes it possible to obtain of layers layout, as well as simulate the adding of layers, and present how to build a prototype.

3.2. 3D printing of model of human head

Third example, is realized for the same model as in the second example, but in this case the applied technology is known under the name of Fused deposition modeling, Fig.7.

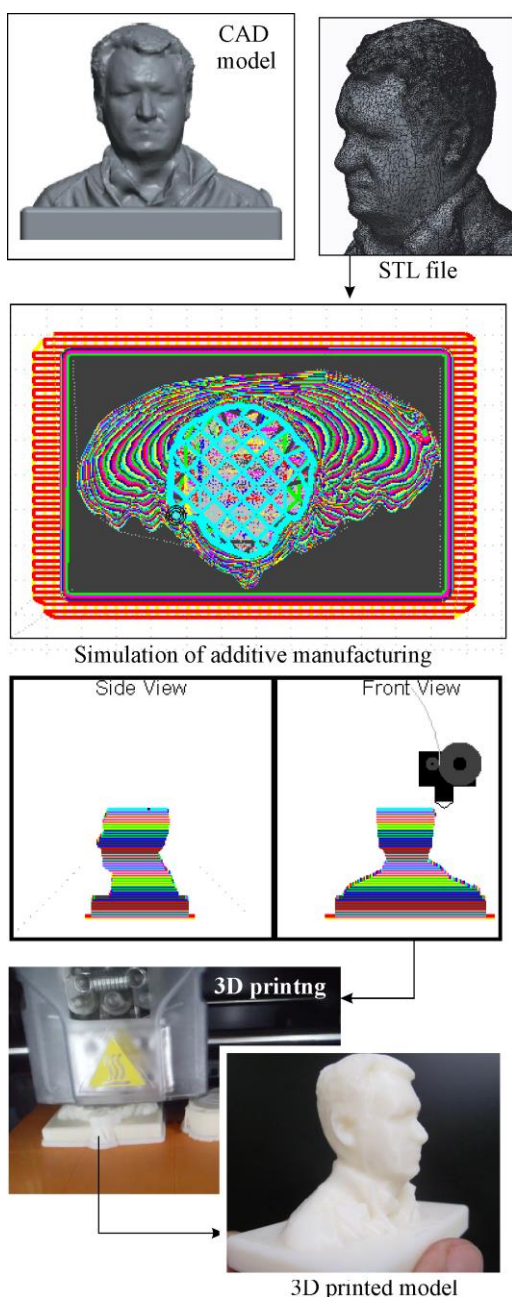
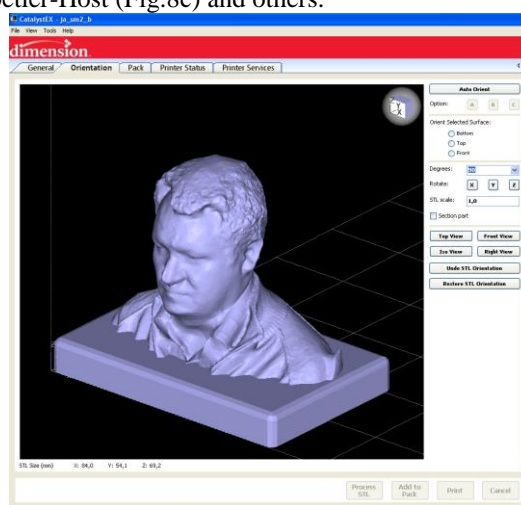


Fig.7: Building the 3D model of the head using 3D printing

Based on the input of the STL file, the G code was postprocessed, and then the simulation of additive manufacturing was performed, in order to finally make a physical model on the 3D printer Stratasys uPrint SE. In order to send the STL model to the 3D print, the software Catalyst EX is used as an interface for communicating with the available printer and which is a recommendation, or basic communication software for printers produced by firm Stratasys.

4. PROGRAMMING, VERIFICATION AND SIMULATION OF 3D PRINTING

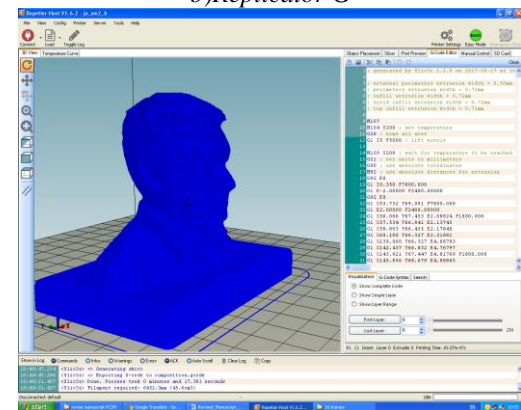
This section presents an examples of programming and program verification obtained for 3D printing. There are various specialized softwares for 3D printing, as already mentioned Catalyst EX (Fig.8a), or Replicator G (Fig.8b), Repetier-Host (Fig.8c) and others.



a) Catalyst EX



b) Replicator G



c) Repetier-Host

Fig.8: Specialized softwares for 3D printing

ReplicatorG [9] and Repetier-Host [10] are simple, open source 3D printing program. These programs represent an interface for communication with additive manufacturing machines. The input into these programs is a STL file based on which prepared additive layers are obtained and the required paths for adding materials. Such programs usually allow:

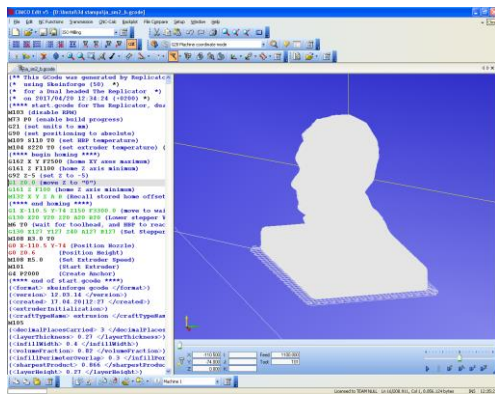
- (i) 3D display of the model being created;
- (ii) scaling the model to the desired size;
- (iii) control of model orientation in the workspace;
- (iv) Automatic or manual basing of the model in the case of making several parts in one production process;
- (v) slicing and forming additive layers;
- (vi) Simulation of the addition of layers and display of the each layers;
- (vii) generating G code for machine.

To verify the obtained G code for the addition of materials, may be used usual CNC editors and simulators, as well as the WEB CNC simulators. In addition, the standard CAD / CAM systems are starting to include Additive Manufacturing option, as is the case with the PTC Creo 4.0.

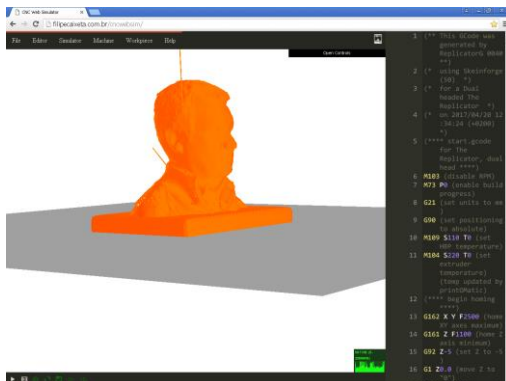
4.1. CNC simulators

The obtained G code based on STL file for Additive Manufacturing, it is possible to verify using commonly CNC editors for simulating the tool path, in this case, the deposit of materials. For example, for the created model from Fig.7, G code is verified by simulation path in two environments: (i) CNC editor CIMCO [11], Fig.9a, (ii) WEB CNC simulator [12], Fig.9b.

Although CIMCO editor not intended for Additive technologies, it enables drawing tool path defined by G code thus enabling successful visualization of models and display simulations path, Fig.9a.



a) CIMCO Editor



b) WEB CNC Simulator

Fig.9: Additive manufacturing simulation

CNC simulator for web browser [12] is capable of generating tool path and also the final 3D workpiece for turning, milling and 3D printing. In this case on Fig.9b is shown simulated path of adding material, for building the model of human head.

4.2. Machine simulation of 3D printing in CAD/CAM environment

Today and commercial CAD/CAM systems are beginning to integrate Additive technology into theirs CAM modules. For example, in a CAD/CAM system PTC Creo [13] from version 3.0 M040 have Additive Manufacturing functionality, Fig 10. 3D printing workflow using a User-Defined printer, or a supported printer Stratasys [5].

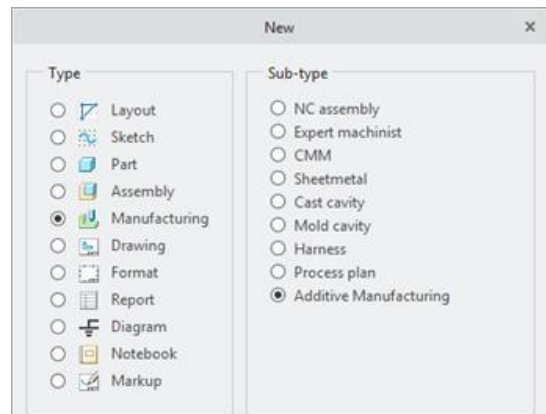


Fig.10: Additive manufacturing in PTC Creo 4.0

A standard characteristic of most CAD/CAM systems is the simulation of the virtual machine tool along a given tool path. For now, there is no possibility of direct simulation of the virtual machine for additive manufacturing, although this is possible realize an indirect way in PTC Creo. This indirect method implies that the 3d printer is modeled in the same way as the milling machine with the same kinematics.

Machine tools for additive manufacturing, or as they are also called 3D printers, can be modeled as a CAD model that includes appropriate kinematic connections. The most common machine tool for additive manufacturing are machine with serial kinematics and three translatory axes. Each of the translatory axes is defined as kinematic connection type Slider in PTC Creo, Fig.11.

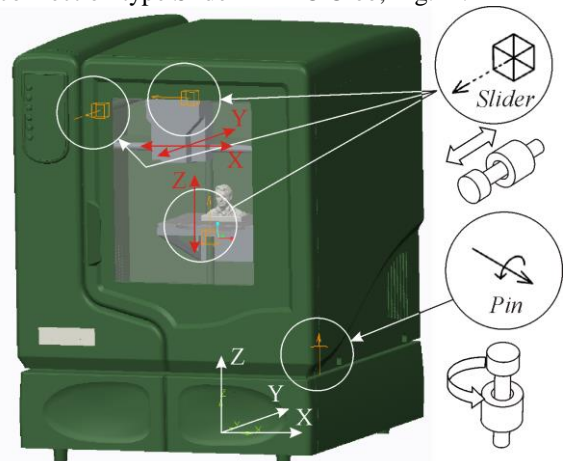


Fig.11: 3D printing machine simulation in PTC Creo environment

Only for opening the cabin door is defined rotary axis as kinematic connection type Pin, which has no influence on simulation process. Such a model is shown for the case of a 3D printer Stratasys uPrint SE plus [14], Fig.11 and Fig.12. The design is very rigid and compact. During the simulation, the machine is treated as if the milling machine, that moves along a path of adding material. To obtain the path of adding material, it is necessary to convert the path of the printing head into G code. Thus obtained path in G code can be converted to the DXF file that is loaded as a tool path into the CAM module by which the printer nozzle is run only for simulation purposes. During the simulation, CAD model of the machine can be loaded, which is made for better visualization, as shown in Fig. 12.

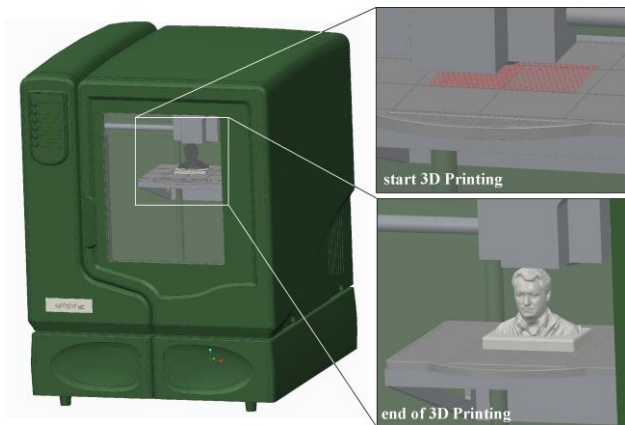


Fig.12: 3D printing machine simulation in PTC Creo environment

5. CONCLUSION

This paper provides an overview of rapid prototyping and manufacturing technology in brief and emphasizes on their ability to shorten the product design and development process.

This paper described several examples of a rapid prototyping and manufacturing of a models of a human head, using new technology, by adding and subtracting material.

In this paper is explained a photogrammetric method of obtaining STL model, using appropriate software.

The paper analyzes the possibility of tool-path simulation by adding a material, as well as the simulation of the machine for additive manufacturing ("3D printers").

REFERENCES

- [1] PHAM, D., DIMOV, S. (2001) *Rapid Manufacturing: The Technologies and Applications of Rapid Prototyping and Rapid Tooling*, Springer Verlag, London.
- [2] PHAM, D., DIMOV, S. (2003) *Rapid prototyping and rapid tooling– the key enablers for rapid manufacturing*, Proceedings of the Institution of Mechanical Engineers, Part C, 217, pp 1–23
- [3] <http://www.3dsystems.com/>, 2015.
- [4] Glavonjic, M., Obradni sistemi za agilne tehnologije, http://cent.mas.bg.ac.rs/nastava/ma_bsc/pdf_nma/ha4nma.pdf, 2013.
- [5] Additive Manufacturing/3D Printing, from [http://www.ptcuser.nl/conf_15/presentations/2-4-Additive%20Manufacturing/1%20PTC%20LiveWork%20Regional%20Event_BENELUX%20Additive%20MfgNov19_2015%20\(1\).pdf](http://www.ptcuser.nl/conf_15/presentations/2-4-Additive%20Manufacturing/1%20PTC%20LiveWork%20Regional%20Event_BENELUX%20Additive%20MfgNov19_2015%20(1).pdf)
- [6] GEBHARDT, A. (2003) *Understanding Additive Manufacturing, Rapid Prototyping–Rapid Tooling–Rapid Manufacturing*, Carl Hanser, Verlag, Munich.
- [7] Autodesk 123D Make, from <http://autodesk-123d-make.en.lo4d.com/>
- [8] Autodesk 123D Catch, from <https://autodesk-123d-catch.en.softonic.com/>
- [9] Replicator G, from, <http://replicat.org/>
- [10] Repetier, from <https://www.repetier.com/>
- [11] CIMCO, from <http://www.cimco.com/>
- [12] CNC WEB Simulator, from <http://filipecaixeta.com.br/cncwebsim/>
- [13] PTC, Creo Parametric, from <http://www.ptc.com/cad/creo/parametric>
- [14] Stratasys uPrint SE Plus, <http://www.stratasys.com/3d-printers/idea-series/uprint-se-plus>

CORRESPONDANCE



Sasa ZIVANOVIC, Prof. D.Sc. Eng.
University of Belgrade
Mechanical Engineering Faculty
Kraljice Marije 16.
11120 Beograd, Serbia
szivanovic@mas.bg.ac.rs

PREDICTION OF THE OPTIMAL MICRO HARDNESS AND CRYSTALLINE SIZE OF NANOSTRUCTURE VIA MACHINING AND NEURO-FUZZY TECHNIQUE

Dalibor PETKOVIĆ
Miloš MILOVANČEVIĆ

Abstract: Materials of nano crystalline are of great interest for the engineers due to its advances mechanical properties such as high strength and high hardness. The main drawback of these materials is high cost incurred during its production. In this paper the method of ANFIS (adaptive neuro fuzzy inference system) was applied to the data resulting from these measurements in order to predict the optimal machining parameters. The main goal is to minimize nanocrystalline structure via machining. The ANFIS process for variable selection was also implemented in order to detect the predominant variables affecting the prediction of micro hardness and crystalline size of the nanostructure via machining.

Key words: ANFIS; prediction; machining; nanostructure; crystalline

1. INTRODUCTION

Materials of nanocrystalline have the highest mechanical properties due to strength, hardness and ductility. Severe plastic deformation is one of the approach for the materials synthesizing. This approach breaks down the microstructure into smaller grains since the ultra-fine grained materials exhibit significantly enhanced mechanical properties.

Another approach is based on materials that have conventional crystalline microstructures. By this approach materials are built up atom by atom, molecule by molecule or cluster by cluster from bottom such as physical vapor deposition and chemical vapor deposition. It is crucial to develop a method for optimizing the nanocrystalline structure via machining process. To obtain optimal machining performance, the minimum crystalline size [1] and the maximum micro hardness [2] are desired. Therefore it is suitable to make a prediction method of the optimal crystalline size [3] and micro hardness [4]. In article [5] was carried out to develop a case depth hardness prediction model where the results indicated that the loss of case depth hardness uniformity was highly influenced by the tempering temperature and the change of cooling rate. The increase in indentation hardness within the plastic zones of macro-indentations was experimentally determined by micro-Vickers indentation and then compared with that predicted by finite element modeling in article [6]. A three-layer backward propagation model was used in article [7] to predict the hardness of Ni-TiN nanocoatings fabricated by pulse electrodeposition where the effect of plating parameters, namely, TiN particle concentration, current density, pulse frequency, and duty ratio on the hardness of Ni-TiN nanocoatings was investigated. It was shown that the

model, with a maximum error of approximately 1.03%, can effectively predict the hardness of Ni-TiN nanocoatings. In paper [8] a feed-forwarded multilayer perceptron artificial neural network framework was used to model the dependence of the grain size of nanocrystalline nickel coatings on the process parameters namely current density, saccharin concentration and bath temperature where the results showed that the current density has the most significant effect and the bath temperature has the smallest effect on the resulting grain size.

In this paper the method of ANFIS (adaptive neuro fuzzy inference system) was applied to the data resulting from these measurements in order to predict the optimal machining parameters. The main goal is to minimize nanocrystalline structure via machining. The ANFIS was applied to select the most influential parameters affecting the prediction of micro hardness and crystalline size. The process, which is called *variable selection*, includes a number of ways to discover a subset of the total recorded parameters that show good capability of prediction. The ANFIS network was used to perform a variable search and thereafter, it was used to examine how 5 parameters influence prediction of micro hardness and crystalline size.

2. METHODOLOGY

2.1. Data collection

Data collection was achieved with CNC Fanuc lathe. The crystalline size of the machined chips are measured on a Rigaku Ultima X-ray diffractometer. The microhardness of the samples was measured by indentation with a Vickers indenter with a 200 g load and 30 s dwell time on

a Mitutoyo micro hardness tester. Scherrer equation has been applied to estimate the size of crystallites [9]:

$$T = \frac{k\lambda}{B \cos\theta} \quad [1]$$

where T is the crystalline size, k is the constant that varies with the method of taking the breath, λ is the wavelength of incident X-rays, B is the width of the peak at half maximum intensity of a specific phase, θ is a Bragg angle.

It is important to fix the parameters that influence the machining output to a greater extent. From the literature [10], the important machining parameters considered are: rake angle, depth of cut, heat treatment, feed and cutting

velocity for which the output response used to measure the machinability is crystalline size and micro hardness. Different levels of machining parameters are chosen to determine the optimal machining parameters to get the desired output response: higher hardness and lower crystalline size. Table 1 shows the all the machining parameters and their corresponding levels.

2.2. Input and output variables

Table 2 shows the 5 input parameters selected for analysis. These parameters are considered potentially influential on prediction of the micro hardness and crystalline size parameters in Table 3.

Table 1: Input parameters

Inputs	Parameters description	Level 1	Level 2	Level 3	Level 4
input 1	Rake angle (degree)	-6	-10	-14	-18
input 2	Depth of cut (mm)	0.2	0.4	0.6	0.8
input 3	Heat treatment (mm)	Annealed	-	-	-
input 4	Feed (mm/rev)	0.1	0.15	0.2	0.25
input 5	Cutting velocity (mm/min)	20	40	60	80

Table 2: Input parameters

Inputs	Parameters description	Min-Max
input 1	Rake angle (degree)	1-4
input 2	Depth of cut (mm)	1-4
input 3	Heat treatment (mm)	1-2
input 4	Feed (mm/rev)	1-4
input 5	Cutting velocity (mm/min)	1-4

Table 3: Output parameters

Output	Parameters description	Min-Max
output 1	Micro hardness (VHN)	462-834.5
output 2	Crystalline size (nm)	28.52-73.39

To build a system with the best characteristics, it is necessary to identify the most relevant and influential subset of parameters and subject these to analysis. This process of selection is usually called variable selection. The purpose of this process is to find a subset of the total set of parameters that have been recorded that show good capability of prediction. Essentially, with neural network as the foundation, we modeled the complex system's architecture in function of approximation and regression. Neural networks are an architecture which is made up of extremely parallel adaptive processing elements. These are interconnected through structured networks. Therefore, the accuracy of the neural network models which are created as a result of this data relies heavily on the accuracy of the chosen sensor data in the representation of the system. To achieve a successful generation and creation of a model which is capable to estimate a special process output, the selection process of the subset of parameters that are really pertinent is crucial. This is achieved in the process of variable selection. As mentioned before, the purpose of this procedure is to find a subset of the total set of parameters that have been recorded to show good capability of prediction [11, 12,

13, 14]. The problems faced in the process of the selection of parameters could possibly be resolved by integrating and applying prior knowledge to segregate and remove parameters that are irrelevant. Otherwise, a more sophisticated manner of approach to the above-mentioned problem is to view it as an optimization procedure through the use of genetic algorithms [15]. The objective here is to select the proper explanatory (input) parameters and thereby reduce and minimize the error that exists between the observed values and the model estimations of the explained variables. Amongst the many neural network system, one of the most used and powerful is the ANFIS; and the ANFIS was employed here, for the purposes of this study, in the variable selection part [16].

3. RESULTS

3.1. Evaluation criteria indices

Predictive performances of proposed model were presented as root means square error (RMSE), Coefficient of determination (R^2) and Pearson coefficient (r). These statistics are defined as follows:

- 1) root-mean-square error (RMSE)

$$RMSE = \sqrt{\frac{\sum_{i=1}^n (P_i - O_i)^2}{n}}, \quad (1)$$

- 2) Pearson correlation coefficient (r)

$$r = \frac{n \left(\sum_{i=1}^n O_i \cdot P_i \right) - \left(\sum_{i=1}^n O_i \right) \cdot \left(\sum_{i=1}^n P_i \right)}{\sqrt{\left(n \sum_{i=1}^n O_i^2 - \left(\sum_{i=1}^n O_i \right)^2 \right) \cdot \left(n \sum_{i=1}^n P_i^2 - \left(\sum_{i=1}^n P_i \right)^2 \right)}} \quad (2)$$

3) coefficient of determination (R^2)

$$R^2 = \frac{\left[\sum_{i=1}^n (O_i - \bar{O}_i) \cdot (P_i - \bar{P}_i) \right]^2}{\sum_{i=1}^n (O_i - \bar{O}_i)^2 \cdot \sum_{i=1}^n (P_i - \bar{P}_i)^2} \quad (3)$$

where P_i and O_i are known as the experimental and forecast values of, respectively, and n is the total number of test data.

3.2. ANFIS prediction

Figure 1 shows scatter plots of ANFIS prediction of micro hardness (Figure 1(a)) and prediction of crystalline size (Figure 1(b)). The better prediction accuracy can be observed for micro hardness prediction than for the crystalline size prediction. This observation can be confirmed with very high value for coefficient of determination. The number of either overestimated or underestimated values produced is limited. Consequently, it is obvious that the predicted values enjoy high level precision.

In order to demonstrate the merits of the proposed models on a more definite and tangible basis, four models' prediction accuracy was compared each other. Conventional error statistical indicators, RMSE, r and R^2 were used for comparison. Table 4 summarize the prediction accuracy results.

Table 4: Statistical results for prediction of micro hardness and crystalline size

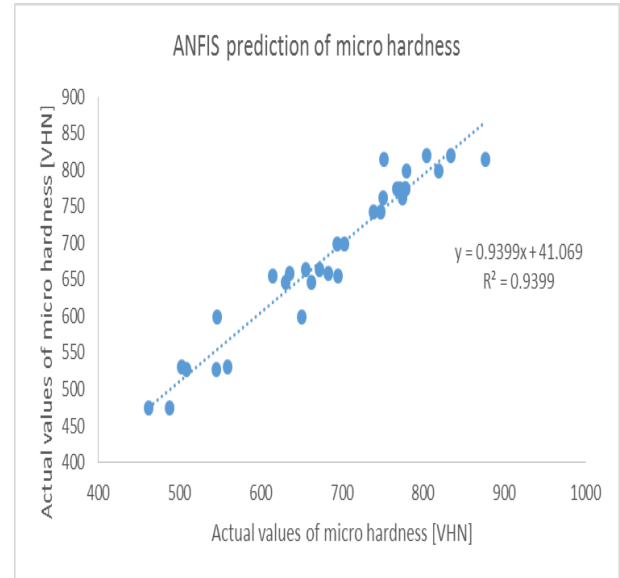
Micro hardness	r	0.969506
	R^2	0.9399
	RMSE	26.58499
Crystalline size	r	0.857226
	R^2	0.7348
	RMSE	6.307403

3.3. Sensitivity analysis

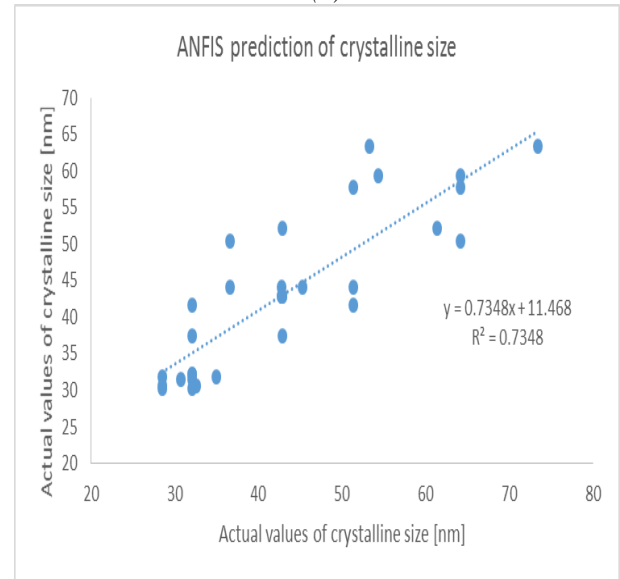
A comprehensive search was performed from the given inputs in order to choose the set of the ultimate optimal combination inputs (Table 1) which has the most impact and influence on the output parameters (micro hardness and crystalline size). Basically, an ANFIS model is built by the functions for each combination and they are then respectively trained for single epoch. Subsequently, the achieved performance is reported. From the outset, the most impactful input in the prediction of the output was

identified and determined, as depicted in Table 5. The input variables with the lowest training errors have the most relevance in regards to the outcome.

As it can be clearly seen from the Table 5, the input variable 4 (feed (mm/rev)) is the most influential for the micro hardness prediction and the input variable 5 (cutting velocity (mm/min)) is the most influential for the crystalline size prediction.



(a)



(b)

Fig. 1: ANFIS scatter plots for prediction of (a) micro hardness and for (b) crystalline size

Table 5: Input parameters influence on micro hardness and crystalline size prediction

Micro hardness	Crystalline size
ANFIS model 1: in1 --> trn=79.8795, chk=132.4067	ANFIS model 1: in1 --> trn=7.9538, chk=14.0770
ANFIS model 2: in2 --> trn=87.6742, chk=117.6481	ANFIS model 2: in2 --> trn=10.1254, chk=16.9335
ANFIS model 3: in3 --> trn=53.2879, chk=126.4379	ANFIS model 3: in3 --> trn=10.1817, chk=14.3752
ANFIS model 4: in4 --> trn=45.9984, chk=174.5915	ANFIS model 4: in4 --> trn=8.3189, chk=14.5005
ANFIS model 5: in5 --> trn=75.6704, chk=172.3097	ANFIS model 5: in5 --> trn=7.9134, chk=18.0515

4. CONCLUSION

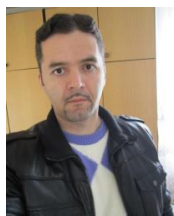
The study carried out a systematic approach to predict the optimal micro hardness and crystalline size by the ANFIS methodology. The simulations also employed MATLAB, and outcomes were checked on the corresponding output blocks. If further research is attempted we recommend polling users for deeper issues to obtain increased reliability. The ANFIS is used to eliminate the vagueness in the information and produces the best machining conditions. The proposed ANFIS model is used to convert the complicated multiple performance characteristics into the optimization of single multi response performance index. As a results, the optimization methodology developed in this research is useful for enhancing the multiple performances characterizing in the production of nanostructure. The ANFIS network was also used to perform a variable search to determine how 5 parameters influence prediction of the micro hardness and crystalline size.

There are many advantages in the use of the ANFIS scheme. Some of the main advantages are: it is adaptable to optimization and adaptive methods, as well as being computationally efficient. ANFIS can be integrated with professional systems and rough sets for use in other applications. Systems that handle more complex parameters can also employ the use of ANFIS, as it is much faster compared to other control strategies. And here is yet another favorable aspect of ANFIS, it conducts the tedious job of training membership functions.

REFERENCES

- [1] Jain, A., & McGaughey, A. J. (2015). Effect of exchange–correlation on first-principles-driven lattice thermal conductivity predictions of crystalline silicon. *Computational Materials Science*, 110, 115-120.
- [2] Thirumalaikumarasamy, D., Kamalamoorthy, K. S., & Visvalingam, V. B. (2015). Effect of experimental parameters on the micro hardness of plasma sprayed alumina coatings on AZ31B magnesium alloy. *Journal of Magnesium and Alloys*, 3(3), 237-246.
- [3] Zhang, Z., Huo, F., Zhang, X., & Guo, D. (2012). Fabrication and size prediction of crystalline nanoparticles of silicon induced by nanogrinding with ultrafine diamond grits. *Scripta Materialia*, 67(7), 657-660.
- [4] Li, K., Yang, P., & Xue, D. (2012). Anisotropic hardness prediction of crystalline hard materials from the electronegativity. *Acta Materialia*, 60(1), 35-42.
- [5] Santhanakrishnan, S., & Kovacevic, R. (2012). Hardness prediction in multi-pass direct diode laser heat treatment by on-line surface temperature monitoring. *Journal of Materials Processing Technology*, 212(11), 2261-2271.
- [6] Branch, N. A., Subhash, G., Arakere, N. K., & Klecka, M. A. (2010). Material-dependent representative plastic strain for the prediction of indentation hardness. *Acta Materialia*, 58(19), 6487-6494.
- [7] Jiang, M., Ma, C., Xia, F., & Zhang, Y. (2016). Application of artificial neural networks to predict the hardness of Ni–TiN nanocoatings fabricated by pulse electrodeposition. *Surface and Coatings Technology*, 286, 191-196.
- [8] Rashidi, A. M., Eivani, A. R., & Amadeh, A. (2009). Application of artificial neural networks to predict the grain size of nano-crystalline nickel coatings. *Computational Materials Science*, 45(2), 499-504.
- [9] Cullity, B. D., & Weymouth, J. W. (1957). Elements of X-ray Diffraction. *American Journal of Physics*, 25(6), 394-395.
- [10] Shankar, M. R., Verma, R., Rao, B. C., Chandrasekar, S., Compton, W. D., King, A. H., & Trumble, K. P. (2007). Severe plastic deformation of difficult-to-deform materials at near-ambient temperatures. *Metallurgical and Materials Transactions A*, 38(9), 1899-1905.
- [11] Castellano, G., & Fanelli, A. M. (2000). Variable selection using neural-network models. *Neurocomputing*, 31(1), 1-13.
- [12] Dieterle, F., Busche, S., & Gauglitz, G. (2003). Growing neural networks for a multivariate calibration and variable selection of time-resolved measurements. *Analytica Chimica Acta*, 490(1), 71-83.
- [13] Cibas, T., Soulié, F. F., Gallinari, P., & Raudys, S. (1996). Variable selection with neural networks. *Neurocomputing*, 12(2), 223-248.
- [14] Andersson, F. O., Åberg, M., & Jacobsson, S. P. (2000). Algorithmic approaches for studies of variable influence, contribution and selection in neural networks. *Chemometrics and intelligent laboratory systems*, 51(1), 61-72.
- [15] Sofge, D. (2002). Using Genetic Algorithm Based Variable Selection to Improve Neural Network Models for Real-World Systems. In *ICMLA* (pp. 16-19).
- [16] Chan, K. Y., Ling, S. H., Dillon, T. S., & Nguyen, H. T. (2011). Diagnosis of hypoglycemic episodes using a neural network based rule discovery system. *Expert Systems with Applications*, 38(8), 9799-9808.

CORRESPONDANCE



Dalibor PETKOVIĆ, Prof. D.Sc. Eng.
University of Niš, Pedagogical Faculty in
Vranje, Partizanska 14, 17500 Vranje,
Serbia
dalibortc@gmail.com



Miloš MILOVANČEVIĆ, Prof. D.Sc. Eng.
University of Niš, Faculty of Mechanical
Engineering, Aleksandra Medvedeva 14,
18000 Niš, Serbia
milos.milovancevic@gmail.com

PREDICTION OF THE FLOW STRESS OF TITANIUM ALLOY LOADED WITH HIGH STRAIN AT VARIOUS TEMPERATURES BY ADAPTIVE NEURO-FUZZY TECHNIQUE

Miloš MILOVANČEVIĆ
Dalibor PETKOVIĆ

Abstract: *In this study the flow stress of titanium alloy (Ti-6Al-4V) under strain and various temperature conditions are analyzed. The flow stresses are measured at mechanical tests for different strain rates at different temperatures. The method of ANFIS (adaptive neuro fuzzy inference system) was applied to the data resulting from these measurements in order to predict the flow stress of titanium alloy loaded with strain and various temperatures. The ANFIS process for variable selection was also implemented in order to detect the predominant variables affecting the prediction of flow stress of titanium alloy.*

Key words: ANFIS; prediction; flow stress; titanium alloy

1. INTRODUCTION

Titanium alloy Ti-6Al-4V is very important in industrial applications. The main characteristics of this alloy is good deformability, low density, high specific strength, corrosion resistance and high temperature strength retention. Since the mechanical characteristics of the alloy is very complex and very sensitive to the processing parameters strain rate and temperature, it is need to make a model for the deformation models of the alloy in relation to the input parameters. There are several numerical, analytical and experimental studies about the loading rate on this material. To understand and evaluate the thermo mechanical property of the titanium alloy, a uniaxial compression test was performed in [1] where it was found significant tension/compression asymmetry in the mechanical response under high strain rate loading. The high strain rate fracturing is characterized by ductile fracture behavior. The plastic deformation behaviors of titanium alloy over wide ranges of strain rate and temperature were investigated in [2] by the quasi-static and dynamic uniaxial compression tests where it was calculated the average standard deviations between the experimental and calculated flow stresses range from 4% to 13%. The residual stress and microstructure in the different depth of titanium alloy have been investigated in article [3] where the results shown that the dislocation interaction dominates the grain refinement process. The surface modification is the main technique to maintain a relatively good mechanical properties and biocompatibility. In article [4], a surface modification using different ceramic shoot was done on the titanium alloy microstructures. Investigation [5] was shown that the laser shock processing could repair the surface defects of titanium alloy structure effectively and reduce the surface roughness with lower laser pulse energy. The flow stress of the titanium alloy increases with increasing equiaxed alpha phase, but decreases with increasing alpha

grain size [6]. The estimated value of plastic zone size at the periphery of rough area is close to the average diameter of the primary grains of the titanium alloy [7]. In article [8] was shown that the limit strain decreases with temperature lowering but strain-rate increasing of the titanium alloy.

The obtained results so far are insufficient and highly time challenging. The main problem is the high strain rate and high temperature properties of the alloy since the alloy is subjected to impact or shock loading in the most crucial structures and components [9]. In other words there are need to develop the deformation model of the alloy for the conditions which seems best suited for the alloy.

Even though a number of new mathematical functions have been proposed for modeling of the plastic deformation behavior of the alloy, in this investigation the main aim is to overcome high nonlinearity of the plastic behavior of the alloy by applying the soft computing method. Artificial neural networks (ANN) can be used as alternative to analytical approach as ANN offers advantages such as no required knowledge of internal system parameters, compact solution for multi-variable problems.

In this investigation adaptive neuro-fuzzy inference system (ANFIS), which is a specific type of the ANN family, was used to predict the dynamic plastic behavior of the alloy or flow stress for different strain rates and in the different temperature range. ANFIS was applied also to select the most influential parameters affecting the prediction of flow stress if the alloy. ANFIS shows very good learning and prediction capabilities, which makes it an efficient tool to deal with encountered uncertainties in any system. ANFIS, as a hybrid intelligent system that enhances the ability to automatically learn and adapt, was used by researchers in various engineering systems [12, 13].

2. METHODOLOGY

2.1. Experimental measurement

Alloy bars Ti-6Al-4V was used in this investigation. The bars has the following chemical composition: 6% Al, 4% V, 0.2% Fe, 0.015% C, 0.008% N, 0.0057% H and 0.15% O. Compression tests are performed for different strain rates ranging from 500 to 5000 s⁻¹ and for different temperatures ranging from room temperature to 1100°C. The experimental procedure is described in [26]. The stress in the specimen is obtained from the strain as the face of the transmitter bar in contact with the specimen. Since the bar is elastic the following equation can be stated:

$$\sigma_s = E_\beta(\epsilon_{T\beta} + \epsilon''_\beta) \quad (1)$$

where ϵ''_β is a pulse which can be determined from strain pulses $\epsilon_{I\alpha}$ and $\epsilon_{T\beta}$ which are recorded as the incident and transmitter bar gauge stations. The pulse changes are caused by transmission through the thermal gradient:

$$\frac{\epsilon_T}{\epsilon_I} = \frac{2E_1}{[E_2 + (E_1E_2)^{1/2}]} \quad (2)$$

where E_1 and E_2 are the moduli of elasticity on the two sides of the bars' thermal gradient. For room temperature tests, the strain, strain rate and specimen stress:

$$\epsilon = \left(\frac{2C_0}{L_0}\right) \int_0^t \epsilon_t dt \quad (3)$$

$$\dot{\epsilon} = \frac{2C_0\epsilon_t}{L_0} \quad (4)$$

$$\sigma = E \left(\frac{A}{A_0}\right) \epsilon_t \quad (5)$$

where C_0 is the longitudinal wave velocity in the bar, L_0 is the effective gage length of the specimen, E is the Young's modulus of the bar, A and A_0 are the cross sectional areas of the bar and the specimen, respectively. Table 1 shows three input and output parameters which are used in this investigation. Output parameter flow stress is determined by measurements and by calculation.

Table 1: Input parameters

Inputs	Parameters description	Values
input 1	True strain	0.1, 0.2
input 2	Temperature (°C)	25-1100
input 3	Strain rate (s ⁻¹)	800-3300
output	Flow stress (MPa)	487.5-1533.7

2.2. ANFIS

Fuzzy inference system in MATLAB software is employed in the whole process of the ANFIS training and evaluation. An ANFIS network for 2 input variables is depicted in Figure 1.

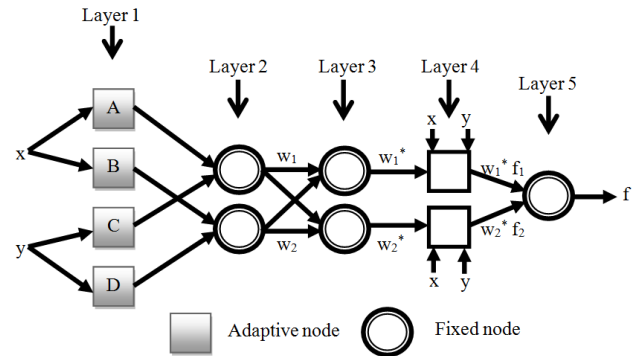


Fig. 1: ANFIS structure.

The fuzzy IF-THEN rules of Takagi and Sugeno's class and two inputs for the first-order Sugeno is employed for the purposes of this study:

$$\text{if } x \text{ is } A \text{ and } y \text{ is } C \text{ then } f_1 = p_1x + q_1y + r_1 \quad (6)$$

The 1st layer is made up of input parameters MFs, and it provides the input values to the following layer. Each node here is considered an adaptive node having a node function $O = \mu_{AB}(x)$ and $O = \mu_{CD}(x)$ where $\mu_{AB}(x)$ and $\mu_{CD}(x)$ are membership functions. Bell-shaped membership functions having the maximum value (1.0) and the minimum value (0.0) are selected, such as,

$$\mu(x) = \text{bell}(x; a_i, b_i, c_i, d_i) = \frac{1}{1 + \left[\frac{(x-c_i)^2}{a_i}\right]^{b_i}} \quad (7)$$

where $\{a_i, b_i, c_i, d_i\}$ is the set of parameters set. The parameters of this layer are designated as premise parameters. Here, x and y are the inputs to nodes.

The membership layer is the second layer. It looks for the weights of every membership function. This layer gets the receiving signals from the preceding layer and then it acts as membership function to the representation of the fuzzy sets of each input variable, respectively. Second layer nodes are non-adaptive. The layer acts as a multiplier for the receiving signals and sends out the outcome in $w_i = \mu_{AB}(x) * \mu_{CD}(y)$ form. Every output node exhibits the firing strength of a rule.

The next layer, the third, is known as the rule layer. All neurons here act as the pre-condition matching the fuzzy rules i.e. each rule's activation level is calculated whereby the number of fuzzy rules is equal to the quantity of layers. Every node computes the normalized weights. The nodes in the 3rd layer are also considered non-adaptive. each of the node computes the value of the rule's firing strength over the sum of all rules' firing strengths in the form of $w_i^* = \frac{w_i}{w_1 + w_2}$, $i = 1, 2$. The outcomes are referred to as the normalized firing strengths.

The 4th layer is responsible for providing the output values as a result of the inference of rules. This layer is also known as the defuzzification layer. Every 4th layer node is an adaptive node having the node function $O_i^4 = w_i^* x f = w_i^* (p_i x + q_i y + r_i)$. In this layer, the $\{p_i, q_i, r_i\}$ is the variable set. The variable set is designated as the consequent parameters.

The 5th and final layer is known as the output layer. It adds up all the receiving inputs from the preceding layer. Thereafter, it converts the fuzzy classification outcomes into a binary (crisp). The single node of the 5th layer is considered non-adaptive. This node calculates the total output as the wholesum of all receiving signals,

$$O_i^5 = \sum_i w_i^* x f = \frac{\sum_i w_i f}{\sum_i w_i} \quad (8)$$

In the process of identification of variables in the ANFIS architectures, the hybrid learning algorithms were applied. The functional signals progress until the 4th layer whereby the hybrid learning algorithm passes. Further, the consequent variables are found by the least squares estimation. In the backward pass, the error rates circulate backwards and the premise variables are synchronized through the gradient decline order.

3. RESULTS

3.1. Evaluation criteria indices

Predictive performances of proposed model were presented as root means square error (RMSE), Coefficient of determination (R^2) and Pearson coefficient (r). These statistics are defined as follows:

1) root-mean-square error (RMSE)

$$RMSE = \sqrt{\frac{\sum_{i=1}^n (P_i - O_i)^2}{n}}, \quad (9)$$

2) Pearson correlation coefficient (r)

$$r = \frac{n \left(\sum_{i=1}^n O_i \cdot P_i \right) - \left(\sum_{i=1}^n O_i \right) \cdot \left(\sum_{i=1}^n P_i \right)}{\sqrt{\left(n \sum_{i=1}^n O_i^2 - \left(\sum_{i=1}^n O_i \right)^2 \right) \cdot \left(n \sum_{i=1}^n P_i^2 - \left(\sum_{i=1}^n P_i \right)^2 \right)}} \quad (10)$$

3) coefficient of determination (R^2)

$$R^2 = \frac{\left[\sum_{i=1}^n (O_i - \bar{O}_i) \cdot (P_i - \bar{P}_i) \right]^2}{\sum_{i=1}^n (O_i - \bar{O}_i)^2 \cdot \sum_{i=1}^n (P_i - \bar{P}_i)^2} \quad (11)$$

where P_i and O_i are known as the experimental and forecast values of, respectively, and n is the total number of test data.

3.2. ANFIS prediction

Figure 2 shows scatter plots of ANFIS prediction of flow stress of titanium alloy. This observation can be confirmed with very high value for coefficient of determination. The number of either overestimated or underestimated values produced is limited. Consequently, it is obvious that the predicted values enjoy high level precision.

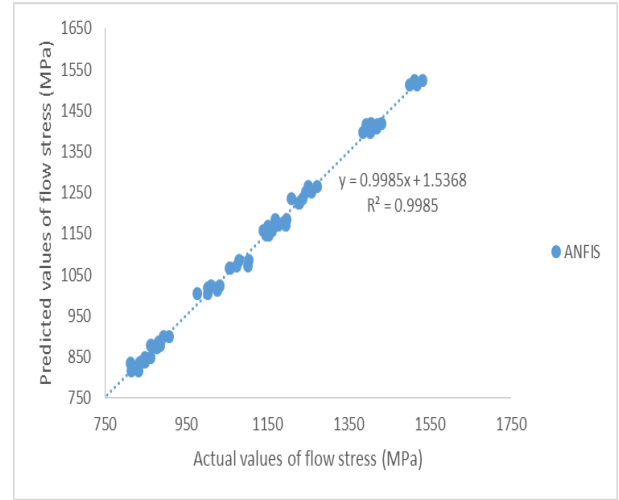


Fig. 2: ANFIS scatter plots for prediction of flow stress of titanium allo

In order to demonstrate the merits of the proposed models on a more definite and tangible basis, four models' prediction accuracy was compared each other. Conventional error statistical indicators, RMSE, r and R^2 were used for comparison. Table 2 summarize the prediction accuracy results.

Table 2: Statistical results for prediction of flow stress of titanium alloy

Flow stress of titanium alloy prediction	r	0.999228
	R^2	0.9985
	RMSE	11.20064

3.3. Sensitivity analysis

A comprehensive search was performed from the given inputs in order to choose the set of the ultimate optimal combination inputs (Table 1) which has the most impact and influence on the output parameter (flow stress of titanium alloy). Basically, an ANFIS model is built by the functions for each combination and they are then respectively trained for single epoch. Subsequently, the achieved performance is reported. From the outset, the most impactful input in the prediction of the output was identified and determined, as depicted in Table 3. The input variables with the lowest training errors have the most relevance in regards to the outcome.

As it can be clearly seen from the Table 3, the input variable 2 is the most influential for the flow stress of titanium alloy prediction and the optimal combination of input variable 2 and 3 is the most influential for the flow stress of titanium alloy prediction.

Table 3: Input parameters influence on flow stress of titanium alloy prediction

One input	Two inputs
ANFIS model 1: in1 --> trn=276.3501, chk=294.4293	ANFIS model 1: in1 in2 --> trn=16.7083, chk=18.3606
ANFIS model 2: in2 --> trn=38.1348, chk=32.8575	ANFIS model 2: in1 in3 --> trn=210.0466, chk=391.6481
ANFIS model 3: in3 --> trn=264.7179, chk=286.0212	ANFIS model 3: in2 in3 --> trn=29.0827, chk=131.6645

4. CONCLUSION

The study carried out a systematic approach to predict the flow stress of titanium alloy by the ANFIS methodology. The plastic deformation behavior of the alloy subjected to high strain rate and under different temperatures has been investigated. The ANFIS is used to eliminate the vagueness in the information and produces the best machining conditions. The proposed ANFIS model is used to convert the complicated multiple performance characteristics into the single multi response performance

index. As a results, the prediction methodology developed in this research is useful for enhancing the multiple performances characterizing in the production of titanium alloy. The ANFIS network was also used to perform a variable search to determine how 3 parameters influence prediction of the flow stress of titanium alloy.

There are many advantages in the use of the ANFIS scheme. Some of the main advantages are: it is adaptable to optimization and adaptive methods, as well as being computationally efficient. ANFIS can be integrated with professional systems and rough sets for use in other applications. Systems that handle more complex parameters can also employ the use of ANFIS, as it is much faster compared to other control strategies. And here is yet another favorable aspect of ANFIS, it conducts the tedious job of training membership functions.

REFERENCES

[1] Li, P. H., Guo, W. G., Huang, W. D., Su, Y., Lin, X., & Yuan, K. B. (2015). Thermomechanical response of 3D laser-deposited Ti-6Al-4V alloy over a wide range of strain rates and temperatures. *Materials Science and Engineering: A*, 647, 34-42.

[2] Chen, G., Ren, C., Qin, X., & Li, J. (2015). Temperature dependent work hardening in Ti-6Al-4V alloy over large temperature and strain rate ranges: Experiments and constitutive modeling. *Materials & Design*, 83, 598-610.

[3] Li, K., Fu, X. S., Li, R. D., Zhou, W. L., & Li, Z. Q. (2015). A mechanism study on characteristic curve of residual stress field in Ti-6Al-4V induced by wet peening treatment. *Materials & Design*, 86, 761-764.

[4] Ahmed, A. A., Mhaede, M., Wollmann, M., & Wagner, L. (2016). Effect of micro shot peening on the mechanical properties and corrosion behavior of

two microstructure Ti-6Al-4V alloy. *Applied Surface Science*, 363, 50-58.

[5] Ren, X. D., Zhou, W. F., Liu, F. F., Ren, Y. P., Yuan, S. Q., Ren, N. F., ... & Yang, T. (2016). Microstructure evolution and grain refinement of Ti-6Al-4V alloy by laser shock processing. *Applied Surface Science*, 363, 44-49.

[6] Luo, J., Ye, P., Li, M. Q., & Liu, L. Y. (2015). Effect of the alpha grain size on the deformation behavior during isothermal compression of Ti-6Al-4V alloy. *Materials & Design*, 88, 32-40.

[7] Liu, X., Sun, C., & Hong, Y. (2015). Effects of stress ratio on high-cycle and very-high-cycle fatigue behavior of a Ti-6Al-4V alloy. *Materials Science and Engineering: A*, 622, 228-235.

[8] Li, X., Guo, G., Xiao, J., Song, N., & Li, D. (2014). Constitutive modeling and the effects of strain-rate and temperature on the formability of Ti-6Al-4V alloy sheet. *Materials & Design*, 55, 325-334.

[9] Kumaraswamy, A., & Rao, V. V. (2011). High strain-rate plastic flow behavior of Ti-6Al-4V from dynamic indentation experiments. *Materials Science and Engineering: A*, 528(3), 1238-1241.

[10] Enayatifar, R., Sadaei, H. J., Abdullah, A. H., & Gani, A. (2013). Imperialist competitive algorithm combined with refined high-order weighted fuzzy time series (RHWFTS-ICA) for short term load forecasting. *Energy conversion and management*, 76, 1104-1116.

[11] Mohandes, M., Rehman, S., & Rahman, S. M. (2011). Estimation of wind speed profile using adaptive neuro-fuzzy inference system (ANFIS). *Applied Energy*, 88(11), 4024-4032.

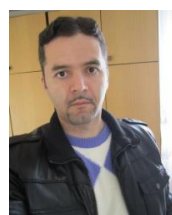
[12] Ata, R., & Koçyigit, Y. (2010). An adaptive neuro-fuzzy inference system approach for prediction of tip speed ratio in wind turbines. *Expert Systems with Applications*, 37(7), 5454-5460.

[13] Jang, J. S. (1993). ANFIS: adaptive-network-based fuzzy inference system. *IEEE transactions on systems, man, and cybernetics*, 23(3), 665-685.

CORRESPONDANCE



Miloš MILOVANČEVIĆ, Prof. D.Sc. Eng.
University of Niš, Faculty of Mechanical Engineering, Aleksandra Medvedeva 14, 18000 Niš, Serbia
milos.milovancevic@gmail.com



Dalibor PETKOVIĆ, Prof. D.Sc. Eng.
University of Niš, Pedagogical Faculty in Vranje, Partizanska 14, 17500 Vranje, Serbia
daliborc@gmail.com

THE INFLUENCE OF THE INPUT PARAMETERS TO THE DIMENSIONAL ACCURACY OF THE 3D PRINTED PROTOTYPE

Obrad SPAIĆ
Aleksandra KOPRIVICA
Mirjana JOKANOVIĆ
Srđan ĆURIĆ

Abstract: *The key of a success, in making the physical prototypes of a good accuracy, is certainly a technology of a rapid prototyping (RP - Rapid Prototyping), by which are, relatively rapidly and inexpensive, produced different classes of a prototype. The RP technology implies a sequence of technological procedures which enable direct production of a complex of physical objects. The digital 3D geometric models are used as inputs. They may be prepared using a CAD program or a technology of a 3D scanning of the existing object and the subsequent treatment of the scanning results. One of the RP technologies, which is prepared by adding a physical model of the material, layer by layer, is 3D printing. Whereas, in 3D printing, the thickness of a layer is selected depending on the desired accuracy of the prototype, this paper analyses the influence of the thickness of the 3D printer to the dimensional accuracy of the prototype, in case when the prototyping is based on the CAD model.*

Key words: 3D printer, dimensional accuracy, prototype.

1. INTRODUCTION

The increasing market globalization, as well as the constant acceleration of the technical - technological progress require from companies increased flexibility in product design. It is essential that companies are oriented to continuous innovation and the creation of new, or changes of the existing products.

In the context of the product development, certainly the most important place takes a phase of the prototype production, where the model of the desired product is made, very representative, with high quality and the possibilities of testing the characteristics.

Although the benefits of 3D printing are at a high level, one of the perceived flaws would be dimensional accuracy, that is, the deviation of the starting model, from the CAD software, to the produced prototype, which was analysed in this paper.

2. THE PROTOTYPE AND THE METHODS OF ITS PRODUCTION

Word prototype represent a derivate of the Greek words "protos" = first and "tipos" = impression of "prototipon" = primitive form. Accordingly, a general definition could be formed as follows: The prototype is the first or original copy of something that is or will be reproduced or developed. However, given the widespread use of the prototype concept in practice, the following comprehensive definition also could be used: A prototype is a first, the original shape, type, example of the product/system or of its part in an appropriate form,

intended for various kinds of tests, testing and use, depending on the characteristics of the prototype and the areas of the implementation of the newly-developed products/systems [1].

For centuries it was thought that the design of a particular product is confirmed with the production of its physical model of the prototype. However, at the present time, fabrication of the prototype, as an important part of the product development process, comprise the activities of the design, optimization and simulation on the computer and also creating a real, tangible and functional part (physical prototype). On one side, there are virtual prototypes, which are studied and analyzed, while on the other hand, there is a physical model of the product, which is used for testing and experiments [2].

Methods for the production of a physical prortotype can be classified into three groups [3]:

- traditional methods (manual and mechanical),
- rapid prorotyping and
- others.

The greatest significance of the traditional method is the ability to create prototypes of the materials that will be used for the production. Traditional methods have some limitations, as for example: the time required for the production of the prototypes, the problems in making a complex object, a large amount of manual labor, a wide variety of technical and practical knowledge which are necessary for the prototypes' production [3].

Rapid prototyping is a general name for several similar technologies which produce physical prototypes directly, from CAD files or other digitized data by layered application of the building material [3].

2.1. Rapid Prototyping

The term rapid prototyping (RP) refers to a series of similar manufacturing processes by which are automatic, with successive application and with bonding layers of building materials, based on the control instruction created directly from CAD files or other digital data without the use of tools, equipment, without the need for additional machining operations, produced physical objects [1].

The process of applying the layers of the building material is commonly performed in a horizontal xy plane, while the process of interconnecting the layers of the building material is performed in a vertical z plane [1]. The overall process may be viewed through the 3 phase [3]:

- pre-processing,
- direct production of prototypes and
- post-processing.

Since the advantages of RP technology are extremely huge, it has resulted in the rapid development, so today we can speak about the tree of RP technologies. A common feature of all technologies is to use method of preparation of layer by layer, and depending on which material is used (liquid, solid, powder), they all may be divided into 2 groups [3]:

1. Techniques of materials addition, for building the physical model, layer by layer. Within this group there are a number of techniques but those that are commonly used in practice are: Stereolithography (SLA), Selective Laser Sintering (SLS), Modeling of the Deposit of Molten Material (FSM), 3D Printing (3DP).
2. The material removal processes, such as milling, which removes the excess material from the block of spatial model, thereby producing the desired physical model.

The characteristics of the previous mentioned technologies are given in the following table.

Table 1: The characteristics of the RP technologies [3]

RP TECHNOLOGY	SLA	SLS	FSM	3DP
Maximum size (mm)	510x510x610	380x330x460	610x510x610	510x610x410
Layer thickness (mm)	0,05-0,3	0,08-0,2	0,05	0,013-0,3
Accuracy (mm)	0,1-0,01	0,03-0,38	0,127-0,254	0,025-0,356
Advantages	Size and accuracy	Accuracy and materials	Price and materials	Speed, price and possibility of making a model in color
Disadvantages	Post-processing and liquid working materials	Size, weight and the price of the system	Speed	Stability of the model

2.1.1. 3D Printing

The work of these systems is based on chemical bonding, adhesive liquids - binder, powdered building materials, whereby physical objects are printed, directly from the 3D CAD environment [4].

The figure 1. illustrates the method of making one layer. The following sections should be noted on the schematic view: on the left side there is a dust storage and a piston for adding material. The roller is shown as a circle, along which is a moving bridge represented as a square. In the middle, there is a working chamber with a platform and on the right there is a hole for accepting the surplus of the material. The bridge can move in both directions and the head moves along the bridge. This makes the possibility for applying the binder in a horizontal plane [5].

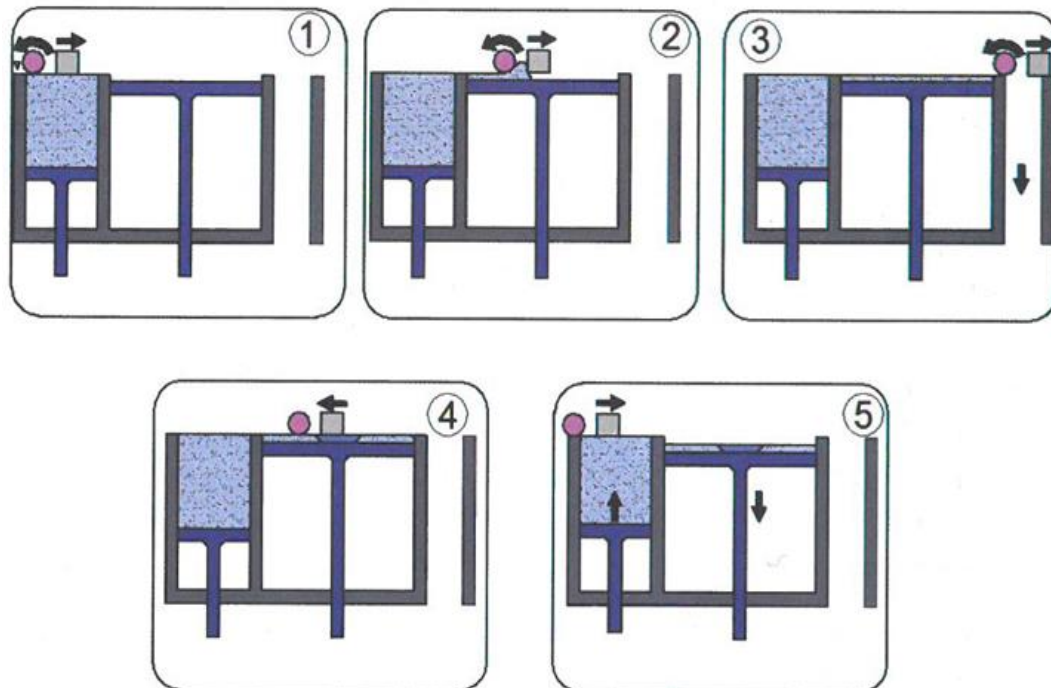


Fig. 1: 3D Printing procedure [5]

In the first operation, the moving bridge, which carries the roller and the print head, moves from left to the right. The roller rotates in the direction shown in (1) and takes away certain quantity of powder. Then, in the second step (2), this powder is drawn into a thin layer over the previously made layer on the platform of the working chamber. At the end of the walk to the right (3), the roller takes away the excess of the powder to the opening that accepts it and enters the repository. In the next step (4), the bridge moves from right to the left, and in the same time the nozzle on the print head of the syringe binds the appropriate points of the current cross-section and thus forms the liquid layer of the model. When the bridge arrives in the extremely left position (5), the piston for adding the material is raised by one step, while the platform is lowered by the thickness of the layer and everything is ready for the re-cycle [5].

Dust to which no binding agent is applied serves as a support. When the process is completed, the finished part is in unbound powder. The platform of the working volume is lifted and the part is removed from the excess powder. The excess material is sucked in and sifted and reused for the next model [5].

The produced prototype, removed from the machine working chamber can be applied for a limited use, while for the full use it is necessary to perform post-processing. Post-processing operations are reduced to the infiltration of the prototype by the appropriate means (wax, cyanoacrylate, two-component epoxy resin, etc.). blasting, painting, lacquering and metallizing for a better visual effect. By adding these agents, the prototype improves mechanical properties and ensures elasticity, all in accordance with the requirements and needs of the customer [5].

3. EXPERIMENTAL RESEARCH

3.1. The prototype production on the ZPrinter 450

The ZPrinter 450 features the latest features that automate and simplify the 3D color printing process. Pleasant design and simplicity, combined with high performance composite materials, have made it possible to use this printer widely. It is also important to emphasize that a precise 450 DPI 3D color prototype model is obtained, five to ten times faster than the others printer for the same purpose. The appearance of the printer is shown in the next figure 2 [6].

The ZPrinter 450 offers the ability to print prototypes of products of various designs, relief maps, human hearts, architectural models (in order for construction workers to have a cleaner picture of design plans, etc.), which puts it on the list of one of the most reliable and high quality printers. The biggest advantage is certainly the ability to print the prototypes in color [6].

The experiment was done in the laboratories at the Production and Management Faculty Trebinje.

Workshop drawing of the object, i.e. the 2D model was developed using the AutoCad 2013 software (figure 3). Based on the 2D model, the 3D model, shown in the figure 4, was also created.



Fig. 2: ZPrinter 450 [7]

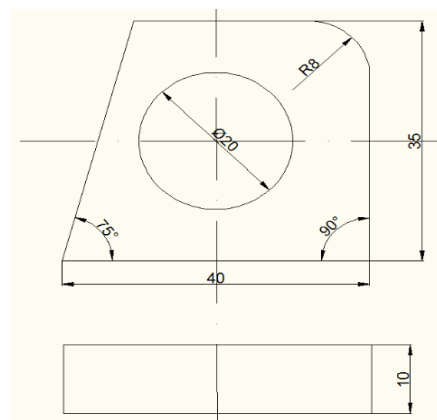


Fig. 3: 2D model

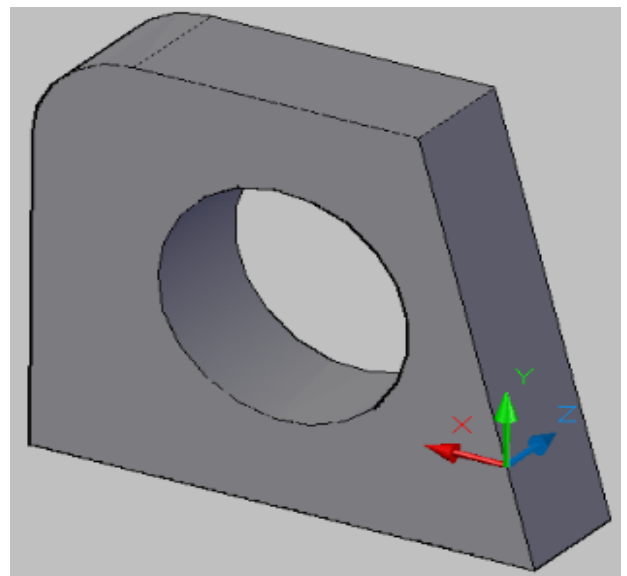


Fig. 4: 3D model

Since there are many factors that can have a different effect on achieving the accuracy of prototype production, it is important to emphasize that the printing was done in the function of varying the thickness of the layer.

The constructed 3D model is converted into a STL file, after which the models, with the different layers' thickness were made.

The size of the layers' thicknesses and number of layers for each model is given in the table 2. Figure 5 shows produced models.

Table 2: The size of the layers' thickness and number of layers

	MODEL 1	MODEL 2	MODEL 3	MODEL 4
Layers' thickness	1.250	1.125	1	0.875
Number of layers	78	87	98	112



Fig. 5: Produced models

Time, required, for all produced models is given in the following table 3.

Table 3: The total required time for models' production

OPERATION	TIME [min]			
	Model			
	1	2	3	4
Pre-processing	10	10	10	10
Direct production	35	40	45	50
Post-processing	50	50	50	50
TOTAL	95	100	105	110

After the models were made, they were accessed by measurement, i.g. their height ($h=35$ mm), length ($l=40$ mm) and thickness ($s=10$ mm).

Positions, at which the measurement was done, are shown in the next figures (figure 6, figure 7, figure 8).

At every position, the dimensions were measured three times and after that their average values were used for the analyses.

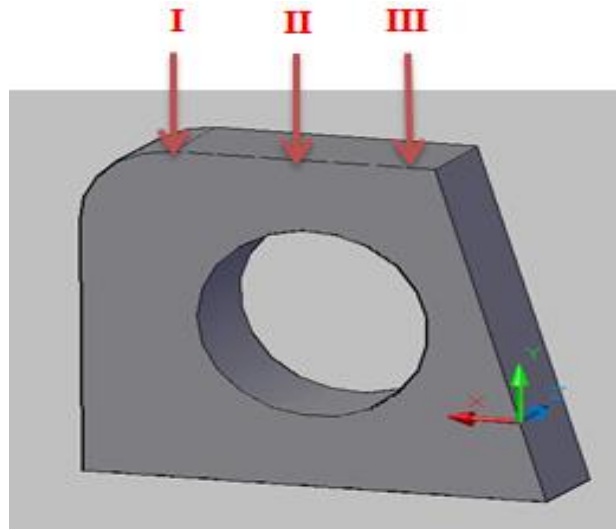


Fig. 6: Height's positions

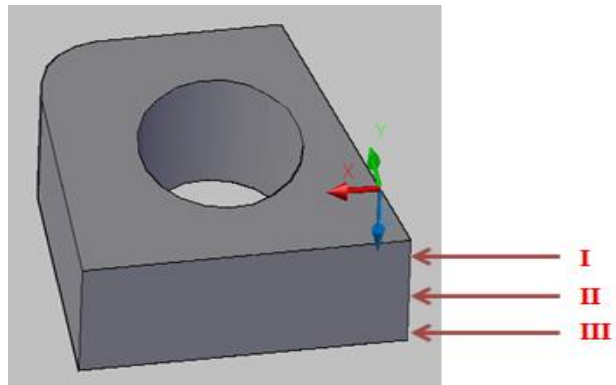


Fig. 7: Length's positions

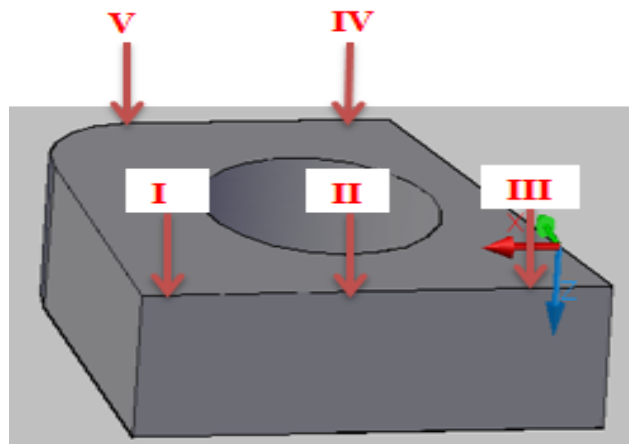


Fig. 8: Thickness's positions

Using Microsoft Excel, while analyzing the data and layer's thicknesses, certain dependences were made. The deviation of the workpieces' thickness, depending on the thickness of the layer, is shown in the figure 9. From the diagram, it can be seen that, contrary to expectation, the deviation is greatest at the lowest value of the thickness of the layer and it decreases with the increasing the layer's thickness.

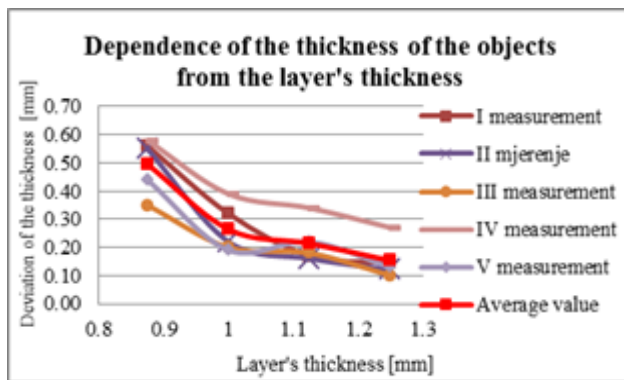


Fig. 9: Dependence of the thickness of the objects from the layer's thickness

The deviation of the height of the workpiece, depending on the layer's thickness, is shown in the figure 10. The diagram shows that the minimum deviation is at the minimum thickness of the layer and that it grows as the thickness of the layer increases. It is interesting to note that the deviation of the workpieces' height at a layer's thickness of 1.125 mm is less than the deviation at a layer's thickness of 1 mm and 1.250 mm.

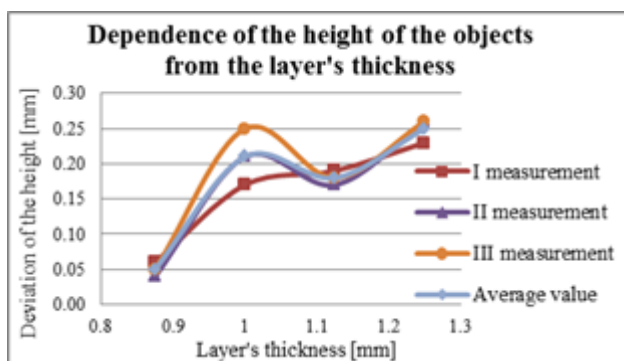


Fig. 10: Dependence of the height of the objects from the layer's thickness

The deviation of the length of the workpiece, depending on the layer's thickness, is shown in the figure 11. The diagram shows that the deviation is minimum at the smallest value of the layer's thickness and that it first grows and then decreases, with the increasing the layer's thickness.

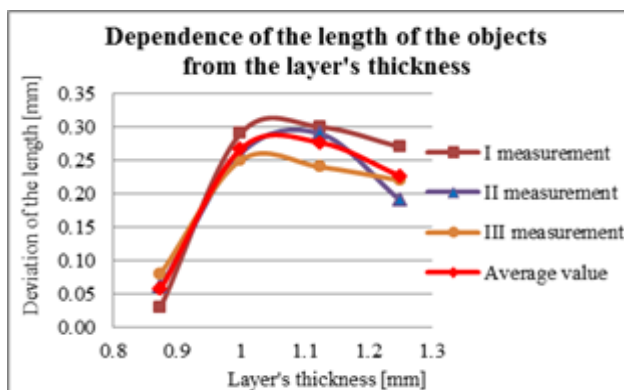


Fig. 11: Dependence of the length of the object from the layer's thickness

Of all geometric dimensions, the slightest deviation from the nominal measure, depending on the layer's thickness, is the angle deviation, which is shown in the diagram in the figure 12. The diagram shows that the deviation is minimum at the smallest value of the layer's thickness and that it first grows and then decreases, with the increasing the layer's thickness.

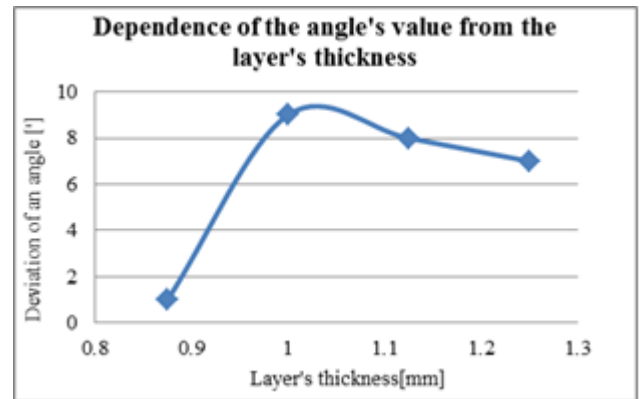


Fig. 12: Dependence of the angle's value from the layer's thickness

4. CONCLUSION

The emergence of 3D printing technologies has already been declared by many as the third industrial revolution, as well as the technologies that will surely mark the 21st century. 3D printing solutions offer the ability to produce very complicated shapes of products and tools in a relatively short period of time, only based on 3D model of the product or tool design. Geometric shapes, which can not be achieved with conventional production technologies, do not pose any problems for 3D printing. In addition, 3D printing also allows the creation of a whole assembly made of parts, which are actually made as one product, so that the installation operation is missing.

Based on 3D prints, future products can be analyzed more efficiently, as well as avoiding potential bugs on products, that, based on a 3D computer model, could not be spotted. Previously said saves both, time and money.

From the analyses carried out, it can be concluded that the deviations of the geometric values from the nominal measure significantly depend on the thickness of the powder's layer. Thus, when creating work items on a 3D printer, the thickness of the powder's layer should be selected depending on the required accuracy of the geometric dimensions.

REFERENCES

- [1] TOPČIĆ, A., TUFEKČIĆ, Dž., CERJAKOVIĆ, E. (2012) *Razvoj proizvodnje*, Univerzitet u Tuzli, Mašinski fakultet u Tuzli, Tuzla
- [2] ŠREDER, R. G. (1999) *Upravljanje proizvodnjom*, Mate d.o.o.
- [3] TOPČIĆ, A., CERJAKOVIĆ, E. (2014) *Izrada prototipa*, Univerzitet u Tuzli, Mašinski fakultet u Tuzli, Tuzla

- [4] PETROVIĆ, B. (1997) *Razvoj proizvoda - istraživanje i primjene*, FTN - Institut za industrijske sisteme, IIS - Istraživački i tehnološki centar, Novi Sad
- [5] TRAJANOVIĆ, M., GRUJOVIĆ, N., MILOVANOVIĆ, J., MILIVOJEVIĆ, V. (2008) *Računarski podržane brze proizvodne tehnologije*, Mašinski fakultet u Kragujevcu
- [6] JOKANOVIĆ, M., KOPRIVICA, A. (2016) *Razvoj proizvoda sa posebnim osvrtom na fazu izrade prototipa*, Zbornik radova Infoteh Jahorina 2016, Univerzitet u Istočnom Sarajevu, Elektrotehnički fakultet Istočno Sarajevo
- [7] <http://infoteh.etf.unssa.rs.ba/zbornik/2013/radovi/STS/STS-14.pdf> (10.07.2017.)

CORRESPONDANCE



Obrad SPAIĆ, Ass. Sc.
University of East Sarajevo
Faculty of the Production and Management
Stepe Stepanovića
89 101 Trebinje, Bosnia and Herzegovina
obradspaic59@gmail.com



Aleksandra KOPRIVICA, degree in Industrial Engineering and Management
University of East Sarajevo
Faculty of the Production and Management
Stepe Stepanovića
89 101 Trebinje, Bosnia and Herzegovina
aleksandra.koprivica@ymail.com



Mirjana JOKANOVIĆ, degree in Industrial Engineering and Management
University of East Sarajevo
Faculty of the Production and Management
Stepe Stepanovića
89 101 Trebinje, Bosnia and Herzegovina
jokanovic.mirjana1@gmail.com



Srđan ĆURIĆ, degree in Industrial Engineering and Management
University of East Sarajevo
Faculty of the Production and Management
Stepe Stepanovića
89 101 Trebinje, Bosnia and Herzegovina
srdjancuric@gmail.com

CUTTING FORCES DURING ULTRASONIC ASSISTED TURNING OF HARD TO MACHINE MATERIAL SPM10

Vladimir PUCOVSKI
Milenko SEKULIĆ
Marin GOSTIMIROVIĆ
Pavel KOVAČ
Borislav SAVKOVIĆ
Darko JOVANOVIĆ

Abstract: In this paper, the results of experiments for ultrasonic assisted turning of hard to machine material SPM10 will be presented. Cutting force values will be shown for various cutting parameters. Ultrasonic assisted turning allows many hard-to-machine materials to be machined with greater material removal rate, prolonged tool life and less affected surface microstructure. Its benefits are beyond dispute and many authors have tested it and graded it as a positive upgrade for conventional machining process. It is found out that while turning the workpiece made of SPM10, cutting forces are reduced when compared with conventional turning.

Key words: ultrasonic assisted turning, cutting forces

1. INTRODUCTION

While machining with ultrasonic vibration assisted turning (UAT), the cutting tool is induced with small vibrations, usually couple of microns, and high frequency, around 20 kHz. Intermittent contact between the cutting tool and the workpiece is the result of this movement which means that cutting forces are generated only during one half-period of vibration. This cutting force is usually higher than those during conventional turning (CT), but average forces in UAT are smaller than those in CT. Ultrasonic assisted turning is a potential technology suitable for machining hard-to-machine metallic and non-metallic materials. Result of ultrasonic assisted turning usage leads to better surface of the machined workpiece, prolonged tool life and more favourable microstructure of the workpiece surface layer. The ultrasonic vibrations can be applied along any of the three cutting directions or along any combinations of them [1]. The most positive effect has been found to be generated during applying vibrations in the tangential direction, which is in the direction of the cutting force.

Main condition for vibration assisted cutting which has to be met to make an effect, is the cutting speed to be less than $v < v_c = 2\pi Af$, where v_c is critical cutting speed, A is an amplitude and f is the frequency of vibrations.

In this paper a short presentation on developed ultrasonic assisted turning device will be presented. Also a brief preview of cutting forces while turning hard-to-machine material SPM10 will be made. Comparison with cutting force values between conventional turning and ultrasonic assisted turning will also be shown.

Ultrasonic vibrational cutting is long known and one of

the first papers were [2] and [3]. As the time went by, the topic started expanding and soon many authors accepted the idea. For example influence on surface roughness in turning with ultrasonic vibrating tool has been later done by [4]. But the idea hit its peak only recently, with the development of technical equipment, mostly electronic controllers and powerful personal computers for simulations and modeling. One of the things that brought novelty is finite element numerical analysis. Among many areas it was also used for research on influence of ultrasonic vibrational cutting on occurrence of chatter during turning [5]. The obtained results from the numerical analysis for some selected points of the stability lobe were compared and validated against the observed experimental results. It was shown that ultrasonic vibration can improve the stability for some cutting conditions, while degrading the stability in others. Hence, the proposed numerical analysis is a valuable tool to aid the designer to predict the effect of ultrasonic vibration on chatter stability [5]. Prior that, one paper analysed the influence of ultrasonic turning on chatter [6] and came to the conclusion that chatter is effectively suppressed irrespective of the tool geometry by vibration cutting. However, in the case of conventional cutting the occurrence of chatter was strongly influenced by the tool geometry. Obviously, vibration cutting achieved a higher cutting stability as compared with conventional cutting. By applying the vibration cutting method, the occurrence of chatter can be reduced significantly [6].

Regarding a theoretical basics of UAT, one of the most in depth paper which is dealing with this subject is [7]. A kinematics model has been developed in the mentioned study for the relative movement between the cutting tool and workpiece in UAT. Among the others, the model

predicts that the cutting tool does not disengage from the workpiece during its cyclic motion and inevitably rubs and presses against the lateral surface remaining after each revolution of the workpiece. [7]. In the second part of this [8] study, a dynamics model has been developed for UAT. The model can theoretically estimate the instantaneous cutting mechanics parameters and forces at various vibration frequencies and amplitudes and for different turning parameters. It is found out that the cutting process is carried out easier at large rake angles due to the lower cutting forces in UAT [8]. Third part [9], which is the final part of this study, is experimentally investigating claims of hypothesis and models stated in two previous works. There was a close agreement between the theoretical and experimental.

The development of new materials such as high-strength metals, composites and ceramics, which are very hard, brittle and abrasive, is demanding progress in the machining techniques. Ultrasonic assisted turning is one of the promising techniques for machining intractable materials. These new materials include Ni and Ti based super alloys, composites, ceramics, glass etc. [10]. Some everyday hard-to-machine materials have been studied and machined with UAT, for example hardened steel SCM440 [11], stainless steel [12], low alloy steel (DF2) [13] and Ti-64 [14]. Others researches are focused on more complex materials like Inconel 718 [15] [16] [17], Ti-15333 [18] [19] or shape memory alloy Nitinol [20] [19]. Some focused their research on materials specially developed for certain purposes, like for example Ti-676-0.9La [21] or Ti-15332Zr-0.9La [22]. Most above mentioned papers reported improvement in machinability of those hard to machine materials with ultrasonic assisted turning.

Regarding abovementioned remarks it is clear that SPM10 hasn't been machined with ultrasonic assisted turning. Because of its acoustic properties, this material is heavily used for production of sonotrodes for ultrasonic welding. While having these optimal properties for usage, SPM10 has a big disadvantage which is a low tool life. To solve this problem a solution has been proposed to machine above mentioned material with ultrasonic assisted turning. By this time only partial experiments have been conducted and results are presented in this paper.

2. EXPERIMENTAL SETUP

At the Faculty of Technical Sciences, Department for Production Engineering a device has been developed for UAT. This project originated as cooperation with Telsonic company from Kac and the Faculty. Telsonic company, which is active in the field of ultrasonic welding, is using SPM10 for ultrasonic sonotrode manufacturing and had the need to improve the production process. The idea was to engage ultrasonic assisted turning and to try to extend tool life and to increase process parameters which would directly lead to shorter manufacturing time.

Sonotrode, which is also the toolholder, is made from steel SPM10 and its dimensions are calculated with respect to acoustic properties given for frequency on

which it will operate. Modeling of acoustic behavior of sonotrode has been performed in Solidworks and the snapshot of final result is shown on Fig. 1. Part of this equipment development has already been presented [23].

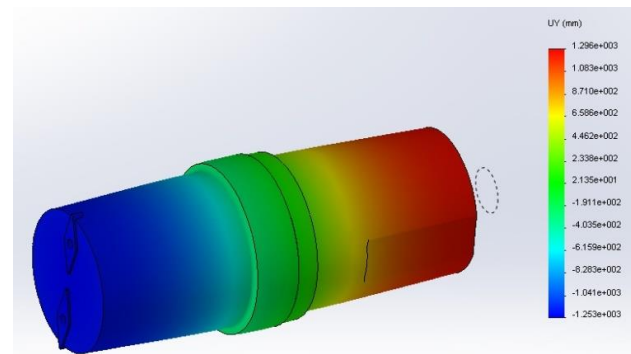


Fig.1: Acoustic properties of tool holder, modeled in Solidworks and result from acoustic analysis

It can be seen that the ratio of input and output amplitude is 1:1, which is 20 μm on 20 kHz. Tool insert was VCGT 11 03 04-UM 1125 by Sandvik Coromant, two pieces which provided symmetric balance during oscillations. Through the brass ring the sonotrode was mounted on steel holder custom made to fit on Kistler 9257A dynamometer and onto the conventional lathe manufactured by Boehringer-Prvomajska.

Classical piezo-electric ultrasonic transducer with 2kW power was used to drive the sonotrode. Telsonic ultrasonic generator type DHG2020 with auto tune option was used to drive the transducer.

Position of ultrasonically assisted turning device mounted on the lathe is shown on Fig 2.

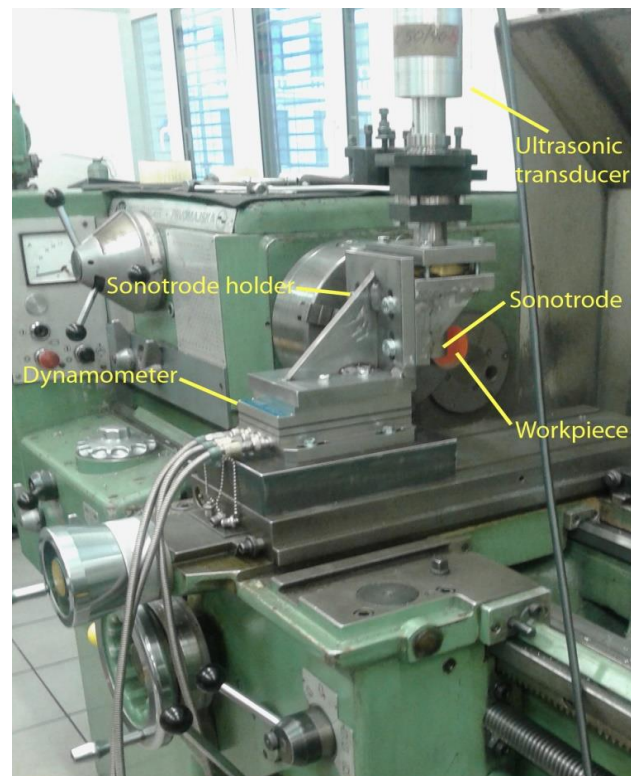


Fig. 2: Assembly of sonotrode on the lathe with Kistler dynamometer and ultrasonic transducer

3. EXPERIMENTAL RESULTS

As it was mentioned before workpiece material, used for this experiment, was tool steel SPM10. Chemical composition of this material is shown in Table 1. Tool insert used for this experiment was VCGT 11 03 04-UM 1125 made by Sandvik Coromant. Machining parameters which were varied are cutting speed v , feed rate s , depth of cut a and the value of the amplitude A . They were all varied on three levels and values in each level are shown in Table 2. Average values of measured cutting forces are shown in Table 3, where F_s is the feed (axial) force, F_p is the passive (radial) force and F_v is the main cutting (tangential) force.

For the experiment the Taguchi L_{18} orthogonal array design was used. During experiments, at the beginning only conventional turning was employed. This phase lasted about 30 seconds and then the ultrasonic vibration was turned on for about the same time. With this kind of approach direct comparison of cutting forces can be

made. Example of cutting forces variation is shown on graph in Fig 3. This example is for experiment number 7 in the Table 3.

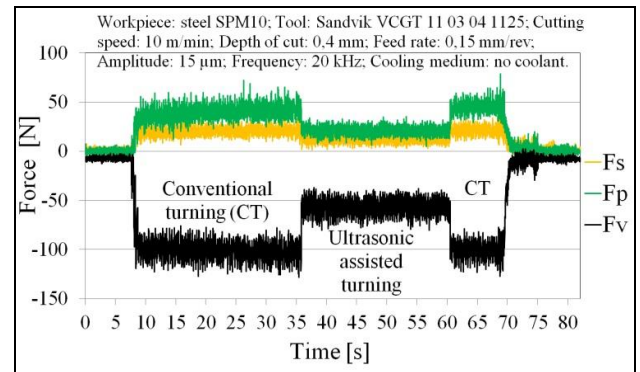


Fig. 3: Cutting forces for CT and UAT

Table 1: Chemical composition of SPM10 tool steel

Chemical element	C	Mn	Si	Cr	V	Mo	S
Value [%]	2,45	0,5	0,9	5,25	9,75	1,3	0,07

Table 2: Levels and values of machining parameters

Symbol	Parameters	Levels		
		1	2	3
A	Cutting speed, v [m/min]	10	20	30
B	Feed rate, s [mm/rev]	0,1	0,15	0,2
C	Depth of cut, a [mm]	0,2	0,4	0,6
D	Amplitude of oscillation, A [μ m]	10	15	20

Table 3: Experiment machining parameters and measured cutting forces for CT and UAT

Number of exp.	Cutting speed, v [m/min]	Feed rate, s [mm/rev]	Depth of cut, a [mm]	Amplitude of oscillation, A [μ m]	Conventional turning (CT)			Ultrasonic assisted turning (UAT)		
					F_s [N]	F_p [N]	F_v [N]	F_s [N]	F_p [N]	F_v [N]
1.	10	0,1	0,2	10	12,82	31,50	62,20	8,67	18,00	38,65
2.	20	0,2	0,6	10	79,92	123,57	244,62	82,58	109,96	220,32
3.	30	0,1	0,4	10	34,70	52,05	104,23	34,8	50,00	99,90
4.	10	0,15	0,2	10	16,80	39,10	77,62	18,12	28,44	53,35
5.	20	0,15	0,6	10	52,11	66,21	149,67	34,42	44,27	101,46
6.	30	0,2	0,4	10	41,08	88,13	164,35	40,18	86,00	160,75
7.	10	0,15	0,4	15	20,60	39,95	100,85	12,27	21,18	57,01
8.	20	0,1	0,2	15	12,11	27,64	57,04	10,25	17,44	40,50
9.	30	0,15	0,6	15	42,20	67,50	130,40	46,24	62,55	113,00
10.	10	0,2	0,4	15	28,33	69,43	134,40	22,47	42,97	86,10
11.	20	0,2	0,2	15	12,30	35,90	86,13	12,90	21,38	59,65
12.	30	0,1	0,6	15	39,45	54,15	115,94	38,45	43,25	91,62
13.	10	0,2	0,6	20	55,12	106,00	210,50	24,60	36,90	97,36
14.	20	0,15	0,4	20	22,66	44,97	93,78	16,00	22,44	51,53
15.	30	0,2	0,2	20	10,70	30,70	62,76	10,79	24,83	51,08
16.	10	0,1	0,6	20	31,76	41,42	108,25	16,98	14,80	49,24
17.	20	0,1	0,4	20	24,60	42,60	85,32	16,00	21,95	43,67
18.	30	0,15	0,2	20	11,24	35,53	66,50	8,44	19,90	42,70

As can be noticed from measured cutting forces values, shown in Table 3, smaller values of cutting forces are generated during ultrasonic assisted turning. Figure 4 show the measured force components during conventional and ultrasonic assisted turning for experiment number 7. The average force is computed by performing a numerical average of the measured force component over time. The average tangential force reduces significantly from 100,85 N to 57,01 N, the radial force reduces significantly from 39,95 N to 21,18 N, the axial force

reduces significantly from 20,6 N to 12,27 N, when the ultrasonic vibration is switched on.

Table 4 shows the results of ANOVA analysis for the main cutting force F_v , because of the tangential force is traditionally referred to as primary cutting force. Results of this analysis is that main effect on cutting force has depth of cut with 40,6% of influence, the next in line is amplitude of oscillation with 23,2% and feed rate with 22,9%. It also suggest that the cutting speed has very little influence on main cutting force with only 6,7%.

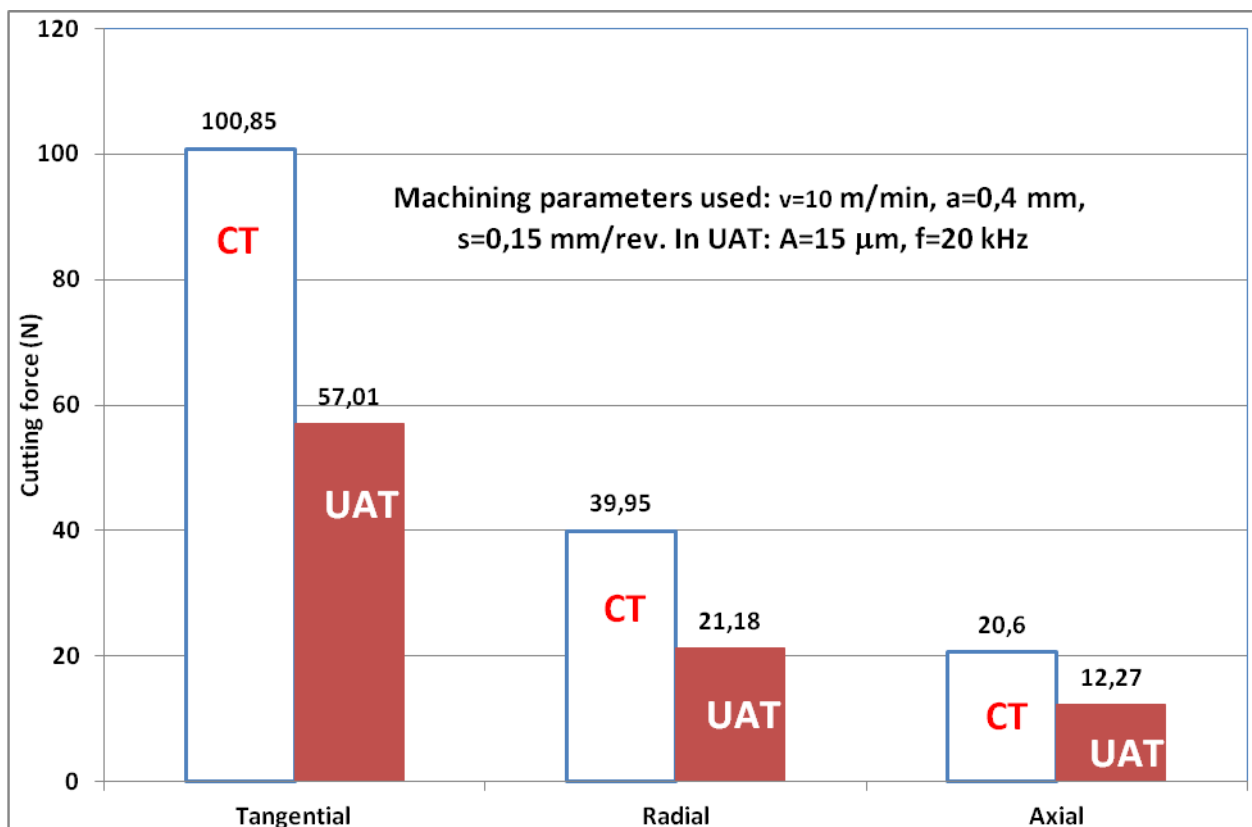


Fig. 4: Cutting forces for CT and UAT

Table 4: ANOVA analysis for the main cutting force F_v

Factor	DOF	Sum of squares	Variance	F-ratio	Pure Sum	Percent %
A (v)	2	24,186	12,093	9,673	21,685	6,726
B (s)	2	76,339	38,169	30,534	73,839	22,904
C (a)	2	133,351	66,675	53,337	130,851	40,588
D (A)	2	77,254	38,627	30,9	74,754	23,188
Other	9	11,249	1,249			6,594
Total	17	322,382				100%

4. CONCLUSION

The overall effectiveness of UAT in the cutting hard to machine material such as steel SPM10 is demonstrated. As can be seen from Table 3 a noticeable reduction in cutting forces has been observed while using ultrasonic assisted turning with comparison to conventional turning. The reduction in average tool force measured for UAT are a result of the intermittent contact between the tool and uncut material. In-depth investigation of process

behaviour is suggested while ultrasonically assisted turning of SPM10. Tool wear is also one of the main

parameters which is to be monitored to see if there is any influence of this technology in tool life duration.

Acknowledgements

The authors would like to thank management and engineers from Telsonic company Kač for their support during design of sonotrode and for providing ultrasonic transducer.

The paper is the result of the research within the project TR 35015 financed by the Ministry of Education, Science and Technological Development of Republic of Serbia.

REFERENCES

- [1] NATEGH, M.J. AMINI, S., SOLEIMANIMEHR, H., ABDULLAH, A., SADEGHI, M.H. (2009) *A Machining Force Model Developed for Ultrasonic Vibration-assisted Turning, through Statistical Analysis of Influential Parameters*, Aerospace Mechanics Journal, Vol. 4, pp 83-91
- [2] BALAMUTH, L. (1966) *Ultrasonic assistance to conventional metal removal* - Ultrasonics, Vol. 4, pp 125-130
- [3] SKELTON, R.C. (1969) *Effects of ultrasonic vibration on the turning process*, International Journal of Machine Tool Design and Research, Vol. 9, pp 363-374
- [4] WANG, L., ZHAO, J. (1987) *Influence on surface roughness in turning with ultrasonic vibration tool*, International Journal of Machine Tools and Manufacture, Vol. 27, pp 181-190
- [5] TABATABAEI, S.M.K., BEHBAHANI, S., MIRIAN, S.M. (2013) *Analysis of ultrasonic assisted machining (UAM) on regenerative chatter in turning*, Journal of Materials Processing Technology, Vol. 213, pp 418-425
- [6] XIAO, M., KARUBE, S., SOUTOME, T., SATO, K. (2002) *Analysis of chatter suppression in vibration cutting*, International Journal of Machine Tools and Manufacture, Vol. 42, pp.1677-1685.
- [7] NATEGH, M.J., RAZAVI, H., ABDULLAH, A. (2012) *Analytical modeling and experimental investigation of ultrasonic-vibration assisted oblique turning, part I: Kinematics analysis*, International Journal of Mechanical Sciences, Vol. 63, pp.1-11.
- [8] RAZAVI, H., NATEGH, M.J., ABDULLAH, A. (2012) *Analytical modeling and experimental investigation of ultrasonic-vibration assisted oblique turning, part II: Dynamics analysis*, International Journal of Mechanical Sciences, Vol. 63, pp. 12-25.
- [9] RAZAVI, H., NATEGH, M.J., ABDULLAH, A. (2012) *Analytical modeling and experimental investigation of ultrasonic-vibration assisted oblique turning, part III: Experimental investigation*, International Journal of Mechanical Sciences, Vol. 63, pp. 26-36.
- [10] BABITSKY, V., ASTASHEV, V. (2007) *Nonlinear Dynamics and Control of Ultrasonically Assisted Machining*, Journal of Vibration and Control, Vol. 13, pp. 441-460.
- [11] XIAO, M., WANG, Q.M., SATO, K., KARUBE, S., SOUTOME, T., XU H. (2006) *The effect of tool geometry on regenerative instability in ultrasonic vibration cutting*, International Journal of Machine Tools and Manufacture, Vol. 46, pp. 492-499.
- [12] MAHDY, S.M.A., GOUDA, M.A., SILBERSCHMIDT, V.V. (2013) *Study of ultrasonically assisted turning of stainless steel and brass alloys*, Journal of Physics: Conference Series, Vol. 451, pp. 012-037.
- [13] NATH, C., RAHMAN, M., ANDREW, S.S.K. (2007) *A study on ultrasonic vibration cutting of low alloy steel*, Journal of Materials Processing Technology, Vol. 192-193, pp. 159-165.
- [14] PATIL, S., JOSHI, S., TEWARI, A. (2013) *Microstructural analysis of Ultrasonic Assisted Turning of Ti alloy Ti6Al-4V*, 8th International Conference on MicroManufacturing, pp. 539-544.
- [15] AHMED, N., MITROFANOV, A.V., BABITSKY V.I., SILBERSCHMIDT, V.V. (2006) *Analysis of material response to ultrasonic vibration loading in turning Inconel 718*, Materials Science and Engineering, Vol. 424, pp. 318-325.
- [16] BABITSKY, V.I., MITROFANOV, A.V., SILBERSCHMIDT, V.V. (2004) *Ultrasonically assisted turning of aviation materials: simulations and experimental study*, Ultrasonics, Vol. 42, pp. 81-86.
- [17] BABITSKY, V., KALASHNIKOV, A.N., MEADOWS, A., WIJESUNDARA, A.A.H.P. (2003) *Ultrasonically assisted turning of aviation materials*, Journal of Materials Processing Technology, Vol. 132, pp. 157-167.
- [18] MAUROTTO, A., ROY, A., BABITSKY, V., SILBERSCHMIDT, V.V. (2010) *Recent developments in ultrasonically assisted machining of advanced alloys*, Proceedings of 4th CIRP International Conference on High Performance Cutting
- [19] MAUROTTO, A., MUHAMMAD, R., ROY, A., BABITSKY, V.I., SILBERSCHMIDT, V.V. (2012) *Comparing Machinability of Ti-15-3-3-3 and Ni-625 Alloys in UA*, - Procedia CIRP, Vol. 1, pp. 330-335.
- [20] AKBARI, J., CHEGINI, A.G., RAJABNEJAD, A.R. (2009) *Ultrasonic assisted turning of NiTi shape memory alloy*, 5th International Conference and Exhibition on Design and Production of MACHINES and DIES/MOLDS, Kusadasi, Aydin, TURKEY
- [21] MUHAMMAD, R., HUSSAIN, M.S., MAUROTTO, A., SIEMERS, C., ROY, A., SILBERSCHMIDT, V.V. (2014) *Analysis of a free machining $\alpha+\beta$ titanium alloy using conventional and ultrasonically assisted turning*, Journal of Materials Processing Technology, Vol. 214, pp. 906-915.
- [22] MAUROTTO, A., SIEMERS, C., MUHAMMAD, R., ROY, A., SILBERSCHMIDT, V.V. (2014) *Ti Alloy with Enhanced Machinability in UAT Turning*, Metallurgical and Materials Transactions, Vol. 45, pp. 2768-2775.
- [23] PUCOVSKI, V., SEKULIC, M., KRAMAR, D., GOSTIMIROVIC, M., KOPAC, J. (2015) *Ultrasonic assisted turning*, 12th International Scientific Conference MMA 2015 - Flexible Technologies, Novi Sad, pp. 29-32.
- [24] BREHL, D.E., DOW, T.A. (2008) *Review of vibration-assisted machining*, Precision Engineering, Vol. 32, pp. 153-172
- [25] SHARMA, V., PANDEY, P.M. (2016) *Recent advances in ultrasonic assisted turning: A step towards sustainability*, Cogent Engineering, Vol. 3:

- [26] AHMED, N., MITROFANOV, A. V., BABITSKY, V. I., SILBERSCHMIDT, V. V. (2007), *Analysis of forces in ultrasonically assisted turning*, Journal of Sound and Vibration, Vol. 308, pp. 845–854.

CORRESPONDANCE



Vladimir PUCOVSKI, Ph.D. student
University of Novi Sad
Faculty of Technical Sciences
Trg Dositeja Obradovića 6
21000 Novi Sad, Serbia
pucovski@uns.ac.rs



Prof. Milenko SEKULIĆ, Ph.D.
University of Novi Sad
Faculty of Technical Sciences
Trg Dositeja Obradovića 6
21000 Novi Sad, Serbia
milenkos@uns.ac.rs



Prof. Marin GOSTIMIROVIĆ, Ph.D.
University of Novi Sad
Faculty of Technical Sciences
Trg Dositeja Obradovića 6
21000 Novi Sad, Serbia
maring@uns.ac.rs



Prof. Pavel KOVAČ, Ph.D.
University of Novi Sad
Faculty of Technical Sciences
Trg Dositeja Obradovića 6
21000 Novi Sad, Serbia
pkovac@uns.ac.rs



Assist. Prof. Borislav SAVKOVIĆ,
Ph.D.
University of Novi Sad
Faculty of Technical Sciences
Trg Dositeja Obradovića 6
21000 Novi Sad, Serbia
savkovic@uns.ac.rs



Darko JOVANOVIĆ, M. Mech. Eng.
Managing Director
Telsonic doo
Kač, Serbia
darko.jovanovic@telsonic.com

THE USE OF MODERN INFORMATION TECHNOLOGIES IN THE EDUCATIONAL PROCESS OF GRAPHIC ENGINEERS AND DESIGNERS

Gojko VLADIĆ
Dragoljub NOVAKOVIĆ
Nemanja KAŠIKOVIĆ
Neda MILIĆ
Sandra DEDIJER

Abstract: *Graphic engineering and design is considered as rapidly growing and changing industry field. Complexity of education in this field may be reflected in understanding and learning structural design and operating ways of graphic equipment, if only conventional educational tools are used. Integration of wide variety of multimedia formats can be helpful supplement to conventional teaching method. With recent development of virtual and augmented reality, web, communication and mobile technologies it become possible to enrich education experience and augmented reality to be used to its full potential in education. The graphic industry equipment (printing presses, folding and cutting machines etc.) reproduced in a 3D virtual environment with ability to disassemble and analyze particles and animations of production processes can provide students with lifelike experiences, mimic the real-life usage scenarios, ensuring deeper immersion in learning process. Thus, this paper aims to present possibilities for integration of augmented reality technology in education of graphic engineers and designers, which can lead to far better comprehension of the subject and improvement of learning process. The concept presented can be easily implemented in other engineering fields as well.*

Key words: *IT technologies, augmented reality, education, graphic engineering, graphic design*

1. INTRODUCTION

Graphic engineering and design is rapidly growing and fast changing industry field. Complexity of education in this field may be reflected in understanding and learning structural design, operating ways of graphic equipment and training for successful organisation of production process. Having in mind that education is the process of facilitating learning, or the acquisition of knowledge, skills, values, beliefs, and habits related to the field the means and media by which the knowledge is conveyed, which may include the classroom, a variety of technologies, independent study, or a combination of approaches plays extremely significant role. Importance of face to face education cannot be underestimated but technological developments during past few decades offer new and exciting possibilities for supplement and further improve the education process [1]. Integration of wide variety of multimedia formats can be helpful supplement to conventional teaching method especially in fast changing fields such as graphic engineering. Recent development of virtual and augmented reality, web, communication and mobile technologies made possible to enrich education experience and to stay up to pace with dynamic changes with employment of these cost effective technologies. Some studies show that online and

classroom learning are essentially equally effective, thus cost effectiveness is bonus [2].

3D virtual environment reproduction of graphic industry production systems (printing presses, folding and cutting machines etc.) offer possibilities to gain overview of production system functionality as a whole, and also to disassemble systems and individual machinery in order analyze subsystems detailed. This provides students with lifelike experiences, mimics the real-life usage scenarios, ensuring deeper immersion in learning process.

Besides higher education vocational training as life long process with aim to improve job performance is where new technologies prove their worth offering possibilities to learn in such a way that it does not interfere with the job: typically, outside work hours and not at a fixed place. The desire to make education less dependent on time and place is mainly related to the increasing number of people who combine study and work in order to stay well prepared for changes in job requirements, to improve career perspectives, and to realize personal growth [3].

There are some optical in adoption of E- learning. Prediction in 1998. was that 50 percent of all workplace training would be delivered online. Today actual percentage in developed countries is about to 15 to 20 percent and significantly less in undeveloped countries. Main advantage of E- learning so far has been eliminating training related travel costs in industry.

Advantages and disadvantages of E-learning must be considered carefully before making the decision of investing in such a system, some of them are given below [4]:

Advantages of E-learning

- Reduction of travel cost and time
- Class work can be scheduled around personal time table
- Students can study wherever and whenever they have access to a computer and internet
- Self-paced learning modules
- Flexibility to join discussions in chat rooms
- Different learning styles in one course
- Students have the option to select learning materials for their level of knowledge and interest

Disadvantages of E-learning

- Problems with motivation
- Isolation and lack of social interaction
- Instructor may not always be available on demand
- Some courses can be difficult to simulate
- Software usage can involve a learning curve
- This form of education may take getting used to
- Slow or unreliable Internet connections influences performance

2. INFORMATION TECHNOLOGIES IN THE EDUCATIONAL PROCESS

There are several different technologies that can be utilized for educational purposes. Basic approach would entail dissemination of the learning materials through electronic media in contrast to classical printed material. Electronic media offer significantly more possibilities for communication, trough multimedia materials (sound, animation, interactivity, etc.). Presentation of the material is usually done on the screen of a computer or a mobile device. Latest technological advancements offer possibilities for reality augmentation or virtual reality utilization. Department for graphical engineering and design has so far developed a significant number of simulations presented in virtual laboratory. There are also mobile application based on augmented reality technology produced in order to help in the engineering field education.

2.1. Multimedia knowledge base with equipment presentation

Developed of knowledge base consists of numerous theoretical materials presented using up to date multimedia technologies. Special addition to the knowledge base is rich library of graphic equipment interactive presentations. These presentations are based on a virtual 3D visualization allows examination of all system elements with the insight into the knowledge base containing information about the theoretical and practical functioning of each element in virtual space. Figure 1 shows one of such presentations regarding the process of packaging prototyping for the particular case of graphic

cutter Aristo Mat 1317 SL. The student is provided with unambiguous information about operation carried out by the device and its basic parts, which significantly facilitates the acquisition of knowledge about the system [5].



Fig. 1. E-learning presentation of Aristo Mat 1317 SL

2.2. Equipment simulation

Different approach to the training is production of functional simulations of graphic equipment. Building on the previous concept of presentation, simulation offers full functionality reproduced in virtual environment.

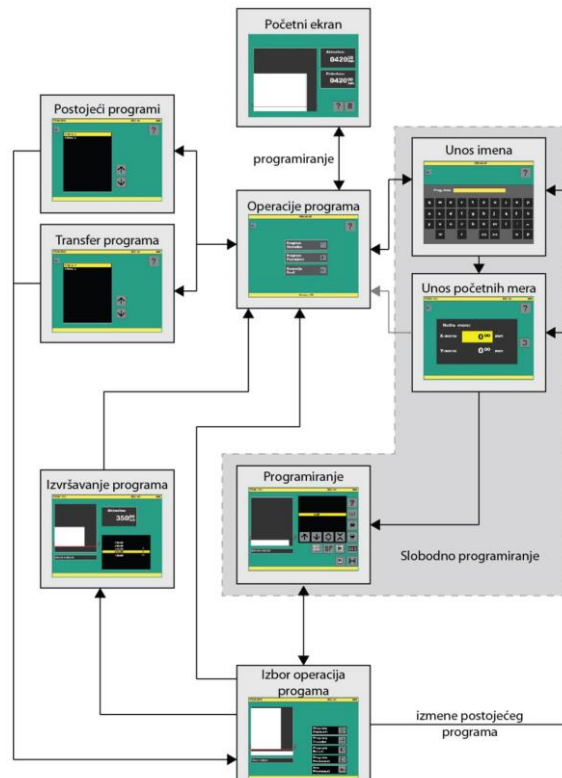


Fig. 2. Simulation operation algorithm

Functional simulation of paper cutting graphical system, which algorithm is shown in figure 2, is problem and project based learning tool. Simulating machine operation and JDF like programming for graphical equipment can prepare trainee for operating real machines by mimicking user interface of graphic equipment. Flash based animation supported by ActionScript programming language offers all the tools needed for creating such simulation [4].

Other simulation based learning tool is HP-200 colorimeter training application shown in figure 3. This application alongside theoretical knowledge regarding color measurements offers the functional simulation of the device with preprogramed tasks for the trainee and appropriate corrections in case of mistake.

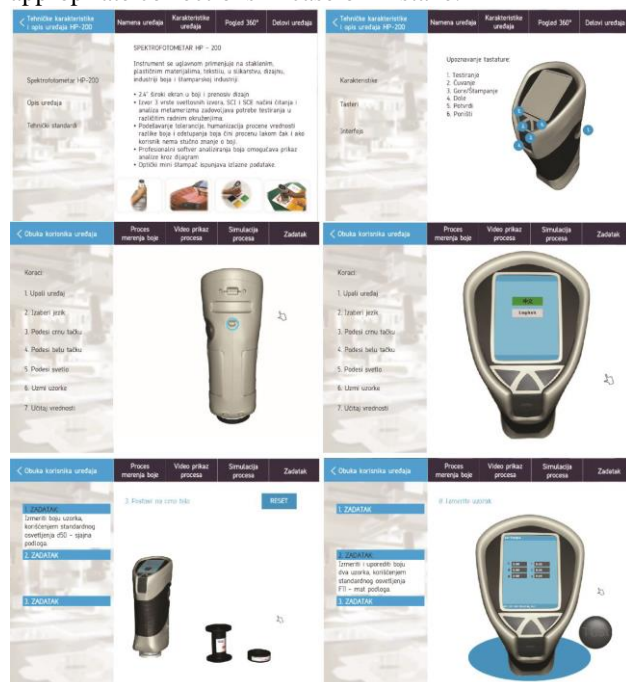


Fig. 3. Simulation of HP-200 colorimeter

Its functionality can prepare trainee for real world problems. Simulation program essentially allows the user to conduct an operations of the process through simulation without actually occupying device, leaving it free for other use. It mimics real world situations and problems to some extent depending on the complexity and versatility of possible problem solutions.

2.3. Augmented reality application for education

Augmented reality technology as an education tool achieved its full potential through advancements of the hardware performance in mobile devices. It made possible capturing the real world images in sufficient quality, processing them, simultaneously processing the virtual content and combining them into augmented reality displayed on the device's screen. Augmented reality basically overlays computer-generated virtual elements onto the real-world images, thus enhancing their informative or entertainment value. Most important characteristic of this concept is that the overlay content is context-sensitive, which means that information displayed is triggered by the real world object in real time. For education field Vision-based tracking technique is especially interesting having in mind that augmented

reality is usually used as an upgrade to existing printed learning materials.

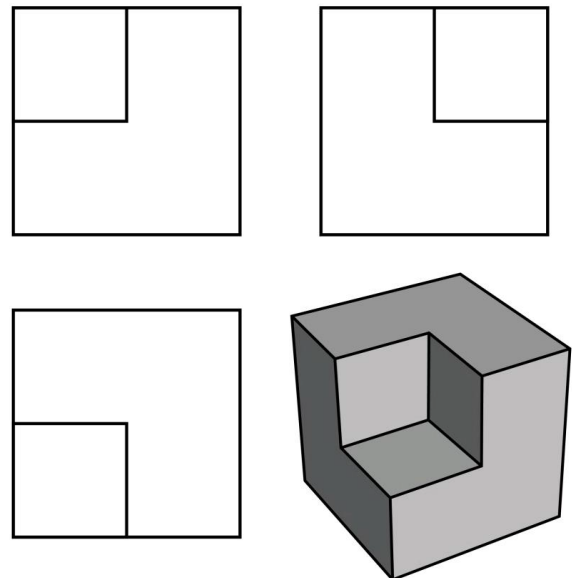


Fig. 4. Interactive 3D model trigger

CADEDU application developed by the Department for graphical engineering and design uses Marker tracking technique, where the corresponding image descriptors are provided beforehand and stored into the database. Application offers integration of augmented reality into the cad modeling and engineering drawing training of designers and offers interactive 3D model augmentation and video augmentations, triggered by the figures 4 and 5. This application intended for Android platform and can be downloaded from the following address:

www.grid.uns.ac.rs/symposium/download/cadedu.apk

When application is installed and run, interactive 3D model triggered by the image shown in figure 4 offers possibility to the user to manipulate the model and to get much better understanding of the object shape [6].

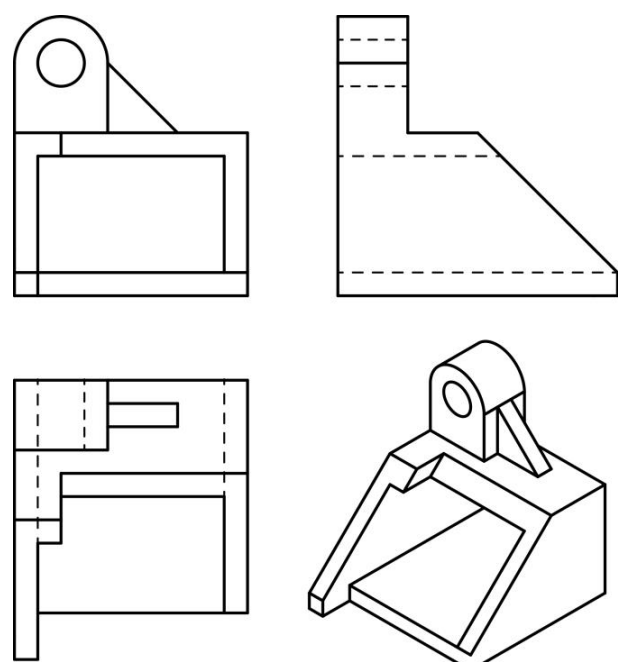


Fig. 5. Video augmentation trigger, placement and creation of the orthographic projections

3. CONCLUSION

This paper presented the possibility for usage of modern information technologies in the educational process of graphic engineers and designers through integration of multimedia material, interactivity and augmented reality technology. The basic approaches are explained followed with examples of applications utilizing that technology. Augmented reality technology as the most recent, offers exciting possibilities for integration with existing teaching materials and optimization of old material to fit better with future trends. Time needed for training on the real machine exploits production resources and by usage of the shown applications this can be changed, freeing up the equipment for other uses. Simulations of the machine operation can save expensive recourses and prevent injuries and equipment destruction by inexperienced trainee.

All the results shown are effort of the small group of authors, with evolvment of the experts in each of the fields mentioned. Future research will be focused on the exploitation of the other possibilities of the augmented reality technology and introduction of virtual reality technology in the educational process.

4. ACKNOWLEDGMENTS

The research is supported by the Ministry of Education, Science and Technology Development of the Re-public of Serbia, project number: 35027 "Development of software model for scientific and production improvement in graphic industry".

REFERENCES

- [1] ROSENBERG, M., STRATEGIE, S. (2001): *Delivering knowledge in the digital age*, Mcgraw-hill professional, ISBN 0-07-136268-1, New York.
- [2] SITZMANN, T.M., et al. (2006): *The comparative effectiveness of web-based and classroom instruction: a meta-analysis*. Personnel psychology, Vol.59 No 3, pp 623-664.
- [3] WIM, J., et al. (2004): *Integrated e-learning, routledgefalmer*, 11 New fetter lane, ISBN 0415335035, London.
- [4] VLADIĆ, G., NOVAKOVIĆ, D., KAŠIKOVIĆ, N., AVRAMOVIĆ, D., (2011): *Development of e-learning platform for graphical equipment operators*, 2nd International Joint Conference on Environmental and Light Industry Technologies, Budapest, Hungary.
- [5] NOVAKOVIĆ, D., PINČJER, I., ĐURĐEVIĆ, S., VLADIĆ, G., KAŠIKOVIĆ, N., NEDELJKOVIĆ, U., (2016): *Improvement of e-learning process of packaging rapid prototyping computer numerical control machine systems*, The Ninth International The 9th International Symposium - KOD 2016 - Machine and Industrial Design in Mechanical Engineering, ISBN 978-86-7892-821-5, Balatonfured, Hungary, pp 19-22.
- [6] VLADIĆ, G., MILIĆ, N., ĐURĐEVIĆ, S., MILOŠEVIĆ, R., STANČIĆ, M., (2016): *Integration of augmented reality into the CAD modeling and*

engineering drawing training of designers, 8th International Symposium on Graphic Engineering and Design, ISBN 978-86-78928-67-3, Novi Sad, Serbia, pp 419-425.

CORRESPONDANCE



Gojko VLADIĆ, Ass. Prof. Ph.D.
University of Novi Sad
Faculty of Technical Sciences
Department of Graphic Engineering and Design
Trg Dositeja Obradovića 6
21000 Novi Sad, Serbia
vladicg@uns.ac.rs



Dragoljub NOVAKOVIĆ, Full Prof. Ph.D.
University of Novi Sad
Faculty of Technical Sciences
Department of Graphic Engineering and Design
Trg Dositeja Obradovića 6
21000 Novi Sad, Serbia
novakd@uns.ac.rs



Nemanja KAŠIKOVIĆ, Assoc. Prof. Ph.D.
University of Novi Sad
Faculty of Technical Sciences
Department of Graphic Engineering and Design
Trg Dositeja Obradovića 6
21000 Novi Sad, Serbia
knemanja@uns.ac.rs



Neda MILIĆ, Ass. Prof. Ph.D.
University of Novi Sad
Faculty of Technical Sciences
Department of Graphic Engineering and Design
Trg Dositeja Obradovića 6
21000 Novi Sad, Serbia
milicn@uns.ac.rs



Sandra DEDIJER, Ass. Prof. Ph.D.
University of Novi Sad
Faculty of Technical Sciences
Department of Graphic Engineering and Design
Trg Dositeja Obradovića 6
21000 Novi Sad, Serbia
dedijer@uns.ac.rs

LASERES WITH THE SOLID EASY AND THEIR APPLICATIONS FOR GRAVING ON TRANSPARENT MATERIALS

Dragana ĐURAŠKOVIĆ
Mileta JANJIĆ

Abstract: LASER is an acronym of English words "Light Amplification by Stimulated Emission of Radiation", which in translation means an increase in light stimulated by radiation emission. In fact, the laser is a light oscillator, that is, a generator of monochromatic, coherent and directional light. The main feature of this light is the possibility of focusing on a small diameter point (<1 mm), which is impossible with natural light [2]. In this paper, the application of solid-core lasers Nd: YAG is shown for sub-surface engraving on transparent materials (crystals).

Key words: Nd: YAG laser, 3D crystal K9, modeling, sub-engraving

LASERI S ČVRSTIM JEZGROM I NJIHOVA PRIMJENA ZA GRAVIRANJE NA TRANSPARENTNIM MATERIJALIMA

Rezime: LASER je akronim od engleskih riječi „Light Amplification by Stimulated Emission of Radiation“, koji u prevodu znači, pojačavanje svjetlosti stimulisanom emisijom zračenja. Zapravo, laser je svjetlosni oscilator, odnosno generator monohromatske, koherentne i usmjerene svjetlosti. Glavno svojstvo ovakve svjetlosti je mogućnost fokusiranja na tačku malog promjera (< 1 mm), što je nemoguće kod prirodne svjetlosti [2]. U ovom radu, prikazana je primjena lasera s čvrstim jezgrom Nd: YAG, za podpovršinsko graviranje na transparentnim materijalima (kristalima).

Ključne riječi: Nd: YAG laser, 3D kristal K9, modeliranje, podpovršinsko graviranje

1. UVOD

Laser je uređaj za stvaranje i pojačavanje koherentnog elektromagnetnog najčešće monohromatskog, usko usmjerenog zračenja. Zasniva se na kvantnim pojavama prilikom prenosa energije zračenjem. Izmjena energije zračenja s atomima ili molekulima aktivnog medija u laseru (plin, kristal, plazma), umjesto apsorbovanjem, odvija se stimulisanom emisijom. To se događa kada se na atom ili molekul u pobuđenom stanju, to jest u stanju u kojem su elektroni na višem energetske nivou, djeluje bijelom svjetlošću ili elektromagnetnim poljem. Laseri se razlikuju prema vrsti aktivnog materijala koji služi za pojačavanje svjetlosti. Za rezanje i graviranje se upotrebljavaju CO₂ i Nd:YAG laseri, koji su dobili ime prema vrsti aktivnog materijala. Značaj svakog lasera je talasna dužina emitovane svjetlosti (λ). Ona je funkcija razlike energetske stanja atoma / molekula aktivnog medija. Uopšteno govoreći CO₂ laseri rade odlično na materijalima koji su slabi provodnici toplote i elektriciteta. Čisti metal i druge reflektivne površine ne

moгу da absorbuju svjetlost generisanu u CO₂ laserima tako dobro kako to mogu, svjetlost generisanu u YAG laserima. Lasersko markiranje ima svaki dan sve veću primjenu u različitim granama industrije. Primjenjuje se u elektronici, automobilskoj industriji, na polju široke potrošnje, a naročito je značajna njegova primjena u medicini. Svake godine se razvijaju nove osobine i poboljšavaju laserski sistemi. Laser proizvodi ekstremno intenzivni snop svjetlosne energije. Da bi gravirao snop se fokusira (kroz specijalno sočivo) u tačku veličine 0.01mm. Fokusirani snop je tako intenzivan da ustvari porizuje površinu materijala, i ostavlja trag ili prolazi kroz materijal i isjeća ga. U oblasti laserskog graviranja najčešće se koriste CO₂ i YAG laseri. CO₂ laser radi na principu podizanja energetske stanja molekula mješavine gasova ugljen-doksida i obično nitrogena i helijuma, dok YAG laseri koriste diodnu pumpu. Predmet istraživanja ovog rada je nastanak, razvoj i primjena čvrstostelnog Nd: YAG lasera za podpovršinsko graviranje u 3d kristalima i drugim transparentnim materijalima.

2. OSNOVNA PODJELA LASERA

Poznato je na hiljade vrsta lasera, ali većina je samo za specijalne istraživačke svrhe.

Osnovna podjela lasera je na:

pulsne lasere, lasere sa čvrstim jezgrom, gasne lasere, poluvodičke lasere, hemijske lasere, lasere s bojilima, lasere sa slobodnim elektronima [7].

3. OBLASTI PRIMJENE LASERA

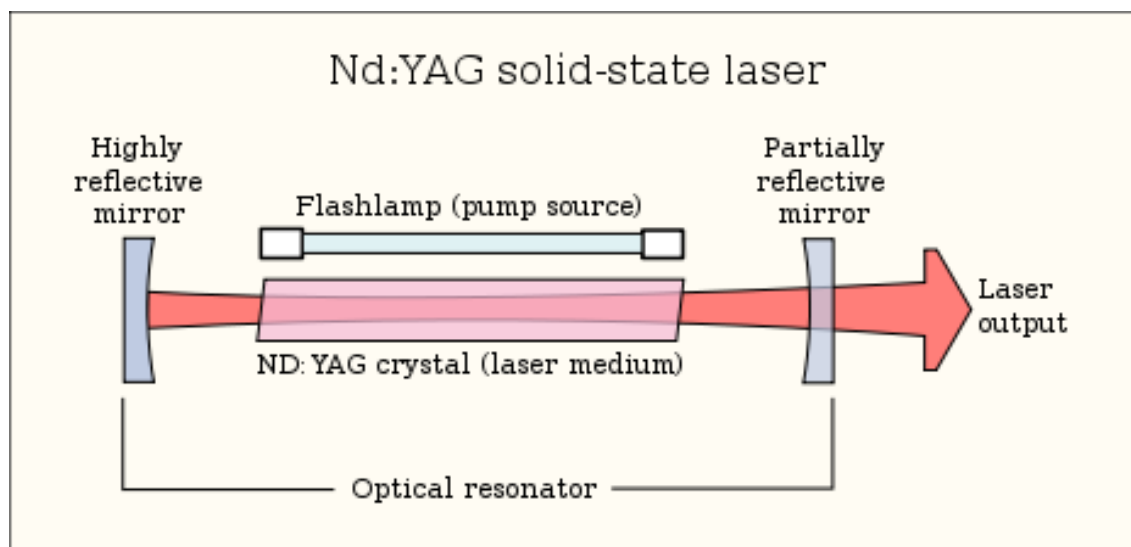
Posljednjih godina primjena lasera je doživjela pravu revoluciju, u gotovo svim oblastima ljudske djelatnosti. U tehnologiji, laser se koristi za finu obradu metalnih površina. U telekomunikacijama za modulirano lasersko zračenje i prenos podataka. Pritom se modulacija može postići promjenom amplitude (intenziteta) zračenja. Prenos je moguć direktnim zračenjem ili vođenjem kroz svjetlo vode (na primjer u telefonskim vodovima). U medicini laser služi ponajviše kao hirurški instrument za precizne operacije (na primjer oka) ili dermatološku obradu, uklanjanje površinskih tumora ili tetovaže, u meteorologiji za mjerenje udaljenosti i brzine pomjeranja oblaka (lidar), u optičkoj astronomiji u uređaju za kompjutersku korekciju deformacije slike izazvane

atmosferskim uticajima, u građevinarstvu za poravnanje terena pri gradnji puteva i nivelaciju, kod protivprovalnih alarmnih uređaja, u optičkim čitačima zvučnih zapisa kod CD-a i DVD-a, kod laserskih pisača i kopirnih uređaja itd. Zbog niske cijene, naročito poluvodičkoga lasera, koristi se i u dječim igračkama. Nd: YAG laser je našao primjenu u sljedećim oblastima: obrada metala, mjerenje udaljenosti, oznaka laserskog nišana, hirurgija, naučna istraživanja, laserska pumpa za ostale lasere (kombinovano sa frekventnim dupliranjem da se dobije zelena svjetlost 532 nm), koji se koristi za podpovršinsko graviranje u 3D kristalima i drugim transparentnim materijalima. Jedan je od najkorištenijih lasera velike snage, obično s impulsima (do dijela nanosekunde).

4. DIJELOVI LASERA

Laser se sastoji od tri osnovna dijela (Sl. 1.):

- Energija za pobuđivanje medija ili laserska pumpa,
- Laserski medij ili laserski materijal,
- Dva ili više ogledala koji stvaraju rezonantnu šupljinu ili optički rezonator [5].



- Sl. 1. Šema tipičnog lasera, koji pokazuje tri njegova osnovna dijela

4.1. Laserska pumpa

Laserska pumpa (engl. *pump source*) je dio koji osigurava energiju za rad lasera. To može biti električno pražnjenje naboja, bljeskalica (engl. *flashlamp*) elektrolyčna svjetiljka, svjetlo sa drugog lasera, hemijska reakcija ili čak eksplozivno sredstvo. Koja će se vrsta laserske pumpe upotrijebiti, zavisi o laserskom materijalu. Tako na primjer, Nd: YAG laser koristi lasersku diodu.

4.2. Laserski medij

Laserski medij (engl. *laser medium*) je glavni određujući pokazatelj na kojoj talasnoj dužini će raditi laser [5]. Može imati linijski spektar ili šire područje spektra. Laserski medij sa širim područjem spektra omogućuje

podešavanje frekvencije spektra (a time i talasne dužine), kod čvrstih materijala, kao što su kristali ili stakla. Tipični čvrsti elementi su itrij-aluminijev granat (YAG), itrij-litij fluorid (YLF), safir (aluminijev oksid) i različita stakla. Primjeri lasera sa čvrstom jezgrom su: Nd: YAG, Ti:safir, Cr: safir (obično poznat kao rubin), Cr:LiSAF (hrom s primjesama litij stroncij aluminij fluorida), Er: YLF, Nd: staklo i Er: staklo. Laseri sa čvrstom jezgrom obično koriste lasersku pumpu sa bljeskalicama ili svijetlom sa drugih lasera.

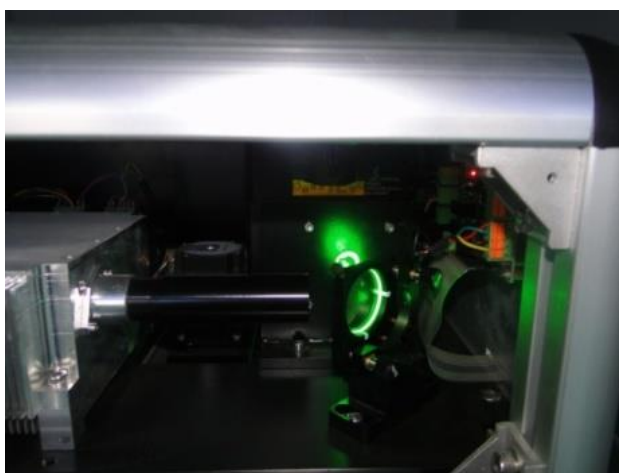
4.3. Optički rezonator

Optički rezonator (engl. *optical resonator*) predstavlja dva paralelna ogledala, smještena oko laserskog medija,

koji omogućuje povratnu vezu svjetla. Na ogledala se stavljaju optički premazi, koji određuju stepen refleksije. Uglavom, jedan je reflektor s visokim stepenom refleksije (engl. *highly reflective mirror*), dok je drugi reflektor s djelimičnim stepenom refleksije (engl. *partially reflective mirror*), koji se još naziva izlazni reflektor, zato što omogućuje da jedan dio svjetla napusti optički rezonator stvarajući izlazni snop lasera (engl. *laser output*) [5]. Svjetlo iz laserskog medija, stvoreno spontanom emisijom usljed djelovanja laserske pumpe, se reflektuje na ogledalu i vraća u laserski medij, gdje može biti pojačan stimulisanom emisijom. Reflektovanje sa ogledala i prolazak kroz laserski medij, može se dogoditi i na stotine puta, prije nego svjetlost napusti optički rezonator. Kod složenijih lasera, koristi se raspored sa 4 ili više ogledala. Konstrukcija i poravnanje ogledala, s obzirom na laserski medij, je od najveće važnosti za određivanje tačne radne talasne dužine i ostalih svojstava lasera.

5. Nd: YAG LASER

YAG laseri za svoj rad koriste diodu pumpu. Nd: YAG je čvrstostelni laser, koji emituje infracrveno zračenje talasne dužine 1064 nm. Laserski snop ovog lasera je moguće usmjeriti prema kristalu sa nelinearnim optičkim svojstvima, čime će se dobiti laserski snop sa fotonima koji imaju dvostruko veću energiju od onih koji su upali u kristal. Tako je dobijena talasna dužina od 532 nm, što odgovara zelenoj svjetlosti (Sl. 2.). Ovaj tip lasera jedini može da ostavi trag na silikonu, kao i plastici [2]. U stanju je da ostavi trag na površini bez mijenjanja strukture površine. Laseri ovih karakteristika se koriste za podpovršinsko graviranje u 3D kristalima. Spadaju u puno skuplju grupu YAG lasera jer koriste "Diode-pumped". Diodni Nd: YAG laser troši manje energije i proizvodi manje toplote, pa je i mnogo efikasniji. Prednosti su mu u odnosu na gasni CO₂ laser, što su diodni laseri daleko dužeg radnog vijeka, a hlade se vazduhom [4].



Sl. 2. Nd: YAG laser

6. SOFTVER

Korišćeni sa odgovarajućim softverom, laseri su sposobni da generišu različite rezolucije. Rezolucija se obično izražava u: tačka po inču (dot per onch) **dpi**, i određuje

kakav će detalj biti postignut; veća rezolucija – sitniji detalj. Međutim, rezolucija, takođe predstavlja i vrijeme za koje će graviranje biti izvršeno, veća rezolucija – više vremena. Većina laserskih sistema je podržana IBM kompatibilnim kompjuterima PC, sa operativnim sistemom Windows. Na raspolaganju je veliki broj programa koji nude neograničene slobode dizajniranja. Vidljiva je orijentacija proizvođača laserskih sistema, da dizajniraju svoje sisteme i prilagode ih da rade sa što većim brojem softverskih programa, tzv. Third-party program [9]. Sve mašine na kojim se radi podpovršinsko graviranje, podržane su kompjuterski. Modeliranje se izvodi u različitim CAD programima (Auto Cad, 3dsMax, Maya). Dxf verziju modela je moguće uvesti u Laser image softver, gdje se vrši priprema modela na način što se prilagođava potrebama mašine.

7. SUB SURFACE LASER ENGRAVING (SSLE)

7.1. Istorija nastanka

Još davne 1917. godine u svom radu «On the Quantum Theory of Radiation» Albert Einstein je dao teorijski koncept i predvidio izum lasera i njegove preteče masera. Maser je uređaj koji radi na jednak način kao i laser, ali u drugom frekvencijskom području. On je izvor mikrotalasa, dok je laser izvor elektromagnetskih talasa u infracrvenom i vidljivom dijelu spektra [3]. Pretekavši nekoliko izvršnih eksperimentalnih grupa, prvi laser napravio je 1960. godine Theodore H. Maiman zaposlen na Huges Research Laboratorie Malibu, California. Njegov je laser emitovao svjetlost talasne dužine 694 nm u pulsnom režimu, a lasersku emisiju je postigao stimulisanom emisijom iz rubinskog kristala pobuđenog svjetlosnom lampom. Nakon toga, laseri se počinju naveliko proizvoditi u eksperimentalnim laboratorijama širom svijeta, dok konačno razvojem tehnologije danas imamo pravu lasersku revoluciju. Podpovršinsko lasersko graviranje je tehnika otkrivena u Rusiji 80-tih godina prošlog vijeka. Prvobitno stvaranje ovih "tačaka" u optičkom staklu je bio problem" Laser Induced Damage" koji je iscrpno studiran. U to vrijeme, ideja je bila da se izabere takav kompozitni materijal u kom će tehničari moći upisati svoje ime. Biran je materijal s kojim je obezbijedena transparentnost sa minimalnom apsorpcijom toplote (Sl.3.) [4]. Ispitivanjem je utvrđena i mogućnost stvaranja komercijalne aplikacije za kontrolisano postavljanje tih tačaka unutar kristala. Tokom godina, nauka je dostigla viši nivo na ovom polju i omogućila dizajniranje slike u kristalu [4]. Devedesetih, Rusi su se pojavili na velikim sajmovima sa staklenim blokovima u kojim su gravirani 2D modeli u obliku poklona. U to vrijeme modeli su bili sastavljeni od oko 200-500 tačaka, tj. imali su krupnije zrno [6]. Ovi dekorativni pokloni su privukli veliku pažnju, ne samo zbog privlačnog izgleda, već i zbog pitanja koji se nametao posmatraču " Kako su oni to uradili ??? " Kasnije se sve više i više kompanija pojavljivalo na sajmovima sa ovim optičkim staklenim blokovima, kao i mašinama za njihovu proizvodnju (Sl.4.).



Sl. 3. Prazan kristal K9

Ova tehnika je gurnuta u drugi plan, tek nakon što je Kemin Du sa Instituta za lasersku tehnologiju u Ahenu-Njemačka, izmislio novi princip. Nova tehnologija je omogućila da se postigne 500 tačaka u sekundi. Nekoliko godina kasnije njegov sledeći izum, zasnovan na tzv. ploči lasera je dostigao astronomsku brzinu obilježavanja od 10 000 tačaka u sekundi. Ovim je drastično smanjena i krupnoća zrna, pa je finija struktura zrna omogućila ravnomjernije stvaranje 3D modela u optički čistom staklu K9 [10]. U stvari, ovako napravljena slika izgleda



Sl. 4. 3D modeli sa finom strukturom

7.3. Kretanje laserskog snopa

Kretanje laserskog zraka označava način na koji se laserski snop kreće da bi gravirao određenu sliku. Većina sistema podržava vektorsko i rastersko kretanje tj. istovremeno kretanje po X i Y osi. Rastersko kretanje, predstavlja kretanje laserske glave napred nazad. Za

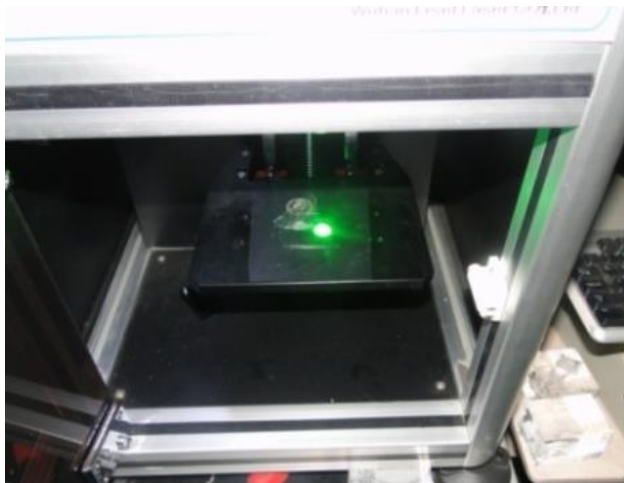
kao skulptura unutar bloka stakla. To je prva tehnika koja omogućava da se stvori "Skulptura" uz pomoć računara (CAD). Po prvi put se dešava da se 3D modeli iz unutrašnjosti računara transformišu u nešto što se pravi izvan njega [6].

7.2. Princip rada

Uobičajeno je da se intenzitet laserskog snopa izražava u Wcm^{-2} . Generalno rečeno: što je veća Watt-aža, snažniji je i laserski snop. Jednostavnije, više snage znači da laser može da gravira brže i dublje na datom materijalu u jedinici vremena. Treba imati na umu i to, da kako će brzo i duboko laser gravirati u mnogome zavisi od samog materijala koji se gravira. Važno je napomenuti, da snaga lasera zavisi i od tipa lasera. Na primer: svetlosni snop koji dolazi od diodnog YAG laser, je približno 10 puta efikasniji nego snop koji dolazi od YAG-a sa fleš lampom. Osobina softvera, koji je priključen uz lasersku mašinu, predstavlja automatsku generaciju polutonskih slika od fotografija koje su skenirane. Da bi se fotografija gravirala, prvo mora da bude konvertovana u polutonove (serija tačaka različitih veličina koje laser može da gravira). Ovo obično podrazumjeva import iz posebnog softvera koji generiše polutonove da bi se kreirale tačke za lasersku obradu. Tako laserski zrak stvara malu mikro pukotinu, a zatim se stvori na desetine hiljada dodatnih mikro pukotina, koji omogućavaju stvaranje 2D ili 3D slike [8]. Graviranje se ne može izvesti bez skenera. Scanner je oprema koja omogućava da crno bijeli dizajn bude transportovan u kompjuter, očišćen od fleka i podešen za graviranje.

vrijeme graviranja, laserski snop se kreće od vrha prema dnu radne površine, dok snop oscilira lijevo i desno (Sl. 5.). Kako se snop kreće sa lijeva na desno, tako se uključuje i isključuje i gravira lik. Pored Watt-aže, ono što determiniše snagu lasera je i veličina tačke laserskog snopa. Kao što je rečeno ranije, laserski snop je koncentrisan i fokusiran na veličinu "vrha igle" pomoću

specijalnog sočiva, koje određuje kolika će količina svjetlosti biti prisutna u određenom polju. Treći tip kretanja je galvanometarski. Sa sistemom baziranom na galvanometru, laserski snop je usmjeren pomoću malih ogledala, koji se kontrolišu galvanometrom. Kako se napon dovede do galvanometra, u ogledalu se proizvodi lik, iznad gravure [1].



Sl. 5. Laserski snop

7.4. Pozicioniranje sočiva

Na koji način se sočivo podešava za fokusnu daljinu, je jedan od elemenata koji se razlikuju od proizvođača do proizvođača. Fokusiranje predstavlja udaljavanje sočiva od materijala za graviranje na određenu distancu, da bi sočivo postiglo tačku na materijalu za graviranje. Ta distanca varira od tipa sočiva i od veličine tačke (spot size). Postoji ručno podešavanje fokusne distance, kada se oslobadjaju zavrtnji na držaču sočiva i ono se fizički pomjera na određenu distancu. Automatski način fokusiranja, podrazumjeva senzor za određivanje fokusne distance. Sve što trebate da uradite je da postavite materijal za graviranje na radnu ploču i mašina će



automatski da postavi sočivo na korektnu fokusnu distancu. Ima različitih uređaja za automatsko fokusiranje, neki na primer imaju mogućnost određivanja fokusa na transparentnim materijalima, a neki čak i na konkavnim (oblim).

7.5. Prednosti i nedostaci galvanometarskog kretanja

Najveća prednost lasera baziranih na galvanometru je brzina. Brzina graviranja je termin koji se odnosi na brzinu kretanja laserske glave preko materijala za obradu i terminise se kao inč na sekund (ips) ili cm na sekund (cps), i odnosi se na kretanje po pravoj liniji. Mnoge mašine imaju podešljivu brzinu, što je korisno za graviranje različitih materijala i različitih dubina graviranja. Ovaj tip lasera ne prolazi horizontalnu putanju, koju mora da prođe mehanički sistem, nego se pojavljuje tamo gdje ima šta da radi tj. eliminiše nepotrebno kretanje. Sledeća prednost ove tehnologije je izuzetno mala potreba za održavanjem. Međutim, ovi sistemi imaju ograničenu radnu površinu, a i koštaju dosta više nego konvencionalni. Radna površina galvanometarskog lasera je reda veličine 300x400x100 mm. Pozicioniranje sočiva je automatizovano. Materijal (optički savršen stakleni blok) se postavlja na radnu ploču, i mašina automatski usmjerava laserski snop kroz transparentni blok na mjesto početka graviranja modela.

8. PRIMJENA GOTOVIH MODELA

Kao rezultat primjene Nd: YAG lasera, sofisticiranom tehnologijom, dobijaju se jako privlačne i nesvakidašnje skulpture oku posmatrača. Interesantno je da je moguće gravirati 3D modele u kristalu, po želji posmatrača i tako ih trajno ovjekovječiti. Dijapazon primjene ove tehnologije je zaista širok. Mogu poslužiti kao prigodni pokloni, kako za fizička tako i za pravna lica, sportske saveze, državne institucije, vjerska obilježja itd. Primjeri modela su prikazani na (Sl. 6.).



Sl. 6. a) Primjeri gotovih modela



Sl. 6. b) Primjeri gotovih modela

9. ZAKLJUČAK

Na kraju se može zaključiti da je ubrzan razvoj tehnike i tehnologije doveo do prave laserske revolucije. Laser je našao svoju primjenu u gotovo svim oblastima ljudske djelatnosti. Posebno mjesto u industriji su našli laseri sa čvrstim jezgrom u koje spada i Nd: YAG laser. Zbog svojih karakteristika (emitovanja zelene svjetlosti 532 nm), našao je primjenu za podpovršinsko graviranje u 3D kristalima i ostalim transparentnim materijalima. Prednosti su mu: velika brzina rada, preciznost, tačnost, lako održavanje, dug vijek. Omogućeno je automatsko kretanje po X i Y osi, kao i podizanje radnog stola po Z osi. Međutim, ove laserske mašine imaju ograničenu radnu površinu 300x400x100 mm, zbog kretanja laserskog zraka, što je njihov nedostatak a i skuplji su od konvencionalnih.

LITERATURA

- [1] ANDREETA, M.R.B.; CUNHA, L. S.; VALES, L. F.; CARASCHI, L. C.; JASINEVICIUS, R.G. (2011) "Bidimensional codes recorded on an oxide glass surface using a continuous wave CO2 laser". *Journal of Micromechanics and Microengineering*
- [2] BAUER, B. (2006) Doktorski rad, Optimiranje parametara laserskog zavarivanja čelika za poboljšavanje; Fakultet strojarstva i brodogradnje, Zagreb.
- [3] BAN, T. (2007.-2008.) Femtosekundni laseri – preciznost u vremenu i frekvenciji, Matematičko-fizički list LVIII 2.

- [4] ĐURAŠKOVIĆ, D.; JANJIĆ, M. (2017) Primjena Nd:YAG lasera za podpovršinsko graviranje u 3D kristalima, KODIP 2017, Budva.
- [5] KOECHNER, W. (1992) *Solid-State Laser Engineering*, 3rd ed., Springer-Verlag.
- [6] PERSAD, R. (2013) *Subsurface Laser Engraving, the Ultimate Glass Decoration Technique*.
- [7] WEBER, MARVIN, J. (1999) *Handbook of laser wavelengths*, CRC Press, [ISBN 0-8493-3508-6](https://doi.org/10.1080/08493350802638666).
- [8] www.engravinglaser.net (2012) Sub Surface Laser Engraving". Engraving Laser./ Retrieved.
- [9] www.graviranje.wordpress.com, 11.05.2014.
- [10] www.princessglassworld.com/world-of-glass-decoration/sub-surface-laser-e.

KORESPODENCIJA



Dragana ĐURAŠKOVIĆ, mr.sci
DM KRISTAL d.o.o.
Vasa Raičkovića 29,
81000 Podgorica, Montenegro
draganadjuraskovic94@gmail.com



Mileta JANJIĆ, Prof. D.Sc. Eng.
University of Montenegro
Mechanical Engineering Faculty
Bul. Džordža Vašingtona bb
81000 Podgorica, Montenegro
mileta@ac.me

**HYDRO AND THERMAL
POWER PLANTS**

DESIGN OF WATER HAMMER CONTROL STRATEGIES IN HYDRPOWER PLANTS

Anton BERGANT
Jernej MAZIJ
Uroš KARADŽIĆ

Abstract: Hydropower plants play an important role in the growth of the renewable energy sector. The main objective of the paper is to present, discuss and assess critical parameters which may cause unacceptable water hammer loads in hydropower plants. Water hammer is caused by flow disturbances in a conduit from one steady state to another. It induces pressure rise or drop in hydraulic systems, rotational speed variation in hydraulic turbomachinery and level fluctuation in surge tanks and air chambers. Design principles of water hammer control strategies (mitigation of excessive loads) are outlined including operational scenarios (closing and opening laws), surge control devices (flywheel, surge tank, regulating valve, air valve, etc.) or redesign of the pipeline components. Water hammer models and solutions are briefly discussed in the light of their capability. Case studies include hydropower plants with long fluid conveying systems (open channels, tunnels) and water hammer control devices (surge tank, regulating valve).

Key words: hydropower plant, water hammer control, surge tank, regulating valve

1. INTRODUCTION

Modern hydropower systems should be able to cover peak demands and to store surpluses of grid energy, in particular that coming from intermittent generators associated with wind and solar power. There are several key parameters associated with the design of a new or refurbishment of aging hydropower plant including safety, efficiency, availability and profitability of the plant. Refurbished plant by definition starts from old basic infrastructure which may raise issues not encountered with new plant: some ageing components cannot be refurbished adequately (in particular civil works), changes in the role of the plant in the energy system (increased operational flexibility), increase of plant output and changes in the environment of the plant. The objective of this paper is to present, discuss and assess the critical parameters which may cause unacceptable water hammer loads in hydropower plants. Flow-induced vibrations (draft-tube surge, rotor-stator interactions) [1] are beyond the scope of this paper. Water hammer is caused by turbine load acceptance and reduction, load rejection under governor control, emergency shutdown and unwanted runaway, and closure and opening of the safety shutoff valve. It induces pressure rise or drop in hydraulic systems, rotational speed variation in hydraulic turbomachinery (turbines, pump-turbines, storage pumps) and level fluctuation in surge tanks and air chambers. Design principles of water hammer control strategies (mitigation of excessive loads) are outlined including operational scenarios (closing and opening laws, limitation of operating conditions), surge control devices (flywheel, surge tank, regulating valve, air valve, etc.), or redesign of the pipeline components. Theoretical elastic and rigid water hammer models and solutions are briefly presented and

discussed. The paper concludes with two case studies including hydropower plants with long fluid conveying systems (open channels, headrace and tailrace tunnels) and water hammer control devices (surge tank, regulating valve).

2. DESIGN PRINCIPLES OF WATER HAMMER CONTROL STRATEGIES

Large transient loads may disturb overall operation of the hydropower plant and damage the system components. Water hammer [2] can be kept within the prescribed limits (e.g. pressure in the flow-passage system, turbine rotational speed, surge tank water level, etc.) with the following methods: (1) alteration of operational regimes, (2) installation of surge control devices in the system and (3) redesign of the flow-passage system layout.

2.1. Alteration of operational regimes

Alteration of operational regimes includes appropriate regulation of the wicket gate and runner blade maneuvers in reaction turbines, and turbine distributor (needle valve) and jet deflector maneuvers in impulse turbines. Typically a two-speed wicket gate closing time function (adding a cushioning stroke) significantly improves reaction turbine safe operation. Opening of runner blades during Kaplan or bulb turbine shutdown (normal, mechanical quick stop, emergency) results in favourable blade operation, improved over-speed performance and reduced negative axial hydraulic thrust. Appropriate setting of closing/opening times of the shutoff valves contributes to safer operation of these devices in emergency and exceptional operating conditions. A draft tube gate can be used to protect axial turbine against runaway. In addition, sluicing operation of the low-head axial turbines can attenuate open channel

waves during transient regimes. Limitation of operating regimes (reduced discharge) is yet another option. This measure may be considered as temporary one before more effective method is devised.

2.2. Installation of surge control devices

Installation of surge control devices in the system alter the system characteristics (shorten the active conduit length, reduce the liquid compressibility, increase the turbine unit inertia). The protective devices that may be installed along the inlet and outlet conduit or added to the hydropower system components include:

- (1) increased turbine unit inertia (adding flywheel to small units, increasing the generator inertia);
- (2) resistors (to absorb excessive power);
- (3) surge tank in headrace and/or tailrace (shortens the active conduit length, improves governing stability);
- (4) air cushion surge chamber (requires compressed air supply);
- (5) pressure-regulating valve (operates synchronously with the turbine wicket gates);
- (6) pressure-relief valve (opens at a set pressure, small units);
- (7) rupture disc (bursts at a set pressure, small units);
- (8) aeration pipe (attenuates water column separation);
- (9) air valve (attenuates water column separation, reduces negative axial hydraulic thrust).

2.3. Redesign of the flow-passage system layout

Redesign of the flow-passage system layout includes:

- (1) change of water conveyance profile (high point);
- (2) change of conduit dimensions (diameter, length);
- (3) different position of system components (valve).

Operational, safety and economic factors are decisive for selection of the type of protection against the undesirable water hammer effects. A number of alternatives should be investigated before the final design. The most convenient water hammer control method in the hydropower plant is the alteration of operational regimes. It is expensive to install additional surge control devices in the system except if this cannot be achieved by the first method. It is rarely feasible to redesign the proposed flow-passage system. Water hammer control devices should operate smoothly in normal operating conditions. These conditions include the turbine start-up, load acceptance, load reduction and total load rejection (mechanical quick stop, electrical emergency shutdown). Emergency conditions are load rejections in which the runner blades (axial and diagonal turbines) fail to operate or partial runaway occurs. The turbine runaway is considered as a catastrophic transient regime. Water hammer analysis should be performed for normal, emergency and catastrophic operating conditions [2].

3. WATER HAMMER ANALYSIS

Water hammer is the transmission of pressure waves along the pipeline resulting from a change in liquid flow velocity (discharge). It leads to higher dynamic loads on plant components during transient operating events (rapid load acceptance and reduction, unit shutdown). This requires a thorough transient analysis. Hydraulic transient analysis is traditionally undertaken with deterministic models [2], [3]

that treat a number of transient regimes based on experience, guidelines and codes. In addition, parametric analysis accounts for uncertain parameters (e.g. friction, wave speed, turbine performance characteristics). These results form the basis for risk analysis to transients in hydropower plant that includes identification of critical regimes, evaluation of the risk (low, high) and risk management (modifications to reduce the risk) [4]. It is clear the scope of analysis is dependent on the type of the machine and complexity of the plant layout.

Water hammer in hydropower plants can be calculated using either elastic or rigid water hammer theory [2], [3]. The elastic liquid column model is used for the systems with relatively long tunnels and penstocks, and systems with rapid transients. Slightly compressible liquid and elastic pipe walls are assumed in the elastic column model. Unsteady flow in closed conduits is described by two one-dimensional equations; the continuity equation and the equation of motion. The hyperbolic set of equations is solved by the method of characteristics. For run-of-river power plants with relatively short inlet and outlet conduits the rigid column model is recommended. In this case the length of the conduit is of the same order as the cross-sectional dimensions. Incompressible liquid and rigid pipe walls are assumed in the rigid column model. Rigid water hammer is described by the one-dimensional equation of motion for unsteady pipe flow. The equation can be solved numerically by using the Runge-Kutta method. Elastic and rigid column equations are solved simultaneously with the boundary condition equations (turbine, valve, surge tank, reservoir, etc.) [2], [3]. The hydraulic turbomachine may undergo turbine, pump or pump-turbine operating modes. The governed turbine boundary condition is described by the turbine (head balance equation, dynamic equation of rotating masses) and the governor (dynamic equation which relates the pump-turbine rotational speed change to the position of the regulating mechanism(s)), and it is coupled with pipeline water hammer equations. The relationship among influential turbine variables is presented in the form of the experimentally predicted characteristics (head, torque, axial force). The complete set of the hydraulic turbomachine-governor-pipeline equations should be used for the case of load reduction in which the turbine speed is regulated by the governor. The governor equations are omitted in analysis for the case of turbine sudden load rejection in which the unit speed change is controlled by the turbine net torque only. The theoretical description of the actual hydropower system invariably introduces assumptions and approximations [5] which may have negligible influence in certain applications but introduce significant systematic errors in other circumstances. Field test cases are needed to verify water hammer models and adequacy of design strategies.

4. CASE STUDY 1: TURBINE EMERGENCY SHUTDOWN IN ZLATOLIČJE HPP

The Slovenian run-off river type Zlatoličje HPP has been recently refurbished. Two old Kaplan turbines were upgraded with new runners of larger output capacity each of 80 MW. Two Kaplan units are embedded into large-scale open channel system (Fig.1). The length of the inlet channel

is of 17,200 m and the outlet channel is 6,200 m long. The channels are of trapezoidal profile with its bottom and side walls concrete lined.



Fig. 1: Layout of Zlatoličje HPP powerhouse, Slovenia



Fig.2: Lowering of 80 MW Kaplan runner in turbine pit; Zlatoličje HPP

Each of the two Kaplan turbines (Fig. 2) is equipped with a pressure regulating valve (PRV). The PRV is comprised of five vertical vanes connected via the rod to servomotor and controlled by the turbine governor. The continuous

measurement of the channel water level at the turbine inlet, and pressures in the turbine scroll case and draft tube indicates that water level oscillations in the two open channels are small and within the prescribed limits during water hammer events. The PRV attenuates free surface waves in both channels [6]. Therefore, the constant water levels at the turbine inlet and the turbine outlet are assumed in water hammer calculations. Analysis of free surface waves in both channels is beyond the scope of this paper. Fig. 3 shows action of the PRV during shutdown from full-load. The detailed plant layout used for water hammer calculations can be found in Bergant et al [6]. The length of the conduit is of the same order as the cross-sectional dimensions and the cross-sectional area is of complex shape. The standard one-dimensional elastic column water hammer model cannot accurately predict the physics of wave transmission and reflection in very short pipelines. The rigid column model is recommended to be used for this case. The dimensions of the inlet conduit, scroll-casing and draft tube used in the one-dimensional rigid water hammer model are expressed as geometrical characteristics $G_u = 0.876 \text{ m}^{-1}$ and $G_d = 0.549 \text{ m}^{-1}$, respectively ($G = \Sigma(L/A)$; L = length, A = area).

Emergency shutdown of the Kaplan turbine unit from 75 MW load is presented as the case of one of the most severe normal operating regimes with respect to large transient loads. The turbine is disconnected from the electrical grid followed by the complete closure of the wicket gates while the runner blades open to their fully open position (Fig. 4(a)). The PRV blades first open to about 90 % opening synchronously with the wicket gate closure (Fig. 4(a)) and then start to close at a very slow rate to its fully closed position. The PRV linear full-stroke closing time is twenty minutes.



Fig.3: Action of pressure regulating valve during turbine shutdown in Zlatoličje HPP

The computed maximum momentary scroll case pressure head (H_{sc}) of 35 m practically coincides with the averaged measured one; there is a reasonable agreement between the calculated and measured draft tube pressure heads too (Fig. 4(b)). The agreement between the computed maximum rotational speed rise of 35 % and the measured one is good too (Fig. 4(c); $n_o = 125 \text{ min}^{-1}$). The maximum scroll case pressure head and the maximum speed rise are within the guaranteed limits (43.9 m and 45 %, respectively).

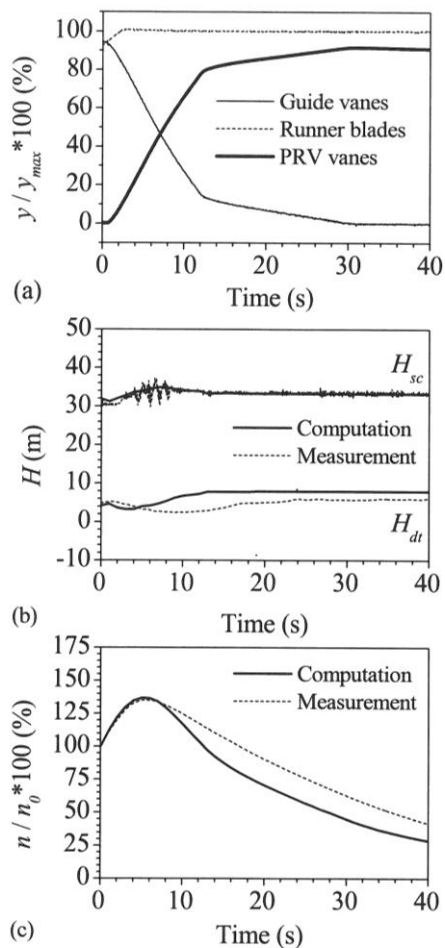


Fig. 4: Emergency shutdown in Zlatoličje HPP ($P = 75$ MW): Guide-vane, runner-blade and PRV-vane servomotor strokes y (a), scroll case and draft tube heads H (b) and unit rotational speed n (c) [6]

5. CASE STUDY 2: TURBINE EMERGENCY SHUTDOWN IN PERUĆICA HPP

Montenegrin Perućica HPP is comprised of a concrete tunnel (length 3335 m, diameter 4.8 m), surge tank (Fig. 5) and three parallel penstocks (Fig. 6) with horizontal-shaft Pelton turbines built at their downstream ends.



Fig. 5: Above-ground layout of the surge tank in Perućica HPP, Montenegro

The maximum water level at the intake is 613 m.a.s.l. and the minimum 602.5 m.a.s.l. The surge tank is of cylindrical type (diameter 8 and 12 m) with an expansion and overflow. At the surge tank intake there is a non-symmetrical orifice. The length of each steel penstock is about 2000 m whereby penstock I feeds two turbine units (A1 and A2) with rated unit power of 39 MW each, penstock II feeds three turbine units (A3, A4 and A5) of 39 MW each and penstock III feeds two units (A6 and A7) of 59 MW each.

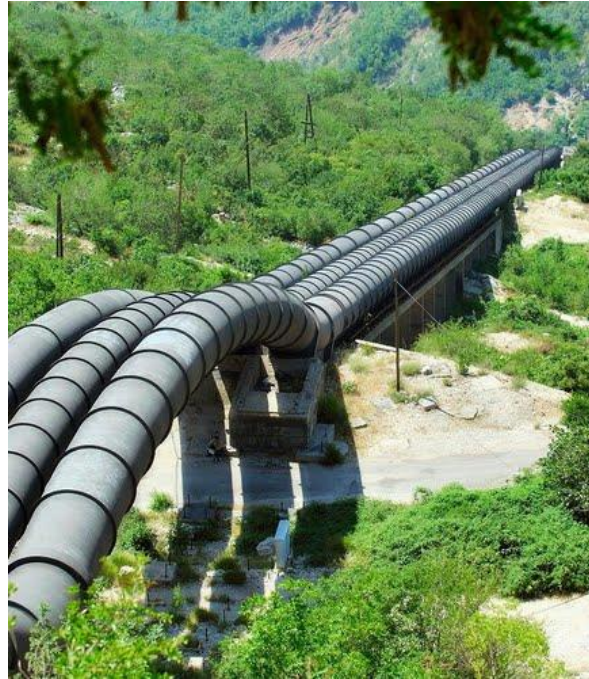


Fig.6: Layout of three parallel steel penstocks in Perućica HPP

All seven turbine units are embedded in powerhouse (Fig. 7) with two tailrace tunnels (one for units A1 to A5, one for units A6 and A7). The runner diameter of twin type turbine units A1 to A5 is 2400 mm and for twin type turbine units A6 and A7 is 2100 mm. Two safety spherical valves are attached to each turbine unit. A detailed description of the Perućica HPP flow-passage system with its all main characteristics can be found in Karadžić et al [7]. Rehabilitation of turbine units has been performed in several stages. This includes supply of new distributors (needle valves) and refurbishment of the pertinent spherical valves (replacement of seals and actuating servomotors) for the first four turbine units, and finally, supply of six new Pelton wheels for 39 MW units and three wheels for 59 MW units.

The standard one-dimensional elastic column water hammer model is used for transient analysis because of long tunnel and penstocks. Method of characteristics based software package with a novel Pelton turbine boundary condition has been validated for a number of typical transient regimes [7] in Perućica HPP. Emergency shutdown of turbine unit A1 from initial power of 39.5 MW is presented in this paper. The corresponding discharge in the penstock I: $8.4 \text{ m}^3/\text{s}$, penstock II: no discharge and penstock III: $22 \text{ m}^3/\text{s}$.



Fig. 7: Perućica HPP powerhouse with seven Pelton turbine units

Numerical and measured heads at the turbine inlet (H) for emergency shutdown of the unit A1 are compared in Fig. 8(b). The computed and the measured total needle closure times are the same (55.3 s - see Fig. 8(a)). Maximum measured head of 557.7 m occurs when the nozzle is fully closed. Head rise for this case is 24.5 m. Maximum calculated head is 556.4 m (two-speed closure; the cushioning stroke is 2.5 %). The maximum calculated head matches the measured one. Calculated and measured heads are much lower than the maximum permissible head of 602 m. Fig. 8(c) shows comparison between computed and measured rotational speed. The maximum measured turbine rotational speed rise of 8.1 % occurs at time of full deflection of the jet (at 1.6 s). The maximum computed turbine speed rise of 8.0 % agrees well with the measured one. After jet deflector deflects all the water into the tailrace, the computed turbine speed decrease reasonably agrees with measured one. The maximum turbine inlet pressure head and the maximum speed rise are within the guaranteed limits.

6. CONCLUSIONS

Water hammer in hydropower plants is caused by turbine load acceptance and reduction, load rejection under governor control, emergency shutdown and unwanted runaway, and closure and opening of the safety shutoff valve. It induces pressure rise or drop in hydraulic systems, rotational speed variation in hydraulic turbomachinery (pumps and water turbines) and level fluctuation in surge tanks and air chambers.

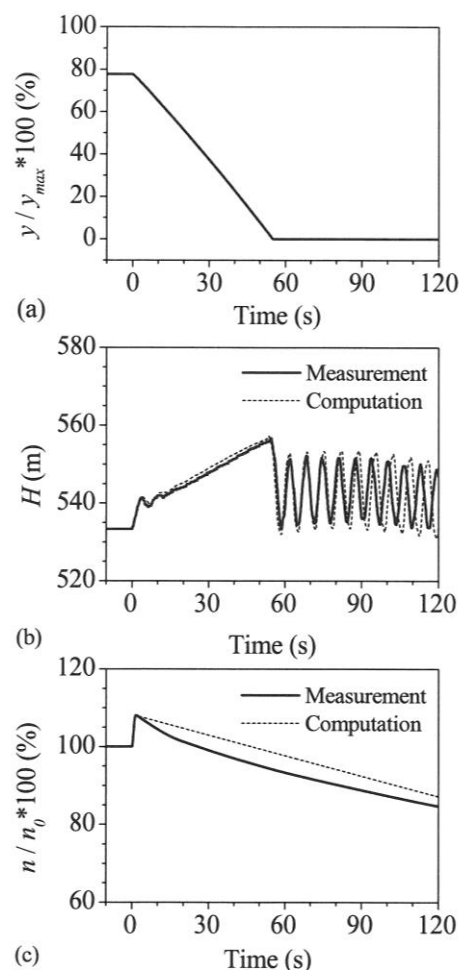


Fig. 8: Emergency shutdown of one Pelton turbine in Perućica HPP ($P = 39.5$ MW): Needle valve servomotor strokes y (a), turbine inlet head H (b) and unit rotational speed n (c) [7]

The paper presents design principles of water hammer control strategies (mitigation of excessive loads) including operational scenarios (closing and opening laws), surge control devices (flywheel, surge tank, regulating valve, air valve, etc.) and redesign of the pipeline components. Classical theoretical water hammer models and solutions are briefly discussed in the light of their capability and availability. Case studies include hydropower plants with long fluid conveying systems (open channels, headrace and tailrace tunnels) and water hammer control devices (surge tank, regulating valve). Due to very long inflow and outflow open channels in Zlatoličje HPP a special vaned pressure regulating device attenuates extreme pressures in Kaplan turbine flow-passage system and controls unsteady flow in both open channels. Water hammer in inlet and outlet short conduits is controlled by appropriate adjustment of the wicket gates and runner blades closing/opening laws. Transients in long tunnel of Perućica HPP are controlled by cylindrical type surge tank with an expansion and overflow. Water hammer in the three penstocks that feed seven Pelton turbines is controlled by appropriate adjustment of the distributor needle valve closing/opening maneuvers.

The agreement between computed and measured results for emergency shutdown cases in both hydropower plants is reasonable. Most important, water hammer control means keep transient pressure heads and turbine rotational speed rise within the prescribed limits.

REFERENCES

- [1] DÖRFLER, P., SICK, M., COUTU, A. (2013) *Flow-induced pulsation and vibration in hydroelectric machinery. Engineer's guidebook for planning, design and troubleshooting*, Springer.
- [2] CHAUDHRY, M.H. (2014) *Applied hydraulic transients*, Springer.
- [3] WYLIE, E.B., STREETER, V.L. (1993) *Fluid transients in systems*, Prentice Hall.
- [4] ZOBELI, A., NICOLET, C., VUANDES, E. (2011) *Risk analysis of the transient phenomena in a hydropower plant installation*, Proceedings of the International Conference "HYDRO 2011", Prague, Czech Republic, CD-ROM, Paper 24.04
- [5] ANDERSON, A., BERGANT, A. (2008) *Issues in 'benchmarking' fluid transients software models*, Proceedings of the 10th International Conference "PRESSURE SURGES", Edinburgh, United Kingdom, pp 519-537
- [6] BERGANT, A., GREGORC, B., GALE, J. (2012) *Numerical and in-situ investigations of water hammer in Drava river Kaplan turbine hydropower plants*,

IOP Conference Series: Earth and Environmental Sciences, Vol.15, Paper 052001

- [7] KARADŽIĆ, U., BERGANT, A., VUKOSLAVČEVIĆ, P. (2009) *A novel Pelton turbine model for water hammer analysis*, Strojniški vestnik - Journal of Mechanical Engineering, Vol.55, No.6, pp 369-380

CORRESPONDANCE



Anton BERGANT, Assoc. Prof, Ph.D.
Litostroj Power d.o.o.
Litostrojska 50
1000 Ljubljana
Slovenia
anton.bergant@litostrojpower.eu



Jernej MAZIJ, B.Sc.
Litostroj Power d.o.o.
Litostrojska 50
1000 Ljubljana
Slovenia
jernej.mazij@litostrojpower.eu



Uroš KARADŽIĆ, Assoc. Prof, Ph.D.
University of Montenegro
Mechanical Engineering Faculty
Bul. Džordža Vašingtona bb
81000 Podgorica, Montenegro
urosk@ac.me

THE NUMERICAL CALCULATION BIFURCATION A6 OF PIPELINE C3 AT HPP “PERUCICA”

Milorad BURIĆ
Radoje VUJADINOVIĆ
Igor KRESOJEVIĆ
Slaviša ĐURIŠIĆ
Marko LUČIĆ

Abstract: This paper presents the results of numerical calculation bifurcation A6 of pipeline C3 at HPP “Perucica”, which was realized in the summer of 2007 and spring of 2008, from the team of experts led by Dr. Milorad Miso Buric, the full professor of the Faculty of Mechanical Engineering in Podgorica and Head of the Center for transport machines and metal constructions (CETIM). The calculations were obtained at the critical points of the internal wall of the bifurcation that is the tension greater than the boundary of the large elongations for Nioval 47 steel, so it was concluded that there were cracks in these places. And indeed, when the protective paint was removed in these places, a large number of cracks were discovered. These cracks were then testing by the Institute of Black Metallurgy from Niksic and performed their analysis. The aforementioned expert team gave a written recommendation to the management of HPP “Perucica” to perform reconstruction of the bifurcation, emphasizing that the situation is very critical. In April 2016, Lahmeyer International GmbH, Germany, in Study of measures and works during Phase II of reconstruction for HPP “Perucica”, explicitly requires the reconstruction of the A6 bifurcation to be carried out, and additional surveys include other parts of the pipeline.

Key words: Numerical calculation of the tension state, critical tension, pipeline, cracks, reconstruction

THE NUMERICAL CALCULATION BIFURCATION A6 OF PIPELINE C3 AT HPP “PERUCICA”

Abstract: U ovom radu su prikazani rezultati numeričkog proračuna račve A6 cjevovoda C3 HE “Perucica” koji je u ljeto 2007. i proljeće 2008. godine realizovao ekspertski tim pod rukovodstvom dr Milorada Miša Burića, redovnog profesora Mašinskog fakulteta u Podgorici i rukovodioca Centra za Transportne mašine i Metalne konstrukcije (CETIM). Proračunom su na kritičnim mjestima unutrašnjeg zida račve dobijeni naponi veći od granice velikih izduženja za čelik Nioval 47 pa se došlo do zaključka da se na tim mjestima nalaze pukotine. I zaista, kada se na tim mjestima skinula farba otkriven je veliki broj pukotina. Ove pukotine je zatim ispitao Institut za crnu metalurgiju iz Nikšića i izvršio njihovu analizu. Gore pomenuti ekspertski tim je dao pismenu preporuku menadžmentu HE “Perucica” da izvrši rekonstrukciju račve naglašavajući da je situacija veoma kritična. U aprilu 2016. godine firma Lahmeyer International GmbH, Germany u Studiji mjera i radova faze II za HE Perucica izričito zahtijeva da se izvrši rekonstrukcija račve A6 a da se dodatnim istraživanjima obuhvate ostali djelovi cjevovoda.

Gljučne riječi: numerički proračun naponskog stanja, kritični naponi, cjevovod, pukotine, rekonstrukcija.

1. UVOD

Na slici 1 je prikazan prostorni model cjevovoda C3 HE “Perucica”. Na njemu se nalazi račva A6 (slika 2.) koja usmjerava vodu na agregate A6 i A7 i predstavlja jedno od najsloženijih i najosjetljivijih mjesta u cjevovodu C3. Ta složenost račve je bila jedan od razloga zašto smo

veoma odgovorno i studiozno pristupili njenom ispitivanju.

U okviru Elaborata(1) ekspertski tim pod rukovodstvom dr Milorada Miša Burića, redovnog profesora Mašinskog fakulteta u Podgorici i rukovodioca Centra za Transportne mašine i Metalne konstrukcije (CETIM) je izvršio numerički proračun račve A6 cjevovoda C3 HE “Perucica”[1].

Proračunom su na kritičnim mjestima unutrašnjeg zida račve dobijeni naponi veći od granice velikih izduženja za čelik Nioval 47 od kojeg je račva napravljena pa se došlo do zaključka da se na tim mjestima vjerovatno nalaze pukotine. I zaista, kada se na tim mjestima skinula farba otkriven je veliki broj pukotina. Ove pukotine je zatim ispitaio Institut crne metalurgije iz Nikšića [2] i izvršio njihovu analizu. Gore pomenuti ekspertski tim je dao pismenu preporuku [1] menadžmentu HE "Perućica" da izvrši rekonstrukciju račve naglašavajući da je situacija kritična. U aprilu 2016.godine firma Lahmeyer International GmbH, Germany u Studiji mjera i radova faze II za HE Perućica [3] izričito zahtjeva da se izvrši rekonstrukcija račve A6 a da se dodatnim istraživanjima obuhvate ostali djelovi cjevovoda

2. NUMERIČKI PRORAČUN RAČVE A6 CJEVOVODA C3

2.1. Granični uslovi

Da bi se uradio detaljan proračun račve napravljen je kompletan prostorni model cjevovoda C3 od temelja T9 do agregata, dužine oko 200 m sa svim postojećim račvama (Slika 1.). Model je urađen veoma precizno i postavljeni su korektno granični uslovi.

Ovakav posao je podrazumijevao pravljenje izuzetno velikog geometrijskog modela, postavljanje mreže ogromnog broja konačnih elemenata, postavljanje velikog broja oslonaca a zatim nanošenje opterećenja od pritiska vode i težine konstrukcije. Ukupan broj konačnih elemenata je 2.429.397 tipa tetraedar i 680 GAP elemenata upotrijebljenih za modeliranje oslonaca. Rezultati dobijeni ovakvim postupkom su opravdali veliki trud, znanje i uloženo vrijeme.



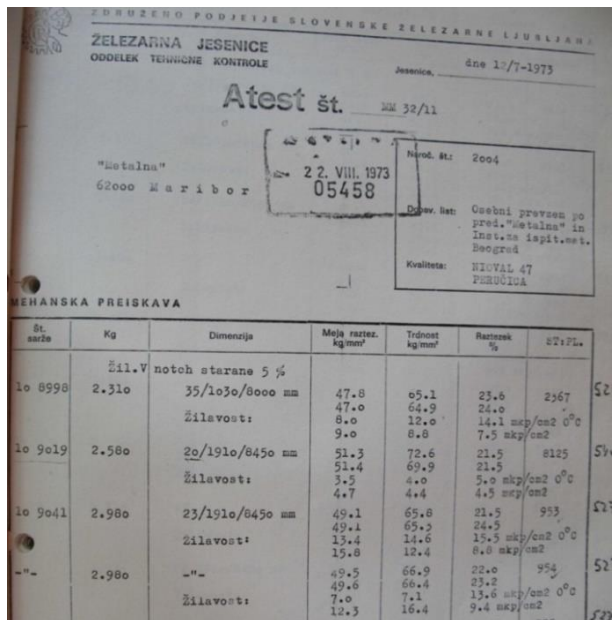
Slika 1. Prostorni model cjevovoda C3 od temelja T9 do agregata

Pri pravljenju geometrijskog modela račve A6 veliku pomoć nam je predstavljala spremnost osoblja HE „Perućica“ da nam stavi na raspolaganje postojeću tehničku dokumentaciju. No uprkos tome nedostajao je dio ove dokumentacije tako da smo je, uz njihovu pomoć, dobili od izvođača radova na ovom cjevovodu „METALNE“ Maribor. Ovo naglašavamo iz tog razloga što je poznato da geometrija konstrukcije dominantno utiče na raspored opterećenja u njoj (prečnici cijevi, debljine limova, geometrija šavova i sl.). Takođe smo mjerenjima na licu mjesta dolazili do neophodnih dimenzija račve. Na taj način smo napravili jedan dovoljno precizan geometrijski model račve.



Slika 2.

Karakteristike materijala od kojih je napravljen cjevovod C3 smo uzeli iz „Dokumentacije o kontroli materijala i kvaliteta izrade cjevovoda pod pritiskom za HE Perućica-treća faza“ koju je uradio Institut za ispitivanje materijala, Beograd 1975 godine. Slika 3 prikazuje fotografiju atesta, a Tabela 1 mehaničke karakteristike mikrolegiranog konstruktivnog čelika NIOVAL 47 od kojeg je izrađen cjevovod C3.



Slika 3.

Za potrebe korišćenog softvera materijal račve A6 je modeliran aproksimativnom krivom očvršćavanja čelika NIOVAL 47. Pošto je kriva nelinearna, u programu je korišćena njena aproksimacija u obliku bilinearne krive napon–deformacija sa uslovnom granicom razvlačenja $R_{0.2}$ i zateznom čvrstoćom R_m koja je prikazana na slici 4.

Table 1: Mehaničke karakteristike NIOVAL 47

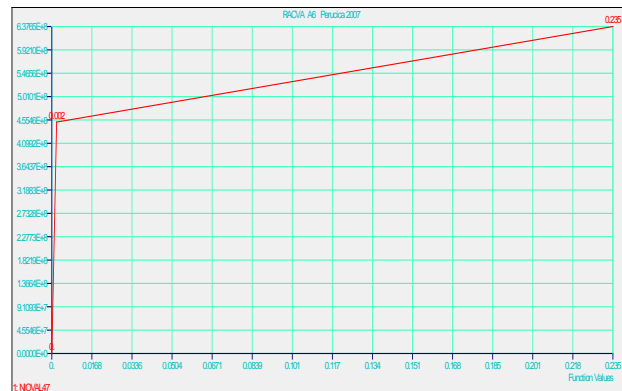
NIOVAL 47	Jedinice	Vrijednost
Modul elastičnosti:	daN/cm ²	$E = 1.95 \cdot 10^6$
Modul klizanja	daN/cm ²	$G = 0.75 \cdot 10^6$
Uslovna granica razvlačenja	daN/cm ²	$R_{0.2} = 4700$
Zatezna čvrstoća	daN/cm ²	$R_m = 6500$
Izduženje	%	$A_{10} = 30.$
Poasson-ov koeficijent		$\mu = 0.3$

Na slici 5 je prikazana mreža konačnih elemenata u zoni račve A6.

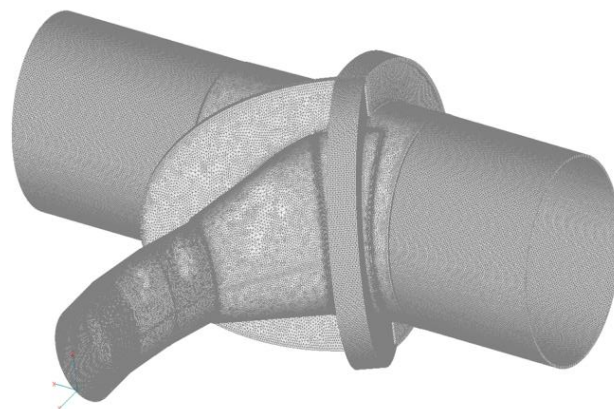
Kao osnovno opterećenje račve se pojavljuje pritisak vode, koji za horizontalnu ravan koja prolazi kroz osu cjevovoda iznosi $p = 50,994$ bar. Ova vrijednost je dobijena mjerenjem. U drugim tačkama po unutrašnjosti cjevovoda pritisak se mijenjao zavisno od prirastaja visinske koordinate (z) u odnosu na centar koordinatnog sistema koji je postavljen na rastojanju od 0.99003 m ispod ose cjevovoda u račvi A6, a po formuli:

$$p = 5099400 + 1000 \cdot 9.81 \cdot (0.99003 - z) \quad (1)$$

Takođe je uzeta u obzir i težina samog cjevovoda.



Slika 4.



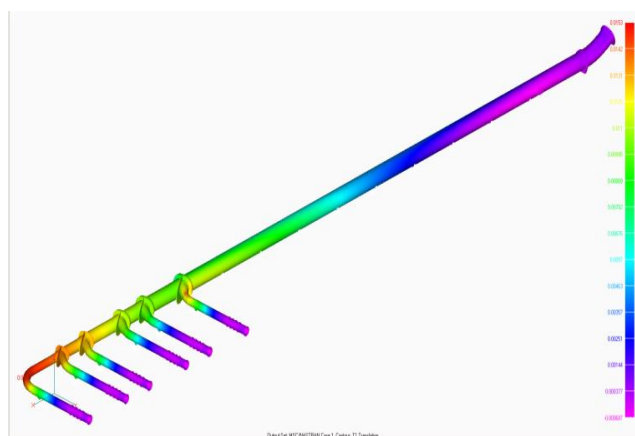
Slika 5.

2.2. Analiza pomjeranja cjevovoda

U prvom koraku smo dobili napone i pomjeranja bez uticaja sila trenja u osloncima. U drugom koraku smo vertikalne reakcije oslonaca množili sa koeficijentom trenja $k = 0.05$ koji odgovara ležištu izrađenom od teflona i nerđajućeg čelika. Zatim smo horizontalne reakcije usmjerili u suprotnom smjeru od rezultante pomjeranja cjevovoda C3 u tačkama ležišta. Na taj način smo dobili nove rezultate napona i pomjeranja koji su bili realniji od dobijenih u prethodnom koraku. Dobijeni rezultat pomjeranja račve A6 u pravcu X-ose je iznosio 16 – 17 mm. Upoređivanje ovog pomjeranja sa stvarnim (izmjerenim) je pokazalo da je stvarno pomjeranje znatno manje i iznosi 10.3 mm. U sledećim koracima smo povećavali prosječni koeficijent trenja u osloncima sve dok nismo dobili pomjeranje koje je jako blizu izmjerenoj vrijednosti (10 – 10.5 mm). Za to pomjeranje je koeficijent trenja iznosio $k = 0.4$. To nam jasno govori o prevelikom otporu koji se javlja u osloncima usled gubitka kvaliteta površina oslonaca (teflon – nerđajući čelik). Napominjemo da je izračunati koeficijent trenja veći i od koeficijenta trenja čelika po čeliku ($k = 0.3$).

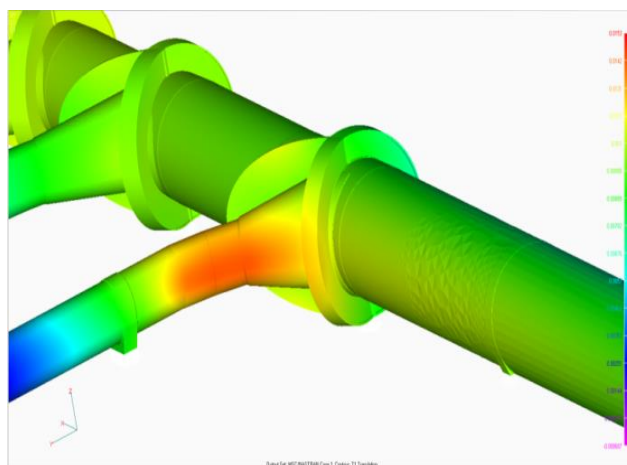
Na ovaj način smo se maksimalno približili stvarnim uslovima rada ovog dijela cjevovoda C3, i na taj način dobili napone i pomjeranja u njemu. Na slikama 6, 7 i 8 su prikazana pomjeranja u X pravcu kako posmatranog dijela cjevovoda C3 tako i same račve A6.

Sa slike 6 se može zaključiti da su maksimalna računska pomjeranja posmatranog cjevovoda 15.3 mm i ostvaruju sa na krivini šeste odvodne cijevi cjevovoda C3.



Slika 6. Pomjeranja cjevovoda C3 u X pravcu

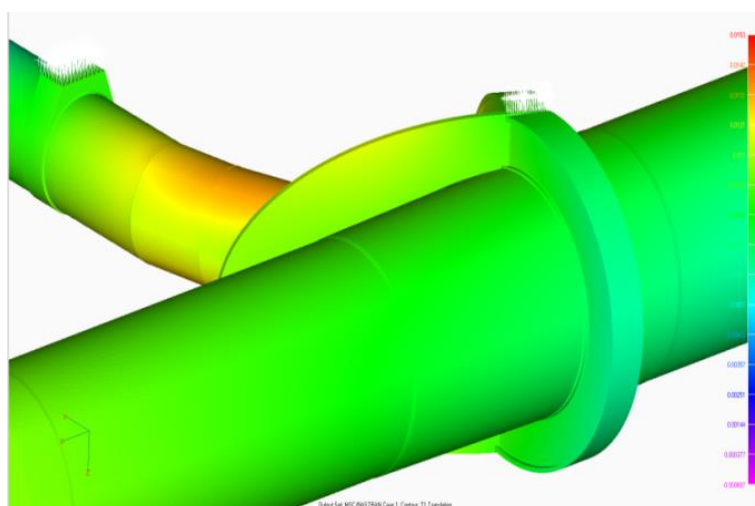
Sa slike 7 se vidi da su značajna pomjeranja i na račvi A6 tj. na krivini prve odvodne cijevi cjevovoda C3. Na tom mjestu maksimalna pomjeranja iznose oko 14 mm.



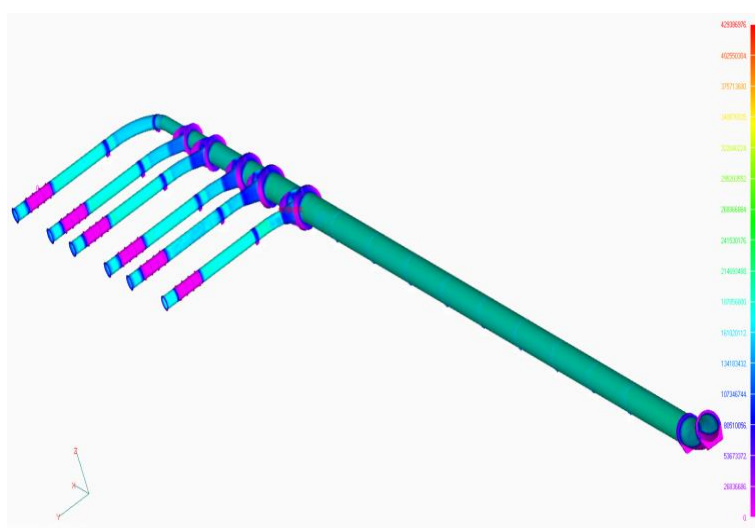
Slika 7. Pomjeranja u X pravcu u zoni račve A6

Na slici 8 se može vidjeti da su računska pomjeranja račve A6 u pravcu X ose, na mjestu mjerenja približna izmjerenim ($\Delta_1 = 10.3$ mm), tj.:

$$\Delta_1 \in (10\text{mm}; 10.5\text{mm}) \quad (2)$$



Slika 8. Pomjeranja u X pravcu u zoni račve A6

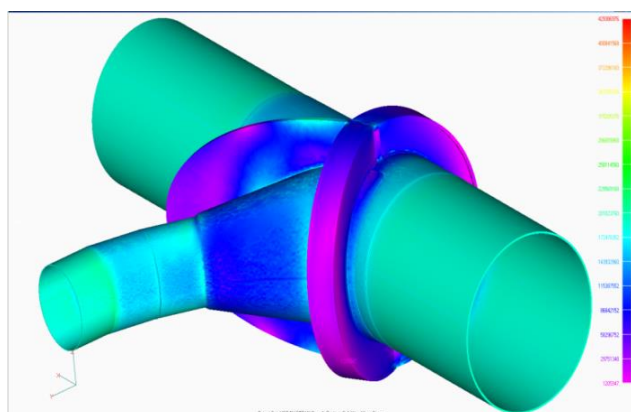


Slika 9. Von – Misesovi naponi na cjevovodu C3

2.3. Analiza naponskog stanja

Globalna slika Von – Misesovih napona posmatranog dijela sistema cjevovoda C3 (slika 9) pokazuje da je u najvećem dijelu, za statička opterećenja, cjevovod dobro dimenzionisan. Međutim, detaljnom analizom naponskog stanja račve A6, dolazi se do zaključaka da na njoj postoje opasne zone za čvrstoću posmatranog cjevovoda.

Prije svega treba istaći činjenicu da se maksimalni Von – Misesov napon $\sigma_{max} = 4293.8 \text{ daN/cm}^2$ nalazi upravo na račvi A6, na mjestu skretanja prve cijevi (slika 11, 12,) i to na njenoj unutrašnjoj površini.



Slika 10. Von–Misesovi naponi u zoni račve A6 (pogled I)

Sa slike 12 se vidi da je mjesto najvećeg napona u zoni uticaja toplote (ZUT) zavarenog šava koji vezuje lim debljine 36 mm za elipsu. Njegova vrijednost je daleko veća od vrijednosti dozvoljenog napona, tj.:

$$\sigma_{maxu} = 4293.8 \text{ daN/cm}^2 > \sigma_d = 2250 \text{ daN/cm}^2 \quad (3)$$

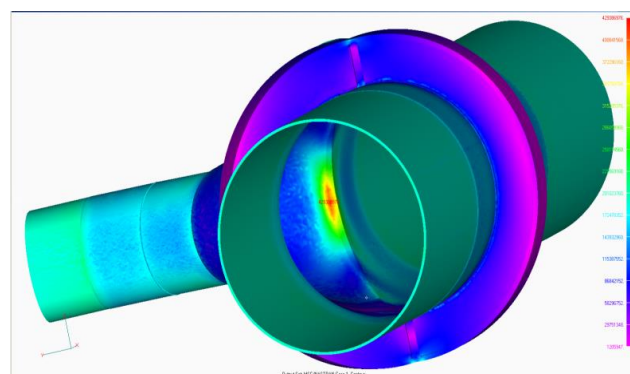
Ovo je svakako kritično mjesto na račvi A6 pa ga treba detaljnije analizirati.

Ako znamo da su dozvoljena dinamička opterećenja u cjevovodu za 10 % veća od statičkih [1], onda možemo pretpostaviti da u dinamičkim režimima rada napon iz izraza (1.3) može postati:

$$\sigma_{din} = 1.1 \cdot 4293.8 \text{ daN/cm}^2 = 4723.18 \text{ daN/cm}^2 \quad (4)$$

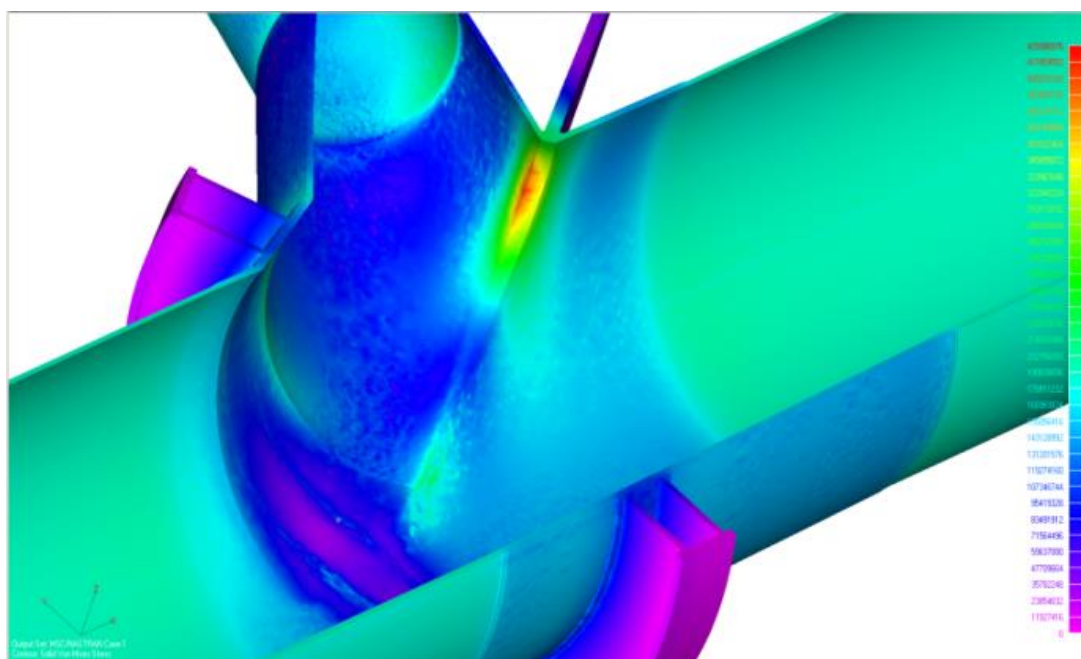
Ovaj napon je veći od napona na granici velikih izduženja za NIOVAL 47, tj.:

$$\sigma_{din} = 4723.18 \text{ daN/cm}^2 > \sigma_v = 4700 \text{ daN/cm}^2 \quad (5)$$

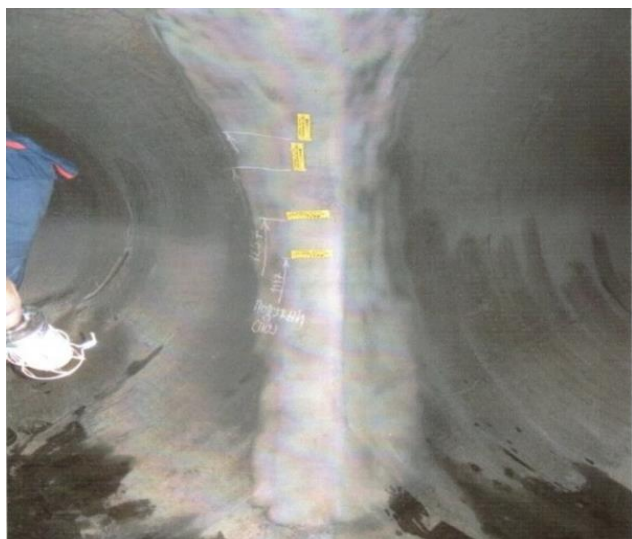


Slika 11. Von–Misesovi naponi u zoni račve A6 (pogled II)

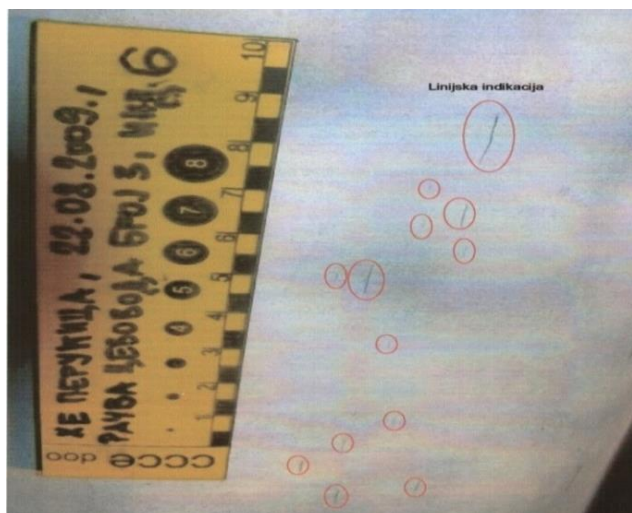
Ovo može biti veoma opasno jer, kao što vidimo sa slike 11, crvena zona u kojoj se nalazi ekstremno visoki napon ima dužinu oko 30 cm. Ovdje se ne radi o naponu u jednoj tački nego o naponu po jednoj liniji (čak i po površini), tako da je vjerovatno došlo do plastičnih deformacija na toj liniji a moguće je da je došlo i do velikih deformacija. Ako su se tu nalazili zaostali naponi na istežanje onda je logična pojava pukotina na toj liniji. Na slikama 13 i 14 su prikazane fotografije pronađenih pukotina koje su analizirane od strane Instituta za crnu metalurgiju iz Nikšića[2].



Slika 12. Von–Misesovi naponi u zoni račve A6(pogled III)



Slika 13 – Zona ispitivanja račve A6



Slika 14 – Pukotine u unutrašnjosti račve A6

3. ZAKLJUČAK

Numeričkim proračunom su dobijeni ekstremno veliki naponi u unutrašnjosti račve A6[1]. Oni su, kao što se to i dokazalo, izazvali pojavu velikog broja pukotina[2]. Iz tog razloga je neophodno rekonstruisati račvu A6 jer postoji opasnost od pucanja cijevovoda.

Ovaj zaključak je, pored niza drugih zaključaka i preporuka, ekspertske tim iznio u elaboratu [1] 2009. godine. Isti zaključak je ponovila firma Lahmeyer International GmbH, Germany u studiji [3] 2016. godine.

REFERENCE

- [1] Elaborat o ispitivanju naponskog stanja u karakterističnim presjecima cijevovoda C3 HE „PERUĆICA“, UNIVERZITET CRNE GORE, MAŠINSKI FAKULTET PODGORICA, CETIM, maj 2009. god
- [2] Izvještaj br. 020000-08/09 o ispitivanju bez razaranja i strukturnoj analizi materijala cijevovoda br.3 (račve A6 i A7), INSTITUT ZA CRNU METALURGIJU „NIKŠIĆ“ 30.09.2009.godine
- [3] [3] Studija mjera i radova faze II za HE Perućica, Lahmeyer International GmbH, Germany, april 2016. god

AUTORI



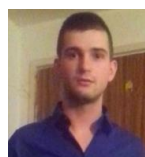
Prof. dr. Milorad Mišo Burić
Univerzitet Crne Gore
Mašinski fakultet
Bul. Džordža Vašingtona bb
81000 Podgorica, Crna Gora
mburic@ac.me



Prof. dr. Radoje Vujadinović
Univerzitet Crne Gore
Mašinski fakultet
Bul. Džordža Vašingtona bb
81000 Podgorica, Crna Gora
radojev@ac.me



Mr.-Ing. Igor Kresojević,
Plantaže, a.d.
81000 Podgorica, Crna Gora
igorkresojevic@gmail.com



Slaviša Đurišić, saobraćajni inž.
Univerzitet Crne Gore
Mašinski fakultet
Bul. Džordža Vašingtona bb
81000 Podgorica, Crna Gora
slavisa.djurisic@gmail.com



Marko Lučić, dipl. maš. inž.
Univerzitet Crne Gore
Mašinski fakultet
Bul. Džordža Vašingtona bb
81000 Podgorica, Crna Gora
Lucic.marko1@gmail.com

ANALYSIS OF ECONOMIC JUSTIFICATION OF CONSTRUCTING A SMALL HYDRO POWER PLANT

Darko SKUPNJAK
Milan VUKČEVIĆ

***Abstract:** This Work presents economic analysis of the project: **SMALL HYDRO POWER PLANT: small hydro power plant "Murino" "Dos's river- Neno's spring" of power 1,5 MW.** To have this project economically treated related to technical elements emerged from technical analysis of the project, it is necessary to determine costs of constructing a small hydro power plant, which are versatile, by their nature. Costs, as one of elements of engineering economy, have provided the required amount of investments. In the work, static and dynamic indicators of economic-financial analysis have been used, based on which an evaluation of economic justification of constructing a small hydro-power plant is given. The analysis is treating reduced production volume for 20% and 30% as possible risk due to change of hydrologic conditions.*

***Key words:** Small hydro power plant, investments, economic-financial analysis, production volume.*

1. INTRODUCTION

Engineering economy is an engineering discipline which has developed techniques which simplify comparison of alternatives on economic base. Engineering projects, which in addition to technical solutions based on scientific knowledge equally need to meet certain economic validities in order to be economically sustainable from one side and payable in overall from the other side, for the one (investor) for who such project is realized with acceptable cost.

In Engineering Economy, the principles and methods which help in precisely defined scientific manner defining and analyzing economic alternatives of project realization have been developed. Based on these analyses, an evaluation is given regarding acceptable solutions no matter they are done by an individual or the team. It is quite difficult to find a balance between technical and economic project feasibility. In particular, a project may be feasible in technical sense, but difficult to be realized in economic sense, or vice versa.

2. PROJECT DESCRIPTION

Small hydro power plant - small hydro power plant "Murino" is placed on the water flow of the Murino river. The Murino river is made of Dos's River and Neno's spring. One tank of water is placed on Dos's river, while the other is placed on Neno's spring on position **1224 m. n. m.** From there, water is transported by free fall to compensation tank for both water flows. The compensation tank of small hydro power plant "Murino"

is placed on the position 1220 m. n. m. Water is transported from both water tanks to compensation tank by derivation pipes. The compensation tank is designed to be on the place where water flow is moved to the pipes by free fall and falling under pressure. From the compensation tank to the place of small hydro power plant which is placed on the position 965 m. n. m., water is transported through the pipes under the pressure.

The analysis of hydro potential and technical calculations has provided selection of the best technical solution in terms of positioning the power plant on the water fall, calculations related to gross, net fall, losses in the pipeline, selection of the turbine type, calculation of required turbine strength, degree of usefulness, strength of generator and the transformer, including elements required for connection to distribution grid.

The investor decided to make the investment of 30% from his own resources and 70% from the loan.

Using the methods of the engineering economy, an analysis of economic justifiability of capital invested in the project of small hydropower plant is made. The economic analysis should show whether the project is sustainable, i.e. to determine interdependency between all economic phenomena and the processes based on economic principles and logics, to explain their generation, former flow and predict future period, to determine optimum direction of the project development, as well as measures which will direct development of the project to desirable, optimal flow. The economic analysis should also show possibility of changing economic parameters no matter they are desirable or undesirable considering their consequences.

3. APPLICATION OF MONEY-TIME RELATION

The term ‘‘capital’’ presents an economic value which is invested in production or some other economic activity aiming to enlarge, i.e. may be used to generate more fortune. Most of engineering economic studies include investment of capital in longer period of time, therefore, the impact of time needs to be taken in consideration. In that sense, it is understandable that one euro values more today than one euro after one or more years, because of the interest (or profit) which can make. Accordingly, the money has higher value over the time [4].

The capital in terms of money, machine, power, material and other elements required for operation of some company may be divided into two basic categories. Equity is capital owned by individuals or the companies that invested their money or the property in some business project or venture hoping to get profit. Loaned capital got from the creditor to invest in projects.

The goal of researches of the engineering economy is the income required to be generated. It researches if the investment with all depending costs emerging over the time, may be covered by the income (saving) of the capital and if this income is acceptable in terms of risk and potential alternative solutions. The key element of this research is time-money relation [1].

3.1. Method of present value

Method of present value PW or net present value (PW) is based on the concept of equivalent value of all cash flows related to some base or initial spot in time.

In order to find a present value in function of interest rate and %, for series of money inflows and outflows, it is necessary to discount future values to present one, using the interest rate in certain period, as follows [1]:

$$PW(i\%) = F_0(1+i)^0 + F_1(1+i)^{-1} + F_2(1+i)^{-2} + \dots + F_k(1+i)^{-k} + \dots + F_N(1+i)^{-N} = \sum_{k=0}^N F_k(1+i)^{-k} \quad (1)$$

where:

- i = effective interest rate or MARR, for calculation period,
- k = index for each period of consideration ($0 \leq k \leq N$)
- F_k = future cash flows at the end of period k ,
- N = number of periods of interest (for example, years).

The Minimum Acceptable Rate of Return (MARR) is the strategic goal of the company and it is defined by top management. Net present value is a sum of discounted net inflows (from economic flow) realized during the project exploitation. Actually, net inflows from economic flow (by years) are multiplied with proper discount factor, and then the sums got like this are added. The result got is an amount of means for reproduction realized in the project in its economic period, from the present point of view. Realization of the investment project is justifiable if PW is positive, i.e. higher than zero. One of the problems when applying this criterion might be choosing a real discount rate. From this reason an interest rate

corresponding to the interest rate of loan is taken for calculation [1].

$$PW(NPV) = \sum_{j=1}^N \frac{F_j}{(1+i)^j} \quad (2)$$

where:

- PW - net present value
- N - project duration
- F_j - net cash flow in the year t
- i - required interest

It refers to an integral and absolute indicator for evaluation of economic profitability and project acceptability. In order to make this project acceptable, net present value needs to be higher than zero, which means that positive project effects exceed the investment costs.

3.2. Method of future value

Future value, FW, is based on equivalent value of all money inflows and outflows at the end of period of consideration by the interest rate which equals to minimum acceptable profit rate [1].

$$FW(i\%) = F_0(1+i)^N + F_1(1+i)^{N-1} + F_2(1+i)^{N-2} + \dots + F_N(1+i)^0 = \sum_{k=0}^N F_k(1+i)^{N-k} \quad (3)$$

3.3. Method of internal rate of return IRR

Method of internal rate is a method which is mostly used in engineering economic analysis. The method requires the interest rate which equals equivalent value of alternative money inflows (incomes and savings) with equivalent value of money outflows (expenditures or costs, including the investment costs). For this method, other names are also used: Investment method, method of cash flows discounts, index of profitability [1].

$$\sum_{k=0}^N R_k(P/F, i\%, k) = \sum_{k=0}^N E_k(P/F, i\%, k) \quad (4)$$

where:

- R_k = net inflows or saving for k years
- E_k = net costs that include any investment cost for k years,
- N = period of project duration

Another method for determining internal profit rate for alternative is to determine i in way that present value equals to zero.

Then IRR is determined from the expression [1]:

$$PW = \sum_{k=0}^N R_k(P/F, i\%, k) - \sum_{k=0}^N E_k(P/F, i\%, k) = 0 \quad (5)$$

It can be said that the internal rate of return is a discount rate which equals present value of negative net inflows (by years) from economic flow to present value of positive inflows, i.e. a discount rate for which PW of project is equal to zero. It indicates the lowest discount rate at which realization of the investment project is justifiable. The internal profitability rate is compared to individual discount rate and must be equal or higher than it.

4. STATIC AND DYNAMIC INDICATORS OF INVESTMENT PROGRAM

The valuation of the investment program means application of certain methods aiming to consider justifiability and acceptability of the project.

It relates to the essential information of the investment project stated in the investment-technical documentation [6].

4.1. Static indicators

This evaluation is done based on data related to one year of full capacity use and maximum use of credit burden.

Method of determining profitability rate only uses representative years of the project lifetime which makes it logically static. The minimum rate of profitability means the minimum selling price acceptable, ie, minimum volume of production in the future, with which the project is still capable to settle all duties. Or more simply, the minimum profitability rate indicates what amount of income you need to receive in order to cover the costs you incurred for the purpose of getting income.

Investments per employee as relation between total investments and number of employees show how much credit and personal resources every employee spends.

Accumulations as relation between accumulation and the investments in assets and turnover show capability of the programme to realize certain accumulation burdened by costs for assets and turnover.

Cost-effectiveness as relation between total income and total expenses shows if a good company meets essential economic postulate in achieving possible results with as less investments as possible, i.e. it shows how much income is realized for 1€ of expenditure...

Long-term loan as relation between the long-term credits and total liabilities is an indicator of a financial structure. This indicator shows how much means from the loan is spent on every euro of liability and in dependence on other indicators and parameters leads to a conclusion whether the company considers impact of financial leverage as a model of realization of a high rate of income to personal resources or it refers to unrealistic evaluation which may question program realization.

4.2. Dynamic indicators

Dynamic indicators are determined based on consideration of certain period of time in which their effects are analyzed.

Dynamic evaluation includes:

- Method of net present value PW,
- Method of internal rate of return IRR,
- Period of financial investment return.

Relative project effectiveness - In addition to net present value as an indicator of the absolute investment income, relative effectiveness is also calculated compared to the investor and relative project efficiency compared to number of employed workers. Relative efficiency of the project compared to the investor is a relation between PW of investment and pre-calculation value. This value, also, has to be positive indicating the amount of material base return of the investor's work against euro investment, while expressed in percentage shows an accumulation rate. Relative efficiency of the project against number of employees shows the amount of contribution provided by every employee to increase material base of the project.

Time frame of the investment return is a period expressed in years during which the discounted annual net inflows of investemnt (from economic flow) will regain total discounted investment. Realization of the project is

justifiable if the deadline for returning the invested means is less or equal to the period of time determined by the credit provider.

5. ECONOMIC-FINANCIAL ANALYSIS

5.1. Investments

Total investment consists of four groups of investments, such as: A. Costs of building object for power generation (construction works and equipment); B. Costs of making technical documentation (research works, designing equipment, designing construction objects); C. Costs of professional services (expert supervision, monitoring); D. Costs of acquiring property rights (lots for power plants, switchyards). Project of small hydro power plant includes **small hydro power plant "Murino" (Dos's River - Neno's spring)** and separately a switchyard for purpose of connecting this hydropower plant to electric-distribution grid, this will be provided further in the study through their costs with exact values of share in the investment.

Table 1: Structure of investment

STRUCTURE OF INVESTMENT	EURO (€)
A. Costs of object building	1,869,279.74
B. Costs of technical documentation	110,578.64
C. Costs of professional services	112,156.78
D. Costs of acquiring property rights	13,084.96
TOTAL INVESTMENT	2,105,100.12

Table 2: Calculation of operation costs

STRUCTURE	EURO (€)
Depreciation	109,099.83
Investment maintenance	16,611.73
Calculation of insurance premium	10,746.60
Labor force	14,328.00
Other non-material costs	3,960.00
TOTAL OPERATION COSTS	154,746.16

Table 3: Projected total annual income

Power supply plant	Small Hydro Power Plant "Murino"
Power on plant exit Ppe (MW)	1,42862
Annual power production (kWh)	4.200.000,00
Incentive price (Group 1) Ppe < 1MW [c€/kWh]	10,44
Incentive price (Group 2) $1 \leq Ppe \leq 3$ MW [c€/kWh]	9,35570 (10,44-7xPpe)
Total power plant (€)	392.939,40
TOTAL	392.939,40 €

5.3. Projection of total income during period of ten years

In conformity with the Investor's intentions, production of small hydro power plant will participate in meeting need for power sources in Montenegro. As a concept, hydro power plant converts power of the water flow to electric power, therefore, hydro power plan operates using current inflows. The fact is that it is not possible to manage production (i.e. production adjusts to current inflow) which indicates that it is necessary to analyze current inflows as precise as possible, i.e. a curve of distribution of average daily flows. Based on that curve, annual production is projected and determined.

5.4. Economic - financial indicators

The table shows economic-financial indicators of the project of constructing a small hydro power plant for different production volumes.

Table 4: Calculation of operation costs (volume 100%)

No	Element of Analysis	Production Volume 100%
1.	Income/year	392.939,40 €
2.	Total investment	2.105.100,12 €
3.	Deadline to return investment	7 god.
4.	Cost-effectiveness	1,52
5.	Accumulation rate	16%
6.	Net present value (PW)	1.697.684,96 €
7.	Internal rate of return (IRR)	14%

Table 5: Calculation of operation costs (volume -20%)

No	Element of Analysis	Production Volume -20%
1.	Income/year	314.351,52 €
2.	Total investment	2.105.100,12 €
3.	Deadline to return investment	8 god.
4.	Cost-effectiveness	1,26
5.	Accumulation rate	12%
6.	Net present value (PW)	554.146,13 €
7.	Internal rate of return (IRR)	8%

Table 6: Calculation of operation costs (volume -30%)

No	Element of Analysis	Production Volume -30%
1.	Income/year	275.057,58 €
2.	Total investment	2.105.100,12 €
3.	Deadline to return investment	10 god.
4.	Cost-effectiveness	1,13
5.	Accumulation rate	10%
6.	Net present value (PW)	-17.623,28 €
7.	Internal rate of return (IRR)	3%

6. CONCLUSION

Using static and dynamic indicators of economic-financial analysis, an objective evaluation of investment is provided based on financial benefits when making a final decision. If all presumed conditions are realized for 100%

of realized production volume used as a base for analyzing economic-financial aspects of the investment, construction of small hydro power plant "Murino" is economically **HIGHLY JUSTIFIABLE**.

The work is analyzing unfavorable possibilities of operation of small hydro power plant "Murino" for the case of reduction of the production volume due to change of hydrologic conditions. Production volumes have been analyzed for 100% (projected), as well as reduced for 20% and 30%.

The risk which objectively exists in case the production of small hydro power plant "Murino" operates with 30% reduced capacity (i.e. negative net inflows) for certain year or years, the investor might, in agreement with the loan provider, overcome problem by using some financial derivatives.

Considering overall economic-financial project, it is highly **FAVORABLE FOR THE INVESTOR**.

REFERENCES

- [1] VUKČEVIĆ, M. (2012) *Engineering measurements*, University of Montenegro, Faculty of Mechanical Engineering Podgorica.
- [2] PAUNOVIĆ, B., ZIPOVSKI, D. (2010) *Business plan (manual for creation)*, Publishing Center, Faculty of Economics, Belgrade.
- [3] ĐUKIĆ, P. (1994), *Essentials of Economics*, Faculty of Technology and Metallurgy Belgrade, Belgrade.
- [4] SULLIVAN, W., BONTADELLI J., WICKS E., (2000) *Engineering Economy*, Prentice-Hall, New Jersey.
- [5] MARKOVIĆ D., PETROVIĆ D., MIHIĆ M. (2012) *Cost-Benefit analysis of electric power production project from renewable sources*, Management Magazine for theory and practice of management, No 64, pp 39-45.
- [6] VUKČEVIĆ M., ZOGOVIĆ S. (2007) *Evaluation of economic profitability of engineering project solutions*, Montenegrin Journal of Economics / Vol 3 No 6 December.

CORRESPONDANCE



Darko SKUPNJAK, M.Sc. Mech.Eng.
Daido Metal Kotor AD
Industrijska zona bb, 85330 Kotor,
Montenegro
skupnjak@daidokotor.com
skupnjak@t-com.me.com



Milan VUKČEVIĆ, Prof. D.Sc. Eng.
University of Montenegro
Mechanical Engineering Faculty
Bul. Džordža Vašingtona bb
81000 Podgorica, Montenegro
milanvu@ac.me

APPLICATION OF PROMETHEE METHOD AS SUPORT IN THE PLANNING PROCESS OF SMALL HYDROPOWER PLANTS

Branka GVOZDENAC UROŠEVIĆ
Budimirka MARINOVIĆ
Radislav BRĐANIN
Željko ĐURIĆ

Abstract: *During the planning of small hydropower plants, besides the energy performances of the possible alternatives, it is necessary to valorize all the other effects of projects construction. This paper gives an insight into the application of multi-criteria decision analysis (MCDA) methods in the planning of small hydropower plants through the creation of the model using the Promethee method.*

Key words: *Multi-criteria decision analysis, Promethee method, small-hydropower plant.*

1. INTRODUCTION

Energy has become one of the most discussed issues in economical, political, social and environmental aspects. Industrialization and technological developments resulted in major environmental concerns. Current and future possible environmental, economical, political and social negative consequences also force the countries to incline towards to renewable energy resources. In this respect, renewable energy has become the answer for sustainable energy planning [1].

Renewable energy decision-making can be viewed as a multi criteria decision-making problem with correlating criteria and alternatives. This task should take into consideration several conflicting aspects because of the increasing complexity of the social, technological, environmental and economic factors [2]. This all because renewable energy alternatives are emerging as a solution for a sustainable, environmentally friendly, cost-effective source of energy.

This work aims to evaluate applicability of multi-criteria decision analysis (MCDA) in order to provide a technical-scientific decision making support. The study propose suitable model for indentifying the most preferable solution for regional energy planning by creating classifications of alternative of small hydropower plants.

Small hydropower plant is a clean source of power, but also small hydropower plants are site specific and need careful planning for project formulation and implementation. Therefore using effective techniques as MCDA tools may become helpful to produce better understanding and results.

The results from the analysis lead to the conclusion that MCDA can be recommended as a decision support tool along with the development of relevant databases to be incorporated into policy and program development procedures [3].

2. MULTICRITERIA DECISION ANALYSIS METHODS IN ENERGY PLANNING

MCDA method is form of integrated sustainability evaluation. MCDA method deal with process of making decisions in the presence of multiple objectives. The objectives are usually conflicting, the solution is highly dependent on the preferences of the decision-maker and must be a compromise [4]. Nowadays, the focus on global environmental protection drives MCDA aid in energy systems [5].

MCDA techniques are being successfully used in many different planning processes: energy resource allocation, energy planning problems, environmental problems. Polatidis et al. [6] developed methodological framework to provide insights regarding the suitability of multi-criteria in the context of renewable energy planning. Loken, 2007 [7] described various MCDA methods for energy planning problems.

MCDA method can provide better understanding and better analysis of decision problems, also. Supriyasilp et al., [8] used MCDA analysis to determinate the advantages and disadvantages of hydropower plant plants in the Ping River Basin. Mladineo et al. [9] used Promethee method to rank locations in order to make the unit costs as low as possible.

2.1. Promethee metod

MCDA with Promethee (Preference Ranking Organisation Method for Enrichment Evaluation) method was used in this paper to analyze the advantage and disadvantage for eight project, based on seven criteria, including technical, socio-economic and environmental aspects. Promethee method uses the outranking principle to rank the alternatives. Basis of this metod is decision matrix:

criteria $C_1 \quad C_2 \quad \dots \quad C_n$
weight $w_1 \quad w_2 \quad \dots \quad w_n$
alternative -----

$$A = \begin{matrix} A_1 \\ A_2 \\ \cdot \\ \cdot \\ A_m \end{matrix} \begin{pmatrix} a_{11} & a_{11} & \dots & a_{1n} \\ a_{21} & a_{22} & \dots & a_{2n} \\ a_{31} & a_{32} & \dots & a_{3n} \\ \dots & \dots & \dots & \dots \\ a_{m1} & a_{m2} & \dots & a_{mn} \end{pmatrix}_{m \times n}$$

where a_{ij} is the performance of j -th criteria of i -th alternative, w_j is the weight of criteria j , n is number of criteria i and m is number of alternatives.

The different alternatives are compared pairwise by considering the deviation between the evaluations of two alternatives on a particular criterion. Based on this deviation, the decision-maker assigns a preference to the best alternative (under that given criteria) expressed by a number between 0 (indicating no preference or indifference) and 1 (indicating outright preference). For small deviations, a small preference to the best alternative is allocated (or possibly even no preference if the deviation is considered negligible), while larger preferences are assigned to larger deviations.

The preference of alternative a_1 over alternative a_2 for a particular criteria C_j can be determined by means of a preference function $P_j(a_1, a_2)$, which expresses the preference as a function of the deviation $d_j(a_1, a_2)$ between a_1 and a_2 on that particular criterion:

$$P_j(a_1, a_2) = F_j[d_j(a_1, a_2)] = F_j[c_j(a_1) - c_j(a_2)]$$

where F_j is a function of the deviation and ensures that $0 < P_j(a_1, a_2) < 1$ [12].

An overall or global preference index

$$\Pi(a_1, a_2) = \frac{\sum_{j=1}^P P_j(a_1, a_2) w_j}{\sum_{j=1}^P w_j}$$

represents the intensity of preference of a_1 over a_2 .

Outranking flows are then calculated in order to rank one alternative against all the other alternatives. The outranking flows for alternative a_1 are given by

$$\phi^+(a_1) = \frac{1}{N-1} \sum_{b \in A} \Pi(a_1, b) - \text{positive outranking flow}$$

$$\phi^-(a_1) = \frac{1}{N-1} \sum_{b \in A} \Pi(b, a_1) - \text{negative outranking flow}$$

and they express how the alternative outranks all the others - positive flow, while negative flow expresses how the alternative is outranked by all the others.

Net outranking flow for each alternative

$$\phi(a_1) = \phi^+(a_1) - \phi^-(a_1)$$

give a complete ranking for the alternatives. The alternatives with the highest net outranking flow value are given the highest rank [12].

Figure 1 presents a flowchart of steps for ranking the proposed solutions of small hydropower plants using the Promethee method of MCDA.

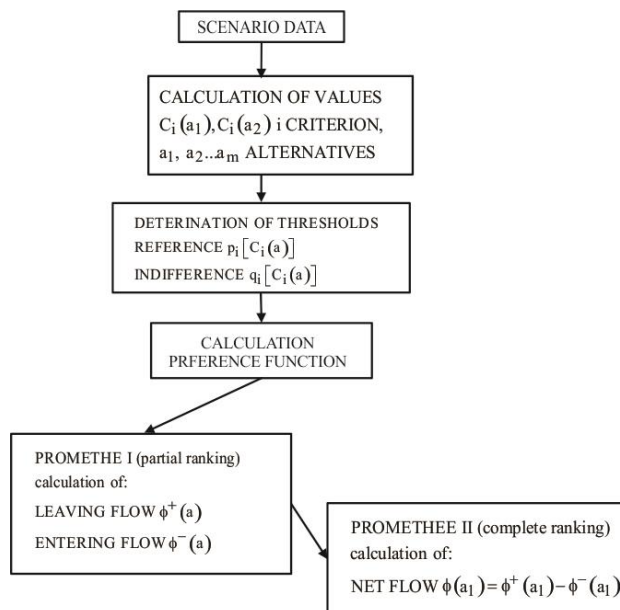


Fig.1: The PROMETHEE ranking method [10]

2.2. Multicriteria analysis for small hydro plants using Promethee method

This example deals with eight small-scale hydropower plants on Vrbas river. The main advantage of small-scale hydropower plants is that they could be easily developed in a short time based on local community participation. In addition, the small-scale hydropower could be used as a main energy resource for rural area as well as a supplementary for the country level. Accordingly, it is important to discover a potential area where is able to develop the small-scale hydropower plant, [11]. Also, small hydropower plants are recognized as a renewable and environmentally sustainable energy source.

MCDA has been applied in order to determinate advantages and disadvantages of the hydropower plants in seven criteria (Table 1.). The criteria enable the alternatives to be compared from a specific viewpoint. The number of criteria to use depends on the availability fo both quantitative and qualitative information and data relating to the potential criteria [12].

Important step in MCDA analysis is criteria weighting [3]. The weights determine how heavily a criteria contributes to the overall score. In this paper criteria weights have been discussed by experts and then the weights were calculated with the AHP (Analytic Hierarchy Process) method. As a consequence of weight assignment, the investment safety and legal abstractacle are the most important criteria in the view of the experts.

The analysis was facilitated by the *Visual Promethee* software.

Table 1: Overview of used criteria

Criterion		Type	Expert weight	Description	Literature
Technical aspect	Installed capacity	Quantitative	0,08	Indicates the potential for generating electrical power	[8]; [11]
	Annual energy production	Quantitative	0,11	High annual energy production means high potential [8]	[1]; [8]; [11]; [12]
Environmental aspect	Flow pattern and amount of flow	Qualitative	0,2	Sites are ranked from the least impact to the most impact on flow pattern and amount of flow as: 1 – sites with an existing infrastructure and reservoir, 2- the sites currently in water resource development plan, 3 – the sites with low head Q based type, 4 – the warway type and 5 – site that is not in the water resource development plan.	[8]; [11]
Socio-economic aspect	Investment cost	Quantitative	0,06	Cost rendered from purchasing the equipment, installation and construction	[1]; [5]; [8]; [10]; [11]
	Investment safety	Qualitative	0,25	Plants are ranked from the least impact on flow pattern and amount of flow [8]	[1]; [8]
	Social acceptability	Qualitative	0,05	Acceptance by the local population regarding the plant	[1]; [5]; [10]; [12]
	Legal abstracte	Qualitative	0,25	If plant is in conservation area or if there are ancient remains in the area project can not be developed.	[8]

2.3. Results and discussion

Figure 2. present the resulting ranking. By MCDA analysis the alternative ranked highest is option MHE 3. The criteria that mostly affected on this result is that it has highest installed capacity, and highest annual energy production and lowest investment cost.



Fig.2: Profile of an alternatives

A sensitivity analysis of the results determined the robustness of the model and the responsiveness of the

rankings to change in the weights assigned to the criteria. [3].

The sensitivity analysis (Table 2) show that the two highest ranked options, MHE 3 and MHE 2, do not change their rank as a result of the change in weights.

Table 2: Stability intervals

Criteria	Weight [%]	Stability intervals	
		Min	Max
Installed capacity	8	0	100
Annual energy production	11	9,08	11,22
Flow pattern and amount of flow	20	0	100
Investment cost	6	5,87	7,32
Investment safety	25	0	100
Social acceptability	5	0	100
Legal abstracte	25	0	100

3. CONCLUSION

Hydropower plant depends on several conditions, and energy planning processes should take into account not only technical but also environmental, economical and social dimension.

The present work proposed MCDA approach to select the best compromise alternative of hydro-power plant, in order to assist policy making for hydropower development. In this way the complexity of a multi-actor energy system can be an asset in planning when using MCDA.

The selection is based on comparison of eight alternatives according to their performances with respect to relevant technical, environmental social and financial criteria. The application the Promethee method of MCDA analysis proved to be a valuable tool to assess and evaluate alternatives.

Analysis of the weight stability intervals, the limits within which its weight can be modified without changing ranking, are very large, except in criteria investment cost and annual energy production.

REFERENCES

- [1] DEMIRTAS O, (2013). *Evaluating the Best Renewable Energy Technology for Sustainable Energy Planning*. International Journal of Energy Economics and Policy Vol. 3, Special Issue, ISSN: 2146-4553, pp.23-33.
- [2] DAIM T, et al. (eds.) (2013). *Research and Technology Management in the Electricity Industry*, Green Energy and Technology, DOI: 10.1007/978-1-4471-5097-8, Springer-Verlag London.
- [3] BRATANOVA A (2015). *Multiple criteria analysis of policy alternatives to improve energy efficiency in industry in Russia*, Doctoral dissertation, IESE Business School.
- [4] POHEKAR S D, RAMACHANDRAN M (2004). *Application of multi-criteria decision making to sustainable energy planning – A review*. Renewable and Sustainable Energy Reviews, 8, pp. 365-381.
- [5] WANG J, JING Y, ZHANG C AND ZHAO J (2009). *Review on multi-criteria decision analysis aid in sustainable energy decision-making*. Renewable and Sustainable Energy Reviews 13, pp. 2263 - 2278.
- [6] POLATIDIS H, HARALAMBOPOULOS D A, MUNDA G, VREEKER R (2006). *Selecting an Appropriate Multi-Criteria Decision Analysis Technique for Renewable Energy Planning*, Energy Sources, Part B: Economics, Planning, and Policy, 1:2, 181-193.
- [7] LOKEN E (2007). *Use of multicriteria decision analysis methods for energy planning problems*. Renewable and Sustainable Energy Reviews 11, pp. 1584-1595.
- [8] SUPRIYASILP T, PONGPUT K AND BOONYASIRIKUL T. (2009). *Hydropower development priority using MCD Method*, Energy Policy 37, pp. 1866 - 1875.
- [9] MLADINEO N, MARGETA J, BRANS J P, MARSHAL B (1987). *Multicriteria ranking of alternative locations for small scale hydro plants*. European Journal of Operational Research 31, pp. 215-222.
- [10] TSOUTSOS T et al. (2009). *Sustainable energy planning by using multi-criteria analysis application in the island of Crete*. Energy Policy 37, pp. 1587-1600.
- [11] WAISURASINGHA C, CHINDAPRASIRT P, SRIAMPORN W, CHUANGCHAM S (2012). *The utilization of geographic information systems and multi-criteria decision making with local community participation for selection of site for micro hydropower project: A case study of Chi river Basin, Thailand*, 33rd Asian Conference on Remote Sensing, ACRS 2012, pp. 1201-1205.
- [12] TROLDBORG M. et al (2014). *Assessing the sustainability of renewable energy technologies using multi-criteria analysis: Suitability of approach for national-scale assessments and associated uncertainties*. Renewable and Sustainable Energy Reviews 39, pp.1173 - 1184.

CORRESPONDANCE



Branka GVOZDENAC UROŠEVIĆ, D.Sc. Eng.
University of Novi Sad
Faculty of Technical Sciences
Trg Dositeja Obradovića 6
21000 Novi Sad, Serbia
brankagvozdenc@uns.ac.rs



Budimirka MARINOVIĆ, D.Sc. Eng.
University of East Sarajevo
Faculty for production and management
Stepe Stepanovića bb
89101 Trebinje, Bosnia and Herzegovina
buda.koprivica@gmail.com



Radislav BRĐANIN, M.Sc. Eng.
University of East Sarajevo
Faculty for production and management
Stepe Stepanovića bb
89101 Trebinje, Bosnia and Herzegovina
radislavbrdjanin@gmail.com



Željko ĐURIĆ, D.Sc. Eng.
University of East Sarajevo
Faculty for production and management
Stepe Stepanovića bb
89101 Trebinje, Bosnia and Herzegovina
zeljkodjuric71@gmail.com

DEVELOPMENT OF WORK PLATFORMS FOR MAINTENANCE OF PENSTOCK HPP PIROT

Dragan MILČIĆ
Miodrag VELIMIROVIĆ
Miodrag MILČIĆ

Abstract: *In order to maintain the high reliability of the HPP Pirot, special attention is paid to maintenance of the system, which consists in the planning of maintenance, maintenance, monitoring of the maintenance process and continual improvement of the maintenance process. In order to improve the maintenance process of the penstock HPP Pirot, a work platform was developed for the maintenance of the penstock. Since the diameter of the pipeline is 3.5, 3.3 and 3.0 m, the conditions for maintaining of the penstock are difficult. For this reason, is development work platform for the transportation of the necessary maintenance equipment, the needs of the upper part of the pipeline. The paper presents the development of a working platform for the maintenance of the penstock of the hydroelectric power plant Pirot.*

Key words: *product development, work platform for maintenance of penstock, HPP Pirot*

1. INTRODUCTION

Hydroelectric power plant "Pirot" is located on the territory of southeastern Serbia, between Pirot and the Bulgarian border, and uses the water of the river Visočica on the profile of the dam "Zavoj". It is a storage (reservoir) type hydropower plants with a tunnel and a pressure pipeline.

Hydroelectric power plant "Pirot" started construction in 1983, while the first aggregate was put into operation in 1990. The accumulation "Zavoj" was created naturally. Big landslide closed the valley of Visočica, turning it into a lake. At the bottom of the lake, the village of Zavoj remained, and the natural dam was used to build an artificial dam with 1.5 million cubic meters of stone, clay and filter material. The accumulation itself is multipurpose.

Its waters are used for:

- electricity production
- acceptance of the flood wave
- water supply
- preventing of water borne deposition
- refining small waters.

Powerhouse of hydroelectric power plant is overhead with 2 vertical aggregates with Francis turbines with power of 80 MW, with command and distribution facilities. Operating time of the plant is 1400 hours per year (4.5-5 hours per day).

Pirot Hydroelectric Power Plant has an inlet tunnel with an entrance building and a tunnel of the control gate. Length of tunnel 9093m, diameter 4.5m. Surge tank

height of 97m, variable diameter from 8 to 15m. Steel pipeline with tunnel section of pipeline of 400 m, total length 2030 m, diameter 3.5 m, 3.3 m and 3.0 m. In front of the power plant it is divided into two branches $d = 1,70$ m.

Preventive maintenance of the HPP Pirot plant is carried out once a year. During this period, the inspection of the penstock is carried out and the necessary work is carried out for the maintenance of the pipeline. Since the diameter of the pipeline is 3 m, these maintenance conditions are difficult. The need for the transport of the necessary maintenance equipment for reaching the upper part of the penstock, required the development of the work platform for the maintenance of the penstock.

The paper presents a new innovative solution for the developed working platform for penstock maintenance based on the defined requirements:

- Launch the work platform with its own weight platform and a winch with a steering wheel and support rollers;
- All platform elements should be so dimensioned that it is possible to smoothly enter the pipeline through the inspection holes, and to quickly assembly;
- The work platform should enable the safe transport of cargo and persons working on the maintenance of the penstock;
- Maximum platform speed of 0.5 m / sec;
- Platform length 3000 mm;
- The width of the work platform should be as high as possible, but so as not to interfere with the movement through the penstock;

- Maximum platform load of 5 kN;
- The work platform should provide a simple and efficient placement system in a horizontal position;
- It is necessary for the winch and the work platform to have a braking system for the effective positioning of the work platform in the desired position along the penstock;
- An integral part of the work platform should include ladders for safe entry-exit onto the platform;
- The winch should be portable and provide easy transport and installation on a horizontal basis;
- The winch drive should be a motor with frequency speed control.

In addition to the above requirements, the following requirements are added:

- The maximum mass of one part of the structure is max 30 kg.
- The solution should ensure efficient positioning of the work platform so as to prevent possible rotation of the platform around the axis of the pipeline.
- High flexibility of the work platform in relation to the change in the slope of the pipeline.
- Achieving a good relationship between quality and price of the construction of the work platform.
- High durability of all elements of the work platform and low maintenance costs.
- High Efficiency and reliability of the work platform's functioning.

In order to fully meet the defined requirements, and especially because the penstock changes the diameter and direction, both vertically and horizontally, an penstock analysis has begun. This analysis was also necessary due to the requirement that the work platform be as wide as possible and not interfere with the movement through the penstock.

2. ANALYSIS OF THE PENSTOCK OF HPP PIROT

The objective of the analysis of the penstock of the HPP Pirot is to generate relevant data necessary for the design of a work platform intended for operation on the maintenance of the penstock of the HPP Pirot.

The length of penstock the pipeline changes the direction (in the vertical and horizontal plane), the diameter and the thickness of the sheet metal. The general appearance of the penstock is given in Fig. 1.

1. The minimum diameter of the penstock through which the moving work platform must move is 3000 mm.
2. The maximum diameter of the penstock through which the moving work platform is moving is 3500 mm.
3. The maximum distance between the two inspection openings on the penstock is 701 m.
4. The minimum slope of the penstock is 0° in the control gate and at the branch in the front of the

machine hall. In both cases, there are extremely short relationships of maximum 10 m.

5. The maximum slope of the inlet pipeline is 11.922055° , which starts at about 294 m in front of the branch. This slope of the pipeline retains at 189 m of its length. The maximum change in the slope of the pipeline is 8.383248° in front of the machine hall.
6. The maximum change in the direction of the pipeline in the horizontal plane is 26.633810° .

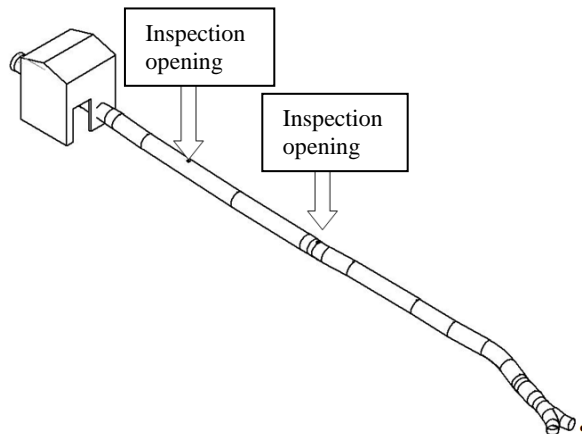


Fig.1: General layout of the penstock from the control gates to the branch in front of the powerhouse

3. CONSTRUCTION OF THE TRANSPORT SYSTEM OF WORK PLATFORM

The work platform, the winch and the accompanying equipment is intended for operation on the maintenance of the penstock of the HPP Pirot. Platform capacity is 5 kN. Down of pipelines work platform moves its own weight. The withdrawal of the platform along the pipeline is realized by a winch. The main parts of the transport system within the pipeline of the HPP Pirot are:

1. Winch,
2. Work platform trolley,
3. Work platform,
4. Support (horizontal) and directional (vertical) rollers,
5. Boundary L profiles, which are mounted along the pipeline.

The work platform consists of the supporting trolleys and the working part of the platform, which are connected with the pin joint that allow the rotation of the platform's workpiece by the angle $< 14^\circ$. This rotation is required to bring the working part of the platform to a horizontal position independent of the inclination of the pipeline. The change of the angle of the workpiece of the platform is achieved by means of hydraulic cylinders, manual pumps and three-stage distribution valve.

The diameter of the pipeline is from 3300 to 3500 mm and the slope of the pipeline is from 2° to 12° . In the pipeline at the control gate, the diameter is 3000 mm. In order to provide a smooth passage of the work platform with a width of 2300 mm and through this narrowest part of the pipeline it is necessary that the height of the stroller be lower than 2142 mm (Fig. 2).

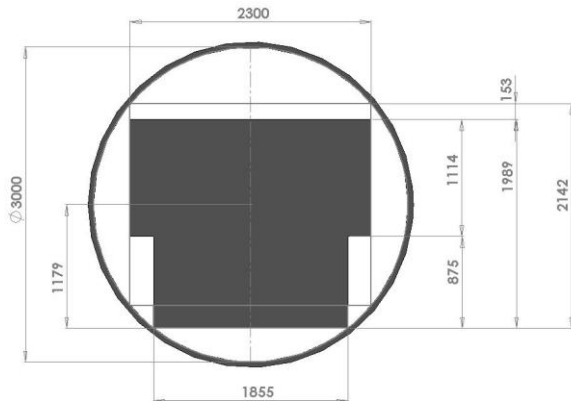


Fig.2: Work platform position in a horizontal pipeline of 3000 mm diameter

The penstock changes the slope in relation to the horizontal, and the platform should maintain a horizontal position. This leads to a change in the height of the work platform while moving through the penstock. The change of the fictive height of the work platform (Fig. 3) is given by the expression (1):

$$H_f = H_k + \frac{L_p}{2} \cdot \sin \alpha + H_p \cdot \sin \alpha \quad (1)$$

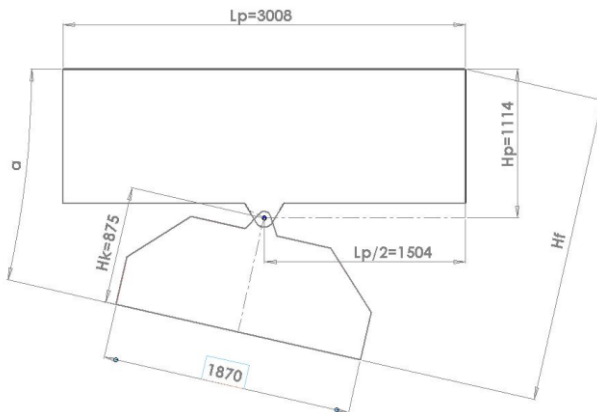


Fig.3. Fictive work platform height

Based on the conducted analysis of the penstock of the HPP Piro, the projected solution of the platform meets the necessary conditions for smooth passage along the entire route of the penstock with a diameter of 3300 to 3500 mm. It is possible to pass through the penstock with a diameter of 3000 mm, but only if it is straight-line without changing the direction, which is also the case in the control gate.

In order to secure the position of the platform in the transverse plane of the penstock and to prevent the rotation of the platform around the axis of the pipeline, the boundaries along the penstock are placed.

Figure 4 shows the model of the work platform in the penstock.

The launching of the platform is achieved by the own weight of the work platform and the winch with a directional and support rollers.

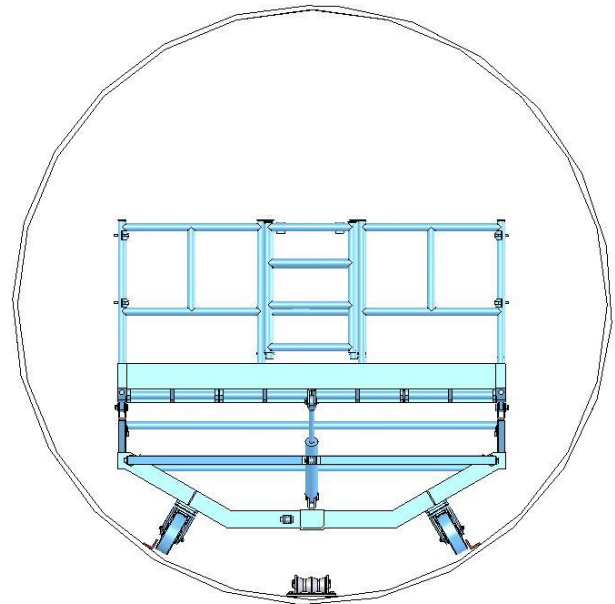


Fig.4: Model of the work platform in the penstock whose possible rotation prevents the boundaries

The platform with two cables is connected to the winch, where one cable is powered and the other one is safety. For the axial positioning of the platform, besides the cable, all the wheels are placed so-called. complete brakes.

In order to prevent possible rotation of the work platform around the axis of the penstock, there are welded screws for mounting the L profile along the entire pipeline as the stops for the work platform wheels.

The work platform is made the basis of the panel-framing combined system made of stainless steel welded, which can be inserted into the penstock through the inspection holes 600 mm in diameter.

The work platform is prefabricated. Connecting parts is done with the screwed and cotter joint. Assembly is simple and quick. All platform elements have a maximum weight of 300 N.

Technical solution the work platform intended for maintenance of penstock of the HPP Piro (Figures 5, 6 and 7) is fully realized (projected and implemented) by the Faculty of Mechanical Engineering in Niš.



Fig. 5: Implemented technical solution of the work platform for maintenance of penstock – position 1



Fig.6: Implemented technical solution of the work platform for maintenance of penstock – position 2

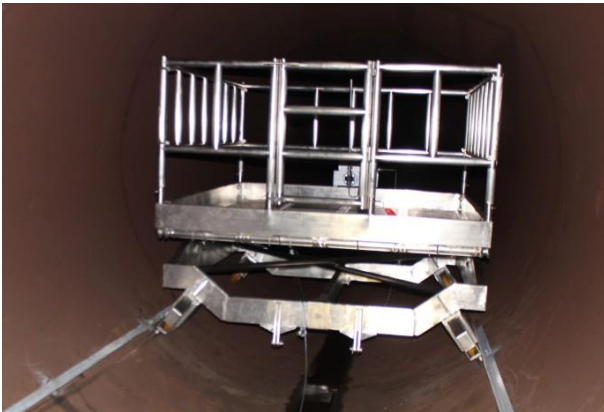


Fig.7: The work platform in the penstock

4. CONCLUSION

HPP Pirot belongs to the system of peaking hydroelectric power plants. In order to maintain the high efficiency of the system, ie the high availability and reliability of the system, special attention has been paid to the maintenance of the system in the HPP Pirot, which consists in the planning of maintenance, maintenance, monitoring of the maintenance process and continuous improvement of the maintenance process. In order to improve the maintenance process of the penstock HPP Pirot, a work platform was developed for the maintenance of the penstock.

User of the technical solution of work platforms for operation on the maintenance of the penstock is the Public

Enterprise of the Electric Power Industry of Serbia Branch of HPP ĐERDAP - Hydroelectric Power Plant Pirot.

Certain results of the technical solution can be applied with similar hydroelectric power plants.

REFERENCES

- [1] McStraw, Bill, Inspection of Steel Penstocks and Pressure Conduits, Facilities Instructions, Standards, and Techniques, Volumes 2-8, September 1996.
- [2] MILČIĆ, D., VELIMIROVIĆ, M., TEMELJKOVSKI, D., NIKOLIĆ, V., MILČIĆ, M., VELIMIROVIĆ, N. (2013) *Technical solution: The work platform for maintenance of penstock HPP Pirot*, Realizer: Faculty of Mechanical Engineering in Niš, User: Public Enterprise of the Electric Power Industry of Serbia Branch of HPP ĐERDAP - Hydroelectric Power Plant Pirot.
- [3] <http://www.djerdap.rs/sr/page/36/HE+Pirot>

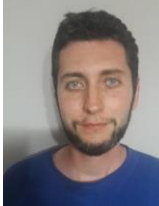
CORRESPONDANCE



Dragan MILČIĆ, Prof. D.Sc. Eng.
University of Niš
Faculty of Mechanical Engineering
Aleksandra Medvedeva 14
18000 Niš, Serbia
dragan.milcic@masfak.ni.ac.rs



Miodrag VELIMIROVIĆ, Ass. M.Sc. Eng.
University of Niš
Faculty of Mechanical Engineering
Aleksandra Medvedeva 14
18000 Niš, Serbia
m_velimirovic@yahoo.com



Miodrag MILČIĆ, Ass. M.Sc. Eng.
University of Niš
Faculty of Mechanical Engineering
Aleksandra Medvedeva 14
18000 Niš, Serbia
miodrag.milcic@masfak.ni.ac.rs

NUMERICAL ANALYSES OF TRASH RACKS CHARACTERISTICS UNDER DIFFERENT EXPLOITATION CONDITIONS IN HYDROPOWER PLANTS

Miloš KRUNIĆ
 Ivan BOŽIĆ

Abstract: This paper represents a research about the influence of different operational conditions on trash racks characteristics. The main goal of the research was to find to how the specific parameters of the trash racks (flow velocity, head loss and head loss coefficient) change in the various exploitation situations. The comparison was done by looking at the cases of the normal flow (flow is perpendicular to the trash rack's frontal area) and inclined flow (flow takes different angles). All of the mentioned cases were analysed by running simulations based on the branch of fluid dynamics called computational fluid dynamics (CFD). In both cases simulations were based on the steady flow, while the normal flow case was analysed with both steady and unsteady flow simulations.

Key words: : trash racks, simulations, conditions, comparison.

1. INTRODUCTION

Trash racks (often called bar screens) are one of the most common and most responsible parts of mechanical equipment in hydropower plants. Their role is highly important, as they need to prevent water debris from passing through them. This is vital because any form of debris can make working parameters of the facility worse, while bigger pieces can do serious damage not only to turbomachines (water turbines), but also to the plant or building itself. They need to be reliable and resistant, because if they get deformed or broken due to accumulation of debris, the process of electricity generation has to stop. Trash racks are located at the intake of the hydropower plant and they can be totally or partially submerged, which depends on the size of the plant and depth of the inlet reservoir.



Fig.1: Trash rack at the intake of the hydropower plant (wilcoxdiving.com).

One of the most important geometric parameters of trash rack is clean span opening, which represents an open area between the bars, and it is usually square or rectangle.

There are different tips on choosing the right dimensions for the opening, but the most important rule is that clean span opening must be smaller than the smallest opening of the water distribution pipe or the inlet of the water turbine. Clean span dimensions also depend on the type of the water turbine and the origin/structure of water debris.

2. HEAD LOSS CALCULATION

One of the most important hydraulic parameters of the trash rack is the head loss. It is defined as the drop of water

level after water flow passes through the bars. If the surface of the trash rack is cleaned and maintained regularly (and all previously mentioned dimensions are well chosen), head loss has the value equal to few centimeters. Head loss can be influenced by the amount of debris, flow velocity in front of the trash, angle of the water flow, and by the hydraulic shape and characteristics of the trash rack. Value can be calculated by using the equation below [2]:

$$h_R = \zeta_R \cdot \frac{v_R^2}{2g} \quad (1)$$

In the equation above, “ h_R ” represents the head loss, “ ζ_R ” represents head loss coefficient, “ v_R ” represents stream velocity in front of the trash rack, and “ g ” stands for gravitational acceleration. For the purpose of research other equations were also used for calculating the head loss value. First equation was developed by Kirschmer and it is based on the geometry of both horizontal and vertical bars of the trash rack [3]:

$$h_R = K \left(\frac{t}{b} \right)^{\frac{4}{3}} \cdot \frac{v_R^2}{2g} \sin \alpha \quad (2)$$

In this equation, factor “K” depends on the cross section shape of trash rack’s bar (see figure 2), “t” stands for bar thickness, while “b” represents the distance between the two bars. Angle “α” is the angle between the trash rack and the river bottom.

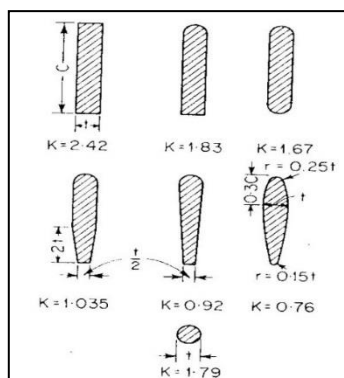


Fig.2: Different values of the “K” factor used in Kirschmer’s head loss formula [3].

Next equation was developed by Beresinsky and it also takes geometry of the trash rack into consideration, while the expression is a bit more complex than those mentioned before [2]:

$$h_R = \zeta_R^{(n)} \cdot K_\delta \quad (3)$$

Where “K_δ” is the factor of flow angle (if the flow is normal than K_δ = 1, otherwise, it depends on the flow angle). “ζ_R⁽ⁿ⁾” is the normal flow head loss coefficients and it is calculated as [2]:

$$\zeta_R^{(n)} = \beta_{OR} \cdot \left(\frac{A_R + A_Z}{A} \right)^{1.6} \cdot \left(2.3 \frac{l}{b} + 8 + 2.4 \frac{b}{l} \right) \cdot \sin \alpha \quad (4)$$

Where “β_{OR}” represents factor that depends on cross section shape of the bar, “A_R” is the area of the trash rack which is occupied by the rack’s elements (bars, frame and mounting guides), “A_Z” is clogged area of the trash rack, while “A” represents the total area of the trash rack, and finally “l” represents length of the bar’s profile.

	β _{OR}		β _{OR}
	0.504		0.18
	0.370		0.15
	0.32		0.26
	0.21		

Fig.3: Different values of the “β_{OR}” factor used in the head loss formula developed by Beresinsky [2].

Finally, the third equation used in this paper was developed by Idel’chik. It can be described as only geometry based since all of the variables (β₂ and ζ) are dependent on trash rack’s bar dimensions [4]:

$$h_R = \zeta_R \cdot \frac{v_R^2}{2g} = \beta_2 \cdot \zeta \cdot \sin \alpha \cdot \frac{v_R^2}{2g} \quad (5)$$

As it was mentioned in the abstract of the paper, results of these calculations were compared to the results obtained by running CFD based analyses. Head loss was calculated as pressure drop (pressure difference in front and behind the trash rack).

3. MODEL USED FOR THE RESEARCH

For the purpose of the research, 3 different trash rack models were made by using the modeling software. The only difference between them is the cross section of the vertical bars – the first model has vertical bars with rectangular shaped cross section, the second model has rectangular cross section with rounded edges, while the third one has round (circular) cross section. The thickness of the bars has the same value (15 mm), cross sections are 30 mm long, and the distance between the bars (clean span opening) is 200 mm.

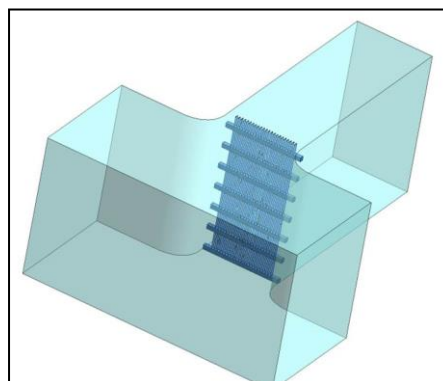
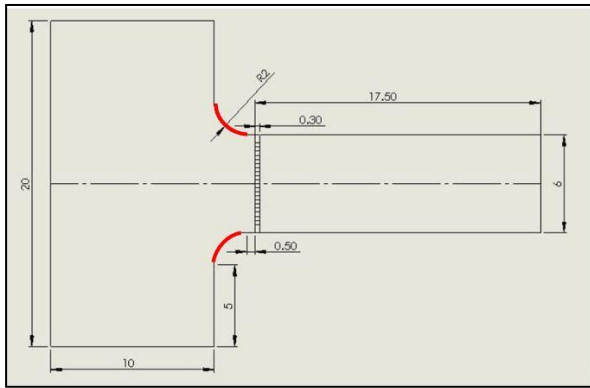


Fig.4: The analysed model of the submerged trash rack [1].

Each of the trash racks is 10m high and 6m wide. Also, each one has 23 vertical bars and 7 horizontal bars. By looking at figure 4, it is clear that model consists of three-dimensional trash rack and the volume that represents the river. Channel behind the trash rack is mostly made of concrete, so it was defined as “wall“, while the “side walls“ of the water volume in front of the trash rack were defined as “symmetry“ (wall which doesn’t affect any of the analyzed parameters). Also, the entrance to the trash rack’s area is rounded, because it is the most common case since it balances negative flow effects (especially in the case of inclined flow). Dimensioned model with red-coloured rounded entrance can be seen in figure 5:



Every simulation had several different stream velocities (from 0.4 m/s to 2 m/s). In every simulation there was an assumption that the trash rack was clean.

4. NORMAL FLOW SIMULATION

The first analysed case was the case of normal flow through the trash rack. All of the three available trash rack models were used, while 7 different stream velocities were selected as input values for CFD based software. Head loss was calculated by using CFD value, and by using equations developed by Kirschmer (2), Berezinsky (3 and 4) and Idel'chik (5).

4.1. Steady flow simulation

Steady flow is theoretical form of fluid flow which is based on assumption that parameters of the flow don't change during the time (they have constant values). When it comes to the simulation setup, it should be noted that unstructured mesh was used (with around 3 million elements) and that SST model (Shear Stress Transport) was used as the turbulence model (because the trash rack was defined as wall). Velocity changes during normal flow can be seen in figure 6:

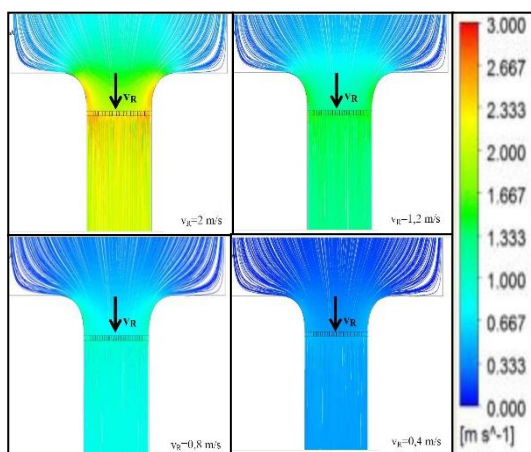


Fig.6: Stream velocity changes for different input velocities during steady normal flow simulations [1].

Results of the simulation are shown as in the following tables and diagrams (the abscissa represents square value

of stream velocity while the ordinate represents head loss):

Table 1: Head loss during normal flow through the trash rack with rectangular shaped cross section of vertical bars [1].

v_R		CFD	Kirschmer	Berezin.	Idelchi k
2	h_R	0.103	0.093	0.15	0.107
	ζ_R	0.506	0.46	0.74	0.52
1.	h_R	0.058	0.052	0.084	0.060
	ζ_R	0.506	0.46	0.74	0.52
1.	h_R	0.037	0.033	0.054	0.038
	ζ_R	0.506	0.46	0.74	0.52
1	h_R	0.026	0.023	0.038	0.027
	ζ_R	0.506	0.46	0.74	0.52
0.	h_R	0.016	0.015	0.024	0.017
	ζ_R	0.506	0.46	0.74	0.52
0.	h_R	0.009	0.008	0.013	0.010
	ζ_R	0.506	0.46	0.74	0.52
0.	h_R	0.004	0.004	0.006	0.004
	ζ_R	0.506	0.46	0.74	0.52

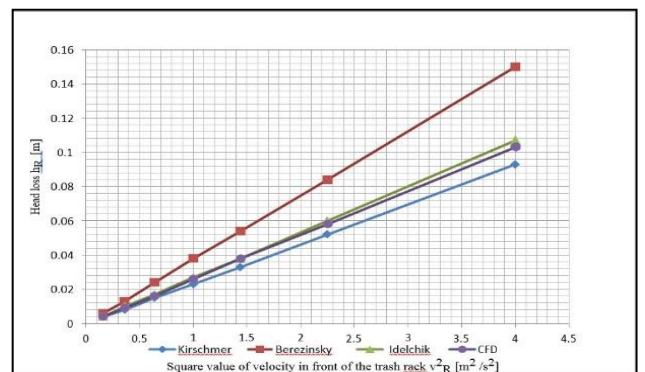


Fig.7: Comparison of head loss values for the case of steady normal flow through the trash rack with vertical bars with rectangular shaped cross section [1].

Table 2: Head loss during normal flow through the trash rack with rectangular cross section of vertical bars (with rounded edges) [1].

v_R		CFD	Kirschmer	Berezin.	Idelchi k
2	h_R	0.103	0.088	0.095	0.081
	ζ_R	0.505	0.43	0.47	0.4
1.	h_R	0.058	0.049	0.054	0.046
	ζ_R	0.505	0.43	0.47	0.4
1.	h_R	0.037	0.031	0.034	0.029
	ζ_R	0.505	0.43	0.47	0.4
1	h_R	0.026	0.022	0.024	0.020
	ζ_R	0.505	0.43	0.47	0.4
0.	h_R	0.016	0.014	0.015	0.013
	ζ_R	0.505	0.43	0.47	0.4
0.	h_R	0.009	0.008	0.009	0.007
	ζ_R	0.505	0.43	0.47	0.4
0.	h_R	0.004	0.0035	0.004	0.003
	ζ_R	0.505	0.43	0.47	0.4

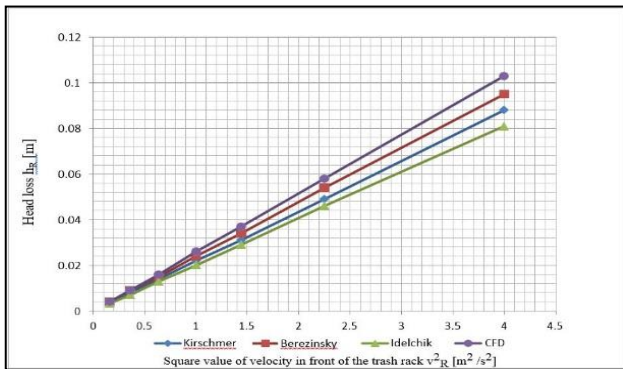


Fig.8: Comparison of head loss values for the case of steady normal flow through the trash rack with vertical bars with rectangular cross section (with rounded edges) [1].

Table 3: Head loss during normal flow through the trash rack with circular cross section of vertical bars [1].

v_R		CFD	Kirschmer	Berezin.	Idelchik
2	h_R	0.108	0.089	0.078	0.079
	ζ_R	0.53	0.44	0.38	0.39
1.5	h_R	0.061	0.050	0.044	0.044
	ζ_R	0.53	0.44	0.38	0.39
1.2	h_R	0.039	0.032	0.028	0.028
	ζ_R	0.53	0.44	0.38	0.39
1	h_R	0.027	0.022	0.019	0.020
	ζ_R	0.53	0.44	0.38	0.39
0.8	h_R	0.017	0.014	0.012	0.013
	ζ_R	0.53	0.44	0.38	0.39
0.6	h_R	0.009	0.008	0.007	0.007
	ζ_R	0.53	0.44	0.38	0.39
0.4	h_R	0.004	0.004	0.003	0.003
	ζ_R	0.53	0.44	0.38	0.39

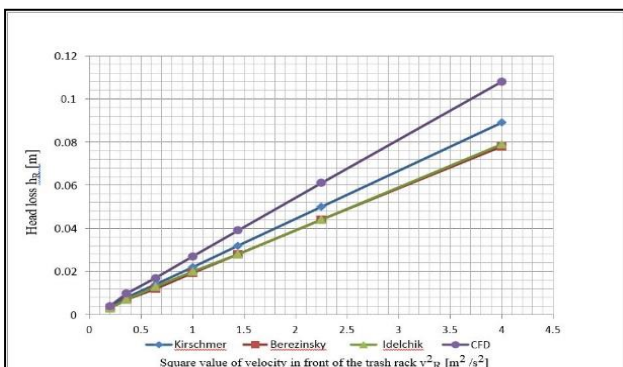


Fig.9: Comparison of head loss values for the case of steady normal flow through the trash rack with vertical bars with circular cross section [1].

As it can be concluded from the obtained results, CFD simulation can be successfully used for determining the value of the head loss caused by the flow parameters and trash rack itself. However, it is highly recommended that those results should be checked by comparing them to the equations and expressions from the literature.

4.2 Unsteady flow simulation

Unsteady (transient) flow is natural case of water flow when all of the flow parameters have different values over the time (unsteady flow can be described as vortical, unstable, chaotic, nonlinear and dissipative). The idea was to compare results of the steady and unsteady simulations of normal flow through the trash rack, so it can be seen whether or not the steady flow simulations are suitable to be used for this level of research (since unsteady simulation needs a far better computer for calculations, more time and memory). It should be noted that 20 seconds of flow simulation took around 15 hours to complete and around 50 GB of hard disk storage room. For that reason, only trash rack with rectangular cross section of the bars was used.

Since the results of unsteady simulations are almost identical to the results of steady simulations presented in Table 1 and Figure 7, only the tabular results are given:

Table 4: Comparison of head loss values from steady and unsteady CFD simulation of the river flow through the trash rack with vertical bars with rectangular shaped cross section [1].

Flow velocity	$h_{R, \text{steady}}$	$h_{R, \text{unsteady}}$
2	0.103	0.104
1.5	0.058	0.059
1.2	0.037	0.038
1	0.026	0.026
0.8	0.016	0.017
0.6	0.009	0.0094
0.4	0.004	0.0042

Table 5: Comparison of head loss coefficient values from steady and unsteady CFD simulation of the river flow through the trash rack with vertical bars with rectangular shaped cross section [1].

Flow velocity	$h_{R, \text{steady}}$	$h_{R, \text{unsteady}}$
2	0.103	0.104
1.5	0.058	0.059
1.2	0.037	0.038
1	0.026	0.026
0.8	0.016	0.017
0.6	0.009	0.0094
0.4	0.004	0.0042

It can be concluded that steady simulation is suitable for usage when it comes to this type of research/simulation. For more complex situations and specific phenomena which could possibly occur, it is recommended to use the unsteady setup of the simulation and run it for a far longer period (measured in days or even weeks).

5. STEADY INCLINED FLOW SIMULATION

It is vital to find out what happens with the flow parameters when river flow is not perpendicular to the trash rack. The case of inclined flow is very common, and

the interesting fact is that the angle of the flow (δ) has different values at different water depth level (this fact was not part of research).

For the purpose of the simulation, 4 value of flow angle were analysed (15° , 30° , 45° , 60°). In CFD simulation's setup 2 intakes were chosen and only trash rack with vertical bars with rectangular cross section was taken into consideration. Inclined flow is presented in figure 10:

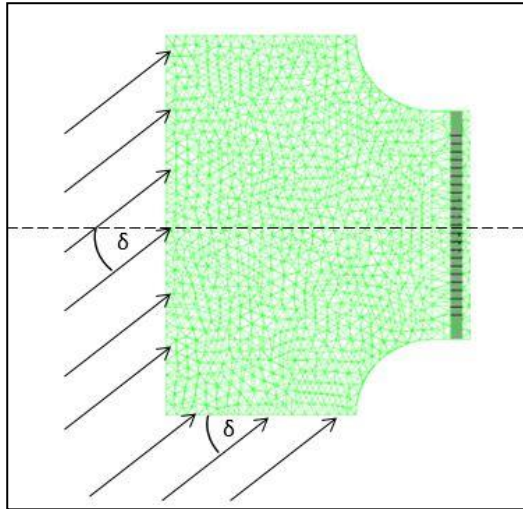


Fig.10: Inclined flow direction at the entrance of analysed model.

Since the entrance to the trash rack's area is rounded, it tends to rectify the flow which means that flow angle does not have that big influence on head loss value. However, after the simulations were done it was clear that flow angle at the entrance of the model (δ) is different than the actual flow angle in front of the trash rack (δ_R). Same applies to the velocity. Like in the case of normal flow (figure 6), velocity change for different flow angles is represented in the following figure ($v_R=2$ m/s):

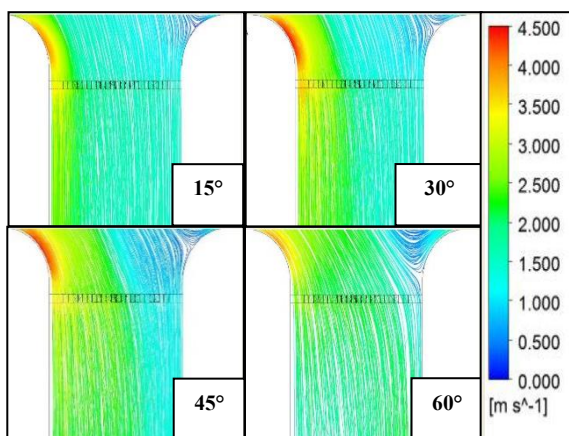


Fig.11: Stream velocity change in case of the inclined flow for different flow angles [1].

Also, when it comes to the head loss calculation in case of inclined flow there is one change to the equation 1: horizontal component of stream velocity (v_z) is used for calculation instead of v_R . Results are given in following tables for 4 different stream velocity values:

Table 6: Flow parameters in case of inclined flow through the trash rack when the angle is equal to 15° [1].

$\delta=15^\circ$				
$v_{R, \text{entr}} \rightarrow v_{R, \text{trash rack}}$	δ_R	v_z	ζ_R	h_R
2 \rightarrow 1.646	10.8	1.676	0.461	0.0657
1.2 \rightarrow 0.987	10.8	1.005	0.459	0.0236
0.8 \rightarrow 0.786	10.7	0.672	0.457	0.0105
0.4 \rightarrow 0.393	10.8	0.336	0.460	0.0026

Table 7: Flow parameters in case of inclined flow through the trash rack when the angle is equal to 30° [1].

$\delta=30^\circ$				
$v_{R, \text{entr}} \rightarrow v_{R, \text{trash rack}}$	δ_R	v_z	ζ_R	h_R
2 \rightarrow 1.746	13.9	1.799	0.463	0.0764
1.2 \rightarrow 1.047	13.9	1.079	0.463	0.0275
0.8 \rightarrow 0.698	13.9	0.719	0.463	0.0122
0.4 \rightarrow 0.388	14	0.359	0.465	0.0031

Table 8: Flow parameters in case of inclined flow through the trash rack when the angle is equal to 45° [1].

$\delta=45^\circ$				
$v_{R, \text{entr}} \rightarrow v_{R, \text{trash rack}}$	δ_R	v_z	ζ_R	h_R
2 \rightarrow 1.728	17.51	1.812	0.473	0.0792
1.2 \rightarrow 1.037	17.38	1.087	0.473	0.0285
0.8 \rightarrow 0.690	17.47	0.724	0.475	0.0127
0.4 \rightarrow 0.346	17.22	0.362	0.479	0.0032

Table 9: Flow parameters in case of inclined flow through the trash rack when the angle is equal to 60° [1].

$\delta=60^\circ$				
$v_{R, \text{entr}} \rightarrow v_{R, \text{trash rack}}$	δ_R	v_z	ζ_R	h_R
2 \rightarrow 1.549	24.53	1.703	0.521	0.077
1.2 \rightarrow 0.928	24.61	1.021	0.523	0.0278
0.8 \rightarrow 0.618	24.60	0.680	0.522	0.0123
0.4 \rightarrow 0.308	24.65	0.339	0.523	0.0031

As it can be seen, head loss values merely change compared to the case of normal flow (when the entrance to the trash rack's area is rounded). However, values of flow velocity are different (lower), so inclined flow can affect parameters behind the trash rack which are, in case of the hydropower plant, the intake parameters of the water turbine.

6. CONCLUSION

Trash racks are very responsible and important parts of hydropower systems. They are exposed not only to the accumulation of water debris, but also to stream velocity and flow angle variations. The purpose of this paper is to represent analyses of different exploitation conditions of the flow through different types of trash racks, and to determine how those conditions change flow and energy parameters.

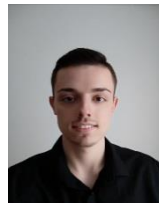
After all analyses were done, a list of conclusions can be written as the summary of the research:

- CFD simulations can be used for calculation of head loss and head loss coefficient in case of the normal flow through the trash rack. However, it is also recommended to calculate those parameters by using different equations, so the results obtained from simulations can be both checked and compared to the calculated ones.
- When it comes to the selection of the cross section shape of trash rack's bars, the head loss value cannot be primary criteria, since the shape barely affects head loss as a parameter. However, economic aspect can be used as criteria since the more complex shape of bar requires more detailed and precise production – so it is more expensive.
- Although real flow is always unsteady (transient), the results show that both steady and unsteady setup of simulation can be used, since in both cases results are almost identical. However, unsteady simulations take way more time to complete, and they require a very powerful computer for running the simulations.
- Building the rounded entrance to the trash rack area is highly recommended since it is shown that the geometry of the entrance rectifies the inclined flow and reduces head loss values variations. It should be noted that rounded entrance also lowers stream velocity, so the inclined flow can still affect the intake parameters of the water turbine, which is behind the trash rack.
- For the future researches, it is recommended to run simulations on supercomputer, so the CFD mesh can be denser (it could be made from tens or hundreds of millions of elements compared to the mesh used in this research which consists of 3 millions of elements).

REFERENCES

- [1] KRUNIĆ, M. (2016) *Numerical analyses of trash racks characteristics under different exploitation conditions in hydropower plants* (in serbian: *Karakteristike rešetki pri uslovima eksploatacije u hidroelektranama*), master thesis, University of Belgrade Mechanical Engineering Faculty
- [2] BENIŠEK, M. (academic year 2015/16) *Hydropower plants and equipment; Part two (lectures)*, (in serbian: *Hidroenergetska postrojenja i oprema; Drugi deo*), University of Belgrade Mechanical Engineering Faculty, pp 12-13
- [3] DAVIS C. V., SORENSEN K. E. (1969) *Handbook of applied hydraulics*, McGraw-Hill, Chapter 24, pp 14-15
- [4] IDEL'CHIK I. E. (1966) *Handbook of hydraulic resistance – Coefficients of local resistance and friction*, U. S. Atomic Energy Commission and National Science Foundation, Washington, pp 325-330

CORRESPONDENCE



Miloš KRUNIĆ, M. Sc. Eng.
University of Belgrade
Mechanical Engineering Faculty
Kraljice Marije 16.
11120 Beograd, Serbia
krune92@gmail.com



Ivan BOŽIĆ, Assist. Prof.Dr.Sci.
University of Belgrade
Mechanical Engineering Faculty
Kraljice Marije 16.
11120 Beograd, Serbia
ibozic@mas.bg.ac.rs

ANALYSIS OF TRANSIENTS IN HYDROELECTRIC POWER PLANTS FOR SPECIFIC OPERATIONAL REGIMES

Jovan ILIĆ
Ivan BOŽIĆ

Abstract: In this paper one of possible working regimes of a hydroelectric power plant is investigated. Analysis of sequential turbine starts and their implementation is one of modern approaches that should be taken into account during building of a new energetic system. In this paper results of simulations and analyses of sequential turbine starts in a hydroelectric power plant „Piroć“ are presented. Those results are compared to a regimes that are currently used in that system. Equations that describes simulations are shortly presented along with method that is used for their implementation.

Key words: water-mass oscillations, transients, sequential starts, hydropower plant working regimes.

1. INTRODUCTION

Hydropower plants, as very flexible systems, occupy top area on electro-energy diagram of a country. Every change in required power is successfully balanced by these power production systems. Power manipulation is done by closing/opening turbine gate and this process has an effect on all elements in a Plant. Various turbine operations such as start-up, shut down, load acceptance or rejection produce transients in hydroelectric power system. Calculation of hydro-mechanic transients during normal, special or emergency working regimes is very important during construction and exploitation of hydropower plant. This phenomenon requires serious approach taking into account possible consequences like human lives and expensive equipment loss. Intense pressure oscillations, during transient state, represent major problem for penstock, turbine regulation and other equipment and that pressure can be several times higher than normal. There are six groups of transient analysis that should be taken into account during construction of a hydropower plant (HPP) and they are represented in table 1. Which analysis needs to be done depends on the elements that hydropower plant possesses. The basis of this paper are water-mass oscillations analyses, although equations that are used for water hammer research are the same. Turbine shut-down, especially in emergency situations, is followed by large pressure oscillations in water supply system. It is of great importance to have precise information on extreme pressure values in system. Analyses of water-mass oscillations are followed by low frequency, but long term oscillations, and by analyzing them designer chooses pipe dimensions and dimensions of the surge tank. In this paper, those analyses are done

Table 1: Types of transient analyses in HPP

No	Analysis	Explanation
1.	WMO	Water-mass oscillations. These analyses are done if there is a surge tank in HPP. These transients are followed by low frequency pressure oscillations in a tunnel (reservoir – tunnel – surge tank).
2.	WH	Water hammer analyses are important for the calculation of pressure oscillations in a penstock (reservoir – pipe – turbine).
3.	TGOV	Turbine governing. These analyses are used to define turbine gate maneuvering while HPP is working and needs power change.
4.	HOCH	Hydraulic oscillations. These researches are done to define possible resonance between quasi-settled oscillations of every element in a HPP.
5.	OPCH	Open channel. This research is done if s HPP has open channel as an element.
6.	LGOV	Level governing. These analyses are most often required if there is more than one HPP on the same flow - cascade.

for a specific HPP, named “Piroć”. With already defined construction and operating modes, there is a better chance of synchronizing equations for simulations of transient regimes in a hydroelectric power system. HPP “Piroć” as a well-equipped hydropower plant is a good example for

analysis so the further on presented results are neither a part of previous design activities nor a part of existing project documents. Therefore, mathematical models were developed and necessary numerical simulations were performed.

2. HPP “PIROT” TRANSIENTS SIMULATION

Hydroelectric power plant “Piro” is located in the south-east of Serbia. This facility is using potential energy from “Zavojsko” lake which has an altitude of 600 m above sea level and presents upper reservoir. Level of the lower water is around 370 m. HPP “Piro” is equipped with two Francis turbines of 40 MW each, rotational speed of 500 rpm, and maximum flow up to 45.6 m³/s. Considering gross head and field topology, this plant has more than eight kilometres of tunnels and around two kilometres penstock of derivation systems. At the end of the tunnel part there is a surge tank placed as one of security elements. Another security element of the plant is synchronous valve which is placed directly on spiral casing. HPP scheme is presented in figure 1 with its main parts.

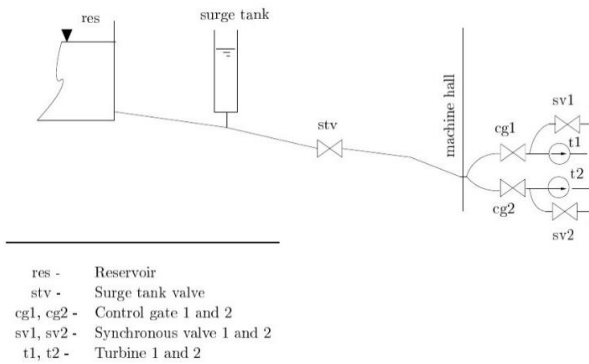


Fig.1: Hydro power plant “Piro” scheme [5]

Equations that are included in this paper along with the ones given in the literature made it possible to form a program for numerical simulations of transients in HPP.

3. EQUATIONS WHICH DESCRIBE TRANSIENTS IN HPP

Analysis of transients in hydro power plants is done through mathematical model that is formed for numerical simulation. Equations that are used are basic equations of fluid mechanics – continuity equation and dynamic equation. These equations were adjusted so they could be successfully implemented in mathematical model. Most of them can be found in literature [1], but for some cases [3] and [4] are recommended. The method of characteristics is used in numerical simulations. The purpose of this method is to convert partial differential equations into solvable normal differential equations. In the researched case, there are two matrices of coefficients and two familiar lines that are defined as Characteristics. These equations of characteristics are:

$$Q_P = C_P - C_a \Pi_P \quad (1)$$

$$Q_P = C_n + C_a \Pi_P \quad (2)$$

where “P” is an index for the next time step, Q is discharge and Π is piezometric head. Coefficients C_P and C_n are defined as:

$$C_P = Q_A + \frac{gA}{a} \Pi_A - \frac{\lambda \Delta t}{2DA} Q_A |Q_A| \quad (3)$$

$$C_n = Q_B - \frac{gA}{a} \Pi_B - \frac{\lambda \Delta t}{2DA} Q_B |Q_B| \quad (4)$$

where “A” is cross-section area of the pipe, “a” is wave velocity, “D” is diameter of the pipe, λ is friction coefficient and Δt is time step which is needed to fulfill criteria of numerical stability. Indices “A” and “B” are defined in previous time step as shown in figure 2.

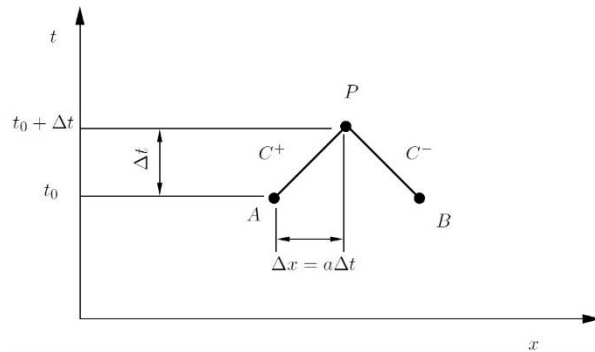


Fig.2: Principle for calculation of next time step by method of characteristics [5]

This method is most commonly used in engineering practice and it is recommended in literature [2]. For this method to be used, boundary conditions must be defined at the beginning and at the end of the pipe in all internal points. Boundary conditions that are used for mathematical modeling of hydroelectric power plant are defined in master thesis [5] and they are not subject of this paper.

4. STABILITY CRITERIA FOR NUMERICAL CALCULATION

Certain conditions must be fulfilled so that method of characteristics can give proper results. Rapidly growing error during calculation indicates numerical instability. Analysis of stability criteria is very complex and there were many recommendations about conditions that should be fulfilled. Recommendation by Perkins is:

$$\frac{\Delta t}{\Delta x} < \frac{1}{a} \quad (5)$$

In addition, Courtan’s researches present that equality in previous equation is also acceptable and recommended. Chaudhry recommends equation (6) which is related to more complex systems [1].

$$\Delta t = \frac{L_i}{a_i n_i} \quad (6)$$

where “L” is pipe length and “n” is number of sections into which pipe is divided.

5. SEQUENTIAL STARTS IN HPP “Piroć”

Series of researches were made during analyses of transients in HPP “Piroć”. Analyses considering water-mass oscillations and water hammer were investigated and part of water-mass oscillations analyses is represented here. One of operating regimes that is investigated is sequential turbine starts. Sequential starts are usually investigated during construction of HPP when low investment is needed. Main feature of these regimes is that minimal time difference between starts of turbine generator units is defined. By doing this restriction it is possible to build up a system with less material and cheaper security elements. Main effect during simultaneous turbine starts is pressure drop, this effect can be mitigated by doing sequential starts. These operation regimes are compared to the simultaneous turbine starts. Change of characteristic parameters during start of both turbines at the same time is shown in figure 3.

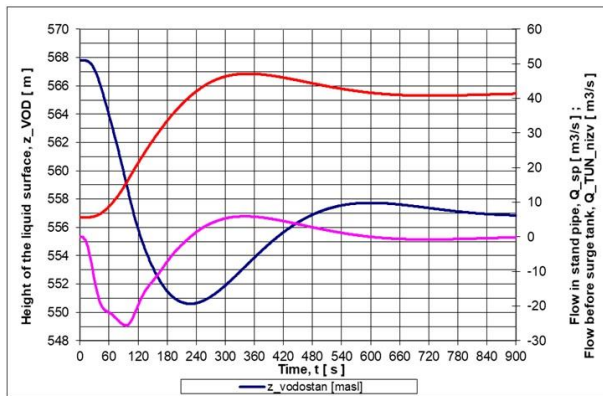


Fig.3: Simultaneous turbine start of two turbine generator units [5]

Change of the height of the liquid surface in the surge tank, change of flow rate in the stand pipe and change of flow before the surge tank are presented. Values of the main parameters that define hydroelectric power plant are: reservoir height $H_{res} = 576$ m, discharge at the start $Q_{start} = 5.8$ m³/s and turbine gate opening duration of 90 seconds. It is shown that minimal height of the liquid surface in the surge tank is 531m. This value defines bottom of the surge tank as it must not be higher than this. Improper construction of the surge tank, in the way that it is higher than it should be, can make catastrophic consequences during air suction in pipe system. In this paper two cases are taken into account. The first is with a delay of 90 s and the second is with a delay of 180 s between starts. In both cases turbine gates were opening to full load in 90 seconds. The opening way of turbine valves gates open is shown in figure 4 for the first case.

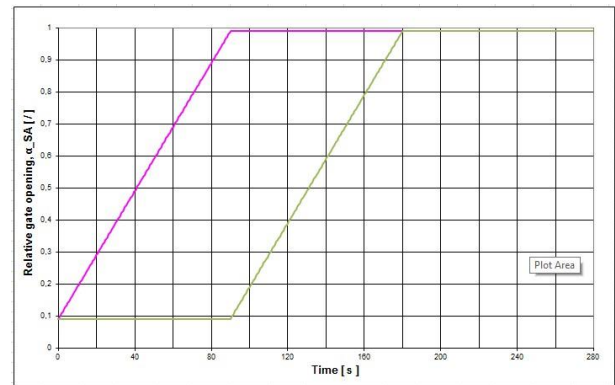


Fig.4: Turbine gates of two turbine generator units during sequential start with 90 s delay [5]

The values of characteristic parameters are shown in figure 5.

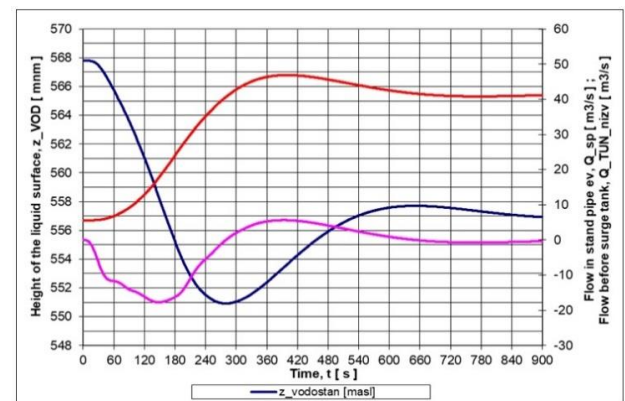


Fig.5: Sequential turbine start of two turbine generator units with a delay of 90 sec [5]

Figure 5 shows that there is no noticeable change in height of the liquid surface of the surge tank during sequential start with delay of 90 s with comparison to the simultaneous start. Further on, in case two, analysis of sequential turbine start with delay of 180 seconds is performed. For the second case where both turbines are also started to full load, the opening way of turbine gates is shown in figure 6.

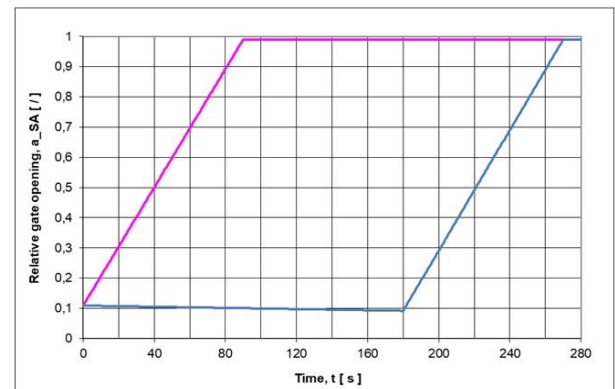


Fig.6: Turbine gates of two turbine generator units during sequential start with 180 sec delay [5]

The values of characteristic parameters for case two are shown in figure 7-

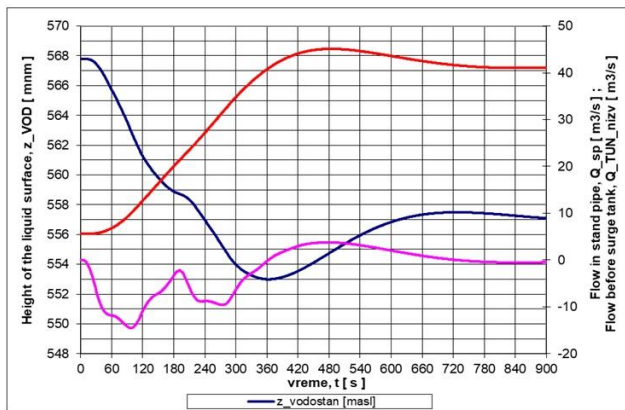


Fig.7: Sequential turbine start of two turbine generator units with a delay of 180 sec [5]

In this case there are visible changes in pressure drop which is defined through height of the liquid surface in surge tank and decreases to 553 m. There is a 2 m difference in height. This difference is not enough for this working regime to be adopted so it would be useful to continue research of this regime on a hydroelectric power plant "Piroć".

6. CONCLUSION

Calculation of fluid transients presents one of the greatest problems and challenges during construction of a hydroelectric power system. Extreme values of parameters that follow these phenomena are investigated and the results are used for the construction of basic elements. Wrong calculation may cause serious casualties and expensive damages of every part of the plant. Analyses of transients are necessary and they are done whenever a new energy system is built. Sequential starts give possibility for HPP building to become cheaper through operating limits and procedures. Sequential turbine starts were part of the master thesis [5] and the level of their examination is shown in this paper. Although it is already clear that these analyses are not very useful for the existing hydroelectric power plants, the idea is to present them and to show the way of their implementation. The more turbine generator units in hydroelectric power plant, the greater the requirement for this type of regime. This paper presents a comparison between simultaneous and sequential turbine starts. Numerical simulations were performed using original software developed within master thesis [5]. This software gave unlimited possibilities for performing tests of any working regimes in a hydroelectric power plant considering water-mass oscillations and water hammer oscillations. Results are showing that these working regimes are useful and should be implemented in a system if needed. Further investigation should be placed in projects for new hydroelectric power plants and in that way these analyses may become valuable.

REFERENCES

- [1] CHAUDHRY, H. (2014) *Applied hydraulic transients*, College of Engineering and Computing, University of South Carolina, Columbia, SC, USA.
- [2] CRNOJEVIĆ, C. (2014) *Mehanika fluida*, University of Belgrade Faculty of Mechanical Engineering, Belgrade (in Serbian)
- [3] IVETIĆ, M. (1996) *Računska hidraulika Tečenje u cevima*, Faculty of Civil Engineering, University of Belgrade, Belgrade (in Serbian)
- [4] КРИВЧЕНКО, Г. (1989) *Расчеты на микроалькмуляторах переходных процессов в гидроэлектростанциях*, Energoatomizdat, Moscow
- [5] ILIĆ, J. (2017) *Transients in hydroelectric power plants – modeling, numerical simulations and analysis of normal, special and emergency working regimes*, M.Sc. thesis, University of Belgrade Faculty of Mechanical Engineering, Belgrade (in Serbian)

CORRESPONDANCE



Jovan ILIĆ, M.Sc. Eng.
University of Belgrade
Mechanical Engineering Faculty
Kraljice Marije 16.
11120 Beograd, Serbia
jovan.z.ilic@gmail.com



Ivan BOŽIĆ, Prof. D.Sc. Eng.
University of Belgrade
Mechanical Engineering Faculty
Kraljice Marije 16.
11120 Beograd, Serbia
ibozić@mas.bg.ac.rs

THE FIRST FLUE GAS DESULPHURIZATION PLANT FOR THE COAL-BURNING THERMAL POWER PLANTS IN SERBIA

Miroslav CRNČEVIĆ
Dragan ŽIVIĆ
Perica KRSTIĆ

Abstract: *The primary goal of environmental protection in the field of energetics in the Republic of Serbia is the reduction of sulphur oxide emission from the large boilers of the thermal power plants. Pursuant to the valid legislation in the Republic of Serbia (Environmental Protection Law – Official Gazzette of RS, no 135/04) and with the purpose of complying with the requirements of the EU directive for large combustion plants (EU Directive no. 2001/80/EC), the first flue gas desulphurization plant, which burns lignite from the Kostolac mine, was built and put into trial operation at TPP Kostolac B (2x350MW).*

This study shows the design and technical solutions, performed works, installed equipment and results received from the guarantee testing of this plant.

Key words: *environmental protection, sulphur oxide, limestone, gypsum*

1. INTRODUCTION

The necessity for building the flue gas desulphurization plant (FGD plant) at TPP Kostolac B came from the obligation to apply the national and international regulation in the field of the environmental protection. Meeting these requirements should provide obtaining the ecology licence, mandatory for the TPP Kostolac B further operation.

Relatively high content of the total sulphur in the Kostolac coal basin (approx. 1,3%) and the access emission of sulphur oxides in flue gasses at TPP Kostolac (5.000 – 7.000 mg/m³), were the reason that the first flue gas desulphurization plant in thermal power plants in Serbia was designed and constructed in TPP Kostolac B. Pursuant to the valid Environmental Law (Official Gazzette of the Republic of Serbia no.135/04) and the National Environmental Programme of the Republic of Serbia, and within the measures of substantial development and environmental management, as one of the primary goals was protecting the environment from the access emission of sulphur oxides from the big burners (EU Directive no.2001/08/EC), Public Enterprise ELECTRIC POWER INDUSTRY OF SERBIA – Belgrade, has concluded the contract with the Chinese company CMEC- Beijing, China for designing, delivery of the required equipment and construction of the flue gas desulphurization plant, created by coal combustion in the boilers of the TPP Kostolac B two units, both having the power of 2 x 348,5 MW.

Based on the Investor's Design Task (PE EPS Belgrade) for preparing the Detailed Design, and the basis for designing and offered and contracted equipment, the Detailed Design was prepared by the designing company

ENERGOPROJEKT Entel-Belgrade. After expert's control of this design and technical documentation, and based on the Report by the Republic Revision Committee and the Design Task, the Building Permit Design was done by the consortium consisted of the companies: 'Kirilo Savic' Institute, Belgrade and Designing company NDC, Belgrade.



Fig.1

2. DESIGN BASIS

The design basis are provided in the Design Task and shown in the following tables.

Table 1: Flue Gas Characteristics

Item	Unit	Parameter
Flue gas temperature	°C	175
Flue gas flow (S.T.P., dry base, Oxygen)	m ³ /h	1469000
Flue gas flow (S.T.P., wet base, Oxygen)	m ³ /h	1830530
Flue gas flow (170°C, wet base, real oxygen)	m ³ /h	2970000
H ₂ O (S.T.P., wet base, Oxygen)	vol. %	19.75
O ₂ (S.T.P., wet base, Oxygen)	vol. %	8
CO ₂ (S.T.P., wet base, Oxygen)	vol. %	11.46
Concentration of SO ₂ (S.T.P., dry base, 6% O ₂)	mg/Nm ³	7661
Concentration of ash (S.T.P., dry base, 6% O ₂)	mg/Nm ³	50
Concentration of SO ₃ (S.T.P., dry base, 6% O ₂)	mg/Nm ³	50
Concentration of HCL (S.T.P., dry base, 6% O ₂)	mg/Nm ³	50
Concentration of HF (S.T.P., dry base, 6% O ₂)	mg/Nm ³	50

Table 2: Limestone characteristics

Parameter	Unit	Base	Gypsum for disposal	Gypsum for the plates
Free moisture	%	dry	≤ 5.0	≤ 5.0
Calcium Carbonate CaCO ₃	%	dry	≥ 89.0	≥ 94.0
Magnesium carbonate MgCO ₃	%	dry	≤ 4.0	≤ 3.0
Silicone dioxide SiO ₂	%	dry	≤ 5.0	≤ 3.0
Iron oxide Fe ₂ O ₂	%	dry	-----	≤ 0.8
Total inert (incl. MgCO ₃)	%	dry	≤ 11.0	≤ 6.0
Particles size analysis	mm	dry	19.05 x 0	19.05 x 0
Bond index (BWI)	KWh/T	as received	≤ 12.0	≤ 12.0

3. DESCRIPTION OF FGD PLANT

3.1. Location of the plant

FGD Plant is located on the vacant area behind the Units B1 and B2 within the TPP Kostolac B. The proposed location has enough space for placing the FGD Plant. The arrangement of the mentioned systems of the plant for flue gas desulphurization using the wet procedure was agreed with the TPP Drmno Urban Plans (TPP Kostolac B) and OCM Drmno, established in the year 1982 and with the arrangement of the new ash and slag transportation system. The requirements for the area needed for building one or two more Units for the TPP Kostolac B were also considered.

The by-product of the flue gas desulphurization process is gypsum. Gypsum disposal area, which cannot be used commercially at time being, will be located in the available area of the closed part of the open cast mine Drmno.

Placing the gypsum disposal site in the exploited part of the open cast mine Drmno is favourable solution in respect of the environmental protection, since it does not require additional space, and provides possible re-usage of the material disposed in such manner. On the area in question a protective foil was put thus preventing the surface waters to reach the ground and the underground waters, figure no.2.

3.2. The designed technology of the plant operation

The TPP Kostolac B FGD Plant designing principles were the following:

1. The proces uses the moist-wet procedure 'from limestone to gypsum',
2. One absorber was designed and installed from each boiler,
3. The designed efficiency of the flue gas desulphurization, being min.97,5%, meets the boiler operation with maximum capacity while burning the designed coal of the lowest quality,
4. CO₂ emission does not goes over 200 mg/Nm³ in designed conditions,
5. One bypass channel for the flue gas was designed for safe functioning of the process with the load up to 100% of the FGD Plant operation,
6. FGD Plant is min.95% disposable,
7. Working life of the Plant is 15 years.

3.3. FGD plant consists of the following systems:

- Limestone storage and limestone slurry preparation system - sorbent,
- Absorber system,
- Flue gas system,
- FGD Plant process building,
- Dewatering system and gypsum transportation system,
- FGD Plant pipe bridges,
- Transportation system,
- Chimney, and
- Electrical installations.

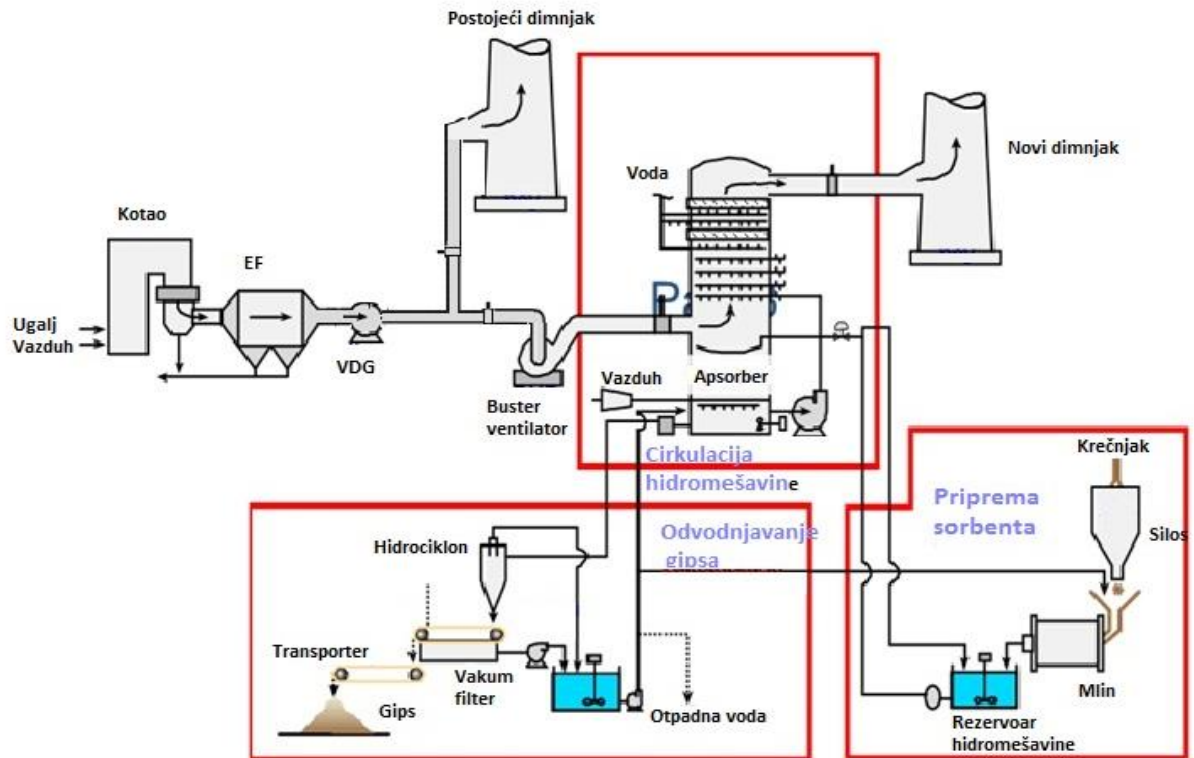


Fig.2. FGD Plant designed process diagram is provided in the following scheme

3.4. Limestone storage and limestone slurry preparation system -sorbent

Limestone slurry preparation system (including limestone storage, grinding and delivery systems) includes:

- Limestone storage with the capacity of about 5040 t, 75m long, 26m wide and 9m high. The limestone is stored up to 4m in height. Limestone storage provides the supplies for approx.7 working days for both Units,
- Limestone is delivered from the warehouse by the wheel loaders to the underground hopper-bunker to the adjacent object for limestone slurry preparation,
- The limestone is transported to the limestone silos via vibration doser and the elevator. Limestone silos, with the effective volume of 2.200 m³, provides the necessary supply of limestone for the continuous operation of both units for 72 hours. The limestone is carried from the silos via belt conveyor to the mill grinders (wet ball mills),
- The limestone is being grinded by the two wet balls mills that provide the needed granulation of the limestone particles. Limestone particles cannot be larger than 44 microns,
- The preparation of the limestone slurry is joint for the both Units, B1 and B2 and the necessary slurry is being provided (30% of limestone and 70% of water) until meeting the requirements for the limestone particles size. Limestone slurry is pumped into the hydrocyclone and separated. The sediment (including also the larger particles) is then returned into the grinder and the upper flow automatically goes into the limestone slurry tank,
- Limestone slurry preparation system is apart from the absorber system,

A large limestone slurry tank is placed near the absorber system. The slurry is being delivered into the absorbers via limestone slurry pumps,

- Limestone suspension accumulating tank and three pumps for limestone slurry were designed and placed near the limestone slurry preparation system.

3.5. Absorber system

One absorber was designed for each Unit. Absorber diameter is 15,3m and reaction basin diameter is 16,9m.

Flue gasses from the boilers enter the absorbers above the liquid level in the absorber reaction basin and they flow upwards with the designed speed of 3,8m/s.

Inside the absorber at the certain levels there are nozzles (sprinklers) for making the limestone slurry fog. Flue gas pass through the spreaded limestone slurry fog thus activating the chemical reaction of purifuing the flue gas from the sulphur oxides and forming the gypsum slurry. Through the two lines of droplets eliminators installed above the line of nozzles, the flue gas pass through and exit the flue gas outlet located at the top of the absorber and move into the clean flue gas channels (fig.3).

Dimensioning of the absorber circulation pump used in the process, must be determined depending on the boiler load and the actual needs for the absorbtion slurry. The slurry that circulates and that has absorbed SO₂, falls into the absorber reaction basin. On the absorber walls in the absorber reaction basin, the four sets of gypsum slurry mixer were installed.

Air Fan (air blower) for oxidation provides the oxygen for the oxidation in the reaction basin. The oxidation air distribution system applies the 'air eruption' principle.

The system for intervent cooling of the flue gas was installed at the flue gas inlet channel into the absorber, for the case of flue gas temperature rising. Each absorber has one emergency water tank located above the gas input into the absorber.

Gypsum slurry is transported from the absorber via discharge pump from to the system for gypsum dewatering.

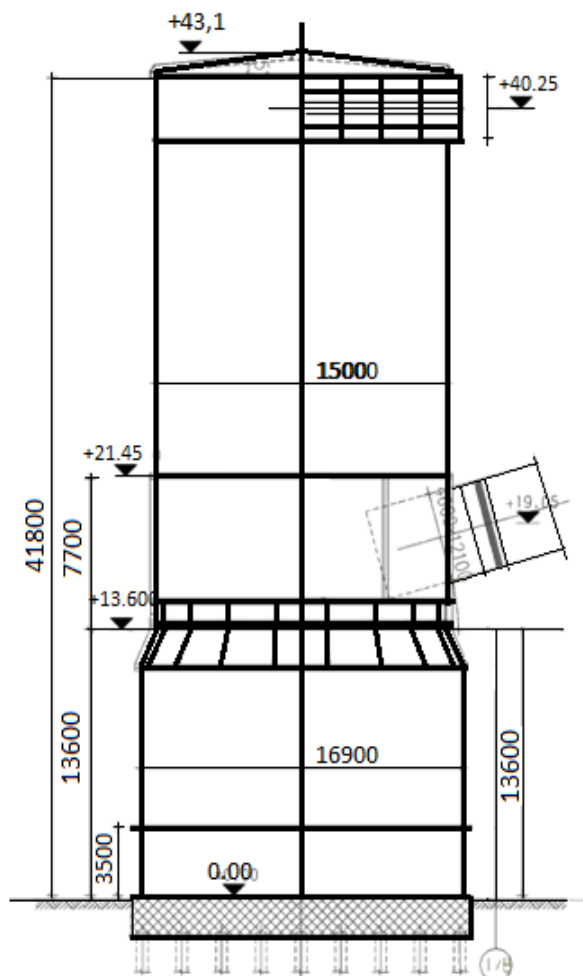


Fig. 3 Absorber

Two sets of liquid level gauges, two sets of pH gauges and one aerometer were designed for each absorber, for measuring and controlling the liquid level, pH measuring and measuring the gypsum slurry thickness.

In the absorber zone, one drainage pit with the mixer and the drainage pump was designed for each unit. The function of the drainage pit is to collect the slurry from absorber discharge and the water used for flushing the equipment and the pipeline and then transport it in the absorber or in the intervent slurry tank.

3.6. Flue gas system

A complete flue gas channels system was provided for each Unit. Into the flue gas system channels for each Unit booster up fans (BUF) were installed in the dry flue gas zone before entering the flue gas into the absorber.

Flue gas system channels mostly consist of the following 4 parts:

- Channel from the FGD fan output to the chimney, including the output bypass channel to the old chimney for the tour around the FGD Plant.
- Input channel into the BUF fan,
- Channel between BUF output and absorber input,

- Channel between the absorber output and the new chimney.

The hot flue gas from the suction fan, under pressure, created by the BUF fan, flows towards the absorber. The flue gas at the absorber input goes through the emergency cooling up to the temperature of <1800C.

Flue gas emergency cooling system was designed at the gas input into the absorber and consists of the water tank, nozzles and the flushing pipeline, water pump, valves and the auxilliary equipment. The pumps are located in the process building of the FGD Plant. Finally, the flue gas goes into the chimney. Temperature of the flue gas at the chimney output is 60 oC

- The stopples, installed in the flue gas system, provide the normal operation of the FGD Plant, as well as some emergency operations, via bypass line.

3.7. Gypsum drainage and transportation system

It consists of the subsystem for drainage (thickening) and gypsum transportation sub-system.

- **Gypsum drainage subsystem**

consists of the two-phased drainage process. The first phase is realized in the gypsum slurry hydrocyclone and the second phase is realized in the vacuum belt filter. Water content in the gypsum after the drainage is approximately < 10% .

Gypsum slurry from the absorber is transported to the gypsum slurry hydrocyclone via absorber discharge pump. in the case of damage or during the overhaul of the absorber, the same pump delivers the gypsum slurry into the emergency tank.

Overflow from the gypsum slurry hydrocyclone automatically enters the waste water hydrocyclone supply tank. After that, it is transported to the waste water hydrocyclone via waste water hydrocyclone supply pump. Outflow of the gypsum slurry hydrocyclone enters the vacuum belt filter for drainage.

Overflow of the gypsum slurry hydrocyclone is transported out the FGD system and the outflow automatically enters the filtrate water tank.

The design implies two vacuum belt gypsum filters.

After the dewatering the gypsum falls into the gypsum storage facility and then is transported via wheel loader from the storage facility to the gypsum discharge bunker.

- **Gypsum belt conveyors subsystem**

is equipped with all the necessary equipment between the underground basket to the disposal area and/or further gas distribution.

Gypsum transportation sub-system consists of the following:

- Underground basket for the gypsum,
- Other equipment for supplying the belt conveyors,
- Belt conveyors C1 to C4 with relay points,
- Remaining equipment (fans, controls, fire protection etc).

Below the underground basket – hopper, a belt feeder/doser was provided, for transporting the gypsum to the one-way belt conveyor. Via four in-line one-way belt conveyors the gypsum will be transported to the disposal area.

Gypsum conveyors consist of the 4 transporters (Cg-1, Cg-2, Cg-3, Cg-4) and 3 towers as the relay points (Tg-1, Tg-2, Tg-3). These towers are armoured concrete and steel constructions supplied with the manual chain cranes and infusion channels (hoppers).

3.8. The subsystems arranged in the process building of the FGD plant are:

- Process-technical water subsystem,
- Compressed air subsystems,
- Limestone slurry tank and the auxiliary equipment.

The subsystems for gypsum dewatering, process water and compressed air subsystem were designed to be used jointly between the Units B1 and B2.

• Process and technology water subsystem

This is the water used from the ash and slag pump station and via underground pipeline transported to the FGD Plant. One process water tank is installed in FGD system and its effective volume is sufficient for the water consumption.

Process water provides the complete FGD system with water, more precisely:

- flue gas and equipment cooling water,
- water for recharging (make-up) the absorber water,
- water for flusing the droplets eliminator,
- water for oxidation air moisture,
- water for flushing the gypsum from the drainage system,
- water for flushing the pipes of the FGD system and
- emergency fire water for FGD system.

• Discharge and drainage subsystem

This subsystem consists of the following equipment:

- two absorber drainage channels,
- one drainage channel in the limestone slurry preparation zone,
- one drainage channel in the gypsum thickening zone,
- one drainage channel in the emergency storage tank zone,
- one drainage channel in the chimney zone.

The mixer on the top and the submerged pump are installed on every drainage channel except the channel located in the chimney zone, where only the pump is installed, without the mixer.

• **Compressed air subsystem** in the FGD Plant consists of the instrumental air and service air used solely for maintainance purposes.

Two new compressors were installed (operating and standby) with the filters, air dryers and necessary armour.

3.9. Transportation system

The system for transportation, storage and mechanical constructions and technology includes:

- Solid materials storage with adequate equipment for transportation and disposal,
- Mechanical construction for transportation means – belt measuring limestone transporter to the grinder; bucket elevators for transporting limestone to the limestone silos; infusion basket and steel bar with the steel separator and vibro doser for the limestone transportation,

- Silo with the deduster on the top for limestone storage,
- Wet balls mills – grinders, as part of the main equipment of the limestone slurry preparation system,
- Mechanical construction for transportation means –belt conveyors for gypsum with adequate subsystems:
 - System for gypsum thickening/dewatering,
 - Process water system and
 - Limestone slurry tank and the auxiliary equipment.

3.10. Chimney

After the detailed technical and economical consideration of the possible design and technical solutions, it was desicec to design and construct a new chimney. Since there is a necessary area near the existing chimney 250m high, a new concrete chimney 177m tall was built and equipped with two cylindric steel pipes, with the diameter of 6,7m and 180m high, with titanium alloy in order to prevent condensate corrosion appearing on the pipe walls. The condensate which appered and is collected is transported via drainage channel into the chimney drainage pit and then via pump into the absorber or the emergency tank.

3.11. Electrical installations

The main supply for the FGD Plant was realized by building the separate 110kV voltage adapter and installing the two redundant transformers with the power of 2x25 MVA and the voltage of 110/6.6kV. For supplying the users of the voltage levels 6,3; 0,4 and 0,23 kV, the necessary number of necessary transformers and substations which are connected via required energy cables.

Safety supply of the priority uses was provided in three manners: double from the network and single from the diesel electric accumulator (DEA).

Supplying the single-current with the power of 30 kW was provided by installing the two lead storage batteries with the capacity of 2x400Ak and the voltage of 220V, which provide the 3 hours of operation for the JSS user with the total power of 30 kVA.

The supply voltage for the FGD Plant control system was provided using the necessary number of adequate apparatus for continuous supply – UPS, supplied from the network from the busbars 0,4/0,23 kV, from the emergency system or storage batteries.

Distribution and Control System (DCS) and Systems for continuous monitoring of gas emission (CEMS) are connected to central control of Units.

The installation of the lights, grounding, lightning protection, video surveillance and telecommunications were done pursuant to the needs of the FGD Plant as a whole.

4. GUARANTEE TESTING RESULTS

The following table shows the results of the conducted guarantee testing:

	Contracted guarantee values	Measured values B1	Measured values B2	Unit																										
Dust matters emission	30	<table border="1"> <tr><td>1</td><td>11,7±1,5</td></tr> <tr><td>2</td><td>11,2±1,5</td></tr> <tr><td>3</td><td>9,8±1,5</td></tr> <tr><td>4</td><td>11,1±1,5</td></tr> <tr><td>5</td><td>11,2±1,5</td></tr> <tr><td>6</td><td>10,2±1,5</td></tr> </table>	1	11,7±1,5	2	11,2±1,5	3	9,8±1,5	4	11,1±1,5	5	11,2±1,5	6	10,2±1,5	<table border="1"> <tr><td>1</td><td>20,7±2,4</td></tr> <tr><td>2</td><td>22,5±2,7</td></tr> <tr><td>3</td><td>23,1±2,8</td></tr> <tr><td>4</td><td>27,6±3,4</td></tr> <tr><td>5</td><td>27,0±3,3</td></tr> <tr><td>6</td><td>24,9±3,0</td></tr> <tr><td>7</td><td>19,9±2,4</td></tr> </table>	1	20,7±2,4	2	22,5±2,7	3	23,1±2,8	4	27,6±3,4	5	27,0±3,3	6	24,9±3,0	7	19,9±2,4	mg/Nm ³
1	11,7±1,5																													
2	11,2±1,5																													
3	9,8±1,5																													
4	11,1±1,5																													
5	11,2±1,5																													
6	10,2±1,5																													
1	20,7±2,4																													
2	22,5±2,7																													
3	23,1±2,8																													
4	27,6±3,4																													
5	27,0±3,3																													
6	24,9±3,0																													
7	19,9±2,4																													
Emission of SO ₂	200	<table border="1"> <tr><td>1</td><td>66,1±11,5</td></tr> <tr><td>2</td><td>64,5±12,3</td></tr> <tr><td>3</td><td>36,7±11,8</td></tr> <tr><td>4</td><td>30,4±11,4</td></tr> <tr><td>5</td><td>70,6±13,9</td></tr> <tr><td>6</td><td>63,7±12,5</td></tr> </table>	1	66,1±11,5	2	64,5±12,3	3	36,7±11,8	4	30,4±11,4	5	70,6±13,9	6	63,7±12,5	<table border="1"> <tr><td>1</td><td>163,0±15</td></tr> <tr><td>2</td><td>148,8±15,4</td></tr> <tr><td>3</td><td>153,3±15,1</td></tr> <tr><td>4</td><td>125,3±15,5</td></tr> <tr><td>5</td><td>191,9±16,4</td></tr> <tr><td>6</td><td>156,7±16,1</td></tr> <tr><td>7</td><td>113,3±16,5</td></tr> </table>	1	163,0±15	2	148,8±15,4	3	153,3±15,1	4	125,3±15,5	5	191,9±16,4	6	156,7±16,1	7	113,3±16,5	mg/Nm ³
1	66,1±11,5																													
2	64,5±12,3																													
3	36,7±11,8																													
4	30,4±11,4																													
5	70,6±13,9																													
6	63,7±12,5																													
1	163,0±15																													
2	148,8±15,4																													
3	153,3±15,1																													
4	125,3±15,5																													
5	191,9±16,4																													
6	156,7±16,1																													
7	113,3±16,5																													
Droplets content	100	23,9	77,8	mg/Nm ³																										
Energy consumption	20.733	19.832,46		kW																										
Noise level	85	<table border="1"> <tr><td>1</td><td>72</td></tr> <tr><td>2</td><td>74</td></tr> <tr><td>3</td><td>78</td></tr> </table>	1	72	2	74	3	78	<table border="1"> <tr><td>1</td><td>66</td></tr> <tr><td>2</td><td>82</td></tr> <tr><td>3</td><td>82</td></tr> </table>	1	66	2	82	3	82	dB														
1	72																													
2	74																													
3	78																													
1	66																													
2	82																													
3	82																													
Limestone consumption	19	<table border="1"> <tr><td>1</td><td>11,1</td></tr> <tr><td>2</td><td>11,6</td></tr> <tr><td>3</td><td>12,1</td></tr> <tr><td>4</td><td>11,8</td></tr> <tr><td>5</td><td>12,8</td></tr> <tr><td>6</td><td>12,4</td></tr> </table>	1	11,1	2	11,6	3	12,1	4	11,8	5	12,8	6	12,4	<table border="1"> <tr><td>1</td><td>13,7</td></tr> <tr><td>2</td><td>13,9</td></tr> <tr><td>3</td><td>11,0</td></tr> <tr><td>4</td><td>11,1</td></tr> <tr><td>5</td><td>11,7</td></tr> <tr><td>6</td><td>12,1</td></tr> <tr><td>7</td><td></td></tr> </table>	1	13,7	2	13,9	3	11,0	4	11,1	5	11,7	6	12,1	7		t/h
1	11,1																													
2	11,6																													
3	12,1																													
4	11,8																													
5	12,8																													
6	12,4																													
1	13,7																													
2	13,9																													
3	11,0																													
4	11,1																													
5	11,7																													
6	12,1																													
7																														
FGD efficiency	>97	<table border="1"> <tr><td>18.03. 2017.</td><td>98,8</td></tr> <tr><td>20.03. 2017.</td><td>99,4</td></tr> <tr><td>21.03. 2017.</td><td>98,8</td></tr> </table>	18.03. 2017.	98,8	20.03. 2017.	99,4	21.03. 2017.	98,8	<table border="1"> <tr><td>11.04. 2017.</td><td>97,3</td></tr> <tr><td>12.04. 2017.</td><td>97,3</td></tr> <tr><td>13.04. 2017.</td><td>97,5</td></tr> </table>	11.04. 2017.	97,3	12.04. 2017.	97,3	13.04. 2017.	97,5	%														
18.03. 2017.	98,8																													
20.03. 2017.	99,4																													
21.03. 2017.	98,8																													
11.04. 2017.	97,3																													
12.04. 2017.	97,3																													
13.04. 2017.	97,5																													

Statements:

Guarantee testing measured values provided within the previous table show that the values are in accordance with the contracted guaranteed values.

The results of the FGD Plan operation reliability must be monitored during the first year of operation of the Units' B1 and B2 FGD Plant. The contracted guaranteed values for the FGD Plant's operation must be exactly or better than 90% x 8.760 h.



Fig.4: Gypsum dump location in the excavated area of the open cast mine Drmno

5. CONCLUSIONS

The results of performed guarantee testing, conducted by the independent and accredited laboratories of the Mining Institute – Zemun and Electrotechnical Institute Nikola Tesla, Belgrade, have shown the adequacy of the selected technology for the plant's operation (wet procedure 'from limestone to gypsum') and proved that TPP Kostolac B FGD Plant including the applied technical solutions and installed equipment, have met the guaranteed technical parameters.

Based on previously performed retrofit of the Units, confirmed guarantee parameters for FGD Plant operation and the installed system for continuous monitoring of gaseous emissions (CEMS), and after completion of construction and commissioning of new waste water treatment plant, TPP Kostolac B shall meet conditions for obtaining the ecology permission for operation.

TPP Kostolac B FGD Plant has been constructed and commissioned as the first such plant in Serbian thermal power plants and may be used as model for obtaining the experience in developing, designing and construction of other similar plants.

REFERENCES

- [1] The design task.
- [2] Design and Technical Documentation
- [3] Guarantee testing report

CORRESPONDANCE



Miroslav CRNCEVIĆ, Mech.. Eng.
IMP Autometika d.o.o
Volgina 15
11000 Belgrade
miroslav.crncevic@pupin.rs



Dragan ŽIVIĆ, Mech. Eng.
JP"EPS" Belgrade
Branch TE-KO Kostolac
Nikole Tesle 5-7
Kostolac
Dragan.Zivic@te-ko.rs



Perica KRSTIĆ, El. Eng.
IMP Autometika d.o.o
Volgina 15
11000 Belgrade
perica.krstic@pupin.rs

THERMODYNAMIC ANALYSIS OF SYSTEM OF LOW-PRESSURE HEATERS THERMO-ENERGY PLANT

Ivana KECMAN
Mirko DOBRNJAC

Abstract: The objective of this paper is an exergy analysis of a system of low-pressure heaters. Low-pressure heaters for which the calculations were made are recuperative heat exchangers. The calculations were made on the basis of data onto the technology scheme for thermal power plant. Using values which are given in a scheme and taking into account that the calculations were made for water, steam, or their mixture, the values of unknown parameters were calculated. After determining the following parameters: temperature, pressure, enthalpy and entropy of water and steam, on the inlet and outlet of all heat exchangers by using the formula for exergy matter flow the values of exergies on the inlet and outlet of low-pressure heat exchangers were calculated. By using the exergy method of thermodynamics analysis exergy efficiency was obtained, and later checked by using entropy method of thermodynamics analysis.

Key words: exergy, water and steam, exergy efficiency, low pressure heater, recuperative heat exchanger

TERMODINAMIČKA ANALIZA SISTEMA ZAGRIJAČA NISKOG PRITISKA U TERMO ELEKTRANI

Abstrakt: Cilj rada je eksregetska analiza sistema zagrijača niskog pritiska. Zagrijači niskog pritiska za koje je rađen proračun su rekuperativni izmjenjivači toplote. Proračun je rađen na osnovu podataka iz tehnološke šeme termoenergetskog postrojenja. Korištenjem vrijednosti datih u šemi i uzimajući u obzir da se radi o vodi, vodenoj pari ili mješavini vode i pare, određene su vrijednosti nepoznatih parametara. Nakon što su određeni slijedeći parametri: temperatura, pritisak, entalpija i entropija, vode i vodene pare na ulazu i izlazu iz svakog zagrijača korištenjem formule za eksergiju toka materije proračunate su vrijednosti eksergija na ulazu i izlazu iz zagrijača niskog pritiska. Koristeći eksergijsku metodu termodinamičke analize dobijen je eksergetski stepen korisnog dejstva, koji je kasnije provjeren entropijskom metodom termodinamičke analize.

Ključne riječi: eksergija, voda i vodena para, eksergetski stepen korisnog dejstva, zagrijač niskog pritiska, regenerativni izmjenjivači toplote

1. UVOD

Na osnovu drugog zakona termodinamke, svaki oblik energije sastoji se od eksergije i anergije. Eksergija predstavlja onaj oblik energije koji se može neograničeno transformisati u rad, dok anergija predstavlja oblik energije koji se ne može prevesti u eksergiju.

Postrojenje u kome bi se realizovali povratni procesi je najbolje sa termodinamičkog gledišta. Međutim, povratni procesi nisu prihvatljivi sa praktičnog aspekta, iz razloga što bi se odvijali beskonačno sporo. Da bi proces u stvarnosti bio povratan bilo bi potrebno da ne bude prisutan ni jedan od uzročnika disperzije energije. Prelaz toplote bi teoretski mogao biti povratni proces samo u slučaju kada bi razlika temperatura bila beskonačno mala.

U stvarnim postrojenjima procesi koji se realizuju trebaju proticati brzinama prihvatljivim za tehničku praksu. Da bi se to moglo postići neophodno je da postoji razlika potencijala, zbog čega su stvarni procesi nepovratni. Pri nepovratnim (realnim) procesima dolazi do gubitka eksergije (rada). Savršenstvo postrojenja u termodinamičkom smislu se određuje prema stepenu njegovog odstupanja od teoretski najboljeg mogućeg (povratnog). Za određivanje eksergetskog stepena termodinamičkog savršenstva koriste se eksergijska i entropijska metoda termodinamičke analize.

U ovom radu su primjenjene obje metode i upoređeni su njihovi rezultati. Na početku rada dobijeni su svi neophodni parametri za svaki od četiri redno vezana zagrijača niskog pritiska. Nakon određivanja parametara dobijeni su stepeni korisnog dejstva, korištenjem obje metode, za jedan zagrijač niskog pritiska (u daljem tekstu ZNP), a zatim za sistem ZNP u cjelini korištenjem samo entropijske metode. Svi rezultati su prikazani tabelarno.

2. EKSERGETSKO I ENERGETSKO PROCJENJIVANJE TERMODINAMIČKOG SAVRŠENSTVA- UPOREDNA ANALIZA

Kao primjer uporednog energetskog i eksergetskog procjenjivanja termodinamičkog savršenstva možemo uzeti parni kotao i kondenzator.

Prema energetskoj analizi najveće gubitke ima kondenzator, skoro dvije trećine, jer se u njemu energija koja je dobijena od goriva odvodi u okolinu. Termodinamički stepen korisnosti kondenzatora prema energetskoj analizi je oko 33%. Dok se u parnom kotlu gubi samo oko 10% od energije unesene u ciklus, sa izlaznim dimnim gasovima i zbog nesavršenosti izolacije. Potpuno drugačiju sliku dobijamo ako iste elemente posmatramo eksergetskom analizom. Naime kotao ima najveću nepovratnost, jer se toplota sa dimnih gasova na vodu i vodenu paru prenosi sa velikim razlikama temperatura što dovodi do znatnih gubitaka eksergije. Za razliku od kotla, sa eksergetskog stanovišta, kondenzator je u velikoj mjeri termodinamički savršeniji, jer se toplota odvodi u okolinu pri znatno manjoj razlici temperatura.

Energetska analiza pokazuje da bi se trebali smanjiti gubici u kondenzatoru, dok eksergetska analiza pokazuje da bi se veća pažnja trebala posvetiti smanjivanju gubitaka u kotlu.

3. EKSERGETSKI STEPEN KORISNOSTI

Termodinamička analiza procesa koji se realizuje u nekom postrojenju se vrši na sledeći način:

1. postrojenje se kontrolnom granicom odvoji od okoline,
2. odrede se eksergije tokova materije i energije koje ulaze i izlaze kroz kontrolnu granicu (figura 1),
3. uporedi se odnos ulaznih i izlaznih eksergija.

U realnim postrojenjima suma izlaznih eksergija je manja od sume ulaznih za iznos gubitaka eksergije. Do gubitaka dolazi usljed nepovratnosti realnih procesa.

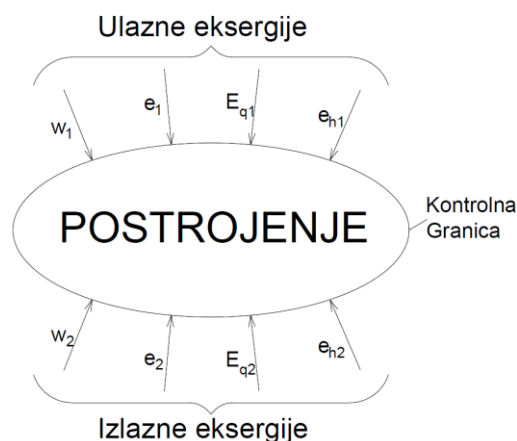


Fig.1: Postrojenje odvojeno od okoline kontrolnom granicom

Odnos izlaznih i ulaznih eksergija naziva se eksergetskim stepenom korisnosti:

$$\eta_e = \frac{\sum Ex_{iz}}{\sum Ex_{ul}} = \frac{\sum Ex_{ul} - D}{\sum Ex_{ul}}, \quad (1)$$

gdje su: η_e - eksergijski koeficijent korisnosti, Ex_{ul} - ulazne eksergije, Ex_{iz} - izlazne eksergije i D - gubici eksergije.

Kod eksergijske metode eksergetski stepen korisnog dejstva računamo na osnovu ulaznih i izlaznih eksergija, dok ga kod entropijske metode računamo na osnovu ulaznih eksergija i gubitaka eksergije.

4. EKSERGETSKA ANALIZA

Tradicionalne metode analize i proračuna složenih termoenergetskih sistema zasnivaju se na prvom zakonu termodinamike. Te metode koriste energetske bilanse za sistem. U principu, energetske bilanse ne daju nikakvu informaciju o internim gubicima. Nasuprot tome, drugi zakon termodinamike uvodi pojam eksergije, koji je koristan u analizi termoenergetskih sistema. Eksergija je mera za ocenu kvaliteta energije, i omogućava određivanje lokacije, uzroka, realnih veličina nastalih gubitaka kao i nastalih ostataka u nekom termičkom procesu.

Sistem zagrijača niskog pritiska čiju eksergetsku analizu vršimo (figura 2) za zagrijavanje osnovnog kondenzata koristi 4 zagrijača niskog pritiska (ZNP 1, ZNP 2, ZNP 3 i ZNP 4).

Imamo dva radna medijuma vodu koja se zagrijava i paru koja se kondenzuje. Voda se kreće od kondenzatora do degazatora prolazeći kroz zagrijače. Dio vode iz kondenzatora ide u ZNP 4, a dio se odvodi u hladnjak šljake. Između ZNP 2 i ZNP 3 se uvodi zagrijana voda iz hladnjaka šljake i odvodi se voda u ekonomajzer gdje se zagrijava i vraća se između ZNP 1 i ZNP 2. Para se dovodi iz turbine niskog pritiska u 4 oduznanja. Para najvišeg pritiska se dovodi u ZNP 1 i nakon kondenzacije se kaskadno odvodi u zagrijač nižeg pritiska ZNP 2 i tako redom do ZNP 4. Kondenzat iz ZNP 4 se odvodi u kondenzator.

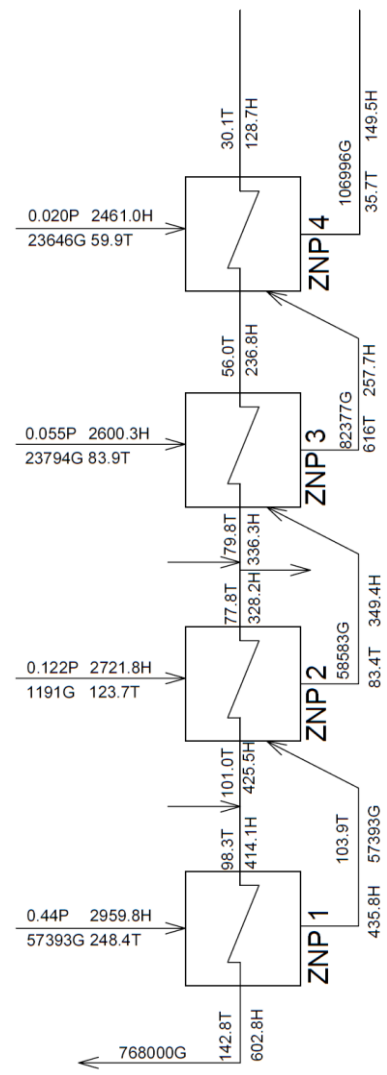


Fig. 2: Tehnološka šema zagrijača niskog pritiska u sklopu termoenergetskog postrojenja

Legenda uz Fig. 2: G –protok [kg/h]; P -pritisak [MPa]; T –temperatura [$^{\circ}\text{C}$]; H –entalpija [kJ/kg].

Jako bitan faktor pri procesu eksergetske analize jeste i usvajanje parametara okoline. Pod parametrima okoline podrazumevaju se referentna temperatura i pritisak. U literaturi se sreće nekoliko modela, ali najčešće se kao referentna temperatura i referentni pritisak usvajaju vrednosti: $T_0=298,15[\text{K}]$, $p_0=1013$ [mbar].

Na osnovu podataka datih na Figuri 2, koristeći se proračunom i programom za računanje parametara vode i pare dobijamo podatke u Tabeli 1.

Tabela 2 dobijena je korištenjem izraza za eksergiju toka materije u slučaju kada se potencijalna i kinetička energija struje fluida mogu zanemariti:

$$Ex = W_{t,max} = H_1 - H_0 - T_0 (S_1 - S_0) \quad (2)$$

gdje su: H_1, S_1 -entalpija i entropija toka materije u stanju neravnoteže sa okolinom; H_2, S_2 -entalpija i entropija toka materije u stanju ravnoteže sa okolinom.

Tabela 1: Pregled parametara ZNP 1

	Temperatura [K]	Entalpija [kJ/kg]	Protok [kg/s]	Entropija [kJ/kgK]
Voda ulaz	371.3	414.1	213.333	1.294
Voda izlaz	415.8	602.8	213.333	1.772
Para ulaz	521.4	2959.8	15.943	7.328
Para izlaz	376.9	435.8	15.943	1.352
Voda na T_0	298	104.92	-	0.3672

Tabela 2: Vrijednosti eksergija ZNP 1

	Eksergija [kJ/kg]	Eksergija [kJ/s]
Voda ulaz	32.9936	7038.62
Voda izlaz	79.2496	16906.55
Para ulaz	780.5616	12444.49
Para izlaz	37.4096	596.42

Odnos izlaznih i ulaznih eksergija naziva se eksergetskim stepenom korisnosti ili koeficijentom termodinamičkog savršenstva pokazujemo proračun na ZNP 1:

$$\eta_e = \frac{\sum Ex_{iz}}{\sum Ex_{ul}} = \frac{16906,55 + 596,42}{7038,62 + 12444,49} = 0,898366 \quad (3)$$

$$\eta_e = 89,84\%$$

Provjeravamo dobijene podatke korištenjem entropijske metode:

$$D = T_0 \cdot \Delta S_s = 298 \cdot (101,973 - 95,275) = 1966,004 [\text{kJ/s}] \quad (4)$$

Gdje su:

$$\Delta S_v = m_v (s_{v,iz} - s_{v,ul}) = 213,333(1,772 - 1,294) = 101,973 [\text{kJ/sK}] \quad (5)$$

$$\Delta S_p = m_p (s_{p,iz} - s_{p,ul}) = 15,943(1,352 - 7,328) = -95,275 [\text{kJ/sK}] \quad (6)$$

$$\eta_e = \frac{\Sigma Ex_{ul} - D}{\Sigma Ex_{ul}} = \frac{19483,11 - 1996,00}{19483,11} = 0,89755$$

$$\eta_e = 89,75\%$$

Tabela 3: Vrijednosti eksergija ZNP 2, ZNP 3 i ZNP 4

Broj ZNP	Ulazna Eksergija [kJ/s]	Izlazna Eksergija [kJ/s]	Eksergetski stepen korisnosti [%]
2	1168,10	1132,81	96,98
3	4042,78	3470,95	85,85
4	1816,30	1112,72	61,26

Ulazne i izlazne eksergije za ZNP 2, ZNP 3 i ZNP 4 su određene na isti način kao i za ZNP 1. Nakon određivanja vrijednosti eksergija dobijen je stepen korisnog dejstva eksergijskom metodom koji iznosi:

$$\eta_e = 87,59\%$$

5. ZAKLJUČAK

Proračun stepena korisnog dejstva za zagrijač niskog pritiska (ZNP) 1 raden je eksergijskom metodom, nakon čega je provjeren entropijskom metodom. Korištenjem eksergijeske metode dobijeno je da je stepen korisnog dejstva 89,94%, odnosno da su gubici 10,16%. Pri provjeravanju rezultata entropijskom metodom dobijeno je da je stepen korisnog dejstva 89,75%, odnosno da su gubici 10,25%. Razlika između dobijenih rezultata je manja od 1% na osnovu čega možemo zaključiti da je proračun sproveden ispravno i da su mala odstupanja pri korištenju različitih metoda.

Za ostale ZNP i za ukupan sistem ZNP korištena je samo eksergijska metoda pri proračunu stepena korisnog dejstva. ZNP 4 ima najveće gubitke 38,74%, a ZNP 2 ima najmanje gubitke 3,02%, dok ZNP 3 ima gubitke 14,15%. Ukupan sistem zagrijača niskog pritiska ima gubitke 12,41%, odnosno stepen korisnog dejstva od 87,59%. ZNP 4 ima prevelike gubitke, zbog toga bi ga trebalo zamjeniti zagrijačem niskog pritiska koji bolje provodi toplotu ili primjeniti neke od ostalih mjera za povećanje stepena korisnog dejstva izmjenjivača toplote. Kao na primjer povećanje koeficijenta prolaza toplote u vidu

izmjene konstrukcije zagrijača ili promjene režima strujanja kroz zagrijač.

REFERENCE

- [1] BIŠNJAKOVIĆ, F. (1970) *Nauka o toplini 1. dio*, Tehnička knjiga, Zagreb, Hrvatska
- [2] PETROVIĆ, P. (2010) *Tehnička termodinamika*, Univerzitet u Banjoj Luci, Mašinski fakultet, Banja Luka, Bosna i Hercegovina
- [3] MITROVIĆ, D., ŽIVKOVIĆ, D., LAKOVIĆ, M. (2010) *Eksergetska analiza rada komponenata termoenergetskog postrojenja*, Univerzitet u Nišu, Mašinski fakultet, Niš, Srbija
- [4] KOZIĆ, Đ., VASILJEVIĆ, B., BEKVALAC, V. (2005) *Priručnik za termodinamiku u jedinicama SI*, Mašinski fakultet, Beograd, Srbija
- [5] CHEMICAL LOGIC, *ChemicaLogic Steam Tab Companion*, Thermodynamic and transport properties of water and steam, version 2.0
- [6] KOZIĆ, Đ. (2007) *Termodinamika - inženjerski aspekti*, Mašinski fakultet, Beograd, Srbija
- [7] ĐORĐEVIĆ, B., VALENT, V., ŠERBANOVIĆ, S., RADOJKOVIĆ, N. (1989) *Termodinamika i termotehnika – Priručnik*, IRO „Građevinska knjiga“, Beograd, Srbija
- [8] ERLACH, B., TSATSARONIS, G., CZIESLA, F. (2001) *A New Approach for Assigning Costs and Fuels to Cogeneration Products*, Int. J. Applied Thermodynamics, vol. 4. (No.3)
- [9] ABBOTT, M. VAN NESS, H. (1972) *Theory and problems of Thermodynamic*, Schaum's Outline Series, Mc Grow- Hill, Book Co., New York, USA

CORRESPONDANCE



B. Sc. Ivana KECMAN, MSc student
University of Banja Luka
Faculty of Mechanical Engineering
Bulevar vojvode Stepe Stepanovića 71
78000 Banja Luka, B&H
ivana933@hotmail.com



PhD Mirko DOBRNJAC, Assoc. Prof.
University of Banja Luka
Faculty of Mechanical Engineering
Bulevar vojvode Stepe Stepanovića 71
78000 Banja Luka, B&H
mirko.dobrnjac@mf.unibl.org

**MECHANICAL SYSTEMS
MONITORING AND
MAINTENANCE**

DETERMINATION OF CRITICAL SIZE OF CORROSION PIT ON MECHANICAL ELEMENTS IN HYDRO POWER PLANTS

Radivoje M. MITROVIĆ
Dejan B. MOMČILOVIĆ
Ivana D. ATANASOVSKA

***Abstract:** Researchers in the field of fracture mechanics, predominantly developing appropriate solution algorithms for problems of solid bodies with cracks. Problems in mechanics generally, related with fracture and fatigue for solid bodies with various geometries of sharp notches, are studied to a much lesser extent. This situation can be explained by analytical difficulties arising in solving problems of elasticity theory for bodies with rounded notches. To solve problems of such class, starting from data on stress concentration in the rounded notch tip with a significant radius of curvature, simplified solutions with are therefore of great importance. Recent years, due to constant rise of computing power and development of numerical methods, re-evaluation of stress concentration factors from a viewpoint of theory of elasticity is present. This is mainly as a feedback from industry, which have requirements toward mega and nanostructures.*

Corrosion represents an important limitation to the safe and reliable use of many alloys in various industries. Pitting corrosion is a form of serious damage on metals surface such as high-strength aluminum alloys and stainless steel, which are susceptible to pitting when exposed to a corrosive attack in aggressive environments. This is particularly valid for dynamic loaded structures.

The basic idea behind this paper is finding links between different scientific and engineering disciplines, which will enable useful level of applicability of existing knowledge. The subject of this paper is application of new method of determine length scale parameter for estimating the mechanistic aspect of corrosion pit under uniaxial/multiaxial high-cycle fatigue loading.

Key words: stress concentration, fatigue, multiaxial fatigue, corrosion pit, critical distance

1. INTRODUCTION

The variation of complex geometries on real mechanical components is in direct relation with local stress concentration phenomena. During recent years different theories have been developed to particularly perform the high-cycle fatigue assessment of notched components without missing the undoubted advantages of linear-elastic finite element solutions.

The magnitude of fatigue damage can be quantified also in terms of linear-elastic notch tip stresses, taking into consideration the high-cycle fatigue only. The advantage of this simplification is that linear-elastic notch root stresses can easily be determined via conventional linear-elastic finite element (FE) models. The main drawback is that this methodology is very straightforward, the resulting level of conservatism is seen to increase as the sharpness of the geometrical feature being assessed increases. Consequently, under relatively large values of the stress concentration factors, this leads to components and structures which are heavier and bigger than necessary, with an end result of inefficient usage of materials and energy efficiency. Further, this simplified approach cannot be used to design against fatigue cracks

and sharp notches, because the resulting linear-elastic local stress fields become singular when crack/notch tip radii are taken equal to zero. The problem increase with complex three dimensional geometries on components subjected with uniaxial/multiaxial loading [1]. Some of the answers for noted problems are solved by Theory of Critical Distances (TCD). TCD represents a family of methods that are all characterized by two main common features: (i) the relevant stress fields are determined by adopting a simple linear-elastic constitutive law to model the mechanical behavior of the material being assessed; (ii) the extent of damage is assessed via an effective stress whose value depends not only on the entire linear-elastic stress fields acting on the material in the vicinity of the crack initiation locations, but also on a material characteristic length [2-4].

The TCD can be applied solely to notches subjected to in-service Mode I fatigue loading. In order to extend its use to those situations involving complex multiaxial load histories, this approach has to be applied along with an appropriate multiaxial fatigue damage model. Researchers [1] has been proven that the highest level of accuracy is obtained by applying the PM along with the so-called Modified Wöhler Curve Method (MWCM) [5,6] and gradient elasticity [7-10], through length scale parameter

ℓ (1). The MWCM is a bi-parametrical critical plane approach, the critical plane being that material plane experiencing the maximum shear stress amplitude τ_a . The MWCM quantifies the extent of fatigue damage not only via τ_a , but also via the mean value, $\sigma_{n,m}$, and the amplitude, $\sigma_{n,a}$, of the stress perpendicular to the critical plane. Recent efforts [7–10] in the mechanics, materials science, and applied physics communities have introduced internal length in phenomenological gradient models to account for internal micro/nanostructures and derive, among other things, non-singular analytical expressions for dislocation/crack fields, as well as to interpret deformation localization phenomena (shear bands, dislocation patterns) along with size effects. As a result further development can be expected by combining gradient elasticity with TCD and MWCM. As to a possible way to determine length scale parameter ℓ , it is evident that gradient elasticity and the TCD share some important features. In particular, both approaches post-process the relevant stress fields by coupling liner-elasticity with an internal length scale parameter which is assumed to be an intrinsic material property. By taking as a starting point these similarities, recently it was proven that length ℓ can directly be estimated from the TCD's critical distance L as follows (1):

$$\ell \approx \frac{L}{2\sqrt{2}} = \frac{1}{2\sqrt{2}\pi} \left(\frac{\Delta K_{th}}{\Delta \sigma_0} \right)^2 \quad (1)$$

Previous equation points that length scale parameter ℓ can directly be estimated from the material plain fatigue limit, σ_0 , and the threshold value of the stress intensity factor range, K_{th} , or through known value of critical distance L . Because both σ_0 and K_{th} are material properties, ℓ is in turn an intrinsic characteristic length which is different for different materials and different load ratios.



Fig 1. General view of cracks initiated from on transition radius and meshing on hydro turbine shaft.

Published results show that gradient elasticity was seen to be capable of accurately modeling, in the fatigue limit condition, the transition from the short to the long-crack regime [11]. Moreover, gradient elasticity applied along with the MWCM was successful in assessing the high cycle fatigue strength of specimens, the estimates falling within an error interval of $\pm 20\%$.

The results in this field open field of application on corrosion fatigue damage assessment. Example for this application is given in [12, 13] which is good example of real component subjected to both uniaxial and multiaxial fatigue loading, with stress concentration – corrosion pit on transition radius, Fig 1. Detail of damage caused by corrosion on transition zone is shown on Fig 2.

2. DESCRIPTION OF APPLIED METHODOLOGY

The theory of critical distances (TCD) has named by Taylor [2] attempts to predict the effect of notches and other stress concentration features by considering the stress field in the region close to the notch tip. This theory requires two parameters, a characteristic distance and a critical stress or strain characterizing failure. In one version of the critical distance theory, termed as the Point Method, the failure occurs when the stress becomes equal to the failure stress at a given distance from the notch root. In the other version of the critical distance theory, termed as the Line Method, the failure is assumed to occur when the stress becomes equal to the failure stress when computed as an average value over a line of given length. The background philosophy lying behind the TCD is described as wish to observe engineering components rather than to test specimens. In practice this meant that we only considered predictive methods which could be applied to bodies of arbitrary shape and size, subjected to arbitrary loadings, containing stress concentration features of arbitrary geometry. This is achieved by measuring material behavior using test specimens containing notches rather than cracks (fatigue threshold ΔK_{th} and toughness Kc using sharp notches rather than pre-cracks) which avoids the difficulties and uncertainties of carrying out standard fracture mechanics tests. The second presumption of successful application of TCD is the existence of an accurate stress analysis of the machine part.

The analysis and assessment of influence of corrosion pit depth on crack initiation was discussed [12-15]. The analysis of the stresses on various dimensions of pits on numerical model, Fig 3 and Fig 4a) was used to evaluate a critical depth of pit for this particular case, Fig 4b).

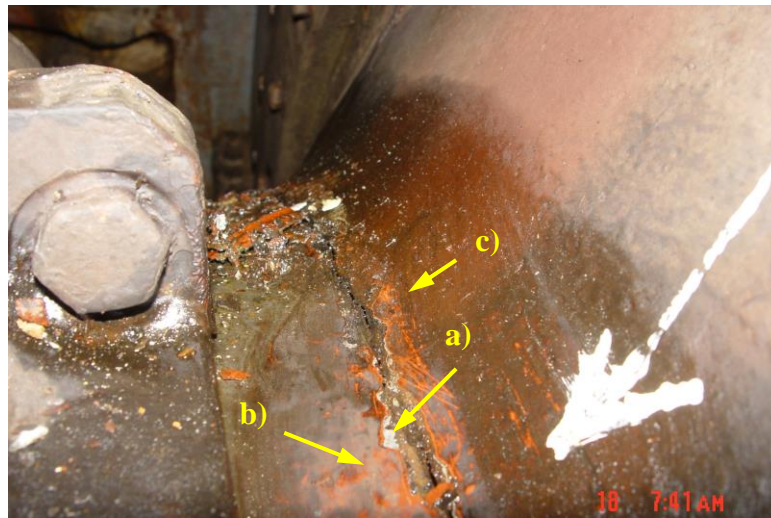


Fig. 2. Close view of the transient flange radius after detecting the crack
 a) main crack, b) anti-corrosive protection layer, c) oil residue on corrosion pits

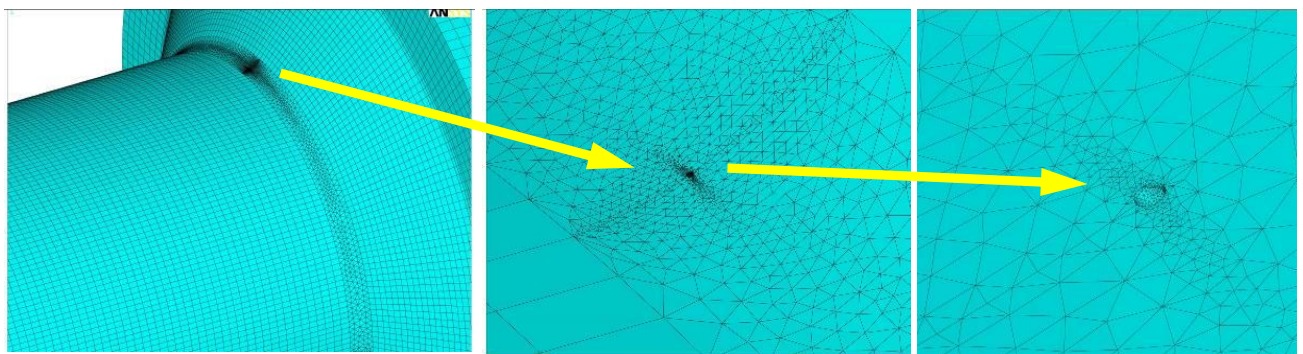


Fig 3. Meshing on hydro turbine shaft. Model of 300 μm radius corrosion pit on 7000 mm long model of turbine shaft.

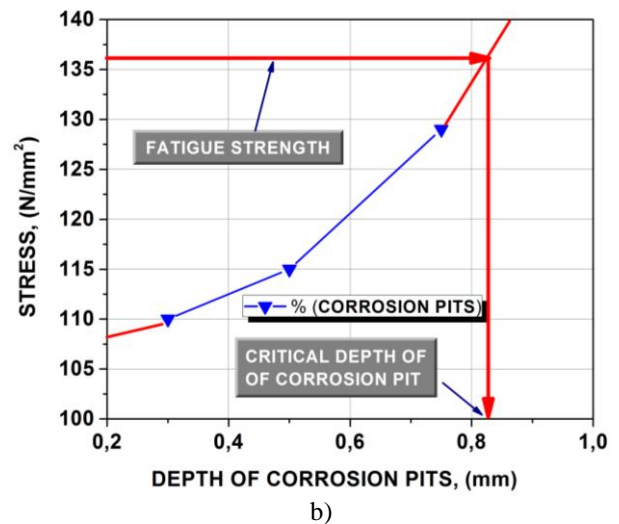
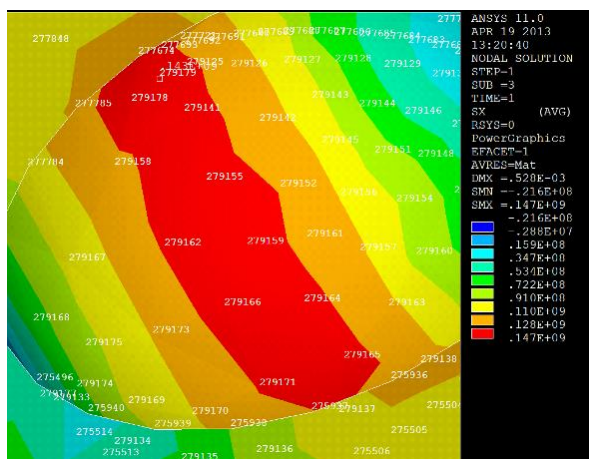


Fig 4. Solution for corrosion pit for $r=300\mu\text{m}$ pit, distance between nodes 277674 and 279165 is $340\mu\text{m}$ a) detail with results; b) extrapolated values of analyzed corrosion pits with marked critical value of corrosion pit]

3. CONCLUSIONS

From the presented and promising results, the general conclusions from gradient elasticity point of view are:

Identification and determination length scale parameter through solid physics arguments from phenomena like fatigue, mechanism-based microscopic models, multiscale simulations, and

experiments, presents the way of enhancing present knowledge of stress concentration.

This is important due fact that coupling gradient elasticity applied along with the MWCM is highly accurate in estimating high-cycle fatigue strength of notched components subjected to both uniaxial and multiaxial fatigue loading. It is also important to underline that application on real components require further research in this area to extend the use of the proposed methodology to the finite lifetime regime.

ACKNOWLEDGEMENT

Parts of this research were supported by the Ministry of Sciences and Technology of Republic of Serbia through Projects TR 35029 and TR 35011.

REFERENCES

- [1] SAVRUK, M.P, KAZBERUK, A., (2017), *Stress Concentration at Notches*, Springer International Publishing, ISBN 978-3-319-44554-0
- [2] TAYLOR, D., (2007), *The Theory of Critical Distances – A New Perspective in Fracture Mechanics*, Elsevier, ISBN–13: 978-0-08-044478-9
- [3] SUSMEL, L., *The theory of critical distances: a review of its applications in fatigue*, Elsevier, Engineering Fracture Mechanics, 75, pp. 1706–1724, 2008
- [4] SUSMEL, L. AND TAYLOR, D. (2006), *Can the conventional high-cycle multiaxial fatigue criteria be re-interpreted in terms of the theory of critical distances?* Structural Durability & Health Monitoring, 2, 91–108
- [5] SUSMEL, L. AND TAYLOR, D, (2008), *The Modified Wöhler Curve Method applied along with the Theory of Critical Distances to estimate finite life of notched components subjected to complex multiaxial loading paths*. Fatigue Fract. Eng. Mater. Struct., 31, 1047–1064
- [6] SUSMEL, L., (2009), *Multiaxial Notch Fatigue*, Elseveir, ISBN: 978-1-84569-582-8,
- [7] ASKES, H., et al, (2012), *Intrinsic material length, theory of critical distances and gradient mechanics: analogies and differences in processing linear-elastic crack tip stress fields*, Fatigue Fract. Eng. Mater. Struct., 36, 39–55, 2012
- [8] SUSMEL, L., ASKES, H., BENNETT, T. TAYLOR, D. (2013), *Theory of critical distances versus gradient mechanics in modeling the transition from the short to long crack regime at the fatigue limit*, Fatigue Fract. Eng. Mater. Struct., 36, 861–869, 2013
- [9] AIFANTIS, E.C. (2014), *Gradient material mechanics: Perspectives and Prospects*, Acta Mech 225, 999–1012
- [10] CHARLTON, T.J, COOMBS W.M, AUGARDE, C.E, (2016), *Gradient Elasticity with the material point method*, Proceedings of the 24th UK Conference of the Association for Computational Mechanics in Engineering 31 March - 01 April 2016, Cardiff University, Cardiff
- [11] BAGNI, S, ASKES, H, SUSMEL, L, (2016), *Gradient elasticity: a transformative stress analysis tool to design notched components against uniaxial/multiaxial high-cycle fatigue*, Fatigue Fract Engng Mater Struct, 39, 1012–1029
- [12] MOMČILOVIĆ, D., et al, (2012), Odanović Z., Mitrović R., Atanasovska I., Vuherer T., *Failure Analysis of Hydraulic Turbine Shaft*, Engineering Failure Analysis, Vol. 20, pp. 54–66
- [13] MOMČILOVIĆ, D., MITROVIĆ R., ATANASOVSKA I, (2016), *Stress Concentration and Fatigue of Materials* (in Serbian), ISBN 978-86-7083-915-1, Faculty of Mechanical Engineering, University of Belgrade
- [14] ATANASOVSKA, I, et al, (2013), *The influence of corrosion on stress concentration factor at shaft to flange radius*, Mechanisms and Machine Science (Book Series), Series Ed.: Ceccarelli Marco, ISSN: 2211-0984, Vol. 13: Power Transmissions, Springer Science + Business Media Dordrecht, ISBN: 978-94-007-6557-3, pp. 657-66, 2013
- [15] MITROVIĆ R., MOMČILOVIĆ D., ATANASOVSKA I., *Assessment of the effect of pitting corrosion on fatigue crack initiation on hzdro turbine shaft*, Advanced Materials Research, ISSN: 1022-6680, Vol. 633, Advances in Engineering Materials, Product and Systems Design (Special topic volume with invited peer reviewed papers only), Editor: Aleksandar Subić, Trans Tech Publications, Switzerland, pp. 186-196.

CORRESPONDANCE



Prof. Radivoje MITROVIĆ, Ph.D.
University of Belgrade
Faculty of Mechanical Engineering
Kraljice Marije 16, 11120 Belgrade
Serbia
rmitrovic@mas.bg.ac.rs



Dejan B. MOMČILOVIĆ, Ph.D.
Institute IMS
Bulevar vojvode Mišića 43
11000 Belgrade
Serbia
dejan.b.momcilovic@gmail.com.



Ivana ATANASOVSKA, Dr.Sc. Eng.
Mathematical Institute of the Serbian
Academy of Sciences and Arts
Kneza Mihaila 36
11000 Belgrade, Serbia
iviatanasov@yahoo.com
iatanasovska@mi.sanu.ac.rs

METHODOLOGY FOR THE REPAIR OF DAMAGES THAT OCCURRED ON THE WELDED JOINTS AT THE BODY OF GUIDE VANE APPARATUS VANES OF THE VERTICAL KAPLAN TURBINE

Miodrag ARSIĆ
Srđan BOŠNJAK
Mladen MLADENOVIĆ
Zoranka MALEŠEVIĆ
Zoran SAVIĆ

Abstract: Vertical Kaplan turbines, with nominal power of 178 MW and manufactured in Russia, have been installed in 6 hydroelectric generating units of hydro power plant 'Djerdap 1'. Experimental tests were carried out by non-destructive methods in order to determine the turbine condition during the rehabilitation of the hydro power plant. Lack of root penetration was detected in V40 welded joints between upper and lower sleeves and bodies of guide vane apparatus vanes. Height of the lack of root penetration was in the range between 5 and 15 mm, while the allowable height of the lack of root penetration is 3 mm, according to the technical conditions. The upper sleeves were made of cast steel 25L (in accordance with GOST 977), while lower sleeves were made of steel forging St 25 (in accordance with standards GOST 1050 for chemical composition and GOST 8479 for forgings).

Methodology for the repair of non-penetrated welded joints between the sleeves and body of the guide vane apparatus vane was composed taking into account the results of ultrasonic testing. By repair methodology it is necessary to, due to the structural solution and service function of guide vane apparatus vanes, specify a large number of details, consider them carefully and carry them out in order to improve safety, because if some of them get overlooked, underestimated or incorrectly perceived, significant problems in turbine operation may occur.

This methodology refers solely to the repair of damaged welded joints between sleeves and bodies of guide vane apparatus vanes.

Key words: sleeve, guide vane apparatus vane, welded joint, lack of root penetration, repair methodology

1. INTRODUCTION

Vertical Kaplan turbines, with nominal power of 178 MW and manufactured in Russia, have been installed in 6 hydroelectric generating units of hydro power plant 'Djerdap 1' [1]. They were designed for the service life of 40 years due to the structural solution, or in other words due to the impossibility to perform periodic inspections and condition analyses. In figure 1 the guide vane apparatus vane is shown. In figure 2 welded joints V40 between the upper or lower sleeve and body of the vane are displayed, while in figure 3 the dimensions of the vane are represented. The repair methodology for non-penetrated welded joints was composed on the basis of ultrasonic testing results.

2. CHEMICAL COMPOSITION AND MECHANICAL PROPERTIES OF PARENT MATERIAL

Chemical compositions and mechanical properties of cast steel 25L, steel forging St 25 and sheet metal MSt 3 of which the shaft sleeves and bodies of guide vane apparatus vanes were made are presented in tables 1 and 2, according to standards GOST 977 [2], GOST 8479 [3], GOST 1050 [4] and GOST 380-60 [5].

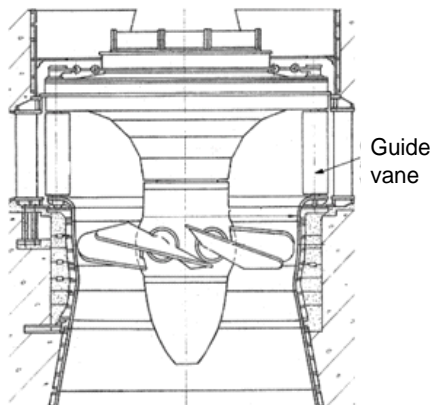


Fig.1: Appearance of a vertical Kaplan turbine with nominal power of 178 MW

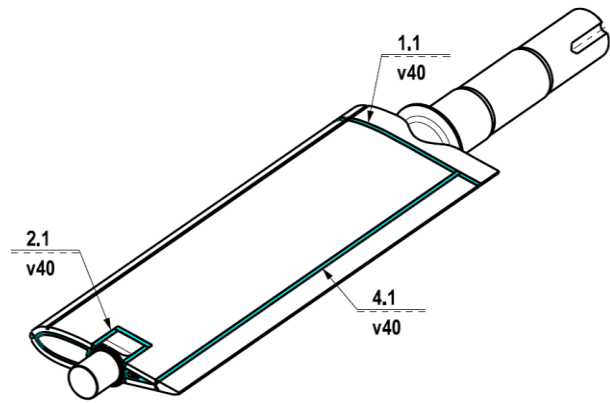


Fig.2: Appearance of a guide vane apparatus vane with marked V40 welded joints

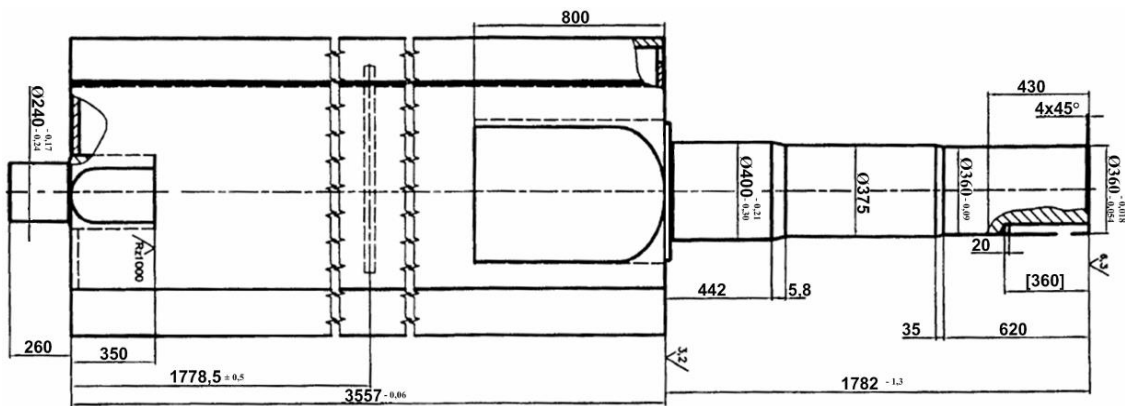


Fig.3: Dimensions of a guide vane

Table 1: Chemical composition, values in [%]

Material	GOST	C	Si	Mn	P	S	Cr	Ni	Cu
25L	997	0.22-0.30	0.20-0.52	0.35-0.80	≤ 0.040	≤ 0.045	< 0.30	< 0.30	< 0.30
St 25	1050	0.22-0.30	0.17-0.37	0.50-0.80	≤ 0.035	≤ 0.04	< 0.25	< 0.25	< 0.25
MSt3	380-60	0.14-0.22	0.12-0.30	0.40-0.65	≤ 0.045	≤ 0.055	< 0.30	< 0.30	< 0.30

Table 2: Mechanical properties of normalized and annealed material

Material	GOST	Yield strength YS [N/mm ²]	Tensile strength TS [N/mm ²]	Elongation A [%]	Contraction Z [%]	Impact energy KCU [KJ/m ²]
25L	997	305-315	520-530	21-23	27-28	62-64
St 25	8479	min 195	min 390	20	50	49
MSt3	380-60	min 206	min 509	43	-	54

3. WELDABILITY ANALYSIS OF PARENT MATERIALS

Weldability of parent materials is limited. Taking into account that cast steel 25L is 60 mm thick, as well as that sheet metal MSt 3 is 36 mm thick, it is recommended to perform preheating and post weld heat treatment even when welding / surface welding is being performed with use of filler material of the same type.

According to Sepherian, preheating temperature for thicknesses up to 200 mm is being calculated on the basis of the chemical composition, table 1.

For thicknesses up to 200 mm and chemical composition of cast steel 25L, necessary preheating temperature during welding calculated according to Sepherian is $T_p = 276 \text{ }^\circ\text{C}$.

$$360[C]_h = 360C + 40(Mn + Cr) + 20Ni + 28Mo =$$

$$= 360 \cdot 0.3 + 40(0.80 + 0.3) + 20 \cdot 0.3 = 158 \quad (1)$$

$$[C]_h = \frac{158}{360} = 0.438$$

$$T_p = 350\sqrt{[C]-0.25} = 350\sqrt{0.876-0.25} = 276^\circ C$$

$$[C] = [C]_h + [C]_d = 0.438 + 0.438 = 0.876 \quad (2)$$

$$[C]_d = 0.005 \cdot d \cdot [C]_h = 0.005 \cdot 200 \cdot 0.438 = 0.438$$

3.1. Selection of welding procedure

Based on experience, the welding / surface welding process carried out through the use of filler wire (procedure 136) was selected due to the fact that significantly lower residual stresses compared to other welding procedures that are based on the use of filled welding electrodes occur.

3.2. Selection of filler material

Repair of non-penetrated welded joints between the sleeves and bodies of guide vane apparatus vanes by welding / surface welding was carried out through the use of filler wire $\varnothing 1.2$ mm [6]. Chemical composition and mechanical properties of weld metal formed through the use of filler wire OK E71T-1 are presented in tables 3 and 4.

Table 3: Chemical composition of weld metal, values in [%]

Filler wire	C	Si	Mn
OK E71T-1	0.06	0.50	1.30

Table 4: Mechanical properties of weld metal

Filler wire	Yield strength YS [N/mm ²]	Tensile strength TS [N/mm ²]	Elongation A [%]	Impact energy KV [KJ/m ²]
OK E71T-1	> 420	510-590	> 22	> 54 (-20 °C)

4. METHODOLOGY OF REPAIR OF NON-PENETRATED WELDED JOINTS

This methodology refers to works carried out during the repair of non-penetrated welded joints between the sleeves and bodies of guide vane apparatus vanes by welding / surface welding.

4.1. Removal of non-penetrated areas in welded joints

Appearance of a non-penetrated area in welded joint V40 is shown in figure 4. Grinding of the section with lowered weld metal thickness should be carried out until reaching the depth which allows easier welding of 2-2.5 mm of sheet metal thickness in root area. Multiple openings with 3 mm in diameter should be drilled in order to check this measure. Length of the section which is being repaired is restricted to 200 mm in one passage in order to reduce the

level of deformations. When it comes to longer sections, the repair should be carried out in several passages. Grinded spots should not have sharp edges and should enable accessibility for deposition of layers by welding. Grinded area should be degreased, dry and clean.

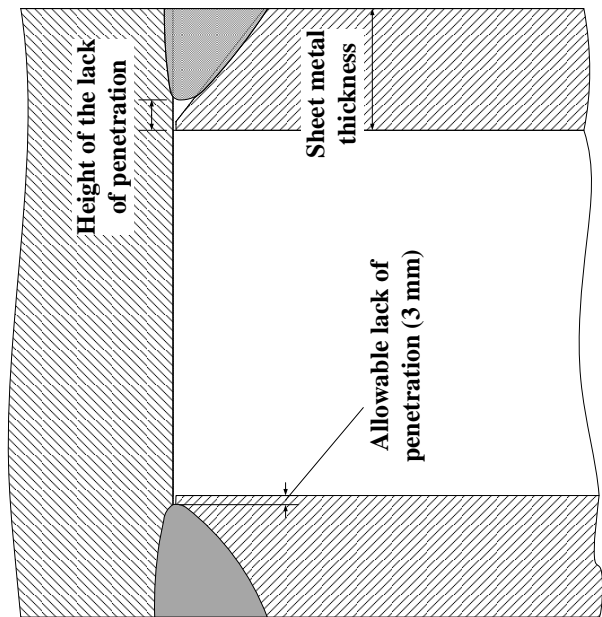


Fig.4: Appearance of welded joints with the lack of root penetration on the side of the upper sleeve of a guide vane apparatus vane

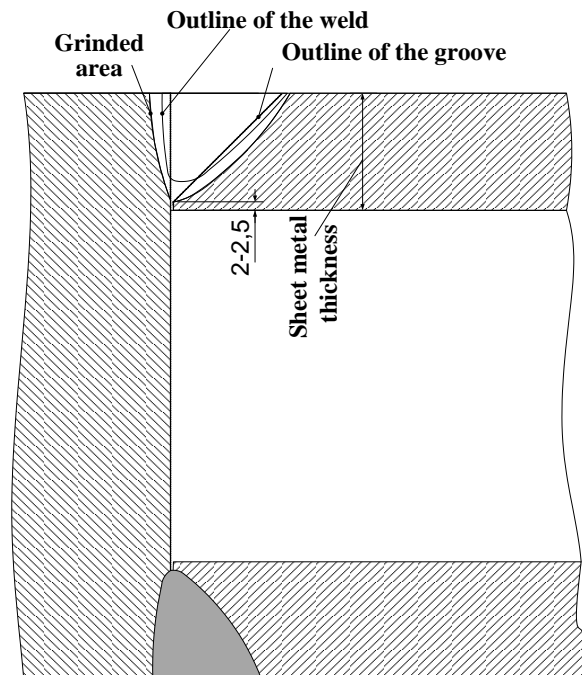


Fig.5: Appearance of the grinded area at the side of the upper sleeve of a guide vane apparatus vane

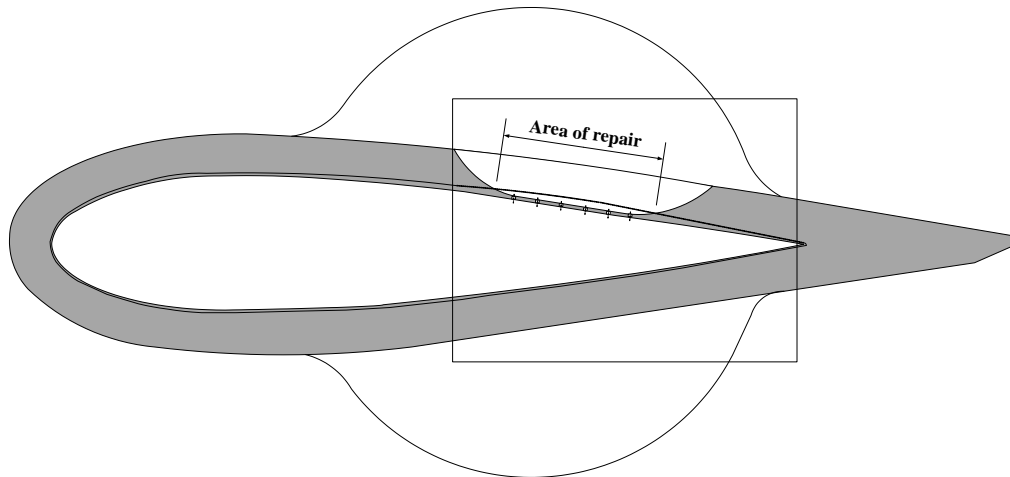


Fig.6: Repair of sections with the lack of root penetration shorter than 200 mm at a guide vane apparatus vane

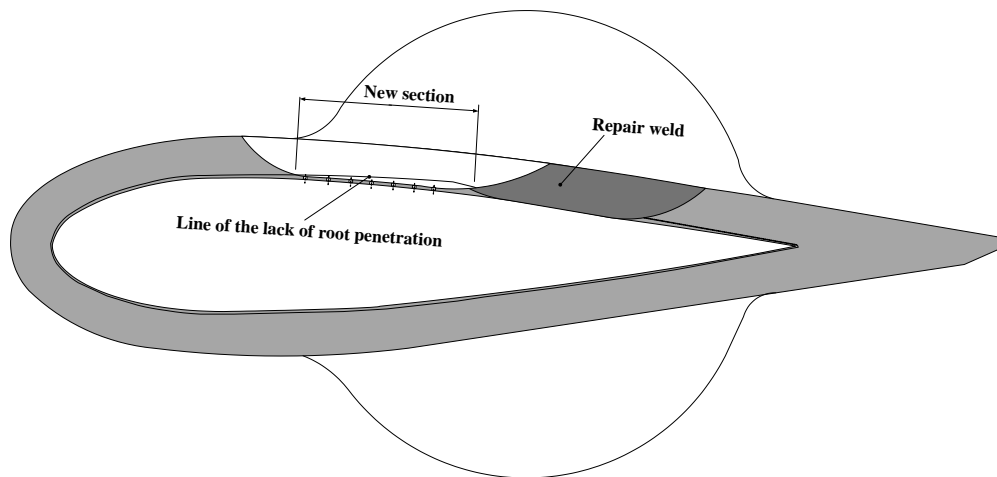


Fig.7: Repair of sections with the lack of root penetration longer than 200 mm at a guide vane apparatus vane

5. METHODOLOGY OF WELDING PROCESS PERFORMED IN ORDER TO REPAIR AREAS WHERE LACK OF ROOT PENETRATION WAS DETECTED

Preheating at max 150°C was performed by using the inductors located 300 mm around the area where grinding was performed, in compliance with Russian literature for cast steel 25L. Preheating temperature was checked by IC thermometers.

Welding was performed in PA position in grinded areas that were located on the same side of the vane, while welding in areas that were located symmetrically on both sides of the vane was carried out by 2 welders in PF position [7].

Welding was performed at ambient temperature greater than 5°C, with no significant air streaming. Weld reinforcement was removed by grinding after the finish of the welding process.

5.1. Parameters of repair welding performed in areas of welded joints where lack of root penetration was detected

Parameters that were used during the welding through the use of filler wire OK E71T-1 are as follows:

- Wire diameter: 1.2 mm;
- Current source:
 - direct,
 - polarity +,
 - voltage 25-28V,
 - current intensity 215-225 A;
- Protective gas:
 - Ar mixture,
 - composition of gas mixture in accordance with EN 439: M3-1 [8],
 - gas consumption 12-15 l/min;
- Welding speed in horizontal position: 0.35-0.45 m/min;
- Wire feed speed in horizontal position: 9.5 m/min;
- Length of the free end of the wire: 10-12 mm;
- Distance between the nozzle and the welding position: 12 mm.

5.2. Procedures that cause decrease of stresses and deformations that occur during repair welding

Following procedures were applied for the decrease of stresses and deformations that occur during repair welding:

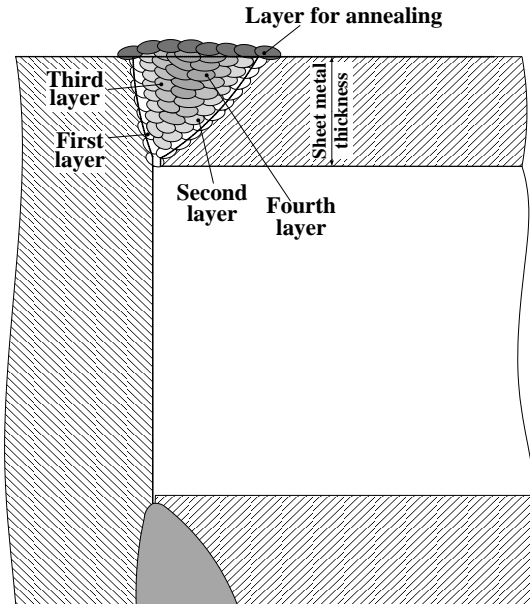


Fig. 8: Appearance of the order of deposition of weld beads along the cross-section of the guide vane apparatus vane

- During the deposition of weld beads system that included overlaying of groove edges, with the finish layer for annealing, which was removed by grinding the face of the weld in order to even it with parent material (figure 8) was applied;
- Every layer was treated by pneumatic hammer with rounded top with diameter of 3 mm;
- After grinding was performed wide area (weld metal, heat affected zone and 10 mm of parent material on every side) of the repair weld was treated by pneumatic hammer with rounded top with diameter of 3-5 mm, during which overlapping of prints was required. After hammering the surface had to be polished.

6. HEAT TREATMENT OF REPAIR WELDS AT GUIDE VANE APPARATUS VANES

Heat treatment was carried out only for guide vane apparatus vanes with the volume of repair welds that exceeds 3000 cm³.

Applied parameters that refer to heat treatment, shown in figure 9, are as follows:

- Heating until reaching $T = 300^{\circ}\text{C} \pm 25^{\circ}\text{C}$ was carried out in 1 hour;
- Heating until reaching $T = 590 \pm 15^{\circ}\text{C}$ was carried out with rate less than 70°C/h ;
- Keeping the temperature at $590 \pm 15^{\circ}\text{C}$ was carried out in 5h;
- Cooling until reaching 250°C was carried out with rate less than 50°C/h ;
- Cooling below 250°C in still air.

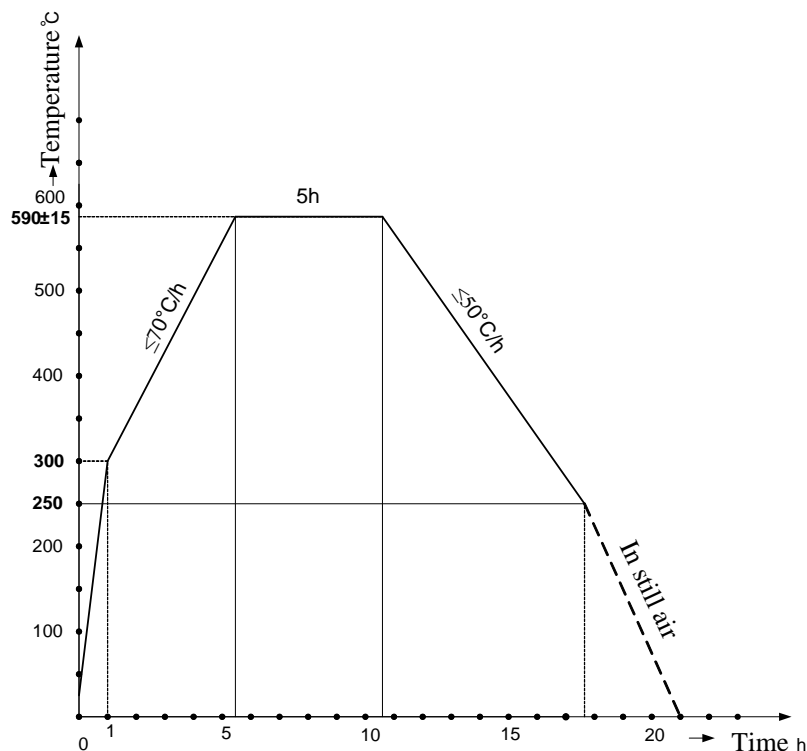


Fig. 9: Diagram that refers to heat treatment of repair welds of guide vane apparatus vanes

7. TESTING OF REPAIR WELDS BY NON-DESTRUCTIVE METHODS

Testing of repair welds by non-destructive methods was carried out after the machining of the weld face and heat treatment were finished.

7.1. Visual testing

Visual testing (VT) of repair welds was carried out before, during and after welding in compliance with standard [9] and acceptability criteria from standard [10] for quality level B.

7.2. Magnetic particle testing

Magnetic particle testing (MT) of repair welds was carried out after the machining of the weld face and heat treatment were finished, in compliance with standard [11] and acceptability criteria from standard [12] for acceptance level 2.

7.3. Ultrasonic testing

Ultrasonic testing (UT) of repair welds was carried out after the machining of the weld face and heat treatment were finished, in compliance with standard [13] and acceptability criteria from standard [14] for acceptance level 3.

8. CONCLUSION

Successfulness of applied methodology for repair of areas of welded joints where lack of root penetration was detected between sleeves and bodies of turbine guide vane apparatus vanes by welding / surface welding at hydro power plant 'Djerdap 1' was confirmed by equipment manufacturer 'Power Machines' from Saint Petersburg, because they gave the guarantee for their use until next rehabilitation of the turbine.

ACKNOWLEDGEMENT

Authors wish to thank the Ministry of education, science and technology of Serbia for supporting the Project TR 35002.

REFERENCES

- [1] LMZ (1973) *Documents of the manufacturer of the upper ring of vertical Kaplan turbine runner guide vane apparatus of hydroelectric generating set A6*. LMZ, Sankt Peterburg.
- [2] GOST 977 (1988) *Steel castings, General specifications*, Russian Standard.
- [3] GOST 8479 (1971) *Structural carbon and alloy steel forgings*, Russian Standard.
- [4] GOST 1050 (1988) *Carbon structural quality steel gauged bars with special surface finish. General specifications*, Russian Standard.
- [5] GOST 380-60 (1988) *Chemical and mechanical properties*, Russian Standard.

- [6] EN ISO 17632-1 (2015) *Welding consumables, Tubular cored electrodes for gas shielded and non, Classification*, T 42 2 P C 1 H5, ESAB, Sweden.
- [7] ISO 6947 (2011) *Welding positions*, International Organization for Standardization.
- [8] SRPS EN 439 (2001) *Welding consumables - Shielding gases for arc welding and cutting*, Institute for Standardization of Serbia.
- [9] SRPS EN 17637 (2012) *Non - destructive testing of welds - Visual testing of fusion-welded joints*, Institute for Standardization of Serbia.
- [10] SRPS EN ISO 5817 (2015) *Welding - Fusion-welded joints in steel, nickel, titanium and their alloys (beam welding excluded) - Quality levels for imperfections*, Institute for Standardization of Serbia.
- [11] SRPS EN ISO 17638 (2012) *Non - destructive testing of welds - Magnetic particle testing of welds*, Institute for Standardization of Serbia.
- [12] SRPS EN ISO 23278 (2011) *Non-destructive testing of welds. Magnetic particle testing of welds. Acceptance levels*, Inst. for Standardization of Serbia.
- [13] SRPS EN ISO 17640 (2012) *Non - destructive testing of welds - Ultrasonic testing - Techniques, testing levels, and assessment*, Institute for Standardization of Serbia.
- [14] SRPS EN ISO 11666 (2012) *Non-destructive testing of welds - Ultrasonic testing - Acceptance levels*, Institute for Standardization of Serbia.

CORRESPONDANCE

Miodrag ARSIĆ, D.Sc. Eng.
Institute for materials testing - IMS
Bulevar vojvode Mišića 43
11000 Belgrade, Serbia
miodrag.arsic@institutims.rs

Srđan BOŠNJAK, Prof. D.Sc. Eng.
University of Belgrade,
Faculty of Mechanical Engineering
Kraljice Marije 16.
11120 Belgrade, Serbia
sbošnjak@mas.bg.ac.rs

Mladen MLADENOVIĆ, Dipl. Ing. Mech.
Institute for materials testing - IMS
Bulevar vojvode Mišića 43
11000 Belgrade, Serbia
mladen.mladenovic@institutims.rs

Zoranka MALEŠEVIĆ, Prof. D.Sc. Eng.
High Tech. School of Professional Studies
Josifa Pančića 11,
34300 Arandelovac, Serbia
zorankamalesevic@msn.com

Zoran SAVIĆ, Dipl. Ing. Mech.
Institute for materials testing - IMS
Bulevar vojvode Mišića 43
11000 Belgrade, Serbia
zoran.savic@institutims.rs

REPAIR WELDING OF GEAR SHAFTS OF SERVICE ROLLERS AT THE ŽELEZARA SMEDEREVO

Drakče TANASKOVIĆ
Branislav ĐORĐEVIĆ
Uroš TATIĆ
Aleksandar SEDMAK
Mirjana OPAČIĆ

Abstract: Presented in this paper are two methods for repair welding of a total of 8 gear shafts (toothed shafts) of service rollers in the "Topla valjaonica" rolling mill within Železara Smederevo. Damage that occurs in these shafts is a consequence of exploitation conditions, which lead to lateral wear of the tooth up to one half of its thickness, due to adhesion and surface fatigue. Shown in the following text are the procedures for repair welding of gear shafts, including manual arc welding (MAW procedure) and the automatic welding procedure (FCAW). In addition, the requirements that need to be fulfilled in order to successfully perform the repair welding, so that the repaired parts can be exploited again, are presented. The techno-economical analysis had confirmed the technological and economical justifiability of applying this repair welding methods, compared to purchasing of new parts.

Key words: repair welding, gear shaft, wear, techno-economical analysis

1. INTRODUCTION

Material loss represents one of the main causes for applying of repair weld procedures. In the case of contact between two or more coupled machine parts, the following mechanisms of material loss can be distinguished: wear, abrasion, erosion. Damages caused by these mechanisms occur on the machine part surface. In addition to these damages, machine part damage can occur along the volume, due to material fatigue [1-4], usually caused by dynamic loads.

In order to make the proper decision about the need for repair welding and the corresponding procedure, it is necessary to develop the requirements and algorithm of the repair welding technology [5, 6]. Each technological procedure for repair welding of a machine part has its own specificities. The general algorithm for repairing of machine parts consists from a series of activities, which should be performed in the following order:

disassembling, specimen cleaning, damage analysis, selection of the repair method, techno-economical analysis, development of technical documentation, development of the technological procedure, specimen preparation, repairing, tests and control, machining to the final dimensions, assembly, running in of the repaired parts.

Shafts made coupled with the gear, i.e. toothed shafts, are typically manufactured from materials used for the manufacturing of gears. These materials include cementation steel or enhanced materials, in accordance with the technical requirements. Finishing of the teeth is performed by milling or grinding, whereas other functional surfaces are always finished by grinding. In addition, shafts to which toothed elements are attached are made of high quality enhanced materials. Shaft samples are made of forgings or rolled material. The model of one such toothed shaft is shown in Figure 1.

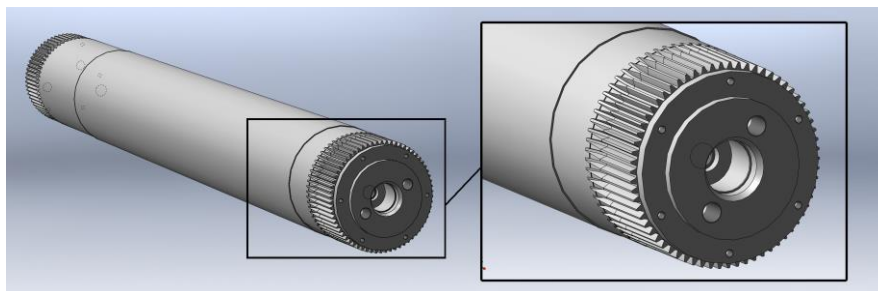


Fig.1: Model of gear shaft

Presented in this paper is the welding technology used on eight toothed shafts, i.e. the repairing of damaged teeth of driving shafts. Damage was caused by the exploitation conditions, and were reflected in form of worn teeth along the lateral profile, until one half of the thickness, due to adhesion and surface fatigue, which affects the connection between the shaft and the coupling. These gear shafts are parts of service rollers of "Topla valjaonica" rolling mill

within Železara Smederevo. Železara Smederevo has 6 facilities with 2 service rollers and 2 support rollers. These driving shafts were manufactured by the German company "Siemag". During exploitation, gear shafts were subjected to variable loads and difficult working conditions at elevated temperatures. In Figure 2, the appearance of the teeth after exploitation and their damage can be seen.

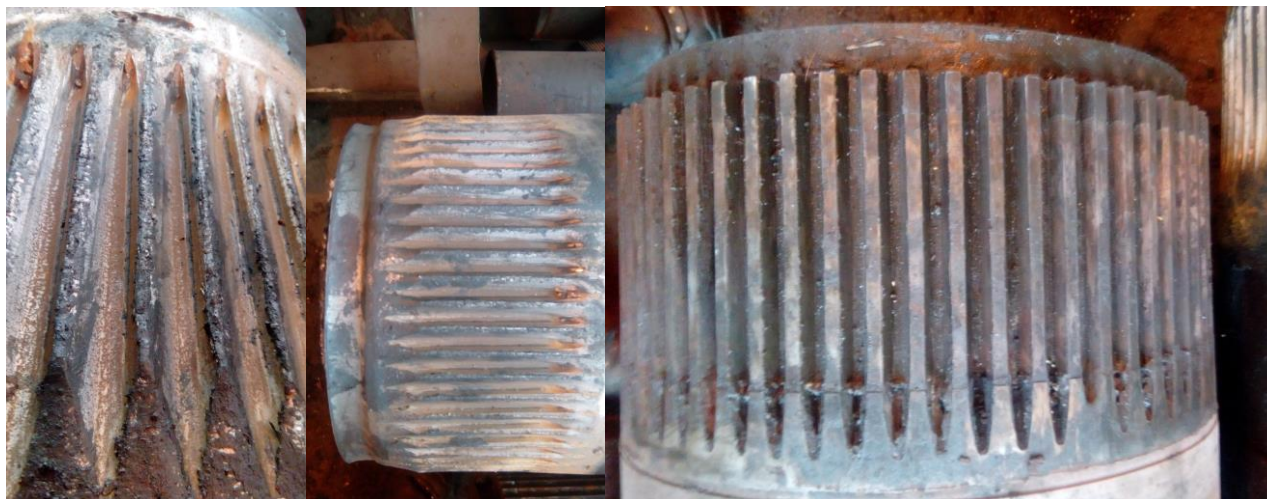


Fig.2: Appearance of some of the gear shafts in the rolling mill „Topla valjaonica“ in Steelwork Smederevo

2. BASE MATERIAL OF GEAR SHAFT

Gear shaft, which were repaired due to damage, were made of steel 42CrMo4. This is an enhancing steel used for machine parts in engines and vehicles, subjected to high levels of load, at elevated temperatures. 42CrMo4 is

alloyed heat treatable steel with a typical tensile strength of 900 - 1200 N/mm². The 42CrMo4 alloy material also has high fatigue strength and good low-temperature impact toughness and low temper brittleness. The chemical composition of 42CrMo4 is given in Table 1, whereas its mechanical properties are given in Table 2.

Table 1: Chemical composition of steel 42CrMo4 [7]

Element	C	Si	Mn	Cr	Mo	P	S
Percentage [%]	0.38-0.45	Max 0.4	0.6-0.9	0.9-1.2	0.15-0.3	<0.025	<0.035

Table 2. Mechanical properties of steel 42CrMo4 [7]

Mechanical properties	Re [N/mm ²]	Rm [N/mm ²]	As %
Values	780	1000	10-14

Taking into account significant probability of residual stresses occurring after welding of parts whose thickness is greater than 30 mm, preheating and tempering after welding are required in order to remove these stresses. In addition, it is recommended to preheat in order to reduce the cooling rate, thus avoiding unwanted micro-structural changes [8-10].

3. REPAIR TECHNOLOGY FOR TOOTHED SHAFTS

During exploitation, gear shafts were subjected to variable loads and difficult working conditions at elevated temperatures. After the load analysis was performed, the development of the welding plan was initiated.

The welding plan begins by determining the reasons for repairing, and for this purpose the following activities are undertaken [5, 6, 11]:

- Selection of the repair procedure
- Calculation of the preheating temperature (if needed)
- Selection of additional materials
- Determining of the number of passes (layers)
- Determining of technological welding parameters
- Determining of the eventual need for additional heat treatment (if necessary)

3.1. Selection of the repair procedure

Repair welding was performed on eight gear shafts of service rollers. Based on the geometry and size of a gear shaft, the possibility of welding and the quality of the base material, as well as on rational welding procedures, two repair welding procedures were selected:

- 1) Flux core arc welding (FCAW procedure)
- 2) Manual arc welding using coated electrodes (MAW procedure).

Seven of the shafts were repaired using the EPP procedure, and one was repaired using the E procedure.

3.2. Selection of additional materials

The chemical composition and mechanical properties of the electrode used for manual arc welding differs from the one used in the FCAW procedure. Based on the map shown in Figure 3, the selection of additional materials for repair welding is made. This selection is made in accordance with the percentage of carbon and other alloying elements, as well as in accordance with damage mechanisms.

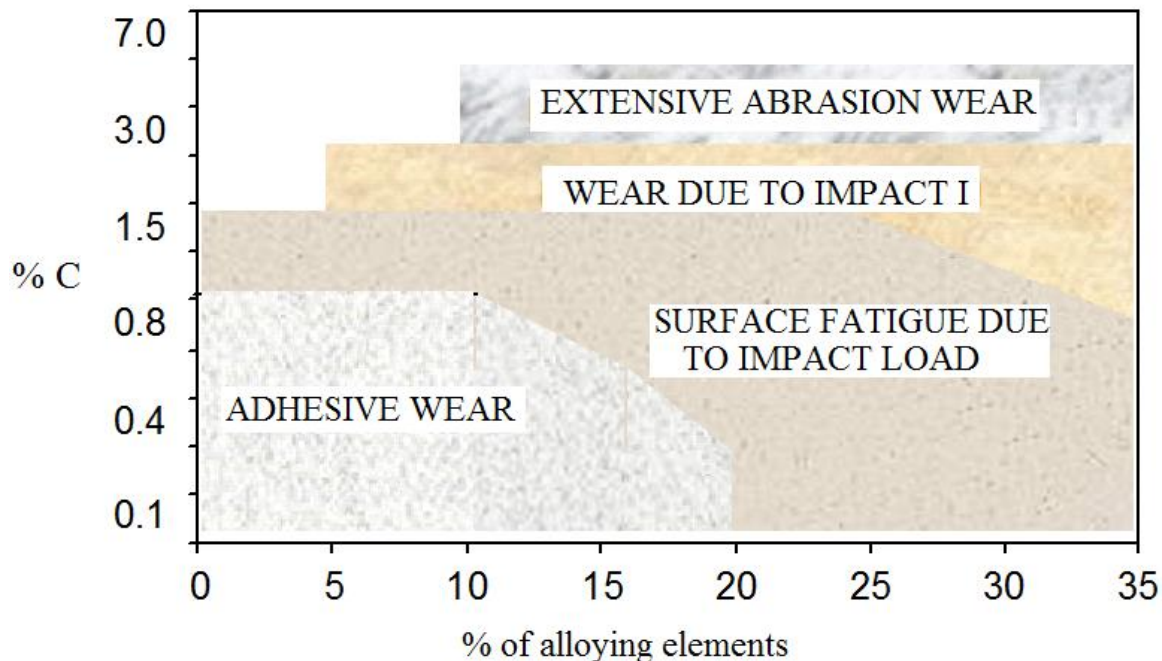


Fig.3: Map of iron based hard repair welding [5]

Taking into account the selected repair procedures, base material quality, geometry and dimensions of the welded surface, geometry after machining, as well as the conditions under which the toothed shaft is working, the following additional materials for each procedure were selected:

- 1) For the flux core arc welding (FCAW), the WLDC 3 \varnothing 3,2 mm wire was used, along with the universal Weldclad powder. WLDC 3 wires are used for general purposes and are characterized by exceptional wear resistance at higher temperatures [12].
- 2) For manual arc welding (E), the following two electrodes were used:
 - Electrode Piva 29/9 R \varnothing 3.25 mm for the applying of the intermediate layer. This is an austenite-ferrite rutile electrode, used for welding of appropriate types of corrosion resistant steels and steel moulds, and for welding of heterogeneous steels, hard manganese steels and steels with poor weldability. It is suitable for repair welding and welding of intermediate layers [13].

- Electrode Piva 430 B R \varnothing 5 mm for the finishing layers. This is a coated base electrode, used for repair welding of worn elements such as gears, axles, crushers, shafts and other machine elements [13]. Welded layers are characterized by high wear resistance and can be machined. Welded layers are pure, without porosity and material toughness is high at low temperatures as well. Hydrogen content in the welded layer is less than ml/100g of metal.

Electrode Piva 430 B and wire WLDC 3 are located in the adhesion resistant area, according to the map shown in figure 3, which partially corresponds to the requirements of the welded layer on the shaft. These electrodes are commercially available, economical and completely meet the welded layer requirements. Commercial designations, electrode manufacturers, chemical composition and mechanical properties of pure weld metal for the electrodes available on the market are presented in table 3 [12, 13].

Table 3: Electrodes used for repair welding procedure: chemical composition and mechanical characteristics

No.	Commercial designation	Manufacturer	Chemical composition %					Mechanical properties		
			C	Mn	Si	Cr	Ni	Re [MPa]	Rm [Mpa]	Hardness
1	PIVA 430 B	FEP Plužine	0.15	1.3	0.7	1.2	/			280-330 HB
2	PIVA 29/9 R	FEP Plužine	0.15	1.2	/	29.0	9.0	500	740-840	230-270 HB
3	WLDC 3	Weldclad	0.12	1.0	0.6	12.2	2.5			33-48 HRC

Before use, these electrodes were dried for two hours at a temperature of 300°C, and were then stored at a temperature of 150°C. On site, the electrodes are kept in accessory driers (quivers).

3.3. Repairing of the toothed shaft

After the additional materials have been selected, the repair welding of damaged gear shafts took place. In the following section of the paper, the activity flow during the repairing is presented, for both procedures.

The first step is the removal of worn-out teeth on one, as well as on both sides (depending on the damage) of the shaft, by machining. Shown in Figure 4 are the shaft dimension before and after preparation, i.e. machining. In this way, the damaged parts of the shaft (teeth) were removed, until the shaft diameter of $\varnothing 380$ mm was achieved. In addition, machining also removed the material along the length until the non-damaged part of the shaft is reached.

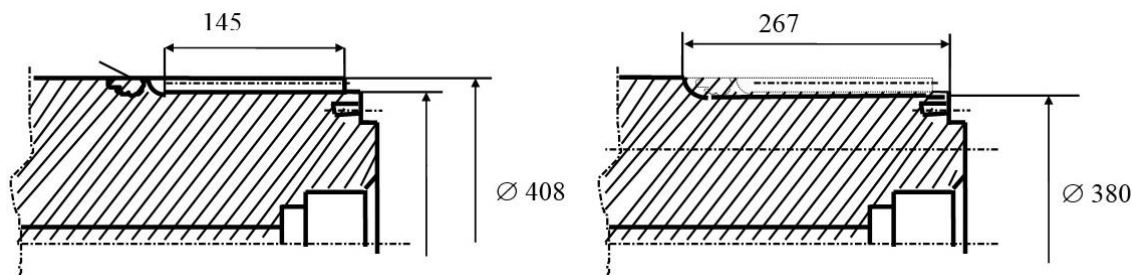


Fig.4: Left) Shaft dimensions before, and Right) after repair welding preparations

The next step involved the testing of the prepared surface for repair welding via magneto-flux in order to detect cracks and other defects which can affect the bond between the parent material and the welded layer.

Taking into account the workpiece thickness, as well as the properties of the base material, heat treatment of the welded joint represents the key position for the successful repairing of the gear shaft. Prior to welding, the shaft is locally preheated to a minimum of 200 mm to the left/right of the welding location to temperatures of 300 ± 10 °C. Preheating temperature was determined according to the Seferian procedure [14, 15].

Repair welding in accordance with the selected procedure and the corresponding additional material (in the case of repair welding using the MAW procedure, a puffer layer is first applied, using the Piva 29/9 R electrode, whereas welding continues with the use of Piva 430 B electrode). In order to overcome the differences in the mechanical properties, an intermediate layer made of a "softer" material is applied, which is common practice in engineering [6, 16, 17]. Parameters of the repair welding process are given in table 4.

Table 4: Welding parameters

Manual arc welding (MAW procedure)		Flux core arc welding (FCAW procedure)	
Electrode diameter	5 mm	Wire diameter	3.2 mm
Welding currency	190 - 230 A	Powder - granulation (Tyler)	8 x 48
Welding arc length	4 - 5 mm	Current type and amperage	(+) do 800 A
Electrode angle relative to the application line	70 - 80°		

Temperature during the repair welding was locally maintained within the range between 280 °C and 300 °C, for its full duration.

The welding process lasted until the removed material was filled (i.e. until the pre-treatment shaft diameter was achieved), with added 3 mm along the generatrix for machining - tooth manufacturing. Welding was performed until a shaft diameter of \varnothing 415 mm was achieved.

After welding, the repaired shaft is tempered in order to reduce residual stresses. The shaft is heated locally to a temperature of 620 °C/h at the rate of 50 °C/h and this temperature is maintain for a period of 3 hours. After 3h, the shaft is subjected to controlled cooling at the rate of 50 °C/h, until the temperature of 150 °C is reached, and at this point the machine is turned off and heat isolation is removed. After that, cooling continues at room temperature.

For the purpose of welded layer quality control, hardness was measured for both cases of repairing (MAW and FCAW procedures). Measured hardness of surfaces welded by the E procedure after heat treatment ranged from 280 to 310 HB, which entirely corresponds to the hardness of the tooth surface before repairing. The hardness of the welded layer on one of the shafts welded using the FCAW procedure is slightly higher and ranged from 320 to 340 HB.

3.4. Techno-economic analysis

Repair welding of working parts can help in achieving significant savings. All repaired shafts from the "Topla valjaonica" rolling mill have been in exploitation for over two years and there are still no signs of damage. The costs of repairing a single shaft, including the manufacturing of all necessary tools were around 1.500 €. The price of manufacturing a new shaft is around 25.000 €. Savings achieved with the use of repair welding in this case was around 200.000 € for all eight shafts, compared to the purchase of new ones. It should be mentioned, that due to their dimensions, delivering and assembling of new shafts would require several months, whereas repair welding can be performed in one week. Production downtime of several month in this facility would cause considerably higher financial losses. Thus it can be concluded that the indirect savings achieved by the use of repair welding is significantly higher than the aforementioned amount.

The conceptual solution for repair welding of machine parts was developed within the Železara Smederevo. A detailed techno-economic analysis determined that a bit over 800.000 € could be saved on an annual level, i.e. that repair welding of spare parts would make up 53% of the price of new parts. Costs mentioned previously also include the purchasing of necessary equipment, adaptation of the industrial hall, additional materials, etc.

4. DISCUSSION AND CONCLUSION

The problem of repair welding cannot and should not be observed purely as compensation of lost dimensions. Significant issues in repair welding occur within the domain of working parts dimension preservation. Enhancing the work surfaces quality is a particular technological problem whose solving needs to include

extensive material science, the metallurgical nature of both base and added materials, which are dictated by the requirements which the applied welded layer must meet. In the example presented here, providing of a high quality weld in the case of toothed shaft repair welding requires the controlling of the following:

- preparation of the shaft for welding
- electrode drying process
- preheating and tempering temperatures
- the repair procedure itself, including the work done by welders or operators.

A high quality welded layer can be expected only in the case that all these elements are in accordance with the prescribed technology. After repair welding, the welded surface is machined, and after that, it needs to be examined in detail, using a non-destructive test method. It should also be noted that repairing of a single machine part cannot be performed an unlimited number of times. Practice had shown that a machine part can be repaired up to 3 or 4 times, thus it would be useful to introduce records about the repair history of any given machine parts, as a form of its "passport", which would contain information about its previous repairs.

In the example presented in this paper, both repair welding procedures that were performed (manual arc welding - MAW procedure, and flux core arc welding - FCAW procedure) were determined as favorable solutions for compensation of materials lost due to wear. Of all the requirements that need to be fulfilled, the most important ones are related to the absence of cracks and notches from the welded layer. In the case defects are detected after the repairing was completed (insufficiently welded surface for the MAW procedure and surface cracks for both procedures), these defects are removed by grinding the surface, or grooving in the case of significant depth of defects, followed by repeated welding in accordance with the technology.

All eight of the repaired shafts were put into back into exploitation and have been working for over two years, still showing no signs of damage, which confirms the justifiability of this technical solution for repairing. Direct financial savings achieved by applying repair welding, compared to the purchase of new shafts can be seen from these examples. Techno-economical analysis had determined that the total amount of around 200.000 € was saved, for all eight shafts, whereas the indirect saving were even greater.

ACKNOWLEDGEMENT

The authors of this paper acknowledge the support from Serbian Ministry of Education, Science and Technological Development for projects TR35040 and TR35011.

REFERENCES

- [1] ANGELOVA, D., YORDANOVA. R., KRASSTEV, D., YORDANOV, B.(2010) *Comparison Of Bending And Rotating Bending Fatigue Of Low-Carbon Steel*, Structural Integrity And Life, ISSN 1451-3749 Vol. 10, No 3

- [2] BAI, Y., WEI-LIANG. J.(2016) *Mechanism of Fatigue and Fracture*, Marine Structural Design, ISBN 978-0-08-099997-5 pp.477-487
- [3] SEONGWOO, W. (2017) *Mechanical System Failures, Reliability Design of Mechanical Systems*, ISBN 978-3-319-50829-0 pp.139-170
- [4] SAKAI, T., NAKAGAWA, A., OGUMA N., NAKAMURA, Y., UENO, A., KIKUCHI, S., SAKAIDA, A (2016) *A review on fatigue fracture modes of structural metallic materials in very high cycle regime*, International Journal of Fatigue, Volume 93, Part 2, pp 339–351
- [5] BAJIC, N., KARASTOJKOVIC Z. (2016) *Contemporary Technology for Surfacing*, Istražičko razvojni centar, ISBN 978-86-89775-01-03
- [6] TANASKOVIĆ, D., ĐORĐEVIĆ, B., ARANĐELOVIĆ, M., SEDMAK, S., SEDMAK, A., ĐUKIĆ, M., TATIĆ, U. (2016) *Repair Welding of Crane Wheels in Steelworks Smederevo*, Advanced Materials Research (Volume 1138), conference: Innovative Technologies for Joining Advanced Materials VIII, pp. 180-185, ISSN 1662-8985, June 02-03, Timisoara, Romania
- [7] Material data sheet, Dr.Sommer Material Technology, Dr. Sommer Werkstofftechnik GmbH
- [8] ERTEK EMRE, H., KAÇAR, R. (2015) *Effect Of Post Weld Heat Treatment Process On Microstructure And Mechanical Properties Of Friction Welded Dissimilar Drill Pipe*, Mat. Res. Vol.18 No.3 São Carlos, ISSN 1980-5373
- [9] BAUER, B., KRALJ, S., MUSTAPIC, A. (2006) *Influence of the welding process on the mechanical properties of the welded joint*, Welding Equipment and Technology, year XVII, ISSN 1221-4639
- [10] STOJAKOVIĆ, D., RAJNOVIĆ, D., ŠIDANIN, L., SABO, B., DAKIĆ, J.(2002) *Influence Of Heat Treatments On Weldability Of Steels With Different Carbon Equivalents*, Zavarivanje I Zavarene Konstrukcije, pp. 41 – 43
- [11] ARSIC, D., LAZIC, V., ALEKSANDROVIC, S., NIKOLIC, R, HADZIMA, B. (2016) *Reparation of the fractured mandrel axle-shaft by welding*, Advances and Trends in Engineering Sciences and Technologies, ISBN 978-1-138-02907-1
- [12] Weldclad Roll welding technology, Material Data Sheet, Doc. No. DS024
- [13] AD Fabrika elektroda „Piva“ Plužine, Dodatni materijali za zavarivanje: katalog
- [14] RADHAKRISHNAN, V.M. (1999) *Carbon equivalent and weldability map*, Transactions- Indian Institute of Metals 52(2):147-151
- [15] JOVIČIĆ, R. (2007) *Analiza uticaja prslina na integritet feritno-austenitnih zavarenih spojeva*, Doktorska disertacija, Mašinski fakultet u Beogradu,.
- [16] POPOVIC, O., PROKIC-CVETKOVIC, R., SEDMAK, A., BUYUKYILDRIM, G., BUKVIC, A. (2011) *The influence of buffer layer on the properties of surface welded joint of high-carbon steel*, MTAEC9, 45(6)579(2011), ISSN 1580-2949
- [17] RATHOD, D. W., SINGH, P., PANDEY, S., SIVANANDAM, A. (2016) *Effect Of Buffer-Layered Buttering On Microstructure And Mechanical Properties Of Dissimilar Metal Weld Joints For*

Nuclear Plant Application, Materials Science And Engineering A 666:100-113

CORRESPONDANCE



Dr Drakče TANASKOVIĆ
Hesteel Serbia Iron & Steel d.o.o.
14 bb, Radinac
11300 Smederevo, Serbia
drakcetanaskovic@gmail.com



Branislav ĐORĐEVIĆ, Research Assistant
University of Belgrade
Inovation center of Faculty of Mechanical Engineering
Kraljice Marije 16
11120 Belgrade, Serbia
brdjordjevic@mas.bg.ac.rs



Uroš TATIĆ, Research Associate.
University of Belgrade
Inovation center of Faculty of Mechanical Engineering
Kraljice Marije 16.
11120 Beograd, Serbia
taticuros@gmail.com



Dr Aleksandar SEDMAK, Full Time Professor
University of Belgrade
Faculty of Mechanical Engineering
Kraljice Marije 16
11120 Belgrade, Serbia
asedmak@mas.bg.ac.rs



Mirjana OPAČIĆ, Research Assistant
University of Belgrade
Inovation center of Faculty of Mechanical Engineering
Kraljice Marije 16
11120 Belgrade, Serbia
mopacicmf@gmail.com

THE CASE OF UNSUCCESSFUL REPAIR WELDING OF A TREIBER ROLL

Drakče TANASKOVIĆ
Branislav ĐORĐEVIĆ
Simon SEDMAK
Uroš TATIĆ
Marko GAJIN

Abstract: Presented in this paper is the case of unsuccessfully performed repair welding of the upper treiber roll in the „Topla Valjaonica“ facility within the Železara Smederevo, currently known today as Hesteel ltd. Inadequate and improperly performed welding technology resulted in the occurrence of a large number of cracks, with the possibility of their propagation to the parent material. The upper and lower treiber roll are parts of the installation whose purpose is to fold the rolled strip and then send it to be further machined. The parent material used for the upper treiber roll was the structural steel S235JO. Repair welding was the consequence of damage that occurred during the exploitation of the roll. Shown in the paper are some of the cracks detected on the welded surface of the upper treiber roll. The analysis of the reasons behind the occurrence of these cracks is presented, and machining was recommended for the purpose of removing of these cracks, along with the use of certain NDT methods.

Key words: repair welding, cracks, preheating, welding

1. INTRODUCTION

Welding and activities related to it represent a process which requires special attention, starting from the design stage, through the development and performing of the technology and up to welded joint control stage, for the purpose of putting the welded or repaired machine part in exploitation. Deviations that occur during each of these stages may result in defects, cracks and deformation due to rapid cooling, along with the occurrence of unwanted metallurgical structures. Welding should be performed entirely in accordance with the welding technology. Presented in this paper is the case of repair welding of the upper treiber roll in the „Topla Valjaonica“ facility within the Železara Smederevo. The upper and lower treiber roll are the driving rolls which are placed in front of each strip coiler. These rolls are used to fold the strip supplied by the output rollers and direct it towards the coiling mandrel. The upper treiber roll is supported by the driver switch cradle. In addition, the treiber roll serves the purpose of providing sufficient tensile force to the strip between the rolls and the coiling mandrel. The diameter of the upper treiber roll is $\varnothing 900$ mm, its calibrated length is 2280 mm, whereas the lower roll diameter is $\varnothing 400$ mm. The geometry and position of the treiber rolls is shown in figure 1.

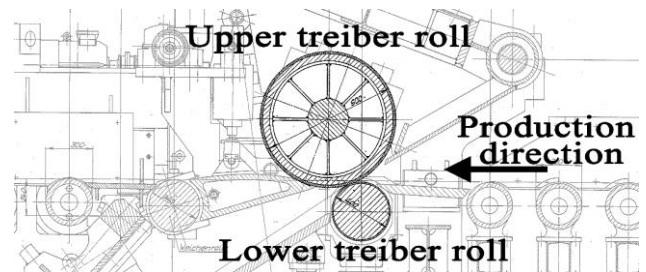


Fig.1: Position and geometry of the upper treiber roll in the production line

Due to exploitation conditions and wear, it was necessary to repair weld the upper treiber roll, as was predicted by the manufacturer. The roll was pre-machined in the mechanical workshop at the Železara Smederevo, to a diameter of $\varnothing 870$ mm. After machining, magnetic flux testing of the whole roll was performed (including the branch and the work surface). The thickness of the welded hard layer should be up to 40 mm, including the intermediary layer, i.e. the diameter of the roll should be $\varnothing 910$ mm. After welding and applying of hard weld layer, the upper roll have to be machined to a diameter of $\varnothing 900$ mm. The following section of this paper contains a detailed overview of all activities performed during welding, as well as the activities performed in order to remove cracks. Repair welding was unsuccessful, resulting in the occurrence of cracks after cooling.

2. PROPERTIES OF THE UPPER TREIBER ROLL PARENT MATERIAL

The parent material of the treiber roll was steel S235JO, a general purpose structural steel with good weldability. Depending on the manufacturing process, chemical composition and relevant application, further letters and classifications might be used to reference particular grades/products of structural steel. This structural steels are used in many ways and their application can be diverse. They are particularly useful because they offer

the unique combination of good welding properties with guaranteed strengths. Structural Steel is an extremely adaptable product and is often favored by the engineer trying to maximize strength or structure while minimizing its weight [1, 2].

The chemical composition of the roll parent material is given in table 1, whereas table 2 shows its mechanical properties.

Table 1: Chemical composition of the roll parent material

Chemical Element	C	Si	Mn	Cr	Ni	Cu	P max	S max
%	0,17	0,3	1,4	/	/	Max 0.55	0,045	0,009

Table 2: Mechanical properties of the roll parent material

Mechanical properties	Tensile strength R_m [N/mm ²]	Yield strength R_e [N/mm ²]	Elongation	Toughness
Values	400-490	245	22	27

It should be noted that steel S235JO does not have the tendency towards neither hot nor cold cracks.

3. WELDING TECHNOLOGY

Repair welding was performed using automated FCAW procedure, with the following additional materials.

- WLDC 9 wire, along with the universal Weldclad powder was used for the puffer layer. This wire is low alloyed flux-cored wire, used for submerged-arc welding for build-up, maintenance and repair. WLDC 9 has excellent hot slag release, especially suitable for continuous welding operations.

Universal Flux is suitable for single and multi-pass welding using single or twin wire technique [3].

- For the hard weld, WLDC 17 wire was used. This wire is fully basic, all mineral, non-alloying agglomerate flux for submerged arc welding wire, used for multilayer surfacing of hot strip mill process rolls including wrapper rolls and has a martensitic matrix [3].

First two layers formed the intermediary layer (puffer), whereas the following three layers represent the hard weld. Layers were applied using the oscillation technique, with weld overlap of 30-35%. Welding parameters are given in table 3. The diameter of the roll after surfacing is \varnothing 910-912 mm.

Table 3: Welding parameters

Layer	Wire	Temperature max	Amperage	Polarity
1	WLDC 9	420 °C	500 – 550 A	-
2	WLDC 9	420 °C	500 – 550 A	+
3	WLDC 17	420 °C	500 – 550 A	-
4	WLDC 17	420 °C	500 – 550 A	+
5	WLDC 17	420 °C	500 – 550 A	+

The roll was not annealed after the repair welding was complete. Cracks have occurred in certain zones. These cracks were grooved by a grinder after surfacing, and it was determined that they cannot be eliminated, along with

the assumption that they propagated into the pre-machined parent material. Shown in figure 2 are some of the cracks (along with the grooved ones), with designated fields (A to G).

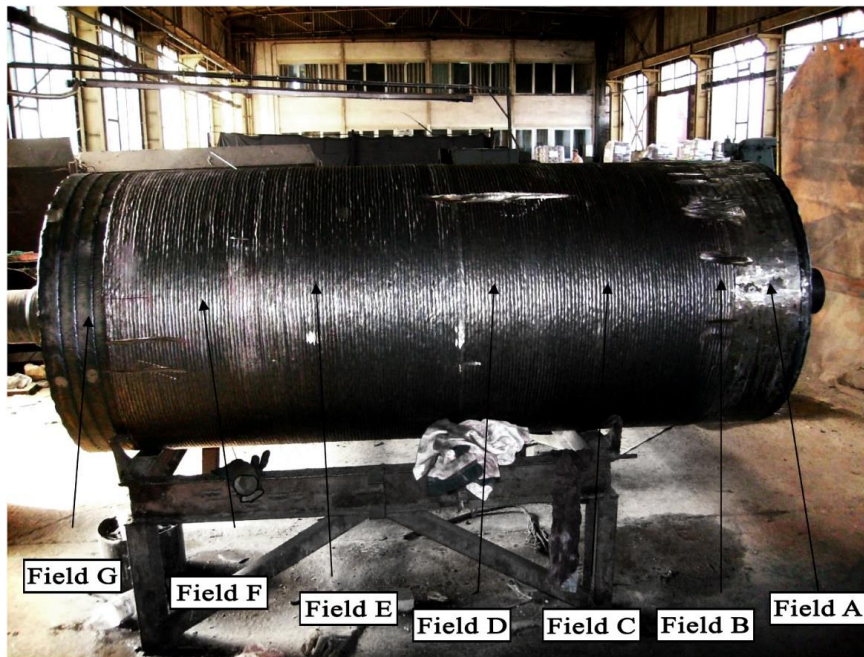


Fig.2: Appearance of treiber roll after repair welding

4. INSPECTION AND CRACK IDENTIFICATION

A total of 46 cracks were detected in the treiber roll after applied repair welding procedure. In addition to these cracks, a number of small mesh cracks were observed in field A, along the full circumference. For the purpose of easier identification, cracks were divided into zones, denoted A to G. Some of these cracks are shown in figure 3.

Field A was ground with a width of 300 mm along the circumference. Small mesh cracks were detected by magnetic flux testing in this field. Field B was 200 mm wide and grooved along the circumference. A total of 19

cracks were detected in this field. Two of the cracks were eliminated by grooving, to a depth of 20 mm. The depth to which the cracks have propagated could not be accurately determined, since there is no documentation about it. Field D, with a width of 300 mm, contained 13 cracks along its circumference. One of the cracks shown in this field was eliminated by grooving to the depth of 25 mm. The depth to which the cracks have propagated could not be accurately determined. Field F was 200 mm wide, and 14 cracks were detected along the circumference, some of which were eliminated by additional grooving, whereas some were not. No cracks were detected in fields C, E and G.



Fig.3: Some of the cracks on the treiber rolls after the surfacing

5. DISCUSSION AND CONCLUSIONS

Cracks have occurred as the result of a lack of preheating, i.e. due to cold surfacing of grooved locations. The cracks are caused by applying the hard weld to an insufficiently preheated, or completely cold surface, even though the welding technology specified that preheating is mandatory. Most of the cracks were located in the reinforced part of the roll, as well as its vicinity. It is well known that parts with thickness greater than 20 mm must be preheated and this is recommended for properly performing welding procedure [4-6].

The treiber roll with defects shown in the previous parts of this paper could not be put back into exploitation. Thus, it is recommended to develop the plan for machining of the welded roll for the purpose of removing of cracks and defects. Due to welded layer thickness, it can be concluded that the operation of removing the whole weld for the purpose of determining of the extent of crack propagation, must be performed in several passes. It is recommended to perform testing using NDT methods on the surface following the removal of each layer, for the purpose of determining the crack depth. It cannot be claimed with certainty that the cracks have propagated into the parent material, since additional crack grooving was performed in order to eliminate them.

In this paper, the significance of preheating prior to repair welding for the purpose of avoiding crack initiation and other types of deformation can be seen. Preheating reduces the cooling rate, which in turn reduces the temperature difference between the cold parent material and the welded layer (which transforms from molten hot phase to a solid phase during the cooling, until the environment temperature is reached).

In addition to technical consequences, this also resulted in economic losses due to additional machining of the treiber roll after welding for the purpose of removing of defects, along with the need for repeated welding.

ACKNOWLEDGEMENT

The authors of this paper acknowledge the support from Serbian Ministry of Education, Science and Technological Development for projects TR35040 and TR35011.

REFERENCES

- [1] <http://www.azom.com>
- [2] PROKIĆ-CVETKOVIĆ, R., POPOVIĆ, O.: Mašinski Materijali 1, izdanje Mašinskog Fakulteta Univerziteta u Beogradu, 2012
- [3] Weldclad Roll welding technology, Material Data Sheet, Doc. No. DS024
- [4] DRAKČE TANASKOVIĆ, BRANISLAV ĐORĐEVIĆ, MIHAJLO ARANĐELOVIĆ, SIMON SEDMAK, ALEKSANDAR SEDMAK, MILOŠ ĐUKIĆ, UROŠ TATIĆ: Repair Welding of Crane Wheels in Steelworks Smederevo, Advanced Materials Research (Volume 1138), conference:8th International Conference on Innovative Technologies for Joining Advanced Materials (TIMA 16), pp. 180-

185, ISBN 978-3-03835-768-1 (ISSN 1662-8985), June 02-03, 2016, Timisoara, Romania

- [5] A. SEDMAK I DR.: Mašinski materijali, 2. deo, Univerzitet u Beogradu Mašinski fakultet, Beograd, 2000.
- [6] ZVONIMIR LUKAČEVIĆ: Zavarivanje, Slavonski Brod 1998.

CORRESPONDANCE



Dr Drakče Tanasković
Hesteel Serbia Iron & Steel d.o.o.
14 bb, Radinac
11300 Smederevo, Serbia
drakcetanaskovic@gmail.com



Branislav Đorđević, Research Assistant
University of Belgrade
Inovation center of Faculty of
Mechanical Engineering
Kraljice Marije 16
11120 Belgrade, Serbia
brdjordjevic@mas.bg.ac.rs



Simon Sedmak, Research Assistant
University of Belgrade
Faculty of Mechanical Engineering
Kraljice Marije 16
11120 Belgrade, Serbia
simon.sedmak@yahoo.com

Uroš Tatić, Research Associate
University of Belgrade
Inovation center of Faculty of
Mechanical Engineering
Kraljice Marije 16.
11120 Beograd, Serbia
taticuros@gmail.com

Marko Gajin
Hesteel Serbia Iron & Steel d.o.o.
14 bb, Radinac
11300 Smederevo, Serbia

MAINTENANCE OF AXIAL BEARING OF KAPLAN TURBINE

Safet ISIĆ
Mensud ĐIDELIJA

Abstract: Axial slide bearing of vertical Kaplan turbines is main bearing element supporting up to several hundreds tones of turbine elements self weights and water column. Because of that, exact assembling and maintenance is of vital significance for turbine correct operating. Problems which could appear in long term operations are damages of segments basements or "white metal" and change of position of bearing housing due to long term loading and subsidence of concrete foundations. This paper presents examples of testing and maintenance of segments of axial bearing and correction of bearing housing position. Effects of corrections and their indicators are also presented.

Key words: Caplan turbine, axial bearing, maintenance,

1. INTRODUCTION

During the planned reconstruction and revitalization of a hydro-aggregate, replacement of all of damaged and worn individual parts and solution of all defects recorded during the exploitation should be done. If possible, application of new constructive solutions could be used, which will improve the operation of certain mechanical assemblies. Axial bearing of hydro aggregate is a very important assembly for reliable and functional work of hydro aggregates. It is loaded by a large scale axial force consisting of the weight of the rotating parts of the hydro-aggregate - a runner with blades, a turbine shaft, a rotor of a generator and a pressure force of the water column above blades of a runner.

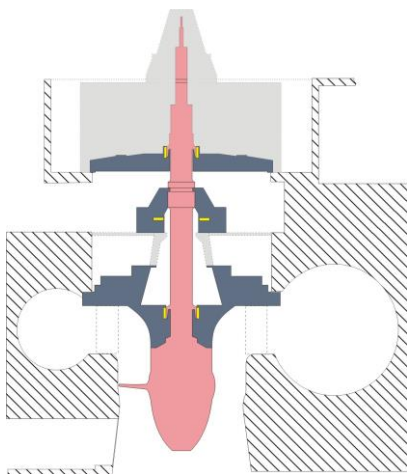


Fig.1: Design of aggregates on HPP Grabovica

Correction of defects on the axial bearing takes significant time needed for preparation due to the design of the hydro-aggregate (Fig. 1), the purchase of spare parts, the execution of the works and commissioning. In this paper

the analysis of previous exploitation work, preparation for reconstruction and revitalization, installation and reconstruction, and analysis of work after the reconstruction of the axial bearing of aggregate no. 1 of HPP Grabovica, designed to carry axial load of 1060 tons are presented.

2. AN OVERVIEW OF EXPLOATATION HISTORY OF AXIAL BEARING

During the 33 years of exploitation, aggregate no. 1 of HPP Grabovica achieved 104,000 operating hours with 9,600 start-ups. In starting and stopping process, when aggregate rotates with rotation speed greater of 80% of the nominal (150 rpm), the oil is fed by high pressure pumps between the sliding surface of the segment and the sliding plate of the axial bearing, to ensure a necessary thickness of the oil film and improve the lubrication and protection of the sliding surfaces of the segment and sliding plate. Regularly, every hour of the aggregate operation, the temperature of the metals base of the four segments and oil are recorded. Capillary-mercury thermometers for measuring the temperature of the metal are placed in openings of 13 mm diameter and length of 400 mm, with an opening axis at the 30 mm from the upper sliding surface of the segment. Temperature value of peace metal base is measured at the distance of 23.5 mm from the contact surface of the segment and sliding plate. To measure the oil temperature, or more precisely – temperature of the oil film, the capillary thermometer is placed in a "wiper", which is attached to the exit side of the sliding plate and used to remove the oil film from the contact with the segment. The base of axial bearing segment is made of cast iron ČL. 0401. The maximum achieved temperatures in the previous exploitation of the hydro-aggregates at these five measuring points are shown in the table 1.

Table 1: Maximum temperature of axial bearing.

Measuring point	Temperature (°C)
Metal segment 1	62
Metal segment 2	59
Metal segment 3	54
Metal segment 4	54
Oil	62

The values of the temperature were taken after a long operation of an aggregate on a power slightly less than the nominal value of 57.5 MW, when the stationary temperature distribution from the upper sliding surface of the segment (having an approximate temperature of the oil film of 62 °C) to the segment steel base in contact with the outer surface of the capillary probe at the distance of is 23.5 mm, is established. Daily oil level in the tank of the axial bearing is controlled. Regularly, annual oil analysis was carried out to verify the physical and chemical characteristics of the oil and preventive detection of the beginning of the wearing process of the sliding surfaces and other surfaces of the axial bearings that are in mutual contact. During the operation of the aggregate, through the glass opening on the bearing housing, it was observed that the oil was foaming, which sometimes caused, at the normal operating level of the oil, a pronounced overflow of the created foam above the inner side of the tank housing and a loss of oil from the tank. In exploitation of the hydro-aggregate, and the axial bearing also, until the reconstruction, there were no defects requiring bigger maintenance, so the axial bearing assembly worked with the equipment installed during the commissioning in 1982.

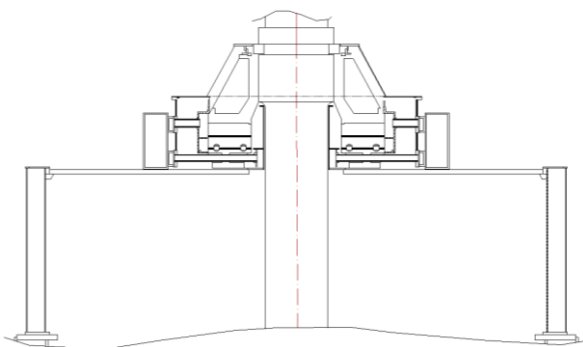


Fig.2: Cross-section of axial bearing assembly of aggregates on HPP Grabovica

3. PREPARATION FOR RECONSTRUCTION

Taking into account the facts stated in the previous chapter, that there were no failures of the axial bearing due to number of working hours and years of exploitation

as well, there were no rebuilding due to the very demanding and time consuming works for repairing possible malfunctions. It is considered the white metal replacement on the all segments, the replacement of the conic support g bolts, the replacement of the bolts for the connection of the conic support to the sliding plate and replacement of the white metal in the oil collector. In the previous solution, the oil collector pushes oil from the tank through eight coolers located around the bearing housing firstly, and then through a routing tube at a diameter of 1400 mm. They are directed to the segment sliding surface between the oil wiper and the beginning part of the sliding plate and the axial bearing segment, applying fresh oil, just after the wiper removed the hot oil film. By analyzing the constructive solution of the bearing, it has been concluded that the routing pipes, due to their position and the low bandwidth of action only partially apply oil to the sliding surface because of segment length of 650 mm. In addition, the processing of the support bearing and bearing ring plate is planned to achieve the required structural horizontality of 0.02 mm/m. This processing is planned because of machining of a horizontal flange of the turbine barrel at which the turbine cap is placed (its upper surface is in fact the support of axial bearing base) which is done because of obtaining structural horizontality.

4. EQUIPMENT DISASSEMBLY

During the dismantling of the axial bearing equipment, it was visually confirmed that, due to incorrect centering, the oil flow through some routing pipes up to 30% ended on the forehead of the oil wiper. Measurements were made of the horizontal support of the support ring plate and ring plate by a precision digital level Sokkia SDLIX and the mechanical level of resolution of 0.02 mm/m. Measuring the bearing plate horizontality by the digital level, a total difference of 0.31 mm between the highest and lowest measuring positions was measured. Measuring points were placed on the inner and outer diameter of each of the sixteen segments (32 measurement values). Tangential and radial slope were measured on the middle of the bearing segments (16 measured values). Tangential slope was ranged from - 0.06 to + 0.06 mm/m, and the radial slope was ranged from - 0.10 to + 0.04 mm/m. Measurement of the horizontal bearing height of the bearing bed - the top surface of the turbine cover - digital level cover was a total loss of 0.41 mm between the highest and lowest point positions measured on the inner and outer diameter of the hoisting rim (32 measurements), while the tangential slope of the midline of the support rim was - 0.12 to + 0.14 mm / m, and the radial slope of the center of the holding of the supporting ob Dressed from - 0.20 to + 0.04 mm/m (16 measured values), where at four measuring points it was not possible to measure the slope because the value was outside the measuring range of the machine gauze. It is important to note that between the support bearing segment and the bearing plate are the bottom bearing bottom mounts and 5 mm height, as well as between the support plate and the bearing base of 16 circular rubber girders and 5 mm in height. The NDT tests of the bearing segments showed

presence of a no acceptable indications in white metal surface.

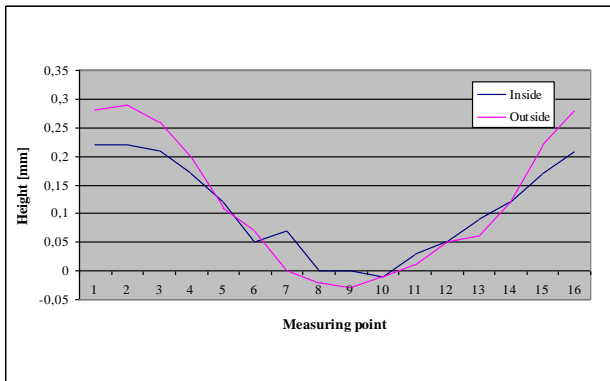


Fig.3: Results of horizontality measurement of the base

5. INSTALATION AND EQUIPMENT RENEWAL

By measuring of the horizontality of the flange in the turbine barrel at which the turbine cover is located, a deviation of 1.7 mm in height has been established. The machining by a special machine mounted on the turbine bolt has been provided to obtain flange horizontality. The machining of the surface of the turbine cover which is attached to this flange in the turbine barrel has also been carried out. The aim of the machining of these two flanges is to achieve the best horizontal position of the axial bearing base. These machining also affected horizontality of the bearing base and bearing ring plate, which also should be processed. With manual processing on the bearing base, the horizontality was reached at 29 measuring points with a deviation of 0.06 mm, while at three measuring points the height was increased by 0.03 mm. Tangential and radial slope of the center of the seating surface were from - 0, 03 to + 0.02 mm/m (16 measured values). The actual horizontality of this surface is probably even better because, due to the manual processing, small local recesses and protrusions on the surfaces have been made.

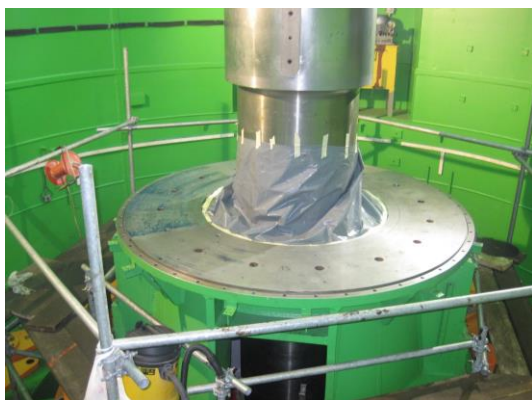


Fig.4: Hand processing of the axial bearing base

With the machining of the bearing plate of the axial bearing, the horizontality of 30 measuring points with a deviation of 0.08 mm was achieved, while the other two

measurement points were increased by 0.02 mm or 0.05 mm. Tangential slope of the middle of the segment area had the values from 0.00 mm/m to 0.02 mm/m (at a single measured position + 0.03 mm/m), while radial slope of the middle of the segment area was from 0.00 to + 0.04 mm/m (at two measuring positions to + 0.06 mm/m among 16 measured values).



Fig.5: Machining of bearing plate

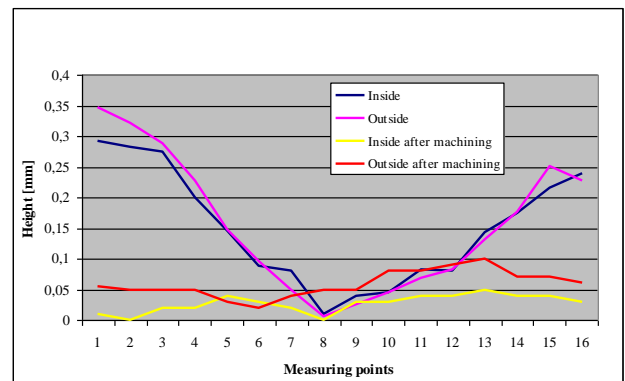


Fig.6: Horizontality of bearing plate before and after machining

Directional pipes are extended between the oil wiper blade and segment to the outer diameter of the 650 mm segment with openings on the upper surface through which fresh oil is applied to sliding plate. White metal (White Metal WM 80 with of 80% tin, 12% antimony, 6% copper and 2% lead) was replaced on the bearing segments. The total thickness of the white metal is 10 mm, with the height of the "cargo tail" in the steel section of the segment of 6 mm. The construction of new capillary-mercury thermometers in four segments (metal segment 1 to metal segment 4) has been arranged in the mutually normal axes. A capillary thermometer with a shorter length is mounted for oil temperature measurement. Cleaning of the system for oil cooling is done before filling of new oil. The new oil of the same viscosity but another producer, with improved physical and chemical characteristics is used. New oil has specially increased oxidative stability, a reduced foaming tendency and high air separation capacity. In the process of the aggregate testing after renewal and revitalization, as well as by monitoring in the real work conditions with power near the nominal, it was found that the metal temperatures of the four segments of the bearing segments and the oil

were significantly less than before the reconstruction, as shown in the table 2.

Table 2: Maximum temperature of axial bearing before and after maintenance i revitalization.

Measuring point	Temperature before (°C)	Temperature after (°C)
Metal segment 1	62	48
Metal segment 2	59	44
Metal segment 3	54	39
Metal segment 4	54	41
Oil	62	37

The average temperature of segment base metal is lower by 14.25 °C. The oil temperature is considerably lower because it is now the value of the oil in the bearing reservoir and before it was the temperature of the oil film in the wiper. After that, it should be noted that measuring of the absolute and relative vibration of the aggregates as well as the noise level in the turbine area, showed that the condition of aggregate 1 of HPP Grabovica can be classified as new equipment.

6. CONCLUSION

For the planned renewal and revitalization of the hydro-aggregate, as well as its individual assembly plants, it is necessary to:

- analyze all possible failures and causes of their occurrence that have been recorded since commissioning,
- analyze daily operating reports with all relevant data on aggregate work,
- implement constructive improvement and modernize existing technical solutions,
- make optimum selection of parts for replacement and revitalization,
- optimize the assembly time of all individual assemblies-planted by compromising the required functionality and reliable future work of the aggregate.

The application of all the above mentioned activities in the mainence of the axial bearing of unit 1 of HPP Grabovica has been resulted in:

- the average lowering segment base metal temperature of the bearing for 14.25 °C, which will considerably prolong the service life of the bearing segments,
- Reduction of the oil film temperature, which will considerably prolong the working life of the bearing oil,
- Reduced oil spillage to prevent oil leakage from the bearing bed reservoir.

These improvements in operation are achieved primarily by:

- modifying the routing pipes which direct cooled oil on a substantially larger sliding surface,
- using oils of better physical and chemical characteristics, and
- achieving the designed horizontality of the base and bearing plate at 90% of area, while two sets of 5 mm thick rubber pads successfully amortize local unbalances (recesses and bulges).

REFERENCES

- [1] Technical documentation of HP Grabovica.
- [2] Tecnical documentation of HP Grabovica turbines (Litostroj).

CORRESPONDANCE



Safet ISIĆ, Prof. D.Sc. Eng.
University Džemal Bijedić” in Mostar,
Mechanical Engineering Faculty
University campus bb
81104 Mostar, BiH
safetisic@gmail.com



Mensud ĐIDELIJA, M.Sc. Eng.
JP Elektroprivreda BiH d.d. Sarajevo
HE na Neretvi Jablanica,
Jaroslava Černija 1
88420 Jablanica, BiH
m.djidelija@epbih.ba

CHALLENGES OF ROLLING ELEMENT BEARINGS FAULT DETECTION BASED ON VIBRATION SIGNAL MEASUREMENT AND ANALYSIS

Ninoslav ZUBER

Abstract: This paper addresses the suitability of vibration monitoring and analysis to detect different types of faults in roller element bearings and presents the result of an industrial evaluation of different vibration signal processing techniques as a method for condition monitoring of roller elements bearings condition monitoring. Different processing techniques are presented and demonstrated on signals acquired from real life industrial applications. Advantages and disadvantages of different techniques having in mind specific limitation have been shown.

Keywords: bearing faults, vibration signal processing, condition monitoring

1. INTRODUCTION AND LITERATURE REVIEW

Roller elements bearings (REB) are the most common components in rotating machines and they are claimed to be one the most responsible elements for machine's unplanned stoppages and failures. Unplanned stops leads to loss of production, high maintenance costs and sometimes to losses of human lives. As a result, development of methods of vibration signal processing, together with the analysis of their applicability in REB diagnostics is very important and attractive. It is essential to detect REB defects as early as possible to avoid fatal breakdowns of machines and to reduce the secondary damage caused by failures.

In the last three decades many papers have been published that deal with methods of REB faults identification. In [9] authors gave a very detailed review of different methods of vibration signals analysis in time and frequency domains, analysis of noise pressure and intensity, shock waves and measurement and analysis of acoustic emission. In [2] some alternative techniques are presented such as shock pulse measurement, oil analysis and particle counting. In [4], [5] and [3] a review of techniques of analysis in time and frequency domains is given. There are many studies that investigate the mechanism of noise and vibration generation in REB ([8], [10], [6], [1], [7]). According to these papers the main cause of noise and vibration inside the REB is a non – uniform stiffness due to the fact that we have a finite number of rolling elements. The number of rolling elements that make a contact with inner and outer race of the bearing and the influence of the bearing loading zone are the parameters that influence the level and frequency content of noise and vibration signals ([8] and [10]). Even if the geometry of the bearing is perfect and if we treat

both races as continuous the change of direction of contact forces generate unwanted noise and vibration.

We can define two types of REB faults: localized and distributed. Distributed faults are result of bearing production, improper mounting technique or abrasive wear ([7]). Localized faults are in the form of discrete cracks on contact surfaces of races and rolling elements. The most common cause of localized faults is a fatigue crack where the crack occurs bellow the contact surface and over the time propagates to the contact surface. Fatigue crack is the result of bearing overload or improper mounting.

2. SIGNAL PROCESSING TECHNIQUES IN REB FAULT DETECTION

In general REB has four components, two races, rolling elements and a cage. When we analyze localized REB fault we seek for discrete faults on these components. Characteristic REB fault frequencies are as follows:

$$FTF = \frac{f_o}{2} \left(1 - \frac{d}{D} \cos \alpha \right) \quad (1)$$

$$BPFO = \frac{f_o N_r}{2} \left(1 - \frac{d}{D} \cos \alpha \right) \quad (2)$$

$$BPMFI = \frac{f_o N_r}{2} \left(1 + \frac{d}{D} \cos \alpha \right) \quad (3)$$

$$BSF = \frac{f_o D}{2 d} \left(1 - \frac{d^2 \cos^2 \alpha}{D^2} \right) \quad (4)$$

where: FTF (cage frequency), BPFO (ball pass defect frequency at the outer race), BPMFI (ball pass defect frequency at the inner race), BSF (defect frequency at the rolling element), d (diameter of the rolling element), D (REB pitch diameter), N_r (number of rolling elements)

and α (contact angle). These equations define REB defect frequencies in the units of harmonic orders (frequency divided by the shaft speed). In general case these frequencies are asynchronous. Also it is worth to mention that these equations assume that there is rolling movement inside the bearings. In real REBs there is always some slip so there is always some difference between calculated and measured REB's bearing frequencies.

In case of existence of indentation or external particle inside a REB, every time the roller element passes over the indentation on a race, a decrease of internal strain will be produced. When a roller element passes over the metal particle that is on the race due to the flaking of the components, there will be an increase of REB internal stresses. These transient forces result in rapid change of accelerations of REB components and as a result shock phenomena are present in the vibration signal. If the size of the fault is large enough, these stress waves can excite the natural frequencies of the REB structure and the REB is "ringing".

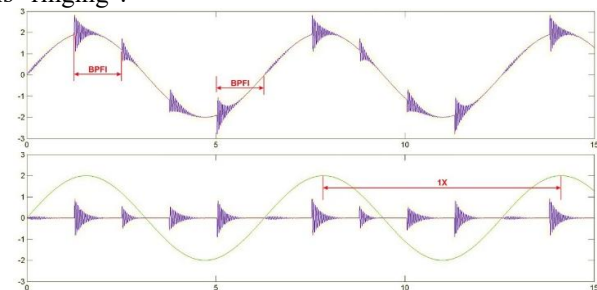


Figure 1 – Vibration time waveform (inner race fault, BPF1) – numerical simulation. Raw and high pass filtered time waveform

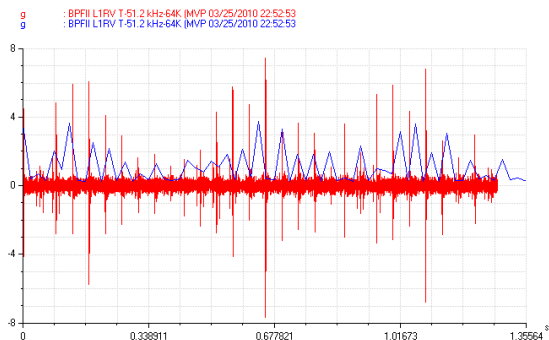


Figure 2 – Vibration time waveform (inner race fault, BPF1) – signal from the real machine

Due to the nature of this mechanism, techniques of applied vibration signal processing used in REB diagnostics should be adequate to identify transient components in acquired signal. These low amplitude high frequency components from the faulty bearings are superimposed with the high amplitude low frequency components from low frequency defects (such as residual imbalance).

Vibration measurement and signal processing for REB fault identification have three different challenges to face with:

1. Low amplitude. Amplitudes of stress waves are very low. A machine generates a high volume of vibration which far exceeds the amplitude of stress wave. Vibration transducer and vibration analyzer may have an excellent dynamic range (for example 90 dB),

however this may not be sufficient. Even if it could be measured it would be quite hard to analyze the raw data. Therefore we need a method that removes the low frequency high amplitude components and focus on the area of interest (high frequency domain)

2. Short duration. The frequency of the stress wave is very high – typically greater than 5 kHz (1-50 kHz). Bearing faults generate repetitive impacts. If we could measure them directly we could calculate the periodicity of impact and relate it to the bearing component.
 3. Measurement issues. Since we are interested in high frequency components of the signal, it is highly recommended to measure and analyze acceleration due to its sensitivity in high frequency region. Also for the purpose of having an adequate transfer function of the system care must be taken when choosing transducer mounting technique (mounting with the stud is preferred).
- To cope with these challenges there are basically four different approaches:
1. Use of accelerometer to amplify high frequency components.
 2. Use of high speed data acquisition to directly capture stress waves.
 3. Use demodulation techniques for capturing high frequency vibration.
 4. Use ultrasound measurements to capture high frequency components.

The most common used methods of vibration signals analysis applied to identification of defected REB are: time waveform analysis, analysis in the frequency domain, techniques of spectral enveloping and demodulation and time-frequency transformations. Techniques of time waveform analysis are focused on extraction of statistical parameters of raw or filtered time waveform signals in order to quantify the transient phenomena. The most common *universal* parameters are: root mean square - RMS, peak-peak value - PP, Crest factor – CF and Kurtosis – Kurt. Crest factor is a ratio of peak and RMS values of the signal while the Kurtosis parameter is the kurtosis is a measure of the "tailedness" of the probability distribution. Kurtosis is also a measure of impulsiveness of the time waveform and is independent of amplitude of the signal. Figure 2 shows a Kurtosis parameter (blue curve) with a time window of 20 msec over a time waveform of a REB with a defect on the inner race.

Transformation of time waveform into frequency domain using the FFT algorithm enables identification of possible typical REB defect frequencies in the signal (BPFO, BPF1, BS and FTF).

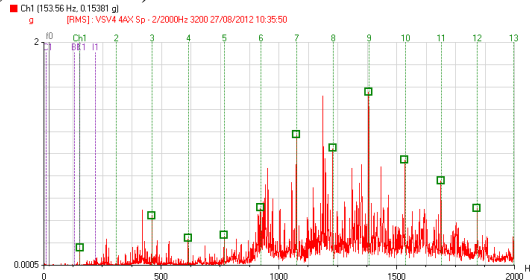


Figure 3 – FFT of a REB with inner race fault, harmonics of BPF1 (400 kW, recirculation fan)

Demodulation / enveloping technique is the advanced signal processing method with its wide application in REB condition monitoring in the early stages of defect development. Repetitive impulses caused by roller elements passage over the indentation could excite REB housing natural frequencies. As a result, frequency spectrum contains peak at the natural frequency modulated by the REB defect frequency. After band pass filtering and signal rectification, envelope spectrum is generated with the sidebands shown as harmonic family. The success of REB fault detection using envelope spectra is highly dependent on filter cut off frequencies. The center frequency of the band pass filter should be near the resonance frequency of the bearing structure which is in general case unknown. This is the main culprit of enveloping in its use for everyday condition monitoring of machines. With faulty REB in case of its localized fault its envelope spectrum should contain sideband components of the REB fault frequency that periodically excited the REB's natural frequency. The envelope spectrum is always analyzed in decibels and if the harmonics of REB's fault frequencies are raised more than 20 dB (power ratio of 1:100) over the carpet noise the bearing is ready to be replaced.

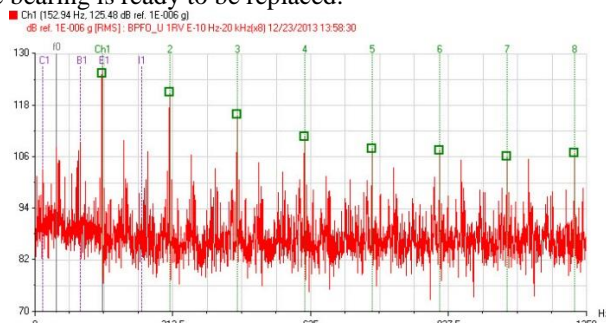


Figure 4 – Envelope spectrum of a REB with inner race fault, harmonics of BPFI (400 kW, recirculation fan)

Methods of time-frequency transformations are widely used in REB's diagnostics due to the nonstationary nature of the impact phenomena. As a result, time-frequency transformations result in signal presentation in both domains – time and frequency. This makes possible to analyze frequency contents nonstationarity over the time. The most common used methods for time-frequency transformations in REB diagnostics are: short time frequency transform - STFT, Wigner – Ville distribution – WVD and wavelet analysis - WA.

3. EVOLUTION OF FREQUENCY SPECTRA COMPONENTS WITH THE REB'S DEFECT GROWTH

In order to get a reliable information from a defective bearing, as is the case in other fields of vibrodiagnostic too, it is necessary to know how fault development affects the recorded vibration signal in time and frequency domain.

Initial stage of fault development begins with the occurrence of fatigue microcrack just below the contact surface of the faulty component. It is necessary to note that the level of degradation is small. Components of the vibration signals that come from a bearing are results of small impacts (shock impulses) and friction that occurs due to the abnormal lubrication. These

components are located in the high frequency region (from 20kHz and above).

The reliability analysis of the existing detection methods gives the following conclusions:

1. High frequency methods (SPM, SpikeEnergy, PeakVue¹) in this stage are very reliable and their scalar representatives will grow together with the fault development.
2. Enveloping / demodulation of acceleration vibration signal, in assumption that the cutoff frequencies are well defined, will, despite the bad signal to noise ratio, detect the existence of fault inside the bearing.
3. Frequency spectra – FFT of the vibration velocity will not detect the bearing fault due to the fact that vibration components are in high frequency region. FFT of acceleration signal could give a very limited information on the bearing fault.
4. Time waveform analysis – generally, for this stage is not useful.

In the second stage of fault development, cracks on the faulty components become larger and wider and therefore the generated impulses could have enough energy to excite the bearing natural frequencies. In this stage the acceleration envelope should give a very clear information on the present defect in the bearing.

The reliability analysis of the existing detection methods gives the following conclusions:

1. High frequency methods – their scalar parameters will still grow together with the fault development.
2. Enveloping / demodulation of acceleration vibration signal will clearly detect the existence of fault inside the bearing.
3. Frequency spectra – FFT of the vibration velocity will not detect the bearing. FFT of acceleration signal will give a very reliable and clear information on the bearing fault.
4. Time waveform analysis – generally, for this stage is not useful.

In the third stage, bearing faults are larger and there could be more of them in comparison with a previous stage. In this phase it is possible to get the bearing seizure. Typical for this stage is a strong excitement of bearing's natural frequencies. Generally the wideband noise will be raised, both, in FFT and envelope spectra.

The reliability analysis of the existing detection methods gives the following conclusions:

1. High frequency methods – their scalar parameters will still grow together with the fault development.
2. Enveloping / demodulation of acceleration vibration signal will detect the existence of fault inside the bearing but the raised noise will start to mask the bearing frequencies.
3. Frequency spectra – FFT of the vibration velocity and acceleration will give a very reliable and clear information on the bearing fault.

¹ These methods are not considered as universal since they require using vibration acquisition devices and softwares from specific vendors. Therefore, they are not analyzed in this paper.

4. Time waveform analysis – generally, is very useful for this stage.

The third stage is generally a point where the bearing should be replaced, if possible. If not the vibration analyst should monitor the vibration parameters of the bearing on weekly basis.

If the bearing is still left in operation, initial faults on one bearing's component will damage the other bearing's components. Due to the indentations smearing, it is possible to get lower high frequency components, compared to the previous stage.

Due to the material flaking loosens in the bearing grows. This directly affects the bearing geometry and this results in noisy operation and changing the bearing defect frequencies.

The reliability analysis of the existing detection methods gives the following conclusions:

1. High frequency methods – they are very unreliable in this stage due to the lowering of high frequency components. The bearing faults develops while the high frequency parameters are decreasing.
2. Enveloping / demodulation of acceleration vibration signal could detect the existence of fault inside the bearing but the raised noise very often mask the useful components.
3. Frequency spectra – FFT of the vibration velocity and acceleration will give a very reliable and clear information on the bearing fault.
4. Time waveform analysis – generally, is very useful for this stage since the impacts and amplitude modulation are visible.

The bearing in the fourth stage must be immediately replaced.

4. EXPERIMENTAL PART AND RESULTS

Case presented in the paper deals with the REB fault on a recirculation fan (Figure 5, REB number 4) in the local can manufacture plant. Machine consists of one 30 [kW] motor that drives the fan using a belt transmission. This machine has been monitored once per year in the last 7 years. The trend of overall acceleration in last three measurements shows the fan REB fault development (Fig 7). On the other hand, trend of overall values of vibration velocities doesn't show much information that an ongoing REB fault development is present.

The REB type is 2218 (manufacturer SKF), so using formulae (1)-(4) and REB dimension data the characteristic defect frequencies in terms of rotating orders are: BS=7.02, BPFO=8.19, BPFI=10.81 and FT=0.43. A detailed analysis of time waveforms and frequency spectra reveals the nature of a fault (Fig. 7). The overall amplitude of last acquired time waveform compared to the time waveform acquired at the same location three years ago is much higher. The unit of time waveform is acceleration so this indicates a presence of strong metal to metal impacts in the signal. Comparison of frequency spectra shows two typical symptoms of a faulty REB:

1. Frequency spectrum is raised by the wide frequency noise which comes from the excessive looseness in the bearing caused by the REB with local faults left in operation.

2. Frequency spectrum shows the nature of the localized fault – there is a modulation around 3998 [Hz] (REB housing natural frequency) with the frequency of 187.5 [Hz]. Since the fan is rotating at 22.9 [Hz], this is the BPFO component of the bearing. Therefore, the nature of the initial localized fault of the REB is the defective outer race of the bearing.

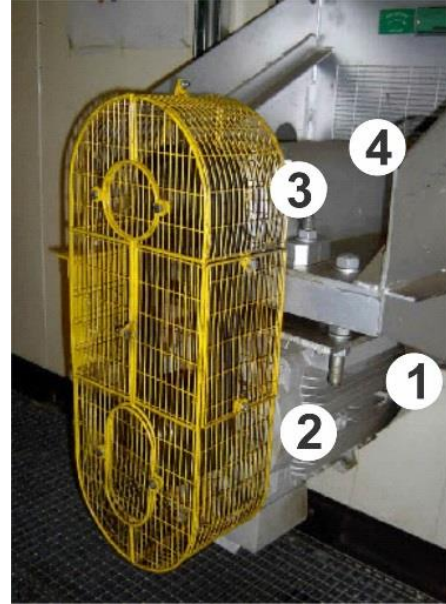


Figure 5. Recirculation fan under the test

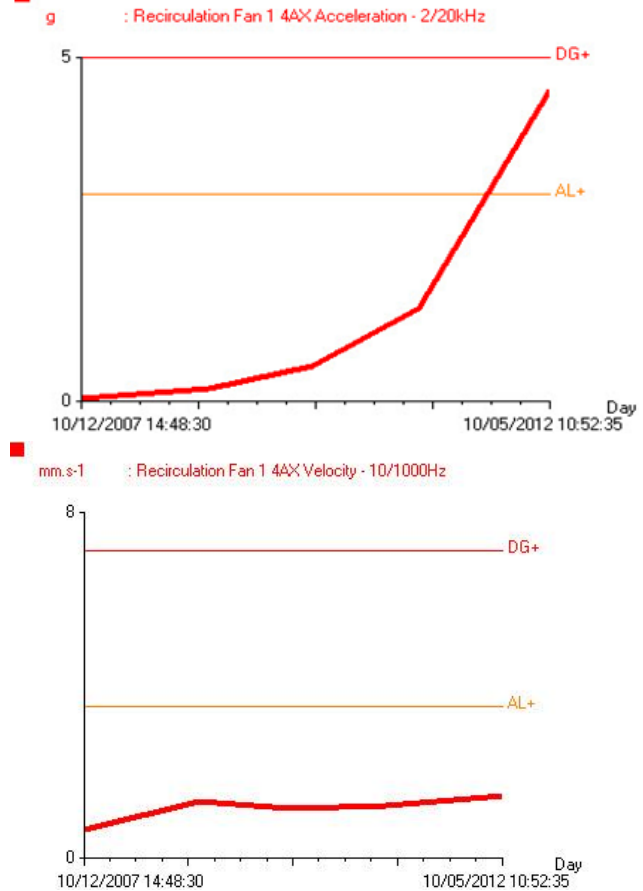


Figure 6. Trend lines for overall acceleration (top) and overall vibration velocity (bottom)

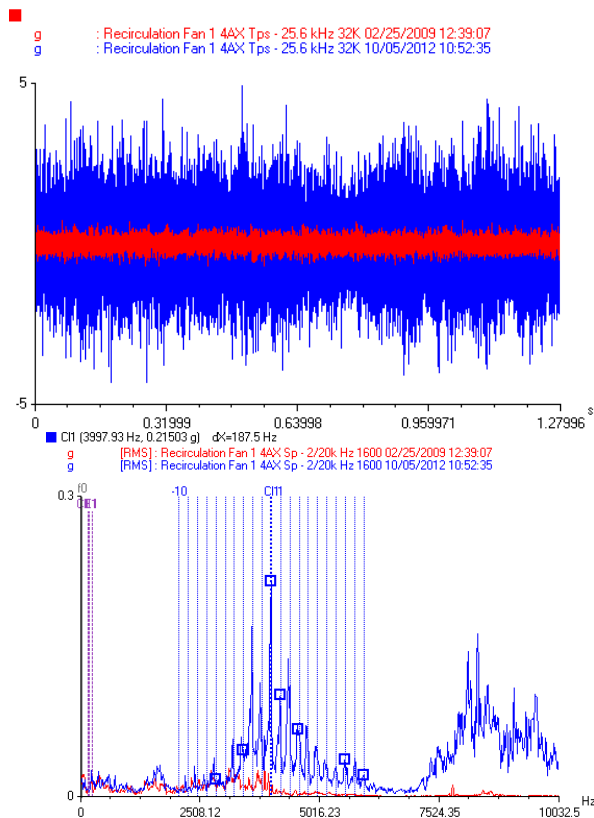


Figure 7. Years 2009 and 2013 measurement comparison on a faulty REB: time waveforms (top) and frequency spectra (bottom)

According to the REB fault development stages explained in the previous section, this REB is considered to work in the last 4th stage of the REB life. As a result of leaving this faulty REB in operation, a failure of frequency inverter and a failure of drive occurred 6 months before the last measurement!

5. CONCLUSION

Vibration analysis is the proven and the most reliable method for identification of faults inside the REB. The success and the content of the information we get from the measurement are highly dependent on the signal processing methods that were applied. The paper demonstrated that there is no unique universal method for monitoring the development of a fault inside the bearing from its mounting up to bearing's wreck. The default measurement setup should include all the explained signal processing techniques in order to identify the REB fault in all developing stages.

REFERENCES

- [1] Choudhury A, Tandon N. A theoretical model to predict vibration response of rolling bearings to distributed defects under radial load. *Trans ASME, Vibr Acoust* 1998;120(1):214±20.
- [2] Kim PY, Lowe IRG. A review of rolling element bearing health monitoring. In: *Proceedings of Machinery Vibration Monitoring and Analysis Meeting*, Vibration Institute, Houston, TX, 19±21 April, 1983. p.145±54.

- [3] Kim PY. A review of rolling element bearing health monitoring (II): preliminary test results on current technologies. In: *Proceedings of Machinery Vibration Monitoring and Analysis Meeting*, Vibration Institute, New Orleans, LA, 26±28 June, 1984. p.127±37.
- [4] Mathew J, Alfredson RJ. The condition monitoring of rolling element bearings using vibration analysis. *Trans ASME, J Vibr, Acoust, Stress Reliab Design* 1984;106:447±53.
- [5] McFadden PD, Smith JD. Vibration monitoring of rolling element bearings by the high frequency resonance technique - a review. *Tribol Int* 1984;17(1):3±10.
- [6] Meyer LD, Ahlgren FF, Weichbrodt B. An analytic model for ball bearing vibrations to predict vibration response to distributed defects. *Trans ASME, J Mech Design* 1980;102:205±10.
- [7] Sunnersjo CS. Rolling bearing vibrations geometrical imperfections and wear. *Sound Vibr* 1985;98(4):455±74.
- [8] Sunnersjo CS. Varying compliance vibrations of rolling bearings. *Journal of Sound and Vibration* 1978;58(3)
- [9] Tandon N, Nakra BC. Vibration and acoustic monitoring techniques for the detection of defects in rolling element bearings a review. *Shock Vibr Digest* 1992;24(3):3±11.
- [10] Tallian TE, Gustafsson OG. Progress in rolling bearing vibration research and control. *ASLE Trans* 1965;8(3):195±207.
- [11] Zuber N., "Automation of rotating machinery failure identification by the means of vibration analysis", PhD Thesis, Faculty of Technical Sciences, University of Novi Sad, 2010.
- [12] Zuber Ninoslav, Bajric Rusmir (2016) Application of Artificial Neural Networks and Principal Component Analysis on Vibration Signals for Automated Fault Classification of Roller Element Bearings, *EKSPLOATACJA I NIEZAWODNOSC- MAINTENANCE AND RELIABILITY*, vol. 18, br. 2, str. 299-306, ISSN: 1507-2711,
- [13] Zuber Ninoslav, Bajric Rusmir, Sostakov Rastislav (2011) Application of vibration signal analysis and artificial intelligence methods in fault identification of rolling element bearings, *TECHNICS TECHNOLOGIES EDUCATION MANAGEMENT-TTEM*, vol. 6, br. 3, str. 841-847, ISSN: 1840-1503,
- [14] Mobius Institute Vibration training manual – CAT III

CORRESPONDANCE



dr Ninoslav ZUBER, Associate Professor
 University of Novi Sad
 Faculty of Technical Sciences
 Trg Dositeja Obradovića 6
 21000 Novi Sad, Serbia
 zuber@uns.ac.rs

SELECTION OF RELIABLE VBRODIAGNOSTIC MODEL ROTATION MACHINES

Ranko ANTUNOVIĆ
 Nikola VUČETIĆ

Abstract: The control parameters of rotary machines are indirect individual sizes associated with structural parameters (vibrations, temperatures, bedding, oil pressure, etc.) and bearers are accurate information about the technical condition of the system. The parameters that bring the most information about the state of the technical system are surely the parameters of vibration, in addition to them, parameters of displacement, temperature, noise, current parameters, oil parameters for lubrication, etc. are also important.

This paper presents the vibrational diagnostic model for the control of rotary machines of large rotary machines, which, with two selected vibrational diagnostic displays, was confirmed as a very reliable diagnostic tool for diagnostic analyzes that were performed in power plants on aggregates during their exploitation. Research has shown that it is possible to carry out the selection and grouping of problems in the operation of rotary machines as well as the vibrodiagnostic methods itself, and thus develop a reliable vibrodiagnostic model for controlling the operation of rotary machines, depending on the class of the machine, or the specificity of the controlled machines themselves.

Key words: Rotary machines, Vibration, Monitoring, Diagnostics

1. INTRODUCTION

Correct measurement, monitoring and analysis of diagnostic parameters relevant to the operation of the machine, especially those that describe the dynamic state and behavior is obtained at any time insight into the mechanical and procedural status of the machine, which is the goal of condition based maintenance.

Occurrence of certain faults on the machine produce a stable excitation which generates a specific oscillatory motion. The outcome of the vibration response analysis reveals the character of the excitation force and determine the cause of machine malfunction Fig. 1.

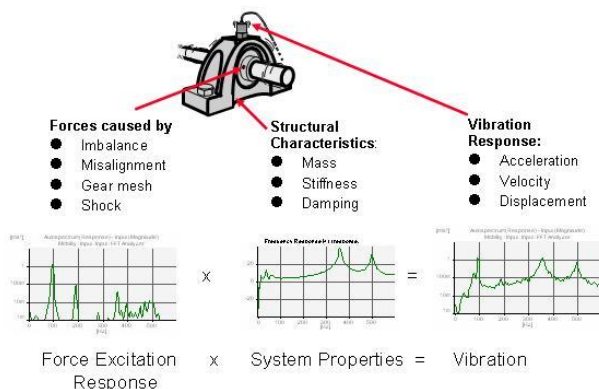


Fig. 1: Dependence of system response to the excitation force

The vibrodiagnostics approach itself lies in the fact that any malfunction in the machine's operation produces a precisely determined vibration. By analyzing the signal from the vibration response we can determine the character of the stimulus force, or identify the cause of the vibrations.

The most common malfunction of rotating machines that we can promptly identify and monitor their further growth, using control-diagnostic systems are: imbalance (asymmetry of weight and rotor geometry changes), misalignment, malfunction roller bearings, failure to recline, resonance phenomena, fault slip beds, malfunctioning electrical origin, failure resulted from an act of aerodynamic and hydraulic power, a malfunction in the belt gears, gear failure, looseness of rotating parts, malfunction due to pulsations, touching (scraping) of the rotor stator, rotor anisotropy etc.

Commonly used vibrodiagnostic methods are: the overall level of vibration analysis, spectral analysis, phase analysis, real-time vector analysis, orbit, DC analysis, the impact impulse method (SPM method), energy analysis, Zoom FFT analysis, CPB analysis, cepstral analysis, SED detection, detection of HFD, LFD detection, SEE technology, modal analysis. It is possible to extract vibrodiagnostic methods used for early detection of causes dynamic problems.

There are some other methods which contribute to a proper identifying of real causes of malfunction. They are: Monitoring and analysis of air gap, analysis of the magnetic flux, analysis of partial discharge, monitoring of parts wear, detection of combustion products, monitoring of system fluids (oil and lubricants, gases, coolants...),

corrosion monitoring (visual methods, gravimetric and electrochemical methods) [1..8].

2. SELECTION OF PROBLEMS AND SELECTION OF THE VIBRODIAGNOSTIC MODEL

Dynamic problem is typical for certain group of machines, depending on their power, rotation, construction, base etc. Using standard ISO 10816 all machines are classified in 4 classes and each class of machines has its recommended and allowed level of vibration, measuring points for vibration, the way of measurement and the selection of parameters for measurement, as shown in Fig. 2.

	Machine		Class I small machines	Class II medium machines	Class III large rigid foundation	Class IV large soft foundation
	in/s	mm/s				
Vibration Velocity Vrms	0.01	0.28				
	0.02	0.45				
	0.03	0.71			good	
	0.04	1.12				
	0.07	1.80				
	0.11	2.80			satisfactory	
	0.18	4.50				
	0.28	7.10			unsatisfactory	
	0.44	11.2				
	0.70	18.0				
	0.71	28.0			unacceptable	
1.10	45.0					

Fig. 2: Vibration Severity Per ISO 10816

Analyzing certain causes of dynamic problems, we can conclude that the certain causes are typical for two types of machines:

- GROUP 1

Machines classes I – in according ISO 10816, Electric machines up to 15 kW

Machines classes II - in according ISO 10816, Medium machines, electric motors with power of 15 to 75 kW without special foundation and rotary machines with a special basis of power up to 300 kW

Characteristics of this group machines has owning rolling-element bearings. The most common causes of the dynamic problem of this group of machines are: imbalance, rolling bearings defects, lack of susceptibility and leakage errors (soft foot, change in stiffness of the foot, relative resonance). Rarely, there are errors of electrical origin, damage to gears, mistakes caused by the action of aerodynamic and hydraulic forces, defects in belt drives, defects caused by pulsation, and the touch of the rotor from the stator

- GROUP 2

Machines classes III - in according ISO 10816, Large machines (over 300 kW) with high frequency and heavy foundations

Machines classes IV - in according ISO 10816, Large machines with low frequency bases (eg turbochargers)

Characteristics of these group machines has owning journal bearings. The most common causes of the dynamic problem on these machines are: imbalance, insensibility, slide bearings defects, reliance errors and resonant phenomena (as a consequence of low frequency bases and inadequate stiffness). Rarely, there are errors of electrical origin, mistakes caused by the action of

aerodynamic and hydraulic forces, stator rotor coupling and anisotropy of the rotor.

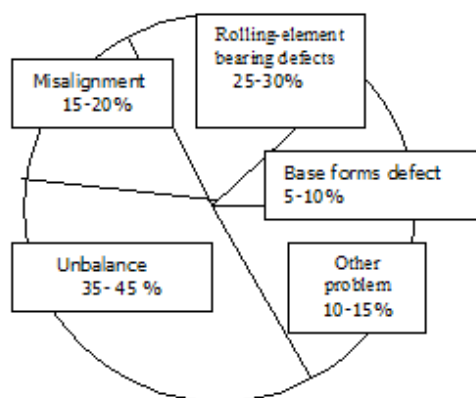


Fig.3: Possibility of certain defect appearance in machines Group 1

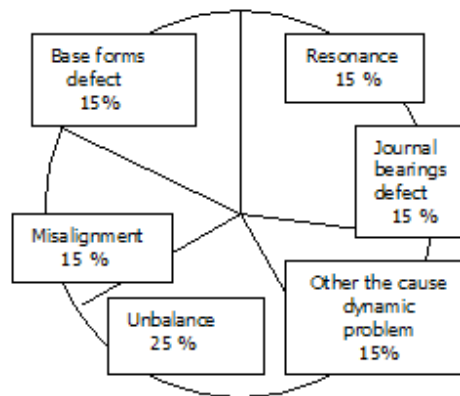


Fig.4: Possibility of certain defect appearance in machines Group 2

During research, we came to conclusion that optimal model could be seen when using four valuable functions:

1. Identifying the cause of dynamic problem
2. Simplicity for use and performance
3. Early detection cause of dynamic problem
4. Economic aspect

The optimal set vibrodijagnostičkih method chosen by this criterion, in addition to the basic set includes: overall level of vibration, spectrum display, signal and image time polar trend, for machines to be used in Group 1 HFD vibration analysis, machine for Group 2: Bode presentation and analysis orbit. [9,10]

In order to have available the necessary data for the diagnostic evaluation and analysis of the technical system must be a system for the collection of all relevant data. The system must allow the display of data in the relevant form (format) in which decisions about the state of the machine, and take appropriate actions to maintain. With the existence of a system for the collection and analysis of relevant data must be a system of management and organizational machinery that clearly defines who gets access to what information, and who on the basis of them take the appropriate decisions.

2.1. Vibro-diagnostic model monitoring

For the purpose of selecting the necessary vibrodiagnostic formats necessary for reliable diagnostic analysis of machines *Group 2*, machines with sliding bearings, here is presented the setting of one vibrodiagnostic control model, ie the necessary vibrodiagnostic displays that need to be monitored and analyzed in different operating modes, correlated with Process and other diagnostic parameters allow a robust diagnostic evaluation of the condition of controlled machines.

- The machine is not in operation

Absolute vibration: total vibrational velocity levels V_{rms} with absolute vibration measurements, spectral display of absolute vibrations.

Rotor vibrations: Position the rotor axis (polar display)

- RunUp and CostDown

Absolute vibrations: the total level of vibration velocity V_{rms} , spectral display (cascade spectrum dependent on the number of rotations), Bode displays of 1X and 2X vibration harmonics (or polar).

Rotary vibration: Total vibrational displacement levels of Ap-p, spectral display (cascade spectrum dependent on the number of rotations), Bode displays of 1X and 2X vibration harmonics (or polar), Polar display of the position of the rotor axis (DC component of the vibration)

- Synchronization and low loading of hydroelectric power plants

Absolute vibrations: Total vibrational velocity levels V_{rms} , spectral vibration display, Polar displays of the 1X and 2X vibration harmonics

Rotor vibrations: total vibrational displacement levels of Ap-p, spectral vibration display, Polar displays of the 1X and 2X vibration harmonics, Polar display of the position of the rotor axis (DC component of the vibration)

- Operating mode

Absolute vibrations: Total vibrational velocity levels V_{rms} , spectral vibration display, Polar displays of the 1X and 2X vibration harmonics.

Rotor vibrations: total vibrational displacement levels of Ap-p, S_{max} , spectral vibration display, Polar displays of the 1X and 2X vibration harmonics, Polar display of the position of the rotor axis (DC component of the vibration), Display Orbit

- Stop the machine

Absolute vibrations: the total level of vibration velocity V_{rms} , spectral display (cascade spectrum dependent on the number of rotations), Bode displays of 1X and 2X vibration harmonics (or polar)

Rotary vibration: Total vibrational displacement levels of Ap-p, spectral display (cascade spectrum dependent on the number of rotations), Bode displays of 1X and 2X vibration harmonics (or polar), Polar display of the position of the rotor axis (DC component of the vibration)

It should also be noted that for reliable diagnostics it is necessary to observe multiple vibrato-diagnostic formats at the same time. Research has shown that the vibrodiagnostic model, which at the same time shows on all bearings the position of the axis of the rotor, the orbit, the spectrum and the polar 1X vibration display, provides reliable diagnosis of the greatest possible number of

possible malfunctions that can arise in the operation of the *Group 2* machine. Of course, To be observed in correlation with the process parameters (the number of rings, forces, etc.) and the total level of vibration, which should also be the second vibrodiagnostic display. These two mixes of vibrodiagnostic representations actually represent an optimal model of vibrodiagnostics for rotary machines of large rotational masses.

3. VIBRODIAGNOSTIC ANALYSIS - CASE STUDY

Vibrodiagnostic analyzes performed on machines of GROUP 2 in real conditions of exploitation with previously shown vibrato-diagnostic model are shown here.

3.1. Vibro- diagnostics of hydroaggregate

The vibrational diagnostic analysis of the hydroaggregate was performed in HPP Višegrad, where the control diagnostic system of the manufacturer Bentley Nevada - GE System1 was installed, shown in Fig. 5.

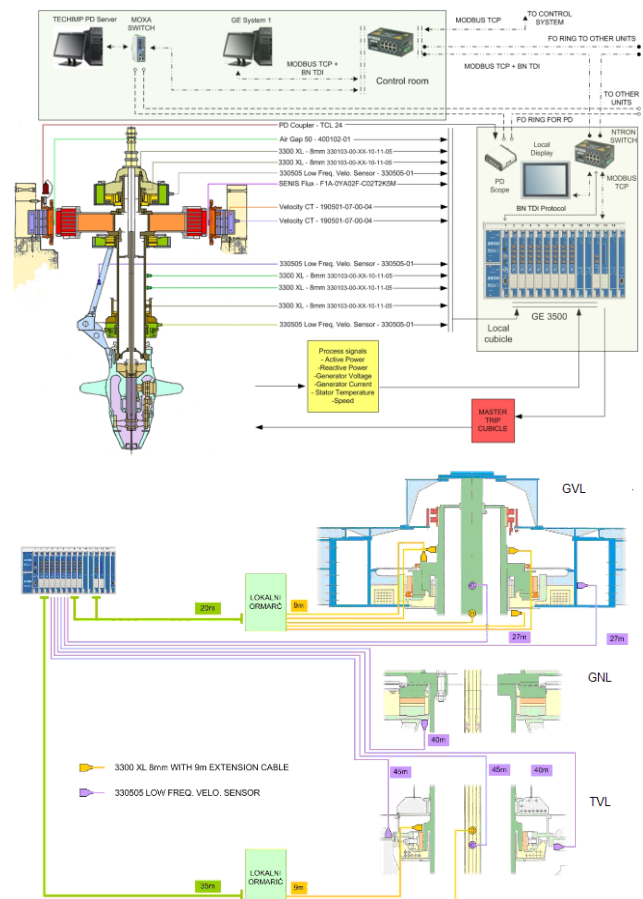


Fig. 5. Display of the installed monitoring and diagnostic system in HPP Višegrad and the location of the vibration sensor installation

In Fig. 6 and Fig. 7, two vibrato-diagnostic views were presented, which were set for the purpose of diagnostic analysis of the condition of the hydro-aggregate number 2. in the mentioned plant [11].

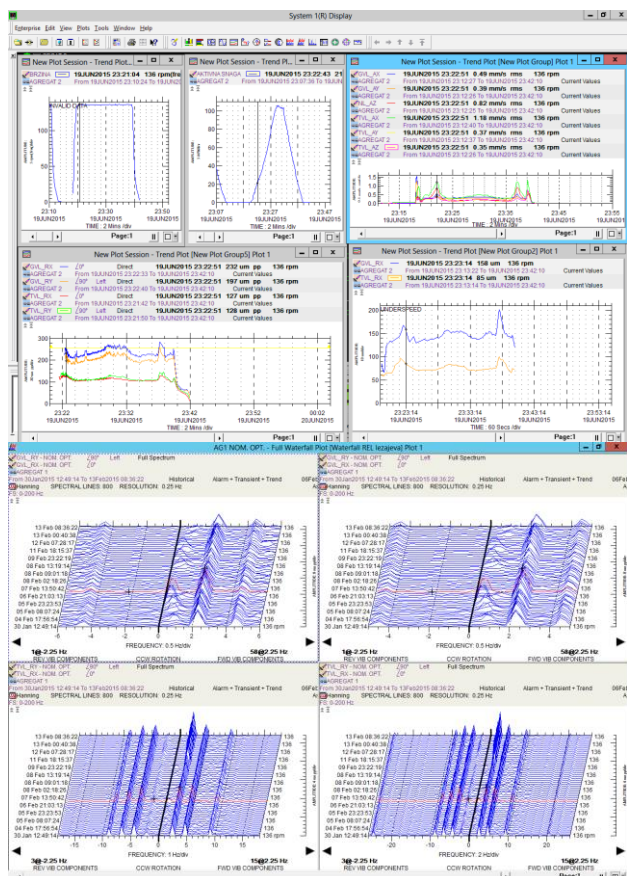


Fig.6. The first vibrodiagnostic display from the hydroaggregate

The most unfavorable dynamic condition of the hydroaggregate is when the hydroaggregate is overturned and stopped in the range of the rotational speed of 50-70 rpm, where sudden vibration jumps occur, shown in the following figure.

This can be characterized as a resonant frequency, most likely it is the lowest critical speed of the rotating circuit or the resonant frequency of the implement because at that moment the blades of the watering device are completely closed, but a deeper correlation analysis of the injection of the hydroelectric power plant should be done and the possibility of installation Stabilizer of the EE system.

From the spectral vibrations, the dominance of the imbalance on the base tone is clearly noticed, and low-frequency vibrations and a slight presence of the 2X harmonics of vibrations are noticed. On the turbine part there is a slight presence of fluid forces, characterized as turbulence of flow and vortex in a diffuser, which mainly occurs with less power and its changes (a detectable frequency of 0.25 Hz and the threshold of high frequency components).

From the spectral vibrations during the deposition of the hydro-aggregate, the presence of oil vortex in the generator bearing, on the small forces of the hydro-aggregate 20-30 MW, is observed, and a significant short-term sudden jump of rotor vibrations develops, this may be due to inadequate bearing clearance.

This turbine part shows a small presence of turbulence flow on turbine blades and vortex in diffuser.

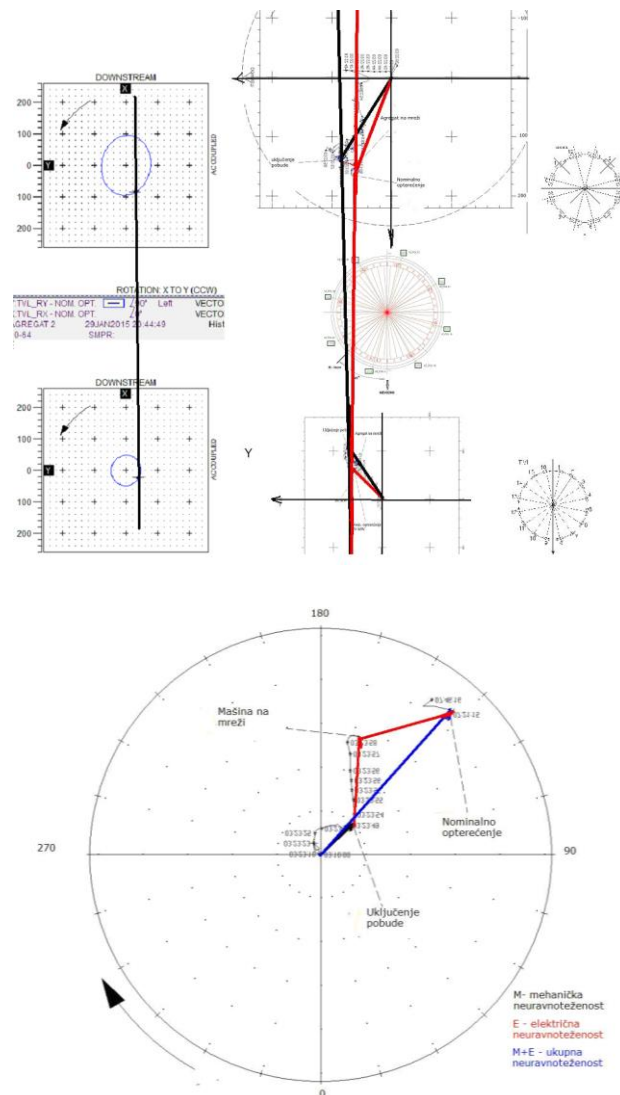


Fig.7. The second vibrodiagnostic display from the hydroaggregate

By analysis the position of the sleeve in the GVL it is clearly noticed that the one-way magnetic field force returns the axis of the rotor to the initial position and thus reduces the displacement of the geometric and inertial axes and the total value of the vibration of the fall. With the increase in load, further shifting of the axis of the sleeve in the bearing occurs, which causes the phase change of the vibration vector 1X, but the overall level of vibration remains the same.

By analysing the polar diagrams, it can be clearly seen that the vectors of mechanical and electrical imbalances are in the protuberances, and that this is the reason for reducing the overall level of vibration. It is noted that phase 1X of the vibration vector changes with increasing power of the hydro-aggregate. There is also the presence of a force of electrical origin (at a frequency of 100 Hz).

From the previous pictures it can be clearly seen that there is a one-way force during the rocking of the hydro-aggregate which moves the rotor of the rotor opposite to the two adjacent bearings, that is, the verticality of the axis of the hydroaggregate is lost, there is obviously a certain degree of clarity in the system.

Also, when the ignition is switched on, the action of the one-way electrical force is clearly seen as a consequence of the magnetic field asymmetry, which further shifts the axis of the generator rotor. If we analyse the displacement of the sleeve in the bearing and taking into account the direction of rotation, the most probable direction and direction of this one-way force, which is perpendicular to the direction of movement of the sleeve in the case of small unidirectional forces, is obtained.

3.2. Vibro-diagnostic of turboaggregate

Vibro-diagnostic analysis of the turboaggregate was performed in TE Gacko based on the diagnostic system COMPASS, which is a product of the company Bruel & Kjaer, Vibro, which serves to monitor the turbine generator's state of mind in the on-line diagnostics and other rotary machines in the off-line Diagnostics and is integrated into the computer control and control system of the production process "OVATION" - the product of the American company Westinghouse. The measurement structure of the diagnostic system is shown. Fig. 8.

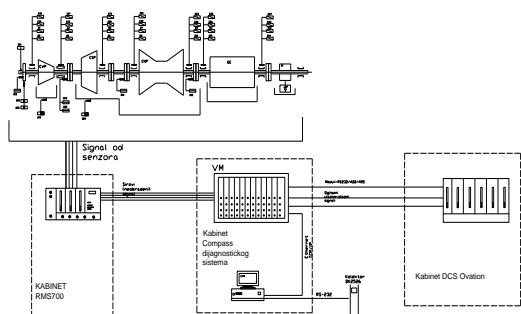


Fig.8. Structure of COMPASS Diagnostic System in TE Gacko

It should be noted that the system measures absolute and rotor vibrations on all turboaggregate bearings, and for the purpose of this analysis, the overall levels and spectral vibrations of those bearings where increased vibration levels are determined are shown.

As a result of the vibrodyagnostics of the turbo-generator, Fig. 9 and Fig.10. The odds are selected two vibrodiagnostic displays.

Table 1.

Bearing s	HOR	VER	AX
	$\sum v_{RMS}$ [mm/s]	$\sum v_{RMS}$ [mm/s]	$\sum v_{RMS}$ [mm/s]
1	3,4	1,8	1,8
2	2,1	1,8	2,1
3	1,4	3,6	2,2
4	2,0	1,9	2,3
5	3,2	2,7	2,1
6	3,3	4,6	6,5
7	3,8	5,8	9,3
8	6,4	5,2	4,1

Spectral analysis

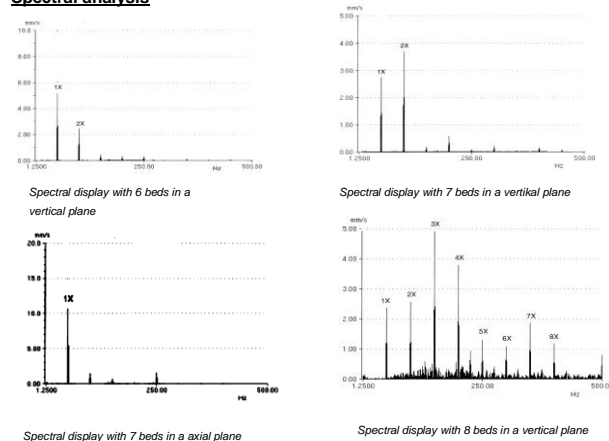
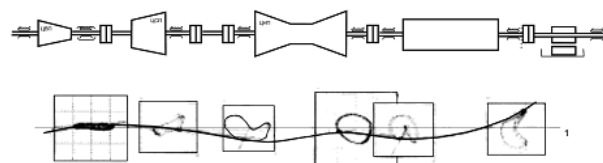


Fig.9. The first vibrodiagnostic display from the turboaggregate

With spectral display is clearly evident that the causes of the problem dimamičkih generator of unbalance and misalignment. In addition, spectrum display with 8 beds indicates that there is slack in this bed. The spectrum on the bearing 7 in the axial direction, there is a lack of stiffness of the bearing in the axial direction. Note: To create a clearer picture of which originate these defects is analyzed polar trend display 1X and 2X harmonic vibration in the radial and axial bearings in the generator.



Polar trend display

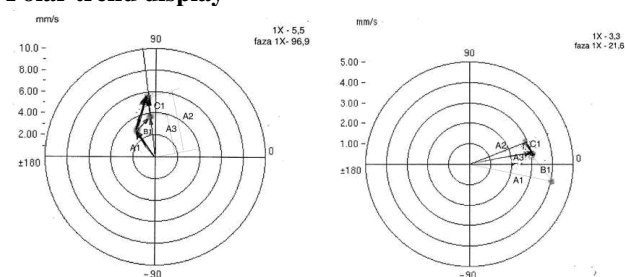


Fig.10. The second vibrodiagnostic display from the turboaggregate

With polar display clearly shows that there is a change of amplitude and phase of the harmonic vibrations 1X with increasing load. This suggests that in addition to the mass asymmetry of the rotor comes up to change the rotor geometry, which may be due to thermal deformation or impact of asymmetric magnetic field. The analysis of polar trend 1X harmonic vibrations in these stages, you can clearly see these effects of these defects:

- Vector of A1-1X harmonic in cold conditions, the number of working without excitation,
- Vector of A2-1X harmonic on full load
- Vector A3 - 1X harmonic after power cuts.

It is observed that the B1-vector thermal imbalance, little influence on the dynamic state (overall vibration level is slightly changed) and C1-asymmetric magnetic field vector, which significantly affects the dynamic state of the machine, therefore it is in phase with the residual mass asymmetry of the rotor in response to the seventh beds.

It is apparent that the thermal imbalance at the reactance power of 91 Mvar, by the intensity is the same as the residual mechanical imbalance on the rotor, but that it is phase-difference by 45 °. By monitoring the trend further changes of the thermal imbalance vector, it can be concluded that by increasing the reactive power, the total vector of the imbalance (vector 1X of the rotor vibrations) would be inadmissible for the further operation of the turbocharger (especially expressed on bearing 7) [12].

4. CONCLUSION

Today, there are a large number of developed and implemented surveillance diagnostic systems in the world, whose software tools give a great opportunity to process and analyze signals, which allow the operator to provide a wide range of possible diagnostic displays that illustrate the existence of a problem and thus provide a diagnostic interpretation of malfunctioning in controlled machines. This is particularly true for a large number of developed and implemented vibrodiagnostic methods. The analysis carried out on aggregates under the conditions of their exploitation, Chapter 3, showed that the set vibrodiagnostic model, shown in Chapter 2.1, provides a reliable and clear analysis of the cause of malfunction in the operation of the controlled aggregates. It should be noted that the developed diagnostic systems do not provide vibrational images in this presented form, which confirms the fact that the knowledge and experience of the diagnostician working with these systems is of crucial importance, which is necessary for this type of diagnostic analysis. Also, the presented vibrodiagnostic model can serve to develop application software that would be tailored to the needs of the operators themselves. It should also be expected that the development of automated diagnostic systems will enable the entire diagnostic process to be automated and accelerated.

This type of machine monitoring in the production process enables us to have an insight into the "health" of the machine at any time, so that we can "control the machines", which is one of the key preconditions for optimizing the production process as a whole.

The development of communications enables the development of remote monitoring (telemonitoring), which enables the appearance of expert consulting firms for the provision of services through remote monitoring. Of course, it would be interesting for the ERS to form a unique diagnostic center, considering energy facilities and built-in surveillance systems.

REFERENCES

- [1] R. Antunović, A. Halep, "DIJAGNOSTIKA I ODRŽAVANJE ELEKTRANA", monografija 1.izd., Mašinski fakultet Istočno Sarajevo 2016
- [2] Bently Nevada, *Predictive maintenance: How the pieces fit together*, Orbit, Vol.7, No.2, June 1986
- [3] A. Muszynska, *Vibrational Diagnostics of Rotating Machinery Malfunctions*, International Journal of Rotating Machinery, 1995, Vol. 1, No. 3-4, pp. 237-266
- [4] R. Antunović, "Advanced methods vibrodiagnostic", Konferencija održavanja KOD-2009, Tivat, Jun 2009. god.
- [5] S. Zelingher, *ON-LINE CONDITION MONITORING AND EXPERT SYSTEM FOR HYDRAULIC PUMP STORAGE UNITS*, CIGRE R11-206, Paris, 1996
- [6] P. Tavner, L. Ran, J. Penman, H. Sedding, *Condition Monitoring of Rotating Electrical Machines*, IET POWER AND ENERGY SERIES 56, Published by The Institution of Engineering and Technology, London, United Kingdom, 2008.
- [7] Michael Flanagan, *Expert System Data Acquisition*, PROFILE Newsletter, Vol.4, No.2, Bruel & Kjar CMS A/S, 1996.
- [8] Berry, J.E. *Illustrated Vibration Diagnostics Chart*. Technical Associates of Charlotte, P.C., 2007.
- [9] Ranko Antunović, Aleksandar Veg, *ANALYSIS OF DYNAMIC BEHAVIOR OF ROTATING MACHINES*, Annals of Faculty Engineering Hunedoara- International Journal of Engineering romania, ISSN: 1584-2665, Hunedoara, No. 9, Vol 2, pp. 205-210
- [10] M. Sarenac, R. Antunovic, "Optimal Model for Vibrodiagnostics of Rotating Machinery", *TEHNIKA*, br.5, 2011, ISSN 0040-2176, pp.759-769,
- [11] V. Šarenac, R. Antunović, M. Plečić, "DIJAGNOSTIC MONITORING OF HYDRO UNITS IN HPP VIŠEGRAD", *PROCEEDINGS OF THE 3rd INTERNATIONAL COMETA2016*, ISBN 978-99976-623-7-8, pp. 465-474
- [12] R. Antunović, *DIAGNOSIS OF ROTOR TURBOGENERATORS THERMAL IMBALANCE*", međunarodni naučno-stručni časopis Tehnička dijagnostika, ISSN 1451-1975, Vol.2, iss.3, pp.48-53, 2003

CORRESPONDANCE



Ranko ANTUNOVIĆ, Prof. D.Sc. Eng.
University of East Sarajevo
Mechanical Engineering Faculty
Vuka Karadžića 30,
73100 East Sarajevo, BiH
rankoantunovicmf@gmail.com



Nikola VUČETIĆ, Ass. M.Sc. Eng.
University of East Sarajevo
Mechanical Engineering Faculty
Vuka Karadžića 30,
73100 East Sarajevo, BiH
vuceticnikola@yahoo.com

VIBRATION ANALYSIS AND REPAIR PROCESS FOR THE VENTILATION SYSTEM FOR SMOKE DRAIN IN THE THERMAL POWER PLANT

Emir NEZIRIĆ
Safet ISIĆ
Edin DŽIHO

Abstract: *Vibrations are common phenomenon in the rotating machinery, which could carry important information about condition of the rotating machinery. All specific failures in rotating machinery have their own characteristics of the vibrations. By measuring and analysis of vibrations cause of increased vibrations could be determined. Since misalignment and rotating looseness have similar frequency spectrum characteristics, it is difficult to determine which one of the failures is present. When cause of increased vibrations is determined, it is possible to plan the future steps for the repairing and neutralising present cause of the possible failure.*

Process of vibration analysis followed by present cause of increased vibration in rotating machinery repairing is presented in this paper through example on the ventilation system for smoke drain in the thermal power plant.

Key words: *vibration analysis, thermal power plant, ventilation system*

1. INTRODUCTION

Reliability of the thermal power plant as one of the mechanical systems is main goal of power producing companies, which causing continuous electricity production. Reliability is achieved when there are no unexpected failures of machines and when it is possible to predict time and cause of machine failure. With those predictions it is possible to plan a future stoppage and possible repairs in the machine system.

Most commonly used method for condition monitoring of the machines in the thermal power plant system is vibration analysis. By measuring frequency and amplitude of the machine vibrations it is possible to determine what is causing that vibration with frequency analysis and how much is machine moving with amplitude analysis.

After determination of main cause of increased vibrations, it is needed to plan future repairs and removal of vibration cause. Since the most loaded elements of rotating machines are the bearings and the couplings, repairs are mostly consisted of replacing those machine parts. Those repairs are mostly time-consuming and the power production is process of high importance, so sometimes it is needed to do some quick repairs to habilitate machine for short-time usage, until repairing process is suitable to carry out.

Process of vibration analysis followed by present cause of increased vibration in rotating machinery repairing is presented in this paper through the example on the ventilation system for smoke drain in the coal-heated thermal power plant Kakanj, Bosnia & Herzegovina.

2. VIBRATION ANALYSIS

Vibrations are common phenomenon in rotating machinery, which could carry important information about condition of the rotating machinery. All specific failures in rotating machinery have their own characteristics of vibrations. Measurements and analysis of the vibratory behavior of the system and vibration changes leads to the detection of problems and faults [1][2].

Most common failure of rotating machinery is misalignment of shafts connected by couplings [1]. Misalignment could be parallel or angular. In practice, misalignment is usually combination of parallel and angular misalignment [1][3][4]. In frequency spectrum of severe misalignment are present orders of rotational frequency (1X, 2X,..) even up to 10X in radial and axial direction.

Other failure with similar characteristics is rotational looseness who could be described as appearance of the clearance between rotating shaft, bearing or housing. Frequency spectrum also contain orders of rotational frequency (1X, 2X, ..) which could also go above 10X [5].

If it is impossible to determine which failure is causing the increased vibrations using frequency spectrum only, sometimes it is necessary to confirm present failure by some other characteristic (waveform, orbit, phase, etc.), by optical observing (opening bearing or coupling) or by physical measurement (misalignment by dials or laser, housing-foundation gap, etc).

3. VIBRATION MEASUREMENTS ON THE VENTILATION SYSTEM

Vibration analysis and repair process for the ventilation system in thermal power plant is shown below. Ventilation system equipment have properties shown in table 1.

Table 1: Ventilation system equipment properties

System name	Smoke drain ventilator (right)
Manufacturer	“Vemos“ Ltd., M. Bistrica, Croatia
Motor serial no.	D-CV-09-100-1
Power	1080 kW
RPM	990 RPM
No. of vanes	8
Ventilator diameter	2500 mm
Shaft lenght	5400 mm
Shaft diameter	440 mm
Journal diameter	160 mm
Type of bearing	Double row cylindrical roller bearing

Ventilation system is shown in fig 1.



Fig.1: Motor flexibly coupled with ventilator

3.1. Location and equipment used for vibration measurements

Vibrations are measured on the housings of the motor and the ventilator bearings in three perpendicular directions: horizontal, vertical and axial. Measurements are marked with L1 and L2 for ventilator bearings, and L3 and L4 for motor bearings. Accelerometers of type KD 37V and KD 41V are used for measurements. Accelerometers are connected to Spider 8 device for data acquisition through M28 power supply. Spider 8 is then connected to the computer, which is used for data recording. Magnetic stands with screws are used for accelerometer mounting on housings, so it is easy to detach them after measuring. Locations of bearings where measurements are done are shown on fig 2.

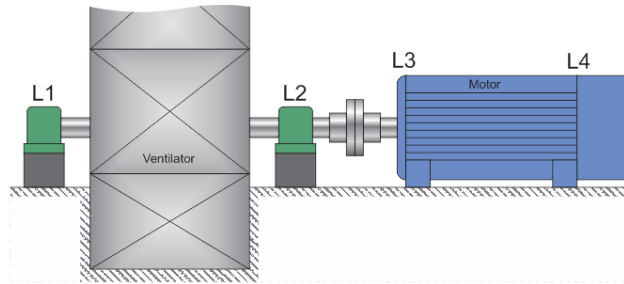


Fig.2: Names of measurement locations

Equipment used for data acquisition and measurement recordings is shown on fig 3., and measurement scheme is shown on fig. 4.



Fig.3: Computer, Spider 8 and M28 power supply

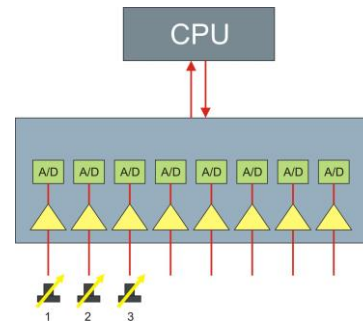


Fig.4: Measurement scheme

On fig. 5. is shown one of the bearing housings with accelerometers attached to the measuring spots.



Fig.5: Bearing housing with accelerometer attached

3.2. Operating modes of ventilation system used for vibration measurements

Vibration testing program is planned to be done with different operating modes of the ventilation system. Operation modes for testing are chosen to be different number of rotations per minute of the ventilator shaft. Operation modes for vibration measurements are shown in table 2.

Table 2: Operation modes for vibration testing

Measurement number	RPM
M1	410
M2	481
M3	547
M4	705

3.3. Results of vibration measurement

Recorded acceleration data is integrated to obtain velocity records, which is used to calculate RMS of velocity. Results of the calculated RMS of velocity of ventilator bearings are shown in table 3., and RMS of velocity of motor bearings are shown in table 4.

Table 3: RMS of velocity on ventilator bearings

RPM	L1 RMS [mm/s]			L2 RMS [mm/s]		
	H	V	A	H	V	A
410	1.7	0.5	0.2	--	--	--
481	2.1	0.7	0.5	--	--	--
547	4.7	3.0	0.5	--	--	--
705	6.1	1.0	2.1	11.2	9.3	3.6

Table 4: RMS of velocity on motor bearings

RPM	L3 RMS [mm/s]			L4 RMS [mm/s]		
	H	V	A	H	V	A
705	5.1	3.9	3.2	5.3	1.9	3.0

As it could be seen, levels of velocity RMS is high on all of measuring points. According to ISO 10816, with 705 rpm machine is graded as class D (vibration could cause damage), since its 11,2 mm/s for horizontal and 9,3 mm/s for vertical measurement on L2 (bearing closer to coupling). Rest of the RMS values are graded as class C (short term operation allowable) according to ISO 10816, since its values are exceed 4,5 mm/s which is lower limit for this class. It is required to determine what is the main cause of this increased vibrations.

4. VIBRATION ANALYSIS

4.1. Waveform analysis

Recorded acceleration data is analyzed by its waveform characteristics. On figs. 6. and 7. Are shown waveforms for bearings L1 and L2 on the ventilator.

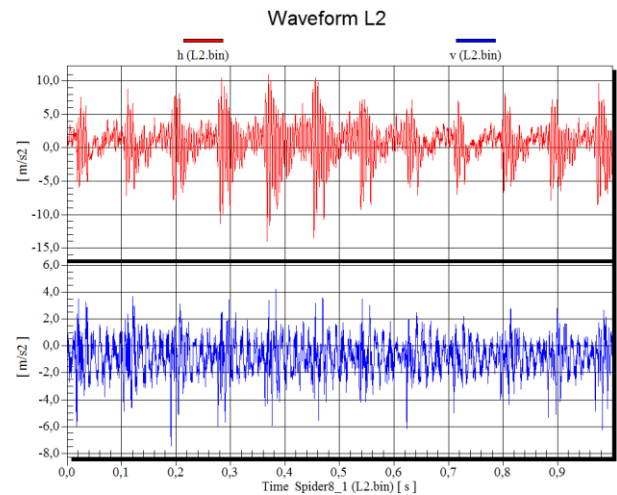


Fig.6: Waveform of acceleration for L2 (H and V)

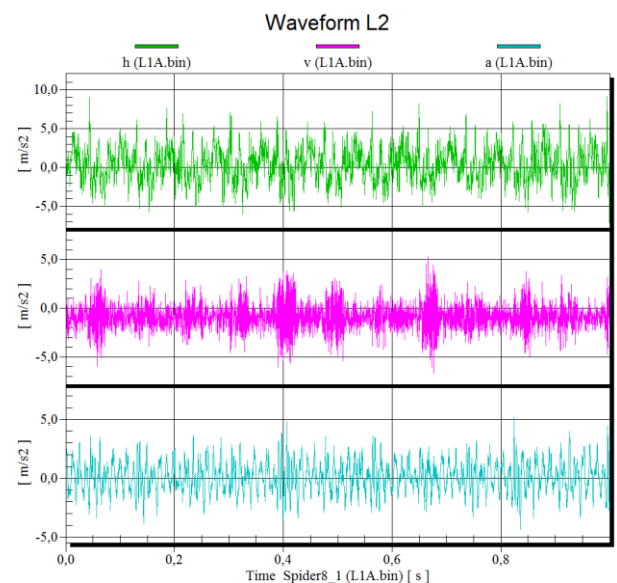


Fig.7: Waveform of acceleration for L1 (H, V and A)

On the waveform for horizontal and vertical direction on bearing L1 some impacts could be noticed, which also transfers to horizontal direction on bearing L2. The shape of letter M and W could be also noticed on the waveform for horizontal direction of bearing L2. Those characteristics could suggest that combination of misalignment and looseness could be main faults of this system.

4.2. Frequency spectrum analysis

From the recorded accelerograms, frequency spectrums are created. On Fig. 8. and Fig. 9. are shown accelerograms for measurements done on ventilator bearings L1 and L2 in range from 0 Hz to 800 Hz when ventilator had 705 rpm.

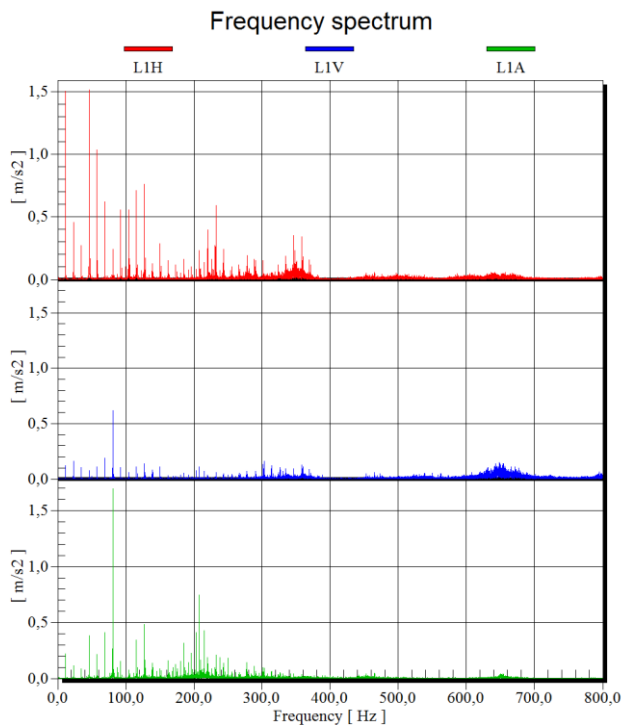


Fig.8: Frequency spectrum of L1 acceleration (0-800 Hz)

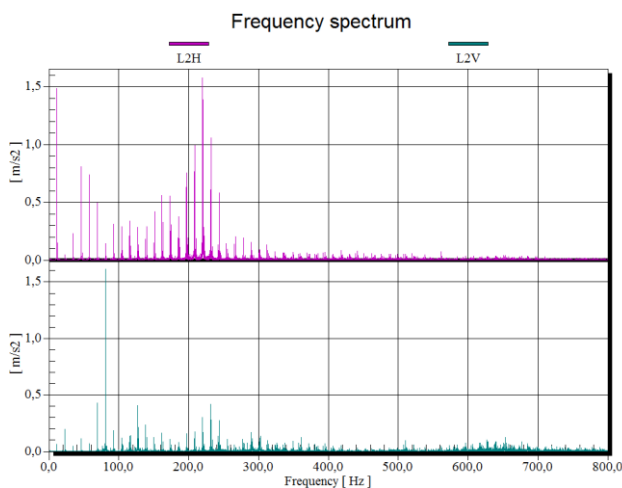


Fig.9: Frequency spectrum of L2 acceleration (0-800 Hz)

On frequency spectrums rotating frequency and its multiple orders are noticeable. It could be also noticed some nonsynchronous frequencies (226 Hz, 346 Hz) where some of them could be bearing frequencies. Some floor noise is raised for frequency spectrum measured on the L1 bearing.

Frequency spectrum characteristics shown on Figs. 8. and 9. are suggesting that possible cause of high vibrations is misalignment and looseness, which already caused bearing failure.

5. REPAIR PROCESS

After main failure is determined, repair process is planned to be done as soon as there is no request for the continuous machine operation. Since that stopping is planned in a few weeks, it is needed to decrease level of vibrations so operation of ventilation system is possible.

First step was to decrease misalignment level. During misalignment measurement, it is noticed that the ventilator shaft journal is radially moving inside bearing closer to the coupling. By measuring radial movement of shaft on both sides of bearing it is concluded that ventilator shaft journal is bent.



Fig.10: Misalignment measurement on coupling

On the coupling of ventilator shaft side is measured that shaft journal is 1 mm bent on that end of shaft. It is concluded that best solution is to distribute that 1 mm of bent shaft journal on 0,5 mm on each sides of motor shaft. Aligning procedure is done with radial and angular measurement (edge – face), where angular misalignment is reduced to <0,05 mm per 100 mm length, and radial misalignment is distributed horizontally and vertically by 0,5 mm.

5.1. Vibration measurement after the quick repair process

After alignment is done, ventilator and motor shafts are coupled. Vibrations on same locations are measured and compared with previous results. Velocity RMS values of vibrations after repair process are shown in table 5.

Table 5: RMS of velocity on ventilator bearings after the quick repair process

RPM	L1 RMS [mm/s]			L2 RMS [mm/s]		
	H	V	A	H	V	A
200	0.8	0.2	0.2	0.7	0.3	0.5
273	1.4	0.2	0.5	1.8	0.4	1.1
365	1.8	0.4	0.5	1.5	0.6	1.9
456	4.1	0.5	1.5	3.6	0.7	2.6
548	2.4	0.4	0.8	2.5	3.2	3.9
640	4.6	1.0	1.3	2.4	1.3	1.3
686	4.4	1.1	1.4	2.3	1.3	1.8

As it could be seen, highest value of vibrations on bearing L1 is decreased from 6.1 mm/s (705 rpm) to 4.6 mm/s (686 rpm), and for bearing L2 is decreased from 11.2 mm/s (705 rpm) to 3.6 mm/s (456 rpm). This drastic reduce of the vibration levels are due to distribution of ventilator bent shaft on both sides of motor shaft.

On Fig. 11 are shown levels of measured vibrations before and after the repair process. This ventilation system belongs to group 1 of machines with nominal power greater than 300 kW and with rigid foundations.

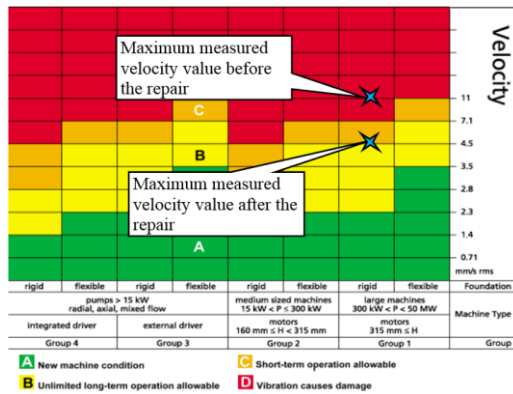


Fig.11: Vibration grade according to ISO 10816 before and after the quick repair process

As it could be seen, before quick repair process, maximum vibration level was larger than 7,1 mm/s which is lowest value of class D, where vibration could cause damage. After the quick repair process, highest value of vibrations was just above the 4,5 mm/s, which is satisfying class C, which allows short-term operation. According to ISO 10816, ventilation system is operable until it is possible to start its main reparation process.

5.2. Vibration measurement after the main repair process

Main repair process started after the few weeks. Ventilator was disassembled and shaft and bearings were examined. It is determined that shaft journal was bent on its end closer to coupling. Since it was bent, it damaged the bearing closer to the coupling and shaft journal was slipping inside. This could be seen on Fig 12., where traces of slipping are visible on bearing inner ring.



Fig.12: Visible traces of skidding on inner ring

Similar traces are visible also on journal where this bearing was mounted. Most possible scenario in this case was that shaft mounted on ventilation system was already bent. Because of that, bearing was loaded over its maximum force and journal grinded inside inner ring of bearing and made some gap, so journal could skid inside the bearing. Since shaft was bent, it acted similar as misalignment. And since it made some gap between journal and bearing inner circle, it also had some frequency spectrum characteristics similar to misalignment frequency spectrum. Velocity RMS values after the main reparation process is shown in table 6.

Table 6: RMS of velocity on ventilator bearings after main repair process

RPM	L1 RMS [mm/s]			L2 RMS [mm/s]		
	H	V	A	H	V	A
200	0.2	0.0	0.1	0.1	0.1	0.1
273	0.2	0.0	0.2	0.1	0.1	0.2
365	0.3	0.1	0.4	0.3	0.0	0.3
456	1.2	0.2	0.6	1.5	0.2	0.7
548	0.8	0.2	1.0	1.3	0.2	0.7
640	1.6	0.4	1.4	1.3	0.5	1.1
731	1.8	0.5	2.1	1.7	0.5	1.7

After the main reparation process where shaft and bearings are changed with new parts, vibrations are measured. It is shown that all vibration levels are classified as A, which is stated as a new machine condition.

6. CONCLUSION

In this paper is shown diagnosing and repairing process of ventilation system in thermal power plant. After this presented analysis, some conclusions could be stated as follows:

- If there are characteristics of vibrations which are similar for some different faults, it is sometimes required to take physical measurements of some possible faults to have full picture of what is happening in the machine.
- It is possible to reduce vibrations on the machine by reducing one of the faults which caused vibrations.
- Reducing machine vibrations could extend its working life, at least until it is possible to fully repair the machine.
- Bearing damage as possible fault in rotational machine could be present with other faults which are probably the cause of bearing failure.
- According to ISO 10816 levels, after the quick repair it is recommended to work with 60% capacity (550 rpm) until the main reparation process is possible, so vibration levels are lower than class C. This is only applied to this ventilation system.
- The main repair process has removed sources of the increased vibrations, so there are no restrictions for operating with this system after the main repair process.

REFERENCES

- [1] PIOTROVSKI J. (2007) *Shaft Alignment Handbook*, Taylor and Francis Group.
- [2] FRISWELL M. (2005) *Models for the condition monitoring of rotating machinery*, Proceedings of the International conference “CONDITION MONITORING”, Cambridge, UK, pp 385-392
- [3] XU M, MARANGONI R.D. (1994) *Vibration analysis of a motor-flexible coupling-rotor system subject to misalignment and unbalance, Part I: Theoretical model and analysis*, Journal of Sound and Vibration, Vol.176, No 5, pp 663-679
- [4] NEZIRIĆ E, ISIĆ S., DOLEČEK V., KARABEGOVIĆ I., (2013) *Vibration analysis of theoretical SDOF model of shaft parallel misalignment*, Journal Technolog, Vol 5. No 4, pp 131-134.
- [5] LI X. (2012) *The Analysis of vibration fault features and vibration mechanism caused by rotating machinery loosening*, Journal Advanced Materials Research, Vol.518-523, pp 3826-3829

CORRESPONDANCE



Emir NEZIRIĆ, D.Sc. Eng.
“Džemal Bijedić” University of Mostar
Mechanical Engineering Faculty
Univerzitetski kampus bb
88000 Mostar, Bosnia & Herzegovina
emir.nezirc@unmo.ba



Safet ISIĆ, Prof.D.Sc. Eng.
“Džemal Bijedić” University of Mostar
Mechanical Engineering Faculty
Univerzitetski kampus bb
88000 Mostar, Bosnia & Herzegovina
safetisic@gmail.ba



Edin DŽIHO, D.Sc. Eng.
“Džemal Bijedić” University of Mostar
Mechanical Engineering Faculty
Univerzitetski kampus bb
88000 Mostar, Bosnia & Herzegovina
edin.dziho@unmo.ba

**SUSTAINABLE
DEVELOPMENT IN THE
ENERGY INDUSTRY**

CONTEMPORARY APPROACH TO AUXILIARY MECHANIZATION OPERATIONS AND MAINTENANCE AT AN OPEN-PIT COAL MINE

Radivoje MITROVIĆ
Dragan JOVANOVIĆ
Gradimir IVANOVIĆ
Dragan STOŠIĆ
Snežana PANTELJIĆ
Dragan STEVIĆ

Abstract: *This paper presents results of a project aimed at improving auxiliary mechanization (“AM”) (bulldozers, excavators, pipelayers, vehicles, etc.) operations and maintenance at the open-pit coal mine Drmno of the TE-KO Kostolac, a subsidiary of Electric Power Industry of Serbia (“EPS”). Business processes supported by ICT (GPS/GPRS system, IS/IT system) were designed and implemented for the needs of the department of auxiliary mechanization. In that way AM managing is provided from the point of readiness and availability at real-time. A basic organizational and technological platform is provided as infrastructure for further enhancements of the GPS/GPRS system of AM and its integration into ecosystem (e.g. open-pit coal mine maps, optimization of the machine paths at open-pit mine, Google maps, sensors for air quality parameters).*

Key words: *auxiliary mechanization, processes, ICT, operations, maintenance, open-pit coal mine*

1. INTRODUCTION

An analysis of current state of an **auxiliary mechanization** (further AM) management system was conducted for the purpose of design, development, implementation and application of modern business processes, information systems (further IS) and information-communication technologies (further ICT) in the AM management sector, (bulldozers, pipe layers, dump trucks, vehicles.....) at open-pit coal mine Drmno of the TE-KO Kostolac, a subsidiary of Electric Power Industry of Serbia (“EPS”), Fig.1,. It was concluded that AM management does not apply modern business such as "end to end" business processes, IS and ICT. Then, basic business goals are defined:

- Readiness increase,ment,
- Availability increase,ment,
- Improvement of operational work and maintenance,
- Development and implementation of modern IS/ICT,
- Management and making decision based on data,
- Costs reduction: operational work, maintenance and spare parts.

For example, Fig.2 shows transport system disposition of tailing and coal, Figures 3, 4, 5 and 6 show paper documents that were used for management of exploitation and maintenance of machines and vehicles (further machines) at the AM.

Starting from the current state and business goals, the design, development, implementation and application of business processes with IS/ICT support with appropriate

software solutions and GPS/GPRS system were carried out, which is given in further text.



Fig.1: The open-pit coal mine "Drmno", Serbia

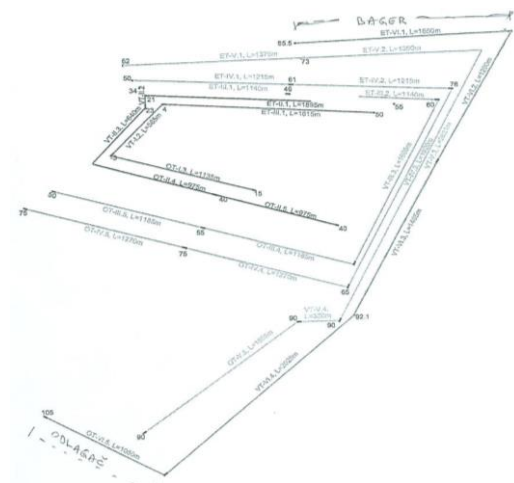


Fig.2: Transport system disposition (year 2011)

POVRŠINSKI KOPOVI KOSTOLAC PK <u>Drmno</u> ZAHTEV ZA RAD br. <u>24</u>	
DATUM <u>27.01.2010.</u> TIP MAŠINE/VOZILA <u>M-1</u> NEDOSTAJU DELOVI br. komada	SADRŽAJ RADA <u>VERIGLA ALI NE MOŽE DA UPRAZI</u> <u>Munot, Nupkobut</u>
ZAHTEV ZA RAD IZDAJE ŠEF SLUŽBE POSLOVODA REFERENT ISPRAVNOSTI	ORGANIZACIONA JEDINICA Eksploatacija mašina: Eksploatacija vozila: Datum: <u>27.01.2010</u> Potpis: <u>[Signature]</u>

Fig.3: Job request for maintenance of machines/vehicles

PD "TE-KO KOSTOLAC" KOSTOLAC Pomoćna mehanizacija		Vrsta mašine <u>M-1</u>	
Radni nalog br. <u>115310</u>		Serijski broj <u>1000</u>	
Stanje broja	Poslije opravka	Stanje mašina	Čista
<input type="checkbox"/>	<input type="checkbox"/>	<input type="checkbox"/>	<input type="checkbox"/>
Predaja mašine na opravku izvršio <u>Nupkobut</u>		datum <u>27.01.10</u>	
Prjem mašine na opravku izvršio <u>Munot</u>		datum <u>27.01.10</u>	

Šifra glavne operacije	Šifra dopunske operacije	Opis operacije	Šifra razine grupe				Izvršena operacija	Šifra izvršio-oca	Šifra kontrolora
			1	2	3	4			
		<u>Zamjena gornjih zupčeva</u>							
		<u>zamjena gornjih zupčeva za zupčevu</u>							
		<u>zamjena ca UT-10.</u>							
		<u>zamjena gornjih zupčeva</u>							
		<u>zamjena zupčeva za razmatranje</u>							

PROBA	Datum	Čas	Ne izvršen oper šifra	Izvršio	Šifra	Potpis
				Mehanizir		<u>Munot 6</u>
Probni vozač	Šifra	Potpis		Mehanizir		<u>Nupkobut 4</u>
Mašinu je preuzeo				Mehanizir		
				Autoelektricar		<u>Nupkobut 1</u>
				Varlac		
				Postovoda		
Mašina je tehnički ispravna za rad glavnih poslova, osim:				Mašina je tehnički ispravna za rad glavnih poslova, osim:		
Kandiciona ispravnost sklopa	Procena šifra rad. MC	Transport	Motor	Menjač	Hidraul.	Š. Mašina

Fig.4: Work order for maintenance

RASPORED RADA POMOĆNE MECHANIZACIJE NA PO DANA 03

Redni broj	Mašina	I smena Mesto rada	II smena Mesto rada	III smena Mesto rada
1	A-1			
2	3	Pos 1/2		
3	4	0/5 + 0/5	0/5	0/5
4	5	0/5 + 0/5		
5	6			
6	7			
7	8			
8	9	0/5 + 0/5	0/5	0/5
9	10	0/5	0/5	0/5

Fig.5: Machines/vehicles Work Schedule at the AM

Vozilo/naziv:	benzin:	benzin:	S. long:	S. long:	Matric:	Stanje:	Prezime i ime:	Potpis:
Mašina br. 10	2/60	1.5/panje	1.5/panje	20w-50	15w-40	DAC	km	Vozaca
Šifra robe:	1302884	1302884	751073	905828	45309	stat		
trošak:	01025000							
PO=464-42/D-43							NE radi	STANOVNIĆ DRAGAN
PO=464-48/D-44	32		2					
PO=133-299/D-78	47							
PO=133-298/D-79	46							
PO=133-297/D-80	56							
PO=133-624/D-81	30							
PO=133-626/D-82	48							
Ukupno:	645		2	2				
Izdato na pumpi								
Bordlević Stanj. mb: 14985								
datum izdavanja: 16.12.2010.godine								
potpis: [Signature]								

Fig.6: Monitoring of fuel consumption

2. CONTEMPORARY MANAGEMENT OF AM AT OPEN-PIT COAL MINE

The design, development, implementation and application of modern approach of AM management at open-pit coal mine "Drmno" are based on improved "end to end" business processes - BP (activities, responsibilities, business events, key performance indicators - KPI and documents), with ICT support (IS/IT, GPS/GPRS). Basic BP are:

- **BPM** - Maintenance, Fig.7: BPM1- Corrective; BPM2- Preventive; BPM3-Combined and BPM4-According to the sub-process condition: Submission for maintenance, Reception (for maintenance), Diagnostics, Work order and Worksheets (Preparation and maintenance execution), Control, Report out (notification from exploitation), Handover.

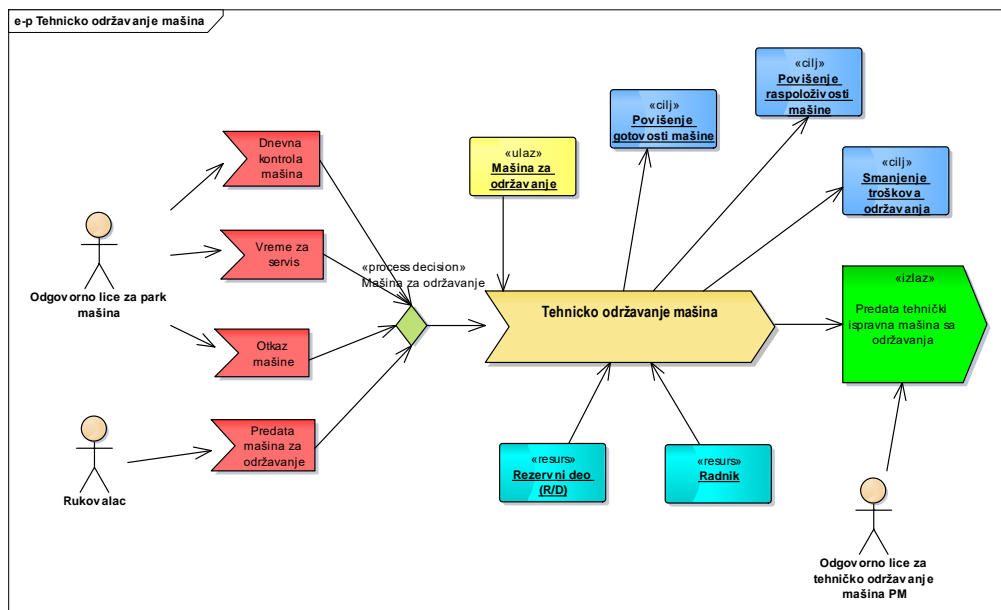


Fig.7: Business process "Technical maintenance of machines and vehicles"

Fig.8: Main menu ICT (ISPM, GPS/GPRS)

– **BP-Exploitation:** BP1- Updating of general and technical characteristics of machines and other general facilities; BP2- Support to annual work schedule by shifts and employee groups; BP3- Daily machines and operations schedule; BP4- Support to fuel management; BP5- Support to lubricant and technical fluids management; BP6- Solving fails of machines on site/service; BP7- Information for operational and top management.

For business processes and sub-processes, appropriate software solutions, i.e. IS for exploitation and maintenance of AM and GPS/GPRS system have been developed and implemented. This provides monitoring of all "end to end" business processes and sub-processes, as well as data and information for AM management. For instance business sub-processes are given for *BP3- Daily machines and workers schedule: BP3.1- Machine status; BP3.2- Daily schedule of machines and BP3.3 - Daily schedule of the operator* and for them software solutions have been developed. By activating, in the Main menu, Fig.8, the drop-down menu "Exploitation" (Daily) Schedule is activated, Fig.9.

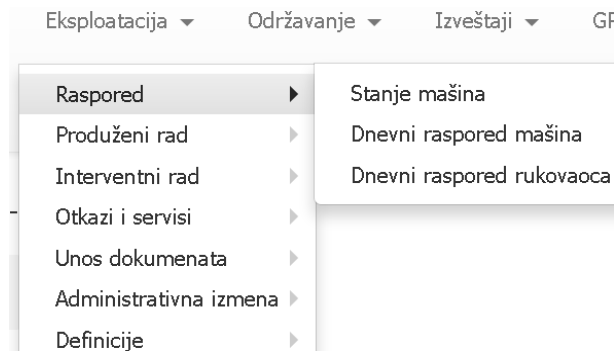


Fig.9: (Daily) Machine and operator schedule

Included activities of machine maintenance are: from submission for maintenance (document Q.Z.EK.10) to delivery of fixed machine/vehicle (document Q.OD.10), using necessary resources (workshops, qualified personnel, spare parts, engine for devices and

machines testing, maintenance, technical documentation, information system for system maintenance management).

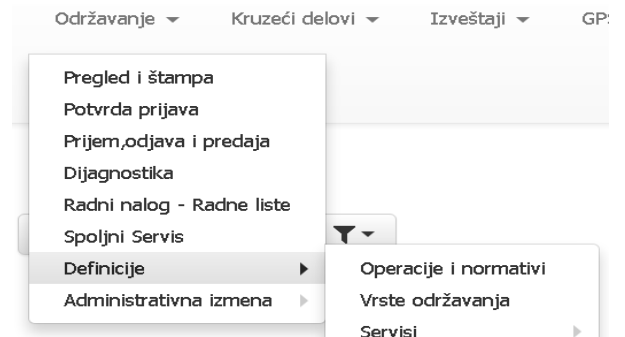


Fig.10: Drop-down menu "Maintenance"

By activating, in the Main menu, Fig.10, the "Maintenance" drop-down menu, maintenance activities with software support is activated, Fig.10. For example, the documents forms BP-" maintenance" which occur in the maintenance process are listed, Figures 11, 12, 13 and 14. Electronic documents can be printed.

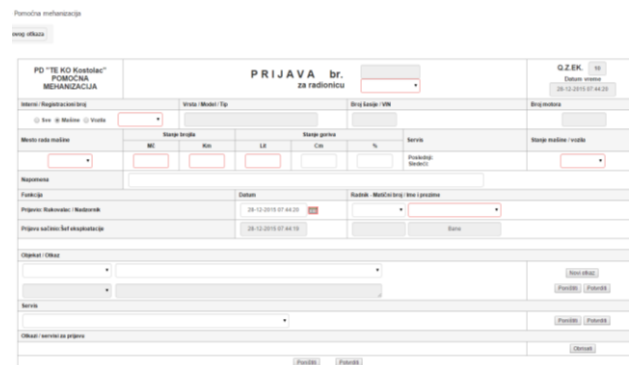


Fig.11: Submission for maintenance (see Fig.3)

Pregled prijavljenih otkaza / servisa - Šef službe									
Prijava otkaza / servisa					Razmotrio prijavu				
R.br.	Mašina	Broj prijave	Pozicija	Otkaz / Servis	Šef eksploatacije	Šef službe	Status		
							Za održavanje	Na čekanju	
1.	Buildozer B / K2 / CAT / D8R	775/15	IV BTO	Menjač - PALI SE LAMPICA ZA KOČNICE	02-10-2015 07:05 - nenad.nikolic	08-10-2015 09:44 - nenad.nikolic	●	●	
2.	Cevopologač / C24 / TD25 / CS-3	147/15	I BTO	Mašina - proveriti otkaz	20-04-2015 14:34 - FilipMF	22-04-2015 12:38 - FilipMF	●	●	
3.	Kombinovana mašina / Skip1 / JCB / 3CX	330/15	Kontejnersko naselje	Kabina i klimatizacija - Lose radi klima.	04-07-2015 14:15 - Nenad	27-07-2015 08:58 - nenad.nikolic	●	●	
4.	Dizalica / AD Tatra 6 / TATRA NJ20 / T-815	111/15	Kontejner pomoćne mehanizacije	Prednji most - PROBLEM SA PUŠTANJEM I PODIZANJEM RUKE.	02-04-2015 09:55 - mladjan.ivkovic	20-04-2015 13:58 - FilipMF	●	●	
5.	Dizalica / AD Tatra 8 / TATRA NJ20 / T-815	674/15	Radionica Drmno	Pneumatski (gume) - pada strela	18-09-2015 09:02 - mladjan.ivkovic		●	●	
				Mašina - labava bolca na kuki	18-09-2015 09:02 - mladjan.ivkovic	22-09-2015 09:22 - Bane	●	●	

Fig.12: Review of reported failure

Pregled Dijagnostike za Radni nalog / Radni nalog

Br.prijave	Interni broj	Mesto održavanja	Održavanje	Objekat rada	Dijagnostika otkaza	Red. servis	Datum	Komentar	R.biti
871/15	B15	Rad_PH MAŠINE	Preventivno	Mašina	Redovni servis	ms1	24.12.2015 07:48:26		0

Broj	Int.broj	Objekat rada	Operacija	Zad.(G)	Prit.(G)	R.grupa	Radnik	Početak(dan/sat)	Završetak(dan/sat)	Izv.	Komentar	Kont.	Zatv.
871/15	B15	Mašina	Operacija	Zad(G)	Prit(G)	Odaberite	Odaberite	Početak(dan/sat)	Završetak(dan/sat)	Odaberite	Komentar	●	●

Fig.13: Menu for definition of Work order and Worksheets (after diagnostics)

PO "TEKOP" Krošćak POMOĆNA MEHANIČARSKA		RADNA LISTA 807/15 Od 12.10.2015 07:15:52 - Radionica: Rad_PM MAŠINE				Q.OD.03 30.12.2015 07:54:34 Bane		
Pozicija Rad_PM MAŠINE		Int. br. ULT10		Vrsta, model, tip Utovarnač-ULT100-CK		VIN -		
Starje brojača		-		Starje goriva		-		
DIO mē		- km		105 L		%		
#	Lokacija rada	Objekat	Šifra	Operacija	Početak	Završeno	Radnik - Overa	Norma [Eas]
1.	Rad_PM MAŠINE	Mehanizam za upravljanje	-	Zamena ložnog cilindra sa vakuum aparatom	12.10.2015 07:19:15	12.10.2015 (Da)	Grubić Mlađa	7.00
2.	Rad_PM MAŠINE	Mehanizam za upravljanje	-	Zamena ložnog cilindra sa vakuum aparatom	12.10.2015 07:20:13	12.10.2015 (Da)	Serafinović Zoran	7.00
3.	Rad_PM MAŠINE	Motor	-	Zamena filtera goriva	13.10.2015 07:32:25	13.10.2015 (Da)	Spasić Bojan	0.50
4.	Rad_PM MAŠINE	Motor	-	Razvodivanje saje gasa	13.10.2015 08:15:41	13.10.2015 (Da)	Spasić Bojan	2.00
Ukupno:							10.50	10.50
#	Otvorio		Kontrolisao		Završio			
1.	Datum 13.10.2015 13:19:45	Ime i prezime nenad nikolic	Datum 13.10.2015 13:19:45	Ime i prezime nenad nikolic	Datum 13.10.2015 13:19:45	Ime i prezime nenad nikolic		
2.	Datum 13.10.2015 13:20:41	Ime i prezime nenad nikolic	Datum 13.10.2015 13:20:41	Ime i prezime nenad nikolic	Datum 13.10.2015 13:20:41	Ime i prezime nenad nikolic		
3.	Datum 13.10.2015 13:33:04	Ime i prezime nenad nikolic	Datum 13.10.2015 13:33:04	Ime i prezime nenad nikolic	Datum 13.10.2015 13:33:04	Ime i prezime nenad nikolic		
4.	Datum 13.10.2015 13:34:29	Ime i prezime nenad nikolic	Datum 13.10.2015 13:34:29	Ime i prezime nenad nikolic	Datum 13.10.2015 13:34:29	Ime i prezime nenad nikolic		

Fig.14.: Worksheet in el. form, can be printed

GPS/GPRS system has been developed and implemented for tracking machines and vehicles work at open-pit mine. The scheme of the system is shown in Figure 15.

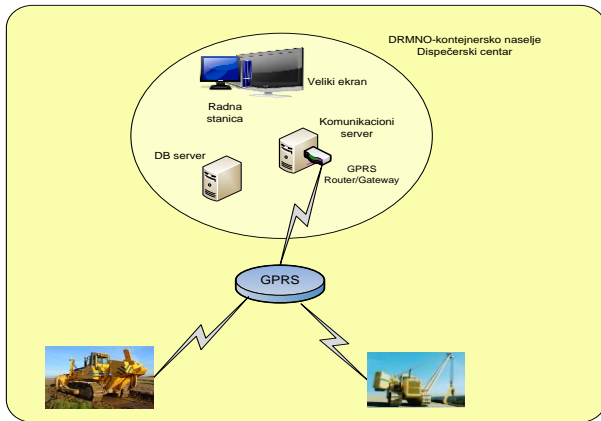


Fig.15: Lay-out of the GPS/GPRS system physical architecture of the at open-pit coal mine "Drmno"

3. RESULT - MANAGEMENT INFORMATION

The business process Exploitation and Maintenance generates documents (with data and information) for managing these processes, in real time. Data and information are available to operational and top management. Choosing the "Reports" option, Fig.9, reports are generated, Fig.16.

For example, Figure 17 shows **readiness**, and Figure 18 shows **availability** of machines and vehicles at open-pit coal mine "Drmno" which are generated currently.

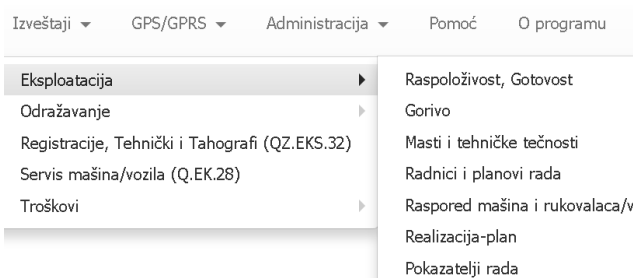


Fig.16: Reports: Exploitation

Readiness (which includes working time and failure-maintenance time) is one of the key measures of successful operation and maintenance of machines on coal mines. Based on readiness, it is possible to plan operation of machines for next year, as well as assessment of new machines purchase, or maintenance system improvement.

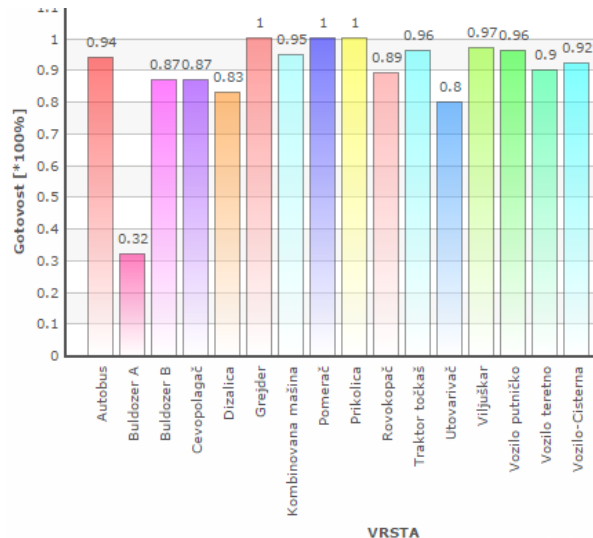


Fig.17: Readiness of AM machines and vehicles at open-pit mine

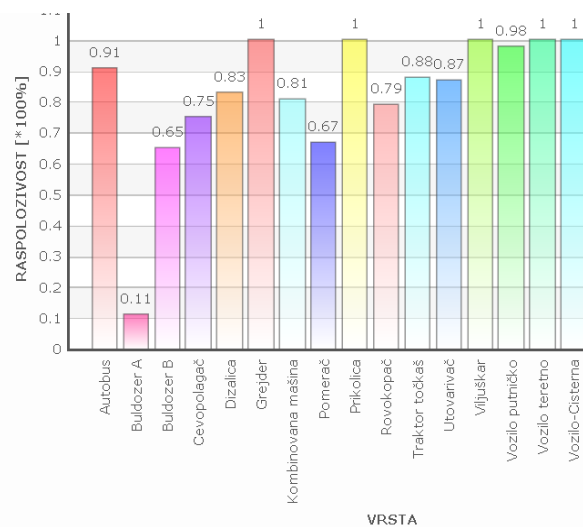


Fig.18: Availability of AM machines and vehicles at open-pit mine

Availability, in %, represents an overview of the correct and canceled machines / vehicles in the current time. Based on the availability, it can be concluded is it possible to carry out daily tasks at open-pit mine or is it necessary to make special efforts to maintains in order to realize daily tasks. From BPM-Maintenance in Fig.19. the document Q.OD.33 is shown- The register of work orders generated based on: Q.Z.EK.10-Submission for maintenance, Fig.11, Q.OD.01-Diagnostics, Q.OD.2- Work Order and Q.OD.03-Maintenance lists.

An overview of **regular services, spare parts costs, as well as other indicators** of exploitation and maintenance of machines and vehicles, are obtained by activating the options shown in Fig.16.

Fuel. One of the main indicators of operation of machines at open-pit mine is **fuel consumption**. Every machine/vehicle has its own card, as well as operators and drivers. Through a mobile computer which is installed on the tank (fuel dispensing at open-pit mine) and using the appropriate communication structure, the data on tank injection and fuel dispensing machines in the field are sent to the server. It is pointed out that the implementation of "BP-fuel consumption" with software support has contributed to the savings that are

measured in hundreds of thousands euros. Figure 21 shows one of the fuel-review reports: monitoring average, total, and average consumption according to normative in %. These values are monitored by machine operators and vehicle drivers.

Application of **GPS/GPRS** provides an overview of all AM machines and BASIC MECHANIZATION machines location by activating option "All" with symbol ✓ in the Control Display, Fig.20. It is possible to display only one type of machine by activating the symbol ✓ (for chosen machines). Choosing-clicking on certain - one machine at open-pit mine in the field "Machine/vehicle data" machine parameters are displayed: positions (GPS coordinates, ID device, time, amount of fuel in the tank). Also, notice about non-announcement of machine at open-pit mine at certain time intervals is given.

It is pointed out that it is possible to see the movement of machines in the mine for any previous period, even for the previous years by activating the "Map" option and entering the period for which an overview of the movement in this field is desired, Fig.20.

PD "TE KO Kostolac" POMOĆNA MECHANIZACIJA		Registar radnih naloga					Q.OD.33		
							Dokument generisan 25.05.2015 08:53		
Radionica	Dat.izdavanja	Vrsta,model, tip	Int.br.	Br.RN	Opis radova	Br.izvr.	Zad.sati	Priz.sati	
Rad_PM MAŠINE	22.05.2015	Cevopolagač SB60	C27	218/15	Motor: Redovan servis na 250 mh	2	8.00	8.00	
					Razvodnik pogona (reduktor): Zamena zaptivne grupe na reduktoru	3	24.00	24.00	
					SUM	5	32.00	32.00	
	22.05.2015	Kombinovana mašina JCB3CX	Skip3	224/15	Motor: Čišćenje sistema za dovod goriva	1	4.00	4.00	
					Radni uređaj: Montaža osigurača na bolci kašike	1	2.00	2.00	
					SUM	2	6.00	6.00	
	22.05.2015	Utovarivač ULT160CK	ULT07	220/15	Motor: Zamena filtera vazduha	1	1.00	1.00	
					SUM	1	1.00	1.00	

Fig.19:" Register of work orders" of the performed maintenance in the workshop

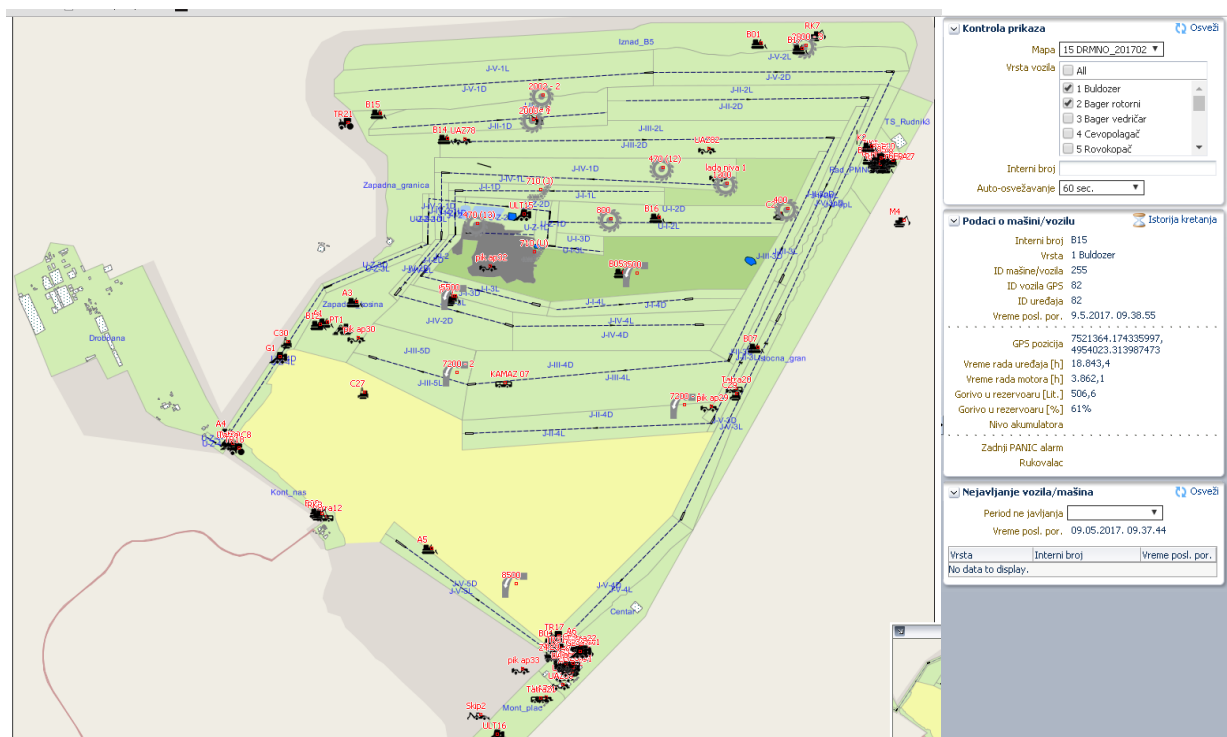


Fig.20: Position of machines at the "Drmno" with disposition of conveyor belts tailings and coal (see Figure 2.)

EPS Ogranak "TE-KO Kostolac" Pomoćna mehanizacija		Potrošnja Evrodizel goriva prema dolivanju na terenu								Q.GO.05 Dokument generisan 10.07.2017 11:52		
Vrsta	Model i tip	Interni broj	Kartica	Dat.dolivanja	Pri km/m ³	Rukovalac	Razl.km/m ³	Doliveno	Spec.potr.	Norm.potr.	Odnos	
Buldozer B	TD25M EHTRA	B10	2762580798	05.07.2017 09:22:22	4,036.00	1010562279	7.00	220.00	31.43	45.00	69.84%	
				04.07.2017 09:33:45	4,029.00	1010562279	8.00	240.00	30.00	45.00	66.67%	
				03.07.2017 09:23:46	4,021.00	1010562279	14.00	345.00	24.64	45.00	54.76%	

Fig.21: Monitoring of fuel consumption (see Fig.6)

4. CONCLUSIONS

Paper presents basics of development, design and implementation of improved management of exploitation and maintenance system of AM machines and vehicles.

Some of the presented documents, that were used for management of the PM (as it is not possible to display all documents due to the space) were shown before the implementation of the modern approach with business processes and the support of ICT (IS/IT, GPS/GPRS) at open-pit mine "Drmno". Business processes of exploitation and maintenance with developed ISPM with adequate software support developed by Business processes and sub-processes as well as developed GPS/GPRS system were exposed. A basic organizational and technological platform is provided as infrastructure for further enhancements of the GPS/GPRS system of AM and its integration into ecosystem (e.g. open-pit coal mine maps, optimization of the machine paths at open-pit mine, Google maps, sensors for air quality parameters).

Some of the results, i.e. REVIEWS and REPORTS, are presented which enable management of AM in real time. All reviews and reports are generated from these processes of AM, in current time.

Developed and implemented processes with software support at the open-pit coal mine "Drmno" can be applied in other mines of various ores (minerals) with possible adjustment.

REFERENCES

- [1] MITROVIĆ, R., JOVANOVIĆ, D., IVANOVIĆ, G., STOŠIĆ, D., PANTELIĆ, S., STEVIĆ, D., STEFANOVIĆ, B., DIMITRIJEVIĆ, at all (2010-2017) *Development and Implementation of Auxiliary Mechanization Operations Management System Based on Technical and Economic Indicators of Operations Supported by Modern Information System /Information Communication Technology, Phase I-V*, Faculty of Mechanical Engineering, University of Belgrade, Progress reports, Institute „Mihajlo Pupin” Belgrade, Auxiliary Mechanization of the TE-KO Kostolac, a subsidiary of Electric Power Industry of Serbia, Kostolac (in Serbian).
- [2] PANTELIĆ, S., IVANOVIĆ, G. MITROVIĆ, R., JOVANOVIĆ, D., STOŠIĆ, D., DIMITRIJEVIĆ, S. (2013) *Improvement of Auxiliary Mechanization Operations Management at an Open-Pit Coal Mine Based on a Process Approach with ICT Support*, in

Subic, A. (eds.), *Advances in Engineering Materials, Product and Systems Design, Advanced Materials Research Vol. 633*, Trans Tech Publications, Switzerland, ISBN 978-3-03785-585-0, pp. 322-334.

Acknowledgement. Research presented in this paper is realized within TR 35030 project supported by the program of technological development of The Ministry of Education and Science of the Republic of Serbia

CORRESPONDANCE



Radivoje MITROVIĆ, Prof. PhD.Sc. Eng.
University of Belgrade
Mechanical Engineering Faculty
Kraljice Marije 16
11000 Belgrade, Serbia
rmitrovic@mas.bg.ac.rs



Dragan JOVANOVIĆ, B.Sc. Eng.
Electric Power Industry of Serbia,
Belgrade
dragan.jovanovic@eps.rs



Gradimir IVANOVIĆ, Prof. PhD.Sc. Eng.
University of Belgrade
Mechanical Engineering Faculty
Kraljice Marije 16
11000 Belgrade, Serbia
givanovic@mas.bg.ac.rs



Dragan Stošić, B.Sc. Eng.
Institute Mihailo Pupin
Volgina 15
11060 Belgrade, Serbia
dragan.stosic@pupin.rs



Snežana PANTELIĆ, PhD. Eng.
Institute Mihailo Pupin
Volgina 15
11060 Belgrade, Serbia
snezana.pantelic@pupin.rs



Dragan STEVIĆ, B.Sc. Eng.
Electric Power Industry of Serbia,
TE-KO Kostolac
Nikole Tesle 5-7
12208 Kostolac, Serbia
dragan.stevic@te-ko.rs

FUEL MANAGEMENT AT AUXILIARY MECHANIZATION OF OPEN-PIT COAL MINE SUPPORTED BY MODERN ICT

Dragan STOŠIĆ
Dragan STEVIĆ
Snežana PANTELIĆ
Nenad NIKOLIĆ
Rastko NEGOIĆIĆ
Filip TODORVIĆ

Abstract: A software application has been developed and integrated within modern ICT environment to support a fuel management process for Auxiliary Mechanization (“AM”) at the open-pit coal mine Drmno of the TE-KO Kostolac, a subsidiary of Electric Power Industry of Serbia (“EPS”). The fuel management process activities are automated as follows: (i) obtaining fuel from the local pump; and (ii) delivering the fuel to vehicles, machinery and fuel storage-tanks at the open-pit mine. To support fueling at open-pit mines software application named “Field Fuel-issuing” was developed and implemented on mobile computers. Data collected for fuel ‘in charge’ and supplied fuel are transmitted to the Auxiliary Mechanization Information System (in Serbian, ISPM) data base via the contemporary communication infrastructure of the TE-KO Kostolac. This data enables fuel management of AM. This approach to fuel management is based on fuel consumption monitoring results expressed by different technical parameters in an on-line data queries and reports, which are discussed in this paper.

Key words: auxiliary mechanization, fuel management data collecting, open-pit coal mine, software application for mobile computers

1. INTRODUCTION

Reduction of fuel consumption of machines/vehicles of Auxiliary Mechanization (AM) is one of the Key Performance Indicators (KPI) of the fuel management process and Auxiliary Mechanization management as a whole [1].

The first update of monitoring, ordering, issuing and reporting modes on fuel consumption of AM at the open-pit coal mine Drmno within the TE-KO Kostolac (henceforth: TE-KO) - a subsidiary of Electric Power Industry of Serbia (“EPS”) was undertaken during the period of 2010-2011 [1, 2]. A contemporary process approach and applied Information and Communications Technologies (ICT) were embedded in the foundations of design, development and implementation solutions. A “Fuel Management Support” process was conceived and a software solution developed and implemented within the Auxiliary Mechanization Information System (ISPM) (for the process and software, henceforth: “Fuel”). From that point on, the ISPM secured the daily insight of fuel consumption (per machine and vehicle, model and type), comparison of issued and registered items within the Work order, as well as monthly, quarterly, semiannual and annual insights in electronic form, which before 2011 was not possible.

Further improvement of the “Fuel” business process was sparked by the global ICT advances (for example: Cloud

computing, Internet of Things, GPS/GPRS, [3]). Ongoing improvements were furthermore instigated by new technologies in the field of refueling, machine and vehicle identification, mobile computer’s data input and system and communications infrastructure updates at the TE-KO, as well as by improved mobile operator’s services and networks. This was acknowledged by the design teams of TE-KO Auxiliary Mechanization, Faculty of Mechanical Engineering and Institute „Mihajlo Pupin“.

In Chapter 2, this paper first presents the “Field Fuel-issuing” Application for mobile computer as a base for further improvement of the “Fuel” business process, with integration into ISPM. Yet, a more ample context of this business process improvement lies in contemporary perception of sustainable mining founded on five supporting pillars: economy, security, environment pollution, productivity and community [4]). Further on, in Chapter 3, the Application in question is described and viewed through its goals, specification of requirements, realization and description of the infrastructure where the Application is running. This infrastructure uses communication resources of the TE-KO ICT infrastructure. Chapter 4 presents and views some of the development and implementation of the Application in question related to management and decision-making support. Conclusion underlines the results related to planning improvements and diminishing of expenditures based on improved data quality of issued fuel to machines in the field obtained in real-time.

2. BUSINESS PROCESS IMPROVEMENT

According to current perception, sustainable mining is founded on five supporting pillars: economy, security, environment pollution, productivity and community.

Taking these pillars for goals, the principle of a multi-goal optimization can be applied to sustainable mining, where all of the goals, opposing each other from immemorial times, are being simultaneously optimized. Furthermore, the optimization process in mining can be conducted in continuity so that the process parameters may adapt to changeable circumstances, such as climate conditions or situations of partial system failures, diminishing thus its functionality [4].

The use of modern information and communication technologies (ICT), as well as of multi-goal optimization in geology, mining engineering, mechanical engineering, ecology and economy may accomplish the goal of creating a frame for a complex mining factory of the future. Such a system would be of use to the superior management of mining organizations enabling them to obtain real-time information and make right decisions.

In contemporary business conditions activities within the fuel management process are mainly automated: refueling from storage-tanks, that is, fuel-issuing to vehicles, machines and fueling-trucks (for further field fuel-issuing). "Field Fuel-issuing" Application for mobile computer was developed and implemented for field refueling at open-pit mines (bulldozers, pipelayers, dump trucks...) which supports automatic identification of machines/vehicles and their operators/drivers through identification cards [1].

The referred Application was developed for industrial mobile computer Psion 8585 which has an option to substitute the keyboard with a screen. This means that the communication between the Application and its user is conducted through the touch screen – by the means of fields on the screen user choses available options or makes data entries. Training for the Psion Application use

is thus greatly simplified, since contemporary smart phones and tablets use the very same functionality.

Via contemporary TE-KO communications infrastructure, data on fuel 'in charge' and issued fuel is transmitted to the ISPM data base. This data gives rise to a more efficient fuel management at the AM Sector. This is related to planning and control of fuel consumption on daily or, for example, monthly bases.

3. MOBILE COMPUTER APPLICATION FOR FIELD FUEL-ISSUING

3.1. The goals of Application development and implementation

The main goals of "Field Fuel-issuing" Application development and implementation are to avoid mistakes and accelerate data input on field fuel-issuing, as well as making such event information available as fast as possible to the ISPM.

The ultimate goal of building an application that monitors field fuel-issuing on mobile computer is to completely substitute paper documents (Q.EK.12 - Record-keeping form for event registration of field fuel-issuing at the open-pit mine, Fig.1). Entering of such an event is made directly through the mobile computer's screen, whereas such data is further on transferred through communication channels to the data base, that is, to ISPM. Thus, the writing of documents in paper form is avoided, as well as the repeated entry of same data to ISPM. This eliminates mistakes during repeated entry and secures faster input, precision and system data availability. To attain this ultimate goal it is necessary to fulfill prior requirements, that is, certified digital signatures, a matter related to the whole of EPS. In this phase, data input is electronic while, instead of a certification body, a responsible person verifies the data in a still faster and easier way rather than by repeated entry of the same in ISPM.

EPS Ogranak TE-KO Kostolac Pomoćna mehanizacija		IZDAVANJE EVRODIZELA NA KOPU IZ CISTERNE br. /						Q.EK.12 Dokument kontrolisan dana:		
		Dana _____, interni br. vozila _____, cisterne _____								
Litara u cisterni					Totalizator [l]					Kontrola
Br. CMS	Br. izdatnice	Stanje	Doliveno	Ukupno	Ukupno izdato	Ostalo	Na početku	Na kraju		
Vreme dolivanja	Pozicija	Br. interni	Br. naloga	Broj [Mč] / [Km]	Izdato [l]	Totalizator [l]	Rukovalac/vozač			Kontrola
							ImePrezime	MB	Potpis	
Izdavalac primio/predao			Podatke u ISPM uneo			Kontrolisao				
ImePrezime	MB	Potpis	ImePrezime	MB	Potpis	ImePrezime	MB	Potpis		

Fig.1: Q.EK.12 - Record-keeping form for field fuel-issuing at the open-pit mine

3.2. Specification of Application requirements

As already stated, the main goal for development and implementation of the “Field Fuel-issuing” Application was to avoid mistakes and accelerate the data input on field fuel-issuing, as well as to secure that such information is rapidly forwarded to ISPM data base. The Application uses Identification Cards (ID) for machines and vehicles, for operators and drivers, as well as for the field fuel-issuer. Activities of “Field Fuel-issuing” are comprised out of three units:

- Fueling of fuel trucks at the fuel storage-tank,
- Field fueling of the machines,
- System’s functions as an Application support.

Last to units will be describe below.

Worker charged with field fuel-issuing (Fuel-issuer), logs into the system (identifies himself) through his ID card. After logging, he has a choice of two functionalities: refueling the fueling-truck or field fuel-issuing. Fig.2 depicts the Fuel-issuer’s scenario of field activities.

All the data entered through this Application is forwarded to the central data base, further used to control field work and to obtain fuel consumption reports.

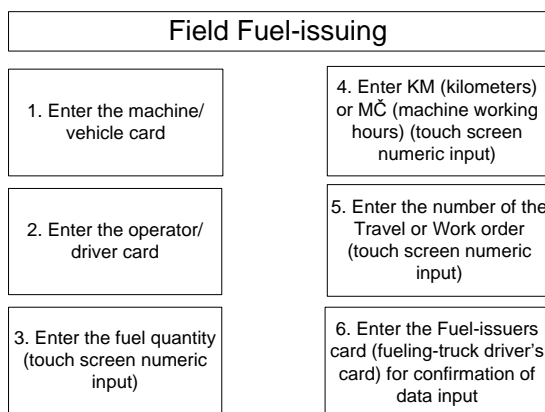


Fig.2: Activities during Field Fuel-issuing

Aside from the Fuel-issuer, the Application has an administrative user whose role is to maintain the ID card codes of machines and vehicles, as well as of the operators and drivers. Administrator is also the only one who can enter data into the system on technical parameters of fueling-trucks (fueling-truck’s internal number, current fuel quantity, fuel type, fueling-truck’s volume) and the initial totalizer value (totalizer – cumulative fuel quantity in liters dispensed from the fueling-trucks). Fig.3 depicts the choice of activities permitted to the Application Administrator for the adjustment of Application parameters. Fueling truck parameters (current system quantity value of fuel) may differ from the actual quantity of fuel in the fueling-truck due to the fuel technological working process (volume changes due to the temperature) or due to the fueling pistol’s precision and fuel issuing. In case of a difference between the real fuel quantity and the system quantity value, obtained from the Application, a Commission for leveling-out the state of fuel quantity in fueling-trucks, determines the real state according to the procedure for technological control, while, through the Administrator’s input console, the Administrator will introduce that data as a fueling-truck’s system parameter.

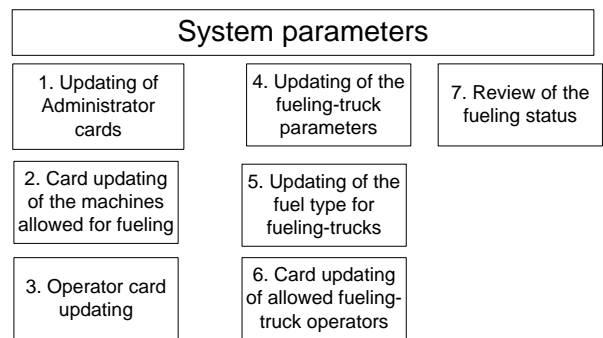


Fig.3: Administrator activities for the adjustment of Application parameters

3.3. Application realization

According to given specification, a system for data recording of field fueling was developed and implemented, as well as for control and report-issuing on fuel consumption of machines and vehicles. Real-time field information significantly contributes to quality decision-making in fuel management (planning and purchasing), as well as in accompanying each units fuel consumption (machine or vehicle), on daily, monthly or annual basis.

The “Field Fuel-issuing” Application accompanies the fuel-issuer’s working process. Fuel-issuer signs-up in the system by introducing his ID card to the reader (screen shot at Fig.4).



Fig.4: Fuel-issuer’s system logging

Next step is the choice of activity: fueling of the fueling-truck or field fuel-issuing (Fig.5).

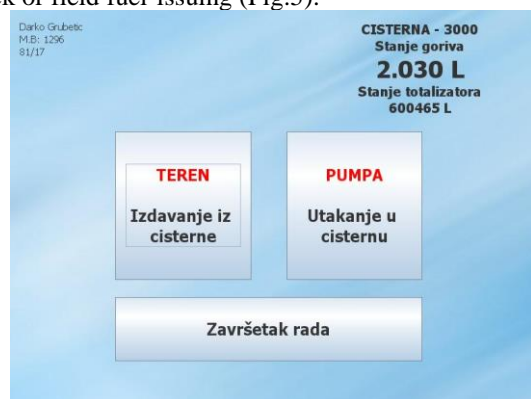


Fig.5: Fuel-issuers choice of activities

The refueling process of fueling-trucks involves the entry of issue-slip’s number and the fuel quantity if refueled system forwards this data (on refueling from a storage-tank) to ISPM through GPRS modem.

According to the field refueling plan and a Fuel-issuer's Work order, fueling-truck's driver and a Fuel-issuer are dispatched to the open-pit mine where, on field locations of the machines, refueling is conducted until completely filling up their tank. The Application provides data input of all of the relevant refueling information:

- Machine/vehicle's ID card;
- Operator/driver's ID card;
- Number of the operator/driver's Work order;
- Quantity of issued fuel;
- Number of machine working hours (MČ) or vehicle kilometers (KM);
- Fuel-issuer's ID card as conformation that all of the data has been entered.

Figures 6, 7 and 8 depict Application's screens as an example of the working process unfolding during a refueling, to be entered by a Fuel-issuer.

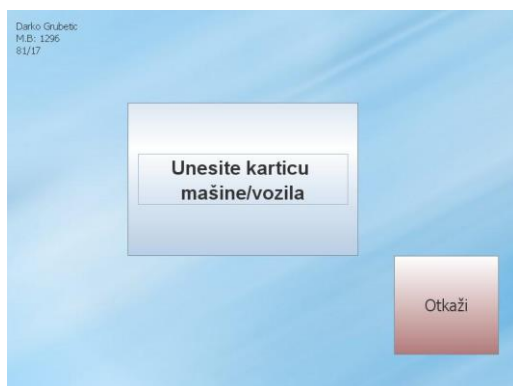


Fig.6: Machine identification through ID card

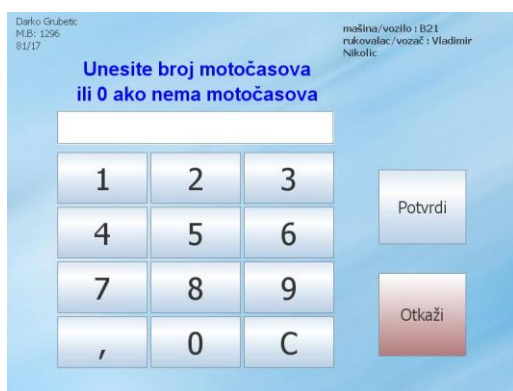


Fig.7: Input of machine working hours



Fig.8: Input of issued liters of fuel

Through a GPRS modem all of this data is sent via communications server to the data base. Aside from this data, system data is also sent to the ISPM:

- Fuel type,
- Date and time of transaction,
- GPS coordinates,
- Internal number of the fueling-truck (in ISPM).

Fuel-issuer confirms entered data by own ID card.

End of shift

When a Fuel-issuer ends his shift, next step is the "Work ending" where, based on the shift data input, on the mobile computer screen the Application presents a review of activities during that shift. Summing up, the following is being presented (Fig.9):

- Fuel state at the beginning of the shift,
- Fueled quantity during the shift,
- Number of fuel storage-tank issuing's during the shift,
- Issued fuel quantity,
- Number of field fuel-issuings,
- Fuel quantity at the end of the shift,
- Totalizer state at the beginning of the shift and
- Totalizer state at the end of the shift.



Fig.9: Data for the Fuel-issuer at the end of the shift

Input of system parameters

According to the requirements specification, the function of system parameters input has been executed. Administrator's role within the system is to enter/delete/update all of the ID cards (operators/drivers and machines/vehicles) and to enter all of the technical fueling-truck parameters as described in Chapter 3.2.

3.4 Infrastructure

Fig.10 depicts the lay-out of the physical architecture of the designed and implemented "Field Fuel-issuing" Application with its major components. TE-KO data center hosts the ISPM application servers (data base, web server and communications server), while the TE-KO communications infrastructure provides for the ISPM accessibility from all of the TE-KO Kostolac locations. Equipment installed in fueling-trucks cabins or in tractors cabins pulling fueling-tanks, is comprised of (Fig.11):

- Mobile computer (Psion company),
- ID card reader, and
- GPRS modem.

Mobile computer (an industrial Psion company PC has been used) works under Windows XP operation system, while the Application itself has been executed in Java development settings. Data from ID cards is stored in data base, while all the information on refueling and fueling is stored in form of xml messages kept in "for sending" and "sent" folders, depending on the message's status.

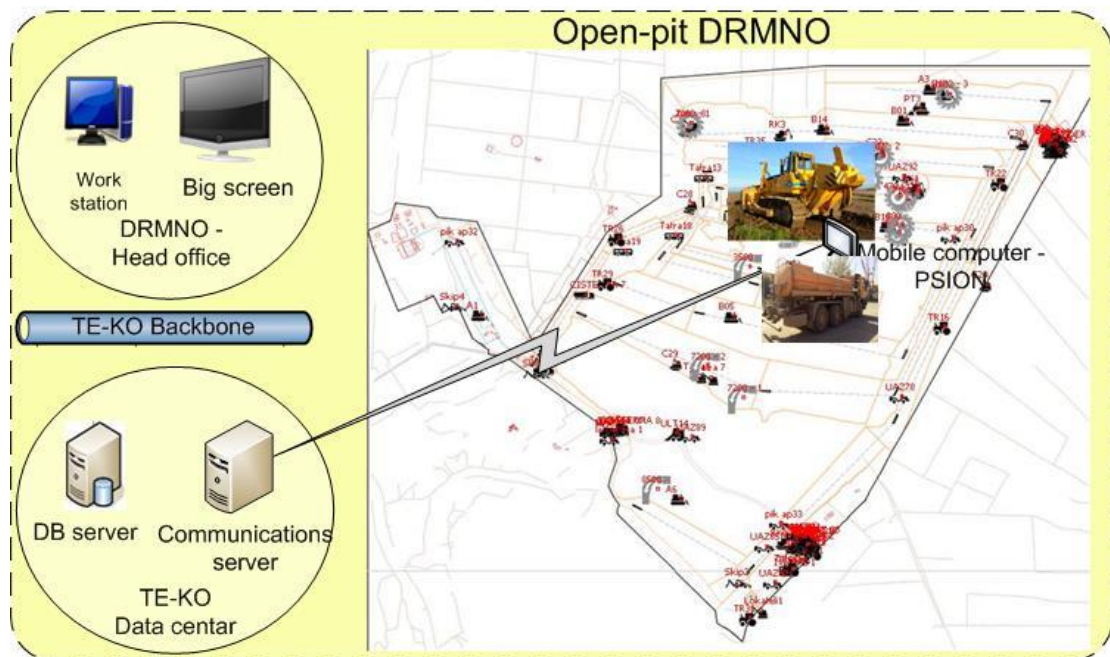


Fig.10: Lay-out of the ISPM physical architecture with “Field Fuel-issuing” Application



Fig.11: Equipment mounted inside a tractor cabin

4. MANAGEMENT AND DECISION SUPPORT

One of the key indicators of the machine/vehicle performance in open-pit mines is the **fuel consumption**. Each machine/vehicle has its own ID card, as well as their operators/drivers. By the means of mobile computers installed on fueling-trucks (open-pit mine field fuel-issuing) and the use of adequate communications infrastructure, data related to the fueling of fueling-trucks and to the fuel-issuing of field machines (refueling from fueling-trucks) is sent to the server.

Fig.12 depicts fuel consumption. This review is generated in real-time and through the use of filters reports can be generated for any required period time since all of the data is stored in ISPM. Reports give the possibility of monitoring the fuel consumption of each the machines, or vehicles, as follows:

- Total consumption for a determined period of machine’s activity,
- Average consumption,
- Average consumption as related to the normative consumption in %.

The referred values are accompanied per machine operator and vehicle driver.

For the control purposes of issued and consumed fuel, a comparison of fuel issued from the fueling-trucks is made by entering data into ISPM from the Q.EK.12 document for registration of field refueling and fuel-issuing events, thus instead of “0.00” in the last column (Fig.13) issued fuel quantities are entered and compared with the automatically entered data from the “Field Fuel-issuing” Application (Fig.13 - Screen form for data verification of field fuel-issuing.)

5. CONCLUSION

Having in mind that AM fuel consumption is one of the key performance indicators of AM management in TE-KO, it is natural for the business process of fuel consumption management to be constantly improving based on the use of latest technologies. “Field Fuel-issuing” Application, developed and implemented on mobile computers, forms part of a system that integrates the identification equipment of machines/vehicles and operators/drivers on contemporary bases. Furthermore, an integration of ISPM data base was undertaken with the contemporary TE-KO communications infrastructure. Thus, the goal of improving data quality was achieved in the sense of precision and faster data accessibility from the sum total of data for decision-making in the process of fuel consumption management. This was accomplished due to the improvement of data quality on machine field fuel-issuing obtained in real-time, presented in action through reviews and reports important for planning fuel provisions.

It is to be noted that, due to the implementation of the up-to-date business process “Fuel Management Support” with developed and implemented software support, great savings have been made in TE-KO.

For further improvement of the business process of fuel consumption management one has to consider that this process is an important model of sustainable mining where the open-pit mines of TE-KO are viewed as a modern future factory.

EPS Ogranak "TE-KO Kostolac" Pomoćna mehanizacija		Petrošnja Evrodizel goriva prema dolivanju na terenu							Q.GO.05 Dokument generisan 10.07.2017 11:52		
Vrsta	Model i tip	Interni broj	Kartica	Dat.dolivanja	Pri km/mč	Rukovalac	Razl.km/mč	Doliveno	Spec.potr.	Norm.potr.	Odnos
Buldozer B	TD25M EHTRA	B10	2762580798	05.07.2017 09:22:22	4,036.00	1010562279	7.00	220.00	31.43	45.00	69.84%
				04.07.2017 09:33:45	4,029.00	1010562279	8.00	240.00	30.00	45.00	66.67%
				03.07.2017 09:23:46	4,021.00	1010562279	14.00	345.00	24.64	45.00	54.76%
Svega za Kartica: 2762580798 (3 zapisa)											
SUMA											
PROSEK											
Svega za Model i tip: TD25M EHTRA (3 zapisa)											

Fig.12: Q.GO.05 Report on fuel consumption according to field fuel-issuing

Br.dokum.	Cisterna	Dat.i vreme	Polozija	Mašina	Radni nalog	Mh/Km	Količina goriva	Totalizator	Rukovaoc	Izdavaoc	Vrsta goriva	Lit/izdat.
93/17	CISTERNA - 3000	05.07.2017 13:08:42		1009756583, ADM2	21/17	13,730.00	310.00	581,740.00	1009501655, Administrativna, 2	1010562279	Evrodizel	0.00
93/17	CISTERNA - 3000	05.07.2017 10:23:24		1009756583, ADM2	76/17	10,019.00	100.00	581,430.00	1009501655, Administrativna, 2	1010562279	Evrodizel	0.00
93/17	CISTERNA - 3000	05.07.2017 10:01:41		3555383524, RK11	98/17	4,873.00	170.00	581,330.00	1009501655, Administrativna, 2	1010562279	Evrodizel	0.00
93/17	CISTERNA - 3000	05.07.2017 09:50:02		2762640462, B17	9/17	7,370.00	160.00	581,160.00	1009501655, Administrativna, 2	1010562279	Evrodizel	0.00
93/17	CISTERNA - 3000	05.07.2017 09:34:35		2762283966, RK3	431/17	12,287.00	200.00	581,000.00	1009501655, Administrativna, 2	1010562279	Evrodizel	0.00
93/17	CISTERNA - 3000	05.07.2017 09:22:22		2762580798, B10	317/17	4,036.00	220.00	580,800.00	1009501655, Administrativna, 2	1010562279	Evrodizel	0.00
93/17	CISTERNA - 3000	05.07.2017 09:06:37		1009412919, B16	128/17	13,163.00	435.00	580,580.00	1009501655, Administrativna, 2	1010562279	Evrodizel	0.00

Fig.13: Screen form for data verification of field fuel-issuing

REFERENCES

- [1] MITROVIĆ, R., JOVANOVIĆ, D., IVANOVIĆ, G., STOŠIĆ, D., PANTELIĆ, S., STEVIĆ, D., STEFANOVIĆ, B., DIMITRIJEVIĆ, S., at all (2010-2017) *Development and Implementation of Auxiliary Mechanization Operations Management System Based on Technical and Economic Indicators of Operations Supported by Modern Information System / Information Communication Technology, Phase I-V*, Faculty of Mechanical Engineering, University of Belgrade, Progress reports, Institute „Mihajlo Pupin“ Belgrade, Auxiliary Mechanization of the TE-KO Kostolac, a subsidiary of Electric Power Industry of Serbia, Kostolac (in Serbian).
- [2] PANTELIĆ, S.D., IVANOVIĆ, G., MITROVIĆ, R., JOVANOVIĆ, D., STOŠIĆ, D., DIMITRIJEVIĆ, S. (2013) *Improvement of Auxiliary Mechanization Operations Management at an Open-Pit Coal Mine Based on a Process Approach with ICT Support*, in Subic, A. (eds.), *Advances in Engineering Materials, Product and Systems Design, Advanced Materials Research Vol. 633*, Trans Tech Publications, Switzerland, pp. 322-334.
- [3] SUN, E., ZHANG, X., LI, Z. (2012) *The internet of things (IOT) and cloud computing (CC) based tailings dam monitoring and pre-alarm system in mines*, *Safety science* 50.4, pp. 811-815.
- [4] ZOGOVIĆ, N., DIMITRIJEVIĆ, S., PANTELIĆ, S., STOŠIĆ, D. (2015) *A Framework for ICT Support to Sustainable Mining - An Integral Approach*, proceedings of the 5th International Conference on Information Society and Technology, ICIST, Kopaonik, Serbia, pp.73-78.

Acknowledgements. Research presented in this paper is executed within TR 35030 project supported by the program of technological development of The Ministry of Education and Science of the Republic of Serbia

CORRESPONDENCE



Dragan Stošić, B.Sc. Eng.
Institute Mihailo Pupin
Volgina 15
11060 Beograd, Serbia
dragan.stosic@pupin.rs



Dragan STEVIĆ, B.Sc. Eng.
Electric Power Industry of Serbia,
TE-KO Kostolac
Nikole Tesle 5-7
12208 Kostolac, Serbia
dragan.stevic@te-ko.rs



Snežana PANTELIĆ, Ph.D. Eng.
Institute Mihailo Pupin
Volgina 15
11060 Beograd, Serbia
snezana.pantelic@pupin.rs



Nenad NIKOLIĆ, B.Sc. Eng.
Electric Power Industry of Serbia,
TE-KO Kostolac
Nikole Tesle 5-7
12208 Kostolac, Serbia
nenad.nikolic@te-ko.rs



Rastko NEGOJČIĆ, B.Sc. Eng.
Electric Power Industry of Serbia,
TE-KO Kostolac
Nikole Tesle 5-7
12208 Kostolac, Serbia
rastko.negojic@te-ko.rs



Filip TODOROVIĆ, B.Sc. Eng.
Electric Power Industry of Serbia,
TE-KO Kostolac
Nikole Tesle 5-7
12208 Kostolac, Serbia
filip.todorovic@te-ko.rs

CONTRIBUTION OF THERMAL POWER PLANT TO THE IMMISION OF PM10 IN THE CENTER OF PLJEVLJA

Vladan Ivanović
 Esad Tombarević

Abstract: Pljevlja is one of the most polluted cities in Montenegro. All the basic elements of the environment in Pljevlja are endangered, and the indicators of the state of their quality are outside the limits permitted by law. The main sources of pollutant emissions in Pljevlja are numerous: the coal mine, power plant, industrial and non-industrial boilers, individual furnaces, road traffic, landfill, etc. Combustion processes have the greatest contribution to emissions - power plant boiler, road traffic, city boiler rooms and individual furnaces. This paper presents the influence of the operation of a nearby thermal power plant on the level of pollution by PM10 particles in the city.

Key words: pollution, emissions, TPP Pljevlja

1. INTRODUCTION

Pljevlja is one of the most polluted cities in Montenegro. The main sources of pollutant emissions in Pljevlja are numerous: the coal mine, power plant, industrial and non-industrial boilers, individual furnaces, road traffic, landfill, etc.

It should be noted that there is a long list of air pollutants in Pljevlja that are systematically monitored in a way that gives a detailed insight into the air pollution situation in Pljevlja. All the basic elements of the environment in Pljevlja are endangered, and the indicators of the state of their quality are outside of the law limits. Air quality in Pljevlja is continuously monitored since mid-2009, in line

with European air quality standards transposed into Montenegrin legislation.

However, in accordance with the contemporary view on this issue, information on PM10 particles, which are recently treated as one of the critical components of pollution in terms of its impact on the health of residents, will be used as a reference pollutant indicator in this paper. Moreover, the measurements show that the level of concentration of this pollutant, in comparison to the others, is convincingly leading in exceeding allowed limit values. The measured PM10 concentrations in Pljevlja, averaged over the months, are given in [1] and are shown in Fig. 1.

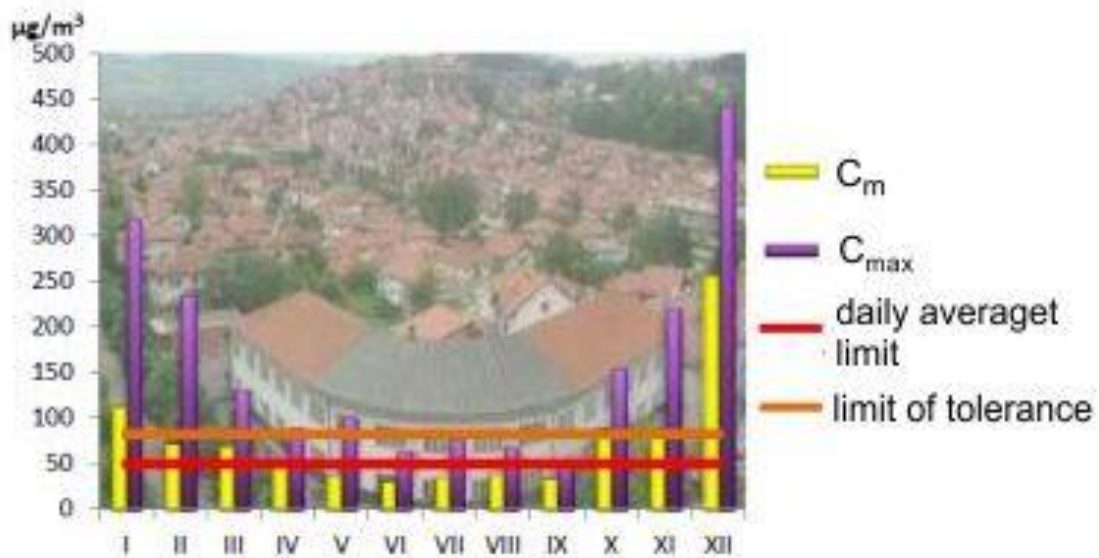


Figure 1. PM10 concentrations in Pljevlja [1]

The average daily values of PM10 concentrations in Pljevlja for the year 2013 [1] exceeded the prescribed limit of 50 $\mu\text{g}/\text{m}^3$ during 177 days (out of 337 days of valid measurements), with the limit of tolerance exceeded during 85 days. The allowed number of exceeding days is 35 (10%). The average annual concentration of 79,51 $\mu\text{g}/\text{m}^3$ was above the prescribed limit value (40 $\mu\text{g}/\text{m}^3$) and the tolerance limit for 2013 (50 $\mu\text{g}/\text{m}^3$). Short-term concentrations exceeding 1000 $\mu\text{g}/\text{m}^3$ were measured several times.

There were 332 days of valid measurements of PM2.5. The average annual concentration was 45,69 $\mu\text{g}/\text{m}^3$, which is above the limit value of 25 $\mu\text{g}/\text{m}^3$ and the tolerance limit for 2013.

Similar values were measured in 2014 and 2015 [1]. Therefore, air pollution by PM10 in Pljevlja is significant, not only because of the measured concentrations, but also because of the large number of days with overruns of allowed values.

From Fig. 1 it can be seen that the concentrations of PM10 in the air during the heating season were significantly higher than the concentrations measured in the period from April to October.

In order to obtain a wider picture of the pollution situation in Pljevlja (and in Montenegro), Podgorica, Nikšić and Pljevlja are compared with several regions in the World in terms of PM10 concentrations in major cities. The comparison is given on Fig. 2. Year-round averaged data on worldwide PM10 concentrations is a result of analysis of 1600 cities [2].

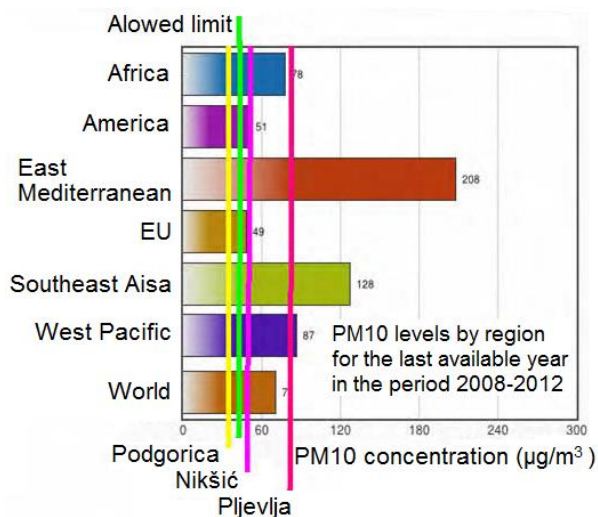


Figure 2. PM10 pollution worldwide [2]

It is clear that other major cities are also highly endangered and that the PM10 contamination problem is present throughout the world, both in developing and developed countries.

2. LOCATION OF TPP IN PLJEVLJA VALLEY

The town of Pljevlja is situated in Pljevlja valley located in the far north of Montenegro. The valley is of irregular shape, approximately 6 km wide and 9 km long. The hills of Maljevac, Velika and Mala Pliješ and Stražica are

elevations in the valley itself, with the heights of up to 900 m above sea level. Elevations that directly surround the valley reach the height of 1100 to 1400 m above sea level.

The valley in which the town of Pljevlja is located is at the altitude of 760 to 770 m above sea. The valley is irregular in shape and extends in the northwest-southwest direction and covers an area of 16 km^2 . The city is located in an area that is approximately 2.5 km in length and 1 km wide. There are several hills in the valley, and the highest is Stražica (840 m altitude). The valley is surrounded by the hills on all sides: Golubinja, Maljevac, Glavica, Bogiševac and Balibeg hill.

The thermal power plant Pljevlja is located in the southwest part of the valley. Its distance from the centre of the town is about 4km. The objects are deployed in a circle that occupies an area of 35,8 ha. The following facilities are located in this area: main building with boiler room and control room, transformers, workshop and warehouse, administrative building, electro-filters with dumper station and rectifier station, 250 m high chimney, pump station with two storage tanks of 2000 m^3 each, chemical water treatment with two reservoirs of demineralized water, auxiliary boiler room, electrolysis station, coal depot with transitional buildings and combined units, cooling tower with pump station, 35/0,4 KV substation and clean water treatment plant.

Coal is transported by dumpers between the mine and the crushing plant, and then by strip conveyors to the coal dump. Coal is then transported by strip conveyors between the coal dump and boiler bunkers in the main object. The capacity of the coal dump is approximately 100.000-120.000 tons.

A pulverized coal-fired boiler of TPP Pljevlja is equipped with a system for preparation of pulverized coal with direct incineration in the furnace. Due to the high moisture and ash content in coal, its grinding in pulverized coal is carried out in ventilation mills. The mixture of powdered coal and air is blown in the furnace at three levels, together with the heated combustion air.

The boiler is of a single drum type, with forced circulation of water and with membrane walls of the furnace. The flue gas tract of the boiler has the shape of Cyrillic letter „II“ - (P). The boiler operates with subsequent reheating of steam. The capacity is 194,44 kg/s, (pressure 13,73 MPa, temperature 540/540 $^{\circ}\text{C}$).

3. CLIMATIC CHARACTERISTICS OF PLJEVLJA

The shape of the valley itself and the characteristic shape of the relief favour longer stay of accumulated cold air, so that the temperature inversions are common.

Pljevlja has pronounced local inversions in lower atmospheric layers, in the colder part of the year, especially in the evenings, when the sky is clear. Their height is up to 50 m. Above this height, a layer with weaker inverse temperature gradients gradually forms, which rises to different heights. In the second half of the night, ground level gradient decreases, in higher layers it increases, and the development of the raised inversion is possible.

The ecological burden of the city area is compounded by the adverse climatic characteristics that prevail in the area of Pljevlja: a large number of silent days, with the frequent occurrences of “cold air lakes” and radiation fogs, especially in the winter months, which reflect on the long-term retention of pollutants and precipitating particles in the atmosphere.

Pljevlja is the city with the highest cloudiness in Montenegro. Cloudiness is increased in the cold part of the year, while in the summer period it reaches a minimum. The fog period in Pljevlja lasts 200 days a

year. According to the available data, the number of foggy days has been rising since 1974, which can be related to the time of construction and opening of industrial facilities, which is especially valid for the discharge of water vapour from the cooling tower of the thermal power plant [3]. Natural conditions cause poor ventilation of Pljevlja basin, which causes fogs to appear and remain for a long time (Fig. 3). Fogs are characteristic in autumn and in winter days, they last long and are very low. In such conditions, the concentration of pollutants in the air increases.



Figure 3. A foggy day in Pljevlja valley [2]

Due to this geographical position, meteorological silence prevails in Pljevlja basin. In the annual distribution of silence, they account for 67%, which means that air currents from all directions amount to 33%. By frequency, the southern and north winds point out, and the eastern wind is the least frequent.

The data [4] obtained from the Hydro-meteorological Institute of Montenegro about the rose of the wind (Figure 4) and silence show that the medium silence lasts 46% of the winter time, and during the summer it lasts 5% of the time, which at the level of the year gives the duration of

silence for 29% of the time. In this consideration, the year is divided into winter lasting from October to April and summer that lasts from May to September.

If the silence data for months during the year are presented graphically, it is obvious that the shape of the curve of PM10 concentration in Pljevlja (Fig. 1) has the character of the silence graph shown in Fig. 5.

For this reason, it would be important to monitor and record relevant weather data simultaneously with concentrations of pollutants.

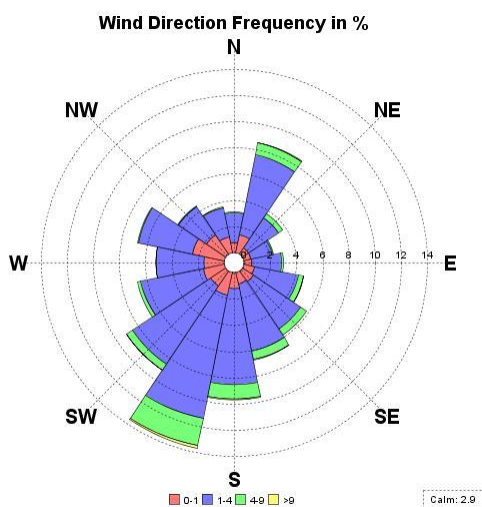


Figure 4. Rose of the winds for Pljevlja [4]

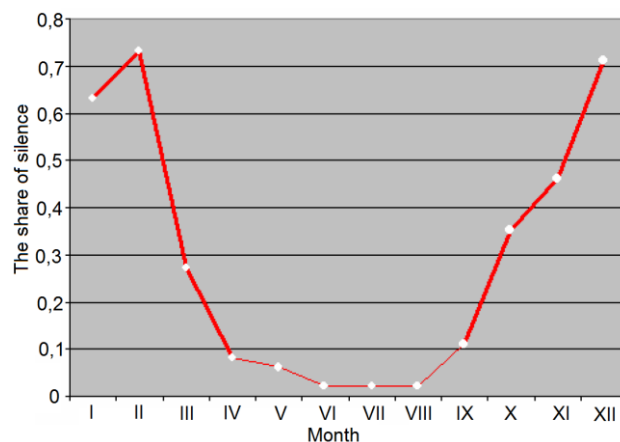


Figure 5. Meteorological silence during the year

4. ENVIRONMENTAL IMPACT OF THERMAL POWER PLANT

All thermal power plants have a major impact on the environment, causing soil, water and air pollution, resulting in excessive noise as well as in large electromagnetic radiation.

The soil is directly polluted by dust from the coal depot, ash blasted by the wind from the ash depot, and by solid particles that are emitted with the flue gas through the chimney and then deposited from the air.

Indirectly, the soil is polluted by precipitations that deposit all the harmful substances from the air (sulphur, nitrogen and carbon oxides and heavy metals) as well as process waste waters coming to the soil.

Water pollution in the thermal power plant can be physical, chemical or radioactive. Physical pollution represents any colour change, blur, temperature or conductivity change. The typical physical pollution of water is due to the insoluble matters (oil, heavy oil, etc.) Chemical pollution of water is caused by ash, wastewater from chemical preparation of water, faecal waters and waters that rinses all the harmful substances from the surrounding surfaces.

Air pollution in the vicinity of the thermal power plant is the result of the combustion of coal in the boiler. There is primary and secondary air pollution by combustion products. Primary sources of pollution are oxides of combustible elements of coal (carbon, sulphur, hydrogen), than heavy metals, dust and aerosols. Secondary pollutants arise as a result of the reaction of primary pollutants with air under the influence of the solar spectrum, where more destructive pollutants can occur. An example is the conversion of NO that occurs in the boiler to NO₂ which is significantly more aggressive.

TPP Pljevlja directly or indirectly affects the quality of air, the watercourse of Vezišnica river and its tributaries, the watercourse of Paleški potok and further on to the water stream of Čehotina downstream of Pljevlja. Also, the impact of the coal mine which inevitably follows the operation of the thermal power plant should not be overlooked. The most pronounced impacts on the environment are through [5]:

- Air pollution with particulate materials, SO₂, NO_x, CO;
- The contribution of greenhouse effect by CO₂ emission;
- Pollution of water and air from ash and slime dump;
- Drying of vegetation caused by acid rain;

- Deposition of sediments and degradation of water in natural streams due to discharge of water from the thermal power plant;
- Soil degradation in the vicinity of the thermal power plant by deposition of fly ash and heavy metals as well.

Lignite from the surface coal mines Borovica and Potrlica with lower calorific value ranging from 6.782 kJ/kg to 12.016 kJ/kg is used as a fuel for TPP Pljevlja. TPP Pljevlja has been in operation since 1982.

The total amount of coal burning in Pljevlja is over 1.800.000 tons a year, of which 1.700.000 burns in TPP, which, in addition to coal, annually consumes about 3.500 tons of oil and 660 tons of chemicals. Based on available data [3], TPP Pljevlja hourly consumes 225 tons of coal, 200 tons of oxygen and emits 230 tons of carbon oxides, 3,57 tons of sulphur oxides, 120 tons of water vapour and 0,36 tons of suspended particles per hour. Also, 44 tons of ash and 5 tons of slag per hour result as the products of combustion.

The height of the chimney of the thermal power plant is 252 m, so that its outlet exceeds 1000 meters above the sea level. Despite the relatively high thermal power plant chimney, increased concentrations of suspended particles are registered during the adverse meteorological conditions in the heating season.

Continuous emission monitoring system is installed on the chimney before the outlet of the gas to the atmosphere. The measuring site is located at the height of the existing platform (67 m).

In addition, continuous measurement of emission concentrations of suspended particles, carbon oxides and sulphur oxides are performed on the chimney. The average values of concentrations measured by the system for flue gas monitoring for the last few years are given in Table 1.

From the above data, it is clear that the thermal power plant invest considerable efforts in reducing the emissions of solid particles. Those efforts have been remarkably successful in recent years, primarily thanks to the reconstruction of the electro filters. Further reduction of sulphur oxide emissions from flue gases from the current approximately 5000 mg/nm³ to less than 150 mg/nm³ is possible only by the construction of a flue gas desulphurisation plant (DeSO_x). The reduction of nitrogen oxide emissions from flue gases from the current cca 600 mg/nm³ to less than 200 mg/nm³ is possible by reconstructing/building a nitrogen oxide reduction plant in outlet flue gases (DeNO_x) with the application of primary and secondary reduction measures.

Table 1. Average emissions from TPP Pljevlja

Pollutants	Unit	Value					MAC*
		2010	2011	2014	2015	2016	
Solid particles	mg/nm ³	82	171	45	35	11	10
SO ₂	mg/nm ³	3229	4729	5610	5308	5384	150
Nox	mg/nm ³	480	473,7	571	668	661	200
CO ₂	%	11,46	10,74	12,5	11,93	11,7	-
CO	mg/nm ³	38	32,5	32	28	23	100

* maximum allowable concentration

5. IMMISIONS EMANATING FROM THE THERMAL POWER PLANT

Pursuant to Article 21 of the Law on air protection [6], the Ministry, in cooperation with the Agency and the local government bodies in whose territory the environment is endangered by pollution, issues an Air quality plan. The aim of the plan is to achieve as soon as possible the concentration values established by the Decree on determination of pollutants, limit values and other air quality standards.

To this end, for the purposes of air quality plan, TECHNE Consulting has completed a study on the impact of air pollution in the municipality of Pljevlja [3]. According to this study, the total emission of pollutants will increase in the coming years (observed by 2020) unless measures are taken to reduce pollution. By implementing a series of proposed measures, by 2020, pollution reduction will be achieved, especially in terms of PM10 suspended particles.

One of the main conclusions is that the influence of thermal power plant is minimal, i.e. among other things that, due to the high chimney, the emission of PM10 from the thermal power plant, does not compromise the air quality in the city. The impact of the emissions from the thermal power plant on the urban area of Pljevlja was estimated using the Calpuff model. Due to the height of the chimney (252 m), the emissions are dispersed in a large area, overtaking the city and settling away from the it (Fig. 6).

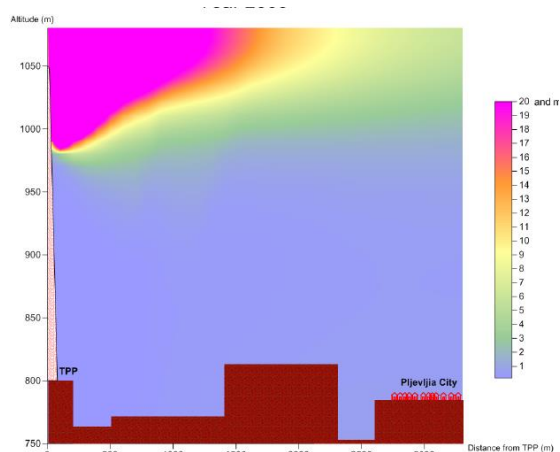


Figure 6. Mean annual concentrations of PM10 coming from TPP only [3]

This Study, although based on the use of sophisticated CFD technology, has a shortage for which it is hard to blame anyone. Input data of pollutant emissions were taken from the literature, i.e. exact data was not measured. On the other hand, when comparing the PM10 concentrations measured over a longer period of time (data from the Environmental Protection Agency of Montenegro) with interruptions in the operation of the thermal power plant (data on interruptions obtained by the courtesy of the thermal power plant operator), no correlation is obtained, which confirms the conclusion in the abovementioned study. This comparison for the year 2013 is graphically shown in Figure 7.

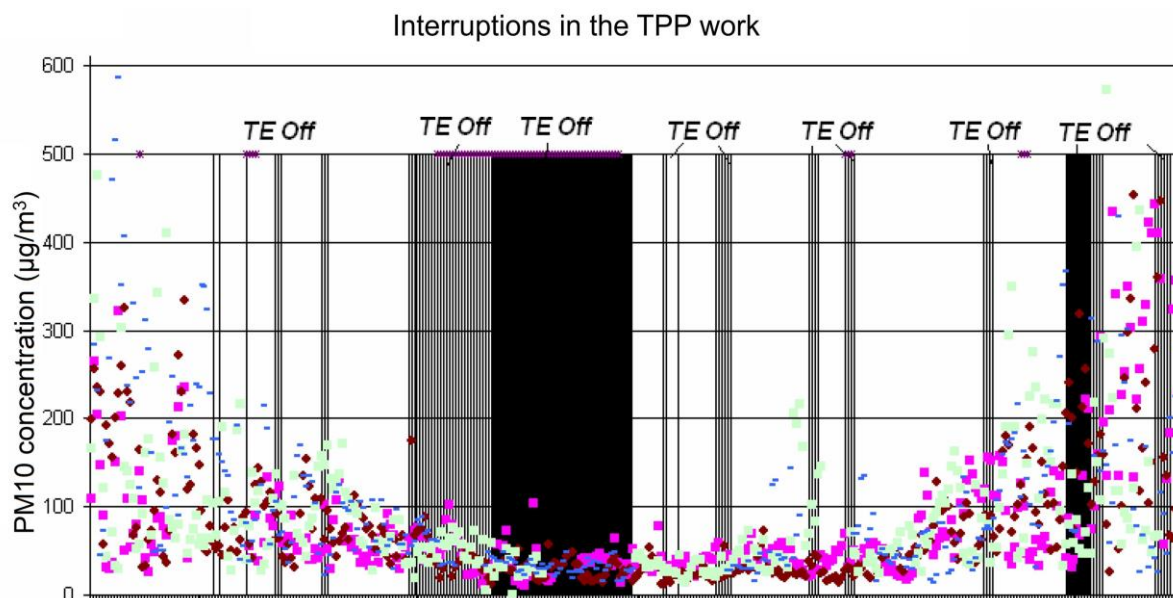


Figure 7. Correlation of interruption in the operation of TPP and PM10 concentration

6. CONCLUSION

All the basic elements of the environment in Pljevlja are endangered, and the indicators of the state of their quality are outside the limits permitted by law. Waste materials emanating from the exploitation of coal, forests, clay, marlstone, electricity generation, etc. results in increased pollution of air, surface and groundwater, as well as in soil degradation and pollution, in accumulation of municipal and hazardous waste, deterioration of the health status of the population, destroying flora and fauna etc.

Combustion processes have the greatest contribution to emissions of pollutants – boiler of thermal power plant, industrial boilers, road traffic, non-industrial boilers in the household and service sector (city boiler rooms and individual furnaces) as well as processes related to extraction, refining and solid fuel transport.

However, the main culprit for excessive PM10 pollution in the winter months (heating season) is not the thermal power plant, but rather small boilers and furnaces in the city itself. Their fuel is primarily lignite, primarily because of its availability and low price. Because of the small height of the chimneys, those boilers and furnaces, in conjunction with adverse weather conditions, fail to disperse the flue gasses out of the city [8].

Solid fuel combustion in households is one of the leading sources of suspended particles in which a high percentage of benzene and benzo(a) pyrene is found. Among solid fuels, combustion of lignite produces the highest amount of pollutants per unit of calorific value. In addition to wood and coal, it is common to use packaging waste in household furnaces, which sometimes results in emission of carcinogenic pollutants such as dioxins and furans.

REFERENCES

- [1] Environmental Protection Agency of Montenegro (2016) *Information on the state of the environment in Montenegro: Report for 2015*, Podgorica, Montenegro (in Serbian)
- [2] Ivanović, V. et al. (2015) *Study for solving the pollution problem in Pljevlja*, University of Montenegro, Faculty of Mechanical Engineering, Centre for Energy, Podgorica, Montenegro (in Serbian)

- [3] Ministry of Sustainable Development and Tourism (2013) *Air quality plan for the municipality of Pljevlja*, Podgorica, Montenegro (in Serbian)
- [4] Institute of Hydrometeorology and Seismology of Montenegro (2014) *Climatic wind roses for Pljevlja for 2010-2013*, Podgorica, Montenegro (in Serbian)
- [5] Vemić, M., Gačević, D. (2015) *Environmental protection program in TPP Pljevlja*, Internal report of Electric Power Company of Montenegro, Pljevlja, Montenegro (in Serbian)
- [6] Law on air protection, Official Gazette of the republic of Montenegro 025/10, 040/11, 043/15, Podgorica, Montenegro (in Serbian)
- [7] Ivanović V., Kovač, D. (2017) *The effects of energy efficiency measures on the reduction of pollution level in Pljevlja*, Proceedings of the 14th International Conference for Maintenance and Production Engineering, KODIP 2017, Budva, Montenegro, pp. 117-121 (in Serbian)
- [8] Ivanović, V., Tombarević, E. (2017) *Modelling of PM10 Immision from Individual Furnaces and City Boiler Rooms in Pljevlja*, Submitted to the 18th International Symposium on Thermal Science and Engineering of Serbia, SIMTERM 2017, Sokobanja, Serbia.

CORRESPONDANCE



Vladan IVANOVIĆ, Prof. D.Sc. Eng.
University of Montenegro
Faculty of Mechanical Engineering
Bulevar Džordža Vašingtona bb
81000 Podgorica, Montenegro
vladaniv@ac.me



Esad TOMBAREVIĆ
University of Montenegro
Faculty of Mechanical Engineering
Bulevar Džordža Vašingtona bb
81000 Podgorica, Montenegro
esadt@ac.me

APPLICATION OF NEW TECHNOLOGIES IN THE DEVELOPMENT AND INCREASE OF WIND POWER PLANT CAPACITY

Isak KARABEGOVIĆ

Abstract: Energy stability and security have become an important issue for each country over the last few years, and the reason for this depends on the economic and social development of each country. Energy and energy systems, in addition to their well-being for the society as a whole, also have negative consequences such as release into the atmosphere of greenhouse gases and carbon dioxide. The world's tendency is to reduce the percentage of carbon dioxide and greenhouse gases which are result as a use of fossil fuels for energy production and this reduction is achieved through the use of renewable energy sources. Renewable energy sources include: biomass, solar energy, geothermal, hydroelectric power and wind. The paper presents a trend of energy production from renewable energy sources over the past ten years, with a special focus on wind power. The trend of development and modernization of the wind power plant from the beginning to the present, the influence of modern-new technologies on the development and implementation of wind power plants as well as the increase in electricity generation capacity has been demonstrated. A review of various design solutions for wind use as renewable energy sources is presented. In the end, a review of the future development of the wind power is utilized by using advanced technologies, i.e. technologies that establish the fourth industrial revolution.

Key words: energy, renewable energy sources, new technologies, wind, wind power plants.

1. INTRODUCTION

The use of fossil fuels in the world has for years caused global climate changes that humanity is now facing. Their use increased carbon dioxide and other greenhouse gases, which caused climate changes. The effects of climate change are already noticeable, such as melting of glaciers, disintegration of the polar ice, melting of permafrost, rising of sea level, which results in the change of the ecosystem. In addition, when nuclear energy is concerned, it has been shown that its production is insecure for the humanity, examples of which are large nuclear accidents such as Fukushima in Japan (March, 2011) and Chernobyl in former Soviet Union [1,2,3, 4,5,6,7,8,11,12]. This has forced the governments of almost all countries in the world to turn towards renewable energy sources. Renewable energy sources play an increasing role in the energy system. Energy evolution is the most ambitious, because it introduces the production of energy from the renewable energy sources, as well as rigorous energy efficiency measures, so that by 2050 the largest share of energy production would be placed on renewable energy sources. Renewable energy sources can be divided into two main categories: traditional renewable energy sources such as biomass and large hydroelectric power plants, and so-called "new renewable energy" such as biomass (bio-fuel, bio-gas), small hydroelectric power plants, solar photovoltaic energy, solar thermal energy, wind power energy, geothermal energy [6,7,21,43,45], and sea energy (tidal energy, waves, and currents). Renewable energy sources are considered to be the future of the energy or

clean energy that will replace fossil fuels and their harmful impact on the environment. In regard to the wind power energy, the development of wind power plants is increasing annually, thus increasing the height of the wind power plants and generator power. In 1980 the height of wind power plant amounted to 15 meters and generator power to 1 MW, while in 2015, with the application and implementation of new technologies in the development of wind power plants, their height reached 178 meters and generator power to 9.0 MW. There is an ongoing research in new technologies, especially nanotechnology, whose implementation in wind power plants will increase the height of wind power plants and wind generator power in the future.

2. ENERGY PRODUCTION IN THE WIND POWER PLANTS WORLDWIDE

The production of wind energy recorded the fastest growth of all renewable energy sources at the beginning of 21st century, so that the capacity increased about seven times in the period 2005-2015. The estimates are that renewable wind energy will have the growth tendency of 21% annually. The long-term technical potential of wind as a renewable energy source will increase, followed by the solution of the structural problems of wind power plants, because wind turbines are currently produced up to 178 meters and 9.0 MW. With future development of new technology, wind power plants will achieve height to 300 meters and 20 MWh [1-3,14]. Installation of wind power plants will occur on large areas and high altitudes, as well as in the oceans where wind resources are rather high.

Constructive solutions of wind power plants will be such that they will be mobile, and will be installed in the areas where the intensity of the wind is very large. The global production capacity of wind energy in the world for the period 2005-2015 is shown in Figure 1. [3-8]

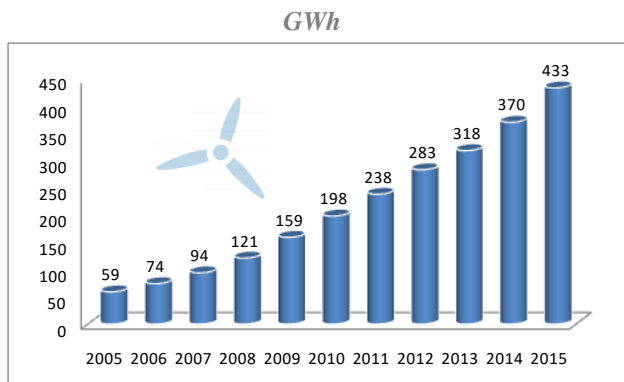


Fig. 1: World production of electricity from wind power plants worldwide for the period 2005-2015

The analysis of the Figure 1 indicates that the production of electrical energy from wind power plants in the world has the growing tendency every year. In 2005, total production was 59 GWh, while in 2015 total production was 433 GWh. We can conclude that in ten years the production of electricity increased about seven times. In order to get a complete picture of the production of electricity from wind power plants we need to conduct an analysis of electricity production by countries in the world. Top ten countries that produce highest percentage of electricity from wind power plants is shown in Figure 2.

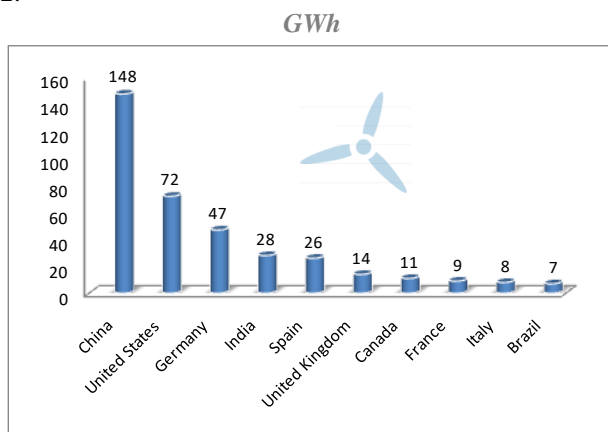
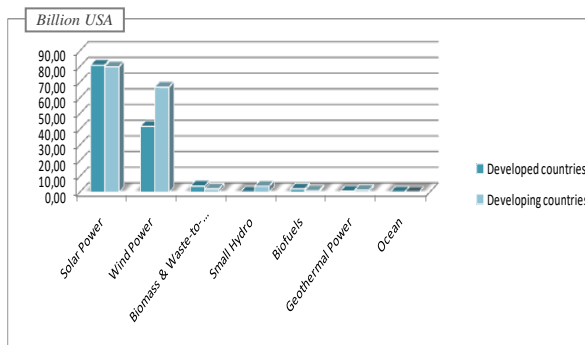


Fig. 2: The produced electricity from wind power plants in ten top countries in the world in 2015 [3]

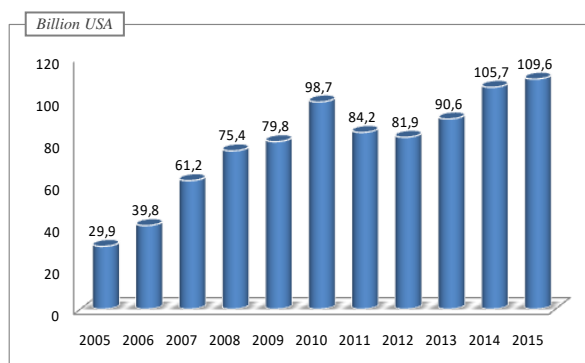
The leading role in the production of electricity from wind power plants in the world belongs to China which produced 148 GWh in 2015, followed by USA with 72 GWh, and Germany with 47 GWh, and other countries: India, Spain, England, Canada, France, Italy, and Brazil with capacities shown in Figure 2.

In regard to global investment in renewable energy sources, investment are constantly increasing since 2005. In 2005 about 73 billion USD were invested worldwide, and in 2015 the tendency of investment has grown to about 286 billion USD [REN 21 RENEWABLES 2016 - Global Report]. The largest investments are directed

towards the solar energy, Figure 3 a), in which developed countries invested about 81 billion USD and developing countries about 80 billion USD in 2015. The second place in investment in renewable energy in the world is held by wind energy utilization, Figure 3b), where investment are increasing continuously every year. In ten years investment in this renewable energy source has increased from about 30 billion USD in 2005 to about 110 billion USD in 2015, and it can be concluded that the investment increased 3.6 times. Predictions are that this tendency of investment in renewable energy sources will continue in the future. The investment in renewable energy has led to the creation of new jobs and employment of workers in renewable energy sector in the world. In 2015 the REEmployed 8.1 million workers [REN 21 Renewables 2016 Global Report], and the tendency of hiring workers in regard to wind energy usage is shown in Figure 4.



a- Developed countries and developing countries in 2015



b- Investing in wind energy

Fig.3: Global new investments in RES technology and wind energy in the developed countries and developing countries in 2015 [3-8]

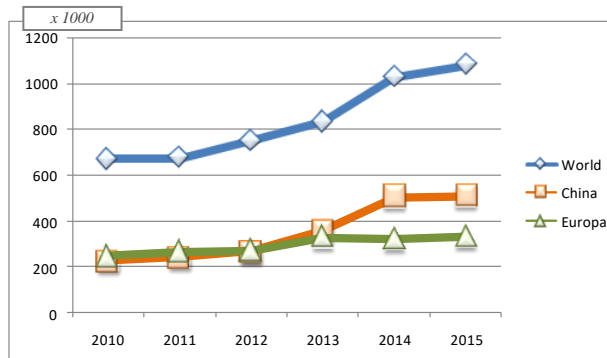


Fig. 4: Employment in the world, China and Europe in technology and wind power plant production for the period 2010-2015 [3-6]

Figure 4 indicates that the tendency of employment in the wind power plants is growing worldwide in the last five years. In 2015 there were approximately 1.081.000 workers in the world. Based on the Figure 4a) we can conclude that more is invested in wind energy by the developing countries in 2015, which is confirmed by Figure 4. We see that China is in the first place in the number of workers in this renewable energy source in last three years. In 2015 there were about 507.000 workers in the use of wind energy (technology and production) which is far more than in Europe. The estimates are that this tendency of employment will continue in the future.

3. THE APPLICATION OF NEW TECHNOLOGIES IN THE DEVELOPMENT AND INCREASE OF CAPACITY OF WIND POWER PLANTS

The world is undergoing the fourth industrial revolution “Industry 4.0”, so that the development of new technologies, such as digital technology, sensor technology and nanotechnology, contribute to the increase of boundaries in use of wind as renewable energy source. Figure 5 shows historical development of wind power plants in the world.

Based on Figure 5 we see the past and the future development of wind power plants in the world. In 1980 the height of wind power plants was only 15 meters, and in 2000 wind power plants reached the height of 112 meters with 1.5 MW generators. The development of new

technologies has favored the development of wind power plants so that in 2015 the largest wind power plant reached the height of 178 meters with 9.0MW generator. The development of new technologies and nanotechnology and its further application in wind power (nanomaterials and machines have already been introduced in the wind industry) aims to improve the durability of components of wind power plants critical elements. One of the element is the blade of turbine where the application of nanotechnology and new materials targets to improve their properties, Figure 6. The basic characteristic of the wind power plants blades that needs to be increased is the resistance and stiffness of the blades. New materials should ensure safe operation and long life operation of wind power plants.

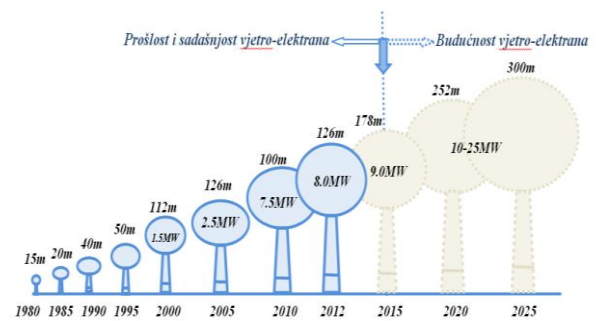


Fig.5: Former and future development of wind power plants in the world [1,2,11]

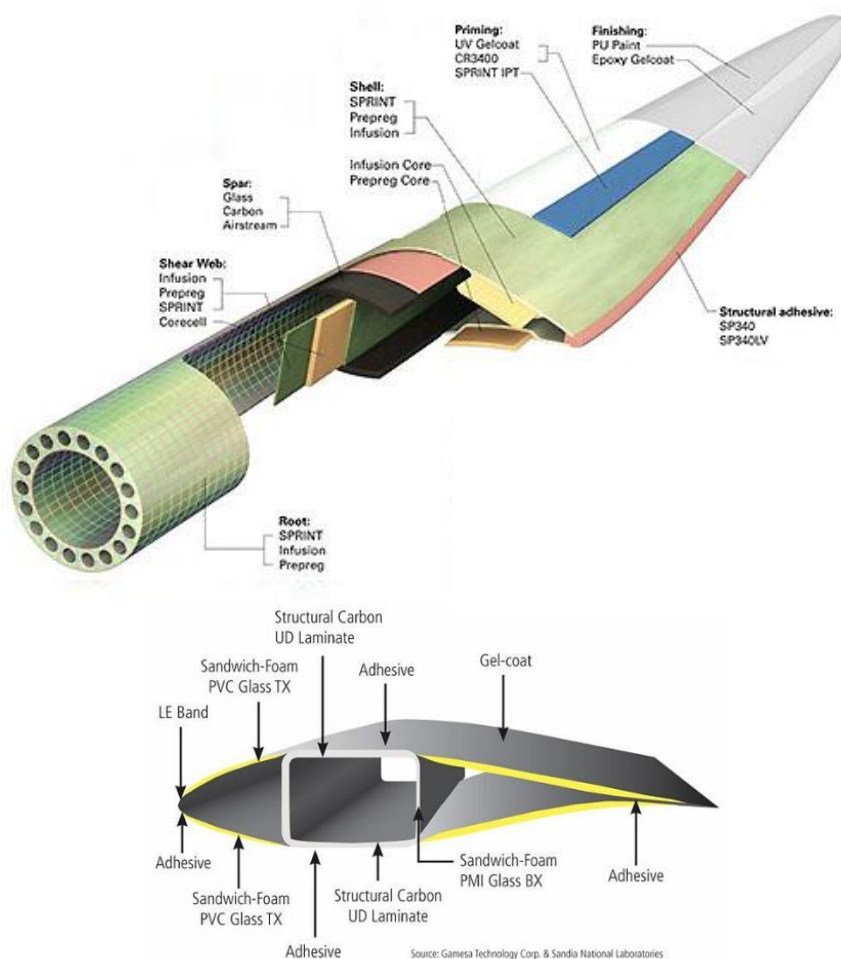


Fig. 6: New generation blades of wind power plants [2]

As is well known, the blades of wind power plants are made of polymer matrix composites. These materials dominate the market for several reasons: low price, smaller ratio of the weight and strength, excellent characteristics of material fatigue, high elastic modulus, high specific strength, as well as the possibility of making very complex geometric shapes that are very important in order to create greater resistance. High quality nanomaterials allow huge challenges and progress in the field of polymer matrix composites that will affect the characteristics of the blades in wind power plants, but also make them easier and rougher. Nanoparticles that are used for coating of blades of wind power plants have good diffusion barrier properties and excellent resistance to water, which is very important in the wind power plants blades. Use of nanoparticles in composite polymers have advantages and increase in: tensile strength up to 40%, modulus of elasticity up to 68%, bending stiffness up to 60%, and improves the fire retarding properties. They also have disadvantages, such as: improper ratio of price and their impact, difficulty in recycling, brittleness, etc. Revolutionary idea for long-term operation of blades of wind power plants is the development of super-hydrophobic and ice-phobic materials, since coating of blades, sensors and measuring equipment with these

materials prevents the formation and accumulation of ice on these elements. The same situation is with the carbon nanotubes (Figure 7 show carbon nanotubes with cylindrical nanostructures) that are 50-110 times stronger and six times lighter than steel, whose coating on blades prevents icing.

Use of nanotechnology (nanoparticles, nanomaterials, and polymer matrix composites) enables the improvement of length of wind power plant blades, Figure 5. The objective is to increase the blades, so as to increase the power produced by wind power plants, because it is proportional to the square of the bladlength. Nanocomposite materials are used in order to develop new generation of blades that will have high performances. Considering the fact that during the operation of wind power plants, wind gusts can impact the blades, all elements of the generator are exposed to static and dynamic loads. Many companies in the world produce generators for wind power plants. In an effort to remain competitive in the market they need to develop and apply new technologies in the production of generators for wind power plants. Figure 8 shows the market share of ten manufacturers of wind power plants in the world in 2015.

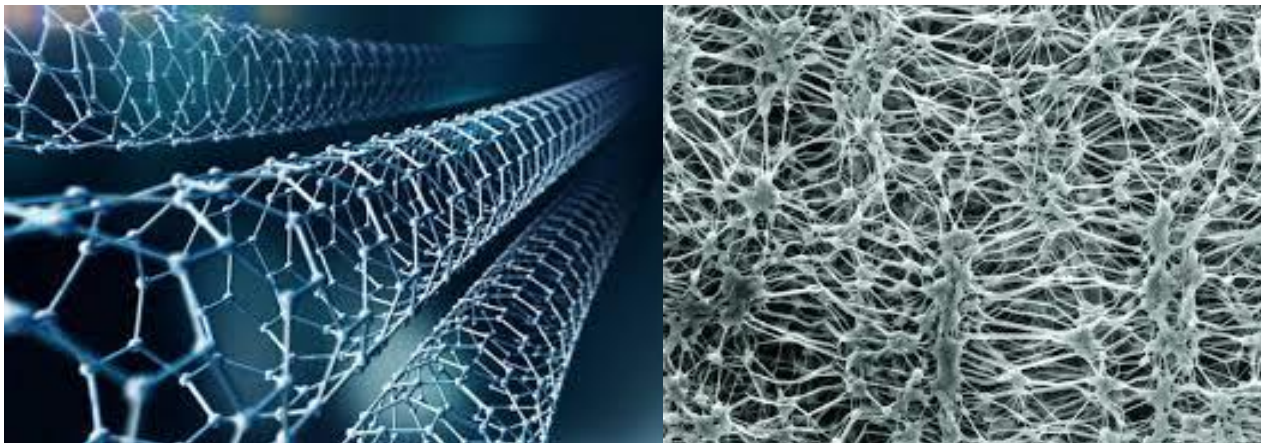


Fig. 7: Carbon nanotubes used in wind power plants [14,15]

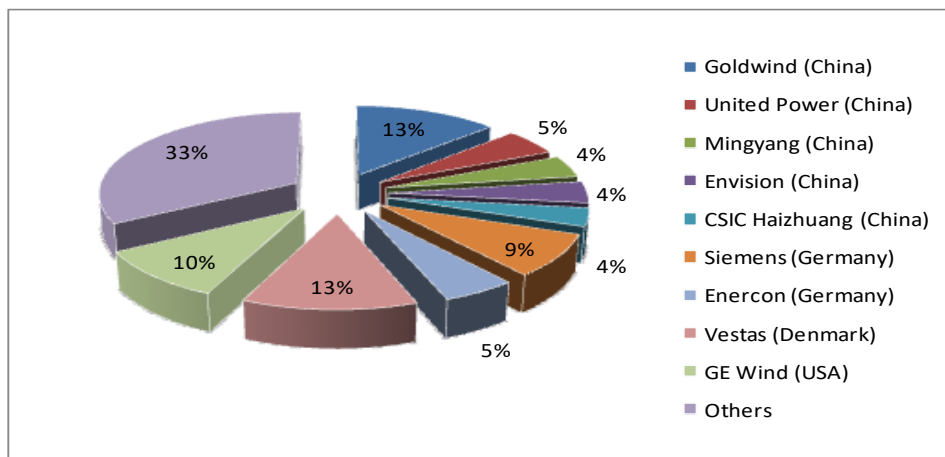


Fig.8: The market share of the ten top manufacturers of wind power plants in the world in 2015 [3]

The analysis of the involvement of the largest manufacturers of wind power plants in the world in 2015 provides us with the conclusion that companies from China are the largest manufacturers of wind power plants and cover 30% of the market. This conclusion confirms the fact that in 2015 China was the biggest producer of electrical energy with 148 GWh.

Due to unstable working conditions, all rotating elements in wind turbines are loaded statically and dynamically, and cracks can occur due to cyclic stress. In addition, it may cause wearing of rotating parts and the creation of localized corrosion. Nanotechnology has developed nano-

lubricants with very low friction which coat the rotating elements in order to reduce the energy loss in them (gears, bearings). Nano-lubricant is the geometric structure of the nanoparticles, which acts as small ball bearings, and is convenient for the protection of the rotating elements against wearing. Wind power plants installed at sea are subject to moisture and water. In order to protect them, new seals based on nanocomponent elastomer have been developed, that protect and prevent the penetration of moisture and water.

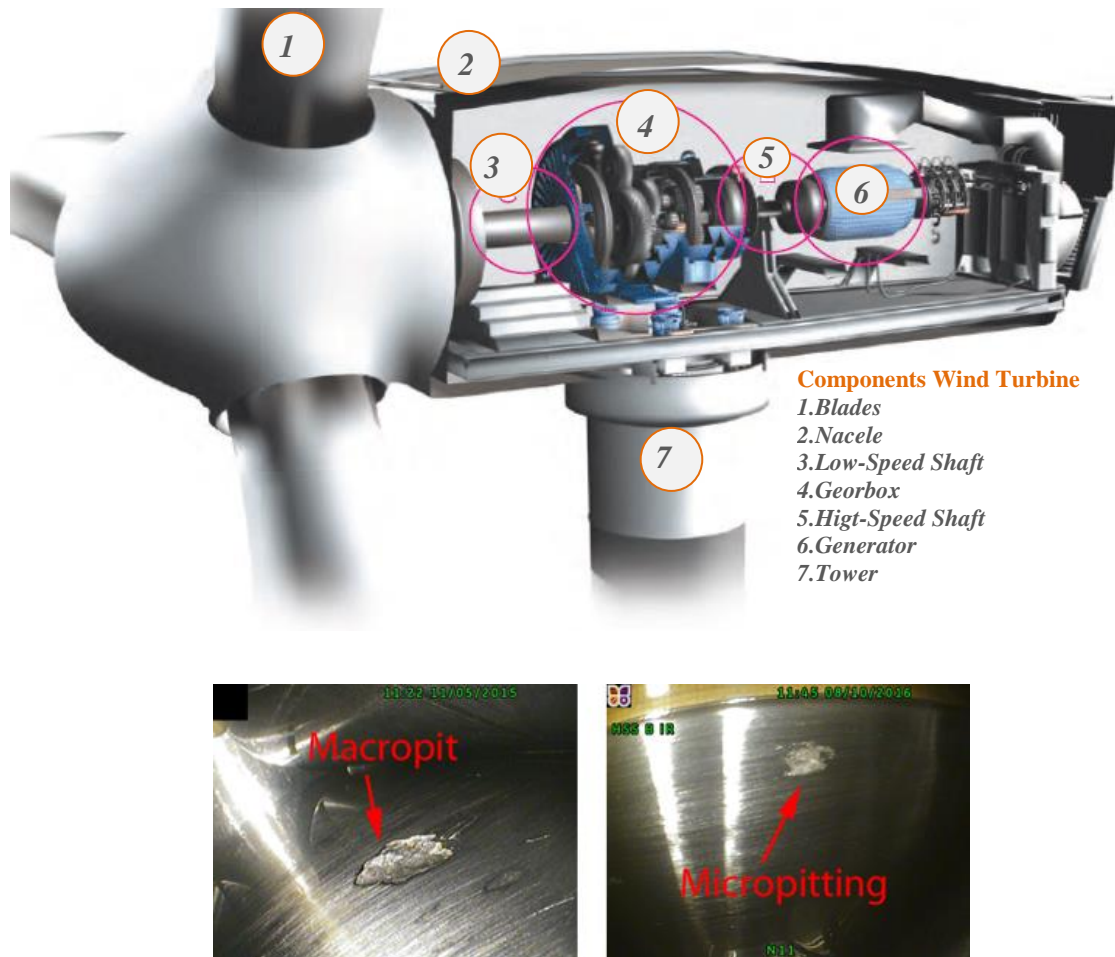


Fig. 9: Wind power plants with components [16]

4. CONCLUSION

The use of fossil fuels in the world has led to global climate change, and many strategies were made to replace fossil fuels with renewable energy sources. One of the renewable energy sources is wind. The use of wind for energy production in the world is increasing every year, and in 2015 it reached 433GWh, with China becoming the largest producer with 148 GWh. Investment in the utilization of wind power energy is constantly increasing and in 2015 it reached about 110 billion USD. In addition, the number of jobs in the use of wind energy in 2015 increased to approximately 1.081 million workers. Investments have been made in technology which uses the wind as a renewable energy source, so that the height of wind power plants and power generators is continuously

increasing. The largest contribution to the increase of the capacity of wind power plants is attributed to the new technologies, which include new materials, nanotechnology and sensor technology. The use of nanoparticles and nanotubes increase the wind power plants blades and their working life. In terms of rotating elements, they increase wear resistance, reduce friction and reduce the formation of localized corrosion and cracking, and thus increase the efficiency of wind power plants. Maintenance and replacement of parts of wind power plants are very expensive, as they contribute to significant delays in installations of wind power plants. The development of new technologies, especially nanotechnology, will provide a greater blade length of which the capacity of wind turbines depends, as well as the production of high power generators in the future.

REFERENCES

- [1] Wolfgang Luther, Sebastian Hummel, Application of Nano-technologies in the Energy Sector, Vol.9. HA Hessen Agentur GmbH, Wiesbaden, Germany, 2008. Pp.6-44.
- [2] Sibujohn, Pravesh malviya, Nanotechnology for Solar and Wind Energy Applications Recent Trends and Future Development, Conference: IEEE International conference on Green Computing and Internet of things, (ICGCIoT 2015), At Greater Noida, Galgotia College of Engineering, October 2015, DOI: 10.1109/ICGCIoT.2015.7380650; pp.181-187.
- [3] Renewable 2016. Global Status Report, Paris: REN21 Secretariat, 2016.
- [4] Renewable 2015. Global Status Report, Paris: REN21 Secretariat, 2015.
- [5] Renewable 2014. Global Status Report, Paris: REN21 Secretariat, 2014.
- [6] Renewable 2013. Global Status Report, Paris: REN21 Secretariat, 2013.
- [7] Renewable 2012. Global Status Report, Paris: REN21 Secretariat, 2012.
- [8] Zäch, Michael, Carl Hägglund, Dinko Chakarov, and Bengt Kasemo. "Nanoscience and nanotechnology for advanced energy systems." *Current Opinion in Solid State and Materials Science* 10, No. 3. 2006. pp. 132-143.
- [9] The Application of Nanotechnology to Energy Production [Online], Available FTP: <http://www.understandingnano.com/nanotechnology-energy.html>
- [10] Top ten wind energy companies in India, 2014. [Online], Available FTP: <http://www.about-alternative-energy.com/Wind-Energy-Companies-India.html>
- [11] Isak Karabegović, Applications Trend of Renewable Energy Sources for Energy Production in the World Wirt Special Reference to Wind Power, *International Journal of Materials Protection*, Vol.58., No.1., Published by Inženjersko društvo za koroziju, SERBIA, 2017., ISSN: 0351-9465, E-ISSN 2466-25-85; COBISS SR-ID 4506626 pp:86-93. (UDC:620.192; doi:10.5937/ZasMat1701086K; www.idk.org.rs/casopis-zastiza-materijala/).
- [12] Isak Karabegović, Applications of Renewable Energy Sources in the World and the EU wirt a Particular Focus on Solar Energy, *International Journal of Advanced Engineering Research and Science*, Vol.3., Iss.11., AI Publications, Jaipur, Rajasthan, INDIA, 2016., ISSN: 2349-6495 (P) / 2456-1908 (O), pp:224-228. (<https://dx.doi.org/10.22161/ijaers/3.11.34>; www.kwpublisher.com).
- [13] www.windpowerengineering.com
- [14] https://hr.rbth.com/science/2015/12/10/nano-cijevis-sibira-najavljuju-dolazak-ugljicnog-stoljeca_549507
- [15] <https://www.quora.com/What-am-I-seeing-when-I-look-at-an-electron-microscope-photograph>
- [16] <http://www.ucsusa.org/publications/catalyst/sp14-how-it-works-wind-power.html#.WRlxtevyjIU>

CORRESPONDANCE



Isak KARABEGOVIĆ, Prof. D.Sc. Eng.
University of Bihać
Technical Engineering Faculty
Irfana Ljubijankića bb
77000 Bihać, Bosnia and Herzegovina
isak1910@hotmail.com

APPLICATION OF RENEWABLE ENERGY SOURCES IN TERMS OF ECONOMIC, ENVIRONMENTAL AND SOCIAL SUSTAINABILITY

Mirjana JOKANOVIĆ
Dušan GOLUBOVIĆ
Blagoje ŠUPIĆ
Aleksandra KOPRIVICA

Abstract: We are witnesses of everyday changes, which can bring the world into the question of survival. On the other hand, the progress and the speed of changes are the keys of success. What is important is that we have to change the human being's life, due to the concept of the sustainable development, which includes three dimensions: ecology, economy and social aspect. This paper gives the analysis of using the renewable energy, through the production of the electricity, including the sustainable development. Through research, attention was paid to analyzing the growth in the share of renewable energy in electricity production, as well as incentives to use renewable energy sources, in the area of Republic of Srpska.

Key words: electricity, renewable energy, sustainable development.

1. INTRODUCTION

Modern life style means much more energy, with the goal to achieve higher effectiveness and comfort. Nowadays, most energy needs are settled using extremely harmful fossil fuels, which, in the future, should be replaced with cleaner energy resources, like renewables or nuclear energy.

Sustainable development is a dominant philosophy which must be respected by every human in a global world, if he/she wants to settle nowadays needs without compromising the ability of future generations to meet theirs [1].

Also, sustainable development means maintaining a balance between use, saving and restoring all resources, and understanding that the generations who are coming will largely depend on our present actions [2].

The paper's topic is very current due to the fact that the development of the renewable energy sources is a major challenge for the future of the whole world.

2. RENEWABLE ENERGY SOURCES

Renewable or inexhaustible sources of energy are those on the Earth, which are available in unlimited quantities. Although, the process of conversion and transformation temporarily spends their quantities, i.e. they can always be restored. Also, they are called alternative energy sources [3]. Renewable energy sources can be divided into several groups, based on similarities, which illustrates figure 1 [3]:

- Solar energy,
- wind energy,
- hydropower,
- earth energy,
- energy from biomass and
- other renewable energy.

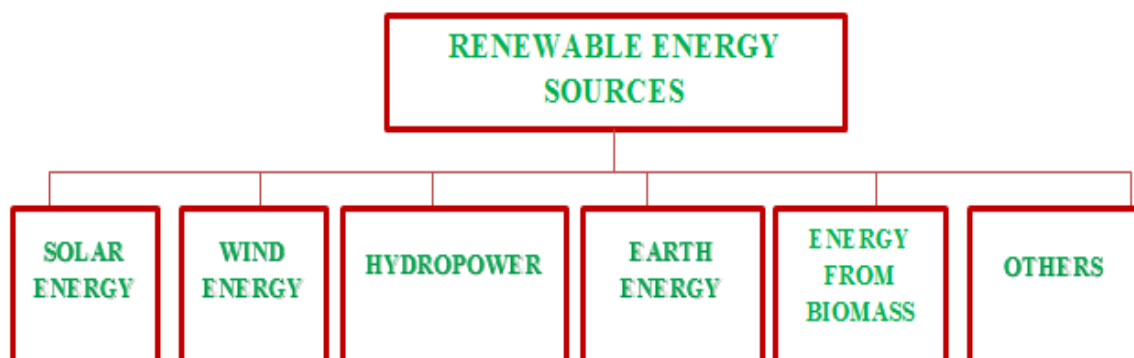


Fig. 1: Renewable energy sources

Knowledge of the relative limitations and exhaustion of conventional, non-renewable energy resources and limited capacity of energy supply from renewable energy sources, have an impact on energy and economic development, forcing all users to rationality and maximum savings [3]. Energy of the future, but not only it, completely should turn to renewable energy sources, which will stop any unreasonable and irreversible exploitation of non-renewable fossil fuels. It is, for sure, Solar energy, created millions of years ago, which humanity consumes in the most unreasonable and the most possible damaging way, often destroying their own environment, which is increasingly becoming a prerequisite for the survival of the civilization. Non-renewable energy sources, such as coal, oil and nuclear energy, by the end of the 21st century will have been replaced with new, renewable, environmentally clean, natural energy sources, especially Solar, wind, water, biomass and geothermal energy [4]. Solar energy can be used actively and passively. The active use of energy means the conversion of solar radiation, directly, into heat or electricity. On the other hand, passive use of energy refers to energy efficiency, in the use of Solar energy, for heating homes and other buildings [3].

Like most of the renewables, wind energy is also derived from solar radiation. Wind energy occurs like a circumstance of a complex process of weather, various soil heating and evaporation of water, which leads to differences in atmospheric pressure, at different geographical positions and movements of air masses from a higher to a lower pressure position [3].

Hydropower plants are plants in which the potential energy of water is first converted into kinetic energy of its flow, then into mechanical energy of the rotation of the turbine shaft and finally into electrical energy, in the generator [5].

Geothermal energy, in a narrow sense, includes only that part of the energy from the ground, which in the form of hot or warm geothermal media (water or steam) passes through the surface of the earth and is suitable for utilization in the original format (for bathing, treatments, etc.) or conversion to other forms (electricity, heat in thermal systems, etc) [5].

Biomass is a biodegradable part of product, waste product from agriculture, forestry and forest industry, plant and animal origin, which use of energy is allowed in accordance with the regulations of environmental protection [6].

In the world, there are attempts to beneficial use of other renewable energy sources. This mainly refers to the energy of seas and oceans [3].

3. SUSTAINABLE DEVELOPMENT

Establishing a balance between economic development and higher standards of living, with the population growth and depletion of natural resources, creates a conceptual basis for a entirely new approach to the development of humanity - sustainable development [1].

According to one of the most commonly used definition, sustainable development is one that meets the needs of humanity in the present, taking care not to jeopardize meeting the needs of those who will live in the future [2].

Sustainable development implies a balance between meeting basic needs and achieving a certain standard of living, with the available natural resources and preservation of the environment. In essence, sustainable development is a process in which there is a harmony between the exploitation of resources, direction of investments, orientation of technological development and institutional change, in order to improve the potential for the satisfaction of human needs, both now and in the future [2].

Many researchers agree that the terms sustainability and sustainable development could be described together as an improving of the life quality, in terms of a healthy environment, ie. improving the social, economic and environmental conditions, for current and future generations [2].

Vollenbroek argued that sustainable development is the balance between available technologies, innovative strategies and laws, passed by the Government of the country. Sustainable development is a challenge, on one hand there is a meeting of the growing needs of humanity to natural resources, energy, food, transport and waste management and on the other hand there are conservation and protection of the environment and basic resources, for the life of future generations and their development. This concept includes the view that in the long run human needs can not be met, without preserving the physical, chemical and biological systems on the planet [2].

Sustainable development encompasses three aspects, which are commonly referred to as pillars of sustainability [2]:

- the economic aspect,
- aspect of the environment and
- social aspect.

Previous illustrates the next figure 2.



Fig. 2: Sustainable development [7]

For the economic aspect it is necessary to ensure economic growth, in order to improve the life quality. The economy is therefore essential for long-term survival of the community. When we talk about sustainability, it is often associated with the aspect of the environment business practices, energy efficiency and sustainable business [2].

For the environmental aspect it is necessary to reduce to a minimum damage of the environment, pollution and exploitation of natural resources. Environmental issues make up the core of sustainable development and they are inextricably linked with the economic and sociological component. Community cohesion with its environment is complex and involves the exploitation of resources and consumption which acts to a local and also global eco-region [2].

For the social aspect it is necessary to ensure fairness in the resource distribution between the rich and poor. Social equality, in terms of sustainability, is usually considered as intergenerational, because the activities taken today affect the life of the community in the future. Sustainable development is aimed at improving the living standards of individuals, with short, medium and long-term preservation of the environment. Its goal is threefold; development which is based on economic efficiency, social justice and sustainable environmental protection. Discussion of the concept of the sustainable development in particular contribute the challenges that come with the vulnerability of the environment. Some of these challenges are: global warming, ozone layer depletion, the greenhouse effect, deforestation, the phenomenon of acid rain, the extinction of plant and animal species and the climate change, as the biggest and the most complex challenge that human society faces today [2].

3.1. Main aspects of the sustainability of the power system

The electricity system consists of generation, transmission, distribution and consumption of the electricity. The main task of this system is a reliable and quality supply of the consumers. This is the largest, most influential, the most necessary and the most widely used technical system, and it is, therefore, the most expensive. Once the electricity is produced in power plants it is handed over to customers. The settlements, cities and finally the whole country are interwoven with power lines that transmit electricity [8].

The electricity system is the most widely used, which follows from its size. The only system which could be compared to the power system is the Internet. But, even comparing it to the Internet, we can say that the power system is more widespread than the Internet because there are places where the electricity is available, but the Internet isn't. As well, to connect to the Internet, in most cases, it is necessary to have the electricity infrastructure. Nowadays, there is a number of 30 main energetic indicators of the sustainable development which are classified according to the three dimensions of the sustainable development [8]:

- economic dimension (16 indicators),
- dimension of the environment (10 indicators),
- social dimension (4 indicators).

Taken together, these indicators can give a picture of the whole energy system, including interconnections and exchanges between the different dimensions of sustainable development, as well as the long-term consequences of the current decisions and behavior.

Changes in the indicators, over the time, show the progress or its absence in relation to the sustainable development.

The next tables 1, 2 and 3 show mentioned indicators.

Table 1: Energy indicators for sustainable development - economic aspect [8]

ECO 1	The use of energy per capita.
ECO 2	The use of energy per unit of GDP.
ECO 3	The efficiency of the energy conversion and the distribution of energy.
ECO 4	The ratio of the energy reserves and production.
ECO 5	The ratio of natural resources and production.
ECO 6	The energy intensity in the industry.
ECO 7	The energy intensity in the agriculture.
ECO 8	Services/energy intensity in the store.
ECO 9	The energy intensity in the households.
ECO 10	The energy intensity of the traffic.
ECO 11	The fuels shares in the electricity and energy.
ECO 12	The energy shares that does not contain carbon in the power generation and energy.
ECO 13	The renewable energy shares in the electricity generation and energy.
ECO 14	The energy prices for end users by sectors and by fuels.
ECO 15	The dependence on energy imports.
ECO 16	The inventories of missing fuels at an appropriate consumption.

Table 2: Energy indicators for sustainable development - environmental aspect [8]

ENV 1	The emissions of greenhouse gases due to the energy production and use per capita and per unit of GDP.
ENV 2	The concentration of the air pollutants in urban areas.
ENV 3	The emissions of air pollutants from the energy system.
ENV 4	The discharge of the contaminated substances in the fluids, from the energy system, including the discharge of oil.
ENV 5	The land where acid rains exceed the allowable limits.
ENV 6	The ratio of the deforestation and the use of energy.
ENV 7	The production of solid waste per unit of produced energy.
ENV 8	The ratio of the correctly deflected solid waste and the total quantity of produced waste.
ENV 9	The solid radioactive waste per unit of produced energy.
ENV 10	The ratio of the solid radioactive waste, which is waiting to be removed, and total produced solid radioactive waste.

Table 3: Energy indicators for sustainable development - sociological aspect [8]

SOC 1	The share of the households without electricity or commercial energy, high dependence on non-commercial energy.
SOC 2	The share of the households income on fuel or electricity.
SOC 3	The energy use in households for each income group and corresponding fuel combination.
SOC 4	The number of accidents and injuries of the produced energy in the chain of the energy production.

4. THE GREEN ENERGY - THE ENERGY OF THE FUTURE

The role of the energy is to encourage the growth and the economic development of the Republic of Srpska, taking into account environmental protection. The development of the energy sector will be achieved by technological development, strengthening of the domestic companies, increasing of the investment and competitiveness of the economy of the Republic of Srpska.

In the Republic of Srpska, the most important renewable energy sources are the energy of the watercourse (in large hydro power plants) and wood (for heating in households). The potential for hydropower development is significant and largely untapped, but in the terms of renewable energy here is emphasis on the smaller streams, i.e. the construction of small hydropower plants. Also, there is a significant potential for using wind, solar, agricultural biomass and geothermal energy, but unfortunately, now they are particularly not used [9].

In the Republic of Srpska, producers of electricity from the renewable energy sources are entitled to incentives. Right at the instigation of electricity, produced from the renewable energy sources and efficient cogeneration, based on the Agreement on mandatory purchase of electricity for the production from the renewables at the guaranteed purchase price for electricity which is delivered to the network, currently achieve 52 companies [9].

The right to an incentive is realized by companies that own hydroelectric power, solar power, biomass or biogas. It is interesting that, at the moment, there are no wind turbines or power plants that utilize the energy of the Earth, during the electricity production, even though the objective conditions exist. Percentage share of various energy plants that are entitled to incentives is shown in the following figure 3.

Figure 4 provides information about the total amount of the mentioned power plants.

Although the percentage share of hydro power plants is lower than the solar plants, the total planned production of the electricity by hydro power plants is about 35 times higher than the solar plants. Also, the total planned electricity production of a biogas plant is about 2 times higher than the total planned production of all 35 solar power plants, although the solar power plants overall strength is much higher than the power of the biogas plant. Above said is shown in the figure 5.

Period, which is analyzed is the time interval of 4 years, from 2012 to 2016. The following figure 6 shows how varied the number of companies that have received the right to incentives, during the said period.

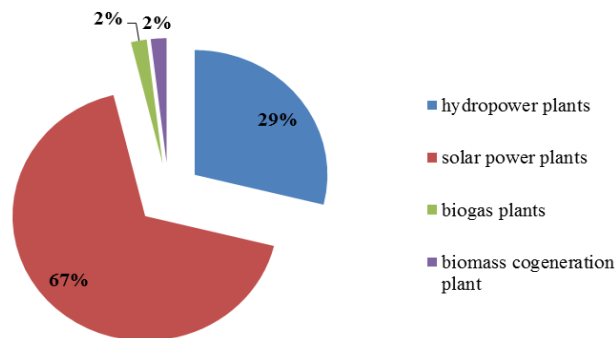


Fig. 3: Percentage share of various energy plants that are entitled to incentives

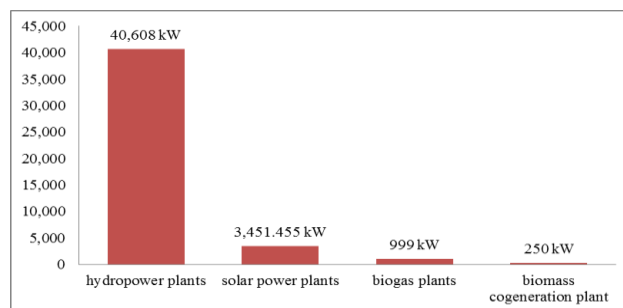


Fig. 4: Total amount of the power plants

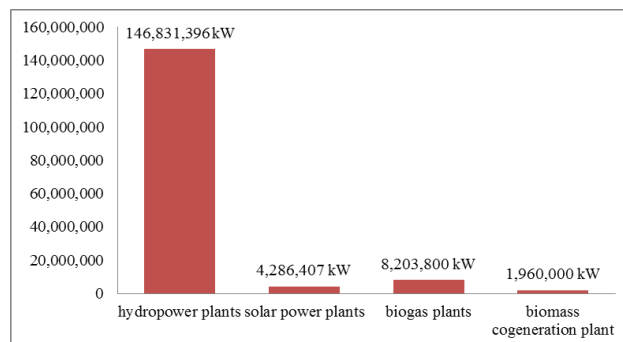


Fig. 5: The total planned electricity production of the power plants

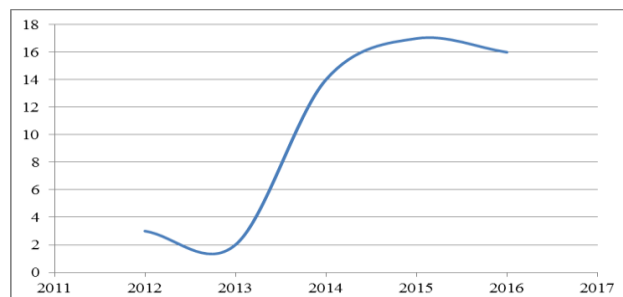


Fig. 6: Curve of the companies that have received incentives during the period 2012-2016

Since 2012, the share of renewable energy is steadily increasing, due to their enormous benefits. Figure 7 shows the share of renewable energy in the system of incentives

in the total consumption of the electricity in the Republic of Srpska and the figure 8 displays it graphically.

	UNIT	YEAR				
		2012.	2013.	2014.	2015.	2016.
<i>Total gross of the electricity production</i>	kWh	3.670.321.440	3.693.716.900	3.682.021.225	3.821.051.340	4.002.584.204
<i>The total electricity production from renewables</i>	kWh	5.049.206	24.650.412	42.095.078	45.143.269	112.902.081
<i>Participation of the renewables in total consumption</i>	%	0,14	0,67	1,14	1,18	2,82

Fig. 7: The share of renewable energy in the system of incentives in total consumption of the electricity in the Republic of Srpska [9]

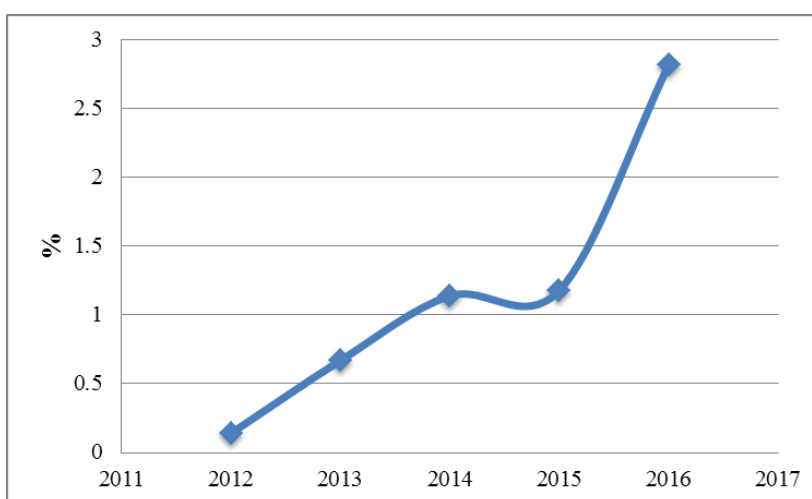


Fig. 8: The growth of the renewable energy sources in the system of incentives in the total consumption of the electricity in the Republic of Srpska

5. CONCLUSION

Humanity today faces great problems in the energy sector. There are growing energy needs of mankind, which is every day more and more increasing. Limited reserves of non-renewable energy sources with its emissions exhaust gases and particulates significantly affect climate change in the world.

Currently, as an environmentally friendly solution there are renewable energy sources. Like all new technologies, at this stage of development, the exploitation of renewable energy economically is not, yet, fully viable. As a result, many countries, with their various measures of incentives are affecting the development and the use of renewable energy sources, including the Republic of Srpska. Republic of Srpska with these measures seeks to

increase the spread of so-called application of the green energy.

Interconnection of economic and socio-cultural development, with the state of the environment, the need for the necessary natural balance, processes and global living conditions, today have become the part of the economic, political, normative-institutional and cultural reality of the modern humanity.

REFERENCES

- [1] NIKOLIĆ Z., PUCAR M., DAKIĆ P. (2006) *Renewable energy on Mount Athos*, Proceedings of the conference Alternative Energy and the future of their application, Podgorica, CANU, vol. 77, Department of Natural Sciences vol 10, pp 109-116.

- [2] VUČIĆEVIĆ, B. S. (2014) *Analysis and assessment of sustainable development of energy systems in the building (thesis)*, University of Niš, Faculty of Mechanical Engineering, Niš.
- [3] NIKOLIĆ, Z., KRAGIĆ R., PETROVIĆ S., ŠAMŠALOVIĆ S. (2010) *Renewable energy sources*, Union of Mechanical and Electrical Engineers and Technicians of Serbia, Belgrade.
- [4] NIKOLIĆ, Z., KRAGIĆ R., PETROVIĆ S., ŠAMŠALOVIĆ S. (2010) *Renewable energy sources*, Union of Mechanical and Electrical Engineers and Technicians of Serbia, Belgrade.
- [5] LABUDOVIĆ, B. (2002) *Renewable energy sources*, Energy marketing, Zagreb.
- [6] POČUČA N. (2015), *The environmental effects of the biomass application*, AGM books, Belgrade - Zemun.
- [7] https://www.google.ba/search?q=sustainable+development&source=lnms&tbn=isch&sa=X&ved=0ahUKEwjdL3EmabUAhUUIIAKHWAAtCIQQ_AUIB&biw=679&bih=468#imgrc=U2ocg41WBdvGZM: (05.06.2017.)
- [8] ANTIĆ D., KRSTIĆ I., ĐORĐEVIĆ A. (2013) *Indicators of the energy performance of the technological systems*, Safety Engineering, Vol 3, pp 151-160.
- [9] POWER UTILITY OF THE REPUBLIC OF SRPSKA (2017) *Report of the achievement of stimulating of the electricity production from renewable energy sources and efficient cogeneration in the Republic of Srpska for December 2016 and for the period January - December 2016*.

CORRESPONDANCE



Mirjana JOKANOVIĆ,
University of East Sarajevo
Faculty of the Production and
Management
Stepe Stepanovića; 89101 Trebinje,
Bosnia and Herzegovina
jokanovic.mirjana1@gmail.com



Dušan GOLUBOVIĆ, Prof. Dr. Eng.
University of East Sarajevo
Mechanical Engineering Faculty
Vuka Karadžića; 71123 East Sarajevo,
Bosnia and Herzegovina
dusan.golubovic54@gmail.com



Blagoje ŠUPIĆ, Ass. Sc. Ecc.
Power Utility of the Republic of
Srpska
Stepe Stepanovića
89 101 Trebinje,
Bosnia and Herzegovina
bsupic@ers.ba



Aleksandra KOPRIVICA,
University of East Sarajevo
Faculty of the Production and
Management
Stepe Stepanovića; 89101 Trebinje,
Bosnia and Herzegovina
aleksandra.koprivica@ymail.com

RESEARCH OF DEVELOPMENT AND PRODUCTION EFFECTS MACHINERY AND ELECTRIC SYSTEM FOR HYDRO POWER PLANTS ON THE BASIS OF ITS TECHNOLOGIES

Zdravko BIJELIĆ
Biljana MILANOVIĆ
Mijana JOVIŠIĆ
Bojan JELAČIĆ

Abstract: *The strategic objective of the Republic of Srpska should be to increase the production of electricity on the basis of new hydropower plants that will use equipment developed and manufactured in their own industry.*

The question that arises is: what kind of effects will be and what projects would be realized as a result of the realization of the set goal.

The effects would be historical, as the Republic of Srpska would get a stable, growing economic development system. First of all, from the classical capital-intensive model of low-power electricity generation, a modern labor – intensive model would be created that would enable the employment of an extremely large number of highly educated engineers of various profiles. Secondly, there would be a significant reduction in the cost of electricity. Reducing the cost of electricity costs means higher profit and the possibility of reducing prices and services in the Republic of Srpska, because electricity is included in the cost of cutting all other products and services. In this way, the products and services of the Republic of Srpska would be significantly more competitive on the export market.

Projects that would be realized through this concept of development are:

- 1. Development and production of turbines.*
- 2. Development and production of generators.*
- 3. Development and production of energy electronics and automation.*
- 4. Development and production of mechanical equipment and*
- 5. Development and production of logistics technology for advanced and other systems.*

Authors have been working for years on research on this extremely complex problem. The results of the research will be presented in the paper and indicated the necessary further directions of the research and the direction of realization of the set strategies and goal.

Key words: *Development, production, system, hydro power, technologies.*

1. INTRODUCTION

The transformation of renewable resources, a certain geographic space, into products that have performance of high level of value is the best known strategy of high intensity of economic development of this area .

If this strategy is implemented at the same time in a very short time, we have a dynamic growth of economic development. Furthermore, if such changes are supported exclusively by domestic knowledge embedded in their own technologies and, ultimately, if such an economy is managed effectively, then this can be called the economy of excellence [6] Today, in conditions of intense and dynamic changes in the environment of the observed entity, the appropriate force, that is, energy for a proactive change within the entity itself, is the system observed from the angle of applied system theory is required. [28] Within the overall economic system, the energy

production sub-system is today the basic subsystem of economic development.

When it comes to the territory of the former Yugoslavia, then it is the production of electricity, and it is a priority production of electricity based on renewable resources and own technologies.¹ The scientific-research project on the basis of which this applied scientific research was created deals with the problem of economic development of the Republic of Srpska, whose central sub-development is the development of the energy sector. Within this sector, viewed from the angle of value, the most important area is the area of renewable resources for the production of electricity. The key renewable source of electricity is the hydro-potential of watercourses. Within the overall problem of development and production of

¹ *This claim, as stated in mathematical terms, is an axiom.*

electricity based on hydro-power, the subject of this work is the production of electricity in hydroelectric power plants that would be built with their own technology, that is, equipped with equipment based on their own development and own production. Through the research published in this paper, the effects of the development and production of mechanical and electrical systems based on their own technologies that make up the hydroelectric power plant and logistic systems for energy transmission (First transfer of hydropower to hydro power plant and other, transmission and transformation from hydroelectric power plant to consumer).

The main goal of the work is to determine possible effects of development and production: turbines, generators, energy electronics and automation, machine equipment and various logistics equipment. The second goal is to create a development model for optimal management of the development and production of hydroelectric equipment. The third goal is for the practically realistic research space, Republika Srpska, to determine the benefits in case of realization of this integrated economic development project and production of the mentioned equipment. The paper sees the exceptional complexity of the research problem and subjects, as well as the huge number of questions that will have to be answered through the implementation of an extremely large number of projects.

The tasks that need to be realized in the paper are not defined. The task assignment is a huge project in itself. It is logical that the work of this volume can not be dealt with in the direction of further research, but in the end, a framework organizational model is defined which could provide effective strategic and operational management of this enormous project enterprise. A number of research hypotheses have been raised in this paper. All hypotheses have been confirmed on the basis of relevant data using the well-known and proven scientific-research methods and techniques. The paper consists of the following parts: Introduction, Problem Analysis, Model Development, Swot Analysis, Research and Conclusion.

2. PROBLEM ANALYSIS

2.1. General about the problem

In times of global economic crisis and the increasing development gap between rich and poor, energy is getting more and more important.² State communities that have their own energy are less vulnerable to the strong effects of the economic crisis, while those who are dependent on energy are increasingly lagging behind in development. Rich western countries that do not have enough of their own energy, through the mechanism of faster technological development and the knowledge-based knowledge in technology, provide energy not only for themselves, but also trade in energy. In this way, they

² *Development and crisis are from the angle of mathematics of the same size of a one-dimensional coordinate system. Development with a positive, and a crisis with a negative change.*

achieve a double effect. The problem of electricity generation must be viewed from the angle of change.

Changes are the only possible solution. The solution is the result of a change activity [1].³

Economy grown on the basis of its own natural potential is able to withstand not only the greatest crisis, but also disasters. Nations that are bravely preserving their natural resources, which are more fully processed in their own country, are visibly advanced in economic development. Resilience in the use of one's own natural resources is shown by the first and the starting conditions for successful development Economy [28].⁴

2.2 Analysis of the current situation

The production of electric power in hydropower plants in all countries formed on the territory of the former Yugoslavia for more than 30 years is realized on the basis of the same capacities, if the construction of an extremely small number of mini hydroelectric power plants is neglected. Considering the age of the equipment and the increased losses in the production, transmission and consumption of the consumer itself, probably the volume of electricity consumption is reduced in comparison with the 1990s of the last century.

The issue is arisen promptly, what will it be using the additional electricity generation? In order to make a correct conclusion we must know that electricity is technically marketed as a product that is embedded in other products and as a commodity for consumption. A state community that wants to develop and grow in the performance of its economic system must develop new production systems in which new added value will be created and in which new people will be motivated to participate in the development and growth of their company and the community as a whole.

3. MODEL DEVELOPMENT

3.1. The new development state of the problem

In this paper, we will only look at the new development state of the problem from the perspective of design, and the implementation of the projected state will be the subject of special work. The first question that arises now is the question that technology uses to transform the old system. From the front of the analysis it is evident that this is a new situation with the new structures, that is, the new production and business system with other structures and processes. It is a technology for change management, reengineering, or the technology of comprehensive systemically integrated development changes based on one's own knowledge. For such a complex set of managerial and technological activities it is inevitable to

³*The activity of change is movement*

⁴*The author of this quotation made a wrong conclusion Except possible drought, ie lack of water, and thus reduced hydropower.regarding the need to save water hydromechanical energy (the exception is dry periods).*

use intelligent business mechanisms and systems of excellence [34]⁵

The new developmentally integrated situation will be the result of developmental changes not only in the management of the electricity generation system, but also in this case, and development changes in the field of their own technological development.

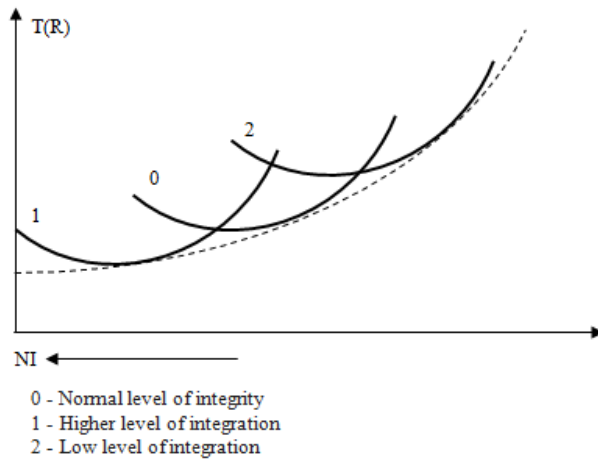


Fig.1: Dependent on cost of integrated management from the degree of integrity of NI. good quality figure with clear lettering

Considered the whole systemic level from a certain entity, the new state of the electricity production system in hydroelectric power plants means new generation of capacities for electrical, mechanical and logistic equipment. At the same time, it means a lot of employment in development and technology, above all the highly skilled technical staff, as well as staff for marketing and sales. The new state of the system is characterized by increased economies of scale, which will result in a reduction in the production cost of the unit of electricity. In this way, economically, they would get a new product that is significantly more competitive on the market.

New corporations that should emerge as a result of a public-private partnership would be socially very responsible and would have developed a corporate governance system.

3.2. Synthesis of effects and limitations

The effects, or the values of the newly developed electricity generation system, would be in the following:

1. New value would be multiplied: through a product that is more competitive, through its own technologies for electricity generation, through the development and conquest of a new product, through new employees who possess a large amount of technological and managerial knowledge of contemporary and traditional character and motivated for long term results In terms of efficiency and effectiveness.

2. A long-term, realistic growth in electricity generation

⁵ It is known that the complexity of the management of a single-hyecharchical system $SU = N!$ And multi-hierarchical system $SU = Nm$ (N is the number of elements in one level, and m is the number of levels).

would be ensured, which would be safe from the aspect of efficiency and effectiveness. This would have a stable and significant growth in the overall economy of the entity or state community concerned. Poverty and developmental differences in wealthy countries and fast-growing economies would soon be reduced.⁶

3. The production of electricity based on equipping hydroelectric power plants with equipment developed and produced by their own technologies based on their own knowledge is the only option for the poor to get out of poverty. To get out of poverty, they will not be helped by administrative membership in the EU or other world and European global institutions. [18]⁷

4. The subject development and production will enable extremely high employment of young highly educated engineers of various profiles and technicians in the processes of operational production of electrical energy and mechanical equipment for the needs of the construction of new hydropower plants. It will be significant that the departure of young highly educated and skilled people to work abroad will be reduced. Some traditional development and production knowledge that is archived in dirty warehouses and heads of a small number of other top researchers and experts who have worked on development projects in former powerful research and development centers and institutes for a long time [6]⁸

⁶ The present state of changes in the economy is primarily the result of financial flows and the impact of global character. The estimate is that today we have ten times higher GDP expressed through financial flows than is real, the result of a real economy. [30] This means that money is the largest commodity and largest demand in the global financial market. Of course, the most beneficial of this greatest benefit are wealthy entities (from a wealthy individual to a rich country). The result of this is the fact that the number of rich people is decreasing, but their wealth grows rapidly, and on the other hand, the number of the poor grows and their Wealth. Those who manage and decide on global financial flows are profit-oriented and secure and strengthen their positions by causing permanent financial and economic crises. However, in essence, the poor have a technological development crisis, better to say catastrophic, or no technological advancement. The current growth rates of the poor at the existing or somewhat higher level of wealth growth are in favor of the rich and are created through the IMF by wealthy countries and wealthy individuals.

⁷ The right solution for the emerging countries in the former Yugoslavia is to turn to their own technological development based on the growth of their own technologies in the field of natural resources. The authors of this paper, not only are not against EU accession, but are also about to do the same as soon as possible, because in this case they would have far fewer bureaucratic barriers in achieving their own technological progress. In addition, it would be easier to get the favorable investment funds needed for the development of their own technologies

⁸ With the disappearance of this generation with the experience of applied development, we are in danger of

5. There is no doubt that the most complex constraint, that is, resistance to the implementation of this historically possible project is expected from the administration and people in the administrative decision-making positions. The most common resistance to implementation will be the result of ignorance and unwillingness, as well as the lack of ability to make such a major change on all levels. The personnel, primarily technical and economic profiles, are to study the model and expand the necessary messages that the project can bring. It is necessary that many people change in order to be able to deal with developmental changes, because the solution is still the most complex social activity. Development is concerned with the design and implementation of the future, the future is always uncertain and full of risk.

6. The realization of this project would mean parallel development of education and continuous learning and education of people. Then the growth of citizens' standards through, increase in consumption, and hence the growth of public revenues. There would be a huge increase in the social responsibility for responsible allocation for projects of social development. An appropriate outcome is also expected in the area of democracy, human freedom and the development of legal security and the reduction of all forms of deviant behavior by individuals and institutions, as well as the growth of all forms of civilized behavior and accountability towards human values.

7. Significant resistance can be expected among university teachers and scientists at the institutes, who do not possess knowledge in the field of applied research and applied development.⁹

3.3. Optimization of technology management

The first author of this paper has developed an enormous number of mathematical models of optimization solving in his long-standing career, dealing with development, various development problems and situations. His scientific point of view is that any sort of complex situation can be mathematically modeled in order to search for the optimum solution. [7].¹⁰

If E is the measure of the efficiency of electricity generation¹¹, and Xi is a set of input factors that affect efficiency. In mathematical form, the dependence of

entering a full developmental discontinuity or worse developmental darkness. Different development agencies will help us in solving this problem, because they are intermediary organizations that sell their knowledge to the poor (Example of footwear sales in Africa [2]).

⁹ It is known that resistance to change decreases with increasing knowledge

¹⁰ Optimization in most cases reduces to the search for an optimal size for the constraint of a specific resource and the size of the parameter that produces the level of engagement of that resource. Also, optimality in the case of development is often the optimal combination of traditional and contemporary values.

¹¹ For the measure of efficiency, it is best to take a newly created value per unit of power or the amount of energy produced at a certain time interval.

efficiency (E) on input variables can be given in the following form:

$$E(X) = F(X_1, X_2, \dots, X_i, \dots, X_n, t) \quad (1)$$

Since the input quantities are subject to change, that is, the function of time, the efficiency (E) will be simultaneously in function of time (t). The key input parameter X is the technology. In addition to the technology, the structure of the parameters Xi will be different depending on the hydroelectric power plant to the hydroelectric plant, from situation to situation.

Since the construction and production of the hydroelectric power plant is a very long-term project, with small fluctuations in the production volume on an annual basis.¹² Time as an independent variable in formula (1) can be excluded.

Technology as a key influencing factor on the effect of electricity generation consists of external and internal (own) technology.

If K is external technology and L is an internal (own) result of our own knowledge and operational work, then the efficiency of electricity production will be a function of these two technologies. We will explain efficiency (E) in the form of costs, and as such, as a sum of the cost of external technology K and internal L, so we will have it:

$$T = K + L = f(L) + L \quad (2)$$

Where the $K = f(L)$ project determined the correlation between external and internal technology.

If there is no correlation between external and internal technology then the cost will be a function of two unrelated variables K and L.

Optimization is now reduced to a differential account of one or two variables. In the case of one variable L - native (own) technology, the optimal solution will be where $(dT / dL) = 0$ and where $(d^2T / dL^2) > 0$.

How is the correlation between external and internal technology

$$K = f(L) \text{ and } T = f(L) + L \quad (3)$$

We will have optimal production of electricity in the hydroelectric power plant where:

$$(DT / dL) = 0 \text{ and } (dK / dL) = -1 \quad (4)$$

In this way we can determine the optimal combination of external K and internal L technology.

The problem of electricity generation can be modeled in mathematical form by setting that the costs of electricity generation are the sum of the costs of investing (I) and operating costs of production.

$$T = T(I) + L \quad (5)$$

$$(DI / dL) + 1 = 0 \text{ and } (d^2I / dL^2) > 0 \quad (6)$$

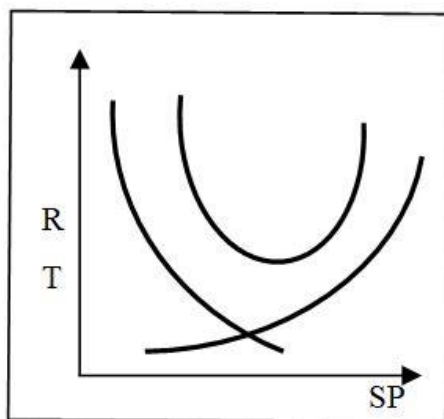
The subject of optimization can be various indicators related to the technology of electricity production in hydroelectric power plants:

- The relation between modern and traditional technology,
- The relation between internal (own) and external technology,

¹² Except possible drought, ie lack of water, and thus reduced hydropower.

- Optimization of automated management,
- Optimization of capacities, more precisely, installed power of turbines and generators.
- Optimization of water flow,
- Optimization of the repair period,
- Optimizing the relationship between investment and operational costs,
- Optimizing the investment risk,
- Optimization of the degree of justification of investment,
- Optimizing investment in knowledge, ie human resources,
- Optimization of the management of the construction phase of the hydroelectric power plant,
- Optimizing the sales price of electricity
- Optimization of quality control and other.

Figure 2 presents a graphic illustration of risk optimization related to the degree of change in the existing initial state Technology. Curve 1 represents the flow of costs due to the rate of change (SP). Curve 2 represents the risk, that is, of the costs of possible non-performance, and they decrease with the growth of the degree of change. Curve 3 is the overall risk and total cost. The optimum level of technology change will be in the lowest cost zone, that is, at the lowest risk zone.



R - Risk
T - Costs
SP - The degree of change

Figure 2: Costs and risks depending on the degree of change

Optimization in this case consists in determining the optimal degree of change. The optimal degree of change is the one with the least total cost (Curve 3).

In conditions of intense and dynamic changes in the environment, we need to be trained for proactive management, that is, behaviors that will constantly lead us to finding optimal solutions. Looking for the optimum flow of the process of replacing external technologies with an internal (own) project is of exceptional complexity, but undoubtedly of enormous benefits, both from the aspect of the economic and from the aspect of social justification.

3.4. Organizational mechanism

The project for the development and production of mechanical and electrical systems and other logistic

systems for the start must be organized as a complex project for which governments of individual countries will make decisions on how to operate. The project should have initial management and operational management. In Serbia, the project could be organized locally in the Ministry of Education and Technological Development, and in the Republic of Srpska within the Ministry of Science and Technological Development.

At a later stage, when the project becomes a reality with sufficient support for functioning, the Ministry of Development or a department should be set up parallel to one of the existing ministries. In parallel with this latest activity, it is necessary to establish at the beginning a public institution for the development of machinery and electrical equipment for new hydropower plants. In the next step, a public institution would be transformed into a modern corporation that would involve various partners in accordance with corporate governance rules.

4. SWOT ANALYSIS

The objective of the SWOT analysis, as well as the overall work of this paper, is to create a critical mass of research and development and research and professional individuals based on argued scientific research and proofs that will follow the goals and possibilities of this paper. This would also be a strategy created through this work. It is known that swot analysis involves an analysis of: power, weaknesses, opportunities and threats related to a particular project or activity.

The strengths of the project are:

The greatest strength of the project is the fact that the former Yugoslavia has a huge amount of unused energy hydro potentials.

We still have a significant amount of knowledge related to the production of electricity in hydropower plants.

We have a critical mass of young engineers of various professions, as well as students at technical faculties, who will be a competent logistical support to the project.

The project provides the possibility of partnerships of interested partners.

Possible phase realization of the project and phase financing.

The Republic of Srpska has exceptional hydro potential for the construction of hydro power plants of various sizes of power.

The disadvantages of the project are:

The biggest weakness of the project is that we do not have a critical mass of people from knowledge and science who are able to understand how important this project is.

Hydroelectric power plants are projects that are cost-effective in the long run, efficient and effective in the long run

The disadvantages are that young people in reality do not have enough competence for development projects. Electricity companies do not allocate depreciation funds to a separate account in order to invest in new projects. Lack of development initiative in ministries and public enterprises in the field of electric power industry. Great financial indebtedness of public utility companies. Abuse in public procurement.

In Republic of Srpska, and partly in Serbia tycoons have been installed in a very important position, from which they have a huge influence on decision-making. Adapting laws to their own needs and abusing public positions for personal interests. On the other hand, the bravest are leaving us. Those who went away significantly reduced the average level of intelligence and abilities to those who remained. It is valid for all areas, and of course for sports.

The possibilities of the project are:

The project can integrate traditional and modern technological and management values of electricity generation by choosing the optimal combination of one and the other values.

Electricity produced in hydropower plants on the basis of own technologies will be much more flexible, and thus significantly more adaptive to the requirements of the market, that is, different buyers.

By incorporating low-cost electricity into other products, it will lead to more competitiveness of exports from the observed space.

The need for a highly educated staff profile will lead to the development of higher education.

Using our traditional values and capabilities, we create conditions for more efficient business in the field of electricity generation and some other products.

The threats of the project are:

At the level of global economy and at the level of smaller economies and economic systems and at the current level, the prevailing speculative financial economy is the realm of the real economy, which is offered by the project. The real biggest threat to the project is the administration, traditional entrepreneurs, holders of political functions and tycoons. They are all short-term oriented both for efficiency and effectiveness, and most often for profit. Problem centralization of decision making. Lack of development organizations.

Problem structure of ministries:

Lack of planning system. Lack of integrated management and decision-making. Lack of the concept of technology development based on its own technologies. The existing higher education system does not educate personnel for development activities. Lack of study programs for economic development, but only a study program for improving operational activities.

5. RESEARCH

5.1. Synthesis of research

Due to the limited scope of work, as well as the complexity of the problems and the projects on which these research is based, the paper gives a shorter shorter synthesis of the research.

The main goal of the work is to determine possible effects of development and production: turbines, generators, energy electronics and automation, machine equipment and various logistics equipment. The second goal is to create a development model for optimal management of the development and production of hydroelectric equipment. The third goal is to determine the effects for the realization of this integrated economic development

project and the production of the mentioned equipment for the practically realistic research space, Republic of Srpska.

The following research hypotheses are set out in this paper:

Basic hypothesis:

Production of electricity in hydropower plants built on the basis of mechanical, electrical and logistic equipment

Which is developed and produced on the basis of its own technologies is a project of economic excellence and a revolutionary-radical character for the premises, that is, entities that have hydropower potential.

Additional hypotheses:

First: For the realization of this revolutionary-radical development project, people who possess the applied research and development skills are needed. They must, in partnership with state institutions, be effective and efficient in the long-term oriented since this is a long-term project. Second: In addition to the exceptional economic and wider social benefits of the project, huge resistance to the realization is expected Project by a large number of powerful and influential individuals and institutions.

Specific hypotheses:

First: Republika Srpska has huge unused hydro power potential, and from that aspect it represents an ideal area for the realization of the project of electricity production in hydroelectric power plants that would be built on the basis of equipment that would be developed and produced by its own technologies. Second: Republika Srpska does not have enough competent human resources to implement the entire project in the Republic of Srpska. Third: The Republic of Serbia has competent human resources, institutions and institutions, and can organically, along with the installation of the necessary organizational mechanism as a partner, stand behind the successful realization of the project of electricity generation based on equipment that would be developed and produced by its own technologies results of the Based on the analysis given in the points: 2. Analysis of the state of the problem, 3. The development of the model, the swot analysis and the research given and published in other projects and scientific research papers [6, 9, 12, 13] can be accepted that all hypotheses Confirmed with high probability using the scientific method of analysis and synthesis and logical conclusion.

5.2. Directions of new research

Research carried out in this paper is of a strategic nature and should serve as a scientific and research logistics to create a scientific and professional climate that it is possible to develop and produce equipment for hydroelectric power plants in the former Yugoslavia that would generate electricity with significantly lower cost price than the situation now. It will be necessary to define a very large number of research projects such as:

1. Development and production of turbines.
2. Development and production of generators.
3. Development and production of energy electronics and automatics.
4. Development and production of machinery and equipment

5. Development and production of logistics technologies for forward and other systems

In particular, new research has to be research related to investment and investment financing, as well as the organizational mechanism necessary for the successful implementation of the project. A special subject of research must be possible resistance to the launch of a power generation project based on equipment that would be developed and produced by its own technologies. One of the key research projects would be the education of personnel for the needs of the new economic system, which is the result of the production of "New Electricity".

6. CONCLUSION

With this work, in the spirit of scientific knowledge, it is clearly revealed and defined what would be the subject of management and decision-making. It would be a new excellent product "new electricity" as a result of systemic creative thinking. With great reliability, it can be argued that the new electricity will have better performance than the electricity transformation that would be produced in hydropower plants built on the basis of equipping equipment from abroad.

The second and most complex question about change and decision making is to translate the system from the current state of the value into a newly created project. The mechanism of transformation using own technologies for the production of hydroelectric equipment is possible with a huge economic and environmental benefit. However, it is indisputable that many of the resistance and problems will be found along the way of project realization. The research carried out in this paper is sufficient for the competent authorities on the basis of the same to determine in the first step the strategy for the production of electricity in hydropower plants based on equipment developed and produced by internal (own) technologies. By entering this model of electricity generation, in the Republic of Srpska and in other countries in the region, in the second phase, the production capacities of the new technological form should be built. This involves the processing of existing raw materials with the use of new electricity. It will be possible to build a large number of industrial capacities for primary and secondary wood processing. In addition to this area, new electricity will also be used in agriculture and the food industry. New electricity will be used for heating in households, in this way we will be less dependent on gas imports. The electricity produced in this way can be used for electrically powered vehicles.

REFERENCES

- [1] ADIŽES, I. (1994) Upravljanje promjenama, Prometej, Novi Sad, Serbia.
- [2] ADIŽES, I. (2009), Kako izaći iz krize, Asee, Novi Sad, Serbia.
- [3] ADIŽES, I. (2005.), Težnja ka top formi, Asee, Novi Sad, Srbija .
- [4] BAJEC, J.& JOKSIMOVIĆ, Lj, (1993) Savremeni privredni sistemi, Ekonomski fakultet, Beograd, Serbia.
- [5] BIJELIĆ, Z: (1981), Control modelling optimal production development, VI ICPR, Novi Sad, Serbia, pp 385- 388.
- [6] BIJELIĆ, Z. i MILANOVIĆ, B., Savremeno upravljanje razvojem, Neobjavljena knjiga, Novi Sad, Serbia.
- [7] BIJELIĆ, Z i BIJELIĆ, M., Matematičko modeliranje optimizacije razvojnih procesa i sistema, Neobjavljena knjiga.
- [8] BIJELIĆ, Z., MILANOVIĆ, B. & JOVIŠIĆ SIMIĆ M. (2017), Industrial system :transformation and development, IS'17, Novi Sad, Srbija.
- [9] BIJELIĆ, Z. (1982), Modeliranje optimalnog planiranja razvoja proizvodnih sistem SYMOPIS'82, Herceg Novi, Serbia, pp 24-28.
- [10] BIJELIĆ, Z. (1990), Optimizacija automatizovanosti testiranja elektronskih uređaja Naučna konferencija IS'90, Novi Sad, Serbia, pp 24-27. Serbia,
- [11] BIJELIĆ, Z. (2014), Matematičko modeliranje razvoja poslovnih sistema i procesa, 2. nacionalna konferencijasa međunarodnim učešćem „Menadžment, sport i turizam“ MASTA-2014, Banja Luka, Bosnia and Hercegovin, pp 83-90.
- [12] BIJELIĆ, Z. (2014), Ograničenja i mogućnosti upravljanja razvojem i krizom Republici Srpskoj, IV Međunarodna konferencije OD KRIZE DO RAZVOJA, Zbornik radova pp 9-28, Banja Luka, 2. B&H.
- [13] BIJELIĆ, Z. & CVIJIĆ, M. (2011), Own production technology as a key out of powerty, Intrnational svojstvu partnera Scientific Conferen CAPITALISM ITRANSITIO Belgrade, Zbornik radova pp 181-190, Serbia.
- [14] BIJELIĆ, Z. (1990), Optimizacija automatizovanosti testiranja elektronskih uređaja, Naučna konferencija IS'90, Novi Sad, Serbia, pp 24-27. Serbia.
- [15] BLANŠAR, K. O'KONER, M. (2003), Upravljanje putem vrednosti, Prometej, Novi Sad, Serbia.
- [16] ČOBELJIĆ, D, (1978), Planiranje privrednog razvoja, Rad, Beograd, Serbia.
- [17] DRAKER, P. (2005), Upravljanje u novom društvu, Asse, Novi Sad, Serbia.
- [18] GALBRAITH, J.(1995), Ekonomija u perspektivi, Mate,Zagreb, Croacia.
- [19] GALOGAŽA, M. (2001), Filozofsko-etički aspekti logičkog upravljanja tržištem poslovanja, MM College, Novi Sad, Serbia
- [20] GALOGAŽA, M. (1999), Strategija društveno-ekonomskog razvoja Republike Srpske, M&M College, Novi Sad, Serbia.
- [21] HORVAT, B. (2007) Dinamičan ekonomski razvoj, ECPD, Beograd, 2007.
- [22] IVOVIĆ, M. (1996), Optimizacija u ekonomiji, Ekonomski fakultet, Beograd, Serbia.
- [23] Jarić, D., Bijelić, Z., Tairova, M., Mohači, T., Savremena analiza privređivanja, 2. Nacionalna konferencija sa međunarodnim učešćem „Menadžment, sport i turizam“ MASTA-2014, Zbornik radova pp 169-176, Banja Luka.
- [24] MEJOVŠEK, M. (2005), Metode znanstvenog istraživanja, Naklada slap, Zagreb, Croacija.

- [25] MILANOVIĆ, B. & BIJELIĆ, Z. (20015), Razvoj modela za upravljanje integrisanom procenom vrednosti, XX internacionalni naučni skup CM 2015, Subotica, Zbornik radova pp 422-444, Serbia.
- [26] MILANOVIĆ, B. & JOVIŠIĆ, M. (2017), Effects of education of entrepreneurs abo financial management, ITRO 2017, Zrenjanin, Serbia.
- [27] MILANOVIĆ, B. & JOVIŠIĆ, M. (2017), Effects of education of entrepreneurs abo financial managemen ITRO 2017, Zrenjanin, Serbia.
- [28] MILOJEVIĆ, A.. (2007), Male hidroelektrane,
- [29] SAZDANOVIĆ. S. (1977), Posleoptimizacija ekonomskih sistema modrlima parametarskog programiranja, Naučna knjiga, Beogrsad, Serbia..
- [30] RISTIĆ |Ž. i KOMAZEC, S.(1996), Globalni finansijski mendžment, Čigoja, Beograd, Serbia.
- [31] SAZDANOVIĆ, S. (1975), Posleoptimizacija ekonomskih sistema modelima parametakog programiranja, Savremena administracija, Beograd, Serbia.
- [32] TOMOVIĆ. R, (1977) , Ograničenja formalne teorije upravljanja sistmima eorije upravljanja, Serbia.
- [33] ZELENKA, R. (2000), Metodologija i tehnologija izrade naučnog i stručnog rada, Ekonomski fakultet, Rijeka, Croacia.
- [34] ZELENOVIĆ, D. (2011), Inteligentno privređivanje, Prometrij, Novi Sad, Serbia
- [35] BIJELIĆ. Z i saradnici, [2014] Projekat razvoja Republike Sroske, Banja Luka, B&H.
- [36] MALE HIDROELEKTRANE, Savey ma[inskih i elektrotehni;kih in/enjera i tehni;ara Jugoslavije, 1984, Arandjelovac.
- [37] Strategija tehnološkog razvoja Jugoslavije, Beograd, 1987.
- [38] Biynis asocijacije ya 21 vijek, Centar za medjunarodno privatno preduzetništvo, Sarajevo.
- [39] Aktuelni energetske projekti Republike Srpske, Ministarstvo industrije, energetike i rudarstva, Banja Luka.
- [40] Postkrizni model privrednog rasta i razvoja Srbije 2011 – 2020, USEID i Fond razvoja ekonomskih nauke.
- [41] Vodič kroz korpus znanja za upravljanje projektima (PMBOK vodič), Prevod FTN Novi Sad.
- [42] Program podrške malim i srednjim preduzećima u Republici Srbiji, Ministarstvo ekonomije i regionalnog razvoja.
- [43] Program upravljanja riječnim slivom za BiH. Progran Evropske unije.

CORRESPONDANCE

Zdravko BIJELIĆ,
 Institut u osnivanju LOGOS
 Novi Sad
 Serbia
bijeliczdravko51@gmail.com

Biljana MILANOVIĆ,
 Ekonomski fakultet Subotica
 Subotica
 Serbia
dusan.golubovic54@gmail.com

Mijana JOVIŠIĆ,
 Univerzitet ALFA-BK
 Beograd
 Serbia

Bojan JELAČIĆ,
 Fakultet tehničkih nauka
 Novi Sad
 Serbia

HYDRAULIC ANALYSIS OF THE WATER SUPPLY SYSTEM IN TOWN NEVESINJE

Stanka D. KULJIĆ
Uroš M. KARADŽIĆ

Abstract: *The water supply network is an essential part of water supply system. It has a task to provide distribution of necessary quantities of water under appropriate pressure from the source to each consumer while keeping the process cost sensitive. In this paper, a hydraulic design of water supply network of the town of Nevesinje, Bosnia and Herzegovina, have been conducted applying an original and newly developed numerical model for simulation and calculation of pipe networks in steady operating conditions. This model is created in Visual Fortran and is used for simultaneous solving of systems of equations which describe a steady flow in pipe networks, regardless of the number of pipes and nodes. The system of equations is solved by the Newton-Raphson Method. The results obtained by the numerical model have been compared with those obtained by means of the commercial software AFT Fathom 6.0. Based on good matching of the compared results it can be concluded that the developed numerical model is applicable in engineering practice.*

Keywords: *hydraulic analysis, numerical modelling, optimization, water supply system.*

1. INTRODUCTION

In accordance with quantities of water required for water supply and characteristics of a water supply network (material performance, position and operating conditions of network facilities, topographic conditions) it is necessary to carry out a hydraulic network design to provide a sufficient amount of water and pressures to fulfill customer demand. The water supply system has to be modeled and analyzed under the various physical and hydraulic parameters or conditions. The hydraulic analysis serves as an efficient decision-support tool for the management, development and reconstruction of the water supply system. Hydraulic modelling is a technique to represent mathematically the water distribution system using software programs and applications. Regardless of technical or other differences among water supply networks that meet needs of various users, there are also similarities that provide a unique approach to their hydraulic analysis based on creation of a mathematical model [1, 2]. The novel contribution of this paper is in its presentation of results obtained from a newly and originally developed numerical code written in Visual Fortran. This model is developed for a hydraulic analysis of water supply networks in steady conditions, regardless of the number of pipes and nodes. In the first part of the paper, the mathematical model of the flow in water supply networks is presented along with the main methods for their numerical solution. In the second part of the paper, were stated the main characteristics of that part of town's water supply network for which the analysis had been done and the results obtained by a developed numerical code (in-house software) are compared with those

obtained by commercial software AFT Fathom 6.0. for the present state of the part town of Nevesinje water supply system. Based on a very good match between them it is concluded that in-house developed software is applicable in engineering practice

The mathematical model of water flow in pipe networks is created by applying the basic laws of Fluid Mechanics to network elements, customizing these laws to specific conditions of movement in certain areas of flow and expressing them in the form of algebraic, differential and integral equations. Resulting equations describe idealized flow field at each point at any time. The changes of the flow field described in this way depend on the initial state, boundary conditions and the value of flow parameters. A solution exists but it cannot be found directly. In these cases, some methods providing approximate solutions are used (empirical methods, theoretical and analytical methods and simulation methods [1, 2]. The most commonly used approach is a numerical simulation that provides approximate solutions of equations of mathematical models obtained by the application of numerical methods. The choice of a numerical method depends on the manner of formulation of a mathematical model.

In order to speed up the calculation, reduce the number of unknowns and increase transparency of results, certain rules and assumptions are used to design a mathematical model of pipeline network which ultimately influences the quality of a numerical simulation. Key assumptions introduced in the hydraulic calculation, under which these laws apply, are as follows [2]:

- the flow is steady
- the fluid is incompressible,

- all variables (flow, velocity,...) were integrated per cross-section of pipes and replaced by corresponding mean values,
- it is admitted that dominant forces are gravity and friction forces,
- number of drain and water supply spots in the network is large and they are fictively reduced into nodes for reasons of simplification,
- pipes and nodes are the main elements of distribution network,
- the assumption is that cross-sections are constant along the pipe,
- other elements of pipe network (fasteners, pumps, etc...) are usually included in calculation through the pressure loss at the points of their installation i.e. local losses that occur at those locations,
- there are two main variables defining the situation in the network: the pressure at certain points and flow rates through the pipes. Piezometric heads presented mostly in network nodes are used instead of pressures. The computational model of a network, obtained in this way, should provide a reliable engineering analysis and hydraulic calculation in spite of being significantly simpler than the real distribution network.

1. MATHEMATICAL MODEL

Pipe networks are system of complex pipelines containing one or more lines in the form of closed circuits whereas consumers are supplied from the nodes through manifolds and branches. While forming a mathematical and numerical model of pipe network it is usually considered that water consumption along the pipe is concentrated in nodes. Then, considering the assumption that the flow is steady, continuity equation for the pipe provides a trivial result $Q = const$. It is commonly assumed that a piezometric head is the same at the ends of all pipes meeting in a node, which eliminates the need to consider the equations for conservation of momentum or energy for nodes. Therefore, only equations of continuity for nodes and energy equation for pipes or conservation equations for momentum are used in the steady flow model of pipe networks [1, 3]. The equation of continuity states that the sum of the flow in each of the nodes is equal to zero.

$$\sum_j \pm Q_{ij} + Q_{ip} = 0 \quad (1)$$

where: Q_{ij} - the flow through the pipe that connects node i and node j , Q_{ip} – nodal consumption assigned to the node i , n_i – number of pipes meeting at node i . Equations of continuity can be written for all network nodes. Out of these there are $i-i_r$ mutually independent equations where, i_r is a number of nodes with known piezometric heads. Number of equations provided in this way is sufficient for solving problems only in the simplest cases of dendritic pipe networks whereas for looped pipe networks additional equations must be set.

In order to form additional equations a second condition is used, i.e. pressure drop (or algebraic sum of all energy losses) per closed contour is equal to zero. This condition arises from the energy (Bernoulli) equation written for the

beginning and the end of each pipe. Based on this condition a following equation can be written for each circle [4, 8]:

$$\sum_{j(l)} \pm \Delta p_{ij(l)} = 0 \quad (2)$$

The pressure drop through the pipes can be calculated using the expression:

$$\Delta p = \rho \lambda \frac{l_{ij}}{d_{ij}} \frac{v_{ij}^2}{2} \quad (3)$$

Where, v - is the velocity (m/s), ρ -density(kg/m³), λ -coefficient of friction, l -pipe length(m), d - diameter of pipe (mm).

If velocity is expressed in terms of the flow rate, $Q = vA$, and piezometric head or head ($H = p/\rho g + z$) are introduced instead of pressure, the equation for the circular cross-section pipe can be written in the form:

$$\sum_l r_{ij(l)} Q_{ij(l)}^0 \left| Q_{ij(l)}^0 \right| = 0 \quad (4)$$

where, r_{ij} is the characteristic of the pipe which is equal to,

$$r_{ij} = 8 \frac{\lambda l_{ij}}{d_{ij}^5 \pi^2 g} \quad (5)$$

where, π -Ludolph's number ($\pi=3,14159$), g -the constant of gravity.

The equation (4) is used to calculate the energy loss along the section of length l_{ij} because differences in piezometric heads and energy differences are the same within the pipes of a constant cross-section.

$$\Delta E_{ij} = \Delta H_{ij} \quad (6)$$

Number of equations formed in this manner is equal to the number of natural loops that not overlap each other. In the cases when there are at least two reservoirs (nodes with known heads), a concept of a pseudo loop is introduced whereas a pseudo loop ends with a single fictive pipe which connects two reservoirs. A pseudo loop might be understood as a usage of the condition that per any path connecting two reservoirs the sum of energy losses is equal to a difference between the levels of these two reservoirs. Number of equations for pseudo loops is equal to $i_r - 1$, and the total number of equations that can be obtained in this manner is $(i + k_l - 1)$ and it is equal to the number of unknown flows in pipes. Number of linear equations is $i - i_r$ and the rest of them are non-linear and can be linearized during the process of solving. For the calculation of a circular network some of iterative methods of calculation are mostly used, which can be obtained by the application of numerical analysis and some numerical techniques for linearization of equations. The most commonly used methods are: the numerical method of minimization, the Hardy-Cross method, the Newton-Raphson method and the linear theory method .

The Newton-Raphson method is based on simultaneous solving of M non-linear equations in the form of

$$\sum_{j(m)} r_{ij} * Q_{ij}^2 = 0 \quad \text{where, } r_{ij} = 8 \frac{\lambda_{ij}}{d_{ij}^5 \pi^2 g} \quad \text{and N linear}$$

equations in the form $\sum_{j=1}^{j_i} Q_{ij} + Q_{ip} = 0$ [1, 3].

The newly developed numerical model is created for the hydraulic analysis of the circular pipe network with simultaneous solving of systems of equations describing steady flow in pressurized pipe networks. Software is created in a Visual Fortran numerical code based on a mathematical and numerical model for solving problems of a steady flow in pipe networks and it is applicable to any water supply network regardless of the number of pipes and nodes [14]. The mathematical model of a steady flow has been reached by the application of equations for conservation of mass for nodes and equations for conservation of momentum for pipes and the formation of systems of equations for the observed pipe network. In this manner, a system of non-linear algebraic equations was obtained whose number is equal to the number of unknown piezometric heads in nodes:

$$\sum_j SGN(H_i - H_j) \left(\frac{(H_i - H_j)}{r_{ij}} \right)^{1/2} + Q_{ip} = 0 \quad (7)$$

For the purpose of linearization (that is solving the system) Newton-Raphson method was applied.

$$\frac{1}{2} \sum_{i=1,2,\dots,(I-I_R)} \frac{H_i^{(k+1)} - H_j^{(k+1)}}{r_{ij} * Q_{ij}^{(k)}} + Q_{ip} + \frac{1}{2} \sum_j Q_{ij}^{(k)} = 0 \quad (8)$$

A resulting system of equations is solved by the iterative approach applying the method of a successive over-relaxation [2,4].

3. DESCRIPTION OF THE WATER SUPPLY SYSTEM

The distribution network operation analysis was performed on the basis of established hydraulic scheme (fig 1.). This scheme was created using the geometry-system, connections of nodes, lengths and diameters of sections, objects in the system and their capacity, and distribution to consumers. All data has been taken from the existing scheme of the water supply system of the town of Nevesinje and consumption data available from a local water supply company.

– During the formation of the mathematical model for the pipeline networks, apart from the previously mentioned basic assumptions in application of fundamental equations of Fluid Mechanics, following simplifications are introduced for the real network, [2,4]: Small individual ports along the pipe are not considered individually but the total flow at all junctions along the

pipe is divided and assigned to neighboring nodes as "nodal consumption"; local losses at regulating valves, pressure reducers and similar elements that actively influence water distribution must be taken into consideration; available pipes of a smaller diameter with the known consumption are excluded and their flows are added to the nodal consumption of the node;

This schematic overview presents all real elements of the water supply system (reservoirs, pump stations, pipelines), and the resulting model comprises the following:

- 32 nodes defined by name, label, terrain elevation and consumption,
- 45 sections defined by name, diameter, length and type of material,
- 1 reservoir determined by the bottom elevation, spillway elevation, elevation of the feeder pipeline, shape etc.

In determination of the total consumption, the water losses in the system that could not be accurately determined, because of lack of data, have been taken into consideration as well. Total specific consumption by the population is adopted to be 210 l/s/day. Average daily consumption is determined based on the billing information obtained from the local water supply company and according to the number of consumers. The overall average household and industry consumption is $Q_{sr} = 38.83$ l/s. Seasonal fluctuations in consumption and daily variations were determined based on available data and a daily coefficient of non-regularity was adopted [4]: for household $k_{dn} = 1.35$, for industry $k_{dn} = 0.75$. Maximum daily consumption is determined based on average daily consumption and adopted daily coefficients of non-regularity i.e $Q_{max,d} = 27.75 * 1.35 + 11.08 * 0.75 = 45.77$ l/s. Daily oscillations of consumption are presented by hourly coefficient of non-regularity. For households it is $k_{max}^h / k_{min}^h = 1.8/0.24$, and for industry $k_{max}^h / k_{min}^h = 1.35/0.70$. Maximum hourly consumption is $Q_{max,h} = 37.46 * 1.8 + 8.31 * 1.35 = 78.646$ l/s. They are relevant for design of distribution network [4]. Spatial distribution of consumption per node was conducted in order to carry out the analysis of the system operation.

4. RESULTS AND DISCUSSION

In this section a comparison of results obtained from the developed numerical model (in-house software) and commercial software for the current condition of the water supply system is given. Firstly, a hydraulic analysis of the present situation has been carried out. On the basis of these results the reconstruction of the system has been suggested. The schematic view of the water supply network of the town of Nevesinje with the applied numerical model is given in Fig. 1 and it presents geometrical characteristics of the pipes and elevations of all nodes. The scheme has been made in commercial software AFT Fathom 6.0 [6].

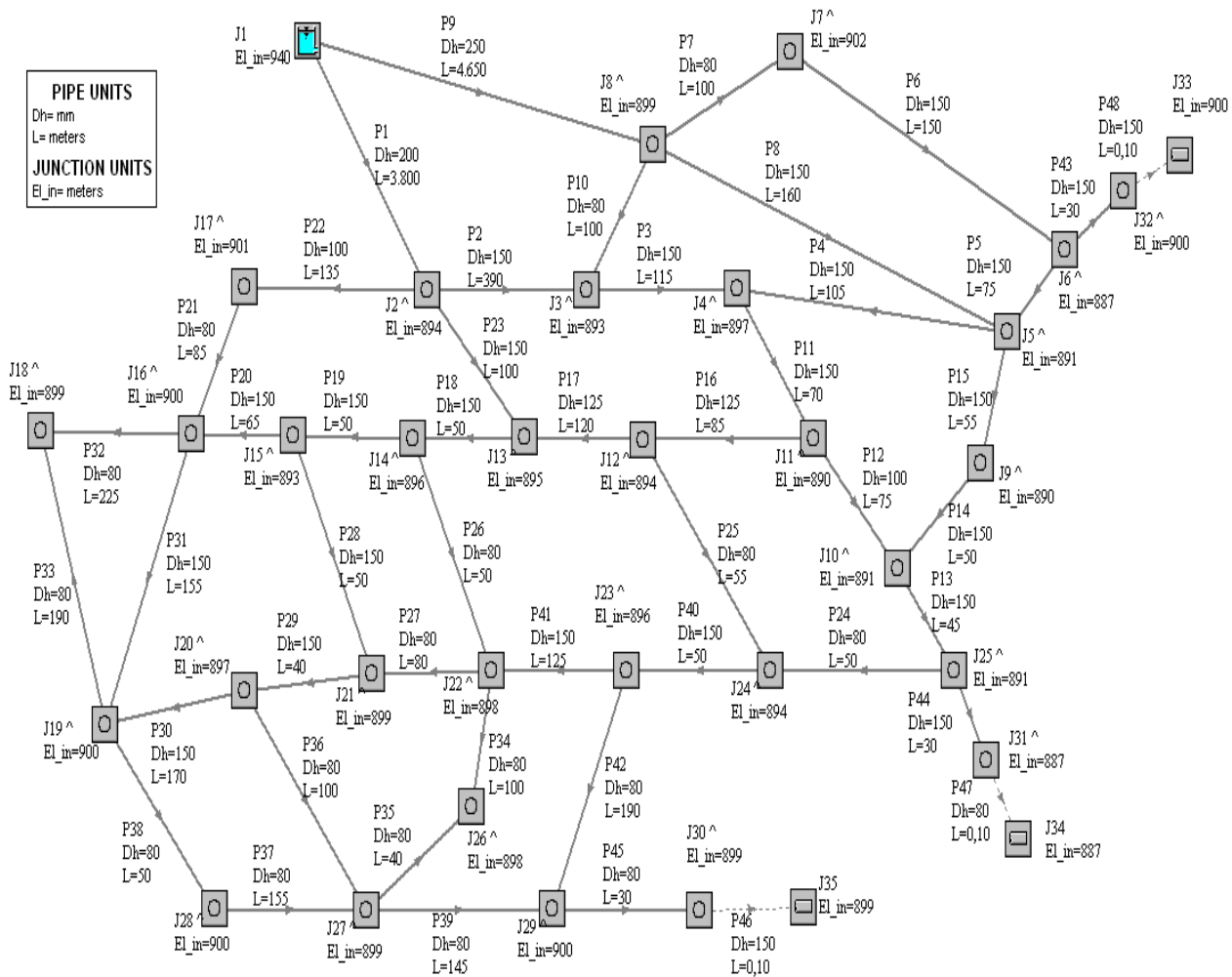


Figure 1: Hydraulic scheme of urban water supply network in the present state,

Note: P1---P49- label tubes, J1 ...J39- label nodes, Dh- diameter of pipe(mm), L- pipe length(m), El_in- geodesic height of nodes(m)

Absolute roughness of asbestos-cement pipes that compose the whole distribution network is 0.06 mm and a flow rate of some nodes is shown in Table 1. Reference node is a node 1 and computational parameters used in all calculation are: coefficient of over-relaxation $\omega = 1.85$ and allowed difference between two consecutive iterations is 0.001. Table 1. and Table 2. present results of calculation of the urban water supply network of the part town of Nevesinje in its current state by applying in-house software and corresponding results obtained using the commercial software AFT Fathom.

The flow rate of the reference node is, $Q = 78.417$ l/s for in-house software and $Q = 78.110$ l/s for AFT Fathom.

Results of the hydraulic analysis of the current system condition showed that the water supply system of the town of Nevesinje has numerous shortcomings.

The calculation of the network in the reconstructed state has been made based on the proposal for the reconstruction of the water supply network and it proved that the water supply network would be able to meet the requirements of the town with respect to the pressure and quantities of water needed.

The obtained results show that the planned reconstruction would provide the elimination of the identified deficiencies in the network. Results of the calculation of

the network obtained using a developed numerical model are in a good agreement with those obtained using commercial software AFT Fathom 6.0. The differences between the obtained values are within tolerable limits and range from 0.0 to 0.1 m/s. The main advantages of using the developed numerical model (in-house software) are the possibility of access to the source code. This enables a user to carry out changes in a program, to adapt, expand and upgrade the program according to his own needs. Unlike the applied commercial software, that has a good graphic platform and allows the user to communicate with the program in an interactive way through appropriate dialogue boxes, the developed numerical model is fairly simple. The data have been entered as well as the results obtained by processing the data are in a written form and currently there is no possibility of graphic display. Precisely, the access to the source code would allow for deficiencies to be eliminated in the future by upgrading the existing program, as well as the precision of the results to be improved if it is necessary. On the basis of the obtained results and a good agreement with those obtained by using the commercial software, it can be concluded that the developed numerical model can be successfully applied in the engineering practice.

Table 1: Results of calculation of the water supply network using the developed numerical code and commercial software AFT Fathom 6.0. for the pipes

Input data			Results given by in-house software		Results given by AFT Fathom 6.0.	
Pipe from-to	L(m)	Dh (mm)	Q (l/s)	v (m/s)	Q(l/s)	v (m/s)
1-2	3800.0	200.0	31.65	1.01	31.53	1.01
2-3	390.0	150.0	2.36	0.13	2.35	0.14
3-4	115.0	150.0	6.15	0.35	6.12	0.35
5-4	105.0	150.0	9.24	0.52	9.20	0.52
6-5	75.0	150.0	0.61	0.04	0.61	0.04
7-6	150.0	150.0	5.08	0.29	5.07	0.29
8-7	100.0	80.0	7.08	1.41	7.06	1.40
8-5	160.0	150.0	29.77	1.69	29.68	1.68
1-8	4650.0	250.0	46.77	0.95	46.58	0.95
8-3	100.0	80.0	7.35	1.46	7.33	1.46
4-11	70.0	150.0	13.78	0.76	13.32	0.76
11-10	75.0	100.0	1.35	0.17	1.35	0.17
10-25	45.0	150.0	11.21	0.64	11.19	0.64
9-10	50.0	150.0	13.80	0.78	13.76	0.78
5-9	55.0	150.0	16.16	0.92	16.11	0.91
11-12	85.0	125.0	9.67	0.79	9.62	0.79
12-13	120.0	125.0	2.64	0.22	2.62	0.22
13-14	50.0	150.0	21.79	1.23	21.74	1.23
14-15	50.0	150.0	16.56	0.94	16.53	0.94
15-16	65.0	150.0	5.44	0.31	5.43	0.31
17-16	85.0	80.0	3.93	0.78	3.92	0.78
2-17	135.0	100.0	6.45	0.82	6.43	0.82
2-13	100.0	150.0	21.52	1.22	21.46	1.21
25-24	50.0	80.0	6.06	1.21	6.05	1.21
12-24	55.0	80.0	4.83	0.96	4.82	0.96
14-22	50.0	80.0	3.22	0.64	3.21	0.64
22-21	80.0	80.0	1.14	0.23	1.13	0.22
15-21	50.0	150.0	9.11	0.52	9.09	0.51
21-20	40.0	150.0	7.78	0.44	7.77	0.44
20-19	170.0	150.0	1.80	0.10	1.81	0.10
16-19	155.0	150.0	5.60	0.32	5.59	0.32
16-18	225.0	80.0	1.31	0.26	1.31	0.26
19-18	190.0	80.0	1.03	0.21	1.04	0.21
22-26	100.0	80.0	3.42	0.68	3.42	0.68
27-26	40.0	80.0	0.53	0.11	0.53	0.11
20-27	100.0	80.0	3.02	0.60	3.02	0.60
28-27	155.0	80.0	1.34	0.27	1.34	0.27
19-28	50.0	80.0	3.38	0.67	3.38	0.67
27-29	145.0	80.0	1.45	0.29	1.45	0.29
24-23	50.0	150.0	8.74	0.50	8.72	0.49
23-22	125.0	150.0	3.44	0.20	3.44	0.19
23-29	190.0	80.0	2.84	0.57	2.84	0.56
6-32	30.0	150.0	2.33	0.13	2.32	0.13
25-31	30.0	150.0	2.24	0.13	2.23	0.13
29-30	30.0	80.0	2.14	0.43	2.14	0.43

Table 2: Results of calculation of the water supply network using the developed numerical code and commercial software AFT Fathom 6.0. for nodes

Input data			Results given by in-house software		Results given by AFT Fathom 6.0.	
Node	Vol. Flow Rate Jct Net (l/s)	Elevation Inlet (m)	Head (m)	Pressure (bar)	Head Inlet (m)	P Static Out (bar)
reservoir	-78.11	940.0	940.0	0.00	940.0	1.01
1	1.29	894.4	922.2	2.73	922.4	3.76
2	3.50	893.0	922.2	2.86	922.3	3.89
3	2.00	896.5	922.1	2.51	922.2	3.54
4	4.90	890.5	922.3	3.12	922.4	4.14
5	2.14	887.0	922.3	3.46	922.5	4.49
6	1.99	902.3	922.4	1.97	922.5	2.99
7	2.52	899.0	925.1	2.56	925.1	3.58
8	2.35	890.0	921.9	3.14	922.1	4.16
9	3.92	890.5	921.8	3.07	921.9	4.09
10	2.35	890.0	921.8	3.12	922.0	4.15
11	2.19	894.0	921.3	2.68	921.5	3.71
12	2.35	895.0	921.3	2.58	921.4	3.60
13	2.00	895.5	920.8	2.48	921.0	3.51
14	2.00	893.0	920.5	2.70	920.7	3.73
15	2.45	900.0	921.4	2.01	920.7	3.04
16	2.51	901.0	920.2	1.98	921.4	3.01
17	2.34	899.4	920.2	2.04	920.4	3.07
18	2.99	900.0	920.3	1.99	920.5	3.03
19	2.95	897.5	920.4	2.24	920.6	3.27
20	2.45	899.4	920.4	2.06	920.6	3.09
21	2.10	898.0	920.5	2.21	920.7	3.24
22	2.45	895.5	920.5	2.50	920.7	3.49
23	2.14	894.4	920.6	2.57	920.8	3.59
24	2.91	890.5	921.6	3.05	921.8	4.08
25	3.95	897.8	919.8	2.16	920.0	3.19
26	2.37	898.9	919.8	2.05	920.0	3.08
27	2.04	899.5	919.9	2.01	920.2	3.04
28	2.15	900.0	919.6	1.92	919.8	2.95
29	2.14	899.0	919.5	2.01	919.7	3.04
30	2.23	887.0	921.6	3.40	921.8	4.43
31	2.32	900.0	922.3	2.18	922.5	3.21
32	0.00	900.0	922.3	2.18	922.5	3.21
33	0.00	887.0	921.7	3.40	921.8	4.43
34	0.00	899.0	919.5	2.013	919.7	3.04

5. CONCLUSION

This paper presents the results of the hydraulic analysis of the water supply network of the town of Nevesinje, Bosnia and Herzegovina, achieved by applying the newly developed numerical model for simulation and calculation of circular water pipeline networks in steady operating conditions. Calculations have been first made for the present system state. The obtained results revealed that the water supply network has many shortcomings and that some parts that do not meet consumers' needs require reconstruction and optimization. The proposal for the reconstruction has been made and new calculations for the modified network state have been carried out demonstrating that the suggested state of the system significantly improves network characteristics and quality of water supply. Verification of the results obtained by the developed numerical model has been carried out by comparison with results obtained by application of commercial software "AFT Fathom 6.0. Based on good matching between two models it is concluded that the developed numerical del can be successfully applied in engineering practice.

REFERENCES

- [1] ROCK, E. B., JEPPSON W. R. and WATTERS,Z. G. (2000) "*Hydrodynamics-Hydraulics of Pipeline Systems*", CRS Press, Boca Raton, Florida, , pp. 85-92.
- [2] IVETIĆ,M. (1995) "*Computer Hydraulics*", Civil book, Belgrade, , pp. 130-132, (in Serbian).
- [3] WHITE, M. F.(2003) "*Fluid Mechanics*", McGraw-Hill Professional, Boston, , pp. 17-18.
- [4] RADOJKOVIĆ, M., KLEM,N. (1989) "*Computer applications in hydraulics*", Civil book, Belgrade, (in Serbian), pp. 263-279.
- [5] Data from JKP "*Water supply system*"(2001) Nevesinje, (in Serbian),
- [6] AFT Fathom, <http://www.aft.com>
- [7] KULJIĆ, S. (2012) "*Numerical calculation of water supply system Nevesinje*", *Master thesis*, , University of Montenegro, Montenegro.

CORRESPONDENCE



Stanka KULJIĆ, M.Sc. Eng.
Secondary School Center
„Aleksa Santic“,
88280 Nevesinje,
Bosnia and Herzegovina,
stanka.kuljic@gmail.com



Uroš KARADŽIĆ, Assoc. Prof, Ph.D.
University of Montenegro
Mechanical Engineering Faculty
Bul. Džordža Vašingtona bb
81000 Podgorica, Montenegro
uros.karadzic@ac.me

SIMPLIFIED EQUILIBRIUM MODEL FOR BIOMASS AND WASTE GASIFICATION

Beno ARBITER
Filip KOKALJ
Aleksandar JOVOVIĆ
Niko SAMEC

Abstract: Gasification of waste with synthetic gas production is an alternative to conventional waste to energy process based on incineration. Depending on predicted composition and quality of synthetic gas (calorific value, supporting process heat/fuel needed) preparation of waste derived fuel or study of process parameters is possible. Because of waste composition diversity there is not enough experimental results for gasification available and synthetic gas composition prediction models are often used to estimate which waste fractions are suitable for gasification.

A simplified thermodynamic equilibrium based prediction model for different waste composition gasification has been developed. A stand-alone computer application of the mathematical models has been developed. Standard numerical methods have been implemented for solving the mathematical problem formulation. Limits set by legislation for implementation of waste gasification technology have been also considered. Model predicted results have been compared with published results for the biomass and some waste types - municipal solid wastes and refuse derived fuels. Accuracy of model predictions and experimental results has been evaluated. Results obtained by stoichiometric model have been presented for most cases of practical use offering main information about produced synthetic gas quality from different kind of waste.

Key words: Biomass, Waste, Gasification, Equilibrium model, Waste – to - Energy

1. INTRODUCTION

The aim of this work is to show that simple equilibrium model is a good enough for prediction of waste gasification process and gasification products for most full scale applications. In the lack of large number of experiment results for waste gasification many authors use equilibrium models also for biomass gasification, as shown by [1], [2], [3]. In literature there are two basic approaches for equilibrium gasification model: stoichiometric and nonstoichiometric or Gibbs energy minimization approach. The last one gives the possibility to include more synthetic gas species into consideration, is more suitable to consider higher process pressures (real gas properties instead of ideal gas) but one is faced with more complex system of nonlinear equations that has to be solved together with much bigger solver convergence stability problems.

Many of waste gasification reactors are operating at or about the atmospheric pressure as well with air as oxidation agent – fluidized bed reactor, updraft and downdraft reactor except of the entrained flow reactor which does not operate at atmospheric pressure and is generally suitable only for fine particle wastes (wood sawdust or sewage sludge) [4].

Mathematical prediction of gasification end products is very useful because it helps to find conditions for the elimination of tar and soot from synthetic gas. Authors [5]

showed that exergetic efficiency is nearby the carbon deposition optimum point.

Industrial Emissions Directive EC 2010/75 [6] covers also gasification of waste. It is requested by that Directive that gasified waste should be handled at least 850°C for 2 s and in case of hazardous waste at 1100°C. At such conditions it could be considered that thermodynamic equilibrium will occur.

Some authors showed that in case of stoichiometric equilibrium model predictions methane is underestimated and carbon monoxide is estimated too optimistic, so the mathematical model should include some form of calibration possibility to overcome this weakness.

Because of all above mentioned it was decided to develop simple stoichiometric equilibrium model for gasification of waste.

2. GASIFICATION MODEL

A stoichiometric equilibrium gasification model has been developed for modeling process conditions with remaining solid phase – solid carbon – at and below carbon boundary point (CBP) and without solid carbon deposition – above CBP. Air, oxygen or oxygen enriched air can be considered as oxidation agent in the model.

Model is based on presumption that all process conditions of the system are steady state. Temperature and pressure are uniform across the observed system. Temperature is high enough and process time is long enough that

thermodynamic equilibrium of the system is achieved. The presumption of an adiabatic system is also fulfilled. Nitrogen and ashes do not participate in chemical reactions. Presence of sulfur is regarded as not high enough to influence the reaction and is accounted as ash. Model is supposed to be valid for gasification temperatures between 800°C and 1200°C and gasification pressure at the level of atmospheric pressure. All gases are regarded as ideal gases. Higher hydrocarbon gases are neglected, only H₂, CO, CO₂, H₂O, CH₄, N₂ and solid carbon as gasification products are taken into account. Primary oxidation reactions are regarded as fast and completely finished.

2.1. Modeling thermodynamic properties of predict species

Specific heats of formation h_{fj}^0 and specific Gibbs energies g_{fj}^0 of species at standard pressure are obtained by [7].

Polynomial correlations for species temperature dependency of specific heat capacity have been implemented, because it has been more suitable for numerical formulation of the model. The temperature dependency of gases heat capacity is calculated according Equation (1), where c_{pj} is the specific heat capacity of a

gas species, T is absolute temperature in Kelvin, c_{pji} are correlation coefficients as obtained by [7].

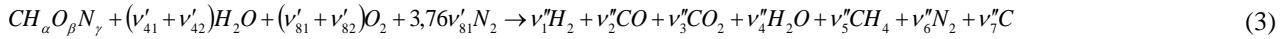
$$c_{pj} = \sum_{i=1}^4 c_{pji} T^{(i-1)} \quad (1)$$

Equation (2) shows the correlation for specific heat capacity of solid carbon – graphite, where, c_{p7} is the specific heat capacity of a solid carbon and c_{p7i} are correlation coefficients obtained by [8].

$$c_{p7} = c_{p71} + c_{p72}T - c_{p73}T^{-3} \quad (2)$$

2.2. Mathematical formulation of the model

Mathematical formulation of the model relies on three sets of equations: mass balance, energy balance and thermodynamic equilibrium of representative chemical reactions. Equation (3) represents summarized reaction of gasification, where v_j' are the stoichiometric coefficients of reactants and v_j'' the stoichiometric coefficients of gasification process products, v_{41}' is the coefficient for moisture, v_{42}' for water steam, v_{81}' for air and v_{82}' for pure oxygen.



Equation (4) represents the relation between supplied air v_8' in the summarized reaction of gasification in connection to equivalence ratio (ER) and hydrocarbon composition of dry ash free waste.

$$v_8' = ER(1 + 0.25\alpha - 0.25\beta) \quad (4)$$

Mass balance

Equation (5) is presenting mass balance for carbon, hydrogen, oxygen and nitrogen, where $[b_{i0}]$ is wet fuel and $[b_{i1}]$, $[b_{i2}]$, $[b_{i3}]$ are composition matrixes of oxidizing agent air, pure oxygen and water steam, presented respectively.

$$[a_{ij}] \cdot [v_j''] = [b_{i0}] + [b_{i1}] + [b_{i2}] + [b_{i3}] \quad (5)$$

$$[a_{ij}] = \begin{bmatrix} 0 & 1 & 1 & 0 & 1 & 0 & 1 \\ 2 & 0 & 0 & 2 & 4 & 0 & 0 \\ 0 & 1 & 2 & 1 & 0 & 0 & 0 \\ 0 & 0 & 0 & 0 & 0 & 1 & 0 \end{bmatrix} \quad (6)$$

$$[b_{i0}] = [1, (\alpha + 2v_{41}'), (\beta + v_{41}'), 0, 5\gamma]^T \quad (7)$$

$$[b_{i1}] = [0, 0, 2v_{81}', 3,76v_{81}']^T \quad (8)$$

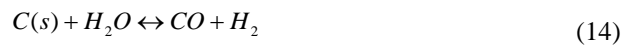
$$[b_{i2}] = [0, 0, 2v_{82}', 0]^T \quad (9)$$

$$[b_{i3}] = [0, 2v_{42}', v_{42}', 0]^T \quad (10)$$

$$[v_j''] = [v_1'', v_2'', v_3'', v_4'', v_5'', v_6'', v_7'']^T \quad (11)$$

Thermodynamic equilibrium of representative chemical reactions

Because of different representative chemical reactions for gasification conditions at, above or below CBP the sets of thermodynamic equilibrium equations are different. Below and at CBP gasification process is described by methane decomposition reaction (12) and equation (15), water gas shift reaction (13) and equation (16) and heterogeneous water gas shift reaction (14), equation (17),



$$f_1 = \Psi_1^3 \Psi_2 - t_1 K_1 \Psi_4 \Psi_5 = 0 \quad (15)$$

$$f_2 = \Psi_1 \Psi_3 - t_2 K_2 \Psi_2 \Psi_4 = 0 \quad (16)$$

$$f_3 = \Psi_1 \Psi_2 - K_3 \Psi_4 = 0 \quad (17)$$

$$\Psi_j = \frac{v_j''}{\sum_{j=1}^6 v_j''} \quad (18)$$

where Ψ_j is mole fraction of component in gas phase, K_r is temperature and pressure dependent equilibrium constant of partial chemical reaction, t_r is calibration coefficient. t_1 is the reflecting underestimation of methane predicting, while t_2 is the reflecting overestimation of carbon oxide.

The above CBP gasification process is described by water gas shift reaction (13) and equation (16) and methane reaction (19) and equation (20).



$$f_4 = \psi_5 - t_4 K_4 \psi_1^2 = 0 \quad (20)$$

Equation (21) is presenting the temperature dependency of equilibrium constant at standard pressure,

$$\ln K_r(T) = -\frac{\Delta G_r^0}{R_m T} \quad (21)$$

where R_m is universal gas constant, ΔG_r^0 is total Gibbs energy of the system for the observed partial gasification reaction given by Equation (22).

$$\Delta G_r^0 = \sum_{j=1}^n (v_j'' - v_j') \Delta g_{f,j}^0 + \sum_{j=1}^n (v_j'' - v_j') R_m T \ln \left(\frac{\prod (v_j'' - v_j')}{\prod (v_j'' - v_j')} \right) \quad (22)$$

$$H_R = H_{f,F}^0 + v_{41}' h_{f4(l)}^0 + v_{42}' \left(h_{f4}^0 + \int_{T_0}^{T_{42}} c_{p4} dT \right) + v_{81}' \int_{T_0}^{T_{81}} (3.76c_{p6} + c_{p8}) dT + v_{82}' \int_{T_0}^{T_{82}} c_{p8} dT \quad (24)$$

where $h_{f4(l)}^0$ is the heat of formation at standard pressure for liquid water (moisture), T_{42} , T_{81} and T_{82} are temperatures of the oxidation agents steam, air and pure oxygen. $\Delta H_{f,F}^0$ is the heat of the formation for fuel, estimated as described in equation (25),

$$\Delta H_{f,F}^0 = LHV_F + \Delta h_{f3}^0 + 0.5 \cdot \alpha \cdot \Delta h_{f4}^0 \quad (25)$$

where LHV_F is the low heating value estimated with equation by [9] and h_{f3}^0 and h_{f4}^0 are heats of formation at standard pressure for carbon dioxide and water in the gaseous phase.

Equation (26) represents the equation for calculation of the enthalpy of the produced syngas, where h_{fj}^0 are standard heats of formation for gaseous species.

$$H_P = v_2'' h_{f2}^0 + v_3'' h_{f3}^0 + v_4'' h_{f4}^0 + v_5'' h_{f5}^0 + \sum_{j=1}^7 \int_{T_0}^T v_j'' c_{pj} dT \quad (26)$$

2.3. Numerical formulation of the model

For solving the system of equations numerical methods have been implemented including Newton Raphson for system of nonlinear equations according equations (27) and (28).

$$\begin{bmatrix} \frac{\partial f_1(k)}{\partial \psi_2} & \frac{\partial f_2(k)}{\partial \psi_5} & \frac{\partial f_3(k)}{\partial v_7''} \\ \frac{\partial f_1(k)}{\partial \psi_2} & \frac{\partial f_2(k)}{\partial \psi_5} & \frac{\partial f_3(k)}{\partial v_7''} \\ \frac{\partial f_1(k)}{\partial \psi_2} & \frac{\partial f_2(k)}{\partial \psi_5} & \frac{\partial f_3(k)}{\partial v_7''} \end{bmatrix} \begin{bmatrix} \Delta \psi_2 \\ \Delta \psi_5 \\ \Delta v_7'' \end{bmatrix} = \begin{bmatrix} f_1(k) \\ f_2(k) \\ f_3(k) \end{bmatrix} \quad (27)$$

$$\begin{aligned} \psi_2(k+1) &= \psi_2(k) + \Delta \psi_2 \\ \psi_5(k+1) &= \psi_5(k) + \Delta \psi_5 \\ v_7''(k+1) &= v_7''(k) + \Delta v_7'' \end{aligned} \quad (28)$$

For better convergence initial guess has been set according equations (29), (30) and (31).

which have to be solved for unknown values ($v_j'' - v_j'$) to minimize ΔG_r^0 .

Energy balance

Equation (23) shows energy balance for reacting system under presumption that moisture of the waste is of standard temperature,

$$H_R + Q_{sup} - Q_{dis} + \eta_{PT} W_{el,sup} = H_P \quad (23)$$

where H_R is enthalpy of reactants, Q_{sup} energy introduced to reactants by heat, Q_{dis} heat loss of reactor, $W_{el,sup}$ power supplied to the system (for instance: plasma gasification), η_{PT} efficiency of converting electrical energy to thermal energy by the plasma torch, and H_P enthalpy of synthetic gas.

Equation (24) is presenting estimation of H_R

$$\psi_2(0) = \frac{0.5}{0.5\gamma + 3.7619v_{41}' + 1} \quad (29)$$

$$\psi_5(0) = 0 \quad (30)$$

$$v_7''(0) = 0 \quad (31)$$

3. RESULTS

At first the model was validated with published model for biomass [2]. Both models have been calibrated and model predicted results have been compared. Later the calculation was made for different types of wastes using these models.

Altafini [1] predicted synthetic gas composition of the Pinus elliotis wood by using nonstoichiometric equilibrium model. The calculated values refer to the sawdust with 10 wt.% water content, reaction temperature of 800°C, heat loss in the gasifier equal to 1 % based on the HHV of the fuel and equilibrium state of chemical reactions. The experimental test results refer to an average of 10 tests performed at the gasifier, where fuel (wood Pinus Elliotis) water content has been approximately 11% and the average reaction temperature was nearly 832°C. Although the H₂-CO content in dry synthetic gas base predicted through model (39.76 vol.%) was higher than the average value of the experiments (34.14 vol.%), the presence of CH₄, C₂H₄ and C₂H₆ in the actual synthetic gas composition, determines higher HHV for it (5.276 kJ/Nm³ as the experimental value against 5.042 kJ/Nm³ for the model calculated value). The H₂ content of the simulations is 6.06 vol. % larger than that of the experimental tests, while the CO content is 0.44 vol. % lower than the experimental value. The higher values in the model simulation for the fuel and the fuel gas masses

determine higher cold gas efficiency for the predicted value than that of the experiments.

Zainal [3] developed stoichiometric equilibrium gasification model for biomass gasification. Heat losses of gasifier were not considered and included in his model. Air gasification model and experimental results of wood with 20% water content at 800°C were compared. Results show that H₂ (21.06 vol. % vs. 15.23 vol. %) and H₂-CO (40.67 vol. % vs. 38.27 vol. %) calculation of the model is higher than the experiment results. CO (19.61 vol. % vs. 23.04 vol. %) and CO₂ (12.01 vol. % vs. 16.42 vol. %) calculation values are lower than experimental results. CH₄ (0.64 vol. % vs. 1.58 vol. %) is quite negligible and CV (4.72 MJ/Nm³ vs. 4.85 MJ/Nm³) calculated and experimental values are quite close to each other.

Jayah [10] made experimental test and stated that heat losses for updraft fixed bed reactor is between 5% and 15% of feedstock HHV.

3.1. Model validation and simulation with wood

There are published results of other models developed for gasification of biomass – wood (cashew nut) which have also been used for the validation of this model.

The CHO syngas system analysis has yield that gasification is taking part above the CDP, so solid carbon is not considered in prediction.

Table 1 presents validation data for 4 runs: run R1 is experimental for downdraft lab-scale gasifier as presented

in reference [10], runs R2 and R3 are reference non-calibrated and calibrated models predictions by [2], while run R4 is calibrated prediction by this model.

As the gasification temperature has been maintained at level of experimental run R1, the ER value for runs of this model calibrated prediction comply better with experiment than reference model. RMS is within 2% what is compared to [11] negligible when taking into account real circumstances (untight gasifier, introduction of air with feedstock stream). As in the reference model gasifier heat losses were not presented, this model has considered it by 5% of fuel LHV. Preserved energy suited good to experiment, specially LHV for this model and RMS for syngas composition. For reference non-calibrated model methane prediction is under estimated and originated from model non considered chemical kinetics. In runs of calibrated models (reference and this model) also carbon-monoxide estimation is calibrated to get results closer to reference experiment.

Table 1 Ultimate analysis of wood [10]

Ultimate analysis [wt. %, daf]				
C	H	O	N	S
50.6	6.5	42.0	0.2	0.0

Table 2 Dry basis synthetic gas composition (vol.%), equivalence ratio (-), gasification temperature (°C), low heating value (MJ/Nm³), dry base synthetic gas yield (Nm³/kg) for wood gasification

run	H ₂ [vol. %]	CO [vol. %]	CO ₂ [vol. %]	CH ₄ [vol. %]	ER [-]	T [°C]	LHV [MJNm ⁻³]	V [Nm ³ kg ⁻¹]
R1[10]	17.0	18.4	10.6	1.3	0.36	827	4.23	2.56
R2[2]	18.0	17.9	11.8	0.1	0.49	827	3.57	2.66
R3[2]	16.8	17.9	12.1	1.1	0.47	827	3.72	2.56
R4	16.7	19.3	11.4	1.3	0.40	827	3.99	2.95

3.2. Model simulation with municipal solid waste

Reference modeled results for downdraft fixed bed gasifier by [2] have been compared with this model prediction.

As presented in Table 5 this model – run R6 (calibrated) has been compared to reference model run R5. Both predictions suit very well except by predicting gasification temperature.

Table 3 Ultimate analysis of referent fuels –MSW [2]

Ultimate analysis [wt. %, daf]				
C	H	O	N	S
51.0	6.8	39.2	2.6	0.4

Table 4 Fraction composition of MSW (wt%) [2]

paper	vinyl, plastics	wood	bio- waste	non- combustable	other
9.8	17.3	4.0	54.2	11.1	4.1

Table 5 Dry basis synthetic gas composition (vol.%), equivalence ratio (-), gasification temperature (°C), low heating value (MJ/Nm³) for municipal solid waste gasification

run	H ₂ [vol. %]	CO [vol. %]	CO ₂ [vol. %]	CH ₄ [vol. %]	ER [-]	T [°C]	LHV [MJNm ⁻³]
R5[2]	16.0	25.0	6.0	0.1	0.40	1100	3.08
R6	16.1	25.2	6.0	0.0	0.40	1062	3.05

3.3. Model simulation with RDF

RDF model calculation results have been compared with our model calculations.

Table 6 Ultimate analysis of referent fuels (wt%)

		Ultimate analysis [wt. %, db]					
run	name	C	H	O	N	S	ash
R8[12]	PE-12	85.0	13.8	0.0	0.0	0.0	0.2
R10	GS3-5	84.4	14.0	0.0	0.0	0.0	0.3
R12	N4	68.1	10.2	14.3	0.0	0.1	0.6

Table 7 presents data for experimental runs for derived fuel gasification to be compared with this model. Gasification results by [12] of runs R8, R10 and R12 are compared respectively with this model prediction runs R9, R11 and R13. Original runs have been performed with air as oxidizing agent at pilot scale bubbling fluidized bed gasifier. RDF originated from MSW and household packaging waste with low moisture content.

While syngas yield data was not presented it could not be compared with model. Due absence of higher hydrocarbons in model this share of carbon converted was considered in methane and LHV has been lower than estimated in experiment by RMS 10% to 25%. In two out of three runs, the composition RMS is quite well calculated with accuracy 3 to 7%.

Table 7 Dry basis synthetic gas composition (vol.%), equivalence ratio (-), gasification temperature (°C), synthetic gas low heating value (MJ/Nm³), dry base synthetic gas yield (Nm³/kg, for RDF gasification)

run	H ₂ [vol. %]	CO [vol. %]	CO ₂ [vol. %]	CH ₄ [vol. %]	C _n H _m [vol. %]	ER [-]	w [wt. %]	T [°C]	LHV [MJNm ⁻³]	V [Nm ³ kg ⁻¹]
R8[12]	27.1	20.1	1.7	2.1	0.5	0.28	1.3	816	6.50	-
R9	24.3	25.8	0.4	0.2	-	0.34	1.3	817	5.86	6.12
R10[12]	29.5	19.9	1.7	2.5	0.7	0.24	1.0	829	7.00	5.14
R11	24.4	24.8	0.6	0.2	-	0.35	1.0	827	5.79	2.35
R12[12]	6.8	3.7	11.1	7.3	4.8	0.22	6.7	869	6.80	-
R13	22.6	24.4	2.6	0.1	-	0.36	6.7	868	5.32	2.35

3.4. Model simulation with plastics

Table 9 presents data for experimental run R14 for waste plastics material gasification by [13] to be compared with this model prediction run R15. Original run have been performed with air as oxidizing agent preheated at 448°C at pilot scale bubbling fluidized bed gasifier with special bed material named olivine, which is acting also as bed catalyst for tar cracking reactions.

Experimental data show presence of solid carbon in syngas at 0.1 g_C/kg_{C_{fuel}}, while model prediction is 0.6 g_C/kg_{C_{fuel}} – it could be accounted to bed material tar cracking reaction for experimental run. Due absence of higher hydrocarbons in model this share of carbon converted was considered in higher carbon monoxide and carbon dioxide presence, while LHV and syngas yield is similar estimated in model prediction as in experiment by RMS 10% to 25%.

Table 8 Ultimate analysis of referent fuels (wt.%)

Ultimate analysis [wt. %, db]						
run	C	H	O	N	S	ash
R14 [13]	79.5	13,1	4.5	0.2	0.1	1.9

Table 9 Dry basis synthetic gas composition (vol.%), equivalence ratio (-), gasification temperature (°C), synthetic gas low heating value (MJ/Nm³), dry base synthetic gas yield (Nm³/kg) for waste plastics gasification

run	H ₂ [vol. %]	CO [vol. %]	CO ₂ [vol. %]	CH ₄ [vol. %]	C _n H _m [vol. %]	ER [-]	w [wt.%]	T [°C]	LHV [MJNm ⁻³]	V [Nm ³ kg ⁻¹]
R14	8.4	5.2	9.6	7.1	5.9	0.21	0.7	810	9.40	3.4
R15	24.8	14.4	4.6	0.4	-	0.21	0.7	800	9.39	3.2

4. CONCLUSION

Simple gasification model is accurate enough for computing process parameter trends and the study of gasification process settings since:

- majority of waste is capable of the gasification at atmospheric pressure - it means that an atmospheric gasification reactor is used (various kind) because of its physical structure and generally bigger particle size.
- only part of waste is capable of gasification and technology runs at elevated process pressure. Entrained flow gasifier is used because parts have to be of the very fine structure – sewage sludge, fine shredded waste, waste biomass pellets.

For the majority of the gasifiers this simple model can be used because of good accuracy that is verified by experimental results and compared with nonstoichiometric model. It is useful tool for process parameter study and selecting the mixture of wastes gasified.

Some waste composition elements and synthetic gas end-product components that are not included in the model are of low concentration. This study also shows that they have no significant impact on the heating value of waste neither on the heating value of produced synthetic gas.

REFERENCES

- [1] Altafini, C.R., Wander, P.R., Barreto, R.M. (2003) *Prediction of the working parameters of a wood waste gasifier through an equilibrium model*, Energy Conversion and Management, Vol. 44, pp 2763-2777
- [2] Jarungthammachote, S., Dutta, A., *Thermodynamic equilibrium model and second law analysis of a downdraft waste gasifier*(2007), Energy, 32, pp 1660-1669
- [3] Zainal, Z.A., Ali, R., Lean C.H., Seetharamu K.N. (2001), *Prediction of performance of a downdraft gasifier using equilibrium modeling for different biomass materials*. Energy Conversion and Management, Vol.42, pp 1499-1515
- [4] Highman, C., (2007). Gasification. GPP
- [5] Ptasinski, K.J., Prins, M., Pierik, A. (2007), *Exergetic evaluation of biomass gasification*, Energy, Vol.32, pp 568-574
- [6] Industrial Emissions Directive EC 2010/75
- [7] Reid, R.C. (1977). The properties of gases and liquids, McGraw-Hill. ISBN 0-07-051790-8
- [8] Perry, R.H. (1999). Perry's chemical engineers' handbook, McGraw-Hill. ISBN 0-07-134412-8
- [9] Channivala, S.A., Parikh, P.P. (2002) *A unified correlation for estimating HHV of solid , liquid and gaseous fuels*, Fuel, Vol. 81, pp 1051-1063
- [10] Jayah, T.H., Aye, L., Fuller, R.J., Stewart, D.F., *Computer simulation of downdraft wood gasifier*

for tea drying (2003), Biomass & Energy, Vol.25, pp 459–469

- [11] del Alamo, G., Hart, A., Grimshaw, A., Lundström, P. (2012) *Characterization of syngas produced from MSW gasification at commercial-scale ENERGOS Plants*, Waste Management, Vol.32, pp 1835–1842
- [12] Arena, U., Zaccariello, L., Mastellone, M.L. (2010) *Fluidized bed gasification of waste-derived fuels*, Waste Management, Vol. 30, pp 1212-1219
- [13] Arena, U., Di Gregorio, F., Amorese, C., Mastellone, M.L. (2011) *A techno-economic comparison of fluidized bed gasification of two mixed plastic wastes*, Waste Management, Vol. 31, pp 1494-504

CORRESPONDANCE

Beno ARBITER, M.Sc. Eng.
University of Maribor
Faculty of Mechanical Engineering
Smetanova ulica 17
2000 Maribor, Slovenia
beno.arbiter@gmail.com

Filip KOKALJ, Prof. D.Sc. Eng.
University of Maribor
Faculty of Mechanical Engineering
Smetanova ulica 17
2000 Maribor, Slovenia
filip.kokalj@um.si

Aleksandar JOVOVIĆ, Prof. D.Sc. Eng.
University of Belgrade
Faculty of Mechanical Engineering
Kraljice Marije 16
11120 Belgrade, Serbia
ajovovic@mas.bg.ac.rs

Niko SAMEC, Prof. D.Sc. Eng.
University of Maribor
Faculty of Mechanical Engineering
Smetanova ulica 17
2000 Maribor, Slovenia
niko.samec@um.si

ANALYSIS COMBUSTION LIGNITE OF GACKO IN THE STEAM BOILER P - 64

Borivoje VUJIČIĆ
Ženja VUJOVIĆ

Abstract: Process of production of electric energy in thermal power plant Gacko has begun in 1983 year. Basic fuel is from surface pit Gacko. Power on threshold of thermal power plant is exclusively in function quality of disposable fuel. Characteristics of Gacko lignite are variable, so that process and conditions for its combustion are different. Coal deposit is in multiple layers (two surface, main layer, and two floor layers). Exploitation of coal from the above mentioned layers and its burning by technology – burning in flight, causes significant changes in firebox itself and combustion products are cubically different. Because of great stastill and untimely detection of the main layer, thermal power plant is constrained to use only lignite from immediate roof zone (shallowest layer). Lignite from immediate roof zone is rich in great amount of silicon, light metals and clay, which significantly slow down speed of combustion and latently consume released heat for evaporation of trapped moisture, as well as for transformation of incombustible material and compound of new oxides. As a consequence is oscillation of disposable power on treshold of thermal power plant, and which most frequently departs from expected.

Key words: combustion, combustion products lignite , steam boiler, firebox

ANALIZA SAGORIJEVANJE GATAČKOG LIGNITA U PARNOM KOTLU P-64

Rezime: Proces proizvodnje električne energije u termoelektrani Gacko počeo je 1983. godine. Osnovno gorivo je iz površinskog kopa Gacko. Snaga na pragu termoelektrane je isključivo u funkciji kvaliteta raspoloživog goriva. Karakteristike gatačkog lignita su varijabilne, tako da proces i uslovi za njegovo sagorijevanje su različiti. Nalazište uglja je u više slojeva (dva površinska , glavni sloj i dva podinska sloja). Eksploataciom uglj iz navedenih slojeva i njegovog spaljivanja tehnologijom - spaljivanje u letu, izaziva značajne promjene u samom ložištu i produkti sagorijevanja su različiti zapreminski. Zbog velikog zaostatka i neblagovremenog otkrivanja glavnog sloja, termoelektrana je prinuđena da koristi samo lignit iz povlatne zone (najplići sloj). Lignit iz povlatne zone je bogat velikom količinom silicijuma, lakih metala i glinom, koji značajno usporavaju brzinu sagorijevanja i latentno troše oslobođenu toplotu za isparavanje zarobljene vlage, kao i za transformaciju nesagorivih materija i sajedinjenje novih oksida. Kao posljedica je oscilovanje raspoložive snage na pragu termoelektrane, a koja najčešće ostupa od očekivane.

Key words: sagorjevanje, produkti sagorjevanja, parni kotao, ložište

1. INTRODUCTION

Rudnik i TE Gacko nalaze se u Gatačkom ugljenom bazenu u jugoistočnom dijelu Republike Srpske. Izgradnja Rudnika i TE Gacko je počela 1974. godine. Izgrađen je rudnik PK Gračanica kapaciteta 2,2 mil. tona uglja godišnje i blok nominalne snage 300 MW. Blok TE Gacko je počeo sa radom 9. februara 1983.god. Termoelektrana posluje u okviru JP Rudnik i Termoelektrana "Gacko" A.D. Gacko i sa maksimalno ostvarenom godišnjom proizvodnjom 1.773 GWh u 2013.

godini, najveći je proizvođač električne energije u Republici Srpskoj.

TE Gacko radi u jedinstvenom elektroenergetskom sistemu RS u mješovitom holdingu Elektroprivreda RS (MH ERS).

Glavna oprema Rudnika i TE Gacko isporučena je uglavnom iz bivšeg Sovjetskog Saveza i montirana u periodu 1977-1983. godine.

Mašinsko-tehnološki dio Termoelektrane "Gacko" čini kondenzaciono-oduzimni blok sa povratnim zatvorenim sistemom hlađenja, projektno instalisane snage 300 MW i raspoložive snage na pragu TE od 276 MW, kompletno sa

svim pratećim pomoćnim objektima i postrojenjima. U Glavnom pogonskom objektu termoelektrane smještena je oprema kotlovske i turbinske postrojenja. Termoelektrana Gacko projektovana je po blok sistemu kotao-turboagregat kao čisto kondenzacijska bez odvajanja pare vanjskim potrošačima. Projektno osnovno

gorivo je lignit kalorične vrijednosti 6 500 KJ/kg do 9.500 KJ/kg, srednje kalorične vrijednosti 8 100 KJ/kg. Za potpalu kotla i održavanje gorenja pri nižim opterećenjima ili pri znatnom smanjenju kalorične vrijednosti uglja koristi se mazut.

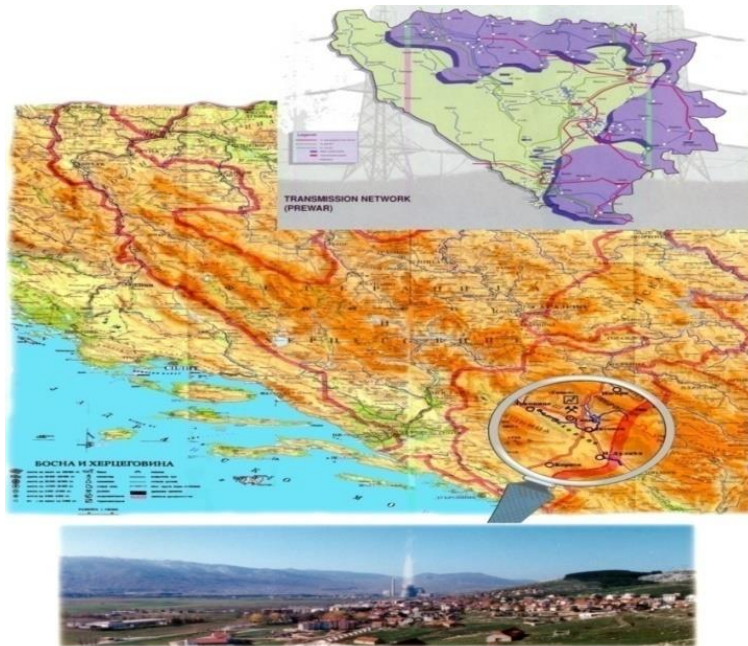


Fig.1. Položaj Rudnika i Termoelektrane Gacko

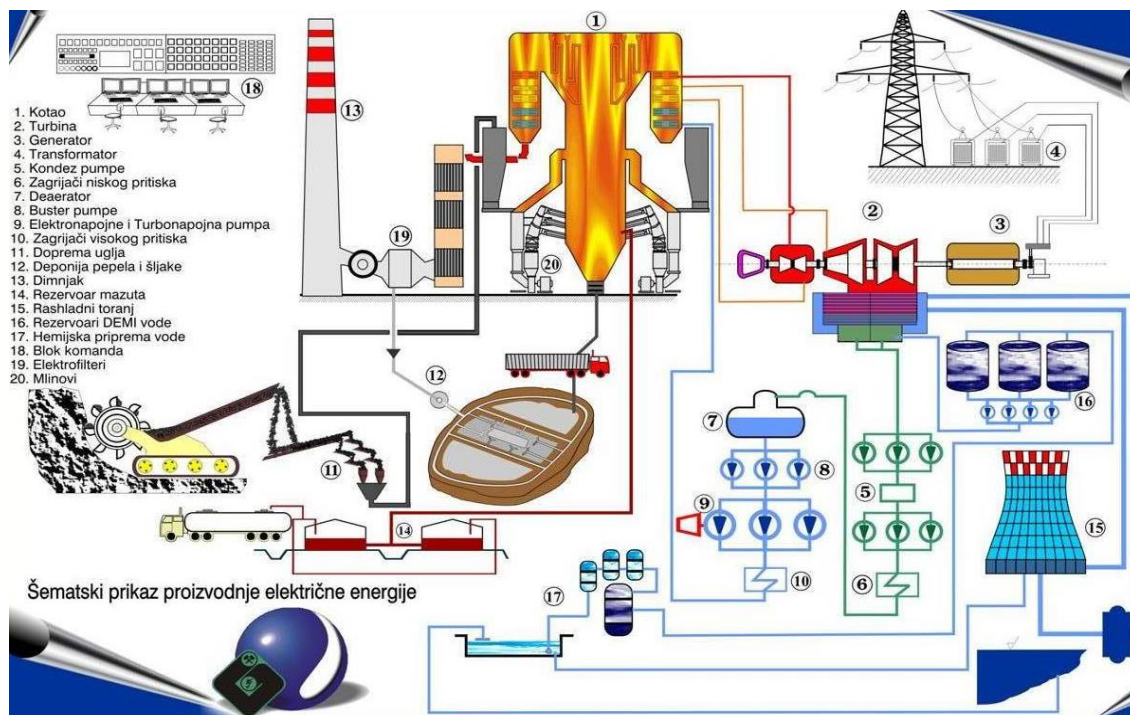


Fig.2. Toplotna šema bloka 300 MW

2. TOPLOTNA ŠEMA BLOKA 300 MW

Tehnološki proces termoelektrane sastoji se u postepenom pretvaranju hemijske energije sagorijevanja goriva u toplotnu i električnu energiju.

Radno tijelo (nosilac toplote) u procesu proizvodnje energije u termoelektrani je voda i vodena para. Gorivo sagorijeva u kotlu i predaje toplotu vodi, voda se pretvara u vodenu paru koja se dodatno pregrijava na račun čega se povećava njena potencijalna energija. Prolazeći kroz protočni dio turbine, para se širi, potencijalna energija

pare pretvara se u kinetičku a kinetička u mehaničku energiju obrtanja rotora. U generatoru se mehanička energija parne turbine pretvara u električnu.

3. SISTEM UGLJENE PRAŠINE

Kotao P-64 je opremljen sa 8 individualnih zatvorenih sistema ugljene prašine sa direktnim uduvavanjem. Sistem ugljene prašine se sastoji od:

1. bunkera sirovog uglja,
2. kombinovanog dozatora-transportera sirovog uglja,
3. usisnog kanala (sa GZO)
4. ventilacionog mlina tipa S 40.50
5. inercionog separatora
6. kanala ugljene prašine, vrtložnika i gorionika
7. šibera, klapni i druge stop i regulacione armature.

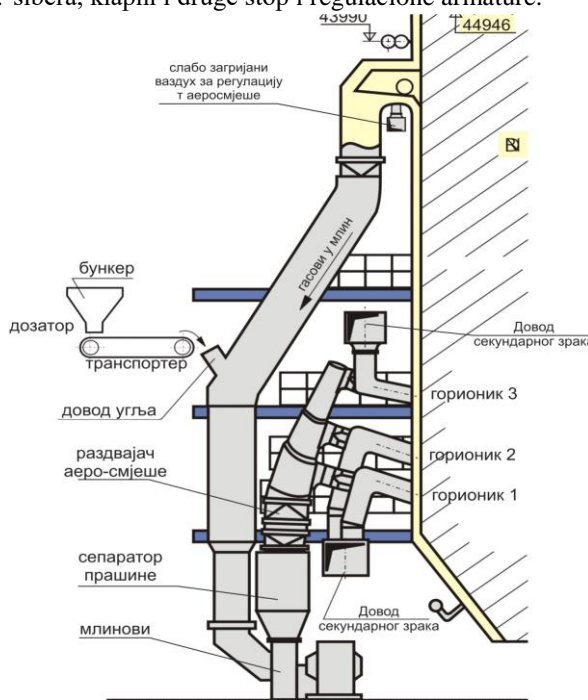


Fig.3.

Princip rada sistema ugljene prašine je sledeći:

Ugalj u potrebnoj količini i sa granulacijom manjom od 40 mm dodaje se u usisni kanal pomoću dozatora i transportera. Pomoću ventilacionog mlina dimni gasovi se sa temperaturom koja odgovara opterećenju kotla (500 - 1000°S) usisavaju u šahtu za uzimanje gasova (GZO).

Pri padanju ugalj predaje vlagu dimnim gasovima, hladi ih do temperature 300-450°S, a sam se suši. Komadi uglja padaju na radno kolo mlina. U mlinu se čestice uglja udarajući u oklop i radne ploče pretvaraju u ugljenu prašinu. Pri mljevenju uglja vrši se njegovo završno sušenje. Smjesa ugljene prašine i dimnih gasova potiskuje se radnim kolom mlina u separator gdje dolazi do odvajanja krupnih čestica prašine od sitnih. Krupne čestice ugljene prašine se recirkulacionim kanalima vraćaju u mlin, gdje se vrši još jedan ciklus mljevenja. Na taj način oko 40-50 % dovedenog uglja u mlin recirkuliše. Separisana ugljena prašina zajedno sa gasovima i vazduhom (aerosmješa) iz separatora usmjerava se prema vrtložniku, gdje dolazi do raspodjele (krupne čestice ugljene prašine idu na periferiju, a manje

ka centru). Na taj način krupne čestice dolaze u donje gorionike, a manje u gornje.

Za normalno sagorijevanje ugljene prašine potrebna je temperatura od 120 - 180°S. Održavanje temperature aerosmješe iza mlina vrši se dodavanjem veće količine uglja ili smanjenjem temperature dimnih gasova za sušenje. U tom cilju umjesto oduzimanja gasova iz ložišta (GZO) dodaje se slabo zagrijani vazduh iz CVZ koji ima temperaturu 120°S. Na dovodu slabozagrijanog vazduha postavljena je regulaciona klapna na koju se daje komanda od regulatora temperature aero-smjese.

U zavisnosti od kvaliteta uglja koji se melje, u radu je 7- 8 mlinova.

- kapacitet mlinova od najmanje 50 t/h,
- ventilaciono dejstvo mlinova >220.000m³/h na 180oC,
- temperatura "aerosmeše" (iza mlina) 120-180 oC,
- finoća mlevenja od najviše 5% ostatka na situ R₁₀₀₀ i 60% na situ R₉₀.

4. PRODUKTIVNA UGLJENA ZONA

U okviru neogene ugljenosne serije ležišta "Gacko" razvijena su tri ugljena sloja veće dubine zalijeganja i povlatna zona (sa tri krovinska ugljena sloja). Svi slojevi su složene strukturne građe. Pri tome su slojevi povlatne zone specifični iz različiti po morfološkim, strukturnim, litofacijalnim i drugim geološkim karakteristikama, jer ugljeni slojevi nemaju kontinuitet u debljini, po pružanju i padu. Slojevi uglja u ležištu "Gacko" se odlikuju sa izrazitom promjenljivošću po vertikalnom međusobnom rastojanju. Ova promjenjivost u vertikalnom pogledu se izražava kroz različito rastojanje između ugljenih slojeva u pojedinim dijelovima ležišta. Na slici Fig. 4. prikazan je geološki stub gatačke ugljenosne formacije (centralni dio ležišta).

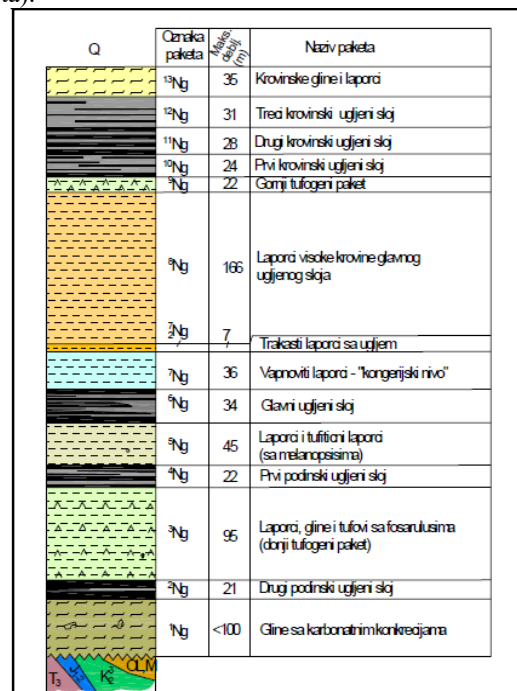


Fig.4. Geološki stub gatačke ugljenosne formacije

5. RESURSI UGLJA KAO ENERGETSKO GORIVO ZA SADAŠNJE I BUDUĆA TE - POSTROJENJA

Geološke rezerve ležišta uglja Gacko iznose cca 330 Mt. Prema aktuelnoj geološkoj dokumentaciji bilansne rezerve iznose ≈185miliona tona sa prosječnom toplotnom vrijednošću od 9,9 MJ/kg i energetskim potencijalom od 545 TWh. Prema obrađenim pokazateljima uspješnosti, bilansne rezerve uglja omogućavaju dugoročno obezbeđenje gorivom sadašnjeg i budućih termoelektrskih postrojenja po povoljnijim ekonomskim uslovima. Ležište uglja Gacko zahvaljujući ukupnoj količini rudnih rezervi i kvalitetu, predstavlja

najznačajniji izvor te sirovine za potrebe termoelektrana u Republici Srpskoj.

Prosječna ugljonosnost, u ležištu uglja Gacko, po pojedinim ugljenim slojevima, samo za glavni sloj, iznosi 9,36 t/m². Za svatri ugljena nivoa prvog podinskog ugljenog sloja, prosječna ugljonosnost iznosi 13,73t/m².

6. REZERVE I KVALITET UGLJA

U tabelama koje slijede prikazane su rezerve i kvalitet uglja u ležištu "Gacko".

U tabeli 1. prikazane su rezerve uglja (bilansne, vanbilansne, potencijalne, ukupne geološke i eksploatacione) u ležištu "Gacko" sa stanjem na dan **31.12.2016. godine.**

Table 1: Rezerve uglja (bilansne, vanbilansne, potencijalne, ukupne geološke i eksploatacione) u ležištu "Gacko"

Ležište	REZERVE UGLJA (tone)				
	BILANSNE (A+B+C ₁)	VANBILANSNE (A+B+C ₁)	POTENCIJALNE (C ₂ +D ₁ +D ₂)	UKUPNO GEOLOŠKE (A+B+C ₁)	EKSPLOATACIONE (A+B+C ₁)
„Gacko“	186.909.806	107.154.000	36.112.000	330.175.806	170.087.923

Table 2:

UZORAK 1-ŠLJAKA IZ HLADNOG LIJEVKA				
Komponenta	%	Komponenta	%	Standardna norma
Al	10.3	S	0.22	ASTM D6349:2009
Ba	0.034	Sr	10.020	
Ca	18.71	SiO ₂	40.83	
Fe	5.24	Ti	0.35	
Mg	1.05			
Mn	0.041			
P	0.11			

Ležište uglja "Gacko"podijeljeno je na 4 eksploataciona polja:

- Centralno polje,
- Istočno polje,
- Povlatna zona i
- Zapadno polje – PK „Gračanica“ (Sjeverna kosina i Gojkovića potok).

Od početka rada termoelektrana je koristila ugalj samo sa jedne lokacije ugljenog basena Gacko. U prethodnom periodu , zbog nemogućnosti razvoja kopa i investiranja u rudnik, kontinuirano snabdijevanje ugljem je bilo ugroženo. Osnovni uzrok je zaostatak u otkrivanju uglja i nemogućnost uzimanja uglja iz glavnog sloja. Kako je već potreba za kontinuiranim procesom proizvodnje el. energije sa jedne strane , a sa druge nemogućnost kontinuiteta obezbijevanja uglja, kao prelazno riješenje se nudilo korišćenje uglja iz povlatne zone Površinsko ležište sa vrlo malim slojem zemljane pokrivke.

U procesu sagorijevanja lignita iz povlatne zone oslobođena energija se troši na zagrijavanje osnovnog fluida, isparavanje preostale vlage iz goriva topljenje i jedinjenje prisutnih metala, stvaranje novih oksida.

Produkti sagorijevanja su pepeo sa vrlo velikom količinom silicumske sadržaja i šljaka. Proces sagorijevanja se dešava u donjem dijelu ložišta znatno niže u odnosu na projektovano, tako da je i pored nastojanja pomoću raspoložive opreme pomjeriti vatrenu loptu prema višim kotama. Kao posljedica takvog položaja dolazi do nemogućnosti održavanja temperature fluida u projektovanim granicama, jer je ugrožena tehnološka temperatura koja štiti cijevni sistem od pregrijavanja i obezbijeduje produkciju tehnološke pare za turbinu u projektovanim parametrima. Kao prvi signal je pad temperature fluida u nisko radijacionom dijelu. Da bi se spriječilo propadanje temperature, i pored opterećenja mlinova i ubacivanja ugljene prašine neophodno je vršiti podršku vatre sa dodatnim tečnim gorivom. U raspoloživom gorivu je veliki procenat balastnih materija (nesagorive materije u vidu gline, vlaga). Poređenjem procesa sagorijevanja uglja iz glavnog sloja i iz povlatne zone u istom parnom kotlu uočavaju se savim novi efekti. Prvi efekat je praćen stvaranjem depozita od jedinjenja silicijuma i aluminijuma kao osnovnih elemenata novonastale legure. Pored ovih nalazi se i niz drugih elementi koji imaju tačku topljenja nižu

1250° C. Za transformaciju i nastajanje novih oksida i legura troši se značajna količina oslobođene toplote, što veoma mnogo umanjuje radijaciono predavanje toplote radnom fluidu i produkciju pare na kotlu, a samim tim i snag na pragu termoelektrane.

Drugi efekat taj, proces stvaranja novih jedinjenja prati i okrupnjavanje čestica koje po svojoj gabaritu i težini završavaju na dnu ložišta. U hladnom lijevku se sustižu i formiraju veće komade koji po gabaritu ne mogu proći kroz kanal za odvod šljake. Posljedica ovoga je začepljenje kompletnog kanala i zaustavljanje rada kotla odnosno bloka. Novonastala legura u hladnom stanju je vrlo visoke tvrdoće i vrlo je teško odstraniti iz ložišta.

Treći efekat se manifestuje u tome da je elektrofilterski pepeo značajno teži, njegova specifična težina je u odnosu na pepeo sagorijevanjem uglja iz glavnog sloja značajno veća. Kao takav stvara veliki otpor pri pneumatskom transportu do silosa, što izaziva zaustavljanje rada sistema. Zaustavljanje pneumatskog transporta izaziva zapunjavanje bunkera ispod elektrofiltera i samim tim nemogućnost rada elektrofilterskog polja. Taj efekat dovodi do povećane emisije čestica u okolinu. Kako je već rečeno proces sagorijevanja lignita sa velikim procentom silicijuma i drugih metala, u kotlu termoelektrane gacko, zahtijeva određenu količinu dodatnog goriva. Kotao je opremljen sa sistemom vodenih duvača, a čija je funkcija uklanjanje naljepaka šljake sa cijevnog sistema. U procesu koji je opisan nije moguće reagovati sa vodenim duvačima zato što dodatno snižavaju temperaturu radnog fluida i ugrožavaju temperaturu koja je u tehnološkoj zaštiti, a samim tim i doprinosi isključenju kotla odnosno bloka. U prethodnom periodu termoelektrana je imala dva neplanska zastoja zbog začepljenja kanala za odvoda šljake iz kotla. Usljed niza analiza i stvaranja mogućnosti za miješanje uglja iz glavnog ugljenog sloja ovaj problem se značajno promijenio. Rad kotla je stabilan, držanje osnovnih parametara je značajno olakšano, ne troši se mazut kao dodatno gorivo, zašljakivanje hladnog lijevka je smanjeno, pomjerena je vatrena lopta prema

projektovanom položaju. Zahvaljujući takvoj komponenti raspoloživog goriva (50% ugalj iz povlatne zone i 50% iz glavnog sloja ostvaruje se planirani obim proizvodnje električne energije.

7. ZAKLJUČAK

Neophodno je obezbijediti kontinuirani rad bloka i proizvodnju električne energije, iz raspoloživog goriva gatačkog basena. Organizaciju sagorijevanja lignita iz povlatne zone vršiti isključivo sa miješanjem lignita iz glavnog ugljenog sloja. Proces zašljakivanja donjeg dijela ložišta kontrolisati sa količinom goriva u ložištu i doziranjem dodatnog goriva (mazuta). Izbjegavati korišćenje lignita sa velikim procentom nesagorivih materija

REFERENCES

- [1] TE GACKO, *Izveštaj o ispitivanju uzoraka - Institutu za rudarstvo i metalurgiju Bor*
- [2] TE GACKO, *Upustvo za eksploataciju bloka*

CORRESPONDANCE



Borivoje VUJIČIĆ, M.Sc. Eng.
ZP "Rudnik i Termoelektrana Gacko" ad
Gračanica bb
89240 Gacko, Republika Srpska,
Bosna i Hercegovina
borivoje.vujicic@ritegacko-rs.ba

Ženja VUJOVIĆ, Eng.
ZP "Rudnik i Termoelektrana Gacko" ad
Gračanica bb
89240 Gacko, Republika Srpska,
Bosna i Hercegovina

STUDENT SESSION

MINI HYDRO POWER PLANT BASED ON PELTON TURBINE

Marko MUMOVIĆ
 Aleksandar TOMOVIĆ
 Vuk VUJOŠEVIĆ
 Marko RAŠOVIĆ
 Vasilije SAMARDŽIĆ
 Nikola ĆIRKOVIĆ
 Radoslav TOMOVIĆ

Key words: power plant, pelton, electric, bucket

Hydroelectric power plant is an electric for the production of electricity obtained by the power of water. Any water turbine is a means of extracting energy from falling water. Different types of turbines prefer different operating conditions. Propeller turbines work best at low head and high flow. Crossflow turbines require medium heads and flows. Pelton turbines work best under conditions of high head and low flow.

For our design of mini hydro power plant, we decided to construct and make the model of Pelton turbine.

Pelton turbine have many advantages. Firstly, because they can utilize high heads, they can produce a lot of power from a small unit. Secondly, they are reasonably to make. Thirdly, a given turbine can be used for a range of heads and flows. Fourthly, Peltons are particularly useful for driving small electrical generators. Even at modest heads, small Pelton wheels can be made to run at high speeds, which allows them to be matched to generators without the need for a belt drive or gearbox to change the speed.

The jet is directed at a wheel, or runner, which has a number of buckets around its edge. The force of the jet on this wheel makes it turn, and gives the output power.

The buckets have the shape of the two cups joined together, with a sharp ridge between them. There is a notch cut out of the bucket at the outside end of the ridge.

The water flows around the insides of the cupes, and exits from the sides of the bucket. The notch allows the jet to pass through the outside edge of the preceding bucket so that the first place it touches each bucket is the end of the splitter.

The power developed in a Pelton wheel completely due to the momentum change of the jet in the buckets. There is no change in water pressure across the runner. Pelton turbines are specified by their Pitch Circle Diameter (PCD). This is the tangential diameter at which the jet centerline passes the wheel.

For making a bucket we used the 3D printer.

Table 1: Setting the task and changing properties

First step: Setting the task and changing properties		
<div style="text-align: center;"> Input product Water from nozzle → Work of turbine → Output product Output voltage </div>		
Properties of input products		Properties of output products
Operation from the nozzle, flow 50 l/min, and pressure 4 bar		Voltage 12V
Additional Requirements		
Fixed requirements: - max dim. a x b x c = 1000 mm x 1000 mm x 1000 mm	Tolerated requirements: - flow 50 l/min - pressure 4 bar - position of nozzle	Wishes: - Bigger current



Fig.1: Buckets

Water is brought down the penstock pipe to a nozzle, and it comes out into the turbine casing as a fast, circular jet.

When choosing a number of buckets for a Pelton turbine the best solution seems to be using as few as possible and to fit them as close to the shaft. The problem is that if there are too few of the buckets some of the water in the

jet will not be caught, and therefore efficiency of the turbine will be smaller. The exact number depends on the bucket design, but is generally between 18 and 22 buckets. The number of buckets can be found by drawing or by using following equations.

$$z_k = \sqrt{\frac{D_1}{d_0}} + 17, \text{ when is } \frac{D_1}{d_0} > 12 \quad (1)$$

$$z_k = 0.4 \cdot \frac{D_1}{d_0} + 16, \text{ when is } \frac{D_1}{d_0} = 12 \quad (2)$$

$$z_k = 0.5 \cdot \frac{D_1}{d_0} + 15, \text{ when is } 6 < \frac{D_1}{d_0} < 35 \quad (3)$$

Calculating the forces on the shaft in a Pelton turbine is relatively straightforward. The main forces come from the water jets, the runner and the shaft weight, the bearings, and the drive system. Formula for the calculation of the jet force:

$$F_{jet} = \frac{T}{n_{jet} \cdot \left(\frac{D}{2}\right)} = \frac{60 \cdot P_{mech}}{\eta_{force} \cdot \pi \cdot n_{jet} \cdot D} \quad (4)$$

D_1 – pitch circle diameter, a diameter where the jet hits the bucket

d_0 – diameter of the nozzle

In this project we have chosen 18 buckets as an optimal number for this application.

If they are numbered make sure that they are numbered consequently. Put the numbers in parentheses flush with the right - hand margin level with the last line of the equation.

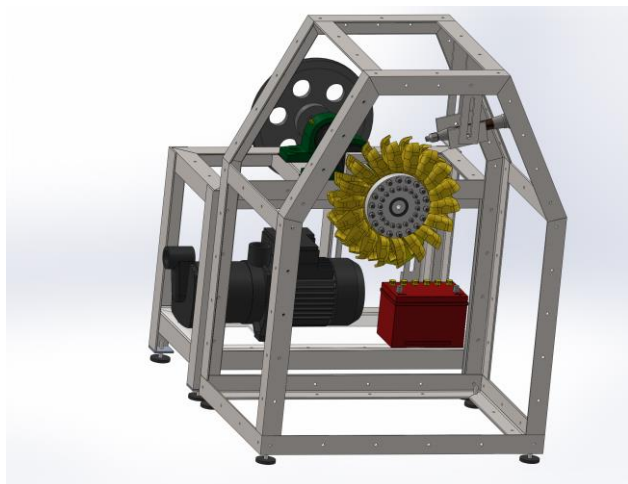


Fig.2: 3D model

REFERENCES

- [1] JEREMY THAKE (2000) *The micro-hydro Pelton turbine manual, Design, Manufacture, and Installation for small-scale Hydropower.*

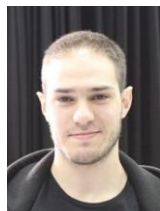
CORRESPONDANCE



Marko MUMOVIĆ, Student
University of Montenegro
Mechanical Engineering Faculty
Bul. Džordža Vašingtona bb
81000 Podgorica, Montenegro
markomumovic@gmail.com



Aleksandar TOMOVIĆ, Student
University of Montenegro
Mechanical Engineering Faculty
Bul. Džordža Vašingtona bb
81000 Podgorica, Montenegro
aleksandartomovic23@gmail.com



Vuk VUJOŠEVIĆ, Student
University of Montenegro
Mechanical Engineering Faculty
Bul. Džordža Vašingtona bb
81000 Podgorica, Montenegro
vukvujosevic7@gmail.com



Marko RAŠOVIĆ, Student
University of Montenegro
Mechanical Engineering Faculty
Bul. Džordža Vašingtona bb
81000 Podgorica, Montenegro
markorasovic2@gmail.com



Vasilije SAMARDŽIĆ, Student
University of Montenegro
Mechanical Engineering Faculty
Bul. Džordža Vašingtona bb
81000 Podgorica, Montenegro
vanja.mika@t-com.me



Nikola ĆIRKOVIĆ, Student
University of Montenegro
Mechanical Engineering Faculty
Bul. Džordža Vašingtona bb
81000 Podgorica, Montenegro
nikola.cir.225@gmail.com



Radoslav TOMOVIĆ, Prof. D.Sc. Eng.
University of Montenegro
Mechanical Engineering Faculty
Bul. Džordža Vašingtona bb
81000 Podgorica, Montenegro
radoslav@ac.me

CONSTRUCTION OF PELTONS MINI HYDROPOWER PLANT MF MOSTAR

Kenan PELKO
Edmin HAKALOVIĆ
Arnel MAKSUMIĆ
Muhamed GOSTO
Jasmina ŠENDRO
Safet ISIĆ

Key words: mini hydropower plants, power transmission

Hydropower or water power is power derived from the energy of falling water or fast running water, which may be harnessed for useful purpose. The water is collected through the blades and piped where it pressurized through the nozzle aimed to hit the hydraulic wheel. The power that spins the wheel will be connected to the electric generator. Electricity is transformed and transmitted through the power transmission network and directed to further use.

The project that we are launching with the construction of a small hydro power plant will give us a new experience, and thus we will also gain new working habits in the field of science.

The task is determined that the project has to be compiled into the dimension space axbxc (1m x 1m x 1m). For the start we'll have to determine which generator and also turbine to choose based on power of water. The water power from the initial conditions (50 l/min = 0.000833 m³/s at 4 bar pressure) is calculated from the formula:

$$P(W) = Q \left[\frac{m^3}{s} \right] \cdot p \left[Pa = \frac{N}{m^2} \right] \quad (1)$$

With the power of water and certain losses on turbine blades, bearing and certain power transformer we would determine the power and the type of electric motor that would turn to the operation mode as a generator. We were planning on using Pelton's type turbine or Turgo's type turbine that would provide us with great efficiency, taking into account that we will be working with small low water flow, and efficiency is playing a big role in this project. We were planning on using pvc materials for the turbine and simple house spoons for the blades of the turbine that would be connected to the turbine wheel.

For calculating diameter of turbine our priority would be to achieve enough momentum for starting entire system, and at the same time to get as much speed as possible for rotation of the turbine so we could harness more power at generator output.

Additionally, we would choose an adequate pair of bearings to bring the power of water, brought to the turbine blades to the generator with as little loss as possible. The turbine would be enclosed with glass or plexiglass so that there would not be water dissipation around the same. On the next picture we have presented hand drawn idea of our project.

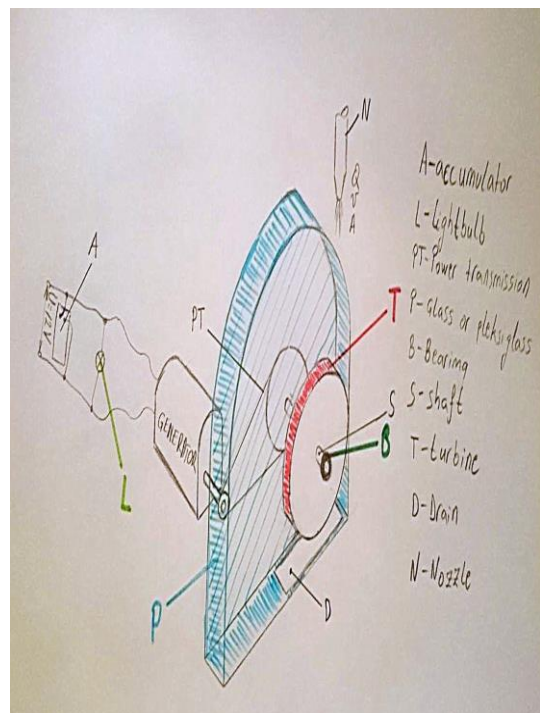


Fig.1: Hand drawn idea of our project

For the start of the project we tried to construct a single blade for peltons turbine and prototype and it went pretty well taking in account that we used simple only simple spoons. We've taken two spoons removed handles and welded bowls of the spoon together to create as similar as possible shape to peltons blade.

The next picture only shows the prototype and if we would be using this type of blades we would do our best to improve them in every possible way.



Fig.2 : Our prototype of blade for peltons turbine

Under the turbine we would construct an opening that would be used as water output from turbine. On the end of the system, that is behind the generator there would be a bulb to signal generation of electricity and battery charger as it is was requested by the task.

On the end of this presentation there will be presented a table with names and price of the used materials. Everything needed for construction of the project would be either purchased on internet or homemade.

Table 1 : Necessary materials for the project

No	Item	Explanation
1.	Generator	The generator is the main thing for this project.
2.	Bearings	They are responsible for the transfer of power from the turbine to pulley.
3.	Belt drive	Transmits power with pulleys to the generator.
4.	Tablespoons	It will be used for making turbine.
5.	Water hose	It serve to bring water to the turbine.
6.	Plexiglas	Preventing the water spray.

REFERENCES

- [1] MARGARETA ZIDAR (2013)
<http://www.menea.hr/wp-content/uploads/2013/12/6-hidroelektrane.pdf>
- [2] Wikipedia, May 2017,
https://en.wikipedia.org/wiki/Pelton_wheel

CORRESPONDANCE



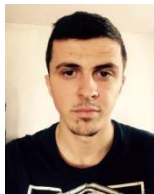
Kenan PELKO, Student
 University of Džemal Bijedić
 Faculty of Engineering
 Univerzitetski Kampus/
 88104, Mostar , Bosnia and Herzegovina
 pelko.kenan@outlook.com



Edmin HAKALOVIĆ, Student
 University of Džemal Bijedić
 Faculty of Engineering
 Univerzitetski Kampus
 88104, Mostar , Bosnia and Herzegovina
 edminhakalovic@hotmail.com



Arnel MAKSUMIĆ, Student
 University of Džemal Bijedić
 Faculty of Engineering
 Univerzitetski Kampus
 88104, Mostar , Bosnia and Herzegovina
 arnelmaksumic96@gmail.com



Muhamed GOSTO, Student.
 University of Džemal Bijedić
 Faculty of Engineering
 Univerzitetski Kampus
 88104, Mostar , Bosnia and Herzegovina
 gosto1337@gmail.com



Jasmina ŠENDRO, Student.
 University of Džemal Bijedić
 Faculty of Engineering
 Univerzitetski Kampus
 88104, Mostar , Bosnia and Herzegovina
 jasmina.sendro@gmail.com



Safet ISIĆ, Prof. D.Sc. Eng.
 University of Džemal Bijedić
 Faculty of Engineering
 Univerzitetski Kampus
 88104, Mostar , Bosnia and Herzegovina
 safet.isic@unmo.ba

ACHIEVING LOW COST, HIGH EFFICIENCY PELTON TURBINE

Enis HABUL
 Armin MUŠIĆ
 Muhamed GRAČIĆ
 Sven BOREC
 Mirsad BERBEROVIĆ
 Emir NEZIRIĆ

Key words: Pelton turbine, hydroelectricity, electricity, sustainability, hydropower

Hydroelectric power is a relatively inexpensive, efficient and sustainable form of energy. Given the increasing focus on developing energy without the use of fossil fuels, hydroelectricity stands as a viable option. Therefore, it is important for today's engineers and scientists to optimize existing hydroelectric technology so that it may better serve as a standard mechanism for generating power.

Specifically, Lester Allen Pelton's "Pelton Wheel" has been in existence since the 1870s, yet remains the preferred design choice for some of the world's largest and most advanced hydroelectric power plants.

We believe the Pelton Turbine is the best candidate for the continued development and reliance on hydroelectric power. Our miniature turbine will demonstrate how this design can be applied at a small scale and built to exact specifications to produce the desired outcome of 12 volts to power a light bulb. Additionally, our Pelton Turbine will prove that reaching the target energy output can be affordable, elegant and compact.

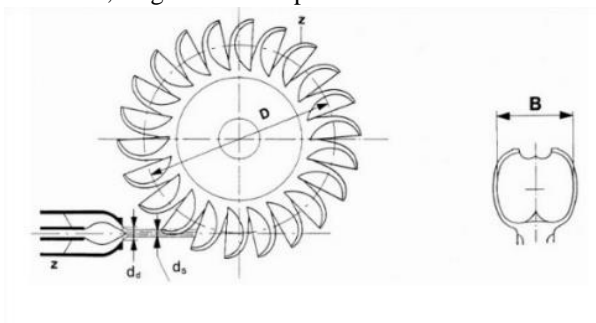


Fig. 1: Diagram of a Pelton Turbine

The Pelton Turbine utilizes buckets instead of paddles, which allows for as much as 95 percent hydraulic

efficiency. We hope ours will achieve 65 percent efficiency. With the given data:

$$Q = 50 \frac{l}{min} = 0.000833 \frac{m^3}{s}, p = 4 \text{ bar}$$

We calculated the maximum power of water:

$$P = \gamma * Q * H = 9.802 \frac{kN}{m^3} * 0.000833 \frac{m^3}{s} * 40.77371 \text{ m} = 326.60 \text{ W}$$

Given the limitations in this specific project, and factoring in some net loss from the max power of water, we hope to obtain 60 W of electricity from our turbine.

To determine the dimensions for our turbine, we had to calculate the diameter of the nozzle, where d_s is the diameter of the nozzle, Q is flow, z is the number of nozzles, and V_a is the real velocity of the jet:

$$d_s = \sqrt{\frac{4 \cdot Q}{z \cdot \pi \cdot V_a}} = \sqrt{\frac{4 \cdot 0.000833}{1 \cdot \pi \cdot 27.44}} = 0.0061 \text{ m} = 6.1 \text{ mm}$$

From there, we determined the diameter of the turbine, where V_1 is the theoretical velocity of the jet, V_a is the real velocity of the jet and C_v is the coefficient of the velocity of the jet (0.98~0.99):

$$V_1 = \sqrt{2 * g * H} = \sqrt{2 * 9.81 * 40.77471} = 28 \frac{m}{s}$$

$$V_a = V_1 * C_v = 28 * 0.98 = 27.44 \frac{m}{s}$$

$$D = 30 * d_s = 30 * 6.1 = 183 \text{ mm}$$

We also calculated the dimensions of the bucket, according to the following diagram:

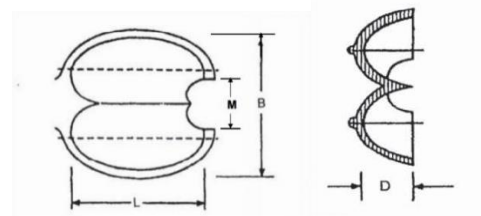


Fig. 2: Dimensions of the bucket

We calculated each of the bucket dimensions according to the following:

$L = 20 \text{ to } 30d_s = 20 * 6.1 = 122 \text{ mm}$
 $B = 25 \text{ to } 50d_s = 20 * 6.1 = 152.5 \text{ mm}$
 $M = 11 \text{ to } 15d_s = 11 * 6.1 = 67.1 \text{ mm}$
 $D = 8 \text{ to } 12d_s = 8 * 6.1 = 48.8 \text{ mm}$

Given these calculations, we determined velocity of the wheel and revolutions per minute:

$$\frac{U}{V_1} = 0.45$$

$$U = V_1 * 0.45 = 28 * 0.45 = 12.6 \frac{\text{m}}{\text{s}}$$

$$n = \frac{U * 60}{\pi * D} = \frac{12.6 * 60}{\pi * 0.183} = 1314 \text{ rpm}$$

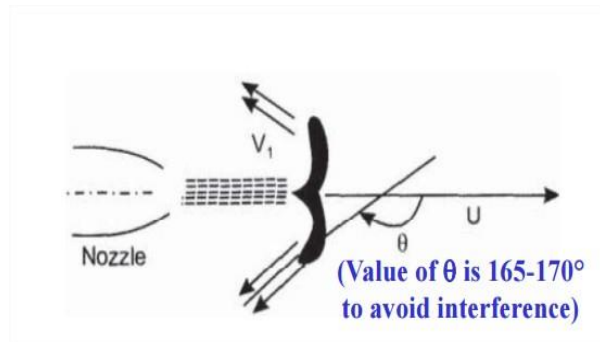


Fig. 3: Velocity of the wheel

To build our turbine, we were faced with three options: Create a mold, use a 3-D printer, or construct it using aluminum piping. Creating and sourcing materials for a mold proved too costly, so we are left to choose between 3-D printing and manual construction. There are pros and cons to both methods:

A 3-D printer is cleaner and simpler. However, the cost and access for 3-D printers is not ideal – it can be expensive and not everyone has ready access to such technology.

Manual construction with aluminum piping involves more labor, but such materials are inexpensive and easy to find.

Even with a focus on reducing cost and complexity, we are confident the Pelton Turbine is the best design for this task.

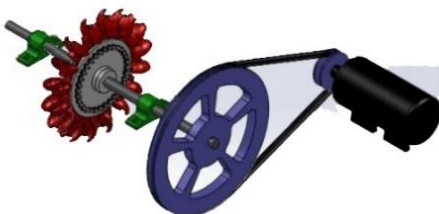


Fig. 4: Diagram of Pelton Turbine mechanism

Hydroelectricity has great use for both large- and small-scale applications. We hope our Pelton Turbine will demonstrate effectively that, even with limited budgeting and resources, it is very possible to generate the necessary amount of electricity to power a light bulb, store energy or perform other minor tasks. Today, with our over-

reliance on fossil fuels, technologies like this are crucial for both sustainability and access to affordable, effective electricity.

CORRESPONDANCE



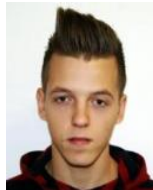
Mirsad BERBEROVIĆ, Student
 “Džemal Bijedić” Uni. of Mostar
 Faculty of Mechanical Engineering
 88104 Mostar, BiH
mirsoberberovic123@gmail.com



Enis HABUL, Student
 “Džemal Bijedić” Uni. of Mostar
 Faculty of Mechanical Engineering
 88104 Mostar, BiH
enis.habul@edu.fit.ba



Armin MUŠIĆ, Student
 “Džemal Bijedić” Uni. of Mostar
 Faculty of Mechanical Engineering
 88104 Mostar, BiH
armin.music@live.com



Muhamed GRAČIĆ, Student
 “Džemal Bijedić” Uni. of Mostar
 Faculty of Mechanical Engineering
 88104 Mostar, BiH
gracicmuhamed@gmail.com



Sven BOREC, Student
 “Džemal Bijedić” Uni. of Mostar
 Faculty of Mechanical Engineering
 88104 Mostar, BiH
sven.borec@gmail.com



Emir NEZIRIĆ, Prof. Dr. Sc. Eng.
 “Džemal Bijedić” Uni. of Mostar
 Faculty of Mechanical Engineering
 88104 Mostar, BiH
emir.nezirc@unmo.ba

HYDROTURBINE MADE FROM RECYCLED SCRAP MATERIALS

Ahmed TAJAR
Samir RUSTEMPAŠIĆ
Amir OMERAGIĆ
Sead IMAMOVIĆ
Alem KARAOSMANOVIĆ
Emir NEZIRIĆ

Key words: hydroturbine, recycling, electric power

The idea for project is to use recycled material in this case it is an Aluminium, which will be taken to make a turbine.



Fig. 1. Recycled materials for turbine parts

Blades of turbine will be made of pipe irregular (D) shape, and the pipe will be cut longitudinally and transversally. Blades will be attached for carrier by screws. The carrier of the blades presents two disks which will be taken from the washing machine. Shaft will be made of steel and have full cross section. For the bearings it will be used standard definition 6004.



Fig. 2. 3D model of turbine

To make carrier of a construction it will be used steel pipe with dimensions 40x40x2. Protection construction of external influences will be provided by plexiglas panels.

On the top of construction it will be made a hole for supply turbine with water, and after it pass turbo blades water will go out on bottom drain pipe.

Dynamo will be situated into the housing of a construction and it will be protected out of water effect. Then it will be mounted on construction by steel carrier. The transfer of the force from turbine to alternator will be realized by two pulleys. Mechanical work on pulley 1 will be transferred with belt to pulley 2 respectively on dynamo.

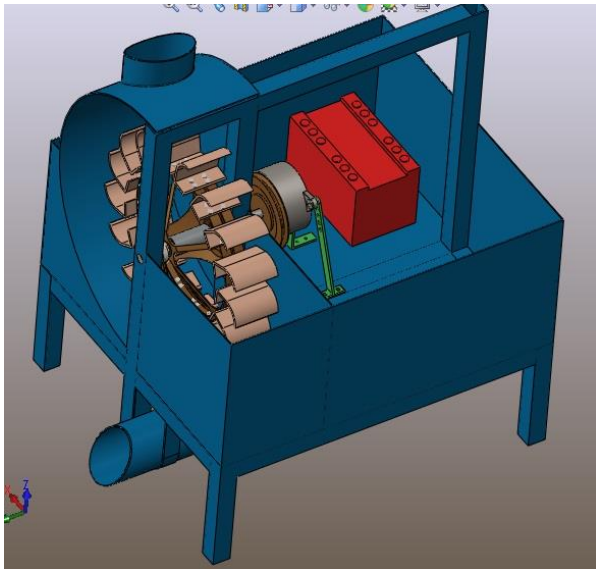


Fig. 3. 3D model of prototype

Table 1. Parts used for power plant

No	Item	Explanation
1.	Irregular (D) shape pipe	Used for turbine blade.
2.	Wash machine pulley	Turbine blade carrier.
3.	Steel pipe with dimension (40x40x2)	Used for main frame.
4.	Automotive dynamo	Producing electric energy.
5.	Plexiglass	Used for covers.

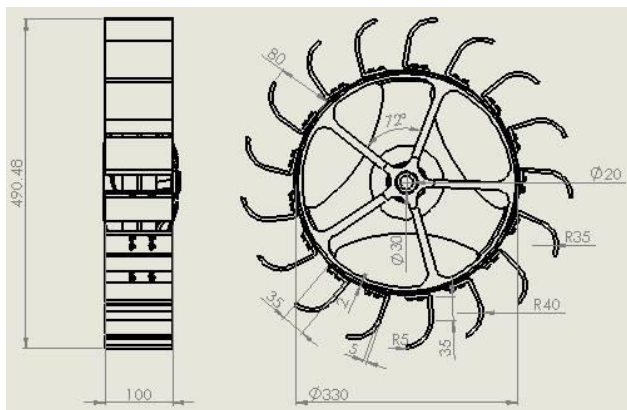


Fig. 4. Drawing of turbine with impellers positions

REFERENCES

- [1] INŽINJERSKO TEHNIČKI PRIRUČNIK Mašinski elementi – Projektovanje, Vol.4 (1979)
- [2] INŽINJERSKO TEHNIČKI PRIRUČNIK Otpornost materijala – Proračun konstrukcija, vol.3 (1979)

CORRESPONDANCE



Ahmed Tajar
University of Mostar
Mechanical Engineering Faculty
Sjeverni Logor
88104 Mostar, Bosnia and Herzegovina
ahmo94@hotmail.com



Samir Rustempašić
University of Mostar
Mechanical Engineering Faculty
Sjeverni Logor
88104 Mostar, Bosnia and Herzegovina
crna_vrana@hotmail.com



Amir Omeragić
University of Mostar
Mechanical Engineering Faculty
Sjeverni Logor
88104 Mostar, Bosnia and Herzegovina
omeragic247@gmail.com



Sead Imamović
University of Mostar
Mechanical Engineering Faculty
Sjeverni Logor
88104 Mostar, Bosnia and Herzegovina
sead.imamovic@hotmail.com



Alem Karaosmanović
University of Mostar
Mechanical Engineering Faculty
Sjeverni Logor
88104 Mostar, Bosnia and Herzegovina
alem_karaosmanovic@hotmail.com



Emir Neziric, D.Sc. Eng.
University of Mostar
Mechanical Engineering Faculty
Sjeverni Logor
88104 Mostar, Bosnia and Herzegovina
emir.nezirc@unmo.ba

MINI HYDRO POWER PLANT

Kenan STARČEVIĆ
Nihad BEŠIĆ
Izet AHMIČEVIĆ
Dragi TIRO

Key words: brief insight into our project.

In the following text, we will briefly refer you to our system and our solution to the problem of "mini hydroelectric power plants". Our way of implementing this project stands for the simplest way to get electricity and maximize the capacity of machine elements used in our project. The project itself gives the possibility of various contralateral performances. Our team is committed to the simplest contractual performance, the better the aesthetics of the project itself, and the great economic convenience of performing it.

First of all, we have decided that all parts used for the project are already used parts (due to economics). In our electricity production system the greatest attention is given to the greater utilization of natural resources (water). By design we decided to accumulate water and increase the water pressure acting on our turbine. Due to the high pressure on the turbine blades, the turbine speed is increased.

The turbine made of lightweight material will be connected to the alternator over the shaft. For the shaft we will use the best material to reduce the power losses we achieve on the turbine. Given that the bearings are paying great attention to the budget and having a great impact on the loss of strength in our case we will strive to choose the best. Through the shaft to the pulley and from the twist to the alternator found on the car waste and our reconstruction, we are coming to the most important part of our system. The alternator will be our "generator" in our mini power generator.

Table 1: Parts

No	Item	Explanation
1.	Bearings	According to our needs and according to the market price, we will cost us < 20 BAM
2.	Bracing pulleys	According to our needs and according to the market price, we will cost us about 50 BAM
3.	Alternator	60 BAM
4.	Box	We did not find out
5.	Shafts	We did not find out

The more efficient transmission of power, torque and torque from the turbine to the pulley and the better the performance of the pulley, the greater the amount of electricity we will have, as well as the budget. With the first practical turbine testing we found that we did not make a mistake when selecting the turbine construction itself. The great advantage of our system is quiet and quiet work. The machine system itself will be protected by a tin-plated construction so that there is no injury to the system. In order to have a better look in use, it will be the best color and varnish.

Below 1.(Parts) are some of the parts that will be used in our project and their prices, and the financial part of the funds is provided by our faculty. By consulting with our mentor, we have found that it is economical and fairly easy to implement, which gives us a certain amount of confidence that this kind of mini-hydro power plant will work. In the forthcoming period, we will work to provide you with a more detailed 3D rendering system that we will model in one of the most up-to-date software, namely SOLID WORKS.

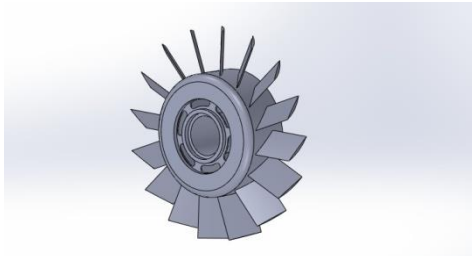


Fig.1: Turbine

In Figure 1(Turbine) is the model of our turbine, drawn in solidworks. In this software we also performed a simulation, which helped us to perform the equation for the output power.

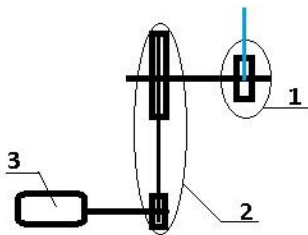


Fig.2: Scheme

In Figure 2(Scheme) we see the schematic representation of electricity generation. The diagram shows the turbine (1), spindle bracket (2), alternator (3). Although not shown in the alternator scheme, part of the energy obtained will be used to work bulbs and the remaining energy to another consumer. Also not shown are constructions and bearings.

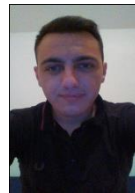
REFERENCES

- [1]JOHN WARD – SMITH, Mechanics of Fluids, Ninth Edition
- [2]MANJGO MERSIDA, FADIL ISLAMOVIĆ (2015), Mašinski elementi 2

CORRESPONDANCE



Kenan STARČEVIĆ
University "Dzermal Bijedic" Mostar
Mechanical Engineering Faculty
Piljužići br.70
74264, Jelah, BiH
kenan_201295@hotmail.com



Nihad BEŠIĆ
University "Dzermal Bijedic" Mostar
Mechanical Engineering Faculty
Babići – Omerbašići bb
75320, Gračanica, BiH
nihad-besic1@hotmail.com



Izet AHMIČEVIĆ
University "Dzermal Bijedic" Mostar
Mechanical Engineering Faculty
Tuzlanskog odreda br.9
75350, Srebrenik, BiH
izet.ahmicevic.2010@gmail.com



Dragi TIRO, prof.dr.
University "Dzermal Bijedic" Mostar
Mechanical Engineering Faculty
Univerzitetski kampus
88104, Mostar, BiH
dragi.tiro@unmo.ba

CNC Plotter

Aleksandar TOMOVIĆ
Vasilije SAMARDŽIĆ
Marko RAŠOVIĆ
Marko MUMOVIĆ
Vuk VUJOŠEVIĆ
Zoran MIJANOVIĆ

Key words: CNC, machine, G-code

Nowadays the machine industry is unimaginable without modern CNC (Computer Numerical Control) machines. CNC machines have more or less the same parts as old, hand-controlled machines. The important difference is the addition of a control (CNC) unit and servo motor to all shafts. CNC calculates the coordinates where the shaft should be and controls the servo motors that move the tool, the turning machine, or the treated part, (milling machine) through the ball screw.

The programming of these machines is done in several ways:

- ISO programming (G-code, M-code, cycles, etc..),
- Dialogue programming (symbols, drawings and many other features),
- CAM programming 3D (complex drawings are transformed into a mechanical program).

For the programming of this CNC machine we used the G-code, the working environment of the Processing program.

To assemble the mechanical part of the CNC plotter, the following materials were used:

- wooden stand,
- two wooden battens (holders),
- two aluminum tetrax holders,
- four steel shafts (shock absorbers of the rear doors on the car) for movement in the direction X and Y axis,
- one aluminum tetrax holder (for marker, movement in the direction of Y axis),
- plywood as a paper base (movement in the direction X axis),
- marker holder, printed on 3D printer
- marker (as writer)
- silk (fishing thread) and two wheels (as a pulley)

As well as parts of electronics:

- Arduino UNO microcontroller
- 2x ULN2003 stepper driver + 2x 5V step motors (for drive in X and Y direction)
- 1x micro servo (to lower marker)
- breadboard
- wires

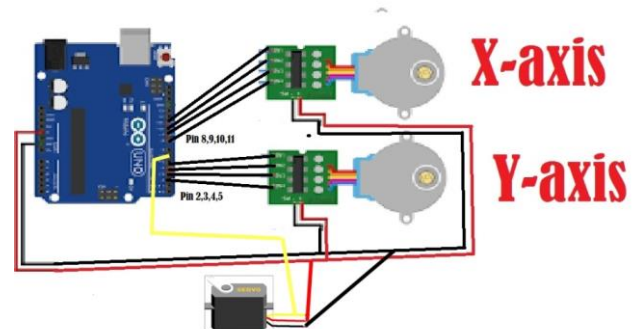


Fig.1: Connection scheme

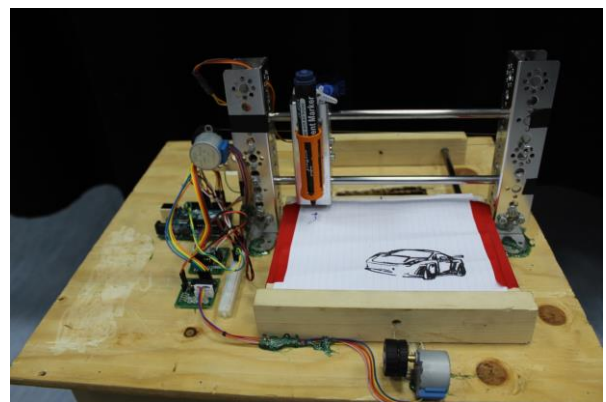


Fig.2: CNC plotter

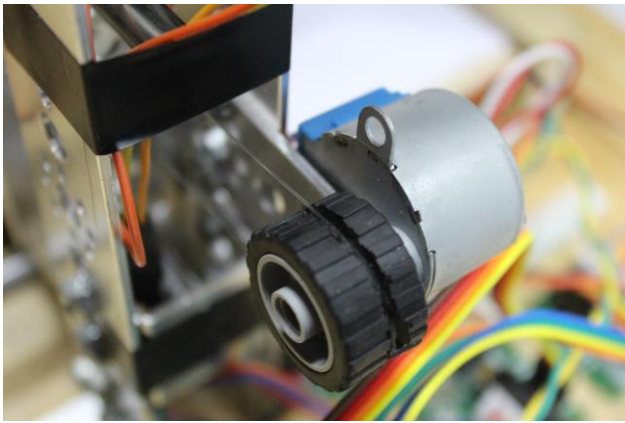


Fig.3: Step motor and a wheel as a pulley (Y axis)

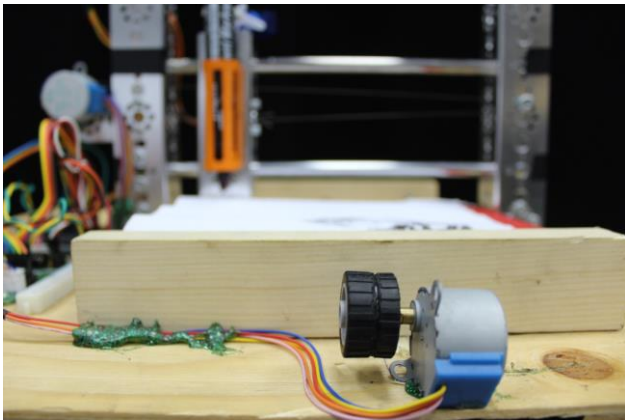


Fig.4: Step motor and a wheel as a pulley (X axis)

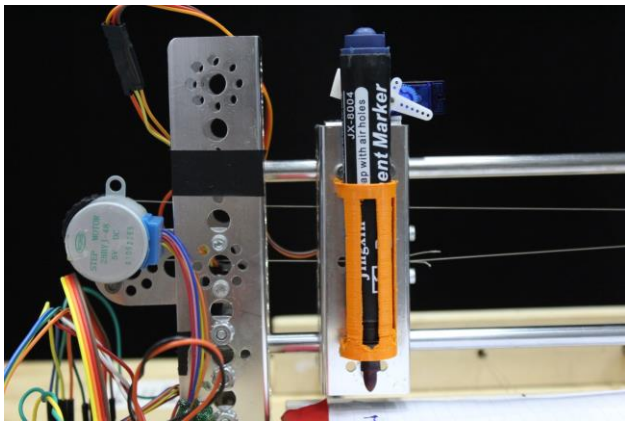


Fig.5: Holder for marker

For the connection between the G-code and the microcontroller we used a program written in the Arduino working environment, and for the operation of the CNC plotter we used the Processing program.

How to Operate and Launch the Program Code:

1. Connect Arduino to the computer, then compile and upload the program (Arduino code) on the development board.
2. Run the program (G-code) in the Development environment Processing.



Fig.6: Drawing of CNC plotter

REFERENCES

- [1] <https://www.youtube.com/watch?v=szXNpI4GydA>.

CORRESPONDANCE



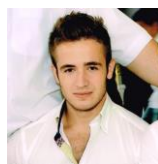
Aleksandar TOMOVIĆ, Student
University of Montenegro
Mechanical Engineering Faculty
Bul. Džordža Vašingtona bb
81000 Podgorica, Montenegro
aleksandartomovic23@gmail.com



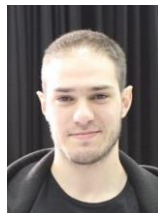
Vasilije SAMARDŽIĆ, Student
University of Montenegro
Mechanical Engineering Faculty
Bul. Džordža Vašingtona bb
81000 Podgorica, Montenegro
vanja.mika@t-com.me



Marko RAŠOVIĆ, Student
University of Montenegro
Mechanical Engineering Faculty
Bul. Džordža Vašingtona bb
81000 Podgorica, Montenegro
markorasovic2@gmail.com



Marko MUMOVIĆ, Student
University of Montenegro
Mechanical Engineering Faculty
Bul. Džordža Vašingtona bb
81000 Podgorica, Montenegro
markomumovic@gmail.com



Vuk VUJOŠEVIĆ, Student
University of Montenegro
Mechanical Engineering Faculty
Bul. Džordža Vašingtona bb
81000 Podgorica, Montenegro
vukvujosevic7@gmail.com



Zoran MIJANOVIĆ, Prof. D.Sc. Eng
University of Montenegro
Faculty of Electrical Engineering
Bul. Džordža Vašingtona bb
81000 Podgorica, Montenegro
zoranm@ac.me

DEVELOPMENT OF A THERMAL POWER PLANT TUBULAR BOILER CLEANING MACHINE

Slavoljub MARKOVIĆ
Dino TIHIĆ
Srđan ĐERIĆ
Biljana MARKOVIĆ

Key words: development, boiler, cleaning, thermal power plant, cleaning

1. INTRODUCTION

This study is made in order to show the potential of innovative mechanised and semi-automatised solutions for a cleaning process, that happens in the boiler section of a thermal power plant, with the supporting analysis for developed solution.

As the cleaning process of these sections of thermal power plants represents very hard labour, it needs a great number of participants, varying from 60 to even a 100, which also means that this process needs a significant amount of financial resources, taking in the fact that the cleaning needs to happen at least 5 times annually. Clothes, tools and the environment that characterizes the cleaning process is shown in Fig. 1.



Fig1. One of the participants in the boiler section carrying a cleaning tool

For this study, the team has made a questionnaire, that was sent to 20 recipients working in this area, some of them being regular participants. Also, the team

investigated the market, seeking existing solutions with the abovementioned function. As a final task, the team will evaluate three possible variants, that will be assessed using methods of variant evaluation, and develop a model of the one that is satisfying the requirements the most.

The team will use several methods in order to determine the functionality and profitability of the machine in question, using the CHECK list, regarding the financial, functional, ergonomic, aesthetic and maintenance requirements, as a starting point. Also, the cleaning process in thermal power plants located in Gacko and Ugljevik will be set as an example and a basis for the analysis.

2. PRODUCT DESCRIPTION AND PURPOSE

The cleaning machine is developed for semi-automatized removal of the sediment rock shown in Fig 2., that's made of sublimated particles of combustion products, which is located on the tubes in the boiler section. These tubes have a "chess" layout, with the vertical and diagonal gaps between them and, while tubes mustn't be damaged, the rock needs to be totally removed from those gaps.



Fig. 2 Sediment rock

To achieve that, the developed machine has a saw-like cutting tool, that is breaking off the chunks of rock while moving through the space between the tubes (approx. 80 mm). Also, the machine possesses the ability to rotate at

the maximum angle of 45 degrees in one or either side, in relation to the ground, allowing the cutting tool to breach through the diagonal gaps filled with sediment.

Although this process leaves some chunks of sediment untouched, that is a small amount, and can be cleaned with the manual tools (ex. "spears").

Through the analysis of variant solutions, few options emerged concerning the mechanism for driving of the cutting blade, two of which were plausible solutions – an electromotor and a pneumatic motor.

The team decided to implement the pneumatic motor as it is cleaner, quieter, with smaller amount of parts and maintenance needed, as well as the fact that the pneumatic lines, with the appropriate pressure, are accessible and free to use in the boiler section.

As for the machine movement, the team settled for the manual labour, because of its simplicity, from the automatization and maintenance aspect, and versatility, as well.

Taking into the account the information from the questionnaire, and information that derived from the simulation, we conclude that the machine:

- Weights approximately 50 [kg],
- Has a light for additional illumination,
- Works in low noise level as possible,
- Has soothing colour,
- Has a modular design with a removable cleaning body,
- Can clean vertical and diagonal gaps,
- Has additional cleaning bodies in the reserve.

3. ADVANTAGES

The team has made an analysis of the market, seeking for the existing solutions and estimating the possible market demand for this type of product, taking into consideration the number of the thermal power plants existing in the vicinity, from which the following can be stated:

- The team failed to find similar existing solutions on the market;
- The market demand for this type of product is significant;

Substantial advantages of this solution are, as follows:

- Modular design,
- Lightweight construction,
- Versatility in different environments,
- Cleanliness,
- Simple design for maintenance, assembly and disassembly,
- Inexpensive parts.

4. CONCLUSION

After the consideration of the acquired information, it can be concluded that:

- The process of cleaning the boiler of a thermal power plant is a very hard labour;
- The process needs to be mechanised, which will make it more cost and time efficient;
- Mechanised cleaning will not eliminate the manual labour, but it will be greatly reduced,

- There is a number of thermal power plants in the vicinity, that could invest in this innovative solution;
- The machine should perform the work more effectively and efficiently compared to the existing method;
- The machine has dimensions compatible with the boiler section, and it must not damage the tubes or the boiler,
- There is a significant demand for the innovative solution on the market,
- The team failed to find another competitive product.

REFERENCES

- [1] MARKOVIĆ, B., MILOVANČEVIĆ, M., JEREMIĆ, D. (2015.) *Upravljanje razvojnim projektima*, Univerzitet u Istočnom Sarajevu, Mašinski fakultet
- [2] MILTENOVIĆ V. (2003) *Integralni razvoj proizvoda*, Univerzitet u Nišu, Mašinski fakultet
- [3] OGNJANOVIĆ M. (2014) *Inovativni razvoj tehničkih sistema*, Univerzitet u Beogradu, Mašinski fakultet

CORRESPONDANCE



Slavoljub MARKOVIĆ
University of East Sarajevo
Faculty of Mechanical Engineering
Vuka Karadžića 30
71126 Lukavica, Istočno Sarajevo
Republika Srpska, Bosnia and
Herzegovina
slavoljubm1970@gmail.com



Dino TIHIĆ
University of East Sarajevo
Faculty of Mechanical Engineering
Vuka Karadžića 30
71126 Lukavica, Istočno Sarajevo
Republika Srpska, Bosnia and
Herzegovina
tihic.dino@gmail.com



Srđan ĐERIĆ
University of East Sarajevo
Faculty of Mechanical Engineering
Vuka Karadžića 30
71126 Lukavica, Istočno Sarajevo
Republika Srpska, Bosnia and
Herzegovina
srdjandjeric95@gmail.com



Biljana MARKOVIĆ, Prof. dr
University of East Sarajevo
Faculty of Mechanical Engineering
Vuka Karadžića 30
71126 Lukavica, Istočno Sarajevo
Republika Srpska, Bosnia and
Herzegovina
biljana46m@gmail.com

MOBILE NXT ROBOT THAT IS MANAGED VIA A BLUETOOTH CONNECTION

Aleksandar TOMOVIĆ
Marko MUMOVIĆ
Vasilije SAMARDŽIĆ
Vuk VUJOŠEVIĆ
Marko RAŠOVIĆ
Marina MIJANOVIĆ MARKUŠ

Key words: NXT, microcontroller, sensors

This robot is managed using the NXT microcontroller. Lego Mindstorms NXT is the second set of Lego Mindstorm collections, which is designed by Lego. The set consists of NXT microcontrollers, various sensors (color sensor, sound, ultrasonic sensor ..) servo motors, as well as cubes of various shapes and sizes, wheels, etc. NXT is a microcontroller consisting of 4 input ports for sensors, 3 output motor ports, and a USB port port, and is shown in Figure 1.



Fig.1: NXT microcontroller

The robot is made of parts from the TETRIX set and the NXT microcontroller. The following parts were used to assemble a robot: TETRIX rails, fixed wheels (drive front wheels), wheels with 2 degrees of freedom (rear wheels), 12V DC TETRIX motor, casing for DC motor, power supply of 12 V, 3000 mAh motors (batteries), DC motor controller for TETRIX, power switch, NXT microcontroller.

DC TETRIX motors are powered by a 12V battery and connected to a DC motor controller for TETRIX, which is connected to the NXT Microcontroller for detecting the motor. The battery is connected to the motor controller via which it drives the motors.

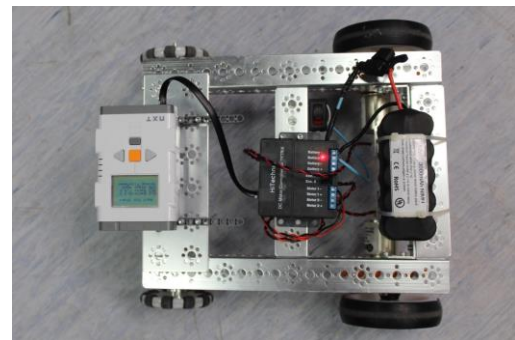


Fig.2: Mobile NXT robot



Fig.3: Batteries

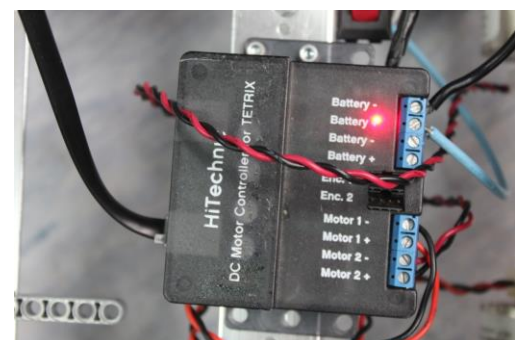


Fig.4: DC motor controller for TETRIX

The mode of communication between the robot and the computer was realized through bluetooth, and the robot was operated via the keyboard.

The program code is written in the RobotC work environment, intended for NXT microcontrollers. Since the RobotC work environment contains pre-existing Joystick libraries, we have used PPJoy program to create a virtual joystick on the keyboard.

First, it was necessary to perform the adjustment and configuration of the PPJoy program, to select the control key.

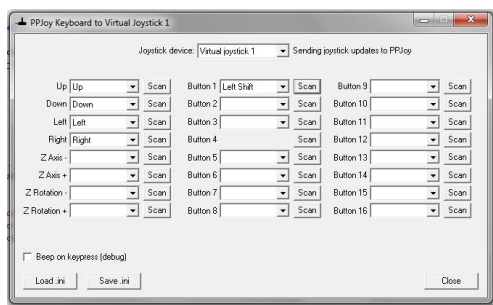


Fig.5: Configuration of PPJoy paramteres

After the start of the RobotC operating environment, it was first necessary to configure the DC TETRIS motor, then download the firmware to the NXT microcontroller via a USB cable. The next step was to compile and upload code on the NXT microcontroller, and then pair with Bluetooth.

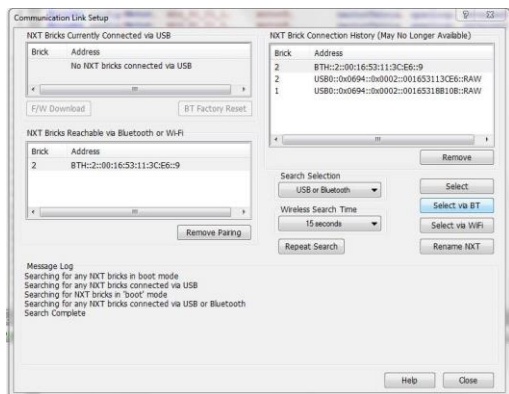


Fig.6: Bluetooth configuration

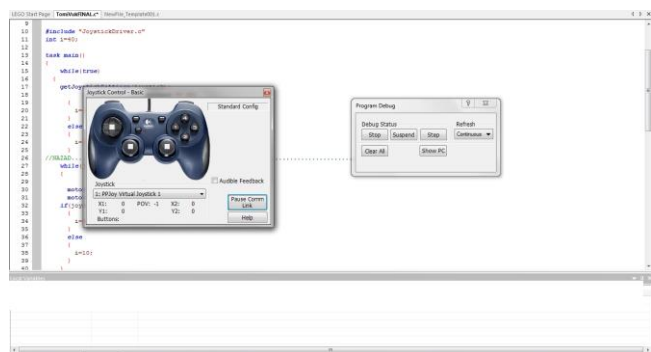


Fig.7: Program start

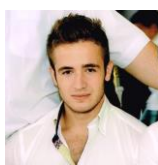
REFERENCES

- [1] http://www.robotc.net/wikiarchive/NXT_Functions_Joystick_Control
- [2] <http://ppjoy.en.malavida.com/>

CORRESPONDANCE



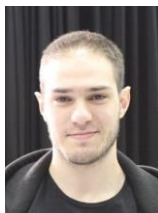
Aleksandar TOMOVIĆ, Student
University of Montenegro
Mechanical Engineering Faculty
Bul. Džordža Vašingtona bb
81000 Podgorica, Montenegro
aleksandartomovic23@gmail.com



Marko MUMOVIĆ, Student
University of Montenegro
Mechanical Engineering Faculty
Bul. Džordža Vašingtona bb
81000 Podgorica, Montenegro
markomumovic@gmail.com



Vasilije SAMARDŽIĆ, Student
University of Montenegro
Mechanical Engineering Faculty
Bul. Džordža Vašingtona bb
81000 Podgorica, Montenegro
vanja.mika@t-com.me



Vuk VUJOŠEVIĆ, Student
University of Montenegro
Mechanical Engineering Faculty
Bul. Džordža Vašingtona bb
81000 Podgorica, Montenegro
vukvujosevic7@gmail.com



Marko RAŠOVIĆ, Student
University of Montenegro
Mechanical Engineering Faculty
Bul. Džordža Vašingtona bb
81000 Podgorica, Montenegro
markorasovic2@gmail.com



Marina MIJANOVIĆ MARKUŠ, Prof.
D.Sc. Eng
University of Montenegro
Mechanical Engineering Faculty
Bul. Džordža Vašingtona bb
81000 Podgorica, Montenegro
marinami@ac.me

TRAINABLE ROBOTIC ARM

Marko MUMOVIĆ
Vuk VUJOŠEVIĆ
Vasilije SAMARDŽIĆ
Aleksandar TOMOVIĆ
Marko RAŠOVIĆ
Zoran MIJANOVIĆ

Key words: Robotic, arm, manipulators

Robotic manipulators have a very wide application today in industry, due to their flexibility and good mobility, and they are very useful in carrying out different tasks from various fields of science and industry.

This project represents the manipulator with 5 degrees of freedom of movement, or 5 independent motors. Control is done by using two buttons located on the breadboard. One button serves to enter the "learning state", while the other serves to start executing the given movements. By pressing the button on the 6th pin, the LED lights up and the robot enters the "learning state", then you need to move the robot arm manually, then press the same button to remember the movement. After pressing button, the robot will then return to the starting position. By pressing on the button, which is on the 7th pin, the robot will repeat the last path which was assigned to it.

This principle is used in a large number of factories all over the world, because if it is necessary for the robot to repeat its movement, or function, all that needs to be done is to manually move it, instead of typing a special code for every robot movement.

For the development of this project, the following material was used:

- Arduino UNO microcontroller
- 5 analogue feedback servo motors
- 2 buttons
- 2 resistors of 1Kohm
- Wires
- Breadboard.

Parts of the robot, respectively the motor housing, are printed on a 3D printer.

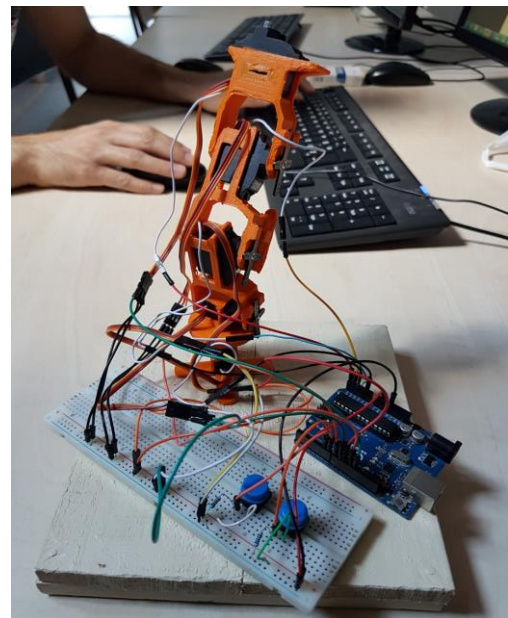


Fig.1: Trainable robotic arm

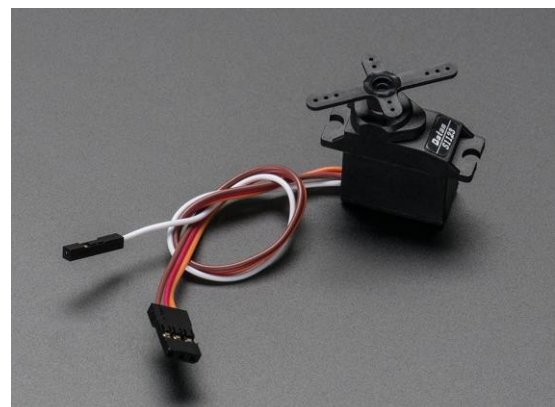


Fig.2: Analogue feedback servo motor

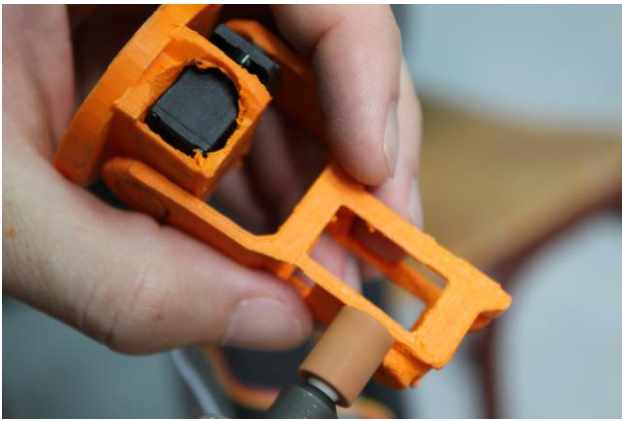


Fig.3: Making the housing for servo motor

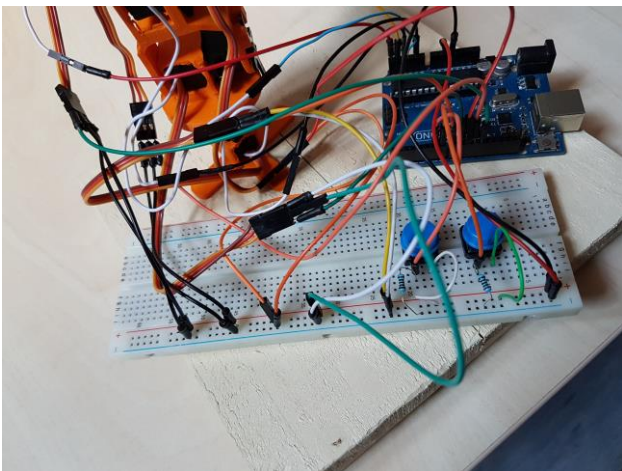


Fig.4: Robotic arm wiring

Connecting a robot to the Arduino is simple. Arduino 5V and GND should be brought on the breadboard. Connect two buttons directly to 5V and through resistor to GND. Analogue feedback servo motors have 4 wires (brown, red, yellow and white). The brown wire is connected on GND, red one on 5V, yellow wire represents motor signal and it connects to desire pin on Arduino, and the white wire represents motor feedback and it connects to the analog pin.

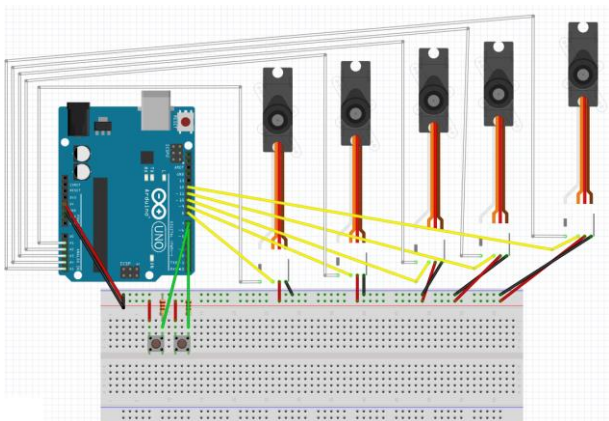


Fig.5: Scheme of connection

The program code is written in the Arduino work environment.

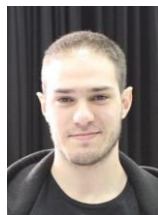
REFERENCES

[1] <https://learn.adafruit.com/trainable-robotic-arm?view=all>

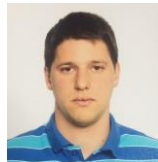
CORRESPONDANCE



Marko MUMOVIĆ, Student
University of Montenegro
Mechanical Engineering Faculty
Bul. Džordža Vašingtona bb
81000 Podgorica, Montenegro
markomumovic@gmail.com



Vuk VUJOŠEVIĆ, Student
University of Montenegro
Mechanical Engineering Faculty
Bul. Džordža Vašingtona bb
81000 Podgorica, Montenegro
vukvujosevic7@gmail.com



Vasilije SAMARDŽIĆ, Student
University of Montenegro
Mechanical Engineering Faculty
Bul. Džordža Vašingtona bb
81000 Podgorica, Montenegro
vanja.mika@t-com.me



Aleksandar TOMOVIĆ, Student
University of Montenegro
Mechanical Engineering Faculty
Bul. Džordža Vašingtona bb
81000 Podgorica, Montenegro
aleksandartomovic23@gmail.com



Marko RAŠOVIĆ, Student
University of Montenegro
Mechanical Engineering Faculty
Bul. Džordža Vašingtona bb
81000 Podgorica, Montenegro
markorasovic2@gmail.com



Zoran MIJANOVIĆ, Prof. D.Sc. Eng
University of Montenegro
Faculty of Electrical Engineering
Bul. Džordža Vašingtona bb
81000 Podgorica, Montenegro
zoranm@ac.me

TACHOMETER BASED ON A HALL EFFECT

Vasilije SAMARDŽIĆ
Vuk VUJOŠEVIĆ
Marko RAŠOVIĆ
Aleksandar TOMOVIĆ
Marko MUMOVIĆ
Marina MIJANOVIĆ MARKUŠ

Key words: Hall, effect, sensor

This project uses the Hall effect sensor that works on the principle of magnetic field detection. Whenever the magnet passes by the sensor, it detects it. It can be used for a lot of different purposes. For example, if we want to detect the closing of the door, we should just connect the magnet to the door, and put the Hall sensor on the doorpost. Whenever the door closes, the sensor would detect the magnetic field.

For the development of this project, the following material was used: Arduino UNO, piece of magnet, Hall effect sensor 44E or US5881 or US1181, 10 Kohm resistor, wires, a casing made on a 3D printer, and LCD display module.

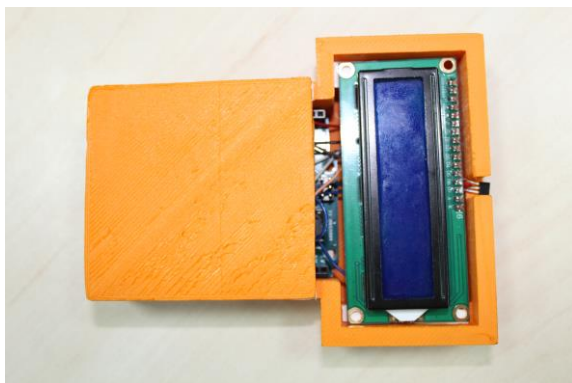


Fig.1: Tachometer based on a Hall effect



Fig.2: Arduino UNO, LCD display

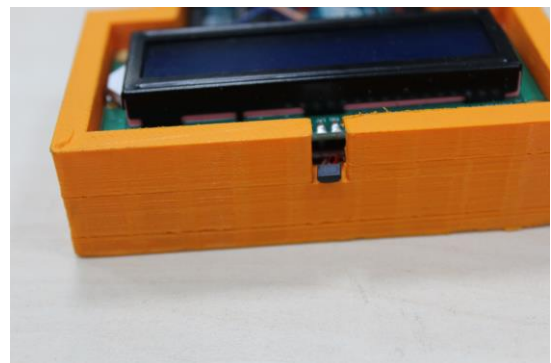


Fig.3: Hall effect sensor

The Hall effect sensor works on the principle of the Hall effect, which says that whenever a magnetic field is placed in the direction normal on the electrical current flow in the conductor, the potential difference is induced. This voltage can be used to detect whether the sensor is near the magnet or not. Arduino can detect the change of this voltage through the interrupt pin, and thus determine whether the magnet is close to the sensor or not. The principle of Tachometer based on the Hall effect is shown in the picture below.

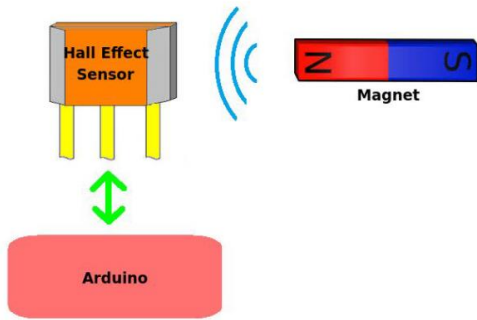


Fig.4: The working principle of Hall effect sensor

There are several types of Hall sensor, and some types are better than others for individual applications. For applications where detection speed is not crucial, a common Hall sensor such as 44E can be used. But for an application that involves high-speed detection, such as in the case of speedometer Hall high-frequency sensors such as US5881 or US1881, should be used.

3-pin Hall effect sensor: VCC (5V), GND and Vout (Signal). Pins are shown in the picture below:

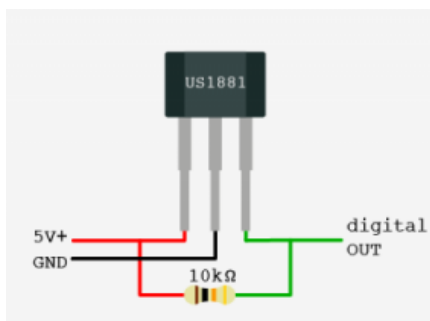


Fig.5: Pins of Hall sensor

Connecting the Hall sensor with Arduino is very simple. The VCC of the sensor is connected to a 5V Arduino pin. The GND of the sensor is connected to the GND pin at Arduino. V_{out} (Signal pins) of the Hall sensor is connected to the interrupt pin of Arduino (digital pin 2). The Hall sensor signal pin is connected to the VCC via a resistor of 10Kohm. Wiring is shown in the picture below.

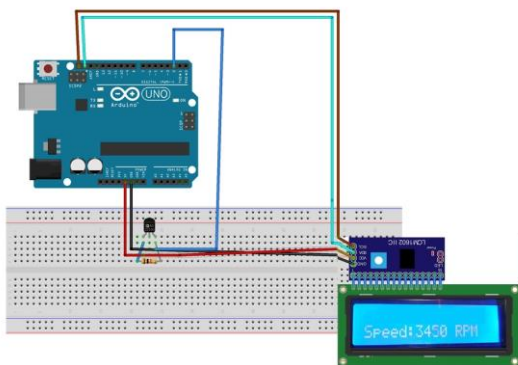


Fig.6: Wiring

The program code for Hall sensor is written in an Arduino program environment.

REFERENCES

- [1] <https://diyhacking.com/arduino-hall-effect-sensor-tutorial/>, accessed 15.5.2017.

CORRESPONDANCE



Vasilije SAMARDŽIĆ, Student
University of Montenegro
Mechanical Engineering Faculty
Bul. Džordža Vašingtona bb
81000 Podgorica, Montenegro
vanja.mika@t-com.me



Vuk VUJOŠEVIĆ, Student
University of Montenegro
Mechanical Engineering Faculty
Bul. Džordža Vašingtona bb
81000 Podgorica, Montenegro
vukvujosevic7@gmail.com



Marko RAŠOVIĆ, Student
University of Montenegro
Mechanical Engineering Faculty
Bul. Džordža Vašingtona bb
81000 Podgorica, Montenegro
markorasovic2@gmail.com



Aleksandar TOMOVIĆ, Student
University of Montenegro
Mechanical Engineering Faculty
Bul. Džordža Vašingtona bb
81000 Podgorica, Montenegro
aleksandartomovic23@gmail.com



Marko MUMOVIĆ, Student
University of Montenegro
Mechanical Engineering Faculty
Bul. Džordža Vašingtona bb
81000 Podgorica, Montenegro
markomumovic@gmail.com



Marina MIJANOVIĆ MARKUŠ, Prof.
D.Sc. Eng
University of Montenegro
Mechanical Engineering Faculty
Bul. Džordža Vašingtona bb
81000 Podgorica, Montenegro
marinami@ac.me

INDEX OF AUTHORS

INDEX OF AUTHORS

A

Ahmičević Izet	459
AL Basaqr Sulaiman	53
Al Sammarraie Amir	53
Antić Igor	135
Antunović Ranko	385
Arbiter Beno	443
Arsić Miodrag	359
Atanasovska Ivana	203,209,355

B

Banić Milan	53, 71,161,175
Berberović Mirsad	455
Bergant Anton	309
Bešić Nihad	459
Bijelić Zdravko	429
Blagojević Jasmina	265
Blagojević Mirko	153,225
Blagojević Vladislav	157
Blanuša Vladimir	241
Borec Sven	76
Bošnjak Srđan	359
Božić Ivan	333,339
Brđanin Radislav	325
Bucha Jozef	81,85
Bukvić Milan	219
Bulatović Radoš	82,195
Burić Milorad	315

Č

Čavić Maja	111, 225
------------------	----------

Ć

Ćirić Ivan	117
Ćirković Nikola	451
Ćurić Srđan	285

C

Ceccarelli Marco	3
Crnčević Miroslav	343
Crnojević Cvetko	169

D

Danko Ján	47, 81
Dedijer Sandra	297
Desnica Elenora	247

Dimchev Georgi	43
Dimić Aleksandar	183
Dimitrijević Branislav	161
Dimitrov Lubomir	43
Dizdar Samir	37
Dobranjac Mirko.....	349
Dukovski Vladimir	259

Đ

Đerić Srđan	463
Đidelića Mensud	375
Đorđević Branislav	365,371
Đorđević Zorica	265
Đurašković Dragana	301
Đurić Aleksija	149,253
Đurić Željko	325
Đurišić Slaviša	315

Dž

Džihó Edin	391
------------------	-----

F

Filová Zuzana	91
---------------------	----

G

Gajin Marko	371
Glišić Aleksandar	343
Glišović Jasna	105
Golubović Dušan	423
Gostimirović Marin	291
Gosto Muhamed	453
Gračić Muhamed	455
Gulan Ladislav	47, 81
Gvozdenac Urošević Branka	325

H

Habul Enis	455
Hakalović Edmin	453
Hedrih (Stevanović) Katica	209
Horváth Dániel	65

I

Ilić Andreja	105, 247
Ilić Jovan	339
Imamović Sead	457
Isić Safet	35,391,453
Ivanović Dečan	59

Ivanović Gradimir	399
Ivanović Lozica	105, 149, 247
Ivanović Vladan	411

J

Janjić Mileta	237, 301
Jelačić Bojan	45, 429
Jelić Vesna	231
Jerz Vladimir	75
Jokanović Mirjana	285,423
Josifović Danica	247
Jovanović Darko	291
Jovanović Dragan	399
Jovanović Janko	82,195
Jovišić Mijana	429
Jovović Aleksandar	443

K

Karabegović Isak	417
Karadžić Uroš	309, 437
Karaosmanović Alem	457
Karuppanan Saravanan	203
Kašiković Nemanja	297
Kämper Klaus Peter	9
Kecman Ivana	349
Knežević Ivan	225
Kokalj Filip	443
Koprivica Aleksandra	285,423
Kostić Nenad	153
Kotlarik Bohumil	91
Kovač Pavel	291
Kozakova Alena	91
Krešić Inga	165
Kresojević Igor	315
Krstić Perica	343
Krunić Miloš	333
Krupejová Daša	91
Kubalová Katarína	91
Kuljić Stanka	437
Kuzmanović Siniša	225

L

Lučić Marko	315
-------------------	-----

M

Maksumić Arnel	453
Malešević Zoranka	359
Marinović Budimirka	325
Marjanović Nenad	153
Marković Biljana	149, 253,463
Marković Slavoljub	463
Markuš Mijanović Marina	129,465,469
Matejić Miloš	105,153,225
Mazij Jernej	309
Mijanović Zoran	461,467
Miladinović Slavica	219
Milanović Biljana	429
Milčić Dragan	53, 329

Milčić Miodrag	329
Milesich Tomáš	81
Milić Neda	297
Miloradović Nenad	135
Milošević Miloš	71
Milovančević Miloš	215,277, 281
Miltenović Aleksandar	71, 161, 175
Miltenović Đorđe	175
Miltenović Vojislav	13
Milutnović Mladimir	157
Mišković Žarko	161
Mitrović Radivoje	161, 355, 399
Mladenović Mladen	359
Mladenović Srđan	157
Momčilović Dejan	355
Movrin Dejan	157
Mumović Marko	451,461,465,467,469
Mušić Armin	455

N

Negoičić Rastko	76, 405
Nezirić Emir	391, 455
Nikolić Nenad	405
Nikolić Vlastimir	117
Nikolov Kiril	43
Novaković Dragoljub	297

O

Ognjanović Milosav	21
Omeragić Amir	457
Opačić Mirjana	365

P

Pantelić Snežana	399, 405
Patil Santosh	203
Pelko Kenan	453
Penčić Marko	111, 225,
Petković Dalibor	277,281
Petrović Emina	117
Petrović Nenad	153
Poós Tibor	65
Pucovski Vladimir	291

R

Rackov Milan	111,175,225
Radosavljević Saša	219
Ranđelović Saša	157
Rašović Marko	451, 461,465,467,469
Rašović Nebojša	165
Risteska Svetlana	259
Ristivojević Mileta	169, 183
Rosić Božidar	183
Rustempašić Samir	457

S

Salih Sabah	53
-------------------	----

Samakoski Blagoja	259
Samardžić Vasilije	451, 461,465,467,469
Samec Niko	443
Savić Zoran	359
Savković Borislav	291
Sedmak Aleksandar	365
Sedmak Simon	371
Sekulić Milenko	291
Simonović Miloš	117
Skoko Dragiša	169
Skupnjak Darko	129,321
Soldat Nataša	231
Sovilj Bogdan	241
Sovilj Nikić Ivan	241
Sovilj Nikić Sandra	241
Spaić Obrad	285
Stamenić Zoran	231
Stamenković Dušan	71
Starčević Kenan	459
Stefanović Marinović Jelena	215
Stević Dragan	399, 405
Stojanović Blaža	105,219,247
Stojić Boris	123
Stošić Dragan	,399, 405
Sulova Janka	469

Š

Šendro Jasmina	453
Šibalić Nikola	129
Šupić Blagoje	423

T

Tabaković Slobodan	189
Tajar Ahmed	457
Tamásh Kornél.....	65
Tanasković Drakče	365,371
Tatić Uroš	365,371
Tica Milan	175
Tihić Dino	463
Tiro Dragi	459
Todorović Filip	405
Tombarević Esad	411
Tomić Miša	161
Tomov Pancho	43
Tomović Aleksandar	451, 461,465,467,469
Tomović Radoslav	37, 82,141,451
Troha Sanjin	215
Tudose Cristina	47
Tudose Lucian	47

U

Ursache Constantin	47
--------------------------	----

V

Veličković Sandra	219,265
Velimirović Miodrag	329
Vladić Gojko	297

Vučetić Nikola	385
Vučina Adisa	37
Vujadinović Radoje	315
Vujanac Rodoljub	135
Vujičić Boro	449
Vujošević Vuk	451, 461,465,467,469
Vujović Ženja	449
Vukčević Milan	129,237,321
Vukoslavčević Petar	27

Z

Zeljковиć Milan	189
Zuber Ninoslav	379

Ž

Živanović Saša	271
Živić Dragan	343
Živković Aleksandar	189

**PRESENTATIONS OF
SPONSOR**

Your partner for renewable and clean energy



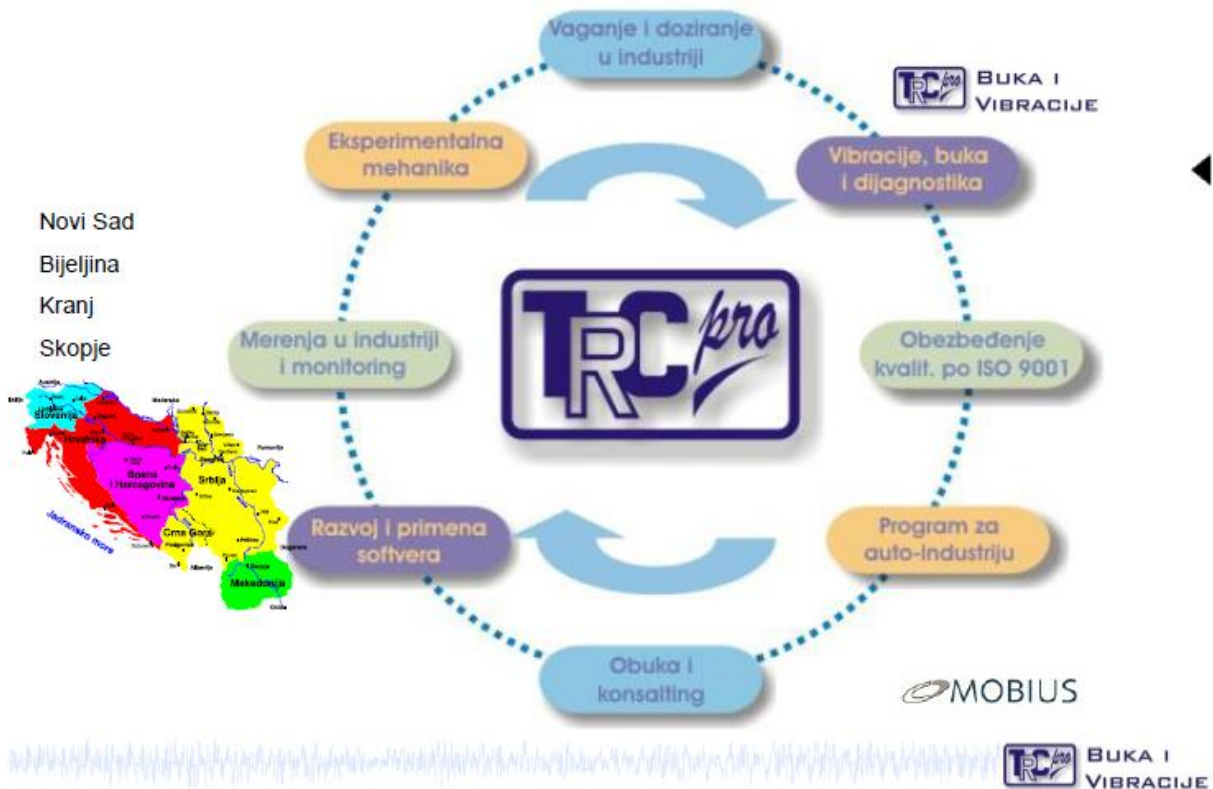
ANDRITZ HYDRO is a global supplier of electromechanical equipment and services (“from water-to-wire”) for hydropower plants. With over 175 years of experience and more than 31,600 turbines installed, we are a market leader for hydraulic power generation.

Water has always been a source of fascination and inspiration. But to us at ANDRITZ HYDRO, it means even more because it represents a constant challenge to create up-to-date technological innovations. Utility companies from all over the world value our know-how and commitment, and trust in the safety

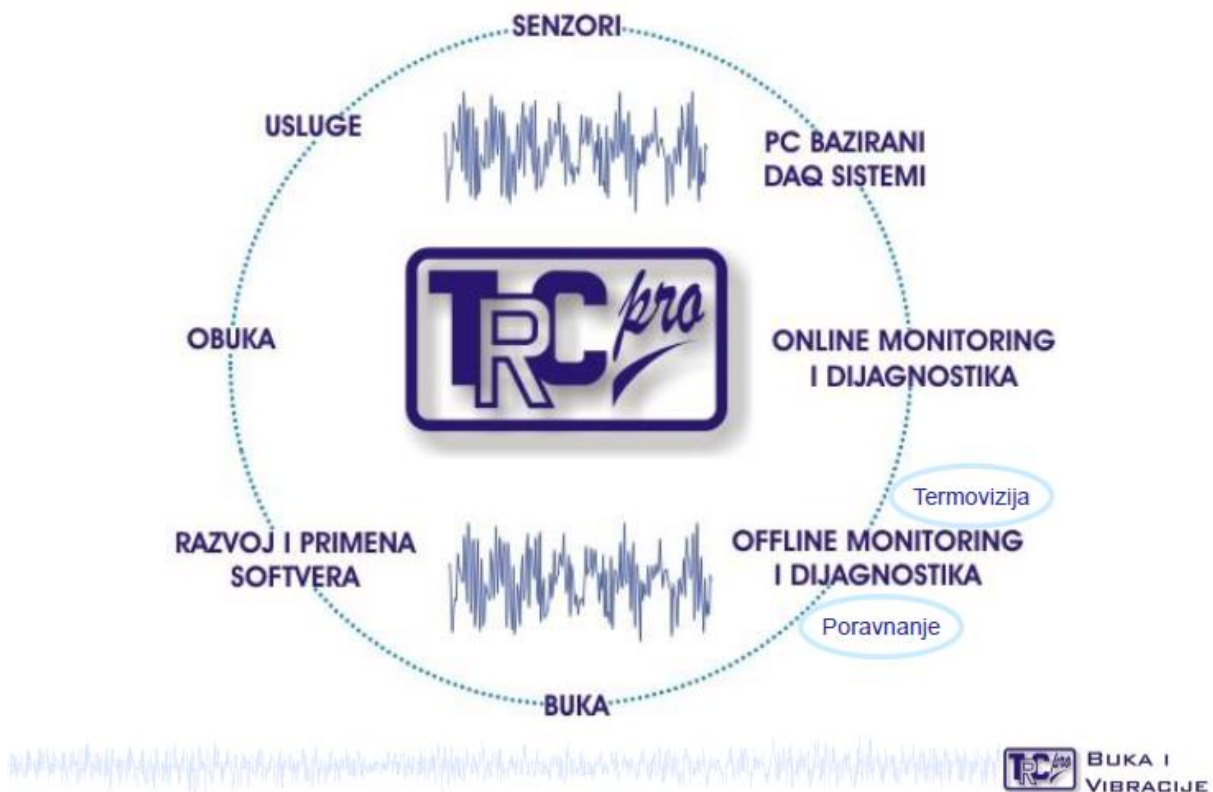
and reliability of our tailor-made energy generation solutions. From equipment for new, turnkey hydropower plants, and the refurbishing and overhaul of existing installations, to comprehensive automation solutions.

We focus on the best solution – “from water-to-wire”.

TRCpro Delatnosti (merenje mehaničkih veličina električnim putem)



TRCpro Delatnosti – Buka i Vibracije



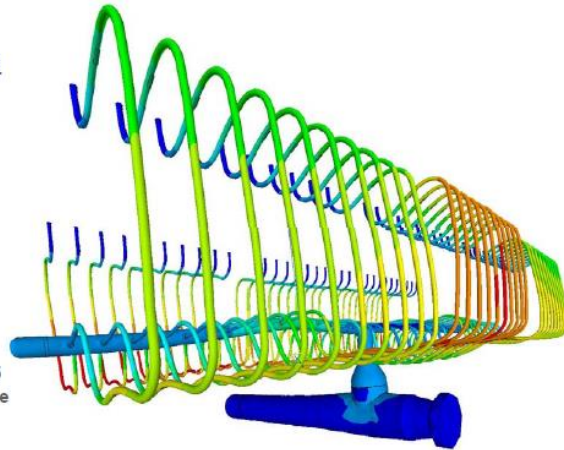
BerDiz Consulting AB was founded in 2004 by CEO Samir Dizdar and Erik Bernesson with head office in Gothenburg.



Erik: +46-733-791328
erik.bernesson@berdiz.se



Samir: +46-704-589275
samir.dizdar@berdiz.se



Office: Ranängsgatan 8-10
416 64Gothenburg
(just off the E6 Olskroken
junction on the south west side)

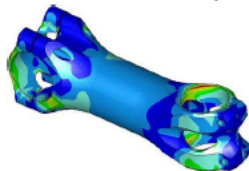
2017-09-06

2

Our Consultancy Services

We have: ANSYS, Peps (Pipestress), Pro-E, CAE-pipe, Mathcad, Inventor, AutoCAD, Relap5

New programs are purchased when necessary.



Mechanical calculations

Ex: Requirement engineering, FEM, stress & strength, pipe and thermal analysis, fatigue, cracks, plasticity, multi-axiality, creep

Mechanical construction

Process construction, Pro-E, Inventor, AutoCAD, CAE Pipe

Programming & HW / Electronics

Analog / digital simulation, EMC electrical engineering, CE-marking, Control systems

Codes used for evaluation

Ex: ASME III, ASME II, ASME VIII, ASME B16, ASME B31.3, KTA, RCC-M, RCC-MRx, EN-13445, EN-13480, Eurocode 2, Eurocode 3, SSG, API:s, TKN, RN, ASCE, AFS, ANSI, ISO, DIN, Colly and more

2017-09-06

6



TREBINJE

In an oasis of greenery with its typical Mediterranean spirit, at the foot of Leotar mountain, lies Trebinje, one of the most beautiful towns in the Republic of Srpska. Its magnificent scenery makes it very attractive for many visitors...

Trebinje is situated in the very south of the Republic of Srpska (Bosnia and Herzegovina), on the crossroads between the towns under the protection of UNESCO (Kotor, Mostar and Dubrovnik), and only 25 kilometers away from the Adriatic coast.

Very favorable traffic-geographical position and Mediterranean climate with a lot of sunny days (260 a year) makes it an ideal place for living or spending a perfect vacation. It also favors cultivation of various agricultural crops.

It has 32 000 inhabitants and occupies an area of 904 square kilometers, at an altitude of 273 meters.

Trebinje is an economic, cultural and tourist center of the East Herzegovina region. It is rather harmoniously built and well planned town.

Throughout its long and turbulent history Trebinje has always been a crossroads and a link between the Mediterranean and the interior of the Balkan Peninsula. The Illyrians, Romans, Slavs, Byzantines, medieval rulers of Serbian Nemanjic state, and then the Ottoman Empire and the Austro-Hungarians all passed this crossroads, and eventually Trebinje became a town on the border of Bosnia and Herzegovina, Montenegro and Croatia.

All these eras and rulers left their traces and marked local culture, both spiritual and material.

The old town "Kastel" was established in the early 18th century on the bank of the river Trebisnjica. Formerly it was a trade and crafts center and this old atmosphere can be felt during the walk through narrow paved streets, tunnels, squares...

The present appearance of the town is an attractive mosaic of closely intertwined Mediterranean and Oriental styles of the past and the modern age.

In the very centre of the town, in Ducic's Street, there is a well known sidewalk cafe 'Platani'. A unique picturesque green market is located near the sidewalk cafe, on the main town square, offering the indigenous agricultural and other products of this region.

